THE PHYSICS OF METALS AND METALLOGRAPHY

VOLUME 8, 1959

VOL.
8
1959

Chief Editor:
S. V. VONSOVSKII

Deputy Chief Editor:
V. I. ARKHAROV

EDITORIAL BOARD:

V. I. ARKHAROV
S. V. VONSOVSKII
V. D. KUZNETSOV
G. V. KURDIUMOV
B. G. LAZAREV
A. G. LESNIK
A. N. ORLOV
V. A. PAVLOV
V. D. SADOVSKII
R. I. IANUS
IA. S. SHUR

Translation Editor:
Prof. Bruce Chalmers

PERGAMON PRESS INC.

NEW YORK . LONDON . OXFORD . PARIS . LOS ANGELES

THE PHYSICS OF METALS AND METALLOGRAPHY

VOLUME 8 1959

CONTENTS

No. 1

		PAGE
The spectrum of elementary excitations of the electron system of a single atom non-conducting crystal. II. The limits of applicability of Dirak's interchangeable Hamiltonian	YU. A. ISYUMOV	1
On the effect of internal interactions on the second moment of the paramagnetic resonance curve in the case of pure spin magnetism	U. KH. KOPVILLEM	6
The change in the internal energy, the thermoelectric force and the specific electric resistance in the plastic deformation of metals	V. N. KUNIN	16
The thermoelectric properties of the alloys Sn-Cd and Pb-Cd	V. A. YURKOV and V. V. NEKRASOV	19
Investigations into the defectoscopy of railway rails in moving magnetic fields. 17. A study of the currents in rails on excitation by a transverse field	V. V. VLASOV	23
The mechanisms involved in the solution and shifting of carbon in ferrite	L. S. LIVSHITS	27
The relief of metal powder grains	YA. YE. GEGUZIN and N. N. OVCHARENKO	32
The influence of additions of palladium on the hydrogen permability of iron	V. I. ARKHAROV and A. A. KRAGINA	37
The dynamics of the heating of a metal when internal transformations are present	E. M. GOLDFARB	44
The changes in fine crystal structure on the disintegration of the saturated solid solution nickel-chromium-aluminium-titanium	V. G. CHERNYI	58
The mechanism of brittle fracture in steel in a notched bar impact bending test	B. S. KASATKIN	65
The influence of length in tubular steel testpieces on deformation and tensile stress	L. G. AFENDIK and L. I. SHEKHTER	73
The effect of hydrogen adsorption in the process of deformation of steel on its mechanical properties	G. V. KARPENKO and R. I. KRIPYAKEVICH	77
The influence of plastic deformation on the internal friction of iron-tungsten alloys	V. S. POSTNIKOV and R. S. LEBEDEV	81
Latent plastic deformation energy of aluminium and copper alloys	M. M. POPOV, E. N. TIKHOMINA, S. M. SKURATOV and E. N. KALININA	87
On the subject of "super-ductility" of alloys	A. A. PRESNYAKOV and V. V. CHERVYAKOVA	96
Influence of stress concentration on fatigue endurance of steel	E. M. SHEVANDIN, L. F. KURDINKOVA and L. M. RUBINSHTEIN	103
Investigation of plastic properties of single crystals of beryllium	P. I. GARBER, I. A. GINDIN, A. I. KOVALEV and YU. V. SHUBIN	110
Investigation of highly heat-conducting and heat-resisting alloys of the Cu-Co-Be system	N. V. MAL'TSEV, V. YE. MIKRYUKOV and CHZHOY SHI-SHAN	119
Letters to the Editor		
Spin electron relaxation in antiferromagnetics	IU. SEIDOV and BERDYSHEV	125
To the question of the complex permeability of magnesium ferrites	L. A. FOMENKO	130
The basic state and the spectrum of elementary excitations of isotropic ferrite	S. V. TIABLIKOV	132
To the theory of vibration spectra of solid solutions	A. N. MEN' and A. N. ORLOV	135
On an error in the handbook "The physico-chemical properties of the elements"	IU. A. BAZHIN, V. A. GLADKODSKII, M. I. OLEINIK and K. P. RODIONOD	139
On the problem of the method of X-ray investigation of substances under high pressure. I. An X-ray tube that can be dismantled	S. A. NEMNONOV, M. I. OLEINIK and A. P. FROLOD	141

VOL.
8
1959

No. 2

	PAGE
On the elastic moduli of a two-phase solid M. A. KRIVOGLAZ and A. S. CHEREVKO	1
Ferromagnetic resonance in uniaxial ferrite with two sub-lattices E. N. IAKOLEV	5
On the structure of the energy bands in ionic crystals M. SH. GITERMAN and S. A. MOSKALENKO	9
Magnetic properties of steels as a basis of magnetic structure analysis G. S. TOMILOV, M. N. MIKHEEV and M. F. POMUKHIN	15
Study of the properties of titanium Alloys. IV. Properties of alloys of the ternary Ti-Al-Fe system I. I. KORNILOV, E. N. PYLAEVA and M. A. VOLKOVA	20
Directional diffusion, due to deformation, of hydrogen in a solid solution and strength of the metal K. V. POPOV and V. A. YAGUNOVA	25
On the kinetics of reactions diffusion in systems with some intermediate prase. I. Macroscopic calculation for a binary system V. I. ARKHAROV	30
Study of a nickel-chromium-aluminium-titanium alloy deformed in the quenched condition V. G. CHERNYI	39
Structure of the energy spectrum of electrons in Fe-Cr- and Fe-Cr-Ni- alloys N. D. BORISOV and V. V. NEMOSHKALENKO	44
On the problem of the influence of alloying on the kinetics of pearlitic transformation L. N. ALEKSANDROV and B. IA. LYUBOV	49
Some properties of the initial stage of plastic deformation. II. The point at which the first slip lines appear and the distribution of their direction. IA. R. RAUZIN	57
X-ray studies of deformations in the crystal lattice of metals deformed at low temperatures V. P. GOLIK, G. A. SIRENKO and V. I. KHOTKEVICH	65
Investigations of rolling texture by an electron-diffraction method IU. I. SOZIN	70
Variation of internal friction and coefficients of elasticity in pure iron with temperature V. M. AMONENKO, B. I. SHAPOVAL and V. V. LEBEDEV	78
Deformation of a plane solid body on phase transition A. M. KOSEVICH and L. V. TANATAROV	83
Some problems in the measurement of microhardness V. M. DOLIDZE	93
A study of the mechanical properties of solids, in particular of metals at absolute temperatures of 4.2°K and below. I. Tensile testing of polycrystalline aluminium (99.3%) O. V. KLYAVIN and A. V. STEPANOV	99
Mechanisms of plastic flow for lead and tin in shear conditions V. I. LIKHTMAN and V. S. OSTROVSKII	107
Influence of a low melting point molten metal on the mechanical properties of single crystals of more refractory metals L. A. KOCHANOVA, V. I. LIKHTMAN and P. A. REBINDER	112
On the nature of internal friction in hardened and tempered steel M. A. KRISHTAL and S. A. GOLOVIN	118
A contribution to the question of the nature of damping of vibrations in hardened and low temperature tempered carbon steel M. A. KRISHTAL and S. A. GOLOVIN	126
Letters to the Editor	
Concerning ferromagnetics with two Curie points V. L. BONCH-BRUYEVICH	132
The influence of plastic deformation on internal friction in iron and an iron-nickel alloy R. S. LEBYEDEV and V. S. POSTNIKOV	134
The influence of boron on the recrystallization of silicon iron V. YE. NEIKMARK and V. M. ROZENBYERG	137
Concerning magnetic anisotropy on the basis of spin-orbit interaction IU. A. IZIUMOV	139
Phase analysis by the superposition method using electron diffraction L. S. PALATNIK and B. T. BOIKO	141

No. 3

	PAGE
Ordering in ternary alloys — O. Mdivani and Gachechiladze	1
The importance of indirect interaction in the theory of magnetization of transition metals and rare earths — A. A. Berdyshev and B. V. Karpenko	10
Concerning binary solid solutions with interatomic bonds of two types — A. N. Men' and A. N. Orlov	17
The Hall effect in iron-nickel alloys near the Curie point — N. V. Bazhanova	22
On the problem of anomalous behaviour of the coercive force of quenched and highly annealed steels — M. N. Mikheev and G. S. Tomilov	26
The laws of intra-crystalline distribution of elements in metal alloys — A. S. Zav'yalov and B. I. Bruk	29
A study of self-diffusion in zirconium and its alloys with tin — V. S. Lyashenko, V. N. Bykov and L. V. Pavlinov	40
The effect of hydrogen on alloy VT-8 with increased creep stress — I. I. Kornilov, C. G. Glazunov and A. M. Yakimov	47
The study of aluminium alloys of the Al-Cu-Mg system in samples of variable composition — L. S. Palatnik, G. B. Fedorov and H. T. Gladkikh	54
Electron microscopic investigation of etching figures in aged aluminium alloys — N. N. Buinov, T. V. Shchegoleva, V. G. Rakin, M. F. Komarova and R. R. Zakharova	62
Homogeneous ageing of unsaturated solid solutions — A. A. Prfsniakov, L. I. Duatova and Iu. F. Kliuchnikov	68
Investigation of the tempering of cold deformed K40NKhM alloy — B. G. Livshits and N. G. Makhukov	73
Transformation of austentite into martensite under high pressure — A. I. Stregulin and L. A. Mel'nikov	79
Structure changes and anomalous temperature dependence of the magnetic properties of Ni-Fe alloys (50% Ni) — M. V. Dekhtyar and N. M. Kazantseva	84
Mechanical properties of nickel-aluminium alloys — V. A. Pavlov and I. A. Pereturina	88
Relationship of creep of nickel-copper alloys to solid solution concentration and deformation conditions — M. G. Gaidukov and V. A. Pavlov	95
Some peculiarities of transformer steel on rapid heating. 2; Kinetics of texture formation — P. D. Izbranov, V. A. Pavlov and H. M. Rodizin	101
Internal friction of metastable solid solutions — B. G. Livshits, Iu. S. Avraamov, V. B. Osvenskii, S. O. Mebzennaia and L. N. Beliakov	107
Determination of the number of arbitrary parameters of the short range order for multicomponent alloys — A. N. Men'	116
Studies of reaction diffusion in binary systems of the "metal gas" type — V. I. Arkharov and E. B. Blankova	119
Some peculiarities in the disposition of corrosion figures in the alloy Al-Zn-Cu — N. N. Buinov and T. V. Shchegoleva	122
Some regularities of the change of forces of the inter-atomic bond in the alpha-solid solutions of systems with electron compounds — G. P. Kushta and O. I. Rybailo	125
Temperature dependence of magnetic properties of the alloy IU 16 (Alfenol) — O. N. A'.tgauzen and I. K. Kupalova	127
The increase in the coercive force of mixed ferrite-chromites of Lithium in the region of the compensation temperature — K. M. Bol'shova and T. A. Yelkina	129
On the polygonal structure of iron-aluminium alloys — B. V. Molotilov	132
On the type of defects in an alpha-leboite — F. A. Sidorenko, P. V. Gel'd and L. B. Dubrovskaya	134
A fine structure in brittle and ductile fracture of E1531 steel tubes in tests of expansion by a cone — E. Iu. Chemadurova	136
On the problem of intermediate carbide phases in carbon steels — N. V. Gudkova and V. P. Kuznetsova	138
Influence of the duration of treatment on the phase composition of iron which has been electrically hardened with graphite — B. P. Kolesnik	141

Electrical conductivity and the Hall effect in iron-silicon alloys containing leboite when subjected to high temperature
A. I. Gol'dberg, V. A. Lipatov and P. V. Gel'd 143

An investigation of pearlite transformation in segregated austentite powder
A. O. Gulyaev and V. D. Zelenova 146

An investigation of intermediate transformation in segregated austentite powder
A. O. Gulyaev and V. D. Zelenova 148

The X-ray *K* absorption at the temperature of liquid nitrogen
S. A. Nemnonov and K. M. Kolobova 150

No. 4

PAGE

Investigation of the stability of cracks in a microscopic model of a crystal
A. N. Orlov 1

The dispersion of current carriers in compounds of the PbS group
I. M. Tsidil'kovskii 16

Superconductivity of metals taking into account overlapping of the energy bands
V. A. Moskalenko 25

The effect of geometrical distortions on the distribution of the background intensity of X-ray and neutron diffraction photographs M. A. Krivoglaz 37

The influence of thermomechanical treatment in which the stresses are created by twisting the sample, on the magnetic properties of the alloy vicalloy
M. G. Iuzhinskaia, Ia. S. Shur and N. N. Iagovkina 52

A magnetic method for the quantitative carbide analysis of carbon steels
Ia. I. Kagan and S. V. Bronin 56

Magnetic properties, electrical characteristics and hardness of high-carbon alloy steels in hardened state M. N. Mikheev and G. .S Tomilov 63

Nickel-cadmium ferrites N. A. Smolkov and S. A. Guschina 76

Generator of ultra-high magnetic fields I. G. Fakudov and E. A. Zavadskii 81

An investigation of reaction diffusion in binary systems of the " metal-gas " type 2
V. I. Arkharov and E. S. Blankova 87

The problem of the state of carbon and iron in steel
I. N. Frantevich, D. F. Kalinovich and I. Io. Kovenskii 93

Treatise on recrystallization of the matrix in the process of decomposition of super-saturated solid solution aluminium-silver R. M. Leriman and M. I. Turchinskaia 98

Electron microscope investigation of the distortion of Guinier-Preston zones in ageing alloys N. N. Buinov 103

Plasticity of transformer steel after heat treatment at temperatures of 300-900°
S. I. Doroshek 109

Carbide eutectic in nickel carbon alloys R. A. Sidorensko 114

An investigation of internal friction in powder products B. Ia. Pines and Den Ge Sen 117

Some features of the recrystallization of transformer steel during rapid heating. 3. The dependence of grain growth rate and activation energy on heating rate
P. D. Izbranov, V. A. Pavlov and N. M. Rodigin 124

Small flow and after-effect deformations of spring phosphor bronze Br OF 6.5-0.15
S. O. Tsobkallo 129

Hardness and brittleness of metal-like compounds
G. V. Samsonov, V. S. Neshpor and L. M. Khrenova 137

On the question of the mechanism of the initial stage of deformation of polycrystal-line metals Y. R. Rausin 145

Letters to the Editor

A study of the reactional diffusion in binary systems of the type "metal-gas". 3
V. I. Arkharov, E. B. Blankova, N. A. Sukhova and R. A. Entelis 150

The change in the electrical resistance of a monocrystal of magnetite in a magnetic field in the region of its low-temperature transformation T. D. Zotov 154

VOL. 8 1959

No. 5

PAGE

On the determination of conditions for the autoradiographic exposure of inhomogeneities in adsorptive concentration
V. S. Galishev, A. N. Orlov and I. A. Shvarte 1

On the effect of fluctuations in the parameters of correlation upon scattering of X-rays and thermal neutrons by solid solutions M. A. Krivoglaz 8

Relaxation absorption of ultrasound in ferromagnetics V. T. Shmatov 27

A diabetic galvanomagnetic and thermomagnetic phenomena in semiconductors. 2. Mixed conductivity V. Ye. Vzdornov and I. M. Tsidil'kovskii 31

On the temperature dependence of the magnetic properties of magnetically textured specimens of MnBi alloy powders
Ia. S. Shur, Ye. V. Shtolts, G. S. Kandaurova and L. V. Rebneva 38

On the reforming of the domain structure of magnetically uni-axial ferromagnetics in a magnetic field Ia. S. Shur, Ye. V. Shtolts and A. A. Glazer 44

On the dependence of the field of a defect of the crack type on the thickness of the covering metal layer V. V. Vlasov and R. Ye. Yer'shov 47

The thermoelectric properties of magnetite in the temperature region of 80-400°K
A. A. Samoklvalov and I. G. Fakidov 52

X-ray study of the temperature dependence of defects in the crystal lattice of metals
G. A. Sirenko and V. I. Khotkevich 57

Some peculiarities in the structure of anomalous effects in powder diffraction patterns of ageing Al-Ag and Al-Ag-Cn alloys R. R. Zakharova and N. N. Buinov 62

Effect of small amounts of admixtures on the diffusion coefficients of polycrystalline materials. 3. Effect of thallium on auto-diffusion of silver
V. I. Arklarov, S. M. Kliutsman and A. N. Timofeev 66

Investigation of the causes of diffusional "activity" of deformed crystalline bodies. 2. On the sintering of electrolytic metals in the light of model tests data
Ia. E. Geguzin and N. N. Ovcharenko 70

To the determination of surface tension on the boundaries of phases I. V. Salli 76

The effect of additions of vanadium on the self-diffusion of iron
M. S. Zelinskii, B. M. Noskov, P. V. Pavlov and E. V. Shitov 79

High temperature study of alloys, the phases of which have identical lattices with nearly the same parameters I. I. Titarenko and B. M. Rovinskii 84

The nature of ζ_2-phase of the system Fe-Si
F. A. Sidorenko, P. V. Gel'd and L. B. Dubrovskaya 88

On the reduction of copper ferrite with graphite
N. M. Stafeeva, V. N. Bogoslovskii, G. I. Chufarov and V. A. Subbotina 93

The effect of vacuum on variation of critical temperatures structure and chemical composition of cast iron
V. P. Chernobrovkin, V. S. Belyaev and A. A. Dobryden' 98

Hot-rolled transformer steel with low specific losses N. F. Dubrov 103

Analysis of the kinetics of two-phase precipitation of Cu-Be alloy by an electrical resistance method A. S. Kagan and Ya. S. Umanskii 108

Study of the patterns of deformation and recrystallization of iron-nickel alloy (48% Ni) in relation to the degree of deformation on cold rolling
M. M. Borodkina and N. P. Gromov 111

The influence of phosphorous on structural transformations and properties of low-alloy electro-technical steel S. I. Doroshek 118

The influence of cold plastic deformation on the modulus of elasticity in carbon steels A. V. Gur'yev 123

Determination of the period of relaxation at the polymorphic transformation of iron R. I. Garbyer and A. I. Kovalev 129

The influence of the temperature of the experiment on the fatigue strength of specimens of carbon steel with stress concentrators under the action of a molten environment of the eutectic Pb-Sw M. I. Chayevskii 132

VOL
8
195

Letters to the Editor

The problem of the mechanism of intercrystalline internal adsorption in dilute solid solutions
V. I. ARKHAROV, B. S. BORISOV, S. D. VANGENGEIM and G. G. TALUTS 135

On additional weakening of X-ray diffraction lines in powder specimens
A. YE. KOVAL'SKII and S. V. SEMENOVSKAIA 138

Dispersion equation for electron plasma in a magnetic field L. I. PODLUBNYI 140

Contribution to the treatment of anomalous effects on X-ray photographs of alloys in the process of ageing R. R. ZAKHAROVA and N. N. BUINOV 142

No. 6

PAGE

Electrical conductivity of ferromagnetic metals in a radio-frequency field
P. S. ZYRYMANOV, T. G. IZYUMOVA and G. V. SKROTSKII 1

The role of dipole-dipole interaction in ferromagnetic resonance IU. A. IZYUMOV 6

Development of metal physics and physics of metallurgy in the Chinese Peoples' Republic during ten years CHOU CHIH-HUNG, KO TSUN and TSIN LIN-CHAO 16

Mechanism of production of internal friction impurity peaks
V. T. SHMATOV and A. V. GRIN 24

The Hall effect in ferromagnetics
V. N. NOVOGRUDSKII, A. A. SAMOKHALOV and I. G. FAKIDOV 28

A method for the direct measurement of magnetic anisotropy in thin films
W. SCHUPPEL, O. STEMME, W. ANDRA and Z. MALEK 30

Electric conductivity of iron at elevated temperatures
V. S. GUMENYUK and V. V. LEBEDEV 38

The temperature relation of the Nernst-Ettingshausen thermomagnetic effect in nickel and ferro-nickel alloys R. P. IVANOVA 42

The X-ray diffraction study of the reduction processes in some ferrites
V. N. BOGOSLOVSKII 47

On the question of concentration inequalities experimentally detected in solid bodies V. I. ARKHAROV 51

A study of the internal friction in powder metallurgical bodies. 4. Specimens from binary powders of noninteracting components Cu-Mo, Cu-W
B. IA. PINES and DEN GE SEN 56

The wear resistance of case-hardened steel and its substructure
I. M. LYUBARSKII, A. P. LYUBCHENKO and G. N. BAKAKIN 61

On the existance of the silicide W Si
N. N. MATIUSHENKO, L. N. YEFIMENKO and D. P. SOLOPIKHIN 67

The fine structure of the intercrystalline transition zones of mild steel
B. S. KASATKIN and G. F. DAROVSKII 70

The formation of a cubic texture in ferro-silicon alloys
CHOU P'EN HSIN, WANG WEI MING and CHENG NEN HUANG 74

The components of specific loss and magnetic permeability of dynamo steels alloyed with phosphorous S. I. DOROSHEK and V. V. DRUZHININ 80

On the nature of the strain hardening which occurs when quench hardended high-speed steel is tempered P. M. YUSHKEVICH 84

The influence of cyclic heat treatment on uranium bicrystals
S. YA. ZALIVADNYI and V. M. MIKHAILOVSKII 91

The failure of a martensite crystal under the simultaneous action of external tensile and compressive stresses A. MASHIN 95

The effect of the original structure and temperature of deformation on phase transformations during plastic formation B. A. APAEV and YU. A. SYSUED 101

Study of the mechanical properties of solids particularly metals, at and below temperatures of 4.2°K. 3. The mechanical properties of iron, titanium, tantalum and 2 steel at and below temperatures of 4.2°K. O. V. KLIAVIN and A. V. STEPANOVA 107

The influence of the size effect on the deformability of metals
I. A. RAZOV, YE. M. SHEVANDIN and A. V. YEFIMOV 113

To the question of the dependence of the hardness on the composition of multi-phase alloys V. P. SHISHOKIN and A. E. NIKEROV 119

Effect of the rate of heating and cooling on the irreversible deformation of iron
S. F. KOVTUN 123

VOL.
8
1959

THE PHYSICS OF METALS AND METALLOGRAPHY

VOLUME 8 1959

CONTENTS

No. 1

		PAGE
The spectrum of elementary excitations of the electron system of a single atom non-conducting crystal. II. The limits of applicability of Dirak's interchangeable Hamiltonian	Yu. A. Isyumov	1
On the effect of internal interactions on the second moment of the paramagnetic resonance curve in the case of pure spin magnetism	U. Kh. Kopvillem	6
The change in the internal energy, the thermoelectric force and the specific electric resistance in the plastic deformation of metals	V. N. Kunin	16
The thermoelectric properties of the alloys Sn-Cd and Pb-Cd	V. A. Yurkov and V. V. Nekrasov	19
Investigations into the defectoscopy of railway rails in moving magnetic fields. 17. A study of the currents in rails on excitation by a transverse field	V. V. Vlasov	23
The mechanisms involved in the solution and shifting of carbon in ferrite	L. S. Livshits	27
The relief of metal powder grains	Ya. Ye. Geguzin and N. N. Ovcharenko	32
The influence of additions of palladium on the hydrogen permability of iron	V. I. Arkharov and A. A. Kragina	37
The dynamics of the heating of a metal when internal transformations are present	E. M. Goldfarb	44
The changes in fine crystal structure on the disintegration of the saturated solid solution nickel-chromium-aluminium-titanium	V. G. Chernyi	58
The mechanism of brittle fracture in steel in a notched bar impact bending test	B. S. Kasatkin	65
The influence of length in tubular steel testpieces on deformation and tensile stress	L. G. Afendik and L. I. Shekhter	73
The effect of hydrogen adsorption in the process of deformation of steel on its mechanical properties	G. V. Karpenko and R. I. Kripyakevich	77
The influence of plastic deformation on the internal friction of iron-tungsten alloys	V. S. Postnikov and R. S. Lebedev	81
Latent plastic deformation energy of aluminium and copper alloys	M. M. Popov, E. N. Tikhomina, S. M. Skuratov and E. N. Kalinina	87
On the subject of "super-ductility" of alloys	A. A. Presnyakov and V. V. Chervyakova	96
Influence of stress concentration on fatigue endurance of steel	E. M. Shevandin, L. F. Kurdinkova and L. M. Rubinshtein	103
Investigation of plastic properties of single crystals of beryllium	P. I. Garber, I. A. Gindin, A. I. Kovalev and Yu. V. Shubin	110
Investigation of highly heat-conducting and heat-resisting alloys of the Cu-Co-Be system	N. V. Mal'tsev, V. Ye. Mikryukov and Chzhoy Shi-Shan	119
Letters to the Editor		
Spin electron relaxation in antiferromagnetics	Iu. Seidov and Berdyshev	125
To the question of the complex permeability of magnesium ferrites	L. A. Fomenko	130
The basic state and the spectrum of elementary excitations of isotropic ferrite	S. V. Tiablikov	132
To the theory of vibration spectra of solid solutions	A. N. Men' and A. N. Orlov	135
On an error in the handbook "The physico-chemical properties of the elements"	Iu. A. Bazhin, V. A. Gladkodskii, M. I. Oleinik and K. P. Rodionod	139
On the problem of the method of X-ray investigation of substances under high pressure. I. An X-ray tube that can be dismantled	S. A. Nemnonov, M. I. Oleinik and A. P. Frolod	141

VOL 8 195

THE SPECTRUM OF ELEMENTARY EXCITATIONS OF THE ELECTRON SYSTEM OF A SINGLE ATOM NON-CONDUCTING CRYSTAL
II. THE LIMITS OF APPLICABILITY OF DIRAK'S* INTERCHANGEABLE HAMILTONIAN

Yu.A. ISYuMOV

The Gor'kii Urals State University

(Received 4 March 1958)

This paper sets out the conditions in which it is possible to use the interchangeable Hamiltonian of Dirak as an arbitrary value of spin.

VOL. 8 1959

As shown by Dirak [1], the part of the energy operator in a system of interacting electrons, which depends on spin, has the form

$$\hat{\mathbf{H}}_{об} = -\sum_{f_1 \neq f_2} I(f_1 f_2) \left\{ \frac{1}{4} + \hat{\vec{S}}_{f_1} \hat{\vec{S}}_{f_2} \right\}, \tag{1}$$

where $\hat{\vec{S}}_f$ is the operator of the spin vector of junction f of the lattice, and $I(F_1 f_2)$ is the interchangeable integral. Equation (1) is obtained from the necessity for an antisymmetrical state of the wave functions of the electron system in relation to the space and spin co-ordinates of the two electrons. It is important to note here that Dirak presented equation (1) especially for $s = ½$ (for electrons), and its generalization to meet the case of arbitrary spin Dirak's method will inevitably lead to difficulties. However, the Hamiltonian is already used in papers (1) to describe systems of particles with an arbitrary spin of $s > ½$ such as, for instance, might be the uncompensated orbitals of atoms.

We will consider the limits of application of the Hamiltonian (1) to the collection of atoms which form a crystal.

Let us take the number of electrons forming the open envelope of an atom as z, while between them there is a weak Russel-Saunders bond such that the atom as a whole could be given a spin number s. The orbital state of these electrons will be given the index λ. The Hamiltonian of the electron system of the metal in a secondary quantum presentation will have the form

$$\hat{\mathbf{H}} = \sum L(f_1 \lambda_1 f_1' \lambda_1') a^+_{f_1 \lambda_1 \sigma_1} a_{f_1' \lambda_1' \sigma_1} + \\ + \frac{1}{2} \sum F(f_1 \lambda_1 f_2 \lambda_2 f_1' \lambda_1' f_2' \lambda_2') a^+_{f_1 \lambda_1 \sigma_1} a^+_{f_2 \lambda_2 \sigma_2} a_{f_2' \lambda_2' \sigma_2} a_{f_1' \lambda_1' \sigma_1}. \tag{2}$$

If the transitions between the various orbital states of the electrons are disregarded, and also the formation of polar states, it could be formulated with the symbols

$$\sum_{\sigma} a^+_{f\lambda\sigma} a_{f\lambda\sigma} = 1; \quad \lambda = \lambda_1, \lambda_2, \ldots, \lambda_z, \tag{3}$$

---

* *Fiz. metal. metalloved.*, 8, No. 1, 1-7, 1959.

so that the Hamiltonian (2) is reduced to

$$\hat{\mathbf{H}} = E_0 - \frac{1}{2} \sum_{(f_1\lambda_1)\neq(f_2\lambda_2)} I(f_1\lambda_1 f_2\lambda_2)\, a^+_{f_1\lambda_1\sigma_1} a_{f_1\lambda_1\sigma_2} a^+_{f_2\lambda_2\sigma_2} a_{f_2\lambda_2\sigma_1}, \tag{4}$$

in which

$$I(f_1\lambda_1 f_2\lambda_2) = F(f_1\lambda_1 f_2\lambda_2 f_2\lambda_2 f_1\lambda_1)$$

is the integral exchangeable between the two electron states. As orbital transitions are not allowed, the spin co-ordinates are single dynamic alternating systems from which it is clear that the Hamiltonian (4) could be expressed through the spin operator. Following Bogolyubov [2], they may be introduced by means of the following ratios:

$$\hat{S}^x_{f\lambda} = \frac{1}{2}\left(a^+_{f\lambda,\,-\frac{1}{2}}\, a_{f\lambda,\,+\frac{1}{2}} + a^+_{f\lambda,\,+\frac{1}{2}}\, a_{f\lambda,\,-\frac{1}{2}}\right),$$

$$\hat{S}^y_{f\lambda} = \frac{1}{2}\, i\left(a^+_{f\lambda,\,+\frac{1}{2}}\, a_{f\lambda,\,-\frac{1}{2}} - a^+_{f\lambda,\,-\frac{1}{2}}\, a_{f\lambda,\,+\frac{1}{2}}\right),$$

$$\hat{S}^z_{f\lambda} = \frac{1}{2}\left(a^+_{f\lambda,\,-\frac{1}{2}}\, a_{f\lambda,\,-\frac{1}{2}} - a^+_{f\lambda,\,+\frac{1}{2}}\, a_{f\lambda,\,+\frac{1}{2}}\right).$$

Hamiltonian (4) may then be expressed in the form

$$\hat{\mathbf{H}} = U_0 - \sum_{(f_1\lambda_1)\neq(f_2\lambda_2)} I(f_1\lambda_1 f_2\lambda_2)\, \hat{\vec{S}}_{f_1\lambda_1}\, \hat{\vec{S}}_{f_2\lambda_2}, \tag{5}$$

where U_0 is an insignificant constant value.

In order to obtain the Dirak operator (1) from formula (5) it must now be written in the form

$$\hat{\mathbf{H}} = U_0 - \sum_{\substack{(f_1\neq f_2)\\ \lambda_1\lambda_2}} I(f_1\lambda_1 f_2\lambda_2)\, \hat{\vec{S}}_{f_1\lambda_1}\, \hat{\vec{S}}_{f_2\lambda_2} - \sum_{\substack{f_1\\ \lambda_1\neq\lambda_2}} I(f_1\lambda_1 f_1\lambda_2)\, \hat{\vec{S}}_{f_1\lambda_1}\, \hat{\vec{S}}_{f_1\lambda_2} \tag{6}$$

and two propositions will be made:

(1) The integral of exchange between two groups is weakly dependent on the orbital state of the electrons, that is

$$I(f_1\lambda_1 f_2\lambda_2) \approx I(f_1 f_2),\ f_1 \neq f_2. \tag{7}$$

(2) The exchange force between the electrons inside the atoms is much greater than that between different atoms, that is

$$|I^0(f\lambda_1 f\lambda_2)| \gg |I(f_1\lambda_1 f_2\lambda_2)|. \tag{8}$$

Then, on the strength of the second proposition, the operator character of the last term of (6) may be ignored and it can be regarded as a constant value and on the strength of the first proposition

Hamiltonian (6) may be expressed by the operator for the total spin of the group

$$\vec{S}_f = \sum_{\lambda} \hat{\vec{S}}_{f\lambda}. \tag{9}$$

Instead of formula (6) we get

$$\hat{\mathrm{H}} = W_0 - \sum_{f_1 \neq f_2} I(f_1 f_2)\, \hat{\vec{S}}_{f_1}\, \hat{\vec{S}}_{f_2}, \tag{10}$$

where

$$W_0 = U_0 - \sum_{f_1\lambda_1 \neq f_2\lambda_2} I^0(f_1\lambda_1 f_1\lambda_2)\, \vec{S}_{f_1\lambda_1}\, \vec{S}_{f_1\lambda_2} - \tag{11}$$

is a constant value.

In formula (11) the values $\vec{S}_{f\lambda}$ are classic vectors of spin. Formula (10) correct to the constant member, coincides exactly with the Dirak Hamiltonian (1), but from here the approximation character of the latter is immediately apparent. The unclosed electron orbital of the atom, consisting of several electrons may be ascribed the total spin s and the Hamiltonian may only be used where it (the orbit) is sufficiently compact and, thanks to the internal exchange interaction, behaves as a whole.

In cases where the electron orbital is "loose", formula (6) will have to be used, or else the more general Hamiltonian (2).

We observe that we are not discussing the approximation of operator (1) which is connected with the non-orthogonal nature of the single-particle electron functions in the crystal, a paper on this has been produced by Slater [3]. This feature leads to configurational interaction with the polar states. As shown by Bogolyubov [2], a number of single-particle functions in a crystal may be made orthogonal, and the energy operator of a system of electrons with a weak addition of polar states may be expanded into a series of staged spin operators, in which case the first term of the expansion will have exactly the form (1).

2. Let us see how the character of the electron orbit affects the spin waves. For simplicity we will observe the ferromagnetic in which all the z electrons in the atom have the same direction of spin, so that their total spin is

$$s = \frac{1}{2} z. \tag{12}$$

(*a*) *The "compact" orbit.* Starting from equation (1) we will use the method of Holstein and Primakoff [4]:

$$S_f^+ = (2s)^{1/2} b_f; \quad S_f^- = (2s)^{1/2} b_f^+; \quad S_f^z = s - b_f^+ b_f; \quad S_f^{\pm} = S_f^x \pm i S_f^y. \tag{13}$$

Then the energy of the weakly-excited state of the system may be presented in the form

$$E = W_0 + \sum_{\mu} E_\mu n_\mu; \quad n_\mu = 0,\ 1,\ 2, \ldots, \tag{14}$$

where

$$E_\mu = 2s \sum_h I(h)\,(1 - e^{ih\mu}) - \tag{15}$$

VOL. 8 1959

of the spin energy of the wave with quasi pulse μ.

(*b*) *The "loose" orbit.* Here we must start from equation (5). Instead of (13) we must use the transformation ($s = \frac{1}{2}$):

$$S_{f\lambda}^{+} = b_{f\lambda};\ S_{f\lambda}^{-} = b_{f\lambda}^{+};\ S_{f\lambda}^{z} = \frac{1}{2} - b_{f\lambda}^{+} b_{f\lambda}. \tag{16}$$

Then the Hamiltonian of the system

$$\hat{\mathbf{H}} = W_0 + \sum_{f_1\lambda_1 \neq f_2\lambda_2} I(f_1\lambda_1 f_2\lambda_2)\,(b_{f_1\lambda_1} b_{f_1\lambda_1} - b_{f_1\lambda_1}^{+} b_{f_2\lambda_2})$$

after diagonalization leads to the true value of the energy

$$E = W_0 + \sum_{\mu} \sum_{j} E_{\mu}^{j} n_{\mu}^{j}, \tag{17}$$

where E_{μ}^{j} is determined from the system of linear homogeneous equations

$$\left[\sum_{f_2\lambda_2\ (\neq f_1\lambda_1)} I(f_1\lambda_1 f_2\lambda_2) + E_{\mu}\right] C(\lambda_1) - \sum_{\lambda_2} \left[\sum_{f_2} I(f_1\lambda_1 f_2\lambda_2)\, e^{i(f_2 - f_1)\mu}\right] C(\lambda_2) = 0, \tag{18}$$

already presented in paper [5].

Thus, instead of one branch of the spin waves we now get z independent branches. As the secular equation of the system (18) in its general form is impossible to resolve, we will look at some idealized cases, when it is possible to get

$$\begin{gathered} I(f_1\lambda_1 f_2\lambda_2) \approx I(f_1 - f_2) = I(h); \\ I^0(f_1\lambda_1 f_1\lambda_2) = I^0, \end{gathered} \tag{19}$$

that is, we actually return to approximation (7). For the energy of elementary excitation we get:

$$\left.\begin{aligned} E_{\mu}^{(1)} &= z \sum_{h} I(h)\,(1 - e^{ih\mu}). \\ E_{\mu}^{(k)} &= z \left[\sum_{h} I(h) + I^0\right];\ k = 2, 3, \ldots, z \end{aligned}\right\} \tag{20}$$

As we are dealing with weak excitation the last branches ($z - 1$) can be ignored as, in view of the value of the exchange integral, greater energy would be required than is excited by them. Now only one branch remains which, bearing in mind relation (12), coincides with result (15) for the compact orbit, as is to be expected.

Let us look at yet another curious analogy. If the solution to system (18) in approximation (19) is sought in the form (by analogy with the way quasi impulse μ was introduced)

$$C(\lambda) = C_0 e^{i\lambda\varphi}, \tag{21}$$

then for the energy of elementary excitations we shall find

$$E_\mu(\varphi) = z\left[I^0 + \sum_h I(h)\right] - z\left[I^0 + \sum_h I(h)\, e^{ih\mu}\right] \Omega_z(\varphi), \tag{22}$$

where

$$\Omega_z(\varphi) = z^{-1} \sum_{\lambda=0}^{z-1} e^{i\lambda\varphi}. \tag{23}$$

Here the value ϕ plays the part of a certain quantum number; the spectrum of ϕ may be determined from the condition (by analogy with the quasi impulse)

$$C(\lambda + z) = C(\lambda), \tag{24}$$

from which it follows that

$$\varphi = \frac{2\pi}{z} n; \quad n = 0,\ 1,\ 2, \ldots,\ (z-1), \tag{25}$$

then

$$\Omega_z(\varphi) = \begin{cases} 1, & n = 0 \\ 0, & n = 1, 2, \ldots, (z-1). \end{cases} \tag{26}$$

It can be seen that, with the values indicated for ϕ one gets all the branches of excitation determined by formulae (20).

Translated by V. Alford

REFERENCES

1. P. Dirak, *Osnovy kvantovoi mekhaniki (Principles of quantum mechanics)* United Scientific and Technical Press 61, (1937).
2. N.N. Bogolyubov, *Lektsii z kvantovoi statisiki (Lectures in quantum statistics)* Kiev, 1949.
3. I.C. Slater, *Rev. Mod. Phys.*, 23, 199, (1953).
4. T. Holstein and H. Primakoff, *Phys. Rev.* 58, 1098, (1940).
5. Ye. Kondorskii, and A. Pakhomov, *Dokl. Akad. Nauk* S.S.S.R. 93, 431 (1953).

VOL. 8 1959

ON THE EFFECT OF INTERNAL INTERACTIONS ON THE SECOND MOMENT OF THE PARAMAGNETIC RESONANCE CURVE IN THE CASE OF PURE SPIN MAGNETISM*

U. Kh. KOPVILLEM

Kazan "V.I. Ul'ianov" State University

(Received 16 September 1958)

The second moment of the paramagnetic resonance curve is calculated in magnetically anisotropic crystals which contain only magnetically equivalent ions. It is assumed that the basic energy level of these ions in the crystalline electric field has a double Kramers degeneration and that only this doublet is occupied. The dependence on the direction of the static magnetic field in relation to the crystal axis, the temperature, the symmetry of the crystalline electric field, the dipole-dipole, anisotropic-exchange and superfine interactions is taken into account. It is shown that the coefficients of the spin Hamiltonian can be used to study the internal interactions in paramagnetics. The application of the formulae obtained is illustrated on the example of the calculation of the width of the paramagnetic resonance line in ethylsulphates and double nitrates of rare earth elements with an uneven number of 4*f* electrons.

I. FORMULATION OF THE PROBLEM

Many authors [1-7] have calculated the second moment of the absorption curve in magnetically isotropical crystals. The formulae obtained in these papers do not, however, take account of the anisotropic g factor, the dependence of the nature of the internal interactions on the temperature or the effects caused by the difference between the direction of the static magnetic field H_0 and the symmetry axis ϵ of the crystalline electric field E. In this paper the derived second moment $\langle(\Delta\nu)^2\rangle$ of the paramagnetic resonance curve is calculated under the following conditions:

(*a*) the g factor is anisotropic,

(*b*) the width of the paramagnetic resonance line is given by the dipole-dipole $\mathbf{H}_1$, the anisotropic exchange $\mathbf{H}_{1ex}$ and the hyperfine $\mathbf{H}_{1sf}$ interactions;

(*c*) the field H_0 has an arbitrary direction to the symmetry axis of the crystal;

(*d*) the spin system consists of N magnetically equivalent ions the basic energy state of which in the field E has a double Kramers degeneration,

(*e*) the spin temperature T is so low that only the basic doublet is occupied;

(*f*) the dependence of the nature of the internal interactions on T and E is taken into account.

In our calculations we used the fact that in the case considered by us the magnetic moment μ_t^k of the ion k in the direction of the axis t can be written in the form [8]

$$\mu_t^k = -\frac{\beta}{2}\left(g_{ta}\sigma_a^k + g_{tb}\sigma_b^k + g_{tc}\sigma_c^k\right), \tag{1}$$

where g_{tl} are the elements of the g tensor; σ_l of the Pauli matrix and β the Bohr magneton. The wave functions $\{\psi_{ov}\}$ of the unexcited spin system can easily be found by solving the secular equation for a certain fictitious operator, the spin Hamiltonian $\mathbf{H}_s$, the proper values of which fully describe the distribution of the lines in the paramagnetic resonance spectrum. Here it is a valuable circumstance that in calculating $\langle(\Delta\nu)^2\rangle$ with the aid of the proper functions $\{\psi_{ov}\}$ of the spin Hamiltonian H_s the derived second moment of the paramagnetic resonance curve proves to be expressed by the coefficients of the spin Hamiltonian which can be measured with great accuracy by the paramagnetic

---

* *Fiz. metal. metalloved.*, 8, No. 1, 8-16, 1959.

resonance methods. In the past ten years these coefficients have been determined for many substances and it has been shown that the number of substances for which the effective spin is equal to ½ is very large. The corresponding data has been published in a number of articles of the nature of previews [4-6].

Therefore, the formula $\langle(\Delta\nu^2\rangle$ can serve both to predict the width of the paramagnetic resonance line and to study the internal interactions in paramagnetics. The latter is of importance for selecting substances for paramagnetic amplifiers and microwave generators.

2. DERIVATION FOR THE FORMULAE FOR THE ZERO AND SECOND MOMENT FOR SINGLE PARTICLE AND TWO PARTICLE OPERATORS

We introduce the following system of rectangular co-ordinates:

(B) ϵ, η and ξ are the main axes of the g tensor;

(C) ϵ', η' and ξ' are the main axes of the tensor A;

(D) x, y and z are a system connected with the direction of the static magnetic field H_0 by the relation $H \parallel z$;

(P) a, b and c, where $c \parallel G$;

(F) a', b' and c', where $c' \parallel (RG)$.

The vector G is directed towards the resulting electron magnetic moment $\mu_\epsilon^{\mathrm{I}}$ of the paramagnetic ion in the field H_0. In the system of co-ordinates B the vector G has the components $G_\epsilon l_\epsilon$, $Q_\eta l_\eta$ and $G_\xi l_\xi$, where l_λ are the directional cosines of the field H_0 and G_λ are the corresponding factors of spectroscopic resolution. The vector RG is directed towards the resulting nuclear magnetic moment $\mu_{\mathrm{nu}}^{\mathrm{I}}$ of the paramagnetic ion. This direction is determined by the magnetic field created at the point of the position of the nucleus by the unpaired electrons of the paramagnetic ion. Using this system of co-ordinates and neglecting items of the second order of smallness in the elements $A_{\lambda\nu}$ of the tensor of the hyperfine spin interaction A one can write the Hamiltonian spin system $\mathbf{H}$, which satisfies all the conditions (a)-(f) in the form

$$\mathbf{H} = \mathbf{H}_0 + \mathbf{H}_1, \tag{2}$$

where $\mathbf{H}_0$ is the non-excited part of the Hamiltonian spin system and H_1 the excited part.

$$\mathbf{H}_0 = \frac{1}{2}\beta G H_0 \sigma_c^{II}, \tag{3}$$

$$\mathbf{H}_1 = \frac{1}{2} R \sigma_c^I I_c^I + Q^{II} + P_{\alpha\beta}^{IIj} \sigma_\alpha^I \sigma_\beta^j, \tag{4}$$

$$G = (l_\lambda^2 G_\lambda^2)^{1/2}, \tag{5}$$

$$RG = (g_\lambda g_\mu A_{\lambda\nu} A_{\mu\nu} l_\lambda l_\mu)^{1/2}, \quad \lambda, \mu \subset B, \ \nu \subset C. \tag{6}$$

In formular (3)-(6) Q is an operator which depends only on the spin of the nucleus I and describes the interaction of the electric quadrupole moment of the nucleus with the gradient of the electric field created by the unpaired electrons of the paramagnetic ion; the upper indices relate to the particles, the lower to the co-ordinate axes; products containing the same index twice should be added up with respect of these indices and for two particle operators P the inequality $j > k$ should be observed.

Subsequently we shall take the direction c for the axis of the quantization of the magnetic moment of the ion, while with the arbitrary direction of the magnetic field H_0 relative to the crystal axis the

proper functions of the non-excited spin system take the form

$$\psi_{0v} = \Big(\prod_{n_v=1}^{K_v} \varphi_1^{(n_v)}\Big)\Big(\prod_{f_v=1}^{N-K_v} \varphi_2^{(f_v)}\Big), \tag{7}$$

where

$$\varphi_1^{(n_v)} \equiv 1 + \frac{1}{2} \rangle \text{ and } \varphi_2^{(f_v)} \equiv 1 - \frac{1}{2} \rangle$$

are the proper functions of the operator

$$\frac{1}{2}\,\sigma_c^v; \quad K_v$$

is the number of ions with energy 0; $N-K_\nu$ the number of ions with energy $G\,\beta\,H_0$.

To calculate the zero M_0 and the second M_2 of the moments of the paramagnetic resonance curve the formulae [2] are used:

$$M_0 = exp\,(-E_t/kT)\,T_r(L_t\,\mu_\alpha\,L_s\,\mu_\alpha), \tag{8}$$

$$M_2 = exp\,(-E_t/kT)\,T_r(L_s\,\mathbf{H}_1\,L_s\,\mathbf{H}_1\,L_s\,\mu_\alpha\,L_t\,\mu_\alpha - 2L_t\,\mathbf{H}_1\,L_t\,\mu_\alpha\,L_s\,\mathbf{H}_1\,L_s\,\mu_\alpha + \\ + L_t\,\mathbf{H}_1\,L_t\,\mathbf{H}_1\,L_t\,\mu_\alpha\,L_s\,\mu_\alpha). \tag{9}$$

Here

$$E_t = K\langle \varphi_1 \left|\frac{1}{2}\,G\,\beta\,H_0\,\sigma_c\right| \varphi_1 \rangle + (N-K)\langle \varphi_2 \left|\frac{1}{2}\,G\,\beta\,H_0\,\sigma_c\right| \varphi_2 \rangle$$

and $E_s\,(K-1)\langle \varphi_1 \left|\frac{1}{2}\,G\,\beta\,H_0\,\sigma_c\right| \varphi_1 \rangle + (N-K+1)\langle \varphi_2 \left|\frac{1}{2}\,G\,\beta\,H_0\,\sigma_c\right| \varphi_2 \rangle -$

is a certain pair of energy levels of the non-excited spin system between which magnetic dipole transitions are possible under the influence of the alternating magnetic field with the frequency

$$\nu_0 = |E_s - E_t|/h; \quad L_t \text{ and } L_s$$

are operators projecting the functions $\{\psi_{v0}\}$ on the sub-spaces $\{\psi_{ov}\}_t$ and $\{_{ov}\}_s$ formed by the proper functions of the levels E_t and E_s respectively. Summation with respect to t should be done for all pairs of levels for which $|E_s - E_t| = h\nu_0$. Formulae (8) and (9) take account of the change in the nature of the internal interactions only as a result of change in the occupation of the non-excited energy levels of the spin system when the temperature changes, which is valid while

$$exp\,\{-\langle \pm|\mathbf{H}_1|\pm\rangle/kT\} \approx 1, \tag{10}$$

where $|\pm\rangle$ are the correct wave functions of zero approximation for the basic Kramers doublet of the paramagnetic ion; k is the Boltzmann constant. Further it is assumed that

$$|\langle +|\mathbf{H}_1|+\rangle - \langle -|\mathbf{H}_1|-\rangle| \ll h\nu_0. \tag{11}$$

Let us examine the case where

$$(h)\ H_t \parallel \alpha,$$

(I) H_0 lies in the plane $\beta\ \gamma$, i.e.

$$\mu_\alpha = -\frac{1}{2}\beta\, g_{\alpha\alpha}\, \sigma_\alpha^{Il}.$$

where $\alpha,\ \beta,\ \gamma \subset B,\ \alpha \nparallel \beta \nparallel \gamma$ and H_t is the radio-frequency magnetic field. Applying formulae (3)-(9) and taking into account

$$\langle (\Delta\nu)^2 \rangle = -\hbar^{-2} M_2 M_0^{-1}, \tag{12}$$

we obtain for the derived second moment $\langle (\Delta\nu)^2 \rangle$ of the paramagnetic resonance curve the following expression:

$$M_0 = \frac{1}{4} N Z^{N-1} \beta^2 g_{\alpha\alpha}^2 (2I+1)^N, \tag{13}$$

$$\langle (\Delta\nu)^2 \rangle = (\hbar^2 Z)^{-1} \sum_{j(\neq I)} \{2exp\,(m)\,(P_{aa}^{Ij2} + P_{bb}^{Ij2} + P_{aa}^{Ij} P_{bb}^{Ij} + P_{bb}^{Ij} P_{aa}^{Ij}) +$$
$$+ [3 + 4exp\,(m) + exp\,(2m)]\, P_{cc}^{Ij2} - 2\,(1 + 3exp\,(m))\,(P_{aa}^{Ij} P_{cc}^{Ij} + P_{cc}^{Ij} P_{bb}^{Ij}) +$$
$$+ 2exp\,(m)\,(P_{ba}^{Ij2} + P_{ab}^{Ij2} - P_{ab}^{Ij} P_{ba}^{Ij} - P_{ba}^{Ij} P_{ab}^{Ij})\} + (3\hbar^2)^{-1} I\,(I+1)\,R^2,$$

where $$Z = 1 + exp\,(2m),\quad m = -G\,\beta\, H_0/kT.$$

In (13) we have omitted terms of the form

$$(Zh)^{-2}\,[exp\,(m) - exp\,(2m)]\, P_{\alpha\beta}^{Ij} P_{\gamma\delta}^{Ik},$$

which contain the lattice sums depending on the form of the specimen. Detailed calculations for ethylsulphates of rare earth elements show that these terms are negligibly small for specimens in the shape of a sphere. This conclusion appears to be valid also for lattices of magnetic ions which have a lower symmetry than the lattice of the ethylsulphates. Formula (13) solves the problem of calculating the quantities $\langle (\Delta\nu)^2 \rangle$ when the conditions (a)-(l) are fulfilled.

3. DERIVATION OF THE SPIN HAMILTONIAN FOR TWO-PARTICLE INTERNAL INTERACTION

(1) The operator of the dipole-dipole interaction has the form

$$\mathbf{H}_{1g} = \mu^I \mu^j / r^{Ij3} - 3\,(\mu^I r^{Ij})\,(\mu^j r^{Ij})\, r^{Ij5}, \tag{14}$$

where r^{Ij} is the radius vector linking the ions I and j. We shall express $\mathbf{H}_{1g}$ by the effective spin $s' = \frac{1}{2}$, for which we substitute (1) in (14). As a result we obtain

$$\mathbf{H}_{1g} = \frac{\beta^2}{4}\,\{g_{l\alpha}^j\, g_{l\beta}^k \delta / r^{jk3} - 3 g_{l\alpha}^j\, r_l^{jk}\, g_{r\beta}^k\, r_r^{jk} / r^{jk5}\}\, \sigma_\alpha^j\, \sigma_\beta^k. \tag{15}$$

For calculations with the aid of formula (15) we use the components of the g tensor $g_{\delta\gamma}$, where the

indices γ and δ serve to indicate the axes of co-ordinates of D and P respectively. In a system of co-ordinates B the g tensor has only diagonal elements which, according to (5), are determined by the relations

$$G_\xi \equiv g_{\xi\xi},\quad G_\eta \equiv g_{\eta\eta},\quad G_\zeta \equiv g_{\zeta\zeta} \tag{16}$$

and, hence, can be measured with great accuracy by paramagnetic resonance methods. To find the elements of the g tensor in the systems of co-ordinates P and D one can proceed in the following manner. Let $\phi_{B\to P}$ and $\theta_{B\to D}$ be the affinors which transform the points of the co-ordinate axis B into the points of the co-ordinate axes P and D respectively. The matrix of the g tensor represented in P and D then assumes the form

$$g_{DP} = \tilde{\theta}_{B\to D}\, g_{BB}\, \varphi_{B\to P}, \tag{17}$$

where $\tilde{\theta}$ is the transposed matrix θ. In the case (h, l) the affinor $\theta_{B\to D}$ describes a revolution around the axis a through the angle θ and the affinor $\phi_{B\to P}$ a revolution around the same axis through the angle ϕ, where

$$\cos\theta = l_\beta^{\text{and}} \cos\varphi = g_{\beta\beta} l_\beta \left(l_\beta^2 g_{\beta\beta}^2 + l_\gamma^2 g_{\gamma\gamma}^2\right)^{-1/2}.$$

The magnetic moment of the paramagnetic ion l in the direction a has the form

$$\mu_\alpha^l = \left(-\frac{1}{2}\beta\right)(g_{DP})_{\alpha\beta}\,\sigma_\beta^l,\quad \alpha \subset D,\ \beta \subset P. \tag{18}$$

It follows from (17) and (18) that the non-zero elements g_{DP} in the case (h, l) have the form (to be specific we assume that $a = \xi$):

$$\begin{gathered} g_{xa} = g_{\xi\xi},\ g_{yc} = \cos\theta \sin\theta\,(g_{\eta\eta}^2 - g_{\zeta\zeta}^2)\,G^{-1}, \\ g_{zc} = \left(g_{\zeta\zeta}^2 \cos^2\theta + g_{\eta\eta}^2 \sin^2\theta\right)^{1/2} = G,\ g_{yb} = g_{\eta\eta} g_{\zeta\zeta}\, G^{-1}. \end{gathered} \tag{19}$$

(2) Let us express the operator of the isotropic exchange interactions

$$\mathbf{H}_{1\,ob} = -2J^{lj}\,S^l\,S^j \tag{20}$$

through the effective spin $s' = \frac{1}{2}$. For this purpose it is necessary to know the true (and not those determined from the spin Hamiltonian) wave functions $|+>$ and $|->$ of the Kramers doublet. To simplify the problem we assume that the field E has the symmetry axis ϵ. Let $|+>$ and $|->$ be the correct proper functions of zero approximation, when $H_0 \parallel \epsilon$. We introduce the designations

$$<+-|2S_\xi^l S_\xi^j|-+> \equiv B^2,\quad <++|2S_\zeta^l S_\zeta^j|++> \equiv A^2.$$

Using the correct wave functions of zero approximation for the case where H_0 forms the angle θ with ϵ we obtain

$$\begin{gathered} \mathbf{H}_{1\,ob} = [J_a^{lj}\delta_{aa} + J_b^{lj}\delta_{ab} + J_c^{lj}\delta_{ac}]\,\sigma_\alpha^I \sigma_\beta^j \delta_{\alpha\beta}, \\ J_b^{lj} \equiv -J^{lj}(B^2\cos^2\varphi + A^2\sin^2\varphi), \\ J_c^{lj} \equiv -J^{lj}(B^2\sin^2\varphi + A^2\cos^2\varphi), \\ J_a^{lj} \equiv -J^{lj}B^2, \end{gathered} \tag{21}$$

where

$$\sin\varphi \equiv \sin\theta \frac{g_{\eta\eta_1}}{G}, \quad \cos\varphi \equiv \cos\theta \frac{g_{\varepsilon\varepsilon}}{G}.$$

After substituting (21) and (15) in (13) we obtain the following general formula for calculating the derived second moment:

$$\langle (\Delta\nu)^2 \rangle = \langle (\Delta\nu)^2 \rangle_g + \langle (\Delta\nu)^2 \rangle_{g-o\delta} + \langle (\Delta\nu)^2 \rangle_{o\delta} + \langle (\Delta\nu)^2 \rangle_{sf}, \tag{22}$$

where the individual items designate the contributions made by the dipole-dipole, dipole-exchange and superfine interactions respectively. In form $\langle(\Delta\nu)^2\rangle_g$ agrees with the expression from (13) enclosed in curved brackets and, in accordance with (19), contains the summation with respect of the lower indices. In the particular case where $H_t \| d$ and $H_0 \| c$ we have

$$\langle (\Delta\nu)^2 \rangle_g = (18Zh^2)^{-1} \sum_{I(\neq j)} \{(B_{aa}^{Ij} + B_{bb}^{Ij})^2 K + \\ + B_{cc}^{Ij2} D - B_{cc}^{Ij}(B_{aa}^{Ij} + B_{bb}^{Ij}) L\}. \tag{23}$$

If the field E has the symmetry axis ϵ formula (23 is simplified and we then obtain

$$x \equiv g_{\eta\eta}/g_{\varepsilon\varepsilon}, \quad H_0 \parallel \varepsilon,$$

$$\langle (\Delta\nu)^2 \rangle_g = (18Zh^2)^{-1} \sum_{I(\neq j)} \{exp(m)(x^4 + 3x^2 + 2) + \\ + 0.5exp(2m) + 1{,}5 + x^2\} B_{\varepsilon\varepsilon}^{Ij2}. \tag{24}$$

The remaining items in expression (21) have the form: $H_t \| a$,

$$\langle (\Delta\nu)^2 \rangle_{o\delta} = 2(Zh^2)^{-1} \sum_{I(\neq j)} \{(J_a^{Ij} + J_b^{Ij})^2 K + J_c^{Ij2} D - J_c(J_a + J_b)\} L, \tag{25}$$

$$\langle (\Delta\nu)^2 \rangle_{g-o\delta} = 4(Zh^2)^{-1} \sum_{I(\neq j)} \{(P_{aa}^{Ij} + P_{bb}^{Ij})(J_a^{Ij} + J_b^{Ij}) K + P_{cc}^{Ij} J_c^{Ij} D - \\ - 0{,}5[P_{cc}^{Ij}(J_a^{Ij} + J_b^{Ij}) + J_c^{Ij}(P_{aa}^{Ij} + P_{bb}^{Ij})] L\}, \tag{26}$$

$$\langle (\Delta\nu)^2 \rangle_{sf} = (3h^2)^{-1} I(I+1) R^2, \tag{27}$$

$$A \equiv 1 + exp(m), \quad K \equiv exp(m), \quad L \equiv 1 + 3exp(m),$$

$$D \equiv 1{,}5 + 2exp(m) + 0{,}5exp(2m),$$

$$m \equiv -G\beta H_0/kT, \quad B_{\alpha\alpha}^{Ij} \equiv -3g_{\alpha\alpha}^2 \beta^2 r^{Ij(-3)} \left\{\frac{3}{2}\gamma_\alpha^{Ij2} - \frac{1}{2}\right\},$$

$$\gamma_\alpha^{Ij} \equiv \cos(r^{Ij}, \alpha).$$

VOL. 8 1959

4. THE DERIVED SECOND MOMENT AND THE WIDTH OF THE PARAMAGNETIC RESONANCE CURVE IN ETHYLSULPHATES AND DOUBLE NITRATES OF RARE EARTH ELEMENTS

Let us examine the nature of the mechanism of widening of the paramagnetic resonance line in concentrated ethylsulphate single crystals and double nitrates of rare earth elements which have an odd number of $4f$ electrons. The crystalline field in these substances is unable fully to suppress the orbital movement of the deep-lying $4f$ electrons, and the magnetism of the ions, which is caused by these electrons, is not purely a spin magnetism. A number of authors [4-5] has shown that in the above mentioned substances the basic energy level of the rare earth ions with an odd number of $4f$ electrons is split up under the influence of the field E into a Kramers doublet, and one can neglect the occupation of all but the basic doublet in the region of helium temperatures.

If follows from this that in paramagnetic resonance experiments all the conditions (a)-(l) are fulfilled in these substances [4, 5, 9-12]. Up to the present, however, measurements of the quantity $\langle(\Delta\nu)^2\rangle$ in magnetically anisotropic crystals have not been made with direct methods [13]. Therefore, we are here compelled to confine ourselves to a comparison of $\langle(\Delta\nu)^2\rangle$ with certain data on the width $\Delta\nu_{1/2}$ of the paramagnetic resonance line. Such a comparison is possible because, in accordance with the statements of many authors [9-12], the form of the line in these substances is nearly of Gauss type, and, hence, the relation [3] is valid:

$$\Delta\nu_{1/2} = 2.35 \langle (\Delta\nu)^2 \rangle^{1/2}. \tag{28}$$

Below we give the formulae for the calculation of the width of the line $\Delta H_{1/2}$ and the derived second moment $\langle(\Delta H)^2\rangle$ as functions of the strength of the static magnetic field H_0.

$$\Delta H_{1/2} = 2.35 \langle (\Delta H)^2 \rangle^{1/2}, \quad \langle (\Delta H)^2 = h^2 (g_{cc}^2 \beta^2)^{-1} \langle (\Delta\nu)^2 \rangle, \tag{29}$$

$$\langle (\Delta H)^2 \rangle_{sf\,\parallel} = I(I+1) A^2 (3\beta^2 g_\parallel^2)^{-1},$$

$$\langle (\Delta H)^2 \rangle_{sf\,\perp} = I(I+1) B^2 (3\beta^2 g_\perp^2)^{-1},$$

$$\langle (\Delta H)^2 \rangle^{ec}_{g,\, H_0 \parallel \varepsilon} = (Za^6)^{-1} 66{,}73 g_\parallel^2 \beta^2 [exp(m)(x^4 + 3x^2 + 2) + 0.5 exp(2m) + 1{,}5 + x^2], \quad x \equiv g_\perp / g_\parallel, \tag{30}$$

a is the side of the cell.

$$\langle (\Delta H)^2 \rangle^{ec}_{g},\ H_0 \parallel \eta = (18Za^6)^{-1} \{(508{,}4 + 1201x^{-4} - 1194x^2) exp(m) + 514{,}3[1{,}5 + 2exp(m) + 0.5exp(2m)] + (603x^{-2} - 88{,}01)[1 + 3exp(m)]\} g_\perp^2 \beta^2. \tag{31}$$

$$\langle (\Delta H)^2 \rangle^{dh}_{g,\, H_0 \parallel \varepsilon} (Za^6)^{-1}\, 1.78 g_\parallel^2 \beta^2 [exp(m)(x^4 + 3x^2 + 2) + 0.5exp(2m) + 1.5 + x^2]. \tag{32}$$

$$\langle (\Delta H)^2 \rangle^{dh}_{g,\, H_0 \perp \varepsilon} = (18Za^6)^{-1} g_\perp^2 \beta \{[13 + 32(x^{-4} - x^{-2})] exp(m) + 13[1.5 + 2exp(m) \quad 0.5exp(2m)] + (16x^{-2} - 3)[1 + 3exp(m)]\}. \tag{33}$$

Formulae (29) contain the main values of the tensor of the hyperfine spin interaction along the

axis of symmetry (the coefficients A) and in the direction perpendicular to this (the coefficients B), while the signs $\parallel$ and $\perp$ indicate the direction of the field H_0 in relation to the axis ϵ. Formulae (30) and (31) relate to the ethylsulphates of the rare earth elements (ES). The grid lattice sums take into account the contribution of over 99 per cent of all neighbours of the paramagnetic ion in the ethylsulphate lattice. In the calculations it was assumed that the axis η is inclined to the side of the nearest magnetic ion in the plane $\eta\,\xi \perp \epsilon$. Formulae (32) and (33) relate to the double nitrates (DH). The sum

$$\sum B_{\varepsilon\varepsilon}^{IJ}$$

for this lattice was obtained directly with the aid of the results of paper [8]. The sums which contain the projections r^{Jf} on the axes ξ and η were calculated under the assumption that the magnetic lattice of the double nitrates has the symmetry axis ϵ and takes account of the contribution from neighbours with an accuracy of 10 per cent.

Table 1. gives the values for $\langle(\Delta H)^2\, G^2$ and $\Delta H_{1/2} G$ calculated with the aid of the formulae (29)-(33). Here it was assumed that the spin temperature $T = 2.5°$K and the wavelength of the radio frequency magnetic field $\lambda = 3.25$ cm. We note that independently of the relation $\langle(\Delta H)^2\rangle_{sf}\langle(\Delta H)^2\rangle^{-1} = k$ the quantity $\langle(\Delta H)^2_{g+sf}\rangle$ is always physically measurable. The quantity $\Delta H_{1/2\,(sf+g)} = 2.35\,\langle(\Delta H)^2\rangle^{1/2}_{g+sf}$ has a meaning only when $k \lesssim 1$. If $k \gg 1$, all components of the hyperfine structure are well resolved and their width depends only on the two-particle and electric interactions.

TABLE 1.

	M^{3+}	H_0	$(\Delta H)^2_g$	A	$\langle(\Delta H)^2\rangle_g + \langle(H)^2\rangle_{sf}$	$\Delta H_{1/2g}$	$\Delta H_{1/2}$ (g+ sf)	Experimental values of $\Delta H_{1/2}$	References
$M^{3+}(C_2H_5SO_4)^3 \cdot 9H_2O$	Ce^{3+}	$\parallel \varepsilon$	20740			338		700	[10]
		$\parallel \eta_i$	$1780 \cdot 10^3$			3140			
	Nd^{3+}	$\parallel \varepsilon$	25 140	143	$303 \cdot 10^3$	374			
				145	$1323 \cdot 10^2$				
		$\parallel \eta_i$	20 380	143	$242 \cdot 10^3$	335		400	[9]
				145	$1064 \cdot 10^2$				
	Sm^{3+}	$\parallel \varepsilon$	1157	147	$24 \cdot 10^4$	79			
				149	$1605 \cdot 10^2$				
		$\parallel \eta_i$	511	147	$452 \cdot 10^3$	54			
				149	$3018 \cdot 10^2$				
	Er^{3+}	$\parallel \varepsilon$	$1174 \cdot 10^3$	167	$1177 \cdot 10^3$	2520	2550		
		$\parallel \eta_i$	55140	167	85440	552	691		
$Mg_3M_2^{3+}(NO_3)_{12} \cdot 24\,H_2O$	Ce^{3+}	$\parallel \varepsilon$	8145			212			
		$\perp \varepsilon$	243			37		40	[11]
	Nd^{3+}	$\parallel \varepsilon$	12440	143	$3324 \cdot 10^2$	263			
				145	$1324 \cdot 10^2$				
		$\perp \varepsilon$	533	143	$3205 \cdot 10^2$	54		170	[12]
				145	$1205 \cdot 10^2$				
	Sm^{3+}	$\parallel \varepsilon$	130	147	$495 \cdot 10^4$	27		75	[12]
				149	$34 \cdot 10^5$				
		$\perp \varepsilon$	123	147	$< 1\,390\,123$	26			
				149	$< 139 \cdot 10^4$				

VOL. 8 1959

In the calculations we neglected the exchange interactions since these substances are in themselves magnetically dilute and the exchange interactions diminish rapidly with increasing distance between the magnetic ions. All parameters of the hyperfine structure and values of the g factor are taken from paper [6].

The table shows that the width of the paramagnetic resonance line can be explained by dipole-dipole interaction only in the ethylsulphates if neodymium and the double nitrate of cerium, which is in agreement with the data of paper [8]. In the remaining cases for which experimental values for $\Delta H_{1/2}$ are known the width of the paramagnetic resonance line is apparently chiefly caused by the electric interactions.

Describing these interactions by the formal Hamiltonian

$$\mathbf{H}_e = \frac{1}{2}(\Delta_\xi^I \sigma_\xi^I + \Delta_\eta^I \sigma_\eta^I + \Delta_\varepsilon^I \sigma_\varepsilon^I).$$

we obtain for $Mg_3Nd_2(NO_3)_{12}\cdot 24\,H_2O\,\Delta_\xi = \Delta_\eta = 0.087\ cm^{-1}$ and for $Mg_3Sm(NO_3)_{12}\cdot 24\,H_2O\ \Delta_\epsilon = 0.011\,cm^{-1}$ (we assume that the parameters Δ_α change from ion to ion and have a Gauss distribution with the centre in point zero). The physical nature of the constant Δ should be established experimentally. We note that if Δ describes the dispersion of the g factor the width of the paramagnetic resonance line should depend on the strength of the field H_0. It is also possible that the widening of the line is caused partly by super-exchange interactions through the water molecules which surround the paramagnetic ions [8].

Concerning the dependence of $\langle(\Delta\nu)^2\rangle_g$ on the temperature in crystals where the field E has a symmetry axis we note the following. In the temperature region where the Zeeman splitting up of the Kramers doublet is of the order of kT the value of $\Delta H_{1/2g}$ diminishes noticeably with decreasing temperature and the rate of this diminution depends on the ratio $g_\perp/g_\parallel$ and the direction of H_0.

(1) If $g_\perp \ll g_\parallel$ the diminution of $\langle(\Delta H)^2\rangle_g$ is always more noticeable in the case of $H_0 \perp \epsilon$ than in the case of $H_0 \parallel \epsilon$.

(2) If $g_\perp \ll g_\parallel$ (or $g_\perp \gg g_\parallel$), the diminution of $\langle(\Delta H)^2\rangle_g$ is particularly noticeable for the case of $H_0 \perp \epsilon$ (or $H_0 \parallel \epsilon$).

(3) For $Ce(C_2H_5SO_4)_3\cdot 9\,H_2O$, where $g_\perp = 0.2$ and $g_\parallel = 3.8$, the value of $\Delta H_{1/2g}$ is for $T = \infty$ and $H_0 \perp \epsilon$ equal to 3280 G, and for $T = 0$ and $H_0 \perp \epsilon$ equal to 176 G.

In conclusion we make the following remarks.

(1) It follows from (13), (15) and (21) that the field E changes the nature of the course of the internal interactions in paramagnetics to a considerable degree, while the symmetry properties of the field E are transmitted to $\langle(\Delta\nu)^2\rangle$ through the coefficients of the spin Hamiltonian. From (19) it is clear that if the direction of the field H_0 does not coincide with the main axes of the g tensor, an additional anisotropy of the dynamic properties of paramagnetic single crystals appears which is caused by the field H_0.

(2) Taking account of the Boltzmann factor leads to the exchange interactions making a contribution to $\langle(\Delta\nu)^2\rangle$ even in the case of real spin ½ and isotropic g factor.

(3) It follows from (13) that the quadrupole interaction Q^{II} does not affect $\langle(\Delta\nu)^2\rangle$. This is because in the first approximation with respect to the parameters of the hyperfine interactions the operator Q^{II} shifts all hyperfine energy levels by one and the same distance and hence, does not change the frequency of the transitions between these levels.

(4) $\langle(\Delta\nu)^2\rangle_{sf}$ does not depend on the temperature. This is because we assumed $H_{sf} \sim H_g$ and because formula (13) contains the inaccuracy (10).

(5) If in (23) we substitute $T = \infty$ and $g_{\alpha\alpha} = \text{const}$. the well known formula (11) is obtained which is given in paper [3] and the contributions (25) and (26) from the exchange interactions vanish, which is also in agreement with the results obtained earlier [3].

I express my gratitude to Professor S.A. Al'tshuler for suggesting this subject and for giving his attention to this work.

Translated by B. Ruhemann

REFERENCES

1. 1. K. Kambe and J.F. Ollom, *J. Phys. Soc. Japan* II, 50 (1956).
   2. M.H.L. Price and K.W.H. Stevens, *Proc. Phys. Soc.* A 63, 36 (1950).
   3. J.H. Van Vleck, *Phys. Rev.* 74, 1168 (1948).
   4. S.A. Al'tshuler and B.M. Kozyrev, *Progress of Physical Sciences* 63, 533 (1957).
   5. B. Bleaney and K.W.H. Stevens, *Repts. Progr. Phys.* 16, 108 (1953).
   6. K.D. Bowers and J. Owen, *Repts. Progr. Phys.* 18, 304 (1955).
   7. G. Ia. Glebashev, *Uchenyye zapiski Kasanskogo gosuniversiteta* 116, kn. 1, p. 121. *Zh. eksp. teor. fiz.* 30, 612 (1956).
   8. J.M. Daniels, *Proc. Phys. Soc.* A 66, 673 (1953).
   9. B. Bleaney, R.J. Elliot and H.D.E. Scovil, *Proc. Phys. Soc.* A 64, 933 (1951).
   10. G.S. Bogle, A.H. Cooke and S. Whitley, *Proc. Phys. Soc.* A 64, 931 (1951).
   11. A.H. Cooke, H.J. Duffus and W.P. Wolf, *Phil. Mag.* 44, 623 (1953).
   12. A.H. Cooke and H.J. Duffus, *Proc. Roy. Soc.* A 229, 407 (1955).
   13. J. Herve, *Arch. Sci. 10, fasc. spec.*, 114 (1957).

VOL.
8
1959

THE CHANGE IN THE INTERNAL ENERGY, THE THERMOELECTRIC FORCE AND THE SPECIFIC ELECTRIC RESISTANCE IN THE PLASTIC DEFORMATION OF METALS*

V.N. KUNIN

Cheliabinsk Institute for the Mechanization and Electrification of Agriculture

(Received 23 February 1958)

Describes the results of measurements of the induced thermoelectric force and the changes in the specific electric resistance of silver and copper in plastic extension from 2 per cent to fracture. The changes in the electric properties of the metal are compared with the amount of the absorbed energy.

The amount of energy absorbed in the plastic deformation of a metal is a measure of its deviation from the state of equilibrium. Therefore it is quite natural to suppose that the changes in the properties of a metal in the process of plastic deformation will in one way or another be connected with this amount.

The number of papers concerned with this question is very limited. Kunin [1] has found that for copper the change in the absolute thermoelectric force is directly proportional to the amount of energy absorbed by the metal. True, the data from which this dependence was derived was obtained by various researchers at different times and on different specimens. Khotkevich, Chaikovskii and Zashkvara [2] have found that the increase in the specific electric resistance for cadmium and lead deformed at low temperatures increases linearily with increase of the latent energy of deformation.

In the present paper are described the results of parallel measurements of the absorbed energy, the induced thermoelectric force and the changes in the specific resistance in the process of plastic deformation. Experiments were made with one and the same series of specimens of electric copper wire and chemically pure silver deformed under identical conditions. Hence, the results of the experiments can be compared with complete reliance on the comparison.

METHOD OF MEASUREMENT AND THE RESULTS OBTAINED

(*a*) *The induced thermoelectric force.* The method for measuring the absorbed energy has already been described in paper [3], therefore, we shall only described the method for measuring the thermoelectric force and the specific electric resistance.

The initial length of the specimens was 100 mm. The initial diameter of the copper specimens was $d_0 = 1.314$ mm and of the silver specimens $d_0 = 1.409$ mm. The extension was effected in a series of stages in the same machine [4] and at the same rate as in the experiments for measuring the absorbed energy. The form of the specimens is shown in Fig. 1. The specimen consists of a deformed arm *A* and an undeformed arm *B*. In this way the thermoelectric force of the deformed metal was measured in relation to the same, but undeformed metal. Vessel *1* contained kerosene, vessel *2* a mixture of melting ice with water. The thermoelectric force was measured with a mirror galvanometer of M-25 type. A variable voltage controlled by the voltmeter *V* could be applied to the specimen circuit. This voltage could be used to calibrate the galvanometer or to compensate for the thermoelectric force to be measured. The thermoelectric force was measured by two methods: (1) from the angle through which the mirror of the galvanometer was turned; (2) by the compression method.

The sensitivity of the arrangement for measurements by the first method was $\gamma_1 = 0.0218$ mV/mm of the galvanometer scale, by the second method $\gamma_2 = 0.00666$ mV/mm of the voltmeter scale. The values of the thermoelectric force obtained by these methods agreed well. The method of measurement was similar to the method used in paper [5].

From the data of the experiments the dependence shown in Fig. 2 between the amount of the energy absorbed by silver in the process of extension and the induced thermoelectric force was plotted. The figure shows that the induced thermoelectric force is directly proportional to the absorbed energy.

* *Fiz. metal. metalloved.*, 8, No. 1, 17-20, 1959.

VOL
8
195

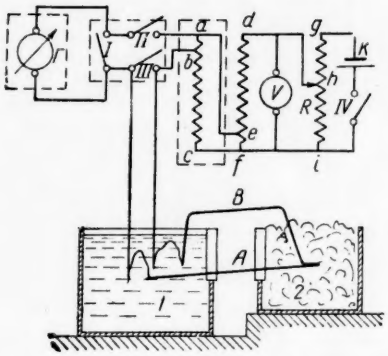

FIG. 1. Schematic drawing of the arrangement for measuring the induced thermoelectric force.

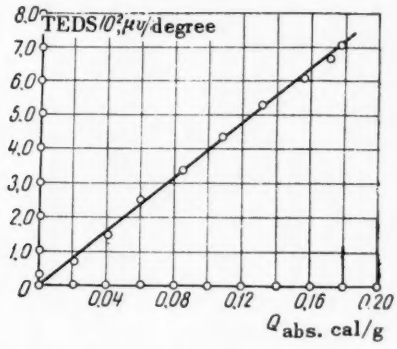

FIG. 2. Dependence of the induced thermoelectric force in mV/degree on the amount of absorbed energy for silver.

A similar result was obtained for copper also. The slopes of the straight line proved to be the same: for silver tan $\alpha = 0.41$ mV. g/cal degree, for copper tan $\alpha_1 = 0.086$ mV . g/cal degree.

Thus, both for silver and for copper the change in the absolute thermoelectric force during the process of plastic deformation is directly proportional to the amount of the absorbed energy.

(*b*) *Change in the specific electric resistance.* One can assume with sufficient accuracy that during the annealing of a cold worked specimen its length does not change. Hence, the volume of the specimen in the process of plastic deformation may also be assumed constant.

Assuming also that during the extension the specimen remains a true cylinder, i.e. that the deformation occurs uniformly over the whole length of the specimen, one can easily obtain an expression for the relative increase in the specific electric resistance during extension

$$\frac{\Delta\rho}{\rho_0} = \frac{\rho_1 - \rho_0}{\rho_0} = \frac{R_1}{R_0}\left(\frac{1}{1+\varepsilon}\right)^2 - 1,$$

where R_0 is the resistance of the annealed specimen; R_1 is the resistance of the cold hardened specimen; ϵ the relative deformation ($\epsilon = \Delta l / l_0$).

The change ρ in the process of extension occurs to the extent of the order of one per cent of the initial value. Therefore it is necessary to measure all the quantities which enter into the formula with great accuracy (the resistance, the initial length and the elongation of the specimen).

The initial length of the specimen was measured from the distance between the clamps of the machine with an accuracy of up to 0.05 mm, the elongation of the specimen Δl from the number of revolutions of the power screw of the machine (taking into account the pitch of the thread) with an accuracy of 0.01 mm. The resistance of the specimens was of the order of 0.001 Ω. In order to exclude the effect of the resistance of the lead wires the resistance was measured with the aid of a double bridge. The scheme of the measurements is shown in Fig. 3.

The resistance of the specimens was measured directly in the clamps *1* and *2* of the machine. The standard resistance R_{st} was a wire from the same lot of metal from which the specimens were made. Since the standard resistance was in the immediate neighbourhood of the specimen their temperatures were the same, hence there was no need for temperature corrections. The working current was taken from the accumulator *3* and measured by the ammeter *4*. With the aid of the rheostat *5* the necessary strength of the working current was maintained. The resistances in the measurement circuit were always the same in pairs: $R_1 = R_2$ and $R_3 = R_4$. Then the resistance of the specimen can be found from the formula

$$R_{spec} = R_{st}\frac{R_1}{R_3} = R_{st}\frac{R_2}{R_4}.$$

The drop in voltage along the specimen was taken off with the aid of two thin copper wires soldered directly to the part of the specimen which was to be elongated. In this way the drop in voltage is not affected by the resistance of current conducting contacts. A mirror galvanometer of M-21 type was used as zero galvanometer. The galvanometer could be shunted with the switch *K*. To exclude the effect of parasitic thermoelectric forces the resistance was measured for both directions of the current and the arithmetic mean of the two measurements was taken. The direction of the working current was changed with the reversing switch *P*. The resistance was measured with an accuracy to

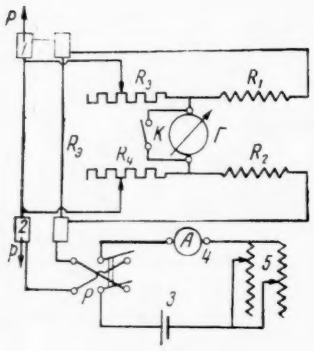

FIG. 3. Schematic drawing of the arrangement for measuring the specific electric resistance during deformation.

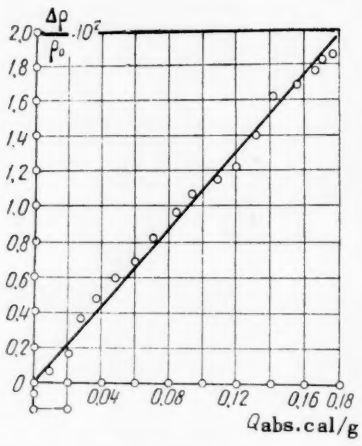

FIG. 4. Dependence between the amount of energy absorbed and the relative increase in the specific electric resistance of silver.

the fourth figure.

The relationship between the amount of energy absorbed and the relative increase in the specific resistance of silver during plastic deformation was plotted from the results of the measurements. Fig. 4 shows that the change in the specific resistance in the process of plastic deformation is directly proportional to the amount of energy absorbed. A similar dependence was obtained for copper also. The coefficient proved to be constant: for copper it was 9.5×10^{-8} Ω cm g/cal, for silver 18×10^{-8} Ω cm g/cal. It goes without saying that the resistance induced by the deformation and the thermoelectric force, being each directly proportional to the absorbed energy, are directly proportional to each other. This result had already been obtained by us in paper [6].

Translated by B. Ruhemann

REFERENCES

1. N.F. Kunin, *Fiz. metal. metalloved.*, 2, 237 (1956).
2. V.I. Khotkevich, E.F. Chaikovskii and V.V. Zashkvara, *Dokl. Akad. Nauk SSSR* 96, No. 3 (1954).
3. V.N. Kunin, *Uchenyye zapiski Cheliabinskogo pedagogicheskogo inst.* 5, No. 1, 93 (1958).
4. V.N. Kunin, *Uchenyye zapiski Cheliabinskogo pedagogicheskogo inst.* 5, No. 1, 107 (1958).
5. N.F. Kunin and N.A. Karelin, *Trud. Cheliabinskogo inst. mekhanizatsii i elektrifikatsii sel'skogo khoziaistva* No. 2, p. 25 (1947).

THE THERMOELECTRIC PROPERTIES OF THE ALLOYS Sn-Cd AND Pb-Cd*

V.A. YURKOV and V.V. NEKRASOV

Archangelsk Institute of Wood Technology

(Received 3 March 1958)

A great deal of research has been devoted to the thermoelectric properties of alloys, a subject of great scientific and practical significance. An example of one of the important applications of the data concerning the thermoelectric properties of alloys is the development of thermoelectric generators and refrigerators under the general direction of Academician Ioffe. In this case it was the material concerning the thermo-electromotive force which was of the greatest significance.

Sometimes however, it is necessary in practice to make use of material which gives no significant thermo-e.m.f. in couple with the metal in question. In the solution of this type of problem, curves of thermo-e.m.f. vs composition of the alloy can be particularly useful. It is not unusual [1-3] to observe points of inversion of the sign of the thermo-e.m.f. on such curves. In this case, obviously, the thermo-e.m.f. of the couple alloy – metal will be equal to zero. This fact makes it desirable to examine systems in which there is a point of inversion of the thermo-e.m.f. sign on the the thermo-e.m.f. composition curve. Such investigations would also serve the purpose of widening our knowledge of the form of thermo-e.m.f. composition curves. For instance, it is believed that in the thermo-e.m.f. composition curves for eutectic systems [4], the latter should have the form of a straight line. Researches have, however, revealed such a large number of exceptions as to make it impossible to speak of this in terms of a rule.

This paper is written with the object of clarifying the form of the curve thermo-e.m.f. composition for the alloys Sn-Cd and Pb-Cd and of explaining how this may be influenced by the conditions of the test. Particular attention will be paid to describing the conditions under which inversion of the thermo – e.m.f. sign is possible.

Metallographically, the systems Sn-Cd and Pb-Cd have already been given sufficient detailed investigation [5]. They are eutectic with limited solubility of the components. The electric properties of these alloys have been given insufficient attention. In particular, the relation between thermo-e.m.f. and the difference in temperature of the hot and cold contacts has not been explained.

METHOD OF CONDUCTING THE EXPERIMENT

Samples of the alloys were prepared by fusing weighed portions of the components in hard glass ampoules evacuated to a pressure in the region of 10^{-3} mm Hg [3]. The components used were Pb and Sn mark (xr) and standard laboratory samples of Cd. Two or three samples of exactly the same composition were used for measuring, in the form of cylinders 5-6 mm across and 50-60 mm long.

The samples were not given any special annealing before measurement as metallographic analysis had shown that they were sufficiently homogeneous and there was no segregation. All the alloys investigated were two-phase systems.

For the measurements of thermo-e.m.f. the samples were compressed between two copper blocks, the temperature of one which was maintained at around 12 ± 2° by a special circulating device. The temperature of the other block varied between 15 and 160°. The temperatures of the blocks were measured by means of copper-constantan thermocouples, the junctions of which were placed in special holes in the base of the blocks. The thermo–e.m.f. of the samples was measured by the usual compensation method. The sensitivity of the apparatus was good enough for the difference in potentials of 3 to 4 μV to be fixed with complete reliability.

From considerations of the accuracy of temperature measurement and difference of potentials, the writers limited themselves to the measurement of thermo-e.m.f., starting with a temperature difference Δt = 20 to 25°. The course of the thermo-e.m.f. composition curves in the range $\Delta t < 20°$ therefore remains unclarified. This is no obstacle to the determination of the position of the point of

*Fiz. metal. metalloved., 8, No. 1, 21-24, 1959.

VOL. 8 1959

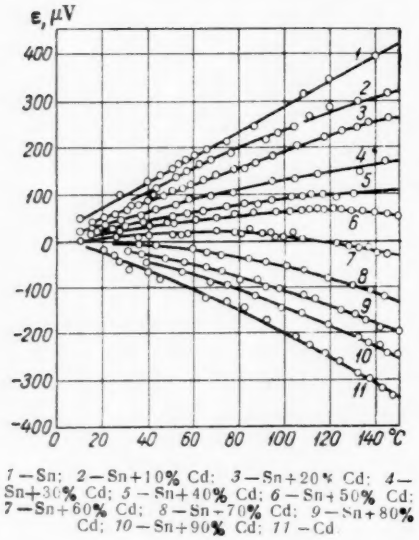

1 — Sn; 2 — Sn + 10% Cd; 3 — Sn + 20% Cd; 4 — Sn + 30% Cd; 5 — Sn + 40% Cd; 6 — Sn + 50% Cd; 7 — Sn + 60% Cd; 8 — Sn + 70% Cd; 9 — Sn + 80% Cd; 10 — Sn + 90% Cd; 11 — Cd

FIG. 1. The relation between the thermo-e.m.f. of Sn-Cd alloys and the temperature difference of the hot and cold contacts.

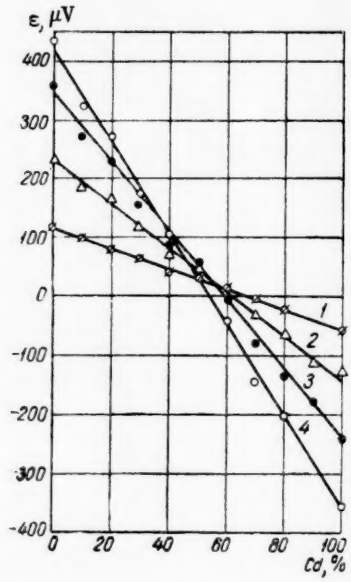

1 — 40°; 2 — 80°; 3 — 120°; 4 — 140°.

FIG. 2. Relation between thermo-e.m.f. of Sn-Cd alloys and their composition at various temperature differences.

inversion on the concentration axis, of the thermo – e.m.f. sign. It seems from the general characteristics of changes in the thermo-e.m.f. of alloys in the field of small temperature differences, that this question is of special interest and could well be the subject of special research. We note that for semiconductors the coefficient of thermo-e.m.f.does not, apparently, depend on the difference in temperature [6]. This cannot be regarded as proven for metal conductors.

RESULTS AND EVALUATION

1. *Alloys Sn-Cd.* The relation between thermo – e.m.f. (ϵ) and temperature difference was investigated for a set of 9 samples which contained 10, 20, 30, 40, 50, 60, 70, 80 and 90 per cent Cd. The results of the measurement of the thermo-e.m.f. of the Sn-Cd alloys at various values of Δt are set out in Fig. 1. The end curves are for pure Sn and Cd. The thermo-e.m.f values were considered to be positive if, in the outer circuit current flowed from the hot to the cold contact.

For pure Sn the relation $\epsilon = f(\Delta t)$ appeared to be linear in the range of Δt variation from 20 to 140°. The coefficient of thermo-e.m.f. $a = \Delta\epsilon/\Delta t$ was equal to 2.97 μV/degree, which is reasonably close to the alloying data [7]. Subsequent increases of the Cd in the Sn led to reduction in the value of the thermo-e.m.f. and in clearly evident loss of linearity of the function $\epsilon = f(\Delta t)$.

The curvature of the curves increased with increasing Cd content. The relation between ϵ and Δt for pure cadmium was clearly non-linear. In the temperature range under investigation therefore, the coefficient of thermo-e.m.f. cannot be regarded as a constant value. For alloys containing 50 % Cd the thermo-e.m.f. in the range $60° < \Delta t < 150°$ hardly moved with variation of Δt.

The relation $\epsilon/\Delta t$ for alloys containing 60 per cent Cd is particularly interesting. For this alloy the curve $\epsilon = f(\Delta t)$ has a clearly visible maximum at which, in the range of Δt variations from 110 to 130° inversion of the thermo-e.m.f. sign was observed. At $\Delta t < 110°$ current in the outer circuit flowed from the hot to the cold contact; at $\Delta t < 130°$ current in the outer circuit flowed in the opposite direction.

To explain the relation between the shape of the thermo-e.m.f. (composition curve and Δt from the data in Fig. 1 ϵ) composition curves were drawn for various values of Δt (Fig. 2). The relation between ϵ and composition was shown to be practically linear, while the inversion of the thermo-e.m.f. sign was observed at various percentages of cadmium. When the difference in temperature was increased the point of inversion shifted in the direction of less content of Cd. At all values of $\Delta t < 130°$ all the straight lines intersected at the same point, appropriate for the alloy containing

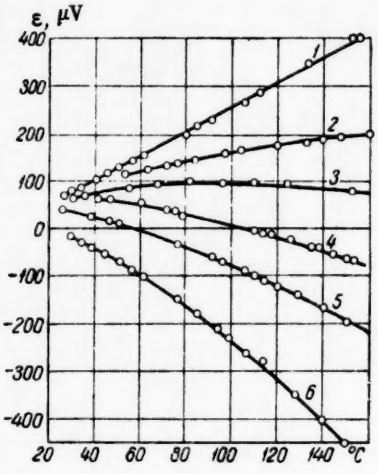

1 — Pb; 2 — Pb + 20% Cd; 3 — Pb + 30% Cd; 4 — Pb + 50% Cd; 5 — Pb + 80% Cd; 6 — Cd.

FIG. 3. Relation between thermo-e.m.f. of Pb-Cd alloys and the temperature difference of the hot and cold contacts.

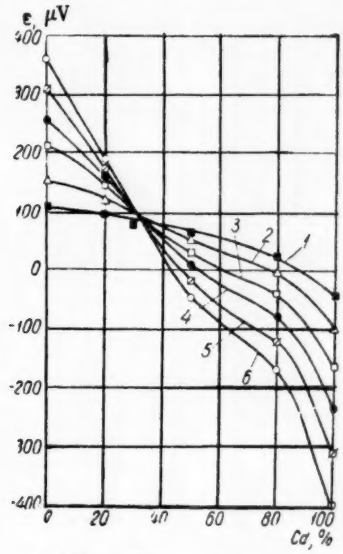

1 — 40°; 2 — 60°; 3 — 80°; 4 — 100°; 5 — 120°; 6 — 140°.

Fig. 4. Relation between thermo-e.m.f. of Pb-Cd alloys and their composition at various temperature differences.

55 per cent Cd. As will be seen from Fig. 3, the thermo-e.m.f. of this alloy should not be dependant on temperature difference. The eutectic alloy does not differ, as regards thermoelectric properties, from the hypo- and hypereutectic alloys.

2. *Alloys Pb-Cd.* In its electrical properties lead has many similarities with tin. In particular, the thermo-e.m.f. of the couple Sn-Pb is practically zero. From this it is to be expected that one would observe inversion of the thermo-e.m.f. sign with a cadmium concentration of 40 to 60 per cent. For this reason only four alloys were prepared, containing 20, 30, 50 and 80 per cent Cd.

The results of the examination of the relation between ϵ and Δt for these alloys are set out in Fig. 3. For lead the relation between ϵ and Δt, within the limits of error for the experiment is, of a linear nature. The coefficient of thermo-e.m.f. was equal to about 2.45 μV/deg, which was somewhat lower than that given in published sources [7]. Additions of cadmium to the lead caused departure from the linear relationship between ϵ and Δt, which increased with increasing Cd concentration. It is clear from a comparison of the family of curves (Figs. 1 and 3) that additions of cadmium change the thermoelectric properties of lead rather more sharply than they do the properties of tin.

It must also be noted that the $\epsilon = f(\Delta t)$ curves for some Pb-Cd alloys do not converge towards the beginning of the co-ordinates. This could be regarded as an indication that, in the range of low values for Δt the relation $\epsilon = f(\Delta t)$ is of a somewhat different nature than for the values $\Delta t < 20$-25°.

From the data in Fig. 3 the values of ϵ were calculated for alloys of varying composition at values: 40, 60, 80, 100, 120, and 140°. The results are set out in Fig. 4. It is easy to see that in this case the curves are of a more complex form and are very different from those in Fig. 2. They have this in common however, that the cadmium content influences the position of the point of inversion of the thermo-e.m.f. sign on the concentration axis. The greater the cadmium content, the smaller the temperature difference at which the inversion is observed. All the curves intersect at more or less the same point, that at which the cadmium content is 30 per cent. The thermo-e.m.f. of this alloy in relation to copper should not be dependent on temperature difference in the range of variations of the latter from 25 to 140°.

CONCLUSIONS

1. The relation $\epsilon = f(\Delta t)$ is linear for Pb and Sn and, but non-linear for Cd.

2. Additions of cadmium change the thermoelectric properties of lead more sharply than they do the properties of tin.

3. In the systems examined, inversion of the thermo-e.m.f. sign occurred both with change in composition of the alloy and with change in the

VOL. 8 1959

temperature difference. The position of the point of inversion on the concentration axis for Cd changes with alteration of the temperature difference. If concentration is increased the point of inversion moves into the field of low cadmium content.

Translated by V. Alford

REFERENCES

1. F.I. Vasenin, *Zh. teor. fiz.*, 25, 81 (1955).
2. D.I. Kon ozenko and V.I. Ustinov, *Zh. teor. fiz.*, 27, 1606 (1957).
3. V.A. Yurkov, *Dokl. Akad. Nauk SSSR*, 91, 891 (1953).
4. Ya.G. Dorfman and I.K. Kikoin, *Fiz. metal.* Gostekhteoretizdat 1934.
5. M. Hansen, *Struktur binarnykh splavov (The structure of binary alloys)* Metallurgizdat, 1941.
6. B.I. Boltaks, *Zh. teor. fiz.* 20, 1039 (1950).
7. A.F. Ioffe, *Tablistsy fizicheskikh konstant (Tables of physical constants)* Moscow-Leningrad, 1928.

INVESTIGATIONS INTO THE DEFECTOSCOPY OF RAILWAY RAILS IN MOVING MAGNETIC FIELDS

17. A STUDY OF THE CURRENTS IN RAILS ON EXCITATION BY A TRANSVERSE FIELD*

V.V. VLASOV

Institute of the Physics of Metals

(Received 12 August 1958)

VOL. 8 1959

It has already been demonstrated that when rails are magnetized longitudinally by a moving U-shaped electromagnet supplied by d.c., the resulting currents are not entirely suitably orientated for discovering the most dangerous transverse cracks in the head of the rail. In particular, the angle of incidence between the current and the defect is very small. For the satisfactory detection of internal transverse cracks in rails the angle of incidence between the current and the defects should be 90° or thereabouts. This could only occur if the current were to flow straight along the head of the rail. In principle it is possible to obtain current flowing in this direction if the rail is magnetized by a moving permanent magnetic field directed across the rail.

Polivanov [2] has studied the currents in rails with magnetization in a transverse field at fairly slow speeds and Sycheva [3] has examined the currents in cylindrical bodies with magnetization at high speeds in a relative weak transverse field [3, 4]. It seems that it would now be interesting to study the currents in rails with relatively powerful transverse magnetic fields moving at relatively high speeds. With no pretensions to a solution of the whole problem, we are going to restrict ourselves to consideration of a general nature regarding the equipment for transverse magnetization of rails, description of its design and an approximate estimate of the current density in one particular case.

CHOICE OF DESIGN FOR THE MAGNETIZING EQUIPMENT

To get current flowing along the head of a rail the best thing is an electromagnet with pole pieces arranged on either side of the neck of the rail and as near as possible to it. However, this type of construction cannot be used owing to the rail fastenings, turnouts and guide rails. For this reason the most acceptable design for practical use might be an electromagnetic equipment above the rail and as near to it as possible.

It is well known that U-shaped and rod electromagnets create a non-homogeneous field. While the external field, according to the differential equation for current density [5], should have a gradient only in the direction of the movement, according to the height of the rail its gradient should, for reasons which are fully understandable be reduced to a minimum. It is therefore desirable to have a field which has a fairly considerable gradient along the rail. In this context we made a study, by means of models, of the field of electromagnets with various configurations of the cores, in which the coefficient of geometrical similarity, equal to the ratio of the corresponding linear dimensions of the original to the model, was taken as 3.5. The purpose of the study was to establish at what geometry of the electromagnet cores the ratio of the field at the points corresponding to the head and sole of the rail would be near to one. The field of the electromagnet was measured in the sectors which correspond to the head and sole of the rail model without the latter being in the role of a magnetized object.

As we are not describing all the investigations we will make the following observations. For U-shaped and rod electromagnets the ratio shown was around 4, while the lowest value, 1.6 was established for the electromagnet whose design is shown in Fig. 1. The core of the electromagnet for magnetizing the model of the rail was wide (120mm) but comparatively thin (1 cm) and had the curved form of a pole piece.

Further, the field created by the electromagnet along the axis X of the perpendicular surface of the diagram shown, was measured without a model of the rail. The results of the measurement are given in Fig. 2. where the field is plotted along the ordinate

* *Fiz. metal. metalloved.*, 8, No. 1, 25-30, 1959.

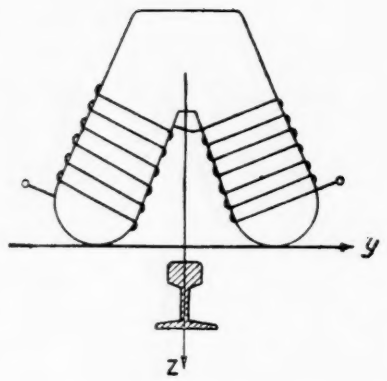

FIG. 1. Diagram of electromagnet and its arrangement relative to the rail.

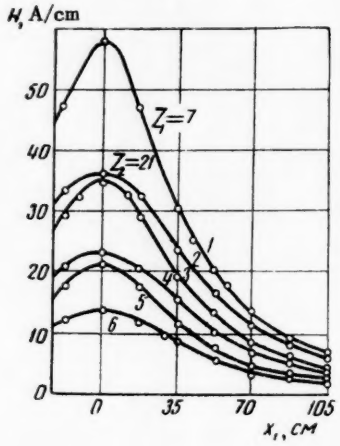

FIG. 2. Relation between the field of electromagnet H for the points corresponding to the surface of the head z_1 and the sole z_2 and co-ordinate X along the rail for m.m.f: 1, - 11; 3, 4 - 7 and 5, 6 - 4 thousand ampere turns. The uneven curves are those for the surface of the head and the even ones, for the sole.

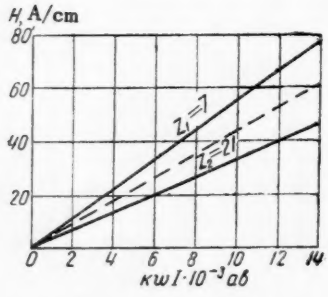

FIG. 3. Relation between electromagnetic field H in the points corresponding to the surface of the head z_1 and sole z_2 at $X = 0$, and the magnetizing ampere turns. Dotted line represents the field in the middle of the rail k is the coefficient of geometrical similarity, w is the number of turns, I is the strength of the current in the model experiments.

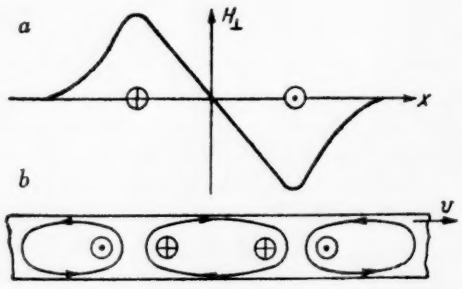

FIG. 4. a — diagram of external fields: b — diagram of eddy currents in duced in the rails on movement of the field.

axis and co-ordinate X along the axis of the abscissa, that is, the distance from the core of the electromagnet along the rail. Here and elsewhere the graphic material presented is applicable to the magnetization of rails in conditions simulated by model experiments. Consequently the point which corresponds to the surface of the rail has $z_1 = 7$ cm and the point corresponding to the sole, $z_2 = 21$ cm. It will be seen from Fig. 2 that the fields in the points corresponding to the head and the sole of the rails are, at one and the same value for the magnetizing ampere turns, fairly strongly differentiated from each other at low X values with increase in X the difference between them diminishes.

The field in the points corresponding to the surface of the head and the sole of the rail is shown in Fig. 3 for $X = 0$, in relation to the magnetizing ampere turns. It can be seen from this illustration that the field of the electromagnet grows with increase in the magnetizing ampere turns, and also the distance between the fields in these two points is increased. If the m.m.f. in 25,000 ampere turns is taken and the co-ordinates of the axes in Fig. 3 are appropriately lengthened, by using extrapolation of

the dotted curve we find that the field in the centre of the rail is equal to 100 A/cm.

To get the best distribution of currents along the rail it is obviously necessary to arrange two electromagnets above it in such a way that they have poles of counter-polarity from one side of the rail. The resulting field will be as shown in Fig. 4a. eddy currents should arise in the process of movement of this field in the rail. They are shown schematically in Fig. 4b in the form of closed lines with arrows indicating their direction. The primary (Fig. 4a) and secondary (Fig. 4b) are represented by circles with crosses or dots indicating the direction of the field in the normal way, to the surface of the drawing.

Fig. 4 shows that the longitudinal component of the current reaches maximum at approximately middistance between the diametrically opposed maxima of the primary field, that is, between the electromagnets. From this illustation it will also be seen that the longitudinal component of the current in the head of the rail between the electromagnets has, as is to be expected, a direction counter to the current beyond this area.

VOL. 8 1959

THE CURRENT DENSITY TO BE EXPECTED IN THE HEAD OF THE RAIL

We will give an approximate estimate of the density of the eddy currents set up in the rails by the moving transverse magnetic field which created in the manner described above, by a system of two electromagnets. It must be noted that these currents are described as inconclusive in the general case, by the integro-differential equation [5]. Therefore, with no claims of rigidity, we make and estimate of the density of the eddy currents by the following elementary method. For simplicity we will take instead of the complex shape of the rail, a plate with the same magnetic properties and electric conductivity. The geometrical dimensions of the plate are, in width and thickness, in correspondence with the height of the rail and thickness of its neck. In other words, we are going to ignore the effects which are introduced into the density of the eddy currents by the projecting portions of the rail, the head and sole.

We will suppose that the magnetic field is dependent only on co-ordinate X which coincides with the longitudinal axis of the plate, and is in no way dependent on the co-ordinates in the direction of which the width and thickness of the plate are assigned, that is $H = H(x)$. When this field moves in the direction X, in the two points diametrically opposed to each other across the width of the plate there appears an electromotive force

$$e = vhB,$$

where e is the e.m.f.; v is the rate of relative movement; h is the width of the plate and B is the magnetic induction.

Ignoring the reduction in the field caused by the eddy currents (which leads to some increase in the estimate of them) it is possible for induction B in the plate, to write the following equation:

$$B = \mu_0 \mu^* H,$$

where H is the external field and μ_0 and μ^* are the magnetic permeability appropriate for a vacuum and a body in which the latter is determined by the relation [6]

$$\mu^* = \frac{\mu}{1 + N(\mu - 1)},$$

where μ is the relative magnetic permeability of the material of the body and N is the demagnetization factor.

For plates magnetized by a transverse field $N = 1$. In this case the permeability of the body $\mu^* = 1$ and $B = \mu_0 H$. Consequently

$$e = \mu_0 vhH.$$

Differentiating this equation according to X, that is, the co-ordinate in the direction of movement, and substituting the derivatives of the final increments, we get

$$\frac{\Delta e}{\Delta x} = \mu_0 vh \frac{\Delta H}{\Delta x}.$$

Ignoring surface effect it is possible for $\Delta e/\Delta x$ to write

$$\frac{\Delta e}{\Delta x} = \rho\delta,$$

where ρ is the specific electric resistance and δ the current density.

Thus we get, for current density, the following relation

$$\delta = \frac{\mu_0 vh}{\rho}\left(\frac{\Delta H}{\Delta x}\right).$$

When rails are magnetized by electromagnets as shown in Fig. 1, the magnetic field with m.m.f. in

25,000 ampere turns amounts to 100 A/cm. Allowing that two electromagnets are used, arranged at a distance of 100 cm from one another, then the system shown in Fig. 4 is acceptable as regards creation of the field. In these conditions the gradient of the field amounts to 2 A/cm².

Inserting this value for the gradient into the last equation, and also $\mu_0 = 12.26 \times 10^{-9}$ in sec/A.cm, $v = 1.25$ cm/sec (45 km/hr), $h = 14$ cm (height of rails) and $\rho = 0.21 \times 10^{-4}$ Ω.cm, we find that the density of the current in the rail should be around 20 A/cm².

ESTIMATION OF CURRENT DENSITY FROM EXPERIMENTAL RESULTS

For the estimate of current density the voltage of the electric field was measured on the surface of the head of the rail model, moving in a transverse magnetic field. For this purpose, the apparatus already described was used for modelling electromagnetic phenomena in rails on magnetization of their moving field sources [7-9]. Two electromagnets of the type shown in Fig. 1 were used and on one side of the rail model the electromagnets had poles of counterpolarity. A diagram of the transverse field arising in the rail model is shown in Fig. 4a. The distance between the electromagnets along the rail model amounted to 16 cm, while in theory they ought to have been about 28.5 cm apart. The experiments were conducted with a m.m.f. of around 6600 ampere turns, which corresponds to 23,000 ampere turns for the magnetization of rails in similar circumstances. The speed of movement of the model was 840 rev/min which corresponds to 45 km/hr for rails.

The results were as follows. The difference in the potential on the surface of the rail model along the centre line between the two electromagnets was 15 mV for a length of 10 cm. Consequently, the voltage of the electric field $E = 1.5 \times 10^{-3}$ V/cm.

As we measured the voltage of the electric field in the direction of the speed of movement, for the density of current in the rails according to the data from the model, we get [5]

$$\delta_1 = \frac{1}{k\rho} E,$$

where δ_1 is the current density, k is the coefficient of geometrical similarity, ρ is the specific electric resistance and E is the voltage of the electrical field on the model.

Inserting in this equation $k = 3.5$, $\rho = 0.21 \times 20^{-4}$ Ω.cm and $E = 1.5 \times 10^{-3}$ V/cm, we find that the density of current in the head of the rail on transverse magnetization by the arrangements outlined, amounts to around 10 A/cm², which is the same value as that obtained by the analytical method described above. Therefore, the current density in rails which have been magnetized transversally by this equipment is, speaking generally, not very great. However, it might be increased a little by increasing the value of the external magnetizing ampere turns. By the same token, if, for example, 100,000 ampere turns are used instead of the 23 indicated above, it should be possible to achieve a current density in the rails of up to 40-50 A/cm² at a speed of movement of the source of magnetic field in the regions of 45 to 90 km/hr.

CONCLUSIONS

An apparatus is described for the induction of eddy currents in rails by means of a transverse magnetic pole. By means of a model the static magnetic field is examined, which is created by the inductor in the absence of movement. An approximate estimate of the density of the current is given, which is induced in the rails when the inductor is moved along them. The values for current density obtained analytically are confirmed by experiment using a model. The possibility of increasing the density of the current in the rails has been demonstrated for the case of transverse magnetization, by increasing the external magnetizing ampere turns.

Translated by V. Alford

REFERENCES

1. V.V. Vlasov, *Fiz. metal. metalloved.*, 7, 159 (1959).
2. K.M. Polivanov, Sbornik. Prob. ferromagnetizma i magnetodinamiki (Problems of ferromagnetism and magnetodynamics) *Akad. Nauk SSSR*, 196, 147 (1946).
3. T.M. Sycheva, *Zh. teor. fiz.* 25, 6, 1132 (1955).
4. T.M. Sycheva, *Trud. Sibirskogo fiziko-tekhnicheskogi inst.* Tomsk. 35, 75 (1956).
5. B.B. Vlasov, *Fiz. metal. metalloved.* 5, 3, 442 (1957).
6. V.K. Arkad'ev, *Elektromagnitnoe protsessy v metallakh (Electromagnetic processes in metals)* 1, United Scientific and Technical Press 120, 121 (1934).
7. V.V. Vlasov, *Fiz.metal.metalloved.* 6, 1, 74 (1958).
8. V.V. Vlasov, *Fiz. metal. metalloved.*, 6, 2, 247 (1958).
9. V.V. Vlasov, *Fiz. metal. metalloved.*, 6, 4, 628 (1958).

VOL
8
195

THE MECHANISMS INVOLVED IN THE SOLUTION AND SHIFTING OF CARBON IN FERRITE*

L.S. LIVShITs

(Received 13 March 1958)

Observation of the processes of reaction diffusion of carbon in welds has shown that their mechanisms are determined by the change in concentration of the carbon in the ferrite on alteration of the carbide-forming elements.

The fact that it is possible to have a variable content of carbon in the ferrite with local changes in the concentration of the atoms of the carbide-forming elements, should also have some effect on the processes of coagulation of carbides on tempering and the transfer from the less stable types of carbide to the more stable ones with a higher content of the alloying elements.

VOL. 8 1959

As a form of reaction diffusion, carbon displacement in steels at temperatures below A_{c1} is associated with either the breakup or the formation of chemical compounds between the carbon atoms and those of the iron or of any carbide forming elements present. The rate of diffusion of carbon when alloyed with various different elements differs considerably [1]. It has also been observed that alloying has some influence on the extent to which the carbon is soluble in ferrite [2]. The introduction of carbide forming elements increases the solubility of carbon in α-iron and, for example, the presence in steel of a carbide-forming element such as vanadium, will lead to concentration of carbon in the ferrite of not less than 0.11 per cent, even after prolonged heating at 700° [2].

From the observations we have pursued of one of the instances of diffusion of carbon in α-iron, it is possible to say that the solubility of carbon in ferrite and the rate of diffusion do not depend only on the qualitative difference in alloying. In alloys with one or other of the carbide-forming elements, their values are connected with the concentration of the latter. Thus the level of solubility of carbon in alloyed ferrite also in most cases determines the possibility of the appearance of a reaction diffusion of carbon in the α-iron.

The basis for this point of view, as derived from trial and experiment, is set out below.

It has been noticed that in welded joints in which the seam and the addition metal had different content of carbide-forming elements, when there is prolonged heating in the range 500-700° a transfer of the carbon occurs in the direction of the element which produces the more stable carbides [3, 4]. In the zone of fusion of the seam with the basic metal, areas of distinct carburization form where there is an element which in the system in question, produces a more stable carbide, and of distinct decarburization in those parts where there are elements which will produce the less stable carbide (Fig. 1).

In the example given in Fig. 1 of welding a chromium steel, the presence of molybdenum in the seam has led, on ten-hours heating at 700° to a transfer of the carbon from the steel to the seam.

Experiment has shown that it is not always the presence in one part of the welded joint of an element yielding more stable carbides which leads to the transfer of carbon. This might also be due to the presence of such an element in another part of the weld. It appears that, for the transfer of carbon from one part of a weld to another, one of the parts (the seam or the basic steel) should contain free atoms of the element which produces stable carbides. By "free" we mean atoms of the carbide-forming element in question which are free to form carbides with a content of carbon increased above that of the basic metal.

To explain this, let us look at a very simple case where a seam containing vanadium is made on a carbon steel. Welded test pieces were subjected to prolonged heating at 700° (10 and 100 hr). In these conditions the existence in the main of carbide of iron type VC [2] may be considered highly probable.

Two types of seam were made on a carbon steel with 0.15 per cent carbon, one with 0.4 and one with 0.9 per cent V. In the first type of seam, after prolonged heating at 700° no signs whatsoever appeared of a transfer of carbon from the welded steel into the seam (Fig. 2); in the second case there was an appreciable shift of carbon from the basic metal

* *Fiz. metal. metalloved.*, 8, No. 1, 31-37, 1959.

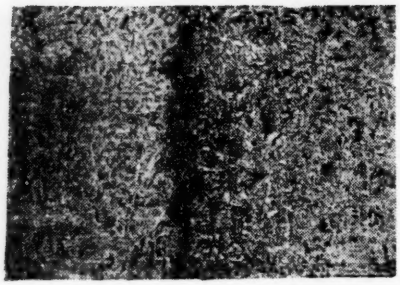

FIG. 1. Fusion sector between steel containing 0.12% C, 1.3% Cr, and the welded seam containing 0.13% C and 1.5% Mo, after heating at 700° for 10 hr; × 200.

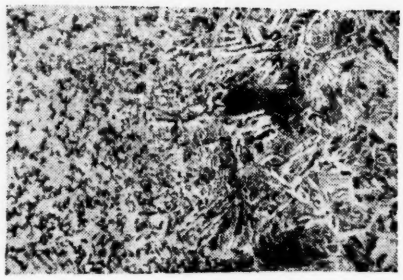

FIG. 2. Fusion sector between carbon steel (0.15% C) and a welded seam containing 0.15% C and 0.4% V, after heating at 700° for 100 hr; × 100.

FIG. 3. Fusion sector between carbon steel (0.15% C) and a welded seam containing 0.15% C and 0.9% V, after heating at 700° for 10 hr; × 100.

into the weld and the formation of a distinct structural heterogeneity on fusion (Fig. 3). The same transfer of carbon was also observed in some other tests in which a seam with a high vanadium content was produced on chromium and molybdenum steel.

In producing a seam with 0.15% carbon (0.69 at.%) and 0.4% vanadium (0.44 at.%), the vanadium was insufficient to combine with the carbon in the metal and form carbide VC. There was an excess of carbon atoms in the seam (0.25 at.%) which thus precluded the necessity (or possibility) of admitting from without (from neighbouring sections of the steel being welded).

In a seam containing 0.15% carbon (0.69 at.%) and 0.9% vanadium (0.98 at.%), free atoms of vandium remained after the formation of carbide VC (0.29 at.%). The presence of these free atoms of an element producing a more stable carbide than that which might be formed in the metal adjoining the seam, also caused a transfer of carbon from the basic steel into the seam, where it combined with the free vanadium atoms.

As the transfer of carbon is in all cases accompanied by decarburization of that part of the weld which has the less stable carbides, and carburization for the part with the alloying element producing the more stable carbides, the process of the reaction diffusion of carbon in ferrite must, in welds, be associated with the decomposition of the less stable carbides in the one part and the formation of more stable carbides in the other part of the weld. In the case under consideration vanadium carbide (or a carbide in which the main part of the metallic atoms was vanadium) was formed in the weld and in the steel there was a decomposition of cementite.

The transfer of the carbon in the ferrite could occur where there is a drop in the carbon concentration of an α-solid solution. It means that, in the part where there are free atoms of the stable carbide-forming element, the concentration of carbon in the ferrite will be lower, and in that part where the carbon is combined in less stable carbides it will be higher.

The difference in the concentration of carbon could be explained by the change in the solubility of carbon in ferrite on alteration of the content of the carbide-forming alloying element. Where there is a high content of the carbide-forming element, when all the carbon in a given sector combines in

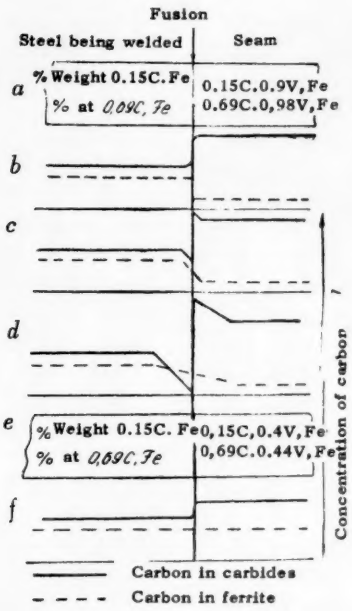

FIG. 4.

the stable carbides and there is an excess of free atoms of the carbide-forming element, the carbon content in the α-iron solution will appear to be low. The carbide former has, so to speak, drawn out the carbon from the solution to form stable carbides.

As long as the process of transfer (removal) of carbon from the solution and its combining with the metallic atoms into carbides of the alloying elements continues, the constitution of the system ferrite-special carbide, will be unstable. The constitution of this system is characterized by a high degree of free energy. This means that when there is a high content of the alloying element corresponding to a low carbon content in the steel, there will be free atoms of the former waiting to absorb fesh additions of carbon. Typical of this kind of constitution is the lowered carbon content in ferrite in comparison to that required for the equilibrium state of an analloyed ferrite.

On the other hand if there is a lot of carbon in the steel and a comparatively low content of the alloying carbide-producing element, all the atoms of the carbide producer will be combined with the carbon. The amount of combined carbon will be increased and also, it seems, in accordance with the equilibrium conditions the corresponding content of carbon in the ferrite.

In general terms the equilibrium conditions of the system ferrite-carbide of an alloying element, may be expressed by the following equation

$$K = m\frac{C_\kappa}{C_f C_l},$$

where C_k is the carbon concentration in the carbides; C_f is the carbon concentration in the ferrite; C_l is the concentration of carbide-forming alloying elements; m is the coefficient which accounts for the influence of temperature and the stability of the carbides formed.

According to the equation presented, in the first of the cases given where there is a small overall content of carbon in the alloy, an increase in the content of alloying elements (increase in the number of free atoms of the carbide former) must lead to an increase in the concentration of carbon in the carbides and a reduction of carbon concentration in the ferrite.

In the second case where there is an unchangeable concentration of alloying elements (C_l) and content of carbon sufficient to form a bond with all the available atoms of the carbide-former, the concentration of carbon in the carbides will increase and there will be a corresponding increase in the ferrite.

Thus the carbon content of the ferrite is dependent on the variable content of carbon in the alloy, (itself dependent on the concentration of the alloying element) the stability of the carbide formed and the temperature.

This viewpoint is confirmed by various data on

VOL. 8 1959

the solubility of carbon in ferrite for a number of steels alloyed with different carbide-forming elements, with a fairly high carbon content.

Paper [2] gives data concerning the solubility of carbon in ferrite after prolonged heating at various temperatures, in several steels containing separately, manganese, chromium, tungsten, molybdenum and vanadium.

If we look at the atomic composition of the alloys and types of carbide established by the writers for each of these alloys, it is apparent that in each case there is a considerable surplus of carbon over and above that which might be bonded with the alloying elements contained. For this reason the writers decided that there was in all cases increased solubility of the carbon in ferrite.

On the basis of the arguments presented above concerning the solubility of carbon in ferrite, it is easy to explain the whole of the process we have described of the reaction diffusion of carbon in welds and the formation of sharp structural heterogeneity in the zone of fusion of the weld with the steel being welded.

As an example let us take a simple case of a weld in carbon steel, which is alloyed with vanadium to a greater amount than is required for bonding into stable carbides which contain the carbon of the seam (Fig. 4). Alloying with vanadium is used for the simplicity by which the system may be observed, where the vanadium is almost all able to combine with the carbon in carbides, and the main type of carbide is the cubic VC which is suitable for calculating the quantity of bonded carbon by atomic percentage.

In this type of weld the quantity of carbon in carbides due to the presence of vanadium in the seam, will be higher than in the welded steel (Fig. 4b), while the quantity of carbon in the ferrite of the seam will, for the reasons set out above (low carbon content in the steel with high vanadium content) be lower than in the ferrite of the unalloyed welded steel.

The fall in carbon concentration on the fusion boundaries immediately after welding will be relatively sharp, if one ignores the fusion in a narrow sector of intermediate compositions (the result of the mixing of the filler metal with the steel under weld) and diffusion processes occurring in the short interval of coling time after welding.

If this weld is heated in the range 500-700°, diffusion processes will arise which are directed towards an equalization of the carbon concentration of the ferrite. By virtue of this there is a transfer of carbon atoms from the ferrite of the welded steel into the ferrite of the seam. This causes a reduction of the concentration of carbon in the ferrite of the basic metal and an increase in that of the seam near to the fusion (Fig. 4c). As the carbon concentration in the ferrite of the basic metal decreases around the seam zone, at the same time the process of solution of the bonded carbon starts up, in order to maintain the equilibrium indicated above, and in this sector the quantity of cementite (pearlite) is reduced. On the weld side, on the other hand, the increase in the carbon concentration of the ferrite leads to the formation of carbides with the free vanadium atoms and in this sector the quantity of carbides will increase (Fig. 4c).

In the further course of this process the quantity of carbides in the zone around the weld will decrease right down to the state at which metallographic analysis would disclose decarburization. Along with this the zone of decarburization will grow, so that the size of the ferrite sector will increase and its carbon will be diffused in the seam (Fig. 4d). On the other side, in the sector of the seam adjacent to the fusion, the entry into the ferrite of all the new carbon atoms will lead to the further formation of vanadium carbides (or, where there are other alloying elements, of carbides in which the atoms of the carbide-forming elements participate) until all (or that number which is able to form carbides) of the vanadium atoms are bonded with the carbon. At the same time there will be an increase in the depth of the carburizing layer, as in the ferrite there will be a further penetration of carbon atoms from the rich into the poorer zones.

The rate at which this process takes place is dependent on a number of factors and, first of all, on the rate of diffusion of the carbon in the ferrite from one part of the weld into the other (in the case on hand, from the welded steel into the seam).

At a given temperature the rate of diffusion may be determined from the gradient of the carbon concentration in the ferrite of the weld and of the basic metal and will in consequence be dependent on the absolute value of carbon concentration in the ferrite of each of the parts. As we have said before, the carbon concentration in the ferrite is dependent not only qualitatively – which element – but also quantitatively, on the nature, of the alloying. For this reason the difference in the concentration of carbon in the ferrite, and the rate of carbon diffusion determinable from it, will depend on the nature and quantity of the alloying element.

In the processes of the coagulation of carbides in the tempering of steel (heating temperature below A_{c1}) transfer of carbon in the ferrite should also take place according to the mechanism outlined above.

The mechanism of these processes may be described as follows. Around the fluctuation zones (or separate carbide particles) with an increased content of atoms of the element which produces the most stable carbide for the system, a zone is formed in which the ferrite has a lower carbon content than that of the rest of the ferrite (as shown above, free atoms of the carbide-forming element will draw the carbon out of the ferrite). The resulting difference in concentration acts as a stimulus for the transfer of carbon atoms from the general mass of the ferrite to the sectors where there is an increased content of carbide-forming atoms.

As soon as carbon atoms from the surrounding ferrite arrive in the area where there are free carbide-forming elements, bonding of the carbon in carbides commences and there is a growth in the carbide particles and once again, draining of the carbon from the adjacent ferrite. This is the way in which the carbides of the more stable and richer alloying elements are formed.

At the same time, in the other system of "less stable carbides – general mass of ferrite", another process should be taking place, in which the reduction in the carbon of the whole mass of ferrite (due to the transfer described, of the carbon to the sectors rich in carbide-formers) will be accompanied by the decomposition of the less stable carbides with the transfer into the general solution of the released carbon atoms. Thus the process of coagulation is at one and the same time connected with the decomposition of the less stable carbides and the formation of the more stable ones with a higher content of the alloying element.

The rate of diffusion of the carbon in ferrite in the conditions we have considered, must be determined from the resulting difference in concentration of solute carbon. As this difference in concentration (of carbon in solution in the general mass of ferrite and in the sectors of ferrite adjacent to the particles rich in alloying element) is dependent on the content of the alloying element, the content of carbon and the type of carbide formed, the rate of diffusion of carbon in ferrite at a given temperature will be dependent on exactly the same factors.

CONCLUSIONS

The process of transfer of carbon atoms in ferrite, as with all diffusion processes, takes place at different concentrations. The difference in the concentration of carbon in the ferrite of different sectors of a steel, is determined by the heterogeneity of the content of the carbide-forming alloying element. In the sectors with a high content of the element which forms the more stable carbides in the system in question, a zone of ferrite will be formed which is poor in carbon. This will occur in a steel with a relatively low carbon content and will be due to the great affinity of this element to carbon. In this zone diffusion transfer of carbon atoms will also take place.

With a high carbon content in a steel containing carbide-forming alloying elements, the equilibrium requirements between the bonded and the free carbon will lead to the quantity of solute carbon in the ferrite becoming greater.

The circumstances described above will explain, for instance, such processes as the coagulation of carbides in tempering and the formation of chemically and structurally heterogeneous conditions in the sector of fusion in some welds.

Translated by V. Alford

REFERENCES

1. S.Z. Bokshtein, *Struktura i mekhanicheskie svoistva legirovannoi stali (The structure and mechanical properties of alloy steel).* Metallurgizdat (1954).
2. A.S. Zavyalov and Ye.Ya. Pavlov, *Sb. Metallovedenie (Compendium on metallography)* Sudpromgiz (1957).
3. V.N. Zemzin, G.L. Petrov and B.I. Bruk, *Sb. Svarochnoe proizvodstvo (Welding)* Lenizdat (1957).
4. L.S. Livhits, L.P. Bakhrakh and S.I. Panich, *Metallovedenie i obrabotka metallov (Metallography and the working or metals)* 8, No. 1 (1958).

VOL. 8 1959

THE RELIEF OF METAL POWDER GRAINS*

Ya. Ye. GEGUZIN and N.N. OVChARENKO
Kharkov State University i/n Gor'kii

(Received 5 April 1958)

In papers [1, 3, 4] tests have been described which were undertaken for the purpose of observing the processes which take place on a free metal surface heated to a high temperature. It has been demonstrated [3] that these processes might well prove to be essential to such phenomena as the sintering of compacts of metal powders. The surface of these compacts is highly developed as regards the dispersion of the original powders.

This paper describes experiments conducted for the purpose of observing the constitution of the surface of powder compacts at high temperatures. The experimental task was dictated by the desire for knowledge concerning the nature of the relief of the powder grain surfaces which lead into pores, that is to say, more detailed information concerning the form of the pores ("fine structure") in addition to those observations conducted earlier for the purpose of studying the process of spheroidization with the aid of macroscopic wire models [6].

This article also includes an account of certain results of experiments conducted for the purpose of providing a clearer definition to existing ideas on the development of the so-called "natural surface roughness".

METHOD AND DESCRIPTION OF THE OBSERVATIONS

Direct observation of the form and constitution of the surface of a pore inside a metal compact is impossible as the compact is not transparent. We therefore resorted to the method of modelling the conditions obtaining in the inside of the pore. One of the surfaces of a powder compact was polished, after which the compact was wrapped in copper foil and annealed at constant temperature.

By this method the compact was annealed in a medium of copper vapour, which means that the polished surface to be examined was in a condition similar to that of the surface of a pore within the body of the compact. Annealing was carried out in a vacuum $\simeq 10^{-3}$ mm Hg. The testpieces were made by pressing electrolytically produced copper powders. The average size of the powders was $\sim 50\ \mu$. The initial porosity of the compact was 35-40 per cent. After annealing, the polished surface of the testpiece was examined under microscopes MIM 6 and MIM 3.

In these experiments the following observations were carried out:

1. The surface which, until the annealing, had been polished, became uneven. The relief of the surface observed after annealing was that of a collection of projections and hollows (macroscopic unevenness). The average distance apart of the macroscopic unevennesses was $\sim 100\ \mu$. Bearing in mind the size of the powders ($\sim 50\ \mu$) and the initial porosity of the compact, it is reasonable to suggest that each of the protuberances observed is connected with a single powder grain. The sort of picture of the surface seen within the field of a metallographic specimen, may be seen from the microphotographs made of the same spot on the specimen with different degrees of defocusing of the lens (Figs. 1a-c) and also with vertical and oblique illumination (Figs. 2a-b). The depth of the "macrorelief" was estimated according to the degree of displacement of the lens on defocusing, which was necessary in order to get the sectors in focus which, when the tops of the protuberances were focused, were themselves completely out of focus. This figure was around $10\ \mu$.

2. Within the limits of each of the "macroscopic" irregularities small unevennesses were observed in the form of steps, which looked like the "natural roughness" already described [1, 3].

In each of the macroscopic irregularities, the natural roughness had a different appearance, according to the orientation of the powder grains in respect to the plane of the specimen. After prolonged annealing (more than 3 hr), on many of the powders roughness was observed in the form of steps with the

* *Fiz. metal. metalloved.*, 8, No. 1, 38-44, 1959

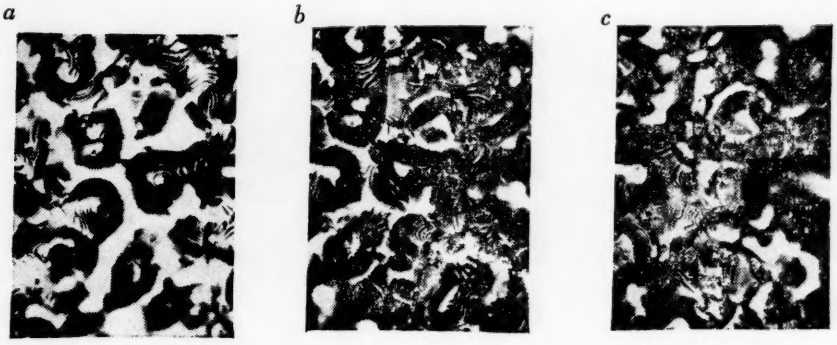

FIG. 1. Surface at the same part of a metallographic specimen, taken at $T = 950^0$, $t = 10$ hr:
a – initial position of lens; b – on focusing to a depth of 6×10^{-4} cm;
c – to a depth of 10×10^{-4} cm; X 666.

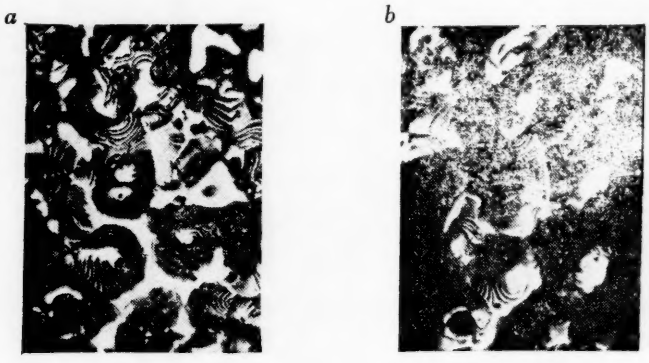

FIG. 2. Surface at the same part of a metallographic specimen taken at $T = 950^0$, $t = 10$ hr;
a – vertical illumination; b – oblique illumination X 75.

following regular shapes: rectangles and triangles, Figs. 3a and b respectively. On the surface of some of these regular shapes, formations were visible which appeared to be a undeveloped flake. The atoms which form this flake come from the gaseous phase (see below). The smallest of the formation observed was 10^{-4} cm (Fig. 3a and Fig. 4). In certain cases natural roughness was observed of a form very far removed from the regular shapes (Fig. 5).

In connexion with this description of our observations we would like to draw attention to the researches reported in recent years, on the constitution of the surface of crystals formed in the process of crystallization from solution or in the process of the evaporation of atoms from the surface on high temperature annealing. The photographs given in Figs. 1 to 7 show that on the surface which is formed, a system of steps takes shape or, in some case, of spirals. In paper [2] there is a description of the spiral and stepped formations on the surface of a natural flake of a NaCl crystal in the process of evaporation. The writer of that paper connected this formation with dislocation arising on the surface of the crystal.

The observations described by us did not include any direct indications as to the role of dislocations in the creation of the stepped structure on the surface of powder grains; it is however possible, that the relief observed of the powders was to some extent occasioned by the presence of dislocation in those grains which had a deformed lattice.

3. Particular interest is attached to the sectors of the metallographic specimen where the meeting of powder grains limits the pore. One of these spots is shown in Fig. 6a-b. Four powder grains, on each of which there is a different form of natural roughness, confine a pore. The surface of this pore consists of separate flat sector.

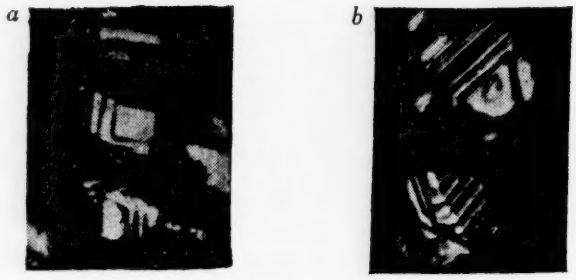

FIG. 3. The form of surface roughness of copper powders with different regular patterns at $T = 950°$, $t = 3$ hr:
a – rectangular; b – triangular X 800.

FIG. 4. Comparative size and shape of formation; X 800.

FIG. 5. Form of natural roughness, X 720.

THE SHAPE OF THE PORES

It is well known that, in the course of the sintering of powder compacts, the process known as spheroidization of the pores occurs. This process can be very distinctly observed on wire models which are modelling a powder body. This process is the result of the straining of the system towards the minimum of free energy and, in particular, towards the minimum of surface energy the value of which, $E_n = \sigma S$ (σ is surface tension, S is surface area) is reduced as the contours of the pore become curved because, at a given volume, the pore will have the minimum surface area when its shape is spherical.

It is obvious however, that reduction of the surface area is not the only way by which the free surface energy may be reduced. The natural roughness which arises leads to an effective reduction in surface tension, due to the development of planes which have less surface tension. The fine structure of the pore therefore, is determined not only by the process of macroscopic spheroidization, but also to the process of the development of natural roughness.

In connexion with what has been written it could be suggested that, in equilibrium conditions, the pore must be a polyhedron bounded by planes of low surface tension and that the form of this polyhedron is determined by the orientation of the grains going into the pore. An example of such a pore (actually a half-pore) is shown in Fig. 6 a-b.

We must point out that observations similar to those described, concerning the form of pores in metal compacts, have been made before [5] in the study of the process of sintering testpieces under investigation. In the later stages of the sintering process pores of cubic shape are quite clearly visible.

THE ROLE OF THE GAS PHASE IN THE EMERGENCE OF NATURAL ROUGHNESS

In one of the previous papers it was shown that the evaporation of a substance from the surface of a testpiece and the consequent condensation of the vapours, plays an essential role in the process of creating the natural roughness. Assuming that the gas phase plays a decisive role in the development of the roughness and that the time t_i, during which the appropriate degree of roughness is established on the surface of the grain, is inversely proportional to the vapour pressure, then between t_i and the temperature of isothermal annealing T_i there should be the following relationship

VOL
8
195

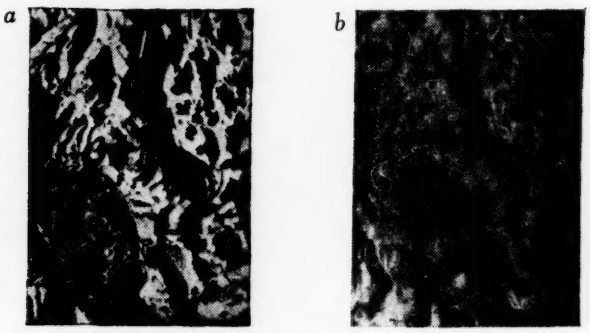

FIG. 6. Sector of a specimen on which some powder grains confine the pore, at $T = 980°$, $t = 4$ hr:
a – arrow indicates junction of four powder grains;
b – same place with lens defocused; X 720.

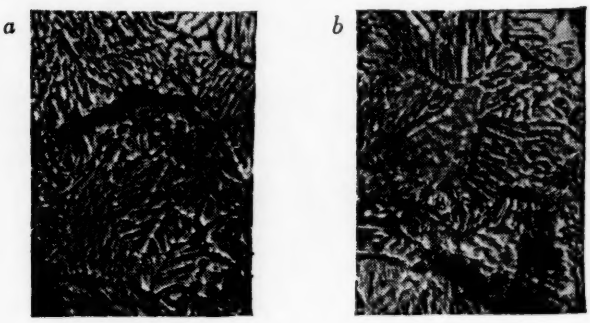

FIG. 7. Form of relief at different annealing conditions;
a – $T = 800°$, $t = 30$ min;
b – $T = 930°$, $t = 20$ sec X 216.

$$\frac{1}{t_i} = A \exp\left(-\frac{Q}{RT}\right),$$

where A is the constant; Q is the heat of evaporation. In this case it should be possible from the slope of the straight line in the co-ordinates

$$\ln \frac{1}{t_i} - T_i$$

to determine the value which, if the assumption regarding the role of the gas phase is correct, should be very close indeed to the figure for the heat of evaporation.

In connexion with these propositions the following tests were carried out.

Similar testpieces produced by pressing copper powders were annealed in an atmosphere of their own vapour at different temperatures (750, 800, 870, 930°), during which the isothermal annealing was periodically interrupted in order to examine the surface under the microscope.

The interval of time t_i was determined by visual identification of the structure on testpieces annealed at different temperatures.

For example, in Figs. 7a and b two structures are shown (the difference in temperatures is 800 and 930°), which, in our analysis we took to be identical.

On the basis of the data obtained by the method described, a graph for the relation

$$\ln \frac{1}{t_i} - \frac{1}{T}$$

(Fig. 8) was constructed and a value for Q determined which was around 80×10^3 cal/mol, which is close to the figure for the heat of evaporation of copper [7]. The value of Q was determined not only from the experimental data, in which the structure shown in Figs. 7a-b, was taken as a "datum", but also from the data of experiments conducted for the purpose of observing the stage at which the appearance of the roughness was marked. In these experiments also, the value obtained for Q was 80×10^3 cal/mol.

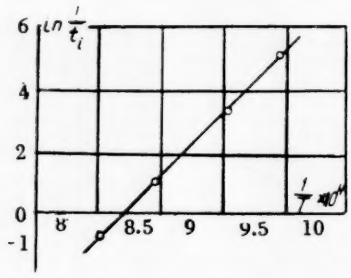

FIG. 8. Relation between $\ln \frac{1}{t_i}$ and $\frac{1}{T}$.

In paper [8], which is dedicated to the study of the figures appearing on the surface of nickel, copper and zinc in the pre-melting range of temperatures, photographs of figures are shown which are similar to ours. The writers call these "evaporation figures" and have concluded that the gaseous phase plays a decisive role in the development of the structure observed.

The results obtained however, do not exclude such a mechanism as surface diffusion, but merely provide evidence that the role of the gaseous phase is essential.

The writers of paper [9] have observed the kinetics of the disappearance of etching figures on the surface of the monocrystal of copper which has the shape of a sphere. The experiments were conducted at temperatures of 700-900°. From the slope of the straight line in co-ordinates

$$\ln \frac{1}{t_i} - \frac{1}{T}$$

in paper [9] the energy of activation of the process was determined and was found to be $Q \simeq 10^3$ cal/mol. In connexion with this value for Q the writer suggests that the disappearance of the etching figure occurs as a result of surface diffusion. In the light of the results of our researches and of those of paper [8], the results given in paper [9] seem a little curious. We note also that the disappearance of etching figures from the surface of a monocrystal of copper having a spheroidal form, as described in paper [9], does not agree with the appearance of similar figures on the surface of spheroidal and cylindrical crystals of rock salt, described in detail by Lukirskii [10].

In conclusion, we would observe that the experiments described in this and previous papers [1, 3] were conducted for the purpose of explaining certain details of the mechanism of the development of natural surface roughness, and did not embrace the problem of the possible role of the processes of partial oxidation and decomposition of the oxides. They do, however, provide evidence that the process of recondensation of a substance is essential in the occurrence of natural surface roughness.

CONCLUSIONS

1. The surface of copper powder compacts acquires, on annealing in copper vapours, a comlex relief which consists of "macroscopic" projections and hollows ($L \simeq 100\ \mu$), each of which is, in its turn, covered by a natural roughness (the length of the steps is $\simeq 0.5\ \mu$).

2. The essential role in the kinetics of the development of the relief observed is played by the process of evaporation and subsequent condensation of the vapours on the surface of the testpiece.

Translated by V. Alford

REFERENCES

1. Ia.Ye. Geguzin and N.N. Ovcharenko, *Dokl. Akad. Nauk SSSR*, 99, 3 (1954).
2. S. Amelincky, Naturwiss. 41, 422 (1954).
3. Ia. Ye. Geguzin and N.N. Ovcharenko, *Izv. Akad. Nauk SSSR, otd. tekh. nauk.* No. 1 (1956).
4. Ia. Ye. Geguzin and N.N. Ovcharenko, *Izv. Akad. Nauk SSSR , otd. tekh. nauk* No. 2 (1956).
5. A. Muller, *Z. Phys.* 96, 307 (1935).
6. Ia. Ye. Geguzin, *Zh. teor. fiz.*, 24, 9 (1954).
7. *Sbornik fizicheskikh konstant (Symposium of physical constants* United Scientific and Technical Press, Moscow-Leningrad. (1937).
8. J. Danko, *J. Metals*, 8, No. 5 (1956).
9. E. Menzel, *Z. Phys.* 132, 508 (1952).
10. P.I. Lukirskii, *Dokl. Akad. Nauk SSSR*, 46, 7 (1945).

THE INFLUENCE OF ADDITIONS OF PALLADIUM ON THE HYDROGEN PERMEABILITY OF IRON*

V.I. ARKhAROV and A.A. KRALINA

Institute of the Physics of Metals Academy of Sciences S.S.S.R.

(Received 18 March 1959)

VOL. 8 1959

From the various deliberations on the subject of the nature of grain boundaries in polycrystalline bodies it may be assumed that, in such a body, diffusion of the various elements must take place with great ease along these areas as compared with diffusion through an undeformed crystal lattice. This has been established experimentally for a number of binary systems. Although in this respect there is still not enough light on the diffusion of hydrogen through polycrystalline metals [1], there is at the same time a lack of arguments which might be set against the possibility of preferred diffusion of the hydrogen along the grain boundaries.

Palladium is known to be particularly permeable to hydrogen. On the other hand, it forms an uninterrupted series of solid solutions with iron. On this basis it may be suggested that the solid solution of palladium and iron (at least at high concentrations of palladium) is more permeable to hydrogen than pure iron.

It has been established by a number of researches in our laboratories that certain dissolved (horophillic) elements, which promote internal adsorption and, because of it, enrich the grain boundaries, exert in such alloys an essential influence on the course of diffusion of a third component from without, as they strengthen (or weaken) the role of intercrystalline diffusion as compared to that of volumetric [2]. This phenomenon has been particularly observed for the diffusion of silver in iron containing palladium [3-6].

It is to be expected from this, that intercrystalline diffusion will be evident to a greater degree in iron which contains some palladium than iron which does not. A similar influence from the palladium is also possible in various alloys based on iron.

With regard to these problems a certain interest attaches to our observations of the diffusion of hydrogen through polycrystalline iron base alloys with palladium, and their comparison with alloys of the same composition but containing no palladium, both with the same coarse, and the same fine, grain.

METHOD OF CONDUCTING THE TESTS

The following materials were used for the experiments: (1) Armco iron, (2) iron with a 0.5 per cent addition of palladium, (3) an austenitic Fe-Cr-Ni alloy (18% Cr, 7.5% Ni) and (4) an austenitic alloy containing the same concentrations of nickel and chromium but with a 0.5 per cent addition of palladium. Armco iron was the basis of all the alloys. The testpieces were forged into bars 10×10 mm in section which were then rolled into plates 0.25 mm thick (in two passes with a 10 hr annealing at 600° in between).

The difference in the thickness of the plates never exceeded 0.01 mm. Testpieces 12×12 mm were cut out of the plates, and were given a preliminary annealing for 50 hr at 600°.

Annealing for the purpose of grain refinement or the reverse then followed. The testpieces were annealed in a vacuum for 10 hr at various temperatures which had been selected so as to produce a series of testpieces from each of the alloys with the same-sized grain. One series was "fine grained" (20-25 μ) and the other, "coarse grained" (280-290 μ). In addition testpieces with "specially coarse" grains were produced from the austenitic alloys (560-580 μ). The annealing temperatures are shown in Table 1.

The size of the grain was determined as the average of the measurements of 120-150 grains on 4-5 samples of every kind on the eyepiece scale of microscope MOM 6 with magnifications of 200, 450 and 850.

The condition of the surfaces of the testpieces was as follows: on one side a metallographic polish was prepared; the other side remained in a state of "post-cold rolling and vacuum annealing".

* *Fiz. metal. metalloved.*, 8, No. 1. 45-52, 1959.

TABLE 1.

Characteristics of materials examined

Material		Annealing temp. °C	Grain size	Characteristic
Composition	Type			
Fe (Armco-iron)	Ferrite without	700 880	25 290	Fine Coarse
Fe+0.5% Pd	Ferrite with	700 880	20 280	Fine Coarse
Fe+18% Cr+7.5% Ni	Austenite without	750 1000 1200	25 290 580	Fine Coarse Very coarse
Fe+18% Cr+7.5% Ni +0.5% Pd	Austenite with	750 1000 1200	25 285 560	Fine Coarse Very coarse

The tests for hydrogen permeability were carried out as follows. Short lengths of glass tubing were soldered on the plate testpieces with picein. This made a small vessel for the electrolytic cell. A 1 per cent solution of sulphuric acid was used as the electrolyte. The testpiece was the cathode (bottom of the vessel) and the anode was a platinmum plate (3 × 8 mm) arranged vertically in the centre of the vessel (the lower edge of the anode was 2 mm from the bottom). During electrolysis the anode rotated on a vertical axis.

The electrolysis took place at a current density of 0.22 A/dm². The under side of the testpiece closely abutted* the opening of the instrument-gas analyser. The diameter of this aperture (10 mm) was determined by the area of the surface of the testpiece (0.785 cm²); it was open at the bottom and facing the gas analyser. On this sector of the surface of the testpiece was the diffusion membrane for that part of the hydrogen which on electrolysis, separated on to the cathode and was diffused through the testpiece into the interior of the gas analyser.

This apparatus was constructed on the lines of a Shakespeare catharometer [7]. The instrument has two chambers, one of which is in communication with the space where the hydrogen falls after being diffused through the testpiece and the other is closed and filled with air.

In each chamber there is a calibrated spiral of platinum wire, 0.02 mm in diameter. These spirals are connected with an electric current on a bridge system in which they are heated by current passing through both parallel branches of the system. A zero reading on the galvanometer connected to the bridge indicates identical composition of the atmosphere in both chambers. As soon as a certain quantity of hydrogen appears in one chamber the heat transfer of the platinum spiral in this chamber is increased, the temperature of the spiral is reduced and, in consequence, its resistance, and the galvanometer dips. We used a M-21 galvanometer with a sensitivity of 10^{-9} A.

The apparatus was previously calibrated on mixtures of hydrogen and air of known composition. For this, the catharometer was connected to a Hoffmann instrument in which were measured the different quantities of hydrogen which had been mixed with air in the inner space of the apparatus (the volume of which was known and remained constant). The galvanometer readings were plotted on a graduated graph along the axis of the abscissa, while on the ordinate axis the percentage concentrations of hydrogen in the mixture with air were shown. Calibration was checked five times while the graduating curve was fully reproduced.

In the tests for the determination of the hydrogen permeability of the alloys under investigation the galvanometer readings were registered at regular intervals and, by means of the graduating curve, a graph was constructed for the increased concentration of hydrogen in the catharometer (that is, the amount diffused through the testpiece) during electrolysis.

* On the picein joint.

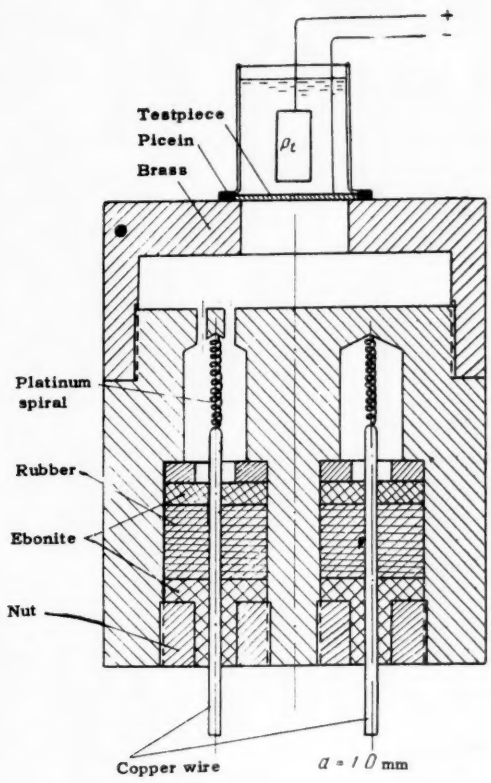

FIG. 1. Apparatus for determination of hydrogen permeability.

RESULTS OF THE EXPERIMENTS

The results of the experiments are shown in Figs. 2-6 in the form of graphs for the relationship between the quantity of hydrogen diffused through the testpiece, and the electrolysis time. These graphs were obtained for each of the four alloys under examination in both fine- and coarse-grained states. In all, ten variations of the material were tested in this way; the tests were repeated for each variant and the graphs were reproduced in their entirety.

On all the graphs the initial period has been noted when the hydrogen progresses at a retarded rate while it is being dissolved in the material of the testpiece up until saturation point*. As this saturation is irregular in sectors which have different permeabilities to hydrogen and also due to variations in its solubility (sectors of varying degrees of lattice distortion, intercrystalline linkages and boundaries of substructure blocks), it is quite possible for the hydrogen to start to emerge from the underside of one part of the testpiece while in another saturation has not yet been reached. For this reason in the initial period the graph curve proceeds with an increasing gradient (convex to the time axis). When saturation has been reached throughout the testpiece the hydrogen passes through it at a constant rate which is determined by the composition and structure of the material. At this stage the graph curve enters a straight line sector and has a constant incline which in its turn is determined by the permeability of the material to hydrogen.

After this the polarization at the cathode starts to take effect and the curve begins to bend, reducing the gradient to the time axis.

The measurements for the tangent of the angle of incline of the straight lines in the graphs are set out in Table 2 in the form of indicators of the hydrogen permeability of the alloys.

EVALUATION OF THE RESULTS

Comparison of the hydrogen permeability of samples with coarse and fine grain, ferritic and

* i.e. up to a state of static steady distribution of the hydrogen throughout the testpiece.

VOL. 8 1959

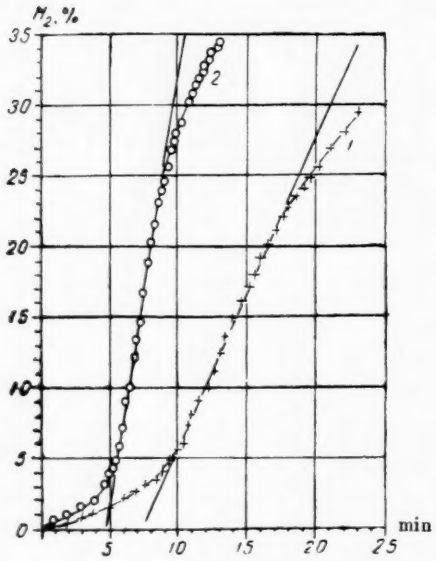

FIG. 2. Relation between amount of hydrogen diffused through the testpiece, and electrolysis time. Fine grain pieces (annealing temp. 700°);
1 – Armco iron (ferrite);
2 – Armco iron (ferrite) with 0.5 per cent palladium.

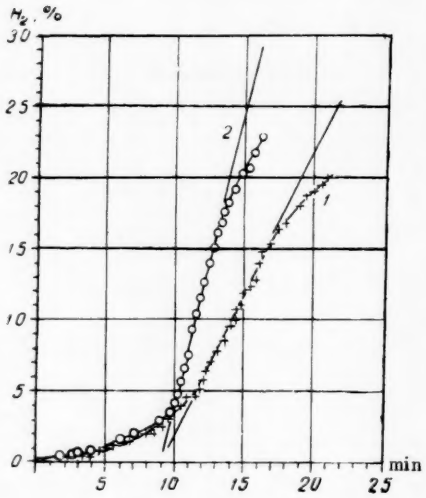

FIG. 3. Relation between quantity of hydrogen diffused through the testpiece, and electrolysis time. Coarse grained samples (annealing temp. 880°);
1 – ferrite;
2 – ferrite; with 0.5 per cent palladium.

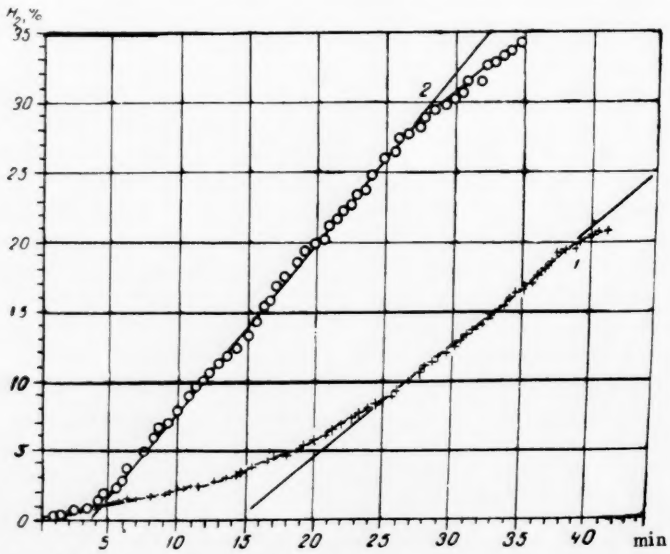

FIG. 4. Relation between quantity of hydrogen diffused through the testpiece, and electrolysis time. Fine grained samples (annealing temp. 750°);
1 – austenite;
2 – austenite with 0.5 per cent palladium.

austenitic structure, palladium additions and without, permits the following conclusions.

In all the tests, of both the ferritic and austenitic alloys, the hydrogen permeability was lowered on transition from fine to coarse grain. From this the conclusion may be drawn that in all these alloys

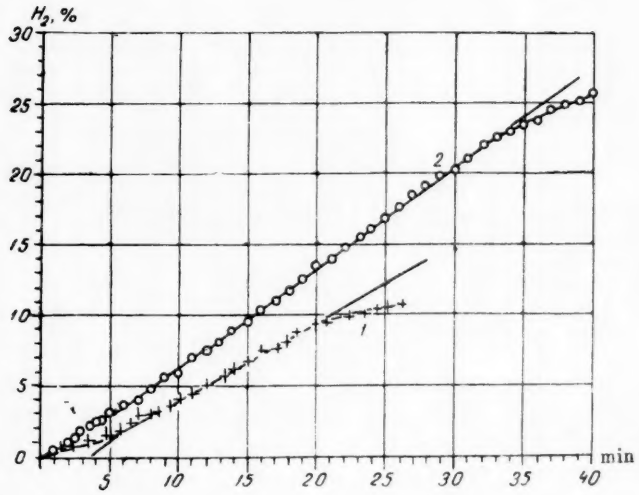

FIG. 5. Relation between quantity of hydrogen diffused through the testpiece, and electrolysis time. Coarse grained samples (annealing temp. 1000°);
1 – austenite;
2 – austenite with 0.5 per cent palladium.

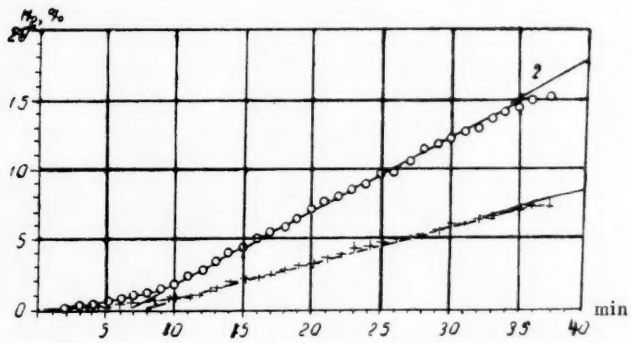

FIG. 6. Relation between quantity of hydrogen diffused through the testpiece, and electrolysis time. Very coarse grained samples (annealing temp. 1200°);
1 – austenite;
2 – austenite with 0.5 per cent palladium.

diffusion of hydrogen proceeds via the grain boundaries to a much greater degree than it does through the grain*.

A comparison of the permeability of alloys with and without palladium with other similar characterisctics (grain size, chemical composition of other elements, type of crystal lattice) shows that the presence of palladium increases the hydrogen permeability.

The hydrogen permeability of austenite is lower than that of ferrite at the same grain size. However, the addition of palladium increases the permeability to practically the same level as that of ferrite with the same grain size but without palladium.

* It is suggested here that the hydrogen permeability through the grain after recrystallization is not essentially different for fine and coarse grained materials. As in our experiments the fine or coarse grain was obtained after recrystallization at different temperatures it may be assumed that in the coarse grain the network of subgrain boundaries is somewhat smaller and the essence of our conclusions remains: hydrogen diffusion occurs to a large degree along the boundaries of the differently oriented crystals, not through them. This is, of course, only significant for high temperature annealing, of which more later.

TABLE 2.

Hydrogen permeability indicators of different alloys

Alloy	Specific hydrogen permeability units		
	With fine grain	With coarse grain	With very coarse grain
Ferrite without	2.24	2.13	—
Ferrite with	6.06	4.11	—
Austenite without	0.81	0.53	0.255
Austenite with	1.21	0.71	0.53

A more detailed comparison of the individual series of results leads to further conclusions.

A given variation in grain size in alloys containing palladium causes a greater diffusion in the hydrogen permeability than is the case for the alloys without palladium, all other characteristics being equal. For example, in armco iron alloyed with palladium, on transition from fine to coarse grain the hydrogen permeability is lowered from 6.06 to 4.11, that is 1.47 times, while a similar change in armco which is not alloyed with palladium reduces the permeability from 2.24 to 2.13, that is, only 1.05 times. In Fe-Cr-Ni austenite containing small additions of palladium the permeability is reduced from 1.21 to 0.71, that is, 1.71 times, while in the same austenite without palladium the reduction is from 0.81 to 0.53, or only 1.53 times. This is an indication that the prevalence of intergranular diffusion, both in ferritic and austenitic alloys is greater where palladium is present. In other words, the increase in hydrogen permeability occasioned by the addition of palladium takes place mainly because of intergranular diffusion.

The following contradictions may be made to these conclusions. The hydrogen permeability of ferrite increases, from the addition of palladium, with fine grain 2.71 times, and with coarse, 1.93 times. For austenite the corresponding figures are 1.50 and 1.34.

The increase in the hydrogen permeability occasioned by the presence of 0.5 per cent palladium in the composition, may be explained in two ways.

(1) A similar quantity of the alloying element in the thickness of the grain and in the intercrystalline zone may lead to different changes in the nature of these media in view of the lack of a structure for the intercrystalline zone which is distinct from that of the regular crystal lattice.

(2) Palladium is diffused volumetrically through a polycrystalline alloy irregularly: it enriches the grain boundaries, that is to say, it promotes intercrystalline internal adsorption.

The second explanation seems more likely to us. It agrees with the conclusions drawn in papers [3-6].

In contradiction to these conclusions it might be said that where there is very considerable coarsening of the austenite grain we observed a greater reduction in the hydrogen permeability in the alloy without palladium (2.08 times) than in the same alloy with palladium (1.54 times). However, we suggest that this contradiction is not real. The fact is that in our experiments the coarsening of the grain was achieved with preheating of the testpieces to very high temperatures. The coarsest grained state at which this contradiction was noticeable was achieved after heating at very high temperatures (1200°) in comparison to those for the less coarse grain (880-1000°) and with fine grain (700-750°).

Heating at higher temperatures leads not only to coarsening of the grain but also, it seems, to the improvement of the sub-crystalline structure, i.e. reduction of overall tension on the sub-crystalline boundaries. It seems likely that, as regards permeability to hydrogen, the role of the latter is similar to that of the intercrystalline boundaries. Thus, with preliminary annealing at the higher temperatures, there is a reduction in permeability not only on account of the general lowering of tension on the intercrystalline boundaries but also because of the reduction in tension of the sub-crystalline boundaries as a result of the improvement in the substructure.

On transition from the fine grain obtained by annealing at 700-750°, to the coarse, obtained by annealing at 880-1000°, it appears to be the first factor which has the overriding influence (in other words, we are suggesting that the change in substructure on annealing at 1000° is slight when compared to that which occurs at 750°).

On transition to very coarse grains, which requires a very high annealing temperature indeed, the most noticeable feature was the intracrystalline improvement of the sub-structure. This occurred

from the most part in the alloys without palladium, as the presence of palladium which is able (on account of its horophillic nature with regard to the iron base of the alloy) to be adsorbed on both the intercrystalline and sub-crystalline boundaries, hinders the processes of improvement of the intragrain block structure. For this reason the intragranular boundaries in comparable austenitic alloys (with and without palladium) appeared, after annealing at 1200°, to be reduced in different degrees. In the alloys without palladium this reduction was clearly greater and the reduction in permeability sharper, than in the alloys with palladium although it might here be suggested that the reduction of the intercrystalline boundaries is the same for both alloys, as at less high annealing temperatures there is a considerable effect on permeability on account of its adsorption.

CONCLUSIONS

1. The hydrogen permeability of iron alloys is increased by additions of 0.5 per cent palladium.
2. The increase in hydrogen permeability caused by additions of palladium occurs for the most part through intercrystalline linkages (boundaries).
3. The hydrogen permeability through the crystals appears to be controlled to a large extent by subboundaries.
4. The influence of palladium on the hydrogen permeability of iron alloys may be explained by the internal adsorption of palladium.

Translated by V. Alford

VOL. 8 1959

REFERENCES

1. R. Berrer, *Diffuziya v tverdykh telakh (Diffusion in solid bodies)* (transl.) Foreign Literature Publishing House, Moscow, 221 (1948).
2. V.I. Arkharov, *Trud. Inst. fiz. met., Urals. fil. Akad. nauk*, 20, 201 (1958).
3. V.I. Arkharov, K.A. Yefremov, C.I. Ivanovskaya, A.K. Shtol'tz and B.A. Yunikov, *Dokl. Akad. nauk.* 89, 269 (1953).
4. V.I. Arkharov and B.A. Yunikov, *Dope. Akad. nauk SSSR*, 1057 (1954).
5. V.I. Arkharov, K.A. Yefremov, S.I. Ivanovskaya, A.K. Shtol'ts and B.A. Yunikov, *Trud.* Foreign Literature Publishing House 16, 56 (1955).
6. V.I. Arkharov, and B.A. Yunikov, *Trud.* Foreign Literature Publishing House 16, 62 (1955).
7. H.A. Daynes, *Proc.Roy.Soc.*, A97, 273 (1920).

THE DYNAMICS OF THE HEATING OF A METAL WHEN INTERNAL TRANSFORMATIONS ARE PRESENT*

E.M. GOL'DFARB

Dnepropetrovsk Metallurgical Institute

(Received 11 March 1957)

The dynamics of the heating of bodies of various shapes has been established, in circumstances where there is internal transformation. This has been done on the basis of a method developed for the momentary regular conditions. Formulae are presented for calculation of the temperature field in various circumstances of heating.

The internal transformation processes in metal alloys are usually accompanied by thermal effects, i.e. the absorption or liberation of the latent heat of transformation. In iron-carbon alloys one of the most substantial effects is that of eutectoid transformation which amounts to 15/cal/kg. pearlite [1]. In thermotechnical calculations for the heating conditions of steels, the thermal effect of transformation is usually reckoned as the mean thermal capacity of the body being heated. In fact, the internal transformations do not flow through the body at the same time, but in stages, as each layer reaches the transformation temperature. For this reason, integral calculation of the thermal effect by the thermal capacity of the body substantially distorts the dynamics of the heating process. As a result of this, the differences in temperature calculated for cross sections of steel ingots is, in a number of cases, 1.5-2.0 times less than is actually the fact (Fig. 1) [2]. In this paper the mechanism of heating a body is examined in various forms and where internal transformations are present.

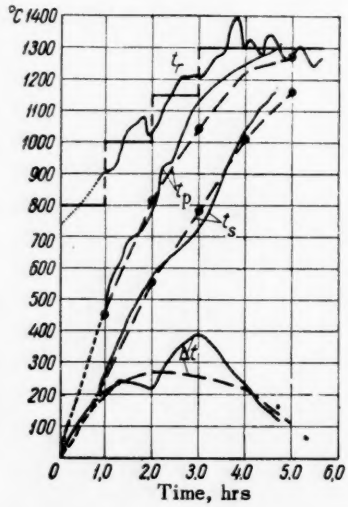

FIG. 1. The heating dynamics of a spring steel ingot in soaking pits: t_p and t_s are the temperatures at the surface and the axis of the ingot; $\Delta t = t_p - t_s$, t_g is the furnace temperature. Solid lines – experimental; dotted lines – calculated.

* *Fiz. metal. metalloved*, 8, No. 1. 53-65, 1959.

THE SOLUTION OF THE PROBLEM

If the known methods of the theory of thermal conductivity are used for solving the problem of the heating of a body where internal transformations are present, substantial difficulties will be encountered. Besides this the possibilities of the theory of thermal conductivity may be considerably widened by the introduction of certain suppositions based on the general mechanism of the process of heating bodies [3, 4].

From a study of the dynamics of heating bodies the process may be divided into two qualitatively differentiated periods, the inertia and the regular. A peculiarity of the inertia period is the continuous change in the thickness of the layer being heated in accordance with the gradual commitment of the body to the process of heating. The regular period is characterized by the fact of the whole body taking part in the heating process while the layer being heated maintains a constant depth.

Given the flow of heat on the surface, a solution to the problem may be reached for the regular period if the rate of heating at different points of the heating layer are taken to be the same, and equal to the mean rate of heating for the whole body. In this case the rate of change of temperature of the body may be directly connected with the arrival of the heat on its surface. This simplification of the problem is equivalent to the presumption of the existence in the heating layer of momentary regular conditions at which the rate of change of temperature is the same at different points in the layer. The inertia period may be represented as a combination of the regular states, differentiated from one another by the varying depths of the layer. This method could be described as that of momentary regular conditions.

VOL. 8 1959

The process of internal transformation is preceded by heating up to the moment at which the surface reaches transformation point. After this the flow of heat directed to the surface will also be used in transformation, accompanied by absorption. In this way we get the heating of a 3-layered body (Fig. 2) consisting of the first layer in which transformation is already complete, the second elementary layer in which transformation is taking place, and the third layer in which transformation has not yet started.

The circumstances of the problem may be represented in the following way:

a) The differential equation for thermal conductivity in the body may be written

$$\frac{\partial t(x,\tau)}{\partial \tau} = \frac{a}{x^{2\nu+1}} \frac{\partial}{\partial x}\left[x^{2\nu+1} \frac{\partial t(x,\tau)}{\partial x}\right], \tag{1}$$

where $t(x, \tau)$ is the temperature at the point with co-ordinate x in a moment of time τ; λ/Cy – the coefficient of temperature conductivity; C – specific heat; λ – the coefficient of thermal conductivity; γ – specific weight; ν – the coefficient of form, for plate $\nu = -\frac{1}{2}$, for a cylinder = 0, for a sphere $\nu = \frac{1}{2}$.

b) The first condition: for a regular heating cycle with constant flow of heat, the distribution of temperature in plate, cylinder or sphere at the moment at which transformation point is reached on the surface will be described by the following equation:

$$t(x, 0) = t_{pr} - \Delta t\left(1 - \frac{x^2}{r^2}\right), \tag{2}$$

where t_{pr} is the transformation temperature; r – the radius of the body; Δt – the difference in temperature across the section of the body equal to

$$\Delta t = \frac{q_1 r}{2\lambda}, \tag{3}$$

where q_1 is the specific flow of heat on the surface.

c) The limiting conditions: on the heating surface of the body the specific flow of heat is equal to

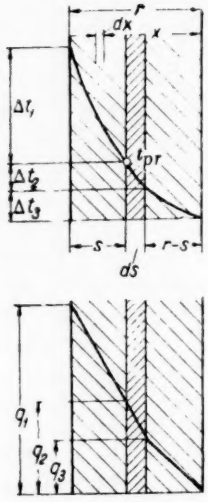

FIG. 2. Heating diagram of a three-layered body.

$$\lambda \frac{\partial t(r, \tau)}{\partial x} = q_1. \tag{4}$$

At a depth s equal to the thickness of the first layer, in which transformation has occurred, the specific flow of heat is equal to q_2

$$\lambda \frac{\partial t(r-s, \tau)}{\partial x} = q_2. \tag{5}$$

At a depth $s - ds$, equal to the combined thickness of the first and second layers, the specific flow of heat is equal to

$$\lambda \frac{\partial t(r-s-ds, \tau)}{\partial x} = q_2. \tag{6}$$

For the second layer $t(x, \tau) = t_{pr}$ we get

$$C\gamma \frac{\partial t(x, \tau)}{\partial \tau} dx - \rho\gamma \frac{ds}{d\tau} = \frac{\lambda}{x^{2\nu+1}} \frac{\partial}{\partial x}\left[x^{2\nu+1} \frac{\partial t(x, \tau)}{\partial x}\right] dx, \tag{7}$$

where ρ is the latent heat of transformation.

The solution to differential equation (1), together with the boundary conditions, should give the relation between the rate of spread of transformation throughout the body, and time, and also, the distribution of temperature across the body at different moments in the process.

Using the theory of analogy we get a solution to the problem of the distribution of temperature in the body in the form of the relation between the following criteria:

a) at constant temperature of the surrounding medium t_0 and a given figure for the coefficient of heat emission

$$\vartheta = f_\nu(F_0, N, B_i, W, \xi); \tag{8}$$

b) with a constant flow of heat q_1

$$\vartheta = \varphi_\nu (F_0, N, W, \xi), \tag{9}$$

where

$$\vartheta = \frac{t(x, \tau) - t_{pr}}{\Delta t}; \quad F_0 = \frac{(2\nu + 2)\, a\, \tau}{r^2}; \quad N = \frac{C \Delta t}{(2\nu + 2)\, \rho}; \quad W = 1 - \frac{s}{r}; \quad \xi = \frac{x}{r}.$$

If we suppose in equations (8) and (9) that $x = s$ and $t(x, r) = t_{pr}$, we get the equation for the dynamics of the heating process in the following criterial form

$$W = \psi_\nu (F_0, N, B_i) \tag{10}$$

or

$$W = \eta_\nu (F_0, N). \tag{11}$$

From the boundary conditions it follows that the temperature field in the first layer is determined by flow of heat q_1 and q_2 and in the third layer by q_3. The specific flows of heat q_1 and q_2 concern the surfaces of heating and cooling of the first layer, which in the ordinary way may be different. For this reason the amount of heat received in the first layer per unit of heating surface, will be equal to

$$(q_1 - q_2 W^{2\nu+1}),$$

and per unit of cooling surface

$$\left(\frac{q_1}{W^{2\nu+1}} - q_2\right).$$

We are taking the rate of heating through the thickness of the first layer to be the same and equal to

$$c_{ni} = \frac{(q_1 - q_2 W^{2\nu+1})\, k_1 (W)}{s \gamma C}, \tag{12}$$

where $k_1 (W)$ is the coefficient of material load on the heating surface, depending on the shape of the layer and the ratio of the internal to the external surface, and equal to

$$k_1 (W) = \frac{(2\nu + 2)(1 - W)}{1 - W^{2\nu+2}}. \tag{13}$$

The special values of coefficient $k_1 (W)$ for plate, cylinder and sphere [3, 4] may be reached if we assume that

$$\nu = -\frac{1}{2},\ 0,\ \frac{1}{2}.$$

The coefficient of material load on the cooling surface $k_1\left(\frac{1}{W}\right)$ is related to coefficient $k_1(W)$

$$k_1\left(\frac{1}{W}\right) = W^{2\nu+1}\, k_1 (W). \tag{14}$$

The heating rate for the second elementary layer ds is equal to

$$c_{n2} = \frac{q_2 - q_3}{C_{usl} \gamma\, ds}. \tag{15}$$

VOL. 8 1959

Here C_{usl} is the nominal specific heat of the elementary layer calculated with the latent heat of transformation, equal to

$$C_{usl} = C + \frac{p}{t_{pr} - t_{sr_2}}, \tag{16}$$

where t_{sr_2} is the mean temperature of the second elementary layer.

The rate of heating of the third layer is equal to

$$c_{n_3} = \frac{(2\nu + 2)\, q_3}{r\gamma C W}. \tag{17}$$

Inserting the value for rate of heating c_{n_1} in differential equation (1), after integration with reference to the boundary conditions, we get the following formulae the temperature field in the first layer:

for $\nu \neq 0$ (plate and hollow sphere)

$$t_1(x, \tau) = t_{pr} + \frac{q_2 W^{2\nu+1} r}{2\lambda\nu}\left\{\left(\frac{1}{W}\right)^{2\nu} - \left(\frac{r}{x}\right)^{2\nu}\right\} + \\ + \frac{(q_1 - q_2 W^{2\nu+1})\, r}{2\lambda}\,\frac{1}{1 - W^{2\nu+2}}\left\{\frac{x^2}{r^2} - W^2 + \frac{W^2}{\nu}\left[\left(W\frac{r}{x}\right)^{2\nu} - 1\right]\right\};$$

for $\nu = 0$ (hollow cylinder) (18)

$$t_1(x, \tau) = t_{pr} + \frac{q_2 W r}{\lambda}\ln\frac{x}{rW} + \\ + \frac{(q_1 - q_2 W)}{2\lambda}\,\frac{1}{1 - W^2}\left\{\frac{x^2}{r^2} - W^2 - 2W^2\ln\frac{x}{rW}\right\}.$$

for Inserting the value for rate of heating c_{n_2} in differential equation (1), after integration we get the formula for the temperature field in the third layer(plate, solid cylinder and sphere)

$$t_3(x, \tau) = t_{pr} - \frac{q_3 r W}{2\lambda}\left[1 - \left(\frac{x}{rW}\right)^2\right]. \tag{19}$$

The temperature difference in the first layer

$$\Delta t_1 = t_1(r, \tau) - t_1(r - s, \tau) = q_2 R + \frac{(q_1 - q_2 W^{2\nu+1})\, s}{k_2(W)\,\lambda}, \tag{20}$$

where $k_2(W)$ is the coefficient of neutralization of the flow of heat in the first layer on the application of external heat, is equal to [3, 4]:

for a plate, cylinder or solid sphere $k_2(W) = 2$;

for a solid cylinder $$k_2(W) = 2\frac{(1 - W)(1 - W^2)}{1 - W^2 + 2W^2\ln W};$$

for a solid sphere $$k_2(W) = 2\,\frac{1 + W + W^2}{1 + 2W}; \tag{21}$$

$$R = \frac{s}{\lambda}\left[\frac{W^{2\nu+1}}{k_2(W)} + \frac{1}{k_2\left(\frac{1}{W}\right)}\right], \tag{22}$$

R is the thermal resistance of the first layer in the stationary state when

$$q_1 = q_2 W^{2\nu+1} k_2\left(\frac{1}{W}\right)$$

is the coefficient of neutralization of the flow of heat in the first layer on cooling from within. The value of

$$k_2\left(\frac{1}{W}\right)$$

could be obtained from the formulae for $k_2(W)$ if the last W is replaced by $1/W$.

The formula for the thermal resistance R may be presented in the form:

for a plate $$R = \frac{s}{\lambda},$$

for a cylinder $$R = \frac{rW}{\lambda} \ln \frac{1}{W}, \tag{23}$$

for a sphere $$R = \frac{rW(1-W)}{\lambda}.$$

Formula (20) for a plate takes the form

$$\Delta t_1 = q_2 \frac{s}{\lambda} + \frac{(q_1 - q_2)s}{2\lambda} = \frac{(q_1 + q_2)s}{2\lambda}. \tag{24}$$

The difference in temperature in the third layer

$$\Delta t_3 = t_3(r - s, \tau) - t_3(0, \tau) = \frac{q_3 rW}{2\lambda}. \tag{25}$$

The mean temperature of the layer is obtained by integration of the distribution of temperature (18) in the following form:

$$t_{sr} = \frac{(2\nu + 2)}{r^{2\nu+2}(1 - W^{2\nu+2})} \int_{Wr}^{r} t(x, \tau)\, x^{2\nu+1}\, dx. \tag{26}$$

Inserting the value for $t(x, r)$, from (18) after integration we get

$$t_{sr1} = t_{pr} + \frac{q_2 s}{k_2\left(\frac{1}{W}\right)\lambda} + \frac{(q_1 - q_2 W^{2\nu+1})s}{k_2(W)\, k_3(W)\, \lambda}, \tag{27}$$

where $k_2(W)$ is the coefficient of neutralization of the temperature in the first layer on heating from without, and equal to [3, 4]:

for a plate $$k_3(W) = 3;$$

for a hollow cylinder $$k_3(W) = 2\frac{(1 - W^2 + 2W^2 \ln W)(1 - W^2)}{1 - W^4 + 4W^2 \ln W}; \tag{28}$$

for a hollow sphere $$k_3(W) = \frac{5}{3}\frac{(1 + W + W^2)(1 + 2W)}{(1 + 3W + W^2)}$$

for a solid cylinder $k_2(W) = 2$ and for a solid sphere

$$k_3(W) = \frac{5}{3}.$$

For plates, from (27) we get

$$t_{sr1} = t_{pr} + \frac{q_2 s}{2\lambda} + \frac{(q_1 - q_2)s}{6\lambda}. \tag{29}$$

VOL. 8 1959

for the third layer, having inserted the values for $t_3\ (x,\ \tau)$ (19) in (26), after integration we get

$$t_{sr_3} = t_{pr} - \frac{q_3 r W}{(2\nu + 4)\lambda}. \tag{30}$$

The formulae deduced for the first layer may be used to calculate the temperature field in the second elementary layer. The thickness ds of the elementary layer is not very great. It may therefore be regarded as flat. This simplification is justifiable for the whole process of transformation with the exception of the final moment of heating a cylinder or sphere $W = 0$, when the elementary layer has the form of a solid cylinder or sphere.

Using (24), the difference in temperature in the second layer is equal to

$$\Delta t_3 = \frac{(q_3 + q_3)\, ds}{2\lambda}, \tag{31}$$

and, using (28) the mean temperature in the second layer is equal to

$$t_{sr_2} = t_{pr} - \frac{(q_2 + q_3)\, ds}{2\lambda} + \frac{q_3 ds}{2\lambda} + \frac{(q_2 - q_3)\, ds}{6\lambda}. \tag{32}$$

From which

$$t_{pr} - t_{sr_2} = \frac{(2q_2 + q_3)\, ds}{6\lambda}. \tag{33}$$

Inserting value (33) into (16) we get

$$C_{usl} = C \frac{6\rho\lambda}{(2q_2 + q_3)\, ds}. \tag{34}$$

Inserting (34) into (15), we get the following formula for the rate of heating of the second layer:

$$c_{n_2} = \frac{(q_2 - q_3)(2q_2 + q_3)}{6\rho\lambda\gamma}, \tag{35}$$

In a regular cycle the rates of heating of the layers will be the same, that is

$$c_{n_1} = c_{n_2} = c_{n_3}. \tag{36}$$

From (36) the relation may be established between the heat flow values q_1, q_2, q_3 for various conditions of heating the three-layered body.

HEATING WITH CONSTANT FLOW OF HEAT ON THE SURFACE $q_1 = \text{const}$

If the value the flow of heat q_1 is known, from $c_{n_1} = c_{n_3}$ we get

$$\frac{q_3}{q_1} = \left(1 - \frac{q_2 W^{2\nu+1}}{q_1}\right) \frac{W}{1 - W^{2\nu+2}}. \tag{37}$$

From condition $c_{n_1} = c_{n_2}$ using formula (37), we get, after conversion, the following equation for the determination of the flow of heat q_2

$$(2-3W^{2\nu+2})\left(1-\frac{q_2W^{2\nu+1}}{q_1}\right)^2-\left(\frac{1}{n}+4-3W^{2\nu+2}\right)\left(1-\frac{q_2W^{2\nu+1}}{q_1}\right)+ \\ +2(1-W^{2\nu+2})^2=0, \tag{38}$$

where

$$\frac{q_1rC}{6\rho\lambda(2\nu+2)W^{4\nu+2}}=\frac{C\Delta t}{3(2\nu+2)\rho W^{4\nu+2}}. \tag{39}$$

From the solution of equation (38) the following formula emerges for the determination of the flow of heat q_2

$$1-\frac{q_2W^{2\nu+1}}{q_1}= \\ =\frac{4(1-W^{2\nu+2})}{\left(\frac{1}{n}+4-3W^{2\nu+2}\right)+\sqrt{\left(\frac{1}{n}+4-3W^{2\nu+2}\right)^2-8(2-3W^{2\nu+2})}}. \tag{40}$$

Inserting (4) into (37) we get the formula for determining the flow of heat q_3

$$\frac{q_3}{q_1}=\frac{4W}{\left(\frac{1}{n}+4-3W^{2\nu+2}\right)+\sqrt{\left(\frac{1}{n}+4-3W^{2\nu+2}\right)^2-8(2-3W^{2\nu+2})}}. \tag{41}$$

The differential equation for the process of heating has the form

$$q_1d\tau=dI, \tag{42}$$

where dI is the change in the heat content of the body in the process of heating and transformation:

$$I=\frac{s\gamma}{k_1(W)}[\rho+C(t_{sr_1}-t_{sr_3})]+\frac{r\gamma C}{(2\nu+2)}t_{sr_3}. \tag{43}$$

For heating with a constant flow q_1 the integration of (42) yields

$$\Delta\tau=\frac{I_k-I_n}{q_1}, \tag{44}$$

where $\Delta\tau$ is the time interval; I_n and I_k – the heat content of the body at the beginning and end respectively of interval of time $\Delta\tau$.

THE INERTIA AND REGULAR PERIODS OF THE TRANSFORMATION

The relationships presented above have been arrived at starting from the assumption that, the moment the temperature on the surface reaches transformation point, distribution of temperature through the depth of the body is established in accordance with the regular cycle, for which $c_{n1}=c_{n2}=c_{n3}$. In actual fact, this state is established, not immediately, but after a certain time. Determination of the duration of heating by formula (44) produces, not the overall heating time, but just the duration of the regular period. To determine the overall duration of the process, the length of the inertia period which precedes the regular one, must be added to the time value obtained from formula (44). The process of heating in the presence of internal transformations also has an inertia

VOL. 8 1959

and a regular period. The inertia period is characterized by lack of transformation in a solid body. Heat applied during this period is practically entirely used up in heating the body. In the regular period there is characteristic gradual spread of transformation throughout the body. Here the heat applied to the body is used partly in transformation and partly in heating. The duration of the inertia period can be determined by the increase in heat content for this period [4]. The heat content of the body at the beginning of the inertia period (in the moment at which the temperature at the surface reaches transformation point) is equal to

$$I_n = \frac{r\gamma C}{(2\nu+2)}\left[t_{pr} - \frac{2}{2\nu+4}\Delta t\right] = \frac{r\gamma C}{(2\nu+2)}\left[t_{pr} - \frac{q_1 r}{(2\nu+4)\lambda}\right], \tag{45}$$

and at the end of the inertia period (in the moment at which the regular period is established throughout) it is equal to

$$I_k = \frac{r\gamma C}{(2\nu+2)}\left[t_{pr} - \frac{2}{2\nu+4}\Delta t_3\right] = \frac{2\gamma C}{(2\nu+2)}\left[t_{pr} - \frac{q_3 r}{(2\nu+4)\lambda}\right], \tag{46}$$

where q_3 is determined from formula (41) for $W = 1$.

From the heat balance equation for the inertia period we get

$$\Delta\tau_{in} = \frac{I_k - I_n}{q_1} = \frac{r^2}{(2\nu+2)(2\nu+4)a}\left(1 - \frac{q_3}{q_1}\right)_{W=1}, \tag{47}$$

where $\Delta\tau_{in}$ is the length of the inertia period.

Substituting the value for q_3 from (41) for $W = 1$, we get, after conversion

$$\Delta\tau_{in} = \frac{r^2}{2(2\nu+2)(2\nu+4)a}\left[\frac{1}{n} + 3 - \sqrt{\left(\frac{1}{n}+1\right)^2 + 8}\right], \tag{48}$$

$$n = \frac{q_1 rC}{6\rho\lambda(2\nu+2)}. \tag{49}$$

Fig. 3 gives the results of the calculations of the dynamics of transformation through a plate, a cylinder and a sphere, for a number of values of the criterion of transformation N. In the first half of the process it is characterized by a linear relationship between the depth of the deformed layer, and time. Computation of the overall duration of the transformation process (Fig. 4) indicates the existence of a linear relationship between

$$\frac{(2\nu+2)a\tau}{r^2} \text{ and } \frac{1}{N}.$$

This relationship may be approximated in the form of the following assymetric formula:

$$\frac{(2\nu+2)a\tau}{r^2} = \frac{1}{2} + \frac{1}{(2\nu+3)N}. \tag{50}$$

Calculations according to this formula are set out in Fig. 4 in the form of solid lines. Calculations of the change in temperature at the surface and axis of a cylinder for the case $N - 1$ are set

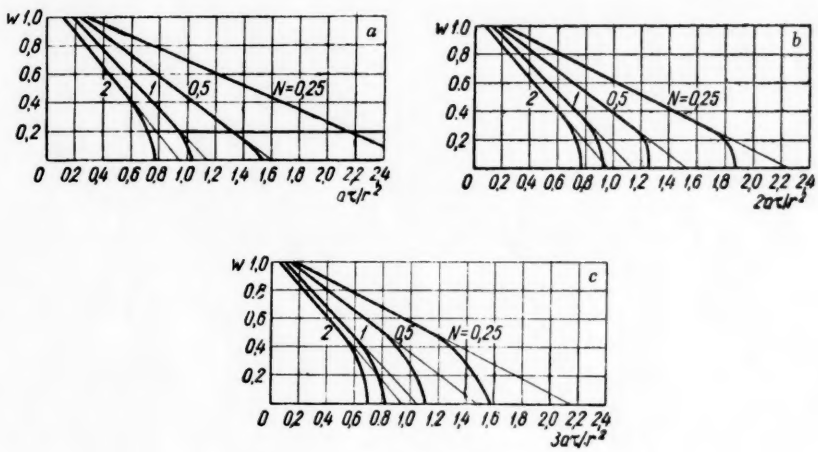

FIG. 3. Dynamics of transformation for a plate (a), cylinder (b) and sphere (c) at different values for the transformation criterion N.

VOL. 8 1959

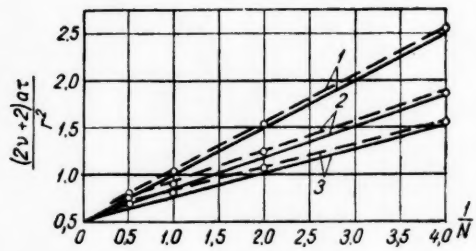

FIG. 4. Relation between a measureless duration of heat and the reciprocal of the criterion of transformation:
1 – for a plate;
2 – for a cylinder;
3 – for a sphere;
Dotted lines – according to formulae (37) – (44);
Solid lines by the asymptotic formula (50).

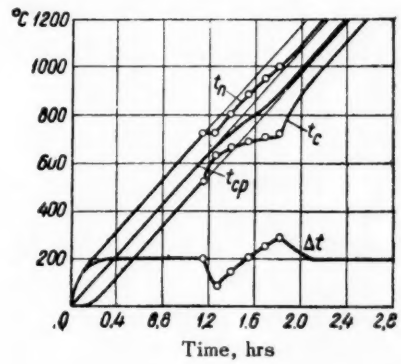

FIG. 5. Results of a heating calculation for a cylinder with diameter 400 mm at constant flow of heat q_1 = 60,000 cal/m² hr, t_{pr} – 720°, λ = 30 cal/m/hr°C, C = 0.15 cal/kg°C, γ = 7500 kg/m³, ρ = 15 cal/kg; t_p and t_s – temperatures at the surface and axis, $\Delta t = t_p - t_s$, t_{sr} – mean temperature.

out in Fig. 5. The heat of the cylinder up to the moment at which its surface reaches transformation temperature and after this temperature is reached at the axis, may be calculated by the usual method [2], but in the transformation range it must be done by the method presented above. It follows from Fig. 5 that the rate of temperature rise at the axis of the cylinder in the process of transformation, will be gradually reduced. This leads to a gradual increase in the difference in temperature through the cylinder. The temperature difference reaches its maximum towards the end of the transformation process, when the temperature at the axis is close to transformation point. After this the temperature starts to equalize throughout the body. The change in the temperature difference through the body in the process of heating indicates the existence that there are two bonds in the curve – at the beginning and at the end of transformation – which is relavent to the experimental data for the heating of ingots (see Fig. 1).

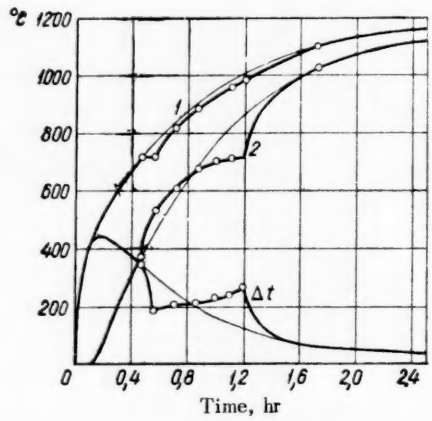

FIG. 6. Results of the calculation of the heating of a cylinder with a diameter 400 mm at constant furnace temperature $t_0 = 1200°$; $\alpha = 200$ cal/m² hr °C, t_p and t_s – temperatures at surface and axis $\Delta t = t_p - t_s$.

HEATING WITH CONSTANT TEMPERATURE OF THE SURROUNDING MEDIUM ($t_0 = \text{const}$)

The flow of heat at the surface is equal to

$$q_1 = \alpha (t_0 - t_p), \tag{51}$$

where t_0 is the temperature of the surrounding medium; t_p is the temperature at the surface; α is the coefficient of heat transfer.

The temperature at the surface is equal to

$$t_p = t_{pr} + \Delta t_1, \tag{52}$$

where Δt_1 is the drop in temperature in the first layer.

Inserting from (52) the values for t_p and Δt_1 into (51) we get

$$q_1 = \alpha \left[t_0 - t_{pr} - q_2 R - \frac{(q_1 - q_2 W^{2\nu+1}) s}{k_2 (W) \lambda} \right]. \tag{53}$$

Using formula (53) and (35), from the condition $c_{n2} - c_{n3}$ we get the following equation for the determination of the flow of heat q_3:

$$\left(\frac{q_3 R_0}{\Delta t_0} \right)^2 (2m^2 + m - 1) - \frac{q_3 R_0}{\Delta t_0} \left(4m + 1 + \frac{m}{n'} \right) + 2 = 0, \tag{54}$$

where

$$m = \frac{(2\nu + 2) \tau_a}{r \gamma C W R_0}, \tag{55}$$

$$n' = \frac{\Delta t_0 \tau_a}{6 \rho \lambda \gamma R_0^2}; \tag{56}$$

τ_a is the accumulation time for the first layer where heating is from the outside [4], equal to

$$\tau_a = \frac{s \gamma C}{k_1 (W)} \left[\frac{1}{\alpha} + \frac{s}{k_2 (W) \lambda} \right]; \tag{57}$$

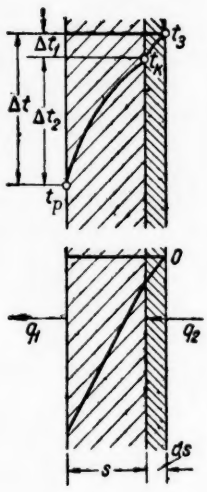

FIG. 7. Cooling diagram for a semi-infinite body.

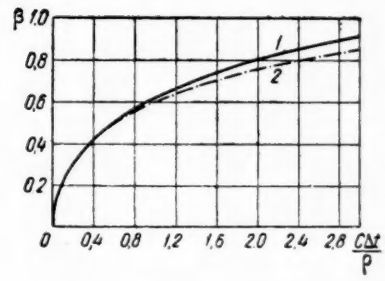

FIG. 8. Relation between coefficient β and $C\Delta t/p$: 1 – in Stefan's solution (77) 2 – from formula (76).

VOL. 8 1959

R_0 is the combined thermal resistance in the first layer and the heat transfer in the surrounding medium.

$$R_0 = \frac{W^{2\nu+1}}{\alpha} + R, \tag{58}$$

$$\Delta t_0 = t_0 - t_{pr}. \tag{59}$$

The solution of equation (54) in relation to q_3 produces

$$\frac{q_3 R_0}{\Delta t_0} = \frac{4}{\left(4m + 1 + \frac{m}{n_1}\right) + \sqrt{\left(4m + 1 + \frac{m}{n_1}\right)^2 - 8(2m^2 + m - 1)}}. \tag{60}$$

Flows of heat q_2 and q_1 are determined from the formulae

$$q_2 = \frac{\Delta t_0}{R_0} - mq_3, \tag{61}$$

$$q_1 = q_2 W^{2\nu+1} + \frac{q_3}{W}(1 - W^{2\nu+2}). \tag{62}$$

Integration of differential equation (42) for the final increase in time $\Delta\tau$ produces

$$\Delta\tau = \frac{I_k - I_n}{q_{1\,sr}}, \tag{63}$$

where q_{1sr} is the mean flow of heat at the surface of the body determined as an arithmetical mean of the beginning and end value of q_1 for the interval of time $\Delta\tau$.

Fig. 6 shows the results of the calculation of the heating of a cylindrical body 400 mm in diameter at a furnace temperature of 1200° and α = 200 cal/m² hr.

EVALUATION OF THE ERROR OF THE METHOD USED

For the purpose of establishing the errors liable in the method used we will consider the process of transformation in a flat semi-infinite body at constant surface temperature. The approximate solution obtained for this case may be compared with the well-known classic solution of the problem by Stefan [5].

The symbol s shall be the depth of the layer in which transformation is taking place, q_1 and q_2 represent the specific flow of heat in heating and in transformation (Fig. 7). Using the system set out above for the solution of the problem, we get the following formula for the rate of heating of the layer

$$c_{n1} = \frac{q_1 - q_2}{s\gamma C}, \tag{64}$$

$$c_{n2} = \frac{q_2}{C_{usl}\gamma\, ds}, \tag{65}$$

where C_{usl} is the conditional specific heat of the elementary layer taking into account the latent heat of transformation:

$$C_{usl} = C + \frac{\rho}{t_{pr} - t_{sr2}}. \tag{66}$$

The mean temperature of the elementary layer t_{sr2} is equal to

$$t_{sr2} = t_{pr} - \frac{1}{3}\Delta t_2 = t_{pr} - \frac{q_2 ds}{6\lambda}. \tag{67}$$

Inserting (67) and (66) we get

$$C_{usl} = C + \frac{6\rho\lambda}{q_2 ds}. \tag{68}$$

For the regular period of the process we get

$$\frac{q_1 - q_2}{s\gamma C} = \frac{q_2}{C_{usl}\gamma\, ds}. \tag{69}$$

The difference in temperature in the first layer is equal to

$$\Delta t = \frac{(q_1 + q_2)\, s}{2\lambda}. \tag{70}$$

Inserting (68) and (70) into (69), after conversion we get the equation for the determination of the flow of heat q_2

$$\frac{s^2 C}{12\lambda^2\rho} q_2^2 + \frac{s}{\lambda} q_2 - \Delta t = 0. \tag{71}$$

From which

$$q_2 = \frac{6\rho\lambda}{sC}\left(\sqrt{1 + \frac{C\Delta t}{3\rho}} - 1\right). \tag{72}$$

The differential equation for the process of heating will have the form (42), where

$$I = s\gamma\,[\rho + Ct_{sr_1}]. \tag{73}$$

The mean temperature of the first layer t_{srl} is equal to

$$t_{sr_1} = t_{pr} - \frac{q_2 s}{2\lambda} - \frac{(q_1 - q_2)\,s}{6\lambda}\,. \tag{74}$$

Inserting (72), (73) and (74) into (42), after integration we get

$$s = 2\beta\sqrt{a\tau}, \tag{75}$$

where

$$\frac{1}{\beta^2} = \frac{1}{3}\left(1 + \frac{2}{\sqrt{1 + \frac{c\Delta t}{3\rho}}}\right) + \frac{\rho}{C\Delta t}\left(1 + \frac{1}{\sqrt{1 + \frac{C\Delta t}{3\rho}}}\right). \tag{76}$$

VOL. 8 1959

In the solution of Stefan's problem in the absence of superheating [5] the parameter is determined as the root of the transcendent equation

$$\frac{C\Delta t}{\rho} = \sqrt{\pi}\beta\, e^{\beta^2}\, erf\,\beta, \tag{77}$$

where

$$erf\,\beta = \frac{2}{\sqrt{\pi}}\int_0^{\beta} e^{-u^2}\,du. \tag{78}$$

The results from calculations by formulae (76) and (77) indicate that the method used is sufficiently satisfactory for the solution of technical problems.

Translated by V. Alford

REFERENCES

1. B.G. Livshits, *Fizicheskie svoistva metallov (Physical properties of metals)* Metallurgisdat (1946).
2. N.Yu. Taits, *Tekhnologiya nagreva stali (The technology of heating steel)* Metallurgizdat (1953).
3. I.D. Semikin, and E.M. Gol'dfarb, *Liteinoe proizvodstvo (Foundry practice)* No. 2 (1956).
4. E.M. Gol'dfarb, *Trud. NTO chernoi metallurgii (Proceedings of the Scientific and Technical Soc. of ferrous metallurgy)* 7, 406 (1956).
5. A.V. Lykov, *Teor. teploprovodnosti (The theory of heat conductivity)* Gosteortekhizdat (1952).

THE CHANGES IN FINE CRYSTAL STRUCTURE ON THE DISINTEGRATION OF THE SATURATED SOLID SOLUTION NICKEL-CHROMIUM-ALUMINIUM-TITANIUM*

V.G. ChERNYI

Institute of Metallophysics AS Ukr. S.S.R.

(Received 25 May 1957)

The fine crystal structure, change in the lattice parameter and hardness on ageing of the alloy, nickel-chromium-aluminium-titanium, have been investigated. The constitution has been studied of the intermetallic phase which separates on disintegration. It has been established that the increased hardness of this alloy on ageing is not connected with the resulting distortion of the crystal lattice of the second type.

As a result of X-ray analyses conducted in recent years the nature, and many details of the structure, of metals in a strain-hardened state have been studied [1-5]. It has thus been established that it is characteristic of the majority of deformed pure metals and alloys for there to be distortion of the second and third type and small fields of coherent dispersion of the X-rays. On heating, the fine crystal structure and mechanical properties of cold deformed metals and alloys undergo a change in the direction of the state which is characteristic of undeformed materials. A similar regularity has been observed in studying hardened steels.

This paper is devoted to the study of the changes in the fine crystal structure and hardness, on the disintegration of the creep-resisting alloy Ni-Cr with Ti and Al.

MATERIAL AND METHOD OF INVESTIGATION

An alloy of nickel-chromium-aluminium-titanium with the following chemical composition was selected for this study: 19.55% Cr, 0.59% Al, 2.38%Ti, 0.035% C, the rest Ni. After extraction the alloy was forged into bars. Cylinders were cut from the bars, with a diameter of 9.5 mm and height of 15 mm, and were given a homogenizing treatment at 1100° for 20 hr. After this treatment, the testpieces were deformed by uniaxial compression by 75 per cent, as the study of the width of the interferential lines on the X-ray pictures requires rather a small grain size. The deformed testpieces were heated to 1080°, held 1.5 hr and then cooled in water. This treatment (quenching after plastic deformation) produces a structure which has continuous lines on the X-ray screen.

The hardened blanks were heated for the same amount of time (4 hr) at various temperatures (400-950°) and for different lengths of time (up to 25 hr) at 700 and 800°. After the final heat treatment the blanks emerged as testpieces for the study of the constitution of the α'-phase, stress of the second type, the size of the mosaic blocks of the basic solid solution and the change in the lattice and hardness parameter.

The constitution of the intermetallic phase formed on the disintegration of the alloy was investigated on powders produced by electrolytic dissolution. Three types of electrolyte were used. No. 1 was composed of citric acids 10 g, sulphate of ammonia 10 g, and water 1000 ml. [6]. No. 2 – solid acetic acid 50 ml, concentrated nitric acid 100 ml. water 1000 ml. The best results were obtained with No.3 which was mixture of Nos. 1 and 2 (3 : 1). The anodic dissolution conditions were – current density 0.1 A/cm², voltage 20-25 V, time 1.5-2 hr. From the poders resulting in the α'-phase, cylindrical testpieces were made in the following way: the powder, mixed with Ramsay paste, was packed into a glass cylinder with a dia. of 0.8 mm, and then half of it was pushed out. Radiographs were made in a an instrument with a barrel dia of 57.2 and 150 mm, on cathode ray tubes with copper radiation.

For the determination of distortion of the second type, the dimensions of blocks D and the permament crystal lattice of the solid solution, X-rays were taken of the cylindrical testpieces 0.5 mm in dia, in the camera with the 150 mm drum in copper illumination. The film was loaded asymmetrically into

* *Fiz. metal. metalloved.*, 8, No. 1, 66-74, 1959.

VOL
8
195

TABLE 1. Results of the X-ray analysis of the intermetallic phase

Heating temperature °C	β_{ist} radians	$D \cdot 10^{-6}$, cm
600	Precipitates separated, whose structure could not be determined	
650		
675		
700	0.0315	0,53
750	0.0125	1,3
800	0.0077	2.2
850	0.00485	3.4
900	0.0185	0.97
910	0.0245	0.68
920		
950	α' phase could not be separated	

the camera.

The dimensions of the α'-phase blocks were determined from the width of line (111), values $\Delta a/a$ and D of the basic solid solution from the width of lines (111) and (331). The crystal lattice period was calculated from the distance between the lines (420). Photometering of the X-ray photograph was carried out on microphotometer MF-2 with a magnification of x 21.

Insertion of corrections for the width of the interferential lines on the $K\alpha$-doublet and the geometry of the picture, as also calculation of the size of the areas of coherent dispersion, were all effected in the manner described in papers [7-9].

We must point out that, in our case, the true width of the lines was calculated with the aid of the formula $\beta^2 = B^2 - b^2$ (B – width of the line corrected for non-monochromatic radiation, b – width of the line in a standard testpiece). The size of the areas of coherent dispersion and the value for distortion of the second type were obtained from the equations:

$$D = \frac{\lambda_{k_\alpha}}{m \cos \vartheta} ; \frac{\Delta a}{a} = \frac{n}{4 \operatorname{tg} \vartheta} , \qquad (1)$$

in which λ is the wave length, θ the angle of reflection, m – diffusion of the line due to dispersion of the blocks (on radiographs of the isolated α'-phase, $m = \beta$; n = the diffusion caused by the presence of distortion of the second type.

Hardness was measured on a Rockwell machine with a diamond cone and 60 kg load (scale A).

THE RESULTS OF THE INVESTIGATION

a) The constitution of the α'-phase separated on disintegration.

Analysis of the X-ray photos of precipitates obtained by anodic dissolution have shown that, in all the cases we have investigated, the only phase separated is that which has a face-centred cubic lattice. As we know, this phase answers to formula $Ni_3(Al, Ti)$ [6].

If the heating temperature is raised to 850°, the width of the lines on the X-ray photo is considerably reduced. The width of line (111) for this instance shows that there is a reduction from 0.916 mm at 700° to 0.268 mm at 850°. Further heating at 900 or 910° causes the lines to expand again; at 900° – B_{izm} = 0.568 mm, at 910° – B_{izm} = 0.728 mm. At temperatures below 700° (600, 650, 675°) and above 910° (920 and 950°) it is not possible to separate the α'-phase. It will be seen from Table 1 that a rise in temperature from 700 to 850° leads to an increase in the size of the blocks of α'-phase in the alloy, amounting to almost 7 times. Thus, while at 700° $D = 0.53 \times 10^{-6}$ cm, after heating at 850° $D = 3.4 \times 10^{-6}$ cm. With further increases in temperature the size of the blocks is reduced, at 900° $D = 0.97 \times 10^{-6}$ cm, and at 910° $D = 0.68 \times 10^{-6}$ cm.

From Table 2 and Figs. 1 and 2 it can be seen how the size of the areas of coherent dispersion of the α'-phase changes at 700 and 800°.

The change takes place in the same way for both temperatures, the blocks gets larger with continuation of the holding time.

b) The fine crystal structure of the basic solid solution.

Study of the interference pictures has shown that, in all the radiographs made from the solid lines, only the lines of the face-centred lattice are present – (111), (200), (220), (311), (222), (400), (331) and (420). On the radiographs both of the quench-hardened alloy and also when tempered at 400, 500, 600, 700, 750, 800, 850 and 900°, all the lines from (220) to (420) are clearly divided into component doublets $K_{\alpha 1}$ and $K_{\alpha 2}$. At higher temperatures spots

TABLE 2. Results of the X-ray analysis of the intermetallic phase

Heating time, hr	$D \cdot 10^{-6}$, cm	
	700°	800°
0.25	α'-phase could not be separated	0.82
0.5		1.3
1.5		1.8
2.0	—	—
4.0	0.53	2.15
6.0	—	2.4
10.0	0.92	—
12.0	—	2.7
16.0	1.05	—
20.0	1.15	—
25.0	1.15	3.4

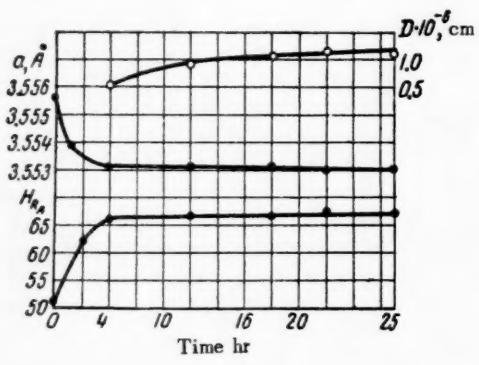

FIG. 1. The change in the size of the α'-phase blocks (D), the crystal lattice parameter (a) and hardness (H_{R_A}) at 700°.

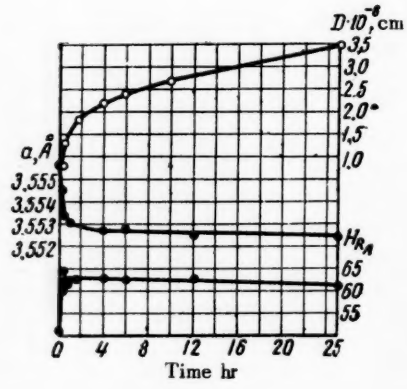

FIG. 2. The change in the size of the α'-phase blocks (D), crystal lattice parameter (a) and hardness (H_{R_A}) at 800°.

appear on the lines. In radiographs of testpieces heated at 500 and 600°, the later lines are somewhat diffused but the doublet still remains separate. Microphotometry confirms the results of a visual analysis of the interference picture which was: line (331) on the radiograph of the alloys tempered at 500 and 600° is wider than that for a quenched piece. After quench-hardening the width of component K_{α_1} of line (331) is 0.659 mm, after heating at 500° the width of the line is 0.905 mm, and after heating at 600° – it is 0.97 mm. The change in the width of line (111) lines is in the region of possible error.

Calculations carried out on the width of lines (111) and (331) show that heating at 500 to 600° leads to an increase in the heterogeneity of the parameter of lattice $\Delta a/a$. At other heating temperatures and in a quenched state $\Delta a/a$ is virtually equal to zero (Table 3).

Determination of the size of the areas of coherent diffusion of the X-rays has shown that if the alloy is heated right to 850° they do not alter in size.

c) Measurement of the crystal lattice period of the solid solution on heating.

The results of the analysis of the parameter of the lattice are given in Figs. 1, 2, 3.

Fig. 3 shows how the crystal lattice parameters of the alloy change when it is heated from 500 to 950°. In the quench-hardened alloy the lattice parameter is equal to 3.5557 Å. Heating to 500-600° leads to practically no change in the parameter. In the region of 600-800° the constant of the crystal lattice is appreciably reduced, and at 800 reaches 3.5527 Å. Above 800° the parameter starts to increase and after heating at 950° a = 3.5546 Å, nearly the same figure as that typical of the quench-hardened state.

The data concerning the change in the parameter

TABLE 3. Results of the X-ray analysis of the solid solution.

Heating temp. °C	$D\times10^{-6}$ cm	$\frac{\Delta a}{a}\times10^{-3}$
Quenching	6.5	0.2
400	6.8	0.25
500	6.9	0.75
600	5.9	0.9
650	—	—
700	7.1	0.35
750	—	—
800	6.8	0.25
850	7.2	—
900	—	—
925	—	—
950	—	—

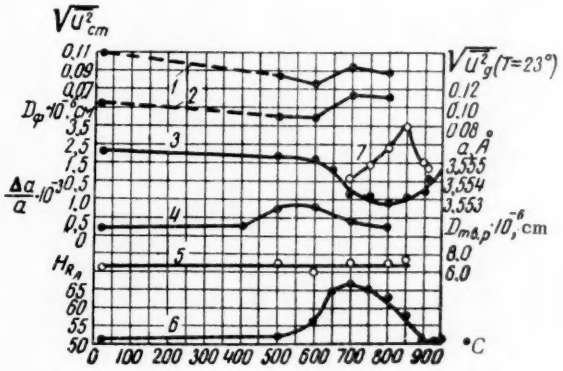

FIG. 3. The change in the characteristics of the alloy in connexion with heating temperature:

$1-\sqrt{\overline{i^2_{st}}}$; $2-\sqrt{\overline{i^2_a}}$; $3-a$; $4-\frac{\Delta a}{a}$; $5-D_{m\&p}$; $6-H_{R_A}$; $7-D_\phi$

of the lattice at constant temperature related to holding time, are given in Figs. 1 and 2. These data show that in the beginning, at low positive temperatures, the parameter quickly grows less, after which no change can be brought about, even after 24 hr soaking. At the absolute value, the constant of the lattice after 25 hr heating at 800° is less than at 700° (at 800° a = 3.5525 Å and at 700° a = 3.5530 Å.

Table 4 shows the constants of the basic solid solution and a'-phase lattices after the same heat treatment.

d) Changes in hardness on disintegration. Fig. 3 shows how the hardness of the alloy changes with increased temperature. Heating up to 600° does not produce any change in the hardness. At 600° and over, the hardness grows, reaching the maximum at 700° (66.3 units). Above 700° the hardness starts to fall and at 900° it is the same as for the quench-hardened alloy.

Figs. 1 and 2 give data concerning the change in hardness in relation to holding time at 700 and 800°. The alloy reaches maximum hardness at 700° after 20 hr heating

(H_{R_A} = 67.5); at 800° after 1.5 hr H_{R_A} = 62.6.

Further continuation of the heating up to 25 hr produces no change, neither at 700° nor 800°.

EVALUATION OF THE RESULTS

Examination of electrolytically separated precipitates has shown that in all cases, on the disintegration of the quench-hardened alloy Ni-Cr-Al-Ti, only the intermetallic phase is separated out, with

TABLE 4. The results of radiographic analysis of the parameters of the crystal lattices of the solid solution and the intermetallic phase

Heat treatment	Lattice period	Lattice cycle A
Quenching Heating at 800°, for 25 hrs	α'-phase Solid solution	3.5843 3.5525

face-centred cubic lattice answering to the formula Ni_3 (Al, Ti) [6]. The value of the constant of the crystal lattice of the α'-phase is higher than that of the solid solution (see Table 4). This is connected with the fact that the α'-phase is enriched to a greater extent by Ti and Al than the solid solution (see paper [1] and our data on the change in the parameter of the lattice).

Table 1 and Fig. 3 give data which show how the size of the blocks of phase Ni_3 (Al, Ti) alter in relation to the heating temperature. The growth of the α'-phase blocks is quite regular from 700 to 800° and is easily understood (at temperatures of 700° and over perceptible diffusion processes commence and coagulation begins).

The refinement of the α'-phase blocks observed after heating at 900 and 910° may be explained in the following way. While being heated at 900-910° the alloy is close to the limit for the solubility of aluminium and titanium by the nickel (two factors indicate this: 1) at 920-950° the parameter is approaching the original state and 2) after heating at 920-950° the α'-phase can no longer be separated out from the alloy). Therefore, despite the fact that at 900-910° diffusion processes are taking place at a considerable rate, the degree of saturation of the alloy is low and the thermodynamic conditions are such that,although α'-phase particles are being formed, their growth is exceedingly small and after 4 hr (holding time at 900 and 910°) their size is not significantly larger.

We will now look at the results of the study of the kinetics of growth of the α'-phase blocks after heating at 700 and 800° (see Table 2 and Figs. 2 and 1). These figures show that the relative change in the size of the blocks at one and the same interval of time but at different temperatures, is not the same. At lower temperatures the blocks begin to increase in size rapidly, after which their growth slows down. At higher temperatures the curve of growth reaches saturation after longer holding times. The relative change in the size of the α'-phase blocks is greater where the heating temperature is higher. Let us turn to the corresponding data. After heating at 700° the crystals of phase Ni_3 (Al, Ti) grow from 0.53×10^{-6} cm after 4 hr holding time to 1.15×10^{-6} cm after 25 hr holding. At 800° the relative change in size is greater (0.82×10^{-6} cm after 15 min heating and 3.44×10^{-6} after 25 hr).

Similar qualitative regularity has been observed in studying the kinetics of the process of carbide formation in carbon and alloy steels [10, 11].

In the quench-hardened state heterogeneity of the lattice parameter is practically non-existent (0.2×10^{-6}), $\Delta a/a$ is not subject to change and after heating at 400° it is (0.25×10^{-3}). Heating at 500 and 600° causes the value $\Delta a/a$ to grow in the basic solid solution (at 500° $\Delta a/a = 0.75 \times 10^{-3}$ and at 600 $\Delta a/a = 0.8 \times 10^{-3}$). With further increases in temperature the distortion is reduced and at 800° the value is 0.25×10^{-3}.

The question arises as to whether the growth in $\Delta a/a$ observed after heating at 500 and 600° is the result of elastic distortion of the lattice (distortion of the second type). It is impossible to supply a precise answer to this question. The growth of $\Delta a/a$ on the disintegration of the saturated solid solutions may be due to elastic distortions of the lattice [12, 13]; it might also be the result of concentrated heterogeneity of the solid solution. The more probable cause for the growth of $\Delta a/a$ after heating at 500 and 600° is the development of heterogeneity in the solid solution through concentration. The reduction of static and dynamic distortions detected in the alloy Ni-Cr-Al-Ti after heating at 500 and 600° rather indicates this [14]. The changes indicated

$$\sqrt{\overline{i^2_{st}}} \text{ and } \sqrt{\overline{i^2_{a}}}$$

are evidence of the redistribution of the atoms of the alloying elements in the solid solution.

The regions of coherent diffusion of the basic solid solution, as already mentioned, do not change in size when heated right up to 850°.

From the analysis it is possible to establish the fact that (see Fig. 3 and Tables 1-4) the high mechanical strength (hardness) after heating in the region of 700-750° is connected neither with the second-type distortion of the lattice of the basic solid solution, nor with the refining of its blocks. In fact, at the temperature mentioned, second type distortion hardly exists.

The great hardness of the alloy cannot be explained by an increase in third type distortion

$$\sqrt{\overline{i^2_{st}}} \quad \text{and} \sqrt{\overline{i^2_a}}$$

shown in Fig. 3 and taken from paper [14]), as the distortion after heating at 700-750° is less than after quench hardening. It is true that the possibility is not excluded that, on the disintegration of the alloy, these distortions in the places where separation of the α'-phase occurs, are considerably higher than the average figures obtained in paper [14], and that this localization may lead to an increase in the hardness of the solid solution.

It is also impossible to explain the increase in hardness by a change in the forces united in the lattice of the solid solution, as after heating at 700-750° the dynamic distortion is considerably higher than after quench hardening.

The main factor leading to an increase in the hardness of the alloy after heating in the region of 700-750° is the formation of a large number of finely dispersed secondary phases of the α'-phase.

The increased hardness of the quench-hardened alloy on heating in the 600-700° range also appears to be attributable to the appearance of the secondary phase.

This is indicated by the changes in the values

$$\sqrt{\overline{i^2_{st}}};\ \sqrt{\overline{i^2_a}};\ a \text{ and } \frac{\Delta a}{a}.$$

Further data, obtained from a study of the properties of the alloy related to holding time at 700 and 800° (see Figs. 1 and 2 and Tables 1-4) pointed to the main part played by the α'-phase in the increase in mechanical strength. It has already been mentioned that after a 4 hr holding time atthese temperatures second-type distortion in the lattice of the solid solution is nil. The absence of distortion after long soaking is indicated by the sharp separation of the $K\alpha$ doublets in the lines of the radiograph. There is no change either in the blocks of solid solution after heating at 700 and 800°. Evidence of this is the fact that even when the alloy is heated for 4 hr at 850° the blocks remain the same as in the quench-hardened state.

Can the great hardness of the alloy be explained in the same way where it contains a finely dispersed intermetallic phase? The answer to this question may be found if use is made of current information on the processes of plastic deformation [15, 4, 5]. The separation of the finely dispersed secondary phase on the disintegration of the saturated solid solutions cause dislocation of the proper structure of the crystal lattice of the basic solid solution. The places where these dislocations occur are, at the same time, the places where the first germ of plastic deformation emerges and the places where its expansion is prevented. The greater the number of these points of dislocation, the greater will be the number of emerging plastic deformations, the smaller the number of atoms taking part in each separate act of deformation and the larger the number of atoms taking part in the resistance to external force. On the disintegration of alloy Ni-Cr-Al-Ti a large amount of the finely dispersed intermetallic phase is separated. Particles of this phase cause a large number of dislocations in the solid solution, of the correct lattice structure. It is precisely this, in connexion with the above, which explains the increase in the hardness of the alloy with the resulting separation of the α'-phase.

What is the connexion between the hardness of the alloy, and the size and number of the blocks of phase $Ni_3(Al,Ti)$? We know from various works [6, 16] that the maximum amount of α'-phase is separated on disintegration in the region of 700-750°. It is this same temperature which, according to our data, is responsible for the great dispersibility of the blocks and for the maximum hardness. At higher temperatures of disintegration, the number of phases in sharply reduced; up to 850° also, the size of the α'-phase particles increases and hardness is reduced. It seems that the refinement which takes place around 900-910° must lead to a renewed growth in hardness. This, however, does not occur, owing to the sharp reduction in the number of intermetallic phases.

We wish to express out thanks to Academician G.V. Kurdyumov and L.G. Khandros for their valuable advice in completing this work.

CONCLUSIONS

1. On the disintegration of quench-hardened alloy Ni-Cr-Al-Ti only the intermetallic face with a face-centred cubic lattice is separated, the parameter of which is greater than that of the lattice of the basic solid solution.

It was possible to separate the α'-phase electrolytically after heating the alloy in the regions of

VOL. 8 1959

700-910° (holding time at each temperature was 4 hr).

At first, after heating at 700-850° blocks of phase Ni, (Al, Ti) grew larger and then, after heating at 900 and 910° they reduced again in size, having reached at 910° a value close to that of the blocks of a'-phase when the alloy was heated at 700°. In this paper an explanation is put forward for the marked refinement of the intermetallic phase blocks.

2. A study of the fine crystalline structure of the alloy has shown that, after heating in the region of 500-600°, the value $\Delta a/a$ increases. This may be the result of the emergence of elastic distortion of the crystal lattice, as also of the concentrated heterogeneity of the basic solid solution. The more probable cause is the appearance in the alloy of heterogeneity in concentration.

The areas of coherent diffusion of the solid solution do not change in size on heating up to 850°.

3. From these investigations and from the data on changes in the forces of bonding and distortion of the third type [14], the conclusion may be drawn that the increase in hardness in the alloy nickel-chromium-titanium is not connected with the emergence of distortion of the crystal lattice of the secondary type nor with the change in the strength of the bond in the lattice of the basic solid solution. The increase in hardness in our case was not accompanied by a change in the size of the areas of coherent diffusion. It is possible that the latter is connected with the smallness of the mosaic blocks in the initial state.

The increase in hardness is due to the emergence of submicroscopic and concentrated heterogeneity in the alloy in the course of the process of disintegration of the solid solution.

Translated by V. Alford

REFERENCES

1. V.A. Il'ina, V.K. Kritskaya and G.V. Kurdyumov, *Problemy metallovedeniya i fiziki metallov.* 2, 222 (1951).
2. V.A. Il'ina, E.Z. Kaminskii, V.K. Kritskaya and R.I. Engin, *Problemy metallovedeniya i fiziki metallov.* No. 3, 178 (1952).
3. G.V. Kurdyumov, V.A. Il'ina, V.K. Kritskaya and L.I. Lysak, Izv. AN SSSR, ser. fizich., 17, 297 (1953).
4. G.V. Kurdyumov, *Problemy metallovedeniya i fiziki metallov.* No. 4, 321 (1955).
5. V.M. Golubkov, V.A. Il'ina, V.K. Kritskaya, G.V. Kurdyumov and M.D. Berkas, *Fiz. metal. metalloved.*, 5/3, 465 (1957).
6. N.I. Blok, A.I. Glazov, O.A. Dubovnikova, S.T. Kishkin and A.S. Lashko, *Zav. lab.* 20, No. 8, 903 (1954).
7. M.P. Arbuzov, *Dokl. Akad. Nauk SSSR*, 73, No. 1, 83 (1950).
8. G.V. Kurdyumov and L.I. Lysak, *Zh. eksp. teor. fiz.*, 17, 997 (1947).
9. L.I. Lysak, *Voprosy fiziki metallov i metallovedeniya Akad. Nauk SSSR*, No. 5, 45 (1954).
10. M.P. Arbuzov, *Voprosy fiziki metallov i metallovedeniya, Akad. Nauk SSSR*, No. 3, 3 (1953).
11. M.P. Arbuzov and V.G. Chernyi, *Dopovidi Akad. Nauk USSR*, No. 3. (1955).
12. S.T. Konobeyevskii, *Zh. eksp. teor. fiz.*, 13, 418 (1943).
13. M.I. Zakharova and N.F. Lashko, *Izv. Akad. Nauk SSSR*, OTN, 7, 1015 (1946).
14. G.V. Kurdyumov and N.T. Travina, *Problemy metallovedeniya i fiziki metallov.* No. 4, 465 (1955).
15. M.V. Yakutovich, *Trud. Inst. fiziki metallov Ural Inst. Akad. Nauk SSSR*, p. 121 (1948).
15. F.F. Khimushin, Ye. F. Trusova and M.I. Gavrilyuk, *Struktura i svoistva splava* EI 437, Oborongiz. *(The structure and properties of alloy* EI 437) (1955).

THE MECHANISM OF BRITTLE FRACTURE IN STEEL IN A NOTCHED BAR IMPACT BENDING TEST*

B.S. KASATKIN

Institute of Electric Welding AS, Ukr. SSR

(Received 1 June 1957)

It has been shown that brittle fracture of steel is preceded by local plastic deformation. The micromechanism of brittle fracture of steel has been described; its development proceeds in the following stages: breakdown of the grains, local slip of the grains in relation to each other, and the formation of twinning and micro-cracks.

Local plastic deformation on the actual base of the notch has no appreciable effect on brittle fracture. Brittle fracture is composed of two stages: in the first stage a series of micro-cracks develop, and in the second – that of the fracture itself – the main fracture progresses along the path of the series of micro-cracks.

VOL.
8
1959

In real crystals, resistance to fracture is much less than in theory. The great divergencies in the figures for resistance to fracture have caused research workers to believe that strength is dependant on defects of structure. This point of view regarding the causes of the lowered technical strength of solids was first propounded and developed by Griffiths.

Attempts were made to use this theory also for the explanation of brittle fracture of metals. However, the problem of the fracture of amorphous materials on the one hand, and metals on the other, must be resolved in two different ways, and this difference is due to the substantially different plastic properties of the materials. In the problem of fracture the most important factors are: 1) the different influences of temperature on the resistance of the material in question to plastic deformation and 2) the differences in the evenness of the course of plastic deformation [1].

In amorphous materials plastic deformation at reduced temperatures may be excluded. If there is no plastic deformation it is not possible to remove local concentrations of stress. As a result of this even a small scratch may cause concentrations of stress which exceed the strength and consequently, lead to local fracture.

On the other side, in metals, resistance to plastic deformation does depend to a small extent on temperature. Passing from room temperature to 10°K the yield point of a metal increases by not more than 5 times [1]. It has been shown by experimental data that brittle fracture is bound to be accompanied by local plastic deformation [2, 3, 11]. For this reason, Griffiths' formula for calculating the brittle fracture resistance of amorphous bodies cannot be directly applied to metals.

The question arises, in what way, once there is local plastic deformation, does the stress in the root of the notch increase to the level of resistance to embrittlement and cause fracture?

Several theories have been put forward to explain this fact. In recent years particular attention has been paid to the theory of "strain hardening" [2], in accordance with which it has been suggested that the plastic deformation in the root of the notch and the strain hardening associated with it, cause the tensile stresses to increase to the value necessary for brittle fracture. In this case it is suggested that the strain hardening should permit an increase in triaxiality as a result of increased concentration of stress in the root of the notch.

According to Davidenkov, brittle fracture always begins with ductile cracks which give rise to a marked concentration of stress and a volume/stress state in the apex [4]. The latter causes a rise in resistance to further mechanical deformation and the stress grows according to the depth of the crack. In these circumstances the stress reaches the same level as the technical cohesive strength and the ductile cracks are discreetly transformed into rupturing cracks which increase the concentration of stress. The jump in stress caused by this increase in concentration, alters the course of the fracturing process, as no further external application of force

* *Fiz. metal. metalloved.*, 8, No. 1, 75-84, 1959.

is required to increase the depth of the brittle crack.

Special significance has been attached by Orowan [5] and Irving [6] to the increased rate of deformation in brittle fracture on the grounds that the rapid distribution of the ductile cracks is the cause of their transformation into brittle ones. However, according to Davidenkov, this proposition is not sound, as for the rapid dissemination of ductile cracks it is necessary to have rapidly progressing plastic deformation, which is not possible without a similarly rapid increase of external force; meanwhile, the transformation of ductile cracks has also been observed at quite small speeds such as those applied, for instance, by a Gagarin press.

At the moment it is considered that the conditions for the propagation of brittle fracture are based on the energy conditions of Griffiths, with the variation according to Orowan [5], regarding the plastic deformation of the layer of metal next to the surface, which forms new cracks. From this point of view, the rapid spontaneous propagation of brittle cracks may be explained by the comparatively small depth of plastic deformation [2, 5].

From all this it is clear that there is still much that is unexplained in the problem of the origin of brittle fracture. It seems therefore, that the study of the micromechanism of brittle fracture and even more, of its initial stages, may prove of considerable use.

THE CAUSE OF MICROCRACKS

We studied the micromechanism of brittle fracture by examining its separate stages in impact bend tests on prismatic testpieces $10 \times 10 \times 55$ mm with a standard notch and with V-shaped notch 2.0 mm deep with a bottom radius of 0.25 mm. The testpieces were of steel A – open-hearth steel M18kp after heat treatment (heating to 1100° 1.5 hr, cooling in the furnace), steel B – standard hot-rolled Bessemer steel B16kp 18 mm thick and steel C – forged blanks 16 mm thick, of technical iron.

The method used for the study of the individual stages of brittle fracture was that of testing the pieces in a ring [7]. By the use of special rings it was possible to bring about deformation of the testpieces in a notch bend test at a predetermined point.

The investigations were carried out as follows. The testpieces, together with the ring, were cooled to a temperature 20-15° below critical point of brittleness for the materials in question. This had been previously established by an impact toughness/temperature diagram. After this the testpiece was quickly transferred in the ring to a Charpy impact machine and deformed by blows of the hammer (15 kg). The extent of deformation was determined from the angle of transverse bend and the deflexion of the piece.

It was established by preliminary tests that there was a definite value for deflexion below which the testpieces are liable to plastic deformation without visible signs of fracture. This value is to a considerable extent determined by the angle of the notch. In testpieces with standard notches brittle fracture was observed with the characteristic instantaneous propagation of the crack and breakdown of the crystals at a deflexion of 0.7 mm or more and angle of bend over 3 to 4°. In testpieces with V-shaped notches on the other hand, this occured at a deflexion of over 0.3 - 0.4 mm.

The experiments were commenced with the study of the "prefacture" stage. For each series of testpieces a value for deflexion on impact bending was selected close to that at which brittle fracture may be observed. From each deformed testpiece a longitudinal specimen was taken from across the centre.

From the metallographic examination of these specimens it was possible to establish the existence of twinning and of microcracks in the microspaces arranged below the notch (Fig. 1). The twinning and microcracks were as a rule observed in those sectors at some distance from the bottom of the notch. At the bottom itself no signs were visible.

Local X-ray structural analysis of the specimens after electrolytic polishing showed that preliminary deformation in the "brittle state" produces a definite change in the interference picture on the radiograph. The X-rays were taken on a special instrument by the back reflection method which gives a dia of 0.10-0.20 mm to the exposed spot [3]. X-rays were made of sectors; right at the notch, 1.5 - 2.0 mm and a considerable distance, from it (Fig. 2).

X-rays of the undeformed sector (a long way from the notch) consist of a number of interference spots. A similar X-ray was made of the sector immediately at the base of the notch; only a small tendency to broadening was noticed in the spots. In the sectors 1.5 mm and more from the notch the interference spots were fewer and more widely spaced and in some cases were already in the stage of transition to interference line. This is a sign of the more intensive breakdown of the grain and accumulation of microstresses in these sectors.

For a more detailed study of the mechanism of brittle fracture we concentrated on some typical cases of microfracture.

Fig. 3 shows a photomicrograph of a grain in which

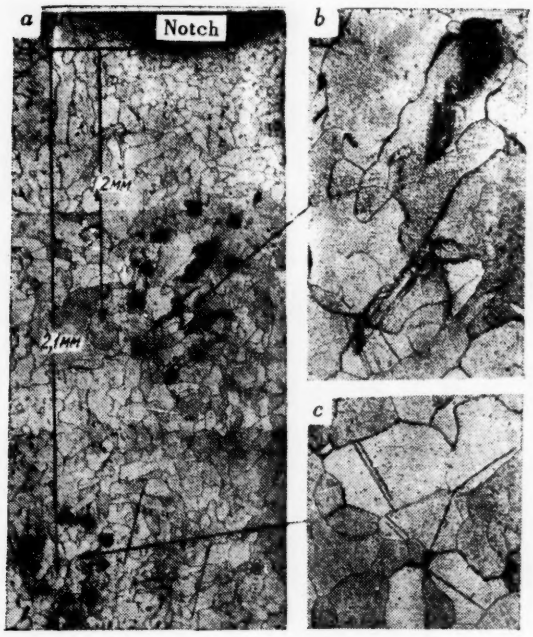

FIG. 1. *a* – brittle "prefrature of a testpiece of steel C with V-shaped notch (longitudinal notch down centre of piece, deformation in a ring at -40°, deflexion 0.3 mm, × 54);
b – micro-cracks and twins 1.2 mm from the bottom of the notch, × 300;
c – group of twins 2.1 mm from bottom of notch, × 300.

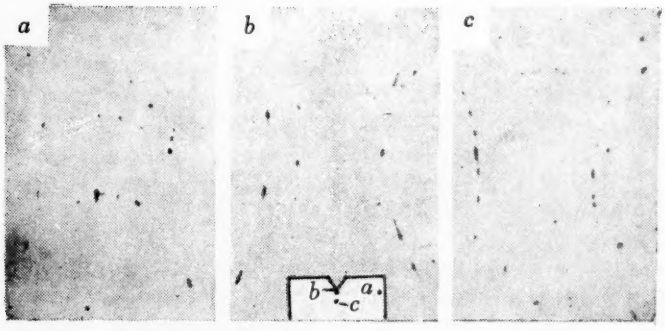

FIG. 2. X-ray photogram of a steel C testpiece (V-shape notch), prior to deformation in a brittle state
a – a long way from the notch;
b – below the notch;
c – 1.55 mm from bottom of notch (in a vertical direction.

there is a chain of microcracks and a series of parallel bands connected by twinning to the plastic deformation which preceded the formation of the microcracks. The grain is divided into two halves by distinct boundaries between the sub-grains. Each half of the grain has a typical well-defined direction of development of microcracks and twins. However, in both cases the angle between these directions is the same, 30° in this instance, which is very close to the angle ($\cos \alpha = 21\sqrt{6}$) between the crystallographic planes (112) and (001) of which (in cold shortness conditions for alpha iron) the

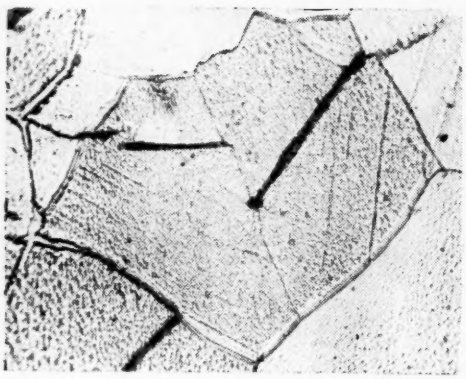

FIG. 3. Elementary slip and series of microcracks in ferritic grain. Steel C, ×850.

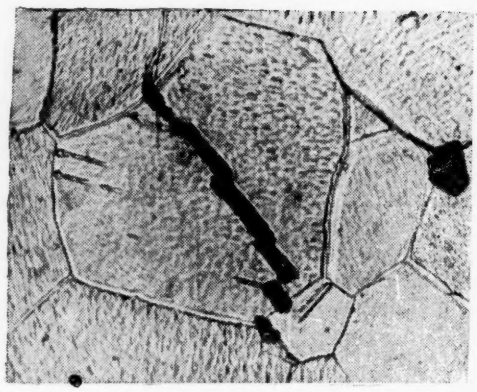

FIG. 4. Elementary slip and microcracks in ferritic grain. Steel C, ×750.

first is the twinning plane and the second, the plane of rupture.

In certain circumstances the boundaries between the sub-grains and the twins may prevent the formation of microcracks, resulting in their formation in stages. This is clearly visible from Fig. 4 which shows microcracks which have progressed in stages. It is easy to see that the stages fall in the direction of the twinning. In this case the angle between the direction of twinning and the microcracks is 37°, which is also very near to the angle between the planes (112) and (001). In certain cases, delay in the development of microcracks at the boundaries of the sub-grains may lead to the development of considerable local plastic deformation (Fig. 5). It is also characteristic that, in the case in question, local plastic deformation developed in that part of the grain where etching had revealed a very small-celled sub-structure the formation of which is apparently connected with the considerable breakdown (formation of blocks) of the grain.

Fig. 6 shows a case of fracture with slip (actually, twinning), originating from the junction of three grains. The wedge shape of the twin is clearly visible in Fig. 6, *b* which was photographed using a slightly different range and focus from that in Fig. 6, *a* in which the cracks and grain boundaries are clearly visible. The direction of twinning coincides with the boundary between the two adjacent grains. It appears that both the twinning and the microcrack were caused by the intermingling of adjacent grains along their boundaries, continuation of which led to twinning.

The role of the twins is interesting as, at the same time, they both promote the formation of microcracks, and prevent their spread. Fig. 7 shows a case of the prevention of a microcrack in a grain

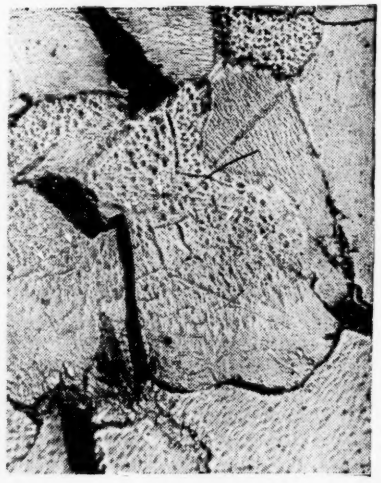

FIG. 5. Microcrack passing into local plastic deformation. Steel C. Subgrain boundary indicated by arrows, ×750.

by twins one of which, the shorter, is apparently responsible for its beginning. In this same grain there is a series of microcracks lying at an angle of 90° to each other.

Thus, in the stage of brittle "prefracture", breakdown of the grains (block formation), local slip along grain boundaries, twinning and formation of microcrack, are observed in the most favourable orientated micro-spaces some distance from the notch.

The process of twinning is particularly noticeable in brittle fracture. Concerning this the hypothesis has been put forward, that brittle fracture of metals subject to cold shortness is due to their ability to undergo mechanical twinning [8,9]. Recent researches however, throw doubt upon the

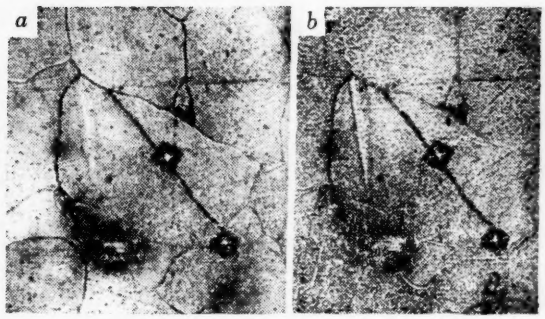

FIG. 6. Local slip from the junction of three grains and microcrack along the grain. Steel C:
a — clearly visible boundaries between grains, and microcracks.
b — microscope setting altered to bring out twins formed from junction of 3 grains, × 334.

VOL. 8 1959

FIG. 7. Two twinning pairs with microcracks between. Several intersecting microcracks starting from the boundaries. Steel B × 300.

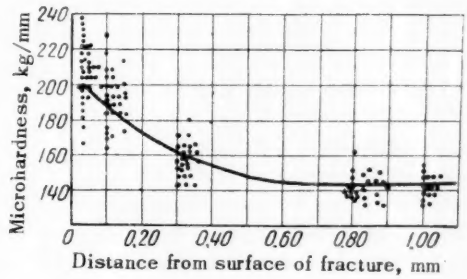

FIG. 8. Microhardness (50 g) of grains at various distances from the surface of brittle fracture (longitudinal section through the centre of the piece of Bessemer steel, a_k = 0.8 kgm/cm²).

accuracy of this proposition [10].

The examinations we carried out on a large number of metallographic specimins taken from the testpieces at the pre-fracture stage, provide a basis for the suggestion that it is the breakdown (formation of blocks) of the grains which is the driving factor. In many cases in which no intensive twinning was observed even after brittle fracture, the process of breakdown was clearly visible *.

Breakdown of the grains also occurs in ductile fracture. In this respect it is particularly interesting to compare X-rays of brittle fracture with those of testpieces loaded a little above their yield point (2 - 4% elongation). The X-rays have this in common that in both cases there is breakdown of the grain. However in the first case the breakdown includes practically all the grains (equal broadening of the individual interferential spots) at the same time as, with brittle fracture, diffraction broadening is disimilar, which is a sign of great irregularity in degrees of breakdown of individual grains.

Microhardness checks have revealed that with brittle fracture there is a noticeable hardening of the grains around the fracture (Fig. 8). With plastic deformation (load a little above yield point), besides the hardening of the grains, to a small extent hardening of their boundaries has been observed [13]; it appears that in both cases, hardening of the grain is connected with the process of their breakdown. Hardening of the boundaries proceeds by virtue of the plastic deformation which is connected with the reversal, interchange of grains relative to one another [13]. This also occurs in brittle fracture but to a much lesser extent.

The micromechanism of brittle fracture may be

* There are two points of view on the nature of grain breakdown: the first, put forward by Stepanov, is based on the loss of elastic rigidity of the structure [11], and the second, on a dislocation mechanism [12].

FIG. 9. Series of microcracks in a notched testpiece at the commencement of total fracture. Steel C, deformation in the ring at − 40°.

presented in the following way.

Under the action of the applied load, shearing deformation starts up in suitably oriented grains, accompanied by breakdown of the grains (Block formation), leading to a change in their form. This in its turn, leads to intermingling of the original grains along their boundaries. The low temperature and high rate of deformation lead to an increase in resistance to slip along the boundaries, which causes an increase in the stresses required to promote slip between the grains. The most favourable conditions for the formation of the precursors of fracture (twinning and microcracks) arise under the action of local loads [11]. Where the metal is in a "brittle" state high stress concentration may result in the slowing down of slip. The manner in which local stresses arise in the case of retardation of slip due to some obstacle (non-metallic inclusions, grain boundary, grain junction) has been described already by Zener [1]. According to this a concentration of stress arises at the point where the slip is impeded, which may lead to one of two consequences: 1) On reaching a value sufficient for the removal of the blockage and furtherance of the slip in the sector adjacent to that of the blockage or in some other favourable direction, twinning may be caused; 2) the concentration of normal stress may reach the critical point which leads to the formation of microcracks.

As the twinning occurs as a result of high concentration of stress and slip in the direction of the twinning plane, spread of the twinning ceases suddenly when it comes up against an obstacle (non-metallic inclusions, sub-grain boundaries etc.) and may also lead to high concentration of normal stresses and the formation of microcracks. Check in the growth of the microcracks may lead to considerable plastic deformation.

The origin and growth of twins and microcracks is dependant on the extent and nature of distribution of stresses which are to a very great extent determined by the orientation and anisotropic properties of the crystal*, while this, in the case under review, may be substantially increased by the process of breakdown of the grain.

THE DEVELOPMENT OF BRITTLE CRACKS

It has been shown above that in the beginning stage of brittle pre-fracture, there is a characteristic appearance in the inner micro-spaces of the metal situated below the notch, of a series of microcracks about the size of one or two grains. With increase and prolongation of the external load, these microcracks extend further in pre-fracture conditions.

Fig. 9 shows a typical photograph of internal cracks in a notched testpiece, just before the commencement of general brittle fracture. The testpiece became deformed in the ring in a "brittle" state. The distribution of separate internal cracks and the existence of necks between them consisting of partially deformed but not fractured grains, is evidence of their independent birth and growth. Another thing which attracts the attention is the presence of a series of twins and microcracks in each micro-space

* A detailed analysis is given in the works of A.V. Stepanov [11].

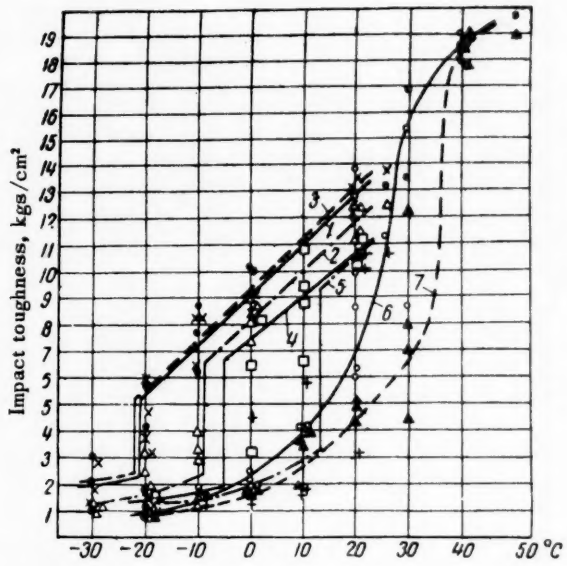

FIG. 10. Relation between impact toughness and the temperature of notched testpieces:
1 – steel B in original state, standard notch;
2 – steel B with preliminary deformation at – 45°. deflexion 0.6 mm;
3 – steel B with preliminary deformation at 20°, deflexion 1.0 mm;
4 – steel A in original state, standard notch;
5 – steel A with preliminary deformation at – 40°, deflexion 0.6 mm;
6 – steel C in original state, V-shaped notch;
7 – steel C, V-notch, with preliminary deformation at – 30°, deflexion 0.25 mm.

in the neighbourhood of the more developed cracks. It is beyond question that these microcracks arose at the same time as those which, under favourable conditions, subsequently achieve significant proportions.

The size of the internal cracks just below the notch is also of interest. Immediately under the notch there are one or two comparatively short cracks, after that some rather longer ones. The length of the subsequent cracks gets progressively less as they get further away from the notch, and the length of the last cracks is equivalent to the width of one to three grains. So, with an overall length of around 5 mm (Fig. 9) for the cracks, the size of individual cracks (proceeding from the notch) is: 0.32: 0,68: 2.24: 1.04: 0.68: 0.36: 0.07: 0.08: 0.05 mm. The same sort of thing has been observed in other testpieces deformed in similar circumstances.

This illustration shows that the most intensive state of stress, sufficient to promote the origin and growth of internal brittle cracks, occurs at a distance of about 1.5 - 2.0 mm from the bottom of the notch. Conditions are quite different in the deformation in the thin layer of metal at the bottom of the notch. Here it is pure slip which develops, due to the surface distribution of the layer [4, 5, 7]. This slip in the surface layer, as may be seen from Fig. 9, and the subsequent formation of ductile cracks, are directly connected with the extension of brittle cracking below this layer. Complete fracture of the testpiece starts with the formation of ductile cracks in the thin plastically deformed surface layer at the bottom of the notch, with subsequent extension through the series of cracks formed immediately before this event.

The picture we have given above of the development of brittle fracture, establishes beyond doubt the validity of the proposition made earlier, that brittle fracture is due to the conditions in which local ductile fracture develops immediately round the notch. In fact, as may be seen from the experimental data, the dominant role in the process of brittle fracture is played by the conditions which determine the start and growth of internal cracks in the micro-spaces arranged some way from the notch.

From this one very important conclusion must be drawn – that brittle fracture cannot in all cases be regarded as an instantaneous process with uninterrupted progress from the first signs of microcracks to total fracture.

In fact, in the pre-fracture conditions described –

the formation of microcracks – it might be halted at any stage and never develop to total fracture. In this case there would, however, be substantial reduction in the original cross section. This may facilitate subsequent brittle fracture under considerably "softer" conditions of loading.

This may be confirmed experimentally by the following date. A series of notched testpieces of steels A, B and C, previously deformed in a brittle state, (see above for conditions of deformation in a ring) were subjected to impact tests at wide intervals of temperature. At the same time for comparison untreated testpieces were tested, and also testpieces of steel B previously deformed in the ring (at deflexion of 1.0 mm) in ductile conditions (+ 20°).

The results, given in Fig. 10, show that preliminary deformation (without visible signs of fracture on the surface) in conditions of brittle fracture, lead to an increase in the dispersion of impact toughness indicators and mixing of the critical temperature for embrittlement 10 to 15° on the side of positive temperatures. These changes cannot be attributed to the ordinary plastic deformation of the root of the notch, as plastic deformation, even to quite a large degree (see curve 3 Fig. 10) cannot be considered in the ductile state at the critical temperature. Here the deciding factor was the formation of internal microcracks below the notch, which also led to increased cold shortness.

CONCLUSIONS

The process of brittle fracture may be divided into two stages.

The first is that of pre-fracture. Typical of this are plastic deformation and, connected with it, the breakdown of the grain, twinning; appearance and development of microcracks in the internal micro-spaces of the metal.

The second stage is that of actual brittle fracture. This stage commences with the formation of ductile cracks in the thin surface layer of metal at the bottom of the notch, the conditions of deformation of which are quite distinct from those prevailing in the internal micro-spaces. After this the fracture progresses along the previously formed internal cracks which are separated from one another by bridges of partially deformed grains.

Translated by V. Alford

REFERENCES

1. C. Zener, *Fracturing of metals*, (1948).
2. A.A. Wells, *Welding Research*, 7, 34 (1953).
3. B.S. Kasatkin and B.A. Movchan, *Izv. Akad. Nauk SSSR, Otd. tekh. nauk* 5, 51 (1956).
4. N.N. Davidenkov, *Metallovedenie i obrabotka metallov (Metallography and the working of metals)* 12, 36 (1956).
5. E. Orowan and D. Felbeck, *Welding Journal*, 570 (1955).
6. G. Irwin, *Fracturing of metals*, (1948).
7. B.S. Kasatkin, *Izv. Akad. Nauk SSSR, Otd. tekh. nauk* 7, 75 (1955).
8. N.N. Davidenkov, *Problema udara v metallovedenie (The problem of impact in metallography) Izv. Akad. Nauk SSSR*, (1938).
9. E.M. Shebandin, *Zh. teor. fiz.* 8, 441 (1938)
10. V.V. Sachkov, and Ya. M. Potak, *Zh. teor. fiz.* 24, 450 (1954).
11. A.V. Stepanov, *Izv. Akad. Nauk SSSR, seroya fiz.*, 17, No. 3, 271 (1953).
12. A.D. Forti, *Neposredstvennoe nabludenie dislokatsiya v kristallakh. (Direct observations of dislocation in crystals)* Metallurgizdat (1956).
13. V.S. Ivanova, *Dokl. Akad. Nauk SSSR*, 94, No. 2, 217 (1954).

THE INFLUENCE OF LENGTH IN TUBULAR STEEL TESTPIECES ON DEFORMATION AND TENSILE STRESS*

L.G. AFENDIK and L.I. SHEKHTER

L'vov Polytechnical Institute

(Received 25 July 1957)

The results are given of investigations into the deformation and stress in the neck of tensile tubular testpieces in dependence of the ratio of the length of the piece to its mean diameter with the same ratio between wall thickness and diameter.

VOL. 8 1959

In paper [1] the experimental data are set out for the deformation in the neck of tubular tensile testpieces and formulae are examined for the determination of stresses. One of the essential conditions for the comparability of this type of test is the maintenance of geometrical similarity of the testpieces. To fulfil this condition for tubular specimens it is necessary to maintain the equality of the ratio between wall thickness and mean dia and also that between the length of the piece and its dia. In the paper mentioned, only partial attention was given in the first dimensional ratio; the influence of the ratio between length and dia on the tensile results as a whole was not examined.

In connexion with the fact that the tensile characteristics obtained by Bridgman in his examination of large plastic deformations [2] were noticeably different from those observed by us, it seems expedient to find the possible cause of this circumstance. Bridgman used short tubes, the gauge length of which was the same as the mean dia. Our tests were conducted both with short testpieces and with some whose gauge length was 4.3 times the mean dia, the ratio of wall thickness to dia remaining the same in both cases.

It has been shown that the ratio of length to mean dia in tubular testpieces is reflected to a considerable extent, particularly for the small ratios considered by us, by the deformation and stress after formation of the neck on tension.

1. THE RELATIONSHIP BETWEEN THE COMPONENTS OF STRESS AND DEFORMATION IN LARGE PLASTIC DEFORMATIONS

In the following the deformation and stress will be considered which occurs in the smallest cross section of a stretched tubular testpiece after formation of local reduction of area (the neck). Axial, radial and hoop stresses are represented by the symbols σ_z, σ_r, $\sigma\theta$, and the corresponding logarithmic characteristics of deformation by e_z, e_1, $e\theta$.

As the directions of the main axes of stress and deformation remain unchanged on tension in this cross section, the existence may be assumed of a proportionality between the deviators of stress and deformation. If here relative volumetric deformation in comparison to components of deformation may be neglected, then, on the basis of the assumption indicated, we get the following equation giving just one relationship between stress and deformation:

$$\frac{e_z}{\sigma_z - \frac{1}{2}(\sigma_\theta + \sigma_r)} = \frac{e_\theta}{\sigma_\theta - \frac{1}{2}(\sigma_r + \sigma_z)} = \frac{e_r}{\sigma_r - \frac{1}{2}(\sigma_z + \sigma_\theta)}. \quad (1)$$

For the surface points of the testpiece $\sigma_r = 0$ as the hoop stress $\sigma\theta$ may be given in relation to axial stress σ_z. For this purpose Bridgman used equation (1). From these equations it follows that

$$\sigma_\theta = \frac{2e_r + e_z}{e_r - e_z} \cdot \sigma_z. \quad (2)$$

In the work outlined above, for the tubular testpieces with small wall thickness compared to radius we used the mean numbers for deformation and stress

* *Fiz. metal. metalloved.*, 8, No. 1, 85-89, 1959.

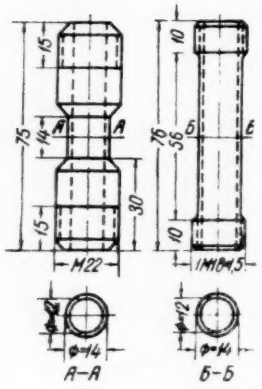

FIG. 1. Dimensions of testpieces used.

FIG. 2. Photograph of longitudinal section in the neck of a testpiece in tension.

and obtained, in particular, exactly the same connexion between means for σ_θ and σ_z as in equation (2).

When subjecting the short tubular testpieces to tension, Bridgman discovered that local reduction occured along the wall thickness in the final stage of stretching. As a result of this, meridional curvature on the inner and outer surfaces had opposite directions. He endeavoured to calculate the stress of this reduction of part of the wall by the same formula as for the neck of wide plates in tension. To what extent this is applicable to long testpieces will be considered below.

2. RESULTS OF THE EXPERIMENTS

Two types of tubular testpieces were used for the tensile tests; they were made of annealed steel type St. 30. Their dimensions are shown in Fig. 1. The external dia and wall thickness was the same for all, 14 mm and 1 mm respectively. Four different lengths were used.

Tension was applied slowly on testing machine IM-4R. On reaching the allotted cross section reduction load was removed for a moment and the external dia and wall thickness were measured. Both external dia and wall thickness were measured in the perpendicularly related directions of least reduction with an accuracy of ± 0.005 mm.

Besides this, tensile tests were conducted on solid cylindrical testpieces with a dia 6 mm and gauge length of 30 mm. The radius of curvature of the neck in a meridional direction, necessary in these circumstances for calculation of stress, could be measured with a satisfactory degree of accuracy by projecting the testpiece on to a screen with a magnification of 40 times.

In processing the experimental data only those tests were used in which rupture occured in the centre portion of the testpiece. In each of the cases referred to at least three pieces were tested.

The process of applying tension to the longer pieces was carried out in the following manner. When the axial elongation approached $e_z \approx 0.20$, the load exceeded maximum and local reduction commenced. For a short time the load was maintained unaltered and then reduced, starting slowly and increasing in speed.

The external dia in the neck grew smaller up to onset of rupture. The cross sectional shape was observed from circle to deviate slightly. Axial elongation in the neck, calculated from the reduction in area, was characterized at the onset of rupture by $e_z = 0.550 - 0.600$. No meridional curvature in an opposite direction to the inner surface of the testpiece was discovered. Fig. 2 is a greatly enlarged photo of the longitudinal section of the piece shortly before rupture, when axial elongation amounted to $e_z = 0.508$. As may be seen from the illustration, the meridional curvature of the walls, both inside and out, has only one direction.

Deformation of the short testpieces was somewhat different. After reaching maximum load and the formation of a neck, the fall in the value of the load proceeded rapidly. At the same time the external dia of the neck was reduced slowly, while just before rupture it ceased to change at all. The external dia after rupture was noticeably greater than with the long pieces.

We did not manage to release the load on the short testpieces before rupture. However, after rupture a small meridional curvature could be observed on the

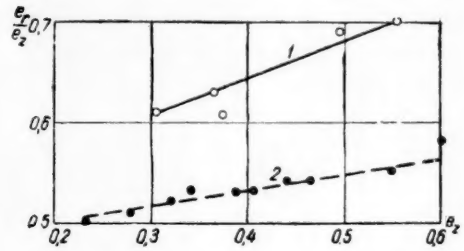

FIG. 3. Curves showing the dependence of ratio e_r/e_z on the components of deformation e_z.

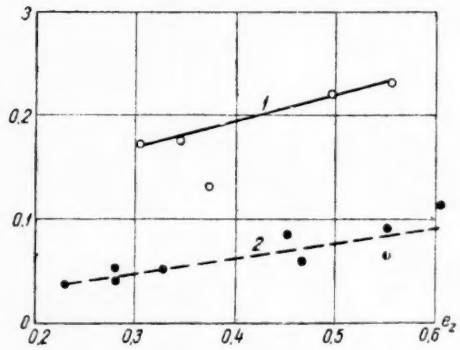

FIG. 4. Curves showing the dependence of ratio σ_θ/σ_z on axial deformation e_z.

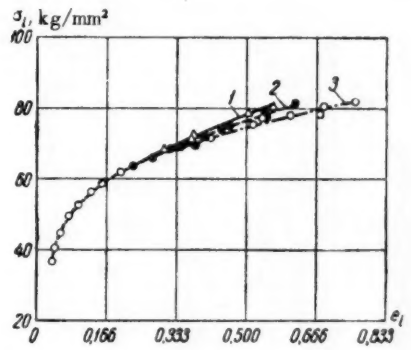

FIG. 5. Curves of tension in the co-ordinates e_i, σ_i.

inner surface, running counter to the curvature on the outer surface.

As a result of this, annular deformation e_θ higher, than in the long ones, while axial deformation was the same e_z.

As stress σ_θ was determined by equation (2) which includes components of deformation, the hoop stress obtained for the two cases investigated was different.

The curves shown in Fig. 3 reflect the dependence of the ratio of the components of deformation, e_r/e_z on the axial deformation e_z. Curve *1* was obtained for the short and curve *2* for the long tubular testpieces. In the first case radial deformation on rupture attained $e_r \approx -0.70\ e_z$, and in the second $-\ e_r \approx -057\ e_z$. (sic)

Fig. 4 shows the stress ratio σ_θ/σ_z at the various figures for axial deformation. Curve *1* was obtained for the short, and curve *2* for the long testpieces. In the final stages of tension the hoop stress σ_θ in the neck of the short pieces was 2–2.5 times greater than that in the testpieces which were 4 times longer. On rupture, in the long pieces $\sigma_\theta = 0.07 - 0.09\ \sigma_z$, and in the short ones $\sigma_\theta = 0.19 - 0.23\ \sigma_z$.

It should be observed however that in the cases investigated, with the same intensity of deformation e_i, there was no substantial difference in the intensities of stress σ_z. Fig. 5 shows the curves of tension in co-ordinates e_i and σ_i. Curve *1* is for the short pieces and curve *2* for the long, while curve *3* is for the solid cylindrical testpieces.

CONCLUSIONS

The data obtained from the investigation of the deformation and stress in the neck of tubular testpieces of varying lengths under tension show that the ratio of mean dia to the length of the testpiece has an essential influence on the effects of tension in those cases where the ratio is not large. The most sensitive values to this ratio were found to be the components of deformation e_r, σ_θ and annular stress σ_θ, and also the meridional curvature of the inner surface.

Where the ratio between the length of the tubes and their mean dia is greater enough, signs of influence disappear. It follows therefore that it may

VOL. 8 1959

only be said for sufficiently long testpieces that the results of a tensile test are reliable. In this context it must also be remembered that the ratio of wall thickness to mean dia also has some influence on the deformation and stress in the neck in tension, on which subject we have previously written a paper [1].

Translated by V. Alford

REFERENCES

1. L.G. Afendik and L.I. Shekhter, *Fiz. Fiz. met. metalloved.*, 2, 538 (1956).

2. P.V. Bridgman, *Investigation of large plastic deformation and rupture*. Foreign Literature Phublishing House, (1956).

VOL
8
195

THE EFFECT OF HYDROGEN ADSORPTION IN THE PROCESS OF DEFORMATION OF STEEL ON ITS MECHANICAL PROPERTIES*

G.V. KARPENKO and R.I. KRIPYAKEVICH

Institute of Engineering and Automatics AS Ukr. SSR

(Received 13 July 1957)

It has been found that, in the process of deformation of steel hydrogen adsorption during galvanic processes occurs along the lines of slip. Hydrogen adsorption in these circumstances leads to loss of plasticity of mild steels and a reduction in the true stress on rupture. UTS and yield stress in such a case remain practically unchanged.

VOL. 8 1959

The hydrogen adsorption of steels observed in etching and various galvanic processes as also in cathodic protection, leads to loss of plasticity by the steel and reduces its resistance to embrittlement. The large number of investigations devoted to the problem of the influence of hydrogen on the mechanical properties of steel have been conducted on the basis of the preliminary adsorption of hydrogen by the metal, after which, in many cases, the effect of the stress of the metal has been examined [1]. We know of no investigations into the effect of hydrogen on the mechanical properties of steel in the process of deformation, although this problem is of absorbing interest.

We carried out tests to examine the action of hydrogen in the process of the deformation of mild steel, on its mechanical process. By means of a special attachment to the tensile testing machine IM-12 (Fig. 1) it was possible to rupture a steel testpiece in electrolyte to which either a cathodic or an anodic potential could be applied at the expense of the external current supply. With this attachment it was possible to determine the mechanical characteristics of the steel in the kinetics of its hydrogen adsorption. When the tensile testpiece was in the role of cathode the anode material could be changed and also the composition of the electrolyte and the density of the current. With the same attachment steel testpieces could be examined during anodic polarization.

In order to provide an opportunity to study the effect of reduction of plasticity, the tests were conducted with mild annealed steel type St. 3 with a pearlite-ferritic structure. 10 mm dia testpieces with a test length of 100 mm, were washed in aviation gasoline and desorbed with activated carbon. Soft steel type St. 3 was used as the anode, and also lead, copper and graphite. For the electrolyte a 26 per cent solution sulphuric acid and 18 per cent solution caustic soda were used. The density of the H_2S04 was 1.18. During polarization the current density changed from 0 to 60 A/dm².

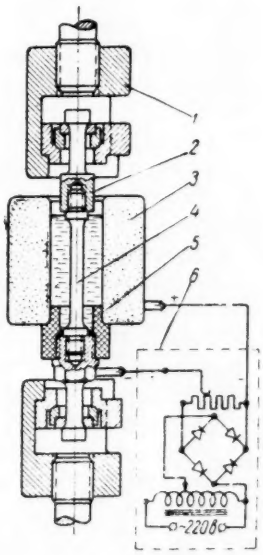

FIG. 1. Diagram of the attachment to tensile testing machine IM 12 for the polarization of tensile testpieces:

1 – terminals;
2 – screw clamps;
3 – graphite container (anode);
4 – testpiece (cathode);
5 – insulating sleeve;
6 – adjustable d.c. supply.

* *Fiz. metal. metalloved.*, 8, No. 1, 90-94, 1959.

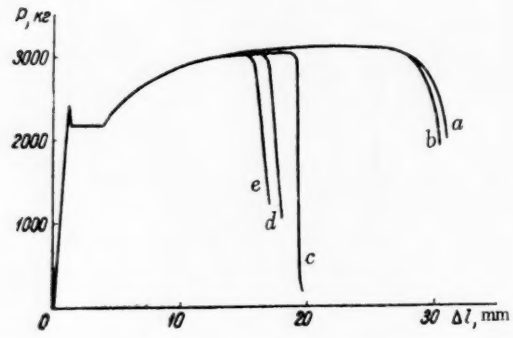

FIG. 2. Effect of polarization of St. 3 on the nature of the tension diagram:
a – in air;
b – during anodic polarization;
c, *d*, *e* – during cathodic polarization; anode is iron.

The test were carried out at a constant rate $v = 2$ mm/min. The current was switched on at the same time as the tensile machine. The electrolyte was poured in immediately before the beginning of the test (from the beginning of pouring the electrolyte to the beginning of the test is about 4 min). The whole test took about 10-15 min. The purpose of the test was to determine the ultimate tensile stress (σ_{prochn}, kg/mm²), the yield stress (σ_{tek}, kg/mm²), the true stress on rupture (σ_{ist}, kg/mm²), percentage elongation (δ 10%) and percentage reduction (ψ %) of steel in the process of its polarization.

Mild steel St. 3 showed, on the application of tensile stress in the air, a clearly defined area of tension with marked elongation and cross-sectional reduction (curve *a* Fig. 2). The same was observed when St. 3 testpieces were put under tension at the same rate in the electrolyte with anodic polarization of the piece. (curve *b*). In the latter case, although the testpiece was covered with a thin scale of oxides, it did not lose its plasticity (Fig. 3, *b*) and the mechanical properties remained the same as in the steel subjected to tension in air (Fig. 3, *a*).

A very different state was observed with the cathode-polarized testpieces. In these pieces the fracture was brittle as the rupture took place along the slip lines, as seen in Fig. 3, *c*. Of the mechanical properties of the cathode-polarized pieces the most noticeable deterioration was in the figures for plasticity ψ and δ 10 and true stress on rupture σ_{ist}; tensile and yield stress remained virtually the same. The curves of tension of these testpieces are shown in Fig. 2 (curve *c*, *d*, *e*).

The tests showed that the change in the plasticity and true stress of a cathode-polarized steel depends on current density, anode material and type of electrolyte. At the same time this dependence has an unusual character (Fig. 4). Similar curves were obtained for the relationship between percentage elongation and true stress, and current density.

Table 1 gives the figures obtained for the mechanical properties of St. 3 in tests in air in electrolyte with the maximum current density at which the maximum effect of the changes in the mechanical properties* was observed.

EVALUATION OF THE RESULTS

In the anodic polarization of steel there is a transition of iron ions into the electrolyte and oxidation of the steel at the expense of the oxygen separated. As apparent from our tests these processes had no influence on the mechanical properties of the steel during its anodic polarization. This may possibly be due to the short duration of the test as the anode polarized steel showed no significant corrosion in the course of the test. It is well-known that corrosion lowers plasticity.

On cathodic polarization, ions of the dissolved metal of the anode were passed on to the steel, together with hydrogen ions. While the change in the nature of the anode in our tests had very little effect on the change in the mechanical properties of cathode-polarized testpieces, this effect was also

* eg., the maximum current density D_k at which maximum reduction in ψ (up to 71.4%) and was observed was $D_k = 5$-15 A/dm² maximum reduction in σ_{ist} (up to 97.7%) was observed at $D_k = 15$-30 A/dm².

VOL 8 195

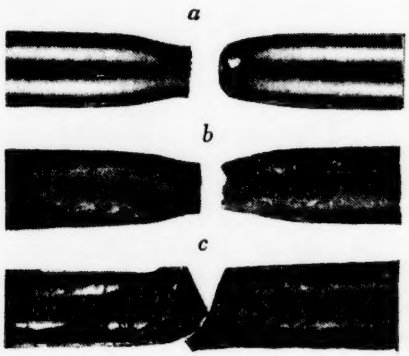

FIG. 3. St. 3 testpieces fractured under different circumstances:
a – in air;
b – during anodic polarization;
c – during cathodic polarization.

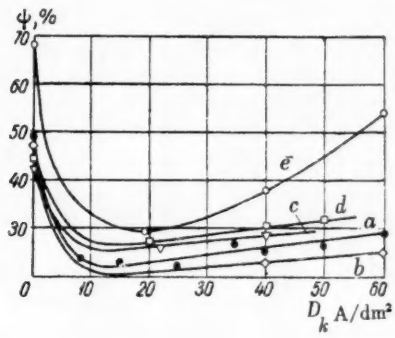

FIG. 4. Relation between relative reduction and current density:
a – copper anode, acid electrolyte;
b – lead anode, acid electrolyte;
c – iron anode, acid electrolyte;
d – graphite anode, acid electrolyte;
e – copper anode, alkaline electrolyte.

TABLE 1. Mechanical properties of St. 3 testpieces

Test conditions		ψ		δ_{10}		σ_{ist}		σ_{tek}		σ_{prochn}	
Anode	Electrolyte	Abs. %	Relative %	Abs. %	Relative %	Abs. kg/mm²	Relative %	Abs. kg/mm²	Relative %	Abs. kg/mm²	Relative %
Cu	NaOH (18%)	28	40.0	24	75	33	38.0	28	100	39	97.5
Cu	H_2SO_4 (26%)	21	30.0	17	53.2	17	19.5	26.5	94.5	39	97.5
Pb	Ditto	20	28.6	16	50	2	2.3	28.5	101.5	38.0	95
Fe	»	25	35.7	18	56.3	15	17.3	27.5	98.2	37.5	93.8
C	»	26	37.2	17.5	54.7	25	28.7	28.5	101.7	37.5	93.8
In air		70	100	32	100	87	100	28	100	40	100

observed for insoluble (lead and graphite) anodes. From this it follows that it is hydrogen, and not the deposited metal, which is responsible for the reduction in plasticity and true stress.

It frequently occurs that considerable residual tensile stresses arise in the layer of deposited metal in electroplating, which reduce the fatigue strength of nickel, chromium and copper plated steel testpieces. However, as shown by our tests [3], steel objects with this type of electroplating have the same plasticity as unplated ones.

Hydrogen ions adsorbed by the surface of a cathode-polarized steel under deformation are reduced to an atomic or molecular state and frequently given off in the form of bubbles of gas, often penetrating the metal along the slip lines caused by the deformation and then, being diffused into the lattice of the metal, transform it to a brittle state. This embrittlement of the metal, according to current opinion, is due both to the strain caused in the lattice and to the pressure

of the hydrogen filling the deffects in the lattice.

After the diffusive penetration of the metal by the hydrogen the tensile forces brought about brittle fracture of the cathode-polarized steel by rupture along those parts of the metal affected by the hydrogen, which fall along the slip planes.

The accuracy of this opinion regarding the mechanism of the phenomenon is confirmed by the external appearance of ruptured cathode-polarized testpieces (see Fig. 3, *c*) and also by the tension curves (see Fig. 2) which bear witness to the lack of influence of the hydrogen on the course of the tension curve up to the upper yield point or on the yield stress itself. Until the commencement of yield (formation of slip) introduction of hydrogen into the lattice would be slight, and would not affect the mechanical properties of the steel. It is relevant to this that the tension diagram until the commencement of yield, and the yield stress itself, remain the same as when the tests are carried out in air. With the commencement of yield, hydrogen penetration occurs along the slip lines to a considerable depth in the metal and, entering into the lattice, transform it into a brittle structure.

The fantastic speed at which the hydrogenation of steel occurs may be explained in this way: in the zone of the slip planes not only is the lattice of the metal distorted, but also a tremendous number of cavities appear, and in the process of their formation hydrogen is sucked in, penetrating the metal at quite a high speed, which exceeds the speed of volumetric, and therefore, boundary diffusion.

The sectors of metal dividing these cavities which, in the ordinary way, lead to increased strength of the slip zone, have distorted lattices and are penetrated by diffusion by virtue of the great activation connected with the distortion of the lattice and the concentration there of up to 99% of the residual energy of deformation. It is well known that the rate of diffusive penetration in distorted activated lattices is somewhat greater than that of the diffusive penetration in volume with properly arranged lattice. Konobeyevski [4] has said that the increase in the rate of diffusion of nickel in deformed copper is more than 1000 times.

CONCLUSIONS

1. The influence of hydrogen on mild steel in the process of deformation amounts to a reduction in plasticity ψ and δ and in the true stress σ_{ist}. Ultimate tensile stress and yield stress are virtually unaltered.

2. The effect of the influence of hydrogen on the stated mechanical properties of steel depends on the density of the current D_k in that it appears at a certain optimum figure for this.

3. Rupture of cathode-polarized testpieces in tension has a brittle character and occurs in the main along the lines of maximum tangential stress (along the slip lines).

Translated by V. Alford

REFERENCES

1. A. Bastien, *Compt. Rend.* 241, No, 24 (1955).
2. M.I. Chaevsky, *Deyaki pitaniya fiziko-khimichnoi mekhaniki metaliv. (Investigation of the physico-chemical mechanics of metals), Akad. Nauk Ukr. S.S.R.*, (1957).
3. G.V. Karpenko, *Vliyanie aktivnykh zhidkikh sred na vynoslivost' stali (The influence of active liquid media on the fatigue of steels), Akad. Nauk Ukr. S.S.R.* (1955).
4. S.T. Konobeyevsky, *Izv. Akad. Nauk S.S.S.R.* No.5 (1957).

VOL 8 195

THE INFLUENCE OF PLASTIC DEFORMATION ON THE INTERNAL FRICTION OF IRON – TUNGSTEN ALLOYS*

V.S. POSTNIKOV and R.S. LEBEDEV
Kemerov State Pedagogic Institute

(Received 30 July 1957)

VOL. 8 1959

Well annealed polycrystalline metals and alloys have low internal friction – 10^{-4} and less [1-3]. In metals and alloys which have undergone preliminary plastic deformation, subsequent measurement has revealed sharply increased internal friction which however, is not permanent, but is strongly dependant on holding time, testing temperature and amplitude of oscillations [4-46].

Despite the not inconsiderable number of works devoted to the study of the influence of strain hardening on the internal friction of pure metals and alloys, the nature of this phenomenon is still far from clear as it is dependent on a number of factors (especially with alloys). These are – nature of cold deformation and degree of strain hardening, holding time, temperature, frequency and amplitude of oscillations, content of impurities and surrounding medium. A no less important reason is the lack of systematic investigation by one particular method, for example, by a low frequency method, a method which, it seems, might yield more material for the understanding of the mechanism of such phenomena, than do high frequency methods. [3].

Of the various investigations listed in the bibliography, 26 were carried out by high frequency methods (investigation of pure metals: tin [10], lead [10], zinc [10, 15, 20], aluminium [12, 19, 30], copper [5, 10, 16, 19, 25, 27], iron [11] and alloys: brass [6, 9, 17, 19, 31, 34], steel [4, 6, 7, 33]) and 21 were carried out by low frequency methods (metals: aluminium [24, 26, 36, 37, 41, 45, 46], silver [46], copper [39, 41, 43], gold [42], iron [22, 35], platinum [38, 46], molybdenum [29] and alloys: brass [13], aluminium - copper [23], aluminium - magnesium [44, 48], nickel - chromium [21]).

This paper is devoted to the study of the influence of strain hardening on the internal friction of binary alloys. For this investigation a low frequency method was used (oscillating frequency 1c/s) with small amplitude torsional oscillation [46]. All measurements were made in a vacuum of 10^{-3} Hg.col. on 300 mm long testpieces, dia 0.7 mm, of iron-tungsten (1.83% and 5% W) on an Armco iron base (0.02% mn; 0.03% Si; 0.02% C; 0.017% S; 0.001% P) with reduction to 5; 15; 25; 30; 40; 60; 80 and 95%. Internal friction for all the testpieces* was measured only on heating (at the rate of $\sim 3.5^{\circ}$/min) after previous annealing at 825°C for 90 min. Besides this, to determine the heat of activation of the process of recovery of internal friction, the isothermal change of the internal friction was studied at the maximum oscillation amplitude for all – 10^{-5}. All the measurements made on the alloy with 1.83% W were made 7 months after reduction while those on the one with 5% W were made in the course of one month.

The unit used as a measure of internal friction was the logarithmetic decrement over π. Accuracy of measurement of internal friction was $\sim 0.05\%$ at low temperatures and 2-3% at high.

RESULTS OF THE MEASUREMENTS

The results of the measurements are set out in Fig. 1-6 and in the table. From these illustrations and tabulated data the following conclusions may be drawn.

1. The internal friction of plastically deformed unannealed Fe-W alloys (Fig. 1, 2) is large when compared with that of the same alloys annealed at high temperatures (Figs. 3, 4). Besides this, as we found in our tests, it is strongly dependent on the rate of heating and the holding time (Fig. 6).

2. The peak of internal friction moves towards higher temperatures in inverse ratio to the amount of previous reduction. The height of the peak depends essentially (Fig. 5, curve *1*, *2*) on the amount of

* *Fiz. metal. metalloved.*, 8, No. 1, 95-101, 1959.

* The testpieces were approved by the Institute of the Physics of Metals and Metallography, Centr. Res. Inst. Ferrous Metallurgy.

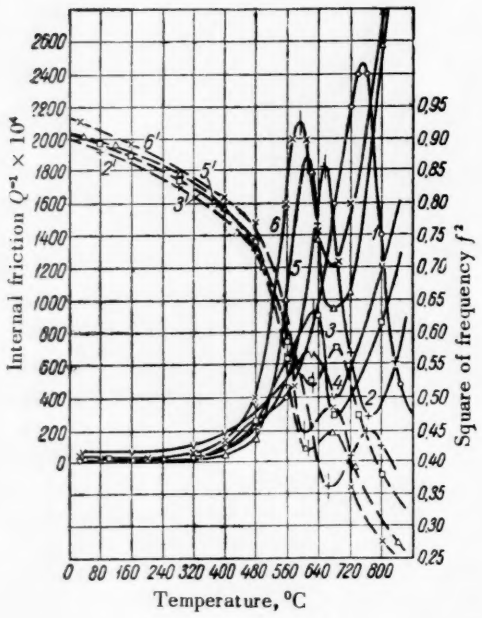

FIG. 1. The temperature relationship between internal friction (1 – 5; 2 – 15; 3 – 30; 4 – 40; 5 – 60; 6 – 80 % reduction) and modulus of elasticity in shear (2′ – 15; 3 – 30; 5′ – 60; 6′ – 80% reduction) of a plastically deformed alloys Fe-W (1.83% W) prior to annealing.

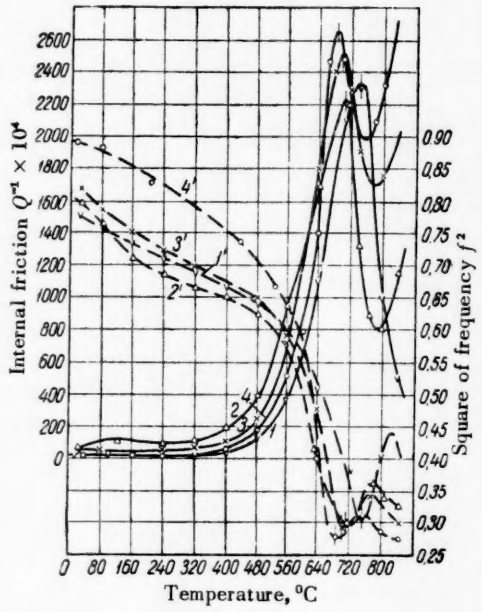

FIG. 2. The temperature relationship between internal friction (1 – 25; 2 – 60; 3 – 80; 4 – 95% reduction) and modulus of elasticity in shear (1′ – 25; 2′ – 60; 3′ – 80; 4′ – 95% reduction) of a plastically deformed alloy Fe-W (5%W) prior to annealing.

reduction, especially for 1.83% W alloys. As may be seen from Fig. 5, the peak is lowest where reduction is about 40-45 per cent.

3. With isothermal soaking at various temperatures, internal friction is reduced in an almost exponential relation to time (Fig. 6).

4. The energy of activation of the process of "recovery" of the alloy Fe-W depends on the concentration of tungsten in the iron and on the extent of previous plastic deformation. As may be seen from the Tables, the energy of activation decreases according to the extent of reduction.

5. The level of internal friction at high temperatures (840°C) is considerably greater in work-hardened alloys than in annealed ones. The high temperature level depends on the amount of deformation, the annealing temperature, and the concentration of W in the iron. The deformation considerably increases the level of internal friction (Fig. 5, curves *3*, *4*), while annealing lowers it (Fig. 5, curves *5*, *6*). Introduction of large amounts of tungsten effects a sharp reduction in internal friction at high temperatures.

6. The level of internal friction at high temperatures is indirectly connected with the strength of the alloy at the same temperature, as is evident from the temperature course of the modulus, of elasticity in shear and the tensile strength at high temperatures (v. Fig. 5, curves *7′* and *8′* and Table 1).

7. The modulus of elasticity in shear at high temperatures is greater for unannealed testpieces than for annealed ones, and at low temperatures the reverse is true (Figs. 1-5).

EVALUATION OF THE RESULTS OF MEASUREMENT

1. As we have seen above, previous plastic deformation of an alloy causes appreciably higher internal friction than exists in annealed ones. The same thing has been observed by other research workers [5, 6, 9-13, 15, 17, 19, 20, 22-24, 26, 27, 29-31, 34-39, 41-46], with the exception of papers [4, 7, 18], which report reduction in the level of internal friction as a result of plastic deformation. In [33], both increase and decrease in internal friction was observed with plastic deformation of steel. Finally, in [16, 17, 21, 25] it was found that internal friction at room temperature, as a function of the degree of work hardening, passes through a minimum and then increases in ratio to load.

Analysis of the work listed above and of the investigations reported in [33] has shown that

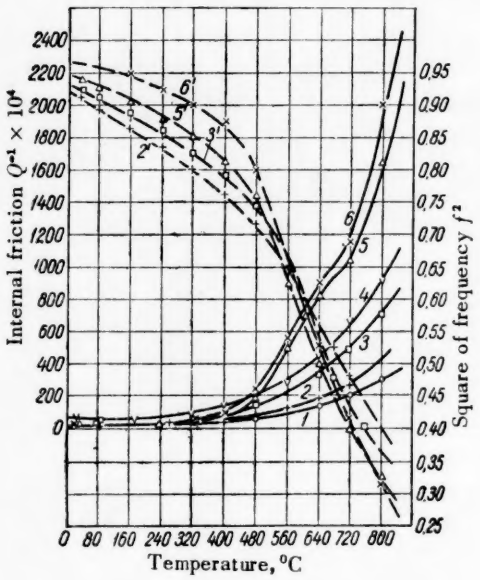

FIG. 3. The temperature relationship between internal friction (1 – 5; 2 – 15; 3 – 30; 4 – 40; 5 – 60; 6 – 80% reduction) and modulus of elasticity in shear (2′ – 15; 3′ – 30; 5′ – 60; 6′ – 80% reduction) of plastically deformed alloy Fe) W (1.83% W) after annealing at 825°.

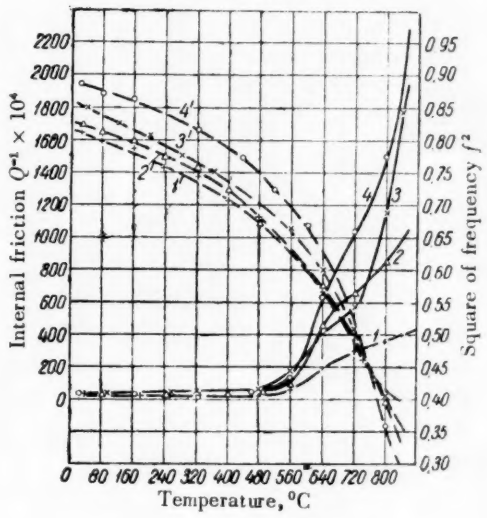

FIG. 4. The temperature relationship between internal friction (1 – 25; 2 – 60; 3 – 80; 4 – 95% reduction) and modulus of elasticity in shear (1′ – 25; 2′ – 60; 3′ – 80; 4′ – 95% reduction) of plastically deformed alloy Fe-W (5% W) after annealing at 825°.

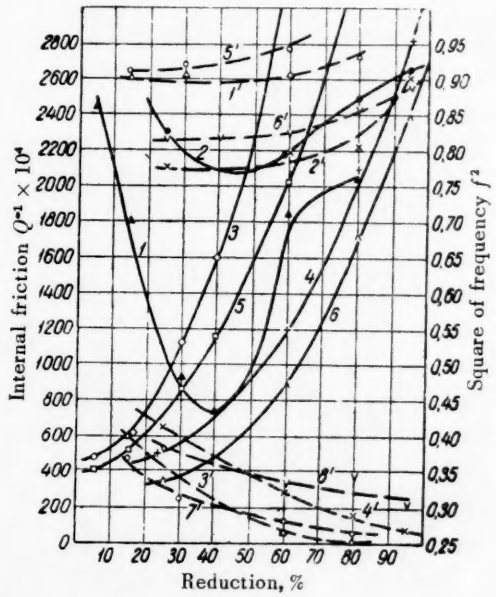

FIG. 5. Relationship between the peak of internal friction (1 – 1.83% W, 2 – 5% W) and its level at 840° (3 – 1.83% W, 4 – 5% W prior to annealing; 5 – 1.83% W, 6 – 5% W after annealing), and the degree of reduction. Relationship between modulus of elasticity in shear (1′, 2′ – 20°; 3′, 4′ – 840° prior to annealing; 5′, 6′ – 20° and 7′, 8′ – 840° after annealing at 825°) and the degree of reduction.

TABLE 1.

W, %	Reduction %	Av. size of grain, mm	Rupturing strength kg/mm² at 25°	Rupturing strength kg/mm² at 840°	Energy of activation cal/mol
1.83	5	0.2	31.0	*	—
	15	0.06	35.5	2.10	5,500
	30	0.055	42.0	1.80	4,200
	40	0.05	44.0	1.65	2,400
	60	0.02	65.0	1.55	—
	80	0.01	78.0	*	1,500
5	25	0.09	58.0	2.20	3,000
	60	0.012	65.0	1.75	2,000
	80	0.010	70.0	1.50	1,400
	95	0.009	81.0	1.43	1,300

* No data due to lack of sufficient number samples with 1.83% W.

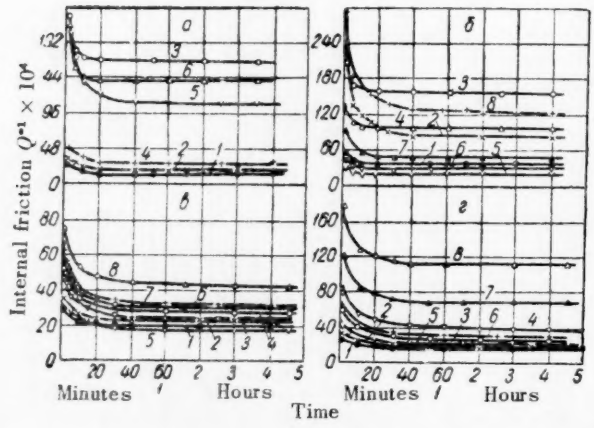

FIG. 6. *a*. Isothermal change in internal friction of alloy with 1.83% W after reduction by 15% (1 – 300; 2 – 329; 3 – 435°) and by 30% (4 – 291; 5 – 367; 6 – 420°) and its relation to time;
b – ditto after reduction by 40% (1 – 213; 2 – 360; 3 – 412; 4 – 460°); and by 80% (5 – 170; 6 – 350; 7 – 400; 8 – 450°);
c, *d* – the same relationship for a 5% W iron-tungsten alloy at various degrees of reduction (from 25 to 95%) and some of their temperatures.

increased internal friction due to plastic deformation is observed in tests where a low stress amplitude ($\sim 10^{-5}$ and less) is used, while the reverse obtains (it is decreased), where the amplitude is great. As regards the maximum of internal friction as a function of the degree of strain hardening, which was observed in [16, 17, 25] at frequencies exceeding 10^3 c/s, it is in all probability a type of thermo-elastic relaxation which is not directly connected with the atomic diffusion and microplasicity which causes anelastic phenomena at low frequencies of oscillation.

The dependence shown above, of the extent of internal friction in deformed testpieces, on amount of strain hardening, testing temperature and soaking time, has already been observed some time ago [41]. It was found that the internal friction of a plastically deformed metal truly a basic contribution !) may be represented by the formula

$$Q = \frac{\alpha\beta\bar{\theta}}{f\,kT}\left[a\,exp\left(-\frac{H}{RT}\right) + b\,exp\left(-\frac{t}{\tau}\right)\right], \quad (1)$$

in which a, β, α, b, k, R are constants; θ is the mean shearing strain acting on the testpiece; f is the frequency of oscillation; T is the absolute temperature; H is the particular parameter characteristic of the possibility of different types of transition of the atoms in the lattice; t is time; τ is the relaxation time of the process of recovery of internal friction.

From this it will be seen that as $t \to \infty$ the value of Q converges with the equilibrium value

$$Q_\infty = \frac{\alpha\beta\bar{\theta}\,a}{f\,kT}\,exp\left(-\frac{H}{RT}\right), \quad (2)$$

appropriate for the given temperature.

The same value

$$Q_t = \frac{\alpha\beta\bar{\theta}\,b}{f\,kT}\,exp\left(-\frac{t}{\tau}\right) \quad (3)$$

defines the supplementary internal friction which occurs after deformation of a metal or alloy. In connexion with the fact that the internal friction of a deformed testpiece is reduced by isothermal soaking at a quicker rate if the temperature is higher, the following relation may be proposed between relaxation time τ and temperature

$$\tau = \tau_0\,exp\left(\frac{E(\sigma)}{RT}\right), \quad (4)$$

in which $E(\sigma)$ is a particular energy of activation for the process of recovery of the internal friction of the deformed testpiece, which is, in its turn, a function of the degree of strain hardening.

Values found for $E(\sigma)$ from the kinetic curves (Fig. 6) are included in Table 1. These values are evidence that, in the process of recovery, no part is played by atomic diffusion, as the energy of activation $E(\sigma)$ of the process of recovery of internal friction is appreciably less than the value for the energy of activation for atomic diffusion.

Using equation (1), it is possible to explain the growth, observed in the tests, of the extent of internal friction on plastic deformation of testpieces, and also its exponential reduction on isothermal soaking, but not the appearance of the maximum on the curve of internal friction of plastically deformed testpieces. In [50] an attempt is made to tackle this question. For internal friction occasioned by the previous deformation of the testpiece, the following equation has been found

$$Q_\sigma = A\,\alpha_0\,exp\left(-\frac{U}{RT}\right)exp\left(-\frac{t}{\tau}\right), \quad (5)$$

in which A is the constant for the values given; α_0 is the mobility of the defect at $T = \infty$; U is the energy of activation of the movement of the defects.

This equation explains the emergence of the maximum of internal friction on the curve of internal friction when the testpiece is heated at certain rate $\gamma = T/t$. In fact, if, in place of temperature T, the figure for $\gamma\,t$ is inserted in formula (5), and the maximum Q is found, one gets the transcedent equation

$$RT_m^2 = E(\sigma)\,T_m = U\,\gamma\tau_0\,exp\left[\frac{E(\sigma)}{RT_m}\right], \quad (6)$$

which defines the position of the maximum on curve $E(\sigma)$. From these equations it is clear that the position of the maximum depends on the rate of heating γ and on the value of $E(\sigma)$, which is itself dependent on the extent of previous deformation. However, what is still not clear is the unusual dependence of the amount of the maximum of internal friction in deformed testpieces on the extent of reduction, as represented in Fig. 5 by curves *1* and *2*. Another point which is still not quite clear is the relation between $E(\sigma)$ and the content of tungsten in the iron lattice 2. The sharp increase in internal friction at high temperatures (both for annealed and unannealed testpieces) is evidence of the important part played at high temperatures by the mechanism [2] described by formula (2). A no less important part is played by viscous flow in the grain boundaries [47, 2]. Insofar as these two mechanisms are mainly responsible for the behaviour of internal friction at high temperatures, its reduction may be due on one side to reduction of viscous flow at the grain boundaries, and, on the other, and particularly at high temperatures, to an increase in the value of parameter H, which characterizes the migration of defects in the lattice of the alloy.

As may be seen from Figs. 3 and 4, the lowest level of internal friction at a temperature of 840° is

VOL. 8 1959

shown by alloy Fe-W (5% W) after previous reduction by 25%. The level of internal friction of this alloy was somewhat less than that of an alloy at the same temperature, which contained 1.83% W and had suffered 5% reduction. Both testpieces (see Table) had the largest grain size. On the other hand, as is also evident from the Table and from Fig. 5 (curves 7′ and 8]), they also show the greatest bonding energy for the atoms of the lattice and the greatest strength at temperatures of 840°.

For this reason the conclusions drawn in papers [3] may be recapitulated: internal friction in alloys at high temperatures may lead to the unusual characteristic of strength at high temperatures. Apparently it may be said for alloys that the greater the creep resistance, the lower the internal friction at high temperatures. This condition is necessary, as witnessed by many tests, but also inadequate, as the adequacy of this statement is still not proven.

In conclusion we would like to express our gratitude to A.Ya. Samoilova for the compilation of the graphs.

Translated by V. Alford

REFERENCES

1. A.S. Nowick, *Progress in Metal Physics*, 4, 1 (1953).
2. V.S. Postnikov, *Zh. eksp. teor. fiz.* 24, 1599 (1954).
3. V.S. Postnikov, *Transactions Kemerov State pedagogic institute*, 1, 191, (1956), *Fiz metal. metalloved*, 4, 343 (1957).
4. E. Körber and M. Hempel, *J. Inst. Eisenforschung*, 22 (1935).
5. R.L. Wegel and H. Walther, *Physics*, 6, 141 (1935).
6. F. Forster and W. Koster, *Z. Metallk*, 29, 116 (1937).
7. L. Kukanov, *Zav. lab.* 6, 722 (1937).
8. C. Zener, *Phys. rev.*, 53, 582 (1938).
9. W. Köster and K. Rosenthal, *Z. Metallk.* 30, 345 (1938).
10. T.A. Read, *Phys. rev.*, 58, 371 (1940).
11. W. Köster, *Arch. Eisenhuttenw.* 14, 271 (1940).
12. W. Köster, *Z. Metall.* 32, 282 (1940).
13. I. Norton, *Trans. AIME*, 137, 49 (1940).
14. C. Zener, *Phys. rev.*, 60, 455 (1941).
15. F. Seitz and T.A. Read, *J. Appl. Phys.* 12, 100 (1941).
16. A.W. Lawson, *Phys. rev.*, 60, 330 (1941).
17. C. Zener, H. Clarke and S. Smith, *Trans. AIME* 147, 90 (1942).
18. W. Hatfield, Z. Rotherham and E. Hawey, *Iron and Steel*, 17, 613 (1944).
19. C.H. Found, *Trans. AIME*, 161, 120 (1945).
20. T.A. Read and E.P. Tyndorll, *J. Appl. Phys.*, 17, 713 (1946).
21. Ch. Boulanger, *Compt. Rend.*, 226, 1170 (1948).
22. T.S. Kë, *Metals technology*, 15, 1 (1948).
23. T.S. Kë, *Phys. rev.*, 21, 420 (1950).
24. T.S. Kë, *J. Metals*, 2, 575; 581 (1950).
25. R.R. Hasguti and T. Hirai, *J. Appl. Phys.*, 22, 1084 (1951).
26. T.S. Kë and C. Zener, *Chinese J. Phys.* 8, 133 (1951).
27. J. Weertman and J.S. Koechler, *J. Appl. Phys.*, 24, 624 (1953).
28. E. Schreuer, Zs. Naturforsch., 8a, 322 (1953).
29. R.E. Maringer, *J. Appl. Phys.*, 24, 1525 (1953).
30. E.G. Standford, *Research* 6, 21 (1953).
31. H. Fusfeld, *J. Appl. Phys.*, 24, 1062 (1953).
32. A.S. Nowick, *Acta Met.*, 25, 1129 (1954).
33. L.A. Glikman and E.A. Khein, *Zh. eksp. teor. fiz.* 24, 400; 560 (1954).
34. W. Köster and E. Stolter, *Zs. Metallk*, 45, 356 (1954).
35. W. Köster, *Arch. Eisenhuttenw.* 25, 569 (1954).
36. G.K. Brook and A.H. Sully, *Acta Met.* 3, 460 (1955).
37. J. Friedel , Ch. Boulanger and C. Crussard, *Acta Met.* 3, 380 (1955).
38. A.S. Nowick, *Acta Met.*, 3, 312 (1955).
39. W. Köster, L. Bangert and W. Lang, *Z. Metallk.*, 46, 84 (1955).
40. J. Weertman, *J. Appl. Phys.*, 26, 202 (1955).
41. V.S. Postnikov and M.M. Belyaev, *Fiz. metal. metalloved.*, 2, 504 (1956).
42. W. Köstner, L. Bangert and J. Hafner, *Z. Metallk.*, 47, 224 (1956).
43. D.H. Niblett and J. Wilks, *Phil. mag.* 1, 415 (1956).
44. A.V. Grin' and V.A. Pavlov, *Fiz. metal. metalloved.*, 4, 103 (1957).
45. A.Ya. Samoilova and V.S. Postnikov, *Dokl. Akad. Nauk SSSR*, 114, 1228 (1957).
46. A.Ya. Samoilova and V.S. Postnikov, *Trans. Keremov State Pedagogic Inst.*, 3 (1957).
47. V.S. Postnikov, *Trans. Keremov. State Pedagogic Inst.*, 1, 211 (1954).
48. A.V. Grin', *Fiz. metal. metalloved.*, 4, 383 (1957).
49. T.S. Kë, *Phys. rev.*, 71, 533 (1947).
50. V.S. Postnikov, *Dokl. Akad. Nauk SSSR* – printing.

VOL 8 195

LATENT PLASTIC DEFORMATION ENERGY OF ALUMINIUM AND COPPER ALLOYS*

M.M. POPOV, E.N. TIKHOMINA, S.M. SKURATOV and E.N. KALININA

(Received 5 August 1958)

A method of determining thermal heat capacity (true and "apparent") was developed and adopted for determining the deformation energy of aluminium and copper alloys (3 and 5 per cent).

Not all the mechanical work used for any kind or any degree of plastic metal deformation is transformed into heat, a part remains in the metal in the form of energy of internal stresses. Therefore, if we denote by H_1 the enthalpy of undeformed and by H_2 that of deformed metal, then

$$H_2 - H_1 = A - Q, \qquad (1)$$

and in addition $A \neq Q$, consequently $H_2 - H_1 = h$ (h – latent energy of deformation).

The presence in deformed metal of excess energy h sometimes explains very considerable differences in a great number of properties of deformed metal compared with those of undeformed; for instance, high diffusion rates of alloy components, increased reaction capacity, change of density, recrystallization capacity and so on.

Latent deformation energy may be determined in two ways:

1) Values A and Q of equation (1) may be measured experimentally; then $h = H_2 - H_1$ is determined as the difference

$$h = A - Q;$$

2) Internal stresses are removed when the alloy is heated and as a result the latent deformation energy is given out as heat. Therefore, if we denote by $H_1^{\vartheta_1}$, $H_1^{\vartheta_2}$ the enthalpies of a deformed alloy in an annealed condition and by $H_2^{\vartheta_1}$ and $H_2^{\vartheta_2}$ of a deformed alloy in an unannealed condition, we get

$$H_2^{\vartheta_2} - H_2^{\vartheta_1} = \sum \int_t^{t+k} Cpd\,\vartheta + l_1 + l_2 \ldots = q_2$$

(stressed)

$$H_1^{\vartheta_2} - H_1^{\vartheta_1} = \sum \int_t^{t+k} C'pd\,\vartheta + l_1' + l_2' \ldots = q_1$$

(unstressed)

whence $q_1 > q_2$,

$$(H_1^{\vartheta_2} - H_2^{\vartheta_2}) + (H_2^{\vartheta_1} - H_1^{\vartheta_1}) = q_1 - q_2. \qquad (2)$$

If we accept that $H_1^{\vartheta_2} = H_2^{\vartheta_2}$ then $q_1 - q_2 = h$, i.e. the latent deformation energy is equal to the difference between the heats of annealing of deformed alloys in the unannealed and annealed conditions. And the heat of annealing is determined by the method of measuring the true (and the "apparent", if the heating of the specimen is accompanied by internal processes) thermal heat capacity described in the work [29]. By determining at the same time the curve of thermal heat capacity – temperature, it is possible to record the temperature or the interval of temperatures, during which the evolution of latent deformation is taking place.

The second method was used in the present work for a corresponding investigation of aluminium and copper alloys (3 and 5%) after deformation (30%) under a drop hammer.

REVIEW OF REFERENCES

Investigations have been carried out on pure metals (see Table 1). Work with alloys (not counting different types of steel) was carried out only by Smith [3], Sato [4] and Tyzhnova [12].

The latent deformation energy was measured by the first of the described methods in most of the works. The second method was employed only by Sato [4] and Abramovich and his colleagues [10].

* *Fiz. metal. metalloved.*, 8, No. 1, 103-114, 1959.

TABLE 1. Data summary of works on latent deformation energy

Reference	Object of investigation	Type of deformation	Work imposed	Method of measuring work	Additional measurements
[1]	Iron (soft)	Elongation	0.02-0.1 cal/g	Elongation diagram	Amount of heat in calorimeter
[2]	Copper, steel, aluminium, (mono and polycrystals)	-do-	1–2 cal/g	-do-	Amount of heat by thermocouple
[3]	Copper, zinc, brass	Wire, original and annealed		Work not measured	Melting temperature
[4]	Copper, silver, aluminium, nickel, iron, steel, brass aluminium and nickel bronze, German silver	Torsion	1–24 cal/g	Torsion diagram	Latent energy 1) on heating curves 2) in calorimeter
[5]	Aluminium and copper annealed	Drawing wire in calorimeter	8–9 cal/g	Drawing work measured	Amount of heat in calorimeter
[6]	Steel, iron and copper	Torsion	Up to 14 cal/g	Torsion diagram	1) Amount of heat by thermo-couple 2) Amount of heat in calorimeter
[7]	Copper	Compression in a press	Up to 3.5 cal/g	Loading curve	Amount of heat by thermo-couple
[8]	Copper, aluminium, lead, tin	-do-	4–8 cal/g	-do-	-do-
[9]	Copper, aluminium, lead	Pendulum hammer	Up to 7 cal/g copper, up to 2 cal/g aluminium	Computed by weight of head and anvil, allowing for rebound	-do-
[10]	Low carbon steel	Upsetting by drop hammer	By 50% of height	Work not measured	"Aparent" thermal heat capacity
[11]	Copper, aluminium, iron	-do-		Weight of head × height (no allowance for rebound losses)	Amount of heat in mercury calorimeter for copper
[12]	Copper and copper-nickel alloys	Compression in a press		Pressure force and specimen height	Amount of heat by thermo-couple

The adopted methods of deformation vary considerably.

Deformation of specimens by striking, as in our work, was carried out only by Shelepukhin [9], Gubkin and Bashilova [11] and Abramovich [10].

Deformation work and the resultant evolution of heat were very carefully measured in the first work, but only pure metals were used in the experiments (Cu, Al, Pb and Sn) and not alloys. The work, computed as the product of the weight of the drop-weight

and the height of drop without a correction allowance (a very considerable one) for the drop-weight rebound, anvil reaction and friction of the guiding mechanism. The measurements were carried out rather roughly. The measurements of the heat, given out as a result of deformation, were carried out just as roughly (a copper specimen was inserted into a calorimeter filled with mercury).

The value of deformation work (related to the weight of specimen) varies considerably in different authors.

An analysis of the works referred to above permits one to make the following observations:

1) latent deformation energy depends on the type of deformation; for instance, for static compression [9, 11] it is less then for dynamic, and in the latter case it depends upon initial stroke velocity [9];

2) latent energy of the deformation of alloys, which are not stabilized solid solutions, is higher than the latent energy of pure metals.

In the work [4, 10] was determined not only the latent deformation energy but also its evolution temperature by heating.

As a result the author [4] arrives at the following conclusions:

1. The greater proportion of internal stresses in pure metals is maintained up to the temperature of recrystallization and suddenly disappears with a simultaneous change of structure. Recrystallization temperature decreases slightly with the increase of the degree of deformation.

2. In solid solutions the disappearance of internal stresses occurs spasmodically at temperatures characteristic for every alloy. The last stage of the disappearance of internal stresses coincides with recrystallization and, in the case of pure metals, depends on the degree of deformation.

Low carbon steel Y1 was studied in work [10]. Deformation of the specimens was performed by upsetting 50 per cent. Measured by Sykes's method was the true and apparent thermal heat capacity of undeformed and deformed specimens with a heating rate of 10-15 degrees/min, whereas Sykes's heating rate was only 1.4 – 1.6 degrees/min. Such a considerable increase of heating rate definitely did not permit the detection of latent deformation energy as the "apparent" thermal heat capacity. As a result it was found that the curves thermal heat capacity – temperature of deformed and undeformed specimens are the same.

SCOPE OF THE INVESTIGATION

An aluminium copper alloy (up to 6% Cu) is a solid solution in aluminium of θ-phase (Al_2Cu), and the solubility of copper in aluminium depends to a large extent on the temperature. This dependence has not been accurately determined and various authors have obtained different answers. On the basis of Dick's and Richardson's work [14] one should, apparently, accept the following data as the more reliable: (see Table 2. below).

Hence, solubility at temperatures around 20°C by extrapolation is about 1%. At temperatures above the equilibrium curve alloys of Al and 6% Cu are homogeneous solid solutions. With very slow cooling (annealing), processes of segregation of one of the components (Al_2Cu) take place in conformity with the reduction of the solubility of copper in aluminium. By very rapid cooling from a temperature, corresponding to complete solution of both components, to temperatures near 20°C, one may succeed in producing an unstable alloy condition, i.e. supersaturated solid solution, which will gradually pass into a stable (two phase) condition.

This transition proceeds slowly at room temperatures (natural ageing) at higher temperatures the transition is more rapid (artificial ageing). A not insignificant number of works have been devoted to the problem of the ageing of aluminium alloys with copper. In works [26, 22] it is asserted that during ageing phase θ (Al_2Cu) is not precipitated suddenly in a super saturated solid solution but an intermediate phase θ' is formed first which in composition corresponds to phase θ but does not yet possess its lattice structure. Phase θ' passes into θ at higher temperatures with different rates for each temperature.

EXPERIMENTAL METHOD

To determine latent deformation energy and the range of temperatures where this energy is given out during the heating of an alloy we adopted the method of measuring the "apparent" thermal heat capacity [29]. This method was used by Gruzin [16] and

TABLE 2.

ϑ, °C	548	430	400	350	300	200
Cu solubility (% weight)	5.65	2.0	1.4	0.95	0.74	0.5

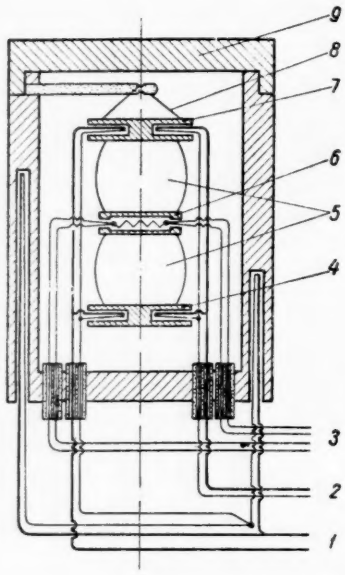

FIG. 1. Diagram of calorimeter and the shell.
1 – leads of differential thermo-couple;
2 – thermo-couple for measuring temperature of calorimeter;
3 – current and potential leads from heating coil;
4 – thermo-couple boxes;
5 – specimens;
6 – heater body;
7 – thermo-couple boxes;
8 – nichrome wire suspension;
9 – shell.

Abramovich [10].

The calorimeter used by us had an unusual form (Fig. 1). Its component parts were:

a heater – silver cylinder 6 (dia 25 mm, height 10 mm), inside this, in a drilled out hollow was a nichrome coil with a resistance of about 4 ohm; current and potential leads were connected to the ends of this coil – 3;

two flat silver boxes 4 and 7 (25 mm dia 4 mm high) – the main junction of the thermo-couples. The studied specimens – 5 consisting before deformation of two cylinders were inserted between the heater and each of the little boxes. Size of undeformed specimens – 20 mm dia, 30 mm high. The whole system (heater, specimens and little boxes with thermo-couples) were tied together with a nichrome wire and suspended inside a massive silver shell – 9 (88 mm dia, height 100 mm, wall thickness 10 mm, weight 4 kg) which was erected inside a tubular electric furnace.

The calorimeter temperature and the difference of the temperatures between the calorimeter and the shell, were measured by chrome-alumel thermo-couples.

The cold junctions of the thermo-couples were placed in well heat-insulated massive metal thermostat blocks, and their temperature was maintained constant within ± .01°.

TESTING THE CALORIMETER

The true thermal heat capacity of silver and aluminium were measured for testing the developed method. The whole calorimetric system consisted in the first case of silver (not counting an insignificant quantity of insulators). As it was intended to study later on specimens of different shapes (deformed and undeformed), silver and aluminium were employed in the form of cylinders.

The purity of silver used for the castings was not high enough (99.2% Ag; .50% Cu, .30% Pb. Fe and Mn – traces) and had a bearing upon the relative accuracy of measuring the real thermal heat capacity, which, in this case was equal ± 1%, whereas for pure metals it is ± .5%. At the same time it was established that the results did not depend on the shape of the specimens used.

A comparison of thermal heat capacity values obtained by us for silver with those found in literature [28] (Moser 1936) disclosed that our data was lower by 2% at 100° and by 6% at 500°.

The aluminium had the following impurities: .2% Fe; .08% Si; .01% each of Zn and Mg; .006% Cu. One pair of aluminium specimens were cast and not subjected to any treatment apart from turning, and the other pair were forged and then turned.

Size of cylinders

	Diameter	Height
1st shape	20 mm	30 mm
2nd shape	30 mm	17 mm

It was established, firstly, that there is no difference in the values of thermal heat capacity of forged or cast aluminium; secondly, a comparison of the obtained data regarding the thermal heat capacity of aluminium with those found in literature (Seekamp, 1931), shows that our data for aluminium differs from that in literature in respect of values and signs in the same way as for silver. The correspondence of these deviation values for aluminium and silver points to the presence of a systematic error in our measurements, evidently due to the unusual type of the calorimeter and also to a possible non-registration of certain thermo-couple recordings. The error could have been easily put right by the introduction

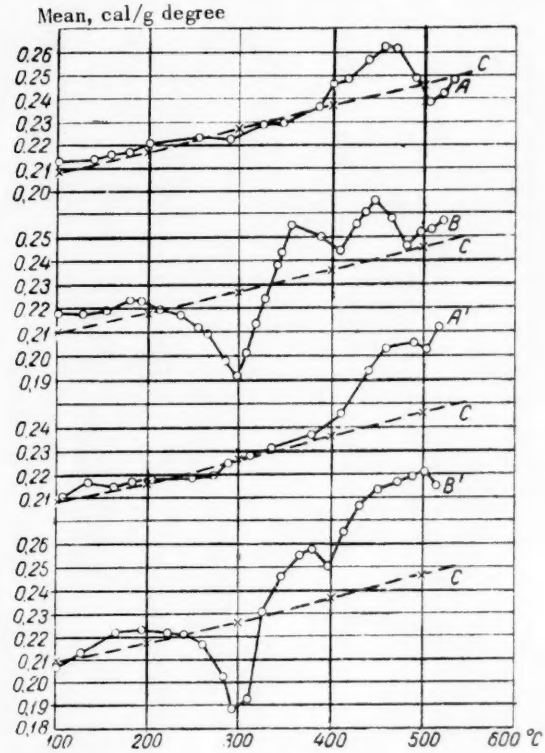

FIG. 2. Thermal heat capacity curves of aluminium alloys with different copper concentrations
A – annealed; B – hardened alloy condition (3% Cu)
A' – annealed; B' – hardened alloy condition (5% Cu)
C – additive curve of thermal heat capacity.

of a corresponding correction, however, for the purposes of this work there was no need to do this: the latent deformation energy is determined as the difference in accordance with formula (2).

RESULTS OF THE EXPERIMENTS

Undeformed specimens

Specimens of alloys of aluminium with copper (≈ 3 – 5% by weight Cu) were used for the investigations.

The original aluminium contained: 99.6% Al; .2% Fe; .1% Mg; .08% Si; .006% Cu. The 3% alloy was produced from this aluminium and a previously prepared hardener (50% Cu) in a graphite crucible in an electric furnace. The alloy was heated to 720° and poured into moulds at 690°, the cooled alloy was then forged and again annealed (5 hr at 460°).

The 5% alloy we succeeded in preparing from purer aluminium and the same hardener. An analysis of the original aluminium disclosed the presence of following impurities: .03% Fe; .006% Si; .02% Mg. The 5% alloy was prepared in the same way as the 3%. Chemical composition of the alloy produced was: 4.45% Cu; .15% Fe; .004% Si; .05% Mg, Zn – traces; the 5% alloy (the same as the 3%) was forged and annealed [5].

Studied were both the annealed and the hardened alloys.

The typical curves of thermal heat capacity – temperature are reproduced in Fig. 2.

The C curve was produced by averaging thermal heat capacity values. Each deviation of the true curves from the average furnish an indication of the presence in the tested specimens of some endothermic (the real curve higher than the average) or exothermic (real curve below the average processes. The movement of the curve of the "apparent" thermal heat capacity of these alloys is very complex (especially for the hardened condition), which testifies to the presence in them of processes accompanied by heat effects.

Annealed condition – two phase system. Up to 360-380° the curves A, A' run close to the additive curve. Above this temperature they rise sharply (process of copper dissolution) and then, near 480°, the curve A comes down again towards the additive curve and the curve A' does not descend

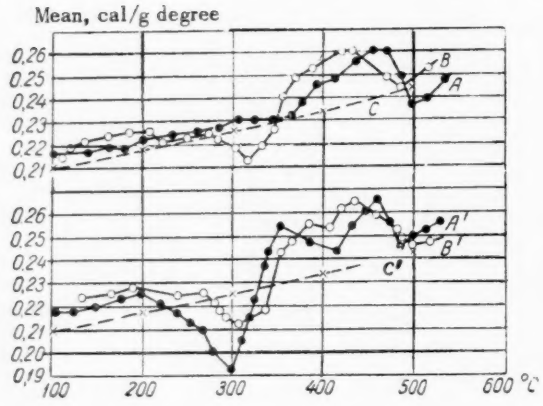

FIG. 3. Values of thermal heat capacity of annealed and hardened specimens of copper-aluminium alloy (3% Cu) for three consecutive heatings;
A – first heating of annealed specimen;
BC – second and third heatings (dark spots) of the same specimen;
A' – first heating of hardened specimen;
$B'C'$ – second and third heatings of the same specimen (coincide).

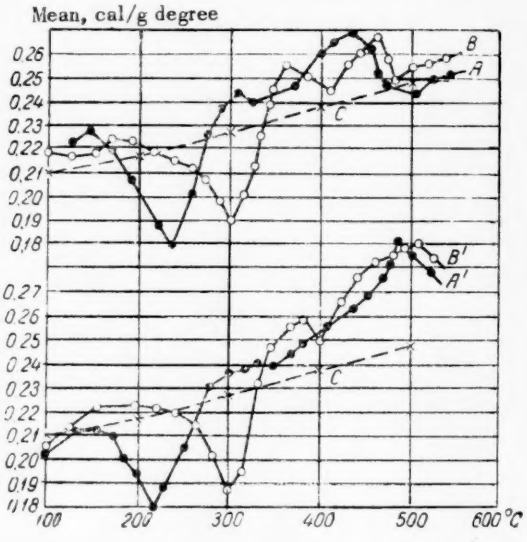

FIG. 4. Thermal heat capacity of copper-aluminium alloy:
A, A' – deformed condition (A – 3% Cu; A' – 5% Cu);
B, B' – undeformed condition (B – 3% Cu; B' – 5% Cu).

towards the additive curve even at the final temperature of the experiment (520°) (the dissolution process has no time to be completed at such heating rates).

Tempered condition – supersaturated solid solution. The curves $B - B'$ closely follow the additive curve in the region of 200-220°. Characteristic for the 220-350° range is the sharp drop of the "apparent" thermal heat capacity, connected with the process of the precipitation of copper from the super-saturated solution.

Above 350° the curves rise very sharply – the dissolution of copper is taking place. At 400°, characteristic for curves B and B', is the existence of a small and sufficiently sharp minimum. Sykes [15] explains this as the thermal effect of the transition of phase θ' to the stable θ phase. Likewise, as in the annealed condition, the B curve approaches the additive in the region of 480°, and this approach is not observed in curve B' (dissolution process is not completed).

Furthermore, one may note, that the curves thermal heat capacity – temperature are always the same for different tempered alloys within the accuracy limits of the measurements, whereas the curves of the annealed – differ up to 7 per cent. Possibly, this may be explained by the shortcomings of the annealing conditions employed by us.

After the measurements of thermal heat capacity the specimen was cooled in the oven, comparatively slowly (from 520° to 80° in 16 hr). The condition of the specimen attained in this way could not be described either as annealed or tempered. Let us call it "half-hardened".

It transpired that a half-hardened condition is reproduced just as well as a hardened. The curve A Fig. 3 characterizes a hardened condition of a 3% alloy; the curves BC and $B'C'$ – the same specimens in a half-hardened condition. These curves, obtained in two experiments; (second experiment – dark spots) are represented by one curve, that is they coincide within the accuracy limits of the measurement. Consequently, even the half-hardened condition is reproduced independently of the fact as to whether the specimen was first annealed or hardened.

Deformed specimens

The deformation of the specimens was carried out

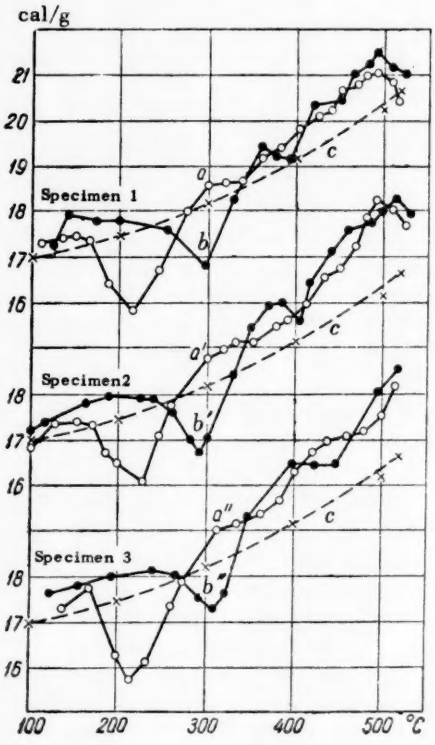

FIG. 5. Thermal heat capacity of specimens of an aluminium and copper alloy (5% Cu) when heated after deformation:
a, a', a'' – first heating,
b, b', b'' – second heating;
C – additive.

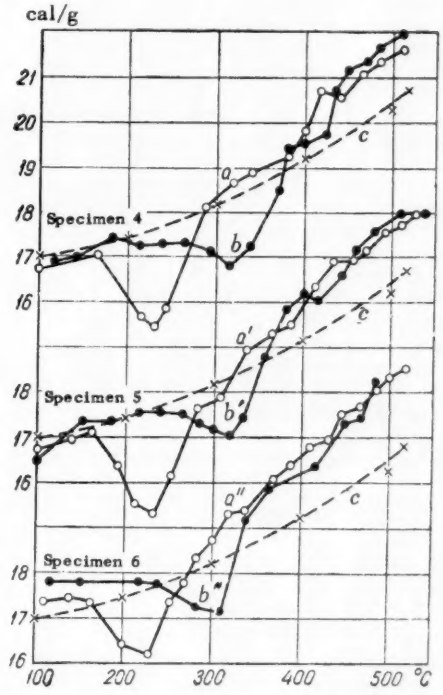

FIG. 6. Thermal heat capacity of specimens of an aluminium and copper alloy (5% Cu) when heated after deformation:
a, a', a'' – first heating;
b, b', b'' – second heating;
C – additive.

in a vertical drop hammer by a free falling drop-weight. Degree of deformation was determined roughly – by the altered height of the specimen. To obtain the same alteration for all samples (30%), the specimens were placed during deformation within a restricting ring, which permitted an alteration of the height of the specimen only by a definite proportion. Only hardened or half-hardened alloys were subjected to deformation because annealed specimens did not yield reproducible thermal heat capacity results.

Let us compare the thermal heat capacity-temperature curves corresponding to deformed and undeformed specimens (Fig. 4). Curves A and A' relate to the deformed specimen, curves B and B' – to the undeformed specimen. Comparing curves A, A' and B, B' one may notice for the deformed condition a sharp shifting of the copper precipitation region in the direction of low temperatures, both for the 3% (A and B) as well as the 5% (A' and B') alloys. This indicates that in a deformed condition the processes connected with diffusion proceed at rates adequate for detection at lower temperatures, than those in the undeformed condition. Furthermore, one may record, that the displacement of the minimum of apparent thermal heat capacity along the temperature axis is by the same amount, irrespective of the composition of the alloy.

It is especially important to note that the difference $q_1 - q_2 = h$, is found to be not a constant value, and is not infrequently, a negative one. This proves that by heating deformed and undeformed alloys to the same temperature an identical thermodynamic condition is not reached, i.e. in equation (2)

$$H_1^{\vartheta_2} \neq H_2^{\vartheta_2},$$

and consequently it is not possible by such a comparison to determine the latent deformation heat as it was done, for instance, by Abramovich and his colleagues.

The latent deformation heat, as it follows from equation (2), may be determined by the "apparent" thermal heat capacity only in such a case, when the ultimate condition of the alloys is the same after

they had been heated to the same temperature, i.e. when

$$H_1^{\theta_2} = H_2^{\theta_2}.$$

If $H_1^{\theta_2}$ is not equal $H_2^{\theta_2}$ for deformed and undeformed conditions, one may still assume that

$$H_1^{\theta_2} \text{ and } H_2^{\theta_2}$$

will be equal or near to each other for two specimens: one first half-hardened and then deformed and the other – also first half-hardened and deformed and afterwards again hardened.

With this assumption the determination of latent deformation heat is reduced to:

1) deformation of half-hardened specimen;

2) determination of

$$H_2^{\theta_2} - H_2^{\theta_1} = q_2$$

after the first heating and

$$H_1^{\theta_2} - H_1^{\theta_1} = q_1$$

for the second and subsequent heatings.

Such experiments were carried out with 6 pairs of specimens of a 5% half-hardened alloy. Thermal heat capacity-temperature curves obtained for several heatings are given in Figs. 5 and 6.

These experiments permit us to draw the following conclusions:

1) For all six pairs of specimens less heat is used up for the first heating than for subsequent heating of the same specimens in the same interval of temperatures, i.e. $q_2 < q_1$.

2) The difference

$$H_2^{\theta_1} - H_1^{\theta_1} = q_2 - q_1 = h,$$

i.e. latent deformation heat, related to 1 g of alloy in these experiments was found to equal:

for 1st. pair of specimens (Fig. 5) 1.9 cal/g;
for 2nd. pair of specimens (Fig. 5) 1.4 cal/g;
for 3rd. pair of specimens (Fig. 5) 2.3 cal/g (average 1.3 ± .6);
for 4th. pair of specimens (Fig. 6) .7 cal/g;
for 5th. pair of specimens (Fig. 6) .4 cal/g;
for 6th. pair of specimens (Fig. 6) 1.0 cal/g.

3) On the curves of the first heating of all 6 specimens it is not possible to mark off the temperature ranges, where the evolution of latent energy was evidenced by a sharp leap; the effect of the evolution of latent energy is "dispersed" along the temperature axis and is therefore not observed. Thus, Sato's assertion, mentioned above, about a spasmodic evolution of latent deformation energy in bounds during the heating of alloys on the example of the Al-Cu alloy, is not confirmed.

As the determination accuracy constitutes ≈ 50%, the adopted method of determining the latent deformation heat permits us to determine only the order of this value and not the value itself if, of course, the deformation work in a drop hammer with a restricting ring was alike for all specimens.

The inaccuracy is explained by the fact that highest value of the latent deformation energy is determined as the difference between two very large magnitudes – the quantities of heat used for annealing the alloy. The value of the latent energy is about 1% of the total quantity of heat required for heating the entire calorimeter system.

Translated by A. Allan

VOL 8 195

REFERENCES

1. H. Hort, *Uer. Deut. In.*, 50, 1831 (1906).
2. W.S. Farren and G.I. Taylor, *Proc. Roy. soc., Lond.*, 107, 422 (1925).
3. C.S. Smith, *Proc. Roy. soc., Lond.*, 125, 619 (1929).
4. T. Sato, *Sc. Rep. Tohoku, Univ.*, 20, 140 (1931).
5. W. Rosenhaim and V. Stott, *Proc. Roy. soc., Lond.* 140, 9 (1933).
6. G.Y. Taylor and H. Quinney, *Proc. Roy. soc., Lond.*, 143, 307 (1933/34).
7. N.F. Kunin and G.V. Senilov, *Trud. Siberian Physico-technical Institue*, 4, 132 (1936).
8. A.A. Fedorov, *Zh. teor. fiz.*, 11, 999 (1941).
9. P.R. Shelepukhin, *Disseratsiya (Tsit. po knige V.D. Kusnetsova' Fizika tverdogo tela'*, (1941).
10. R.A. Abramovich, P.L. Gruzin, G.V. Kurdiumov and R.I. Entin, *Zh. teor, fiz.*, 11, 1083 (1941).
11. S.I. Gubkin and N.I. Bashilova, *Symposium:, Deformiruyemost' tsvetnykh splavov (Deformation of*

non-ferrous alloys) Iz. Akad. Nauk SSSR, (1947).
12. N.V. Tyzhnova, *Zh. teor. fiz.*, 16, 1389 (1946).
13. *Struktura binarnykh splavov (Structure of binary alloys)* 1, 104 (1941).
14. E.H. Dick and H.H. Richardson, *Z. Metallk.* 18, 196 (1926).
15. C. Sykes, *Proc. Roy. soc., Lond.*, 148, 422 (1935).
16. P.L. Gruzin, *Zav. lab. (The factory laboratory)* No. 11, 1266 (1938).
17. P.D. Merica, *Trans. Amer. Inst. Min. Met. Eng.*, 99, 13 (1932).
18. J. Jeffries, *Inst. Met.*, 22, 329 (1919)
19. Kanno, *Sc. Rep. Tohoku, Univ.*, 11, 269 (1922).
20. D. Hanson and L.V. Gaylor, *J. Inst. Met.*, 24, 201 (1920); 26, 321 (1921); 27, 267 ; 28, 213 (1922); 30, 139 (1923).
21. R. Karnop and G. Sachs, *Zs. Phys.*, 49, 480 (1928).
22. M.I. Zakharova, *Dissertatsiya, Moscow State University,* (1948).
23. S.T. Konobeyevskii, *Zh. eksp. teor. fiz.*, 13, 185 (1943).
24. N. Swindell and C. Sykes, *Proc. Roy. soc., Lond.*, 168, 237 (1938).
25. S. Kokubo and K. Honda, *Sc. Rep. Tohoku Univ.*, 19, 365 (1930).
26. G. Wassermann and J. Weerts, *Metallwirt.*, 14, 605 (1935).
27. C. Sykes, *J. Inst. Metals*, No. 2, 257 (1936).
28. H. Moser, *Phys. Zs.*, 37, 737 (1936).
29. M.M. Popov and G.L. Gal'chenko, *Zh. obs. khim.* 21, No. 12. (1951).

VOL.
8
1959

ON THE SUBJECT OF "SUPER-DUCTILITY" OF ALLOYS*

A.A. PRESNYAKOV and V.V. CHERVYAKOVA

(Received 25 May 1959)

Some new facts relating to super-ductility in the systems Al-Zn and Al-Cu are quoted in this article and a conclusion is drawn about the connexion of this phenomenon with the crystalline lattice condition of the alloys.

The phenomenon of super-ductility, first referred to in work [1] as the result of a new mechanism of ductile deformation, called by Bochvar [2] "solution-precipitation", is of considerable theoretical interest from the point of view of a relationship between the mechanical properties of an alloy and its structure and, what is particularly important, the alteration of this structure during the deformation process at increased temperatures.

As it is known from the papers [3, 4] the application of external stress under conditions of raised temperatures is accompanied by profound changes in the structure of solid solutions. A stressed condition, by promoting a rearrangement of atoms of the components of the alloy, facilitates the processes of segregation, the formation and growth of a nucleus of a new stable phase for the particular phase conditions. The movement of atoms arising in molten elements, because of an increasing diffusion in the direction of the gradient of stresses, in its turn, reduces internal stresses and thus leads to a reinstatement of the normal condition of the crystalline lattice distorted during the process of ductile deformation. All these processes find a reflection in the origination of a special alloy condition as a result of a combination of certain definite deformation conditions.

Certain data relating to super-ductility are quoted in this work, which were obtained in the course of a systematic study of the influence of temperature on the ductility of aluminium alloys.

A super-ductility effect was observed by us in a cast eutectic alloy of Al-Cu (33% Cu) during its static tension in the region of 500° and higher [5]. Tests of this alloy in a homogeneous and hardened condition, as well as of cast specimens under dynamic loading, did not disclose any traces of this effect.

Microphotographs of a eutectic alloy, shown in Figs. 1 and 2, offer an idea of the coarse structure of cast eutectics, characterized by a needlelike structure of the lamellae, elongated towards the centre of the casting (Fig. 1a) and of the uniform fine crystalline structure of the same alloy after homogenization (Fig. 2). To discover the character of the microstructure at the moment of deformation, when the alloy displays super-ductility, a microsection of the specimen was heated to 525°, held at this temperature for 15 min and then hardened. As a result of this treatment the needlelike grain in some places (Fig. 1b) lost its clear outline and the texture of a casting, although the general character of a coarse structure has not changed. It should be mentioned that further polishing of the microsection for 3-5 min changed considerably the microstructure of the alloy (Fig. 1, c-d). Partial segregation had taken place; along the edges of the needlelike grain are seen formations of the second phase.

In some places one can still see traces of the needlelike outlines (Fig. 1, c) but in others (Fig. 1, d) where the casting orientation was already lost during the heating, no traces are left of the former coarse structure.

Microphotograph in Fig. 3a characterizes the structure of the same alloy after tension at 525° (one of the temperatures at which super-ductility is observed). A highly dispersed uniform structure illustrates the profond changes in the structure of the alloy which have taken place during the process of deformation.

The microstructure of the homogenized eutectic, as well as of the one hardened after deformation had not changed at all (Fig. 2a). At the same time the degree of ductility has not left the limits of usual values [5].

The appearance of super-ductility during the stretching of a cast aluminium eutectic could not be explained by a mere change of solubility in a solid

* *Fiz. metal. metalloved.*, 8, No. 1, 114-122, 1959.

VOL
8
195

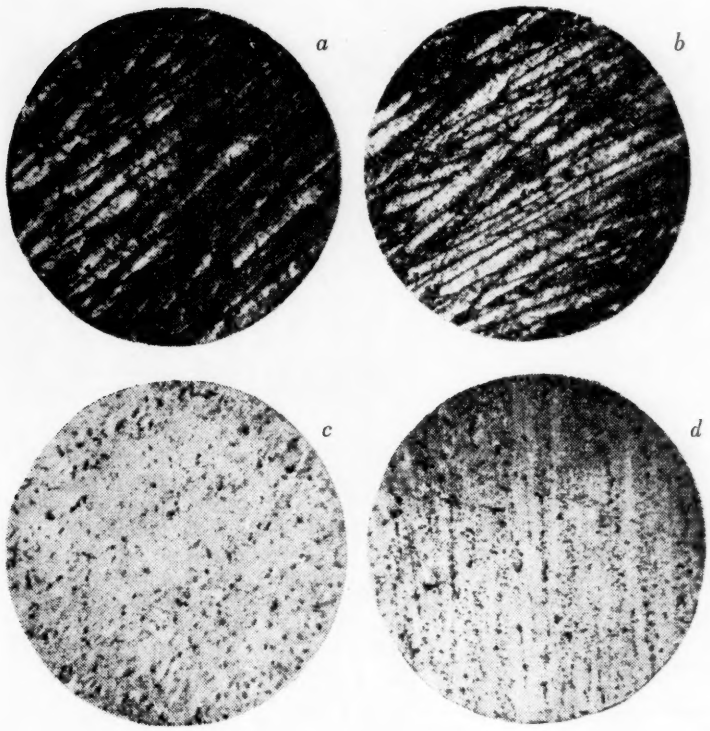

FIG. 1. *a* – microstructure of cast eutectic Al-Cu in ordinary conditions;
b – microstructure of cast eutectic Al-Cu after heating to 525° and keeping at that temperature for 15 min (after additional polishing for 3-5 min);
c, *d* – microphotographs of microsection.

condition, because in a homogenized and hardened alloy, characterized by a finer structure and consequently a larger contact area of the interacting phases, the mentioned effect was not observed.

Describing the solution-precipitating mechanism of ductile deformation Bochvar [2] mentioned the possibility of the appearance of super-ductility purely because of the precipitating stage in the course of deformation, if the solution was accomplished beforehand.

For a clarification of the mechanism leading to the appearance of super-ductility in such a case, experiments were carried out for the study of the crystalline structure of eutectic Al-Cu, when passing from a cast to a deformed condition (when super-ductility arises) by means of X-ray structure analysis and by the method of micro-hardness.

When casting specimens of a eutectic alloy, to a certain extent a hardened "melt" was obtained with a much higher concentration of copper in it compared with an equal weight of a saturated solid solution, with a coarse structure of large blocks [6]. This may be seen in Fig. 4, a-b and is confirmed by a parameter study of a solid solution of copper in aluminium*.

High temperature deformation produces an intensive segregation of metastable eutectic accompanied by a sharp increase of the cubic phase parameter and the appearance of a fine uniform structure (Fig. 3). Such a break-up should be accompanied by a great diffusion movement of the atoms, in accordance with the peculiarity of the mechanism and the kinetic energy of eutectic segregation [7].

When studying Al-Zn systems, alloys were tested with a contents of Zn shown in Table 1.

The method of preparing Al-Zn alloys and the testing of the specimens did not differ from those adopted for Al-Cu alloys.

* Eutectic Al-Cu, shown in Fig. 4, was obtained by pouring it on to a polished surface, in order to avoid a distortion of its structure when analyzing the metastable alloy in the original condition.

VOL. 8 1959

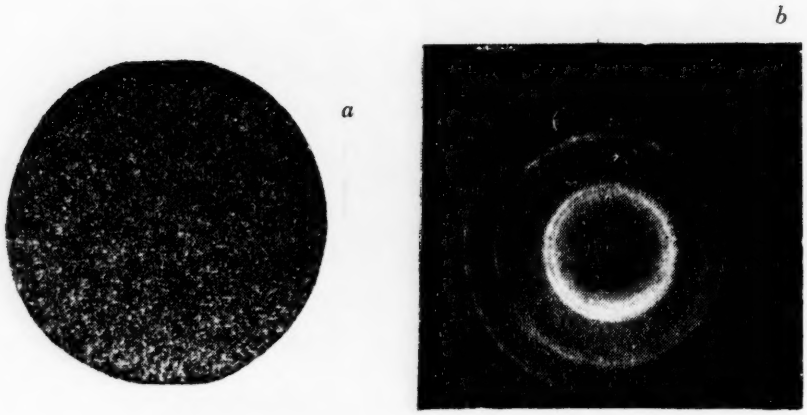

FIG. 2. *a* – microstructure of eutectiferous alloy Al-Cu in a homogenized state and ordinary conditions;
b – X-ray diagram of homogenized Al-Cu eutectic.
Etching reagent – 20% NaOH solution; × 96.

TABLE 1. Zinc content of the alloys

Alloy mark	Zinc content, %	Alloy mark	Zinc content,%
41	5.0	76	76.0
15	15.0	78	78.0
42	23.5	79	79.0
43	34.2	47	80.0
44	48.1	82	82.0
45	57.8	48	88.6
46	71.6	95	95.0

The thermal treatment routine was the following: homogenization at 400° (excluding 82-95 alloys) for 168 hr. Alloys 82-95 were kept for the same time at 350°. Quenching from temperatures of 400; 375 and 300° (2 hr exposure) in ice water.

Alloys containing 71 to 88 per cent Zn proved to be super-ductile tested in a quenched condition. Greatest elongation was noted, as in work [1], in the alloy containing 80 per cent Zn. Contraction, equal to 1.00 in this alloy, was observed beginning at 20° (although elongation did not then exceed 66.8 per cent).

At a higher temperature the value δ increased sharply, reaching more than 648 per cent at 250 and 275° (it was not possible to rupture the specimens at those temperatures because of testing equipment capacity). At 300° ductility dropped sharply, maximum elongation amounted to 148 per cent and it was observed in the 82 per cent Zn alloy; elongation of the 80 per cent Zn alloy at 300° was 60 per cent.

As shown in Fig. 5, the ductility isotherms, given for the interval 57.8 – 88. 6 per cent Zn, form typical single spots up to a temperature of 275°, corresponding to an 80 per cent Zn composition, and the top ones are located on the isotherms corresponding to 275 and 250°.

The microstructure of an alloy, containing 80 per cent Zinc, hardened from 375° (Fig. 6a) and then heated to 250° and kept at that temperature for 15 min before deformation (Fig. 6b), is characterized by a well dispersed structure with unevenly distributed sections where breaking up of the solid solution is noticed. An intensive break up with noticeable (without special instruments) heat evolution occurs during the first few minutes after hardening of the eutectoid alloy (which conforms to the data in papers [8, 10]) up to a certain degree of stability, which is, probably, maintained up to the moment of deformation (i.e. in our working conditions from 30 min to 24 hr and more). Final segregation takes

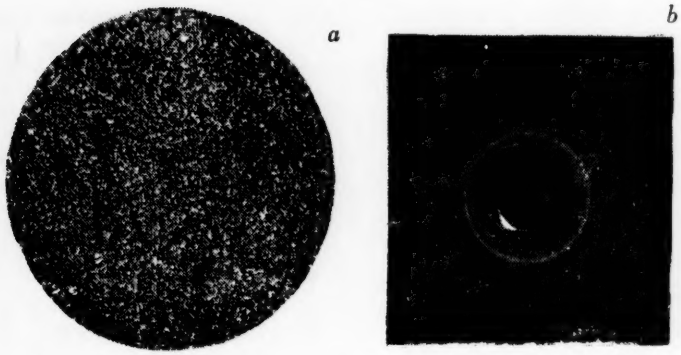

FIG. 3. *a* — structure of a cast Al-Cu eutectic after tension at 525°, *b* — X-ray diagram of a cast Al-Cu eutectic after tension at 525° and the appearance of super-ductility.

VOL. 8 1959

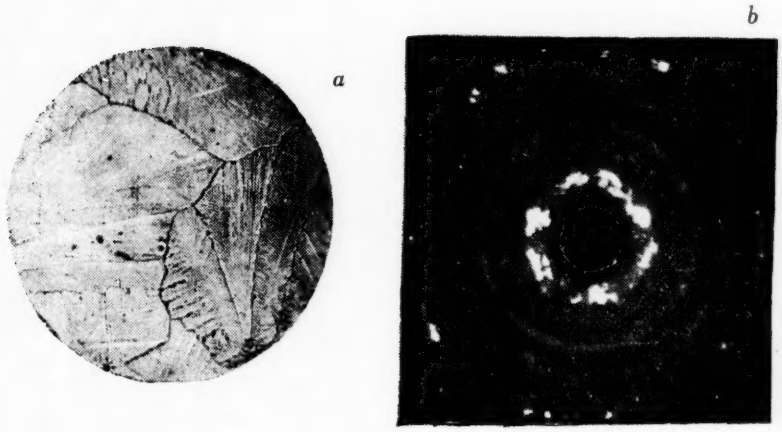

FIG. 4. *a* — microstructure of Al-Cu eutectic, poured on to a polished surface (without polishing and etching) × 96; *b* — X-ray diagram of cast Al-Cu eutectic, obverse view.

place during the process of deformation at increased temperatures. The structure of the alloy obtained in this way (Fig. 6a) is very uniform and highly dispersed.

The super-ductility effect does not depend qualitatively on the hardening temperature (300; 375 or 400°) so long as the hardening takes place above the transformation temperature (275°); however, quantitatively this effect becomes apparent more sharply with hardening from 400 and 375°, than with hardening from 300°.

Cast and homogenized alloys produce only a "splash" of super-ductility within a narrow temperature interval contiguous to the temperature of the eutectoid transformation. (i.e. a sharp rise of the ductility curve and just as sharp a transition to the brittle state at a small change of temperature). However, the ductility parameters in such a case never attain a value, which is observed when testing alloys of the "eutectoid interval" in a hardened condition.

It is particularly necessary to record the change of strength of hardened alloys in a super-ductility state. As mentioned already, a slight but still noticeable load is only fixed during the first moment of elongation, and then the dynamometer pointer drops to zero reading and the entire deformation process, in a state of super-ductility continues at this reading of the instrument. The alloys have the lowest strength (as it is seen in Fig. 7) at a temperature of 275° and then the strength begins to increase in the region of 300°, and with a further rise of temperature a gradual steady reduction of strength is again observed.

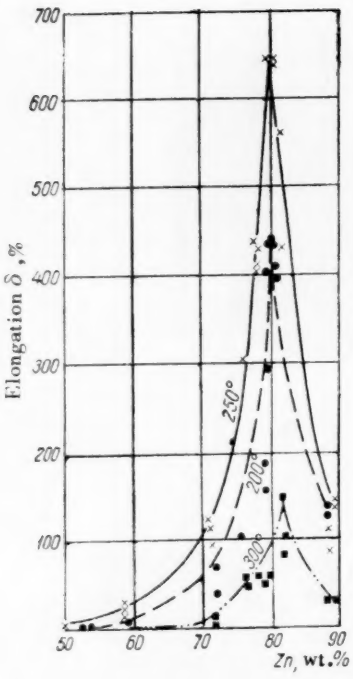

FIG. 5. Al-ZN plasticity isotherms, depending upon zinc concentration, when tested in a condition hardened from 375°.

Thus, as shown by the results of the examination of the systems Al-Cu and Al-Zn, a necessary condition for the appearance of super-ductility, is the existence of metastability in the whole mass of crystals of the alloy under examination and a rate of deformation, commensurate with the rate of their break up at sufficiently high temperatures, ensuring the necessary mobility of atoms.

If a eutectiferous alloy Al-Cu is poured into a graphite mould, which has not been specially heated beforehand, this leads to a certain degree of fixing of the eutectiferous alloy. As proof of eutectic metastability in a cast condition, serve the sharp change of the structure of the alloy and the parameter of α-solution as a result of subsequent high temperature processing: either prolonged homogenizing annealing or a short time heating and deformation with the appearance of a condition of super-ductility.

Super-ductility, which occurs during the testing of a number of hardened alloys in the system Al-Zn, is obviously the results of a powerful diffusional movement of atoms, which accompanies the segregation process of a solid solution, in the direction of the applied load. The presence and the kinetics of this segregation were at one time studied in the papers [11-13]. Hansen, on the basis of these investigations came to the conclusion that during the eutectoid segregation of β-crystals "recrystallization arises, caused by an intensive diffusional process". Apparently this process, intensified by the influence of temperature, attains additional speed and a definite direction under the influence of an applied external load.

The alloy deforms during complete absence of an arrangement order and an unusually low deformation resistance.

The decisive part of eutectoid segregation in this phenomenon is confirmed by the following facts:

1. When hardening takes place at temperatures below 275°, when metastability combined with eutectoid transformation is absent, super-ductility disappears as well.

2. Super-ductility is not observed during deformation of hardened specimens heated to 300°; tests at this temperature characterize ductile properties of a highly alloyed balanced solid solution.

3. Super-ductility is more sharply pronounced when hardening from higher temperatures, which in such a case is naturally explained by a higher degree of metastability of the alloy and consequently, greater mobility of the atoms during segregation.

4. Homogenized alloys, containing almost the completely segregation phase prior to deformation, as a rule, do not display a special condition. A slight effect observed when they are tested near the transformation temperature is probably due to an insufficient stabilization degree during the process of homogenization.

5. Ductility depends on the mass of the substance capable of segregation. A eutectoid alloy consists of such an "active" mass; the more an alloy differs from a eutectoid composition, the greater is the quantity of "inert" mass, which does not participate in segregation and impedes the intensity of diffusional flow; at a certain eutectoid content, super-ductility disappears completely.

6. A cast alloy possesses a considerable degree of metastability, which is the cause of the phenomenon of super-ductility in eutectic Al-Cu, despite its coarse structure in comparison with the structure of a homogenized alloy. Crystallization of Al-Zn in ordinary conditions [8], distorts considerably the composition of the crystals, which is the most important cause for the absence of an uninterrupted even flow of atoms within the whole volume during deformation.

7. Segregation of metastable eutectic Sl-Cu as well as eutectoid Al-Zn, probably occurs in two stages. The first stage in both cases proceeds

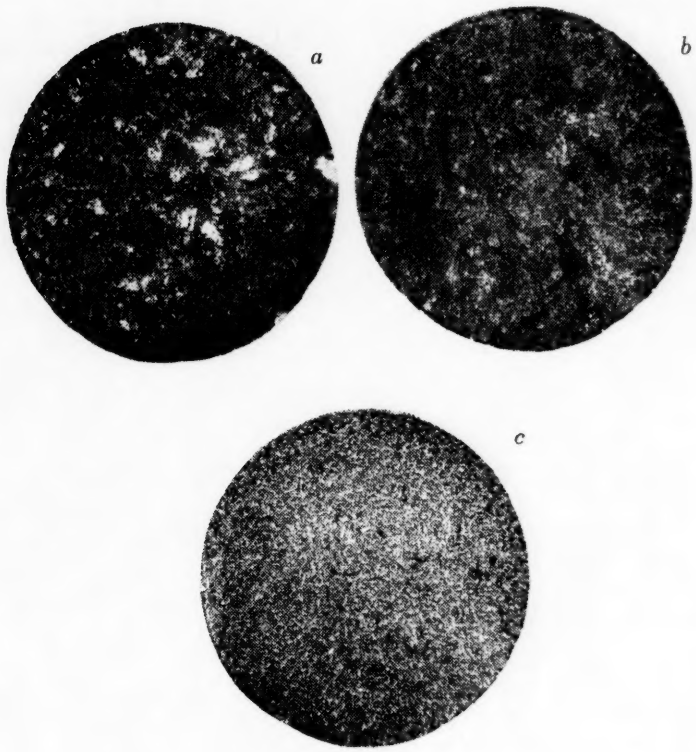

FIG. 6. *a* – microstructure of aluminium alloy containing 80 per cent Zinc, hardened from 375°;
b – microstructure of this alloy, heated to 250° (after hardening from 375°) and kept at that temperature for 15 min;
c – microstructure of alloy, containing 80 per cent Zinc after deformation at 260° in a hardened condition. Etched with 20 per cent solution of NaOH; × 96.

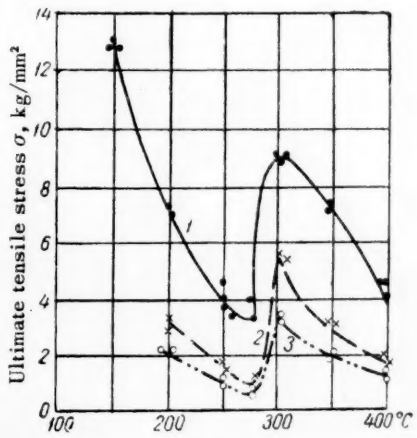

FIG. 7. Change of strength depending on temperature of some alloys in the system Al-Zn, when tested in a hardened condition;
1 – 71 per cent Zn;
2 – 76 per cent Zn;
3 – 80 per cent Zn.

VOL. 8 1959

spontaneously without external influence: in the eutectic Al-Cu, during the process of crystallization, and in the eutectoid Al-Zn, during the hardening process (proved by X-ray interferences, characterizing the presence of two phases in the alloy). The second segregation stage, or complete stabilization of the alloy proceeds only at high temperatures and the application of stresses of a definite magnitude. Obviously, super-ductility arises at this stage.

8. Sharp reduction of strength, accompanying super-ductility, is evidently connected with a weakening of the interatomic bond, taking place during the reconstruction of the crystalline lattice.

In this way, data about super-ductility, obtained by us in the course of a systematic study of aluminium alloys, leads to the conclusion of the connexion of this phenomenon with the condition of the crystalline lattice of the alloy and certain definite processes inside it, occurring as a result of temperature changes and the application of stresses.

Translated by A. Allan

REFERENCES

1. A.A. Bochvar and Z.A. Sviderskaya, *Izv. Akad. Nauk SSSR, Department of technical Sciences,* No. 9 (1945).
2. A.A. Bochvar, *Izv. Akad. Nauk SSSR, Department of technical Sciences,* No. 5 (1948).
3. S.T. Konobeyevskii, *Zh. expt. teor. fiz.,* 13, No. 6 (1943).
4. K.A. Osipov, *Izv. Akad. Nauk SSSR, Department of technical Sciences,* No. 9 (1949).
5. A.A. Presnyakov and V.V. Chervyakova, *Izv. Akad. Nauk SSSR, Department of technical Sciences,* No. 3 (1958).
6. A.A. Presnyakov and V.V. Chervyakova, *Vestnik Akad. Nauk SSR,* No. 12 (1958).
7. A.A. Bochvar, *Issledovanie mekhanizme ikinetiki Kristallizatsii Splavov evtektieheskogo tipa (Analysis of the mechanism and kinetics of the crystallization of alloys of a eutectic type) United Scientific and technical Press, Moscow, Leningrad,* (1933).
8. V. Fuss, *Metallurgia aliumima i Yego splavov (Metallurgy of aluminium and of its alloys)* Moscow, (1937).
9. Bauer und Heidenheim, *Z. Metallk,* 8, 221 (1924).
10. J. Rosenheim, *J. Inst. Met. London,* 30, 3 (1921).
11. Frankel und Wachsmith, *Z. Metallk,* 20, 162 (1930).
12. Frankel und Spanner, *Z. Metallk,* 19, 58 (1927).
13. Schmidt und Wasserman, *Metallwirtschaft,* II, 386 (1932).
14. M. Khansen, *Struktury binarnykh splavov (Structure of binary alloys) Metallurgizdat,* (1941).

VOL 8 195

INFLUENCE OF STRESS CONCENTRATION ON FATIGUE ENDURANCE OF STEEL*

E.M. SHEVANDIN, L.F. KURDINKOVA and L.M. RUBINSHTEIN

(Received 25 May 1958)

VOL. 8 1959

Fatigue failures occur, as a rule, at points of stress concentrations, caused either by the geometrical contours of the construction (cut-outs intermittent jointing, sharp re-entrant angles etc) or the structure of the metal (natural cracks, scale inclusions, porosity etc). Therefore, a systematic study of the problem of the influence of stress concentrators on the fatigue endurance of steel, is undoubtedly of some interest.

Some investigators [1-9] have established the unfavourable role of stress concentrators and the considerable lowering of the fatigue endurance of steel, connected with it. It is partially shown in these investigations that the effective coefficient of stress concentration differs from the theoretical by a degree the greater, the higher the property possessed by the steel of reducing stress concentration peaks by local plastic deformation and, consequently, the lower its sensitivity to notching.

These investigations also contain about the relationship of the sensitivity to stress concentration and the character of sectional stress distribution, the gradient of stresses and size of the component.

In the present work changes ot fatigue endurance of steel were studied during a successive sharpening – reduction of the radius of the notch base.

MATERIAL AND INVESTIGATION METHOD

Hot rolled steel sheets 10-12 mm thick, mark St. 3, 20G. 30G and SKS-1 (see Table 1) were used for the investigations.

Tests were made in tension – compression and cyclic bending, in both cases with a symmetrical cycle with a base of 5×10^6 cycles and additionally on smaller bases.

Tests of the first kind were carried out on a Losenhausen pulsator of 5t. capacity and of the second kind on small machines of the Löhr-Schenk type. Centering of specimens during tension-compression tests was ensured by grips of a special design, and their working reliability was checked several times by statistical loading of the specimens by means of resistance extensometers pasted to the opposite sides of the specimen. For bending tests, centering of the specimens was ensured by the construction of the collets of the testing machines and a corresponding setting of the specimens; the beat did not exceed 0.01 to 0.02 mm.

For the tension-compression and bending tests, plain and notched specimens were used (Figs. 1 and 2). Radius of the notch of the notched specimens used in tension-compression tests varied from 2.5 to 0.05 mm, and for bending tests – from 3.0 to 0.1 mm.

The specimens in tension-compression tests were produced by special technology, and dimensional symmetry in relation to the axis was ensured with an accuracy of ± 0.01 mm. Each notched specimen was checked under a microscope in respect of the symmetry of the side notches in relation to the axis and the degree of coincidence of their bases along the vertical. Only such specimens were chosen for the tests, whose corresponding deviation did not exceed 0.05 mm. The absence during tests of scattered data, exceeding the normal, confirmed the sufficient accuracy in the preparation of the specimens and reliability of their centering.

RESULTS OF THE TESTS AND THEIR CONSIDERATION

Graphs, characterizing the basic dependence of the fatigue endurance of steel on the magnitude of the concentration of stresses during tension-compression and bending, are shown by the co-ordinates ultimate endurance – stress concentration coefficient, and also by co-ordinates ultimate endurance – inverse value of the notch radius $1/\rho$ (in mm^{-1}). The last method of plotting was utilized, because the coefficient of the concentration of stresses is basically characterized by the magnitude $1/\rho$, whose determination is easier that that of the full value α_k.

The results of the tension-compression tests are shown in Figs. 3-4. The bending test results are characterized by curves of the same kind and they

* *Fiz. metal. metalloved.*, 8, No. 1, 122-130, 1959.

TABLE 1. Mechanical characteristics of steel tested in fatigue endurance

Steel	Elongation limit σ_m kg/mm²		Temporary resistance σ_B kg/mm²		True shear resistance S_k, kg/mm²		Relative elongation σ_s, %		Relative compression ψ, %	
	With the grain	Across the grain	With the grain	Across the grain	With the grain	Across the grain	With the grain	Across the grain	With the grain	Across the grain
St. 3	23.0	24.5	42.5	44.5	91.0	86.0	30.5	28.5	65.0	58.0
20G	42.0	44.5	64.0	67.0	159.0	129.0	24,5	26,5	71.5	55,5
30G	48.5	47.0	72,0	71,5	152.0	120.0	23.0	19.0	67.5	51.0

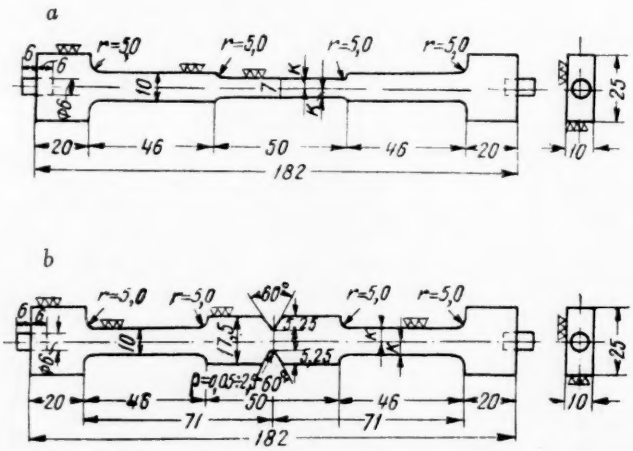

FIG. 1. Diagrammatic representation of specimens for tests in tension – compression:
a – plain specimen; *b* – notched specimen.

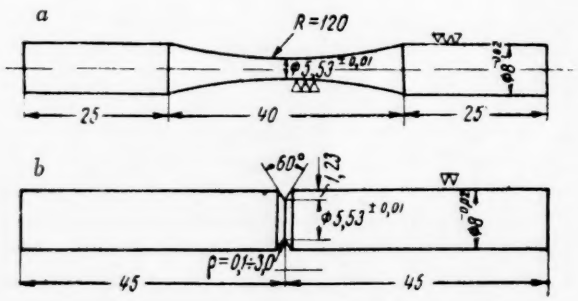

FIG. 2. Diagrammatic representation of specimens for cyclic bending tests:
a – plain specimen; *b* – notched specimen.

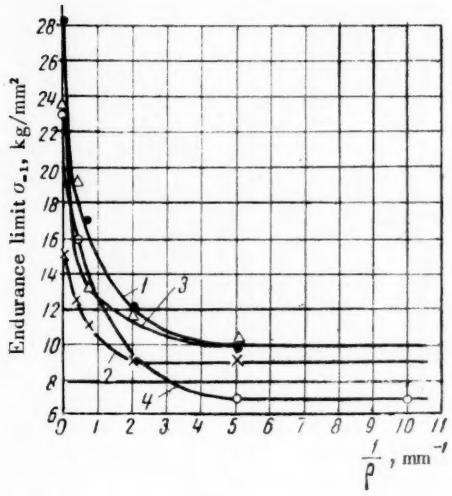

FIG. 3. Curves of limit of endurance changes, determined on a 5×10^6 base in tension-compression depending on the inverse value of the notch radius base, for different types of steel:
1 – SKS-1;
2 – St. 3;
3 – 20G;
4 – 30G.

are, therefore, only shown in the comparative diagram, Fig. 5.

The character of all test diagrams, both in tension-compression and in bending, is the same: with a reduction of the notch radius and a rise of inverse value of ρ, and also with an increase of the stress concentration coefficient the endurance limit decreases, however, at a certain $1/\rho$ and $\alpha_{k\sigma}$ value this reduction stops and further on, the endurance limit continues to stay practically at a constant level. This is correct in an equal degree for tests on a 5×10 base, and on any other base.

The observed features are evident especially clearly in the diagram plotted on logarithmic co-ordinates. It should be generally noted that the curves

$$\delta_{-1} = f(\alpha_k)_{\text{and}} \sigma_{-1} \varphi\left(\frac{1}{\rho}\right)$$

on usual or on logarithmic co-ordinates are almost completely identical with the normal fatigue curves on co-ordinates $\sigma - N$ or $\sigma - 1\,\text{g}N$.

The endurance limit, corresponding to the attainment of the lowest level for the particular base, i.e. a level when the curve

$$\sigma_{-1} f = (\sigma_k) \quad \text{or} \quad \sigma_{-1} = \varphi\left(\frac{1}{\rho}\right)$$

begins to run parallel to the abcsissa axis, may be termed the extreme endurance limit and may be denoted σ_{-1np}. The greatest radius of the notch base, which corresponds to $\sigma_{-1}np$, it is convenient to call the limiting radius of the notch base and denote it by ρ_{pn}. The extreme endurance limit corresponding to the base 5×10^6 and practically equal to the value, found on a base of 10^7 cycles, has a minimum magnitude and characterizes the minimum possible value of fatigue endurance.

It follows from what has been said that the normal fatigue curve, obtained during the tests of specimens with a notch of limiting sharpness, is also the curve of the extreme endurance limits for a changing test base.

Analogous with the usual fatigue curves, the left branch of curves

$$\sigma_{-1} = \varphi\left(\frac{1}{\rho}\right)$$

in the logarithmic system of co-ordinates (S. Fig.4) may be characterized by the equation

$$\sigma_{1i}^{K} \cdot \frac{1}{\rho_i} = \sigma_{-1np}^{K} \cdot \frac{1}{\rho_{np}} = \text{const},$$

Where K – cot of the angle of inclination of the

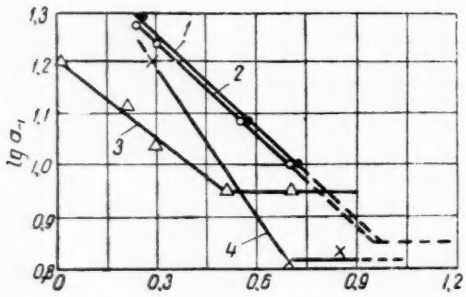

FIG. 4. Curves of limit of endurance changes, determined on a base of 5×10^6 cycles in tension-compression depending on the theoretical coefficient of stress concentration on logarithmic co-ordinates for different types of steel:

1 – SKS-1;
2 – 20G;
3 – St. 3;
4 – 30G.

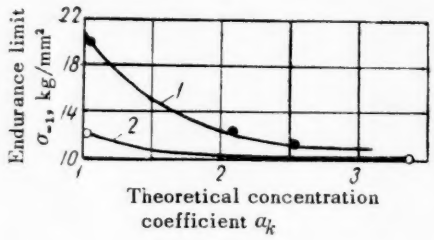

FIG. 5. Comparative curves of limit of endurance changes of St. 3 steel, determined in tension-compression and cyclic bending depending on the theoretical stress concentration coefficient:

1 – bending;

2 – tension-compression.

branch of the curve under consideration; σ_{-1np} – extreme value of fatigue endurance; ρ_{np} – value of the limiting radius of the notch base, corresponding to the break in the curve and its emergence on to the horizontal level.

The dependence σ_{-1} and m $1/\rho$ may be also expressed in the following way

$$\sigma_{-1} = a\,\sigma_{-1\,np} + bA\,exp\left(-\frac{m}{\rho}\right),$$

Where $m = 1/K$ – tangent of the angle of inclination of the left branch of the curve; A – original ordinate; a and b – constants, determining boundary conditions;

With $\rho \geqslant 0.2$ mm $a = 0$, $b = 1$

With $\rho < 0.2$ mm $a = 1$, $b = 0$

Correlations, analogous to those quoted, may be also obtained for curves

$$\sigma_{-1} = f(\sigma_k)$$

plotted on logarithmic co-ordinates.

In accordance with the obtained data it is possible to draw the following principal conclusions:

The extreme endurance limit, determined on a base of 5×10^6 cycles (or 10^7 cycles), during tension-compression may drop to very low magnitudes. This limit does not greatly depend on the compression of the steel and is located in the interval 7 – 9 kg/mm² for those of the tested types of steel, for which the endurance limit (plain specimens) fluctuates from 17 – 28 kg/mm².

If the greatest divergence of the endurance limits in the first case amounts to about 25 per cent, then in the second it is about 60 per cent. The position is about the same with regard to endurance limits determined on a 10^5 cycles base and other bases.

For bending tests a higher magnitude is obtained for the minimum value of the extreme fatigue limit than for tension-compression and averages 12 – 14 kg/mm² (see Fig. 5). However, the drop of the endurance limit when going over from plain to notched specimens with a notch of limiting acuteness, in the case of bending, on the contrary comes out higher than in tension-compression. If in the latter case the ratio

$$\frac{\sigma^p_{-1}}{\sigma^p_{1\,np}}$$

has a value of 2.0 – 2.5, then in the first case –

$$\frac{\sigma^u_1}{\sigma^u_{1\,np}}$$

= 2.5 – 3.0. Therefore, when comparing fatigue limits of plain specimens, the excess of σ^u_{-1} compared to σ^p_{-1} is larger than a similar excess in the case of specimens with a limiting acute notch. If in the first case the ratio of endurance limits is 1.5 – 1.8, then in the second it is 1.3 – 1.5. This divergence is particularly noticed when compared with the absolute difference

$$\left|\sigma^u_{-1} = \sigma^p_{1-}\right|,$$

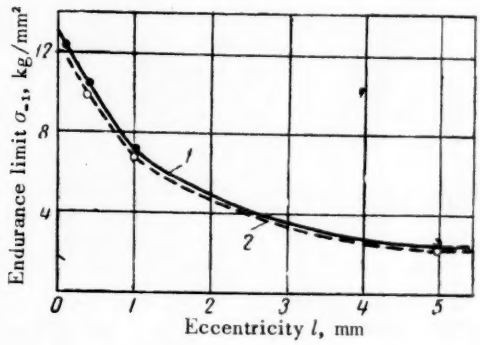

FIG. 6. Dependence of endurance limit, determined in tension-compression of notched specimens (steel type St. 3), on excentricity in accordance with experimental data:

1 – experimental curve;
2 – theoretical curve.

VOL. 8 1959

which is the same for plain and notched specimens, correspondingly 12 – 16 and 4 – 6 kg/mm².

The mentioned feature of the influence of a bend on the value of fatigue endurance may be explained by the presence of a gradient of stresses. The presence of a notch, more so of an acute one, creates the appearance at its apex of a gradient of stresses, a very sharp one both during bending and tension-compression. In such conditions the favourable influence of a stress gradient, especially due to bending, may play a considerably less important part, than on plain specimens.

Although the adduced conclusions are quite obvious and agree with literature data [1, 2], they may, however, raise some doubts because of the difference in the shape of the specimens used in bending and tension-compression tests.

To obtain additional material we carried out tension-compression tests on notched specimens with a varying eccentricity of load application and, correspondingly, with a changing gradient magnitude due to bending. The tests were carried out on specimens of the usual shape with symmetrical side notches on both sides with a base radius $\rho = 1$ mm ($a_k = 2.5$). The centre of the working section of the notches was placed axially or with an eccentricity in relation to the centre line of the specimen.

Under the influence of eccentricity the endurance limit drops and more considerably in the region of slight eccentricities (Fig. 6). However, the difference between the theoretical and the experimentally determined influence of eccentricity on fatigue endurance is very small, which indicates the slight influence of the gradient due to bending in the presence of a notch. This conforms to the data of gradient influence quoted above and confirms the conclusions drawn from it.

The lowering of fatigue endurance by a light notch is considerably less than it should be in accordance with the theory of elasticity and as a result of this the effective coefficient of stress concentration K_σ comes out smaller than the theoretical $a_{K\sigma}$. By increasing the acuteness of the notch this difference gets smaller and attains its minimum magnitude at the limiting radius of the notch base.

With a further reduction of the radius of the base of the notch the magnitude K_σ remains practically unaltered, and $a_{K\sigma}$ increases continuously, as a consequence the difference between K_k and $a_{K\sigma}$ also gets larger.

When appraising steel by the magnitude of the coefficient of sensibility to a cut

$$\eta = \frac{K_{\sigma-1}}{a_{k\sigma-1}}$$

one obtains curves shown in Fig. 7. From these curves, in accordance with what has been stated, it follows that with very small ρ and large $a_{k\sigma}$ the value of the coefficient of sensibility to a cut η is converging on zero. It is seen quite clearly that in a less durable steel (St. 3) sensibility to a cut is lowest, and in this steel the growth of the coefficient of sensibility with an increase of the radius of the notch or a reduction of $a_{k\sigma}$ proceeds much slower than in the more durable steels: 20G and SKS-1. However, for all types of the studied steels, the most important increase of the sensibility coefficient occurs in the region of low values of the

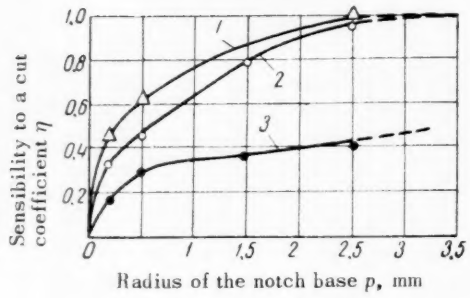

FIG. 7. Dependence of the sensitivity to a cut coefficient on the radius of the notch base for different steels:
1 – SKS-1;
2 – 20G;
3 – St. 3.

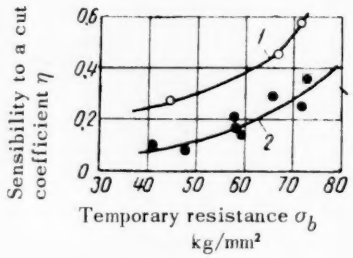

FIG. 8. Dependence of the sensitivity to a cut coefficient on temporary resistance (ρ = 0.5 mm):
1 – specimens cut in the rolling direction;
2 – specimens cut across the rolling direction.

radius of the notch base.

The great capacity of steel to reduce peaks of stress concentrations for account of local plastic deformation, especially with very sharp notches, when $\eta \cong 0$, is an important property of steel. In less durable steel, in accordance with the data in the works [2, 5], this capacity of lowering the magnitude α_k, is seemingly, larger and the value of the coefficient of sensibility to a notch, correspondingly smaller. However, the difference for the compared types of steel is not very large.

The lesser sensitivity to cut of the less durable steels is characterized on the curves

$$\sigma_{-1} = f\left(\frac{1}{\rho}\right) \text{ and } \sigma_{-1}\varphi\ (\alpha_{k\sigma})$$

by a more gentle slope of the left hand branch than for a stronger steel. As a result of this, the limiting radius of the notch base of the less durable steels come out somewhat larger and the limiting theoretical stress concentration coefficient – smaller than for stronger steels. For instance, for St. 3 steel ρ_{np} = 0.5 mm, $\alpha_{k\sigma np}$ = 3.3, and for steels 20G and SKS-1, correspondingly ρ_{np} = 0.25 mm and $\alpha_{k\sigma np}$ = 4.7. Generally, however, for a majority of steels during tension-contraction and bending ρ_{np} = 0.2 – 0.3 mm, $\alpha_{k\sigma np}$ = 4.0 – 5.0 and $K_{\sigma np}$=2.5–3.0.

It should be assumed that with a geometrically similar increase of size, the magnitude of the limiting radius of the notch base should grow in proportion to the changes of size.

In Fig. 8 are placed side by side the curves of sensitivity to a notch of specimens cut along and across the rolling direction. Sensitivity to a cut with the given σ_B is considerably less in the cross grained than in the long grained specimens and with a reduction of durability the relative difference η is increasing in both specimens, whereas the absolute divergence η is at the same time getting slightly smaller.

This phenomenon should be due to a relatively larger size of grain of cross cut specimens compared to those cut in the rolling direction.

It should be mentioned that in a as much as the data, which was examined, was obtained for one and the same material from specimens differing only in respect of their orientation in relation to the direction of rolling, it serves as very convincing proof of the known dependence of the sensitivity to a cut on the size of grain.

Comparing the fatigue endurance curves of plain specimens and specimens with a notch of limiting sharpness, tested in tension-compression as well as in bending, one may point out one particular feature, previously established [10] and mentioned in work [11]: with a large number of reversal cycles (N), the endurance limit of specimens with a sharp notch is less than that of plain specimens. With a small N this difference drops, and with

$$N \leqslant 10^3 - 10^4$$

the correlation of endurance limits of the specimens mentioned may have different inverse signs. This is explained by the intensive influence of stress concentration in case of a large number of cycles and the prevailing influence of the volume of stressed condition, associate with the growing strength of metals in a ductile condition, compared with the influence of stress concentrations during a smaller number of cycles.

CONCLUSIONS

1. With an increased sharpness of the notch and

a growing coefficient of stress concentration both in bending and in tension-compression a drop occurs in the fatigue endurance of low carbon and low-alloy steels, which drops to the extreme value, and practically remains unaltered in the event of a further sharpening of the notch.

2. The maximum radius of the notch base, corresponding to the attainment of the extreme magnitude of fatigue endurance, may be termed the limiting. In bending and tension-compression, for specimens with a section areas of 30 – 60 mm², it has a value of about 0.3 mm (0.2 – 0.5 mm).

3. The noted peculiar features are characteristic for the endurance limit with any base, whereas the extreme endurance limit, established on a base of 5×10^6 cycles (if it is accepted equal τ_{-1} on a base of 10^7 cycles) for steel has a minimum value. Therefore, the usual fatigue curve for specimens with a notch of limiting sharpness is simultaneously the curve of extreme fatigue limits for changing test bases.

4. The stress gradient influence results in an increased fatigue endurance in bending compared with tension-compression. However, a positive influence of a gradient through bending proves to be important for plain specimens and comparatively less so for notched, which have a sharp stress gradient, due to a concentration of stresses because of the notch.

5. The coefficient of sensitivity to a notch increases with the increase of the strength of steel. The greatest increase of this coefficient in absolute magnitude is obtained in the presence of light notches and a low coefficient of stress concentrations, whereas the greatest increase of relative magnitude occurs in the presence of sharp notches and a high stress concentration coefficient.

6. Sensitivity to a cut increases with the increase of the radius of the notch base and in the region of small radii this growth proceeds more intensively.

7. Sensitivity to a cut, with a given durability, is greater for specimens cut along the rolling direction, compared with those cut across the rolling direction, which may be explained by the anisotropy of the grain size; in the first case the grain is comparatively smaller.

Translated by A. Allan

VOL. 8 1959

REFERENCES

1. S.V. Serensen, *Symposium Povysheniye prochnocsti detalei mashin (increasing the durability of machine compoents) Izd. Akad. Nauk SSSR,* p. 46 (1949).
2. S.V. Serensen, V.P. Kogayev, L.A. Kozlov and P.M. Shneiderovich, *Nesushchaiye sposobnost' i raschety detalei mashin (Carrying capacity and computation of machine details) Mashgiz,* (1954).
3. N.N. Afanas'yev, *Z. teor. fiz.*, 10, No. 19 (1940).
4. R. Peterson, *Bulletin ASTM* No. 1, (1945).
5. R. Peterson and S. Timoshenko, *60-th Anniversary volume,* (1938).
6. G.V. Uzhik, *Metody ispytanii metallov i detalei mashin na vynoslivost' (Methods of testing endurance of metals and machine details) Izd. Akad. Nauk SSSR,* (1948).
7. F. Körber, M. Hempel and K. Mitteil, *W Inst.* 21, 336 (1939).
8. R. Mailänder, *Techn. Mitteil. Forschungsberichte Auhang* (1939).
9. H. Buchner, *Forshungs a.d. Ingen.-Wes.* 9, 1 (1938).
10. W. Finch, *Proc. ASTM,* 52 (1952).
11. L.M. Shkolnik, *Zh.teor.fiz.*, 24, No. 3, 517 (1954).

INVESTIGATION OF PLASTIC PROPERTIES OF SINGLE CRYSTALS OF BERYLLIUM*. II†

P.I. GARBER, I.A. GINDIN, A.I. KOVALEV and Yu.V. SHUBIN
Physico-Technical Institute of USSR Academy of Sciences

(Received 24 December 1957)

Data available in references [2-5] concerning slip in beryllium are scarce and contradictory. The data mainly refer to polycrystalline materials. Some authors [3-5] consider that no slip occurs in beryllium at room temperature. However, slip along the basal (0001) plane in specimens of previously twinned single crystals of beryllium was found not only at room temperature but also at lower temperatures [1]. In the present work the processes of slip were studied in single crystals of beryllium which had not been previously twinned and the relationship between the processes of slip and fracture of beryllium crystals in a wide range of temperature elucidated.

SPECIMENS INVESTIGATED AND EXPERIMENTAL PROCEDURE

Specimens were prepared from a single crystal beryllium block grown by slow solidification of the liquid metal in vacuum. The purity of the starting material was 99.7 per cent. The block was cut on a grinding machine with an electric corundum disc of the "D" brand. The work-hardened layer was removed by etching in aqueous solution of hydrofluoric acid. The specimens were in form of rectangular prisms, 3.5 × 4.0 × 7.0 mm. Two side faces (3.5 × 7.0 mm face of the *a* type and 4.0 × 7.0 mm face of the *b* type) were polished. Crystals had no distortions judging by appearance of the Laue pictures.

Experiments were conducted in conditions of straining by compression on a special press [6] with a constant rate of deformation (0.03 mm/sec) at temperatures: −253, −196, +20, 400, 600 and 800°C.

Specimens were orientated so that the basal (0001) plane was inclined at an angle of 45 ± 1.5° to the axis of compressive forces (Fig. 1). The side face of the specimen was parallel (with an accuracy of 30′) to the prismatic plane of the first order $(1\bar{1}00)$, hence to the diagonal of the first order $[11\bar{2}0]$.

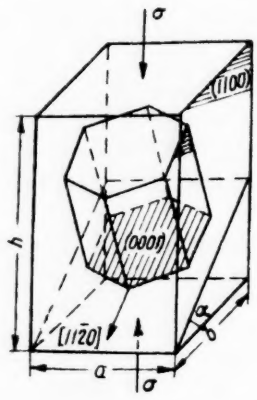

FIG. 1. Crystallographic orientation of monocrystalline specimens of beryllium. The *a*-type plane (plane of drawing) is inclined at an angle of 45° to the basal plane (0001). The $[1\bar{1}20]$ direction and the $(\bar{1}100)$ plane are parallel to the side plane of the *b*-type.

Elements of plasticity and fracture were identified by traces of distorted bands and cracks disclosed on the previously polished faces of specimens. The results were plotted on the standard stereographic projection of the basal plane of the crystal. The X-ray structural examination method was used for the orientation of specimens and for an additional verification of the elements of slip and fracture.

The pattern of the basal slip-bands was also examined by means of electron microscope (magnification 10,000). For this purpose replicas were made by evaporation of quartz in vacuum. Contrast was obtained by evaporating chromium on the specimen surface [8]. The quartz film and the contrast-making layer of chromium were removed from the specimen surface by using gelatin.

RESULTS OF INVESTIGATIONS

Metallographic examination of the surface of the

---

* *Fiz. metal. metalloved.*, 8, No. 1, 130-139, 1959.
† See [1].

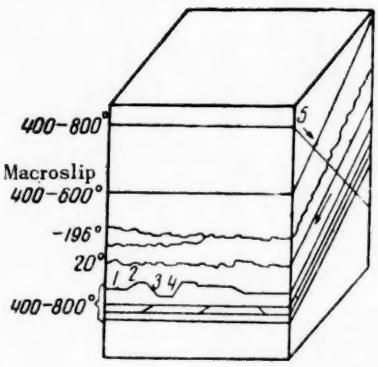

FIG. 2. Schematic representation of the outward appearance of slip-traces in berryllium at various temperatures:
1 – trace of slip on the basal plane (0001);
2 –5 – traces of pyramidal slip on the $(11\bar{2}4)$, $(\bar{1}103)$, $(\bar{1}102)$ and $(\bar{1}\bar{1}21)$ planes.

compressed specimens showed that in a wide range of temperatures (from – 196° to + 800°) slip on the basal plane (0001) occurred in the single crystals of beryllium oriented as described above. The character of slip-bands depends on temperature. At – 196° the basal slip is disclosed in the form of fine slightly branched wave-shaped lines; the slip develops with increase of stress as shown mainly by the occurrence of new fine slip-bands. In cases where there is an inclusion on the polished microsection, e.g. a grain of beryllium oxide, the first slip-bands originate near the inclusion. On its appearance the band does not cross the whole section of the specimen but with increased deformation it extends through the whole width of the single crystal. In specimens deformed at higher temperatures no bands of branched structure are observed, the slip is of a more pronounced crystallographic nature. At the *a*-type faces (see Fig. 1) the regime of straight lines occur oriented parallel to the basal plane. From 20° upward the slip-bands exposed on the *b*-type plane are strictly straight lines. In Fig. 2 the slip-bands are schematically shown as they appear in the single crystals of beryllium at various temperatures.

The photo-micrographs of the specimen faces after compression at 20°C are shown in Fig. 3, *a* - *b*, and the interference microrelief pictures of these faces in Fig. 3, *c*-*d*. The traces of slip on the *a*-type faces (Fig. 3 *a* and *d*) are wave-shaped, on the *b*-type faces (Fig. 3, *a* and *c*) linear and inclined at an angle of 45° to the axis of compression. The slip takes place in the $[11\bar{2}0]$ direction hence the interference picture of the *b*-type face undergoes no displacement across the traces of slip.

In the electron-microscopic examination the slip-bands are resolved as lamellae. At temperatures of – 196° and + 20° the lamellae are 0.1 and 0.3 μ thick respectively* (Fig. 4); at higher temperatures they are a little thicker (0.5 μ at 400°). The increase in stress does not noticeably affect the thickness of the lamellae but results in the increase of their number. The amount of shear in the lamellae is approximately equal to the thickness of the lamellae and does not depend much on the extent of deformation. The amount of shear can be easily estimated by the displacement of the scratch which intersects the slip-band on the *b*-type face (Fig. 5). The trace of the slip-band on the face of *a*-type is lamellar. However, from 20°C upwards the relative shear of some bands is increasing appreciably. The macroscopic deformation is mainly developing just within these bands (especially at 400° and higher). Stresses at which the bands of great relative shear occur depend on temperature; they decrease with rise of temperature approaching the value of the yield strength at a temperature of 600°C.

With rise of temperature the total number of slip-bands decreases and the magnitude of the shear in some bands increases. The total thickness of the "lamellae" amounts to 5-6 micron. The shear within the lamellae reaches 100 micron, that is the tangent to the angle of shear in the bands with large relative shear is approximately equal to 20. Instead of lamellar distinct step-like bands are obtained on the surface of the *a*-type face. These bands form the clearest traces on the *b*-type faces; on the *a*-type faces the displacements of interference fringes correspond to the traces in conformity with the above stated shear. The regions between two such slip-traces contain a great number of fine slip-bands in which the displacement of interference fringes is insignificant. The occurrence of a large relative shear in an individual band affects the mechanical deformation curve and results in the change of its slope.

In Fig. 6 the mechanical deformation curves of beryllium at various temperature are given. It is evident that the decrease of temperature results in the increased slopes of the curves. This is in good agreement with the observed rise of the latent energy of plastic deformation with drop of temperature [9]. Since the slip is localized in individual lamellae, it should follow that the latent energy of deformation is also accumulated mostly within these lamallae, in which distortions evidently reach their

* At – 196° cracks and fracture nuclei are visible at the edge of the slip-band.

VOL. 8 1959

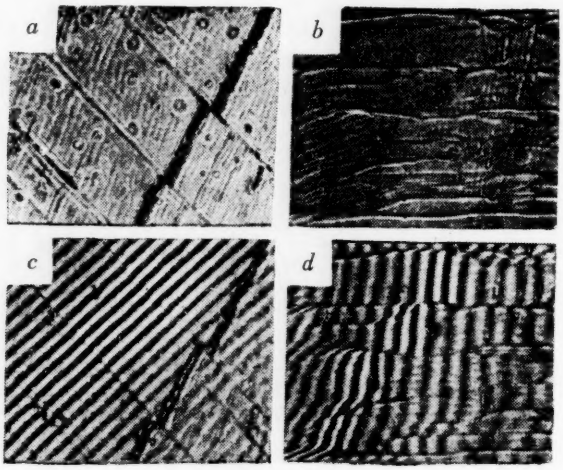

FIG. 3. Microstructure of slip-band traces:
a – traces on the *b*-type face;
b – traces on the *a*-type face;
c – *d* – interference relief picture of corresponding faces. The broad black strip intersecting the slip-lines on the *b* face is the scratch preliminarily made.
Displacements of the scratch can be clearly seen on the bands of large relative shear. Temperature of tests + 20°. Compression deformation 4.9 per cent; × 432.

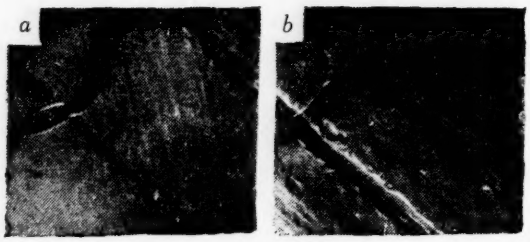

FIG. 4. Slip-bands on the *b*-type plane (the shear plane):
a – after 3.4 per cent compression at – 196°;
b – after 3.9 per cent compression at + 20°.
The slip-bands are intersected by microcracks on the prism plane of the II type ($1\bar{1}\bar{2}0$);
× 8,000.

limits quicker at lower temperatures. This should explain the fact that at low temperatures a great number of slip-bands occur with small relative shear in each. The slip-bands with large relative shear develop only at high temperatures.

The yield strength in basal slip was determined as the compression stress corresponding to the occurrence of the first traces of slip. An appreciable rise of yield strength takes place at low temperatures. Thus, at – 196°C the yield point is 44 kg/mm² while at 20° it is 19 kg/mm². From 20°C towards higher temperatures the yield strength slowly decreases. In the range from 600 to 800°C the yield strength remains constant (Fig. 7, curve δ_s). A permament deformation of the crystal develops before the occurence of slip-bands. For example, at – 196° a permanent deformation of 3 per cent precedes the basal slip. At – 253° the specimen breaks without developing slip-bands, its permanent deformation amounts to 2.7 per cent. The initial stage of deformation at low temperatures (– 196, – 253°) is associated with the formation of blocks

FIG. 5. Break of the scratch on slip-bands. The face of *b*-type. Temperature of test + 20°. Compression deformation 1.5 per cent; × 10,000.

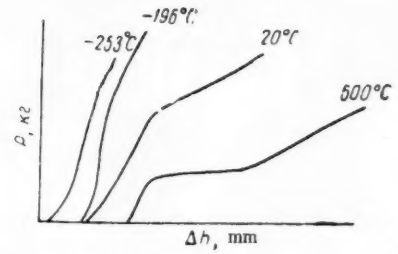

FIG. 6. Load-strain curves for single crystals of beryllium (the curves for various temperatures are displaced along the abscissa). 1 mm on the abscissa corresponds to 6D μ of deformation, 1 mm on the ordinate axis corresponds to 18 kg of load.

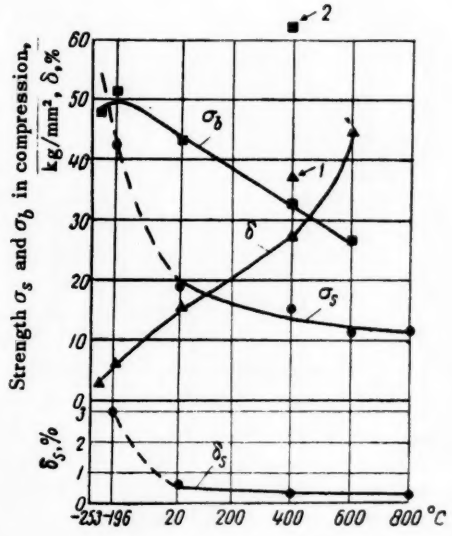

FIG. 7. The variation of mechanical characteristics of single crystals of beryllium with temperature:

σ_s – yield stress in compression;

σ_b – compression strength;

δ – overall permanent compression;

δ_s – permanent compression preceding the appearance of the first slip-bands.

of a mosaic structure. On the X-ray photographs taken of the deformed specimen a split in the spots of the Laue diffraction pattern is found which indicates that the crystal is broken into fragments of varying orientation. This disorientation of the blocks as compared with the initial orientation of the crystal is rather small. The blocks hamper the process of basal slip and increase the resistance

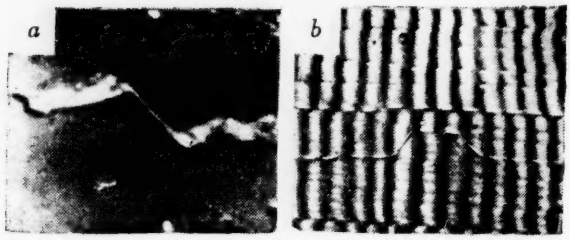

FIG. 8. Prismatic slip in single crystals of beryllium (see Fig. 2):
a — the trace of slip on the face of *a*-type. The 1.2 per cent compression at 20°; × 10,000;
b — trapezial slip on the face of *a*-type. The 1.5 per cent compression at 400°; × 432.

to shear in the specimen. The part of deformation which precedes the occurrence of the slip-bands decreases with the raised temperature of test (see Fig. 7, curve δ_s).

The wavy shape of slip-bands at low temperatures may be attributed to the effect of the blocks formed. With rise of temperature the slip-bands acquire a more pronounced crystallographic character, no block formation is observed. From 20° upwards the electron microscope resolves straight regions of the wave-shaped traces of slip having a strictly crystallographic orientation (Fig. 8, *a*). At 400°C and higher temperatures the straight regions are clearly shown by means of metallographic microscope (Fig. 8, *b*). Examination of the projections produced on the *a*-type face (Fig. 1) indicated that prismatic slip occurrs in beryllium, especially at high temperatures; individual prisms bound by the planes belonging to the zone of the slip direction $[11\bar{2}0]$ move relative to one another. Most often the translation takes place along the basal plane (0001). However, the (0001) stages are separated by the $\{(1\bar{1}04)\}$ and $\{(1103)\}$ planes. The $\{(1\bar{1}02)\}$ planes occur less frequently (see Fig. 2). As a result of prismatic slip, the trapezoidal traces are obtained on the *a*-type faces formed e.g. from a pair of traces of the (0001) plane and of the pyramidal planes of the first order $(1\bar{1}02)$ and $(1\bar{1}03)$. An example of such a slip-band is shown in Fig. 8,*b*. Interferometric investigations showed that the difference in level of separate stages may reach a value of 0.5 micron. By comparing the electron-microscopic with the metallographic photographs of various regions of the crystal surface (Fig. 8,*a*,*b*) it is easy to see that the structure of fine and coarse prismatic slip-bands is similar.

The prismatic slip evidently originates as a result of the fact that the basal plane of beryllium is not a particularly densely packed plane (the ratio c/a in beryllium is 1.567, in zinc — 1.85, in cadmium — 1.88; in dense packing this ratio should be equal to 1.63). The other planes belonging to the zone with the $[1\bar{1}20]$ axis do not differ much in their density of packing from the basal planes.

Before deforming a specimen, slight scratches were made parallel to its axis on some carefully polished microsections. After deforming and shadowing,pictures were taken of the bands intersected by the scratch on the replicas. In this way a picture of the slip lamellae intersected by the scratch was obtained (Fig. 5). In one case it was established that the displacement of one scratch was appreciably greater than that of the neighbouring one intersecting the same slip-band. It was found by calculation that the difference in displacements of these scratches amounted to 5 per cent of the initial distance between them.

If we assume that in straining the compression takes place on one side of the band and the expansion on the other [10], the permanent deformation then should amount to ± 2.5 per cent. This appreciably exceeds the amount of deformation corresponding to the yield strength at the temperature given. Consequently, the irregularity of slip along one and the same band may lead to the plastic deformation in compression and expansion along the direction of slip and in some cases to the rupture of material between two adjacent slip-bands. The surfaces of such ruptures must be so oriented that their traces on the *b*-type plane should intersect the slip-bands. Just this type of rupture was found in the experiments described here at a temperature range from −196° to + 20°C.

In Fig. 4 the electron-microscopic photographs and in Fig. 9 the photomicrographs of the surface parallel to the plane of shear are shown (with the pictures of transverse cracks). These first nuclei of fraction are oriented parallel to the prism edge

VOL 8 195

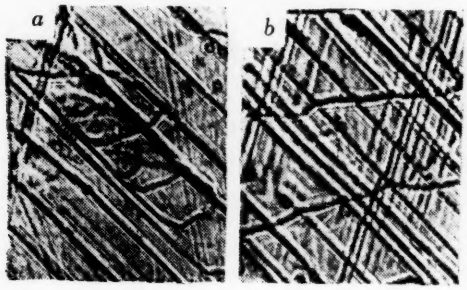

FIG. 9. Photo-micrographs of transverse microfractures occurring as a result of irregular shear in slipping along the slip-bands. The *b*-type face:
a – fracture along the $(\bar{1}\bar{1}20)$ plane (see Fig. 4);
b – fracture along the $(1\bar{1}\bar{2}2)$ plane. Temperature of test + 20°, compression deformation 5.2 per cent; × 432.

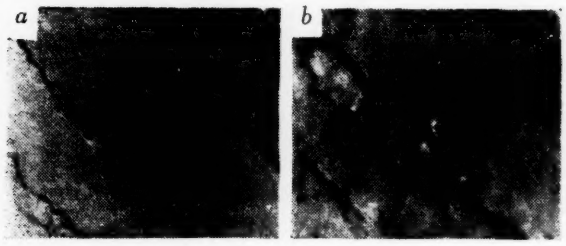

FIG. 10. Slip-traces of polygonized single crystal of beryllium. The wavy shape of the slip-traces and the blocks of polygonization. The procedure of treatment: 0.6 per cent compression at 20°, annealing at 800° for 3 hr, repeated 0.8 per cent compression at 20°; × 8,000.

of the II order – $(\bar{1}\bar{1}20)$ and to the pyramid planes of the II order – $(\bar{1}\bar{1}22)$ and $(\bar{1}\bar{1}23)$. Further straining leads to the break of continuity in individual weakened regions of basal slip* and the main rupture develops by transferring from one basal slip-band to the next. At 400° and higher the rupture is of a more definite crystallographic nature, shear becomes more regular, slip of individual bands takes place with a very large relative shear and ends with the rupture along the basal plane (0001). Fracture along the twinning plane $(1\bar{1}24)$ happens very rarely.

In Fig. 7 the compression strength (σ_b) and the overall residual compression (δ) as the functions of temperature are shown. The strength was determined by the multi-step straining until the first crack appeared shown by the drop of the $P-\Delta h$ curve. It was found that the breaking stress at – 253° is lower than that at – 196°. With rise of temperature the breaking strength drops and the ductility continuously increases.

Quite a number of experiments were performed in order to explain the nature of basal slip in the specimens which had undergone a two-stage straining at 20° with intermediate annealing at high temperature. The specimens were first strained at 20° by 0.5 per cent (until the appearance of first slip-bands), then annealed in vacuum at a temperature of 800° during 3 hours and again compressed at 20°. With higher straining new slip-bands occurred. Their character changed sharply. The traces of bands became curved, very fine and by their appearance resembled those usually occurring at – 196° (Figs. 10 and 4, *a*). Some traces as if avoiding obstacles, split into two branches. The curved and branched slip-traces on the shearing plane are the result of polygonization which took place during the heating of the previously deformed crystal. Individual blocks of polygonization can be seen on the electron-microscopic photographs (Fig. 10,*b*). The polygon-

* In work [8] the formation of transverse rupture within the slip-band itself was noted.

TABLE 1. Crystallographic elements of slipping, twinning and fracture and the temperature range of their development

Elements and character of plasticity and fracture	Temperature range of development, °C	Remarks
Formation of the blocks of mosaic structure	– 253, – 196	At 20° and higher, formation of blocks feebly marked
Slipping:		
a) Basal (0001), $[11\bar{2}0]$	– 196, + 800	
b) Pyramidal		
$\frac{\{(11\bar{0}4)\} \text{ and } \{(1103)\}}{[11\bar{2}0]}$	20 – 800	
$\frac{(\bar{1}\bar{1}02)^*}{[1120]}$	400 – 800	At 400 – 800° fault formation and slip along $(\bar{1}\bar{1}2\bar{1})$ occur
Twinning:		
$\{(2\bar{3}12)\}$	– 253 – 400	
$\{(\bar{1}\bar{1}02)\}, \{(\bar{2}\bar{2}03)\}$	– 253 – 20	
$(11\bar{2}4)$	20 – 600	
Fracture:		
a) Basal (0001)	– 253 – 800	Sometimes along the twinning plane $(11\bar{2}4)$
b) Prismatic $(\bar{1}\bar{1}20)$	– 196 – 400	
c) Pyramidal $(\bar{1}\bar{1}22)$ a. $(\bar{1}\bar{1}23)$	20 – 400	

* This kind of pyramidal slip was earlier detected in magnesium [13].

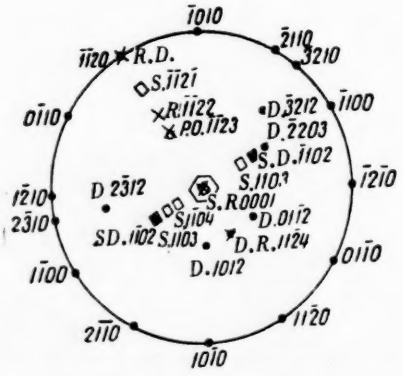

FIG. 11. Standard stereographic projection of the basal plane (0001) of a single crystal of beryllium:

□ *S* – crystallographic members of slip;
• *D* – crystallographic members of twinning;
× *R* – crystallographic members of fracture;
o *O* – direction of the axis of the crystals investigated.

ization of a single crystal of beryllium leads to the increase of its yield strength by over 30 per cent*.

* The increase of yield strength by annealing was already noted in twinning single crystals of calcite [11].

The polygonization is a result of the blocks being formed in the process of deformation at room temperature and lower. The block structure is exposed in annealing, the angle of the subgrain mosaic structure increases and the stress, localized in individual regions of the deformed crystal, released.

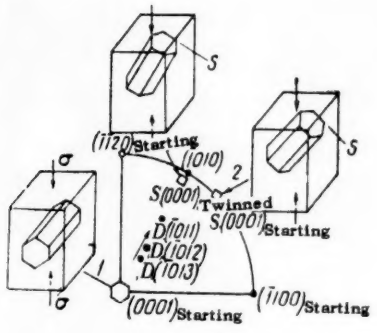

FIG. 12. Orientation of single crystals of beryllium: position 1 and 1′ – crystals in which slip on the basal plane occurred after twinning all over the body; position 2 – crystals in which the slip occurred without preliminary twinning.

In compressing the specimens investigated, mechanical twins occur near the gripping surfaces, that is, in the places where stresses are concentrated. For the chosen orientation of the beryllium specimens a great number of various twinning planes develop. With raised temperature of testing, the number of twinning planes varies. The greatest number of sets of twinning planes was found at 20° (see Table 1). This fact contradicts the assumption that the presence of intersecting twinning planes is the indication of brittleness of beryllium, because the number of various twinning planes decreases at the temperatures at which beryllium becomes more brittle.

The comparison of mechanical properties of the single crystals of beryllium of the *O* orientation (Fig. 11) with the properties of the single crystals previously twinned all over the crystal and having an orientation close to *O* (Fig. 12) renders it possible to draw the important conclusion that the previous twinning has a favourable effect on the strength and ductility of the crystal. In the crystals twinned at 400° this effect is not strongly displayed. In such crystals the relative shear in specific lamellae reached $\gamma = 200$.

In Fig. 7 the arrows 1 and 2 mark the points which refer to the ductility and the strength respectively when basal slip occurs in the crystal which was previously twinned completely. As shown the increase in ductility reaches 35 per cent and in strength 80 per cent. Critical shearing stresses in the specimens of different orientation but twinned along similar planes are different. The twinning process is accompanied with an appreciable strengthening at the boundaries of the laminae formed. The thickness of twins is small and it increases with temperature (2 μ at – 253° and 10 μ at 400°). The violation of the law of critical shear stresses and the increased strengthening in straining the specimens with the *O* orientation should evidently be closely related to the effect of the blocks being formed in the initial stage of compression.

We express our gratitude to B.G. Lazarev for valuable advice throughout this work.

CONCLUSIONS

1. Crystallographic elements and mechanical characteristics of various kinds of plasticity and fracture in beryllium single crystals were determined at the temperature range from – 253 to + 800°C (see the Table and Fig. 11).

2. It was established that in a wide range of temperatures (from – 196 to + 800*) slip on the basal plane (0001) in the [11$\bar{2}$0] direction is the principal kind of plastic deformation in beryllium.

3. The slip in beryllium is substantially different from that in other hexagonal crystals:

a) in addition to slip on the basal (0001) plane, slip is observed on the pyramidal planes of the I order (known as prismatic slip) mainly in the [11$\bar{2}$0] direction.

b) The traces of slip-bands are wavy and branched lines. The wavy shape of the lines can be explained by the formation of the blocks of mosaic structure(low temperatures) on one hand and by the

* Traces of basal slip in microspaces occur at – 253°. However, owing to the formation of blocks and to high yield strength at – 253°, the slip does not cross the whole section of the specimen.

VOL. 8 1959

complicated crystallographic structure of the bands caused by prismatic slips on the other (high temperatures).

4. Beryllium has a great number of various crystallographic systems of twinning. The mechanical twinning is not responsible for the increase in brittleness of beryllium.

5. Twinning of the whole crystal results in the increase of its ductility and strength during the subsequent slipping.

6. An irregularity in the shear along the band of basal slip was found which caused the appearance of microcracks on the planes of prisms and pyramids of the II type. Thus, the brittleness of beryllium is connected with a great number of cleavage planes which are strongly manifest, at low temperatures in particular, owing to irregular shear.

Translated by B. Cynk

REFERENCES

1. R.I. Garber, I.A. Gindin, V.S. Kogan and B.G. Lazarev, *Fiz. metal. metallov.*, 1, 529 (1955).
2. H. Sloman, *J. Inst. of Metals*, 49, 365 (1932).
3. A. Kaubmann, P. Gordon and D. Lillie, *Trans. Am. Soc. of Met.*, 42, 785 (1950).
4. H. Hausner and P. Pinto, *Trans. Am. Soc. of Met.*, 43, 1052 (1951).
5. G. Raynor, *J. Royal Aer. Soc.*, 50, 390 (1946).
6. R.I. Garber, I.A. Gindin, M.G. Konstantinovskiy, N.I. Malik, L.M. Polyakov and V.I. Startsev, *Zav. Lab.*, 7, 857 (1953).
7. R.I. Garber, I.A. Gindin, V.S. Kogan and B.G. Lazarev, *Izv. Akad. Nauk SSSR, ser fiz.*, 20, 639 (1956).
8. R.I. Garber and A.I. Kovalev, *Dokl. Akad. Nauk SSSR*, 86, 901 (1952).
9. V.I. Khotkevich, D.F. Chaykovskiy and V.V. Zashkvara, *Zh. Fiz. metal. metallov.*, 1, 206 (1955).
10. I.V. Obreimov and M.V. Shubnikov, *Zh. russk, fiz.-khim. obshch.*, 9, 818 (1927).
11. R.I. Garber, *Zh. eksp. teor. fiz.*, 16, 923 (1946).
12. R.I. Garber, S. Ya. Zalivadnyy and V.I. Startsev, *Dokl. Akad. Nauk SSSR*, 58, 571 (1947).
13. A. Chandhuri, N. Graut and J. Norton, *J. Met.*, 5, 712 (1953).

INVESTIGATION OF HIGHLY HEAT-CONDUCTING AND HEAT-RESISTING ALLOYS OF THE Cu-Co-Be SYSTEM*

M.V. MAL'TSEV, V. Ye. MIKRYUKOV and CHZHOY SHI-SHAN

"M.V. Lomonosov" Moscow State University

(Received 7 February 1958)

In this paper the results of experimental investigations are given on thermal and electric conductivities, strength, hardness of the Cu-Co-Be system and the constitution of the Cu-CoBe system constructed.

VOL. 8 1959

Heat-resisting and highly heat-conducting alloys have recently become of appreciable importance, in particular those based on copper. In their preparation great attention is paid not only to their strength and heat-resistance but also to thermal conductivity.

Heat-resistant alloys are not only age-hardening but their chemical composition is complex. They are usually many-component systems. It is known that for ageing alloys both the change in solubility of components with temperature and the physico-chemical properties of the precipitating phase in the process of thermal treatment are important.

It is of interest to have the copper-base ternary alloys studied which belong to the pseudo-binary copper-chemical compound section. The hardness and melting point of metal chemical compounds are usually high. An increase in the solubility of a chemical compound in solid copper with temperature is a necessary condition for the quenched alloy to be hardened by ageing. Since beryllium and cobalt from the chemical compound CoBe of high hardness and melting point, it is reasonable to assume that this compound may serve as a hardner of copper alloys. The present work is devoted to the study of structural and physico-chemical properties of this system.

THE CONSTRUCTION OF THE CONSTITUTIONAL DIAGRAM

The chemical compound CoBe can serve as a hardner of copper alloys only when the pseudo-binary system Cu-CoBe is present. Its existance can be proved by X-ray structure analysis. Two systems of lines were obtained on the X-ray pattern obtained in X-ray examination of the alloy powder of Cu + 3.5% Be + 22.9% Co (i.e. 26.4 % CoBe) one of which belongs to the face-centred cubic lattice of solution α based on copper and the other to the body-centred cubic lattice of the CoBe chemical compound. Examination of the microstructure also confirmed the existence of two phases in the alloy: α solid solution and the CoBe chemical compound.

Thirteen alloys were prepared (Table 1) for the construction of the equilibrium diagram of the pseudo-binary system Cu-CoBe. (Actual gravimetric data obtained by analysis of the chemical compositions of the alloys differed from the data calculated in the 4th decimal place).

Electrolytic copper, cobalt and binary alloy Cu-Be (Cu + 6 % Be) served as starting materials. Melting was carried out in a furnace with graphite heater and crucibles under the barium chloride flux. Ingots cast in pig-iron moulds were homogenized and forged with 50 per cent upset. From the billets thus deformed, testpieces for further investigations were prepared.

The constitution diagram was constructed by means of microscopic examination and differential thermal analysis. For this purpose the alloys were heated to various temperatures and soaked for a sufficiently long time to reach equilibrium (the heating procedure is shown below) and then quenched in cold water.

Temperature of heating, °C:

990 900 800 700 600 500

Soaking, hours:

7 12 48 60 100 130

By microscopic examination the solubility limits

* *Fiz. metal. metalloved.*, 8, No. 1, 140-146, 1959.

TABLE 1. Chemical composition of alloys investigated, CO: Be = 6.54%

Nos. of alloys	Contents of components, % by weight		
	Be	Co	CoBe
1	0.1	0.65	0.75
2	0.2	1.31	1.51
3	0.3	1.96	2.26
4	0.4	2.62	3.02
5	0.5	3.27	3.77
6	0.6	3.92	4.52
7	0.7	4.58	5.28
8	0.8	5.23	6.03
9	0.9	5.89	6.79
10	1.0	6.54	7.54
11	1.3	9.50	10.80
12	2.0	13.10	15.10
13	3.5	22.90	26.40

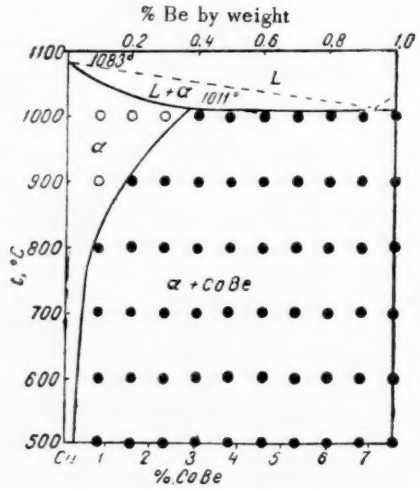

FIG. 1. The pseudo-binary Cu-CoBe system.

of the CoBe chemical compound in copper was determined for various temperatures. The differential thermal analysis was carried out by means of Le Chatelier – Saladin pyrometer. The solidus of the system in question was determined from the results of the analysis; liquidus was not constructed.

The constitution diagram of the pseudo-binary system Cu-CoBe constructed (Fig. 1) belongs to the eutectic type, the eutectic point being 1011°C. It is evident from the diagram that the CoBe chemical compound dissolves in copper in large quantities (about 2.7 per cent by weight at the eutectic point). The solubility sharply decreases with drop of temperature.

THERMAL TREATMENT AND MECHANICAL PROPERTIES OF THE ALLOYS

The thermal treatment of the pseudo-binary alloy system Cu-CoBe was carried out by the following procedure: quenching in water from 990° for two hours, then tempering at 470 and 500°. It was found that all the alloys belonging to the pseudo-binary Cu-CoBe system are highly strengthened, their hardness increases by 3-4 times. Better results were obtained by tempering at 470°. The alloy Cu + 0.3% Be + 1.96% Co displays the same temper-hardening effect as the alloys with higher contents of Be and Co. Thus, the above quantity of beryllium and cobalt

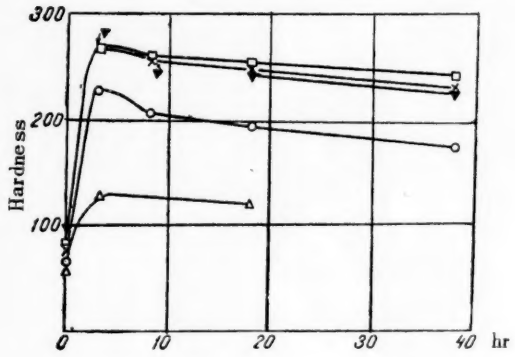

FIG. 2. Relation between hardness of alloys and duration of tempering at 470°C:

△ — 0.1% Be; 0.65% Co; 0.75% CoBe. ○ — 0.2% Be; 1.3% Co; 1.5% Co Be. ▽ — 0.3% Be; 1.96% Co; 2.26% CoBe. □ — 0.4% Be; 2.62% Co; 3.0% CoBe ▲ — 0.7% Be; 4.58%Co; 5.28% CoBe.

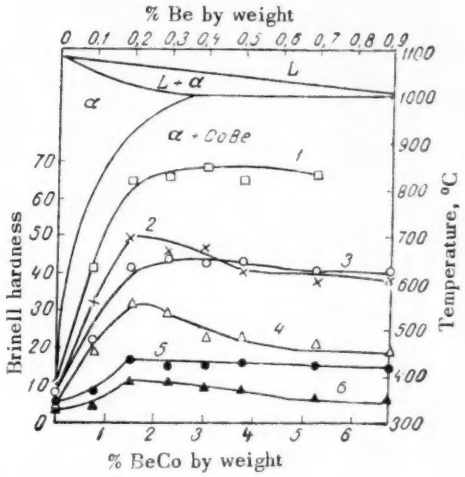

FIG. 3. Variation of hardness of alloys of the Cu-CoBe system with composition in the aged state:
1 — at 600° for 30 sec; 2 — at 600° for 1 hr;
3 — at 700° for 30 sec; 4 — at 700° for 1 hr;
5 — at 800° for 30 sec; 6 — at 800° for 1 hr.

is sufficient for obtaining peak mechanical properties of alloys of the Cu-CoBe pseudo-binary system. This can be explained by the fact that the two-phase structure is already formed in the quenched alloys containing more than 0.3 per cent Be and more than 1.96 per cent Co. (Fig. 1). The supersaturation of the solid s dution with higher content of Be and Co after quenching is not changed effectively. The super-saturation is evidently similar to that in the quenched alloy of Cu + 0.3 per cent Be + 1.96 per cent Co.

The following results were obtained for mechanical properties of alloys from the Cu-CoBe radial system investigated after their thermal treatment (quenching from 990°, tempering at 470° for 3 hr): σ_b = 76 kg/mm², σ_s = 69 kg/mm², δ = 3 per cent.

High temperatures of the solidus and tempering (470°) of the alloys and the great increase of hardness at the first instant followed by a slight decrease indicate that the alloys belonging to the Cu-CoBe pseudo-binary system are capable of retaining their strength at high temperatures. The results of hardness tests of long (1 hr) and short (30 sec) duration at temperatures of 600, 700 and 800°C (Fig. 3) indicate that the alloys of the Cu-CoBe pseudo-binary system are heat-resistant.

THERMAL AND ELECTRIC CONDUCTIVITIES OF THE ALLOYS OF Cu-CoBe RADIAL SECTION OF THE Cu-Be-Co SYSTEM

The thermal and electric conductivities were measured in the alloys of the system having the following composition (Table 2).

It is evident from the constitutional diagram (see Fig. 1) that the solubility of the chemical compound increases with temperature. The thermal treatment of the alloys of this system should, therefore, affect their thermal and electric conductivities. For this reason the alloys were studied in both quenched and temper-hardened states. The thermal treatment of the alloys is described above.

It should be noted that the age-hardened alloys after 6 hr are not in equilibrium both at the tempering and room temperatures. The solid solution contains more solute than required for the equilibrium composition. This fact substantially affects the thermal conductivity and the electrical resistance, also their variation with temperature when the alloy is slowly heated up to and above the tempering temperature.

The electrical resistance of the quenched alloys is 2-2.5 times that of the temper-hardened alloys. The resistivity of the quenched testpieces measured in the temperature range of 250-500° decreases approximately to 2/3rd of the value at 250°. This drop in resistivity is due to the decomposition of the solid solution with precipitation of the CoBe chemical compound (Fig. 4).

The alloy containing 99.25 per cent Cu, 0.1 per cent Be and 0.65 per cent Co is an exception. The resistivity of this alloy, up to 200°C, is half that of

VOL. 8 1959

TABLE 2. Contents of components in alloy investigated, % by weight

Cu	Be	Co	Cu	Be	Co
99.25	0.10	0.65	96.23	0.50	3.27
98.49	0.20	1.31	94.45	0.70	4.58
97.74	0.30	1.96	93.21	0.90	5.89
96.98	0.40	2.62	—	—	—

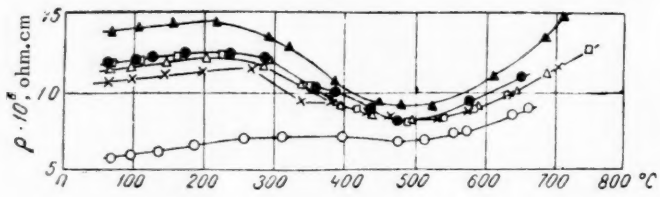

FIG. 4. Relation between resistivity and temperature for the Cu-Be-Co alloys in the quenched state:

○ — Cu + 0.1% Be + 0.65% Co; × — Cu + 0.2% Be + 1.31% Co;
△ — Cu + 0.3% Be + 1.96% Co; □ — Cu + 0.4% Be + 2.62% Co;
◇ — Cu + 0.5% Be + 3.27% Co; ▲ — Cu + 0.9% Be + 5.86% Co.

the alloy which has maximum solubility of the chemical compound in copper at eutectic point. At higher temperatures the solid solution of this alloy also decomposes and the CoBe chemical compound is precipitated but in smaller quantities than in alloys containing, in their quenched state, more of the CoBe compound in solid solution. For this reason the variation in resistivity of the former with rise of temperature from 260 to 500° differs from that for the remaining alloys. The resistivity of the alloy containing 99.25 per cent Cu, 0.1 per cent Be and 0.65 per cent Co in the above temperature range remains practically constant while decreasing in other alloys (see Fig. 4).

The value of resistivity and its variation with temperature in the alloys of the Cu-CoBe pseudobinary system in non-equilibrium state is evidently conditioned by two sources: the decomposition of solid solution and the change of resistivity with temperature. The former lessens the resistivity (see Fig. 4).

The opposite effects of the above two sources have just resulted in obtaining the variation of resistivity with temperature shown in Fig. 4. In the alloy containing 99.25 per cent Cu, 0.1 per cent Be, 0.65 per cent Co the influence of these sources at temperatures from 260 to 500° are equal in value and opposite in sign. The resistivity of this alloy remains practically constant with the rise of temperature. However, in the alloys of different composition the effect of the solid solution decomposition on the decrease of resistivity predominates the usual rise of resistivity with temperature. In these alloys, therefore, the resistivity decreases in the temperature range of 250-500°C. For temperatures above 500°, the temperature is the principal factor affecting the resistivity of alloys of the Cu-CoBe system; with rise of temperature the resistivity increases.

Thus, at raised temperatures the alloys belonging to the radial section of the Cu-CoBe system should represent a two-phase non-equilibrium system of α + CoBe mechanical mixture. In this system the variation of specific resistance with content of CoBe must be linear. In Fig. 5 the isotherms of resistivity of the alloys from the radial section of the Cu-CoBe system are shown as measured after quenching (from 990°).

It is apparent from Fig. 5 that the change of resistivity is linear (in alloys containing from 1.5 to 6.78 per cent CoBe). The alloys of the Cu-CoBe system, therefore, represent a mechanical mixture α + CoBe.

The resistivity of alloys belonging to the radial section of the Cu-CoBe system (containing up to 7 per cent CoBe) in the aged state of previously quenched alloys increases in the whole range of temperature investigated (from room temperature

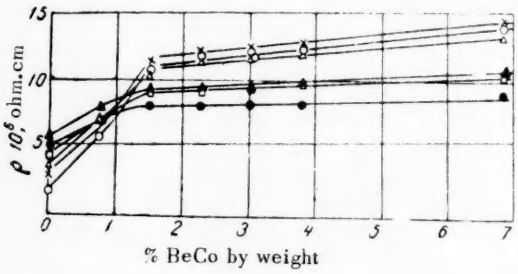

FIG. 5. Isotherms of resistivity for alloys of the Cu-CoBe radial section of the Cu-Co-Be system measured after quenching:

○ — 100°; × — 200°, △ — 300°; □ — 400°; • — 500°; ▲ — 600°.

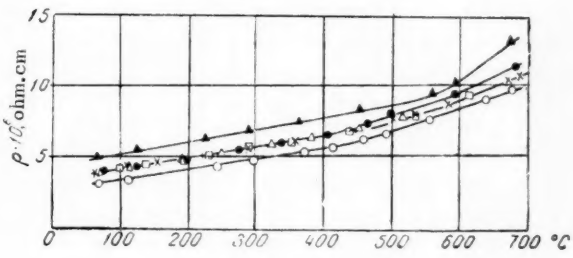

FIG. 6. Relation between resistivity and temperature for alloys of the Cu-CoBe section in the tempered state (470°) after quenching:

○ — Cu+0.1% Be +0.65% Co; × — Cu+0.2% Be +1.31% Co;
△ — Cu+0.4% Be +2.62% Co; □ — Cu+0.5% Be +3.27% Co;
• — Cu+0.7% Be +4.58% Co; ▲ — Cu+0.9% Be +5.89% Co

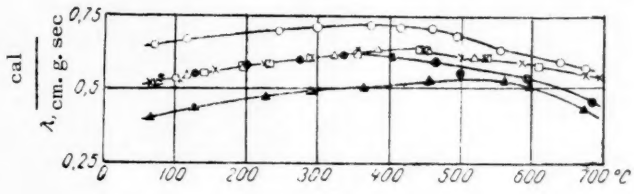

FIG. 7. Relation between thermal conductivity and temperature for alloys of the Cu-CoBe radial section in the tempered state (470°) after quenching:

○ — Cu+0.1% Be +0.65% Co; × — Cu+0.2% Be +1.31% Co;
△ — Cu+0.4% Be +2.52% Co; □ — Cu+0.5% Be +3.27% Co;
• — Cu+0.7% Be +4.58% Co; ▲ — Cu+0.9% Be +5.89% Co.

to 700°, Fig. 6). This can be explained by the fact that in the age-hardened alloys the decomposition of the solid solution when heated proceeds less rapidly than in the "as quenched" condition. In this case a general increase in resistivity with temperature is still noticeable despite the fact that the decomposition of solid solutions lowers the resistivity.

The resistivity of alloys containing Cu, Be and Co in the quantities given in the following table

Cu	98.49	96.98	96.23
Be	0.20	0.40	0.50
Co	1.31	2.62	3.27

coincides in the temperature range from room temperature to 700° and its value approximately amounts to 1/2-2/5 the value of the quenched testpieces as measured up to 300°.

It was shown above that the resistivity decreases with precipitation of the chemical compound from solid solution. For this reason the resistivity of the tempered alloys is 1/2-2/5 that of the quenched.

Different rate of solid solution decomposition (with precipitation of chemical compound) in the alloys with different content of the CoBe chemical compound disolved in copper (at the same temperature), non-equilibrium state of the system and the decrease in resistivity by the decomposition of solid solution have just resulted in obtaining the same value of resistivity in the wide range of temperatures.

The method of investigating the thermal and electric conductivities of metals and alloys developed by us [1-3] made it possible to simultaneously determine on the same testpiece the temperature dependence of both the ratio of thermal conductivity to electric conductivity and the electric conductivity itself. It was found that Wiedemann-Franz ratios obtained experimentally for the above alloys in the age-hardened state are in good agreement with the theoretical relation:

$$\frac{\lambda_E}{\chi T} = 2.45 \times 10^{-8} \text{ W.ohm/deg}^2.$$

In deriving Wiedemann-Franz ratio and in theoretical explaining of the process of heat conduction it was assumed that the conduction of heat and electricity in metals is carried out by electrons alone. A heat conduction by the lattice of metal was not taken into consideration. Since the Wiedemann-Franz ratio obtained experimentally for the Cu-CoBe alloys investigated coincides with its theoretical value, it can be accepted that in these alloys the process of conduction is practically maintained by electrons alone.

The thermal conductivity of the alloys investigated increases with temperature (Fig. 7). At a temperature of 400° the ratio of the thermal conductivity of the alloys to that of copper λ/λ_{Cu} reaches 55-77 per cent. The increase of thermal conductivity of the Cu-CoBe alloys with rise of temperature can be explained by proceeding from Wiedemann-Franz relations. In this case the thermal conductivity is determined by the relationship:

$$\lambda_E = 2.45 \times 10^{-8} \chi T \text{ W/cm.deg.}$$

Consequently, the thermal conductivity and its variation with temperature are determined by the product χT. The tests show that for the alloys of the alloys of the Cu-CoBe radial section the product χT increases with rise of temperature up to 400°, which leads to the increase of thermal conductivity and with further rise above 400° the product χT gradually decreases and consequently so does the thermal conductivity (see Fig. 7).

CONCLUSION

1. The composition diagram of the pseudo-binary Cu-CoBe system is constructed.

2. The strength and hardness of the alloys of this system investigated.

3. The thermal and electric conductivities of alloys of the Cu-CoBe radial section of the Cu-Be-Co system investigated. It is established that the alloys tempered after quenching have higher thermal and electric conductivities than copper. The variation of non-dimensional quantities λ/λ_{Cu} and χ/χ_{Cu} are similar and their numerical values equal. With rise of temperature these ratios increase and at 400° reach the value amounting to 55-77 per cent of that for copper. These ratios also indicate that Wiedemann-Franz ratio holds also in conditions when λ and χ separately deviate from the theoretically calculated relationship.

4. Wiedemann-Franz ratio is applicable to pure metals, homogeneous and heterogeneous metal alloys if the process of their thermal conductivity is mainly maintained by electrons.

Translated by B. Cynk

REFERENCES

1. V. Mikryunov, *Vest. M.G.U. (Bulletin of Moscow State University), ser. mat., mekh., astr., fiz., khim.*, No. 2 (1956).

2. V. Ye. Mikryunov, *Vest. M.G.U. (Bulletin of Moscow State University), ser. mat., mekh., astr., fiz., khim.*, No. 2 (1957).

3. V.Ye. Mikryunov, *Vest. M.G.U. (Bulletin of Moscow State University), ser. mat., mekh., astr., fiz., khim.*, No. 3 (1957).

LETTERS TO THE EDITOR

SPIN-ELECTRON RELAXATION IN ANTIFERROMAGNETICS*

Iu. SEIDOV and A. BERDYSHEV

Urals A.M. Gor'ki State University

(Received 26 June 1958)

If a system of spin waves of an antiferromagnetic is by some means taken out of the state of thermal equilibrium it may restore this state as a result of the combined action of several mechanisms. In particular, in antiferromagnetic metals and alloys one can point to three basic mechanisms of restoring the equilibrium in a system of spin waves: collisions of the spin waves with each other, their interaction with phonons and interaction with conductivity electrons.

The first two mechanisms have been discussed by Tsukernik [1]. We have studied the third mechanism. As the basis for the calculation we have assumed an *s-d* exchange model [2, 3]. The energy operator of the system of the $s + d$ electrons has the form [2, 3]†

$$H = -\frac{1}{2}\sum{}' J(\vec{n}_1, \vec{n}_2)\, a^+_{n_1\sigma_1} a_{n_1\sigma_2} a^+_{n_2\sigma_2} a_{n_2\sigma_1} - \\ -\frac{1}{N}\sum e^{i\vec{n}(\vec{k}_2-\vec{k}_1)}\, a^+_{n\sigma_1} a_{n\sigma_2} a^+_{k_1\sigma_2} a_{k_2\sigma_1}, \tag{1}$$

where $J(\vec{n}_1, \vec{n}_2)$ is the *d-d* exchange integral; $J(\vec{n}_1, \vec{n}_2) < 0$; $I(\vec{k}_1, k_2)$ is the integral of the interaction of the *d* electrons with the states $\vec{k}_1$ and $\vec{k}_2$ of the conductivity electrons; $a_{n\sigma}$ and $a_{k\sigma}$ are Fermi statistics operators. Let us go over from the Fermi amplitudes $a_{n\sigma}$ to spin operators by the well known formulae [4] and from these to spin deviation operators b_n with the aid of Ziman's formalism [5]:

$$a^+_n(-)\,a_n + a^+_n\,a_n(-) = s^x_n/s \approx (2s)^{-1/2}(b_n + b^+_n);$$
$$a^+_n(-)\,a_n(-) - a^+_n\,a_n = s^z_n/s = \frac{1}{s}\,e^{i\vec{\omega}\vec{n}}(s - b^+_n\,b_n);$$
$$i\,[a^+_n(-)\,a_n - a^+_n\,a_n(-)] = s^y_n/s \approx (2s)^{-1/2}\,ie^{i\vec{\omega}\vec{n}}(b_n - b^+_n);$$
$$a^+_n(-)\,a_n(-) + a^+_n\,a_n = 1. \tag{2}$$

Here $\vec{\omega}$ is the vector of the reciprocal lattice so that $e^{i\vec{\omega}\vec{n}}$ is + 1 at the nodes of one sub-lattice and − 1 at the nodes of the other. The *d* part of operator (1) H_{dd} coincides with Ziman's (24). The proper values of H_{dd} were found with the method of the canonic equations for the movement of the operators [3] and are in agreement with Ziman's proper values. The substitution for the diagonalization of H_{dd} has the form

---

* *Fiz. metal. metalloved.*, 8, No. 1, 147-160, 1959.

† Here and further on summation over all lower indices is understood.

$$b_n = \left(\frac{N}{2}\right)^{1/2} \sum_{\mu} \left[\left(\frac{A_\mu}{E_\mu} + 1 \right)^{1/2} e^{i\vec{\mu}\vec{n}} \xi_\mu + \left(\frac{A_\mu}{E_\mu} - 1 \right)^{1/2} e^{-i\vec{\mu}\vec{n}} \xi_\mu^+ \right], \tag{3}$$

where

$$F_\mu = (A_\mu^2 - |B_\mu|^2)^{1/2}; \quad B_\mu = -s \sum_{\langle h \rangle} J(\vec{h}) (1 \quad \sigma_h) e^{i\vec{\mu}\vec{h}};$$
$$A_\mu = B_\mu + 2s \sum_{\langle h \rangle} J(\vec{h}) \sigma_h + g\beta H_a; \tag{4}$$

ξ_μ are Bose statistics operators; $< h >$ means summation over the closest neighbours, $\sigma_h = e^{i\vec{w}\vec{h}}$; H_a is the field of the magnetic anisotropy; E_μ is the energy of the spin wave with vector μ for $H = 0$.

The sum of the energy operators of the conductivity electrons and the energy of the s-d exchange consists of two parts. The first part

$$H_{sd}^{(2)} + H_{sd}^{(4)} = \sum \left[E_k + \frac{1}{4} I(\vec{k}, \vec{k}) \right] a_{k\sigma}^+ a_{k\sigma} +$$
$$+ \frac{1}{4} \sum I(\vec{k}, \vec{k} - \vec{w}) [a_{\vec{k}}^+ a_{k-w} - a_{\vec{k}}^+ (-) a_{k-w} (-)] -$$
$$- \frac{1}{2sN} \sum I(\vec{k}_1, \vec{k}_2) e^{in(\vec{k}_2 - \vec{k}_1 + \vec{w})} b_n^+ b_n [a_{k_1}^+ a_{k_2} - a_{k_1}^+ (-) a_{k_2} (-)] \tag{5}$$

describes the translation energy of the conductivity electrons "submagnetized" by the field of the spin waves. (5) can be diagonalized by the same method as H_{dd}. As a result it turns out that the level of the s-electrons are split into two sub-bands and that the width of the gap between them is in proportion to the magnetization of the sub-lattices [3, 6]. Here we shall not examine this effect but confine ourselves to making an estimate of the effect of the s-d exchange interaction with the free conductivity electrons. This interaction is described by the second part of the operator of the s-d exchange interaction.

$$H_{sd}^{(3)} = -\frac{1}{2} (2sN)^{-1/2} \sum I(\vec{k}_1, \vec{k}_2) e^{in(\vec{k}_2 - k_1)} \{ [(1 - e^{i\vec{w}\vec{n}}) b_n +$$
$$+ (1 + e^{i\vec{w}\vec{n}}) b_n^+] a_{k_1}^+ (-) a_{k_2} + [(1 - e^{i\vec{w}\vec{n}}) b_n^+ + (1 + e^{i\vec{w}\vec{n}}) b_n] a_{k_1}^+ a_{k_2} (-) \}. \tag{6}$$

Substituting (6) in expression (3) we obtain an operator which describes the inelastic collisions of the conductivity electrons with the spin waves; in each of these individual collisions a spin wave either emerges or is absorbed. Let us write out the first of the four members of this expression

$$\frac{1}{4} (2sN)^{-1/2} \sum E_\mu^{-1/2} I(\vec{k}_1 \vec{k}_2) e^{i(\vec{k}_2 - \vec{k}_1 + \vec{\mu})\vec{n}} [(A_\mu + E_\mu)^{1/2} (1 - e^{i\vec{w}\vec{n}}) +$$
$$+ (A_\mu - E_\mu)^{1/2} (1 + e^{i\vec{w}\vec{n}})] a_{k_1}^+ (-) a_{k_2} \xi_\mu.$$

The change in the number of spin waves per unit time is found in the usual manner [7]*

* Here and further on $\hbar$ stands for the Plank constant divided by 2.

$$\frac{dn_\mu}{dt} = \frac{\pi}{16sh} \sum |I(\vec{k}_1 \vec{k}_2)|^2 E_\mu^{-1} \left\{ A_\mu + \sqrt{A_\mu^2 - E_\mu^2} \right) \delta(\vec{k}_2 - \vec{k}_1 + \vec{\mu}) -$$
$$- \left(E_\mu + \sqrt{A_\mu^2 - E_\mu^2} \right) \delta(\vec{k}_2 - \vec{k}_1 + \vec{\mu} + \vec{w}) \Big\} \cdot$$
$$\cdot [n_\mu (n_{k_1} - n_{k_2}) + n_{k_1} (1 - n_{k_2})] \delta(E_{k_2} - E_{k_1} + E_\mu),$$

where n_k is the Fermi distribution, n_μ the Bose distribution.

Hence we find for the average relaxation time

$$w_{c-s} = \frac{1}{\tau_{c-s}} = \frac{\pi}{16sh} \left(\sum_\mu n_\mu \right)^{-1} \sum E_\mu^{-1} |I(\vec{k}_1 \vec{k}_2)|^2 \cdot$$
$$\cdot \left[\left(A_\mu + \sqrt{E_\mu^2 - A_\mu^2} \right) \delta(\vec{k}_2 - \vec{k}_1 + \vec{\mu}) - \left(E_\mu + \sqrt{A_\mu^2 - E_\mu^2} \right) \cdot \right. \tag{7}$$
$$\left. \cdot \delta(\vec{k}_2 - \vec{k}_1 + \vec{\mu} + \vec{w}) \right] exp \frac{E_{k_2} - \zeta}{kT} n_{k_1} n_{k_2} \delta(E_{k_2} - E_{k_1} + E_\mu).$$

VOL. 8 1959

The denominator in (7) is equal to

$$\sum n_\mu = \frac{\pi N}{S2} \left(\frac{kT}{zI} \right)^3.$$

Let us now calculate the numerator.

Let

$$A_1 = \frac{13}{4hsN} \left(\frac{zI}{kT} \right)^2.$$

Then $w_{c-s} = A_1 (w_1 - w_2)$. The first item here describes simple transitions, the second transitions analogous to the transfer processes of the theory of phonon resistance; we shall not discuss these latter processes. To calculate ω_1 we go over from summation to integration in the wave number space. For a simple cubic lattice

$$A_\mu + \sqrt{A_\mu^2 - E_\mu^2} = zJ [1 + (1 - \mu^2)^{1/2}], \; I(\vec{k}_1, \vec{k}_2) = 2\alpha' + \beta' (k_1^2 + k_2^2),$$
$$\alpha' = \frac{1}{2} I_0, \; \beta' = I_1.$$

Then

$$\omega_1 = \frac{4N^2}{(2\pi)^4} \int (1 + \sqrt{1 - \mu^2}) \left\{ \alpha'^2 + \alpha' \beta' [k^2 + (\vec{k} - \vec{\mu})^2] exp \frac{E_k - E_\mu - \zeta}{kT} \right.$$
$$\left. \cdot \left(exp \frac{E_k - \zeta}{kT} + 1 \right)^{-1} \left(exp \frac{E_k - E_\mu - \zeta}{kT} + 1 \right)^{-1} k^2 dk \, \mu \, d\mu \, d \cos \vartheta_{k\mu} \right.,$$

where it is assumed that $k \equiv ka, \mu \equiv \mu a$; I signifies the absolute value of the d-d exchange integral; I_0 and I_1 are the s-d exchange integrals within one atom and between neighbouring atoms respectively. Let us assume that $I_1 < I_0 < j$. It follows from the law of the conservation of energy

$$E_{k-\mu} - E_k + E_\mu = 0 \quad \text{that} \quad \cos \vartheta_{k\mu} = (zJ + A\mu/2Ak,$$

where A is the transfer integral of the single electron theory. Let us go over to dimensionless

variables

$$x = \frac{E_k - \zeta}{kT}, \quad y = \frac{E_\mu}{kT}, \quad E_k = Ak^2, \; E_\mu = zJ\mu.$$

Then

$$w_1 = A_2 \int_{-x_1}^{\infty} \frac{dx}{(e^x + 1)} \int_0^{y_2} \left\{1 + \sqrt{1 - (kTy/zJ)^2}\right\}$$
$$\left\{1 + \frac{\beta'}{A\alpha'} [2(kTx + \zeta) - kTy]\right\} \frac{e^{x-y}}{e^{x-y} + 1} dy,$$

where $A_2 = (NkT\alpha')^2/(2\pi)^4 zJA^2$. The limits of integration are determined by the conditions $\mu > 0$, $k > 0$, $|\cos\vartheta_{k\mu}| \leqslant 1$. Therefore, the region of integration is the upper angle of the first square of the plane

$$(xy) \; -x_1 < x < \infty, \; 0 < y < y_2, \text{ where } x_1 = \frac{1}{kT}\left[\zeta - \left(\frac{zJ}{2A}\right)^2\right] \text{and} y_2 = \frac{zJ}{kT}\left(2k - \frac{zJ}{A}\right).$$

At low temperatures one can in the expression under the integral sign neglect the dependence on y and let y_2 approach infinity. This gives a sufficiently accurate result. Then the integral with respect of y is calculated in an elementary way and

$$w_1 = A_2 \int_{-x_1}^{\infty} \frac{dx}{(e^x + 1)} \ln(e^x + 1)\left[1 + \frac{\beta'}{A\alpha'}(\zeta + kTx)\right].$$

The latter integral is calculated with method [2]. We find finally

$$w_{c-s} = \frac{39(\alpha' J)^2}{16kTh(\pi A)^2}\left\{3\left(1 + \frac{\beta'}{\alpha'}\frac{\zeta}{A}\right) + kT\frac{2\beta'}{A\alpha'}\ln 2\right\}.$$

We assume that $\beta' < \alpha'$. Hence, discarding members with β'/α' we get

$$w_{c-s} \approx \frac{117}{64\pi^2}\frac{(JI_0)^2}{hkTA^2} = \frac{117}{64\pi^2}\frac{I_0^2\vartheta_{Nk}^2}{hz^2A^2}.$$

For a rough quantitative estimate we substitute

$$A \approx 10^{-12}, \; I_0 \approx 10^{-14} \; [2], \; \vartheta_N = \frac{zI}{k} \approx 10^2$$

then

$$w_{c-s} = \frac{1}{\tau_{c-s}} \approx \frac{10^8}{T}.$$

Translated by B. Ruhemann

REFERENCES

1. V.M. Tsukernik, *Fiz. metal. metalloved.*, 4, 566, (1957).
2. Ye.A. Turov, *Izv. Akad. Nauk SSSR, ser. fiz.* 19, 462 (1955).
3. S.V. Vonsovskii and A.A. Berdyshev, *Izv. Akad. Nauk SSSR, ser. fiz.* 18, 328 (1954).
4. A.A. Berdyshev and K.V. Shitikova, *Fiz. metal. metalloved.*, 7, 21 (1959).
5. I.M. Ziman, *Proc. Phys. Soc. A*, 65, 540 (1952) (There is a translation in the collection *Antiferromagnetism*, I. Leningrad (1956).
6. Iu. Irkhin, *Fiz. metal. metalloved.*, 6, 214; 586 (1958).
7. J. Achiejer, *Journ. of Physics USSR* 10, 217, (1946).
8. N.N. Bogoliubov, *Lektsii z kvantovoi statistiki (Lectures on quantum statistics)*, Kiev (1949).

VOL.
8
1959

TO THE QUESTION OF THE COMPLEX PERMEABILITY OF MAGNESIUM FERRITES*

L.A. FOMENKO

(Received 12 June 1958)

Chiron and Prache [1] have described the results of measurements of the magnetic spectrum of Mg ferrite with an initial magnetic permeabiiity of μ_a = 9 G oersted^{-1} in the frequency range of 100–3000 M Hertz. The experimental data was presented in the form of a curve $q' = \varphi_1(q'')$ using the frequency f as parameter. Here the significance of q' and q'' is related to the complex magnetic permeability $\mu' = \mu - j\rho'$ of the ferrite matter in the following manner:

$$q' + jq'' = (\mu_a - 1)/(\mu' - 1),$$

whence we obtain

$$\mu - 1 = (\mu_a - 1)\frac{q'}{q'^2 + q''^2}; \quad \rho' = (\mu_a - 1)\frac{q''}{q'^2 + q''^2}. \tag{1}$$

The curves $\mu' = \varphi_2(f)$, were calculated by us from the data of paper [1] and are given in the figure.

The results of the experiments were in the work referred to integrated in the region of ratio frequency dispersion (for $f < 500$ MHertz), contrary to the conclusions of Rado [2] and the gyromagnetic resonance according to Snoek [3], and in the region of ultra frequency dispersion (for 500 – 2800 MHertz) by other mechanisms. This point of view was, however, based on very loose assumptions concerning the singularity of the gyromagnetic resonance frequency and the equality sign between the mechanism describing the general change in the average values of μ' in the range of

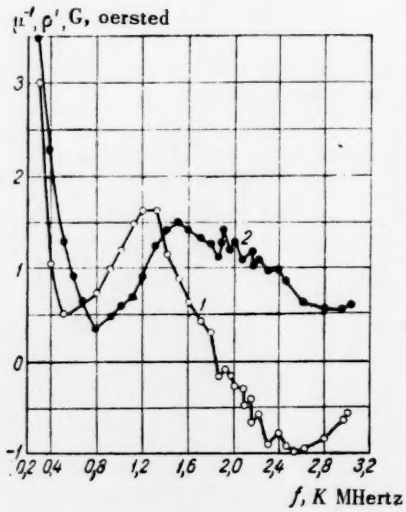

FIG. 1. Magnetic spectrum of Mg ferrite after the data of paper [1]:
1 – dispersion curve;
2 – absorption curve.

* *Fiz. metal. metalloved.*, 8, No. 1, 150-152, 1959.

500 – 2800 MHertz (including the change of the sign of $(\mu_1 - 1)$), and the mechanisms describing the fluctuations of these parameters at 1800 – 2800 MHertz, and therefore, (being apparently inspired by the somewhat unusual form of the curves presented in paper [1]) cannot be accepted when the mechanism of the phenomena are discussed.

From a study the curves $\mu' = \phi_2(f)$ it follows that the average resonance frequency of the ultra high frequency dispersion $f_0 = f_f \approx 1850$ MHertz, where f_f is the frequency for which $(\mu_1 - 1 = 0)$. The frequency $f_f > f_u$ ($f_u \approx 1550$ MHertz is the average frequency of the maximum absorption) and is not equal to the frequencies for the maximum and minimum value of μ (~ 1250 and 2600 MHertz), which is as it should be according to the theory for an oscillating system with noticeable damping and frequency dependent parameters μ and ρ' (because of the effect of the radio frequency dispersion and the distribution of the gyromagnetic resonance frequencies within a certain frequency range).

The value for f_f agrees satisfactorily with the values for this frequency obtained for ferrites of similar composition in the paper by Rado, Folen and Emerson [4] and also (in as much as in polycrystalline specimens the anisotropy parameter is effectively increased [5]) with the value for the average ferromagnetic resonance frequency $f_{0vr} = 940$ MHertz if it is calculated with formula (2) and the data: first order anisotropy parameter $K_1 = -2.5 \times 10^4$ erg/cm³ and magnetic saturation $I_s \approx 100$ G for magnesium ferrite [4]*.

$$f_{0\,vr} = \frac{ge}{4\pi mc} H_i = \frac{1}{1{,}5\pi} \frac{ge}{2mc} \frac{K_1}{I_s} \approx 3.74 \frac{K_1}{I_s}. \qquad (2)$$

The agreement obtained for the results makes it possible to describe the ultra high frequency dispersion in Mg ferrite [1] as gyromagnetic resonance; as far as the radio frequency dispersion is concerned the possibility of describing it as resonance of the same type must evidently be discarded, which leaves the possibility of explaining it according to papers [2, 4] by processes of boundary shifts. Concerning the fluctuations of the values of μ' noted in paper [1], if they are not caused by the errors of measurement or the effect other dispersion mechanisms, one may note that in part their appearance may be caused by the distribution of the gyromagnetic resonance frequencies.

Translated by B. Ruhemann

REFERENCES

1. B. Chiron and P.M. Prache, *Cables et Transmission* 10, No. 1, 73 (1951).
2. G.T. Rado, R.W. Wright, and W.H. Emerson, *Phys. rev.* 80, 273 (1950).
3. J.L. Snoek, *Phys. the Hague* 14, 207, (1948).
4. G. T. Rado, U.J. Fole and W.H. Emerson, *Convention on ferrites of the I.E.E.*, 2174 R (1956).
5. L.A. Fomenko, *U.F.N.* 64, 669 (1958).
6. J. Smit and H.P. Wijn, *J. Adv. in Electron a. Electron Phys.* 6, Acad. Press N.Y. (1954).
7. C. Kittel', *Ferromagnitnyi rezonans, (Ferromagnetic resonance)* I.I. Leningrad-Moscow 18 (1952).

* This formula is derived [6] from the fact that in ferrites K_1 is negative and the axes of [111] type are axes of slight magnetization. With Kittel's formula we also get a similar value $f_{0vr} = (1/\pi)$ (ge/2mc) $(K_1/I_s \approx 5.58$ $(K_1/I_s = 1410$ MHertz). Both formulae are derived without taking account of the damping effect, the effective increase in K_1, the "natural" distribution of the gyromagnetic resonance frequencies (due to the inhomogeneity of the material, magnetic interaction and other causes) and the "effective" distribution of the latter (due to the frequency dependence of μ and ρ' because of the effect of radio frequency dispersion).

THE BASIC STATE AND THE SPECTRUM OF ELEMENTARY EXCITATIONS OF ISOTROPIC FERRITE*

S.V. TIABLIKOV

"A.V. Steklov" Mathematical Institute

(Received 28 July 1958)

The spin-wave treatment of ferrites on the basis of the Néel model has recently been carried out in papers [1, 2, 3 - 6]. In these papers functions of T^2 and $T^{3/2}$ were respectively obtained in these papers for the temperature dependence of the magnetization. In paper [6] it was noted that this depends on differences in the approximations made in introducing the ferrite model.

Following [6] we examine the case which covers both groups of the results mentioned. We shall consider a ferrite as an aggregate of two sub-lattices placed one inside the other and characterized by the number of nodes N_i and the spin moments s_i of the nodes (i is the number of the sub-lattice). The Hamiltonian is written in the form:

$$\mathbf{H} = -\frac{1}{2}\sum I(f_1 - f_2)(s_{f_1}, s_{f_2}) - \frac{1}{2}\sum I(g_1 - g_2)(s_{g_1}, s_{g_2}) - \\ - \sum I(f \quad g)(s_f, s_g) - \mu_1 \sum (H, s_f) - \mu_2 \sum (H, s_g), \tag{1}$$

where the indices f and g relate to the first and second sub-lattice, while for the exchange integrals it is proposed that

$$I(f_1 - f_2),\ I(g_1 - g_2) > 0;\ I(f - g) < 0.$$

In order to be specific we shall also assume that the magnetic moments of the sub-lattices satisfy the condition

$$M_1 - M_2 = N_1\mu_1\sigma_1 - N_2\mu_2\sigma_2 > 0, \tag{2}$$

where σ_i means the spin of the node of sub-lattice i.

For the energy of the basic state in zero approximation as a function of the strength of the external field H we obtain:

$$E_0 = \begin{cases} \varepsilon - H_e\sqrt{M_1M_2} - (M_1 - M_2)H, & 0 \leqslant H \leqslant H_1; \\ \varepsilon - H_e\dfrac{M_1^2 + M_2^2}{2\sqrt{M_1M_2}} - \dfrac{\sqrt{M_1M_2}}{2H_e}H^2, & H_1 \leqslant H \leqslant H_2; \\ \varepsilon + H_e\sqrt{M_1M_2} - (M_1 + M_2)H, & H_2 \leqslant H; \end{cases} \tag{3}$$

$$\left(\varepsilon = -\frac{1}{2}N_1\overline{I}_{11} - \frac{1}{2}N_2\overline{I}_{22}\right).$$

* *Fiz. metal. metalloved.*, 8, No. 1, 152-154, 1959.

Here the following designations are introduced:

$$H_1 = H_e \frac{M_1 - M_2}{\sqrt{M_1 M_2}}; \quad H_2 = H_e \frac{M_1 + M_2}{\sqrt{M_1 M_2}};$$
$$H_e = \sqrt{\frac{\sigma_1 \sigma_2}{\mu_1 \mu_2}}\, \bar{I}_{12} \bar{I}_{21}; \tag{4}$$
$$\bar{I}_{ij} = I_{ij}(\nu)|_{\nu=0} = \sum I(h_i - h_j)\, e^{i(h_i - h_j)\nu}|_{\nu=0}; \quad (i, j = 1, 2).$$

The expression for the magnetization in zero approximation is easy to obtain from (3) by differentiation in respect of H.

The expression for the spectrum of the elementary excitations depends on the range of values in which H lies. For "weak" fields ($0 \leqslant H < H_1$) we get for the two branches of the spectrum (corresponding to the number of sub-lattices) with a precision down to members of the order of ν^2:

$$E_\nu^{I,\,II} = \pm (c + \alpha\nu^2) + \sqrt{C^2 + D^2 + \beta\nu^2},$$
$$C = \frac{1}{2}(\mu_1 - \mu_2) H - \frac{1}{2}(\mu_1 + \mu_2)(H_1 - 2H); \tag{5}$$

$$D^2 = 4\mu_1\mu_2 H(H_1 - H); \quad \alpha = \alpha_{11}\sigma_1 - \alpha_{22}\sigma_2;$$
$$\beta = \{(\mu_1 + \mu_2) H_2 - (\mu_1 - \mu_2)(H_1 - 2H)\}(\alpha_{11}\sigma_1 + \alpha_{22}\sigma_2) +$$
$$\pm 2\sqrt{\frac{\alpha_{12}\alpha_{21}}{N_1 N_2}}\{M_1(H_2 - H_1) + M_2(H_2 + H_1)\}; \tag{6}$$
$$(\alpha_{ij}\nu^2 \cong \bar{I}_{ij} - I_{ij}(\nu)).$$

Substituting $N_1 = N_2$; $\sigma_1 = \sigma_2$; $\mu_1 \neq \mu_2$, in (6) we get $(\mu_1 - \mu_2)\ H_2 = (\mu_1 + \mu_2) H_1$ and (5) takes on the form

$$E_\nu^{I,\,II} = \pm\{(\mu_1 + \mu_2) H + \alpha\nu^2\} + \sqrt{\{(\mu_1 - \mu_2)^2 H + 4\mu_1\mu_2 H_1\} H + \beta\nu^2}. \tag{7}$$

In that case $E_\nu \sim \nu$ for $H = 0$. In the papers by Vonsovskii and Seidov [1, 2] the following specific case was in fact discussed.

If we substitute $\mu_1 = \mu_2$; $\sigma_1 = \sigma_2$; $N_1 \neq N_2$, in (6), (5) takes on the form

$$E_\nu^{I,\,II} = \pm\{\mu(2H - H_1) + \alpha\nu^2 + \sqrt{(\mu H_1)^2 + \beta\nu^2}, \tag{8}$$

which corresponds to the approximation of Kondovskii, Pakhomov, Shiklosh [3-5] and also to paper [6].

The case of the general formula (5) and also the somewhat more specific formula (8) yield a temperature dependence of $T^{3/2}$, while the case of formula (7) yields a dependence of T^2. One may therefore think that in ferrites in fields $H \leqslant H_1$ the magnetization will depend on the temperature rather according to the $T^{3/2}$ law than to the T^2 law, since the case of formula (7) is very special.

Translated by B. Ruhemann

VOL. 8 1959

REFERENCES

1. S.V. Vonsovskii and Iu.M. Seidov, *Izv. Akad. Nauk SSSR, ser. fiz.* 18, 319 (1954).
2. Iu.M. Seidov, *Kand. dissertatsiia, Azerb. gosuniversitet*, Baku (1956).
3. Ye.I. Kondorskii, A.S. Pakhomov and T. Shiklosh, *Dokl. Akad. Nauk SSSR* 109, 931 (1956).
4. T. Shiklosh, *Kand. dissertatsiia M.G.U., fizfak* (1955).
5. T. Shiklosh, *Acta Phys. Hung.* 7, 141 (1957).
6. S.V. Tiablikov, *Fiz. metal. metalloved.*, 3, 3 (1956).

VOL
8
195

TO THE THEORY OF VIBRATION SPECTRA OF SOLID SOLUTIONS*

A.N. MEN' and A.N. ORLOV
Physics of Metals Institute of the Academy of Sciences of the USSR
Sverdlovsk Agricultural Institute

(Received 25 August 1958)

To calculate the spectrum of the frequencies of the elastic vibrations of a one-dimensional model of a binary solid solution in the process of ordering we employed the method of effective atoms [1, 2]. For the investigation of the vibration spectrum of a three-dimensional binary solid solution of isotopes Lifshits and Stepanova [3] also intoduce the effective masses into the discussion. The method of effective atoms is applicable when the difference in the mass of the atoms of various kinds $M_j - M_{j'}$ and the difference in the coefficients of the elastic bond

$$A^{jj'}_{qq'} - A^{j''j'''}_{qq'}$$

are small, as a result of which the changes in the vibration spectra of an ideal single atom crystal of given symmetry caused by the atoms not being the same and by the deviation of their distribution in the lattice sites from the state of order may be regarded as small disturbances. The idea of the method is that by suitable selection of the zero approximation ("effective" fulness of the ordered lattice) the corrections of the first order of smallness to the spectrum of the frequencies can be reduced to vanishing point.

In the present note we wish to draw attention to the fact that the method of effective atoms both to the one-dimensional and to the three-dimensional case not only when the bond coefficients are the same but also when they are different and in the presence of any number of atoms in the elementary cell.

Let us consider a lattice consisting of N cells ($l = 1, 2, \ldots, N$) containing ν nodes each ($a = 1, 2, \ldots, \nu$) in which $N\nu$ atoms of r kinds ($j = 1, 2, \ldots, r$), close to their neighbours, are so disposed that the masses and bond coefficients satisfy the above mentioned conditions. We write the equations for the oscillations of the true lattice in which the atoms are present in arbitrary concentrations and distributed over the nodes in an arbitrary order, in the form [4]

$$(\hat{L} + \varepsilon\hat{\Lambda})\,\psi = E\,\psi, \tag{1}$$

where the components of the vector ψ

$$\psi^{\xi}_{al} = A^{\xi}_{al}\, e^{-i\omega t} \tag{2}$$

represent the distribution of the atoms in the node a of the cell l in the direction of the axis ξ ($\xi = 1, 2, 3$). Substituting (2) in (1) gives, as is well known, a system of $3N\nu$ linear equations for determining the amplitude $A^{\xi e}_{al}$, which we write in the form $(\hat{L}' + \varepsilon\hat{\Lambda}')\,A = EA$. Its secular equation has the form

$$\Delta\,(x) = 0, \tag{3}$$

---

* *Fiz. metal. metalloved.*, 8, No. 1, 154-156, 1959.

VOL. 8 1959

where $x = \omega^2$. We enumerate the $3N\nu$ radical equations (3) by $k = 1, 2, \ldots, 3N\nu$ and designate the corresponding proper functions by ψ^k. For the sake of brevity we shall occasionally designate the totality of indices l, by one letter, either p or q. In this way the (three-dimensional) component ψ^k which refers to the atom l, a is written ψ^k_p.

Now we introduce the effective lattice into the discussion, which is defined as follows. In the node a of any of its cells there is an atom with the mass.

$$\overline{M}_a = \sum_j M^j P^j_a, \tag{4}$$

where M^j is the mass of the atom of kind j and P^j_a the probability of a node of the a kind being occupied by an atom of the j kind

$$P^j_a = N^j_a / N_a, \tag{5}$$

where N_a is the number of nodes of kind a in the whole lattice, N^j_a the number of a nodes occupied by atoms of the j kind. The coefficient of the quasi-elastic bond of the atoms in the nodes l, a and l', a' is equal to

$$\overline{A}_{la,\, l'a'} = \sum_{j,\, j'} P^j_a P^{j'}_{a'} A_{jj'la l'a'}. \tag{6}$$

The determinant of the matrix of the operator L is a characteristic polynominal for the ordered lattice of which the proper function is designated by ψ^k_0.

The elements of the matrix $\varepsilon\hat{\Lambda}'$ have the form

$$(\varepsilon\hat{\Lambda}')_{pp'} = x\,\varepsilon\Lambda^{(1)}_{pp'} + \varepsilon\Lambda^{(2)}_{pp'}, \tag{7}$$

where

$$\varepsilon\Lambda^{(1)}_{pp'} = m_p \delta_{pp'}, \tag{8}$$

$$\varepsilon\Lambda^{(2)}_{pp'} = -\sum_{p''} \alpha_{pp''}\delta_{pp'} + \alpha_{pp'}(1 - \delta_{pp'}), \tag{9}$$

$$m_p = M_p - \overline{M}_a \tag{10}$$

(M_p is the mass of the atom situated in node p)

$$\alpha_{pp'} = A_{pp'} - \overline{A}_{pp'}. \tag{11}$$

We shall assume that the differences (10) and (11) are of the same order of smallness as ϵ.

According to the theory of excitations [5]

$$x_k = x_0 + \varepsilon\, x\, \Lambda^{(1)}_{kk} + \varepsilon\Lambda^{(2)}_{kk} + 0(\varepsilon^2) + \ldots,$$

where $x_0 = \omega_0^2$ is the proper frequency of the effective lattice and the matrix elements $\Lambda_{kk} = (\hat{\Lambda}\psi^k_0,\ \psi^k_0)$ are formed with the aid of the proper functions of the effective lattice ψ^k_0 (of zero approximation). We shall show that for our selection of the zero approximation in the form (4), (6), $\Lambda^{(1)}_{kk}$ and $\Lambda^{(2)}_{kk}$ tend

to zero. For this purpose we write (7) out, substituting (8) and (9)

$$\Lambda_{kk} = \sum_q [(x m_q - \sum_{q'} \alpha_{qq'}) \psi_{0q}^k + \sum_{q''} \alpha_{qq''} (1 - \delta_{qq''}) \psi_{0q''}^k] \psi_{0q}^k = \\ = x \sum_q m_q |\psi_{0q}^k|^2 - \sum_{q,q'} \alpha_{qq'} |\psi_{0q}^k|^2 = x \sum_q m_q - \sum_{q,q'} \alpha_{qq'}. \tag{12}$$

We transform the first item in the right hand part of (12)

$$\sum_q m_q = \sum_q M_q - \sum_q \bar{M}_\alpha = \sum_j M^j \sum_\alpha N_\alpha^j - \sum_\alpha \bar{M}_\alpha N_\alpha. \tag{13}$$

Substituting (4) and (5) in (13) we get

$$\sum_q m_q = 0. \tag{14}$$

Similarly, one can show that

$$\sum_{q,q'} \alpha_{qq'} = 0.$$

VOL. 8 1959

In this way, the spectrum of the frequencies of a solid solution with arbitrary concentrations, degree of ordering and number of atoms in the elementary cell agrees, with an error of small values of the order of ϵ^2, with the spectrum of the ordered solid solution of the effective atoms the properties of which are determined by formulae (4) and (6). The dependence of the probabilities P_α^i on the concentration c_j and the parameters of long range order η_α are in the case of a binary solid solution determined by the formulae given, for example, by Smirnov [6], and in the case of multi-component formulae by one of us [7].

In certain cases the dependence of the maximum (characteristic) frequency ω_m in the spectrum of a solid solution on c_j and η_α is of interest. If the components of the solid solution have similar properties this dependence can be determined if ω_m for the corresponding ordered solid solution is known as a function of the mass of the atoms and the bond coefficients. In particular, for a body centered cubic lattice [8]

$$\omega_m^2 = D (M_1^{-1} + M_2^{-1}), \tag{15}$$

where D is the known sum of the second derivatives of the energy with respect of the inter-atomic distances. Limiting our calculation to the interaction between nearest neighbours only and for the case of a binary solid solution substituting the effective masses for M_1 and M_2 in (15), which are expressed by c and η, we obtain the function $\omega_m (c, \eta)$ which in form agrees with the formulae obtained earlier for the one-dimensional case [1, 2]. Hence, the conclusions drawn in these papers are valid also for the three-dimensional lattice.

Translated by B. Ruhemann

REFERENCES

1. A.N. Men' and A.N. Orlov, *Dokl. Akad. Nauk SSSR* 90, 753 (1953).
2. A.N. Men' and A.N. Orlov, *Fiz. metal. metalloved.*, 7, 335 (1959).
3. I.M. Lifshits and G.I. Stepanova, *Zh. eksp. teor. fiz.*, 31, 156 (1956).
4. I.M. Lifshits, *Zh. eksp. teor. fiz.*, 12, 117 (1942).
5. I.M. Lifshits, *Dokl. Akad. Nauk SSSR* 48, 83 (1945).
6. A.A. Smirnov, *Zh. eksp. teor. fiz.*, 17, 730 (1947).
7. A.N. Men', *Fiz. metal. metalloved.*, 7, 633 (1959).
8. M. Born, M. Geppert-Maier, *Teoriia tverdogo tela (Theory of Solids)* p. 175, O.N.T.I. (1938).

VOL
8
195

ON AN ERROR IN THE HANDBOOK "THE PHYSICO-CHEMICAL PROPERTIES OF THE ELEMENTS"*

Iu.A. BAZHIN, V.A. GLADKOVSKII, M.I. OLEINIK and K.P. RODIONOV
Institute of Metal Physics of the Academy of Sciences of the USSR

(Received 12 September 1958)

In the handbook on the basic physico-chemical properties of the elements of the periodic system [1] the following incorrect formula for calculating the variation of the melting point of metals as a function of pressure is given without any kind of explanation:

$$p = 95,1\lambda D \lg \frac{T}{\theta}, \tag{1}$$

where λ is the latent heat of fusion; T the absolute melting temperature; D the density; θ is not explained.

On the basis of this formula the authors come to the quite erroneous opinion that such metals as silver, copper and others will melt at room temperature if they are subjected to the corresponding pressure.

For example, on p. 97 the authors write: "An increase in the pressure of 1 atm. causes a lowering of the melting point of silver by 0.12°. Hence, at 1400 atm. silver should melt at ordinary temperatures ..." etc.

These conclusions of the authors of the handbook are in contradiction not only to the general propositions of thermodynamics but also to all existing experimental materials.

If we turn to the Clausius-Clapeyron equation

$$\frac{dT}{dp} = \frac{T(V_1 - V_2)}{\lambda}, \tag{2}$$

where V_1 and V_2 are the average specific weights of the metal in the liquid and solid states respectively, one can easily see that for the majority of metals the melting temperature should increase with pressure, which agrees with experimental observations. Exceptions are germanium, bismuth and gallium in which a volume contraction occurs on melting.

Assuming that in the region of not very high pressures the latent heat of fusion of the metal and the volume change on melting do not change materially with the pressure, one can after slight transformations of equation (2) obtain a formula somewhat similar to formula (1):

$$p = -42,7 \frac{\lambda}{\Delta V} \ln \frac{T}{T_p}, \tag{3}$$

where p is the pressure in kg/cm²; ΔV the change in the specific volume on melting in cm³/g; T the melting temperature of the metal at atmospheric pressure in °K; T_p the melting temperature of the metal under pressure in °K; λ the latent heat of fusion in cal/g.

Like the Clausius-Clapeyron equation, this formula is well confirmed by all experimental data obtained in the study of metals under high pressure [2, 3]. In the modern phenomenological theory of solids the connexion between the melting temperature of metals and the pressure is also well described by the following relations [4-6]:

---

* *Fiz. metal. metalloved.*, 8, No. 1, 157-158, 1959.

$$T_p = C \frac{V_{mp}}{\varkappa_{mp}}, \tag{4}$$

$$T_p = C_1 V_{mp}^{2/3} m \theta_p^2, \tag{5}$$

$$p = \left(\frac{T_p}{T}\right)^B - 1, \tag{6}$$

where V_{mp} is the specific volume of the solid phase at the melting point at the given pressure; $\varkappa_{mp}$ the compressibility at the melting point at the given pressure; C, C_1, A and B are positive, constant empirical coefficients; m the mass of the atom; θ_p the Debye temperature at the given pressure.

An examination of formula (4) and (5) shows that the melting temperature increases with increasing pressure since the compressibility of the metal decreases with pressure considerably faster than the specific volume, while θ_p^2 increases with increasing pressure much faster than the specific volume of the metal decreases. Formula (6) also indicates a rise in the temperature with increasing pressure.

As far as formula (1) is concerned, allegedly derived from "thermodynamic relations", it is clear from a comparison of it with formula (3) that it contains gross errors and leads to obviously absurd results.

Translated by B. Ruhemann

VOL 8 195

REFERENCES

1. M.P. Slavinskii (revised by A.Ye. Vol), *Fiziko-khimicheskiye svoistva elementov (The physico-chemical properties of the elements)* Metallurgizdat (1952).
2. P. Bridgman, *Fizika vysokokh davlenii (High pressure physics)* O.N.T.I. (1935).
3. V.P. Butuzov, G.P. Shakhovskii and M.G. Gonikberg, *Tr. Inst. kristallografii* No. 11, 233 (1955).
4. J.J. Gilvarrym *Phys. rev.* 102, No. 2, 308 (1956).
5. F. Simon, *Zs. f. Electrochem.* 35, 618 (1929).
6. F. Lindemann, *Phys. Zs.* 11, 609 (1910).

ON THE PROBLEM OF THE METHOD OF X-RAY INVESTIGATION OF SUBSTANCES UNDER HIGH PRESSURE*
1. AN X-RAY TUBE THAT CAN BE DISMANTLED

S.A. NEMNONOV, M.I. OLEINIK and A.P. FROLOV

Institute of Metal Physics of the Academy of Sciences of the USSR

(Received 4 December 1958)

VOL. 8 1959

In the X-ray examination of substances under high pressure the primary beam and the rays diffracted from the substance to be investigated must pass through the walls of the high pressure vessels (beryllium, diamond) and through the medium which applies the pressure. These requirements, and also the application of filters or in some cases monochromatizers cause considerable increases in exposure time. For photographs under high pressure with a BSV-4 tube the exposure may take more than ten hours.

Starting from the particular requirements of the X-ray method of investigation under high pressure and in order to reduce the exposure time, an X-ray tube has been designed and made at the Institute of Metal Physics of the Academy of Sciences of the USSR, which can be dismantled and has been tested in operation for two years. The tube is simple to make and operate and ensures a steady vacuum (of the order of 10^{-5} mm) and can also be used for ordinary X-ray investigations. The tube produces a very powerful beam of X-rays which reduces the exposure time considerably and makes it possible to obtain pure radiation from various anodes.

The schematic drawing of the tube is shown in Fig. 1. The cathode carries a high voltage and in our arrangement is connected to an URS-70 X-ray machine the hydraulic blocking system of which is connected in series with the cooling of the TsVL-100 diffusion pump. The position of the leads *8* for feeding the filament and the focussing cap *7* are adjusted during the assembly of the tube; the fine adjustment of the hot filament *6* in relation to the focussing screen (of tantalum) *5* is done under vacuum conditions with the aid of the siphon device *9*; tungsten wire of 0.2 mm diameter is used as filament. The anode *2* can be dismantled and is easily replaced by another without dismantling its cooling part *1* before the diffusion pump, which is cut off by means of the siphon valve *10*, has cooled down. The distance from the anode to the window is 16 mm; a narrow beam of X-rays is employed, which is obtained by projecting a linear focus under an angle of 8° 40′ to the surface of the anode. This, side by side with other factors here mentioned, shortens the time of exposure (see the X-ray photographs in Fig. 2, 3). By virtue of the fact that the surface of the anode is in a horizontal position the maximum intensity of radiation can be used under the same angle (8°40′) in two opposite directions through the corresponding windows.

The body of the tube has three openings *3* for the outlet of the X-rays. The tube operates with a linear focus of 12 × 0.4 mm; it is also possible to use an even thinner focus. The windows are made from lithium membrane *4* of 0.8-1.0 mm thickness, which causes the minimum absorption of the X-radiation in the material of the window†. The lithium membrane is obtained by flattening a piece of lithium to the required thickness between steel slabs. These windows work for a long time with vacuum in the tube and with a light coating of vaseline oil on the outside. Because of the plasticity of the lithium the vacuum seal does not require additional washers. Replacing the windows takes only 10-15 min.

---

* *Fiz. metal. metalloved.*, 8, No. 1, 158-160, 1959.

† A lithium window of 1 mm thickness absorbs only 9 per cent of CrK_α radiation, while aluminium foil of 0.01 mm absorbs 33 per cent of the same radiation [1].

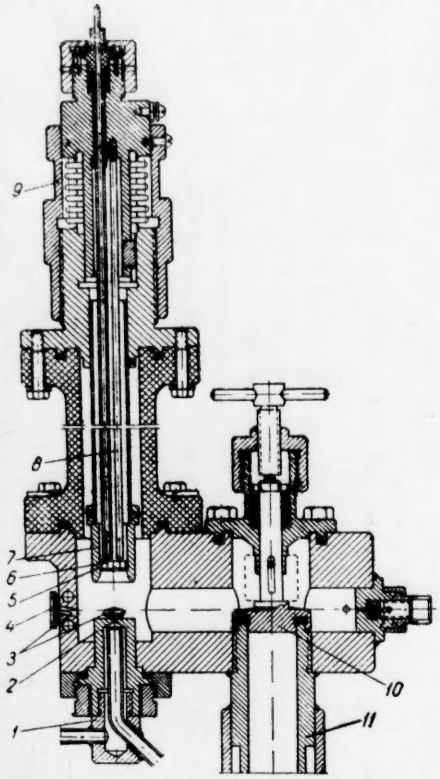

FIG. 1. Schematic drawing of X-ray tube.

FIG. 2. X-ray photograph of copper taken in a cylindrical camera of 57.3 mm diameter from a specimen of 0.4 mm diameter; voltage 30 kV; current 26 mA; exposure 2 min.

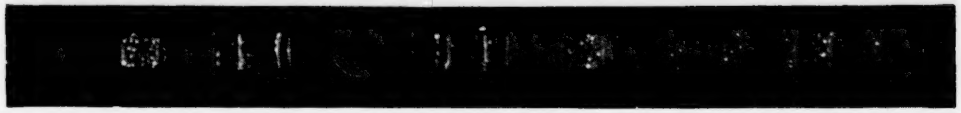

FIG. 3. X-ray photograph of an organic substance taken in a special camera for X-ray investigations under high pressure of 68.8 mm diameter using the corresponding filters; voltage 30 kV; current 26 mA; exposure 1 hr 30 min (round diaphragm of 0.3 mm).

VOL 8 1958

To eliminate oil vapour from the pump the connecting tube *11* has external water cooling and inside it is placed a hollow copper cylinder 70 mm high with two screens of semi-circular shape. This device makes for a more stable vacuum since without this trap a penetration of oil vapour into the body of the tube is observed. The high vacuum pump is connected to the low vacuum by means of a rubber tube fastened with a simple lever clip.

Translated by B. Ruhemann

REFERENCES

1. K. Lonsdale, *Kristally i rentgenovskiye luchi (Crystals and X-rays)* I.I.L. (1952).

VOL.
8
1959

No. 2

	PAGE
On the elastic moduli of a two-phase solid — M. A. KRIVOGLAZ and A. S. CHEREVKO	1
Ferromagnetic resonance in uniaxial ferrite with two sub-lattices — E. N. IAKOLEV	5
On the structure of the energy bands in ionic crystals — M. SH. GITERMAN and S. A. MOSKALENKO	9
Magnetic properties of steels as a basis of magnetic structure analysis — G. S. TOMILOV, M. N. MIKHEEV and M. F. POMUKHIN	15
Study of the properties of titanium Alloys. IV. Properties of alloys of the ternary Ti-Al-Fe system — I. I. KORNILOV, E. N. PYLAEVA and M. A. VOLKOVA	20
Directional diffusion, due to deformation, of hydrogen in a solid solution and strength of the metal — K. V. POPOV and V. A. YAGUNOVA	25
On the kinetics of reactions diffusion in systems with some intermediate prase. I. Macroscopic calculation for a binary system — V. I. ARKHAROV	30
Study of a nickel-chromium-aluminium-titanium alloy deformed in the quenched condition — V. G. CHERNYI	39
Structure of the energy spectrum of electrons in Fe-Cr- and Fe-Cr-Ni- alloys — N. D. BORISOV and V. V. NEMOSHKALENKO	44
On the problem of the influence of alloying on the kinetics of pearlitic transformation — L. N. ALEKSANDROV and B. IA. LYUBOV	49
Some properties of the initial stage of plastic deformation. II. The point at which the first slip lines appear and the distribution of their direction. — IA. R. RAUZIN	57
X-ray studies of deformations in the crystal lattice of metals deformed at low temperatures — V. P. GOLIK, G. A. SIRENKO and V. I. KHOTKEVICH	65
Investigations of rolling texture by an electron-diffraction method — IU. I. SOZIN	70
Variation of internal friction and coefficients of elasticity in pure iron with temperature — V. M. AMONENKO, B. I. SHAPOVAL and V. V. LEBEDEV	78
Deformation of a plane solid body on phase transition — A. M. KOSEVICH and L. V. TANATAROV	83
Some problems in the measurement of microhardness — V. M. DOLIDZE	93
A study of the mechanical properties of solids, in particular of metals at absolute temperatures of 4.2°K and below. I. Tensile testing of polycrystalline aluminium (99.3%) — O. V. KLYAVIN and A. V. STEPANOV	99
Mechanisms of plastic flow for lead and tin in shear conditions — V. I. LIKHTMAN and V. S. OSTROVSKII	107
Influence of a low melting point molten metal on the mechanical properties of single crystals of more refractory metals — L. A. KOCHANOVA, V. I. LIKHTMAN and P. A. REBINDER	112
On the nature of internal friction in hardened and tempered steel — M. A. KRISHTAL and S. A. GOLOVIN	118
A contribution to the question of the nature of damping of vibrations in hardened and low temperature tempered carbon steel — M. A. KRISHTAL and S. A. GOLOVIN	126
Letters to the Editor	
Concerning ferromagnetics with two Curie points — V. L. BONCH-BRUYEVICH	132
The influence of plastic deformation on internal friction in iron and an iron-nickel alloy — R. S. LEBYEDEV and V. S. POSTNIKOV	134
The influence of boron on the recrystallization of silicon iron — V. YE. NEIKMARK and V. M. ROZENBYERG	137
Concerning magnetic anisotropy on the basis of spin-orbit interaction — IU. A. IZIUMOV	139
Phase analysis by the superposition method using electron diffraction — L. S. PALATNIK and B. T. BOIKO	141

ON THE ELASTIC MODULI OF A TWO-PHASE SOLID*

M. A. KRIVOGLAZ and A. S. CHEREVKO

Institute of Metal Physics of the Academy of Sciences, U. S. S. R.

(Received 17 July 1958)

The elastic properties of a two-phase solid are considered. Formulae for the modulus of close compression (hydrostatic stresses) and the shear modulus are derived for the cases in which the concentration of one of the phases is low or in which the concentrations can be arbitrary provided that the values of the moduli of the first and second phase are close to each other. It is shown that the concentration dependence of the moduli of elasticity may differ greatly from linearity.

VOL. 8 1959

In this paper the elastic properties of a mixture of two solid phases are considered. The solution of the analogous problem for mixed liquid phases [1] has shown that the compressibility of an emulsion is equal to the arithmetic mean of the compressibility of its components. As will be shown below, in the case of mixed solids the formulae for the moduli of elasticity are found to be more complex and, in contrast with a view which has often been expressed (see e.g. [4]), their concentration dependence is not linear. The case is considered when the particle sizes of each phase are appreciably greater than the lattice constant, so that the deformation and stresses in these particles can be determined with the aid of the macroscopic theory of elasticity. On the other hand, it is assumed that the particle sizes at least in one phase are sufficiently small compared with the dimensions of the specimen (or with the length of the elastic wave if the moduli are used for determining the rate of ultrasonic vibration). Examples of such systems are age-hardening alloys (at least in the later stages of ageing), eutectics, alkali-halide crystals containing colloidal particles of precipitated alkali metals, solid bodies containing micro-cavities, and the like.

We shall consider the elastic properties of each phase in approximation to an elastic isotropic continuum. The problem leads to determination of the macroscopic modulus of hydrostatic stresses K_c and of the macroscopic shear modulus μ_c of a mixed solid with given moduli K_1, μ_1, K_2 and μ_2 of the first and second phase and with volume concentration of the second phase c. As, in the general case, this problem is extremely complex, we will confine ourselves to the consideration of two special cases. In the first case, the system consists of small spherical inclusions of a secondary phase, the concentration of which is very low ($c \ll 1$). In the second case, the concentration can be arbitrary but the elastic moduli of both phases differ little from each ($|K_1-K_2| \ll K_1; |\mu_1-\mu_2| \ll \mu_1$), so that it is possible to use the theory of perturbations, confining ourselves to the second approximation. In this case the results obtained appear to be applicable not only to isotropic particles, but also to polycrystalline structures consisting of slightly anisotropic crystals.

To start with, we wish to consider the case of low concentration of the second phase when the mean distance between the particles is great compared with their dimensions. We shall determine the field of deformation about a spherical particle of the second phase of radius R, which is present in an appropriately large elastic isotropic body (the first phase). Let, at large distances from the sphere, the components of the tensor of stresses σ_{ij} be equal to σ'_{ij}. Then to determine the tensor of deformations u_{ij}, it is necessary to find a solution to the

* *Fiz. metal. metalloved.* 8, No. 2, 161-164, 1959.

equations of elasticity (see e.g. [2]);

$$(1-2\sigma_1)\Delta\vec{u}_1+\operatorname{grad}\operatorname{div}\vec{u}_1=0,$$
$$(1-2\sigma_2)\Delta\vec{u}_2+\operatorname{grad}\operatorname{div}\vec{u}_2=0, \quad (1)$$

where $\vec{u}_1$ and $\vec{u}_2$ are displacement vectors for the first and second phases, σ_1 and σ_2 are Poisson coefficients for these phases, in boundary conditions

$$\vec{u}_1=\vec{u}_2;\quad \sigma_{ij}^{(1)}e_j=\sigma_{ij}^{(2)}e_j \quad (2)$$

($\vec{e}$ is the unit vector normal to the surface of the sphere, $\sigma_{ij}^{(1)}$ and $\sigma_{ij}^{(2)}$ are the stresses in the first and second phases) on the surface of the sphere and

$$\sigma_{ij}^{(1)}=\sigma_{ij}' \quad (3)$$

at infinity. We shall adopt a co-ordinate system with its origin at the centre of the sphere. Then, the solution to these equations assumes the following form

$$u_i^{(1)}=A_1 s\,\delta_{ij}+\frac{B_1 s}{r^3}(\delta_{ij}-3e_ie_j)+$$
$$+\frac{1}{2\mu_1}(\sigma_{ij}'-s\,\delta_{ij})+ \quad (4)$$
$$+\frac{C_1}{r^3}[3(\sigma_{ik}'-s\,\delta_{ik})e_ke_j+$$
$$+3(\sigma_{jk}'-s\,\delta_{jk})e_ie_k-2(\sigma_{ij}'-s\,\delta_{ij})]+$$
$$+\frac{D_1}{r^5}(\sigma_{kl}'-s\,\delta_{kl})[35e_ie_je_ke_l-5\varphi_{ijkl}+\psi_{ijkl}]-$$
$$-\frac{E_1}{r^3}(\sigma_{kl}'-s\,\delta_{kl})[15e_ie_je_ke_l-3\varphi_{ijkl}+\psi_{ijkl}].$$

$$u_{ij}^{(2)}=A_2 s\,\delta_{ij}+B_2(\sigma_{ij}'-s\,\delta_{ij}),$$

$$s=\frac{1}{3}(\sigma_{xx}'+\sigma_{yy}'+\sigma_{zz}');$$

$$A_1=\frac{s}{3K_1}+\frac{2cs}{3K_1}\cdot\frac{(1-2\sigma_1)(K_1-K_2)}{2K_1(1-2\sigma_1)+K_2(1+\sigma_1)};$$
$$A_2=\frac{s(1-\sigma_1)}{2K_1(1-2\sigma_1)+K_2(1+\sigma_1)};$$
$$B_1=R^3(A_2-A_1);$$

$$B_2=\frac{15(1-\sigma_1)}{4[\mu_1(7-5\sigma_1)+2\mu_2(4-5\sigma_1)]}; \quad (5)$$

$$C_1=-8E_1(1-\sigma_1);$$

$$D_1=\frac{(4B_2\mu_1-1)R^5}{24\mu_1(4-5\sigma_1)};\quad E_1=\frac{15D_1}{R^2};$$

$$\varphi_{ijkl}=e_ie_j\delta_{kl}+e_ie_k\delta_{jl}+e_ie_l\delta_{jk}+$$
$$+e_je_l\delta_{ik}+e_ke_l\delta_{ij}+e_je_k\delta_{il},$$

$$\psi_{ijkl}=\delta_{ij}\delta_{kl}+\delta_{ik}\delta_{jl}+\delta_{il}\delta_{jk}.$$

Here the quadratic summands in A_1 and the linear summands in A_2 with respect to c are rejected.

Substituting expressions (4) in the formula

$$\sigma_{ij}=2\mu\,u_{ij}+3K\frac{\sigma}{1+\sigma}u_{ll}\delta_{ij}, \quad (6)$$

connecting the stresses and deformations, it is possible to find the stresses in both phases. It is not difficult now to find the macroscopic moduli of hydrostatic stresses and shear for the systems K_c and μ_c. These quantities are naturally defined with the aid of formulae

$$\bar{\sigma}_{ii}=3K_c\bar{u}_{ii};\ \bar{\sigma}_{ij}=2\mu_c\bar{u}_{ij}\ \text{when}\ i\neq j, \quad (7)$$

where $\bar{\sigma}_{ij}$ and $\bar{u}_{ij}$ are the mean values of the components of tensors $\bar{\sigma}_{ij}$ and $\bar{u}_{ij}$.

In determining $\bar{u}_{ij}$ and $\bar{\sigma}_{ij}$ for a system consisting of a large number of small spherical second-phase inclusions embedded in the first phase, the fact may be used that the distances between the spheres are great (considerably greater than the radii of the spheres) and the deformation can be determined by superposition of the deformations (4) produced by the various spheres. It should be noted that in the neutralization of $u_{ij}^{(1)}$ a value different from zero is obtained only by summands $A_1 s\,\delta_{ij}$ and $\frac{1}{2\mu_1}(\sigma_{ij}'-s\,\delta_{ij})$. Carrying out the neutralization and taking into account formulae (4)-(7), we obtain the following expressions for K_c and μ_c

$$K_c=K_1\left[1+\frac{3(1-\sigma_1)(K_2-K_1)}{2K_1(1-2\sigma_1)+K_2(1+\sigma_1)}c\right], \quad (8)$$

$$\mu_c=\mu_1\left[1+\frac{15(1-\sigma_1)(\mu_2-\mu_1)}{\mu_1(7-5\sigma_1)+2\mu_2(4-5\sigma_1)}c\right]. \quad (9)$$

In the special case when the moduli of elasticity for the inclusions are considerably greater than the moduli of elasticity for the

VOL 8 195

basis phase, that is, when $K_2 \gg K_1$ and $\mu_2 \gg \mu_1$,

$$K_c = K_1\left(1+3\frac{1-\sigma_1}{1+\sigma_1}c\right);$$
$$\mu_c = \mu_1\left(1+\frac{15}{2}\times\frac{1-\sigma_1}{4-5\sigma_1}c\right). \quad (10)$$

In the opposite case when $K_2 \ll K_1$ and $\mu_2 \ll \mu_1$ (this limiting case is found in particular in the presence of micro-cavities)

$$K_c = K_1\left(1-\frac{3}{2}\times\frac{1-\sigma_1}{1-2\sigma_1}c\right); \quad (11)$$
$$\mu_c = \mu_1\left(1-15\frac{1-\sigma_1}{7-5\sigma_1}c\right).$$

It is clear from the formulae presented that, generally speaking, the magnitudes of K_c and μ_c may differ greatly from the mean magnitudes

$$\bar{K} = K_1 + c(K_2 - K_1);$$
$$\bar{\mu} = \mu_1 + c(\mu_2 - \mu_1), \quad (12)$$

determined by the displacement rule. Thus, for instance, at $\sigma_1 = 0.3$ and with $K_2 \gg K_1$ $K_c - K_1 = 1{,}6K_1c$ instead of the considerably higher value of K_2c corresponding to formula (12), and with $K_2 \ll K_1$ $K_c = K_1(1-2{,}6c)$ instead of $\bar{K} = K_1(1-c)$. Further, it follows from formulae (10) and (11) that, if the moduli of elasticity for the components differ greatly among each other, then for $c \ll 1$ or $1-c \ll 1$ the curve K_c (or μ_c) passes below the straight line $\bar{K}$ (or $\bar{\mu}$) and this curve shows a much more pronounced gradient in the portion where the corresponding modulus is higher.

We now wish to consider the case when the concentration c is arbitrary and the moduli of elasticity for the first and second phases differ little from each other. In this case it is possible to use the method of the theory of perturbations [3] for the elastic properties of a polycrystal consisting of slightly anisotropic crystal grains. With an accuracy up to the second approximation of the theory of perturbations [3], the expression for the components of the tensor of the macroscopic moduli of elasticity Λ_{ijkl} for an inhomogeneous solid body, in which correlation between the inhomogeneities is absent, can be written in the form

$$\Lambda_{ijkl} = \bar{\lambda}_{ijkl} - \frac{3(\bar{K}+2\bar{\mu})}{5\bar{\mu}(3\bar{K}+4\bar{\mu})}\overline{\Delta_{ijpq}\Delta_{pqkl}} + \quad (13)$$
$$\frac{3\bar{K}+\bar{\mu}}{15\bar{\mu}(3\bar{K}+4\bar{\mu})}\overline{\Delta_{ijpp}\Delta_{qqkl}},$$

where Λ_{ijkl} is the mean value of the components of the tensor of the moduli of elasticity and λ_{ijkl} the difference between the value of λ_{ijkl} in a given point and $\bar{\lambda}_{ijkl}$. Using this formula for the case considered of a mixed solid of elastically isotropic phases, the particles of which are distributed at random, after some transformations we obtain the expressions for

$$K_c = \bar{K}\left[1-\frac{1+\bar{\sigma}}{3(1-\bar{\sigma})}\left(\frac{K_1-K_2}{\bar{K}}\right)^2 c(1-c)\right], \quad (14)$$
$$\mu_c = \bar{\mu}\left[1-\frac{2(4-5\bar{\sigma})}{15(1-\bar{\sigma})}\left(\frac{\mu_1-\mu_2}{\bar{\mu}}\right)^2 c(1-c)\right], \quad (15)$$

where $\bar{K}$ and $\bar{\mu}$ are determined by formulae (12).

For low values of c, the expressions (14) and (15) coincide with expansions of the expressions (8) and (9) by powers of $K_1 - K_2$ and $\mu_1 - \mu_2$, if in the last expansions we confine ourselves to quadratic terms. As might have have been expected, in the second approximation of the theory of perturbations, K_c and μ_c depend quadratically on the concentration c. It is clear from formulae (14) and (15) that, in the case considered, the curves $K_c(c)$ and $\mu_c(c)$ should have positive curvature and lie below the straight line $\bar{K}(c)$ and $\bar{\mu}(c)$. It should be noted that formulae (14) and (15), as can be easily understood, are also valid (with an accuracy up to and including the second approximation of the theory of perturbations) for a polycrystalline mixed solid in which the crystal of each phase have slight anisotropy different from zero. Here K_1, μ_1, K_2, μ_2 should be understood to indicate the moduli of elasticity for polycrystals of the first and second phases, and $\bar{K}$ and $\bar{\mu}$ are determin as previously by formulae (12). With the a of formula (14) it is not difficult to determine also the moduli of elasticity for

VOL. 8 1959

crystal in which the separated second phase is oriented in a definite manner relative to the crystal axis. As the components of the macroscopic tensor of the moduli of elasticity will depend on the orientation of the precipitates, measurement of the moduli of elasticity in such a system gives an independent method of determining this orientation.

The results obtained agree qualitatively with experimental data given in [4] on Young's modulus* for eutectics. In agreement with these data, Young's moduli for the systems Ag-Cu, Cd-Zn, Al-Sn depend linearly on c. In these systems the ratios $\frac{|K_1-K_2|}{K}$ and $\frac{|\mu_1-\mu_2|}{\mu}$ are less than ½. Therefore, in agreement with (14) and (15), the deviations of E_c from the mean value of $\bar{E}$ do not exceed 2-3 per cent and lie within the experimental errors. In the Pb-Sn system Young's modulus for lead is three times less than that for tin. Therefore, in agreement with the results obtained, substantial deviations from linearity are observed in the curve plotting the dependence of E_c, and in agreement with (10) and (11) the curve E_c is bent more in that portion where E_c is higher.

Translated by H. Nowottny

REFERENCES

1. M.A. Isakovich, *Zh. eksp. teor. fiz.*, 18, 907 (1948).
2. L.D. Landau and E.M. Lifshits, *Mekhanika sploshnykh sred (Mechanics of continuous media)*, Costekhteoretizdat (1953).
3. I.M. Lifshits and L.N. Rozentsveig, *Zh. eksp. teor. fiz.* 16, 967 (1946).
4. W. Koster and W. Rauscher, *Z. Metallk*, 39, 111 (1948).

* Young's (macroscopic modulus for mixed solids is expressed for the moduli of hydrostatic stresses and shear by the usual formula

$$E_c = \frac{9K_c\mu_c}{3K_c+\mu_c}.$$

FERROMAGNETIC RESONANCE IN UNIAXIAL FERRITE WITH TWO SUB-LATTICES*

E. N. IAKOVLEV

Institute of High-Pressure Physics of
the Academy of Sciences, U. S. S. R.

(Received 9 October 1958)

Resonant frequencies are calculated in this paper for two orientations, along the axis of easy magnetization and perpendicular to this axis, in a constant magnetic field.

VOL. 8 1959

The resonant frequencies for ferrite with uniaxial symmetry have been calculated already [1]. The authors of that paper obtained resonance formulae under the assumption that ferrite consists of one sub-lattice. For a model with two sub-lattices the calculation was carried out elsewhere [2]. In that case a magnetic field was considered set up only along the axis of easy magnetization. In the present paper resonance formulae will be obtained for the following model.

Suppose that ferrite consists of two ferromagnetic sub-lattices. The complete magnetic moment of the first sub-lattice is $\vec{M}_1$ and of the second $\vec{M}_2$. Exchange between atoms belonging to different sub-lattices has an antiferromagnetic character, whereas interaction inside each sub-lattice is ferromagnetic. In addition to this interaction of exchange, there exists an interaction responsible for anisotropy. In the given case uniaxial anisotropy is presupposed. The axis of anisotropy is OZ. Each direction perpendicular to OZ is a direction of difficult magnetization.

The invariant form of energy for the given system of two ferromagnetic sub-lattices can be written thus*

$$F = -\frac{1}{2}A_1M_1^2 - A\vec{M}_1\vec{M}_2 - \\ -\frac{1}{2}A_2^2M_2^2 - \frac{1}{2}\Delta_1M_{1z}^2 - \\ -\Delta M_{1z}M_{2z} - \frac{1}{2}\bar{\Delta}_2M_{2z}^2. \qquad (1)$$

In expression (1) the constants A_1, A_2 and A are proportional to the exchange integrals; A_1, $A_2 > 0$ (ferromagnetic interaction and $A < 0$ (antiferromagnetic interaction). The choice of parameters Δ_1, $\Delta_2 > 0$, $\Delta < 0$ ensures the minimum of energy in the direction OZ. As the exchange energy is considerably higher than the energy of anisotropy, the ratio $\left|\frac{\Delta}{A}\right| \ll 1$.

Let us suppose that the ferrite specimen has the shape of an ellipsoid of rotation. The axis of rotation coincides with the OZ axis. In this case the demagnetizing field of the specimen has the form

$$H_{\sim\alpha} = -N_\alpha (M_{1\alpha} + M_{2\alpha}) \quad (\alpha = x, y, z)$$
$$N_x = N_y = N \quad N_z \neq N.$$

If in (1) the energy of the specimen in the demagnetizing field is taken into account, then only the constant (A, $A_{1,2}$ Δ, $\Delta_{1,2}$) is changed and no new terms are added.

In this way, expression (1) represents the energy of uniaxial ferrite which has the shape of an ellipsoid of rotation. Completing the description of the model, we consider in expression (1) the energy of the moments in

* *Fiz. metal. metalloved.* 8, No. 2, 165-169, 1959.

* As the problem consists in finding the natural frequency of a process uniform in volume, the gradient of magnetization ∇M need not be considered.

the external field – $H(\vec{M}_1+\vec{M}_2)$.

We then proceed in the following manner. On the basis of the condition of minimum energy of F, we determine the equilibrium positions of the magnetic moments $\vec{M}_1$ and $\vec{M}_2$. The moments about the equilibrium positions effect small precessions

$$\delta\vec{M}_i(t)=\vec{M}_i(t)-\vec{\overline{M}}_i,\quad |\delta\vec{M}_i(t)|\ll\vec{\overline{M}}_i,$$
$$\delta M_{i\alpha}(t)=\delta M_{i\alpha}e^{i\omega t}\quad (i=1,2;\ \alpha=x,\ y,\ z).$$

The frequencies of the precessions are found from the equations of movement

$$\vec{M}_i=\gamma_i[\vec{M}_i\cdot\vec{H}_i]$$
$$\gamma_i=g_i\gamma\quad \gamma=\frac{e}{2mc}\quad (i=1,2); \tag{2}$$

where g_i are the g factors of the first and second sub-lattice, and $\vec{H}_i$ the effective magnetic fields acting on each sub-lattice.

The effective fields are determined from equations

$$H_{i\alpha}=-\frac{\partial F}{\partial M_{i\alpha}}\quad (i=1,2;\ \alpha=x,\ y,\ z).$$

The amplitudes of the precessions are always considered to be low: $\left|\frac{\delta M}{M_i}\right|\ll 1$ and are considered only in linear approximation.

We wish to carry out the calculation for the case when the external magnetic field is set up perpendicularly to the axis of easy magnetization.

Field set up perpendicularly to the axis of easy magnetization. From the expression for the energy of the system, which in the given case has the form

$$F=-A\vec{M}_1\vec{M}_2-\frac{1}{2}\Delta_1M_{1z}^2-$$
$$-\Delta M_{1z}M_{2z}-\frac{1}{2}\Delta_2M_{2z}^2-$$
$$-H_x(M_{1x}+M_{2x})+\text{const},$$

we find the equilibrium values of moments $M_{i\alpha}$.

In determining the equilibrium values it is considered that the energy of anisotropy is substantially less than the exchange energy $\left|\frac{\Delta}{A}\right|\sim\varepsilon\ll 1$ and that the external field does not exceed in its order of magnitude the field of anisotropy.

The energy of the system is laid out in powers of the small parameter ϵ. In approximation at zero in respect of ϵ, the minimum of the energy is satisfied by any pair of moments $\vec{M}_1$ and $\vec{M}_2$ anti-parallel in respect of each other. The direction in space is not considered in the given case.

In a first approximation in respect of ϵ, the magnetic moment $\vec{M}_1$ is also anti-parallel to the moment M_2, but the direction in the plane of the external field and of the axis of anisotropy is already fixed by the field and the axis of anisotropy. The magnetic moments in the given case are determined by formulae

$$M_{1x}^0=M_1\sin\varphi_{10};$$
$$M_{2x}^0=-M_2\sin\varphi_{10};\ \sin\varphi_{10}=\varkappa H_x, \tag{3}$$

where

$$\varkappa=\frac{M_1-M_2}{\Delta_1M_1^2+\Delta_2M_2^2+2|\Delta|M_1M_2},$$

and φ_{10} is the angle between $\vec{M}_1$ and the axis of anisotropy OZ.

In this approximation the intensity of magnetization of ferrite does not differ from that of a ferromagnetic with a resulting magnetic moment equal to $|M_1|-|M_2|$.

If the energy in the second order in respect of ϵ is considered, then a difference arises in the behaviour of a ferromagnetic and a ferrite. In this case the intensity of magnetization of the sub-lattices is determined with an accuracy up to the first order in respect of the anisotropy.

The contribution of the calculated corrections to the intensity of magnetization is insignificant (proportional to ϵ). However, the corrections $\varepsilon M'_{1x}$ and $\varepsilon M'_{2x}$ must be known for the determination of the resonant frequencies.

The most natural method of determining M'_{1x}, M'_{2x} appears to be the direct substitution of the values of $M_{i\alpha}=M_{i\alpha}^0+\varepsilon M'_{i\alpha}$ in the expression for the energy, followed by minimization of the energy. However, M_{ix} could not be found directly, and a small parameter δ was first introduced which characterizes the deflexion of the moment

from the anti-parallel orientation. Then with new variables ϕ_1 and δ, δ is determined from condition $\frac{\partial F}{\partial \delta} = 0$ and M'_{1x} from condition $\frac{\partial F}{\partial \varphi_1} = 0$ (Here φ_1, φ_2 are the angles formed by $\vec{M}_1$ and $\vec{M}_2$ with the OZ axis, and $\delta = \varphi_2 - \varphi_1 - \pi$).

By this method the following expressions are found for M_{ix}

$$\varepsilon M'_{1x} = -\frac{\delta}{\alpha \cos \varphi_{10}} (d_2 \cos 2\varphi_{10} - H_x M_2 \sin \varphi_{10}); \quad H_x < H' \tag{4a}$$

$$\varepsilon M'_{2x} = -\frac{\delta}{\alpha \cos \varphi_{10}} (d_1 \cos 2\varphi_{10} + H_x M_1 \sin \varphi_{10}); \quad H_x < H' \tag{4b}$$

$$M_{1x} = |M_1|; \quad M_{2x} = -|M_2| \quad H_x > H'. \tag{4c}$$

Here

$$d_i = \Delta_i M_i^2 + |\Delta| M_1 M_2 \quad \alpha = d_1 + d_2. \quad i = 1,2,$$

$$H' = \frac{1}{\chi} + h.$$

(the magnitude of h is proportional to the square of ϵ and therefore is neglected).

From formulae (4a) and (4b) it is clear that the relative orientation of the moments does not remain constant if the magnitude of the external magnetic field is changed.

We now proceed to the determination of the natural frequencies from the equation of motion (2). Substituting the equilibrium values of the moments (see formulae (3), (4a), (4b)) in the expression of motion, we obtain very cumbersome expressions.

It is more convenient to operate in a co-ordinate system rotated about the OZ axis through an angle ϕ_{10} which is determined by relation $\sin \varphi_{10} = H_z \chi$. This direction is that of the resulting intensity of magnetization if the magnetic moments are so distributed as to be strictly anti-parallel. In the shifted co-ordinate system the projections of the magnetic moments on the OZ axis are integrals of movement with an accuracy up to the first order in respect of ϵ. In the new co-ordinate system the elementary but cumbersome calculations are therefore simplified.

From the equations of movement (2), the following expressions are obtained for the resonant frequencies in a field set up perpendicularly to the axis of anisotropy.

*Radio frequency range**

$$\omega_{r\perp} = \omega_{r0} \cos \varphi_{10}, \quad H_x < H', \quad H' = \frac{1}{\chi} \tag{5a}$$

$$\omega_{r\perp} = \{\gamma'^2 H_x^2 - \omega_{r0} \gamma' H_x\}^{1/2}, \quad H_x > H',$$

$$\omega_{r0} = \frac{d_1 + d_2}{S_1 - S_2}; \quad \gamma' = \frac{M_1 - M_2}{S_1 - S_2}; \quad M_i = \gamma_i S_i \; (i = 1,2).$$

Infra-red frequency range

$$\omega_{i\parallel} = \sqrt{-\chi^2 H_x^2 D} \quad H < H', \tag{6a}$$

$$\omega_{i\perp} = \omega_{i0} - L - \gamma'' H \quad H > H', \tag{6b}$$

where

$$\omega_{i0} = |A| \gamma_1 \gamma_2 (S_1 - S_2) + C;$$

$$C = \frac{d_2 S_1^2 + d_1 S_2^2}{(S_1 - S_2) S_1 S_2};$$

$$L = C + E$$

$$\gamma'' = \frac{S_1 \gamma^2 - S_2 \gamma_1}{S_1 - S_2};$$

$$E = \frac{S_1 S_2}{2(S_1 - S_2)} (\Delta_1 \gamma_1^2 + \Delta_2 \gamma_2^2 + 2(\Delta) \gamma_1 \gamma_2),$$

$$D = \frac{1}{2(S_1 - S_2) S_1 S_2 (M_1 - M_2)} \{2(d_2 M_1 + d_1 M_2)$$

$$(S_1^2 - S_2^2) + S_1^2 S_2^2 (M_1 - M_2)$$

$$(\Delta_1 \gamma_1^2 + \Delta_2 \gamma_2^2 + 2|\Delta| \gamma_1 \gamma_2)\}.$$

The field parallel to the axis of easy magnetization. In the case when the field magnitude does not exceed $H_1 \sim |A|(M_1 - M_2)$ [3], [3], the magnetic moments distributed along the axis of anisotropy OZ are $M_{1z} = M_1$; $M_{2z} = -M_2$.

* The index r relates to radio frequencies and the index i to infra-red frequencies.

VOL. 8 1959

In fields greater than H_1, reversal of the moments occurs. We shall consider in the given case only the region of fields in which the moments are antiparallel ($H \ll H_1$). Then the resonant frequencies are determined by the following expressions

Radio frequency range

$$\omega_{r\parallel} = \omega_{r0} + H\gamma', \quad \gamma' = \frac{M_1 - M_2}{S_1 - S_2}; \quad \omega_{r0} = \frac{d_1 + d_2}{S_1 - S_2}. \tag{7}$$

Infra-red frequency range

$$\omega_{i\parallel} = \omega_{i0} - H\gamma'', \quad \gamma'' = \frac{S_1\gamma_2 - S_2\gamma_1}{S_1 - S_2}; \quad \omega_{i0} = |A|\gamma_1\gamma_2(S_1 - S_2) + C. \tag{8}$$

Proceeding to the analysis of the formulae obtained (5)-(8) for the two field directions, we can draw the following conclusions.

(a) In the radio range the expressions for the resonant frequencies (5), (7) coincide, to an accuracy up to the coefficients, with the expressions obtained for one sub-lattice ($S = \Delta_2 = \Delta = 0$, see [1]). Previously this has not been apparent, especially if it is considered that in the case of a field set up perpendicularly to the axis of easy magnetization the angle between the moments $\vec{M}_1$ and $\vec{M}_2$ does not remain constant. However, as shown by the calculations, the resonant frequencies are not sensitive to a small change of the angle between the moments.

The practical result obtained from the present calculation is that, in the radio frequency range, the concept of one sub-lattice can be used with an adequate degree of accuracy.

(b) The other branch of the spectrum, the range of infra-red frequencies, can naturally not be obtained on the basis of the idea of one sub-lattice. This branch essentially depends on exchange interaction between sub-lattices (6) and (8). As the forces of anisotropy are substantially less than the exchange fields, the dependence of resonant frequencies on anisotropy and field is small. However, in an approximation to the compensation point [4] ($S_1 \to S_2$) the term (see (6), (3)) proportional to A is reduced and the contribution from the anisotropy and the field becomes more important. It seems anisotropy to determine the resonance in this range of the spectrum. However, the experimental investigations of ferrites at the compensation point do not yet allow comparison between calculated formulae and experimental data.

The author is deeply grateful to L. F. Vereshchagin, S. V. Tyablikov and E. A. Turov for their valuable advice in connection with this work.

Translated by H. Nowottny

REFERENCES

1. M. T. Weiss and P. W. Anderson, *Phys. Rev.* 98, 4, 925 (1955).
2. F. Brown and Park, *Phys. Rev.* 93, 3, 381 (1954).
3. S. V. Tyablikov, *Fiz. metal. metalloved.*, 3, 3, (1956).
4. R. K. Wangsness, *Amer. J. Phys.*, 24, 60 (1956).

ON THE STRUCTURE OF THE ENERGY BANDS IN IONIC CRYSTALS*

M. Sh. GITERMAN and S. A. MOSKALENKO

"A. M. Gor'kii" Urals State University

(Received 8 June 1958)

The structure of the electron band and three unfilled bands in crystals of the alkalihalide type is investigated with consideration of the degeneration of the electron states at the nodes of the halide, and of the possibility of the movement of the current carrier along the ions of both types. The approximate diagonalization of the Hamiltonian of the multi-electron problem is studied and a group-theory method is used for investigating the structure of the bands in some directions of K-space.

VOL. 8 1959

A calculation of inter-electronic interaction in crystals has been carried out in the polar Shubin-Vonsovskii model [1]. On the basis of this model a great number of static and kinetic effects in metals and semiconductors were considered by Vonsovskii and his co-workers [2] and satisfactory agreement with experimental data was obtained. Appropriate mathematical treatment for these investigations is provided by the method of secondary quantization which, in its application to the problem of a crystal, was developed by Bogolyubov and Tyablikov [3]. It was, however, the simplest case of *s*-electrons which was considered in that paper and excited states were not taken into account. The calculation of one undegenerate *p*-state was carried out by Seigov and Galishev [4]; this showed overlapping of the energy bands in the spectrum of elementary excitations even at zero approximation. In all the work referred to above the degeneration with respect to the magnetic quantum number was neglected and thus it was not possible to obtain, for instance, the anisotropy of the effective masses of the current carrier and some other effects.

The generalization of the polar model for the case of ionic crystals (of the alkali halide type) has been carried out by us elsewhere [5]. The present paper is devoted to the same problem and special consideration will be given, firstly, to the calculation of the degeneration of the electron states and the halide nodes and, secondly, to the possibility of the movement of the current carrier for each sign in respect of both cations and anions. The first of the effects referred to defines essentially the properties of the energy spectrum of the holes, in particular, the anisotropy of their effective masses. The second effect leads to a change in the shape and position of the energy bands in a crystal, that is, it influences the properties of the current carrier. It is particularly natural to calculate this effect, in view of the fact that recently the properties of the excess electron in the NaCl crystal [6] and also those of the holes in KCl and NaCl [7] have been studied in detail. These works serve thus as a zero order approximation for our problem.

We wish to solve the problem on the basis of secondary quantization, although it can also be solved in configuration space by the Heitler-London method. For simplicity, we shall neglect the crystal-lattice vibrations, since the effects which interest us are not associated with electron-phonon interaction, although the latter can lead to a substantial addition to our calculation.

Thus, we consider an ideal crystal lattice

* *Fiz. metal. metalloved.* 8, No. 2, 170-175, 1959.

of cubic symmetry with two types of nodes g and h, occupied respectively by positive and negative ions which are considered immobile. In the ground state we have maximum random distribution of electron density; there are no valence s-electrons about the nodes of type g (alkali), but at the nodes of type h (halide) we find six electrons each in the p-state, which are characterized by the magnetic quantum number $m = 0, \pm 1$ and spin $\sigma = \pm 1/2$. Excitation of the system is associated with a decrease in the randomness of charge distribution and with the appearance of elementary excitations with charge of opposite sign. By analogy with the single-electron theory, these excitations will in the following be called electrons and holes, and accordingly we shall speak of electron and three-hole energy bands.

The energy operator for our problem has, on the basis of secondary quantization, the following form [2]

$$H = \sum L(\alpha\alpha')\, a_\alpha^+ a_{\alpha'} + \frac{1}{2}\sum F(\alpha_1\alpha_2\alpha_1'\alpha_2')\, a_{\alpha_1}^+ a_{\alpha_2}^+ a_{\alpha_2'} a_{\alpha_1'}, \tag{1}$$

where summing is carried out over all indices α which take the values g, s, σ and $hm_i\sigma$; $i = 1, 2, 3$. Terms of the type $L(\alpha\alpha')$ in (1) describe the additive side of the Hamiltonian – the kinetic energy of the electrons and the interaction with the ionic sub-system, and terms of the type $F(\alpha_1\alpha_2\alpha_1'\alpha_2')$ – the coulomb and exchange interaction of the electrons with each other.

In order to find the energy spectrum of the system it is necessary, first, to bring (1) into the quadratic form of the Fermi operators a_α, and then to transform the quadratic form into the canonical form (to diagonalize the operator (1)); this determines the energy of the elementary excitations reflecting the collective properties of the multi-electron system. The first part of the described problem – writing (1) in a quadratic form with consideration of our choice of ground state – is carried out for weakly excited states of the system by neutralizing the more essential quadratic terms in (1), transforming them into quadratic terms and discarding the less essential fourth terms. This treatment has been carried out repeatedly for models close to ours (see, for instance, section 1 of [8]) and, to save space, is here omitted.

Further, for a clear account of the translation symmetry of the problem, we go over to K-space after laying out the operators a_α in a Fourier series. Finally we obtain

$$H = \sum_{k,\sigma} A(sk)\, a_{ks\sigma}^+ a_{ks\sigma} + \sum_{k,m,\sigma} B(mk)\, a_{km\sigma}^+ a_{km\sigma} + \sum_{k,m,\sigma} C(msk)\, a_{ks\sigma}^+ a_{km\sigma} + \sum_{k,m,\sigma} D(msk)\, a_{km\sigma}^+ a_{ks\sigma} + \sum_{k_1 m_i m_j \sigma} \varepsilon(m_i m_j k)\, a_{km_i\sigma}^+ a_{km_j\sigma}. \tag{2}$$

We shall not write out the explicit form of coefficients $A \ldots E$, which can be expressed easily by coefficients L and F (1), because they are too cumbersome. For the diagonalization of (2) it is simplest to use the Bogolyubov-Tyablikov method [3], which is easily generalized for the case of Fermi particles. In agreement with this method, the diagonalization of (2) is accomplished by linear replacement of operators

$$a_{k\alpha\sigma} = \sum_{\nu=0}^{3} u_{\alpha\nu}(k)\, \xi_{k\nu\sigma} \quad (\alpha = 0, 1, 2, 3)$$

by the ortho-normalized amplitudes $u_{\alpha\nu}(k)$, which are adopted from the condition of conversion to zero of the coefficients with undiagonalized operators $\xi_{k\nu\sigma}$ in (2). This gives a system of linear uniform equations for the determination of energy $E_\nu(k)$ and amplitude of transformation $u_{\alpha\nu}(k)$

$$E_\nu(k)\, u_{\alpha\nu}(k) = \sum_{\beta=0}^{3} G_{\alpha\beta}(k)\, u_{\beta\nu}(k); \tag{3}$$

$$\alpha = 0, 1, 2, 3,$$

where $G_{\alpha\beta}$ indicates the set of coefficients $A \ldots E$. For the system (3) to be capable of solution, it is necessary that the following determinant is equal to zero:

$$|G_{\alpha\beta}(k) - E_\nu(k)\, \delta_{\alpha\beta}|:$$

$$\begin{vmatrix} A(sk) - E_\nu(k) & C(m_1sk) & C(m_2sk) & C(m_3sk) \\ D(m_1sk) & B(m_1k) - E_\nu(k) & \varepsilon(m_1m_2k) & \varepsilon(m_1m_3k) \\ D(m_2sk) & \varepsilon(m_2m_1k) & B(m_2k) - E_\nu(k) & \varepsilon(m_2m_3k) \\ D(m_3sk) & \varepsilon(m_3m_1k) & \varepsilon(m_3m_2k) & B(m_3k) - E_\nu(k) \end{vmatrix} = 0. \tag{4}$$

VOL 8 195

This is a fourth-order equation in respect of E_ν. Clearly, calculation of the higher excited states in the theory of ionic crystals would lead simply to higher orders for equation (3). Since the exact solution of equation (3) (and this applies with even greater force to equations of higher orders for calculating subsequent excited states) is extremely laborious, it is convenient to use for the solution of (3) an approximate method based on expansion of coefficients $G_{\alpha\beta}$, eigen values E_ν and amplitudes $u_{\alpha\nu}$ in powers of a small parameter. Current carriers of a given sign move basically in the same sub-lattice formed by ions of the opposite sign and transfer only rarely to ions of another sub-lattice. The small parameter τ will for our problem account for the ratio of the probabilities of transit of the current carrier between ions of the two sub-lattices (expressed in formula (2) by coefficients $C(msk)$, $D(msk)$, for the probabilities of transit within the limit of one sub-lattice $A(sk)$, $B(mk)$, $(m_i m_j k)$ in (2). This corresponds to an approximation of the close relationship between current carrier and crystal lattice. The expansions referred to above assume the form

$$E_\nu = E_\nu^0 + \tau E_\nu^I + \tau^2 E_\nu^{II} + \ldots;$$
$$u_{\alpha\nu} = u_{\alpha\nu}^0 + \tau u_{\alpha\nu}^I + \tau^2 u_{\alpha\nu}^{II} + \ldots . \qquad (5)$$

Coefficients $A(sk)$, $B(mk)$, $(m_i m_j k)$ are quantities of zero order in respect of τ, and $c(msk)$, $D(msk)$ are of the first order. Substituting (5) in (4), we obtain the following equations with approximation at zero

$$(A(sk) - E_\nu^0)\, u_s^0 = 0,$$
$$(B(m_1 k) - E_\nu^0)\, u_{m_1}^0 + \varepsilon(m_1 m_2 k)\, u_{m_2}^0 + \varepsilon(m_1 m_3 k)\, u_{m_3}^0 = 0,$$
$$\varepsilon(m_2 m_1 k)\, u_{m_1}^0 + (B(m_2 k) - E_\nu^0)\, u_{m_2}^0 + \varepsilon(m_2 m_3 k)\, u_{m_3}^0 = 0, \qquad (6)$$
$$\varepsilon(m_3 m_1 k)\, u_{m_1}^0 + \varepsilon(m_3 m_2 k)\, u_{m_2}^0 + (B(m_3 k) - E_\nu^0)\, u_{m_3}^0 = 0.$$

The unfilled energy bands are determined from the last three equations in (6). The energy spectrum for some points and directions in k-space can be determined analytically by methods of group theory. It is not difficult to determine also the corresponding amplitudes of transformations $u_{\alpha\nu}(k)$, which are necessary for calculating the corrections for the energy in high orders of the theory of perturbations. It follows from the symmetry of a crystal that for the coefficients of equation (6) the following equalities exist

$$L(m_i m_j k) = L(G^{-1} m_i,\ G^{-1} m_j,\ G^{-1} k),$$

where G is any element of the symmetry group of the crystal. The wave functions of the p-shell of the anions are selected in the form: $xf(r)$ and $zf(r)$, that is under the action of symmetry operations they are transformed as co-ordinates x, y, z.

$L(-m_i m_j k) = -L(m_i m_j k)$ and so on. The results are as follows (see Fig. 1):

(1) At the most symmetrical point of $\vec{K}$-space $\vec{K} = 0$ (the wave-vector group in this point contains the greatest number of elements) three energy bands coincide: $E_r = B(m_r 0)$: $r = 1, 2, 3$. The amplitude of the linear transformation $u(o)$ are arbitrary with an accuracy up to the conditions of normalization.

(2) For direction (1,0,0) in $\vec{K}$-space the energy bands split into undegenerate $E_1(k) = B(m_1 k)$ and two-fold degenerate $E_{2,3}(k) = B(m_2 k) + \varepsilon(m_2 m_3 k)$.

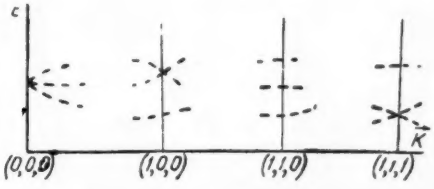

Fig. 1. Diagrammatical representation of energy levels at some points of the Brillouin zone.

For the first band, for instance, the amplitudes of transformation $u_{11}^0 k) = 1$; $u_{21}^0 = u_{31}^0 = 0$ etc.

(3) For direction (1, 1, 0) in K-space degeneration is completely removed, and three energy bands are present.

$E_{1,2}^0(k) = B(m_1 k) \pm \varepsilon(m_1 m_2 k)$, $E_3^0(k) = B(m_3 k)$.

For the third unfilled band, for instance,

the amplitudes in approximation at zero:

$u^0_{13} = u^0_{23} = 0,\ u^0_{33} = 1$ etc.

(4) For direction (1, 1, 1) in K-space one undegenerate band is obtained

$$E^0_{2,3}(\kappa) = B(m_2 k) + 2\varepsilon\ (m_1 m_2 k)$$

and one two-fold degenerate field

$$E^0_{2,3}(k) = B(m_2 k) - \varepsilon\,(m_2 m_3 k).$$

The amplitudes in approximation at zero, for instance for the first unfilled band are

$$u^0_{11} = u^0_{21} = u^0_{31} = \frac{1}{\sqrt{3}} \quad \text{etc.}$$

In a first approximation of the theory of perturbations the corrections of the energy are equal to zero, and in a second approximation we obtain

$$E^{II}_0(k) = C(m_1 sk)\, u^1_{m_1 0} + C(m_2 sk)\, u^1_{m_2 0} + C(m_3 sk)\, u^1_{m_3 0}, \tag{7}$$

$$E^{II}_r(k) = \frac{|C(m_1 sk)\, u^0_{m_1 r} + C(m_2 sk)\, u^0_{m_2 r} + C(m_3 sk)\, u^0_{m_3 r}|^2}{E^0_r - A(sk)};$$

$$r = 1, 2, 3.$$

The amplitudes $u^1_{m_i 0}$ are determined from first-order equations of the theory of perturbations, and neglecting the coefficient $\epsilon(m_i m_j k)$ equal in order of magnitude to the width of an unfilled band, compared with $A(sk)$-$B(mk)$ - of the order of the width of the forbidden band, we have

$$u^1_{m_i 0} = -\frac{D(m_i sk)}{B(m_i k) - A(sk)}. \tag{9}$$

Thus, the correction of the electron energy band is found to be equal to

$$E^{II}_0(k) = \frac{|C(m_1 sk)|^2}{A(sk) - B(m_1 k)} + \frac{|C(m_2 sk)|^2}{A(sk) - B(m_2 k)} + \frac{|C(m_3 sk)|^2}{A(sk) - B(m_3 k)}. \tag{10}$$

This magnitude is nearly always positive, whereas the corrections of the unfilled bands (8) are nearly always negative. The displacement of the unfilled bands in some directions of K-space can be obtained by using the above calculation of amplitudes in approximation at zero.

We now proceed to an analysis of the results obtained.

1. In approximation at zero the energies of electrons moving along anions and the energies of holes moving along cations are determined independently from (6). Such problems were solved in previous works [6, 7]. The wave functions of holes were selected in (7) in the form of a linear combination of functions of the 3p-shell of an isolated Cl pattern according to Hartree with some coefficients determined by the variation method. Thus it was found that the width of the unfilled band which is essential for conductivity amounts to 1.5 eV in KCl and 2.17 eV in NaCl, and the effective masses (in the direction perpendicular to the cube diagonal (111) and lengthwise to this diagonal) are for NaCl = $\mu_\perp = 0{,}98$ m, $\mu_\parallel = 0{,}54$ m; and for KCl respectively 4.56 and 0.47 m. These results agree with other data and they show that it is permissible to use the Hartree functions of isolated atoms for similar calculations; this is connected with their small - compared with the inter-atomic distance - quantum-mechanical radius.

In another paper [6] the corresponding magnitudes for the electron energy bands in NaCl are determined, for which modified Hartree functions, which attenuate more rapidly at larger distances, of the sodium atom are used. The results, however, do not agree with experimental data: for the base of the conductance zone a value of 1.9 eV was obtained instead of the experimental value of 0.5 eV; and the low value of 0.59 m was obtained for the effective mass. From this it must be concluded that in calculations of this nature the wave functions of isolated atoms should not be used and that the modified treatment proposed in [6] does not produce correct results.

2. Formulae (7)-(10) give corrections for the calculations in work referred to above. Corrections for the unfilled bands were found to be nearly always negative and the correction for the energy of the electron band to be positive.* By the group-theory methods

* If subsequent excited states at the g nodes are taken into account, this correction may show reversal of sign.

VOL 8 195

referred to above, an explicit form for the displacement of energy bands for some directions in K-space may be obtained.

3. Numerical estimates which, on the basis of secondary quantization, are connected with a concrete choice of basic functions defining coefficients L and F in (1) would be of very great interest. Approximations which are fundamental for the method used (the break in the set of functions for obtaining (1)) lead to some variation problem, and it is therefore expedient to select basis functions of the concept of secondary quantization which more adequately correspond to real electron states in a crystal (cf. also [6]). The use of wave functions of isolated atoms for these calculations were found to be unpromising also in [6] where overlap integrals for similarly charged ions were essential. The difficulties are increased in our case, since on the basis of these functions it is necessary to calculate integrals relating to the nearest neighbours in the crystal lattice. If the wave functions of electrons in a crystal will be determined in some form or other, then numerical calculations in the given framework do not present any difficulties in principle and, in contrast with single-electron work, they will not be connected with any supplementary concepts (for instance, on the calculation of exchange forces).

4. Consideration of the degeneration of electron states thus leads to the anisotropy of the effective masses of the current carrier and to a change in the shape and position of the energy bands. These effects are also influenced by taking into account in our calculations the movement of the current carrier at the nodes of both cations and anions. It may be stated that in homo-polar semiconductors of the germanium type the anisotropy of the effective masses of the current carrier is due to the nature of the chemical bond [8].

Thus, both in the case of the homo-polar crystals of the germanium type and in the case of the alkali halide type, spin-orbital interaction does not appear to be a necessary factor for producing anisotropy of the effective masses of the current carrier.

The present paper offers a general multi-electron approach to the problem of the degeneration of electron states in crystals; a small parameter is introduced which allows the practical treatment of the calculation of the energy spectrum for the many-electron system in binary crystals; attention is directed to the close connexion with papers [6, 7], which allows the results of those papers to be corrected. A method of numerical calculations is pointed out, which is associated with the general problem of electron wave functions in a crystal*.

Translated by H. Nowottny

REFERENCES

1. S.P. Shubin and S.V. Vonsovskii, *Sov. Phys.*, 7, 292 (1935), 10, 348 (1936).
2. S.V. Vonsovskii, *Adv. Phys. Sci. Moscow*, 48, 289 (1952); Jubilee collection of papers, IFM (1958) (In preparation)
3. N.N. Bogolyubov. *Lektsii po kvantovoi statistike, (Lectures on quantum statistics)* (in Ukrainian) Kiev (1949).
4. Yu.M. Seidov and V.S. Galishev, *Zh. eksp. teor. fiz.* 30, 695 (1956).
5. S.A. Moskalenko and M.Sh. Giterman. *Optika i spektroskopiya, (Optics and Spectroscopy)* 3, No.8 (1958); *Fiz. metal metalloved.* 5, 364 (1957); 6, 930 (1958).
M.Sh. Giterman, P.S. Zyryanov and G.G. Taluts, *Zh. eksp. teor. fiz.*, 35, 1532 (1958).
6. K.B. Tolpygo and O.F. Tomasevich, *Adv. Phys. Moscow*, 3, 145 (1958).
7. T.Io Kucher, *Zh. eksp. teor. fiz.* 34, 394

* In [9] 3 s- and p-valence bands in the KCl crystal are calculated with consideration of their interaction between themselves and with the internal valence bands. Numerical calculations carried out with the aid of calculating machines on Hartree functions of isolated ions show the convenience of taking into account the above interaction. The results of the calculation agree qualitatively with the presuppositions of our work. In [9], however, the intersection of the valence bands with the conduction band, which is taken into account in our work and doubtless corresponds more closely to reality, is neglected.

(1958), 35, 1049 (1958).
8. A.G. Samoilovich and K.D. Tovstyuk, *Zh. teor. fiz.* 27, 1753 (1957).
9. L.R. Howland, *Phys. Rev.*, 109, 1927 (1958).

VOL
8
195

MAGNETIC PROPERTIES OF STEELS AS A BASIS OF MAGNETIC STRUCTURE ANALYSIS*

G. S. TOMILOV, M.N. MIKHEEV and M.F. POMUKHIN

Institute of Metal Physics of the Academy of Sciences, U.S.S.R.

(Received 13 October 1958)

On the basis of an investigation carried out on magnetic and mechanical properties of a number of structural and instrument steels after quenching and tempering in a wide range of temperatures, and also on the basis of an investigation on the temperatures dependence of the magnetic properties of steels (in the range from -196 to + 300°C), a new magnetic method is proposed for quality control in the heat-treatment of steel parts subjected to high-temperature tempering (350-700°C).

VOL. 8 1959

Present-day large-scale production of steel parts, used in machine construction, with high performance requirements and the heat-treatment which in some form or other is associated with it demand that, on the one hand, high-productivity automatic lines be used and, on the other, a method of controlling as efficiently as possible the quality of heat-treatment; this method should ensure 100 per cent control of the product in the flow line and should be non-destructive. Present methods of selective testing of parts in respect to their hardness or microstructure do not fully ensure the elimination of scrap in large-scale production and, far from facilitating the setting-up of automatic heat-treatment lines, they even work against them.

Of all the non-destructive methods of quality control for the heat-treatment of steel parts, it is the magnetic method which is most productive and simple and, at the same time, assists complete automation of the process of heat-treatment and of the quality control of this treatment.

Several magnetic devices are known which allow selective or constant non-destructive control of the quality of thermal treatments (quenching, tempering, annealing); they operate by measuring some magnetic properties present in the product, for instance coercive force or permeability [1-6].

However, the use of magnetic methods of control in practice should be most effective if magnetic devices are incorporated in automatic flow lines of thermal treatment.

STUDY OF MAGNETIC PROPERTIES AND HARDNESS IN STRUCTURAL AND INSTRUMENT STEELS

Before one sets out to design magnetic control apparatus or an automatic flow line incorporating heat-treatment and the quality control of this treatment, it is necessary to study the relationship between the magnetic and mechanical properties and the microstructure in a given steel.

The relationship between magnetic and mechanical properties (for instance, between coercive force and hardness, has a completely defined physical basis. As a rule, when the phase composition remains unchanged (for instance, in pure pearlitic or pure martensitic conditions) the coercive force increases as the hardness increases. If, as a result of inadequate heating of a part prior to quenching, troostite or pearlite is present in the structure together with martensite, it is found that both hardness and coercive force are lowered. If after quenching to martensite a part is tempered,

* *Fiz. metal. metalloved.* 8, No. 2, 176-180, 1959.

both its coercive force and its hardness are, as a rule, reduced depending on the degree of tempering (temperature and holding time). On the basis of these general rules, there arises indeed a practical possibility of using a magnetic method for the quality control of the heat-treatment of steel parts.

However, in some steels these general rules are not observed. Thus, for instance, uniform reduction in hardness is, in a certain range of temper temperatures (200-600°C), accompanied by a non-uniform change in coercive force (first increase, then decrease). This is explained by the formation or decomposition of non-magnetic or weakly magnetic phases such as residual austenite and carbides [7].

In structural steels with low contents of carbon and alloying elements, a direct connexion between hardness and coercive force is often observed over the entire range of treatment temperatures and the magnetic control method can therefore be used without difficulty by measuring any one magnetic characteristic (single-parameter method [3-5, 8]). In the case of high-carbon unalloyed and alloy steels the use of the single parameter method is found inadequate. For instance, the magnetic method for the control of the quench quality in ball-bearing parts (steel ShKh15) by measuring the coercive force does not allow separation of scrap due to overheating from sound products or from scrap due to inadequate heating. This is explained by the peculiar gradient of the change in the coercive force as a function of the quench temperature: the coercive force increases as the quench temperature rises to 800°C, it remains unchanged while the temperature is further increased to 850°C and drops substantially during marked overheating (850-950°C [9]).

However, we turned to another magnetic property – saturation magnetization I_s – and succeeded in overcoming this difficulty, and it can be stated that the magnetic control of quench quality for bearing rings has now been mastered [10]. This experimental development was taken up by the Institute of the Bearing Industry (ENIIPP) and has been introduced in a number of other ball-bearing works [11].

Similar difficulties are encountered when magnetic methods are introduced for the control of temper quality.

Fig. 1 and 2 show magnetic properties (H_c and I_s), hardness (R_c) and electrical resistance (ρ) for two typical steels after quenching and subsequent tempering from various temperatures.

The chemical compositions of the investigated steels are shown in Table 1.

It is seen in Fig. 1 that, in the batches of steel ShKh15 specimens which were subjected to quenching from different temperatures, the electric resistance and hardness as well as magnetic properties show a different behaviour after tempering from various temperatures.

For quenching with underheating (780°C) or normal quenching to microcrystalline martensite (850°C), coercive force and hardness show maximum and electric resistance minimum values compared with higher quench temperatures. Saturation magnetization is lowered with an increase in quench temperature as a result of the increased amount of residual austenite.

As the temper temperature is increased, the hardness and electric resistance values drop nearly uniformly. An exception is made by the coercive force which shows a slight maximum at 500-525°C.

A more marked change is observed for all properties as a result of tempering at 100-

TABLE 1

Composition of steels studied

Steel	Contents, wt.%							
	C	Cr	Mn	Si	W	Ni	S	P
ShKh15	1.00	1.50	0.30	0.30	–	–	0.020	0.027
40KhN	0.40	0.60	0.60	0.25	–	1.10	–	–

VOL. 8 1959

250°C; this is associated with stress relief of the second type and with decomposition of residual austenite.

For quenching with overheating (900-1080°C), on the other hand, the initial properties (coercive force, hardness, saturation magnetization) are relatively low owing to the large quantity of residual austenite.

Tempering at 150-250°C leads to a subsidiary maximum for the coercive force in the range 200-220°C and to nearly complete decomposition of the residual austenite. Following tempering at 300-650°C the values of coercive force, intensity of magnetization and hardness remain higher than with normal quenching from 850°C, but a subsidiary maximum of the coercive force at 550°C shows up more clearly.

The properties of steel 40 KhN show similar changes (Fig. 2). The values of the coercive force are lower compared with those in steel ShKh15.

The coercive force values observed at temperatures ranging from -196 to +300°C are shown in Figs. 3 and 4.*

At observation temperatures $T \geqslant 220°C$ (above the Curie point for carbides) the maximum value of the coercive force was observed in the region of 400°C tempering. At all temperatures above 400°C the coercive force drops steadily and does not show any further maximum values.

The disappearance of subsidiary maxima of coercive force (at 550-600°C) and the formation of a new maximum in the region of $T \geqslant 220°C$ can generally be explained by Kondorskii's theory of inclusions [12], when

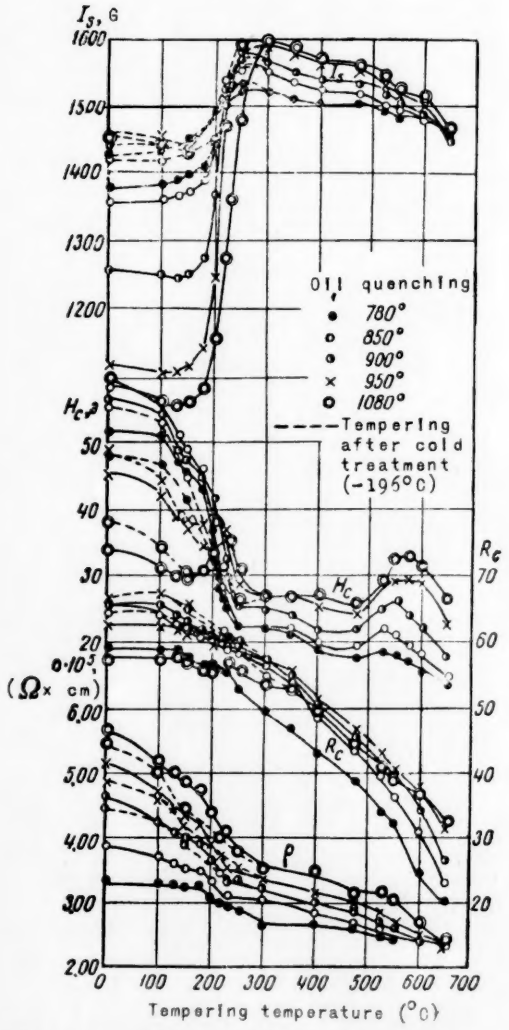

Fig. 1. Magnetic, electric and mechanical properties of steel ShKh15 after quenching and tempering from various temperatures.

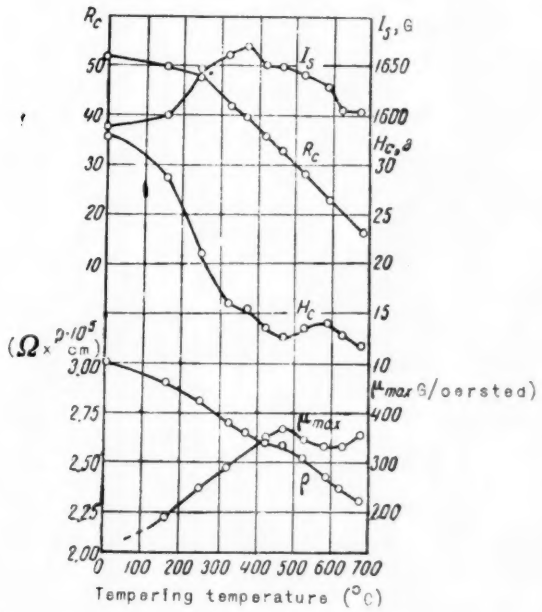

Fig. 2. Magnetic, electric and mechanical properties of steel 40KhN after quenching and tempering from various temperatures.

* The coercive force was measured at various temperatures by means of an astatic magnetometer; a small tubular furnace was placed into one of its solenoids. A thermocouple was located very close to the specimen. The accuracy of measurement and of constancy of temperature was ± 3°.

weakly magnetic carbides differing in their degree of dispersion and intensity of magnetization appear as inclusions.

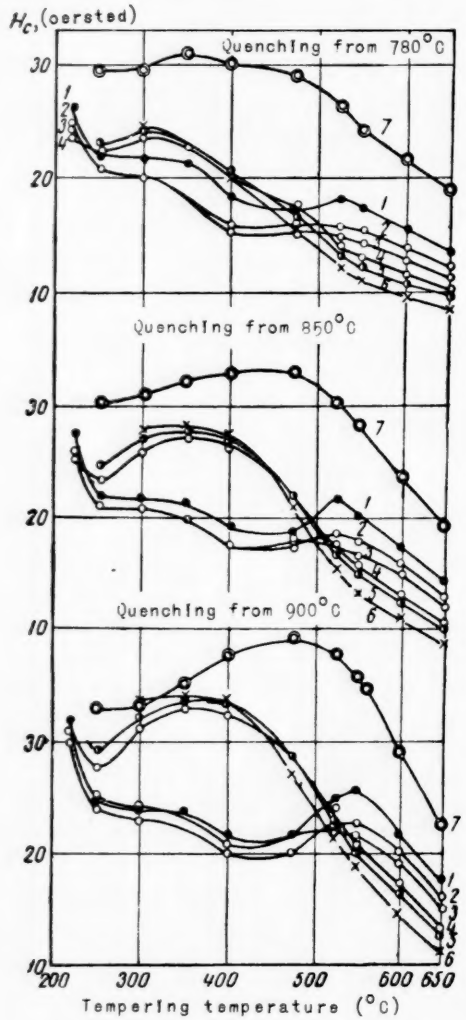

Fig. 3. Coercive force of steel ShKh15 (quenched and tempered from various temperatures) as a function of the temperature of observation: 1 at 20°C; 2 at 100°C; 3 at 150°C; 4 at 220°C; 5 at 250°C; 6 at 300°C; 7 at -196°C (liquid nitrogen).

The temperature measurements of coercive force afford a deeper understanding of the physical nature of the connexion between magnetic and mechanical properties in steels and they can be widely used in practice for magnetic analysis under works conditions. This is of special importance in cases when measurements at room temperature are unreliable for separating temper scrap from the sound products.

For magnetic control in automatic flow lines the measurements of coercive force can be carried out either immediately at the temper temperature or at any lower temperature. All that matters is that the temperature is not lower than 220°C and that it does not differ too widely from this figure.

It is understood that the control of quench quality should be carried out up to tempering by means of measuring (manually or automatically) the coercive force or permeability and intensity of magnetization at the works temperature. Only parts which are quenched normally must be admitted for tempering. Otherwise the results of inspection following the tempering may be incorrect.

In the temper temperature range between 250 and 350°C, as seen in Fig. 3, the coercive force observed at $T \geqslant 220$°C (curves 4 and 5) increases. This does not prevent the use of magnetic control provided that too violent

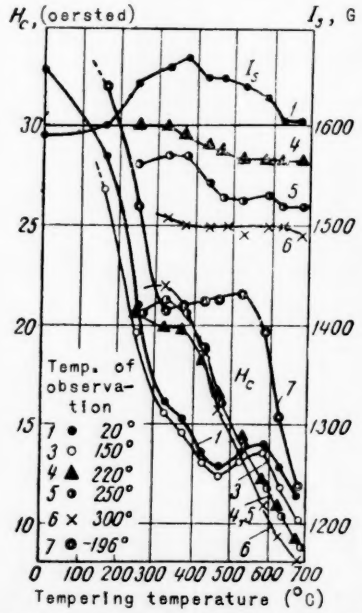

Fig. 4. Coercive force of steel 40 KhN (quenched and tempered from various temperatures) as a function of the temperature of observation: 1 at 20°C; 2 at 100°C; 3 at 150°C; 4 at 220°C; 5 at 250°C; 6 at 300°C; 7 at -196°C (liquid nitrogen).

temperature fluctuations are avoided.

In conclusion it should be noted that several types of automatic apparatus for coercivity measurements have been described

in the literature. The apparatus, which requires no operator, allows continuous measurement of the coercive force of parts produced in any automatic flow line [13-14].

CONCLUSIONS

Supplementary to existing magnetic methods for the quality control of the heat-treatment of steel parts quenched to martensite and subjected to high-temperature tempering, an automated magnetic method is proposed for control in automatic flow lines at observation temperatures not below 220°C. For steels in which the coercive force changes in a non-single-valued manner as a function of the tempering temperature, the proposed method of control ensures sufficiently accurate separation of scrap over nearly the entire range of tempering temperatures. The magnetic properties and hardness of two typical steels after quenching and tempering from various temperatures are given, and also the coercive force at different temperatures of observation (from -196 to +300°C),

Translated by H. Nowottny

REFERENCES

1. S.V. Vonsovskii and M.N. Mikheev, *Zav. lab.* No.10, 1221 (1957).
2. R.I. Yanus, *Trud. Inst. fiz metal Urals fil Akad. nauk SSSR*, No.12, p.150 (1949).
3. A.V. Nifontov, *Zav. lab.* No.8, 924 (1935).
4. M.N. Mikheev, *Zav. lab.*, No.10, 155 (1938).
5. A.N. Rabinovich, *Annotatsiya raboty kafedry tekhnologii mashinostroeniya, stankov i instrumentov (Notes on the work of the Faculty of the technology of machine construction, machine tools and instruments).* L'vov Polytechnical Inst. (1956).
6. F. Forster, *J. Soc. Non-destructive Testing*, 31, Sept.-Oct. 1956.
7. M.N. Mikheev, L.N. Zhukova and G.S. Tomilov, *Trud. Inst. fiz metal Urals fil. Akad. nauk SSSR*, No.15, p.90 (1954).
8. P.H. Zhukova and M.I. Mikheev, *Zh. teor.fiz.* 18, 167 (1948).
9. M.N. Mikheev, I.A. Kuznetsov, V.A. Kryukova and B.K. Neizvestnov, *Fiz. metal. metalloved.* 3, 229 (1956).
10. M.N. Mikheev, G.S. Tomilov, M.F. Pomykhin, K.G. Rzyankin and V.A. Utkina. *Zav. lab.* No.5, 549 (1956).
11. Gosudarstvennyi soiuznyi nauchno-issledovatel'skii i eksperimental'nyi institut podshipnikovoi promyshlennosti (ENIIPP) (Scient. Res. and Developm. Inst. of the Bearing Industry) *Obmen tekhnicheskim opytom (Exchange of technical experience)*, No.12, 376 (1958).
12. E.I. Kondorskii, *Dokl. Akad. Nauk SSSR*, 13, 5 (1948).
13. V.M. Frantsevich and L.A. Fridman, *Zav. lab.* No.5, 590 (1956).
14. M.N. Mikheev, *Zav. lab.*, No.2, 73 (1949).

VOL. 8 1959

STUDY OF THE PROPERTIES OF TITANIUM ALLOYS

IV. PROPERTIES OF ALLOYS OF THE TERNARY Ti-Al-Fe SYSTEM*

I.I. KORNILOV, E.N. PYLAEVA and M.A. VOLKOVA

Baikov Institute of Metallurgy

(Received 25 March 1958)

Titanium, the new light-weight, high-strength material, plays an important part in the production of new heat-resisting materials. For this reason, great importance is attached to the study of phase diagrams of the titanium systems [1-3]. For the solution of practical problems in the application of titanium alloys it is very important to establish the laws according to which the mechanical properties at elevated temperatures of these alloys change in relation to chemical composition and structure or in relation to the phase diagram. In conjunction with a study of the phase diagrams of the titanium systems [4,5] we undertook a systematic investigation of the strength at elevated temperatures of the titanium alloys [6, 7]. These problems are important both for the development of the theory of strength at elevated temperatures and for the solution of the practical problems involved in the development of new titanium alloys.

The present paper gives the results obtained in the study of the strength at elevated temperatures of titanium alloys of the ternary Ti-Al-Fe system.

On the basis of the study of the phase diagram of the ternary Ti-Al-Fe system, the regions of phases α, β, α+TiFe, $\alpha+\gamma$ and γ were established at temperatures of 1150, 1100, 1000, 800 and 550°C in the titanium corner of the diagram [8].

The solid solutions of aluminium and iron in β- titanium at 1100°C occupied considerable space. The ternary solid solutions on the basis of α-titanium at 550°C in the system studied are arranged in the form of a narrow band on the side of the Ti-Al system. The iron contained in the ternary α-solid solution amounts to 0.5 wt. per cent.

Fig. 1 shows the phase diagram at a temperature of 550°C.

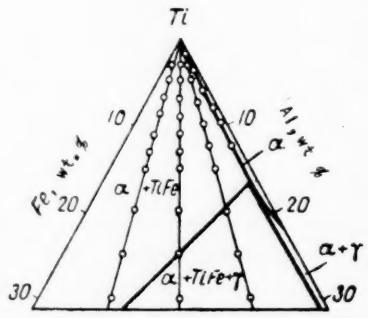

Fig. 1. Iso-thermal section through part of the ternary system Ti-Al-Fe at 550°C.

The alloys were prepared by the powder-metallurgy method. After pressing, the specimens were sintered in a vacuum under the following conditions: slow heating up to 1100°C, holding for 100 hours and cooling in the furnace to room temperature. The compositions of the alloys studied are shown on the three radial sections containing up to 20% Al and Fe (see Fig. 1) with constant aluminium/iron ratios of 3:1, 1:1 and 1:3. Alloys of the section parallel to the Ti-Al side with contents up to 0.5% Fe and up to 8% Al were also studied.

The investigation of the heat-resistant ternary alloys was carried out by the centrifugal method [9]. The tests were conducted at 550°C at a stress of 15 kg/mm^2; the test time was 100 hours. The alloys from the region of the α-ternary solid solutions and adjacent region (up to 0.5% Fe) were distinguished by their high strength at elevated temperatures compared with the

* *Fiz. metal. metalloved.* 8, No.2, 182-186, 1959.

VOL
8
195

alloys found in the clearly two-phase region α + TiFe with separation of the second phase in the form of large inclusions.

For the set of alloys with high strength at elevated temperatures on a basis of ternary α-solid solutions of titanium the test temperature was increased by 50°C after each cycle of 250 hours. The test conditions adopted for these alloys were as follows:

At 550°C σ – 15 kg/mm^2 = 250 hours
At 600°C σ – 15 kg/mm^2 = 250 hours
At 650°C σ – 15 kg/mm^2 = 250 hours
At 700°C σ – 15 kg/mm^2 = up to fracture.

The measure adopted for the strength at elevated temperatures was the change in the deflexion (in mm) in relation to the time of deformation and the time necessary for reaching a given deflexion at the test temperature and at constant initial stress.

Fig. 2 shows the changes in deflexion for alloys, the compositions of which are indicated on the radial sections. These alloys were tested at 550°C while stressed at 15 kg/mm^2 for 100 hours. It is clear from the curves obtained that minimum strength at elevated temperatures is shown by the alloys of the two-phase region on the side of the Ti-Fe system (curves 1 and 2).

The microstructure of the alloy containing 3.75% Al and 11.25% Fe is shown in Fig. 3.

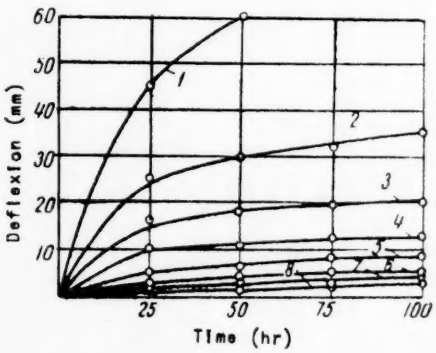

Fig. 2. Deflexion (mm) plotted against time (hr) for parallel-section alloys.
Curve 1: Alloy containing 2.5% Al, 7.5% Fe 90% Ti;
2: 3.75% Al, 11.25% Fe. 86% Ti;
3: 6.5% Al, 6.5 Fe, 87% Ti;
4: 7.5% Al, 7.5% Fe, 85% Ti;
5: 7.5% Al, 2.5% Fe, 90% Ti;
6: 3.75 Al, 1.25% Fe, 95% Ti;
7: 7.5% Al, 0.5% Fe, 92% Ti;
8: 8,0% Al, 0.5% Fe, 91.5% Ti.

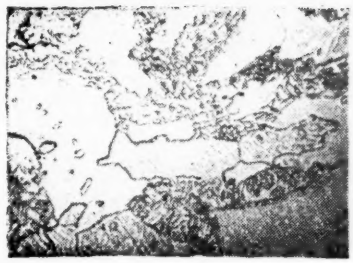

Fig. 3. Microstructure of an alloy containing 3.75% Al, 11.25% Fe, after annealing at 550°C for 500 hr. x 160.

The light regions correspond to the α-phase and the dark to areas between the grains filled with eutectoid α – TiFe. These alloys contain three times more iron than aluminium; at 550°C they are found to be not heat-resistant. Alloys in which the iron/aluminium ratio is 1:1 are more heat-resistant and, when strained, show less deflexion (curves 3 and 4 in Fig. 2) than the preceding alloy compositions. The micro-structure of an alloy containing 6.5% Al and 6.5% Fe (Fig. 4) shows α-solid solution crystals in a eutectoid (α + TiFe) matrix. When the alloy compositions approached the region of the saturation limit of the α-solid solution, the alloys acquired higher heat resistance than alloys which were clearly two-phase, and their deflexions were insignificant. This is clearly shown by the curves plotting the deflexions (curves 5 and 6 in Fig. 2). The microstructure of these alloys is similar to that of an alloy containing 3.75% Al and 1.25% Fe (Fig. 5); it consists of polyhedrons of the ternary α-solid solution with inclusions of α + TiFe eutectoid along the grain boundaries.

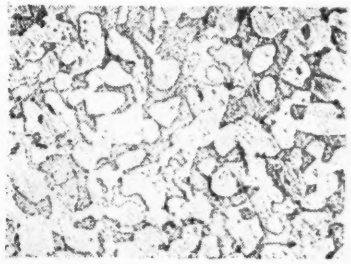

Fig. 4. Microstructure of an alloy containing 6.5% Al, and 6.5% Fe after annealing at 550°C for 500 hr. x 160.

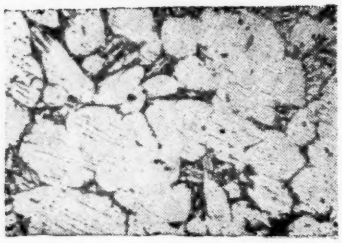

Fig. 5. Microstructure of an alloy containing 3.75% Al and 1.25% Fe after annealing at 550°C for 500 hr. x 160.

Of all the investigated ternary alloys of the Ti-Al-Fe system, high heat-resistance was shown by parallel-section alloys containing 0.5% Fe and from 1 to 8% Al. These alloys exhibited least deflexions on straining compared with the other alloys studied (curves 7 and 8 in Fig. 2).

In their phase structure, these alloys correspond to the boundary region of the transition from the single-phase region of the ternary α-solid solution to the two-phase α + TiFe region.

For a test time of 100 hours at 550°C, creep was low for a number of alloys and their deformation quite insignificant. In this connexion, the test temperature was increased by 50°C after every 250 hours, while the same stress of 15 kg/mm^2 was maintained. The general total test time for these alloys at temperatures of 550, 600, 650 and 700°C was 875 hours.

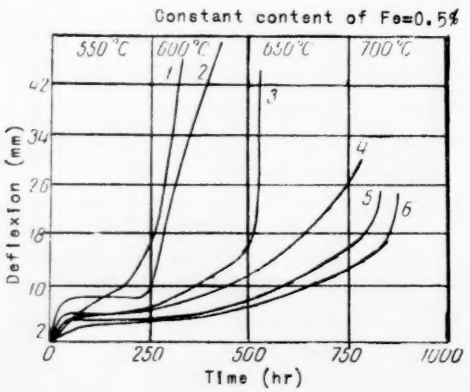

Fig. 6. Curve 1: Pure titanium
2: Alloy containing 1% Al, 0.5% Fe, 98.5% Ti;
3: Alloy containing 3% Al, 0.5 Fe, 96.5% Ti;
4: Alloy containing 5.5% Al, 0.5% Fe, 94% Ti;
5: Alloy containing 7.5% Al, 0.5% Fe, 92% Ti;
6: Alloy containing 8% Al, 0.5% Fe, 91.5% Ti.

Curves plotting the change in deflexion with time are shown in Fig. 6 for alloys of parallel section. The curves show the lowest heat-resistance for pure titanium. Pure titanium deformed more rapidly than titanium alloys containing iron and aluminium.

Ternary alloys with increasing aluminium contents showed a corresponding increase in heat-resistance. Of this series of alloys those containing 7.5 and 8% Al and 0.5% Fe showed the highest strength at elevated temperatures. At temperatures below 650°C their deformation was negligible and they began to be deformed only at temperatures between 650 and 700°C.

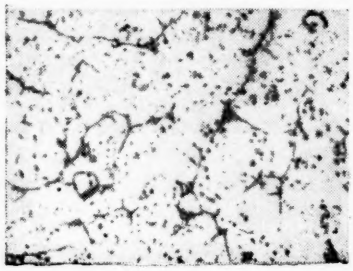

Fig. 7. Microstructure of an alloy containing 7.5% Al and 0.5% Fe after testing by the method of deflexion; x 160.

Fig. 7 shows the microstructure of an alloy containing 7.5% Al and 0.5% Fe after heat-resistance testing; it presents a solid-solution polyhedron with a small amount of precipitate of a finely dispersed phase along the grain boundaries and in the grain interior. The microstructures of the other alloys of this section are similar.

The results of these investigations show that, just as in the binary Ti-Al system [8], aluminium increases the heat-resistance of ternary alloys in those regions of the phase diagram in which the matrices of these alloys are ternary α-solid solutions and alloys from the region of the limit of saturation.

With a view to confirming these results, it was considered interesting to study alloys in which the aluminium contents were kept constant at 1, 4 and 8 per cent while the iron contents were varied from 0.5 to 10 per cent. In agreement with the phase diagram (Fig. 1), these alloys are found in the transition region between ternary solid solutions and

two-phase alloys of eutectoid structure. The influence of the change in the iron content (up to 10 per cent) on the heat-resistance of ternary alloys is shown in Fig. 8, which gives the times when a deflexion of 5 mm was reached by these alloys when tested by the centrifugal method at 550°C at a stress of 15 kg/mm². Three curves are plotted showing the influence of iron on alloys containing, respectively, 1, 4 and 8 Al.

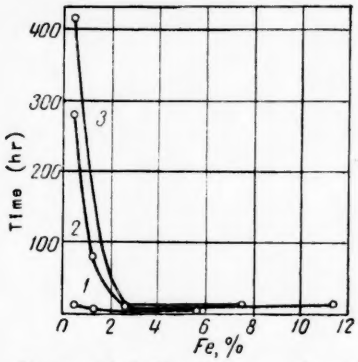

Fig. 8. Change of deflexion as a function of time for alloys of parallel section.
Curve 1: 1% Al and variable Fe contents
2: 4% Al
3: 8% Al

It is seen in Fig. 8 that ternary alloys containing from 0.5 to 1% Fe (from the b boundary region between the α-phase and the α + TiFe phase) have maximum heat-resistance and alloys containing more than 1% Fe (the region α + TiFe) have a reduced strength at high temperatures. Heat-resistance is substantially reduced as the iron content goes up, the alloys containing more than 2 per cent iron show low values of heat-resistance and high plasticity at 550°C.

The relationship between the heat-resistance of titanium alloys [4, 6, 7], and also of alloys of the ternary system Ti-Al-Fe, and their composition and structure is found to be in agreement with the regular changes of heat-resistance in systems based on aluminium iron and nickel [10-12]. This confirms the views expressed in an earlier publication by one of the authors of the present paper on the physico-chemical theory of high-temperature strength [13].

CONCLUSIONS

1. The heat-resistance of titanium alloys is found to be a function of alloy composition and structure of the ternary Ti-Al-Fe system.

2. Alloys with the highest heat-resistance are found in the border zone of saturation and super-saturation of the titanium ternary α-solid solution.

3. Transition to ternary alloy compositions from the two-phase structure (α – TiFe) produces a lowering in heat-resistance with an increase in plasticity. The low heat-resistance of alloys of this region is explained by their eutectoid structure and low temperature of transformation in the region of β-solid solutions.

4. The highest heat-resistance is shown by alloys containing between 3 and 8 per cent aluminium and up to 0.5 per cent iron.

5. As the aluminium content is increased in the ternary alloys while the iron content is kept constant at 0.5 per cent, the heat-resistance of the alloys is increased and their plasticity decreased.

6. Alloys with aluminium contents of 1, 4 and 8% and iron contents varied from 0 to 10% show that the maximum heat-resistance of the ternary alloys corresponds to the compositions found in the phase diagram of the ternary Ti-Al-Fe system in the transition region between the ternary α-solid solution and that of the two-phase α + TiFe.

Translated by H. Nowottny

REFERENCES

1. N.V. Eremenko, *Titan i ego splavy (Titanium and its alloys)*. Published by Academy of Sciences of U.S.S.R. (1955).
2. I.I. Kornilov, *Uspekhi khimii*, 22, 530 (1954).
3. I.I. Kornilov and L.B. Budberg, *Uspekhi khimii*, 25, 12 (1956).
4. I.I. Kornilov, E.N. Pylaeva and M.A. Volkova, *Izv. Akad. nauk SSSR, OKhN*, No.7 (1956).
5. I.I. Kornilov and N.G. Boriskina, *Dokl. Akad. Nauk SSSR*, 108, 1083 (1956).
6. I.I. Kornilov and V.S. Vlasov, *Izv. Akad. nauk. otd. tekh. nauk.* 4, 31 (1958).
7. I.I. Kornilov and V.S. Vlasov, *Izv. Akad. nauk. otd. tekh. nauk.* 7, 136 (1958).
8. I.I. Kornilov, E.N. Pylaeva and M.A. Volkova, *Zh. neorgan. khim.* 3, 6, 1932 (1958).
9. I.I. Kornilov, *Izv. SFKhA Akad. nauk. SSSR*, 18, 72 (1949).

VOL. 8 1959

10. I.I. Kornilov, L.I. Pryakhina and T.F. Chuiko, *Izv. SFKhA Akad. Nauk SSSR*, 19, 437 (1949).

11. I.I. Kornilov, R.S. Mints and S.D. Onoprienko, *Dokl. Akad. Nauk SSSR*, 88, No. 4, 683 (1953).

12. I.I. Kornilov and L.B. Budberg, *Dokl. Akad. Nauk SSSR*, 110, No. 1, 73 (1955).

13. I.I. Kornilov, *Dokl. Akad. Nauk SSSR*, 67, No. 6, 1057 (1949).

DIRECTIONAL DIFFUSION, DUE TO DEFORMATION, OF HYDROGEN IN A SOLID SOLUTION AND STRENGTH OF THE METAL*

K. V. POPOV and V. A. YAGUNOVA

East Siberian Branch of the Siberian Section
of the Academy of Sciences, SSSR

(Received 7 July 1958)

The magnitude of the hydrogen pressure in micro-defects of steel 20, which is necessary for the spontaneous formation of blisters in the surface layer of specimens during cathodic polarization in an electrolyte, is estimated, the diffusion coefficient for hydrogen in steel is calculated and one of the theories of hydrogen embrittlement is confirmed.

VOL. 8 1959

Hydrogen can enter steel, when the metal is in the solid state, either from electrolyte during etching or cathodic polarization, or from a gas phase containing hydrogen, especially at elevated temperatures and pressures. Moreover, steel when solidified can retain part of the hydrogen dissolved in the metal when it was melted.

Hydrogen absorption of steel is accompanied by modification of many of its properties. One of the most typical effects of hydrogen on steel is the development of hydrogen embrittlement at low rates of deformation. The physical nature of hydrogen embrittlement has not yet been studied thoroughly enough and it is therefore too early to formulate a complete theory of this phenomenon.

Several hypotheses exist concerning hydrogen embrittlement; The following appear to be most widely known.

1. The hypothesis of internal pressures forming in micropores as a result of directional diffusion of hydrogen during plastic deformation [1].

2. The hypothesis of inhibition of dislocations due to hydrogen atom clusters at sufficiently slow loading and at a sufficiently high temperature [2].

3. The hypothesis of surface activation by adsorbed hydrogen which decreases surface energy and facilitates propagation of cracks [3-5].

It is the purpose of the present work to estimate the possibility of hydrogen embrittlement being formed in accordance with the first hypothesis.

Prepared ten-notch bar specimens, 8 mm in diameter, of steel 20 were exposed to saturation in normal aqueous solution of sulphuric acid with arsenic accelerator addition. While the specimens were being saturated, blisters appeared on their surface (still prior to testing) spheroidal in shape, and cracks were observed below these blisters (Fig. 1). The formation of such blisters clearly contradicts the result obtained elsewhere [6] according to which hydrogen does not under any circumstances develop pressures high enough to fracture the metal.

For a blister to increase, it is necessary that in the crack a pressure arises which is

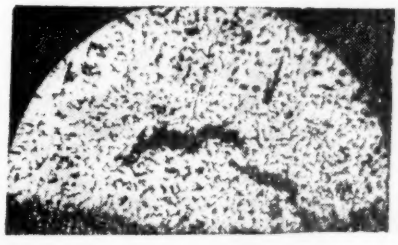

Fig. 1. Cross-section through a blister at the surface of a steel 20 specimen after electrolytic saturation with hydrogen. x 90.

* *Fiz. metal. metalloved.* 8, No. 2, 187-192, 1959.

high enough to set up, in the metal below the crack, stresses which are not less than the yield stress. If the yield stress of the test metal and the basic parameters of the defect formed are known, it is not difficult to estimate the pressure arising during the propagation of a crack.

The portion of the material covering the crack can be regarded, to a certain approximation which is adequate for an estimate calculation, as the wall of a thick-walled spherical container (Fig. 2). The tangential

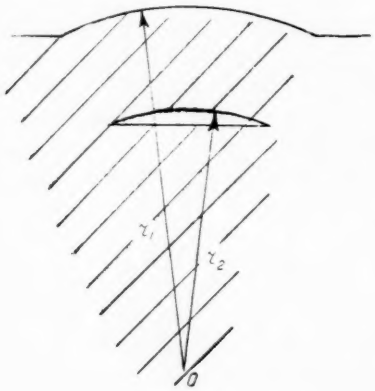

Fig. 2. Diagrammatic representation of a spherical blister, which corresponds to the formation of the actual defect shown in Fig. 1.

stresses in such a wall are calculated [7] according to the formula

$$\sigma_t = \frac{P_2 r_2^3 - P_1 r_1^3}{r_1^3 - r_2^3} + (P_2 - P_1)\frac{r_1^3 r_2^3}{2r^3\left(r_1^3 - r_2^3\right)}, \quad (1)$$

where σ_t are the tangential stresses, P_1 the external pressure, P_2 the internal pressure, r_1 the radius of curvature of the external surface, r_2 the radius of curvature of the internal surface, and r the distance between the centre of the sphere and the point at which the stress is determined.

Assuming that σ_t is equal to the yield point for steel and neglecting the quantity P_1 which is known to be small compared with P_2 we determine the stress at the internal surface of the sphere ($r = r_2$). Substituting the appropriate values in equation (1), we obtain

$$\sigma_s = \frac{P_2\left(2r_2^3 + r_1^3\right)}{2\left(r_1^3 - r_2^3\right)}. \quad (2)$$

Solving equation (2) with respect to P_2 and substituting the experimentally found values of σ_s = 24 kg/mm^2, r_2 = 0.60 mm and r_1 = 0.85 mm, it is seen that the pressures at which a blister can increase must be not less than 25 kg/mm^2 or 2500 atmospheres.

To establish the possibility that the internal defects are filled with hydrogen up to the critical pressure for the time of deformation, it is necessary to determine the diffusion coefficient for hydrogen in the investigated steel at room temperature. This determination is carried out with the aid of the following experiment.

Two sets of specimens, 8 mm in diameter, are subjected to cathodic polarization in an electrolyte under strictly defined conditions. Polarization time is one hour for the first test series and two hours for the second. It was established by parallel tests that specimens polarized for identical times show showed the same total hydrogen contents. The hydrogen-impregnated specimens (two for each measurement) were machined on a lathe to diameters of 6, 4 and 2.5 mm. Two specimens were left in the unmachined condition. Measures were taken to prevent the specimens from becoming heated during the lathe work. In the cylinders prepared in this way, representing in their cross-sections portions

TABLE 1

Hydrogen content in specimens

Polarization time (hr)	Hydrogen content (ml.H_2 per 100 g of metal), in specimens with dia. (mm)			
	8	6	4	2.5
1	3.4	1.1	0	–
2	4.8	3.2	2.0	1.3

of the original 8 mm specimen, the hydrogen content was determined by the method of vacuum hot extraction. The same determination was carried out also on the unmachined specimens. The mean values from two measurements of the hydrogen content in these specimens is shown in Table 1.

The distribution of hydrogen over the specimen cross-sections calculated from the data of Table 1, is well described by the parabolae shown in Fig. 3. Curve 1 corresponds to polarization for one hour and curve 2 for two hours. The equations of these parabolae are as follows:

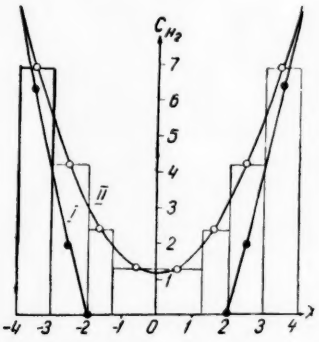

Fig. 3. Distribution of hydrogen over the cross-section of steel specimens after saturation for 1 hour (curve 1) and 2 hours (curve 2).

$$\text{Curve } 1 - C = -2.6 - 0.73X^2$$

$$\text{Curve } 2 - C = 1.1 - 0.48X^2$$

where C is the hydrogen content in steel in ml./100 g of metal and X the distance from the axis of the specimen in mm. On the basis of the experimental data we calculate the mean rate of diffusion through a cylindrical surface (6 mm in dia.) imagined to be inside and coaxial with the 8-mm specimen. The mean rate of diffusion is determined by equation

$$\bar{p} = \frac{\Delta M}{\Delta \tau S} = \frac{M_2 - M_1}{(\tau_2 - \tau_1) S}, \qquad (5)$$

where p is the mean rate of diffusion, M_1 and M_2 the quantities of hydrogen contained inside the cylinder considered after polarization for times τ_1 and τ_2 respectively, and S the side surface of the cylinder.

The total quantity of hydrogen inside the cylinder is defined by equation

$$M = CV, \qquad (6)$$

where C is the mean relative hydrogen content in the metal inside the cylinder considered and V the volume of this cylinder.

Substituting in equation (5) values of M determined from equation (6), we obtain

$$\bar{p} = \frac{(C_2 - C_1) V}{(\tau_2 - \tau_1) S}. \qquad (7)$$

It is found by computation that the mean rate of diffusion is equal to 5.7×10^{-10} g/cm^2 sec. Diffusion rates close to this value were obtained in work on armco-iron [8].

To determine the concentration gradient of hydrogen in the specimens, we differentiate equations (3) and (4) and obtain

$$\left(\frac{dc}{dx}\right)_{\tau=1} = 1{,}46X, \qquad (8)$$

$$\left(\frac{dc}{dx}\right)_{\tau=2} = 0{,}96X. \qquad (9)$$

Hence the mean value of the hydrogen concentration gradient will be

$$\left(\overline{\frac{dc}{dx}}\right) = 1{,}21X. \qquad (10)$$

If $X = 3$, the mean concentration gradient will amount to 3.63 ml. H/100 g x mm or 2.5×10^{-4} g/cm^4.

Substituting in the general diffusion equation

$$p = -D\frac{dc}{dx} \qquad (11)$$

the values of p and $\frac{dc}{dx}$ found by experiment and solving this equation with respect to D, it is found that the diffusion coefficient is equal to 2.3×10^{-6} cm^2/sec.

We now determine the minimum width h of a crack which, for a deformation time of 60 sec, can be filled with hydrogen up to a pressure of 2500 atm by way of diffusion from solid solution grains adjoining the crack.

To do this, we assume that the width of the crack is substantially less than its other two dimensions and that its walls are parallel to each other (Fig. 4). We single out on the surface of the crack an arbitrary surface element of area

VOL. 8 1959

ΔS. Bearing in mind that the filling of the crack with hydrogen takes place on both sides, it is found that the rate of diffusion inside a volume element of the crack bounded by

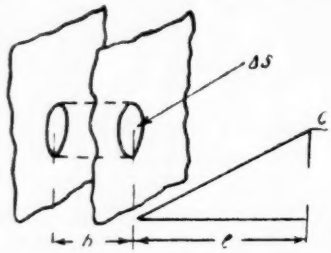

Fig. 4. Diagram illustrating the filling of a crack.

areas ΔS and equal to ΔSh will be equal to

$$\Delta \bar{p} = 2D\left(\frac{\overline{dc}}{dx}\right)\Delta S. \qquad (12)$$

For a deformation time t there will diffuse into a volume element of the crack a quantity of hydrogen

$$m = 2D\left(\frac{\overline{dc}}{dx}\right)\Delta S t. \qquad (13)$$

We shall assume that for time t at the surface of the crack the hydrogen content in the solid solution is reduced to zero. Neglecting the non-linearity of the hydrogen distribution over the specimen cross-section, we assume that on the small length the hydrogen content in the metal increases rectilinearly with the distance from the crack and attains its mean value for a given specimen at distance l from the crack. Then the quantity of hydrogen transferred during time t from the solid solution into the volume element of the crack is determined by equation equation

$$m = cl\Delta S. \qquad (14)$$

The mean value of the concentration gradient for hydrogen during time t will be

$$\left(\frac{\overline{dc}}{dx}\right) = \frac{c}{\frac{l}{2}}. \qquad (15)$$

Substituting this value of the gradient in equation (13), we obtain

$$m = 4D\frac{c}{l}\Delta S t. \qquad (16)$$

Eliminating l from equations (14) and (16), we determine the quantity of hydrogen transferred into the volume element of the crack during time t

$$m = 2c\Delta S\sqrt{Dt}. \qquad (17)$$

To enable pressure P to arise in the incipient crack as a result of diffusion, the volume element of the crack bounded by areas ΔS on its surface should be equal to

$$\Delta V = \frac{m}{\mu}\frac{RT}{P}, \qquad (18)$$

where μ is the molecular weight of the gas, R the gas constant, and T the absolute temperature.

Hence the width of the crack will be

$$h = \frac{mRT}{\mu P \Delta S}. \qquad (19)$$

Substituting in equation (19) the values m from equation (17), we obtain

$$h = \frac{2cRT}{\mu P}\sqrt{Dt}. \qquad (20)$$

On the basis of a deformation time of 60 sec and substituting this value of t in equation (20) together with the values of c, D and P obtained by experiment, it is found that the width of the crack is equal to 0.6×10^{-5} cm.

It is calculated in [9] that the width of incipient cracks in the metal is of the order of 1×10^{-4} cm. Probably this width is less by 1-2 orders of magnitude. It is therefore reasonable to think that for a time of static deformation of the order of one minute a pressure of 2000-3000 atm can arise in incipient cracks.

Taking into account that the rate of diffusion is higher in deformed than in undeformed metal [10] and that the time of deformation often exceeds 60 sec, it can be assumed that in incipient cracks at the very beginning of their propagation the pressure reaches values which are significantly higher than that calculated by us for a well-developed crack.

The estimate calculation shows that directional diffusion of hydrogen to microdefects in the structure during the time of plastic

deformation can be one of the causes of hydrogen embrittlement in steel.

Translated by H. Nowottny

REFERENCES

1. F. de Kazinezi, *J. Iron and Steel Inst.*, 177, 85 (1954).
2. P. Bastien and P. Asou, *Rev. Met.*, 49, 837 (1952).
3. Ya.M. Potak, *Khrupkie razrusheniya stali i stal'nykh detalei (Fractures due to embrittlement in steel and steel components)*, Oborongiz (1955).
4. L.M. Pevzner, V.E. Sadovskaya, T.K. Zilova, S.S. Volkova and Ya.M. Potak, *Metalloved i obrabotka metal*, No.3, 5 (1956).
5. P. Bastien and P. Asou, *Compt. Rend.*, 229, 549 (1949).
6. V.F. Loshkarev, *Stal'*, 16, No.8, 734 (1956).
7. N.M. Belyaev, *Soprotivlenie materialov (Strength of materials)*, Gostekhteoretizdat (1950).
8. N.I. Tugov, *Diffuziya elektroliticheskogo vodoroda cherez zheleznye plastinki v shchelochnykh rastvorakh (The diffusion of electrolytic hydrogen through iron plates in alkaline solutions)*. Author's summary of dissertation, published by Academy of Sciences, Usbek.S.S.R., Tashkent (1954).
9. Ya.I. Frenkel', *Vvedenie v teoriyu metallov (Introduction to the theory of metals)*, Goslekhleoretizdat (1950).
10. H. Schumann, *Metallurgie und Giessereitechn.*, 3, No.10, 420 (1953).

VOL. 8 1959

ON THE KINETICS OF REACTION DIFFUSION IN SYSTEMS WITH SOME INTERMEDIATE PHASES 1. MACROSCOPIC CALCULATION FOR A BINARY SYSTEM*

V.I. ARKHAROV

Institute of Physics of Metals of the Academy of Sciences, U.S.S.R.

(Received 27 April 1959)

The kinetics of reaction diffusion is considered in the steady state for a binary system with some intermediate phases when, on the boundaries between layers of reaction products, chemical reactions are completed by phase transformation and the growth of one of the contact layers takes place not only on account of the quantity of components retained on a given boundary by opposed diffusion currents but also partly on account of the other layer.

EXPOSITION

The kinetics of reaction diffusion in a binary system containing one chemical compound was considered by Tammann and Rocha [1], and also (in greater detail) by Frenkel' and Sergeev [2]. In these papers the problem was simplified by assumptions which are admissible only for a narrow range of special cases. The problem demands, therefore, to be considered for more complex conditions. If a binary system made up from different substances contains several chemical compounds (intermediate phases), then the zone, formed in such systems, of chemical reaction products ("scale") through which diffusion takes place is found to be many-layered.

Each layer consists of one phase and is characterized by particular values, which differ for the various layers, of partial diffusion coefficients of the components.

The kinetics of the process of reaction diffusion in such a system is completely determined by the kinetics of the component processes, and in particular of the diffusion of each component across each layer and of the growth of each layer by means of chemical reactions on the boundaries of this layer.

On which side a layer grows and whether on one side only or on both, at what rate and how these rates of growth differ in the various layers – the solution to these problems depends on the relation between the partial rates of diffusion in the two components of a layer and on the relation between the partial rates of diffusion in the various layers.

The calculation of the kinetics of reaction diffusion is further complicated by the following fact. In the general case, in a chemical reaction at any intermediate boundary between the layers the quantity of components retained at this point by opposed diffusion currents may not correspond to the stoichiometric composition of the phases in both contact layers. Therefore, a certain quantity of the substance of one of the contact layers is involved in the chemical reaction; accumulation of the other layer will take place at this point not only on account of quantity of the components, which is supplied by diffusion, but *partially on account of the neighbouring layer.*

GENERAL PICTURE OF REACTION DIFFUSION IN A BINARY SYSTEM WITH SOME INTERMEDIATE PHASES

We shall consider the reaction diffusion in a binary system made up of Me and O components which may form (at the diffusion temperature)

* *Fiz. metal. metallov.* 8, No.2, 193-204, 1959.

VOL 8 195

a series of solid chemical compounds:

$$Me_{m_1}O_{n_1},\ Me_{m_2}O_{n_2},\ \dots\ Me_{m_i}O_{n_i},\ \dots\ Me_{m_s}O_{n_s}.$$

We shall assume that (1) each of these compounds can show a small deviation from stoichiometric composition which allows diffusion of Me and O through a layer of any such phase, and (2) the solubility of O in Me and of Me in O is small and can be neglected in the calculations (this approximates our calculation to the case of reaction diffusion which is much more interesting in practice, when one of the components (Me) is a solid metal and the other (O) a chemically active gas; processes of gas corrosion and of chemico-thermal treatment of metals belong to this case). The component O will be called oxygen.

We shall consider the process of reaction diffusion at the stage when scale has formed on the metal; the scale is made up of an accumulation of layers each consisting of one phase (with a concentration gradient for Me and O which is the maximum allowed by the limits of the deviation of the phase from stoichiometrical composition) and the order of phase distribution over the layers corresponds to the systematic change in the contents of components of the phase composition.

We shall suppose that

$$\frac{m_1}{n_1} > \frac{m_2}{n_2} > \dots > \frac{m_h}{n_h} > \frac{m_i}{n_i} > \frac{m_j}{n_j} > \dots > \frac{m_s}{n_s}. \tag{1}$$

In this way an order is established for numbering the layers of the scale, beginning with the layer next to the metal and ending with the external layer which is open to the action of the gas component.

Thus we obviously have for the first component (Me)

$$m_0 = 1,\ n_0 = 0, \tag{1'}$$

and for the second

$$m_{s+1} = 0,\ n_{s+1} = 1. \tag{1''}$$

Considering the transit of the diffusion components across the boundary between the layers, we shall indicate these boundaries by a double index consisting of the number of layers which join at this boundary in the sequence which corresponds to the direction of the diffusion of the component considered.

We introduce the following symbols of quantities considered for the time interval dt and for the unit area of surfaces of separation of the layers:

dQ^{Me}–Quantity of metal crossing the boundary 01 between metal and scale;

dQ^{O}–quantity of oxygen crossing the boundary $s+1$, s between the gas component and the scale (entering from the gas component into the adsorption layer at the outer scale surface);

dQ_i^{Me}–quantity of metal transferred across boundary hi and diffusing through the ith layer to its opposite boundary ij;

dQ_i^{O}–quantity of oxygen transferred across boundary ji and diffusing through the ith layer to its opposite boundary ih;

dq_{ij}^{Me}–quantity of metal retained by chemical reaction at boundary ij during transit across this boundary;

dq_{ji}^{O}–quantity of oxygen retained by chemical reaction at boundary ji during transit across this boundary.

According to these definitions one may write

$$dQ_s^{Me} = dq_{s,s+1}^{Me};\quad dQ_1^{O} = dq_{10}^{O}. \tag{2}$$

This indicates absence of volatilization of metal from the scale into the gas component and of dissolution of hydrogen in the metal.

Further, according to the meaning of the notation introduced

$$dQ^{Me} = \sum_{i=0,\ j=1}^{i=s,\ j=s+1} dq_{ij}^{Me};\quad dQ^{O} = \sum_{j=s+1,\ i=s}^{j=1,\ i=0} dq_{ji}^{O}, \tag{3}$$

$$dQ_j^{Me} = dQ_i^{Me} - dq_{ij}^{Me};\quad dQ_i^{O} = dQ_j^{O} - dq_{ji}^{O}. \tag{4}$$

For convenience of notation we shall assume from now on that the ratio between the atomic weight of Me and O is introduced by a factor in values of m_k entering into all calculated formulae (apart from chemical symbols of phases $Me_{m_k}O_{n_k}$).

DETAILS OF INITIAL CONDITIONS FOR CALCULATING THE RATE OF GROWTH OF SCALE LAYERS AT THEIR BOUNDARIES

The quantities of Me and O retained at the

boundary between the ith and jth layers by chemical reaction form new accumulations of some of these layers, depending on the extent to which the ratio between the quantities of components retained at this point approximates to the stoichiometric composition of the ith or jth layer. The following five different cases are then possible.

I. If

$$\frac{dq_{ij}^{Me}}{dq_{ji}^{O}} = \frac{m_i}{n_i}, \qquad (5a)$$

then the quantities of components retained at the given boundary form compound $Me_{m_i}O_{n_i}$, i.e. accumulation of the ith layer occurs.

II. If

$$\frac{dq_{ij}^{Me}}{dq_{ji}^{O}} = \frac{m_j}{n_j}, \qquad (5b)$$

then compound $Me_{m_j}O_{n_j}$ is formed, i.e. accumulation of the ith layer occurs.

If neither (5a) nor (5b) is satisfied, then one of two processes will occur: (1) either the retained quantities of Me and O will grow until stoichiometric composition of one of the two layers in contact at this point is reached by some portion of the substance of the second layer combining with these quantities, i.e. the first of the two given layers will grow not only on account of the quantities of Me and O retained at the boundary but partially also on account of the other layer, (2) or the retained quantities of Me and O will be so distributed as to form partly $Me_{m_i}O_{n_i}$ and partly $Me_{m_j}O_{n_j}$, i.e. both layers will grow. Thus the following three cases are possible.

III. If

$$\frac{dq_{ij}^{Me}}{dq_{ji}^{O}} > \frac{m_i}{n_i}, \qquad (5c)$$

then accumulation of the (deeper) ith layer will occur partly on account of the jth layer (which is closer to the external surface).

IV. If

$$\frac{dq_{ij}^{Me}}{dq_{ji}^{O}} < \frac{m_j}{n_j}, \qquad (5d)$$

then accumulation of the jth layer will occur partly on account of the ith layer.

V. If

$$\frac{m_i}{n_i} > \frac{dq_{ij}^{Me}}{dq_{ji}^{O}} > \frac{m_j}{n_j}, \qquad (5e)$$

then accumulation of both layers will occur. In this case the distribution of Me and O retained from the diffusion flow between both layers is described by relations

$$\frac{v\,dq_{ij}^{Me}}{v'\,dq_{ji}^{O}} = \frac{m_j}{n_j} = a; \quad \frac{w\,dq_{ij}^{Me}}{w'\,dq_{ji}^{O}} = \frac{m_i}{n_i} = b,$$

where v, v', w, w' are regular fractions, and $v+w = 1$; $v' + w' = 1$.

Introducing the notation $\frac{dq_{ij}^{Me}}{dq_{ji}^{O}} = \chi$, we can write $\frac{v}{v'} = \frac{a}{\chi}$; $\frac{w}{w'} = \frac{b}{\chi}$.

Hence we obtain

$$v = \frac{a}{\chi}\,\frac{\chi - b}{a - b}; \quad w = \frac{b}{\chi}\cdot\frac{a-\chi}{a-b};$$

$$v' = \frac{\chi - b}{a - b}; \quad w' = \frac{a-\chi}{a-b}.$$

If χ is close to a, then v and v' are close to unity and w and w' close to zero, i.e. the jth layer accumulates principally, and the ith layer, if χ is close to b. In case III diffusion of the metal from the interior towards the external surface of the scale predominates over diffusion of hydrogen from the outside into the scale interior, towards its boundary with the metal; in case IV the reverse occurs, diffusion of the hydrogen predominates over diffusion of the metal.

We now set down the basic relations for the calculations of rates of growth of the layers in each of the five cases indicated.

In case I the growth of the ith layer at the boundary ij is expressed by equation

$$dq_{ij}^{Me} + dq_{ji}^{O} = \rho_i\,dx_i, \qquad (6a)$$

where ρ_i is the density of the substance of the ith layer ($Me_{m_i}O_{n_i}$), and dx_i is the increase in thickness of the ith layer. On the other boundary of the ith layer (hi) there will be neither an increase nor a decrease of the ith layer. In this way the ith layer will grow only on one side, at its

"external" boundary. In case I we have

$$dQ_1^O = dq_{10}^O = 0;\ dQ^{Me} = dQ_1^{Me}.$$

In case II one-sided growth of the ith layer will occur, analogously, on its "internal" boundary hi expressed by

$$dq_{hi}^{Me} + dq_{ih}^O = \rho_i dx_i. \qquad (6b)$$

For this case we have

$$dQ^O = dQ_s^O;\ dQ_s^{Me} = dq_{s,gaz}^{Me} = 0.$$

In case III it is necessary for the formation of the new accumulation of the ith layer at its boundary with the jth layer to add a certain quantity of the substance of the jth layer to the quantities of components which are retained at this point from the opposed diffusion flow; this addition contains a quantity of metal $d\varepsilon_j^{Me}$ and a quantity of hydrogen $d\varepsilon_j^O$. In this way, the accumulation of the ith layer at the boundary ij contains

$$dq_{ij}^{Me} + dq_{ji}^O + d\varepsilon_j^{Me} + d\varepsilon_j^O = \rho_i dx_i'', \qquad (6c)$$

where dx_i'' is the increase in thickness of the ith layer at the boundary ij.

At the boundary between the ith layer and the (deeper) hth layers a decrease in the thickness of the ith layer (dx_i') will occur which is due to the addition of a portion of the substance of the ith layer to the new accumulation of the hth layer formed at the boundary hi. This decrease is expressed by relation

$$d\varepsilon_i^{Me} + d\varepsilon_i^O = \rho_i dx_i'. \qquad (7)$$

The total change in the thickness of the ith layer is

$$dx_i = -dx_i' + dx_i''. \qquad (8)$$

Thus the following relations will apply to the case considered

$$\frac{dq_{ij}^{Me} + d\varepsilon_j^{Me}}{dq_{ji}^O + d\varepsilon_j^O} = \frac{m_i}{n_i};\quad \frac{dq_{hi}^{Me} + d\varepsilon_i^{Me}}{dq_{ih}^O + d\varepsilon_i^O} = \frac{m_h}{n_h}; \qquad (9)$$

$$\frac{d\varepsilon_j^{Me}}{d\varepsilon_j^O} = \frac{m_j}{n_j};\quad \frac{d\varepsilon_i^{Me}}{d\varepsilon_i^O} = \frac{m_i}{n_i}; \qquad (10)$$

$$d\varepsilon_j^{Me} + d\varepsilon_j^O = \rho_j dx_j', \qquad (7')$$

where ρ_j is the density of the substance of the jth layer and dx_j' the decrease in the thickness of this layer at the boundary ij.

We observe that in the case considered, $dQ_1^O \neq 0$) the first, i.e. the internal, layer of scale will grow on both of its boundaries; for its internal side, instead of a relation of type (7) the change occurring will be

$$dq_{01}^{Me} + dq_{10}^O = dq_{01}^{Me} + dQ_1^O = \rho_1 dx_1', \qquad (11)$$

and

$$\frac{dq_{01}^{Me}}{dQ_1^O} = \frac{m_1}{n_1} \qquad (12)$$

and therefore

$$dx_1' = \frac{1}{\rho_1}\,\frac{m_1 + n_1}{n_1}\,dQ_1^O. \qquad (13)$$

The magnitude of dx_1'' is found from general formulae of type (6c), (9), (10). In contrast with the general expression (8), the general increase in the thickness of the first layer will be

$$dx_1 = dx_1' + dx_1''. \qquad (14)$$

For the change in thickness of the external (sth) layer of scale we obtain the relations

$$dq_{s,s+1}^{Me} + dq_{s+1,s}^O = dQ_s^{Me} + dq_{s+1,s}^O = \rho_s dx_s'', \qquad (15)$$

and

$$\frac{dQ_s^{Me}}{dq_{s+1,s}^O} = \frac{m_s}{n_s} \qquad (16)$$

and hence, from (15) and (16)

$$dx_s'' = \frac{1}{\rho_s}\cdot\frac{m_s + n_s}{m_s}\,dQ_s^{Me}. \qquad (17)$$

The magnitude of dx_z' is found from general formulae of type (6c), (7), (9), (10), and of dx_s from (8).

In case IV for the change in thickness of the ith layer relations will apply which are similar to those obtained for case III, with this difference that growth occurs at the boundary hi and decrease, in favour of the next (jth) layer, at the boundary ij; the parts played by Me and O in this process are the reverse of those in case III. The first layer in case IV grows only on its internal

VOL. 8 1959

side (on the boundary with the metal), while the internal (sth) layer increases on both sides. The relationships between changes in thickness and quantities of components participating in the reactions are established by analogy with formulae (11)-(17).

In case V we have a combination of the relations of type (6a) and (6b), with consideration of the details given by way of explanation of the description of case V, that is the growth of the ith layer at the boundaries ij and hi is expressed, respectively, by equations

$$\left.\begin{aligned} w_{ij}\,dq_{ij}^{\mathrm{Me}} + w'_{ji}\,dq_{ji}^{\mathrm{O}} &= \rho_i\,dx_i'' \\ v_{hi}\,dq_{hi}^{\mathrm{Me}} + v'_{ih}\,dq_{ih}^{\mathrm{O}} &= \rho_i\,dx_i' \end{aligned}\right\} \qquad (6d)$$

Here the indices to coefficients v, v', w, w' indicate the boundaries to which they relate. The general increase in thickness will be

$$dx_i = dx_i' + dx_i''. \qquad (8')$$

CALCULATION OF THE RATE OF GROWTH OF SCALE LAYERS FOR THE CASE THAT DIFFUSION OF THE METAL PREDOMINATES OVER DIFFUSION OF THE GAS COMPONENT

It is proposed to carry out the calculation of the kinetics of reaction diffusion for case III; the calculation for case IV can be made completely analogously by reversing the parts played by Me and O; calculations for cases I and II offer no difficulty in view of the simplicity of the basic relation; for case V the calculation is similar to case III with this difference that relation (8) applies instead of (8).

We observe that case III comprises gas corrosion of a number of metals (in particular high-temperature oxidation of iron and many ferrous alloys) which are not resistant at high temperatures; consideration of case III will therefore have practical interest for the study of methods of combating corrosion.

From equations (7), (9) and (10) it follows that

$$\rho_i\,dx_i' = \frac{m_i + n_i}{m_h n_i - m_i n_h}\cdot(n_h\,dq_{hi}^{\mathrm{Me}} - m_h\,dq_{ih}^{\mathrm{O}}). \qquad (18)$$

We introduce

$$\alpha_i = \frac{1}{\rho_i}\cdot\frac{m_i + n_i}{m_h n_i - m_i n_h}. \qquad (19)$$

when

$$dx_i' = \alpha_i(n_h\,dq_{hi}^{\mathrm{Me}} - m_h\,dq_{ih}^{\mathrm{O}}). \qquad (20)$$

From equations (6c), (9) and (10) it follows that

$$\rho_i\,dx_i'' = \frac{m_i + n_i}{m_i n_j - m_j n_i}(n_j\,dq_{ij}^{\mathrm{Me}} - m_j dq_{ji}^{\mathrm{O}}) \qquad (21)$$

We introduce notation

$$\beta_i = \frac{1}{\rho_i}\cdot\frac{m_i + n_i}{m_i n_j - m_j n_i}. \qquad (22)$$

then

$$dx_i'' = \beta_i(n_j\,dq_{ij}^{\mathrm{Me}} - m_j\,dq_{ji}^{\mathrm{O}}). \qquad (23)$$

Indicating the diffusion coefficients of Me and O through the substance of the kth layer by D_k^{Me} and D_k^{O} respectively, the thickness of the kth layer by x_k, and the drop in concentration at this thickness by Δc_k, we can write

$$dQ_k^{\mathrm{Me}} = D_k^{\mathrm{Me}}\frac{\Delta c_k}{x_k}\,dt;\quad dQ_k^{\mathrm{O}} = D_k^{\mathrm{O}}\frac{\Delta c_k}{x_k}\,dt. \qquad (24)$$

We introduce the notations

$$H_k = (n_R D_k^{\mathrm{Me}} + m_k D_k^{\mathrm{O}})\,\Delta c_k, \qquad (25)$$

$$\gamma_i = \alpha_i\frac{m_h n_j - m_j n_h}{m_i n_j - m_j n_i}. \qquad (26)$$

Then from (8), (20), (23) and substituting (4) in (24), we obtain

$$\frac{dx_i}{dt} = -\frac{\alpha_i H_h}{x_h} + \frac{\gamma_i H_i}{x_i} - \frac{\beta_i H_j}{x_j}. \qquad (27)$$

Taking into account (1′) and (1˜), and also the equalities $\Delta c_0 = 0$ and $\Delta c_{s+1} = 0$, we can see that at $i = 1$ the first term on the right-hand side of (27) becomes zero; at $i = s$ the third term becomes zero.

The solution to the problem of finding the time-dependence of the thickness of each layer presents, in a general form, great mathematical difficulties. Only for the simplest case of single-layer scale is the problem solved easily and we have

$$\frac{dx_1}{dt} = \frac{\gamma_1 H_1}{x_1} = \frac{1}{\rho_1}\,\frac{m_1 + n_1}{m_1 n_1}\,(n_1 D_1^{Me} + m_1 D_1^{O})\,\frac{\Delta c_1}{x_1}\,. \tag{28}$$

Hence

$$a_1 = \sqrt{2\gamma_1 H_1} = \left.\begin{aligned} x_1 &= a_1\sqrt{t} \\ &\sqrt{\frac{2(m_1+n_1)\left(n_1 D_1^{Me} + m_1 D_1^{O}\right)\Delta c_1}{\rho_1 m_1 n_1}} \end{aligned}\right\} \tag{29}$$

In other words, the well known parabolic law of growth is obtained.

For double-layer scale the system of (27) is is represented in the form

$$\left.\begin{aligned} \frac{dx_1}{dt} &= \frac{\gamma_1 H_1}{x_1} - \frac{\beta_1 H_2}{x_2} \\ \frac{dx_2}{dt} &= -\frac{\alpha_2 H_1}{x_1} + \frac{\gamma_2 H_2}{x_2}\,. \end{aligned}\right\} \tag{30}$$

Hence, introducing the notation

$$\frac{dx_k}{dt} = \varphi_k \tag{31}$$

and

$$\gamma_1\gamma_2 - \alpha_2\beta_1 = P_{II}, \tag{32}$$

we obtain

$$x_1 = \frac{P_{II} H_1}{\gamma_2\varphi_1 + \beta_2\varphi_2}\,; \quad x_2 = \frac{P_{II} H_2}{\alpha_2\varphi_1 + \gamma_1\varphi_2} \tag{33}$$

or

$$\left.\begin{aligned} x_1\frac{dx_1}{dt} &= \frac{P_{II} H_1}{\gamma_2 + \beta_2\dfrac{\varphi_2}{\varphi_1}}\,; \\ x_2\frac{dx_2}{dt} &= \frac{P_{II} H_2}{\alpha_2\dfrac{\varphi_1}{\varphi_2} + \gamma_1}\,. \end{aligned}\right\} \tag{34}$$

If during the thickening of the layers the ratio between the rates of growth is kept constant for both layers

$$\frac{\varphi_2}{\varphi_1} = \omega = \text{const}, \tag{35}$$

then the growth of each layer follows a parabolic law

$$x_1 = a_1\sqrt{t};\quad x_2 = a_2\sqrt{t};$$

$$a_1 = \sqrt{\frac{2P_{II} H_1}{\gamma_2 + \beta_1\omega}}\,; \quad a_2 = \sqrt{\frac{2P_{II} H_2}{\alpha_2\dfrac{1}{\omega} + \gamma_1}}\,. \tag{36}$$

and

$$\frac{x_2}{x_1} = \frac{a_2}{a_1} = \omega. \tag{37}$$

For a three-layer scale, writing out analogously the system of equations (27) and introducing the notation

$$\gamma_1\gamma_2\gamma_3 - \beta_1\alpha_2\gamma_3 - \gamma_1\beta_2\alpha_3 = P_{III}, \tag{32'}$$

we obtain

$$\left.\begin{aligned} x_1 &= \frac{P_{III} H_1}{(\gamma_2\gamma_3 - \beta_2\alpha_3)\varphi_1 + \beta_1\gamma_3\varphi_2 + \beta_1\beta_2\varphi_3} \\ x_2 &= \frac{P_{III} H_2}{\alpha_2\gamma_3\varphi_1 + \gamma_1\gamma_3\varphi_2 + \gamma_1\beta_2\varphi_3} \\ x_3 &= \frac{P_{III} H_3}{\alpha_2\alpha_3\varphi_1 + \gamma_1\alpha_3\varphi_2 - (\beta_1\alpha_3 - \gamma_1\gamma_2)\varphi_3} \end{aligned}\right\} \tag{33'}$$

or

$$\left.\begin{aligned} x_1\frac{dx_1}{dt} &= \frac{P_{III} H_1}{(\gamma_2\gamma_3 - \beta_2\alpha_3) + \beta_1\gamma_3\omega_{21} + \beta_1\beta_2\omega_{31}} \\ x_2\frac{dx_2}{dt} &= \frac{P_{III} H_2}{\alpha_2\gamma_3\dfrac{1}{\omega_{21}} + \gamma_1\gamma_3 + \gamma_1\beta_2\omega_{32}} \\ x_3\frac{dx_3}{dt} &= \frac{P_{III} H_1}{\alpha_2\alpha_3\dfrac{1}{\omega_{31}} + \gamma_1\alpha_3\dfrac{1}{\omega_{32}} - (\beta_1\alpha_2 - \gamma_1\gamma_2)} \end{aligned}\right\}, \tag{34'}$$

where

$$\omega_{21} = \frac{\varphi_2}{\varphi_1}\,; \quad \omega_{31} = \frac{\varphi_3}{\varphi_1}\,; \quad \omega_{32} = \frac{\varphi_3}{\varphi_2} = \frac{\omega_{31}}{\omega_{21}}\,. \tag{35'}$$

If during the thickening of the layers the ratio between the rates of growth are kept constant for layers ω_{21} and ω_{31} (and consequently also ω_{32}), then the growth of each layer in particular follows a parabolic law

$$x_1 = a_1\sqrt{t};\quad x_2 = a_2\sqrt{t};\quad x_3 = a_3\sqrt{t}$$

$$\left.\begin{aligned} a_1 &= \sqrt{\frac{2P_{III} H_1}{(\gamma_2\gamma_3 - \beta_2\alpha_3) + \beta_1\gamma_3\omega_{21} + \beta_1\beta_2\omega_{31}}} \\ a_2 &= \sqrt{\frac{2P_{III} H_2}{\alpha_2\gamma_3\dfrac{1}{\omega_{21}} + \gamma_1\gamma_3 + \gamma_1\beta_2\omega_{32}}} \\ a_3 &= \sqrt{\frac{2P_{III} H_3}{\alpha_2\alpha_3\dfrac{1}{\omega_{31}} + \gamma_1\alpha_3\dfrac{1}{\omega_{32}} - (\beta_1\alpha_2 - \gamma_1\gamma_2)}} \end{aligned}\right\}. \tag{36'}$$

and

VOL. 8 1959

$$\frac{x_2}{x_1} = \frac{a_2}{a_1} = \omega_{21};\quad \frac{x_3}{x_1} = \frac{a_3}{a_1} = \omega_{31};$$
$$\frac{x_3}{x_2} = \frac{a_3}{a_2} = \omega_{32} = \frac{\omega_{31}}{\omega_{21}}. \qquad (37')$$

The problem for a greater number of scale layers is solved by analogous treatment.

In the more general case, it is in fact not possible to maintain constant ratios for the rate of growth of the layers, i.e. the magnitudes of type ω will depend on time. In this case we shall not find a parabolic, but some other law for the growth of the layers, depending on the form of function $\omega(t)$. For instance, for two-layer scale at $\frac{\varphi_1}{\varphi_2} = \omega = kt$ (k being a constant) we obtain

$$\left.\begin{aligned} x_1^2 &= \frac{2P_{II}H_1}{\beta_1 k}\ln(\gamma_2 + \beta_1 kt) + C_1 \\ x_2^2 &= 2P_{II}H_2\left[\frac{t}{\gamma_1} - \frac{\alpha_2}{\gamma_1^2}\ln(\gamma_1 t + \alpha_2)\right] + C_2. \end{aligned}\right\} \qquad (38)$$

For a three-layer scale, the position may be more complex: the ratios between the rates of growth of layers ω_{21} and ω_{31} may be different functions of time. It is easily seen that, if they show simple proportionality of time, logarithmic laws similar to (38) will apply for the growth of the layer.

For the cases when the growth of the scale layers satisfies a parabolic law the relationship between the kinetic coefficients a_i and the diffusion coefficients is expressed by the following equation.

For a two-layer/scale we obtain from (36) and (37)

$$\left.\begin{aligned} H_2 &= (n_2 D_2^{Me} + m_2 D_2^{O})\Delta c_2 = \\ &= \frac{a_1}{2P_{II}}(a_1\gamma_2 + a_2\beta_1) \\ H_1 &= (n_1 D_1^{Me} + m_1 D_1^{O})\Delta c_1 = \\ &= \frac{a_2}{2P_{II}}(a_2\gamma_1 + a_1\alpha_2). \end{aligned}\right\} \qquad (39)$$

Similarly, for a three-layer scale we obtain from (36′) and (37′)

$$\left.\begin{aligned} H_1 &= (n_1 D_1^{Me} + m_1 D_1^{O})\Delta c_1 = \\ &= \frac{a_1}{2P_{III}}[(\gamma_2\gamma_3 - \beta_2\alpha_3)a_1 + \gamma_3\beta_1 a_2 + \beta_1\beta_2 a_3] \\ H_2 &= (n_2 D_2^{Me} + m_2 D_2^{O})\Delta c_2 = \\ &= \frac{a_2}{2P_{III}}[\gamma_3\alpha_2 a_1 + \gamma_1\gamma_3 a_2 + \gamma_1\beta_2 a_3] \\ H_3 &= (n_3 D_3^{Me} + m_3 D_3^{O})\Delta c_3 = \\ &= \frac{a_3}{2P_{III}}[\alpha_2\alpha_3 a_1 + \gamma_1\alpha_3 a_2 - (\beta_1\alpha_2 - \gamma_1\gamma_2)a_3. \end{aligned}\right\} \qquad (39')$$

The kinetic coefficient a_i can be determined experimentally from observations of the growth of scale layers. Since the expressions in letter notation remaining on the right-hand sides of (39) and (39′) are defined by stoichiometric indices, atomic weights of components and phase density values for the scale (i.e. they can first be calculated), the diffusion characteristics of scale layers H_i in (39) and (39′) can be determined.

SEPARATE DETERMINATION OF PARTIAL DIFFUSION COEFFICIENTS IN LAYERS OF SCALE

More thorough experimental procedure allows separate determination of D_i^{Me} and D_i^{O} from kinetic data. For this purpose the method of inert markers must be used, that is macroscopic particles of a chemically inactive substance (which does not take part in the reaction diffusion) are deposited in some form on the surface of the specimen before reaction diffusion sets in or at some stage during this diffusion.

To start with, it is possible in this way to arrive at a determination of D_l^{O} by studying the growth of the internal sub-layer of the first scale layer, i.e. measuring the magnitude dx'_l/dt.

In many cases when diffusion of the metal predominates over diffusion of the second component (in particular, during high-temperature oxidation of iron, during sulphiding of

copper), the internal sub-layer of the first layer is clearly revealed in the macrosctructure of the scale even without inert markers by the appearance of a specific brittleness which is due to more pronounced diffusion of of the metal outwards.

$$\frac{dx_1'}{dt} = \alpha_1 D_1^{O} \frac{\Delta c_1'}{x_1'}, \qquad (40)$$

where $\Delta c_1'$ is the drop in concentration at the thickness of the internal sub-layer. Here it is assumed that the diffusion coefficient of hydrogen through the phase $Me_{ml}O_{nl}$, which makes up the first layer of the scale, is identical for both of its sub-layers.

From (40) we obtain

$$D_1^{O} = \frac{1}{\alpha_1 \Delta c_1'} \cdot x_1' \frac{dx_1'}{dt}.$$

If $\Delta c_1'$ is constant, then the growth of the internal sub-layer follows a parabolic law

$$x_1' = a_1' \sqrt{t}; \quad a_1' = \sqrt{2\alpha_1 \Delta c_1' D_1^{O}}$$

and

$$D_1^{O} = \frac{(a_1')^2}{2\alpha_1 \Delta c_1'}. \qquad (41)$$

$\Delta c_1'$ is also determined experimentally (for instance, by measuring the lattice constants of the phase $Me_{ml}O_{nl}$ on both sides of the internal sub-layer separated from the scale during its preparation; see [3]).

Substituting (41) in (25) at $k = l$, we find

$$D_1^{Me} = \frac{H_1}{n_1 \Delta c_1} - \frac{m_1}{n_1} \cdot \frac{(a_1')^2}{\alpha_1 \Delta c_1'}.$$

H_l is determined according to the first equation of the set of equations of type (39) or (39′).

By supplying inert markers on the external surface of the scale formed and measuring the rate of their "growth" during the subsequent process of reaction diffusion, i.e. the magnitude dx_s''/dt, it is possible similarly to define D_s^{Me} from formulae (17) and (24) with consideration of (22)

$$\frac{dx_s''}{dt} = \beta_s D_s^{Me} \frac{\Delta c_s'}{x_s''}. \qquad (43)$$

where $\Delta c_s''$ is the drop in concentration on that portion of the thickness of the external layer or scale x_s'' which lies between the inert markers and the external surface. Since, on the internal side of the external layer during the reaction diffusion, the phase composing the external layer is transformed into the phase composing the layer of the lower level, the inert markers appear at a definite instant $t = t_1$ at the boundary $(s, s+1)$; we therefore can put

$$\left(\frac{\Delta c_s''}{x_s''}\right)_{t=t_1} = \frac{\Delta c_s}{x_s}.$$

Then

$$\left(\frac{dx_s''}{dt}\right)_{t=t_1} = \beta_s D_s^{Me} \frac{\Delta c_s}{x_s},$$

$$D_s^{Me} = \frac{1}{\beta_s \Delta c_s} x_s \left(\frac{dx_s''}{dt}\right)_{t=t_1} \qquad (44)$$

If here x_s and x_s'' grow according to a parabolic law

$$x_s = a_s \sqrt{t}; \quad x_s'' = a_s'' \sqrt{t},$$

then

$$D_s^{Me} = \frac{a_s a_s''}{2\beta_s \Delta c_s}. \qquad (41')$$

Δc_s is determined by the width of the zone of homogeneous phase $Me_m O_n$ in the phase diagram of the Me-O system at T of diffusion, a_s and a_2'' are determined experimentally. Substituting (41) in (25) at $k = s$, we find

$$D_s^{O} = \frac{H_s}{m_s \Delta c_s} - \frac{n_s}{m_s} \frac{a_s a_s''}{\beta_s \Delta c_s}. \qquad (42')$$

H_s is expressed with the aid of an equation obtained completely analogously to (39) or (39′). By a completely analogous procedure it is possible to determine D_i^{Me} and D_i^{O} separately for each intermediate layer. For this purpose, inert markers must be supplied to the external surface of the scale formed and the process of reaction diffusion must be continued up to the moment when the markers appear at the level of boundary ji. At this moment it is possible to begin the measurement of dx_i''/dt. Further determination is carried out just as for the sth layer.

"EFFECTIVE" COEFFICIENTS OF REACTION DIFFUSION

The kinetics of reaction diffusion is usually characterized by the overall quantities of "gain" in a specimen (together with the scale) for diffusion time (Q^{O}) and of "loss in weight" in the specimen after the scale is removed from it at the end of the test (Q^{Me}), or by quantities dQ^{Me}/dt and dQ^{O}/dt, where dQ^{Me} and dQ^{O} are determined by equations (3).

If the total drop in concentration over the entire scale thickness x is indicated by Δc, then the "effective" partial coefficients of reaction diffusion $D^{Me}{}_{eff}$ and $D^{O}{}_{eff}$ can be proposed for consideration according to equations

$$\frac{dQ^{Me}}{dt} = D^{Me}_{eff}\,{}_{x} \; ; \quad \frac{dQ^{O}}{dt} = D^{O}_{eff}\frac{\Delta c}{x}. \tag{45}$$

If the entire scale in general and each layer in particular grow according to a parabolic law, then

$$x = a\sqrt{t}; \quad x_i = a_i\sqrt{t};$$
$$Q^{Me} = 2D^{Me}_{eff}\frac{\Delta c}{a}\sqrt{t}; \quad Q^{O} = 2D^{O}_{eff}\frac{\Delta c}{a}\sqrt{t}. \tag{46}$$

Total scale weight amounts to

$$G = \sum_{i=1}^{s} x_i\rho_i = Q^{Me} + Q^{O} = \left[\sum_{i=1}^{s} a_i\rho_i\right]\sqrt{t} = \tag{47}$$
$$= 2\frac{\Delta c}{a}\left(D^{Me}_{eff} + D^{O}_{eff}\right)\sqrt{t}.$$

Substituting here expressions a_i according to (36) or (36′), we obtain a relation between the partial diffusion coefficients of Me and O in the separate scale layers and the effective coefficients of diffusion. In particular, for double-layer scale

$$\rho_1\sqrt{\frac{n_1D_1^{Me} + m_1D_1^{O}}{\gamma_2 + \beta_1\omega}} +$$

$$+ \rho_2\sqrt{\frac{n_2D_2^{Me} + m_2D_2^{O}}{\gamma_1 + \alpha_2\dfrac{1}{\omega}}} =$$

$$= \frac{2\Delta c}{a\sqrt{2}\,P_{II}}\left(D^{Me}_{eff} + D^{O}_{eff}\right).$$

Translated by H. Nowottny

VOL 8 195

REFERENCES

1. G. Tammann, and H.J. Rocha, *Z. Anorg. Chem.*, 199, 289 (1931).
2. Ya.I. Frenkel' and M.I. Sergeev, *Zh. eksp. teor. fiz.* 9, 189 (1939).
3. V.I. Arkharov and K.M. Graevskii, *Zh. teor. fiz.* 14, 132 (1944).

STUDY OF A NICKEL-CHROMIUM-ALUMINIUM-TITANIUM ALLOY DEFORMED IN THE QUENCHED CONDITION*

V.G. CHERNYI

Institute of Metal Physics of the Academy of Sciences, U.S.S.R.

(Received 6 March 1958)

In a previous work [1] the changes have been studied which occur in the fine crystal structure during the decomposition of the super-saturated solid solution of Ni-Cr-Al-Ti (an alloy of type EI437). The present paper gives data on the influence of plastic deformation on the ageing of this alloy.

VOL. 8 1959

TEST MATERIAL AND METHODS USED

An investigation was carried out on specimens of a nickel-chromium-aluminium-titanium alloy of the following composition: 0.035% C, 19.55% Cr, 2.38% Ti, 0.59 Al, remainder Ni. Cylinders, 0.5 mm in dia. and 15 mm high, were cut from rod obtained after melting and forging; the cylinders were then homogenized for 20 hr at a temperature of 1100°C. After homogenization the specimens were heated for the quench treatment up to 1080°C, held at this temperature for half an hour and cooled in water. The as-quenched cylinders were subjected to 80 per cent reduction by uniaxial compression. From the deformed disks thus obtained specimens were prepared for *x*-ray study, electrolytic dissolution and hardness measurements.

To obtain the dimensions required for the tests, the specimens were prepared by etching and polishing after a final heat treatment (heating at temperatures between 500 and 950°C).

The work was concerned with the investigation of:

1. the condition of the intermetallic phase precipitated during the decomposition of the alloy;
2. the fine crystalline structure of the basic solid solution (lattice distortions of the second type and dimensions of zones of coherent scattering of *x*-rays);
3. the change in the lattice constant of the basic solid solution during heating;
4. hardness.

The second phase precipitating in the decomposition of the alloy was studied in powders obtained by electrolytic dissolution [1]. The dimensions of blocks* of intermetallic phase, lattice constants, magnitude of distortions of the second type and dimensions of mosaic blocks of the basic solid solution were determined by *x*-ray study, as described in the previous paper [1]. The *x*-ray patterns were obtained in cameras with 57.2 and 150 mm drum diameters on electron tubes with K_α copper radiation.

Hardness was measured on a diamond-cone Rockwell machine under 60 kg load (scale *A*).

EXPERIMENTAL RESULTS

Analysis of the *x*-ray patterns for powders obtained by anodic dissolution from specimens heated each for 4 hr at temperatures of 550-850°C and for different times at 700°C showed that in all cases the intermetallic phase precipitating in the decomposition of the deformed alloy was face-centred cubic. This intermetallic phase which corresponds to the formula Ni_3 (Al, Ti) is customarily called the α'-phase [2, 3].

* *Fiz. metal. metalloved.* 8, No.2, 205-210, 1959.

* The regions scattering *x*-rays coherently.

The results of the investigation are shown graphically in Figs. 1 and 2.

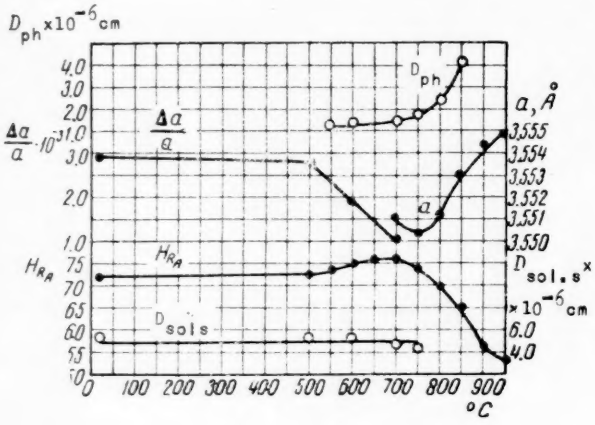

Fig. 1. Hardness H_{R_A}, distortion of second type $\Delta a/a$, dimensions of mosaic blocks $D_{sol.s.}$, lattice constant a' of the solid solution, and dimension of regions of coherent scatter of α' phase D_{ph} plotted against heating temperature, for the alloy deformed in the quenched condition.

The curves in Fig. 1 show the changes, which occur when the deformed alloy is heated, in lattice distortions of the second type, dimensions of the zones of coherent scattering, lattice constant, hardness and dimensions of intermetallic phase. The changes in the dimensions of blocks of the precipitated phase and in hardness as a function of heating time at 700°C are shown in Fig. 2.

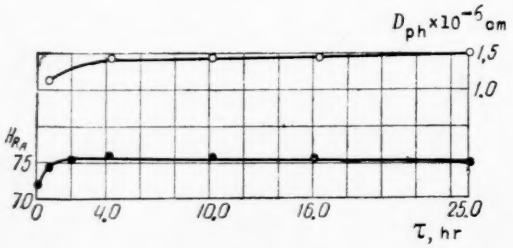

Fig. 2. Dimensions of regions of coherent scatter α' phase D_{ph} and hardness H_{R_A} plotted against holding time at 700°C, for the alloy deformed in the quenched condition.

EVALUATION OF RESULTS

Fig. 3 gives the curves for the change in

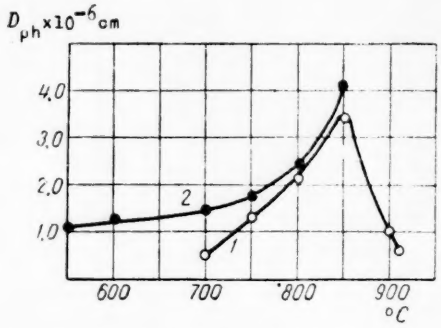

Fig. 3. Change in the dimensions of regions of coherent scatter of the α'-phase during heating for the as-quenched alloy and the alloy deformed after quenching.
1. As-quenched alloy, 2. Deformed alloy.

the size of α'-phase blocks as a function of heating temperature in the deformed and in the as-quenched alloys [1]. In the deformed alloy the second phase appears after heating at lower temperatures compared with the as-quenched alloy. Thus, in the alloy which was deformed after quenching the α'-phase was observed at 550°C, and the size of its blocks was in this case higher than in the as-quenched alloy after heating at 700°C (for the alloy deformed at 550°C $D = 1.1 \times 10^{-6}$ cm and for the alloy quenched from 700°C $D = 0.53 \times 10^{-6}$ cm).

A difference is observed in the character of the change with increasing temperature for blocks of the $N_3(Al,Ti)$ phase. In the as-quenched alloy the blocks increase in size constantly as the temperature rises from 700 to 850°C. In the deformed alloy they remain practically unchanged at first at temperatures of 550-700°C, whereas they show the same intensive growth as in the as-quenched alloy in the same temperature range (750-(750-850°C).

The lattice constant of the intermetallic phase precipitated from the deformed alloy is the same as in the as-quenched alloy, that is, it is equal to 3.584 Å.

Considering the character of the change in the magnitude of the α'-phase blocks after the specimens were heated in the range of 550-750°C, we can imagine that the alloy experienced decomposition resulting in the separation of an intermetallic phase apparently even during the deformation. The fact that the α'-phase was not observed after

the deformation of the alloy can hardly serve as a proof of its absence; it is more likely that it points to a shortcoming of the method of anodic dissolution. The results of the work of Zakharova [4] are in favour of the idea that the alloy is decomposed under the action of deformation.

It was shown in this work [4] that the lattice constant in the quenched Al-Si solid solution was changed substantially after deformation (decomposition took place) and that it remained constant subsequently during heating up to a definite temperature. Another change in the lattice constant was observed after heating at those temperatures at which the lattice constant of the as-quenched alloy was changed likewise. The α'-phase blocks of the Ni-Cr-Al-Ti alloy deformed after quenching change in a similar manner.

As the dimensions of the α'-phase blocks are greater in the alloy deformed after quenching than in the as-quenched alloy at identical temperatures, and as the presence of the second phase is observed in the deformed alloy at lower temperatures, a conclusion may be drawn as to the accelerating effect of deformation on decomposition. More intensive decomposition of the deformed alloy is also indicated by the change in its lattice constant during heating (Fig. 4): during the ageing of the alloy deformed after quenching the change in the lattice constant of the solid solution is substantially more pronounced than during the ageing of the as-quenched alloy.

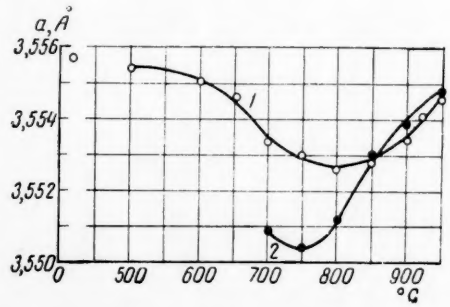

Fig. 4. Change of lattice constant as a function of heating temperature for an as-quenched alloy and an alloy deformed in the quenched condition. 1. As-quenched alloy; 2. Deformed alloy.

When the alloy deformed after quenching was heated at 700°C, the α'-phase was observed after shorter holding times compared with the as-quenched alloy (Fig. 5). Thus, in the deformed alloy the presence of the α'-phase was observed after a holding time of 20 min (compared with 4 hr for the as-quenched alloy) and the size of the particles of the α'-phase changed appreciably less with longer heating times. Whereas in the as-quenched alloy, when the holding time is increased, the second-phase blocks more than double in size, their growth is insignificant in the deformed alloy – from 1.1×10^{-6} cm after 25 min of heating to 1.5×10^{-6} cm after heating for 25 hr. It is characteristic that, for identical holding times at 700°C, the size of the blocks of intermetallic phase is greater in the deformed than in the as-quenched alloy (see Fig. 5).

Comparison of the data on the change in the size of the α'-phase blocks at 700°C for the as-quenched and for the deformed alloy, and also comparison of the temperature dependence of the growth of the blocks show clearly that decomposition is considerably more intense in the deformed alloy.

The results presented in Figs. 1 and 2 indicate the consequences of plastic deformation of the quenched alloy and the manner in which some of its properties change during heating.

As a result of deformation considerable distortions of the second type $\Delta a/a = 2.9 \times 10^{-3}$ arise in the alloy (in the quenched alloy, distortions are practically absent) and its blocks are changed. It has already been pointed out that in all probability deformations produce decomposition with separation of an intermetallic phase. Also the hardness of the alloy is increased after deformation, $H_{R_A} = 72$ (for the quenched condition the figure is 51.3). As a rule, static distortions in the lattice of a solid solution are increased during deformation [5, 6].

The present investigation as well as the data of other authors on the influence of plastic deformation on properties in materials [5, 6] lead to the conclusion that the increase in strength (hardness) during the deformation of a quenched alloy is due, firstly, to the formation of submicro-inhomogeneities in the structure of the solid solution and, secondly, probably to the separation of the intermetallic phase.

VOL. 8 1959

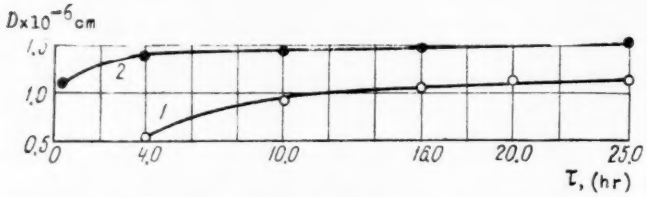

Fig. 5. Change in the dimensions of regions of coherent scatter of the α'-phase as a function of heating times at a temperature of 700°C for an as-quenched alloy and an alloy deformed in the quenched condition.

When the alloy deformed in the quenched condition has been heated at 600-700°C, a further increase in hardness is observed (see Fig. 1). In this temperature range, distortions of the second type are removed rapidly and a large quantity of second phase is separated out. Blocks of the solid solution are not changed in the temperature range of the increase in hardness. Possibly at these temperatures (by analogy with the as-quenched alloy [7]) some increase in dynamical distortions occurs because of the transfer of alloying elements from the basic solid solution to the α'-phase.

At 600-700°C there is hardly any increase in static distortions. This can be explained in the following way. The static distortions in the deformed alloy are large and it is therefore probable that they will be further increased during the precipitation of the second phase. However, if $\sqrt{\overline{u_{cm}^2}}$ will also increase, this occurs only in the initial stages of decomposition [7] which take place in the deformed alloy, in any case below 550°C.

Thus the conclusion may be drawn that the hardness of the deformed alloy after heating at 600-700°C is increased only because of the precipitation of a large quantity of highly dispersed intermetallic phase (at these temperatures considerably more α'-phase is precipitated than after heating at 550-600°C). This conclusion is arrived at from results obtained when the alloy properties were studied after various holding times at 700°C. On x-ray patterns of specimens heated for 10 and more hours at this temperature, the ratio of the width of lines $\frac{\beta_{(331)}}{\beta_{(111)}}$ is less than the ratio of the secants of the reflection angles of these lines; this indicates that distortions of the second type are almost completely absent. The hardness of the alloy is not decreased after a holding time of 25 hr.

The relationship between the increase in hardness and any changes in the structure is discussed in the previous paper [1].

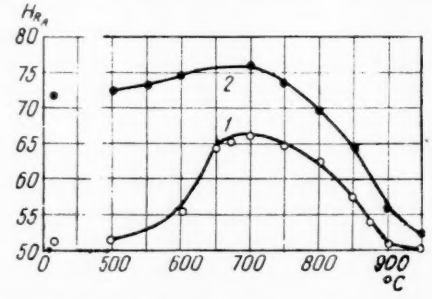

Fig. 6. Change in hardness during heating for an alloy in the as-quenched condition and an alloy deformed after quenching.
1. As-quenched alloy; 2. Deformed alloy.

Comparison of the hardness curves for the as-quenched alloy and for the alloy deformed in the quenched condition (Fig. 6) shows that the hardness of the deformed alloy is in all cases, even at 700-950°C, higher than that of the as-quenched alloy. In [8] it was found that the strength properties of the work-hardened (δ = 10%) alloy E1437A were higher than when this alloy was not work-hardened, even directly at the elevated temperatures.

It would seem that the greater hardness of the deformed alloy compared with the as-quenched alloy after heating at 700-950°C can be explained by the following facts. Firstly, in the deformed alloy the decomposition is more complete and also a larger quantity of intermetallic phase is precipi-

tated (this is indicated by the change in the lattice constant of the solid solution during decomposition (see Fig. 4)). Secondly, the dimensions of the blocks of solid solution are smaller in the deformed than in the as-quenched alloy. Thirdly, the static distortions in the lattice of the deformed alloy must be assumed to be higher even after heating at 700°C and above than the distortions in the as-quenched alloy.

In conclusion, we once again consider the reasons for the increase in hardness during deformation and ageing. Comparison shows that, with different methods of hardening, the mechanical properties of an alloy of type EI437 change under the action of various factors. Thus, if the increase in hardness during plastic deformation is mainly due to the occurrence of considerable distortions of the second type (and apparently also of the third type [5,6]) and to refinement of the mosaic blocks, then the increase in hardness during the ageing of the as-quenched alloy takes place as a result of the precipitation of a large quantity of highly dispersed secondary phase and is not connected with the occurrence of lattice distortions and the change in the dimensions of blocks of basic solid solution. The data obtained in the investigation of the alloy deformed in the quenched condition are even more instructive. Hardness increases during deformation mainly as a result of the occurrence of lattice distortions and of the breaking-down of the solid-solution blocks. The increase in hardening observed after heating at 600-700°C in the deformed alloy is associated only with the precipitation of intermetallic phase. The fact that in both cases a submicro-inhomogeneous structure is formed in the material is common to both types of hardening. This impedes the flow of plastic deformation and naturally leads to improved mechanical properties.

VOL. 8 1959

CONCLUSIONS

1. In the decomposition of a Ni-Cr-Al-Ti alloy deformed in the quenched condition, an intermetallic phase with face-centred cubic lattice is precipitated in the temperature range studied. The lattice constant of the intermetallide is greater than that of the basic solid solution.

2. Plastic deformation accelerates the decomposition of the alloy: the presence of the α-phase in the deformed alloy is observed at a lower temperature than in the as-quenched alloy. The change of its lattice constant also points to a more complete decomposition in the deformed alloy.

3. The increase in hardness during deformation of the as-quenched alloy is due to the formation of a submicro-inhomogeneous structure (occurrence of lattice distortions of the second and third types and breaking-down of the blocks) in the basic solid solution and possibly in the second-phase precipitate.

4. The increase in the hardness of the alloy deformed in the quenched condition after heating in the temperature range of 600-700°C is apparently due to the precipitation of a large quantity of highly dispersed second phase and is not connected with a change in the magnitude of distortions of the second type and in the dimensions of the blocks of basic solid solution.

Translated by H. Nowottny

REFERENCES

1. V.G. Chernyi, *Fiz. metal, metalloved.* 8, No.1 (1958).
2. N.I. Blok, A.I. Glazova, O.A. Dubovikova, S.T. Kishkin and A.S. Lashko, *Zav. lab.* 20, No.8, 903 (1954).
3. R.R. Khimushin, E.F. Trusova and M.I. Gavrilyuk, *Struktura i svoistva splava EI437 (Structure and properties of alloy EI437)* Oborongiz (1955).
4. M.I. Zakharova, *Zh. teor. fiz.* 5, 1158 (1935).
5. G.V. Kurdyumov, R.A. Il'ina, V.K. Kritskaya and L.I. Lysak, *Prob. metalloved i fiz metal,* 4, 339 (1955).
6. V.A. Il'ina and V.K. Kritskaya, *Prob metalloved i fiz. metal.,* 4, 425 (1955).
7. G.V. Kyrdyumov and N.T. Travina, *Prob. metalloved i fiz. metal,* 4, 465 (1955).
8. S.T. Kishkin, A.M. Sulima and V.P. Stroganov, *Issledovanie vliyaniya naklepa na mekhanicheskie svoistva i struktura splava EI437 (Investigation of the influence of work-hardening on the mechanical properties and structure of alloy EI437).* Trud. Ordzhonikidze, MAI, No.7, Oborongiz (1956).

STRUCTURE OF THE ENERGY SPECTRUM OF ELECTRONS IN Fe-Cr- AND Fe-Cr-Ni ALLOYS*

N.D. BORISOV and V.V. NEMOSHKALENKO

Institute of Metal Physics of the Academy of Sciences, U.S.S.R.

(Received 6 March 1958)

The changes are studied which occur in the structure of the energy spectrum of electrons of the "outer" energy bands in an Fe-Cr alloy when the chromium alloy component is partly replaced by nickel.

A good deal of experimental data on the structure of the energy spectrum of electrons in iron-chromium alloys has by now accumulated [1]. However, since alloys with large chromium contents are always brittle and show poor workability, it is of special interest to consider the set of problems dealing with the addition of a third component to iron-chromium alloys, to improve their technological properties without lowering their strength at elevated temperatures.

The present work has been undertaken with a view to determining the typical changes which occur in the structure of the energy spectrum of the electrons, when the chromium component is partly replaced by nickel in an iron-chromium alloy on an iron basis. The materials adopted for the investigation were (electrolytic) chromium, iron and nickel of high purity, and the following alloys were prepared from them: Fe-Cr (55% Fe) and Fe-Cr-Ni (58.4% Fe and 15.4% Ni).

The work was carried out on a high-intensity x-ray spectrograph having a radius of curvature of the quartz crystal (prism face) of 500 mm [2]. The method used is similar to that described in [1].

1. The investigation was directed to the K_{β_5}-lines of chromium, iron and nickel, due to the transfer of electrons from the conductivity band to the K-level, in combination with the short-wave K'_{β}-satellite, and the K_{β_1}-lines of the same elements due to the transfer of electrons from the $3p$-layer to the K-level in combination with the long-wave $K_{\beta'}$-satellite. The above spectrum lines were obtained at 1000°C from pure chromium, iron and nickel and from the Fe-Cr and Fe-Cr-Ni alloys. The lines of the K_{β}-group for iron and nickel were obtained in the fourth, and for chromium in the third order of reflection. Scatter in the specified ranges of the spectrum amounted to 3.88 XE/mm for Cr, 2.44 XE/mm for Fe and 3.03 XE/mm for Ni.

In Table 1 calculated data are listed concerning the wavelengths and energy values in Rydberg of the maxima of lines of the K_{β}-group for chromium, iron and nickel, as determined on the basis of spectrographic measurements.

Figs. 1, 2 and 3 show the microspectrographs of K_{β_5}-lines for chromium, iron and nickel, obtained at a temperature of 1000°C from the pure metals. It is seen in the figures that only in the case of the K_{β_5}-band is the shortwave branch free from superposition of the $K_{\beta'''}$-satellite and can be considered in the pure form. For iron the $K_{\beta'''}$-satellite is clearly super-imposed on the shortwave branch of the K_{β_5}-band. Finally, complete superposition of the two $K_{\beta'''_1}$ and $K_{\beta'''_2}$-satellites on the K_{β_5}-band is observed in nickel.

In the present work, for the determination of the width of the FeK_{β_5}-band the complex contour was decomposed into its component parts by a method described previously [1]. The width of the K_{β_5}-band was determined as the sum of two components $T = T_1 + T_2$, where T_1 is the width of the shortwave branch, measured on the side of maximum intensity, and T_2 calculated from formula

* *Fiz. metal. metallov.* 8, No.2, 211-215, 1959.

$$T = \frac{\gamma_2}{1 - \frac{1}{n^{1/2}}}, \qquad (1)$$

where γ_{2n} is the width of the long-wave branch of the K_{β_5}-band, measured at different sections of its contour, at

$$\frac{I_{max}}{I_n} = \frac{S_{max}}{S_n}.$$

The value obtained for the width of the K_{β_5}-band was corrected for the band-widening due to the final width of the K-level of the chromium and iron atoms (a) and for the angle

TABLE I

Wavelength and energy values of K_β-lines for chromium, iron and nickel

Metal studied	Line symbol	Source of data	Specimen temperature (°C)	λ	
				XE	ν/R
Chromium	$CrK_{\beta'''}$	Tabulated	—	2061.40	442.07
	CrK_{β_5}			2065.53	440.97
	CrK_{β_1}			2080.60	437.98
Iron	$FeK_{\beta'''}$		—	1738.60	524.14
	FeK_{β_5}			1740.54	523.56
	FeK_{β_1}			1752.99	519.84
Nickel	$NiK_{\beta'''}$		—	1484.10	614.03
	NiK_{β_5}			1485.30	613.52
	NiK_{β_1}			1497.08	608.70
Chromium	$CrK_{\beta'''}$	Experimental	700—1000	2060.90	442.15
	CrK_{β_5}			2066.57	440.96
	CrK_{β_1}			2080.52	438.00
Iron	$FeK_{\beta'''}$		300—850	1738.10	524.29
	FeK_{β_5}			1740.48	523.57
	FeK_{β_1}			1752.98	519.84
	$FeK_{\beta'''}$		1000	1738.00	524.33
	FeK_{β_5}			1740.38	523.60
	FeK_{β_1}			1752.98	519.84
Nickel	$NiK_{\beta'''_2}$		1000	1485.50	613.85
	NiK_{β_5}			1485.55	613.42
	NiK_{β_1}			1497.08	608.70
Alloy Fe-Cr	$CrK_{\beta'''}$		1000	2061.10	442.13
	CrK_{β_5}			2066.81	440.91
	CrK_{β_1}			2080.52	438.00

VOL. 8 1959

TABLE I *(contd.)*

Metal studied	Line symbol	Source of data	Specimen temperature (°C)	λ	
				XE	ν/R
Alloy Fe-Cr *cont.*	$FeK_{\beta'''}$			1737.60	524.44
	FeK_{β_5}			1740.47	523.58
	FeK_{β_1}			1752.97	519.85
Alloy Fe-Cr-Ni	$CrK_{\beta'''}$	Experimental	1000	2061.50	442.03
	CrK_{β_5}			2066.95	440.88
	CrK_{β_1}			2080.52	438.00
	$FeK_{\beta'''}$			1737.90	524.34
	FeK_{β_5}			1740.55	523.55
	FeK_{β_1}			1752.98	519.84
	$NiK_{\beta'''}$			—	—
	NiK_{β_5}			1485.52	613.43
	NiK_{β_1}			1497.08	608.70

of incidence of the rays on the photographic film (b). The values of these corrections are shown in Table 2.

The corrected value for the width of the K_{β_5}-band was admitted for $T_{max} = (E_{max} - E_o)$, i.e. the maximum kinetic energy of the electrons in the outer energy band.

Table 3 gives the comparative calculated data for T_1, T_2 and T_{max} of the width of the K_{β_5}-bands for chromium and iron, taken from both the pure metals and the Fe-Cr and Fe-Cr-Ni alloys, and the Fermi and base energies of their 3*d*-bands (in Rydberg). The values of these energies for chromium, iron and nickel in pure metals and in the Fe-Cr and Fe-Cr-Ni alloys were calculated according to the data

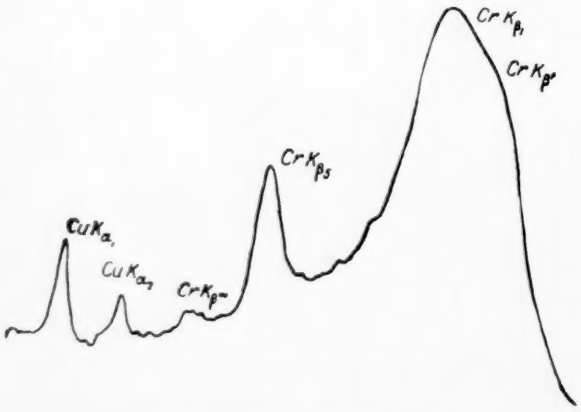

Fig. 1. CrK_{β_5}-band taken from pure chromium at a temperature of 1000°C.

Fig. 2. FeK_{β_5}-band taken from pure iron at a temperature of 1000°C

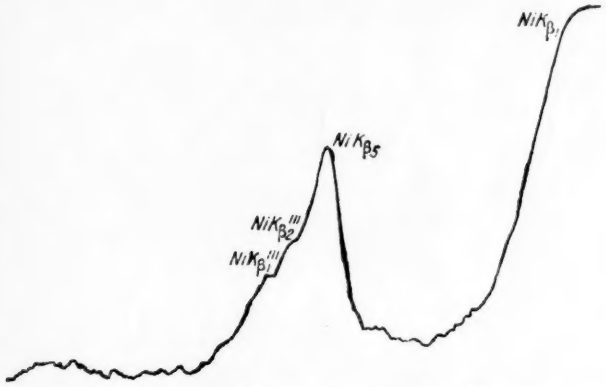

Fig. 3. NiK_{β_5}-band taken from pure nickel at a temperature of 1000°C

of Table 1 and the data for the width of the K_{β_5}-bands shown in Table 3. For the energy of the K-level of chromium, iron and nickel atoms the following values were admitted: 441.10 and 613.64 Rydberg.

TABLE 2

Corrections for widening of the band

Correction	Material studied	
	Iron	Chromium
a	1.8	1.7
b	0.09	0.13
a+b	1.89	1.83

It is clear from the data shown in Tables 1 and 3 that the width of the CrK_{β_5}-band obtained from pure chromium increases as the temperature rises. For iron in the magnetic transformation region during $\alpha_f \rightarrow \alpha_n$, transition, the width of the FeK_{β_5}-band shows a definite increase of 0.9 + 0.1 eV. The position of the maximum of the FeK_{β_5}-line remains unchanged.

The $\alpha \rightarrow \gamma$ phase transformation produces an insignificant reduction in the width of the FeK_{β_5}-band and is accompanied by a considerable change in Fermi energy from 0.20 Rydberg for Fe α to 0.17 Rydberg for Fe γ.

The width of the CrK_{β_5}-band is increased when chromium is introduced into the alloy and attains a higher value for the Fe-Cr alloy compared with the Fe-Cr-Ni alloy; for iron, on the other hand, the corresponding value is decreased and reaches a lower value in the Fe-Cr alloy.

The Fermi energy for the Fe-Cr alloy amounts to 0.19 and for the Fe-Cr-Ni alloy to 0.22 ν/R.

Phase transformation in pure iron, and also the introduction of chromium, iron and nickel in the alloy produces a marked change in the position of the maxima of the $K_{\beta'''}$-satellites for chromium, iron and nickel and a noticeable change in the relative intensities of the K_{β_5} and $K_{\beta'''}$-lines. Thus, for pure chromium $SK\beta_5/SK\beta'''$ amounts to 13.4 while for the alloy it drops to 6.0. For iron the magnitude of this effect is markedly less,

TABLE 3

Object studied	Specimen temperature (°C)	$\mathcal{T}_{K_{\beta_5}}$ (eV)			$\nu/R3d$	
		T_1	T_2	T_{max}	E_f	E_0
Chromium	700	1,7	8,5	8,4	0,14	0,76
	1000	1,7	8,9	8,8		0,79
Iron	300	1,8	10,1	10,0	0,20	0,94
	650	1,8	10,1	10,0		0,94
	850	1,8	11,0	10,9		1,00
	1000	1,8	10,8	10,7	0,17	0,97
Никель	1000	—	—	—	0,22	—
Fe in Fe-Cr alloy	1000	1,8	9,4	9,3	0,19	0,87
Cr in Fe-Cr alloy		1,8	10,6	10,6		0,92
Fe in Fe-Cr-Ni alloy	1000	1,8	9,7	9,6	0,22	0,82
Cr in Fe-Cr-Ni alloy		1,8	10,0	10,0		0,96
Ni in Fe-Cr-Ni alloy		—	—	—		—

the corresponding figures being 4.0 and 3.1. It is, however, difficult to study the $K_{\beta''}$-satellites because of their low intensity.

The position of the maximum of the K_{β_1}-lines remains unchanged in all cases.

Translated by H. Nowottny

REFERENCES

1. N.D. Borisov, V.V. Nemoshkalenko and A.M. Fefer, *Izv. Akad. nauk SSSR*, Physics series, 21, No.10, 1424 (1957).
2. N.D. Borisov and Ya.M. Fogel', *Zh. teor. fiz.* 7, No.2, 164 (1937).

VOL
8
195

ON THE PROBLEM OF THE INFLUENCE OF ALLOYING ON THE KINETICS OF PEARLITIC TRANSFORMATION*

L.N. ALEKSANDROV and B.Ia. LYUBOV

Mordovian State University, Institute of Metallography and Physics of Metals TsNIIChM

(14th July 1958)

The influence of alloying on the kinetics of pearlitic transformation is explained on the basis of an analysis of the equations of kinetic curves calculated for the cases when the process is limited by (a) the rate of polymorphous $\gamma \rightarrow \alpha$ transformation, (b) the rate of diffusion of carbon, and (c) the rate of diffusion of the alloying elements. During alloying the principal influence on the kinetics of pearlitic transformation is shown by the change in the difference between the values of the activation energy for the $\gamma \rightarrow \alpha$ transformation and of the activation energy for carbon diffusion.

For the majority of alloy steels the process determining the kinetics of pearlitic transformation is the re-ordering of the lattice $Fe_\gamma \rightarrow Fe_\alpha$, whereas for unalloyed and low-alloy steels the determining process is the carbon diffusion, and for some alloy steels (for instance molybdenum steels) the diffusion of the alloying element.

VOL. 8 1959

The kinetics of pearlitic transformation in alloyed austenite has been discussed at length in previous work [1-4] and different opinions are held about the reasons for the influence of alloying elements on the kinetics of pearlitic transformation.

Pearlitic transformation is a basic process in hypoeutectoid and hypereutectoid as well as eutectoid steels, since the excess ferrite (or cementite) separated during the first stages of transformation leads to a eutectoid composition being attained in the alloy.

Transformation in a small portion (5 per cent) of austenite of hypoeutectoid composition, for which it is still possible to consider that decomposition is limited by separation of ferrite, is considered in [5]. Further transformation in austenite is eutectoid. We shall estimate the time of complete transformation in a sufficiently large portion η of the initial austenite from the time of pearlitic transformation in a given volume V_0. The volume of new phase $V(t)$ for the phase transformation taking place in time t is described by expression [6]

$$\frac{V(t)}{V} = 1 - exp\left[-\int_0^t I(\xi) f_0 (t-\xi)\, d\xi\right], \quad (1)$$

where I is the rate of formation of nuclei of the new phase (the number of nuclei per unit volume in unit time), and f_0 the volume of the growing nucleus of the new phase.

In conditions of isothermal decomposition, neglecting the time-dependence of I and taking into account the constancy of the lateral growth rate v for pearlitic grain, we find from equation (1) in the case of pearlitic transformation

$$\frac{V(t)}{V_0} = \eta = 1 - exp\left(-\frac{\pi}{2} I v^3 t^4\right). \quad (2)$$

For the kinetic curve of pearlitic transfor-

* *Fiz. metal. metalloved.* 8, No.2, 218-224, 1959.

mation in steel we obtain

$$t = \left[-\frac{3\ln(1-\eta)}{\pi I v^3} \right]^{1/4}. \qquad (3)$$

To explain the influence of alloying elements on the kinetics of pearlitic transformation, it is necessary to elucidate the dependence of quantities of I and v on the concentration of the alloying additions and the temperature of transformation T.

According to the prevailing ideas on the mechanism of pearlitic transformation, the growth of pearlite takes place either without prior diffusion of the alloying elements in austenite or is directly associated with their redistribution. In the first case, there is formed during eutectoid decomposition a two-phase lamellar structure of period s_o consisting of ferrite and cementite containing an addition quantity which differs little from that in the initial austenite. The centres of the new phase are nuclei of cementite Fe_3C. In the second case, the lamellar structure formed consists of ferrite and carbide, and the centres of the phase will be carbide nuclei, for instance of type $(FeMe)_7C_3$ or $(FeMe)_3C$. The nucleation rate of the new phase can in both cases be determined from formula [7].

$$I = \frac{\alpha}{v_0} \left(\frac{RT}{h} \right) e^{-\frac{W}{RT}} e^{-\frac{U}{RT}}, \qquad (4)$$

where

$$W = \frac{1}{3} \sigma s_{cr}; \; s_{cr} = 4\pi \rho_{cr}^2;$$

$$\rho_{kp} = \frac{2\sigma}{\Delta F_0}; \; \frac{\alpha}{v_0} \approx 1 \frac{\text{mol}}{\text{cm}^3};$$

here W is the work of formation of a critical nucleus, $\triangle F_0$ the change in free energy during formation of a unit volume of the new phase, σ the surface tension at the interphase boundary, and U the activation energy for the process of re-ordering the austenite into the cementite lattice (or the carbide lattice, if the second case occurs).

The value of α is determined by the type of solid solution and varies between 1 and 10. For steels one can put $\alpha \approx v_0$ – the specific volume (7 cm^3/mol). The rate of lateral growth of pearlitic grain, that is the rate at which the edges of the ferrite and cementite (or carbide) blocks, which form the alloyed pearlite, move forward into the original alloyed austenite, is determined by the rate of the slowest of the processes necessary for the formation of pearlite. In the case that a ferrite-cementite structure is formed, such processes are the re-ordering of the iron lattice and the diffusion of carbon in the alloyed austenite, which leads to a change in its distribution from uniform c_o in the initial phase to 0.04 per cent in the ferrite and 6.67 per cent in the cementite blocks. With immediate formation of a ferrite-carbide structure, there should, apart from re-ordering of the iron lattice and of carbon diffusion, also occur diffusion of the alloying element leading to a high concentration of this element in the carbide.

We shall estimate the rate of growth of pearlite grain which results from each of these processes. For the rate of growth of the nucleus of the new phase, which is accomplished by re-ordering of the solid solution lattice, a general equation was obtained in [8]

$$\frac{dn}{dt} = -\frac{n^*}{h} e^{-\frac{u}{kT}} \frac{d\Delta F_n}{dn}, \qquad (5)$$

where $\triangle F_n$ is the change in the free energy of the system during the formation of a nucleus of the new phase containing n particles, and n^* the number of atoms on the surface of the nucleus.

In view of the fact that the edges of the ferrite and cementite regions are displaced at a uniform rate, it will be sufficient to consider the moving front of one of them.

We shall consider a region of the austenite-pearlite boundary, neglecting the curvature of the surface, at the ferrite front with an area of a cm^2. If the pearlite front is displaced in the direction OX, then dx/dt defines the rate at which it moves and dx/dt a the increase in the volume of ferrite in unit time. To pass in equation (5) from the number of atoms of the new phase to its volume, that is to the volume of the ferrite formed, we divide n by the Avogadro number N and multiply by the value of specific volume v_o.

$$\frac{d}{dt}\left(\frac{n}{N}v_0\right) = \frac{dV}{dt} = \frac{dx}{dt}a,$$

hence

$$\frac{dx}{dt} = \frac{1}{a}\frac{dn}{dt}\left(\frac{v_0}{N}\right);$$

correspondingly

$$\frac{d\Delta F_n}{dn} = \frac{\Delta F_0 v_0}{N};\quad n^* = \frac{a}{\pi\left(\frac{d}{2}\right)^2};$$

where d is the diameter of the iron atom. Omitting the minus signs for the change in free energy, we obtain from (5) for the rate of growth of pearlitic grain ($U = Nu$)

$$\frac{dx}{dt} = \frac{4\Delta F_0}{\pi h d^2}\left(\frac{v_0}{N}\right)^2 e^{-\frac{U}{RT}}. \qquad (6)$$

From equation (6) the rate of growth of pearlitic grain during transformation can be calculated directly for eutectoid unalloyed and any alloy steel, so that, in contrast with previously proposed [4,9] equations for the rate of growth of pearlitic grain, (6) contains no empirical constants determined from experimental values of this rate.

In equation (6) the value of ΔF_0 is determined by the change in free energy and of U by the activation energy of transformation $Fe\gamma \rightarrow Fe\alpha$. Clearly, the transformation $Fe\gamma \rightarrow Fe_3C$ has its own energy of activation. However, the regular and continuous growth of the pearlitic front bears witness to the closeness of the values of these energies and the difference in them can be neglected to a first approximation. In a more rigorous analysis, especially in the case of formation of special carbides, the values of quantities U in equations (4) and (6) should be distinguished, bearing in mind that the rate of growth will be limited by a slower re-ordering corresponding to the higher activation energy (transformation $Fe\gamma \rightarrow Fe\alpha$ during the formation of the ferrite-carbide mixture).

In [5] the activation energy of the $\gamma \rightarrow \alpha$ transformation in steel containing 0.5% C was put at 35 kcal/mol. In eutectoid steel the increase in the carbon content (0.8%C) decreases the lattice binding energy for iron according to the law [10]*

$$U = U_0(1 - 0{,}4C_C\%),$$

alloying can considerably increase U not only as a result of the increase of binding forces in γ-iron during the introduction of alloying elements but also as a result of the reduction of the carbon content in eutectoid alloy steel. A decrease of U during alloying is also possible.

Alloying with chromium increases the activation energy of the $\gamma \rightarrow \alpha$ transformation by the linear law 11

$$U = U_0(1 + 0{,}044C_{Cr}\%).$$

Calculation according to equation (6) of the rate of the growth of pearlite during eutectoid transformation in unalloyed steel at 700°C gives 0.03 cm/sec; this figure is some hundred times higher than the experimentally observed/values for this rate. In chromium steels (8.5% Cr, U = 47 kcal/mol) the rate of 1×10^{-5} cm/sec obtained by calculation is much closer to the value observed by experiment.

In this way, analysis of expression (6) shows that, just as in the case of the growth of ferrite grains which was considered in [5], also during pearlitic transformation the introduction of alloying elements can slow down significantly the rate of lattice reordering for $Fe\gamma \rightarrow Fe\alpha$ and ensure that the latter process limits the rate of pearlitic grain growth.

We shall compute the rate of growth of pearlitic grains, which is due to diffusion of carbon in alloyed austenite, according to the results of [12]. The very considerable influence on diffusion of concentration stresses arising during the eutectoid decomposition of solid solutions will be taken into account. During pearlitic transformation in unalloyed steel, the rate of grain growth is determined by [12]

* In a first approximation we assume that the change of the values of U during alloying corresponds to the change during alloying of the activation energy of self-diffusion of iron. The coefficient of this linear dependence on the carbon content of 0.4 (more precisely 0.45) is obtained by using the conversion rule established in [10] and we obtain for Q = (69 -7 C at.%) kcal/mol in weight percentage: Q = 69 (1 -0.4 C wt.%) kcal/mol.

VOL. 8 1959

$$v = \frac{4\pi D_0}{s_0 \lambda}\left(1 + \frac{v_0 \bar{c} \omega^2 E}{RT}\right) e^{-\frac{Q}{RT}}, \qquad (7)$$

where Q is the activation energy of the diffusion of carbon in austenite, D_o the pre-exponential factor of the diffusion coefficient, ω the coefficient of the dependence of the lattice constants on the carbon concentration ($\omega = 0.2$), E the modulus of elasticity, c the mean concentration of carbon before the pearlite front,

$$\bar{c} = \frac{c_0 + c_{af} + c_{ac}}{3};$$

(c_{af} and c_{ac} are the concentrations of carbon in austenite at the edges of the ferrite and cementite plates respectively); the value of λ is found by solving the transcendental equation $\Phi(\lambda, b) = \frac{c_{af} - c_{ac}}{c_c - c_f}$, which is represented graphically in [12]; c_c and c_f are the concentrations of carbon in cementite and ferrite. The values of b are determined from the temperature of transformation and the carbon concentration in the original austenite

$$b = \left(\frac{7}{27} + \frac{RT}{9 v_0 \bar{c} \omega^2 E}\right)^{-1}$$

On alloying, the following values are changed in (7): Q, D_o, s_o, λ, b, c_{ac}, c_{af} and c_c (with formation of carbides). From an estimate of the influence of alloying on these quantities one can draw a conclusion on the change of the rate of growth of the ferrite-cementite or ferrite carbide mixtures. For the determination of c_{ac} and c_{af} we take into account

$$c_{ac} = c_{ac}^{\infty};\ c_{af} = c_{af}^{\infty} e^{\frac{v_c}{v_0}\frac{\Delta F_0}{RT}}. \qquad (8)$$

Determination of the equilibrium concentrations of carbon at the boundary plane between the austenite-cementite (carbide and austenite-ferrite phases (c_{ac} and c_{af}) is carried out by extrapolation of the boundaries of the γ-region in the iron-carbon equilibrium diagrams [13], for different alloy steels with varying addition contents in the subcritical temperature range.

Calculations according to formula (7) give, for the rate of pearlitic transformation in unalloyed steel, values close to the experimental. For chromium steel (8.5% Cr) calculation of the rate gives higher values than those observed by experiment.

We now turn to the calculation of the rate of pearlite growth during the formation of the ferrite-carbide mixture, which is limited by diffusion redistribution of the alloying element in austenite. The regular layered structure of pearlite points to a periodicity in the concentration field of the alloying element before the pearlite front with the same period of s_o. The function $c(x, y)$ sought for, which is independent of time, is the solution to the diffusion equation which in the co-ordinate system moving together with the pearlite front at a rate v along the OX axis assumes the form

$$D\left(\frac{\partial^2 c}{\partial x^2} + \frac{\partial^2 c}{\partial y^2}\right) + v\frac{\partial c}{\partial x} = 0. \qquad (9)$$

We solve the equation by the method used in [12]. The changed boundary conditions correspond to the distribution of the alloying element in carbide c_k, in ferrite c_f, in austenite at the carbide surface c_{ar} and at the ferrite surface c_{af}. Mass equilibrium at the austenite-carbide and austenite-ferrite boundaries is expressed by relations

$$\begin{aligned}(c_k - c_{ak})\, v &= D\left(\frac{\partial c}{\partial x}\right)_{x=0,\ y=0},\\ (c_f - c_{af})\, v &= D\left(\frac{\partial c}{\partial x}\right)_{x=0,\ y=\frac{s_0}{2}}.\end{aligned} \qquad (10)$$

For rate v we obtain equation

$$v = \frac{4\pi D_{ok}}{\lambda_k s_0}(1 + k)\, e^{-\frac{Q_k}{RT}}, \qquad (11)$$

where D_{ok} and Q_k are the diffusion parameters of the alloying element in austenite, λ_k is determined from equation $\Phi(\lambda_k, b) = \frac{c_{af} - c_{ak}}{c_k - c_f}$; $1 + k$ is the correction for concentration stresses (which does not exceed 10). The values of λ_k are not less than 0.5. This follows from the fact that the difference $c_k - c_f$ in the denominator of $\Phi(\lambda_k, b)$ is greater than the difference between c_k and c_o. The content of the (carbide-forming) alloying element in ferrite is decreased, and

the difference $c_{af}-c_{ak}$ in the numerator is less than c_k. This follows from the fact that, although at the ferrite surface the austenite is enriched in alloying element, its concentration at this point will be less than in carbide, as a result of the greater difference in the volumes formed. Thus, the values of $\Phi(\lambda_k, b)$ are limited by $\frac{c_k}{c_k - c_0}$, and this ensures that $\lambda > 0{,}5$ even at $c_0 = \frac{1}{3} c_k$ for transformation temperatures right down to 500°C and therefore for higher temperatures. We therefore can write

$$v = \frac{4\pi D_{ok}}{\lambda_k s_0}(1+k)\, e^{-\frac{Q_k}{RT}} < \frac{80\pi D_{ok}}{s_0} e^{-\frac{Q_k}{RT}}. \quad (12)$$

In chromium steel (c_o = 8.5% Cr) the carbides $(FeCr)_7C_3$ or, at lower temperatures $(FeCr)_3C$ are formed. According to the data of [14], D_{ok} = 10 cm²/sec and Q_k = 75 kcal/mol. At a decomposition temperature of 700°C, s_o attains values of 1 x 10^{-4} cm. The inequality (12) gives

$$v < 10^{-11} \text{ cm/sec}$$

In this way, pearlitic transformation in chromium steels cannot be limited by diffusion redistributions of chromium, since the rate of pearlitic grain growth would be 6-7 orders of magnitude less than the observed value. In this case carbide formation takes place in the cementite-ferrite mixture which has formed already. Apparently the position is similar for alloying additions such as manganese, nickel and some other elements with high activation energies of diffusion. In a number of cases, e.g. when alloying molybdenum, the rate of pearlite growth is apparently determined by the diffusion of alloying elements. Calculation of the rate of pearlite growth during decomposition of austenite (675°C) on the basis of equation (11) for molybdenum steel (0.5% Mo) shows that in this case $v = \sim 10^{-9}$ cm/sec (D_{ok} = 0.1 cm²/sec, Q_k = 59 kcal/mol [6]). Experimental determination of the rate of pearlite growth for this steel gives 2 x 10^{-6} cm/sec [15]. In molybdenum steels the possibility exists that austenite is decomposed directly into ferrite and special carbides. This problem, however, requires special consideration.

In agreement with the fact that the rate of pearlite growth can be determined by any one of three possible processes, the kinetic curve for pearlitic transformation is expressed by one of three corresponding equations.

If the rate of pearlitic transformation is determined by the process of re-ordering the iron lattice, then we obtain by formulae (3), (4) and (6) for the kinetic curve the equation

$$t = \frac{Nhd}{2v_0\Delta F_0}\left[-\frac{3\pi^2 N^2 d^2 \Delta F_0 \ln(1-\eta)}{4\alpha v_0 RT}\right]^{1/3} \exp\frac{\frac{1}{4}W + U}{RT}. \quad (13)$$

If carbon diffusion is the process determining the kinetics, then we obtain by formulae (3), (4) and (7) the equation

$$t = \frac{1}{2\pi}\left[-\frac{3v_0 h s_0^3 \lambda^3 \ln(1-\eta)}{4\alpha(1+k)^3 D_0^3 RT}\right]^{1/3} \exp\frac{\frac{1}{4}(W+U) + \frac{3}{4}Q}{RT}. \quad (14)$$

In the case of the alloying element determining the diffusion effects, the equation of the kinetic curve will be of the form (14), and the magnitude of parameters Q, D_o, λ, W, U and others should be replaced by values corresponding to the diffusion of the alloying additions and to the formation of carbides.

Analysis of equations (13) and (14) shows that in alloying the main influence on the kinetics of pearlitic transformation will be exerted by the change in the magnitudes of W, U and Q which are found in the exponent. The change in the difference $U - Q$ during alloying is the criterion which determines the type of kinetics of pearlitic transformation and the possibility of describing it by formula (13) or formula (14). Variation of the temperature of transformation can also lead to a change in the type of kinetics for identical contents of alloying element, as a result of changes in the values of the

VOL. 8 1959

magnitudes entering in the factor preceding the exponent in formulae (13) and (14): ΔF_0, s_0, T, λ, k.

On the basis of the ideas set out above we shall carry out the calculation for the kinetic curves of 50 per cent transformation of austenite in unalloyed and chromium steels.

In unalloyed steel [12]:

$$c_{af}^{\infty} = 0{,}8 + 0{,}013\ (996 - T);$$
$$c_{ac}^{\infty} = 0{,}8 - 0{,}002\ (996 - T); \qquad (15)$$

$\Delta F_0 = RT\ [0.538\text{-}0.0007\ (T\text{-}273)]$;
$D_0 = 0.1^2$ cm /sec; $Q = 31300$ cal/mol.
In the temperature range 720-600°C at $c_0 = 0.5\%$ C the value of b changes from 1.2 to 1.8. From the curve of function

$$\Phi(b, \lambda) = \frac{c_{af} - c_{ac}}{c_c - c_f},$$

given in [12] we find the values of λ for various temperatures of transformation. $E = 2 \times 10^5$ kg/cm^2.

The surface tension at the boundary of the austenite and cementite phases is

$$\sigma = 48 + 0{,}3\ (720° - t°\ \text{C})\ (\text{erg/cm}^2)$$

$$s_0 = \frac{15}{996 - T} \times 10^{-4}\ \text{см}.$$

In Fig. 1, curve 1 corresponds to the kinetic curve of 50 per cent transformation of austenite [17] and curve 3 to the kinetic curve calculated from equation (14). Calculations from equation (13) (curve 2) give for the transformation time in unalloyed steel considerably lower values, which point to the fact that in the given case pearlitic transformation is not limited by the rate of polymorphous transformation $\gamma \rightarrow \alpha$ and, consequently, is determined by carbon diffusion.

For alloy steel containing 0.5% Cr and 0.4% C we find [13]

$$c_{af}^{\infty} = 0{,}45 + 0{,}016\ (1108 - T),$$
$$c_{ac}^{\infty} = 0{,}45 - 0{,}002\ (1108 - T), \qquad (16)$$

Alloying with chromium increases D_0 to 0.21 cm^2/sec and Q to 39 kcal/mol. We put the surface tension at the alloyed austenite/alloyed cementite boundary at 29 + 0.28 (700° - t° C) erg/cm^2. The calculation of s_0 is carried out with consideration of the influence of alloying. Data given in [4] show that alloying with elements retarding the diffusion of carbon can increase s_0 by a factor of 1.5-2; we calculate ΔF_0 by the method given in [5]. When the transformation temperature is changed from 700 to 600°C, ΔF_0 changes from 47 to 136 kcal/mol, the value of b from 1.7 to 2.1, and the values of λ from 0.84 to 0.62.

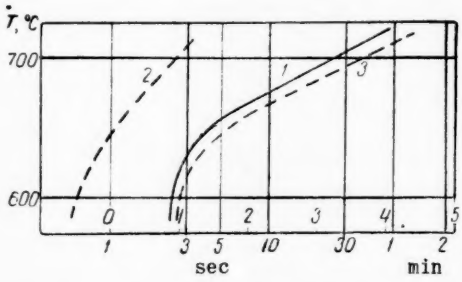

Fig. 1. Curves characterizing the kinetics of isothermal decomposition of austenite in unalloyed steel.

1 – Experimental data; 2 – Calculated on the basis that the re-ordering of the iron lattice $\gamma \rightarrow \alpha$ is the controlling factor.
3.– Calculated on the basis that carbon diffusion is the controlling factor. 50 per cent transformation.

The kinetic curve for 50 per cent transformation of austenite in the chromium steel considered is shown by curve 1 in Fig. 2 from the data given in [18]. Curve 2 corresponds to the calculation according to equation (13). Calculations according to equation (14) (curve 3) give, for the given chromium steel, values for the transformation time which are by 3-4 orders less than those obtained by experiment. In agreement with the results of [1], this confirms the opinion that in alloy steels the factor determining the kinetics of pearlitic transformation can be the re-ordering of the lattice Fe$\gamma \rightarrow$ Feα, whereas in unalloyed and low-alloy steels the kinetics of pearlitic transformation is determined by carbon diffusion.

Comparison between the changes in the activation energy of diffusion [6] and the activation energy of re-ordering during alloy-

ing with chromium shows that the kinetics of pearlitic transformation in chromium steels is determined by the kinetics of polymorphous transformation for chromium contents above 2.5 per cent.

At the same time, the results of the present investigation show that the assumptions made by the authors of [9], that the re-ordering mechanism has a controlling effect during eutectoid transformation in unalloyed carbon steel, cannot be regarded as correct.

This assumption of [9] is due to the fact that the usual explanation of pearlitic transformation in high-purity eutectoid unalloyed steels by the mechanism of carbon diffusion is inadequate. Calculation of the influence of concentration stresses, arising during pearlitic transformation, on diffusion give good agreement of the values of the rate of pearlite growth derived from equation (7) and those obtained by experiment, whereas in [9] empirical constants are adopted to force the equation describing pearlite growth to tie up with experimental curves.

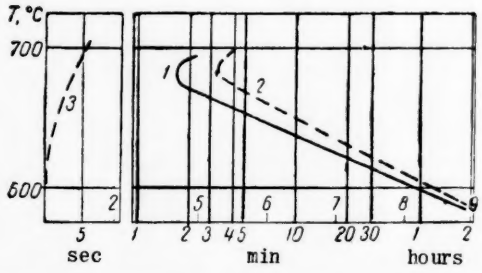

Fig. 2. Curves characterizing the kinetics of isothermal decomposition of austenite in steel containing 0.4% C and 8.5% Cr.
1 – Experimental data 2 – Calculated on the basis that the re-ordering of the iron lattice $\gamma \rightarrow \alpha$ is the controlling factor. 3 – Calculated on the basis that carbon diffusion is the controlling factor. 50 per cent transformation.

It should be noted that (in the absence of experimental data) in the present work a certain arbitrariness in the choice of values of σ, and the possibility that the changes in free energy during the formation of centres of the new phase can be defined more precisely than has been done here, cannot reflect on the general conclusions obtained, since the magnitude of the work of formation of the critical nucleus W enters in equations (13) and (14) in identical powers and, therefore, does not determine the relative distribution of the calculated curves 2 and 3.

Consideration of cases when diffusion is determined by alloying elements, when carbides are formed immediately, requires more detailed study of the thermodynamics of carbide formation.

Translated by H. Nowottny

REFERENCES

1. R.I. Entin, *Prob. metalloved. i fiz. metal (Problems of Metallography and Physics of Metals)*, vol. 4, 239 (1955).
2. M.E. Blanter, *Metalloved. i obrabotka metal.* No. 4, 2 (1955).
3. R.I. Entin, *Metalloved i obrabotka metal.*, No. 9 and 10, 2 (1956).
4. R.F. Mehl and W.C. Hagel, *Progress in Metal Physics*, vol.6, 74 (1956).
5. L.N. Aleksandrov and B.Ya. Lyubov, *Prob. metalloved. i fiz. metal. (Problems of Metallography and Physics of Metals)*, vol. 5, 317 (1958).
6. Ya.S. Umanskii, B.N. Finkel'shtein, M.E. Blanter, C,T. Kishkin, N.S. Fastov and S.S. Gorelik, *Fiz. metalloved. (Physical Metallography)* Metallurgizdat, pp. 261 and 276 (1955).
7. D. Turnbull and J. Fisher, *J. Chem. Phys.*, vol. 17, 71.
8. B.Ya. Lyubov, *Dokl. Akad. nauk. SSSR*, vol. 72, 273 (1950).
9. Y. Frye, E. Stansbury and D. McElroy, *Trans AIME*, vol. 197, 219 (1953).
10. P.L. Gruzin, Yu.V. Kornev and G.V. Kurdyumov, *Dokl. Akad. nauk. SSSR*, vol. 80, 49, (1951).
11. P.L. Gruzin, *Dokl. Akad. nauk SSSR*, vol. 100, 65 (1955).
12. L.N. Aleksandrov and B.Ya. Lyubov, *Dokl. Akad. nauk SSSR*, vol. 74, 1081 *Prob. metalloved. i fiz. metal. (Problems of Metallography and Physics of Metals)* vol. 2, 256 (1951).
13. E. Bein, *Vliyani legiruyushchikh elementov na svoistva stali, (Influence of Alloying Elements on Properties of Steel)* Metallurgizdat, p.127 (1946).
14. P.L. Gruzin, *Probl. metalloved. i fiz. metal (Problems of Metallography and Physics of Metals)* vol.4, 475 (1955).
15. R.W. Parcel and R.F. Mehl, *Trans AIME*, vol.

VOL. 8 1959

194, 771 (1952).

16. A.I. Gardin and A.P. Gulyaev, *Zh. teor. fiz.* vol. 23, 2001 (1953).

17. H.F. Bolkhovitinov, *Metalloved. i termicheskaya obrabotka (Metallography and Heat Treatment)* Mashgiz, p. 167 (1958).

18. L.I. Kogan and R.Io Entin, *Prob. metalloved. i fiz. metal, (Problems of Metallography and Physics of Metals)* vol. 2, p. 204 (1951).

VOL
8
195

SOME PROPERTIES OF THE INITIAL STAGE OF PLASTIC DEFORMATION
II. THE POINT AT WHICH THE FIRST SLIP LINES APPEAR AND THE DISTRIBUTION OF THEIR DIRECTIONS*

Ia. R. RAUZIN

All-Union Scientific Research Institute for Railway Transport

(Received 12 March 1958)

VOL. 8 1959

THE POINT AT WHICH SLIP LINES FORM

It is generally believed that plastic deformation in polycrystalline metals starts in grains which are oriented most favourably relative to the direction of acting forces. Accordingly, under uniaxial loading conditions the first traces of deformation (the slip lines) appear therefore in those grains in which the planes of easiest slip coincide with maximum shear stresses, i.e. at an angle of 45° relative to the direction of the applied force. Such an idea arose by analogy with the deformation of single crystals in which the effort required for slip formation is least in the case when planes packed most closely with atoms, i.e. preferred slip planes, coincide with maximum shear stresses.

The extended application of this idea from single crystals to polycrystalline metals has long since met with objections [1, 2]. Shapov [3] has shown by experiment that an idea of this nature concerning the formation of slip lines rests on insufficient grounds. He observed that slip lines first appear in large grains or in clusters of fine grains having closely related crystallographic orientations. Subsequently Hanson and Wheeler [4] also observed the first slip lines in large grains. Our own investigations on tensile-stressed aluminium have shown likewise that the generally held opinion on the appearance of the first slip lines is inaccurate.

This can be observed easily in a specimen in which the grain dimensions are not uniform along the specimen length. In the fine-grained portion of a specimen having grains with a very favourable orientation relative to the direction of acting forces (cube plane** (001) in the microsection plane, direction (110) at an angle of 45° to the tension force), no slip lines were found; whereas under identical strain large grains with quite different orientations were heavily marked with slip lines.

A study of elongated specimens having non-uniform grain sizes will also show readily that the first slip lines appear in larger grains with different orientations, among them such orientations as are clearly unfavourable for slip. Of the fine grains in the same specimen, a great number of which had orientations considered to be favourable for the development of slip, not a single one showed slip lines.

Generally, the first slip lines appear in coarse grains in both iron and aluminium. As in the previous case, this can be observed either on one and the same specimen when it contains grains of different sizes (Fig. 1) or when straining several specimens in which the grain size of one differs from that of another. In the latter case, the coarser the grain the lower was the strain required for revealing the first slip lines.

Fig. 2 shows the degree of deformation at which the first slip lines occur plotted against the grain size in polycrystalline iron (0.04% C, 0.07% Mn, 0.13% Si, 0.12% Cu) and aluminium (99.46% purity Al).

* *Fiz. metal metalloved.* 8, No. 2, 225-234, 1959.

** Grain orientation was determined by the method of etch pits.

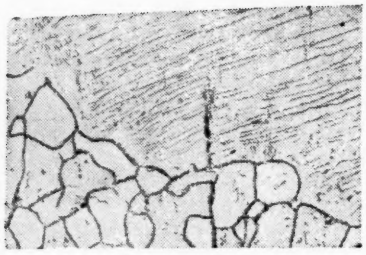

Fig. 1. Slip lines in coarse grain (0.5 mm) of the iron specimen (0.04% C). In fine grains (0.07-0.08 mm) slip lines are absent. x 220.

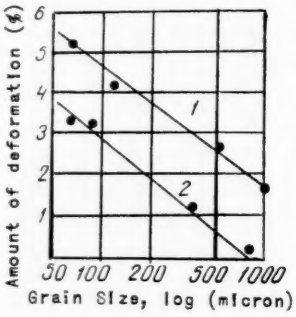

Fig. 2. Degree of deformation at which the first slip lines in polycrystalline aluminium (curve 1) and iron (curve 2) are formed plotted against grain size.

THE DIRECTIONS OF SLIP LINES

The above observations have shown that for tension the coincidence of preferred slip planes with the maximum shear component of an applied stress does not appear an adequate criterion for the formation of the first slip lines in grains. Incipient slip does not develop in fine grains although, in particular in aluminium, in 15-20 per cent of the grains the preferred slip planes are arranged much more favourably relative to the direction of acting forces. In other words, the formation of the first slip lines is not determined only by the coincidence of preferred slip planes with maximum shear stresses occurring in a specimen but it depends also on other conditions and, in particular on the grain size.

Without entering at this point into an explanation of this phenomenon, we note the fact which has been observed previously [1, 3] that the direction of the first slip lines in grains does by no means always form an angle of 45° with the direction of the applied force and in some cases does not coincide with the direction of planes offering the least resistance to slip in a grain.

An investigation was carried out to determine the start of the appearance of the first slip lines in commercial-purity aluminium. Ten polished sections were prepared from the side surface of fractured specimens and the directions of 55 primary slip lines were determined on them, i.e. lines formed at that stage of deformation when there were no more than ten grains with slip lines* on the entire side surface of the strained specimen.

Forty-four lines pass through the cube diagonal (Fig. 3), five through the cube edge (Fig. 4) and six through the octahedron edge. Thus, in spite of the fact that in each specimen grains with an orientation very favourable to slip were present and that the quantity of such grains was less less than 15-20 per cent, only part of the first slip lines coincided with preferred slip planes. A considerable quantity of primary slip lines (approximately 10 per cent) passed parallel to the cube edge; this showed that they did not coincide with preferred slip planes. Further, the slip lines sometimes cut across grains which were clearly unfavourably oriented relative to the applied force, while adjacent grains with an orientation more favourable for slip remained intact.

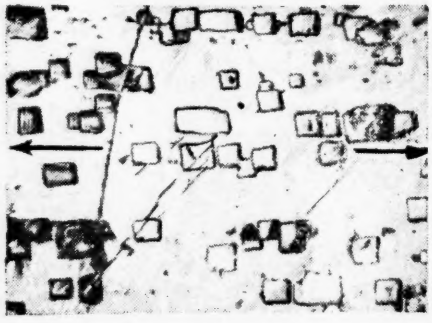

Fig. 3. Direction of slip lines in aluminium grains favourably oriented for slip. The direction of tension is indicated by arrows.

* The area of a microsection was 3 x 20 mm, and the total quantity of grains on one microsection $1 \times 10^4 - 2 \times 10^4$.

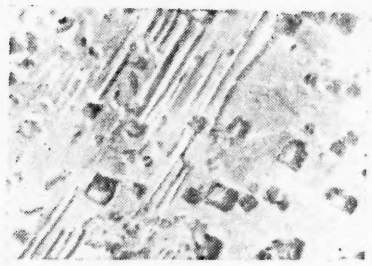

Fig. 4. Slip lines in aluminium grains in which slip does not coincide with a preferred slip plane.

The majority of the primary slip lines was found along the cube face diagonal and the octahedron edge, that is, it coincided with preferred slip planes. However, the direction of maximum stresses (angles of 45° or 135°) but formed various angles between 20 and 160° with the direction of the applied force.

As was to be expected, the large majority (approximately 80-90 per cent) of the slip lines pass through preferred slip planes but, as a rule (approximately 70 per cent), their direction does not coincide with the direction of maximum shear stresses in the specimen.

The fact that, in the presence of grains with favourable orientation relative to the direction of the applied force, first slip lines appear in grains with unfavourable orientation shows that maximum shear stresses in the slip plane do not coincide with the direction of maximum shear stresses in the specimen if it is regarded as an ideal elastically isotropic body. This cannot be confirmed concerning the difference in the direction of the first slip lines. The difference in the direction of first slip lines which has been observed on the microsection plane does not offer any basis for an estimate of the distribution of slip planes in space.

METHODS OF THREE-DIMENSIONAL ANALYSIS OF PLASTIC DEFORMATION IN POLYCRYSTALS

To estimate the distribution laws for directions of forces acting on grains in space on the basis of slip traces in these grains*, it is necessary to establish a relation between the three-dimensional distribution of slip planes and their intersections with the microsection plane, i.e. the slip lines observed by us, the quantity and direction of which can be calculated.

For this purpose a solution must be found to the following geometrical problem. A great number of planes (slip planes) exists for which the law of the distribution of their directions in space is unknown. All these planes intersect with a certain plane (the microsection plane) and the distribution of the directions of the lines of intersection (slip lines) is known. It is required to map the three-dimensional distribution of the slip planes.

The solution of this problem was carried out in co-operation with A.G. Spektor.

Let the direction of the slip planes in space be characterized by the normals to this direction n_1, n_2, n_3. All the normals are transposed parallel to themselves through some point O on the axis of the specimen and a sphere is described about this point with radius equal to unity (Fig. 5). The direction of a normal will be defined by two angles Φ and ϕ. All normals lying at an angle Φ to the specimen axis form a cone with its apex in point O. The intersection of normals corresponding to this angle with the sphere will give an arc pp_1p. Thus, if the deformation is symmetrical with the xx_1 axis, the density of the points of intersection between the normals and the sphere over the entire arc pp_1p, corresponding to the condition Φ = const., will be identical.

The position of a given normal n is defined by angle ϕ which characterizes the divergence of the normal from the plane $xp_1p_2x_1$.

We introduce the distribution function of the density of directions

$$K = \frac{1}{N}\frac{dN}{d\Phi} = \frac{dn}{d\Phi} \simeq \frac{\Delta n}{\Delta \Phi}, \qquad (1)$$

where N is the total number of the normals (slip planes), dN the number of normals inclined to the xx_1 axis at an angle lying

* We are here concerned with primary slip lines characterizing forces which act in the initial stage of plastic deformation.

VOL. 8 1959

between Φ and $\Phi + \Delta\Phi$, and $dn = \frac{dN}{N} \simeq \Delta n$ the fraction of the number of normals directed at this angle.

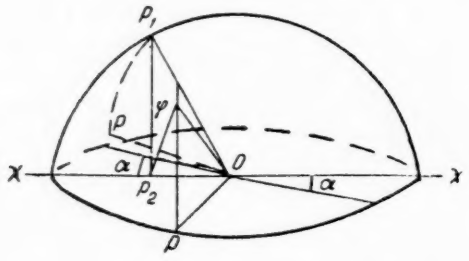

Fig. 5. Diagram showing the distribution of the directions of normals to the slip planes in space. Specimen axis xx_1.

Taking structural symmetry into account, we shall consider only one octant of the sphere of directions of normals, which is characterized by angles $0<\Phi<90°$; $0<\varphi<90°$.

We divide the sphere of directions of normals into a series of narrow bands corresponding to an interval of angles $\Delta\Phi = 10°$ or $\pi/18$ radian. The corresponding values of distribution function of the density of directions of normals K_0^{10}, K_{10}^{20}, K_{20}^{30}... (the indices indicate the limits of angles Φ) may be accepted as constants within the limits of each band.

We indicate by α the acute angle between the slip line on the microsection plane and the xx_1 axis (Fig.5) and calculate the number of slip lines inclined towards the xx_1 axis by an angle $\geq \alpha$. These lines will be formed by slip planes, the normals to which form with the specimen axis an angle of $\Phi<(90-\alpha)$, independently of their second co-ordinates ϕ.

The number of such normals will be

$$n'_{\alpha>\alpha} = \Delta\Phi \sum_{\gamma=0}^{\gamma=90-\alpha-10} K_\gamma^{\gamma+10}. \qquad (2)$$

Not all normals forming with the specimen axis an angle of $\Phi>(90-\alpha)$, will be connected with such slip lines. For this to occur, angle ϕ must lie within the limits

$$0<\varphi<\varphi_m, \text{ where } \varphi_m = \arcsin\frac{\cot\alpha}{\tan\Phi}.$$

The number of these normals for each angle of ϕ will be proportional to the quantity ϕ_m.

If for each band corresponding to $\varphi_m = \frac{\Pi}{2}$, we have $K_\Phi^{\Phi+10}$ normals, then for angle ϕ_m we obtain $K_\Phi^{\Phi+10}\ \frac{\varphi m}{\Pi/2}$ normals.

Hence for such angles we obtain the number of slip lines

$$n''_{\alpha<\alpha} = \Delta\Phi\ \frac{2}{\Pi} \sum_{\gamma=90-\alpha}^{\gamma=90} K_\gamma^{\gamma+10} \arcsin\frac{\cot\alpha}{\tan\Phi}, \qquad (3)$$

where $\Phi = \gamma + 5°$.

The number of normals corresponding to the angle of slip lines lying between α and $\alpha+\Delta$ can be expressed by equation

$$n_\alpha^{\alpha+\Delta\alpha} = a_1K_{80}^{90} + a_2K_{70}^{80} + a_3K_{60}^{70} + \ldots + a_nK_{90-\alpha-10}^{90-\alpha}. \qquad (4)$$

The coefficients a can be readily calculated from the set of equations (2) and (3).

For each interval of angles α an equation of type (4) can be written, Hence we have a system of nine equations of type (4) for determining the nine unknown quantities K_0^{10}, K_{10}^{20}... The solution of this system leads to a system of series of type

$$K_0^{10} = aN_0^{10};$$
$$K_{10}^{20} = bN_0^{10} + cN_{10}^{20};$$
$$\ldots\ldots\ldots$$
$$K_{80}^{90} = fN_0^{10} + gN_{10}^{20} + \ldots + hN_{80}^{90},$$

where K is a quantity proportional to the number of slip planes the direction of which lies within the limits of angles indicated by the indices, N is the relative number of slip lines on a plane, which lie within the limits of the angles indicated by the indices, and a, b, ..., h are numerical coefficients.

INVESTIGATION OF THREE-DIMENSIONAL MAPPING OF PLASTIC DEFORMATION IN IRON AND ALUMINIUM

Starting from the problem posed above of

VOL. 8 1959

determining the three-dimensional distribution of directions of slip planes in the initial stage of plastic deformation, the directions of slip lines relative to the direction of the axis of the specimen stressed in tension were determined experimentally in those grains in which these slip lines first appeared. The following procedure was adopted. The specimens were stressed in tension up to low amounts of deformation when on the polished surface prepared on one side of the specimen one or at most two grains with slip lines were observed under the microscope. The number of such grains did not exceed ten for each specimen surface measuring 4.5 by 25 mm for iron and 3.0 by 20 mm for aluminium.

The angles were determined by means of a protractor placed on the ground glass of the photographic camera. The accuracy of measurement was ± 5°. For each curve showing the distribution of angles of slip lines on a plane, the direction of 100 to 200 lines was determined in 15 to 20 specimens subjected to the initial stage of straining in tension. Lines were determined for angles varying from 0 to 180° and distribution curves were plotted for this entire range. As the distribution of lines in the 0-90° and the 90-180° range was, as a rule, symmetrical, the calculations were based on the sum of lines of symmetrical direction.

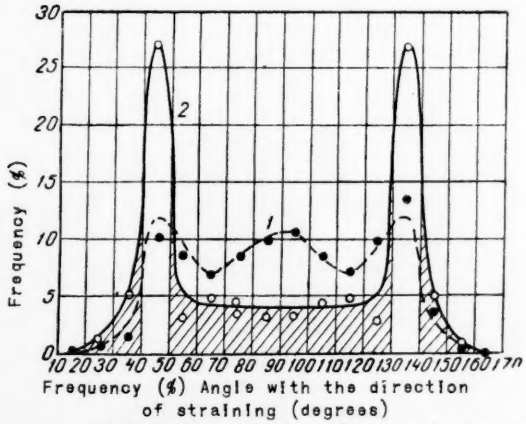

Fig. 6. Distribution of directions (relative to the specimen axis) of slip lines on the plane of the microsection (curve 1) and of slip planes in space (curve 2) for forged fine-grained iron.

In Figs. 6-9 the broken lines show the distribution of the directions of primary slip lines, i.e. slip lines in those grains in which slip deformation started during tensile stressing, for the following four cases:

1. Fine-grained armco iron, carefully forged and annealed at 900°C (mean grain diameter 0.07-0.08 mm),
2. Coarse-grained armco iron forged and annealed at 1180°C (mean grain diameter 0.6-1.0 mm),
3. Aluminium (99.46% Al) deformed and annealed at 280°C (mean grain diameter 0.06 mm),
4. Coarse-grained iron, hot-rolled (mean grain diameter 0.07-0.08 mm).

The continuous lines in Figs. 6-9 show the distribution in space of the directions of slip planes in which slip began. The abscissa indicates the angles formed by the direction of slip lines (broken curves) or slip planes (continuous curves) and the direction of the specimen axis or (what is the same) the direction of the action of the applied force. The ordinate gives the relative number of cases of a given direction as a percentage of the total number of cases.

The distribution of slip lines on a plane for fine-grained forged iron (Fig. 6) is characterized by the presence of lines of almost all directions, with the exception of low angles formed with the specimen axis. A small preference is shown by the direction forming angles of 45 and 135° with the direction of the applied load (the specimen axis).

After conversion carried out by the method described above the preferred orientation of slip planes oriented at angles of 45 and 135° to the direction of straining is clearly increased. However, these directions of the slip planes along which the deformation in the grains starts are not the only ones to appear. In almost half the grains (45 per cent) slipping begins at various angles below 45° (above 135°) and in the intermediate range (50-130°)*.

In the case of very coarse-grained iron (Fig. 7), the amount of grains showing first slip planes at an angle of 45° (135°) is increased to 72 per cent. The coincidence in the directions of the majority of planes in which slipping begins with the direction of

* The relative amount of these directions is indicated in Figs. 6-8 by the shaded areas.

maximum shear stresses in the specimen becomes more marked. However, even in this case the direction of primary slip lines does not coincide with the direction of maximum shear stresses in 28 per cent of the grains.

A relatively high percentage of this coincidence is also found in fine-grained aluminium (Fig. 8). The more pronounced preference of the 45 and 135° directions is here observed even on the specimen plane. Metallographic study of the etch pits showed in this case the presence of a preferred development of orientation more favourable for slip at an angle of 45° to the specimen axis. Calculation of the distribution of slip planes in space revealed a marked increase in the amount of primary slip planes at angles of 45 and 135° (72 per cent). However, in 28 per cent of the grains affected by primary slip the slip planes did not coincide with the direction of maximum shear stresses.

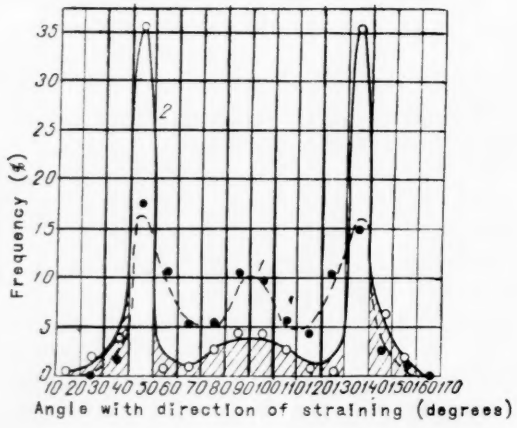

Fig. 7. Distribution of the directions (relative to the specimen axis) of slip lines on the plane of the microsection (curve 1) and of slip planes in space (curve 2) for forged coarse-grained iron.

An interesting picture is presented by hot-rolled iron in which the beginning of the appearance of slip traces during deformation was observed directly after the hot-rolling without any further treatment of the metal.

Fig. 9 shows the diagram for the distribution of the directions of slip lines in grains affected by primary slip in polar co-ordinates. The magnitudes proportional to the number of cases coinciding with the given direction are indicated along the radius of each direction.

Here a preferred direction of slip lines is clearly revealed on the plane of the microsection at an angle of 90° to the direction of the specimen axis and close to this direction. Calculations have shown that the slip planes which give such a distribution of directions of slip lines on the microsection form angles of 45° and 60-65° to the specimen axis and angles symmetrical to them. The three-dimensional distribution of slip planes on which slip began (Fig. 9) clearly indicates these two preferred directions. One of them coincides with an angle of 45° to the direction of the action of the tensile force and therefore reflects the action of maximum shear stresses in the specimen, whereas the second preferred direction diverges substantially from this, forming an angle of 60-65° with the direction of straining. This can be explained on the assumption that in the material studied some preferred orientations of likely slip planes were found, i.e. that texture was present.

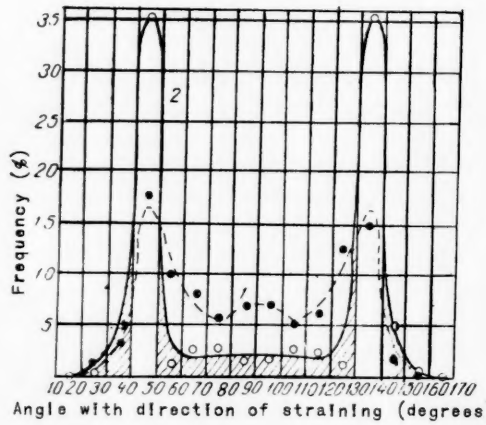

Fig. 8. Distribution of the directions of slip lines on the surface of the microsection (curve 1) and of slip planes in space (curve 2) for strained and annealed fine-grained aluminium.

Preliminary X-ray studies, carried out in co-operation with I.V. Vikker, likewise offer grounds for assuming the presence of texture in the hot-rolled iron investigated. Fig. 10 shows X-ray patterns taken under completely identical conditions for iron radiation; a Laue-type camera was used with a special device for obtaining small-angle reflection.

Comparison of the X-ray patterns shows clearly that they differ in so far as preferred

crystal orientation (texture) is present in that for rolled iron (Fig. 10a), while this cannot be observed in that for forged iron (Fig. 10b). By metallographic investigation using the method of three-dimensional analysis as described above it is possible not only to determine the trends of texture in the material but to arrive at some estimate of the character of this texture.

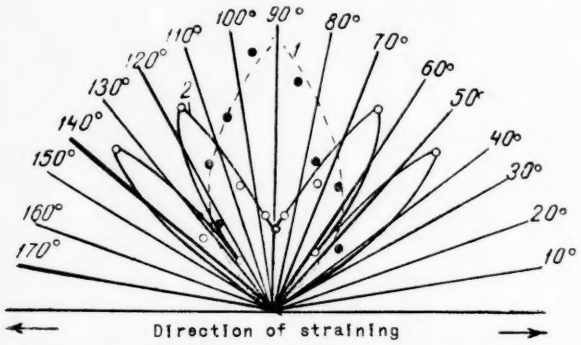

Fig. 9. Distribution of the directions of slip lines on the plane of the microsection (curve 1) and of slip planes in space (curve 2) for hot-rolled armco iron.

In particular, in hot-rolled iron the preferred directions of primary slip planes form an angle of 60-65° with the direction of the specimen axis. If rhombic dodecahedron planes [2], being most close-packed, are likely slip planes for iron, then such a preferred direction of first slip planes corresponds (within the limits of accuracy of the measurements) to the direction which should be formed by the preferred location of the (112) plane in the rolling plane (i.e. parallel to the specimen axis). This agrees with X-ray results obtained at the time by Kurdjumow and Sachs [5] who established that the (112) orientation very frequently lies in the rolling plane.

DISCUSSION OF TEST RESULTS

As mentioned above, plastic deformation in polycrystalline material should in accordance with our ideas start in grains which are most favourably oriented relative to the direction of the applied force, that is in which likely slip planes are found at an angle of 45° to the direction of the action of the tensile load. The first slip planes should therefore coincide with likely slip planes and be found at an angle of 45° to the direction of the applied force.

However, investigations have shown that in some cases, for instance when the grain size is not uniform, slip occurs first in large grains, independent of their orientation. In metals with uniform grain size, cases occur when the first slip planes do not coincide with the likely slip planes. Often the direction in which slip first occurs does not coincide with the direction of maximum shear

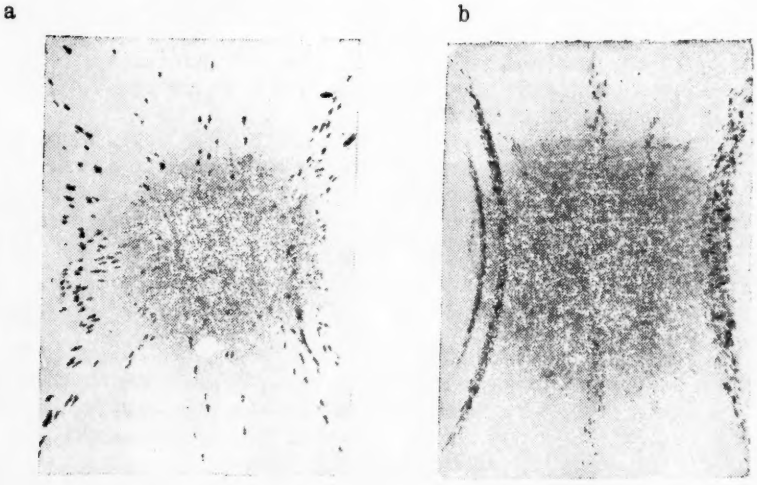

Fig. 10. X-ray patterns of rolled (a) and forged and annealed (b) iron of commercial purity. Grain size in both cases 0.07-0.08 mm.

VOL. 8 1959

stresses in the specimen. The amount of such grains in which the direction of the first slip planes differs by angles of various degrees from the direction of maximum stresses in the specimen amounts to nearly half the total (45 per cent). In uniformly coarse-grained iron this quantity is considerably less (28 per cent).

These facts can be explained on the basis of the following ideas. The direction of slip planes in grains of polycrystalline material is determined, not by maximum shear stresses in the specimen, but by a combination of forces which act on each individual grain from the direction of the neighbouring grains and accumulate under the influence of the complex interaction which takes place between the grains. An externally applied force is not transmitted mechanically to the individual grains, as in a uniform isotropic medium, but is largely redistributed among them. Such a redistribution of forces, which is associated with a difference in the form and orientation of the grains, could explain the scatter in the directions of the first slip planes. However, it does not explain why this scatter changes with the grain size and why the slip lines occur earlier in large than in small grains. As the dimensions of grains determine the extent of the intergranular transition layer it is natural to turn to a consideration of the influence of this layer on the initial stage of deformation.

Grains can act on each other only across transition layers which take up the pressures arising between grains of different orientations. As a result of these pressures there occurs deformation of the transition layers and the grains tend to shift relative to each other. This tendency is also stimulated by a difference in the shape of the grains and by the lack of coincidence of the centres of gravity of the grains with the resulting force acting on each grain [6].

As was shown experimentally for iron and aluminium [7], at this stage of deformation no slip has been observed as yet. Later, when the transition layers harden and the opportunity for the displacement of whole grains is gone, slip deformation due to the effect of increasing forces in the grains starts in those directions which were being built up as a result of the interaction described above between the various grains. These directions together with the direction of likely slip planes determine the direction of the first slip planes on which slip takes place in a grain.

In the case of large grains where intergranular displacement of grains is difficult and the grain boundaries impede slip inside the grains relatively little slip processes begin earlier than in fine grains, independent of their orientation*. In coarse-grained metals external forces are transmitted to individual grains with fewer changes in direction and, consequently, the preferred direction of first slip planes coincides to a large extent with the maximum shear stresses in the specimen.

In textured metals the general scatter of the directions of primary slip is influenced by the texture which to a significant degree controls the preferred direction of the first slip planes.

The author wishes to thank Professor N.P. Shapov for his help and advice concerning the discussion of the work.

Translated by H.E. Nowottny

REFERENCES

1. N.P. Shapov, *Zh. teor. fiz.*, 1, No.4 (1931).
2. V.D. Kuznetsov, *Fizika tverdogo tela (Physics of solids)*, 2 (1941).
3. N.P. Shapov, *Trud. inst. materialov NIS NKPS* No.127, 25 (1930).
4. D. Hanson and M. Wheeler, *J. Inst. Metals*, 45, 229 (1931).
5. G. Kurdjumow and G. Sachs, *Z. Phys.* 62, 593 (1932).
6. I.M. Pavlov, *Teoriya prokatki (Theory of rolling)* p.458, Metallurgizdat (1950).
7. Ya.R. Rauzin and A.R. Zheleznyakova, *Fiz. metal. metalloved.* 3, No.2 (1957).

* Slip processes begin earlier also in severely elongated non-equiaxed grains, even if they are comparatively fine [7].

VOL 8 195

X-RAY STUDIES OF DEFORMATIONS IN THE CRYSTAL LATTICE OF METALS DEFORMED AT LOW TEMPERATURES*

V.P. GOLIK, G.A. SIRENKO and V.I. KHOTKEVICH

Ukraine Institute of Metals

Kharkov State University

(Received 9 April 1958)

Microdeformations and the size of the coherent scattering region were studied by a harmonic analysis method in Fe, Al and Pb, deformed at room temperature and 77°K. It was shown that the most intense build-up of microdeformations and scaling-down of coherent scattering regions occurred at the very beginning of the deformation. Lowering the temperature of deformation leads to a further increase in microdeformations and decrease in coherent scattering regions.

The microstresses which arise are compared with yield strength at the corresponding temperatures. An estimate is given of the elastic energy of residual microdeformations.

VOL. 8 1959

1. A study of the deformation of metals at low temperatures, when to a large extent the effect of relaxation is excluded, is of definite interest, widening our ideas of the nature of plastic deformation and of the mechanism of creation and build-up of deformations of the crystal lattice which occur here.

A large amount of work devoted to the X-ray study of plastic deformation in metals is known. However the overwhelming majority of it was carried out at room temperature. Only a small amount of work is known in which plastic deformation and X-ray studies were carried out at liquid nitrogen temperatures and below [1-5].

The present work was done with the aim of studying the structural changes which arise in plastically deformed metals on decreasing the deformation temperature from room temperature to 77°K.

2. For the investigation massive specimens of commercially pure iron and aluminium and spectrally pure lead were selected. Before deformation the specimens were carefully annealed to give a fine-crystalline, deformation-free structure, and their surfaces were etched. Deformation was by uniaxial compression at room temperature or liquid nitrogen temperature. In the latter case the specimen was immediately transferred (in liquid nitrogen) to the previously cooled low temperature X-ray camera, with no intervening heating.

A diagramatic cut-away view of the camera is shown in Fig. 1. Cooling of the specimen during the exposure time was effected by a simple and reliable method, partial immersion of the rotating specimen in liquid nitrogen. Simultaneously, liquid nitrogen was poured over the sample from above, by means of a simple device. Temperature variation of the specimen under these conditions did not exceed $\pm$ 0.2°. Exposure of specimens deformed at room temperature was carried out in the same camera without cooling.

The back reflection photo method was used in the X-ray examination, with a sharp focus tube with an adjustable focal point and a compartmented cassette, ensuring constant conditions of exposure and processing for the X-ray photos. The direction of the X-ray beam was along the axis of compression. The (211) line of iron, the (420) line of aluminium and the (620) line of lead, taken

* *Fiz. metal. metalloved.*, 8, No.2, 235-239, 1959.

in chromium, cobalt, and iron radiation respectively, were investigated.

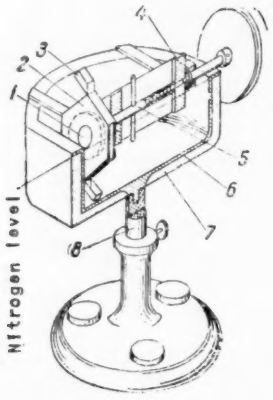

Fig. 1. The low-temperature camera: 1, specimen; 2, specimen holder; 3, "scoop" for polishing the specimen with liquid nitrogen on exposure; 4, shaft; 5, rod; 6, bath with liquid nitrogen; 7, thermal insulation; 8, ebonite pillar, 9, nitrogen level.

In Fig. 2 are shown X-ray photos and their photometric traces from the (211) lines of annealed and deformed iron.

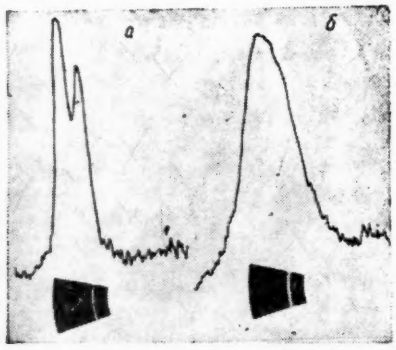

Fig. 2. X-ray photos and their photometric traces, of the iron (211) line, taken at 77°K. (a) Before deformation. (b) After 2% deformation of the specimen at 77°K.

3. Structural changes caused by plastic deformation of the metal were investigated by harmonic analysis of the forms of the interference lines on X-ray photos of polycrystalline specimens [6, 7]. If different-order reflections are obtained on the X-ray photo from a single crystallographic plane, this method allows us to distinguish between the effects of "fine dispersion" and "microdeformations" which cause line broadening on the photo, that is, allows us to fully characterize the state of the crystal lattice of the deformed specimen. In practice however it is not always possible to get different-order reflections. Therefore in the present work, an approximate method [8] of separating the effects of fine dispersion and microdeformations, from the broadening of a single line, is used, not taking into consideration the size distribution of the coherent scattering areas.

4. The relation between coherent scattering region size D and relative deformation $\frac{\Delta d}{d}$ per cent derived by this method for the metals investigated, deformed at room and low temperatures, is shown in Fig. 3. Even for small deformations (2-5 per cent) formation of a very finely dispersed structure takes place, with a coherent scattering region size of about 10^{-5}cm. With increase in degree of deformation the size of these regions decreases comparatively little (by 2-3 times).

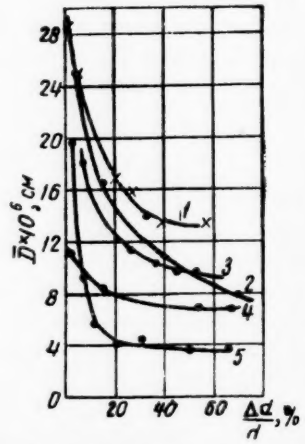

Fig. 3. Variation of coherent scattering region size with degree of deformation: (1) Al at +20°; (2) Al at -196°; (3) Fe at +20°; (4) Fe at -196°; (5) Pb at -183°.

Graphs in Figs. 4 and 5 show the relation between size of microdeformation (displacement) $\sqrt{\overline{\Delta L^2}}$ and the spacing L for iron and aluminium deformed at room temperature and low temperatures. There is a similar relation for lead deformed at a low temperature

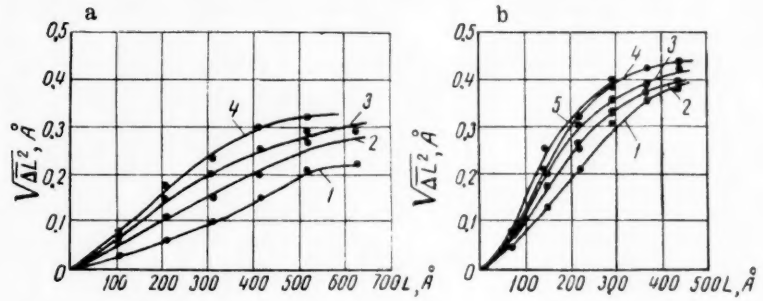

Fig. 4. Variation in microdeformations with spacing for Armco iron specimens deformed at (a) room and (b) low temperature. (a) At room temperature: 1, 2%; 2, 7%; 3, 20%; 4, 26%; 37%; 45%; 59%; (b) At low temperatures: 1, 2%; 2, 14%; 3, 34%; 4, 57%; 5, 66%.

($\sqrt{\overline{\Delta L^2_{max}}} = 0{,}3$ Å). From these graphs it follows also that the basic effect of deformation of the crystal lattice is shown at the very beginning of the deformation ($2 \leqslant \frac{\Delta d}{d} \leqslant 5\%$); further deformation does not lead to significant changes in the displacements. Here low-temperature deformation creates larger microdeformations. Thus for example in iron deformed by 2 per cent at low temperatures the displacement reaches 0.38 Å, while deformation by 60 per cent at room temperature corresponds to a value $\sqrt{\overline{\Delta L^2}} = 0.32$ Å.

It is possible that the form of the graphs shown should be attributed to the fact that for large deformations the overwhelming part of the deformation work is given up in the form of heat and only an insignificant quantity goes over into the energy of deformation of the crystal lattice. Such a result is in accordance with known results about latent energy of deformation [9], where the basic effect of storage of latent energy of deformation occurs in the initial stages of deformation.

In Fig. 6 are shown results of a determination of relative microdeformations $\varepsilon = \frac{\sqrt{\overline{\Delta L^2}}}{L}$ in aluminium deformed at the temperature of liquid nitrogen, which allow us to judge the uniformity of deformation. There is a similar graph for iron and lead. As is seen from Fig. 6, the relative microdeformation ϵ is substantially non-uniform and increases with increase in degree of deformation, passing through a maximum. Thus the maximum value of relative microdeformation ϵ_{max} grows with increasing degree of deformation and decrease in deformation temperature and is reached at shorter and shorter distances. Lowering the temperature of deformation from room temperature to 77°K for similar relative deformations increases ϵ_{max} for aluminium and iron by about twice (for aluminium from 0.7×10^{-3} to 0.4×10^{-3}, for iron 0.9×10^{-3} to 1.7×10^{-3}). The greatest value of ϵ_{max} for lead, deformed at the temperature of liquid nitrogen, is 0.8×10^{-3}. It is of interest to note that in work [8], ϵ_{max} for a high-carbon steel quenched and tempered at 250° reaches a value of 5×10^{-3}.

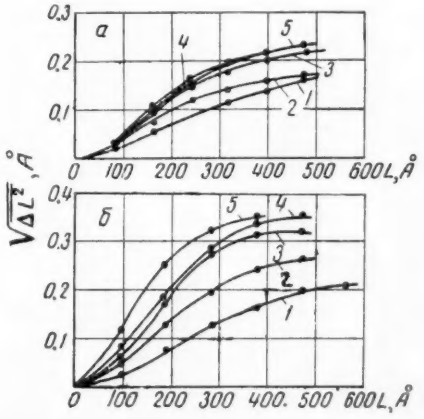

Fig. 5. Variation of spacing microdeformations with spacing for deformed aluminium specimens: (a) at room temperature; 1, 2%; 2, 4%; 3, 20%; 4, 27%; 5, 39%; 62%; (b) low temperature; 1, 4%; 2, 14%; 3, 33%; 4, 52%; 5, 69%.

VOL. 8 1959

From the relative mean microdeformation results and values of modulus of elasticity in a given crystallographic direction, microstresses in the specimens were calculated. Values determined for this quantity $\bar{P}$, for iron and aluminium deformed by 60 per cent at room temperature, were 17.5 and 4 kg/mm^2 respectively. Lowering the temperature of deformation to 77°K, in accord with the relative microdeformation results increased $\bar{P}$ to approximately double (34.3 and 10 kg/mm^2). For lead, deformed at the temperature of liquid nitrogen, the largest value of $\bar{P}$ was 1.9 kg/mm^2.

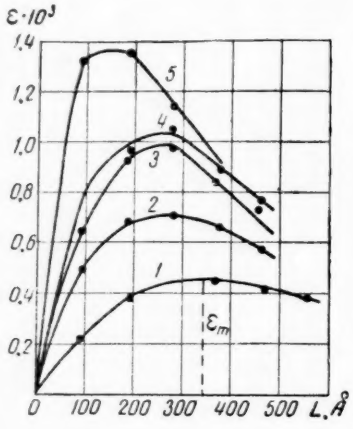

Fig. 6. Graph of relative deformation as a function of spacing for aluminium specimens deformed at 77°K: 1, 4%; 2, 14.5%; 3, 33%; 4, 52%; 5, 69%.

An attempt was made to compare values of the microstresses arising P with the yield strength σ_m for iron and aluminium specimens deformed at room temperature and a low temperature.

The field strength is determined by the so-called non-specimen method [10, 11] from the radius of raised material around a conical impression on the surface of the specimen. The impression is made with a diamond cone at room temperature and 77°K. The experiments showed that values of microstresses $\bar{P}$ calculated were always less than the yield strength and were equal to 0.2-0.3 σ.

For the same specimens under the same conditions the Brinell hardness H_B was measured.

Comparison of values derived for yield strength and hardness with microdeformations $\bar{\epsilon}$ shows that change of σ_I and H_B are related linearly with microdeformations of the lattice both at room and low temperatures. For iron, deformed at 77°K, this relation is shown in Fig. 7. Results derived agree well with those from work [12] for cold-rolled iron and aluminium. It is necessary, however, to emphasize that in such comparisons one should always bear in mind that the quantities σ_T and H_B are averaged over large volumes, while the microdeformations are measured in a layer of thickness $\sim 10^{-5}$cm for the given crystallographic direction, using in calculation of the microstresses the corresponding values of modulus of elasticity E_{hkl}.

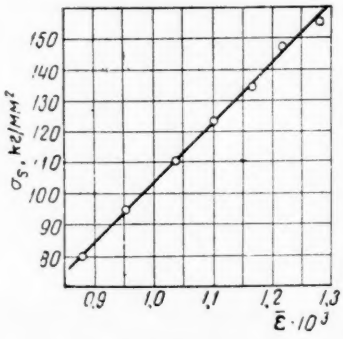

Fig. 7. Variation of yield strength with microdeformation size for iron deformed at 77°K.

The results derived allowed an estimate to be made of the average value of energy of elastic deformation due to the microstresses. For lead, aluminium and iron deformed by 50 per cent at 77°K, these energies were about 0.02, 0.09 and 0.34 cal/mol respectively.

Comparing these figures with values of latent energy of deformation for the given metals received by different authors [13], it is easy to see that as indeed we should expect, the energy of elastic deformation makes up only a fraction of a per cent of the whole latent energy of deformation; this result agrees with results published for non-metallic crystals [14].

Translated by D.G. Noel

REFERENCES

1. V.I. Khotkevich, *Zh. tekh. fiz.*, 22, 3, 474 (1952).

2. Iu.S. Terminasov and V.F. Mindukshev, *Kristallografia*, 2, 4, 514 (1957).
3. C. Barret, *Phys. Rev*, 72, 245 (1947).
4. A. Kelly and W.T. Roberts, *Acta Met.* 3, 1, 96 (1955).
5. W.B. Pearson, *Canad. J. Phys.*, 33, 8, 473 (1955).
6. B. Ia. Pines, *Ostrofokusnyie rentgenovskiie trubki i prikladnoi rentgenostrukturnyi analiz*, Gostekhizdat (1955).
7. B.E. Warren and B.L. Averbach, *J. Appl. Phys.*, 21, 6, 595 (1950); 23, 4, 497 (1952).
8. B. Ia. Pines, *Dokl. Akad. Nauk SSSR*, 103, 4 (1955).
9. V.I. Khotkevich, E.F. Chaikovskii and V.V. Zashkvara, *Fiz. metal. metalloved*, 1, 2, 206 (1955).
10. F.F. vitman, N.A. Zlatin, V.A. Stepanov and L.M. Shestopalov, *Zh. tekh. fiz.* 24, 3, 388 (1954).
11. N.A. Shaposhnikov. *Mekhanicheskiie ispytaniia metallov*, Mashgiz, 1954.
12. N.I. Sandler. Rentgenograficheskoie isledovaniie iskazhenii kristallicheskoi reshetki kholodnokatanykh zehleza i aliuminiia, *U.N I.I.M., No.* 2, p. 284 (1956).
13. M.A. Bol'shanina and V. Ie. Panin. In coll. Issledovaniia po fizike tverdogo tela, *Izd. Akad. Nauk. SSSR*, p. 206 (1957).
14. A.I. Garber, *Zh. eksp. teor. fiz.*, 6, 2, 177 (1936).

VOL.
8
1959

INVESTIGATION OF ROLLING TEXTURE BY AN ELECTRON-DIFFRACTION METHOD*

Iu. I. SOZIN

Kazan Branch of the Academy of Sciences of the U.S.S.R.

(Received 9 May 1958)

Methods of obtaining and interpreting electron diffraction pictures from the surface of a rolled metal are examined. A determination of the rolling texture of aluminium is given.

In investigation of the textures of worked metals the basic tool is the X-ray method. It is sufficiently simple for determining axial texture [1, 2], but a good deal more complicated for determining bounded textures, for example rolling texture. This applies both to the rotation curve method [1] and, particularly, to the pole figure method [1, 2, 5]. The method where a photograph is taken from "reflected" electrons, judging by the literature [7, 8], is used only in study of axial texture and has for this certain advantages over the X-ray method.

In the present work an attempt has been made to determine by electron diffraction methods a more complex bounded texture; rolling texture. In this the electron diffraction method, due to certain features of the diffraction of electrons [3], has as explained below certain advantages over X-ray methods. It allows a full determination, by a simple method, of the rolling texture of a cubic-system metal, from a single diffraction picture taken on reflection from the surface of the specimen.

THE ELECTRON DIFFRACTION PICTURE OF ROLLED ALUMINIUM

As determination of a single axis, which is the case for axial texture, enters into determination of rolling texture, it is necessary to dwell on the basic features of the electron diffraction picture for such a texture.

We will examine the electron-diffraction picture in the form of a "section" on a given scale of the sphere of projections of planes of a textured polycrystal exactly as it is done for X-ray work [2] (Fig. 1). The specimen, in the form of a plate, is placed

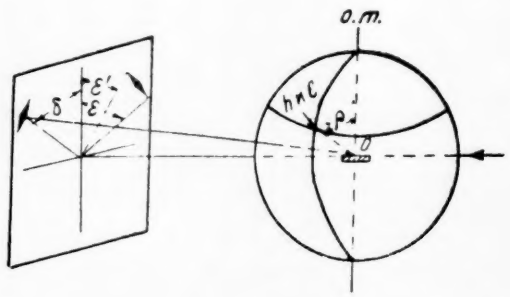

Fig. 1. Formation of an electron reflection picture for axial texture. *O.m.* is the texture axis.

horizontally at the point O. Thus the texture axis is vertical and perpendicular to the rays which are glancing along the surface of the specimen. The poles of different planes form circles for complete texture and belts of positions for incomplete texture. For simplicity we will examine only the first case.

For the electron waves the glancing angle θ in the Bragg formula

$$2d \sin \theta = n\lambda \qquad (1)$$

is close to 0°, and if in all the calculations we take $\theta = 0$, the error will be very small.

The circle of possible reflections will be

* *Fiz. metal. metalloved.*, 8, No. 2, 240-248, 1959.

a great circle, the plane of which is perpendicular to the rays and contains the texture axis.

Planes parallel to the plane of the specimen give a single reflection at the intersection of the vertical line of the electron diffraction picture and the corresponding Debye half-ring (the diatropic maximum). The remaining planes which are in a reflecting position give two reflections each at the corresponding rings. The diatropic maximum gives the indices of the texture axis immediately if the Debye rings are indexed. The azimuthal angle δ on the diffraction picture for a given reflection is approximately equal to the angle ρ between the texture axis and the normal to the plane which gives rise to this reflection. This follows from Polyani's formula

$$\cos\delta = \frac{\cos\rho}{\cos\theta} \qquad (2)$$

when $\theta = 0$.

The values of the angles can be calculated from the formula

$$\cos\rho = \frac{hu + kv + lw}{\sqrt{h^2 + k^2 + l^2}\,\sqrt{u^2 + v^2 + w^2}} \qquad (3)$$

or taken from the work [1]. In the case of absent diatropic maxima or parts of reflections left unexplained the texture axis may be found by one of the methods used in X-ray work [1]. Thus the axis may be found by a comparison of values from tables of the angles calculated from formula (3) for assumed texture axes [u, v, w] and normals to planes [h, k, l] with the values of the angle δ found experimentally from the electron diffraction picture.

This method gives a rapid solution if reflections are taken with the smallest possible values of the experimental angles. Here the field of search for the texture axis is appreciably lessened, since it is only necessary to look among the directions close to the plane normals which give the appropriate reflections. In the case where reflections on the octahedron and cube rings are present, we also recommend finding the axis from two equations of type (3). There is also a method of finding the texture axis using a stereographic net [1].

Calculation of the texture scattering angle α is also simpler than in the X-ray method [4]. The formula used

$$\cos\varepsilon' = \frac{\cos(\rho - \alpha)}{\cos\theta}, \quad \sin\varepsilon = \frac{\sin(\rho + \alpha)}{\cos\theta}$$

for $\theta = 0$ transforms to the simple formula (see Fig. 1) of

$$\alpha = \frac{\varepsilon - \varepsilon'}{2}. \qquad (4)$$

THE ELECTRON REFLECTION PICTURE FOR ROLLING TEXTURE

As distinct from the axial case, in rolling texture there are at least two axes; in many cases of textures there will be more. On rolling, one of the crystallographic planes lies parallel to the surface of the specimen. The normal to this plane is one of the texture axes. It coincides with the normal to the surface of the sprcimen, which is labelled, as usual, *NR*. The direction of rolling, labelled *WR*, will be the second axis. In determining texture one must find the crystal directions parallel to *NR* and *WR*, and also to *QR*, the transverse direction perpendicular to the first two (in future the axes will be labelled with these symbols).

Let us examine the section of a spherical projection, considering the rolling texture as two axial textures, with axes *NR* and *WR*, superimposed (Fig. 2). The specimen is placed so that the plate is horizontal, the rays travel parallel to its surface in the transverse direction. The axes *NR* and *WR* are perpendicular to the beam. The circle of possible reflections lies in the plane containing these two directions.

The poles of the planes (*hkl*) which are in reflecting position must at the same time lie on the circles of positions of the *NR* and *WR* axes and on the great circle of possible reflections. In other words, the normals to the reflecting planes must lie in the plane of the circle of possible reflections.

In the drawing these conditions are satisfied by the normals of the plane (hkl). Although the poles of the plane $(h_1k_1l_1)$ also lie on both circles of positions, the circle of reflections does not pass through them simultaneously, and consequently reflection is not possible. Thus reflection is possible

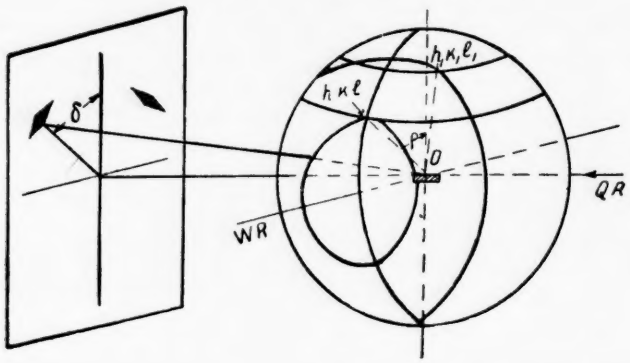

Fig. 2. Formation of electron reflection picture for rolling texture.

only from planes of zones, the axis of which is parallel to the beam, i.e. *QR*. In view of the small differences in glancing angle, given by formula (1), the always present scattering of texture axes, and also the divergence of the beam, reflections will be produced not only by given (hkl) planes but also by others with different indices, and consequently different values of *d*, belonging to the same zone. In certain cases, again due to the scattering of texture axes, reflections may be received from planes not lying in this "basic" zone. This feature is useful however, in determination of the angle of scattering of the texture.

Thus both the normal [hkl] to the reflecting plane (hkl) and the axes *NR* and *WR* lie in the plane of the circle of possible reflections. Since the axes *NR* and *WR* are perpendicular to each other, the angles formed by the normal [hkl] with these axes add up to 90°. This means that on the diffraction picture there will be reflections only from planes (hkl) the normals [hkl] of which satisfy this condition, while the planes themselves belong to the zone including the axis *QR*. The presence of such reflections is sufficient for a determination of texture axes, since for this it is not necessary to have reflections from all poles of the sphere of projection.

The method of interpretation of the electron diffraction picture and determination of rolling texture will be understood on examination of the diffraction picture given below as a concrete example.

THE ELECTRON DIFFRACTION PICTURE OF ROLLED ALUMINIUM

The investigation was carried out on a mark EM-4 electron diffraction apparatus with an accelerating potential of 40 kV with one focusing electromagnetic lens. Calibration of the apparatus was carried out by taking photos of magnesium oxide, precipitated from the vapour. Photos for this calibrating method were taken also by reflection simultaneously with the substance being investigated, which considerably increased accuracy [12]. Non-reflection calibration photos would be of little use, since they would give an appreciably different value of the constant $z\lambda$.

Let us examine the diffraction picture of rolled aluminium, with a deformation of 83 per cent. Preliminary treatment of the specimen consisted of subjection to anode solution in a phosphorus-chromium electrolyte under controlled conditions (current density of 0.1 A/dm^2, temperature 80°, time 5-16 hr), after which it gave a strong and sharp texture diffraction picture (Fig. 3). The relative positioning of the reflections on it are the same as on a weak diffraction picture of a similar specimen etched in HCl. A more detailed description of the electro-chemical side of the question is given in work [10]. In the present case only the method of interpretation of the texture of aluminium rolled to a high degree of deformation is described. Results of the interpretation are given in Table 1, each row of which corresponds to

VOL 8 195

some pair of reflections (or to a reflection for $\delta = 0$) of the diffraction picture. The interpretation is carried out as follows.

Fig. 3. Electron diffraction photo of cold-rolled aluminium; deformation 83%.

1. Measure the half-ring as usual and calculate from the normal formula

$$L\lambda = rd; \qquad (5)$$

The values of interplanar distances d (more strictly d/n, where n is the order of reflection) are compared with tables, allowing the substance giving the diffraction picture to be identified with that assumed (see tables).

2. The ring can also be indexed from the table. In the case where indices of reflecting planes are absent these may be assumed in the order of growth of the squared term $h^2 + k^2 + l^2$, taking into account the type of lattice (of extinctions, governed by the structural factor).

3. Check the indexing either from the formula

$$d = \frac{a}{\sqrt{h^2 + k^2 + l^2}},$$

(a = lattice constant) or from the relation

$$\frac{d_{100}}{d_{hkl}} = \frac{r_{hkl}}{r_{100}}. \quad \text{(see table)}$$

4. Measure on the diffraction photo the azimuthal angle δ for all reflections. It is approximately equal to the angle ρ between the unknown *NR* and the normal to the reflecting plane.

5. From the presence of diatropic maxima, and their absence, find the assumed axis *NR* by the methods described above. In the present case there is one such reflection in the ring (022). Consequently, a direction of the [110] type is a possible axis.

6. Take a given ring, for example the closest to the centre (111) and check the experimental angle δ with the angle ρ calculated [110] and the normal [111] to the plane (111). Try here different combinations of the indices [11$\bar{1}$] with [110]. For this one can use tables (see [1], p. 283) or calculate ρ from formula (3).

The angle δ differs greatly from ρ (35° instead of 25°). Consequently, in addition to being orientated with the axis *NR*, [110] must be orientated with other axes than *NR*.

The same result is found on trying the (022) ring, we get

$$\delta = \rho = 60°.$$

The reflecting plane has indices (101) or of a similar crystalline form, giving from formula (3) the same angle with the [110] direction.

Thus we have got a second proof that [1$\bar{1}$0] is the axis *NR*.

7. We may further find *QR* as the zone axis of the planes (110) and (101). The indices of it will be the minors of the matrix $\left\|\begin{smallmatrix}1&1&0\\1&0&1\end{smallmatrix}\right\|$, that is [1$\bar{1}$1] or [$\bar{1}$11].

8. By the same rule we find *WR* as the line of intersection (zone axis) of the planes *NR* (110) and *QR* (111)*. The matrix $\left\|\begin{smallmatrix}1&1&0\\1&1&1\end{smallmatrix}\right\|$ gives the indices of *WR*, [11$\bar{2}$].

All the texture elements are found from the diatropic maximum and one pair of reflections. They satisfy the conditions explained above, that is all three directions are mutually perpendicular, the reflecting plane (101) lies in the same zone as the planes (110) and (11$\bar{2}$), perpendicular to the texture axes.

9. These axes also explain the reflections on the (133), (024), and (224) rings; for them one could repeat what has been said above.

10. In finding *WR* and *QR* one may proceed a little differently. To be precise, using the

* For brevity we will characterize the planes by their normals since in the cubic system they have identical indices.

TABLE I

Values calculated from electron diffraction picture of rolled aluminium with $L\lambda = 30.71$

No. of reflection	Radius of Debye ring on diffraction photo	Interplanar distance		Ratio of interplanar distances		Index of ring	Azimuthal angle of reflection on Debye ring	Table value of angle between lines *NR* & [hkl]	Angle between lines *WR* & [hkl]	Index of reflecting plane	Indices of texture axes		
	r	d (measured)	d (tables)	$\left(\frac{d_{100}}{d_{hkl}}\right)$ (experiment)	$\left(\frac{d_{100}}{d_{hkl}}\right)$ (tables)	hkl	δ	ρ		hkl	*NR*	*WR*	*QR*
1	13.1	2.34	2.33	1.74	1.73	111	25°	25°10′	64°50′	111	225	–	–
2	15.0	2.045	2.02	2.00	2.00	002	30°	29°30′	60°30′	001	225	–	–
3	21.25	1.440	1.429	2.84	2.83	022	0°	0°	90°	110	110	Diatropic maximum	
4	21.25	1.440	1.429	2.84	2.83	022	60°	60°	30°	101	110	–	–
5	21.25	1.440	1.429	2.84	2.83	022	60°	60°30′	29°30′	110	225	–	–
6	25.0	1.227	1.218	3.33	3.32	113	4°	4°30′	85°30′	113	225	–	–
7	25.0	1.227	1.218	3.33	3.32	113	31°	31°	59°	131	110	–	–
8	25.0	1.227	1.218	3.33	3.32	113	55°	54°45′	35°10′	113	225	–	–
9	26.3	1.167	1.167	3.49	3.46	222	25°	25°10′	64°50′	111	225	–	–
10	30.3	1.012	1.010	4.00	4.00	004	29°	29°30′	60°30′	001	225	–	–
11	33.2	0.925	0.927	–	–	133	10°	13°11′	79°79′	331	110	–	–
12	33.2	0.925	0.927	–	–	133	47°	47°	42°50′	331	225	–	–
13	34.25	0.897	0.9037	–	–	024	12°	18°11′	71°79′	120	110	–	–
14	34.25	0.897	0.9037	–	–	024	49°	50°40′	39°10′	021	110	–	–
15	37.25	0.8240	0.8249	–	–	224	~5°	6°20′	84°	112	225	–	–
16	37.25	0.8240	0.8249	–	–	224	30°	30°	60°	121	110	–	–
17	39.50	0.7775	0.7777	–	–	333	27°	25°10′	64°50′	111	225	–	–

VOL 8 1955

tables of work [1], it is possible without calculation to determine that the [110] axis forms an angle $\rho = 60°$ with the normal to the plane (101), and the line $[1\bar{1}2]$, being perpendicular to [110], forms with the same normal an angle ρ of 30°. Consequently $[1\bar{1}2]$ is the texture axis *WR*. *QR* may be found as the zone axis of any two of the three planes (110), $(1\bar{1}2)$ and (101).

11. The larger part of the reflections remain unexplained however, which means there is a second group (or groups) of orientated crystallites. The *NR* axis of this group we find as follows. On the (113) ring there are reflections with a very small angle δ, so *NR* must be sought among the directions close to [113]. This method appreciably decreases the number of directions among which *NR* should be looked for.

It will be found that the axis *NR* is [225], forming angles with the octahedral (111) and cube (001) planes equal to the angles δ on the diffraction picture. The plane (225) did not give a diatropic maximum, so it must be on the (4,4,10) ring which is not on the diffraction picture. (The last ring on is (333)).

12. The axis *WR* [554], and the axis *QR* $[1\bar{1}0]$ may be found by the methods examined. The presence of this group of texture axes explains the majority of the electron diffraction photo reflections, whereupon agreement of calculated ρ with experimental δ is very good.

13. In addition, a group with orientations *NR* [110], *WR* $[\bar{1}11]$, and *QR* $[\bar{1}12]$ may be discovered, explaining reflections seven and fourteen. Thus one may draw the conclusion that the texture of aluminium is multiple with three groups of orientated crystals, A, B and C.

TABLE 2

	NR	*WR*	*QR*
A	225	554	110
B	110	112	111
C	110	111	112

14. It is easy to see that all the reflecting planes in the given group belong to one zone with zone axis *QR*. For example, planes (001) and (331) (rows 2 and 12), orientated relative to the A group of axes, belong to a zone with zone axis $[1\bar{1}0]$.

15. It should be noted that the reflection $\delta = 60°$ on the (022) ring is well explained both by the A group and the B group axes, since it comes, possibly, from planes belonging to both groups. An argument in favour of this conclusion is that this reflection has an appreciably larger intensity than the diatropic maximum on the same ring.

16. The presence on certain rings only of reflections belonging to a given group of orientations is explained as follows. For example, on the (111) and (002) rings there are no reflections due to the axes *NR* = [110] and *WR* = $[1\bar{1}2]$; calculation of the angles or data in work [1] shows that no normal to the planes $\{111\}$ or $\{001\}$ forms angles with these axes whose sum is 90°, and consequently none of these planes is in a reflecting position.

17. The texture scattering angle in the *QR* plane, perpendicular to the beam, is determined usually from the angular width of the reflections (formula (4)). For example, for A orientations it has a value of the order of 5-7°.

Interpretation of the electron diffraction picture and determination of texture is basically complete. One should dwell further on exceptions which occur to the arrangement examined.

REFLECTIONS FROM PLANES NOT BELONGING TO THE BASIC ZONE

On our diffraction picture there are two pairs of such reflections, explained by the B group axes, on the (133) and (024) rings (see rows 11 and 13). The planes giving them do not match up with any group. Assumption of the presence of other orientations also does not explain them. In both cases the experimental angle δ appreciably departs from the calculated angle ρ. These reflections belong, evidently, to planes not belonging to the zone with axis *QR*, but which due to the texture scattering none-the-less fall in a reflecting position. For this these planes must form a small angle with the beam direction, that is *QR*.

VOL. 8 1959

Let us take, for example, the reflection No. 11 ($\delta = 13°$, $\rho = 10°$), the reflecting plane (331) and find this angle. The plane passing through the beam direction $[\bar{1}11]$ and the normal $[331]$ to the reflecting plane we find using the matrix $\left\|\begin{matrix}\bar{1}11\\331\end{matrix}\right\|$, which gives $(12\bar{3})$. Similarly we find the line of intersection of this plane and the reflecting plane: $\left\|\begin{matrix}1\bar{2}3\\331\end{matrix}\right\|$ gives $[11,8,9]$. The angle between this direction and the $[\bar{1}11]$ direction will be that sought, equal to 7°. The size of this angle gives an idea of the scattering of the texture axis in planes which are perpendicular to the film plate and which contain the beam. This cannot be determined directly with a photograph taken with a beam passing in the cross direction. In the given case the angle of scattering in the $(1\bar{2}3)$ plane is evidently not less than 7°. Since this plane is close to the plane *WR*, $(11\bar{2})$, then in the latter this angle will be approximately the same, as may be shown by direct calculation. For simplicity we find this angle in the *WR* plane.

There remains to be explained the displacement of the reflections, that is the difference between δ and ρ. For this we will take the line of intersection $[1\bar{2}3]$ of the reflecting plane (331) and the plane *QR* $(\bar{1}11)$, we find the plane (541) passing through the *QR* direction $[\bar{1}11]$ and the line $[1\bar{2}3]$. The plane (541) belongs to the basic zone with axis $[\bar{1}11]$, that is, is in a reflecting position. If there were a ring on the diffraction picture (10, 8, 2), there would be found on it reflections with $\delta = \rho' = \left(\begin{matrix}\hat{1}10\\541\end{matrix}\right) =$ = 11°. If the plane (541) had an interplanar distance the same as the plane (331), then there would be a reflection on ring (133) with such a δ. Both are non-existent. In actual fact, due to texture scattering, part of the (331) planes are positioned as in ideal orientation the (541) planes are positioned, and so give an angle $\delta \approx 10°$. The same result is derived if the angle between the lines $[1\bar{2}3]$ and *WR* $[1\bar{1}2]$ is found. For simplicity of calculation we should proceed just so. The displacement of reflection No. 13 from (120) plane is explained similarly. Angle $\delta = 12°$, calculation gives $\rho = 18°$, the angle found by the method described gives $\rho' = 11°20'$. The angle ρ' for these two reflections, and also corrected angles with a second axis are given by the second figure with a dash.

Such an interpretation of reflections must necessarily be made with great care, since behind such "extra" reflections may lie undiscovered orientations.

DISCUSSION OF RESULTS

On the question of the rolling texture of aluminium the X-ray literature evidence [5, 6, 9, 11] is not in full agreement.

Orientation B was found in the majority of works, being the most stable, and taken as basic. Often the orientation (112) $[11\bar{1}]$,* close to orientation A, is found. A recent work [11] contains the following indefiniteness. It was found that parallel to the plane of rolling is the plane (112) or (113). But the plane (225) lies between them, and evidently by its determination this indefiniteness is removed. The C orientation has not been noted by X-ray methods, covered up, possibly, by the other stronger orientations. It has been established ([6], p. 497), that rolling may be examined as a superimposition of a compression normal to the rolling plane and a stretching in the direction of rolling. Orientation C serves as an expression of this position, it appears, in so far as compression and stretching of aluminium are characterized by axial textures with axes $[110]$ and $[111]$ respectively.

The good agreement of experimental results for all rings and reflections with those calculated allows us to think about the correctness of the orientations found.

The question arises, is it justifiable to speak of the texture of a metal on the basis of the texture of its surface? It has been established ([6], p 498) that leaves of a thickness up to 1 mm have a uniform cross-sectional texture. In the case examined the specimens had a thickness of 0.25 mm and less. Consequently, the texture of the deep

* The abbreviated texture symbol: first, the plane parallel to the plane of rolling, second, the direction parallel to the direction of rolling.

layers is the same as the surface.

In thick leaves the cross-sectional textures were different [6], but in this case the electron diffraction method is useful since in many cases the surface texture is important, and not the deep layers.

The electron diffraction method in the form applied has certain advantages over the X-ray method. It has the characteristics:

(a) Comparative simplicity of texture determination method

(b) Accuracy of determination of the axes

(c) The determination is made from all the Debye rings on the photograph. They are governed by the fact that, firstly, electron waves have a very short wavelength, the glancing angles are close to zero, the beam travels parallel to the surface of the specimen and reflection is from the planes of a zone, the axis of which is parallel to the beam; secondly, the combination of these factors creates favourable conditions for getting a simple diffraction pattern.

Thus investigation of a limited texture, in particular the rolling texture of a cubic system metal, may be carried out with a single electron diffraction photograph, taken by reflection in a transverse direction.

Translated by D.G. Noel

VOL. 8 1959

REFERENCES

1. R. Gloker, *Rentgenovskie luchi i ispitaniie materialov*, Leningrad – Moscow, Gostekhteoretizdat (1932).
2. V.I. Arkharov, *Kristallografiia zakalki stali*, Metallurgizdat (1951).
3. Z.G. Pinsker, Diffraktsii electronov, *Izd. Akad. Nauk SSSR* (1949).
4. V.I. Arkharov and F.P. Butra, *Zh. tekh. fiz.*, 10, 1691 (1940).
5. G.S. Zhdanov, *Issledovaniie kristallicheskikh orientirovok v metallakh i splavakh s pomoshch'iu poliusnykh figur*, Metallurgizdat (1934).
6. V.S. Barrett, *Struktura metallov*, Metallurgizdat, (1948).
7. M.M. Umanskii and V.A. Krylov, *Zh. eksp. teor. fiz.*, 6, 684 (1936).
8. K.M. Gorbunova and N.A. Shishakov, *Izv. Akad. Nauk SSSR*, ser. fiz., 17, 242 (1953).
9. A.E. Briukhanova, *Zh. tekh. fiz.*, 9, 1954 (1939).
10. O.I. Avdeieva and V.A. Dmitriiev, *Elektricheski i ul'trazvukovyie metody obrabotki*. Doklady na III, Vsesoiuznom coveshchanii, book 49, No. 2, 3 (1958).
11. Gokyu Isao and Abe Hideo. *J. Japan Inst. Metals*, 21, No. 8 (1957).
12. Iu.I. Sozin, *Kristallografiia*, 3, 6, 748 (1958).

VARIATION OF INTERNAL FRICTION AND COEFFICIENTS OF ELASTICITY IN PURE IRON WITH TEMPERATURE*

V.M. AMONENKO, B.I. SHAPOVAL and V.V. LEBEDEV

Technical Physics Institute of the Academy of Sciences of the Ukr.S.S.R.

(Received 9 June 1958)

Apparatus was constructed and the temperature dependence of internal friction, Q^{-1}, in high-purity iron was measured. The value of Q^{-1} for pure iron was appreciably higher than for Armco iron or other sorts of iron investigated earlier.

The internal friction of many metals has been studied in comparative detail for materials of purity 99.99 per cent. Iron of such a degree of purity has not been studied, and measurements of its internal friction have been made either on Armco iron (99.7 per cent pure [1] or on Puron [2]. This latter had a very small non-metallic impurity, excluding oxygen, the content of which was up to 0.04 per cent.

To study the nature of the internal friction peaks of iron it is necessary to make measurements on metal of higher purity.

PREPARATION OF SPECIMENS AND METHOD OF MEASUREMENT

The specimens were prepared from pure iron prepared by vacuum distillation, by a method devised in the Technical Physics Institute of the Academy of Sciences of the Ukr. S. S. R. Purification of iron from impurities by this method involved distillation in a high vacuum and condensation of the metal vapour on a surface heated to 1200-1300°. The iron vapour was condensed out in a condensation column fixed directly on the vapourizing crucible.

The surface of the condensation column was covered with pure iron foil, previously annealed in a high vacuum, Along the axis of the column, in the shape of a truncated hollow ceramic cone, there was a temperature gradient. In the lower part of the column, close to the crucible, the temperature reached 1300°, and in the upper part, 1100°. Such a temperature distribution along the height of the column was achieved by the appropriate thermal shielding, and also by independent heating with a resistance furnace. With the given temperature gradient the purest iron condensed out on the lower and middle zones of the condensation surface, and it was this that was used in the present work.

Vapourization took place at 1600° from an alundum crucible. The resulting iron condensate was remelted in a high vacuum and poured into a cast-iron mould. Ingots weighing 5 kg were cut into pieces 120 mm long with a cross-section 15 x 15 mm, from which the specimens were later prepared.

Plastic deformation of the iron investigated did not occur, since for this it would be essential that the iron be heated in air to become contaminated with gaseous impurities. The percentages of the main impurities in the iron are shown in Table 1.

Before measurement the specimens were annealed in a vacuum of 10^{-5} mm Hg at 900° for 2 hr and cooled together with the oven.

Measurement of internal friction was made by counting the number of free torsional oscillations the specimen made before its initial amplitude of oscillation was reduced to half.

The specimens were fixed rigidly by one end in the stand. They were prepared in the form of cylinders of dia. 10 mm and length 100 mm. The working part of the specimen was a part

* *Fiz. metal. metalloved;* 8, No.2, 249-254, 1959.

TABLE 1

Percentage of main impurities in iron

Metals	C	O_2	N_2	S	P	Mn	Mg	Ni	Al	Cu
Armco iron	0.04	0.011	0.003	0.03	0.01	0.14	0.001	0.01	0.005	0.2
Vacuum-prepared iron ..	0.03	0.001	0.0005	0.003	0.001	0.0054	0.0001	0.01	0.005	0.007
Distilled iron	0.003	0.003	0.0001	0.001	0.001	0.0007	0.0001	0.008	0.001	0.0006

in the centre of length 20 mm cut down to a dia. of 3 mm. Such a form of specimen allowed harmful losses in the supports to be reduced to a minimum, and also excluded the supporting areas from the temperature zone on

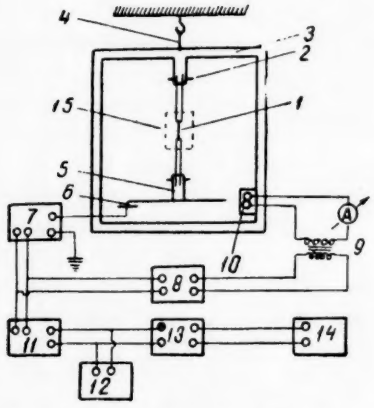

Fig. 1. Layout of apparatus.

heating the specimen [7].

The internal friction of iron was measured in a vacuum with the intention of excluding losses due to air friction, and also to avoid formation of an oxide film on the surface of the iron during heating. To decrease undesirable energy losses of the deformed specimen 1, due to its fixings at the clip 2 and the body of the apparatus 3, the whole was suspended from supports by the thin cord 4 [3]. The layout of the experiment is shown in Fig. 1.

The lower part of the specimen was fixed by a clip to the cross-member 5, by means of which the initial oscillation of the specimen was produced.

The specimen was heated by the resistance heater 15, of double-wound tungsten wire on an alundum former.

To cut down radiation losses the heater was shielded by sheet molybdenum screens. The temperature was controlled with a platinum-rhodium thermocouple. Non-uniformities in heating along the specimen did not exceed 5°. Oscillations were excited on the self-oscillating system principle [4]. Oscillations of the specimen caused a periodic change in capacitance of the condenser 6, the moving plate of which was fixed to the cross-member, and the fixed plate to the case. Changes in the capacitance of the condensers were changed by the transformer 7 into electrical oscillations. These oscillations were fed through the power amplifier 8 and the output transformer 9 to two solenoids 10, which, attracting to themselves the cross-beam armature, rotated the specimen (in the diagram one solenoid only is shown).

Use of solenoids instead of electromagnets allowed losses due to movement of the cross-beam armature in the residual magnetic field of an electromagnet to be cut out. In addition, use of the capacitance pick-up instead of an induction feeler excluded energy losses due to movement of the feeler in a magnetic field.

All the above measures significantly lowered losses in the apparatus and increased the sensitivity of measurements. Thus, in specimens having a low internal friction, values of $Q^{-1} = 7—8.10^{-5}$ were received.

In the measuring channel, a system proposed by Tsobkallo and Chelnokovyi [5] was used. The system consists of a linear amplifier 11, a voltmeter 12, an amplitude discriminator 13 and a scaling circuit 14. Use of this method allows a lot of information to be collected and combines speed of measurement with good accuracy. The frequency of oscillation of a specimen at room temperature was 40 c/s.

VOL. 8 1959

Measurement was made as follows: on switching in the excitation channel the specimen-pick-up-solenoid system oscillated at the resonant frequency.

The amplitude of the oscillations was regulated by the excitation current and measured by the voltmeter 12, previously graduated in amplitude measurement units. In these measurements the maximum angle of rotation of 3′ corresponded to a value of 100 V.

The corresponding threshold of discrimination was fixed, then the excitation system was switched out and simultaneously the scaling circuit switched in. The number of oscillations corresponding to a fall in amplitude of half was counted on the scaling circuit scale.

All measurements were made at a relative deformation at the surface of the specimen not exceeding 5×10^{-5}. The deformation caused by the weight of the cross-arm did not exceed 10^{-6}.

RESULTS OF THE EXPERIMENT

Curves 1 and 2 of Fig. 2 show the change in internal friction with temperature for pure iron, curve 2 referring to change in Q^{-1} for a specimen in a magnetic field. From curve 1 it follows that the internal friction of pure iron is almost unchanged in the temperature range 20-300°; beginning at 300° it regularly increases, showing the typical trend of a specimen with large grains.

Also the absolute value of internal friction at room temperature is appreciably higher than for Armco iron and for other pure metals and amounts to 5×10^{-3}.

As we know, on excitation of elastic oscillations in ferromagnetics there occurs within them a periodic change in orientation of the resultant spins of the areas of spontaneous magnetization. Due to this there occurs hysteresis of deformation relative to mechanical stress, causing damping of the elastic oscillations.

As a check that the abnormally large internal friction of pure iron is caused by magneto-mechanical hysteresis, and not by energy losses in the apparatus, measurements were made with an applied external magnetic field of 100 oersted.

Results of these measurements are shown in curve 2, from which it is seen that Q^{-1} with an applied magnetic field decreases by more than an order of magnitude, being 4×10^{-4} at room temperature. The character of the overall trend is retained.

According to Akulov's theory, the conclusions of which were confirmed experimentally by Gorskii [8], losses on magneto-mechanical hysteresis are proportional to the cube of the amplitude, and for a relative deformation of 10^{-5} must be insignificant.

Actually, as results of other authors and our results below, show, in the case of Armco iron magneto-mechanical hysteresis losses for a deformation of 10^{-5} do not make any appreciable contribution to internal friction, which is due to other factors. It is obvious that in this case a domain boundary, locked by impurity atoms in the iron, is not in a condition to be displaced by such a small stress.

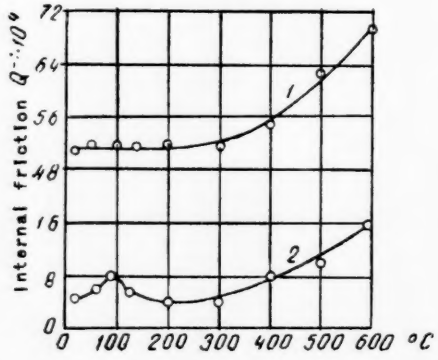

Fig. 2. Dependence of internal friction on temperature for pure iron, without a magnetic field, and with a magnetic field of 100 oersted.

In the case of pure iron however, in which there are appreciably fewer impurities, such a displacement is possible even under the action of a very small stress.

From curve 2 it is also seen that application of an external magnetic field reveals a small internal friction maximum in the region 75-100°.

To elucidate the nature of these maxima measurements were made on ordinary Armco iron, the results of which are shown in Fig. 3 (curve 1). Internal friction in Armco iron has a maximum in the same temperature range, but in absolute magnitude this maximum is much bigger. The identical position of both these maxima points to the fact that

they are of the same nature.

Iun Pao-tsui and Ke Tin-sui [6], studying internal friction in Armco iron, detected just such a maximum, caused by displacement of intrusion carbon atoms in a stress field at a temperature of 35-40°. They measured Q^{-1} at room temperature and oscillation frequency of 2 c/s. Since on increasing frequency an internal friction maximum for a relaxation process of this type must be displaced onto the high-temperature side, then as calculation shows at a frequency of 40 c/s. it should be found at a temperature of 80-90°, which coincides with results found. From this we may conclude that the maximum on curve 1 of Fig. 3, and consequently of curve 2 on Fig. 2, is caused by intrusion atoms of carbon.

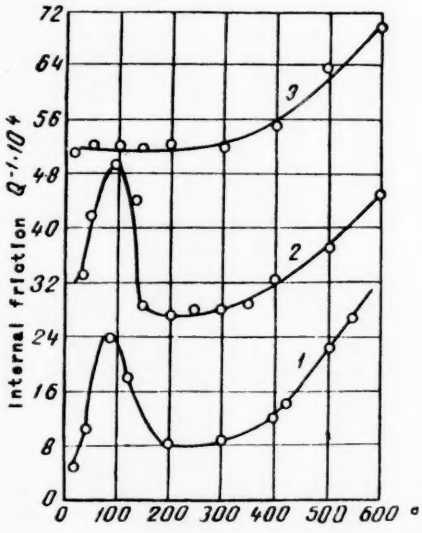

Fig. 3. Temperature dependence of internal friction for iron of various purities.

Comparing the heights of the peaks, one may determine carbon content in a solid solution for pure iron. It turns out equal to 0.002 per cent. Results of chemical analysis give a value of 0.003 per cent. Evidently not all the carbon in the iron is in a solid solution. It is possible that part of it is adsorbed in the mass of a grain. The nature of the adsorption zones is not clear. Iun Pao-tsiu and Ke Tin-sui [6], for example, make the suggestion that crystal defects act as adsorption zones.

Curve 2 of Fig. 3 shows the temperature dependence of internal friction for Armco iron remelted in a vacuum.

From the table it is seen that remelting appreciably lowers the content of gases and volatile impurities, a fact expressed by the position of curve 2 relative to curve 1 of Fig. 2. Curve 2, while retaining the same shape as curve 1, is a good deal higher. Such an increase in the background of the internal friction is caused, evidently, by magneto-mechanical hysteresis losses which increase with increase in purity of the material, in particular with the elimination of gases and non-metallic inclusions. As remelting in a vacuum eliminates carbon only to an insignificant extent, the peak due to the presence of carbon is in this case fully retained.

Curve 3 of Fig. 3 is curve 1 of Fig. 2 and is drawn here for comparison. Comparison of curves 1, 2, and 3 of Fig. 3 shows graphically the change in magnetic properties of iron with increasing purity.

THE ELASTIC CONSTANTS

This method of determining internal friction allows us to measure the modulus of rigidity of the metal investigated with good accuracy, by finding the frequency of free torsional vibrations. In calculating the moduli of elasticity the resonant frequency of torsional and bending vibrations is determined and these subsequently converted to G and E.

As in the case of internal friction measurements, the system is excited at the resonant frequency, and the specimen completes oscillations in a strictly determined given time. The number of oscillations corresponding to the given time is counted and recorded by the scaling device.

The accuracy of measurement of the frequency determined in this manner is very high and depends only on the accuracy of the stop-watch with which the time of the experiment is determined.

The results of the measurements are given in Fig. 4, from which it is seen that the value of the modulus of elasticity E for pure iron decreases almost linearly with temperature, a small deviation which is visible beginning only at 600°. The same applies to

the modulus of rigidity G. From the temperature dependence of E and G was found the relation for Poisson's ratio μ.

In Fig. 4 results for E and G are shown by dotted lines, taken from the work of Garber and Kovalev [7] investigating the moduli of elasticity and rigidity of Armco iron. The differences in the curves, particularly in the temperature range above 450°, may, it seems, be explained by the specimens having different degrees of graininess. In our case, that is for specimens with coarse grains, stress relaxation on the grain boundaries is insignificant, while in the case of fine-grained structures it reaches an appreciable

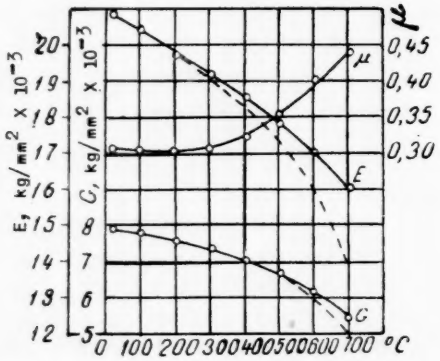

Fig. 4. Variation of elastic constants of pure iron with temperature.

value, leading to a decrease in the values of the moduli.

It is possible also that here a difference is shown up in the vibration frequencies at which the measurements were made.

CONCLUSIONS

1. The variation of internal friction of iron (99.99 per cent) with temperature is similar to the variation of other metals on measurement with coarse-grained specimens.

The absolute value of internal friction over the whole temperature range investigated is several times higher than that for Armco iron, and also that for other metals.

2. The high value of Q^{-1} for pure iron is caused by losses in magneto-mechanical hysteresis, arising upon periodic deformations in a region of very small stresses.

Application of an external magnetic field lowers the size of the internal friction by more than an order of magnitude.

3. Not all the carbon in pure iron is in the form of a solid solution.

4. In the temperature range 20-700°, the ordinary modulus of elasticity and the modulus of rigidity vary almost linearly.

Translated by D. G. Noel

REFERENCES

1. V.S. Postnikov, *Fiz. metal. metalloved.*, 4, 344 (1957).
2. Collection. *Uprugost' i neuprugost' metallov*, Foreign Literature Publishing House (1957).
3. G.S. Pisarenko. Kolebaniie uprugykh sistem s uchetom rasseianiia energii v materiale, *Izd. Akad. Nauk. Ukr. S.S.R.*, p. 200 (1955).
4. V.A. Zhuravlev, *Zav. lab.*, 14, No.5, 614 (1948).
5. S.O. Tsobkallo and V.A. Chelnokov, *Zh. tekh. fiz.*, 24, 499 (1954).
6. Iun Pao-tsui and Ke Tin-Sui, *Fiz. metal. metalloved*, 4, 407 (1957).
7. R.I. Garber and A.I. Kovalev, *Zav. lab.* 24, No. 4, 477 (1958).
8. F.K. Gorskii, *Zh. tekh. fiz.*, 20, No. 9 (1950).

VOL 8 195

DEFORMATION OF A PLANE SOLID BODY ON PHASE TRANSITION*

A.M. KOSEVICH and L.V. TANATAROV

Technical Physics Institute of the Academy of Sciences of the Ukr.S.S.R.

(Received 25 June 1958)

A study was made of the deformations and stresses caused by the movement of the boundary between two solid phases of different specific volumes. It is assumed that the relative change in volume of a body upon phase transition exceeds the values of deformation corresponding to the limits of elasticity for both phases. The residual deformations of the specimen are calculated after full transition of its structure from one phase to the other.

VOL. 8 1959

Recently there have appeared a series of works devoted to investigation of the change in shape of a solid-body specimen upon allotropic transformations [1]. A theoretical examination of this phenomenon is complicated to a large extent by the large number of factors influencing it, and also by its dependence on the very kinetics of phase change.

In the present work an attempt has been made to evaluate deformation of a flat solid specimen on the basis of a purely macroscopic examination of mechanical stresses and deformations due to change of specific volume with change of phase.

SECTION 1. STATEMENT OF PROBLEM

We will examine an isotropic layer of infinite extent of a solid body of thickness $2h$. Let the body be in the solid phase I, and let the surface of the specimen be subjected to a uniform heating so that the temperature of the surface attains, and then exceeds, the phase transition temperature T_0 to the solid phase II. Then when $T \gg T_0$ in the specimen, layers of the new phase II will be formed, beginning at both surfaces (the transition I → II is beginning), whereupon the phase interfaces,** as is seen from symmetry considerations, are planes at an equal distance from the median plane of the specimen. If we choose a system of coordinates so that the axis OX is perpendicular to the plane of the layer and the origin is in the median plane of the specimen (Fig. 1), then the interfaces will correspond to $x = \pm x_0$.

In the study of the deformation of the specimen we will assume that thermal stresses are negligible compared to stresses caused by the change in specific volume upon phase change. This allows us to examine indepen-

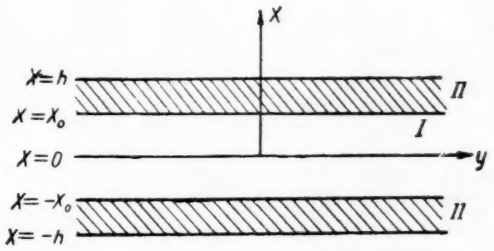

Fig. 1. Disposition of the boundaries between two phases ($x = \pm x_0$) in a layer of thickness $2h$.

* *Fiz. metal. metalloved.* 8, No. 2, 255-267, 1959.

** It is obvious that one can talk about the interface of two phases only in the case of a slab the thickness of which exceeds a certain limiting value, depending on the surface heating conditions and on the kinetics of the phase transformation. Since a phase change can take place in a fixed temperature interval ΔT near T_0, then, for example, on heating at a constant rate such a limiting value of the thickness h is $\sqrt{\chi \Delta T/S}$, where χ is the coefficient of thermal diffusivity and S is the rate of heating.

dently the problem of thermal conductivity (the problem of the speed of movement of the phase interface) and the problem of the deformations of phases I and II.

The rate of movement of the phase interface, that is the dependence of x_0 on time t ($x_0 = x_0(t)$), we will find from the known solution of the plane problem of freezing [2]. It turns out that $h - x_0 = \alpha\sqrt{t}$, where α is a coefficient depending in a complex manner on the coefficient of thermal conductivity and the thermal diffusivity of both phases and on the latent heat of the phase transition.

Thus our problem boils down to a determination of deformations u_{ik} and stresses σ_{ik} in the slab for a given position of the phase interface x_0.

We will denote the relative change in volume of the body on occurrence of the transition I $\rightarrow$ II by $3\epsilon_0$, where ϵ_0 is the relative change in linear dimensions of the body (for convenience we will take $\epsilon_0 > 0$).

Having fixed our aim of investigating the purely mechanical side of the phenomenon, we will assume the following mechanism of movement of the phase interface.

Let at the boundary $x = x_0$ an infinitely thin deformed layer of phase I go over to phase II. After transition to the new phase the layer of solid is "stuck" to phase I. We will find the geometrical deformation of this phase II layer so that the undeformed state corresponds to the state in which a layer would be after a free phase transition (i.e. upon a relative change of volume of $-3\epsilon_0$). Then the transition of the layer to phase II will be accompanied by an additional extension along OY (or OZ) by the relative value of ϵ_0. We will go over to a mathematical formulation of the problem for the phase change I $\rightarrow$ II.

It is clear that stresses and deformations depend only on the co-ordinate x, that is they are even functions of x. Also we can take it that all oblique elements of the tensors of deformation and stress are equal to zero. Then in the absence of three-dimensional forces the single equilibrium equation will have the form

$$\frac{d\sigma_{11}}{dx} = 0. \tag{1}$$

To this one must add the single non-identical equation of consistency

$$\frac{d^2 u_{22}}{dx^2} = 0. \tag{2}$$

Due to the fact that the phases have different properties and are under different physical conditions, one must examine two regions: the regions of phase I ($0 < x < x_0$) and the region of phase II ($x_0 < x < h$). Quantities referring to the phase I (or II) regions we will denote by the corresponding superscripts.

Let us formulate the boundary conditions.

1. Absence of an external force on the upper and lower surfaces

$$\sigma_{11}^{II} = 0 \quad \text{when } x = h. \tag{3}$$

2. Absence of a principal vector of external forces at the ends

$$\int_0^{x_0} \sigma_{22}^{I}\, dx + \int_{x_0}^{h} \sigma_{22}^{II}\, dx = 0. \tag{4}$$

3. Continuity of σ_{11} at the phase interface

$$\sigma_{11}^{I} = \sigma_{11}^{II} \quad \text{when } x = x_0. \tag{5}$$

4. Discontinuity of the components u_{22} at the phase interface due to the change of specific volume with change in phase

$$u_{22}^{II} - u_{22}^{I} = \epsilon_0 \quad \text{when } x = x_0. \tag{6}$$

From equation (1) and boundary conditions (3) and (5) it follows that $\sigma_{11}^{I} = \sigma_{11}^{II} = 0$.

$\sigma_{22} = \sigma_{33}$ are non-zero σ_{ik} components. To determine σ_{22} (and also the elements of the tensor u_{ik}) it is necessary to establish the connexion between the tensors σ_{ik} and u_{ik}. Since we have assumed that the deformation and stresses arising upon phase transition exceed the elastic limits of the substance, the connexion between σ_{ik} and u_{ik} can be linear, and is dependent on the type of deformed state of the body (loading or unloading).

Since the layer of phase II is created extending in the YOZ plane, then in proportion to the movement of the phase interface into the depth of the specimen it will be constrained in this plane, that is, its

deformation u_{22}^{II} will be lessened, the phase I stuck to it being simultaneously compressed. Thus it is clear that the change of deformed state upon movement of the phase interface corresponds to loading in phase I and unloading in phase II. From this the relations between σ_{ik} and u_{ik} will be different in phase I and II.

In the phase I region (the inner layer), the condition of load, according to the "unified curve" hypotheses [3], may be presented in the form

$$u_{22}^{I} - u_{11}^{I} = g_1(\sigma_{22}^{I})\,\sigma_{22}^{I}, \tag{7}$$

where $g_1(\sigma)$ denotes a certain function independent of the type of loading. To equation (7) should be added the elasticity relation between relative change in volume and hydrostatic pressure in the body

$$u_{11}^{I} + 2u_{22}^{I} = 2K_1\sigma_{22}^{I}, \tag{8}$$

where K_1 is the compressibility factor of phase I.

From (7) and (8) one can express σ_{22}^{I} in terms of u_{22}^{I},

$$\sigma_{22}^{I} = \psi_1(u_{22}^{I}). \tag{9}$$

The function $\psi_1(u)$, generally speaking, may be arbitrary, but we will assume that for small values of u it has a linear relation

$$\psi_1(u) = \alpha_1 u \quad \text{for } u \to 0, \ (\alpha_1 = \text{const}). \tag{10}$$

In the phase II region (outer layers) we must use the unloading relations. First we will assume that the residual deformations and stresses correspond to elastic areas (the other possible case will be examined in section 5). Then we may take the relation between stress and deformation to be linear

$$\sigma_{22}^{II} - \sigma_0^{II} = \alpha_2(u_{22}^{II} - u_0^{II}), \ \alpha_2 = \text{const} \tag{11}$$

(σ_0^{II} and u_0^{II} are those values of σ_{22}^{II} and u_{22}^{II} with which loading begins in the phase II region). Strictly speaking, equation (11) describes unloading only for $\sigma_{22}^{II} > 0$. If $\sigma_{22}^{II} < 0$, then in phase II loading, of the opposite sign, occurs. But on the strength of the assumptions made above about residual deformations, loading in phase II, following immediately on unloading, is also described by equation (11).

Since the onset of loading corresponds to the phase interface,

$$\sigma_{22}^{II} = \sigma_0^{II}, \ u_{22}^{II} = u_0^{II} \quad \text{for} \quad x = x_0. \tag{12}$$

Since σ_0^{II} and u_0^{II} arise upon formation of the new layer of phase II, which is accompanied by appreciable geometric deformation at the boundary $x = x_0$ then σ_0^{II} and u_0^{II} must be connected by a non-linear relation.*

$$\sigma_0^{II} = \varphi_2(u_0^{II}). \tag{13}$$

The relations (9), (11) and (13) together with those given at the beginning allow us to determine the deformations and stresses in both phases.

SECTION 2. ANALYSIS OF DEFORMATIONS AND DISPLACEMENTS

From equation (2) it follows that

$$u_{22}^{I} = a_1 x + b_1, \ u_{22}^{II} = a_2 x + b_2, \tag{14}$$

where a and b are constants.

First region ($0 < x < x_0$). Since u_{22}^{I} must be an even function of x, then $a_1 = 0$ and

$$u_{22}^{I} = b_1 = \text{const}. \tag{15}$$

From (15), and also from (9) and (8) it is easy to find the component u_{11}^{I}, which turns out to be constant, and consequently

$$u_1^{I} = u_{11}^{I} x + f_1(y), \ u_2^{I} = b_1 y + f_2(x), \tag{16}$$

where f_1 and f_2 are arbitrary functions. Putting

$$u_1^{I} = 0 \text{ for } x = 0, \ u_2^{I} = 0 \text{ for } y = 0,$$

we get from (16)

* We assume that on change of phase all non-elastic stresses in phase I are removed, but elastic stresses may remain. Therefore reconstruction of the crystal on change of phase in a thin layer of it is accompanied by elastic stresses which lead to the appearance of the initial linear part of the curve $\sigma = \varphi_2(u)$.

VOL. 8 1959

$$u_1^{\mathrm{I}} = u_{11}^{\mathrm{I}} x, \quad u_2^{\mathrm{I}} = by. \tag{17}$$

Second region ($x_0 < x < h$). From (14) assuming that

$$u_2^{\mathrm{II}} = 0 \text{ for } y = 0$$

it follows that

$$u_2^{\mathrm{II}} = (a_2 x + b_2)\, y. \tag{18}$$

If we take into account that $u_{12}^{\mathrm{II}} = 0$, then from (18), it is easy to derive

$$u_1^{\mathrm{II}} = -\frac{1}{2} a_2 y^2 + f_3(x). \tag{19}$$

Since $u_{11}^{\mathrm{II}} = \text{const.}$, then the displacement u_1^{II} at $x = x_0$ must be independent of y. From this it follows that $a_2 = 0$ and therefore

$$u_{22}^{\mathrm{II}} = b_2 = \text{const.} \tag{20}$$

From relations analogous to (8), and equation (11), it is possible to find u_{11}^{II} independently of (19), allowing us to find the arbitrary function $f_3(x)$ in (19). It turns out that

$$u_1^{\mathrm{II}} = 2(K_2 a_2 - 1) b_2 x + 2K_2 \int_{x_0}^{x} (\sigma_0^{\mathrm{II}} - a_2 u_0^{\mathrm{II}})\, dx + \text{const}, \quad u_2^{\mathrm{II}} = b_2 y. \tag{21}$$

The constaht in (21) may be found from the condition

$$u_1^{\mathrm{II}}(x_0) = u_{11}^{\mathrm{II}} x_0.$$

SECTION 3. RESIDUAL DEFORMATIONS AND STRESSES IN THE SPECIMEN

For a solution of the problem it is necessary to find the constants b_1 and b_2, and also the unknown function $v(x) = u_0^{\mathrm{II}}(x)$. The constant b_2, it follows from (12), is given by the value of the function $v(x)$ at the point $x = x_0$

$$b_2 = v(x_0).$$

The constant b_1 is expressed in terms of b_2 from (6). Thus the problem reduces to finding the function $v(x)$. Using the boundary condition (4), we get an equation for $v(x)$

$$x_0 \psi_1[v(x_0) - \varepsilon_0] + a_2(h - x_0)\, v(x_0) + \int_{x_0}^{h} [\varphi_2(v(x)) - a_2 v(x)]\, dx = 0. \tag{22}$$

Differentiating (22) with respect to x_0 and grouping the terms, we have

$$\varphi_2(v) - \psi_1(v - \varepsilon_0) - \{[\psi_1'(v - \varepsilon_0) - a_2] x_0 + a_2 h\} \frac{dv(x_0)}{dx_0} = 0. \tag{23}$$

As (23) fixes v as a function of x_0, in future it will be convenient to denote the argument simply by x.

Considering v as an independent variable, we look for x as a function of v. Then from (23) we have

$$\frac{dx}{dv} - p_1(v)\, x = q_1(v), \tag{24}$$

$$p_1(v) = \frac{\psi_1'(v - \varepsilon_0) - a_2}{\varphi_2(v) - \psi_1(v - \varepsilon_0)};$$

$$q_1(v) = \frac{a_2 h}{\varphi_2(v) - \psi_1(v - \varepsilon_0)}. \tag{25}$$

We will write the solution of equation (24) in the following form:

$$x(v) = \exp[-F_1(v)] \left\{ h - \int_{v}^{\varepsilon_0} q_1(v') \exp[F_1(v')]\, dv' \right\},$$

$$F_1(v) = \int_{v}^{\varepsilon_0} p_1(v')\, dv'. \tag{26}$$

Here the obvious condition $x(\varepsilon_0) = h$ is used.

Formula (26) expresses the function $v(x)$ in an implicit form.

We will calculate the residual deformation u_{22}^{II} corresponding to a position of the boundary $x_0 = 0$, that is the quantity $v(0)$. To do this we put $x(v)$ equal to zero and get an equation for $v(0)$.

$$h = \int_{v(0)}^{\varepsilon_0} q_1(v) \exp[F_1(v)]\, dv. \tag{27}$$

Substituting the expression $q_1(v)$ from (25), this equation can be written in the

form

$$\frac{1}{\alpha_2} = \int_{v(0)}^{\varepsilon_0} \frac{F_1(v')\,dv'}{\varphi_2(v') - \psi_1(v' - \varepsilon_0)}. \qquad (28)$$

It is characteristic that the residual deformation of the specimen in the *YOZ* plane (the quantity $v(0)$) does not depend on the thickness of the layer h and is fully defined in terms of the relation between stress and deformation in both phases*.

It is easy to check that if ϵ_0 does not exceed the limits of elasticity of phase II, i.e. if $\varphi_2(v) = \alpha_2 v$, then $v(0) = 0$. It is very easy to see this by putting (28) in a somewhat different form

$$\frac{\varphi_2(\varepsilon_0)}{\alpha_2} = \qquad (29)$$

$$= \int_{v(0)}^{\varepsilon_0} exp\left\{-\int_{v}^{\varepsilon_0} \frac{\alpha_2 - \varphi_2'(v')}{\varphi_2(v') + \psi_1(\varepsilon_0 - v')}\,dv'\right\} dv$$

In other words, for elastic deformations in phase II the specimen takes up exactly that shape that it would have after simultaneous phase transition throughout its whole thickness. This result is completely independent of the type of function $\psi_1(v)$, that is of the properties of phase I.

To elucidate the limits within which $v(0)$ must be, we will assume that the function $\rho_2(v)$ regularly increases and its graph is similar to the curve shown in Fig. 2, that is we will consider that

$$0 < \varphi_2'(v) \leqslant \varphi_2'(0) = \alpha_2. \qquad (30)$$

Using the inequality (30), it is easy to get from (29) that

$$v(0) < \varepsilon_0\left[1 - \frac{\varphi_2(\varepsilon_0)}{\alpha_2\varepsilon_0}\right]. \qquad (31)$$

The physical significance of the quantity $v^* \equiv \varepsilon_0\left[1 - \frac{\varphi_2(\varepsilon_0)}{\alpha_2\varepsilon_0}\right]$ can be appreciated from Fig. 2.

On the other side, it can be shown that $v(0) > 0$. For a more obvious confirmation of this inequality we will examine first the residual stresses in the specimen. According to (11), the residual deformation, σ_{22}^{ocm}, is given by the formula

$$\sigma_{22}^{ocm} = \alpha_2 v(0) + \varphi_2(v(x)) - \alpha_2 v(x). \qquad (32)$$

Since for $x_0 = 0$ the whole specimen is in phase II, from (4) it follows that

$$\int_0^h \sigma_{22}^{ocm}\,dx = 0,$$

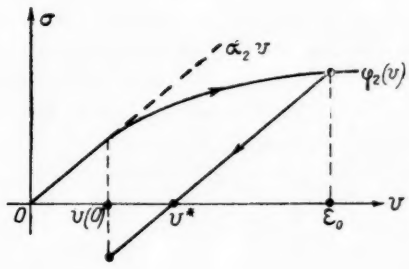

Fig. 2. Graph of stress σ against deformation v arising in a new phase (continuous line) and of unloading law (dotted line, passing through the point

which is possible only in the case where σ_{22}^{ocm}, as a function of x, changes sign between $x = 0$ and $x = h$ (or $\sigma_{22}^{ocm} = 0$, but this is possible only for elastic deformations, when $v(0) = 0$ and $\phi_2(v) = \alpha_2(v)$. As follows from (30) and (32), σ_{22}^{ocm} can change sign only at $v(0) > 0$.

Thus for inelastic deformations

$$0 < v(0) < \varepsilon_0\left[1 - \frac{\varphi_2(\varepsilon_0)}{\alpha_2\varepsilon_0}\right], \qquad (33)$$

the equal sign applying only for elastic deformations. This means that the longitudinal dimensions of the specimen (dimensions in the *YOZ* plane), after the phase change examined, where the boundary of phase transition moves from the surface, exceed the dimensions of a specimen in which the phase transition was completed simultaneously throughout its whole thickness.

As to residual deformation in the transverse direction (in the direction of the axis *OX*) this is determined from formula (8), using (32). From this formula it follows that u_{11}^{ocm} is a function of x, that is differs along the thickness of the slab.

* See footnote on page 83.

VOL. 8 1959

SECTION 4. RESIDUAL DEFORMATIONS AND STRESSES IN THE REVERSE PHASE TRANSITION (II → I)

Let the specimen go back again from phase II to phase I (II→I). It is assumed that the phase interface moves as before from the surface into the specimen. The process of deformation on reverse phase transition depends essentially on the initial mechanical state of the specimen (before the phase interface is created). We will assume that before the reverse phase change the specimen is subjected to prolonged annealing, as a result of which residual stresses (from the direct transition) are completely removed. It is necessary first to explain what changes in mechanical state annealing leads to. We will consider that on annealing (relaxation) the relation between stress and speed of deformation is given by Maxwell's equation

$$\frac{\partial u_{22}}{\partial t} = \beta_1 \sigma_{22} + \beta_2 \frac{\partial \sigma_{22}}{\partial t} \qquad (34)$$

(β_1 and β_2 are multiplying constants characterizing the material of the specimen).

From the saint tenant equation of consistency (formula 2 it follows that u_{22} is independent of x, i.e.

$$\frac{\partial u_{22}}{\partial x} = 0. \qquad (35)$$

Also condition (4) must be satisfied

$$\int_0^h \sigma_{22}(x, t)\, dx \equiv 0. \qquad (36)$$

Integrating (34) with respect to x from 0 to h for given t and using (35) and (36), we get

$$h \frac{\partial u_{22}}{\partial t} = 0 \quad \text{when} \quad \frac{\partial u_{22}}{\partial t} = 0. \qquad (37)$$

Thus $u_{22} = v(0)$, i.e. u_{22} is unchanged as a result of annealing.

Differentiating (34) with respect to x and using (35) and (36), it is easy to see that σ_{22} increases exponentially with time (as $exp\left(-\frac{\beta_1}{\beta_2} t\right)$). The changes in volume are elastic so the relation* $\sigma_{ii} = 3Ku_{ii}$, is also correct for the relaxation medium, i.e.

$$2\sigma_{22} = 3K(u_{11} + 2u_{22}).$$

After annealing however $\sigma_{22} = 0$, consequently $u_{11} = -2u_{22}$ or in our case $u_{11} = -2v(0)$.

Investigation of deformation and stresses in the specimen on reverse phase transition from phase II to phase I is made just the same as the investigation of the direct process (I→II). The only change is that in all the formulae the superscripts denoting phase I or II change places. The condition $u_{22}^{II} - u_{22}^{I} = \varepsilon_0$ at the phase interface, however, is unchanged. As a result the following equation is derived for the function $w(x_0) \equiv u_{22}^{I}(x_0)$ (x_0 is the coordinate of the phase interface)

$$x_0 \psi_2(w(x_0) + \varepsilon_0) + \alpha_1 (h - x_0) w(x) + \int_{x_0}^{h} \{\varphi_1[w(x)] - \alpha_1 w(x)\}\, dx = 0.$$

Making a calculation similar to that given in Section 3, we find the equation giving in an implicit form the relation $w = w(x_0)$:

$$x_0(w) = exp[-F_2(w)]\{h - \int_{-\varepsilon_0}^{w} q_2(w') exp[F_2(w')]\, dw'\};$$
$$F_2(w) = \int_{-\varepsilon_0}^{w} p_2(w')\, dw', \qquad (38)$$

where

$$p_2(w) = \frac{\alpha_1 - \psi_2'(w + \varepsilon_0)}{\psi_2(w + \varepsilon_0) - \varphi_1(w)},$$
$$q_2(w) = \frac{\alpha_1 h}{\psi_2(w + \varepsilon_0) - \varphi_1(w)}.$$

Putting $x_0(w) = 0$, we get the equation for residual deformations $u_{22}^{ocm} = w(0)$

$$\int_{-\varepsilon_0}^{w(0)} exp\left\{-\int_{-\varepsilon_0}^{w} \frac{\alpha_1 - \varphi_1'(w')}{\psi_2(w' + \varepsilon_0) - \varphi_1(w')} dw'\right\} dw = \frac{v_1(\varepsilon_0)}{\alpha_1}. \qquad (39)$$

Similarly to the above (see Section 3), from (39) it follows

$$0 > w(0) > -\varepsilon_0\left[1 - \frac{\varphi_1(\varepsilon_0)}{\alpha_1 \varepsilon_0}\right]. \qquad (40)$$

* This relation is also a consequence of Maxwell's, or other more general, equations describing relaxation processes.

The total residual deformation u_{22}^{ocm} is evidently compounded of $v(0)$ and $w(0)$, i.e.

$$u_{22}^{ocm} = v(0) + w(0). \tag{41}$$

Unlike u_{22}^{ocm}, the total residual deformation before annealing u_{11}^{ocm} is a function of x.

We will give the expression for total residual deformation u_{22}^{ocm} for the case when the stress-deformation curve of the reformed phase consists of two parts: an inclined part corresponding to elastic deformation, and a horizontal part corresponding to inelastic deformation (accompanied by reconstruction of the lattice)

$$\varphi(u) = \alpha u, \ (0 < u < e_s);$$

$$\varphi(u) = \sigma_s = \text{const}; \ (u > e_s).$$

We will also suppose that $e_1^s + e_2^s > \varepsilon_0$, where where e_1^s and e_2^s are the deformations at the elastic limit for both phases. Then in (29) we may put $\psi_1(u) = \alpha_1 u$, and in (39) $\psi_2(u) = \alpha_2 u$. In this case

$$u_{22}^{ocm} = e_2^s - e_1^s - \frac{1}{1-\gamma}\left\{e_2^s\left(1-\gamma+\gamma\frac{\varepsilon_0}{e_2^s}\right)\right.$$

$$\left[1-\gamma\left(1-\gamma+\gamma\frac{\varepsilon_0}{e_2^s}\right)^{\frac{1-\gamma}{\gamma}}\right] + \tag{42}$$

$$\left. + \frac{e_1^s}{\gamma}\left(\gamma-1+\frac{\varepsilon_0}{e_1^s}\right)\left[\gamma-\left(\gamma-1+\frac{\varepsilon_0}{e_1^s}\right)^{\gamma-1}\right]\right\},$$

where $\gamma = \frac{\alpha_1}{\alpha_2}$.

If we assume in addition that the mechanical properties of the two phases differ little, expression (42) simplifies considerably. In fact putting

$$\xi = 1-\gamma, \ \eta - \frac{e_s^2 - e_s^1}{e_s^2}$$

and limiting ourselves to the first terms of the expansion of u_{22}^{ocm} in ξ and η ($|\xi| \ll 1$, $|\eta| \ll 1$), we get

$$u_{22}^{ocm} = (\varepsilon_0 - e_s)\left\{2\left(1-\ln\frac{\varepsilon_0}{e_s}\right)\xi - \eta\right\}.$$

SECTION 5. THE CASE OF PHASE TRANSITION WITH A LARGE CHANGE IN SPECIFIC VOLUME

The essential point of the preceding examination was the assumption that residual deformations after the phase change do not exceed the values corresponding to the limit of elasticity. The mathematical expression of this was the linear variation of stress with deformation in the new phase. It is obvious that such an assumption may be unjustified for a large difference in specific volumes of the two phases, that is for a large value of ε_0, when after unloading there may occur considerable loading in the new phase.

We will examine a specific case when $\varepsilon_0 \gg e_s$, and the variation of σ_{22} with u_{22} in the phase II region (see Section 1) cannot be linear for $\sigma_{22} < 0$ (for loading). For simplicity of calculation we will assume that the deformation process is described by the following relations. The curve $\sigma_{22} = \varphi_2(u_{22})$, relating to the loading of a thin layer of material upon formation of the new phase, and the mechanical loading curve for deformation of the opposite sign $\sigma_{22} = \psi_2(u_{22})$ are made up of two parts each (Fig. 3): the first part is a straight line for loading or unloading (Hooke's Law)

$$\sigma_{22} - \sigma_{20} = \alpha_2(u_{22} - u_{20}),$$

and the second part is some curve (A and B in Fig. 3) not passing through the origin. In actual fact transition from the first part to the second is always smooth, and the curves are regular, but it is convenient to consider that there are two intersecting lines. The points of intersection of the straight line $\sigma_{22} = \alpha_2 u_{22}$ with each of the curves determines the limit of elasticity (σ_s, e_s).

Any mechanical state of the specimen in phase II during the I→II transition can correspond on the diagram $(\sigma_{22}^{II}, u_{22}^{II})$ only to points lying between curves A and B of Fig. 3. Unloading in phase II is described by the equation (see Fig. 3):

$$\sigma_{22} - \sigma_{20} = \alpha_2(u_{22} - u_{20}); \ (u_{22}^{*} < u_{22} < u_{20});$$
$$\sigma_{22} = \psi_2(u_{22}); \ (u_{22} < u_{22}^{*}), \tag{43}$$

where u_{22}^{*} is the deformation at the intersection of the straight line denoting unloading with curve B. It is for the given curves A and B, u_{22}^{*} is the function $u_{20} : u_{22}^{*} = U(u_{20})$.

Putting as before $u_{20} = v(x_0)$, it is easy to

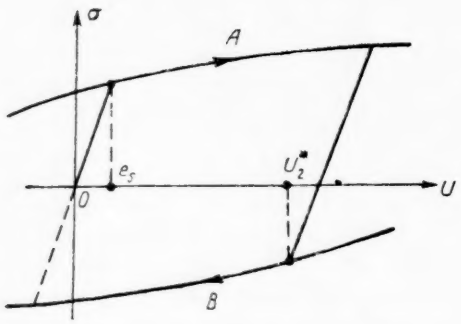

Fig. 3. Graph of stress σ against deformation v arising in the new phase when there is a large change in specific volume (curve A), and of the law of mechanical loading upon deformation of the the opposite sign (curve B).

derive the equation for the function $v = v(x)$, or, what amounts to the same thing, for the function $x = x(v)$:

$$\frac{dx}{dv}[\varphi_2(v) + \psi_1(\varepsilon_0 - v)] + x(v)[\alpha_2 - \psi_1'(v - \varepsilon_0)] = \alpha_2 h, \quad v^* < v < \varepsilon_0; \tag{44}$$

$$\frac{dx}{dv}[\varphi_2(v) + \psi_1(\varepsilon_0 - v)] + x(v)[\alpha_2 - \psi_1'(v - \varepsilon_0)] - x(W(v))[\alpha_2 - \psi_2'(v)] = \psi_2'(v)\, h, \quad v < v^*, \tag{45}$$

where $v^* = U(\varepsilon_0)$, and W is the reverse function to U.

The boundary conditions for equations (44) and (45) are as earlier: $x(\varepsilon_0) = h$. The residual deformation $u_{22}^{ocm} = v(0)$ is also determined as before.

We have already investigated equation (44). As to equation (45), this reduces to a differential equation of the first order with a retarded argument. As we know [4], the solution to such an equation is single-valued if the behaviour of the function sought is given in a certain interval of values of the independent variables adjacent to the examined interval on the least-value side. In our case the behaviour of the function sought in the given interval is given by the solution of equation (44).

For the arbitrary functions ψ_2, ψ_1 and φ_2 the solution of equation (45) cannot be presented in a closed form, however in the theory of such equations [4] there are methods worked out for their integration (for example integration by steps).

As an illustration of the method of calculation we will examine the simplest case, similar to Prandtl's method, when curves A and B (Fig. 3) and symmetrically placed lines parallel to the axis u_{22}, and the curve $\sigma = \psi_1(u)$ has the same form as the curve $\sigma = \psi_2(u)$. We will introduce a new variable

$$v = v^* - 2te_2^s, \tag{46}$$

and also put $y(t) = \frac{1}{h}x(v)$. Then negative t corresponds to equation (44), and positive t to equation (45).

We will consider that the elastic properties of both phases differ little; then $2e_2^s > e_1^s$. Then with the new variables equations (44) and (45) take on the form:

$$\frac{1}{2}[1 + 2\gamma(1+t)]\frac{dy}{dt} = (1-\gamma)y(t) - 1, \quad -1 < t < -1 + t_0; \tag{47}$$

$$\frac{1}{2}\left(1 + \frac{\sigma_1^s}{\sigma_2^s}\right)\frac{dy}{dt} = y(t) - 1, \quad -1 + t_0 < t < 0; \tag{48}$$

$$\frac{1}{2}\left(1 + \frac{\sigma_1^s}{\sigma_2^s}\right)\frac{dy}{dt} = y(t) - y(t-1), \quad t > 0. \tag{49}$$

Here $t_0 = \frac{e_1^s}{2e_2^s}$, $\gamma = \frac{\alpha_1}{\alpha_2}$.

The initial condition for equation (47) is written in the form $y(-1) = 1$.
From (47) and (48) we find

$$y(t) = \{1 - \gamma[1 + 2\gamma(1+t)]^{\frac{1-\gamma}{\gamma}}\}\frac{1}{1-\gamma}, \quad -1 < t < -1 + t_0;$$
$$y(t) = C_0 e^{\frac{t}{B}} + 1, \quad -1 + t_0 < t < 0, \tag{50}$$

where

$$B = \frac{1}{2}\left(1 + \frac{\sigma_1^s}{\sigma_2^s}\right),$$

$$C_0 = exp\left(\frac{1 - t_0}{B}\right)\left\{\frac{1}{1-\gamma}[1 - \gamma(2B)^{\frac{1-\gamma}{\gamma}}] - 1\right\}.$$

In order to explain the behaviour of $y(t)$ for $t > 0$, it is essential to solve (49), using the behaviour of $y(t)$ for $-1 < t < 0$, given by formula (50).

Using the substitution

$$y(t) = e^{\frac{t}{B}} z(t) \tag{51}$$

We bring equation (49) to the form

$$\frac{dz(t)}{dt} = -\Lambda z(t-1); \quad \Lambda = \frac{e^{-\frac{1}{B}}}{B}. \tag{52}$$

If we denote $z_0(t)$ the function $z(t)$ for $-1<t<0$ ($z_0(t)$ is found from (50) and (51)), the solution of equation (52) for t, lying in the interval $n < t < n+1$ ($n = 0, 1, 2, \ldots$), is expressed by the formula

$$z(t) = -$$

$$-\Lambda\left\{\sum_{K=0}^{n-1}(-\Lambda)^K \frac{1}{K!}\int_{-1}^{0} z_0(\tau)(t-\tau-K-1)^K d\tau + \right.$$

$$\left. + (-\Lambda)^n \frac{1}{n!}\int_{-1}^{t-n-1} z_0(\tau)(t-\tau-n-1)^n d\tau\right\} + \tag{53}$$

$$+ (C_0+1)\sum_{K=0}^{n}\frac{(-\Lambda)^K (t-K)^K}{K!}.$$

For example, for the interval (0, 1) formula (53) gives:

$$z_1(t) = 1 + C_0 - \frac{1}{1-\gamma}(1 - e^{-\frac{t}{B}}) +$$

$$+ (0 < t < t_0);$$

$$\frac{\gamma}{1-\gamma}\int_0^{t/B}(1+2\gamma B\tau)^{\frac{1}{\gamma}-1} e^{-\tau} d\tau,$$

$$z_1(t) = C_0[1 - \Lambda(t-t_0)] + \tag{54}$$

$$+ e^{-\frac{t}{B}} - \frac{\gamma}{1-\gamma}(1 - e^{-\frac{t_0}{B}}) +$$

$$+ \frac{\gamma}{1-\gamma}\int_0^{t_0/B}(1+2\gamma B\tau)^{\frac{1}{\gamma}-1} e^{-\tau} d\tau, \quad (t_0 < t < 1).$$

The expressions (50) and (53) or (54) allow us in principle to determine the residual deformation $v(0)$. Actually, as is apparent from (46), the first (smallest) zero of $z(t)$, coinciding with a zero of $y(t)$, gives the single-valued $v(0)$. This quantity can be evaluated only numerically for given values of the elastic constants. However as equation (47)-(49) for a determination of $y(t)$ do not contain h, the zero of $z(t)$ is independent of h, and consequently the residual deformation $v(0)$ is also independent of the thickness of the slab (as long as h exceeds a certain limiting value*)

Residual deformation in the reverse phase transition (II→I) can be studied in an exactly similar manner.

If the elastic properties of both phases are almost the same, the expression for $y(t)$ may be simplified, expanding it in powers of the small quantities

$$\xi = \frac{\alpha_2 - \alpha_1}{\alpha_2} = 1 - \gamma, \quad \eta = \frac{e_2^s - e_1^s}{e_2^s} = 1 - 2t_0$$

and limiting ourselves to the first terms of the expansion. It is easy to check that for $|\xi| \ll 1|\eta| \ll 1$, the root of the equation $y(t) = 0$ lies in the interval $(-1 + t_0, 0)$, that is on the linear part of the unloading curve. In connexion with this for calculation of the residual deformation $v(0)$, formula (29) may be used, directly, substituting in it $\varphi_2 \equiv \sigma_2^s$. An elementary calculation shows that the resulting residual deformation after the direct (I → II) and then the reverse (II → I) phase transitions is equal to

$$u_{22}^{ocm} \doteq -e_s\{1{,}90\eta + 0{,}78\xi\}.$$

Translated by D.G. Noel

REFERENCES

1. B.G. Lazarev, A.I. Sudovtsov and A.P. Smirnov *Fiz. metal. metalloved;* in the press. S.F. Kovtun, *Fiz. metal. metalloved:* in the press.
2. A.N. Tikhonov, A.A. Samarskii. *Uravneniia matematicheskoi fiziki,* Gostekhizdat (1951).
3. L.M. Kachanov, *Osnovy teorii plastichnosti,*

* See first footnote

Gostekhteoretizdat (1956).

4. A. D. Myshkis, *Lineinyie differentsial'nyie uravneniia s zapazdyvaïushchim argumentom*, Gostekhteoretizdat (1951).

VOL
8
195

SOME PROBLEMS IN THE MEASUREMENT OF MICROHARDNESS*

V. M. DOLIDZE

Institute of Physics of Akad. Nauk. of the Georgian S.S.R.

(Received 10 February 1958)

VOL. 8 1959

Methods used in the microhardness examinations of materials, in spite of their wide use and simplicity, contain a number of points, which are not quite clear. The problems of the relationship between microhardness and load of standard specimens are undoubtedly the most vulnerable points in these methods.

It is clear from the numerous papers that the law of similarity loses its validity in the majority of cases of microhardness measurement. Not only quantitative, but also qualitative discrepancies exist between the data of different authors on the relationship between microhardness and load. Even at a very early stage in the development of the method, investigators began to obtain results differing greatly from one another as to the nature of the relationship between microhardness and load.

At first these results were obtained for different materials with the aid of different instruments and methods for preparing the surfaces [1]. Later, however, it turned out that these discrepancies had deeper roots. Differing results were obtained not only for different but also for the same material. Thus, for example, many investigators obtain relationships between the microhardness and load for a fresh rock salt crystal shear plane which differ qualitatively from one another. [2-5].

The discrepancies existing in the microhardness values for rock salt cannot be attributed to the fact that the indenter is not the correct geometric shape or to errors in the indentation measurements, or to the difference in hardness of the different materials. We are firmly convinced that the sole reason for the variation lies in the divergence of the applied force from the nominal. Hence it follows that either the instruments themselves are unsuitable and cannot give reliable results for the loads under consideration, or that the experimenters still do not know how to use these instruments correctly.

Standard specimens must be chosen and introduced in order to solve the problem of the relationship between microhardness and load. Until there is a relationship between the microhardness of some material and the load which is suitable for all investigators, its use as a standard does not give results of any value. A second important requirement of standard specimens is that they can be reproduced easily or that their microhardness values remain constant with time.

An attempt to select standard specimens from polycrystalline materials [6] is very unlikely to succeed on account of the heterogeneity of these materials and the difficulty involved in preparing microsections. As is known [3, 7], mechanical grinding and polishing of the surfaces exerts considerable influence on the microhardness value.

The proposal of Gogoberidge [2] to use a fresh cleavage plane of rock salt as a standard merits attention. Rock salt crystals can be used with success as a standard for loads of 10 g and more. In the case of smaller loads, however, the use of this standard encounters serious difficulties, owing to the absence of a universally adopted viewpoint in its hardness at these loads. It is obvious that a single point of view cannot be obtained by agreement relative to any mean value. Only an experiment carried out under very strict conditions can solve the problem in theory or at least narrow down the range of discrepancies in hardness values.

An attempt is made in this paper to obtain new results for the relationship between

*Fiz. metal metalloved. 8, No. 2, 268-273, 1959.

microhardness and load for the cleavage surfaces of crystals by more accurate definition of the adjustment of the instrument and the lowering of the indenter on to the specimen under test.

EXPERIMENTAL METHODS OF MEASUREMENT

The tests were carried out on PMT-3 instruments. A diamond pyramid with a square base and with an angle of taper of 136° was used as the indenter.

When the PMT-3 instrument is adjusted according to the manufacturer's instructions, the relative errors in the determination of the microhardness under small loads may reach a considerable magnitude. For more accurate adjustment of the instrument we used a method of visual observation of the positive of the indenter with respect to the surface of the specimen after it had been lowered without load. The observation was carried out with the aid of a microscope (x 25) which was directed at a small angle to the surface of the specimen (Fig. 1). Cleavage planes of rock salt, bismuth or zinc (metal crystals are more convenient, as they are better reflectors) served as the surface. The position of the indenter tip relative to the surface of the specimen may be accurately established by observing the diamond tip and its image in the mirror surface of the specimen in the microscope. Since the apparent distance between the tip and its image is twice as great as the distance of the tip from the surface of the specimen, the effective magnification of the microscope is 50.

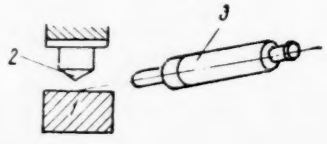

Fig. 1 Diagram of the arrangement of the microscope for observing the process of introduction: 1 – testpiece; 2 – indenter; 3 – microscope.

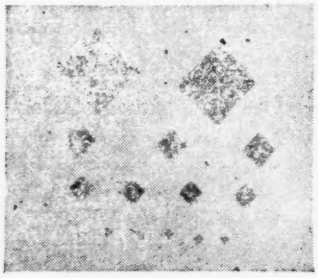

Fig. 2 Indentations on the cleavage surface of a freshly sheared signdl crystal under loads of; 0; 0.5; 1; 5 g; x 464.

When the instrument is adjusted, as is expected, the indenter lowered without load remains noticeably above the surface of the specimen. The oscillation of the indenter caused by the very small vibrations of the instrument, which are difficult to eliminate, can be seen very clearly during this observation. The instrument is adjusted by lowering the loading mechanism until the point of the freely lowered indenter and its mirror image coincide at one point. In this case the diamond tip can be arranged with respect to the testpiece surface with an accuracy of up to $\pm 2\mu$, which corresponds to a deviation in loads of ± 0.03 g. We preferred to have an error on the side of the smaller value, so the loading mechanism was set roughly 2 mm lower, in order that the indenter always gave the same indentations on the soft material without load. These indentations were small and in all cases corresponded to a load not larger than 0.1 g (checking was carried out by interpolating the curve of the relationship between microhardness and load). Hence we assumed that the maximum deviation in the magnitude of the load under the described adjustment was ± 0.1 g.

The speed with which the pyramid is lowered should also exert an influence on the size of the indentations obtained. In our case, the quoted microhardness values are obtained as a result of imposing the dynamic load on to the static. The latter circumstance should have no importance in the case of a sufficiently deep indentation on account of the rapid absorption of kinetic energy of the mechanism being lowered in the top layers of the surface, but is important in the range of minimum loads. In our opinion, the major part of the substantial divergency in hardness values at low loads which have been obtained by different investigators, are the result of the different speeds at which the indenter has been lowered and the different masses of the part of the loading

mechanism, which is lowered, for instruments of every type.

In our measurements the process of the introduction of the indentor into the specimen was observed through the microscope referred to above. The introduction was made in the following way: at first the indenter was lowered comparatively quickly, but when the tip was close to the specimen surface it was lowered on to the surface as slowly as possible. After short training the technique of lowering the indenter at the necessary low speed can be mastered.

The methods described for adjusting the instrument and introducing the indenter on to the specimen, should undoubtedly substantially reduce the errors caused by inaccuracy in the adjustment of the instrument and the imposition of the dynamic load. In actual fact, hardly any scatter was observed in the sizes of the indentations obtained, even at a load of 0.5 g, using the method described above. It was so slight that it lies well within the range of errors in the measurement of the diagonals. The forms of the indentations obtained on the cleavage plane of a bismuth crystal under loads down to 0.5 g, are shown in Fig. 2.

VOL. 8 1959

RESULTS OBTAINED

Measurements were made on a single crystal specimens of rock salt, zinc and bismuth. The microhardness was measured on the cleavage surface of all the specimens both for a freshly sheared fragment, for testpieces annealed after cleavage at 100°C for 5 hr,

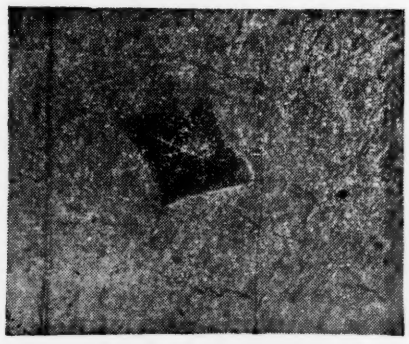

Fig. 3 Indentation on the basal plane of a zinc single crystal obtained after annealing for 5 hr at 100°C. Load 50 g; x 408.

and also on the surface of testpieces aged at room temperature for several days. Since no substantial difference in the hardness values for these testpieces was detected, data is only given below for the untreated fresh cleavage planes.

The hardness of the zinc single crystals was measured both on a basal plane and also on a prismatic plane of the first order. The difference in their microhardness is also slight, so here microhardness values are only given for the basal cleavage plane.

Investigations were carried out on two instruments with the aid of which completely identical results were obtained. The summits at the tops of the diamond pyramids were 0.6 and 0.7 m.

As Schulz and Hanemann [8], showed, when the diamond pyramid is rotated about its axis different hardness values are obtained for the same crystal planes. In our investigations no substantial change was observed in the size or shape of the indentations when the pyramid was rotated about its own axis for indentations with diagonals less than 15 μ. Noticeable distortions were observed for zinc and bismuth in the case of large indentation sizes. These distortions comprise the deviation of the indentation from the correct square shape. We shall not discuss all the shapes observed for the distortion of the indentations. We only note that when the indenter is oriented in a certain direction on cleavage planes of zinc and bismuth the distortions often take place along one diagonal. In this case the indentations are of a rhombic form. (Fig. 3). The length ratios of the diagonals are roughly equal: for zinc – 1.3; for bismuth – 1.12. In the experiments with zinc and bismuth only indentations which had a rhombic form were measured. After both diagonals had been measured the microhardness was calculated from their geometric mean value.

As can be seen from Tables 1, 2 and 3, the microhardness in all the cases considered depends mainly on the load applied and increases when the loads are reduced.

In order to be more conclusive about the results of the increase in microhardness in the range of minimum loads the loading mechanism was lowered slightly more than in the case of accurate adjustment. The errors caused in this case by the deviation of the

TABLE I

Microhardness values for a fresh cleavage section of rock salt.
Plane (100)

Load, q	Indentation diagonal mk	Microhardness, kg/mm^2	Measurement errors, %	
			plus	minus
0.5	5.82	27.2	11	31
1	8.68	24.5	8	18
2	12.7	23.0	4.5	9.5
3	15.65	22.7	4.5	7.5
4	18.6	21.5	4.5	6.0
5	21.4	20.1	2.5	3.5
10	30.5	19.9	2.5	2.5
20	43.9	19.2	2.5	2.5
50	71.3	18.2	1.0	1.0
100	102	17.7	1.0	1.0

TABLE 2

Mean microhardness values for a fresh cleavage section of a zinc single crystal.
Plane (0001)

Load, q	Indentation diagonal, mk		Microhardness kg/mm^2	Measurement errors, %	
	long	short		plus	minus
0.5	3.01	3.01	102	17	37
1	4.65	4.65	86.0	15	25
2	7.12	7.12	73.0	9.6	15
3	8.74	8.74	73.0	5.5	8.0
5	12.0	12.0	65.0	3.0	4.0
10	20.4	17.8	51.0	2.0	2.5
20	30.1	23.6	51.0	5.0	5.0
50	51.1	39.7	45.0	4.4	4.4
100	77.2	60.7	39.0	5.0	5.0
150	94.8	73.7	39.0	5.0	5.0
200	118	86.2	37.5	5.3	5.3

load and by the speed with which the pyramid was lowered can only give the microhardness values given below. The increase in microhardness can only be caused by the scatter in indentation sizes under a constant load, the negligibility of which has already been shown. *

The relationships produced between the indentation sizes and load satisfy the Mayer rule to a good approximation in which $P = ad^n$ (P is the load, d is the indentation diagonal and a and n are constants for the material under investigation). In Fig. 4 it is shown that the relationship between $\log P$ and $\log d$ is roughly of a straight line form. The values of the constants a and n calculated by a method of smallest squares, are given in Table 4, from which it can be seen that on passing from a comparatively soft material to a harder one the constant a increases while n diminishes.

* Flexible restoration of the indentations is not discussed here.

TABLE 3.

Mean microhardness values for a fresh cleavage section of a bismuth single crystal.
(Plane III)

Load, g	Indentation diagonal, mk		Microhardness kg/mm^2	Measurement errors, %	
	long	short		plus	minus
0.5	6.38	6.38	22.7	9.0	29
1	9.62	9.62	20.0	7.5	17.5
2	14.6	14.6	17.3	5.8	10.8
3	19.4	17.6	16.3	6.0	8.6
5	24.3	22.5	17.0	6.0	7.0
10	36.0	31.6	16.2	6.0	6.0
20	52.0	45.2	15.7	6.0	6.0
50	82.5	76.2	14.7	4.0	4.0
100	116	107	14.9	3.3	3.3

VOL. 8 1959

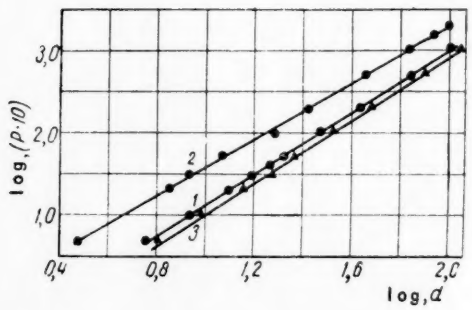

Fig. 4. Relationship between *log P* and *log d* for: 1 – rock salt; 2 – zinc; 3 – bismuth.

It can be concluded from the above that the investigated cleavage planes of crystals of rock salt, bismuth and zinc satisfy all the requirements made of standard specimens for microhardness testing; it can be assumed that zinc and bismuth single crystals, together with rock salt single crystals can be successfully used as standards, especially under low loads (10 g and less). Their microhardness depends little on the ageing at room temperature. A suitable surface without any noticeable strain hardening is obtained easily and rapidly by cleavage. The surfaces produced are very clean and convenient for measuring the indentations in reflected light. No roughness (at least larger than 200 A) is detected when the indentations are checked with an interference microscope. It is also not difficult to produce single crystal zinc and bismuth specimens. Single crystals of bismuth can be produced by sucking the melt into glass test tubes. Methods of producing single crystals of zinc are not complicated and have been well developed [9-11].

TABLE 4

Values of the constants calculated by the least square method.

Single crystals	a, kg/mm^2	n
Rock salt	16.8	1.88
Zinc	71.1	1.72
Bismuth	12.5	1.90

I should like to express my sincere thanks to academician E.L. Andronikashvil of the Akad. Nauk. SSSR for his constant advice on this work, to my scientific fellow workers D.M. Chigninadze, I.A. Nashkidashvil and G.I. Natsvlishvil for valuable discussion of the work.

CONCLUSIONS

A new method of adjusting the PMT-3 instrument and for introducing the diamond pyramid into the specimen under test is proposed. These methods take longer than the normal, but their use is expedient, especially for work in the field of small loads, where it is

extremely difficult to obtain accurate results by the normal method.

The relationships between the microhardness values and load are given in the interval from 0.5 to 100 g for the cleavage planes of crystals of rock salt, bismuth and zinc. It appeared that in all cases the microhardness increases when the load is reduced. The relationship between the size of the indentation and the load is in good agreement with the Mayer ratio. The numerical values of the constants a and n are given.

Opinion is expressed that single crystal testpieces of bismuth and zinc can be successfully used together with rock salt crystals as standard materials for microhardness tests.

Translated by A.H.R. Langmead

REFERENCES

1. B.S. Ioffe, *Zh. teor. fiz.*, 19, 189 (1949).
2. D.B. Gogoberidze, and N.A. Kopatskii, In book; Mikrotverdost' (Microhardness) *Izd. Akad. Nauk. SSSR* (1951).
3. A.A. Bochvar In book: *Mikrotverdost' (Microhardness)*, Izd. Akad, Nauk, SSSR (1951).
4. V.A. Egorov, In book: *Mikrotverdost' (Microhardness)*, Izd. Akad. Nauk. SSSR (1951).
5. O.N. Mgebrian, D.M. Chigvinadze and Ts.M. Salikvadze, *Proceedings of Akad. Nauk. Gruz. S.S.S.R.*, 12, 457 (1951).
6. E.M. Shevtsova and T.V. Lebedeva, In book: *Microtverdost' (Microhardness)*, Izd. Akad. Nauk. SSSR (1951).
7. A.A. Bochvar and O.S. Zhadaeva, *Izd. Akad. Nauk. SSSR, otd. tekh. nauk* 3, 341 (1947).
8. F. Schulz and H. Hanemann; *Z. Metall*, 33, 134 (1941).
9. D.M. Chigvinadze, *Proceedings of Akad. Nauk. Gruz. S.S.R.*, 9, 19 (1948).
10. D.M. Chigvinadze, *Zh. teor. fiz.* 25, 805 (1955).
11. B.N. Bushmanov, *Fiz. metal. metalloved*, 4, 310 (1957).

VOL 8 195

A STUDY OF THE MECHANICAL PROPERTIES OF SOLIDS, IN PARTICULAR OF METALS AT ABSOLUTE TEMPERATURES OF 4.2°K AND BELOW. 1. TENSILE TESTING OF POLYCRYSTALLINE ALUMINIUM (99.3%)*

O.V. KLYAVIN and A.V. STEPANOV

Leningrad Physico-Technical Institute Akad. Nauk. SSSR

(Received 11 July 1958)

A description is given of the experimental methods used for tensile testing different materials at temperatures of 4.2°K and below. The results are given, which were obtained for 99.3 per cent polycrystalline aluminium in the annealed and unannealed conditions at temperatures of 4.2 and 1.6°K.

VOL. 8 1959

The relationship between the strength and ductility and the temperature in the 4.2-1.6°K interval was found.

The ductility and strength of solid bodies are functions of the temperature. Data on the ductility and strength at extremely low temperatures close to the absolute zero, are fundamental characteristics, without knowledge of which it is impossible to formulate correct theoretical assumptions on these properties.

All theoretical estimations of the strength and ductility of solid bodies have been carried out up till now without taking into account the thermal movement, that is they give an idea of these properties at extremely low temperatures. Naturally the findings should be compared with the experimental data relating to low temperatures. As there is no experimental data available on the mechanical properties of solid bodies at very low temperatures the theoretical estimates of the strength characteristics were compared with the experimental data available, which referred to "high" temperatures. It is clear that a comparison of this kind may lead to false conclusions as to the agreement or disagreement of the results of theory and experiment.

Data on the mechanical properties of solid bodies at very low temperatures are also very important from the practical point of view, especially in the selection of materials.

We knew of only three papers on the study of the ductility of solid bodies at liquid helium temperatures. These are the paper by Polany and Meissner [1], which is devoted to the study of the ductility of single crystals of zinc and cadmium, and papers [2, 3], on copper. Here also mention should be made of papers [4-7].

In spite of the importance of the data on the study of the ductility of solid bodies carried out in papers [1-7], the volume of these investigations clearly do not apprehend the importance of the problem. We knew of no paper in which comprehensive stress-strain diagrams had been made and strength characteristics found for materials in the range of liquid helium temperatures. On that ground we began systematic investigations of the mechanical properties of solid bodies at temperatures of 4.2°K and below.

The first stage of the investigations was the development of an apparatus for testing a number of materials and obtaining their stress-strain diagrams up to breaking loads at temperatures of 4.2°K and below.

Polycrystalline aluminium (99.3 per cent) in annealed and unannealed conditions was tested at the following temperatures: 1.6°K (liquid helium under evacuation), 4.2°K (the boiling point of liquid belium), 78°K (the boiling point of liquid nitrogen), 300°K (room temperature). The tests at 78 and 300°K were carried out in order to correlate

* *Fiz. metal. metalloved.* 8, No. 2, 274-281, 1959.

the results of our tests obtained at 1.6 and 4.2°K with the reference data which refer to higher temperatures.

APPARATUS AND TEST CONDITIONS

A problem in the investigation was the plotting of the stress-strain and stress-rupture diagrams for the testpieces at liquid helium temperatures. At this stage of the work the object was not the accurate investigation of the initial section of the stress-strain diagram. These initial conditions also determined the choice of the measuring apparatus.

Tests were carried out on an Stepanov [10] machine, adapted for measuring at liquid helium temperatures (Fig. 1). The bottom part of the machine containing the testpiece was accommodated in a Dewar vessel (vacuum flask jacket) containing liquid helium, which in turn was accommodated in a Dewar vessel containing liquid nitrogen. The testpiece was placed directly in liquid helium*. Appliances were included in the design of the machine for preventing leakage of the gaseous helium.

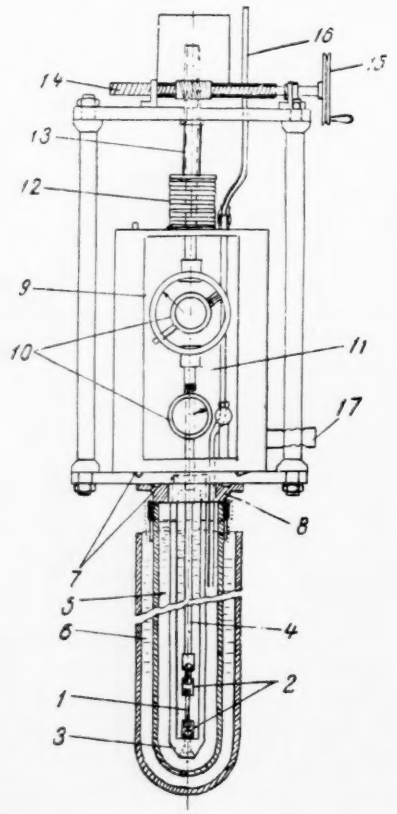

Fig. 1 Diagram of the machine for tensile testing testpieces at liquid helium temperatures

The dimensions of the testpieces were determined by the necessity of making that part of the machine, which is immersed in helium, as small as possible, but at the same time sufficiently rigid and strong, as the introduction of large amounts of metal into the liquid helium makes it difficult to produce low temperatures.

The force was measured with the aid of an elastic dynamometer, the deformation of which was measured by readings from a dial taken to an accuracy of ± 0.005 mm. The elongation of the testpiece was found by measuring the displacement of the upper rod of the machine and reading from a dial to an accuracy of up to ± 0.01 mm. The elastic deformations of the machine, which were calculated from the stress-strain diagrams, were taken into account, this is especially important in the case of low ductility materials. The dimensions of the testpieces before and after the deformation were measured by an MIR-12 microscope with an accuracy of up to ± 0.005 mm.

The temperature of the experiment was determined from the helium vapour tensions. The elongation rate was in the range of from 0.4 to 1.6 mm/min. At liquid helium temperatures the time for pulling ductile testpieces, for example aluminium, from the beginning of the experiment to rupture was about 14 min.

3-4 testpieces were tested at temperatures of 1.6 and 4.2°K.

The data of tests on separate testpieces (standard specifications [8]) are given in Table 1. In this case, if the deviation from the mean value for all tests at the given temperature does not exceed 7 per cent, the data given is that of a typical test. If the maximum deviations in the behaviour of the separate testpieces are considerably, either these maximum values are given or the cases are specially mentioned.

For all testpieces tested at the given temperature the characteristics given in

* The testpiece was also placed directly in the liquid nitrogen during testing in this medium.

VOL 8 195

TABLE I

Strength characteristics of annealed aluminium testpieces.

Number of experiments	T, °K	σ_b, kg/mm²	σ_z, kg/mm²	s_b, kg/mm²	s_k, kg/mm²	ψ_b, %	ψ_k, %	ε_k, %	Literature source
4	1.6	30	30	34	151/105	10	78	37	Data of this paper
5	4.2	32	30	45	115*/70	30	57	47	
3	78	16	8	21	70/58	26	89	42	
8	300	8	5	9	54/20	18	95	29	
–	20	35	–	–	76	–	66	45	Data of [4] s_k is calculated from [8]
–	78	21	–	–	49	–	75	42	
–	300	12	–	–	31	–	86	29	
–	300	–	–	–	14	–	85	20	[9]
–	348	–	–	–	13	–	83	24	
–	408	–	–	–	11	–	88	32	
–	583	–	–	–	4	–	97	39	
–	673	–	–	–	2	–	99	42	
–	783	–	–	–	1	–	99	45	
–	873	–	–	–	0.6	–	100	42	
–	933	Melting point of aluminium							

* The value of s_k is calculated from paper [8], as the test piece broke at an angle of 45°.

Tables 1 and 2, with the exception of the true tensile strength s_k differ little from one another (± 7 per cent). Both the maximum and minimum of the values observed for a_k are given in Tables 1 and 2. The values of ξ_k are given in the stress-strain diagram. The testpieces were in the shape of wires with heads, with a working length of l = 20 mm and a diameter of from 1.2 to 1.6 mm. The testpieces were made on a lathe. After they were taken from the lathe the surface of the working part was not subjected to further treatment. More or less uniform cutter traces were left on the surfaces of the testpieces to a depth of 1-2 μ.

RESULTS OF THE INVESTIGATION

Polycrystalline annealed aluminium (99.3 per cent). Testpieces of length 20 mm and diameter 1.2 mm were cut from grade AD-1 aluminium wire of the following composition: 0.5% Cu; 0.3% Fe; 0.35% Si; other admixtures about 0.1% and annealed in a vacuum of about 10^{-4} mm of Hg at 300°C for one hour with subsequent cooling in the furnace for 3-4 hr. The test results for the testpieces are given in the form of stress-strain curves* in Fig. 2 and in Table 1.

As the test results showed, the ductility of the aluminium is maintained right down to very low temperatures. At 1.6°K the stress-strain diagram has an unusual shape: several drops, shown in Fig. 2** apear on it before rupture.

Curious changes in the nature of the fracture are observed when the temperature is reduced. At 78°K fracture takes place with

* In all the figures stress-strain curves are given for testpieces on which maximum value were observed for a_k and ϵ_k.

** The question of the structure of the drops will be discussed in a separate paper.

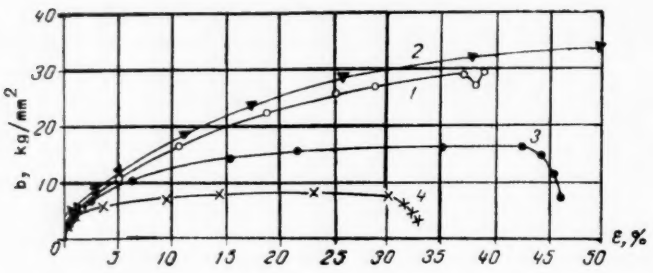

Fig. 2. Stress-strain curves for testpieces of annealed aluminium at different temperatures of: 1-1.6; 2-4.2; 3-78; 4-300°K.

hardly any neck formation.

The surface of the rupture on the ruptured testpiece is seen to be inclined at an angle of approximately 45° (±2°) to the axis of the testpiece.

The elongation up to fracture, is almost completely uniform, very small local necking, which is stretched out toward the area of fracture is seen (Fig. 3). At 1.6°K rupture again takes place with the formation of a neck, somewhat smaller than at room temperature and the temperature of liquid nitrogen.

In Fig. 4 the change in the nature of the rupture of the testpieces depending on the temperature is shown. Here photographs of the silhouettes of the places of rupture at different temperatures* are shown.

It should be emphasized that five repeated tests were carried out, which all gave the same result, so that the phenomenon, shown in Fig. 3, should be considered not as chance, but as a fair representation of the work.

The area of the testpiece at the moment of rupture was determined thus: the contour of the rupture point was drawn with the aid of a drawing device during microscope observation, and the area of this contour, after allowing for the magnification, was taken as the area at the moment of rupture. In this case the testpiece was placed on the microscope so that its axis was parallel to the axis of the microscope. The contour of the area of rupture was always irregular in shape. The area determined in this way was always less than the area determined from the diameter of the narrowest point of rupture, if it is assumed that its contour is round (the universally accepted method of determining the area at the moment of rupture).

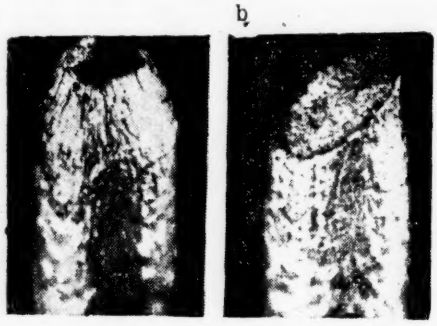

Fig. 3. Photographs of annealed aluminium testpieces, which ruptured at temperatures of: a – 1.6; b – 4.2°K; X 20.

The values of s_k obtained for 300°K, as can be seen from Table 1, are higher than the reference data. This difference is partly caused by the fact that our area at the moment of rupture was determined differently from that in the accepted method. It is also possible that the error in the determination of the force at the moment of rupture was determined differently from the accepted method. It is also possible that it is an error in the determination of the force at the moment of rupture. Should the material to be tested be ductile, a dynamometer of smaller inertia should be used for determining

* The silhouettes of the places of rupture for all the materials investigated are taken at the same magnification. The difference in the diameters of the ruptured testpieces, which is visible on the photographs, is produced as a result of the different degree of plastic deformation, which takes place at different temperatures.

the force at the moment of rupture.

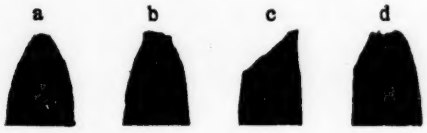

Fig. 4. Silhouette photographs of the points of rupture on annealed aluminium testpieces at temperatures of: a – 300; b – 78; c – 4.2 and d – 1.6°K.

Thus, it is quite possible that we have overestimated the values of s_k given in Table 1 and in other cases in our tests on ductile testpieces. These observations for s_k refer also to aluminium in the unannealed condition.

It can be seen from Fig. 4 that a reduction of the temperature to 4.2°K leads to an increase in the strength characteristics of the process of deformation (the growth in the shear strength) together with a considerable increase in the elongation before rupture.

The elongation is increased by increasing its uniform section. In this way, the reduction in temperature stabilizes the process of flow. The localization of deformations, which leads to the formation of a neck at "low" temperatures, is only possible under much larger loads than at "high" temperatures.

The increase in the strength of the aluminium when the temperature is reduced can be seen from the Table 1. At 1.6°K s_k is of the order of 150 kg/mm^2, which does not differ very much from the theoretical tensile strength of aluminium determined as $0.1E$ (where E is Young's modulus, which is equal to 800 kg/mm^2 for low temperatures).

Obviously, there is also a temperature relationship for the ductility and strength for temperatures even lower than 1.6°K (this problem still requires experimental examination). Therefore still higher strength values may be expected in the case of tests carried out at temperatures lower than 1.6°K.

We found it more convenient to represent the strength temperature relationship not as the function $s_k = f(T)$, where T is the absolute temperature, as is usual, but as the function $1/s_k = f(T)$. The reasons for this are the same as those for which the results obtained in the study of the temperature relationship of the electrical properties of metals are given in the form of the dependence of the conductivity and not the electrical resistance on the temperature.

An attempt was made to establish the form of the relationship

$$1/s_k = f(T)$$

The data for establishing such a relationship is inadequate, therefore this attempt should be regarded as a preliminary consideration of the data obtained.

The results of further investigations can introduce a change here.

The values of $\ln 1/s_k$ depending on $1/T$ are given in Fig. 5. The graph is plotted from the data of papers [4, 9] and this paper, both the maximum and minimum values of s_k being used. The results are plotted as two straight lines.

It can be seen from Fig. 5 that in the strength temperature relationship there are two sections – the "high" temperature (20-78°K) zone and the "low" temperature (20°K and below) zone. In both zones the experimental data satisfy the relationship

$$\frac{1}{s_k} = A \cdot e^{-\frac{B}{T}}, \qquad (1)$$

but with different values for the constants A and B.

In the low temperature zone the influence of the temperature on the strength is considerably weaker than in the high temperature zone, but it exists all the same.

On extrapolating this relationship to the theoretical strength value $s_k = 800$ kg/mm^2, we see that it can be achieved at 0.3°K (extrapolation for the maximum values of s_k) or at 0.5°K (extrapolation for the minimum minimum values of s_k). It is clear that this temperature will alter, if other values are obtained in subsequent experiments for the magnitudes of s_k.

Unannealed polycrystalline aluminium (99.3 per cent). The polycrystalline aluminium testpieces were not annealed. The influence of the temperature was even greater in this case than for annealed testpieces.

Ductility was preserved right down to 1.6°K. The elongation up to rupture increased considerably when the temperature was reduced. Thus at 1.6°K a strain hardened

VOL. 8 1959

aluminium testpiece stretches five times more before rupture than at 300°K. At 4.2°K there is no difference between the behaviour of a strain hardened testpiece and one which has not been strain hardened.

Consequently, the localization of deformation in strain hardened crystals at high temperatures and the low ductility before rupture are also determined by the defects created prior to this by plastic deformation in the testpiece.

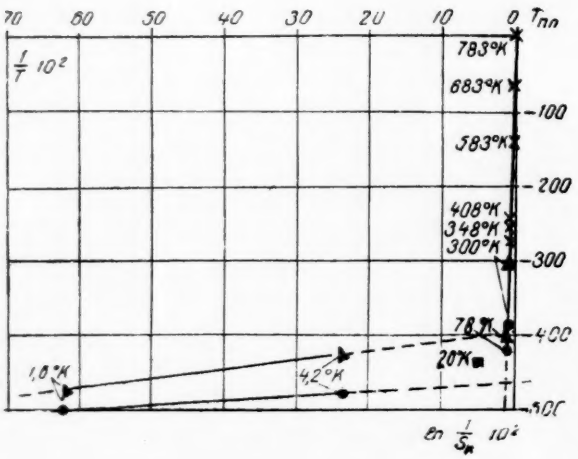

Fig. 5. Relationship between the logarithm of the reciprocal value of the true tensile strength and $1/T$ (T – temperature in absolute units).

• – for the maximum values of s_k; ▲ – for the minimum values of s_k; x – according to the data of paper [4]; ■ – according to the data of paper [9])

The test results are given in Fig. 6 and Table 2.

The drops on the stress-strain diagrams at 1.6°K are sharper than for annealed aluminium and occupy a considerable portion of the stress-strain curve.

The change in the nature of the rupture with temperature is seen in Fig. 7, in which are shown photographs of the silhouettes of the places of rupture of testpieces at different temperatures. The form of the rupture at 4.2°K is different to those at 78 and 1.6°K.

CONCLUSIONS

1. Considerable plastic deformation before rupture is observed in industrially pure aluminium (99.3 per cent) even at 1.6°K. In certain cases this plastic deformation considerably exceeds the magnitude of deformation observed at 300°K.

2. Sharp drops were observed on the stress-strain diagrams for aluminium at 1.6°K.

3. A change in the nature of the rupture was observed for aluminium in the range from 4.2 down to 1.6°K.

4. The temperature strength relationship may be divided into two parts (cf. Fig. 5).

5. A temperature influence on the properties of strength and ductility was observed in the interval of temperatures from 4.2 to 1.6°K. Obviously, it must also appear at even lower temperatures. Hence follows the necessity of studying the strength and

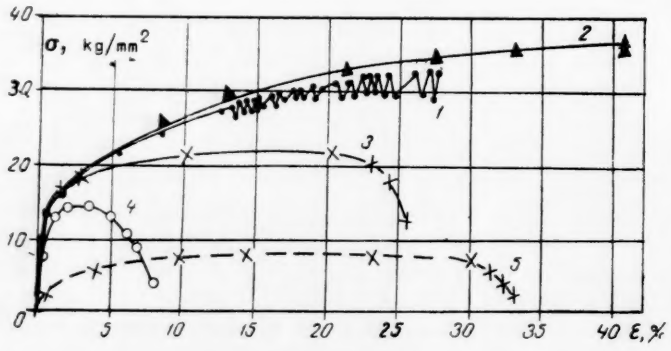

Fig. 6. Stress-strain curves for unannealed aluminium testpieces at different temperatures of:
1 – 1.6; 2 – 4.2; 3 – 78; 4 – 300; 5 – 300°K (annealed).

TABLE 2

Strength characteristics of unannealed aluminium testpieces

Number of experiments	T, °K	σ_b, kg/mm²	σ_z, kg/mm²	s_b, kg/mm²	s_k, kg/mm²	ψ_b, %	ψ_k, %	ε_k, %
3	1.6	35	35	42	198/178	16	82	26
2	4.2	37	36	49	89*/77	24	29	38
2	78.0	21	12	25	76/66	15	83	24
3	300.0	14	4	14	44/38	1	91	7

* s_k - is calculated from paper [8], as the test piece broke at an angle of 45°

VOL. 8 1959

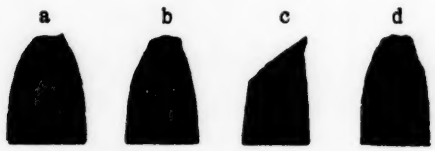

Fig. 7. Silhouette photographs of the points of rupture of unannealed aluminium testpieces at different temperatures of: a - 300; b - 78; c - 4.2; d - 1.6°K.

ductility properties at still lower and ultra-low temperatures.

6. The true tensile strength is seen to increase when the temperature is reduced for pure metals, the absolute values of the true tensile strength at 1.6°K being close to the theoretical strength values. The strength of heavy-gauge aluminium testpieces at low temperatures is practically equal to the strength of thread-like crystals - (whiskers), which have anomalously large strength values (this was attributed to the peculiar properties of thread-like crystals). There is no data for aluminium "whiskers" in the reference literature, but their strength barely exceeds the strength of silver "whiskers" ($\simeq$ 180 kg/mm²) and of copper ($\simeq$ 300 kg/mm²). [11].

Translated by A.H.R. Langmead

REFERENCES

1. W. Meissner, P. Polany and E. Schmid, *Z. Phys.* 66, 477 (1930).
2. T.H. Blewitt, *Phys. Rev.*, 91, 145 (1953).
3. T.H. Blewitt, R.R. Coltman and I.K. Redwan, Rep. Conf. *"Defects in Crystalline Solids"*, London, (1955).
4. V.I. Kostenets *Zh. teor. fiz.* 16, 515 (1946).
5. I.W. Glen, *Phil. Mag.*, No. 5, May (1956).
6. V.I. Khotkevich and V. Golik, Book dedicated to the 70 year old academician A.F. Ioffe, *Izd. Akad. Nauk. SSSR* (1950).
7. V.I. Khotkevich, *Fiz. metal. metalloved.*, 3, 2 (1956).
8. N.A. Shaposhnikov, *Mekhanicheskie ispytaniia metallov (The mechanical testing of metals)*, Moscow-Leningrad, Mashgiz, p.133 (1954).

* Papers have recently been published on the tensile testing of aluminium at 4.2°K. Some of the phenomena observed by us, in particular, the presence of sharp drops on the stress-strain diagrams, were shown in these papers independently of our results.

We still cannot agree with the explanation of the nature of these sudden drops on the stress-strain diagrams given by Basinski [12], in spite of the fact that as far back as 1933 Stepanov [13] attempted to explain the phenomena accompanying plastic deformation in crystals as "local" evolutions of the heat of deformation.

9. Encyclopaedia handbook *"Mashinostroenie" ("Engineering")*, 3, p. 313 (1947).
10. A.W. Stepanow, *Phys, Z. Sowjetunion*, 8, 25 (1935).
11. S.S. Brenner, *J. Appl. Phys.*, 27, No. 12, 1484 (1956).
12. Z.S. Basinski, *Proc. Roy. Soc.*, 240, 229 (1957).
13. A.W. Stepanow, *Phys. Z. Sowjetunion*, B45, H. 4-5 (1933).

VOL
8
195

MECHANISMS OF PLASTIC FLOW FOR LEAD AND TIN IN SHEAR CONDITIONS*

V.I. LIKHTMAN and V.S. OSTROVSKII

Institute of Physical Chemistry of Akad. Nauk. SSSR

(Received 27 February 1958)

The general rheological mechanisms of the plastic flow of tin and lead in shear conditions are established. A constant maximum value of plastic viscosity, which does not depend on the stress, is found at low stresses. Under large stresses the sharp drop in the plastic viscosity with the growth of the shear rate results in a shear stress, which is independent of the rate of deformation. When the temperature is increased the plastic viscosity is naturally reduced as a result of the increase in the flow rate of the metal and the reduction of the creep limit.

VOL. 8 1959

Knowledge of the main rheological characteristic of metals – the effective viscosity – is either contradictory or non-existent 1. A knowledge of the rheological properties of metals can be very useful for processes of deformation and working, especially in the study of creep phenomena, the limiting creep stress and in the pressure shaping of metals.

According to the nomenclature proposed by P.A. Rebinder, the metal should be in the form of structuralized systems which have a dense crystal structure and, in consequence, a perfect contact between the structural elements (the crystals [2]). These structures, if they are capable of plastic (residual changes in shape, are characterized by the very high values of effective viscosity in the region of low stresses (up to 10^{20} poise) and the sharp reduction in the viscosity (by 8-10 powers) in a comparatively short interval of stresses, which corresponds to the practical creep limit.

Pure metals and the majority of alloys are capable of plastic changes in shape, owing to the high ductility of the crystals forming them. However the smaller the capacity of polycrystalline metals for large plastic deformation the greater is the ductility of the individual grains. This is explained by the fact that the maximum ductility is peculiar to those metal single crystals, which have one slip plane, for example, single crystals of the hexagonal system – zinc, cadmium or magnesium. An increase in the number of possible slip planes leads to a reduction in the ductility and an increase in the strength (single crystals of the cubic system). But the presence of one solitary system of slip in metals of hexagonal structure leads to an increase in the brittleness of the polycrystalline testpieces as a result of the grains interlocking with adjacent grains. In metals of cubic structure, for which there are 12 possible slip systems, this grain interlocking only slightly reduces the ductility of the polycrystalline testpieces in comparison with that of single crystals.

Metals with a crystal structure also have singular thixotropic properties, connected with the restoration of the structure disturbed during deformation. The feature of these properties is that the structures of the metals disturbed during deformation are always accompanied by an increase in the yield strength (strain hardening), and the restoration of the disturbed structure in the deformed metals is always connected with a reduction in the yield strength (relaxation, recrystallization), whereas in systems with a coagulation structure (clay solutions and other colloidal systems) restoration of the structure partially destroyed in the flow is always accompanied by an increase in the yield point and yield strength.

In all processes of deformation and work-

* *Fiz. metal. metalloved.* 8, No.2, 282-287, 1959.

ing the metal acts like a viscous medium, the flow of which is analogous to the flow of a viscous liquid. This analogy can be traced very easily to soft metals, for example, to lead or tin, when a hole is punched through them. If a cylindrical tin or lead testpiece is cut along the generatrix and a square grid is placed on the obtained flat surfaces, and then if these two halves are joined and a hole is punched through the least diameter, then the distribution of the rates of deformation in the metal, which may be estimated from the shape of the grid after punching, will not differ in principle from that for the flow of a viscous liquid [3]. Hence, it would seem that under certain conditions of deformation the crystal structure of the metals does not play an important part, and in these cases the mechanical properties of the metals may be given by the Newton equation $P = \eta \times v$, where η is the viscosity. However the numerous attempts to determine the magnitude of η for different metals have invariably led to a large scatter in the viscosity values for any one metal (by 5-6 powers) depending on the conditions under which the experiment has been carried out.

Attempts to improve the agreement of the viscosity values for η for a wide interval of stresses by introducing the yield strength P_m into the Newton formula (that is the transition to the Bingham equation $P - P_m = \eta \times v$) do not lead to positive results [1].

We made a study of the rheological properties of metals (lead and tin) under conditions of simple stress, which occur during pure shear deformation.

We used two types of instrument. The first was designed on the basis of an analogical instrument by Andrade [4]. A diagram of the instrument and the testpiece are given in Fig. 1. The testpieces tested on this instrument are in the form of disks, which are secured at the circumference and in the centre. The load (considerably below the yield strength) which causes rotation of the central part of the disk, is applied to the disk via a central clamp with the aid of a lever. A groove was cut between the circumference and central clamps in the free part of the disk on both sides with a forming cutter so that the cross-section of the cut was regularly reduced as it moved outwards from the centre, thus providing constancy of the shear stress in any cross-section of the groove. Analysis of the stressed state in this testpiece shows that after the load is applied a pure shear deformation is generated in the groove.

A diagram of the second instrument and the shape of the testpieces are given in Fig. 2. We used this instrument mainly for experiments in the presence of different surface active agents. We had established preliminarily that both instruments give results which are in full agreement.

Tin and lead were chosen for the investigation. The mechanical properties of these metals have been studied by many authors in conditions of shear deformation.

After they had been machined the testpieces were subjected to special heat treatment – annealing in an inert atmosphere, in order that the mean grain size was not below a certain threshold value in accordance with the criterion of Amfiteatrova and Iampolskii for the optimum action of a surface active agent [5]. The flow curves of lead are given in Fig. 3 at loads which are different, but constant for each individual experiment. Here a single flow curve is given for lead in a 0.2 per cent solution of oleic acid in vaseline oil under a stress of 0.26 kg/mm^{-2}

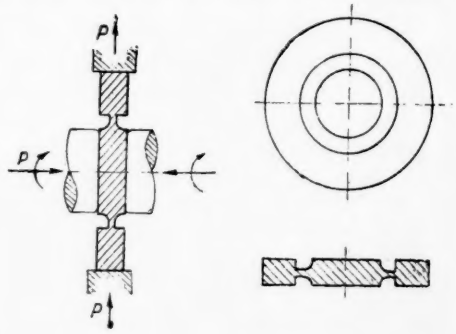

Fig. 1 Diagram of the intrument and testpiece.

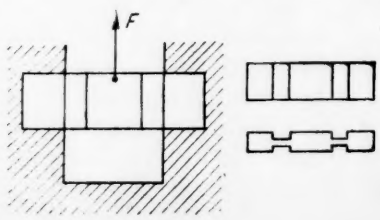

Fig. 2 Diagram of the instrument and testpiece.

Two zones of creep are clearly seen on these curves – the zone of unsettled flow at a reduced rate and the zone of steady flow at a constant minimum rate v_m. The magnitude of v_m increased with the increase in stress, and also at the given stress, in the presence of a surface active agent. Removal of the load leads to a slight elastic recovery and to a very slight elastic secondary effect. An analagous flow is also observed for tin, but at somewhat higher stresses.

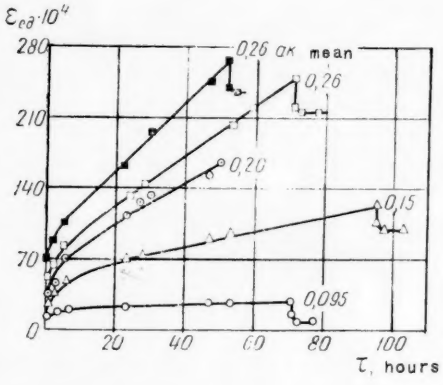

Fig. 3 Curves for the flow of lead at corresponding stresses (kg × mm^{-2})

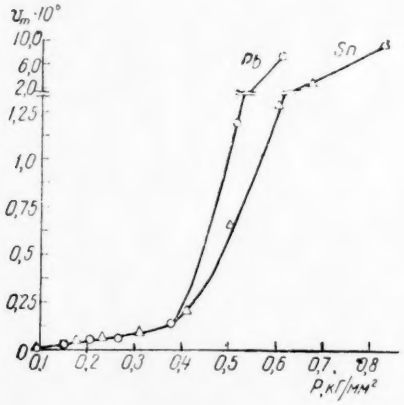

Fig. 4 Relationship between the steady flow rate of tin and lead and the applied stress

The relationship between the rate of steady flow v_m and the applied stress P are given in Fig. 4 for lead and tin.

Attention is drawn first of all to the fact that the initial sections of these curves are rectilinear, that is, in a certain comparatively narrow interval of low stresses, the steady flow rate v_m is directly proportional to the applied stress P. At the same time a noticeable flow of tin or lead only begins when a certain stress P_0 is reached, which can be called the creep limit. the magnitude of the creep limit, ultimately mainly depends on the accuracy with which the deformation is read off and in our experiments was equal to: for lead 0.095 kg × × mm^{-2} and for tin about 0.09 kg × mm^{-2}. Thus in the interval of stresses adjoining the creep limit, the expression $P - P_0 = \eta_0^* \cdot v_m$, in which the viscosity η_0^* remains constant. It has been shown experimentally [6, 7] that there is no creep limit for single crystals of tin ($P_0 = 0$) and the initial plastic flow rate is proportional to the applied stress over a fairly wide range of stresses right down to the yield point: $P = \eta v_0$ where η is the viscosity, which keeps a constant, very high magnitude in the above interval of stresses.

The value of the maximum plastic viscosity η for tin single crystals may be calculated from the data of papers [6, 7]: $\eta = P/v_0 = 3.2 \times 10^{13}$ poise. Calculation of the maximum plastic viscosity of polycrystalline tin from the curve of Fig. 4 gives $\eta_0^* = \frac{P - P_0}{v_m} = 3 \times 10^{14}$ poise. A similar value of η_0^* is also obtained for lead.

As was to be expected, the maximum plastic viscosity of polycrystalline tin proved to be an order above the corresponding viscosity of the single crystal.

It should be mentioned that estimation of the viscosity from the initial plastic flow rate, although it has the advantage, that it gives a viscosity value for metal, which has not been strain hardened, at the same time it has the substantial disadvantage, that it is very difficult to measure accurately the magnitude of the initial rate. If for single crystals, in which there is practically no zone of elastic deformation, the initial plastic flow rate can still be accurately changed, then for polycrystalline metals the errors in the measurement of the initial rate are so large that it is impossible to use this value for determining the viscosity.

In the zone of steady plastic flow, when

the rate of deformation remains constant over a long period of time, its magnitude can be measured very accurately. In this case the viscosity values calculated using the constant steady flow rate are found to be rather higher than for a metal which has not been strain hardened.

The relationship between the plastic viscosity $\eta_0^* = \frac{P - P_0}{v_m}$ of tin and lead and the stress are given in Fig. 5. The maximum constant value of η_0^* is observed in a small interval of stresses near the creep limit. When the stress increases the magnitude of η_0^* drops continuously and is reduced by 2-3 powers for stresses of 0.7-0.8 kg × mm^{-2}.

A graph is given in Fig. 6 for the relationship between the steady plastic flow rate of lead and the stress in the zone of comparatively high stresses. When the stress is about 0.7 kg × mm^{-2}, the curve giving this relationship rises very steeply and its direction becomes almost parallel to the flow rate axis. On continuing the section of the rheological curve, where it is asymptotically approximated to a straight line before it intersects the stress axis, we obtain a certain stress P_m, which may be taken as the practical yield point (according to Bingham). In actual fact, even in the case of a small advancement from P_m of several hundred kg × mm^{-2} in the direction of higher stresses, the plastic flow rate of lead increases very sharply. It is impossible to exceed the stress P_m by any large magnitude, as in this case the testpiece has already begun to rupture during the experiment (after 20-30 hr).

The magnitude of the plastic viscosity for this zone of high stresses may be written as:

$$\eta_m^x = P - P_m/v_m.$$

But as $P/v_m = \eta$, where η is the effective (Newton) viscosity, then $P_m/v_m = \eta - \eta_m^x$. If $\eta_m^x \ll \eta$, which is also the case in the given zone of stresses, then $P_m = v_m \times \eta$, that is the product of the steady flow rate and the effective viscosity remains constant and equal to the practical yield point. This mechanism, is, apparently, based on the known experimental fact that the shear stress

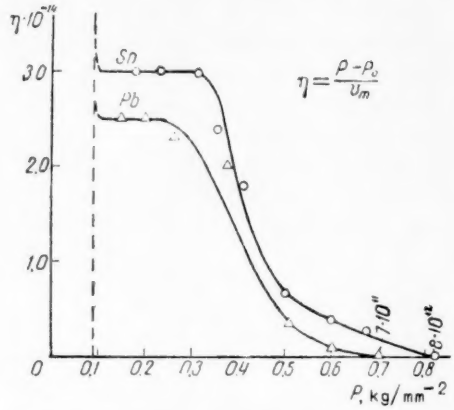

Fig. 5 Relationship between the plastic viscosity of tin and lead and the applied stress

of the metals is independent of the rate of deformation over a wide interval of such rates.

Thus, the effective viscosity of the metals investigated, which is determined according to Newton as $\eta = P/v_m$, alters with respect to the applied stress (falling when it increases) and cannot therefore be a physical parameter characteristic for the given metal. The plastic viscosity of the metal, determined by F. F. Shvedov, as $\eta_0^x = P - P_0/v_m$, in the interval of stresses adjoining the creep limit P_0, remains at a constant value, which does not depend on the applied shear stress, and is then reduced when the stress increases. This very large constant value

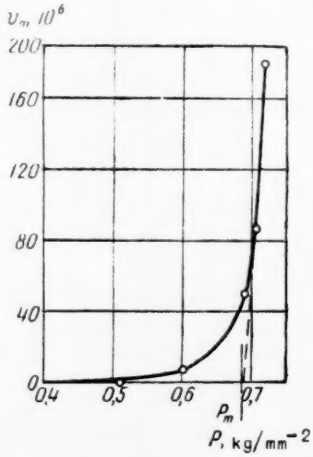

Fig. 6 Relationship between the steady flow of lead and the applied stress in the region of comparatively high stresses.

for the plastic viscosity may be used as a physical characteristic for the metal. In the zone of high stresses close to the shear stress the stress itself was used as the physical characteristic of the metals investigated by us, as in this stress zone the viscosity is inversely proportional to the rate of shear and the shear stress as a result, turns out to be independent of the rate of deformation.

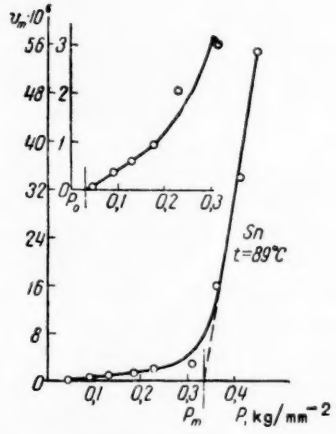

Fig. 7 Relationship between the steady flow rate of tin and the applied stress at 89°C.

The relationship between the steady plastic flow rate of tin at 89°C and the applied shear stress is given in Fig. 7. Here a direct proportionality is also observed between v_m and P in the interval of stresses, adjoining the creep limit. But the creep limit itself P_0 is only equal to 0.03 kg x mm^{-2} at this temperature, which is considerably displaced in the direction of smaller stresses. Calculation of the constant maximum plastic viscosity η_0^* in this stress interval gives $\eta_0^* = P - P_0/v_m = 1.5 \times 10^{13}$ poise, that is at 89°C the viscosity η_0^* turns out to be an order lower than at room temperature.

We should like to express our sincere thanks to academician P.A. Rebinder for his valuable assistance in discussing the results of this paper.

Translated by A.H.R. Langmead

REFERENCES

1. V.D. Kuznetsov *Fizika tverdogo tela (Solid state physics)*, 4, Tomsk. (1941).
2. P.A. Rebinder, *Tezisy doklada na tektonofizicheskom soveschchanii, (The proceedings of the structural physics conference, Institute of earth physics of Akad. Nauk SSSR*, Moscow ((1957).
3. Z.G. Zaks, *Prakticheskoe metallovedenie (Practical metallurgy)*, United Scientific and Technical Press, Moscow (1938).
4. E.N. da C. Andrade and K.H. Jolliffe, *Proc. Roy. Soc.*, A213, 3 (1952).
5. T.A. Amfitestrova and B.Ia. Iampol'skii, *Proc. Akad. Nauk. SSSR.* 82, 5 (1952).
6. B. Chalmers, *Proc. Roy. Soc.* A156, 427 (1936).
7. V.I. Likhtman, P.A. Rebinder and G.V. Karpenko, *Vliianie Poverkhnostno-aktivnoi sredy no protsessy deformatskii metallov, (The influence of surface active agents on the process of deformation in metals)*, Akad. Nauk. SSSR, Moscow (1954).

VOL. 8 1959

THE INFLUENCE OF A LOW MELTING POINT MOLTEN METAL ON THE MECHANICAL PROPERTIES OF SINGLE CRYSTALS OF MORE REFRACTORY METALS*

L. A. KOCHANOVA, V. I. LIKHTMAN and P. A. REBINDER

Institute of Physical Chemistry Akad Nauk S. S. S. R.

(Received 15 October 1957)

Up to the present, the study of the influence of low melting point metals on the mechanical properties of refractory metals and alloys has been carried out using polycrystalline specimens, testing in compression, bend or torsion. The most general result of these experiments is that, in the presence of a molten metal environment, the plasticity and strength of the specimens being deformed in this medium undergo a sharp decrease [1-9].

It has also been discovered that the magnitude of this effect of decreased plasticity and strength under the influence of a fused metal, depends to a great extent on the nature of the metal being deformed, and the nature of the surrounding low melting point molten environment.

In the opinion of some authors [2, 3, 13] molten metals which form solid solutions or intermetallic compounds with the basic metal exert a great effect, whereas the absence of interaction between the basic metal and the molten environment leads to a considerable decrease in the magnitude of the effect. Moreover, the action of the molten metal depends on the mechanical characteristics of the original specimen. The higher its strength and hardness, the sharper will be the action of the medium [4, 7, 8]. Brittle rupture can take place in both the elastic and plastic field, depending on the elastic limit of the steel [7].

The conditions under which the experiments are carried out, plays a substantial role: the character of the stressed state, the rate of deformation or the rate of applying the load, the amount of time for which the specimen is in contact with the molten medium and the temperature at which deformation takes place. Thus, for example, the influence of the molten medium does not appear under the action of compressing stresses [1], but it is very prominent under the action of tensile stresses [1-9]. The effectiveness of the action increases when the rate of applying the load or the rate of deformation is decreased and also with increasing the time for which the specimen is in contact with the molten medium prior to testing [1-5]; the effectiveness of the action of the molten medium grows rapidly with increasing the temperature of the experiment [1, 7-9].

The experimental data concerning the influence of molten metals on the mechanical properties of refractory metals has not yet been exhaustively explained. Many authors put these phenomena down to normal intercrystalline corrosion, suggesting that the molten medium, diffusing along the grain boundaries, by some mechanism or other, weakens the bond between the grains [2-4, 10-12].

Of great importance for the correct understanding of the phenomenon of the decrease in the strength of metals under the influence of fused low melting point metals are the works of Kishkin [7] and Potak [8], which emphasize the connexion between these phenomena and the decrease in the strength of metals due to adsorption effect. The decrease in the strength of solids due to adsorption effect [15] is the best known manifestation of the physicochemical interaction between an external medium and a solid which is being deformed [16]. This effect, as is known, is explained above all by the fact that surface-active substances, by lowering the surface

* *Fiz. metal. metalloved.* 8, No. 2, 288-293, 1959.

VOL 8 195

energy of a solid, promote the onset of plastic shear and the formation of various defects at lower stresses. The primary, initial action of adsorption comes down to the fact that surface-active substances, by penetrating into the developing surface defects – microscopic cracks – and being adsorbed on the walls, promote the further development of the defects, which leads to the premature failure of the solid.

The drop in the strength due to adsorption should, obviously, grow as the interphase surface energy on the boundary between the solid and the environment decreases; since the magnitude of the interphase surface energy determines the probability and the work of the formation, in the deformation process, of the surface defect nuclei of shearing or rupturing.

The effects of decreased strength and facilitated deformation due to adsorption are kinetic in character, in connexion with which the biggest influences exerted by an external medium due to adsorption, as was shown in works [17-19], are observed in the case of protracted action by favourable stressed states – under conditions of creep, endurance or fatigue strength.

Organic surface-active substances – the normal active components of lubricants – can be used only at low temperatures. Considerably more active, giving rise to a bigger drop in the surface tension of metals, that is to say more easily adsorbed, are surface-active, comparatively low melting point metals and alloys.

The occurrence of quite small values of interphase surface tension σ_{12} on the boundary between two phases corresponds, according to Volmer's concept [14], to a spontaneous dispersion up to particles of colloidal dimensions under the action of thermal motion. Moreover a thermodynamically stable colloidal solution is formed – a suspension or an emulsion – ultimately a dispersed two-phase system consisting of two mutually saturated phases in equilibrium. The increase in surface energy with such a dispersion is quite small and is fully compensated by the increase in the entropy of the system due to the equal distribution of particles throughout the whole volume of the medium.

An approximated condition for spontaneous dispersion results in the fact that $\sigma_{12} < \sigma_m$, where $\sigma_m = \frac{kT}{\delta_m^2}$ (δ_m — average size of a mosaic block $\approx 10^{-6}$ cm), or the dispersion criterion $D_i = \sigma_{12}\,\delta_m^2/kT$ should fulfil the condition $Di < 1$ [20, 21]. At high temperatures spontaneous dispersion can take place even at stresses which are not very low: $\sigma_{12} \approx 0.1$ erg cm^{-2}. Usually with an increase in temperature, moreover, σ_{12} also decreases sharply as a result of the increase in mutual solubility. The extreme case of the critical point, according to Mendeleyev $\sigma_{12} = 0$, corresponds to the disappearance of the colloidal phase, that is to say to unlimited mutual solubility with the formation of a true (single-phase) solution.

In the case of big values of σ_{12} ($\sigma_{12} > \sigma_m$), dispersion cannot be self-induced, that is to say it only takes place under the influence of external forces, but in this case the strength of a solid in a given liquid phase $(P_m)_A$ is decreased all the more in comparison with the strength in vacuo $(P_m)_0$, the more σ_{12} is decreased. In this case the conditional dispersion criterion is:

$$D_i = (\sigma_{12} \cdot S_m - \beta P \cdot v_m)\, kT < 1,$$

and the magnitude of the effect of decreased strength, determined under conditions of brittle rupture by the expression:

$$\frac{(P_m)_0 - (P_m)_A}{(P_m)_0} = \frac{\sigma_1 - \sigma_{12}}{\sigma_1},$$

can reach very considerable values.

The study of the rules and mechanism of the influence of molten metals on the mechanical properties of refractory metals is best carried out on single crystal specimens, firstly because here there are no grain boundaries to complicate the study of these phenomena, and also because single crystal metals possess high plasticity, as a result of which an increase in brittleness and a decrease in strength should manifest themselves especially clearly.

For the experiment, single crystals of zinc and cadmium were chosen, molten tin and lead were chosen as surface-active media.

The single crystals of zinc (99.99%) and

VOL. 8 1959

cadmium (99.999%) up to 30 cm long and 0.5-0.6 mm in dia. of various orientation were grown by a method of zonal crystallization [19] developed in our laboratory.

Spheres (up to 1 mm in dia.) were fused onto the ends of working specimens 15 mm in length by means of bringing them in contact with a fused platinum coil. By means of these spheres the specimen was fixed in the clamps of a Polanyi instrument. All the experiments were carried out in tensile conditions with a constant deformation rate of v = 10-15%/min^{-1}. The temperature of the crystal was kept constant in the course of the experiment with an accuracy of ± 5°C. To avoid oxidation in experiments at increased temperatures, the specimens were surrounded by a thick layer of graphite powder.

The metallic medium in the form of a thin layer 5 μ in thickness was deposited electrolytically on the surface of the single crystal being studied. The thickness of the electrolytic coating was determined by weighing. In order to obtain a tin - lead coating on the zinc specimens with a given content of the constituents, electrolytic layers of tin and lead were deposited alternately on the surface of the single crystal in a specified weight ratio. The single crystals with their deposited layer of low melting point metal were placed in a tube filled with finely dispersed graphite powder and held prior to the experiment at 250°C for 4 hr.

Using a metal coating in the form of a thin layer gives many advantages. Firstly it ensures considerably more rapid saturation with molten metal coating by the metal being deformed in its medium at a given temperature of the experiment. Secondly, a small quantity of the metal being investigated is dissolved in the thin layer, down to 350°C for zinc and 270°C for cadmium, in such a way that one can disregard the decrease in dia. of the specimens which takes place when this happens. As the check experiments which were carried out at 250°C showed, the tension diagrams of single crystals of zinc in a tin bath saturated with zinc coincide with the tension diagrams for zinc coated with an electrolytically deposited layer of tin.

Fig. 1 shows tension diagrams in true stresses at various temperatures for single zinc crystals coated with a layer of tin, and also uncoated. As can be seen from Fig. 1 the influence of the film of tin on the mechanical properties of a single crystal of zinc at room temperature is very insignificant. The film has some strengthening action in the initial region of flow, whilst the plasticity of the single crystal remains unchanged. With an increase in temperature up to 300°C the action of the layer of fused tin, whilst not giving rise to significant

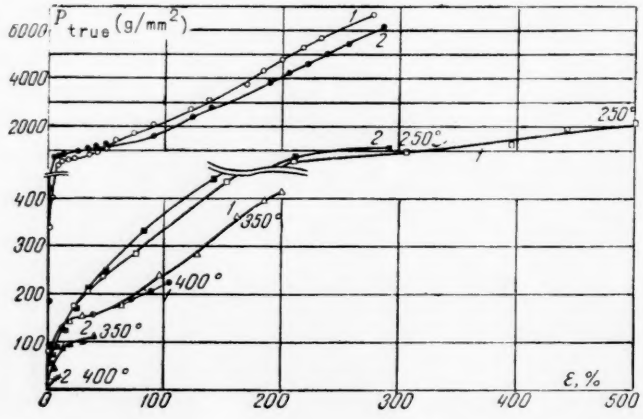

Fig. 1 Graph showing the dependence of true stress $P = P_0\left(1 + \frac{\varepsilon}{100}\right)$ on elongation per unit length ϵ of single crystals of zinc (χ_0 = 44°) without an external coating (curve 1), and coated with a film of tin (curve 2).

deviations from the tension diagram for an uncoated single crystal of zinc in the initial region of flow, leads, with further deformation of the specimens, to a drop in their plasticity and to a decrease in true strength, that is to a decrease in the rupture stress calculated on the true cross-section of the specimen at the moment of rupture. At higher temperatures a sharp drop in the plasticity and strength of the specimens takes place.

The effect of fused tin on single crystals of zinc as a function of temperature is shown in Fig. 2. The relative decrease in the amount of deformation at the moment of rupture of specimens coated with tin ϵ_a in comparison with the deformation at the moment of rupture of uncoated single crystals of zinc ϵ_0 was taken as a measure of the effect and was expressed as a percentage:

$$\frac{\varepsilon_0 - \varepsilon_a}{\varepsilon_0} \times 100\%.$$

The relative decrease in the true rupture stress of the specimens deformed in the molten environment P_A in relation to the true rupture stress of specimens without a metal coating P_0 was the measure used for the weakening action of the medium, expressed as a percentage: $\frac{P_0 - P_A}{P_0} \times 100\%$.

Together with this, the very character of the rupture is changed: from plastic in air, it becomes brittle in an active medium. Therefore the drop in the rupture stress of zinc under the influence of tin calculated according to the rupture area is even more sharply expressed, and the effect is a change in character. The sharp influence of temperature, in the region of 300-400°C, is obviously connected with the increased solubility of the zinc in the liquid tin (45 per cent at 350°C and 92 per cent at 400°C), which promotes a sharp decrease in the interphase tension.

In the same way, the influence of molten lead-tin alloys (with a varied tin content) on the tension diagram of single crystals of zinc was studied. Fused lead by itself, proved to be comparatively mildly surface-active in relation with zinc and did not give rise to a decrease in strength and plasticity in these conditions. Fig. 3 shows than even comparatively small additions of a surface active layer to the molten environment gives rise to a rather sharp drop in the strength and plasticity of single crystals of zinc. This effect reaches a limit at 20 per cent tin, and a further drop is noticed only with a tin content of more than 80 per cent – when approaching pure tin, which is obviously connected with the sharp increase in the solubility of zinc in such molten environments.

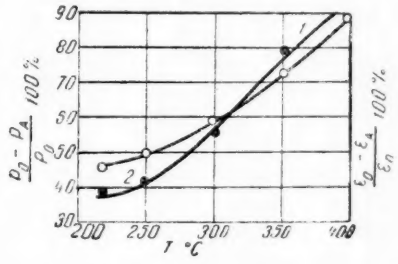

Fig. 2. The temperature dependence of the magnitude of the effect due to the action of tin for single crystals of zinc ($\gamma_0 = 44°$):

$$1 - \frac{\varepsilon_0 - \varepsilon_A}{\varepsilon_0}(T); \quad 2 - \frac{P_0 - P_A}{P_0}(T).$$

We held single crystals of zinc, coated with a thin layer of tin, at 400°C without stressing for a duration of time corresponding to our experiments and then placed them in liquid lead at the same temperature. Then, with sufficiently long holding in the fused lead, the action of the tin disappears entirely and the normal strength and plasticity of the single crystals are

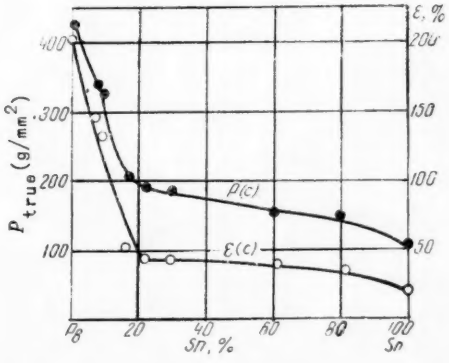

Fig. 3. The dependence of true strength P_m and the greatest elongation ϵ_m before rupture in single crystals of zinc ($\chi_0 = 42°$) on the concentration of tin in the alloy and of tin with lead at 350°C.

restored. These tests indicate the absence of any noticeable role played by the diffusion of tin into zinc (Fig. 4).

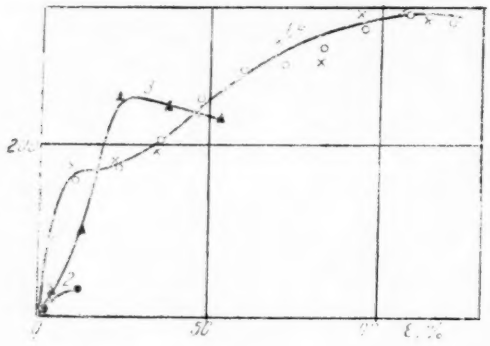

Fig. 4. Restoration of plasticity and strength of single crystals of zinc ($\chi_0 = 38°$) coated with tin after holding them prior to tension in a molten environment of lead at 400°C: diagrams $P - \epsilon$ at 400° for uncoated single crystals of zinc (curve 1); for single crystals of zinc coated with tin (curve 2); for single crystals of zinc coated with tin after preliminary holding for half an hour (curve 3) and for 4 hr (curve 4) in a molten environment of lead prior to tension.

Obviously the penetration of tin, and in connexion with this the drop in δ_{12} as well, takes place only along the developing surface defects – the nuclei of shears and rupture.

We also obtained significant effects of a decrease in strength and plasticity on single crystals of cadmium in the presence of liquid tin (Figs. 5,6). The inherent tendencies of the action of liquid tin, which were established on single crystals of zinc are reproduced entirely on single crystals of cadmium as well.

The results which we obtained, point directly to the very important circumstance that the action of surface-active molten metal environments is not connected with the presence of grain boundaries in a refractory metal. This action is also found on single crystals of metals when there are no intercrystallite boundaries, and can reach a significant size under favourable temperature conditions. This conclusion, of course, does not mean that grain boundaries in a polycrystalline metal do not play any part at all in the effect which is occasioned by the action of a molten environment. They can play a very considerable role and in some cases even a decisive role, however it should be borne in mind that a surface-active fused metal

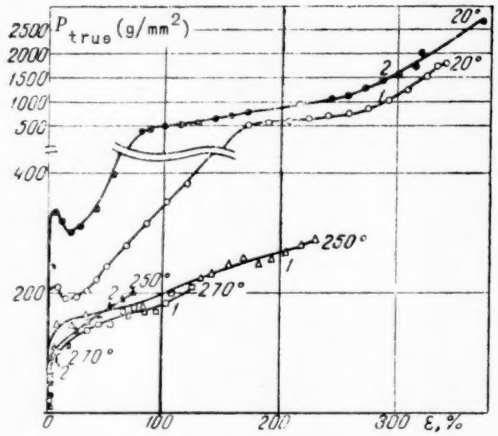

Fig. 5. The dependence of true stress P on the elongation per unit length ϵ in single crystals of cadmium ($\chi_0 = 39°$), without an external coating (1) and coated with a thin film of tin (2).

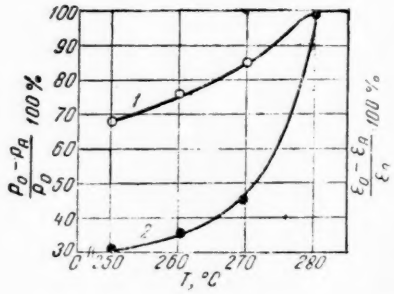

Fig. 6. The magnitude of the effect due to the action of a film of tin in single crystals of cadmium ($\chi_0 = 39°$) depending upon the temperature.

environment can lower the strength and plasticity of an individual grain as much as required as a result of a sharp decrease in the interphase surface tension. In the presence of such a strong surface-active substance as a molten metal is for a refractory one, even very small normal stresses lead to the formation and development of cracks, and the latter to the brittle rupture of the metal. For this to happen, it is only necessary for the kinetics of crack development to correspond to the kinetics of pene-

tration of a surface-active fused environment into the metal along these cracks.

Translated by J.J. Cornish

REFERENCES

1. W. Goodrich, *J. Iron and Steel Inst.*, 132, 43 (1935).
2. R. Genders, *J. Inst. Metals*, 37, 215 (1927).
3. G. Austin, *J. Inst. Metals*, 58, 173 (1936).
4. Z. Ewijk, *J. Inst. Metals*, 56, 241 (1935).
5. H. Miller, *J. Inst. Metals*, 37, 183 (1927).
6. E. Zuch, P. Gregory and R. Eborall, *J. Inst. Metals*, 83, 347 (1954-55).
7. S.T. Kishkin, V.V. Nikolenko and S.I. Ratner, 24, 8, 1455 (1954).
8. Ia.M. Potsk, and I.M. Shcheglakov, *Zh. tekh. fiz.*, 1955, 25, 5, 897.
9. R. Eborall and P. Gregory, *J. Inst. Metals*, 84, 81 (1955-56).
10. H. Hartley, *J. Inst. Metals*, 37, 193 (1927).
11. J. Andrews and R. Higgins, *J. Inst. Metals*, 27, 185 (1922).
12. E. Rhead, *Metall. Inst.*, 18, 365 (1921).
13. E. Daniels, *Trans. Faraday Soc.*, 31, 1277 (1935).
14. M. Volmer, *Z. Phys. Chem.*, 125, 151 (1927).
15. P.A. Rebinder, Report at the sixth congress of Russian physicists, Moscow, 1928; P. Rehbinder, *Z. Phys*, 72, 191 (1931).
16. V.I. Likhtman, *Vest. Akad. Nauk SSSR*, 9, 8 (1956).
17. P.A. Rebinder and V.I. Likhtman, *Dokl. Akad. Nauk SSSR*, 56, 723 (1947): V.I. Likhtman, *Usp. fiz. nauk*, 54, 6 (1954).
18. V.I. Likhtman, *Usp. fiz. nauk*, 37, 3 (1949).
19. V.I. Likhtman, P.A. Rebinder and G.V. Karpenko Vliianiye poverkhnostno – aktivnoi sredy na protsessy deformatsii metallov (The influence of a surface-active medium on the process of deformation in metals) *Izd. Akad. nauk SSSP*, (1954).
20. P.A. Rebinder, Report at the permanent colloquium on solid phases of variable composition together with the Moscow colloquium on colloids, Moscow, 1956.
21. P.A. Rebinder, V.I. Likhtman and L.A. Kochanova *Dokl. Akad. Nauk SSSR*, 111, 1278 (1956).

VOL. 8 1959

ON THE NATURE OF INTERNAL FRICTION IN HARDENED AND TEMPERED STEEL*

M.A. KRISHTAL and S.A. GOLOVIN

Tula Engineering Institute

(Received 28 February 1958)

A study was made of internal friction due to relaxation in hardened and tempered steels mark U7A and U9A. On the basis of the data obtained and work [1] the diffusion coefficients and the activation energy were computed. This showed that the peak of internal friction at 228-255° is brought about by diffusion events of carbon in austenite under the action of stresses.

The work of many steel components which have been subjected to hardening and tempering is accompanied by an alternating load at increased temperatures. It is therefore interesting to study the nature of relaxation phenomena in hardened and tempered steels. Investigations similar to these can also assist the further development of the theory of hardening and tempering steel.

Works [1, 2] give the results of measuring internal friction in carbon steels subjected to hardening and tempering at 100-600°. Steels were studied containing 0.015, 0.28, 0.35, 0.46 and 0.58 per cent of carbon. In all these steels, apart from the one containing 0.015 per cent C, a sharply defined peak of internal friction was observed at a temperature of about 200°.

With an increased carbon content in hardened steels the height of the peak increased; with an increased tempering temperature the height dropped and at 600° the peak disappeared. The author of works [1, 2] connects the appearance of the peak of internal friction with the presence of martensite in the steel, and its decrease and disappearance in tempering – with the decay of martensite.

In the present work specimens of high carbon steels in the form of wire were chosen for investigation; their composition is given in Table 1. The choice of the steels indicated was influenced by the fact that in them, bigger effects of the internal friction were expected in comparison with low carbon steels. Furthermore, these steels (type V-1) are used extensively in practice for making springs.

Testpieces 0.8 mm in diameter and 320 mm in length were investigated. Vacuum annealing was carried out at 1000° for 2 hr prior to hardening. The annealed specimens were subjected to hardening from 800° and to tempering for one hour at temperatures of 100, 200, 250, 350, 450, 500 and 700°.

Internal friction was measured on a vacuum type torsional pendulum RKF-MIS-1 at vibrational frequencies of $\omega_1 = 1.33$ and $\omega_2 = 2.08$ c/s.

The results of the measurements are given in Figs. 1 and 2.

Fig. 1 summarizes the data for steel

TABLE 1

The composition of the steels investigated, (%)

C	Mn	Si	S	P	Cr	Ni,Ti	Cu
0.71	0.47	0.34	0.02	0.03	Trace	–	Less than 0.1
0.92	0.24	0.26	0.02	0.03	Trace	–	"

* *Fiz. metal. metalloved.* 8, No.2, 294-301, 1959.

VOL 8 195

containing 0.71 per cent C, Fig. 2 – 0.92% C. From Figs. 1 and 2 the presence of peaks of internal friction can be seen at temperatures of 220-260°. An increase in the tempering temperature leads to a lowering of the peaks, which is in accordance with the results of works [1, 2]. Fig. 3 shows how the heights of the peaks of internal friction are dependent on tempering temperature for the steels investigated. The values obtained can be plotted on straight lines with only a small amount of spread.

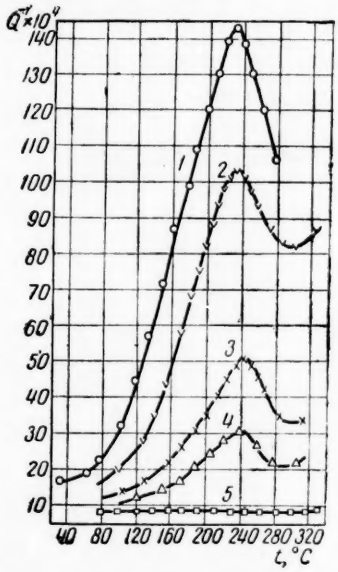

Fig. 1. Temperature trend of internal friction in specimens of steel containing 0.71% by weight of carbon:
1 – hardening from 800°; 2 – tempering at 200°;
3 – tempering at 350°; 4 – tempering at 450°;
5 – annealing at 1000°.

Table 2 and Figs. 4 and 5 show the dependence of the temperature and size of the peaks for a frequency of the order of one cycle per second upon the carbon content in hardened steels. The table contains data obtained in the present work and in work [1]. Both values rise almost linearly with the increase in the carbon content.

It is interesting to determine the nature of the peaks of internal friction at the temperatures indicated. Hardened steel consists of a mixture of martensite and a certain amount of residual austenite. The

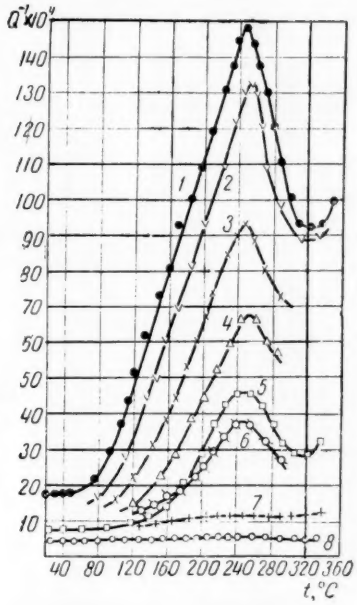

Fig. 2. Temperature trend of internal friction in specimens of steel containing 0.92% by weight of carbon:
1 – hardening from 800°; 2 – tempering at 100°;
3 – tempering at 250°; 4 – tempering at 350°;
5 – tempering at 450°; 6 – tempering at 500°;
7 – tempering at 700°; 8 – annealing at 1000°;

presence of the peak can be explained by relaxation along the grain boundaries and diffusion in the martensite or in the less strong austenite induced by stresses. However the mobility of carbon atoms in these phases is substantially different and it is impossible to expect the disposition of diffusion peaks over martensite and austenite at one and the same temperature.

Unfortunately there is no straightforward information available about the diffusion of carbon in martensite. If one assumes that the diffusion rate of carbon in martensite is

TABLE 2

The dependence of the temperature and size of peaks on the carbon content

Carbon content (%)	$Q^{-1}_{max}\ 10^4$	t (°C)
0.46	125	192
0.58	135	208
0.71	143	230
0.92	148	248

VOL. 8 1959

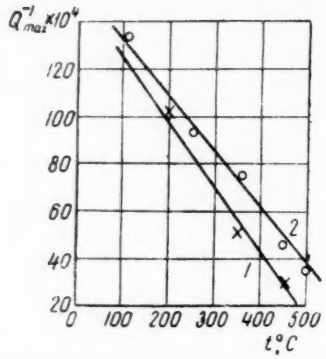

Fig. 3. The influence of the tempering temperature of hardened steel on the peak of internal friction at 200°:
1 – 0.71% C; 2 – 0.92% C.

not vastly different from its diffusion rate in ferrite, and if one calculates the temperature at which the mean time between jumps of a carbon atom will correspond to the relaxation time for selected vibrational frequencies, this temperature is found to be around 100°. In actual fact in work [3] the peak of internal friction, connected with transformations in martensite, was observed at 130° and disappeared at 170°. The data in Table 2 and Figs. 1 and 2 show that the temperatures at which maxima of internal friction were observed in the present investigation were considerably higher than 130°. Therefore it is quite probable that the peaks of internal friction at 200-260°, which are observed in hardened and tempered steels, are connected with diffusion events in austenite induced by stresses.

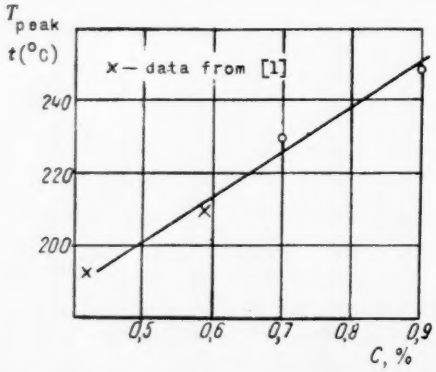

Fig. 4. The dependence of the temperature of the peak of internal friction in hardened steels on their carbon content at $\omega \cong 1$ c/s.

It can be seen from Fig. 5 that in hardened steel the size of the peak increases linearly with the increase in carbon content (average values of the content of residual austenite in steels are taken from work [4]. The growth of the maximum of internal friction is in accordance with the increase in the content of residual austenite and is accompanied by a decrease in the martensite content in the steels. In order to evaluate the amount of residual austenite in the steels investigated, magnetometric measurements were carried out. At the temperature of the peaks the intensity of magnetization of steel containing 0.9 per cent carbon is about 85 per cent of the intensity of magnetization of a steel containing 0.7 per cent carbon. This confirms experimentally the correctness of the the data set forth in Fig. 5.

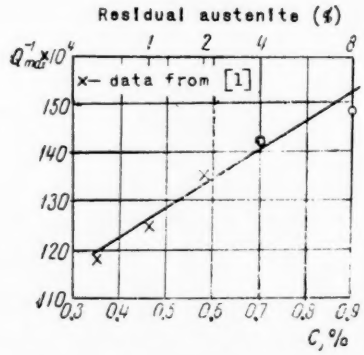

Fig. 5. The dependence of the peak of internal friction in hardened steels on their content of carbon and residual austenite ($\omega \cong 1$ c/s).

With an increase in carbon content, the temperature corresponding to the maxima of internal friction in hardened (Fig. 4) and tempered steels rises practically linearly as well.

To confirm the data and considerations which have been set forth concerning the nature of the peaks of internal friction, diffusion coefficients and activation energies corresponding to the positions of these peaks were calculated. To determine activation energies additional measurements of internal friction were carried out at a vibrational frequency of 2.08 c/s. Figs. 6 and 7 give the curves obtained for hardened and tempered steels containing 0.71 and 0.92 per cent carbon at various frequencies.

The values of the diffusion coefficients

and activation energies compare well with the data of various authors on the diffusion coefficients and activation energies of the diffusion of carbon in austenite.

Many works [5-8] have been devoted to the measurement of the coefficients of diffusion of carbon in austenite. The most complete data are presented in works [6 and 7] in which the investigations were carried out on specimens welded from two steels containing different amounts of carbon and subjected to long homogenizing. The calculations were carried out by the Matano method, taking into account the influence of the concentration of diffusing carbon on the value of the diffusion coefficients. The data obtained in works [6 and 7] characterize the coefficients of diffusion of carbon in unstressed austenite in equilibrium which are expressed by the formulae:

$$D_C^{\gamma} = (0.07 + 0.06\%\ C)\ exp\left[-\frac{32{,}000}{RT}\right], \quad (1)$$

$$D_C^{\gamma} = 0.04 + 0.08\%\ C)\ exp\left[-\frac{31{,}350}{RT}\right]. \quad (2)$$

Coefficients of diffusion of carbon in austenite previously subjected to hardening are determined in work [8]. Measurements were carried out at 1000, 960 and 930°. To avoid the influence of high temperature homogenizing on the elimination of hardening effects in austenite the metallographic method was used, which demands soaking from 5 to 20 min at 930-1000°. The results presented in work [8] for austenite obtained after single hardening, give, on calculation, a formula which characterizes the values of diffusion coefficients in stressed austenite with defects due to hardening:

$$D_C^{\gamma} = 0{,}4exp\left[-\frac{36{,}600}{RT}\right]. \quad (3)$$

The average carbon content in the austenite amounted to 0.7-0.8 per cent.

Calculation of diffusion coefficients using data from internal friction was carried out employing the formula in work [9]:

$$D = \alpha\frac{a^2}{\tau}, \quad (4)$$

where a is the crystal lattice constant; τ the time, dependent upon the relaxation time and α is the geometry factor, which is determined by placing around an interstitial atom the neighbouring points of a crystal lattice into which it can travel. For a face-centred lattice $\alpha = 1/12$, for a body-centred lattice $\alpha = 1/24$. The value of τ was taken as being equal to $^3/_2\,\tau_R$ ($\tau_R = \frac{1}{\omega}$ the relaxation time [9]).

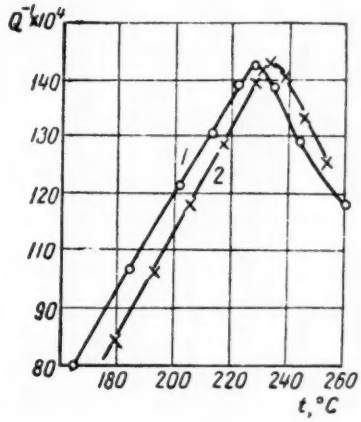

Fig. 6. Temperature trend of internal friction in specimens of steel containing 0.71% by weight of carbon at different frequencies. Hardening from 800°:
1 – at ω = 1.33 c/s; 2 – ω = 1.81 c/s.

Tables 3, 4, 5 and 6 indicate the values of the diffusion coefficients of carbon in austenite for hardened and low temperature tempered steels computed by formulae (1)-(4).

The data in Tables 3, 4 and 5 show the contrast between the values of diffusion coefficients of carbon in austenite determined from peaks of internal friction, and the values computed using formula (3) for the same temperatures. The expected diffusion coefficient of carbon in martensite is five orders bigger. This again bears witness to the fact that the peaks of internal friction in hardened and low temperature tempered steel are explained by diffusion of carbon in residual austenite induced by stresses. The values of the diffusion coefficients calculated by formulae (1) and (2) are correctly one order bigger. The data obtained correspond to the results of work [8], according to which the diffusion rate of carbon in austenite which has been subjected to hardening, is less than in austenite which

VOL. 8 1959

has not been subjected to hardening. With a view to confirming this fact further, the internal friction of testpieces of steel with a carbon content of 0.92 per cent, twice subjected to hardening from 800°C was measured.

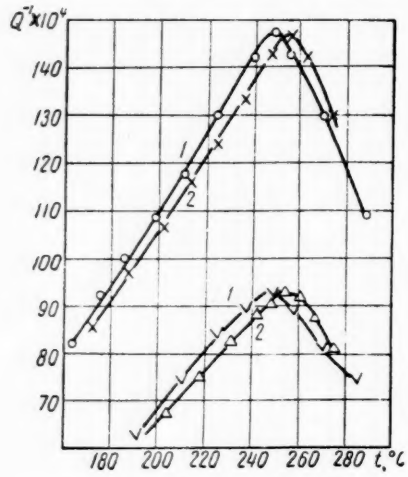

Fig. 7. Temperature trend of internal friction in specimens of steel containing 0.92% by weight of carbon at different frequencies.
Hardening from 800°.
1 – ω = 1.33 c/s; 2 – ω = 2.08 c/s
Tempered at 250°:
1 – ω = 1.33 c/s; 2 – ω = 2.08 c/s.

Fig. 8 shows curves obtained at a frequency of 2.08 c/s for specimens subjected to single and double hardening. The second hardening leads to the maximum being displaced to the higher temperature region, which testifies to increased stability of residual austenite in a twice-hardened specimen. Calculations showed that the second hardening leads to a further decrease in the diffusion coefficient of carbon in austenite. This decrease is twice the size of that resulting from the first hardening.

Thus the stressed state and the defects which are created in hardened and low temperature tempered steel lead to a slowing down of the diffusion of carbon in residual austenite.

It should be noted that in the steel with 0.92 per cent carbon the diffusion coef-

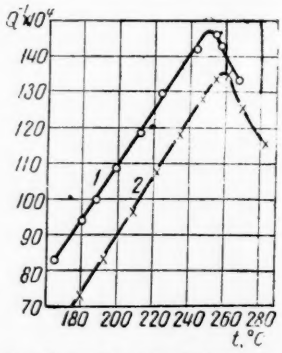

Fig. 8. Temperature trend of internal friction in specimens of steel with 0.92% C, subjected to single and double hardening at a frequency of 2.08c/s: 1 – single hardening; 2 – double hardening.

TABLE 3

Values of the diffusion coefficients of carbon for steel with 0.92% C

Temperature of peak (°K)	Diffusion coefficients by formulae (cm^2/sec)			Heat treatment	Frequency c/s	D_c^{γ} by formula (4) $\left(\frac{cm^2}{sec}\right)$
	(1)	(2)	(3)			
521	4.9×10^{-15}	7.2×10^{-15}	1.59×10^{-16}	Hardening from 800°	1.33	5.97×10^{-16}
528	6.2×10^{-15}	11.2×10^{-15}	2.53×10^{-16}	Hardening from 800°	2.08	9.3×10^{-16}
521	4.9×10^{-15}	7.2×10^{-15}	1.59×10^{-16}	Hardening and tempering at 250°	1.33	5.97×10^{-16}

TABLE 4

Values of the diffusion coefficients of carbon for steel with 0.71% C

Temperature of peak (°K)	Diffusion coefficients by formulae (cm^2/sec)			Heat treatment	Frequency c/s	D_c^{γ} by formula (4) $\left(\frac{cm^2}{sec}\right)$
	(1)	(2)	(3)			
501	1.41×10^{-15}	2.36×10^{-15}	0.505×10^{-16}	Hardening from 800°	1.33	5.93×10^{-16}
505	1.78×10^{-15}	3.06×10^{-15}	0.695×10^{-16}	Hardening from 800°	1.81	8.1×10^{-16}
521	4.64×10^{-15}	8×10^{-15}	1.59×10^{-16}	Hardening and tempering at 350°	1.33	5.93×10^{-16}

VOL. 8 1959

TABLE 5

Values of the diffusion coefficients of carbon for steel with 0.58% C [1]

Temperature of peak (°K)	Diffusion coefficients by formulae (cm^2/sec)			Heat treatment	Frequency c/s	D_c^{γ} by formula (4) $\left(\frac{cm^2}{sec}\right)$
	(1)	(2)	(3)			
481	3.56×10^{-16}	5.6×10^{-16}	0.138×10^{-16}	Hardening	1.0	4.46×10^{-16}
490	6.48×10^{-16}	11×10^{-16}	0.225×10^{-16}	Hardening and tempering at 100°	1.0	4.46×10^{-16}
500	11.3×10^{-16}	23×10^{-16}	0.496×10^{-16}	Hardening and tempering at 200°	1.0	4.46×10^{-16}

TABLE 6

Values of the diffusion coefficients of carbon for steel with 0.46% C [1]

Temperature of peak (°K)	Diffusion coefficients by formulae (cm^2/sec)			Heat treatment	Frequency c/s	D_c^{γ} by formula (4) $\left(\frac{cm^2}{sec}\right)$
	(1)	(2)	(3)			
460	0.71×10^{-16}	1.22×10^{-16}	2×10^{-18}	Hardening	1.0	4.02×10^{-16}

TABLE 7

The results of calculating H and Q by formulae (1)-(3)

Carbon content (%)	Temperature of peaks		Heat treatment	$H\left[\frac{\text{cal}}{\text{g atm}}\right]$	$Q\left[\frac{\text{cal}}{\text{g atm}}\right]$ by formulae		
	at 1.33 (c/s)	at 2.08 (c/s)			(1)	(2)	(3)
0.92	521	528	Hardening from 800°	34,800	32,000	31,350	36,600
	521	529	Hardening and tempering at 250°	30,490	32,000	31,350	36,600
0.71	501	505*	Hardening from 800°	39,000	32,000	31,350	36,600

* $\omega_2 = 1.81$ c/s

ficients, which were calculated using the peaks of internal friction, are regularly nearer to those calculated using formula (3) than in the steel with 0.71 per cent carbon. The exception is the diffusion coefficient of the specimen with 0.71 per cent carbon which had been subjected to tempering at 350°. This, apparently, can be explained by the coherent binding of the tempered martensite and carbides with the original residual austenite, which leads to its being additionally strengthened.

In the steel with 0.46 per cent carbon a correspondence of the diffusion coefficients calculated by formulae (1), (2) and (4) is observed. With a decrease in the carbon content, the residual austenite is found to be less stressed.

If the peak of internal friction is in fact explained by diffusion of carbon in austenite there ought to be a correspondence between the activation energies H, computed from internal friction, and Q, using formulae (1)-(3). The activation energy was computed using the formula from [10]:

$$H = T_1 T_2 \frac{2.3R \log \frac{\omega_2}{\omega_1}}{T_2 - T_1}, \qquad (5)$$

where T_1 and T_2 are the temperatures of the peaks corresponding to frequencies ω_1 and ω_2.

Table 7 compares the results of calculating H and Q by formulae (1), (2) and (3).

The data from Table 7 show a satisfactory correspondence between the activation energies determined by using internal friction and the data on the diffusion of carbon in austenite.

CONCLUSIONS

1. A study was made of internal friction in hardened and tempered steels containing 0.71 and 0.92 per cent carbon.
2. Maxima of internal friction were observed at temperatures of 228-255° which drop with an increase in tempering temperature and a decrease in the carbon content.
3. The size of the peaks increases almost linearly with the increase in the amount of residual austenite in the hardened steel.
4. The temperature of the peaks increases linearly with the increase in the amount of carbon in the steel.
5. Calculations of the diffusion coefficients and activation energies showed that the presence of peaks of internal friction should be connected with diffusion of carbon in residual austenite.
6. The correspondence was shown between the values of the diffusion coefficients measured by the method of internal friction in hardened and low temperature tempered steel, and the values determined by the metallographic method, in austenite obtained from the hardened state.
7. The maximum of internal friction in a

twice hardened specimen is displaced to the high temperature region.

We wish to express our gratitude to Professors B.N. Finkel'shtein, Iu.V. Piguzov, L.F. Usovoi and I.N. Chernikova for their help in carrying out the measurements of internal friction.

Translated by J.J. Cornish

REFERENCES

1. I.N. Chernikova, *Fiz. metal. metalloved.*, 5, 102 (1957).
2. I.N. Chernikova, *Fiz. metal. metalloved.*, 5, 176 (1957).
3. T.S. Ke and I.L. Ma, *Acta Phys. Sinica*, 11, No.6, 479 (1955).
4. A.P. Guliayev, *Termicheskaia obrabotka stali (Heat treatment of steel)*, Mashgiz., pp 126 and 272 (1953).
5. P.L. Gruzin, V.G. Kostogonov and P.A. Platonov, *Prob. metalloved. fiz. metal.*, No.4, p 517 (1955).
6. K. Wells and R. Mehl, *Metals Technology*, No. 8 (1940).
7. M.E. Blanter, *Zav. lab.*, Vol. 3 (1946).
8. M.A. Krishtal, *Metalloved. obrab. metal.*, No. 7, 20 (1957).
9. A.D. Le Kler, *Usp.fiz.metal.*, No.1, 224 (1956).
10. A.S. Novik, *Usp.fiz.metal.*, No.1, 7 (1956).

VOL. 8 1959

A CONTRIBUTION TO THE QUESTION OF THE NATURE OF DAMPING OF VIBRATIONS IN HARDENED AND LOW TEMPERATURE TEMPERED CARBON STEEL*

M.A. KRIShTAL and S.A. GOLOVIN

Tula Engineering Institute

(Received after abridgement 22 *August 1958)*

Measurement was carried out of the damping of torsional vibrations in hardened and low-temperature-tempered specimens of steel type 50A and U7A with successive straining after single and double hardening, cold working at -196°, and at increased temperatures. It is shown that the damping out of vibrations in the steels investigated is connected with the presence of residual austenite and its decay induced by tempering. At increased temperatures the possibility of the development of internal friction due to relaxation was noted.

Measurements carried out earlier [1, 2] of internal friction due to microplasticity in heat treated steels type 50A and U7A, and also of internal friction due to relaxation in steels U7A and U9A, showed the substantial influence of residual austenite in hardened and low temperature tempered specimens on the damping capacity of steel.

The present investigation was undertaken with the aim of developing this position further. Measurements of the damping of torsional vibrations were carried out on specially treated specimens of the steels which were studied before, 50A and U7A (of the table). These types of steel were selected in connexion with their wide use for making components of machines which are subjected to vibrations in the course of their work.

The damping of the torsional vibrations in the testpieces being investigated was measured on an instrument which recorded vibrograms with a tensometer (Fig. 1).

The frame 2 was suspended in the operating position on a caprone thread 1. The specimen 7 was firmly fixed in the upper (or lower) part of the frame and in the cross-beam 3 which undergoes torsional vibrations together with the specimen. The specimen was twisted by turning the cross-beam around the axis of the specimen by means of a pair of electro magnets *M*, which travelled along centring supports. The vibrations of the system specimen - cross-beam were recorded by means of wire or dynamic pick-ups *D* onto an oscillograph.

The resistance furnace 6 allowed the specimen to be heated to 360° with intervals of 10°. The design of the furnace enabled

TABLE 1

Composition of the steels investigated

Type of steel	Content of elements (%)					
	C	Mn	Si	S	P	Cr
50A	0.49	0.34	0.54	0.024	0.019	0.19
U7A	0.70	0.23	0.18	0.021	0.026	trace

* *Fiz. metal. metalloved.*, 8 No.2, 302-308, 1959.

the specimen to operate in an atmosphere of protective gas. Thus the design of the instrument permitted the temperature change of the vibration damping to be determined.

The investigations were made on specimens 7 mm in dia. which are often used for research such as this. Each curve was plotted on the data for three to five specimens, and ten vibrograms were taken of each specimen. Prior to hardening, the specimens were annealed for one hour, then subjected to quench hardening (steel U7A at 800°, steel 50A at 860°) in water and tempering for one hour at various temperatures.

The influence of successive straining on vibration damping in hardened and tempered specimens was also studied. The measurements showed that when straining low temperature tempered specimens the damping capacity is not changed. Figs. 2 and 3 show a decrease and then stabilization of the vibration damping in hardened specimens of steel 50A and U7A with straining connected with successive measurements. The measurements are more noticeable in the hardened specimens of steel U7A (Fig. 2) than in specimens of steel 50A (Fig. 3) with high torsional stresses on the periphery of the specimen. When the measurements of the vibration damping are repeated the stability of the readings increases as a result of decreasing the stresses and the carbon content. For example, for steel 50A at σ = 15 kg/mm^2 practically no decrease in vibration damping is observed (Fig. 3). The phenomena described are connected with cold hardening of the residual austenite with successive straining of the specimen. When the influence of the residual austenite on the damping capacity of the specimens is substantial, a decrease in the quantity of residual austenite leads to a decrease in the vibration damping. Actually, it is shown in work [2] that tempering up to 200° increases the rigidity of the specimens, that is to say it decreases the capacity to damp out vibrations. In as much as cold working is accompanied by additional transformation of residual austenite into martensite [3] it was expected that such specimens would possess less damping capacity.

The specimens were cooled in liquid

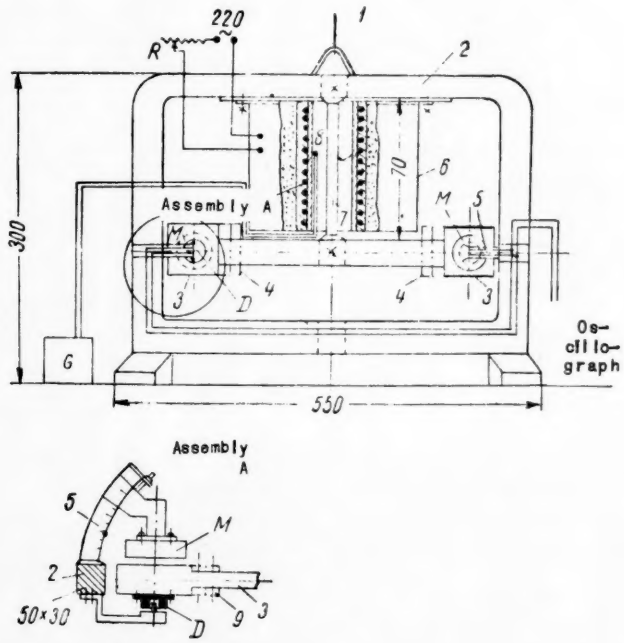

Fig. 1. Diagram of the instrument for determining damping of torsional vibrations: 1 – caprone thread; 2 – steel frame; 3 – cross-beam; 4 – changeable weights; 5 – centring support; 6 – furnace; 7 – specimen; 8 – thermocouple; 9 – furnace winding; *M* – electromagnet; *D* – dynamic pick-up; *R* – rheostat; *G* – galvanometer.

nitrogen to -196° and were held for an hour. Figs. [4] and 5 show the change in vibration damping in hardened and low temperature tempered specimens of steel 50A and U7A before and after cold working depending upon the torsional stresses on the periphery of the specimen. As was expected, the cold working led to a decrease in the damping capacity of the steel, which confirmed the concept about the influence of residual austenite. Hardened and low temperature tempered specimens (100°) subjected to cold working, damp out their vibrations almost to the same extent as specimens of steel hardened and tempered at 200° (the lower curves in Figs. 4 and 5 are the same as for tempering at 200°). Thus cold working gives nearly the same result as tempering, leading to practically complete decay of residual austenite. The considerable increase in the rigidity of specimens of steel U7A after cold working in comparison with specimens of steel 50A is explained by the higher content of residual austenite in steel U7A.

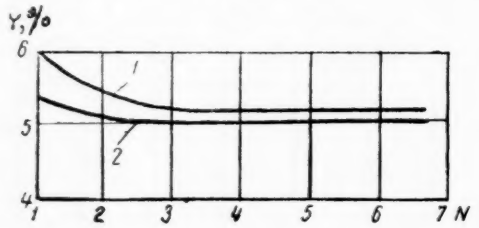

Fig. 2. Change in the damping of torsional vibrations in hardened specimens of steel U7A with successive straining:
1 – at a stress of 17 kg/mm^2:
2 – at a stress of 15 kg/mm^2.

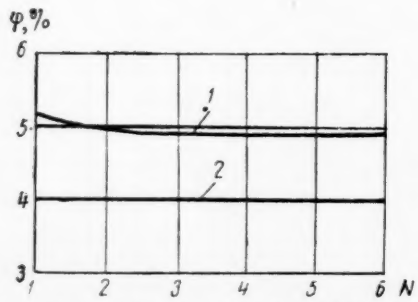

Fig. 3. Change in the damping of torsional vibrations in hardened specimens of steel 50A with successive straining: 1 – at a stress of 17 kg/mm^2; 2 – at a stress of 15 kg/mm^2.

In specimens of the same steels which had been subjected to higher temperature tempering at 400 and 500° there was practically no change in the damping capacity after cold working, which is connected with the absence in them of residual austenite. As follows from the data presented, it is expedient to cold work specimens in which residual austenite is retained after tempering.

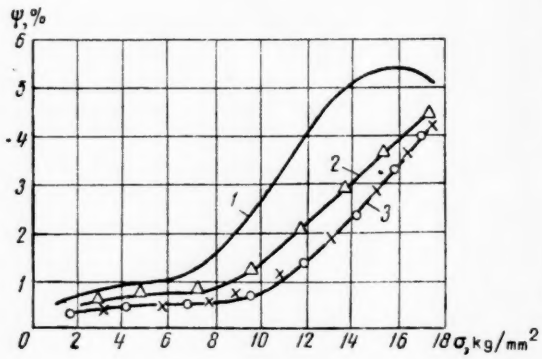

Fig. 4. Change in the damping of torsional vibrations in heat treated specimens of steel U7A: 1 – hardening from 800°; 2 – hardening + tempering (100°); 3 – working of hardened specimens (1) cold working at -196° (x); working of low temperature tempered specimens (2) cold working at -196° (o).

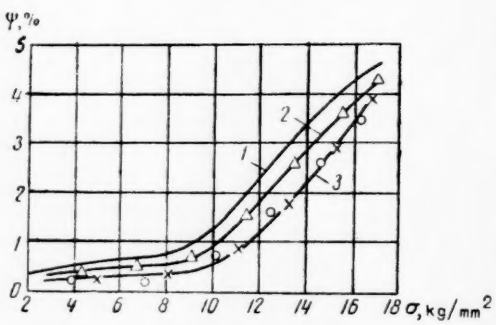

Fig. 5. Change in the damping of torsional vibrations in heat treated specimens of steel 50A: 1 – hardened from 860°; 2 – hardening and tempering (100°); 3 – working of hardened specimens (1) cold working at -196° (x); working of low temperature tempered specimens (2) cold working at -196° (o).

Hardening creates a considerable amount of residual stresses in steel. Therefore with a second hardening, conditions arise under

which austenite is retained in the specimen than after single hardening. Therefore a twice hardened specimen possesses greater rigidity than a specimen hardened once (Fig. 6).

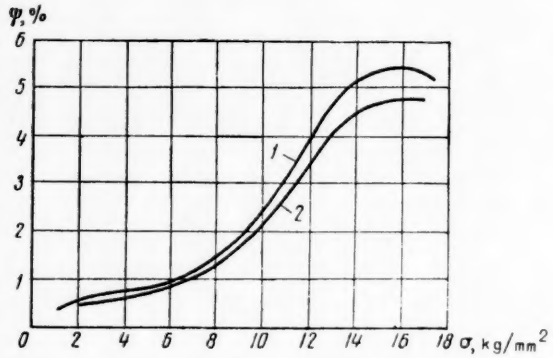

Fig. 6. Damping of torsional vibrations in specimens of steel U7A: 1 – single hardening; 2 – double hardening.

The work of steel components which have been subjected to hardening and tempering is often accompanied by an alternating load at increased temperatures. Therefore the temperature change and the nature of internal friction due to microplasticity in the steels under investigation are of interest. Fig. 7 shows the temperature trend of vibration damping in specimens of hardened (curve 1) and low temperature tempered (curve 2) steel U7A. Internal friction due to microplasticity increases with increasing the temperature, and at a temperature of about 290° it reaches its maximum value in hardened specimens, after which it decreases. As can be seen from Fig. 7, such an increase of the damping of torsional vibrations due to temperature, is more apparent for hardened specimens and less apparent for tempered specimens, which allows this fact to be connected with relaxation in austenite caused by stresses. At the highest heating temperature (350°) the curve for the tempered specimen does not have a maximum.

From the temperature of the peak of internal friction it is possible to calculate the value of the diffusion coefficient of carbon in that phase which is responsible for the relaxation process. Such a calculation can be carried out by the technique set forth in works [4-6]. The calculation allows one to assess the part played by diffusional relaxation in the formation of the maximum of internal friction on the curve for hardened steel. Calculations using diffusion peaks for a specimen of large diameter were carried out in work [7].

The diffusion coefficient is determined by the formula in [1, 4]:

$$D_C^{\gamma} = \alpha \frac{a^2}{\tau}, \qquad (1)$$

where α is the coefficient, for a face-centred lattice equal to 1/12;

a is the lattice constant;

$\tau = {}^3/_2 \tau_R \left(\tau_R = \frac{1}{\omega}\right.$, ω is the vibrational frequency when measuring).

The present measurements were carried out at a frequency of 29 periods per second. The lattice constant of austenite for steel U7A is equal to 3.58 Å. The results of the calculation by formula (1) give the value of the diffusion coefficient as equal to 12.99×10^{-15} cm²/sec.

It is necessary to compare the result obtained with the value of the diffusion coefficient of carbon in hardened austenite measured by another method as was done in work [1], in which a formula was presented for determining the values of D_C^{γ} in hardened austenite which was obtained on the basis of converting the data from work [8] obtained at higher temperature:

$$D_C^{\gamma} = 0.4 exp\left[\frac{36,600}{RT}\right]. \qquad (2)$$

The feasibility of the extrapolation to low temperatures is given in work [1].

The value of the diffusion coefficient at the maximum on curve 1 of Fig. 7 ($\sim$290°) using formula (2) is found to be equal to 2.5×10^{-15} cm²/sec, that is, of the same order as when calculating by formula (1).

It is possible to assess the diffusion coefficient of carbon in austenite which has not been hardened by the data from work [9]. For steel with 0.7 per cent carbon content a similar conversion gives $D_C^{\gamma} = 7.10^{-3}$ cm²/sec at 290°. This latter value of the diffusion coefficient differs substantially from that measured on the basis of experimental data using formula (1). A comparison of the

values of diffusion coefficients of carbon in austenite allows one to think that a certain part may be played by diffusional relaxation in the formation of the maximum on curve 1 of Fig. 7.

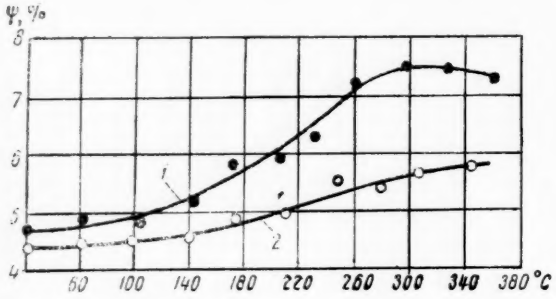

Fig. 7. Temperature trend of damping of torsional vibrations in hardened and low temperature tempered steel U7A:
1 – hardening (200°) at a stress of 18 kg/mm^2;
2 – tempering (100°) at a stress of 17 kg/mm^2.

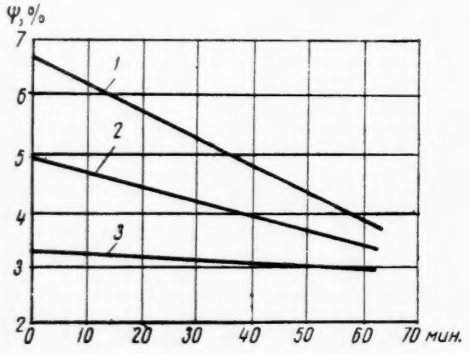

Fig. 8. The dependence of the damping of torsional vibrations on the duration of holding hardened specimens of steel U7A at a tempering temperature of 200° and at stresses of:
1 – 18; 2 – 16; 3 – 14 kg/mm^2.

Side by side with the continuous measurements of vibration damping in hardened specimens dependent upon temperature, tests were carried out at 200° in the course of of the tempering process. In this case an increase in the rigidity of the steel was expected resulting from the decay of residual austenite. The results obtained are presented in Fig. 8; the measurements were carried out every ten minutes for an hour.

The data obtained show a linear decrease in vibration damping with time, which is connected with the decay of residual austenite at the tempering temperature.

CONCLUSIONS

1. A study was made of the damping of torsional vibrations in hardened and tempered steel U7A and 50A with successive straining, and also after cold working, single and double hardening, at room temperature and with continuous heating to 360°.

2. In the hardened steel with the highest carbon content (U7A) at high stresses, a decrease in vibration damping appears when straining the specimens.

3. Cold working of hardened and low temperature tempered specimens (right up to 200°) leads to a decrease in the damping capacity of the steel.

4. A second hardening of the specimens decreases their capacity to damp out vibrations.

5. Measurements of the vibration damping in hardened specimens of steel U7A showed the presence of a temperature maximum on the curve at $\sim$ 290° with continuous heating. Calculations of the diffusion coefficients for steel U7A showed, according to the data of the present work and work [1], that a certain role is played by relaxation in the austenite due to diffusion.

6. The experimental data testify to the significant influence exerted by residual austenite on the damping capacity of hardened and low temperature tempered steel of the types investigated.

Translated by J.J. Cornish

REFERENCES

1. M.A. Krishtal and S.A. Golovin, *Fiz. metal. metalloved.*, 8, 294 (1959),
2. M.A. Krishtal and S.A. Golovin, *Nauch. dokl. vysshei shkoly, otd. metallurgiia*, No.2 (1959).
3. A.P. Gulyayev, *Termicheskaia obrabotka stali (Heat treatment of steel)* Mashgiz. (1953).
4. A.D. Le Kler, *Usp. fiz. metal.*, No.1 (1956).
5. A.S. Novik, *Usp. fiz. metal.* p.7, No.1, (1956).

6. C.A Wert, *J. Appl. Phys.*, 21, (11), 1196 (1950).
7. V.A. Pavlov, N.F. Kriuchkov and I.D. Fedotov, *Fiz. metal. metalloved.*, 5, Vol.2, 371 (1957).
8. M.A. Krishtal, *Metalloved. obrab. metal.*, No. 7, 20 (1957).
9. K. Wells and R. Mehl, *Metals Technology*, No.8 (1940).

VOL.
8
1959

LETTERS TO THE EDITOR

CONCERNING FERROMAGNETICS WITH TWO CURIE POINTS*

V.L. BONCH-BRUYEVICH

Lomonosov Moscow State University

(Received 10 November 1958)

Previously it has been shown [1] that structural defects of a definite type can play the part of "centres of demagnetization" in ferromagnetics; in the vicinity of such defects, local levels of spin are formed, that is to say the localization of "left-handed" spins (orientated opposite to the original direction) is energetically advantageous. Such systems, obviously, are characterized by elementary perturbations of two types: – by normal spin waves and by "right-handed"spins in the defects. Let us signify by z the maximum number of left-handed spins capable of being localized at one defect, and let us assume for the sake of simplicity that the energy connected with the change in spin orientation of each of them ΔE is not dependent upon the number of the remainder. Then the average number of right-handed spins in the vicinity of a given defect will be [2]:**

$$n = \frac{1}{e^{\frac{\Delta E}{kT}} - 1} - \frac{z+1}{e^{\frac{\Delta E}{kT}(z+1)} - 1}. \qquad (1)$$

Further, let the concentration of defects of the type in question be c. Then for spontaneous magnetization at a temperature of T we shall obtain:

$$M = M_0\{1 - f(T) - 2zc + 2cn\}, \qquad (2)$$

where $f(T)$ is the function, which is determined by the average number of spin waves; M_0 is the constant. In particular, when $z \geqslant 2$, $T \ll T_c$ (T_c is the normal Curie point) the equation (2) takes the form of:

$$M = M_0\{1 - 2cz + 2ce^{-\frac{\Delta E}{kT}}\}. \qquad (3)$$

As was pointed out in work [1] the concept about local levels of spin remains in force even with rather large concentrations of defects. Therefore, in principle the occasion would be possible when;

$$1 - 2cz < 0, \qquad (4)$$

but when $T \gg T_0 > 0$ the whole of the brace in formula (3) becomes positive ($T_0 \ll T_c$). This would imply that at absolute zero a given substance (on the strength of the demagnetizing influence of the defects) is not ferromagnetic, but at a certain temperature T_0 (the lower Curie point) it is transformed into a ferromagnetic thanks to the change in spin orientation in the local levels (the condition when $T_0 \ll T_c$ ensures the proper smallness of the demagnetizing influence of the spin waves). Thus a ferromagnetic with two Curie points is obtained.** For T_0 we obtain, obviously:

$$T_0 = \frac{\Delta E}{k} \cdot \frac{1}{\ln \frac{2c}{2cz-1}} \qquad (5)$$

From this it is clear that the conditions for the existence of such a substance are rather

---

* *Fiz. metal. metalloved.* 8, No.2, 309-310, 1959.

** In the corresponding formula in work [1], instead of z, the symbol Nz has been figured erroneously, where N is the total number of defects. This error, as can easily be understood, does not influence the results of [1] except the last result (the sixth) which is incorrect.

* The possible existence of two Curie points in ferromagnetic semiconductors was discussed in work [3] in which, however, a completely different mechanism of the phenomenon was being studied.

inflexible: apart from the inequality of $T_0 \ll T_c$ the following must also take place:

$$\frac{1}{2c} < z < \frac{1}{2c} + 1. \qquad (6)$$

Apparently the predicted effect of the disappearance of ferromagnetism at low temperatures should be sought in solid solutions of non-ferromagnetic substances in ferromagnetic substances. Actually, as was remarked in work [1], the dissolved atoms can be regarded as structural defects as soon as they are lined up in an irregular manner (the concentration c must be sufficiently small so that occasions are rare when dissolved atoms are directly adjacent to one another; in as much as z, apparently, is of the order of the co-ordination number, this does not contradict the condition in (6)).

It must be emphasized however, that local levels of spin are not always formed in such solutions – it depends on the nature of the solute and the solvent. Unfortunately it is not possible to express the conditions for the existence of local levels indicated in work [1] by directly observable physical-chemical characteristics without resorting to more or less clumsy models.

Translated by J.J. Cornish

REFERENCES

1. V.L. Bonch-Bruyevich, *Fiz. metal. metalloved.* 2, 215 (1956).
2. Ter Haar, *Physica*, 18, 199 (1952).
3. S.V. Vonsovskii and Ye.N. Agafonova, *Sbornik, posviashchennyi semidesiatiletiiu Akademika A.F. Ioffe (Symposium dedicated to the seventieth birthday of Academician A.F. Ioffe)* Izd. Akad. nauk SSSR, Moscow, 1950.

VOL. 8 1959

THE INFLUENCE OF PLASTIC DEFORMATION ON INTERNAL FRICTION IN IRON AND AN IRON-NICKEL ALLOY*

R.S. LEBYEDEV and V.S. POSTNIKOV

Kemerovo State Pedagogic Institute

(Received 6 March, 1959)

The present work investigates the influence of plastic deformation on internal friction in iron-based alloys by the same method and under the same conditions as before [1], with the one difference however that the heating rate was slightly higher, namely: $\gamma = 6°/\text{min}$. The error in measuring internal friction at high temperatures was reduced to $\sim$1 per cent. The results of investigation on electrolytic iron at rooling reductions of 8, 17, 30, 47, 70 and 92 per cent, and on iron-nickel alloy (armco iron – 4% Ni) at rolling reductions of from 20 to 80 per cent, are presented in Figs. 1-5 and in the table. The specimen was annealed at 825° for one and a half hours.

From Figs. 1-5 and the tabular data concerning the dependence of internal friction in iron and iron-nickel alloy on the degree of prior deformation, the heating speed and the duration of isothermal holding, one can draw basically the same conclusions as for iron-tungsten alloy [1]. The same can also be said about the connexion between the level of internal friction and the strength of the alloy at high temperatures. However, for internal friction in the iron-nickel alloy there are some characteristic peculiarities.

As can be seen from Fig. 3, internal friction in the iron-nickel alloy has two maxima, whereas internal friction in the iron-tungsten alloy has one maximum, which disappears completely when measurements are repeated after annealing at high temperature. The first maximum of internal friction in the iron-nickel alloy almost completely disappears after high temperature annealing, but the second does not. Consequently the first maximum depends basically on prior deformation, and is connected with the phenomenon of recrystallization. It is easy to convince oneself of this, by determining the activation energy from pure shear by the curve $Q^{-1}(T)$ when changing the vibrational frequency (cf the table), and then comparing

TABLE 1

Results of the investigations on iron-nickel alloy

Extension (%)	Average diameter of grains (mm)	Rupture stress (kg/mm²)			Activation energy (cal/mole)		
		Before annealing	After annealing		Restoration Q^{-1}	I maximum	II maximum
		25°	25°	840°*			
20	0.028	56.4	33.7	1.09	4600	62,000	69,000
40	0.025	60.0	35.0	1.01	4200	58,000	65,000
50	0.023	61.5	35.8	0.97	3700	56,000	63,000
60	0.021	63.0	37.0	0.93	3300	55,000	62,000
70	0.019	64.0	37.9	0.84	2900	53,000	60,000
80	0.018	67.0	39.0	0.85	2700	51,000	59,000

* Heating, as in work [1] was carried out by an electric current.

* *Fiz. metal. metalloved.* 8, No.2, 310-314, 1959.

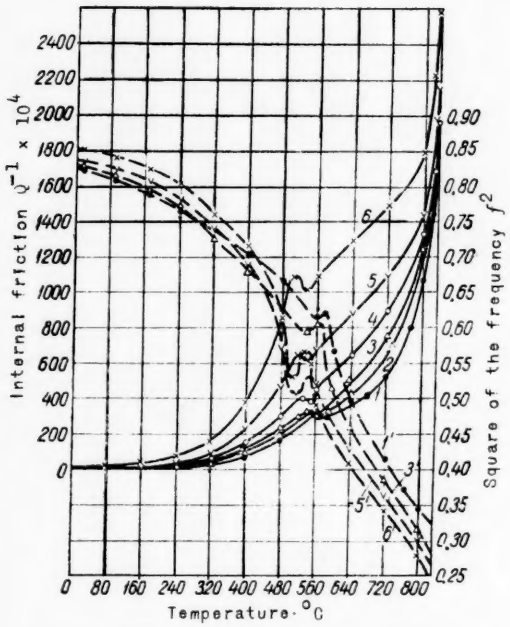
Internal friction $Q^{-1} \times 10^4$
Square of the frequency f^2
Temperature °C
0 80 160 240 320 400 480 560 640 720 800
1 1' 2 3 3' 4 5 5' 6 6'

Fig. 1. The temperature dependence of internal friction (curves 1-6) and the modulus of elasticity in shear (curves 1'-6') of plastically deformed iron:
1,1' - 8; 2 - 17; 3,3' - 30; 4 - 48; 5,5' - 70; 6,6' - 92% extended.

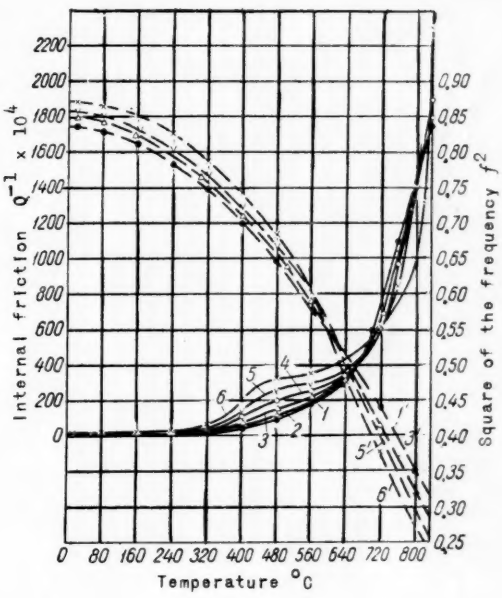
Internal friction $Q^{-1} \times 10^4$
Square of the frequency f^2
Temperature °C
0 80 160 240 320 400 480 560 640 720 800
1 1' 2 3 3' 4 5 5' 6 6'

Fig. 2. Temperature dependence of internal friction and the modulus of elasticity in shear of annealed electrolytic iron after annealing at 825°:
1,1' - 8; 2 - 17; 3,3' - 30; 4 - 48; 5,5' - 70; 6,6' - 92% extended.

the data obtained with those of other researchers [2].

The appearance of the second maximum, which does not disappear, even after annealing, is apparently connected with grain boundary relaxation, because the height of the peak depends substantially upon the grain size of the testpiece. As can be seen from the table, the activation energy of this process is slightly greater than the activation energy of the recrystallization process. Both these activation energies decrease monotonously when increasing the degree of plastic deformation. Just as the recrystallization temperature for the iron-tungsten alloy lies in the region of 660-720° [1,2], so the second maximum for this alloy can be expected at a temperature higher than 840°. But measurements of internal friction were not carried out at temperatures higher than this.

As a result of comparing internal friction in the iron-nickel alloy with that in the iron-tungsten alloy at a temperature of 840°, for example for specimens with a 20 per cent extension and for rupture stresses at the same temperature, it can be seen that the level of internal friction can serve as a sort of characteristic of the strength of the alloy at high temperature. Other researchers have reached the same conclusion [3] when measuring the internal friction of the alloys nickel-titanium and nickel-chromium.

With regard to the activation energy of the process of restoring the internal friction with isothermic holding, which is determined in the same way as in work [1] by kinetic curves, its value as before, is considerably less than the activation energy of diffusion, and even less than the activation energy of recrystallization. On the strength of this circumstance it can be concluded that the process of restoring the internal friction of pure metals and alloys is not diffusional, but takes place in another way. It is still a little early to talk about the mechanism of dislocation in the process of restoration [4-6], because there is not sufficient ex-

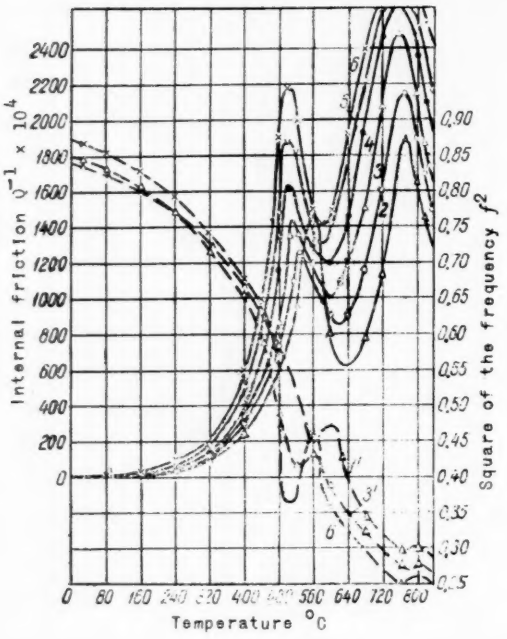

Fig. 3. Temperature dependence of internal friction (curves 1-6) and the modulus of elasticity in shear (curves 1'-6') of plastically deformed iron-nickel alloy:
1,1' – 20%; 2 – 40%; 3,3' – 50%; 4 – 60%; 5 – 70%; 6,6' – 80% extended.

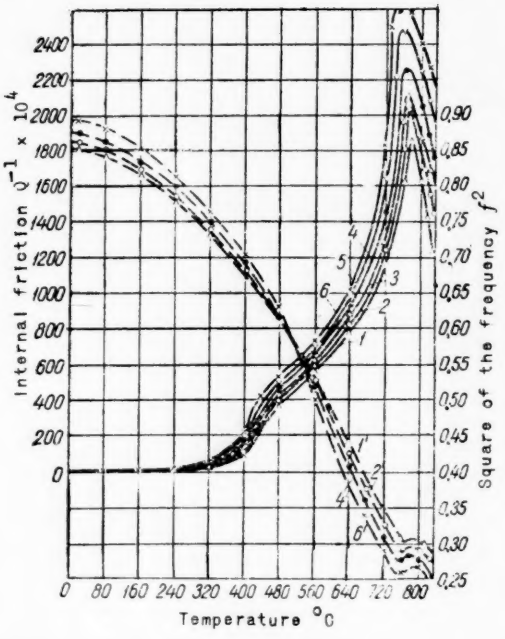

Fig. 4. Temperature dependence of internal friction and the modulus of elasticity in shear of iron-nickel alloy after annealing at 825°:
1,1' – 20%; 2,2' – 40%; 4,4' – 60%; 5 – 70%; 6,6' – 80% extended.

perimental material or reliable information on the value of the activation energy of the movement of the dislocations or on the dependence of their mobility upon temperature.

Translated by J.J. Cornish

REFERENCES

1. V.S. Postnikov and B.S. Lebyedev, *Fiz. metal. metalloved*, 8, No.1 (1959).
2. L.I. Kogan and R.N. Entin, *Probl. metalloved. fiz. metal.*, 2, 214 (1951).
3. E.Z. Kaminskii and V.M. Rozenbyerg, *Sbornik. Issledovaniye po zharoprochnym splavam. (Research into heat resisting alloys. – Symposium)* 2, 34 (1957).
4. A.S. Nowick, *Progress in Metals Physics*, 4, 1 (1953).
5. G. Loschner, *Technik*, 11, 289 (1956)
6. V.S. Postnikov, *Usp. fiz. nauk*, 66, 43 (1958).

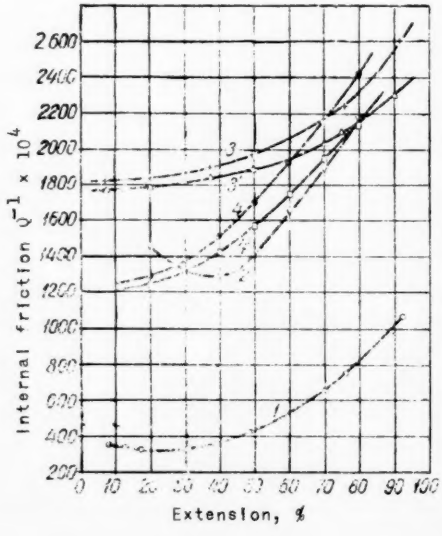

Fig. 5. The dependence of the internal friction peak (1 – Fe, 2 – Fe–4% Ni) and its level at 840° on the amount of extension (3,3' – Fe; 4,4' – Fe–4% Ni) before and after annealing. Vibrational frequency ~0.6 periods/sec.

VOL 8 195

THE INFLUENCE OF BORON ON THE RECRYSTALLIZATION OF SILICON IRON*

V.Ye. NEIMARK and V.M. ROZENBYERG

(Received 16 October 1958)

We have studied the influence of boron on the kinetics of recrystallization in an iron-silicon alloy containing 3% Si, 0.03% C, 0.2% Mn, 0.01% P. A study was made of the alloy without boron, and also containing 0.003%, 0.005% and 0.01% B.

The study of recrystallization after cold rolling to 60 per cent extension was carried out by the X-ray method. The commencement of recrystallization corresponded to the appearance of the characteristic "pin points" on the X-ray photograph. Data are given in Fig. 1 which show the connexion between temperature and time, both of which are necessary for the commencement of recrystallization. It can be seen from the graph that T and τ, as is usual in recrystallization, are connected by the exponential dependence $\tau = A\exp(Q/RT)$ (A is the pre-exponential multiplier, depending upon the mechanism of the process; R is the gas constant; Q is the activation energy of the process).

By using the data obtained, one can determine the temperature of the commencement of recrystallization at a selected annealing time, the activation energy of the recrystallization and the value of the pre-exponential multiplier. The dependence of the corresponding data on the concentration of boron is shown in Fig. 2.

The temperature at which recrystallization begins (for holding one hour) changes in a complicated way, passing through the maximum at a boron concentration of 0.005 per cent. A similar character of the concentration depedence of the temperature of recrystallization is well known [1]. In the present case, the increase in the temperature of recrystallization when introducing up to 0.005% B, because of the very small quantities of the latter, cannot be explained by a change in the forces of interatomic bonds.

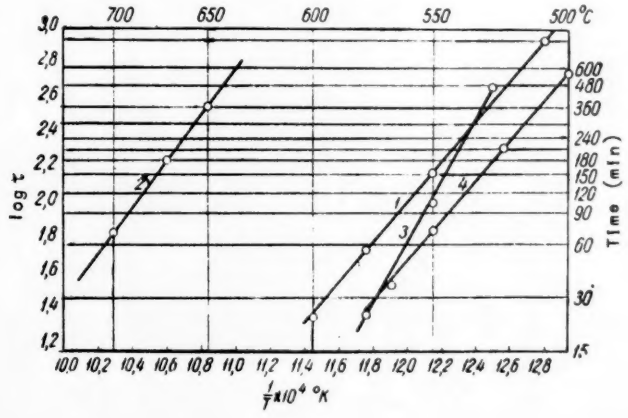

Fig. 1. The connexion between the temperature and the time of commencement of recrystallization in the alloys investigated: 1 – 0.003% B; 2 – 0.005% B; 3 – 0.01% B; 4 – without boron.

* *Fiz. metal. metalloved.* 8, No.2, 314-316, 1959.

Apparently the introduction of boron leads to a decrease in the value of the surface

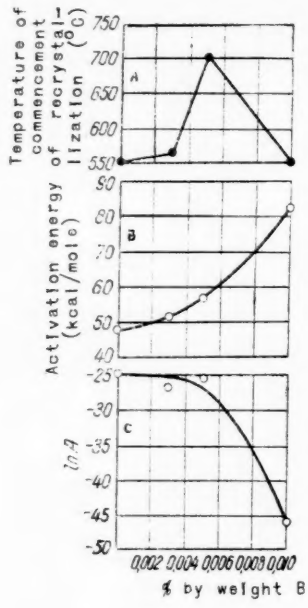

Fig. 2

tension of the grains. The fall in the temperature of the commencement of recrystallization in the alloy containing 0.01% B can be explained by the transition of the alloy into the two-phase region, which is confirmed by metallographic observations. The presence of particles of the second phase can simplify the nucleation of new grains in recrystallization and lower its temperatures.

As can be seen from Fig. 2b, the activation energy of the process increases continuously by increasing the concentration of boron. It is a curious fact that the value of Q increases when the temperature of the commencement of recrystallization decreases for the alloy with 0.01% B. A similar increase in the activation energy of recrystallization, when the temperature of recrystallization decreases, was proved in work [2] when studying the influence of carbon on the recrystallization of iron-nickel-manganese austenite. The difference in character of the concentration dependence of individual parameters of recrystallization of complex solid solutions, in which one of the elements is dissolved by a sort of implantation, requires special study.

Translated by J.J. Cornish

REFERENCES

1. V.I. Ivyeronova, Sborn. *Primeneniye rentgenovskikh luchei k issledovaniiu materialov (The application of X-rays to the study of materials)*, Mashgiz, p.34 (1949).
2. E.Z. Kaminskiĭ and V.M. Rozenbyerg, *Fiz. metal. metalloved.* 6, No.6, 1036 (1958).

CONCERNING MAGNETIC ANISOTROPY ON THE BASIS OF SPIN-ORBIT INTERACTION*

Iu. A. IZIUMOV

A.M. Gor'kii Urals State University

(Received 11 November 1958)

VOL. 8 1959

It is accepted that magnetic anisotropy in ferromagnetic crystals is the consequence of two effects: spin-orbit interaction, and the action of the crystalline field linking the electron orbits of the atoms with the crystallographic axes. Other anisotropic interactions cannot explain the sharp drop in the anisotropy constants with temperature. On the basis of these considerations Vonsovskii [1] gave a qualitative explanation of the temperature dependence of the anisotropy constants of cobalt, but the quantitative theory runs up against great difficulties due to ignorance of the distribution of orbital moment throughout the crystal.

However, the constancy of the g factor over a wide range of temperatures indicates that the distribution depends only slightly upon temperature. By using this fact we can give a semi-phenomenological treatment of magnetic anisotropy in the sense that the exchange interaction between electrons is examined according to microscopic theory, and the effect of the orbits on electron spin is replaced by a certain effective orbital magnetic field, which, however, changes from point to point in the crystal.

In the co-ordinate system linked, with the axes of the lattice the Hamiltonian of the system of N spins, which correspond to the lattice points, is written as:

$$\hat{\mathbf{H}} = \hat{\mathbf{H}}_0 + \hat{\mathbf{H}}_1,$$

$$\hat{\mathbf{H}}_0 = -\sum_{f_1 \neq f_2 \alpha} I(f_1 - f_2) S^{\alpha}_{f_1} S^{\alpha}_{f_2}; \qquad (1)$$

$$\hat{\mathbf{H}}_1 = -2\mu_0 \sum_{f\alpha} H^{\alpha}_f S^{\alpha}_f,$$

where S^{α}_f is the spin operator; $I(f_1 - f_2)$ is the effective exchange integral; H^{α}_f is the component of the orbital magnetic field at point f; μ_0 is the Bohr magneton; $\alpha = x, y, z$.

For the future it is convenient to transform to the co-ordinate system whose axis z' is directed along the magnetization vector, so that:

$$S^{\alpha}_f = \sum_{\alpha'} C_{\alpha\alpha'} S^{\alpha'}_f, \qquad (2)$$

where $C_{\alpha\alpha'}$ is the transformation matrix. Limiting oneself to the case of low temperatures, in the new co-ordinate system one may transform from spin operators to Bose operators b_f and express the Hamiltonian through their Fourier components $b_{\vec{k}}$ ($\vec{k}$ is the quasi-impulse) as:

$$\hat{\mathbf{H}}_0 = \sum \varepsilon_{\vec{k}} b^{+}_{\vec{k}} b_{\vec{k}}; \quad \varepsilon_{\vec{k}} = 2s \sum_{\vec{h}} I(\vec{h})(1 - e^{i\vec{h}\vec{k}}).$$

$$\hat{\mathbf{H}}_1 = \sum_{\vec{k}_1 \vec{k}_2} L^{z'}(\vec{k}_2 - \vec{k}_1) b^{+}_{\vec{k}_1} b_{\vec{k}_2} - \sum_{\vec{k}} (L^{+}_{\vec{k}} b_{\vec{k}} + \qquad (3)$$

$$+ L^{-}_{\vec{k}} b^{+}_{\vec{k}}) - \frac{1}{N} \sum_{f\alpha} H^{\alpha}_f C_{\alpha z'},$$

where

$$L^{\pm}_{\vec{k}} = \mu_0 \left(\frac{2s}{N}\right)^{1/2} \sum_{f\alpha} H^{\alpha}_f e^{\pm i\vec{f}\vec{k}} (C_{\alpha x'} \mp i C_{\alpha y'});$$

$$L^{z}(\vec{k}) = \frac{2\mu_0}{N} \sum_{f\alpha} H^{\alpha}_f e^{i\vec{f}\vec{k}} C_{\alpha z'}.$$

Regarding $\hat{H}_1$ as a perturbation, the free energy can be calculated as an $\hat{H}_1$ series, using the thermodynamic theory of perturbations [2],

* *Fiz. metal. metalloved* 8, No. 2, 316-318, 1959.

$$F = F_0 + F_1 + F_2 + \dots$$

$$F_1 = \langle \hat{\mathbf{H}}_1 \rangle ; \qquad (4)$$

$$F_2 = \frac{1}{2}\{\beta \langle \hat{\mathbf{H}}_1 \rangle^2 - \int_0^\beta \langle e^{\lambda \hat{H}_0} \hat{\mathbf{H}}_1 e^{-\lambda \hat{H}_0} \hat{\mathbf{H}}_1 \rangle d\lambda\},$$

where $\langle \dots \rangle$ signifies expectation over the statistical ensemble with Hamiltonian H_0; $\beta = (kT)^{-1}$ (k is the Boltzmann's constant). Substituting the expression (3) in (4) and carrying out the calculations indicated, we shall find the dependence of free energy on the angles.

From the requirement of symmetry for a uniaxial crystal the following must be true:

$$F = F_0 + K_1 \cos^2\theta + \dots , \qquad (5)$$

where θ is the angle between the magnetization vector and the crystal axis, and the first constant of anisotropy is called K_1. Comparing (5) with the expression obtained from (4) leads to the equations:

$$\sum_f \mathbf{H}_f^\alpha = 0, \qquad (6)$$

$$K_1 = 2\mu_0^2 s \sum_{\vec{k}} \frac{\Lambda(\vec{k})}{\varepsilon_{\vec{k}}} - \frac{4\mu_0^2}{N} \sum_{\vec{k}_1 \vec{k}_2} \frac{\Lambda(\vec{k}_1 - \vec{k}_2)}{\varepsilon_{\vec{k}_1} - \varepsilon_{\vec{k}_2}} \langle n_{\vec{k}_2} \rangle , \qquad (7)$$

$$\Lambda(\vec{k}) = |H_{\vec{k}}^z|^2 - |H_{\vec{k}}^x|^2; \quad H_{\vec{k}}^\alpha = \frac{1}{\sqrt{N}} \sum_f H_f^\alpha e^{i\vec{f}\vec{k}}. \qquad (8)$$

In formula (7) $\langle n_{\vec{k}} \rangle$ is the Bose function of distribution for spin waves. $H_{\vec{k}}^z$ and $H_{\vec{k}}^x$ are magnitudes analogous to Fourier components for the orbital magnetic field of the crystal.

In this way, constants of anisotropy are expressed by magnitudes which are determined by the distribution of orbital moments in the crystal. In spite of the fact that the overall orbital effective field in a crystal is on the average equal to zero (expression (6)), the fluctuations of this field at individual points in the crystal lead to anisotropy.

To obtain the temperature dependence of K_1 it is necessary to know the function $\Lambda(\vec{k})$. It is not possible to find it within the framework of the present theory; at present the theoretical determination of the distribution of orbital moment offers a very difficult problem. Some general ideas about this can be obtained from an analysis of the crystalline and magnetic symmetry group of a crystal.

Apart from this, some data can be obtained from a comparison of the experimental temperature curve of K_1 with the theoretical expression (7). In particular if it is admitted that K_1 decreases with temperature according to the law $\sim T^{3/2}$ (to which a phenomenological calculation often leads), then one must accept $\Lambda_{\vec{k}} \sim \frac{1}{k} + \dots$ These questions will be discussed in another paper.

I wish to express deep gratitude to E. A. Turov for his valuable advice in the compilation of this paper, and to Corresponding Member of the Academy of Science of the U.S.S.R., S.V. Vonsovskii for discussing the results.

Translated by J.J. Cornish

REFERENCES

1. S.V. Vonsovskii, *Zh. eksp. teor. fiz.*, 8, 1104 (1938).
2. S. Nakajima, *Advances Phys.*, 4 (No.6), 363 (1955).

PHASE ANALYSIS BY THE SUPERPOSITION METHOD USING ELECTRON DIFFRACTION*

L.S. PALATNIK and B.T. BOIKO

A.M. Gor'kii Khar'kov State University and
V.I.Lenin Polytechnic Institute

(Received 25 January 1959)

VOL. 8 1959

The absence of a method of quantitive phase analysis using electron diffraction restricts the possibility of studying in detail processes which are taking place in thin films and surface layers of metals and alloys. The peculiarities of analysis by the electron diffusion method prevent the use of the techniques of such well known methods of X-ray phase analysis as the mixing method, the independent standard method and their various modifications.

In the present work a method is suggested for quantitive phase analysis by electron diffraction which is a further development of the superposition method in roentgenography [1]. However in contrast to the X-ray method of superposition in which an alternate exposure of movable free structural components (of standard specimens) is achieved on one and the same X-ray photograph by means of a fixed X-ray beam, in the electron diffraction method of superposition the primary electron beam us displaced while the specimens to be exposed remain fixed. In this way an oscillating beam creates two displaced diffraction pictures on one and the same photographic plate. Alternate displacement of the primary electron beam is achieved by supplying rectangular potential pulses from a pulse generator onto deflecting plates positioned between the diaphragm and the object in the electron diffraction camera (Fig. 1).

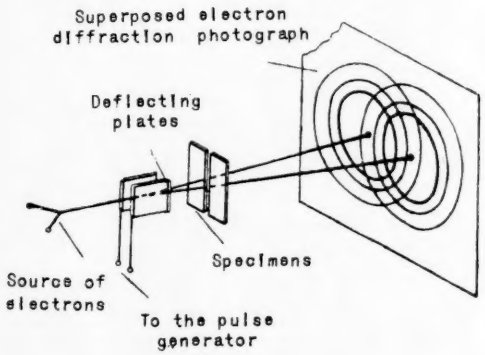

Fig. 1 Diagram for taking electron diffraction superposed photographs

In the present work an electron diffraction camera designed by Pines and Bublik was used [2].

The extent of the displacement of the primary electron beam on the object and consequently on the diffraction picture as well can be changed at will by changing the pulse height. By changing the duration of the pulse or the frequency at which it is supplied, it is possible to obtain a superposed diffraction picture, which is displaced in relation to the basic diffraction picture, with the required ratio between the intensities of the diffraction maxima being compared. The use of electromagnetic pulses ensures the complete inertness of the electron beam displacement. At a given ratio of exposure times (τ_1 and τ_2) the other photographic conditions with basic and deflected beams (the stability of the accelerating voltage, and consequently the wavelength λ and the action of the electron beams on the photographic plates) will be the same, thanks to the sufficiently high frequency of the pulse supply; ν = 10 kc/s. At an exposure time of 1-2 sec such a frequency gives 10,000 – 20,000 displacements

* *Fiz. metal. metalloved.* 8, 2, 318-320, 1959.

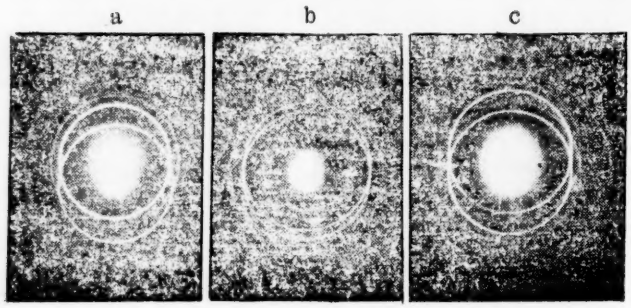

Fig. 2 a – superposed electron diffraction picture for Al + Bi at $\tau_1 = \tau_2$; b – superposed electron diffraction picture for Bi + Bi at $\tau_1 = \tau_2$; c – superposed electron diffraction picture for Al + Al at $\tau_1 = \tau_2$.

of the primary electron beam.

The technique being described permits a superposed diffraction picture to be obtained either from two different films or from one film. The electron diffraction pictures given in Fig. 2 can serve as an example of superposed diffraction pictures such as this.

The suggested method of electron diffraction phase analysis can be used in two ways.

By the first way, auxiliary superposed calibration pictures of a two-phase system are obtained first (cf. Fig. 2a). Reflections from two free structural components of the alloy being studied are alternately exposed on these diffraction pictured within a sufficiently small time interval. The optimum amount of displacement is selected in such a way that the lines of diffraction being compared do not coincide on the superposed diffraction pictures. For each two-phase system to be studied, one can take beforehand a series of superposed calibration diffraction pictures, differing from one another by a gradual change in the relation of the intensities of the lines being compared, which is accomplished by varying the exposure times τ_1 and τ_2. By a contrast of the intensities of the lines on the superposed calibration diffraction picture and on the diffraction picture of the heterogeneous alloy (two-phase mixture), the ratio of phase concentrations in the alloy by volume is determined.

The method of obtaining a superposed electron diffraction picture from two films can be used for other purposes as well.

By obtaining two displaced diffraction pictures of one and the same metal from two films, one can study the influence exerted by the conditions under which the film was prepared, its thickness and so on, upon the expansion and intensity of the lines of diffraction. In this case one can contrast one and the same line on the basic and the displaced diffraction pattern of a superposed electron diffraction photograph obtained from two different specimens. One of these specimens can be a film of metal obtained under certain standard conditions, and the other, a film of the same metal obtained by varying the conditions of evaporation, condensation, heat treatment and so forth. When $\tau_1 = \tau_2$ the conditions of taking electron diffraction photographs of these two films will be identical.

By the second way of using the suggested method, the quantity of one or another phase in a heterogeneous alloy (mixture) is determined by the threshold of response of the corresponding diffraction lines, in the same way as it is done in X-ray spectral analysis. The threshold of response of the diffraction lines is determined under selected photographing conditions by electron diffraction photography using the method of superposing two neighbouring portions of a specimen which contains only one (free) structural constituent of the alloy cf. Fig. 2(b-c)). The quantity of a given phase in a heterogeneous alloy is determined automatically when any one diffraction line, whose theshold of response is known, is situated at the limit of visual range. If, under selected photographing conditions, the diffraction lines of the heterogeneous alloy

VOL 8 195

being investigated are intense enough, the displaced superposed diffraction picture weakens to the point where the intensity of any diffraction line reaches the threshold of response. The phase concentration can be found in this case from the ratio $y = na$ (y is the concentration; n is the multiplicity factor of the weakening of the displaced diffraction picture; a is the predetermined threshold of response of the diffraction line in percentage by volume.

The second way of using the suggested method can be employed with particular effectiveness when studying oxidation, chemical and heat treatment of single-constituent films of metal and so on.

Translated by J.J. Cornish

REFERENCES

1. L.S. Palatnik, *Izv. Akad. Nauk. SSSR ser. fiz.*, 5, 134 (1951).
2. B.Ia. Pines and A.I. Bublik, *Zh. tekh. fiz.*, 24, 1139 (1954).

VOL.
8
1959

No. 3

		PAGE
Ordering in ternary alloys	O. Mdivani and Gachechiladze	1
The importance of indirect interaction in the theory of magnetization of transition metals and rare earths	A. A. Berdyshev and B. V. Karpenko	10
Concerning binary solid solutions with interatomic bonds of two types	A. N. Men' and A. N. Orlov	17
The Hall effect in iron-nickel alloys near the Curie point	N. V. Bazhanova	22
On the problem of anomalous behaviour of the coercive force of quenched and highly annealed steels	M. N. Mikheev and G. S. Tomilov	26
The laws of intra-crystalline distribution of elements in metal alloys	A. S. Zav'yalov and B. I. Bruk	29
A study of self-diffusion in zirconium and its alloys with tin	V. S. Lyashenko, V. N. Bykov and L. V. Pavlinov	40
The effect of hydrogen on alloy VT-8 with increased creep stress	I. I. Kornilov, C. G. Glazunov and A. M. Yakimov	47
The study of aluminium alloys of the Al-Cu-Mg system in samples of variable composition	L. S. Palatnik, G. B. Fedorov and H. T. Gladkikh	54
Electron microscopic investigation of etching figures in aged aluminium alloys	N. N. Buinov, T. V. Shchegoleva, V. G. Rakin, M. F. Komarova and R. R. Zakharova	62
Homogeneous ageing of unsaturated solid solutions	A. A. Presniakov, L. I. Duatova and Iu. F. Kliuchnikov	68
Investigation of the tempering of cold deformed K40NKhM alloy	B. G. Livshits and N. G. Makhukov	73
Transformation of austentite into martensite under high pressure	A. I. Stregulin and L. A. Mel'nikov	79
Structure changes and anomalous temperature dependence of the magnetic properties of Ni-Fe alloys (50% Ni)	M. V. Dekhtyar and N. M. Kazantseva	84
Mechanical properties of nickel-aluminium alloys	V. A. Pavlov and I. A. Pereturina	88
Relationship of creep of nickel-copper alloys to solid solution concentration and deformation conditions	M. G. Gaidukov and V. A. Pavlov	95
Some peculiarities of transformer steel on rapid heating. 2; Kinetics of texture formation	P. D. Izbranov, V. A. Pavlov and H. M. Rodizin	101
Internal friction of metastable solid solutions	B. G. Livshits, Iu. S. Avraamov, V. B. Osvenskii, S. O. Mebzennaia and L. N. Beliakov	107
Determination of the number of arbitrary parameters of the short range order for multicomponent alloys	A. N. Men'	116
Studies of reaction diffusion in binary systems of the "metal gas" type	V. I. Arkharov and E. B. Blankova	119
Some peculiarities in the disposition of corrosion figures in the alloy Al-Zn-Cu	N. N. Buinov and T. V. Shchegoleva	122
Some regularities of the change of forces of the inter-atomic bond in the alpha-solid solutions of systems with electron compounds	G. P. Kushta and O. I. Rybailo	125
Temperature dependence of magnetic properties of the alloy IU 16 (Alfenol)	O. N. Al'tgauzen and I. K. Kupalova	127
The increase in the coercive force of mixed ferrite-chromites of Lithium in the region of the compensation temperature	K. M. Bol'shova and T. A. Yelkina	129
On the polygonal structure of iron-aluminium alloys	B. V. Molotilov	132
On the type of defects in an alpha-leboite	F. A. Sidorenko, P. V. Gel'd and L. B. Dubrovskaya	134
A fine structure in brittle and ductile fracture of E1531 steel tubes in tests of expansion by a cone	E. Iu. Chemadurova	136
On the problem of intermediate carbide phases in carbon steels	N. V. Gudkova and V. P. Kuznetsova	138
Influence of the duration of treatment on the phase composition of iron which has been electrically hardened with graphite	B. P. Kolesnik	141

Electrical conductivity and the Hall effect in iron-silicon alloys containing leboite when subjected to high temperature
A. I. Gol'dberg, V. A. Lipatov and P. V. Gel'd 143

An investigation of pearlite transformation in segregated austentite powder
A. O. Gulyaev and V. D. Zelenova 146

An investigation of intermediate transformation in segregated austentite powder
A. O. Gulyaev and V. D. Zelenova 148

The X-ray *K* absorption at the temperature of liquid nitrogen
S. A. Nemnonov and K. M. Kolobova 150

VOL.
8
1959

VOL
8
19

ORDERING IN TERNARY ALLOYS*

O. MDIVANI and T. GACHECHILADZE

Tbilsk State University, Institute of Electronics,
Automation and Telemechanics Akad. nauk Gruz. S.S.S.R.

(Received 6 May 1958)

In the present work, an attempt has been made to extend formally the long-range order theory of binary alloys to the case of ternary alloys. It has not been possible to extend the long-range theory of Bragg and Williams directly to the problem of evaluating the Curie point, of ternary alloys, owing to mathematical difficulties. In order to describe the equilibrium properties of a ternary alloy it is necessary to introduce four order parameters [2, 3] the calculation of the free energy is then carried out in the normal manner. The conditions for equilibrium lead to a system of four transcendental equations relating the parameters of long-range order.

VOL. 8 1959

In the case of the binary alloys, the Curie point is obtained from the equation:

$$s = \text{th}\,\frac{V_0 s}{2kT}\,.$$

In the case of ternary alloys, it was not possible to calculate the Curie point from the analysis of the system of transcendental equations, equivalent to the above equation, owing to the awkwardness of the expressions. It is therefore impossible to derive a closed expression by these means. It will be shown later that, near the Curie point, it is possible to establish certain relations (starting from general considerations) between the four parameters of long-range order. These will enable us to obtain an approximate expression for the Curie point.

DEFINITION OF THE PARAMETERS OF THE SHORT-RANGE. PASSAGE TO THE LIMIT

We will consider a ternary alloy containing atoms of type A, B and C, and we let the corresponding concentrations be n_1, n_2 and n_3, respectively. Let us choose some site as a centre and consider another point whose co-ordinates with reference to the centre are (l, m, n). We can then introduce the following parameters of short-range order, after the manner of Cowley [4]:

(a) If atom A is in the centre:

$$\alpha^{2(1)}_{lmn} = 1 - \frac{P^{2(1)}_{lmn}}{n_2}\,,\quad \alpha^{3(1)}_{lmn} = 1 - \frac{P^{3(1)}_{lmn}}{n_3}\,. \tag{1a}$$

(b) If atom B is in the centre:

$$\alpha^{1(2)}_{lmn} = 1 - \frac{P^{1(2)}_{lmn}}{n_1}\,,\quad \alpha^{3(2)}_{lmn} = 1 - \frac{P^{3(2)}_{lmn}}{n_3}\,. \tag{1b}$$

* *Fiz. metal. metalloved.*, 8, No.3, 321-329, 1959.

(c) If atom C is in the centre:

$$\alpha_{lmn}^{1(3)} = 1 - \frac{P_{lmn}^{1(3)}}{n_1}, \quad \alpha_{lmn}^{2(3)} = 1 - \frac{P_{lmn}^{2(3)}}{n_2}, \tag{1c}$$

where $P_{lmn}^{i(f)}$ is the probability that if an atom j is at the centre then at the site (l,m,n) we find atom i ($i, j \equiv$ A, B, C $\equiv 1, 2, 3$).

It is easy to see that:

$$n_1 P_{lmn}^{2(1)} = n_2 P_{lmn}^{1(2)}, \quad n_1 P_{lmn}^{3(1)} = n_3 P_{lmn}^{1(3)}, \quad n_2 P_{lmn}^{3(2)} = n_3 P_{lmn}^{2(3)}. \tag{2}$$

Moreover:

$$\begin{aligned} P_{lmn}^{1(1)} &= n_1 + n_2 \alpha_{lmn}^{2(1)} + n_3 \alpha_{lmn}^{3(1)}, \\ P_{lmn}^{2(2)} &= n_2 + n_1 \alpha_{lmn}^{1(2)} + n_3 \alpha_{lmn}^{3(2)}, \\ P_{lmn}^{3(3)} &= n_3 + n_1 \alpha_{lmn}^{1(3)} + n_2 \alpha_{lmn}^{2(3)}, \end{aligned} \tag{3}$$

and

$$\alpha_{lmn}^{1(2)} = \alpha_{lmn}^{2(1)}, \quad \alpha_{lmn}^{1(3)} = \alpha_{lmn}^{3(1)}, \quad \alpha_{lmn}^{2(3)} = \alpha_{lmn}^{3(2)}. \tag{4}$$

Since an atom at the position (l, m, n) belongs to a given, say ith, shell ($i=1,2,\ldots$) and since there is no significance to co-ordinates of a site but only in its distance from the centre, we will write the index i in place of the indices (l,m,n).

It is said that there is a long-range order in the alloy if the α_i parameters tend to finite values when i becomes very large [4]. Our ultimate problem will be to find the limiting values of the short-range order.

To illustrate the procedure of passing to the limit, let us consider the structure $(\alpha^2\beta\gamma)$. In this case we have, in all, four sublattices: two for α-sites and one each for the β - and γ-sites.

We will define the long range order parameters in the following form:

$$S = \frac{2}{4}\frac{l_{11} - n_1}{1 - n_1} + \frac{1}{4}\frac{l_{22} - n_2}{1 - n_2} + \frac{1}{4}\frac{l_{33} - n_3}{1 - n_3}. \tag{5}$$

S is a sort of mean value of the order parameters of the respective sublattices.

We have denoted the mean fractional numbers of atoms of type i on the kth sublattice by l_{ik}. These nine quantities are connected by five linear relations. Hence it is clear that, by choosing as independent any four l_{ik}, it will be possible to express the remaining quantities in terms of these four. However, as shown in reference [2], this choice is not arbitrary: we cannot choose as independent variables any four non-diagonal l_{ik} at the same time. In our example we will choose as independent: l_{12}, l_{31}, and l_{23}, in addition to S. Hence for the stoichiometric relationship:

$$\begin{aligned} l_{11} &= \tfrac{1}{7}(4 + 3s - l_{12} - 2l_{31} + 2l_{23}), \quad l_{21} = \tfrac{1}{7}(3 - 3s + l_{12} - 5l_{31} - 2l_{23}), \\ l_{22} &= \tfrac{1}{7}(1 + 6s - 2l_{12} + 10l_{31} - 3l_{23}), \quad l_{13} = \tfrac{1}{7}(6 - 6s - 5l_{12} + 4l_{31} - 4l_{23}), \\ l_{33} &= \tfrac{1}{7}(1 + 6s + 5l_{12} - 4l_{31} - 3l_{23}), \\ l_{32} &= \tfrac{1}{7}(6 - 6s - 5l_{12} - 10l_{31} + 3l_{23}). \end{aligned} \tag{6}$$

VOL 8 195

We note, during the examination of the limiting values, that the main *a posteriori* probablities will depend only on the average state of order in the crystal. This occurs on the average state of order in the crystal. This occurs when the ith site is very distant from the centre ($t \to \infty$), and therefore we can neglect the influence of the centre.

The passage to the limit is accomplished as follows:

(1) If an α-site is central, then

$$\alpha_{i\,even}^{2(1)} = 1 - \frac{P_{i\,even}^{2(1)}}{n_2} \to 1 - \frac{l_{12}}{n_2}; \quad \alpha_{i\,even}^{3(1)} = 1 - \frac{P_{i\,even}^{3(1)}}{n_3} \to 1 - \frac{l_{31}}{n_3}. \tag{7}$$

The limiting values are actually such that in an even shell about an α-site, all sites will also be α-sites. Therefore the limiting value of the probability $P_{i\,even}^{2(1)}$ gives the probability that an atom B falls on α-site expressed in terms of the long-range order parameters. In a similar way we obtain the probability $P_{i\,even}^{3(1)}$

(2) If a β-site is central, then:

$$\alpha_{i\,even}^{2(1)} = 1 - \frac{P_{i\,even}^{2(1)}}{n_2} \to 1 - \frac{1}{2n_2}(l_{22} + l_{23}), \quad \alpha_{i\,even}^{3(1)} = 1 - \frac{P_{i\,even}^{3(1)}}{n_3} \to \\ \to 1 - \frac{1}{2n_3}(l_{32} + l_{33}). \tag{8}$$

Here the reasoning is the same as in the first case, but inasmuch as a β-site is now central, an even shell contains both β- and γ-sites. Consequently, the limiting value of $P_{i\,even}^{2(1)}$ will be equal to the sum of the probabilities of finding an atom B on a β-and on a γ-site of the ith shell, expressed in terms of the long-range order parameters. This sum must be divided by two since the numers of β- and γ-sites are equal. This is the result of the fact that $P_{i\,even}^{2(1)}$ is the probability of an atom B falling in the ith shell, regardless of the type of site. In a similar way, we obtain the limiting value for $\alpha_{i\,even}^{3(1)}$.

(3) On the basis of the first two sub-cases, we conclude that if a γ-site is central:

$$\alpha_{i\,even}^{2(1)} \to 1 - \frac{1}{2n_2}(l_{22} + l_{23}), \; \alpha_{i\,even}^{3(1)} \to 1 - \frac{1}{2n_3}(l_{32} + l_{33}). \tag{9}$$

Examination of these three sub-cases allows us to write finally:

$$\alpha_{i\,even}^{2(1)} \to \frac{\frac{1}{2} l_{11}\left(1 - \frac{l_{21}}{n_2}\right) + \frac{1}{4}(l_{12} + l_{13})\left[1 + \frac{1}{2n_2}(l_{22} + l_{23})\right]}{\frac{1}{2} l_{11} + \frac{1}{4}(l_{12} + l_{13})}, \\ \alpha_{i\,even}^{3(1)} \to \frac{\frac{1}{2} l_{11}\left(1 + \frac{l_{21}}{n_3}\right) + \frac{1}{4}(l_{12} + l_{13})\left[1 - \frac{1}{2n_3}(l_{32} + l_{33})\right]}{\frac{1}{2} l_{11} + \frac{1}{4}(l_{12} + l_{13})}. \tag{10}$$

II. Similarly, on examining the case when atom B is in the centre, we obtain:

$$\alpha_{i\,even}^{1(2)} \to \frac{\frac{1}{2} l_{21}\left(1 - \frac{l_{11}}{n_1}\right) + \frac{1}{4}(l_{22} + l_{23})\left[1 - \frac{1}{2n_1}(l_{12} + l_{13})\right]}{\frac{1}{2} l_{21} + \frac{1}{4}(l_{22} + l_{23})},$$

$$\alpha_{i\,even}^{3(2)} \to \frac{\frac{1}{2} l_{21}\left(1-\frac{l_{21}}{n_2}\right)+\frac{1}{4}(l_{22}+l_{23})\left[1-\frac{1}{2n_3}(l_{32}+l_{33})\right]}{\frac{1}{2} l_{21}+\frac{1}{4}(l_{22}+l_{23})}. \tag{11}$$

III. Finally, on considering atom C in the centre, we obtain:

$$\alpha_{i\,even}^{1(3)} \to \frac{\frac{1}{2} l_{31}\left(1-\frac{l_{11}}{n_1}\right)+\frac{1}{4}(l_{32}+l_{33})\left[1-\frac{1}{2n_1}(l_{12}+l_{13})\right]}{\frac{1}{2}\ l_{31}+\frac{1}{4}(l_{32}+l_{33})},$$

$$\alpha_{i\,even}^{2(3)} \to \frac{\frac{1}{2} l_{31}\left(1-\frac{l_{21}}{n_2}\right)+\frac{1}{4}(l_{32}+l_{33})\left[1-\frac{1}{2n_2}(l_{32}+l_{33})\right]}{\frac{1}{2} l_{31}+\frac{1}{4}(l_{32}+l_{33})}. \tag{12}$$

Substituting relations (6) in equations (10), (11) and (12), we obtain:

$$\begin{aligned}
\alpha_{i\,even}^{1(2)} = \alpha_{i\,even}^{2(1)} &\to \frac{1}{49}(49-4ab-2cd),\\
\alpha_{i\,even}^{1(3)} = \alpha_{i\,even}^{3(1)} &\to \frac{1}{7}(7-4l_{31}a-2ce),\\
\alpha_{i\,even}^{2(3)} = \alpha_{i\,even}^{3(2)} &\to \frac{1}{7}(7-8l_{31}b-2de).
\end{aligned} \tag{13}$$

By quite similar reasoning we obtain:

$$\alpha_{j\,odd}^{1(2)} = \alpha_{i\,odd}^{2(1)} \to \frac{1}{49}(49-2ad-4bc),$$

$$\begin{aligned}
\alpha_{i\,odd}^{1(3)} = \alpha_{i\,odd}^{3(1)} &\to \frac{1}{7}(7-2ae-4l_{31}c),\\
\alpha_{i\,odd}^{2(3)} = \alpha_{i\,odd}^{3(2)} &\to \frac{1}{7}(7-8l_{31}b-2de),
\end{aligned} \tag{14}$$

where:

$$\begin{aligned}
a &= 4+3s-l_{12}-2l_{31}+2l_{23},\\
b &= 3-3s+l_{12}-5l_{31}-2l_{23},\\
c &= 3-3s+l_{12}+2l_{31}-2l_{23},\\
d &= 1+6s-2l_{12}+10l_{31}+4l_{23},\\
e &= 1-2l_{31}.
\end{aligned} \tag{15}$$

It is easy to verify that these limiting values are the averages over the corresponding sublattices.

Further, it is convenient to introduce the following symbols:

$$\varepsilon_1 = l_{12}-\frac{1}{2},\ \varepsilon_2 = l_{31}-\frac{1}{4},\ \varepsilon_3 = l_{23}-\frac{1}{4}. \tag{16}$$

It is clear that, as the system tends toward complete disorder:

$$\varepsilon_1,\ \varepsilon_2,\ \varepsilon_3 \to 0.$$

In terms of these new symbols, formulae (13) and (14) reduce to:

VOL 8 195

$$\begin{aligned}
\alpha^{1(2)}_{i\,odd} &= -\alpha^{1(2)}_{i\,even} \to -\frac{8}{49}(9s^2+\varepsilon_1^2-10\varepsilon_2^2+4\varepsilon_3^2-6s\varepsilon_1+\\
&+9s\varepsilon_2+12s\varepsilon_3-3\varepsilon_1\varepsilon_2-4\varepsilon_1\varepsilon_3+6\varepsilon_2\varepsilon_3),\\
\alpha^{1(3)}_{i\,odd} &= -\alpha^{1(3)}_{i\,even} \to \frac{8}{7}(-2\varepsilon_2^2+3s\varepsilon_2-\varepsilon_1\varepsilon_2+2\varepsilon_2\varepsilon_3),\\
\alpha^{2(3)}_{i\,odd} &= -\alpha^{2(3)}_{i\,even} \to \frac{16}{7}(-5\varepsilon_2^2-3s\varepsilon_2+\varepsilon_1\varepsilon_2-2\varepsilon_2\varepsilon_3).
\end{aligned} \tag{17}$$

THEORY OF SHORT-RANGE ORDER. RELATIONS BETWEEN THE LONG-RANGE ORDER PARAMETERS NEAR THE CURIE POINT

If correlations exist in the alloy, then we can calculate the change in the free energy caused by fixing any one atom in the centre:

$$F-F_0=(U-U_0)-T(S-S_0),$$

where $(U - U_0)$ is the change in the configurational energy and $(S - S_o)$ is the corresponding change in entropy. The configurational energy consists of the energy of interaction between pairs. We have, in all, the following energies of interaction: V_{IJ}^{12}, V_{IJ}^{13}, V_{IJ}^{23}, V_{IJ}^{11}, V_{IJ}^{22} and V_{IJ}^{33}, where I denotes a given site in the ith shell, and J - one in the jth shell. We can calculate the change in the configurational energy caused by fixing an atom of type A, B or C in the centre by summation, over all the possible pairs, of the expression for the mean change in energy of a single pair. This process is carried out as follows: firstly, determine all the possible configurations and the corresponding mean values of the energy for an (IJ) pair. We also carry out analogous calculations for the atoms of type B and C. Finally, taking into consideration the *a priori* probabilities of atoms A, B or C being in the centre, we obtain the final formula for the change in energy:

$$\begin{aligned}
U-U_0=\frac{1}{3}\sum_I\sum_J\{&n_1n_2[2(1-n_3)\alpha_I^{2(1)}\alpha_J^{2(1)}+n_3(\alpha_I^{2(1)}\alpha_J^{3(1)}+\alpha_I^{3(1)}\alpha_J^{2(1)}+\\
&+\alpha_I^{2(1)}\alpha_J^{3(2)}+\alpha_I^{3(2)}\alpha_J^{2(1)}-\alpha_I^{3(1)}\alpha_J^{3(2)}-\alpha_I^{3(2)}\alpha_J^{3(1)})]V_{IJ}^1+\\
&+n_1n_3[2(1-n_2)\alpha_I^{3(1)}\alpha_J^{3(1)}+n_2(\alpha_I^{2(1)}\alpha_J^{3(1)}+\alpha_I^{3(1)}\alpha_J^{2(1)}-\alpha_I^{2(1)}\alpha_J^{3(2)}-\\
&-\alpha_I^{3(2)}\alpha_J^{2(1)}+\alpha_I^{3(1)}\alpha_J^{3(2)}+\alpha_I^{3(2)}\alpha_J^{3(1)})]V_{IJ}^2+n_2n_3[2(1-n_1)\alpha_I^{3(2)}\alpha_J^{3(2)}+\\
&+n_1(-\alpha_I^{2(1)}\alpha_J^{3(1)}-\alpha_I^{3(1)}\alpha_J^{2(1)}+\alpha_I^{2(1)}\alpha_J^{3(2)}+\alpha_I^{3(2)}\alpha_J^{2(1)}+\alpha_I^{3(1)}\alpha_J^{3(2)}+\\
&+\alpha_I^{3(2)}\alpha_J^{3(1)})]V_{IJ}^3\},
\end{aligned} \tag{18}$$

where the summation extends over all the atoms of the lattice, that is, over all the possible values of the co-ordinates (l, m, n) and (l', m', n'), denoted as summation over I and J. The change in entropy, caused by fixing the position of an atom A, B, or C, is:

$$S-S_0=k\log\frac{w}{w_0},$$

where w is the number of permutations of atoms for which the order parameters α_i have given values; w_o is a constant.

Let atom A be in the centre. If there are c_i atoms in the ith shell around it then, out of these, $c_i(n_1+n_2\alpha_i^{2(1)}+n_3\alpha_i^{3(1)})$ are of type A, $c_in_2(1-\alpha_i^{2(1)})$ are of type B and $c_in_3(1-\alpha_i^{3(1)})$ are of type C. Such a distribution can be achieved in:

$$w_{A,i}=(c_i)!\,\{[c_i(n_1+n_2\alpha_i^{2(1)}+n_3\alpha_i^{3(1)})]!\cdot$$
$$\cdot[c_in_2(1-\alpha_i^{2(1)})]!\,[c_in_3(1-\alpha_i^{3(1)})]!\}^{-1}\quad\text{ways}$$

In a similar way we obtain $w_{B,i}$ and $w_{C,i}$.

In the expression for entropy, it is convenient to substitute the summation over I for the summation over i. After this substitution, the entropy is written as:

$$\begin{aligned} S = -k \sum_I \{ & n_1 n_2 (1-\alpha_I^{2(1)}) \log n_2 (1-\alpha_I^{2(1)}) + n_1 \\ & (n_1 + n_2\alpha_I^{2(1)} + n_3\alpha_I^{3(1)}) \log (n_1 + n_2\alpha_I^{2(1)} + n_3\alpha_I^{3(1)}) + \\ & + n_1 n_3 (1-\alpha_I^{3(1)}) \log n_3 (1-\alpha_I^{3(1)}) + n_1 n_2 (1-\alpha_I^{2(1)}) \log n_1 (1-\alpha_I^{2(1)}) + \\ & + n_2 (n_2 + n_1\alpha_I^{2(1)} + n_3\alpha_I^{3(2)}) \log (n_2 + n_1\alpha_I^{2(1)} + n_3\alpha_I^{3(2)}) + \\ & + n_2 n_3 (1-\alpha_I^{3(2)}) \log n_3 (1-\alpha_I^{3(2)}) + n_1 n_3 (1-\alpha_I^{3(1)}) \cdot \log n_1 (1-\alpha_I^{3(1)}) + \\ & + n_2 n_3 (1-\alpha_I^{3(2)}) \log n_2 (1-\alpha_I^{3(2)}) + n_3 (n_3 + n_1\alpha_I^{3(1)} + \\ & + n_2\alpha_I^{3(2)}) \log (n_3 + n_1\alpha_I^{3(1)} + n_2\alpha_I^{3(2)}) \}. \end{aligned} \tag{19}$$

Equilibrium values of the α-parameters are determined by conditions for minimum free energy:

$$\delta F = \delta u - T\delta S = 0. \tag{20}$$

In the expression (20) we use Cowley's approximation [4]: we shall consider all the parameters α_I to be independent of each other. As a result, we obtain an infinite system of transcendental equations determining the equilibrium values of the α-parameters:

$$\begin{aligned} -kT \log & \frac{\left(1 + \frac{n_2}{n_1}\alpha_I^{2(1)} + \frac{n_3}{n_1}\alpha_I^{3(1)}\right)\left(1 + \frac{n_1}{n_2}\alpha_I^{2(1)} + \frac{n_3}{n_2}\alpha_I^{3(2)}\right)}{\left(1-\alpha_I^{2(1)}\right)^2} = \\ & = \frac{2}{3} \sum_J \{ [2(1-n_3)\alpha_J^{2(1)} + n_3(\alpha_J^{3(1)} + \alpha_J^{3(2)})] V_{IJ}^1 + \\ & \quad + n_3(\alpha_J^{3(1)} + \alpha_J^{3(2)})(V_{IJ}^2 - V_{IJ}^3) \}, \end{aligned} \tag{21}$$

$$\begin{aligned} -kT \log & \frac{\left(1 + \frac{n_2}{n_1}\alpha_I^{2(1)} + \frac{n_3}{n_1}\alpha_I^{3(1)}\right)\left(1 + \frac{n_1}{n_3}\alpha_I^{3(1)} + \frac{n_2}{n_3}\alpha_I^{3(2)}\right)}{\left(1-\alpha_I^{3(1)}\right)^2} = \\ & = \frac{2}{3} \sum_J \{ [2(1-n_2)\alpha_J^{3(1)} + n_2(\alpha_J^{2(1)} + \alpha_J^{3(2)})] V_{IJ}^2 + \\ & \quad + n_2(\alpha_J^{2(1)} + \alpha_J^{3(2)})(V_{IJ}^1 - V_{IJ}^3) \}, \end{aligned} \tag{22}$$

$$\begin{aligned} -kT \log & \frac{\left(1 + \frac{n_1}{n_2}\alpha_I^{2(1)} + \frac{n_3}{n_2}\alpha_I^{3(2)}\right)\left(1 + \frac{n_1}{n_3}\alpha_I^{3(1)} + \frac{n_2}{n_3}\alpha_I^{3(2)}\right)}{\left(1-\alpha_I^{3(2)}\right)^2} = \\ & = \frac{2}{3} \sum_J \{ [2(1-n_1)\alpha_J^{3(2)} + n_1(\alpha_J^{2(1)} + \alpha_J^{3(1)})] V_{IJ}^2 + \\ & \quad + n_1(\alpha_J^{2(1)} - \alpha_J^{3(1)})(V_{IJ}^1 - V_{IJ}^2) \}, \end{aligned} \tag{23}$$

where the quantities V_{IJ}^{ν} ($\nu = 1, 2, 3$), involved in formula (18), (21), (22) and (23) are:

$$\begin{aligned} V_{IJ}^1 &= \frac{1}{2}(V_{IJ}^{11} + V_{IJ}^{22}) - V_{IJ}^{12}, \\ V_{IJ}^2 &= \frac{1}{2}(V_{IJ}^{11} + V_{IJ}^{33}) - V_{IJ}^{13}, \\ V_{IJ}^3 &= \frac{1}{2}(V_{IJ}^{22} + V_{IJ}^{33}) - V_{IJ}^{23}. \end{aligned} \tag{24}$$

It is easy to see that the limiting form of equations (21), (22) and (23) can be written

as:

$$-kT\log\frac{\left(1+\frac{1}{2}\alpha^{2(1)}_{even}+\frac{1}{2}\alpha^{3(1)}_{even}\right)\left(1+2\alpha^{2(1)}_{even}+\alpha^{3(2)}_{even}\right)}{\left(1-\alpha^{2(1)}_{even}\right)^2}= \tag{25}$$

$$=\frac{1}{6}\left\{\frac{3}{2}\left(6\alpha^{2(1)}_{odd}+\alpha^{3(1)}_{odd}+\alpha^{3(2)}_{odd}\right)V_1+\frac{1}{2}\left(\alpha^{3(1)}_{odd}-\alpha^{3(2)}_{odd}\right)(3V_2-V_3)+\ldots\right\},$$

$$-kT\log\frac{\left(1+\frac{1}{2}\alpha^{2(1)}_{even}+\frac{1}{2}\alpha^{3(1)}_{even}\right)\left(1+2\alpha^{3(1)}_{even}+\alpha^{3(2)}_{even}\right)}{\left(1+\alpha^{3(1)}_{even}\right)^2}=$$

$$=\frac{1}{6}\left\{\frac{3}{2}\left(6\alpha^{3(1)}_{odd}+\alpha^{2(1)}_{odd}+\alpha^{3(2)}_{odd}\right)V_2+\frac{1}{2}\left(\alpha^{2(1)}_{odd}-\alpha^{3(2)}_{odd}\right)(3V_1-V_3)+\ldots\right\}, \tag{26}$$

$$-kT\log\frac{\left(1+2\alpha^{2(1)}_{even}+\alpha^{3(2)}_{even}\right)\left(1+2\alpha^{3(1)}_{even}+\alpha^{3(2)}_{even}\right)}{\left(1-\alpha^{3(2)}_{even}\right)^2}=$$

$$=\frac{1}{3}\left\{\frac{1}{2}\left(2\alpha^{3(2)}_{odd}+\alpha^{2(1)}_{odd}+\alpha^{3(1)}_{odd}\right)V_3+\frac{3}{2}\left(\alpha^{2(1)}_{odd}-\alpha^{3(1)}_{odd}\right)(V_1-V_2)+\ldots\right\}. \tag{27}$$

In these equations we have, for simplicity, put: $n_1=\frac{1}{2}$; $n_2=n_3=\frac{1}{4}$; $V_\rho\equiv V^{\rho}_{IJ+1}$ ($\rho=1, 2, 3$). The terms that have not been written out included those V_{IJ} for which $J=I+2, I+3, \ldots$ that is, the interactions with second, third, etc. neighbours. The α-parameters in these expressions, are, furthermore, functions of the long-range order.*

Separating these equations according to the degrees of the long-range order, and restricting ourselves to the first non-zero terms, we obtain the following equations which are true in the vicinity of the Curie point:

$$\begin{aligned}
&-\frac{8}{49}a_{11}(9s^2+\varepsilon_1^2-10\varepsilon_2^2+4\varepsilon_3^2-6s\varepsilon_1+9s\varepsilon_2+12s\varepsilon_3-3\varepsilon_1\varepsilon_2-4\varepsilon_1\varepsilon_3+6\varepsilon_2\varepsilon_3)+\\
&+\frac{8}{7}a_{12}(-2\varepsilon_2^2+3s\varepsilon_2-\varepsilon_1\varepsilon_2+2\varepsilon_2\varepsilon_3)+\\
&+\frac{16}{7}a_{13}(-5\varepsilon_2^2-3s\varepsilon_2+\varepsilon_1\varepsilon_2-2\varepsilon_2\varepsilon_3)=0,\\
&-\frac{8}{49}a_{12}(9s^2+\varepsilon_1^2-10\varepsilon_2^2+4\varepsilon_3^2-6s\varepsilon_1+9s\varepsilon_2+12s\varepsilon_3-\\
&-3\varepsilon_1\varepsilon_2-4\varepsilon_1\varepsilon_3+6\varepsilon_2\varepsilon_3)+\frac{8}{7}a_{22}(-2\varepsilon_2^2+3s\varepsilon_2-\varepsilon_1\varepsilon_2+\\
&+2\varepsilon_2\varepsilon_3)+\frac{16}{7}a_{23}(-5\varepsilon_2^2-3s\varepsilon_2+\varepsilon_1\varepsilon_2-2\varepsilon_2\varepsilon_3)=0,\\
&-\frac{8}{49}a_{13}(9s^2+\varepsilon_1^2-10\varepsilon_2^2+4\varepsilon_3^2-6s\varepsilon_1+9s\varepsilon_2+12s\varepsilon_3-\\
&-3\varepsilon_1\varepsilon_2-4\varepsilon_1\varepsilon_3+6\varepsilon_2\varepsilon_3)+\frac{8}{7}a_{23}(-2\varepsilon_2^2+3s\varepsilon_2-\varepsilon_1\varepsilon_2+\\
&+2\varepsilon_2\varepsilon_3)+\frac{16}{7}a_{33}(-5\varepsilon_2^2-3s\varepsilon_2+\varepsilon_1\varepsilon_2-2\varepsilon_2\varepsilon_3)=0,
\end{aligned} \tag{28}$$

where

$$\begin{aligned}
&a_{11}=9(1-2x_1),\quad a_{12}=1-3x_1-3x_2+x_3,\\
&a_{22}=9(1-2x_2),\quad a_{13}=2-3x_1+3x_2-x_3,\\
&a_{33}=2(2-x_3),\quad a_{23}=2+3x_1-3x_2-x_3,
\end{aligned} \tag{29}$$

*For a similar process of passage to the limit for binary alloys, see Cowley, [4].

$$x_i = \frac{V_i}{6kT}, \quad i = 1, 2, 3. \tag{29 contd.}$$

We can eliminate the temperature from the system of equations (28). We then obtain two relations between the four parameters of the long-range order. This means that we can, for example, express ϵ_1 and ϵ_2 as functions of s and ϵ_3. It is easy to prove that in the approximations which we restricted ourselves in (28), (that is, to the accuracy of terms of the third order with respect to the long-range order parameters) we obtain the following relations:

$$\begin{aligned} \varepsilon_1 &= 3s + 2\varepsilon_3 \\ \varepsilon_2 &= 0. \end{aligned} \tag{30}$$

Applying relations (30) to the quantities l_{ik}, we obtain:

$$\begin{aligned} &l_{11} = \frac{1}{2}, \; l_{12} = \frac{1}{2} + 3s + 2\varepsilon_3, \; l_{21} = \frac{1}{4}; \\ &l_{22} = \frac{1}{4}, \; l_{31} = \frac{1}{4}, \; l_{13} = \frac{1}{2} - 3s - 2\varepsilon_3, \\ &l_{33} = \frac{1}{4} + 3s + \varepsilon_3, \; l_{23} = \frac{1}{4} + \varepsilon_3, \; l_{32} = \frac{1}{4} - 3s - \varepsilon_3. \end{aligned} \tag{31}$$

CALCULATION OF THE CURIE POINT

It is easy to see, that from the long range order theory [2], that by restricting ourselves to the interactions between the nearest neighbours we obtain the following relations for the configurational energy of the alloy.

$$E = E_0 + N \sum_{i,\, l,\, k,\, m=1}^{3} Z_{km} n_k l_{ik} l_{lm} V^{il}. \tag{32}$$

Here: Z_{km} is the number of nearest neighbours, of type m, around an atom of type k; E_0 is a constant; V^{il} is the energy of interaction between the atoms i and l.

Substituting formula (31) in (32), we obtain:

$$\frac{E - E_0}{N} = B_1 s^2 + B_2 s\varepsilon_3 + B_3 \varepsilon_3^2, \tag{33}$$

where:

$$\begin{aligned} B_1 &= 18\left(V^{13} - \frac{V^{11} + V^{33}}{2}\right) = -18V_2, \\ B_2 &= 6\,(-2V^{11} - V^{33} + V^{12} + 3V^{13} - V^{23}) = 6\,(V_3 - V_1 - 3V_2), \\ B_3 &= -4V^{11} - V^{22} - V^{33} + 4V^{12} + 4V^{13} - 2V^{23} = 2\,(V_3 - 2V_1 - 2V_2). \end{aligned} \tag{34}$$

To calculate the configurational entropy, we avail ourselves of a formula derived in [2]. The configurational free energy then takes the form:

$$\frac{F - F_0}{N} = B_1 s^2 + B_2 s\varepsilon_3 + B_3 \varepsilon_3^2 + kT \sum_{i,\, k=1}^{3} n_k l_{ik} \log l_{ik}. \tag{35}$$

The equilibrium values of S and ϵ_3 are obtained from the equations:

$$\frac{\partial F}{\partial s}=0 \quad \text{и} \quad \frac{\partial F}{\partial \varepsilon_3}=0,$$

or

$$\frac{kT}{8}\log\frac{1-18s-8\varepsilon_3}{1+18s+8\varepsilon_3}=-6V_2 s+(V_3-V_1-3V_2)\varepsilon_3,$$

$$\frac{kT}{8}\log\frac{1-6s-8\varepsilon_3}{1+6s+8\varepsilon_3}=3(V_3-V_1-V_2)s+(V_3-3V_1-V_2)\varepsilon_3. \tag{36}$$

From the first equation of the system (36) we find ϵ_3 approximately a function of s (as before, with a limitation to terms of third order):

$$\varepsilon_3 \approx -\frac{-6V_2+\frac{9}{2}x}{(V_3-V_1-3V_2)+2x}s. \tag{37}$$

Then the second equation of this system gives:

$$s=\frac{1}{2\left[4\dfrac{-6V_2+\frac{9}{2}x}{(V_3-V_1-3V_2)+2x}-3\right]}\operatorname{th}\left\{\frac{4}{x}\left[3(V_3-V_1-V_2)-(V_3-3V_1-V_2)\frac{-6V_2+\frac{9}{2}x}{(V_3-V_1-3V_2)+2x}\right]s\right\}. \tag{38}$$

Hence, by the usual method [1], which in our case leads to a quadratic equation, we find the Curie point.

One of the roots*

$$T_c=\frac{2V_1+2V_2+V_3}{4k}\left\{1+\sqrt{1+8\frac{(V_1^2+V_2^2+V_3^2)-2(V_1V_2+V_1V_3+V_2V_3)}{(2V_1+2V_2+V_3)^2}}\right\} \tag{39}$$

is greater than zero for positive V_1, V_2, and V_3, therefore it is taken as the Curie point. The second root must be discarded, because it is positive only for a limited region of values of V_1, V_2 and V_3. On the other hand, the long-range order theory should not impose any limitations on the values of V_1, V_2 and V_3.

Translated by Z. Kowszun

REFERENCES

1. W. Bragg and E. Williams, *Proc. Roy. Soc.*, A145, 669 (1934).
2. O. Mdivani, *Zoobshcheniia Akad. Nauk Gruz. SSSR*, 21, 653 (1958).
3. K.F. Wojciechowski, *Acta Phys.* Polonica, 15, 429 (1950).
4. J. Cowley, *Phys. Rev.*, 77, 669 (1950).

* We assume that the expression inside the radical is not negative.

VOL. 8 1959

THE IMPORTANCE OF INDIRECT INTERACTION IN THE THEORY OF MAGNETIZATION OF TRANSITION METALS AND RARE EARTHS*

A. A. BERDYSHEV and B. V. KARPENKO

"A.M. Gor'kiy" Uralsk State University

(Received 6 August 1958)

1. FERROMAGNETISM

The second approximation of the perturbation theory in the *s-d* exchange model of transition metals leads to the appearance of indirect interaction between the *d*-electrons. In calculating these interactions, the existence of ferromagnetism becomes possible when the direct bond is absent, i.e. when the *d-d* exchange integral is negative. The influence of indirect interaction on spontaneous magnetization is discussed.

The ferro- and antiferromagnetism of transition metals is usually explained by the change in interaction between electrons of the inner atomic *d*-shells. If the exchange integral for the interaction between near neighbours is positive, then the metal is found to be antiferromagnetic. This treatment of magnetic properties meets with a series of difficulties. Without considering all the problems relevant here (see [1]), we will mention only two cases. Firstly, a large proportion of the experimental data cannot be explained by means of the Bethe-Slater curve of the exchange integral for the transition metals [1], as the majority of theoretical estimates of the exchange integral leads to its negative sign [2]. Secondly, it has been shown previously [3] that dilute alloys of manganese in noble metals are ferro- or antiferromagnetic. In these alloys, atoms of the transition metal are dispersed at such large distances from each other that a direct exchange bond between them is completely absent. Similarly the ferro- or antiferromagnetism of rare-earth metals cannot be explained by an extraordinarily weak direct bond between magnetically active electrons. All this led us to seek other possible mechanisms of the exchange bond. One such mechanism is the indirect exchange interaction proposed by Zener [1]. In the present work the influence of indirect interaction on the problem of ferromagnetism is examined.

1. The calculation will be carried out within the limits of the *s-d*- exchange model for transition metals, [4, 5]. The Hamiltonian of a ferromagnet, describing the interaction of conductivity electrons with spin-orbitals, has the form [4]:

$$H = H_0 + H_1 + H_2,$$
$$H_0 = \sum E_k a_k^+ a_k + \sum E_k a_k^+(-)\, a_k(-) + \sum \varepsilon_g b_g^+ b_g, \qquad (1)$$
$$H_1 = -N^{-1} \sum I(\vec{k}_1, \vec{k}_2) b_g a_{k_1}^+ a_{k_2}(-)\, \delta(k_2 - k_1 + g) + \text{remaining terms},$$

* *Fiz. metal. metalloved.* 8, No. 3, 330-336, 1959.

Where

$$H_2 = -\sum I(k, k)\, a_k^+(-)\, a_k(-) + \frac{1}{N}\sum I(\vec{k}, \vec{k}_2)\, b_{g_1}^+ b_{g_2}\Big[a_{k_1}^+(-)\, a_{k_2}(-) - \\ - a_{k_1}^+ a_{k_2}\Big]\delta(\vec{k}_2 - \vec{k}_1 + \vec{g}_2 - \vec{g}_1). \tag{2}$$

Here, $E_k = Ak^2$ is the translational energy of the conductivity electrons; A, is the transfer integral; $\epsilon_g = Jg^2$, is the energy of spin-orbital; $\vec{k}$ and $\vec{g}$, quantum numbers of electron and spin-orbital (in the case of a stationary lattice); J, is the d-d exchange integral; $I(\vec{k}_1, \vec{k}_2)$, the s-d interaction integral; a_k and $a_k(-)$ are Fermi operators for the second quantization of the conductivity electrons, with orbital quantum number k, and projected spins of $+\frac{1}{2}$ and $-\frac{1}{2}$, respectively; b_g, is Bose's operator; N, is the number of points in the lattice. In the preceding work on the s-d exchange model [4, 5], in the energy spectrum of the examined system of s-d electrons, only cases where H_0 and H_2 are additive have been considered. This corresponds to a decrease, to the first approximation in the energy correction of the perturbation theory, The importance of "triplet" terms in the energy spectrum was not apparent and only some distinct kinetic processes have been studied with their help. The purpose of the present work is to explain the influence of these terms on the energy spectrum of a system and on its magnetization. We shall examine the operator H_0 in the role of a non-perturbing operator. The oblique part of the full energy operator [1] gives the energy of the system with a correction, to the first approximation, from the perturbation theory. The correction, to the second approximation, in the term H_1 is calculated by the usual method;

$$W = \sum_{N_k'}{}' \frac{|(H_1)_{N_k N_{k'}}|^2}{E^0_{N_k} - E^0_{N_k'}}$$

and it is equal to :

$$W = \frac{1}{2N}\sum \frac{|I(\vec{k}, \vec{k} - \vec{g})|^2}{E_k - E_{k-g} - \epsilon_g} N_k^+(1 - N_{k-g}^-) + \frac{1}{2N}\sum \frac{|I(\vec{k}, \vec{k} - \vec{g})|^2}{E_k - E_{k-g} - \epsilon_g} n_g N_k^+ - \\ \frac{1}{2N}\sum \frac{|I(\vec{k}, \vec{k} - \vec{g})|^2}{E_k - E_{k-g} - \epsilon_g} n_g N_{k-g}^- + \frac{1}{2N}\sum \frac{|I(\vec{k}, \vec{k} + \vec{g})|^2}{E_{k+g} - E_k - \epsilon_g} N_k^-(1 - N_{k+g}^+) - \\ \frac{1}{2N}\sum \frac{|I(\vec{k}, \vec{k} + \vec{g})|^2}{E_{k+g} - E_k - \epsilon_g}(n_g + 1) N_k^- + \frac{1}{2N}\sum \frac{|I(\vec{k}, \vec{k} + \vec{g})|^2}{E_{k+g} - E_k - \epsilon_g}(n_g + 1) N_{k+g}^+$$

where N_k^- and N_k^- are the quantum numbers of the conductivity electrons; n_g is the quantum number of the spin-orbital. The same expression can be obtained by the method of canonic transformation [6]: $\mathbf{H} \to e^{i\Phi}\mathbf{H}e^{i\Phi}$. Expanding $exp \pm i\Phi$ into a series, we find:

$$\mathbf{H} = \mathbf{H}_0 + \mathbf{H}_1 + \mathbf{H}_2 - i[\Phi, \mathbf{H}_0] - i[\Phi, \mathbf{H}_1] - i[\Phi, \mathbf{H}_2] - \frac{1}{2}[\Phi, [\Phi, \mathbf{H}_0]] - \ldots$$

We have the function Φ in the form of H_1 with undetermined coefficients. These are obtained from the conditions: $H_1 - i$; $[\Phi H_0] = 0$.

$$\mathbf{H} = \mathbf{H}_0 + \mathbf{H}_2 - \frac{i}{2}[\Phi, \mathbf{H}_1] + \ldots$$

The above are terms of this sum and lead to (3).

In the following work we will examine the indirect interaction energy of the conductivity electrons with each other, as described by the terms in equation (3), when these contain the product of the quantum numbers, $N_k^+ N_{k1}^-$. It is not necessary to neglect these terms, but their

VOL. 8 1959

inclusion complicates the calculations and does not change the quantitative conclusions of our work.

Thus the total energy of the system of electrons in the external magnetic field, with the first and second order approximation, is equal to:

$$E=\sum(\varepsilon_g+g_0\mu H)n_g+\sum(E_k^+-\mu H)N_k^+ +\sum(E_k^-+\mu H)N_k^- -N_{g0}\mu H, \tag{4}$$

where:

$$E_k^+ = E_k - \frac{I_k}{N}\sum n_g + \frac{1}{N}\sum_g \frac{|I(\vec{k},\vec{k}-\vec{g})|^2}{E_k - E_{k-g}-\varepsilon_g}(n_g+1),$$

$$E_k^- = E - I_k + \frac{I_k}{N}\sum n_g - \frac{1}{N}\sum_g \frac{|I(\vec{k},\vec{k}+\vec{g})|^2}{E_{k+g}-E_k-\varepsilon_g} n_g.$$

Here g_0 is Lande's factor; μ is Bohr's magneton; $I_k \equiv I(\vec{k},\vec{k})$.

The expression for energy (4) appears typical of all problems which are connected with the study of interaction of particles of fields of two types. This expression is characteristic, since in it are terms containing the action of quantum numbers of one type on the other. Calculation of these terms by means of statistical estimations of the physical characteristics of the system, involves approximations, since, on introducing the quantum number of one type into an appropriate distribution function, we find that the second quantum number enters the result of the first operation non-linearly. Thus, in order to introduce the remaining parameters, it is necessary to linearise, we will indicate below one method of approximate statistical calculation of the magnetization of the system, involving the use of the energy spectrum, (4).

The exact dependence of the s-d exchange integral $I(k_1, k_2)$ on k_1 and k_2 is not known. According to the work of Bonsovski and Trubov [4]:

$$I(\vec{k}_1,\vec{k}_2)=I_0+I_1(k_1^2+k_2^2),$$

where: I_o and I_1 are the s-d exchange integrals within the atom, and with the neighbouring atoms, respectively. On the other hand, proofs have been expressed in certain works [7] to the effect that, with small spin numbers, this integral depends only slightly on the spin number. Therefore, near the boundary of the Brillium zone, it sharply drops to zero. In the present work, we will confine ourselves to the approximation $I(\vec{k}_1,\vec{k}_2)=I_0=\text{const}$, this has also been done in other works [7]. In order to shorten the amount of working, we will introduce the expressions:

$$E_k^+ = E_k + \frac{1}{N}\sum_g E_{kg}^+ n_g + \varepsilon_{sd},\quad E_k^- = E_k - I_0 + \frac{1}{N}\sum_g E_{kg}^- n_g, \tag{5}$$

where:

$$E_{kg}^+ = -I_0 + \frac{I_0^2}{E_k - E_{k-g}-\varepsilon_g},\quad \varepsilon_{sd}^0 = \frac{I_0^2}{N}\sum_g \frac{1}{E_k - E_{k-g}-\varepsilon_g},$$

$$E_{kg}^- = I_0 - \frac{I_0^2}{E_{k+g}-E_k-\varepsilon_g}.$$

2. In order to find the degree of magnetization we will calculate the statistical sum:

$$Z = exp\frac{Ng_0\mu H}{kT}\sum_{n_g=0}^{\infty}\sum_{N_k^+=0,1} exp-\frac{1}{kT}\Big\{\sum(\varepsilon_g+g_0\mu H)n_g + \sum(E_k^+-\mu H)N_k^+ + \sum(E_k^-+\mu H)N_k^-.$$

When summing the quantum numbers of electrons, it is necessary to examine the constancy of the full number of conductivity electrons. To this end we will introduce, under the summation sign, the Kroneker's symbol, δ, expressed in the form:

$$\delta_{\left(\sum N_k^+ + \sum N_k^- - N\right),0} = \frac{1}{2\pi}\int_0^{2\pi} exp\, i\varphi\left(\sum N_k^+ + \sum N_k^- - N\right) d\varphi.$$

Then the summation that we are interested in can be obtained directly, and we have:

$$Z = exp\,\frac{Ng_0\mu H}{kT}\sum_{n_g} exp - \frac{1}{kT}\sum_g (\varepsilon_g + g_0\mu H)\, n_g \cdot \frac{1}{2\pi}\int_0^{2\pi} d\varphi\, exp\, N\left\{-i\varphi + \right.$$
$$+\frac{1}{N}\sum \ln\left[1 + exp\left(i\varphi - \frac{E_k^+ - \mu H}{kT}\right)\right] + \frac{1}{N}\sum \ln\left[1 + exp\left(i\varphi - \right.\right. \qquad (6)$$
$$\left.\left. - \frac{E_k^- + \mu H}{kT}\right)\right]\Bigg\}.$$

We will now make one further approximation, by expanding the logarithmic function inside the integration sign into a series and limiting ourselves to its linear terms only. For the electrons with "+" spin orientation:

$$\ln\left\{1 + exp\left[i\varphi - \frac{1}{kT}\left(E_k + \frac{1}{N}\sum_g E_{kg}^+ n_g + \varepsilon_{sd}^0 - \mu H\right)\right]\right\} =$$
$$= \ln\left[1 + exp\left(i\varphi - \frac{E_k - \mu H}{kT}\right)\right] - \frac{\frac{1}{N}\sum_g E_{kg}^+ n_g + \varepsilon_{sd}^0}{kT\left[exp\left(\frac{E_k - \mu H}{kT} - i\varphi\right) + 1\right]}$$

We also have a similar expression for electrons with "−" spin orientation. We substitute these expressions in (6) and change the order of integration and summation. Then, a summation for all n_g gives:

$$Z = exp\,\frac{Ng_0\mu H}{kT}\,\frac{1}{2\pi}\int_0^{2\pi} d\varphi\, exp\, N\,[w_s(\varphi) + w_d(\varphi) + w_{sd}(\varphi), \qquad (7)$$

where:

$$w_s(\varphi) = -i\varphi + \frac{1}{N}\sum\left\{\ln\left[1 + exp\left(i\varphi - \frac{E_k - \mu H}{kT}\right)\right] + \ln\left[1 + exp\left(i\varphi - \right.\right.\right.$$
$$\left.\left.\left. - \frac{E_k - I_k + \mu H}{kT}\right)\right]\right\},$$
$$w_{sd}(\varphi) = -\frac{I_0^2}{N^2 kT}\sum \frac{(E_k - E_{k-g} - \varepsilon_g)^{-1}}{exp\left(\frac{E_k - \mu H}{kT} - i\varphi\right) + 1},$$
$$w_d(\varphi) = -\frac{1}{N}\sum_g \ln\left\{1 - exp - \frac{1}{kT}\left[\varepsilon_g + g_0\mu H + \right.\right.$$
$$\left.\left. + \frac{1}{N}\sum_k \frac{E_{kg}^+}{exp\left(\frac{E_k - \mu H}{kT} - i\varphi\right) + 1} + \frac{1}{N}\sum_k \frac{E_{kg}^-}{exp\left(\frac{E_k - I_k + \mu H}{kT} - i\varphi\right) + 1}\right]\right\},$$

The integral in (7) is calculated by the "crossing" method, see [8], and it gives:

$$Z = exp\, N\left\{\frac{g_0\mu H}{kT} + w_s(\varphi_0) + w_d(\varphi_0) + w_{sd}(\varphi_0)\right\},$$

where φ_0 is the root of the equation:

$$w_s'(\varphi_0) + w_d'(\varphi_0) + w_{sd}'(\varphi_0) = 0$$

or the relation: $i\varphi_0 = \zeta/kT$, in the equation:

$$\sum_k [f(E_k-\mu H)+f(E_k-I_0+\mu H)]=N-\frac{1}{NkT}\sum N(E_g)\left[E_{kg}^{+}\frac{\partial f(E_k-\mu H)}{\partial \zeta}+\right.$$
$$\left.+E_{kg}^{-}\frac{\partial f(E_k-I_0+\mu H)}{\partial \zeta}\right]-\frac{I_0^2}{N}\sum\frac{\frac{\partial f(E_k-\mu H)}{\partial \zeta}}{E_k-E_{k-g}-\varepsilon_g}.$$

The last equation defines the chemical potential of the conductivity electrons; it can be seen from it that, as a result of the interaction between the conductivity electrons and the spin orbitals, the chemical potential is defined in a more complicated form than in the case of free electrons. We will consider this problem later.

The statistical sum breaks down into a sum of three terms:

$$Z_s=exp\left\{\frac{\zeta N}{kT}+\sum\left[\ln\left(1+exp-\frac{E_k-\zeta-\mu H}{kT}\right)+\right.\right.$$
$$\left.\left.+\ln\left(1+exp-\frac{E_k-I_0-\zeta+\mu H}{kT}\right)\right]\right\},$$

$$Z_{sd}=exp-\frac{I_0^2}{NkT}\sum\frac{f(E_k-\mu H)}{E_k-E_{k-g}-\varepsilon_g},$$

$$Z_d=exp\left\{\frac{Ng_0\mu H}{kT}-\sum_g\ln\left[1-exp-\frac{1}{kT}(\varepsilon_g+g_0\mu H+\Delta_1+\Delta_2)\right]\right\},$$

where:

$$\Delta_1=I_0/N\sum_k[f(E_k-I_0+\mu H)-f(E_k-\mu H)],$$
$$\Delta_2=\frac{I_0^2}{N}\sum_k\left[\frac{f(E_k-\mu H)}{2A_{kg}\cos\upsilon-(A+J)g^2}-\frac{f(E_k-I_0-\mu H)}{2A_{kg}\cos\upsilon+(A-J)g^2}\right]. \quad (8)$$

In these expressions $f(E)$ is Fermi's distribution function; $N(E_g)$ is Base's distribution function, $E_g=\varepsilon_g+g_0\mu H+\Delta_1+\Delta_2$ is the energy of the spin orbital, modified by the s-d exchange interaction. Δ_1 is a correction to the first approximation, Δ_2 is to the second. The free energy of the system is:

$$F=-kT\ln Z=F_s+F_{sd}+F_d,$$
$$F_s=\zeta N-kT\sum\left[\ln\left(1+exp-\frac{E_k-\zeta-\mu H}{kT}\right)+\ln\left(1+exp-\right.\right.$$
$$\left.\left.-\frac{E_k-I_0-\zeta+\mu H}{kT}\right)\right], \quad (9)$$
$$F_{sd}=\sum\frac{I_0^2}{N}\frac{f(E_k-\mu H)}{E_k-E_{k-g}-\varepsilon_g},$$
$$F_d=-Ng_0\mu H+kT\sum\ln(1-exp-E_g/kT).$$

3. The magnetic moment of the system of electrons is equal to the sum of three terms:

$$M=-\partial F/\partial H=M_s+M_{sd}+M_d,$$

We will examine these terms separately. Spontaneous magnetization of the d-electrons is equal to:

$$M_d=Ng_0\mu\left[1-\frac{1}{N}\left(1+\frac{\Delta_1'+\Delta_2'}{g_0}\right)\sum_g N(E_g)\right],$$

where:

$$\Delta_1=\Delta_0+\Delta_1'\mu H,\ \Delta_2=\Delta_2^0+\Delta_2'\mu H.$$

For small values of wave numbers g (low temperature) we have, limiting ourselves to the square terms in g:

$$\Delta_0 = \frac{I_0^2}{4\pi^2 A}\sqrt{\frac{\zeta}{A}}\left[1-\frac{\pi^2}{24}\left(\frac{kT}{\zeta}\right)^2\right], \Delta_1^! = \frac{I_0}{2\pi^2 A}\sqrt{\frac{\zeta}{A}},$$

$$\Delta_2^0 = -\Delta_0 + \frac{I_0^2(A^2+3J^2)}{48\pi^2 A^2\sqrt{\zeta A}}\left[1-\frac{\pi^2}{16}\left(\frac{kT}{\zeta}\right)^2\right]g^2, \ \Delta_2^! = 0.$$

then:

$$E_g = J_{eff}g^2 + g_0\mu H, \tag{10}$$

where the effective "d-d exchange integral" J_{eff} is defined by the relation:

$$J_{eff} = J + J^{(s)} = J + \frac{I_0^2(A^2+3J^2)}{48\pi^2 A^2\sqrt{\zeta A}}\left[1-\frac{\pi^2}{16}\left(\frac{kT}{\zeta}\right)^2\right]. \tag{11}$$

From equations (10) and (11) it can be seen that, in our approximation, the inclusion of the s-d exchange interaction leads to the fact that the energy of the spin orbital has changed in its essential form when compared with the exchange model. Firstly, the energy correction, to the second approximation, has led to the substitution of an effective integral instead of the integral for the d-d exchange bond. The magnitude of this effective integral depends on the Fermi energy and a transfer integral for the conductivity electrons. Secondly, the effective exchange integral depends only to a small extent on temperature. This appears to be the consequence of using a temperature dependent distribution function for the conductivity electrons. Finally, the energy correction, to the second approximation, completely cancels the effect of the energy correction to the first approximation, so that the "zero" energy, Δ_0, of the spin orbitals, whose influence on magnetization has been studied previously [4,5], disappears completely.

Neglecting now the small correction $\Delta_1^! \ll 1$ in the spontaneous magnetization of d-electrons, we obtain the well known law $T^{3/2}$.

$$M_g = Ng_0\mu\left\{1-0{,}1174\left(\frac{T}{\theta}\right)^{3/2}\right\}, \ 2k\theta = J_{eff}. \tag{12}$$

In the preceding work [4,5], in which the influence of the s-d exchange interaction on the magnetization of the d-electrons was studied, it was shown that the correction, Δ_0, to the energy E_g, which appears to be a correction to the first approximation, leads either to an exponential dependence of M_d on T at large values of Δ_0, or to small deviations from the $T^{3/2}$ law at small values of Δ_0. Our results in (10) and (12) show that this correction is fully compensated by the correction to the second approximation, and therefore the s-d exchange interaction does not lead to any deviation from the $T^{3/2}$ law. This is in contrast to the conclusions obtained in the work [4,5]. As a result of the energy correction to the second approximation, we use the effective "exchange" integral (11) instead of the direct bond integral J_{dd}. This effective integral consists of two parts: the direct bond integral, and the "integral" of indirect interaction $J^{(s)}$. The latter is always positive, and therefore it is not required that J_{dd} should be always positive for the existence of ferromagnetism. Ferromagnetism can also exist when $J_{dd} = 0$ (rare earths and dilute alloys of manganese [7]), and also when the exchange integral is negative. The condition for ferromagnetism now is the more general relation: $J_{eff} = J + J^{(s)} > 0$.

The last two terms in the expression for the magnetic moment of a system of electrons, hitherto left unexamined, are easily calculated and assume the form:

$$M_s + M_{sd} = \left[\frac{N\mu I^0}{4\pi^2 A}\left(\frac{\zeta}{A}\right)^{1/2} + \mu^2 N\frac{H}{\pi^2 A}\left(\frac{\zeta}{A}\right)^{1/2}\right] + \frac{3N\mu}{64\pi^2}\frac{I_0^2}{\zeta A}\left(\frac{\zeta}{A}\right)^{1/2}.$$

The first and third terms of this equation express the "submagnetism" of the conductivity electrons in terms of the "field" of inner electrons, and gives the spontaneous magnetic moment of the conductivity electrons. Its magnitude is determined by the magnitude and sign of the s-d exchange integral, I_o. The second term gives the normal Pauli paramagnetism of the conductivity electrons.

In conclusion, we observe that the effective exchange integral (11), as a result of our approximations, is found to depend on temperature, and that with an increase in temperature its magnitude decreases. However, in order to explain the transition of ferromagnetism into antiferromagnetism, observed in the rare earths and dilute alloys of manganese, this dependence on temperature must be quite small. Moreover, all the methods of derivation are based on the assumption that the magnetization of a system deviates little from the maximum, and therefore we cannot make any conçlusions applicable at high temperatures, In the high temperature region it is necessary to apply other methods, for example the method of the energetic centre of mass.

Translated by Z. Kowszun

REFERENCES

1. C. Zener and R. Heikes, *Rev. mod. phys.*, 25, 191 (1953). (see also C. Zener, *Sb. Problemy sovremennoi fiziki*, No.5, (1952).
2. H. Kaplan, *Phys. rev.*, 85, 1058 (1952); E.P. Wolefrath, *Nature*, 163, 57 (1949).
3. Owen, Brown et al, *Phys. Rev* , 102, 1501 (1956); F.A. Otter et al, *Franklin Inst.*, 260, 75 (1955).
4. S.V. Vonsovskii and E.A. Turov, *Zh. eksp. teor. fiz.*, 24, 419 (1953); E.A. Turov, *Zh. eksp. toer. fiz.* 25, 352 (1953).
5. S.A. Berdyshev and Yu.A. Iziumov, *Fiz. met. metalloved.* 5, 552 (1957).
6. Y. Kitano and H. Nakano, *Prog. Theor. Phys.*, 9, 370 (1953).
7. K. Yosida, *Phys. Rev.*, 106, 893 (1957); 107, 396 (1957). T. Kasuya, *Prog. Theor. Phys.*, 16, 45 (1956).
8. M.A. Leontovich, *Statisticheskaia fizika*, Gostekhizdat, sect. 5 (1944).

CONCERNING BINARY SOLID SOLUTIONS WITH INTERATOMIC BONDS OF TWO TYPES*

A.N. MEN' and A.N. ORLOV

Institute of Physics of Metals, U.S.S.R. Academy of Sciences
Sverdlovsk Agricultural Institute

(Received 4 September 1958)

A calculation has been made of the free energy F of a binary solid solution with interatomic bonds of two types, for example, localized bonds, covalent with the participation of d-electrons (strong bonds) and unsaturated (weak) bonds. The equilibrium numbers of strongly and weakly bonded pairs of neighbouring atoms of different sorts have been found for a given temperature from the condition of minimum F. Given the known relationships between the energies of strong and weak bonds, the numbers of pairs of different types depend on temperature non-monotonically. It is suggested that this effect (together with the change of concentration of current carriers) may cause the anomalous temperature variation of electrical resistivity in some alloys of transition metals.

VOL. 8 1959

1. The concept of the energy of a crystal in the form of the sum of the energies of pair interactions of atoms is widely used in the theory of binary alloys. In this it is assumed that the energy of interaction of a given pair is determined only by the sort of atoms composing it. At the same time, this energy depends, generally speaking, on the nature and disposition of all the atoms surrounding the given pair XY. Even if we limit ourselves by considering the interaction of the pair XY with their nearest neighbours only, the energy of the pair V_{XY} may assume a number of values $V^{(i)}_{XY}$, where i denotes the number of configurations surrounding the pair XY. It is possible to attempt to allow for this circumstance by regarding crystal energy, not as the sum of all the possible combinations of X, Y, i, but as the sum of the energies of the complexes formed by each atom with its nearest neighbours**, the energy of each complex in its turn being taken as equal to the sum of the energies $V^{(\alpha)}_{XY}$, appertaining to one pair of atoms of a given sort XY in a complex of type α. The complexes differ in the composition and disposition of the atoms in the first co-ordination sphere of the central atom. The energy $V^{(\alpha)}_{XY}$ depends on the type of complex, inasmuch as combined electron orbits of different types are formed [1] depending on the way in which the central atom is surrounded. If the energy levels of the atoms composing the complex are near (almost degenerate), the formation of resonant orbits is possible. This case is realized in pure metals. If the levels are distant, then resonance is less probable, but localized, covalent bonds may be formed under known conditions. If the atoms of the complex do not have sufficient electrons to ensure the saturation of all localized covalent bonds, some of them will remain unsaturated.***It may be expected that this

* *Fiz. metal. metalloved.* 8, No.3, 337-341, 1959.

** Obviously, allowing for the fact that each atom pair belongs to several complexes simultaneously.

*** We do not dwell here on the clarification of the conditions under which the coexistence of unsaturated and localized, covalent bonds is more advantageous from an energy standpoint than the formation of resonant, non-localized bonds. This question demands separate investigation.

will lead to comparatively stable local distortions of the valent angles and the interatomic distances in the complex. The distances between the atoms which have entered into the covalent bonds will be less, but the energy of interaction more, than between neighbouring atoms of the same sort not bonded covalently. Thus interatomic bonds of two types arise, which we shall arbitrarily term weak and strong, denoting their energies by $V_{ij}^{(1)}$ and $V_{ij}^{(2)}$.*

In this connexion it is of interest to generalize the well-known system of calculating the energy of a solid solution in the approximation of pair interactions for the cases when there are formed: (a) resonant, covalent bonds and (b) localized, covalent (strong) and unsaturated (weak) bonds. We shall restrict ourselves to an examination of the second of these cases.

It is to be expected that in case (b) the differences of the energies $V_{ij}^{(\alpha 1)}-V_{ij}^{(\alpha 2)}$ of different bonds in identical complexes are considerably greater than the differences of the energies $V_{ij}^{(\alpha,l)}-V_{ij}^{(\alpha' l)}(l=1,2;\ \alpha\neq\alpha')$, of identical bonds in different complexes. Therefore, in what follows the index α will be omitted (which it is not possible to do in case (a)). Thus the problem will be reduced to the calculation of the energy of a solid solution with localized interatomic bonds of two types.**

In this connexion the following two possibilities are open:

(1) The full number of electrons n which participate in the formation of strong bonds is given and does not depend on the form of the atomic neighbourhoods (AA, AB, BB), so that the only possibility is the redistribution of these electrons according to pairs of three types. The number n may be, for example, the sum of all the s- and d-electrons in an alloy of the transition metals. If it be assumed that two electrons participate in the formation of one strong bond, then

$$\frac{n}{2}=\sum_{i,j}Q_{ij}^{(2)}, \qquad (1)$$

so that in this case supplementary condition (1) is imposed on the numbers of strong bonds $Q_{ij}^{(2)}$

(2) The number n is not a constant, but depends on the numbers of pairs $Q_{ij}^{(2)}$, in conformance with (1) and is determined from this equation after finding the equilibrium values of $Q_{ij}^{(2)}$ which in their turn are functions of temperature T and of the energies $V_{ij}^{(l)}$. The dependence of n on T may, within the framework of the usual two-zone s-d model, be interpreted in the following manner. During the redistribution of A and B atoms with respect to the lattice points and the corresponding change of the numbers $Q_{ij}\sum_{l=1}^{2}Q_{ij}^{(l)}$, mixing of the levels in the d-band (and also in the s-band) occurs, as a result of which the Fermi level is displaced and redistribution of the electrons occurs according to the s- and d-states. In this treatment the d-electrons bring about strong bonds and the s-electrons weak bonds. As a result of the distinction of the A and B ions, the density of the s-electrons in the crystal is not constant and the energies $V_{ij}^{(1)}$ of the weak interactions brought about by them depend on i and j. The second case is examined in the present note.

2. The free energy (allowing for the interaction only of the nearest neighbouring atoms and not allowing for thermal vibrations) may be written in the form [3]

$$F=-\sum_{e}\sum_{i,j}Q_{i,j}^{(l)}V_{ij}^{(l)}-kT\ln\left[h\Big(\sum_{i,j}Q_{ij}\Big)!\ \Big/\prod_{l\,ij}Q_{ij}^{(l)}!\right] \qquad (2)$$

where, as is easily shown, the multiplier h does not depend on $Q_{ij}^{(l)}$, but depends only on the co-ordination number z and on the concentration of atoms $c_A=N_A/N$ and $c_B=1-c_A$ (the full number of atoms in the crystal $N=N_A+N_B$. For definiteness we shall take $c_A\geqslant c_B$. Between the numbers Q_{ij} and N_i the following relationships exist:

$$\begin{aligned} Q_{AA}\quad Q_{AA}^{(1)}+Q_{AA}^{(2)}&=(N_A z-Q_{AB})/2,\\ Q_{BB}=Q_{BB}^{(1)}+Q_{BB}^{(2)}&=(N_B z-Q_{AB})/2,\\ Q_{AB}&=Q_{AB}^{(1)}+Q_{AB}^{(2)}. \end{aligned} \qquad (3)$$

For independent parameters we shall select $Q_{AA}^{(1)}$, $Q_{AB}^{(1)}$, $Q_{BB}^{(1)}$ and $Q_{AB}^{(2)}$. By expressing the

* $V_{ij}^{(l)}$ denotes the absolute value of the energy.

** Calculation of non-localized bonds of an electrostatic nature in alloys was carried out in a paper by Lesnik [2].

remaining parameters in terms of these, with the help of (3), and substituting for them in (2), we obtain by the usual method from the conditions $\partial F/\partial Q_{ij}^{(l)} = 0$ the equilibrium values of the probabilities* $P_{ij}^{(l)} = Q_{ij}^{(l)} / \frac{1}{2} Nz$

$$P_{ii}^{(1)} = (c_i - L_{AB} P_{AB}^{(2)})/L_i,$$

$$P_{ii}^{(2)}(L_i - 1)\ P_{ii}^{(1)}\ (i = A, B), \tag{4}$$

$$P_{AB}^{(1)} = (L_{AB} - 1)\ P_{AB}^{(2)},$$

$$P_{AB}^{(2)} = \{[(c_A - c_B)^2 + \tag{5}$$

$$+ 16\, c_A c_B \varphi]^{\frac{1}{2}} - 1\}/L_{AB}(4\varphi - 1),$$

where $\varphi = L_A L_B e^{\theta}/L_{AB}^{(2)}$, $L_i = 1 + exp[(V_{ii}^{(2)} - V_{ii}^{(1)})/kT]$ $(i = A, B)$,

$$L_{AB} = 1 + exp[-(V_{AB}^{(2)} - V_{AB}^{(1)})/kT],$$

$$kT\theta = V_{AA}^{(1)} + V_{BB}^{(1)} - 2V_{AB}^{(2)}.$$

Since, as a rule, it is impossible to determine the numbers of pairs $Q_{ij}^{(1)}$ and $Q_{ij}^{(2)}$ separately by experiment, we shall be examining only full numbers of pairs Q_{ij} and the corresponding probabilities $P_{ij} = \sum_l P_{ij}^{(l)}$.

3. Proceeding to the investigation of the temperature dependence of P_{AB}, we shall find the limiting values of P_{AB} when $T = 0$ and $T = \infty$. In the expressions

$$V_{AA}^{(2)} - V_{AA}^{(1)} = k\alpha,\ V_{BB}^{(2)} - V_{BB}^{(1)} = k\beta,\ V_{AB}^{(2)} - V_{AB}^{(1)} = k\gamma,$$
$$e^{1/T} = y,\ V_{AA}^{(2)} \quad V_{BB}^{(2)} - 2V_{AB}^{(2)} = k\nu, \tag{6}$$

φ has the form

$$\varphi = y^{\nu + 2\gamma - \alpha - \beta}(1 + y^{\alpha})(1 + y^{\beta})(1 + y^{\gamma})^{-2}. \tag{7}$$

From (7) and (4) it is evident that

$$\lim_{T \to \infty} P_{AB} = \frac{1}{3}[1 + 12 c_A c_B)^{\frac{1}{2}} - 1] = P_{\infty}, \tag{8}$$

$$\lim_{T \to \infty} P_{AB} = \begin{cases} 0 & (\nu > 0) \\ P_{\infty} & (\nu = 0) \\ 2c_B & (\nu < 0). \end{cases} \tag{9}$$

To clarify the change in P_{AB} (T) at intermediate values of T, we shall note that in the expression

$$\frac{dP_{AB}}{dT} = \frac{dP_{AB}}{d\varphi}\frac{d\varphi}{dT} \tag{10}$$

the first factor is always negative. We shall further examine separately some possible cases.

(a) $V_{ij}^{(1)} = V_1$, $V_{ij}^{(2)}$ Here $d\varphi/dT$ becomes zero at the points T which are the roots of the equation

$$(1 + y^{\alpha})[\gamma(1 + y^{-\beta}) - \beta(1 + y^{-\gamma})] =$$
$$= y^{\alpha - \beta}(1 + y^{\beta})[\alpha(1 + y^{-\gamma}) - \gamma(1 + y^{-\alpha})]. \tag{11}$$

Possible types of the relation P_{AB} (T) are presented on Fig. 1 as the curves *1-8*. Corresponding energy values are shown in Table 1. On curves *2*, *3*, *7*, *8* the number of extrema may be more than is shown on the diagrams, depending on the number of roots of equation (11).

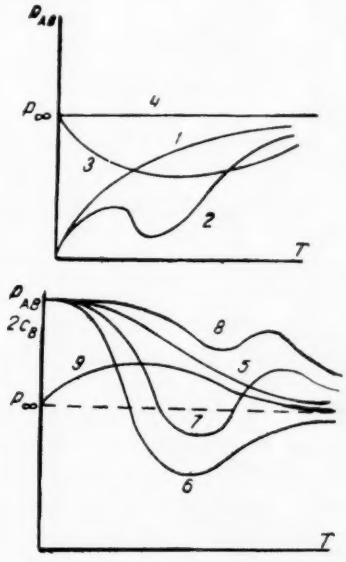

Fig. 1. Possible types of dependence of P_{AB} on T.

(b) $V_{ij}^{(2)} = V_2$, $V_{ij}^{(1)}$ various. In this case curves of types *3* and *9* are possible under the conditions shown in Table 1.

(c) $V_{ii}^{(1)} = V_{ii}^{(2)}$, $V_{AB}^{(1)} < V_{AB}^{(2)}$. P_{AB} is represented by a curve of type *3*, on which there is a single extremum at the point

* The radical sign is determined from the condition that at any temperature T $Q_{AB}^{(2)}$ should have a positive value.

VOL. 8 1959

TABLE 1

Case	Type of Curve	Energy values	
	1	$\alpha > \gamma,\ \beta > \gamma$	$V_{AA}^{(2)} > V_{AB}^{(2)},\ V_{BB}^{(2)} > V_{AB}^{(2)}$
a	2	$\alpha \leqslant \gamma \geqslant \beta$ $(\alpha + \beta > 2\gamma)$	$V_{AA}^{(2)} \geqslant V_{AB}^{(2)} \geqslant V_{BB}^{(2)}$ $\left(V_{AA}^{(2)} + V_{BB}^{(2)} > 2V_{AB}^{(2)}\right)$
	3	$\alpha \leqslant \gamma \geqslant \beta$ $(\alpha + \beta = 2\gamma)$	$V_{AA}^{(2)} \geqslant V_{AB}^{(2)} \geqslant V_{BB}^{(2)}$ $(V_{AA}^{(2)} + V_{BB}^{(2)} = 2V_{AB}^{(2)}$
	4	$\alpha = \beta = \gamma$	$V_{ij}^{(2)} = V_2$
	5	$\alpha < \gamma,\ \beta < \gamma$	$V_{AA}^{(2)} < V_{AB}^{(2)},\ V_{BB}^{(2)} < V_{AB}^{(2)}$
	6* 7 8	$\alpha \gtrless \gamma \gtrless \beta$ $(\alpha + \beta < 2\gamma)$	$V_{AA}^{(2)} \gtrless V_{AB}^{(2)} \gtrless V_{BB}^{(2)}$ $(V_{AA}^{(2)} + V_{BB}^{(2)} < 2V_{AB}^{(2)})$
б	3	$\alpha < \gamma,\ \beta < \gamma$	$V_{AB}^{(1)} < V_{AA}^{(1)},\ V_{AB}^{(1)} < V_{BB}^{(1)}$
	4	$\alpha = \beta = \gamma$	$V_{ij}^{(1)} = V_1$
	9	$\alpha > \gamma,\ \beta > \gamma$	$V_{AB}^{(1)} > V_{AA}^{(1)},\ V_{AB}^{(1)} > V_{BB}^{(1)}$

* Cases 6-8 differ with respect to the numbers of roots of equation (11).

$$T = T_C = \gamma \left[\ln \frac{2\gamma - \nu}{-\nu}\right],\ (\nu < 0{,}2\ \gamma + \nu > 0). \quad (12)$$

In all cases P_{AB} as a function of concentration c_A has a maximum when $c_A = \frac{1}{2}$. It is possible to show that, when there are extrema of $P_{AB}(T)$, T extremum does not depend on c_A.

3. By substituting the equilibrium values of $Q_{ij}^{(l)}$ in the expression for energy and differentiating it with respect to T we shall obtain the heat capacity $C(T)$. Investigation of this expression shows that in some cases $C(T)$ has an extremum, in particular, a minimum.

As is well known [4], the probabilities P_{AB} determine the magnitude of the specific residual electrical resistance of the alloy, equal to

$$\rho = C_1 - C_2 P_{AB}. \quad (13)$$

Since the magnitudes c_i 0 do not depend on T, a maximum is to be expected on the curve $\rho(T)$ at the point where $P_{AB}(T)$ has a minimum and vice versa.

The anomalies found on the curves $P_{AB}(T)$ and $C(T)$ are similar in form to anomalies on the curves of electrical resistance and heat capacity of solid solutions in which the K-state is formed (see, for example, [5]). Our calculations show that in some cases allowing for the redistribution of atoms during a temperature change is sufficient to explain these anomalies and there is no need for hypotheses concerning a change in the number of current carriers. However, we shall note that experimental data [6] on electrical conductivity and Hall's coefficient show, apparently, that both phenomena occur during the formation of the K-state.

Attention should be drawn to the fact that, in agreement with the model examined by us, the stability region of concentration heterogeneities ($P_{AB}(T)$ anomalies) has a boundary not only on the high temperature side but also on the low temperature side. It is also interesting that the theory permits the existence in one and the same alloy of several anomalies in various temperature ranges.

Translated by R.D.M. Hegarty

REFERENCES

1. L. Pauling, *Proc. Roy. Soc.*, 196, 343 (1949).
2. A.G. Lesnik, *Vopr. fiz. metal. metalloved.*, 5, 104 (1954).
3. T. Muto and K. Takagi, *Solid State Phys.*, 1, 193 (1955).
4. M.A. Krivoglaz and Z.A. Matysina, *Zh. eksp. teor. fiz.*, 28, 61 (1955).
5. H. Thomas, *Z. Phys.*, 129, 219 (1951). B.G. Livshits, Sh. Sh. Ibrazimov, Yu.Z. Avraamov and Yu.K. Konev, *Issledovaniya po zharoprochnym splavam, (Investigations of Heat-Resisting Alloys)* 2, 171 (1957) published by U.S.S.R. Acad. of Sci.
6. W. Koster and P. Rocholl *Z. Metallk*, 48, 485 (1957).

VOL. 8 1959

THE HALL EFFECT IN IRON-NICKEL ALLOYS NEAR THE CURIE POINT*

N.V. BAZHANOVA

Moscow Institute of Railway Transport Engineers

(Received 1 November 1958)

As is well known, the magnitude of the Hall effect in a ferromagnetic, as distinct from non-ferromagnetic metals, at least in the technical magnetization region, depends on its magnetic state, on its magnetization and not on the magnitude of the magnetic field. However, after technical magnetic saturation is reached, the Hall effect in a ferromagnetic continues to change when the external magnetic field is increased. By what is the Hall effect in a ferromagnetic determined in this region of magnetic fields which exceed the magnetic saturation field? Measurements made by us on iron-nickel alloys of the invar group [1] showed that the Hall e.m.f. in these alloys, after the attainment of technical magnetic saturation, rises with increase of magnetic field and this rise is determined mainly by the increase in magnetization of a technically saturated ferromagnetic, that is, by the rise in its true magnetization.

The compositions of the iron-nickel alloys investigated were as follows: 30.5 per cent by weight Ni-69.5 per cent by weight Fe; 32 per cent by weight Ni-68 per cent by weight Fe; 34.7 per cent by weight Ni-65.3 per cent by weight Fe; 37 per cent by weight Ni-63 per cent by weight Fe; 38 per cent by weight Ni-62 per cent by weight Fe and 40 per cent by weight Ni-60 per cent by weight Fe. The procedure for measuring the magnetization and Hall e.m.f. in these alloys was described in reference [1].

Within the range of magnetic fields used in these experiments (from 0 to 2000 oersteds) the magnetic field was observed to have no influence on the magnitude of the Hall effect in the ferromagnetic. This made it possible to describe the Hall effect in ferromagnetics by the formula [2]:

$$E=R_tI_t+R_iI_i, \qquad (1)$$

where E is the magnitude of the Hall e.m.f. calculated per unit of length between the Hall electrodes and per unit of current density in the specimen [3]; I_t and I_i are, respectively, the technical and the true magnetization of the specimen; R_t and R_i are the Hall constants.** While the dependence of the Hall e.m.f. in a ferromagnetic on its true magnetization I_i is of a strictly linear character, the dependence of the Hall e.m.f. on the magnetic field in a technically saturated ferromagnetic may be non-linear as well as linear. It will be linear if the susceptibility of the para-process does not depend on the magnetic field H and non-linear if the susceptibility of the para-process does depend on the magnetic field. Thus, near the Curie point [1] the following relationship holds good between the Hall e.m.f. E and the magnetic field H:

$$H=aE+bE^3, \qquad (2)$$

where a and b are coefficients which do not depend on H. However, as experiment shows, the coefficients a and b are functions of temperature.

If the coefficients a and b are determined experimentally for a ferromagnetic at a fixed temperature, it is possible to calculate the $E(H)$ curve from them by using equation (2). Such curves were calculated for all the iron-nickel alloys investigated. The curves calculated for a number of temperatures near

* *Fiz. metal. metalloved.* 8, No.3, 342-345, 1959.

** In the general case, a third term in this formula – R_0H – should be borne in mind.

VOL 8 195

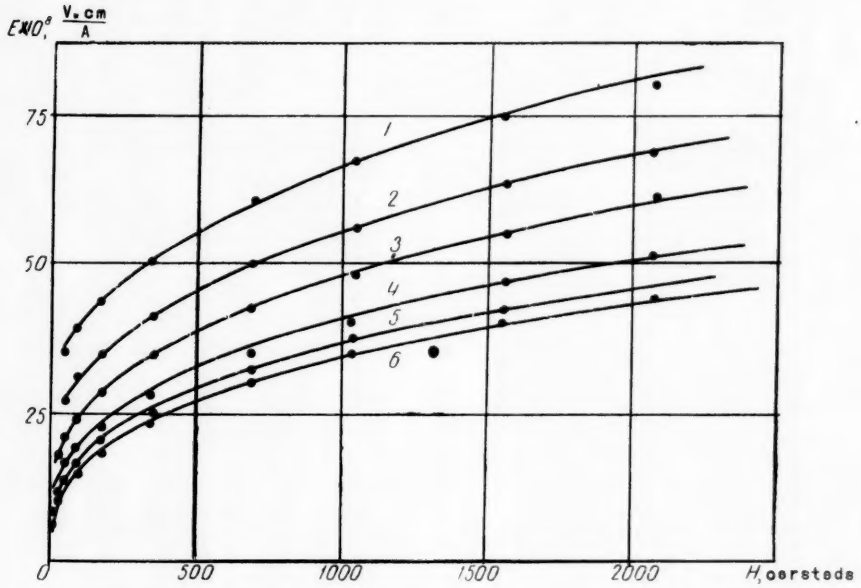

Fig. 1. Dependence of the Hall e.m.f. E on the magnetic field H in an alloy 37 per cent by weight Ni, remainder Fe, for a number of temperatures near the Curie point (calculated and experimental curves):
1 – 226°; 2 – 231°; 3 – 236°; 4 – 240°; 5 – 243°; 6 – 245°C.

the Curie point (θ = 245°) are shown in Fig. 1 (alloy; 37 per cent by weight Ni, remainder Fe); the experimental values of the Hall e.m.f. are marked by dots. As is evident from the graph, the relationship between the Hall e.m.f. and the magnetic field expressed by equation (2) accurately reflects the course of the Hall effect near the Curie point when, due to the small values of the anisotropic and magnetostriction constants, technical saturation is attained in weak magnetic fields. The curves presented in Fig. 1 give the variation of the Hall e.m.f. in relation to the intensity of the magnetic field. This variation is controlled by the para-process, which is essentially non-linear.

It should be noted that the completely satisfactory results given by equation (2) and also the strict proportionality between the Hall e.m f. and the magnetization in the para-process region near the Curie point, where the magnetization does not depend linearly on the magnetic field, indicates that the Hall e.m.f. changes only as a result of the change of true magnetization of the ferromagnetic in magnetic fields stronger than the magnetic saturation field.

The Hall constant R_i may be determined experimentally, as follows from equation (1), if the dependence of the Hall e.m.f. on the true magnetization I_i is known. In the true magnetization region, this relationship is a straight line the tangent of whose angle of slope gives the magnitude of the constant. Experiment shows that for all the alloys investigated this constant is a quantity practically independent of temperature (for temperatures less than 0). Fig. 2 shows the constant R_i plotted against temperature for some of the alloys investigated.

The fact that R_i is independent of temperature near the Curie point makes it possible to estimate the temperature variation of coefficients a and b in equation (2). As was shown in reference [1], coefficients a and b may be written in the following form:

$$a = \frac{\alpha}{R_i} \text{ and } b = \frac{\beta}{R_i^3},$$

where and are coefficients occurring in the equation for the true magnetization of ferromagnetics [4]. It is to be expected

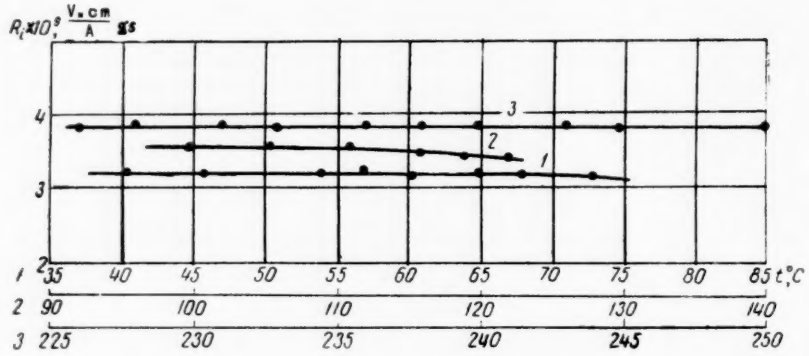

Fig. 2. Dependence of constant R_i on temperature for a series of Fe-Ni alloys near the Curie point:
1 - 30.5 per cent by weight Ni, remainder Fe; *2* - 32 per cent by weight Ni, remainder Fe; *3*- 37 per cent by weight Ni, remainder Fe;
($\theta_1 = 68°$; $\theta_2 = 119°$; $\theta_3 = 245°$).

that, under the condition that R_i is independent of temperature, the variation of coefficients a and b with temperature will be the same as the variation of coefficients and β with temperature 5 . As is evident from Figs. 3 and 4, this is confirmed by experiment.

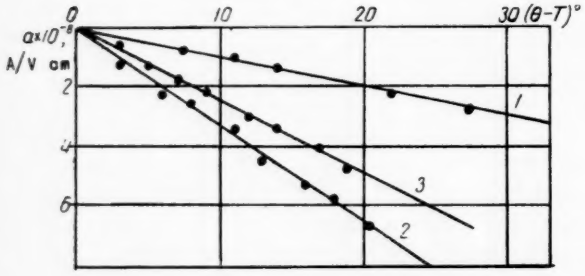

Fig. 3. Dependence of constant a on temperature:
1 - 30.5 per cent by weight Ni, remainder Fe;
2 - 34.7 per cent by weight Ni, remainder Fe;
3 - 37 per cent by weight Ni, remainder Fe
($\theta_1 = 68°$; $\theta_2 = 194°$; $\theta_3 = 245°$)

The relationships between the coefficients a, α, R_i and b, β, R_i enable the constant R_i to be calculated from the coefficients α, a, β, and b, which can be determined from two independent measurements. Of the two pairs of coefficients (α, β and a, b) the coefficients β and b are determined experimentally with a greater degree of accuracy than the coefficients α and a. Therefore the relationship $R_i = \sqrt[3]{\frac{\beta}{b}}$ was chosen for the calculation of the constant R_i. The values of R_i obtained in this way were in good agreement with the experimental values of this coefficient. Experimental and calculated values of the constant R_i for a number of alloys presented in the table for comparison.

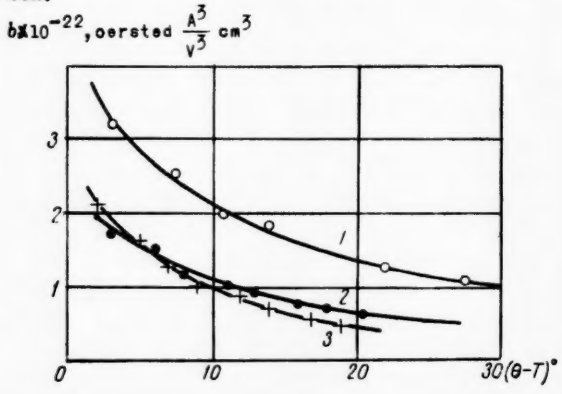

Fig. 4. Dependence of constant b on temperature:
1 - 30.5 per cent by weight Ni, remainder Fe;
2 - 34.7 per cent by weight Ni, remainder Fe;
3 - 37 per cent by weight Ni, remainder Fe.

The quantitative agreement of the constant R_i calculated in this way with the values of R_i determined by experiment (from a graph of the Hall e.m.f. against magnetization) is obvious and is an argument in favour of the correctness of the relationships stated for for the coefficients.

TABLE 1

Alloy 30.5 by weight % Ni, remainder Fe, θ = 68°			Alloy 34.7 by weight % Ni, remainder Fe, θ = 194°			Alloy 38 by weight % Ni, remainder Fe, θ = 260.5°		
t, °C	Values of R_i		t, °C	Values of R_i		t, °C	Values of R_i	
	experimental	calculated		experimental	calculated		experimental	calculated
10.5	3.20×10^{-9}	3.11×10^{-9}	173.5	3.40×10^{-9}	3.35×10^{-9}	251.0	3.95×10^{-9}	3.75×10^{-9}
46.0	3.20×10^{-9}	3.10×10^{-9}	178.0	3.40×10^{-9}	3.30×10^{-9}	253.0	3.85×10^{-9}	3.60×10^{-9}
57.0	3.20×10^{-9}	3.05×10^{-9}	181.0	3.40×10^{-9}	3.35×10^{-9}	258.0	3.80×10^{-9}	3.45×10^{-9}
65.0	3.20×10^{-9}	3.03×10^{-9}	186.0	3.30×10^{-9}	3.35×10^{-9}	263.0	3.80×10^{-9}	3.60×10^{-9}
73.0	3.15×10^{-9}	3.05×10^{-9}	191.0	3.30×10^{-9}	3.35×10^{-9}	270.0	3.70×10^{-9}	3.60×10^{-9}

I express my sincere thanks to D.I. Volkov, under whose direction this work was carried out.

Translated by R.D.M. Hegarty

1. N.V. Bazhanova, *Zh. eksp. teor. fiz.* 33, 567 (1957).
2. D.I. Volkov, *Vest. mosk. gos. univ.* 3, 65 (1954).
3. I.K. Kikoin, *Sov. Phys.* 9, 1 (1936); G.P. Priporova, *Issledovaniye effekta Kholla v zhelezonikelovom splave s polozhitel'noy striktsiyey (Investigation of the Hall effect in an iron-nickel alloy with positive striction)* (dissertation), Gor'kiy Pedagogic Institute, 1950.
4. B.L. Ginzburg, *Zh. eksp. teor. fiz.* 17, 833 (1947).
5. K.P. Belov and A.N. Goryaga, *Fiz. metal. metalloved.* 2, 3 (1956).

VOL. 8 1959

ON THE PROBLEM OF ANOMALOUS BEHAVIOUR OF THE COERCIVE FORCE OF QUENCHED AND HIGHLY ANNEALED STEELS*

M.N. MIKHEEV and G.S. TOMILOV

Institute of the Physics of Metals Akad. Nauk SSSR

(Received 3 January 1959)

It is shown that the anomalous behaviour of the coercive force of quenched and highly annealed steels is connected with the shape, saturation magnetization and mean size of the carbides present. This agrees with the theory of inclusions [4].

A series of works [1-3] has been dedicated to the problem of the nature of the coercive force of annealed steels in relation to the observation of their structure and mechanical properties. Kondorskii [4] examines the theory of coercive force of steels on the basis of the most general idea of the physics of magnetic phenomena.

In works [1-3] the main importance in the mechanism of hysteresis of highly annealed plain carbon or alloy steels is given to the internal interphase surface area (carbide, ferrite, austenite), and also to the dispersion of the blocks of the α-phase [2]. In the series of works [1-6], the anomalous behaviour of the coercive force of steels, annealed at 500-600°C, is explained by dispersion hardening in connexion with precipitation and isolation of the carbide phases.

The present work represents an attempt to elucidate the anomalous behaviour of the coercive force occurring in highly annealed martensitic steels, on the basis of a theory developed by Kondorskii [4].

In the general theory [4], two extreme examples are considered:

(I) The case of relatively small, non-magnetic inclusions, which have the mean diameter $d_{cp} \geqslant \delta$, the mean demagnetizing factor in the direction of the field N, and volume fraction v. Only those inclusions whose mean diameter satisfies the relation $\delta < d_{cp} < d_s$ are included in the volume fraction v. Here δ is the thickness of domain wall d_s is the diameter of a magnetization nucleus, which can grow when $H = H_0$.

Taking into consideration only the energy of the magnetic field of the inclusions A_2, (which in this case is many times greater than the energy A_1, connected with the increase of the interface area), theory [4] gives an estimate of the value of the critical field H_0 by the formula:

$$H_c \sim H_0 \simeq C \frac{N \cdot I_M}{4} v^{2/3} < H_s(d_{cp}) = \frac{C_1 \gamma}{2 C_2 I_M d_{cp}}. \quad (1)$$

Here I_M is the saturation magnetization of the ferrite matrix; C, C_1, C_2 are constant coefficients, approximately equal to one; γ is the surface energy of the boundary, which at room temperature is approximately equal to 2.5 ergs/cm^2

(II) The case of relatively large inclusions. For uniaxial materials:

$$H_c \sim H_0^{\tau} \approx \frac{\gamma}{2 I_s d} \beta^{2/3}.$$

where β is the total concentration of inclusions of all sizes.

$$H_c \sim H_0 = C \frac{N (I_M - I_k)^2}{4 I_M} v^{2/3},$$

where $H_s(d_{cp})$ is the starting field, at which the magnetization nuclei, arising in the large inclusions for which $cd > d_{cp}$ begin to grow.

$H_0(\sigma_i)$ is part of the critical field, defined by the gradients of the internal fields.

* *Fiz. metal. metalloved.* 8, No.3, 346-348, 1959.

For cubic materials, such as iron or highly annealed steel, the expression for the critical field follows Kersten's formula [5]:

$$H_c \sim H_0 \approx \frac{\gamma}{2I_s d} \beta^{2/3}. \qquad (2)$$

For the problem under consideration when the inclusions are found to be carbide phases exhibiting various degreed of magnetization, it is possible to rearrange formula (1) in the form:

$$H_c \sim H_0 = C \frac{N(I_M - I_k)^2}{4I_M} v^{2/3}, \qquad (1')$$

where I_k is the saturation magnetization of the inclusions.

If we take into account that the thickness of the wall is 0.5×10^{-5}cm. [7], we have, on the average, equal numbers of 180° and 90° neighbourhoods, and assuming that the sizes of the carbide inclusions in the region of annealing 400-650°C vary within the limits of 10^{-5}-10^{-4}cm. [see 8], it becomes clear that we can expect to find the maximum concentration of inclusions when annealing at 350-400°C.

When annealing at 400°C, the process of precipitation and separation of carbide phases is in the main complete, and the process of spherodization (transformation of the plate form into globular form) and coarsening begins. During coarsening the large particles grow at the expense of the small, energetically less favourable, particles. The process of coarsening as is known, is completed during annealing at 700°C for the majority of plain carbon and low-alloy steels.

The results of measurements of the magnetic properties of many structural and high-carbon steels, and also the temperature dependence of the magnetic properties, agree well with the data from the theory [4].

In Fig. 2 of the work [13], the values of the magnetic properties, hardness, and electrical resistance at room temperature, of a typical structural steel 40XH, are given in relation to the annealing temperature.

The temperature dependence of the magnetic properties is shown in Fig. 4 of the work [13], and from it can be seen that at the temperature of observation $t > 220$°C, when all the carbides are practically paramagnetic, the maximum coercive force is found in samples annealed at about 320°C.

In samples annealed at all temperatures above 400°C, the coercive force increases monotonically and almost linearly with an increase in annealing temperature.

The saturation magnetization of the matrix I_m, observed at 300°C remains practically constant in the whole annealing interval 400-650°C (curve 6 in Fig. 4 of the work [13]). Meanwhile the saturation magnetization at room temperature (curve 1) falls strongly with an increase in the temperature of annealing. While the quantity of the carbide phase present hardly changes at all during annealing above 400°C its magnetization ought to decrease.*

It is clear from the formula (1') that if we consider the change in the coercive force at room temperature with an increase in the temperature of annealing, then the dominating factor is the difference in magnetization between the matrix and the carbides $(I_M - I_k)$. This stage, as the initial concentration of coagulation v hardly changes, but the mean demagnetization factor N_{cp} decreases (from $N_{cp} = \frac{4\pi + 0}{2} = 2\pi$ at 400°C to $N_{cp} = \frac{4}{3}\pi$ at 600°C), the difference in magnetization $(I_M - I_k)$ increases with the temperature of annealing. On the whole we have a decrease in the coercive force up to annealing temperature 450°C.

It is natural to expect that beginning at some temperature, about 450-500°C, the rate of increase of N becomes zero (that is $N = \frac{4}{3}\pi = \text{const}$), and the rate of increase of $(I_M - I_k)$ becomes greater than the rate of decrease of the concentration v; then the coercive force will increase with the temperature of annealing until the rate of decrease in v becomes greater than the rate of increase of the difference $(I_M - I_k)$. Above this annealing temperature the decrease in the coercive force should begin, resulting from a sharp increase in size of the carbide particles, and the secondary domain structure arising in the inclusions [9]. In this case the coercive force is defined by formula (2).

* This decrease depends both on the carbide transformation [11], and on the alloying of cementite [12] and the formation of special non-ferromagnetic carbides.

VOL. 8 1959

The trend of the temperature dependence of $H_c(t)$ shown in Fig. 4 of work [13] in the region of anneal $T > 600°C$ fully supports this.

Investigations [2, 8 and 10] and similar works have great practical importance in the resolution of the problem of the strength of manufactured articles. The investigation of magnetic properties and their temperature dependence in these observations will help us to understand more quickly the mechanism of durability and so it will facilitate the solution of this important problem.

Translated by Z. Kowszon

REFERENCES

1. R.C. Dean and C.Y. Clayton, *Trans. Amer. Soc. Metals*, 26, 237 (1938).
2. K.F. Starodubov, *Problemy metallurgii Akad. Nauk SSSR*, 442, (1953).
3. N.N. Sirota, *Trud. NTO Chernoi metallurgii*, 6 152 (1955).
4. E.I. Kondorskii, Dokl. akad. nauk SSSR, 63, 5 (1948); 68, 1 (1949).
5. M. Kersten, *Grundlagen einer Theoris der koerzitivkraft*, Leipzig (1943).
6. V.S. Mec'kin, *Ferromaghitnyye splavy*, State Publishing House of Science and Technology (1937).
7. E. Lifshits, *Zh. eksp. teor. fiz.* 15, 97 (1945).
8. Proceedings *Am. Soc. Testing Materials*, 54, 568 (1954).
9. H.J. Williams, R.M. Bozorth and W. Shockley, *Phys. Rev.*, 75, 155 (1949).
10. E.N. Sokolov and V.D. Sadovskii, *Trud. inst. fiz. metal. Urals. fil. akad. nauk.* 18 (1956).
11. B.A. Apayev, *Dokl. akad. nauk. SSSR*, 107, 5 (1956).
12. B.G. Livshits and K.V. Popov, *Zav. lab. lab.* No.2, 157 (1950).
13. G.S. Tomilov, M.N. Mikheev and M.F. Pomukhin, 8, copy 2 (1959).

THE LAWS OF INTRA-CRYSTALLINE DISTRIBUTION OF ELEMENTS IN METAL ALLOYS*

A. S. ZAV'YALOV and B. I. BRUK

(Received 6 August 1958)

VOL. 8 1959

The processes taking place within the grains of solid solution alloys, which sometimes pro produce heterogeneity in the composition due to enrichment or removal from the peripheral zones of the crystallites of individual components, have a marked effect on the physical and mechanical properties of the alloys.

However, existing experimental data are not sufficient to establish the essence and mechanism of these processes. Up to the present time, it has not been decided whether the development of these processes follows those general thermodynamic rules on which the phase diagrams are based, or whether they follow other rules which do not correspond directly with ideas arising from the phase rule. Whereas there is no doubt that liquation heterogeneities of composition become uniform during heating of the alloy, the effect of temperature on the redistribution of the elements relative to the surface layers of the crystallites has not yet been fully clarified.

Extensive use has been made of the theoretical ideas developed by Arkharov [1-4]. The basic principle of these ideas is the fact that the enrichment of inter-phase surfaces with impurities lowering the surface energy of the phases (the so-called horophilic impurities) shown by Gibbs, can extend in polycrystalline aggregates to a monatomic layer. According to Arkharov the thickness of layers enriched with horophilic or impoverished by the so-called horophobic (i.e. increasing the surface energy) impurities reaches several thousands of atomic distances and therefore the phenomena governing the regularities of formation and growth of the nuclei of new phases take place mainly within the limits of these layers.

One of the basic ideas of the Arkharov theory, determining the effectiveness of its application to various phenomena and processes taking place in alloys, is the supposition that the concentration in the enriched layer is linked with the bulk solubility of the impurity and changes with temperature in a similar way to the change in solubility. This means that, for a weak change in the bulk solubility, over a certain temperature range there should be a weak change (of the same sign) of the average concentration of the Gibbs layer in the same temperature range and for a strong change (of the same sign) of the average concentration in the Gibbs layer.

These ideas were used by their authors to explain a number of phenomena and processes taking place during the heat treatment of alloys. The interpretation of most of the phenomena was rather convincing, although as yet there has been no reliable experimental support for these ideas.

The method of contact radiography, which is used in the present work, cannot pretend to give a complete answer to the problem of intra-crystalline distribution of elements in alloys. Nevertheless, this method has two special features which are very useful in the study of this problem. In the first place the radiography method makes it possible to detect in solid solution concentration heterogeneities which cannot be detected metallographically; in the second place, the radiographic method makes it possible with comparatively small magnifications to fix the concentration of element in very fine structural volumes, since the radiation acting on the emulsion, being scattered from the point of localization of the radioactive material in all directions, produces a region of darkening

* *Fiz. metal. metalloved.* 8, No. 3, 349-361, 1959.

which is much greater than the radiating section itself.

We calculated [5] the minimum thickness of a layer, enriched with radioactive carbon, at an austenite grain boundary which was able to develop a zone of preferential darkening on the photographic emulsion. The calculation showed that with the usual nuclear photo-emulsions and the usual exposures and concentrations of the radioactive carbon in the alloy, the minimum thickness of such a layer does not exceed 10^2-10^3 interatomic distances.

Fig. 1. An autoradiograph for the boundary contact of steels (tempering 600°C – 4 hr); × 4.

The application of the radiographic method to the study of the distribution of impurities in iron alloys is much more effective when working with the radioactive isotope of carbon. This is not only because the low energy of the β-spectrum of the ^{14}C isotope makes it possible to obtain sufficiently clear radiographs but also because the distribution of carbon in iron alloys is very closely bound up with the distribution of the alloying elements.

For example, carbon has a tendency to concentrate in zones which are enriched with carbide-forming elements, which is shown by the autoradiograph in Fig. 1, taken with a bimetallic specimen tempered at 600°C, containing radioactive carbon. One half of the specimen is an alloy of iron with 3 per cent chromium, the other half is a low-carbon unalloyed steel. Before tempering, the carbon was distributed uniformly in the unalloyed component of the bimetallic specimen. As follows from this autoradiograph, during tempering the carbon diffused energetically from the deep layers of the unalloyed steel to the boundary where it fused with the alloyed steel; only the chromium contained in the alloyed half of the specimen could cause the carbon to do this.

When the alloy has zones enriched with non-carbide-forming elements, these zones are low in carbon, which diffuses from them into zones which are less rich in these elements. This is confirmed by the photomicrograph of Fig. 2, which shows that carbon diffused from the surface layer, which was rich in silicon, into the deep zones. Similar results were obtained when the surface layer of steel was saturated with phosphorus, aluminium and other non-carbide-forming elements.

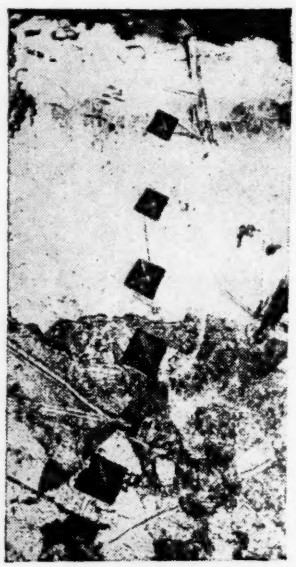

Fig. 2. The microstructure of a carbon steel with 0.21 C after its surface saturation with silicon for 30 hr at 1050°C; × 330.

When steel with a high content of non-carbide-forming elements is carburized, in a number of cases this redistribution of carbon takes place and it collects in certain zones in the form of graphite surrounded by decarburized zones. Fig. 3 gives the microstructure of a steel containing 4.4% Si after it had been carburized for 30 hr at 1000°C. It is of interest that no graphite separates in the layer at the outer surface of a specimen having the highest carbon content.

The highest quantity of graphite separation was found at a distance of 0.5-0.65 mm from the outer surface (the total thickness of the cemented layer is 3.2 mm). During carburiza-

tion, the silicon from the surface layer was apparently "driven back" to the deeper layers, in which its graphitizing effect was much more pronounced. This conclusion is

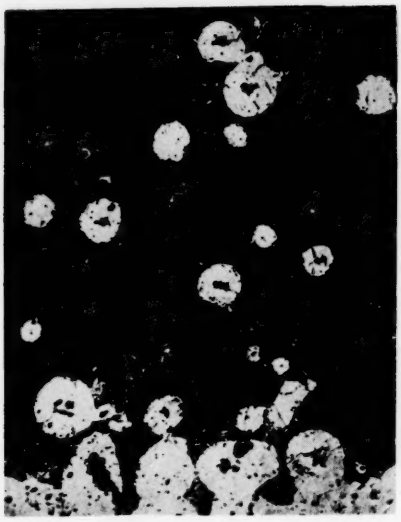

Fig. 3. The microstructure of a carburized layer of steel containing 4.4 per cent silicon, cooled slowly after cementation; x 140.

also confirmed by the chemical analysis of the layers.

Not only is the silicon able to reduce the carbon content of zones which are rich in silicon, but carbon can also have a similar effect on the redistribution of silicon. The difference in their mutual effect is quantitative rather than qualitative, probably depending on the difference in the diffusion coefficients.

The connexion between the distribution of carbon and the alloying elements is very clearly shown by the radiographic method.

The ^{14}C isotope was introduced into alloys of iron alloyed separately with silicon, molybdenum and tungsten, the concentrations of which were less than their solubility limit in iron in some cases and in others the concentrations exceeded this limit. The quantities of the isotope were sufficient to give clear radiographic images of the distribution of carbon on the photoemulsion. The total carbon concentration in the alloys was 0.06-0.13%. Due to the rapid cooling of the ingots after smelting, their structure in most cases showed a clearly expressed dendritic heterogeneity.

We will consider first of all the distribution of carbon in alloys of iron with silicon. Fig.4 gives an optical photograph (a) and an autoradiograph (b) of an iron alloy containing 19.5% Si, the structure of which contains a phase enriched with silicon (apparently the η-phase Fe_3Si_2). A comparison of these photographs shows that where there is silicon intermetallide (the lightly etched part on the optical photograph) there is practically no carbon; on the other hand, in the sections which are low in silicon content, which are clearly the inter-axial dendrite zones in this particular case, there is a noticeable accumulation of carbon.

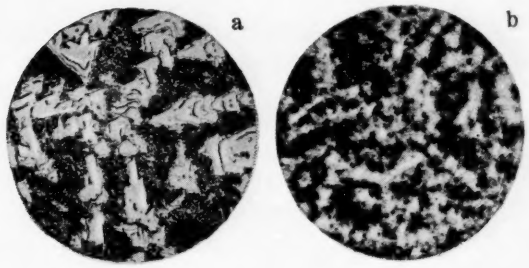

Fig. 4. The distribution of carbon in an iron alloy containing 19.5% Si:
a – optical photograph; x 30; b – autoradiograph; x 20.

Fig. 5. The distribution of carbon in an iron alloy containing 9.2% W:
a – optical photograph; x 45; b – autoradiograph; x 30.

These results agree with data for the distribution of carbon in a plastically worked alloy with a relatively even distribution of the silicon (with its concentration less than the solubility limit for iron). As shown by the autoradiograph of Fig.8, in this alloy the carbon concentrates mainly at the

ferrite grain boundaries, i,e. it is "drawn" from the central zones of the crystallites to their periphery.

We therefore see that in alloys of iron with non-carbide-forming elements (silicon), the carbon tends to concentrate in sections with a low silicon concentration. At the points of separation of intermetallic compounds which are rich in silicon, the carbon is absent, which is probably due to the negligible solubility of carbon in these compounds; when there is no phase enriched with silicon, the carbon "is drawn" (diffuses) to the grain boundaries.

We will now deal with the distribution of carbon in alloys alloyed with carbide-forming elements.

The optical photograph (a) and the autoradiograph (b), given in Fig.5 refer to an alloy of iron with 9.2% W and 0.1% C cooled in air after solidification. The fact that the shape and disposition of the dark sections on the autoradiograph are completely analagous to the microstructure indicates that all of the carbon in the alloy is in the tungsten-containing component, which is visible under the microscope, forming a complex iron-tungsten carbide or possibly, a homogeneous mixture of this phase with the tungstide Fe_2W.

Fig.6 shows an autoradiograph of an iron-tungsten alloy, the concentration of which (1.9 per cent) is less than its solubility limit in iron. In this case, as shown by the autoradiograph, the distribution of carbon (more accurately the carbides) is uniform, which is apparently due to the uniform distribution of the alloying element itself in the alloy.

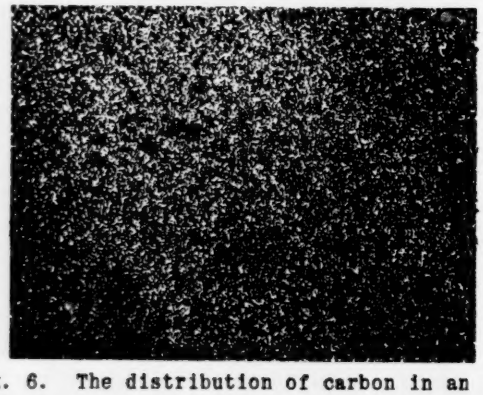

Fig. 6. The distribution of carbon in an iron alloy containing 1.9% W (autoradiograph); x 100.

Thus, in iron-tungsten alloys, the carbides are distributed in such a way that the disposition of the carbon corresponds to the disposition of the alloying element.

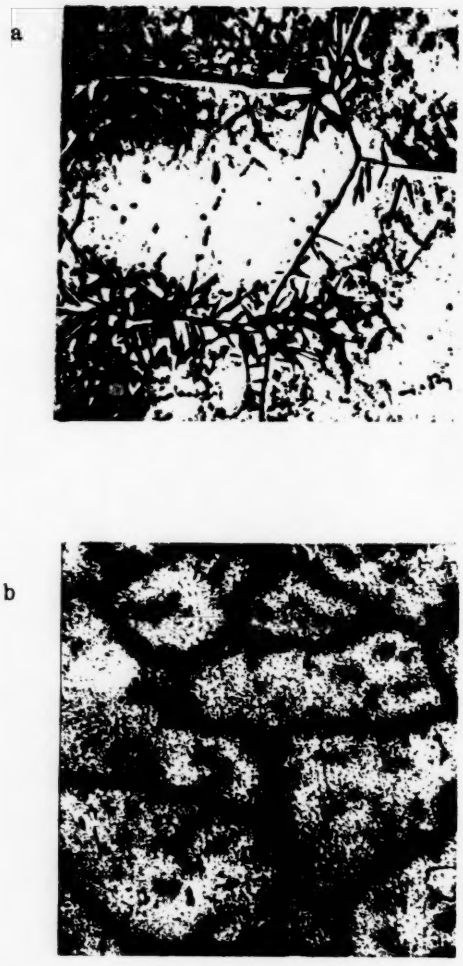

Fig. 7. The distribution of carbon in an alloy of iron containing 15% Mo:
a – optical photograph; x 150; b – autoradiograph; x 50.

A similar regularity is found in alloys of iron with other carbide-forming elements. For example, Fig.7 gives an optical diagram (a) and a autoradiograph (b) of an iron alloy with 15% Mo. The structure of this alloy should have an ϵ-phase enriched with molybdenum, or, possible rich in molybdenum carbide. It can be seen from the autoradiograph that the carbon concentrates at the

α-phase grain boundaries, i.e. apparently in the zones most likely to contain an intermetallic compound or molybdenum carbide. The optical photograph clearly shows the presence of a needle-shaped component in these zones.

Summarizing the results obtained, it can be stated that the distribution of comparatively small amounts (0.06-0.13 per cent) of carbon in iron alloys with different alloying elements shows the following regularities.

In the alloying of iron with non-carbide-forming elements in amounts exceeding the limiting solubility in iron, which results in the formation of an intermetallic compound enriched with this element (its separation in a structurally free state), the carbon is concentrated in those structural components which contain the smallest quantities of the alloying element.

In the alloying of iron with non-carbide-forming elements in amounts not exceeding the limiting solubility in iron, due to which the alloying element is distributed relatively uniformly in the alloy, the carbon is "drawn" from the alloy to the surface of separation between the crystal formations.

In the alloying of iron with carbide-forming elements, the carbon is distributed in accordance with the disposition of the carbide-forming element; if the concentration of the latter exceeds the limiting solubility in iron, then the carbon is concentrated at the places of separation of the compounds enriched with the alloying element, if the concentration of the element does not exceed the limiting solubility in iron, and the element is distributed relatively uniformly in the alloy, then the carbon in the carbide phase is also distributed uniformly.

It can therefore be concluded that if the application of the ^{14}C isotope makes it possible to establish the mode of distribution of carbon in iron alloys containing different alloying elements, then this distribution should undoubtedly be connected with the distribution of the alloying elements in the alloy.

Bearing in mind the established connexion between the distribution of carbon and the distribution of the alloying elements, and also taking into account the result (found by calculation) that the radiographic method can be used to detect layers which are enriched with carbon, where the thickness is 10^2-10^3 interatomic distances [5], we will attempt to establish certain regularities for the distribution of elements in microscopically small boundary volumes of alloys of iron with carbon and various alloying elements.

We will consider an alloy of iron with 4.4% Si [5,6]. It follows from the Fe-Si phase diagram that an alloy of this composition should be single-phase up to the line of the solidus. The distribution of carbon in this alloy (in amounts of 0.03 per cent)* after various types of heat treatment shows up clearly on the autoradiographs given in Fig.8.

With slow cooling of the alloy from 970°C and with tempering of the hardened alloy at 590° there is a perfectly clear concentration of carbon at the grain boundaries. Due to quenching of the alloy from 950 and 1200°C, the distribution of the carbon relative to the grain boundaries is homogeneous (at least in volumes exceeding 10^2-10^3 interatomic distances).

The fact that in unalloyed iron containing 0.035% C which has been tempered after quenching, the carbon distribution does not show any noticeable tendency to concentration at the grain boundaries (Fig.9), indicates that this concentration of carbon in the iron alloy with 4.4% Si, in the annealed and tempered states, is due to the presence of silicon. Enrichment of the grain boundaries with carbon in an alloy containing 4.4% Si, after tempering at 590°C and the absence of such enrichment after quenching from 1200 and from 900°C is apparently connected with the fact that with increase in temperature, the limiting solubility of carbon in the ferrite of the composition indicated increases and at 900°C exceeds (probably by a considerable margin) 0.035 per cent.

These experimental data therefore do not confirm the opinion that the concentration of the dissolved element in boundary volumes of monatomic thickness should change with increase in temperature in accordance with the curve for the volume solubility of this

* In iron-silicon alloys, containing about 0.03% C, the region of the γ-solid solution tapers off completely at 3% Si.

VOL. 8 1959

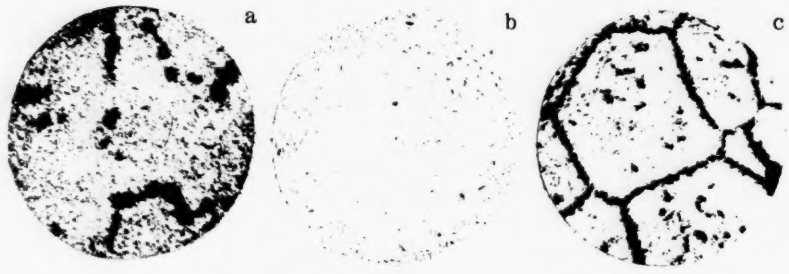

Fig. 8. The microscopic distribution of carbon in an iron alloy containing 4.4% Si (autoradiograph); x 65:
a – slow cooling from 970°C; b – quenching from 950°C; c – quenching from 1200° and tempering at 590°C, 10 hr.

element in the alloy [1-4]. The solubility of carbon in ferrite alloyed with silicon increases with temperature and the concentration of carbon in the boundary volumes decreases.

If we consider that the main "motivating factor" leading to concentration of elements at the crystallites surface is the surface energy, then the decrease in the role of this factor with increase in temperature should follow from the known expression

$$\left(\frac{\partial F}{\partial T}\right)_p = -S.$$

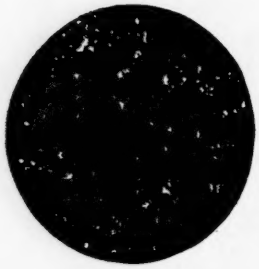

Fig. 9. The distribution of carbon in unalloyed iron with 0.035% C after quenching from 1200° and tempering at 590°C, 10 hr. Autoradiograph, x 65.

Since the entropy is always positive, the free energy decreases with increase in temperature. The decrease with temperature of the factor causing concentration of the element at the grain boundaries should naturally lead to a reduction in the concentration process.

The processes of concentration at the crystallite boundaries are often identified with adsorption phenomena, consisting of enrichment of the surface layer relative to the bulk concentration. In this case, the reduction in the effect of preferential enrichment of the surface layers by the adsorbing material with temperature is also apparent. This is supported by the well-known Gibbs' adsorption equation.

$$\Gamma = -\frac{c}{RT}\frac{\partial \sigma}{\partial c},$$

where Γ is the excess of the substance per unit surface; $-\frac{\partial \sigma}{\partial c}$ – is the change in the surface tension with change in the bulk concentration of the substance.

It follows from this equation that increase in temperature leads to a reduction in the amount adsorbed on the interface.

Thus, both the results of the experiments, and the simple thermodynamic considerations indicate that the factors which promote solute enrichment of the interface regions separating solid solution crystallites decrease with increasing temperature.

This conclusion holds when, in accordance with the phase diagram, the solubility of the component increases with increasing temperature. In the comparatively rare cases when the increase in temperature leads to a reduction in the solubility of the component (as for example in certain concentration regions of the copper-zinc system) the enrichment of the surface layers of solid solution crystallites with impurities should increase with increase in temperature.

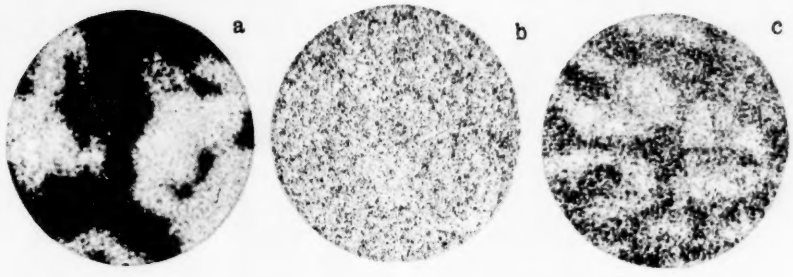

Fig. 10. The microscopic distribution of carbon in iron alloys containing 15% Mo (autoradiograph); x 100.
a – slow cooling after crystallization; b – quenching from 1250°C;
c – quenching from 1250° and tempering at 800°C, 15 hr.

In studying further the intra-crystalline distribution of impurities, we will deal with the distribution of small amounts of carbon (0.06 per cent) in an iron alloy containing 15 per cent molybdenum. Due to the slow cooling of an alloy containing 15% Mo, the carbon, after the crystallization is concentrated near the grain boundaries (Fig. 10a).

In water quenched from 1250°C, the carbon is distributed evenly, as can be seen from the autoradiograph of Fig. 10b. It would therefore appear that either the carbon-enriched layer does not exist at the grain boundaries, or that its thickness does not exceed 10^2-10^3 interatomic distances.

It follows from the autoradiograph of Fig. 10c that tempering the alloy after quenching from 1250°C again leads to a noticeable concentration of carbon at the grain boundaries.

This type of carbon distribution can also be seen in the heat treatment of an iron alloy containing 12 per cent tungsten (Fig. 11). Slow cooling from high temperatures and tempering after quenching from 1250°C leads to a concentration of the carbon at the grain boundaries; high temperature quenching leads to a relatively uniform distribution of carbon in the volumes of the solid solution crystallites.

The observed features of the distribution of carbon in Fe-Mo alloys and Fe-W alloys can be explained in the regularities of the phase state of these alloys in various temperature regions. Alloys of the selected composition (Fe + 15% Mo and Fe + 12% W) at 1250°C are single phase, α-solid solutions. The uniform distribution of carbon (shown by the radiographic method) in alloys which have been quenched from 1250°C may be an indication, as explained at the beginning of this

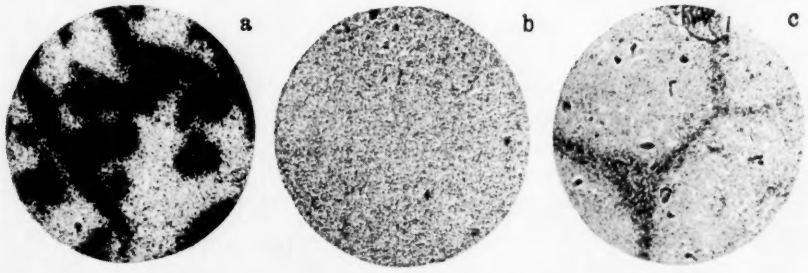

Fig. 11. The microscopic distribution of carbon in iron alloys containing 12% W (autoradiograph), x 100:
a – slow cooling after crystallization; b – quenching from 1250°;
c – quenching from 1250° and tempering at 800°C, 15 hr.

VOL. 8 1959

article, of the uniform distribution of molybdenum and tungsten in alloys at this temperature. It can therefore be assumed that in the temperature region in which the solid solution is the only phase, both the molybdenum and the tungsten are distributed either uniformly relative to the grain boundaries, or the non-uniformity is localized within a layer of less than 10^2 interatomic distances.*

If the concentration of tungsten in the alloy does not exceed the limit of its solubility in α-iron, then if follows from Fig.6 that the distribution of carbon in an alloy which was cooled from high temperatures is uniform, which presumably indicates the uniform distribution of tungsten in the alloy. Similar results are obtained in the iron-molybdenum alloy.

We therefore conclude that the distribution of molybdenum and tungsten in Fe-Mo alloys and Fe-W alloys follows the same laws which proceed directly from the phase diagrams of these binary alloys. In the region of existence of a single-phase solid solution (α) the distribution of these elements in the grain is uniform (in the sense of the word already used above). In the region of a two-phase state, the phases enriched with molybdenum (ϵ) and tungsten (β) are concentrated at the ferrite grain boundaries, "pulling" carbon to these volumes.

Experimental confirmation that intermetallic compounds separate at the grain boundaries of super-saturated solid solutions makes it possible to give the following thermodynamic treatment to processes that lead to the concentration of elements in the surface volumes of crystallites.

The increased level of the free energy in volumes adjoining the grain boundaries facilitates the setting up of atomic groups which are essential for the formation of nuclei of the new phase. In the case of alloys however, the formation of nuclei of the new phase. In the case of alloys however, the formation of nuclei requires the presence not only of energy fluctuations, as for single-component systems, but also fluctuations in the composition. In the case of the formation of Fe_3Mo_2 intermetallides (containing above 50 weight % Mo) and and Fe_2W (containing over 60 wt % W) it is very likely thermodynamically that there is a preceding displacement of the molybdenum and tungsten atoms to the grain boundaries, increasing the possibility of formation of composition fluctuations which are essential for the formation of nuclei for the new phase.

As regards the energy state of the alloys under consideration, being heated to 1250°C, the level of the free energy of the α-phase at this temperature is much lower than the level of the free energy of intermetallic compounds, due to which there is little probability of the formation of nuclei of these phases along the grain boundaries. It is quite apparent that if the energy state of the system prevents the formation of nuclei of a phase enriched with some element along the grain boundaries, then to an equal extent it hinders (or at least reduces the possibility of the enrichment of the grain boundaries with this element. In other words, the processes by which the grain boundaries are enriched in molybdenum and tungsten is in direct connexion with the formation of phases enriched by these elements, proceeding from the phase diagrams. Enrichment by these alloying elements of polyatomic layers along the grain boundaries of an alloy can only take place under those temperature and concentration conditions which precede the separation from the solid solution of phases enriched with molybdenum and tungsten.

The experimental results given in this paper indicate that processes of heat treatment of metallic alloys can cause the displacement of some components of these alloys to the grain boundaries of the solid solution, leading to a reduction in their surface energy. This displacement is bound up with those thermodynamic laws on which the phase diagrams are based. Consequently, the character of the displacement of alloy components towards the grain boundaries, completely determined by those temperature and concentration conditions in which the alloy exists, can be found directly from the phase diagram. If, due to change in its tempera-

* A similar result for a γ-solid solution was obtained in paper [5] in connexion with two other carbide-forming elements – chromium and manganese.

ture or the ratio of components in it, a single-phase alloy is at the stage directly preceding the separation of a new phase, then there should be concentrated along the boundaries of the crystallites of this alloy, or along the boundaries of smaller crystal formations, for example, mosaic blocks (also close to the final surfaces of separation, when dealing with a liquid alloy), those components of the alloy with which the separating phase is enriched in comparison with the initial solid solution.

It follows from this that there is no justification for relating some elements to the class of horophilic elements with respect to the solvent element, and others to the horophobic class when dealing with multi-atomic layers of the solid solution. In the single-phase region of the phase diagram, the same component of the alloy can either be horophilic with respect to the solvent element or horophobic for a different ratio of components or even with the same ratio but at different temperatures.

Considering for example the region of a γ-solid solution on the iron-carbon diagram, we should consider that the carbon in the alloy, whose composition is close to the *ES* line, is horophilic with respect to the iron and horophobic in an alloy close to the composition of the *GS* line.

In fact, the probability of composition fluctuation required for the formation of the nucleus of a new phase, enriched with some element, sharply decreases with increase in the number of atoms concerned in the fluctuation. It has been found for example, that in an iron-carbon alloy of eutectic composition, the probability of formation of a group of atoms corresponding in composition to the formula Fe_3C decreases by 4×10^4 times when the number of iron atoms in this grouping increases from 24 to 48 and another 7.5×10^8 times when this number increases from 48 to 96.

It should also be remembered that for a given degree of supercooling, there is a thermodynamically possible growth of nuclei, only of those exceeding in dimensions a fixed critical value. It is therefore quite apparent that in austenitic alloys, the carbon concentration of which corresponds to the *ES* line for a given temperature in one case, and in another to the *GS* line, the carbon will tend in one case to concentrate at the grain boundaries, thereby increasing the probability of formation of cementite nuclei, and in the other will tend to leave the grain boundaries, increasing the probability of formation of nuclei of the alpha-phase. During slow cooling of a post-eutectoid iron-carbon alloy, cementite forms along the grain boundaries, and in the case of a low carbon alloy, ferrite forms; with slow cooling of an alloy with the exact eutectoid composition, pearlite forms, i.e. the carbon is evenly distributed over the whole of the grain. Depending on its content in the alloy, the same element can therefore be distributed differently within the limits of the grain.

Similarly, we cannot ascribe to zinc a constant horophilic or horophobic property with respect to copper. Changing the concentration of zinc and copper in any isothermal through the phase diagram for these alloys, for any single-phase region of this diagram we will have those ratios of component concentrations for which the zinc, according to the above simple thermodynamic ideas, will tend either to enrich the grain boundaries of the solid solution or to deplete them.

CONCLUSIONS

The experimental results given in this paper and in papers [5, 6] indicate that the distribution of elements in metal alloys obeys the following laws.

1. If for a given temperature the content of the element does not exceed its limiting solubility in the solvent metal, then this element is distributed relatively evenly, over the whole of the crystallite, showing no tendencies to preferential concentration at the peripheral or internal volumes of the crystallite.

2. If the content of the element at a given temperature exceeds its limiting solubility in the solvent metal, then the excess quantities of this element will be concentrated at the boundaries of the crystal formations of the alloy in the form of a phase enriched with this element or in a structurally free state. With change in

VOL. 8 1959

temperature of the alloy, in accordance with the phase diagram, the components may be concentrated either in the boundary zones (with reduction in the limiting solubility of the elements) or distributed more evenly within the limits of the crystallite (with increased solubility of the element).

3. If, due to change in temperature or concentration conditions, a single phase alloy is at the stage preceding the separation of a new phase, then along the crystallite boundaries of this alloy or along the boundaries of the smaller crystalline formations, for example, mosaic blocks (and to an equal extent near to the final surfaces of separation in the liquid alloy) those components of the alloy concentrate with which the separating phase is enriched in comparison with the original phase.

4. The presence in the alloy of some elements affects the intra-crystalline distribution of other elements.

(A) If the alloy is formed by a metal solvent and two other elements, the bond strength between the atoms of which is weaker than between them and the atoms of the metal solvent (an indication of which is the inability of these elements to form compounds with one another in the alloy), then:

in the first place, enrichment of the grain boundaries and other crystalline formations by one of these elements (which is the case when its concentration in the alloy exceeds the limiting solubility in the metal solvent), causes a reduction in the content of the other element in the boundary zones; secondly, a relatively uniform distribution of one of these elements over the whole volume of the crystallite (which is the case when its concentration in the alloy does not exceed the limiting solubility in the metal solvent), causes redistribution of the second element as a result of which it enriches the boundaries of the crystalline formations.

This is found, for example, in alloys of iron with silicon and small amounts of carbon. If the silicon concentration is such that a silicon-enriched phase forms, then the sections containing this phase have a reduced carbon content. In the case where the concentration of silicon does not exceed the limit of its solubility in iron, the grain boundaries of the solid solution are enriched with carbon.

(B) If the alloy is formed with a metal solvent and two other elements, the bond strength between the atoms of which are stronger than between them and the atoms of the metal solvent (an indication of which is their ability to form compounds with one another in this particular alloy) then: firstly, enrichment of the grain boundaries and other crystalline formations with one of these elements (which is the case when its concentration in the alloy exceeds the limiting solubility in the metal solvent), causes enrichment of the boundary zones with the other element also;

In the second place, the relatively uniform distribution of one of these elements over the whole volume of the crystallite (which is the case when its concentration in the alloy does not exceed the limiting solubility in the metal solvent) slows down the process of redistribution of the excess quantities of the second element, resulting in enrichment of the boundaries of the crystalline formations with this element.

This is observed, for example, in alloys of iron with carbide-forming elements (Cr, Mo etc.) and carbon. In the case when the concentration of the carbide-forming elements does not exceed the limits of its solubility in iron, the redistribution of carbon towards the boundaries between the grains is hindered. When there are phases enriched with carbide-forming elements along the grain boundaries, the carbon concentrates in the sections which are enriched with the carbide-forming elements.

5. The investigation shows that when considering the boundary layers of poly, atomic thickness, it is not possible to consider some elements to be horophilic and the others to be horophobic with respect to the metal solvent. The tendency of components to concentrate along the grain boundaries or, on the other hand, to diffuse from the peripheral to the central volumes of the grains is determined not by any constant property of a given element with respect to the solvent element, but by the ratios of the concentrations of components for a given temperature, determined by the phase diagram, and in systems with more than two components by the difference in the bond forces between the elements,

forming the alloy. According to the phase diagram for the alloy, the same element in different temperature regions and for different concentrations of components of a single-phase system can be distributed preferentially both at the surface and in the internal volumes of the crystallites.

Translated by J. Thompson

REFERENCES

1. V.I. Arkharov, *Trud. Inst. fiz. met. Urals. fil. akad. nauk.* SSSR, No.8 (1946).
2. V.I. Arkharov, *Trud. All Union Central Scientific Research Inst. MTM* No.5, 26 (1946).
3. V.I. Arkharov, *Trud. Inst. fiz. met. Urals. fil. akad. nauk.* SSSR, No.14 (1954).
4. V.I. Arkharov, *Trud. Inst. fiz. met. Urals. fil. akad. nauk.* SSSR, No.16 (1955).
5. A.S. Zav'yalov and B.I. Bruk, *Metallovedenie, sb. statei (Metallography, Collection of Articles)* Sud promgiz (1957); *Fiz. metal. metalloved,* 5, No.1 (1958).
6. A.S. Zav'yalov and B.I. Bruk, *Dokl. Akad. Nauk* SSSR, 115, No.1 (1957).

VOL.
8
1959

A STUDY OF SELF-DIFFUSION IN ZIRCONIUM AND ITS ALLOYS WITH TIN*

V. S. LYASHENKO, V.N. BYKOV and L. V. PAVLINOV

(Received 13 September 1958)

The self-diffusion in zirconium in α- and β- regions is studied with the use of the radioactive isotope ^{95}Zr. The activation energy of self-diffusion in α- and β-zirconium is 52,000 and 38,000 cal/g atom respectively. Alloying zirconium with tin raises the activation energy of self-diffusion in α-zirconium. The maximum value of activation energy (75,000 cal/g atom) is obtained for an alloy containing 2,39 per cent weight of tin.

Zirconium possesses good nuclear-physical properties and a comparatively high resistance to corrosion in water at temperatures up to 360°. However, the use of zirconium is limited to a considerable degree by its low mechanical and anticorrosive properties at increased temperatures (400-500°) [1].

It is known [2] that the speed of softening of metals and alloys depends on the mobility of the atoms, determined by the energy of interatomic reaction. The energy of interatomic reaction can be evaluated by the known values of a series of physical parameters, including the activation energy of self-diffusion.

The published data on self-diffusion in zirconium [3-5] do not agree with one another. From the work published for zirconium, there are considerable variations from the known rules of the process of diffusion. This is probably explained by the effect of certain factors which were not taken into account. One of these factors could be, for example, predominant boundary diffusion, the presence of which is confirmed in the present study.

An increase in the energy of interatomic reaction can be obtained by alloying. In the present work the effect of the addition of tin on the activation energy in zirconium is studied. The choice of tin in the capacity of an alloying element is explained by the fact that there are indications in the literature of the favourable effect of tin on the resistance of zirconium to corrosion.

METHOD OF EXPERIMENT

For the study zirconium iodide (99.6 per cent) was used, with the basic additions: Hf-0.07%, N-0.014%, Fe-0.04%, Si-0.05% (hardness not more than 55 Rn), smelted in an electric arc furnace type MIFI-9-3 in an atmosphere of argon. Under the same conditions binary alloys of zirconium were smelted, containing 1.30, 2.39 and 3.54 per cent weight of tin. All the specimens were subjected to homogenizing anneals at a temperature of 1000° for a duration of 5 hr.

The specimens had dimensions of 10 x 10 x x 20 mm. For determining the coefficient of self-diffusion in zirconium, radioactive isotope ^{95}Zr was used, which was evaporated onto the specimens in a vacuum. At the time of evaporation the specimens were situated on the water-cooled cover of the chamber with a residual pressure of 10^{-3} mm Hg. The activity of the specimens amounted to 20,000-25,000 impulses per minute. The deposited film of the isotope of zirconium became compact, 0.5-1 μ thick, calculated by the increase in weight.

The diffusional anneal at temperatures of 650-827° took place in evacuated quartz capsules. At temperatures of 918-1260° the specimens were annealed in a quartz capsule with continuous evacuation (residual pressure

* *Fiz. metal. metalloved.* 8, No.3, 362-369, 1959.

VOL 8 195

approximately 5 × 10^{-4} mm of Hg.).

At temperatures of 1325-1500° the diffusional anneal was carried out in a vacuum furnace with a tungsten heater (residual pressure approximately 5 × 10^{-4} mm Hg.). Two specimens were annealed simultaneously, with their active sides placed together. To prevent possible oxidation, the specimens were covered with zirconium shavings in all cases. The anneal was carried out continuously, the time of heating and cooling of the specimens was accounted for by introducing the corresponding correction. The diffusion anneal in the β-region was from one to thirty hours (depth of penetration 200-300 μ). In the α-region the accuracy of the measurements of the coefficients of diffusion lies at the limit of sensitivity of the method as the depth of penetration for annealing from 222-1076 hr amounted to 30-60 μ.

The temperature was measured by a Pt-Pt-Rh thermocouple. The deviation of the temperature from the set value did not exceed ± 5°.

The layers were removed on a polishing disk. The thickness of the layer was measured by the difference in the thickness of the specimen before and after the removal of the layer on a vertical optical comparator type IZV-1. This instrument ensures an accuracy of ± 1μ. However, because of the possible nonparallelism of the layers removed, the actual error in measuring the thickness of a layer is estimated at 2-3μ. In the α-region the thickness of the layer was measured by the instrument IZV-1 and calculated by the change in weight of the specimens, weighed with an accuracy of ± 0.0001g. In this instance the error in the measurement of the thickness of the layer did not exceed 1μ.

The integral activity of the specimens was measured on a rigidity meter B-2 with the use of a facing meter type MST-17. The duration of each measurement amounted to 10 min. γ-radiation of niobium, a product of the disintegration of Zr-95, was accounted for by the use of a filter.

The coefficient of absorption of β-radiation of zirconium measured with the use of aluminium filters, proved to be 350 cm^{-1}. The coefficient of self-diffusion was measured by the method of the removal of layers and the determination of their specific activity by the variation of the integral activities of the specimen before and after the removal of the layer [6].

In accordance with the primary and boundary conditions for the specimens studied, the solution of the diffusion equation can be put into the form

$$\ln\left(\frac{\Delta In}{\Delta x_n} + \mu In\right) = -\frac{x_n^2}{4Dt} + \text{const},$$

where In is the integral activity after the removal of a layer of thickness xn; μ is the coefficient of absorption of β-radiation of zirconium.

The value $\ln\left(\frac{\Delta In}{\Delta xn} + \mu In\right)$ is a linear function of x^2. The tangent of angle α, formed by this line with the abscissa equals $1/4Dt$. Then the calculation formula will have the form: $D = \frac{1}{4t \times \tan\alpha}$.

The expression obtained is correct for volume diffusion. For boundary diffusion, as follows from the given analysis of Fisher [7], the logarithm of the concentration should be a linear function of the first power of the depth of penetration.

The calculation formula for the coefficient of boundary diffusion has the form

$$D_{gr} = \frac{2}{\delta}\sqrt{\frac{D}{\pi t}}\left[\frac{d(\ln c)}{dx}\right]^{-2},$$

where δ the width of the boundary of the division; D is the coefficient of volume diffusion.

The relative error in the determination of the coefficient of volume diffusion by the described method does not exceed 14-15 per cent. Besides this, in the β-region substantial diffusion occurs rapidly, resulting in an inaccuracy in the measurement of the time of annealing (7-8 per cent). The relative error of the determination of the activation energy of self-diffusion for α- and β-zirconium is 5 and 2 per cent, respectively.

EXPERIMENTAL DATA AND THEIR DISCUSSION

The data for measuring the coefficients of self-diffusion in zirconium are presented in

Table 1 and Figs. 1 and 2 (650-827° for the α-phase; 918-1500° for the β-phase).

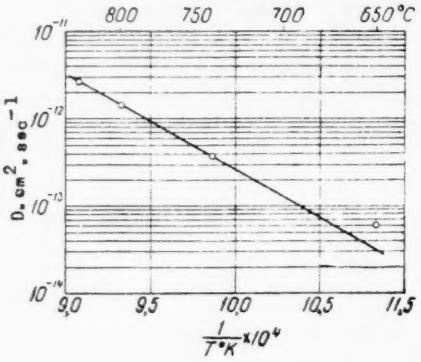

Fig. 1. The temperature dependence of the coefficient of self-diffusion in α-zirconium.

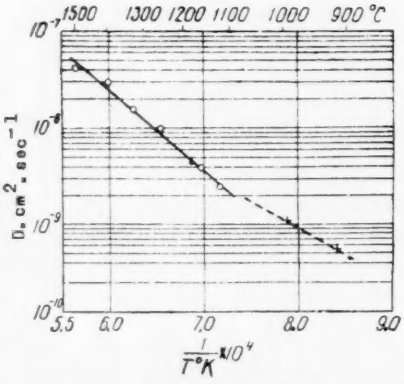

Fig. 2. The temperature dependence of the coefficient of self-diffusion in β-zirconium.

The temperature dependence of the coefficient of self-diffusion, calculated graphically and by the method of least squares, can be represented by the equations:

$$D = 5.9 \times 10^{-2} \exp\left(-\frac{52\,000}{RT}\right) \text{ cm}^2/\text{sec} \quad (\alpha\text{-phase})$$

$$D = 2.4 \times 10^{-3} \exp\left(-\frac{38\,000}{RT}\right) \text{ cm}^2/\text{sec} \quad (\beta\text{-phase})$$

The coefficients of self-diffusion at 918 and 996°, determined from the graph of the dependence of $\log\left(\frac{\Delta I}{\Delta x} + \mu I\right)$ on x^2, do not lie on the straight line, and are rather larger in value than those extrapolated from the equation for the β-phase. The causes of this deviation will be discussed later.

From Fig. 1 it is seen that the experimental point at 650° does not lie on the general straight line carried through the points 740, 800 and 827°. This is explained by the lower accuracy of the determination of the coefficient of self-diffusion at 650°, as the depth of penetration at this temperature for 540 hr amounts, in all, to 10 μ.

The published data and results of the present work show that the process of self-diffusion in zirconium is characterized by certain deviations from the known rules. It is known, for example, that for many pure metals a simple correlation takes place between the activation energy of self-diffusion and the melting point ($Q = 40T_{mel.}$) [8]. For zirconium, from the data of the present work, the deviation from this correlation goes beyond the limit of possible experimental errors. The activation energy, calculated from the formula $Q = 40T_{mel.}$, is equal to 85,000 cal/g-atom for zirconium.

The correlation established in the work [9]

TABLE 1

α-phase		β-phase	
Temperature, °C	D, cm²/sec	Temperature, °C	D, cm²/sec
650	6×10^{-14}	918	$5 \times 5 \times 10^{-10}$
740	$3 \times 6 \times 10^{-13}$	996	$1 \times 1 \times 10^{-9}$
800	$1 \times 4 \times 10^{-12}$	1118	$2 \times 16 \times 10^{-9}$
827	$2 \times 7 \times 10^{-12}$	1162	$3 \times 8 \times 10^{-9}$
		1260	$9 \times 8 \times 10^{-9}$
		1325	$1 \times 5 \times 10^{-8}$
		1400	$2 \times 9 \times 10^{-8}$
		1500	$4 \times 2 \times 10^{-8}$

between the activation energy of self-diffusion and the heat of sublimation does does not take place either. For many pure metals $Q=(0.6\text{-}0.7)E_{subl}$. The value of activation energy, calculated by this formula, is also equal to approximately 85,000 cal/g-atom for zirconium.

The work carried out does not give the opportunity to establish reasons to explain the deviations from the indicated rules. One can only suppose that boundary diffusion has a marked effect on the process of diffusion in the temperature interval studied. Prevalent boundary diffusion is observed at temperatures of 918 and 996°. Whether the diffusion occurs through the volume of the grain or at the boundaries can only be judged by the character of the dependence of the logarithm of concentration on the depth of penetration.

In Fig. 3 is represented the dependence of the logarithm of concentration (more accurately of the value $\frac{\Delta I}{\Delta x}+\mu I$, which is proportional to the concentration) on x^2 for the specimens annealed at 918, 996 and 1260°. In Fig. 4, for the same specimens, is represented the dependence of $\log\left(\frac{\Delta I}{\Delta x}+\mu I\right)$ on the first power of the penetration distance. From these graphs it is seen that the experimental points for a temperature of 918° lie on the straight line in the co-ordinates $\log\left(\frac{\Delta I}{\Delta x}+\mu I\right)-x$. This bears witness to the fact that, at a temperature of 918°, prevalent diffusion takes place on the boundaries. The experimental points at a temperature of 1260° (and also at higher temperatures) lie on a straight line in the co-ordinates $\log\left(\frac{\Delta I}{\Delta x}+\mu I\right)-x^2$. Consequently, at 1260° and higher temperatures diffusion through the volume of the grain is predominant in the diffusional flow. At a temperature of 996°, as is seen from Figs. 3 and 4, the experimental points do not lie in a straight line either in the co-ordinates

$$\log\left(\frac{\Delta I}{\Delta x}+\mu I\right)-x,$$

or in the co-ordinates

$$\log\left(\frac{\Delta I}{\Delta x}+\mu I\right)-x^2.$$

This means that at 996° the diffusion at the boundaries flows at a greater speed than through the volume of the grain, but the diffusional streams are equal in size.

The value of the coefficient of boundary diffusion at a temperature of 918°, calculated with the use of the Fisher formula, equals 10^{-4} cm^2/sec.

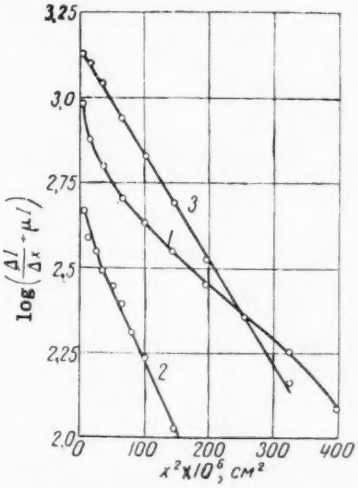

Fig. 3. The dependence of the logarithm of concentration on the square of the depth of penetration. (1 – at 918°; 2 – at 996°; 3 – at 1260°).

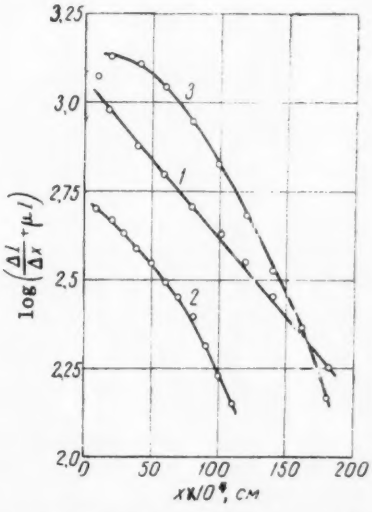

Fig. 4. The dependence of the logarithm of concentration on the depth of penetration. (1-at 918°; 2-at 996°; 3-at 1260°).

The relationship of the coefficient of boundary diffusion to the coefficient of volume diffusion is equal to 2×10^5.

It is difficult to suppose that the prevalent boundary diffusion at 918° and partly at

996°, is explained by diffusion at the borders of the grains, as the size of the grains in the specimens used amounted to 3-4μ. Therefore the supposition of Gruzin and others seems more correct [5], considering that the high level of diffusional mobility at temperatures up to 1200° depends on the intragranular surfaces arising during allotropic transformation. The appearance which takes place here is probably similar to that described in the work [10].

Because of the slight impurities in the zirconium, when cooling from the β-phase a needle-shaped structure of the martensite type is formed (as is shown in the work [11] an oxygen content of 0.07-0.10 per cent is sufficient to obtain the needle-shaped structure). The presence of the needle-shaped structure in the specimens studied is shown in Fig. 5. When a specimen which has a needle-shaped structure is heated to the temperature of the diffusional anneal, new surfaces of division in the β-phase arise, with the breaking of the correct periodicity of the structure of crystals of β-zirconium crystals, which leads to a rise in the diffusion coefficient. Only at temperatures higher than 1100° is the breaking up of the structure eliminated, caused by the phase transformation.

In the work the effect of the addition of tin on the parameters of self-diffusion of zirconium is studied.

TABLE 2

Addition Sn, %	D_o, cm^2/sec^{-1}	Q, cal/g-atom
1.30	5.0	62000
2.39	2.1×10^3	75,000
3.54	10	64,000

The graph of the dependence of the diffusion coefficient of zirconium on the temperature in the alloys studied is shown in Fig. 6. The parameters of the diffusion of zirconium are presented in Table 2.

The data of Table 2 show that the addition of tin up to 2.4 per cent causes a rise in the activation energy, reaching a value of 75,000 cal/g-atom with a content of 2.39 per cent of tin. With a tin content of 3.54 per cent the value of the activation energy decreases, though it exceeds in size the value of the activation energy of pure zirconium.

Fig. 5. The microstructure of a specimen of zirconium after tempering at 1500° for 1 hr, speed of cooling 100°/min; × 200.

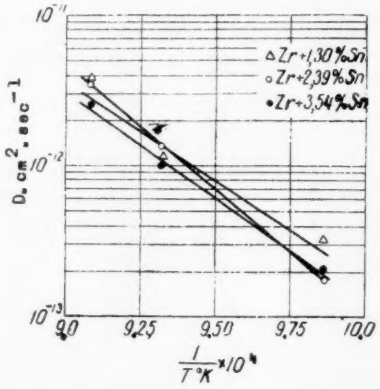

Fig. 6. The temperature dependence of the diffusion coefficient in alloys of zirconium with tin.

The dependence of the values of Q and log D_o on the tin content are shown in Figs. 7 and 8. In Fig. 9 is shown the dependence of log D_o on the activation energy.

From the figure it is seen that the experimental points lie satisfactorily on a straight line. The equation of this straight line has the form

$$\log D_o = aQ - b,$$

$a = 1.94 \times 10^{-1}$ g-at/cal^{-1},

$b = 11.4$ g-at/cal^{-1}.

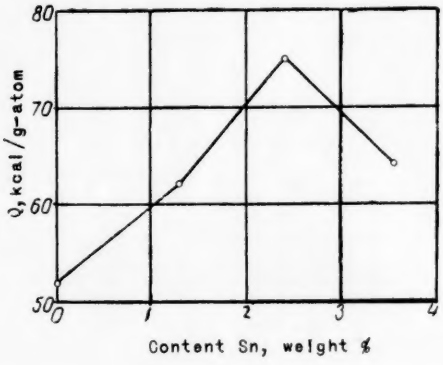

Fig. 7. The dependence of the activation energy on the content of tin

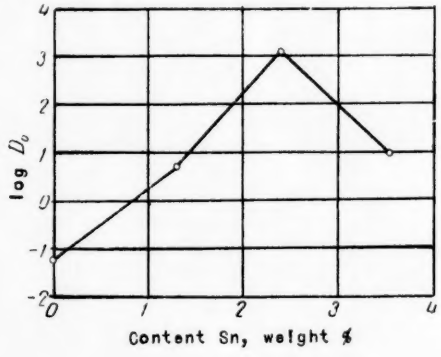

Fig. 8. The dependence of $\log D_0$ on the tin content.

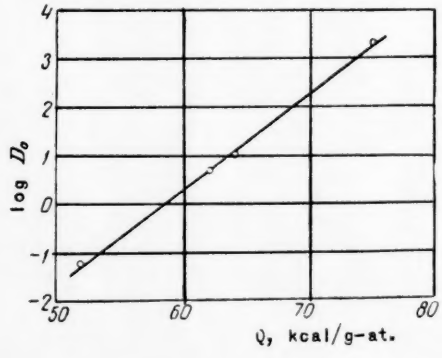

Fig. 9. The dependence of $\log D_0$ on the activation energy.

CONCLUSIONS

1. The equation of the temperature dependence of the self-diffusion coefficient in zirconium has the form:

$$D = 5.9 \times 10^{-2} \cdot exp\left(-\frac{52\,000}{RT}\right) \text{ cm}^2/\text{sec} \quad (\beta\text{-phase})$$

$$D = 2.4 \times 10^{-3} \cdot exp\left(-\frac{38\,000}{RT}\right) \text{ cm}^2/\text{sec} \quad (\beta\text{-phase})$$

2. In the temperature interval 900-1100° there is prevalent boundary diffusion. The ratio of the coefficient of boundary and volume diffusion at 918° equals 2×10^5.

3. Data are obtained on the effect of tin on the parameters of self-diffusion in α-zirconium. The addition of tin up to 3.5 weight per cent raises the activation energy in the temperature interval 740-827°. Also, the greatest value of activation energy (75,000 cal/g-atom) is obtained for an alloy containing 2.39 per cent Sn.

4. A comparison of the values of $\log D_0$ and the corresponding values of activation energy shows that $\log D_0$ depends linearly on Q. The equation representing this dependence has the form:

$$\log D_0 = 1.94 \times 10^{-4} \times Q - 11.4.$$

Translated by Coleman

REFERENCES

1. G.L. Miller, *Zirconium*, Moscow, Institute of Foreign Literature (1955).
2. G.V. Kurdyumov, V.A. Il'ina, V.K. Kritskaya and L.I. Lisak, *Izv. Akad. Nauk SSSR, Physics series*, 17, No.3 (1953).
3. H.I. Wheeler, *Progress Report* 20-172, Jet Propulsion Laboratory, California Institute of Technology, Apr. 8, 1952.
4. B. Lustman, *Metallurgy of Zirconium* (1955).
5. E.V. Borisov, U.G. Godin, P.L. Gruzin, A.I. Evstyukhin and V.S. Emel'yanov, *Report on the All-Union scientific technical conference on the use of radioactive and stable isotopes and radiation in the national economy and science*, Moscow (1957).
6. P.L. Gruzin, *Dokl. Akad. Nauk SSSR*, 36, No.2 (1952).
7. J.C.J. Fisher, *Appl. Phys.*, 22, No.1, 74 (1951).
8. V.Z Bugakov, *Diffusion in metals and alloys*, Moscow-Leningrad., State Scientific and

VOL. 8 1959

Technical Foreign Literature Publishing House (1949).

9. S.D. Gertsriken and I.A. Dekhtyar, *Questions of physics of metals and metallography*, Kiev (1950).
10. P.L. Gruzin, E.V. Kuznetsov and G.V. Kurdyumov *Problems of the physics of metals and metallography*, Moscow, State Scientific and Technical Publishing House, 494 (1955).
11. E. Kheies and A. Kaufman, *Zirconium*, 4, 2, Moscow, Foreign Literature Publishing House (1955).

VOL
8
195

THE EFFECT OF HYDROGEN ON ALLOY VT-8 WITH INCREASED CREEP STRESS*

I.I. KORNILOV, C.G. GLAZUNOV and A.M. YAKIMOV

(Received 21 June 1958)

In the present work the effect of different contents of hydrogen and oxygen on the structure and mechanical properties of the alloy VT-8 of system Ti-Al-Mo is studied.

VOL. 8 1959

In the study of titanium and its alloys in recent times a great deal of attention has been divided to the question of the effect of hydrogen on the structure and properties of titanium. It is known that titanium with a low content of oxygen stands up well to prolonged loads, and the metal with a higher content of hydrogen is subject, in these conditions, to sudden, brittle disintegration. Hydrogen can contaminate titanium at all stages of the technological process of the preparation of manufactured articles, beginning with the preparation of the sponge, right up to obtaining the finished article. At the present time a series of measures has been developed to enable us to obtain a metal with a decreased hydrogen content, namely: the use of vacuum melts, the improvement of pickling baths and the use of an oxidizing atmosphere for heating the articles when forging and rolling.

It has been established by many investigations that the cause of the embrittlement of technical titanium and alloys with α-structure is the precipitation of a hydride phase [1-3]. The mechanism of the embrittlement of alloys with the two phase structure $\alpha + \beta$ has remained unclear until the present time, as the hydride phase has not been observed in this category of alloys [4-7]. In the work [8, 9] on the study of the effect of hydrogen on the structure and properties of alloys of the system Ti-Al-Cr and Ti-Al-Cr-Mo it is shown that the mechanism of hydrogen embrittlement is different for the various alloys and, in the main, depends on the chemical composition of the alloy and the content of hydrogen. Thus, for example, in the alloy VT-3 of the system Ti-Al-Cr, the presence of hydrogen within the limits 0.015-0.035 per cent hastens the eutectoid disintegration of the residual β-phase with the formation of intermetallic $TiCr_2$. With a higher hydrogen content (0.05 per cent and higher) the residual β-phase is stabilized at room temperature, but in the process of subsequent ageing at 400 and 450° for 100 hr it suffers disintegration with tne formation of titanium hydride. In the alloy VTZ-1 of the system Ti-Al-Cr-Mo with a hydrogen content within the limits 0.005-0.12 per cent no disintegration of the residual β-phase was observed. Thus, from these two examples, it is seen that the character of hydrogen embrittlement changed in relation to the hydrogen content and the composition of the alloys.

The present work is a continuation of the work on the study of the effect of hydrogen on the properties of the industrial alloys of titanium with the structure $\alpha + \beta$.

The aim of the present investigation is to study the effect of various hydrogen contents on the properties of alloy VT-8 with increased creep stress (deforming not more than 0.2 per cent in 100 hr with a stress of 24 kg/mm^2 at a temperature of 500°).

The following melts of alloy VT-8 were studied:

1. Melt 7: 6.3% Al; 2.9% Mo; 0.12% Fe; 0.08% Si; 0.1% O_2, with hydrogen contents of 0.005; 0.015; 0.025; 0.05 and 0.08 per cent.
2. Melt 8: 6.3% Al; 3.25% Mo; 0.20% Fe; 0.07% Si; 0.2% O_2, with hydrogen contents of

* *Fiz. metal. metalloved.* 8, No.3, 370-377, 1959.

0.005; 0.015; 0.025; 0.05 and 0.08 per cent.

3. Melt 10-1; 6.6% Al; 3.0% Mo; 0.05% Fe; 0.04% Si; 0.1% O_2, with hydrogen contents of 0.005; 0.015; 0.025 per cent.

4. Melt 10-3; 6.6% Al; 3.0% Mo; 0.05% Fe; 0.04% Si; 0.3% O_2, with hydrogen contents of 0.005; 0.015; 0.025 per cent.

The saturation of the alloys with hydrogen took place in a specially constructed universal installation for saturating metals with gases and the analysis of hydrogen. The purest hydrogen was obtained by the thermal dissociation of titanium hydride. The temperature of saturation is 700°.

The melts of alloy VT-8 with various oxygen contents were obtained by alloying titanium dioxide. An identical initial structure of the specimens after hydrogenation was guaranteed by the subsequent thermal treatment, carried out in electric furnaces with an atmosphere of air.

The thermal treatment of alloy VT-8 consisted of annealing at 880° for one hour and subsequent cooling in air.

The study of the mechanical properties was carried out on specimens of Gagarin type with a rate of extension of 2.5 mm/min (Fig. 1). The properties of the specimens were studied in the initial (880°-1 hr) state, after ageing the prepared specimens at 500° for 100 hr and after ageing the specimens under a stress of σ = 10 kg/mm^2 at 500° for 100 hr. The yield strength increased after ageing from 112 to 125 kg/mm^2 and changed little with an increase in the hydrogen content.

The characteristics of ductility, especially the amount of reduction in area, decrease markedly with an increase in the hydrogen content up to 0.015 per cent in the initial state. With a further increase in the hydrogen content up to 0.025 per cent, the ductility once again increases. After ageing a smooth decrease in ductility was observed with the increase in the hydrogen content. The effect of the speed of testing during extension on the mechanical properties of alloy VT-8 with a varying hydrogen content was also studied. Earlier we were shown the powerful effect of the speed of testing on the mechanical properties of titanium alloys, A test of alloy VT-8 was carried out with a hydrogen content of 0.005 to 0.05 per cent at three speeds of extension: 0.017; 11.3 and 48.2 mm/min both in the initial state and after ageing the prepared specimens at 500° for 100 hr (Fig. 2).

From Fig.2 it is seen that the yield strength at extension speeds of 0.17 and 11.3 mm/min practically did not change. With an increase in the speed of the test to 48.2 mm/min the yield strength increased from 109 to 117 kg/mm^2. A significant increase in the yield strength after ageing was noted (up to 122 kg/mm^2). In the studied range of concentration, hydrogen does not have any effect on the yield strength, either in the initial state or after ageing. The speed of the test has a strong effect on the characteristics of ductility. The minimum amount of reduction in area is independent of the hydrogen content both in the initial state and also after ageing; it is observed at testing rate of 0.17 mm/min.

At testing speeds of 0.17 and 11.3 mm/min the minimum ductility in the initial state is observed with a hydrogen content of 0.015 per cent. After ageing a sharp decrease in the amount of reduction in area is observed with a hydrogen content of 0.05 per cent (ψ = = 15.4 per cent) and tests with a speed of 0.17 mm/min.

The effect of hydrogen within the limits 0.005 to 0.08 per cent on the impact property of alloy VT-8 was also studied at room and low (-78°-196°) temperatures (Fig. 3). At all the investigated temperatures the impact property decreased markedly with an increase in the hydrogen content up to 0.025 per cent and then changes little up to 0.08 per cent of hydrogen. At a temperature of -196° a sharp fall in impact property is observed in all the studied interval of hydrogen concentration (2.4 instead of 4.7 kg/mm^2 at room temperature). Articles manufactured from alloy VT-8 can be reliably used at temperatures as low as -78°.

Thus, the temperature of the experiment has a significantly greater effect on the impact property of the alloy than the change in the hydrogen content.

A metallographic study of alloy VT-8 with a varying hydrogen content was carried out. At room temperature the alloy has a two-phase structure $\alpha + \beta$. The effect of hydrogen on the structure of alloy VT-8 consists of the

VOL 8 195

enlargement of the structural components with the increase in the hydrogen content (Figs. 4 and 5) and also, apparently, an increase in the quantity of untransformed β-phase and its stabilization.

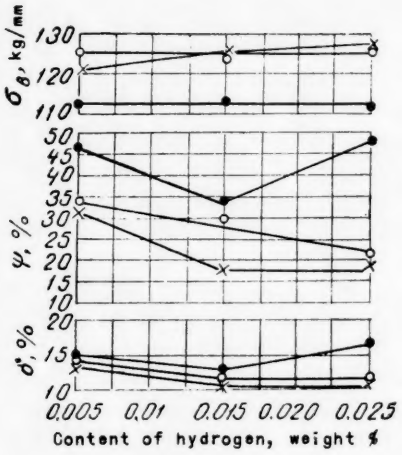

Fig. 1. The dependence of the mechanical properties of alloy VT-8 on the hydrogen content.

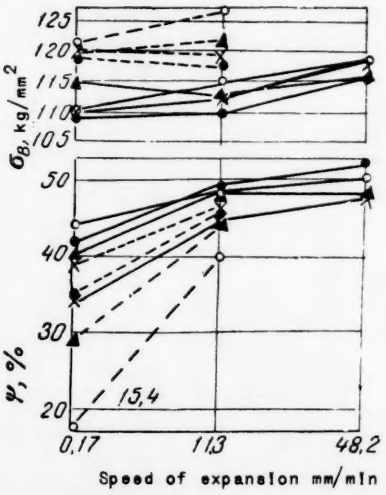

Fig. 2. The dependence of the mechanical properties of alloy VT-8 on the hydrogen content and the speed of test. Solid line-annealing at 880° for 1 hr. Broken line-annealing at 880° for 1 hr and at 500° for 100 hr.

The study of the combined effects of hydrogen and oxygen on the mechanical properties of alloy VT-8 also presented great interest. From published data it is known that in the presence of an increased quantity of oxygen hydrogen has a significantly stronger embrittling effect on the properties of titanium and its alloys. This is connected primarily with the fact that interstitial elements (for example nitrogen and oxygen) significantly lower the solubility of hydrogen in titanium.

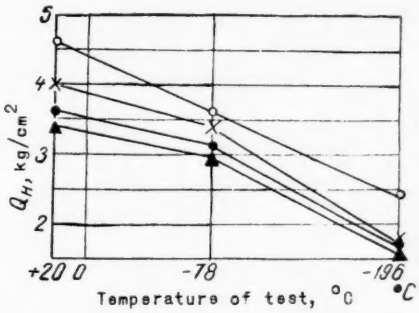

Fig. 3. The relation of the impact resistance of alloy VT-8 to the hydrogen content and the temperature of the experiment.

Fig. 4. Alloy VT-8, containing 0.005% hydrogen; x 500.

Fig. 5. Alloy VT-8, containing 0.08% hydrogen; x 500.

In Figs. 6 and 7 are shown the results of the experiment on the tensile properties of two melts of alloy VT-8, containing 0.1 and 0.3 per cent of oxygen respectively, in relation to the hydrogen content. Specimens

were tested in the initial state, after ageing at 500° for 100 hr and after ageing under a stress of 10 kg/mm^2 for the same time and at the same temperature. From the comparison of these two graphs it is seen that hydrogen has a significantly greater effect on the properties of the alloy VT-8 with the higher oxygen content.

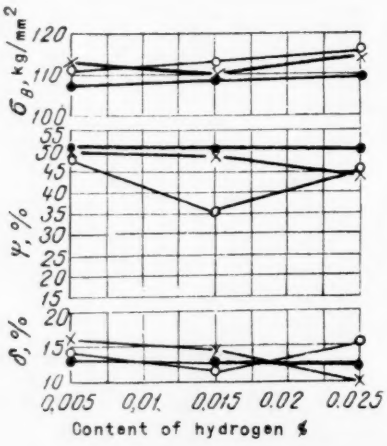

Fig. 6. The relation of the mechanical properties of alloy VT-8 to the hydrogen content with an oxygen content of 0.1%.

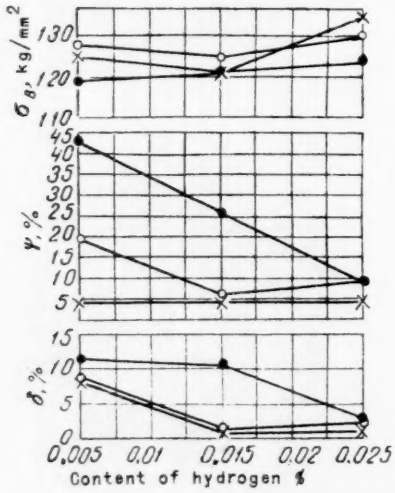

Fig. 7. The relation of the mechanical properties of alloy VT-8 to the hydrogen content with an oxygen content of 0.3%.

In the alloy with an oxygen content of 0.1 per cent the effect of hydrogen within the limits 0.005 to 0.025 per cent on the yield strength is insignificant, both in the initial state and after ageing. The characteristics of ductility for this alloy are sufficiently high. The elongative is of the order of 10-15 per cent and the amount of reduction in area is 37-52 per cent.

However, the picture changes sharply with an increase in the oxygen content in the alloy to 0.3 per cent. If, in the initial state, with a content of hydrogen of 0.005 per cent and oxygen of 0.3 per cent, the ductility is sufficiently high (δ = 12 and ψ = 43 per cent), then after ageing it is sharply lowered. With an increase in the hydrogen content to 0.015 per cent and higher and an oxygen content of 0.3 per cent the ductility falls catastrophically. Thus, oxygen significantly reduces the thermal stability of alloy VT-8.

The reason for the great embrittlement of the alloy with 0.3 per cent of oxygen is seen by the detailed study of the microstructure of these two alloys. In Figs. 8 and 9 are shown the photomicrographs of two alloys of VT-8 with a content of 0.1 and 0.3 per cent of oxygen and various hydrogen contents.

From the photomicrographs shown it is seen that in an alloy with 0.1 per cent of oxygen the structure hardly changes with a change in the hydrogen content from 0.005 to 0.025 per cent.

In an alloy with 0.3 per cent of oxygen the structure remains heterogeneous with the increase in the hydrogen content. In the structure is observed a large quantity of untransformed α-phase on the borders of the grains and its coagulation in the ageing process, which leads to a sharp brittleness of the alloy.

In the work a study was carried out on the effect of hydrogen on the creep of alloy VT-8. Two melts of alloy VT-8 were studied with a content of 0.1 and 0.2 per cent of oxygen and 0.005; 0.015 and 0.025 per cent of hydrogen at 500° for 100 hr and at a stress of 10 kg/mm^2. An increase in residual deformation was noted with the increase in the hydrogen content from 0.005 to 0.025 per cent (Table 1).

With the increase in the oxygen content the absolute values of residual deformation decrease. With the aim of defining more accurately the effect of oxygen on the amount

TABLE 1

The relation of residual deformation to the content of oxygen and hydrogen in the alloy

Content of oxygen in the alloy %	Content of hydrogen in the alloy %	Amount of residual deformation %
0.1	0.005	0.112
	0.015	0.120
	0.025	0.197
0.2	0.005	0.080
	0.015	0.100
	0.025	0.100

Note: In the table are shown the average values from the results of the test of three specimens per point.

VOL. 8 1959

of residual deformation of alloy VT-8, additional tests were carried out with specimens of two melts with a content of 0.1 and 0.3 per cent of oxygen and 0.025 per cent of hydrogen at 500° for 25 hr and at a stress of 50.0 kg/mm^2. The results obtained showed that in an alloy with 0.1 per cent of oxygen the amount of residual deformation equals 1.75 and 1.84 per cent for 25 hr, and in an alloy with 0.3 per cent of oxygen-0.76 and 0.78 per cent. Thus, the increase in the oxygen content contributes to a rise in the creep resistance of this alloy,

Together with the study of the mechanical properties and microstructure a test was carried out on the phase composition* of alloy VT-8 with various hydrogen contents. The presence of residual β-phase, explained by the presence of molybdenum and hydrogen in the alloy, did not give rise to doubt. However, it is extremely difficult to identify it by metallographical investigation. It was necessary to explain whether the residual β-phase was stable and under what conditions

TABLE 2

The effect of hydrogen on the residual β-phase in alloy VT.8 with various thermic treatment.

Thermal treatment	Content of hydrogen, weight %	Parameter of the unit cell of the beta-phase
880°-1 hr.	0.005	3.244
880°-1 hr.-500°-100 hr.	0.005	3.212
880°-1 hr.	0.015	3.260
880°-1 hr.-500°-100 hr.	0.015	3.212
880°-1 hr.	0.025	3.259
880°-1 hr.-500°-100 hr.	0.025	3.240
880°-1 hr.	0.080	3.277
880°-1 hr.-500°-100 hr.	0.080	3.264

Note: The phase composition of the deposit -β.

* Work carried out jointly by N.I. Blok, A.I. Hlazova and N.F. Lashko.

its disintegration was observed. With the aid of the electrolytic method of the separation of phases in titanium alloys it is possible to isolate the β-phase from the basic hard solution and then subject it to X-ray analysis. The results of the phase analysis of the anode precipitations formed from alloy VT-8 are presented in Table 2.

The presence of residual β-phase in the the structure of alloy VT-8 with a content of hydrogen within the limits 0.005-0.08 per cent was confirmed by the phase analysis. From the data presented it is seen that with a low hydrogen content (0.005 and 0.015 per cent) the residual β-phase in the initial state is less stable than with a greater hydrogen content. In the process of the subsequent ageing at 500° for 100 hr the parameter of the unit cell of the β-phase sharply decreases, especially with 0.015 per cent hydrogen, which indicates the redistribution of molybdenum between the α- and β-phases of the alloy.

With the increase in the hydrogen content in the alloy the residual β-phase stabilizes during the ageing process. Thus, the decrease

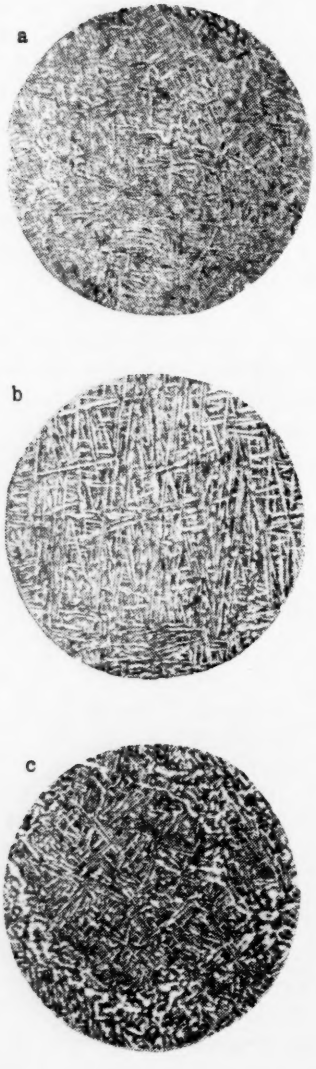

Fig. 8. Alloy VT-8, containing 0.1% oxygen and various hydrogen contents: a – 0.005%; b-0.015%; c-0.025%.

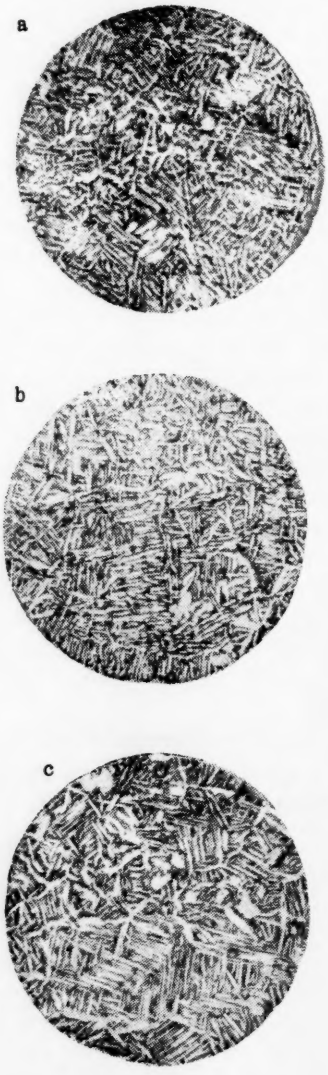

Fig. 9. Alloy VT-8, containing 0.3% oxygen and various hydrogen contents: a-0.005%; b-0.015%; c-0.025%.

in the ductility of alloy VT-8 with a hydrogen content of 0.015 per cent is connected with the disintegration of the unstable β-phase and the re-distribution of molybdenum between the α- and β-phases. The decrease in the ductility after ageing in the alloy with a high hydrogen content is apparently connected with the residual β-phase being made brittle by the hydrogen. From Table 2 it is also seen that with the increase in the hydrogen content in alloy VT-8 the parameter of the unit cell of the β-phase increases. No other phases were observed in alloy VT-8 in the interval of hydrogen concentrations 0.005-0.08 per cent.

CONCLUSIONS

1. The study of the effect of hydrogen within the limits 0.005-0.05 per cent on the mechanical properties of alloy VT-8 showed that with a hydrogen content of 0.015 per cent a marked decrease in the ductility characteristics is observed, which is connected with the presence of unstable β-phase in the structure and its disintegration.

2. The effect of hydrogen (0.005-0.05 per cent) on the tensile properties of alloy VT-8 at different speeds was studied.

At low testing speeds the ductility of alloy VT-8 decreases significantly, especially with an increase in the hydrogen content. The yield strength of alloy VT-8 rises from 109 to 117 kg/mm^2 with an increase in the testing speed from 0.17 to 48.2 mm/min respectively (with an hydrogen content of 0.005 per cent).

3. The impact resistance of alloy VT-8 at room and low temperatures (-78° and -196°) changes comparatively little with the hydrogen content within the limits 0.005 to 0.08 per cent. The temperature of the test has a much greater effect than the hydrogen content within limits up to 0.08 per cent.

4. With higher quantities of oxygen the hydrogen has a much greater negative effect on the properties of alloy VT-8.

5. The effect of hydrogen on the creep of alloy VT-8 at 500° for 100 hr was studied. With the increase in the hydrogen content the amount of residual deformation grows. Oxygen increases the creep resistance of alloy VT-8.

6. The phase analysis of alloy VT-8 with various hydrogen contents confirmed the presence in the structure of residual β-phase.

At low hydrogen contents (up to 0.015 per cent) the residual β-phase is unstable, and in the process of ageing re-distribution of molybdenum comes between the α- and β-phases. With an increase in the hydrogen content the stabilization of the residual β-phase and an increase in the parameter of its unit cell is observed.

Translated by R.J. Coleman

REFERENCES

1. G.A. Lenning, C.M. Graighead and R.I. Jaffee, *J. Metals*, 6 (3), 367 (1954).
2. G.A. Lenning, J.W. Spretnak and R.I. Jaffee, *J. Metals*, 8, No.10, 1235 (1956).
3. R.I. Jaffee, G.A. Lenning and C.M. Graighead, *J. Metals*, 8, No.8, 907 (1956).
4. R.J. Kotfila and E.F. Erbin, *Met. Progress*, 60 (4), 128 (1954).
5. H.D. Kessler, R.G. Sherman and J.F. Sullivan, *J. Metals*, 7 (2), 242 (1955).
6. Burte, Erbin, Hahn, Seeger, Kotfila and Wruck, *Metal Progress*, 67 (5), 115 (1955).
7. E.J. Ripling, *J. Metals*, 8, (5), 502 (1956).
8. I.I. Kornilov, S.G. Glazunov and A.M. Yakimova *Izv. Akad. Nauk SSSR*, Foreign Literature Publishing House, No.9 (1958).
9. N.I. Blok, A.I. Glazova, N.F. Lashko and A.M. Yakimova, *Izv. Akad Nauk SSSR*, Foreign Literature Publishing House, No.12 (1958).

VOL. 8 1959

THE STUDY OF ALUMINIUM ALLOYS OF THE Al-Cu-Mg SYSTEM IN SAMPLES OF VARIABLE COMPOSITION*

L.S. PALATNIK, G.B. FEDOROV and H.T. GLADKIKH

(Received 28 June 1958)

The results of the study of microhardness and X-ray phase analysis are reported for alloys from the aluminium corner of the Al-Cu-Mg system having a copper and magnesium content from 0.5 per cent to 5.0 per cent.

It is shown that under certain conditions alloys are formed which are not in the equilibrium state. The equilibrium could be obtained by annealing of samples or by condensation of metals on a hot support.

Alloys from the aluminium corner of the Al-Cu-Mg system have been investigated by many authors [1-7]. The phase diagram of this system has been studied by Urazov, Petrov and Berg [4-5] and according to their data, aluminium solid solutions can be in equilibrium with the phases Θ ($CuAl_2$), S(Al_2CuMg), T(Al_6CuMg_4), Z(Al_3Mg_2).

It seemed reasonable to us to carry out several investigations of alloys from the aluminium corner of the Al-Cu-Mg system on samples of variable composition, using Vekshianskii [8] method and to compare the results obtained with those given in the literature.

Simultaneously a method related to the specific preparation and study of comparatively thick (massive) samples of variable composition of the given system was developed.

METHODS OF PREPARING AND STUDY OF SAMPLES VARYING IN COMPOSITION

(a) Sample preparation. The samples varying in composition were prepared in a vacuum by simultaneous evaporation and condensation of components from three cylindrical evaporators [9-10], placed at a distance of 70 mm from the collector in apices of equilateral triangles circumscribed by a circle of 60 mm diameter.

The evaporation conditions for the collector were chosen so that the total of CuMg concentrations were within a range of 0.5-16.0 per cent.

The distribution functions under these evaporation conditions were determined photometrically [11] for each of the metals, on the basis of which the calculation of concentrations were carried out by a graphic method [12].

Steel and polished aluminium disks of 140 mm diameter were used as collectors.

(b) Condensation on the steel collector. After obtaining the necessary vacuum ($\sim 10^{-5}$ mm Hg) for the removal of absorbed gases, the collector was heated to about 100°C, then cooled down by running water and a layer of condensation was formed. It was observed that during condensation of the system on the polished steel collector which had been previously cleaned with hot alkali, disruption occurred which was accompanied by detachment of the sample from its base, owing to internal stresses brought about during the condensation process, when the sample reached a certain thickness.

When the collector was sufficiently pickled with concentrated nitric acid, one obtained samples in which the adhesion with the support was increased, (probably as a result of the development of a rought condensation surface) and was sufficient for measurement of microhardness. However, the relatively uneven surface slowed down the measurement of microhardness. To eliminate this defect,

* *Fiz. metal. metalloved.* 8, No.3, 378-386, 1959.

several experiments were carried out using, first, a polished collector and later, corrosion resistant aluminium.

(c) Condensation on aluminium collector. The base used was aluminium and this was chosen for the following reasons: a similar thermal expansion coefficient of aluminium and its condensate should provide smaller internal stress in the layer, while a thick aluminium oxide film, probably, should impede mutual diffusion between the condensate and the plate. As the aluminium oxide is firmly bonded with the metal, one might expect that the condensate layer will also by firmly bonded with the aluminium oxide.

Good results were obtained by the following experimental conditions. The collector was heated in a vacuum up to 400°C and was kept at that temperature for about 15 min. Condensation was carried out by holding the support first at 400°C for 5 min and after that at 50°C for 100-110 min. In this case the sample of 150-170 μ, with mirror smooth surfaces and very firm bond with the plate, were used.

(d) Methods of studying the samples. Samples of varying composition were studied by the microhardness and X-ray analysis. Microhardness was measured on the PMT-3 instrument by stresses of 20 g and 40 g weight. X-ray photographs were taken by radiation of a ferrous anode using an iron filament source and Shlif (Schliff) method in a chamber of 85 mm diameter.

The samples were subjected to annealing in a vacuum at various temperatures.

THE RESULTS OF INVESTIGATIONS

The samples, obtained by precipitation on the cold steel collector were examined by the microhardness method in the concentration range from 0.5-6.0% Mg and 0.5-6.0% Cu through 0.3-1% Cu and Mg along the section, C_{31} (Fig. 1), along which the copper and aluminium concentrations ratio remained stable (0.005; 0.010; 0.015 etc.) Simultaneously with the microhardness measurements, qualitative X-ray phase diagrams were made. Microhardness was measured two weeks after preparation of samples.

Owing to the condensation on the cold support, the samples had very small size crystals ($\sim 10^{-6}$cm). Therefore, in this case macrohardness and not microhardness were measured [13].

According to the measurement data, a diagram (Fig. 1) of the microhardness of the aluminium alloys was constructed in which the

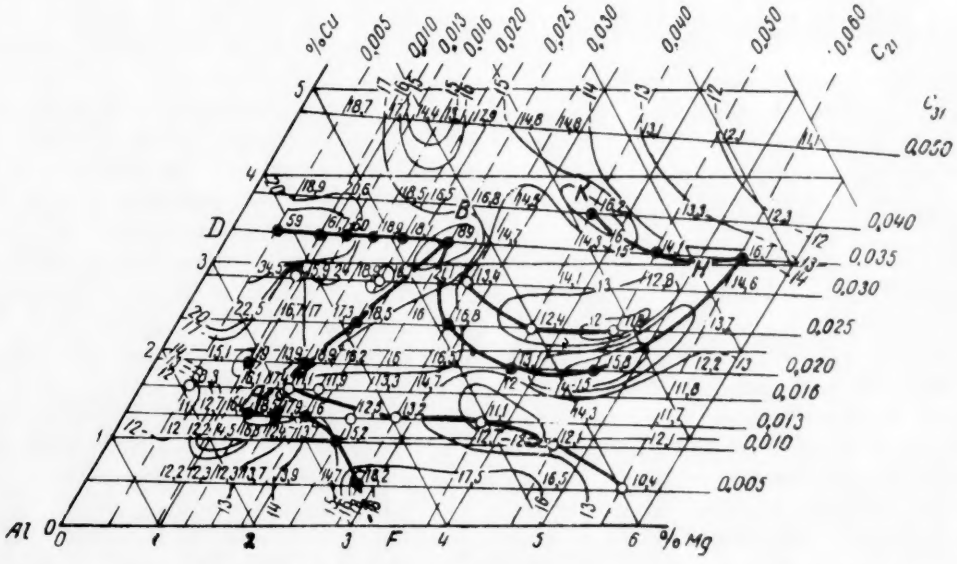

Fig. 1. The microhardness chart of aluminium alloys of the Al-Cu-Mg system (before annealing).

microhardness values are given in relative units ($H_{abs.}$ = 38.9 $H_{rel.}$ kg/mm^2). The microhardness diagram shows five lines, *AB*, *BD*, *BH*, *AF*, *HK* of maximum hardness. Between lines *AF*, *BH* and *HK* are lines of minimum microhardness. Besides showing maximum and minimum lines of microhardness there are separate lines for maximum microhardness at concentration of 1.9% Cu and 1.0% Mg with $H_{rel.}$ = 19.0 and minimum at concentrations of 1.6% Cu and 0.5% Mg with $H_{rel.}$ = 8.3.

The high microhardness at concentrations of 3.3% Cu, 2.4% Mg with $H_{rel.}$ = 89 and 3.4% Cu, 1.3% Mg with $H_{rel.}$ = 60 (Fig. 2 curve 1) was localized in a very narrow region of concentrations, in which at maximum microhardness Mg and Cu form an alloy at stoichiometric ratio as 2:1 and 1:1 respectively.

If one takes into consideration that great microhardness at these points disappears after annealing for 4 hr at 150°C (Fig. 2 curve 2), one can assume formation of metastable intermetallic compounds Al_xCuMg_2 and Al_xCuMg which are responsible for great hardness of alloys.

It was impossible to detect those compounds by X-ray, probably, because in alloys they are in a finely dispersed state and in small concentration. The phase diagram for alloys containing 3.3% Cu and 2.4% Mg, are shown in Table 1. Only very diffuse lines of α-solid solution (and iron base) are present in X-ray photographs, indicating the great dispersion of crystals ($\sim 10^{-6}$cm) and presence of internal stresses.

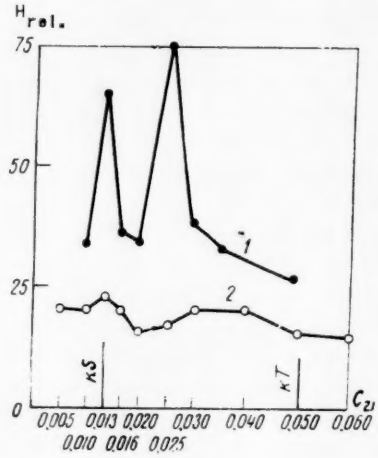

Fig. 2. Profile C_{31} = 0.035: 1 – before annealing; 2 – annealing 150°C (4 hr).

After 4 hr of annealing at 150°C marked changes were observed in microhardness values within the region investigated. Splitting of the maxima line *AD* occurs. The maxima hardness disappears at concentrations 3.3% Cu, 2.4% Mg and 3.4% Cu, 1.3% Mg and on this basis one

TABLE 1

X-ray structure data for 3.3% Cu; 2.4% Mg and 94.3% Al alloy

Before annealing			Annealing 250°C		
Interplanar spacing *d*, Å	Intensity of interference lines, *I*	Phase	Interplanar spacing *d*, Å	Intensity of interference lines, *I*	Phase
2.33	Weak	α-solid sol.	2.33	Strong	α-solid sol.
–	–	–	2.28	Weak	*S*
–	–	–	2.18	V. Weak	*S*
2.02	Weak	α	2.02	Weak	α
2.01	Medium	Fe base	2.01	Medium	Fe base
–	–	–	1.98	Weak	*S*
1.430	V. Weak	α	1.430	Medium	α
1.428	V. Weak	Fe	1.428	V. Weak	Fe
1.219	V. V. Weak	α	1.219	Medium	α
1.168	Weak	α	1.168	Medium	α
1.166	Weak	Fe	1.166	Weak	Fe
1.01	Weak	α, Fe	1.01	Medium	α, Fe

can draw a conclusion about decomposition of the above metastable compounds Al_xCuMg_2 and Al_xCuMg.

General reduction of microhardness and displacement of maxima towards Al-S phase and Al-T phase of the equilibrium diagram occurs after annealing at 200°C for 4 hr. The widths of lines for α-solid solution is reduced, which is obviously connected with a reduction of internal stresses and partial decomposition of the supersaturated solid solution.

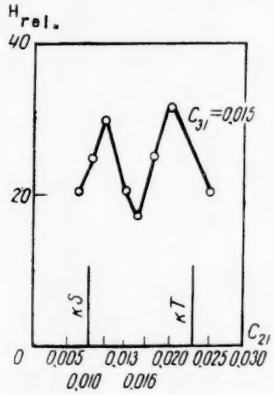

Fig. 3. Profile C_{31} = 0.015, annealing 250°C.

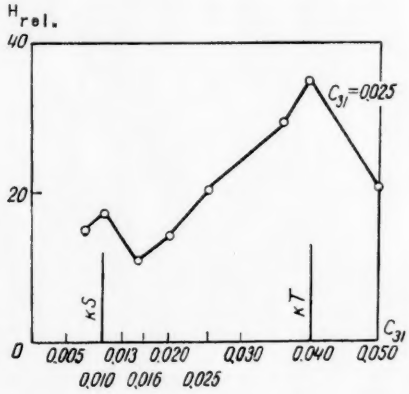

Fig. 4. Profile C_{31} = 0.025, annealing 250°C.

After annealing at 250°C for 4 hr the microhardness maxima (Figs. 3, 4 and 5) are disposed along lines Al in *S*-phase and Al in *T*-phase, while at the same time the microhardness increases faster along the line Al in *S*-phase than along the same line in the *T*-phase.

X-ray diagrams show the phases to be in equilibrium within the studied region (3). The temperature of 250°C prove to be sufficient for greatly relieving the stresses. Some widening of lines of the α-solid solution appearing on the X-ray pictures, are probably due to small crystal dimensions.

The microhardness distribution obtained at 250°C remains stable even when the annealing temperature is raised to 400°C.

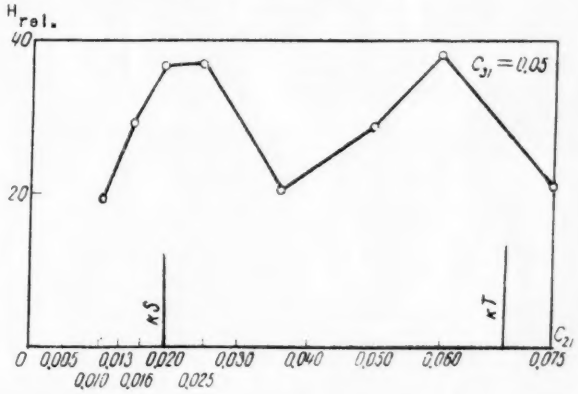

Fig. 5. Profile C_{31} = 0.050, annealing 250°C.

On X-ray pictures, taken after annealing at 300°C for 4 hr, the phase lines formed after annealing at 250°C become clearer, appearing to duplicate those of the Θ-phase.

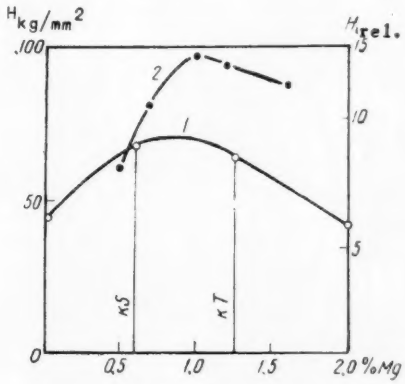

Fig. 6. Comparative microhardness curves on profile Cu – Mg = 2%. 1. Data from literature (7); 2. Experimental data

After annealing at 350°C and 400°C for 4 hr the X-ray pictures of samples varying in composition do not differ from those obtained with massive samples of corresponding composition.

An analysis of the data shows that the state of the samples before annealing, is very unbalanced. When the annealing temperature is increased-greater equilibrium is obtained in the samples. The appearance of lines of maximum microhardness on the *S*- and *T*-phase lines and the appearance on the X-ray picture of lines of phases, known from the equilibrium diagram, allow us to assume that annealing at 250°C puts the system into a state which is sufficiently close to equilibrium.

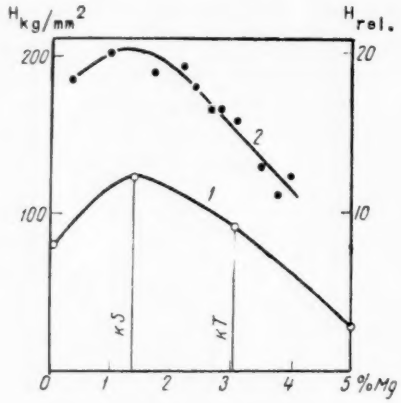

Fig. 7. Comparative microhardness curves on profile Cu – Mg = 5%. 1. Data from literature 2. Experimental data

It is essential to note that extremely high microhardness numbers are obtained in the above measurements. The data given in the literature (8), shows that the tensile strength of the condensed aluminium layer exceeds by 4-5 times the strength of rolled aluminium foil of the same thickness.

Satisfactory qualitative agreement with some of the compared points and sections of experimental data from the literature 6-7 has been observed with regard to hardness

TABLE 2

X-ray data for alloys, condensed on the hot collector 200°C

Composition of alloys								
6.9% Cu; 1.8% Mg; 3% Al			1.9% Cu; 4% Mg; 93.6% Al			1.5% Cu; 15% Mg and 83.5% Al		
d, Å	*I*	phase	*d*, Å	*I*	phase	*d*, Å	*I*	phase
3.15	V. weak	Θ	2.33	V. strong	α-solid sol.	2.45	V. weak	Z
2.38	Medium	Θ	2.28	Medium	S	2.40	V. weak	T
2.33	V. strong	α-solid sol.	2.18	Weak	S	2.33	V. weak	α solid sol.
2.28	Medium	S	2.02	Strong	α	2.27	Medium	T
2.18	Weak	S	1.98	Weak	S	2.15	V. weak	Z
2.14	Weak	Θ	1.93	V. V. weak	S	2.10	V. weak	Z
2.12	Medium	Θ	1.47	V. V. weak	S	2.06	V. weak	T
2.02	Strong	α	1.43	Strong	α	2.02	Strong	α
1.98	Weak	S	1.27	V. V. weak	S	1.97	Medium	T
1.91	Medium	Θ	1.219	Strong	α	1.95	V. weak	T
1.89	Medium	Θ	1.168	Weak	α	1.47	V. weak	Z
1.68	V.V. weak	Θ	1.01	Weak	α	1.430	Strong	α
1.64	V.V. weak	S	–	–	–	1.219	Strong	α
1.61	V. weak	Θ	–	–	–	1.168	Medium	α
1.470	V.V. weak	S	–	–	–	1.01	Weak	α
1.43	Strong	α	–	–	–	–	–	
1.40	V.V. weak	S	–	–	–	–	–	
1.39	Weak	Θ	–	–	–	–	–	
1.27	V.V. weak	S	–	–	–	–	–	
1.23	Weak	Θ	–	–	–	–	–	
1.219	Strong	α	–	–	–	–	–	
1.19	V. weak	Θ	–	–	–	–	–	
1.168	Weak	α	–	–	–	–	–	
1.01	Weak	α	–	–	–	–	–	

VOL 8 195

VOL. 8 1959

TABLE 3

Composition of alloys

6% Cu; 0.8% Mg and 93.2% Al			6% Cu; 1.6% Mg and 92.4% Al			0.64% Cu; 4.8% Mg and 94.56% Al			1.3% Cu; 4.7% Mg and 94% Al		
d, Å	J	Phase	d, Å	J	Phase	d, Å	J	Phase	d, Å	J	Phase
3.15	Weak	θ	2.40	Weak	S	2.40	Weak	T	2.40	Medium	T
2.38	Strong	θ	2.33	Very Strong	α-solid sol.	2.33	Very Strong	α-solid sol.	2.33	Very Strong	α-solid sol.
2.33	Very Strong	α-solid sol.	2.28	Medium	S	2.28	Medium	S	2.27	Medium	T
2.14	Medium	θ	2.11	Very very weak	S	2.27	Very Weak	T	2.02	Very very weak	α
2.12	Strong	θ	2.02	Strong	α	2.06	Very Weak	T	1.97	Very very weak	T
2.02	Very Strong	α	1.98	Very very weak	S	2.02	Strong	α	1.43	Strong	α
1.91	Strong	θ	1.93	Very very weak	s	1.98	Very Weak	S	1.42	Weak	T
1.89	Medium	θ	1.68	Very very weak	S	1.97	Very Weak	T	1.219	Strong	α
1.61	Weak	θ	1.47	Very very weak	S	1.92	Very Weak	S	1.168	Medium	α
1.51	Very Weak	θ	1.43	Strong	α	1.75	Very Weak	T	1.01	Weak	α
1.43	Strong	α	1.41	Medium	S	1.55	Very Weak	T	–	–	–
1.41	Weak	θ	1.219	Strong	α	1.47	Very Weak	S	–	–	–
1.39	Weak	θ	1.21	Weak	α	1.43	Strong	α	–	–	–
1.35	Weak	θ	1.168	Medium	α	1.41	Weak	S	–	–	–
1.23	Weak	θ	1.01	Weak	α	1.36	Very Weak	T	–	–	–
1.21	Strong	α	–	–	–	1.219	Strong	α	–	–	–
1.19	Very Weak	θ	–	–	–	1.21	Weak	S	–	–	–
1.168	Medium	α	–	–	–	1.168	Medium	α	–	–	–
1.13	Very very weak	θ	–	–	–	1.01	Weak	α	–	–	–
1.10	Very very weak	θ	–	–	–	–	–	–	–	–	–
1.09	Very very weak	θ	–	–	–	–	–	–	–	–	–
1.07	Weak	θ	–	–	–	–	–	–	–	–	–
1.06	Weak	θ	–	–	–	–	–	–	–	–	–
1.03	Weak	θ	–	–	–	–	—	–	–	–	–
1.02	Weak	θ	–	–	–	–	–	–	–	–	–
1.01	Weak	α	–	–	–	–	–	–	–	–	–

of aluminium alloys after natural ageing (Figs. 6, 7). Our measurements show that two microhardness maxima occur in Al-*S*-phase at 1.9% Cu, 1.0% Mg, and 3.4% Cu 1.3 to 1.6% Mg.

In paper [7] in the same diagram section are shown hardness maxima at concentrations of 1.9% Cu, 1.1% Mg, and 3.42% Cu, 1.61% Mg. Satisfactory agreement is also observed with the data of some other authors [6].

X-RAY EXAMINATION OF SAMPLES, CONDENSED ON A HEATED ALUMINIUM BASE

Temperature of base 200°C. Selective X-ray pictures were taken from portions differing in phase composition (Table 2).

Only lines of phases known to be in the equilibrium diagram are seen on X-ray photographs. They are sufficiently distinct and strong, though a little wider than those obtained with massive samples. The greatest widening of the lines are observed in *T*- and *Z*-phases when crystals diameters are $\sim 10^{-5}$cm.

Temperature of base 400°C. X-ray pictures taken from various sections of the sample (Table 3) have a similar appearance to those of massive samples of corresponding composition with course crystalline structures, though in the samples of variable composition larger crystals of *T*- and *Z*-phases are encountered. Formation of a texture takes place in Θ, *S*, *T*- and *Z*-phases.

It should be noted that *X*-ray pictures show lines of all phases when Mg is present, (*S*, *T* and *Z*). At the same time, by evaporation of only Mg, it is difficult to provide the condensation conditions even at room temperature, because of the very low critical condensation temperature of Mg($-195 < T_{cr} < -90$) [14]. This confirms Vekshinskii's supposition that such metals as magnesium, cadmium and zinc are impurities, which prevent full condensation on the surface of other metals.

The example (Tables 2, 3) show that deviations in phase composition from those of the equilibrium diagram is observed by condensation on the base heated at 200°C and 400°C. Therefore, the phase equilibrium composition is practically immediately established during the preparation process of samples.

The fact that condensation on a preheated base gives an equilibrium state at a lower temperature (200°C), than annealing does (250°C 4 hr), can be explained by a different mechanism of diffusion. The equilibrium state is obtained during the annealing process by means of the volume diffusion, which demands a high temperature for a long time. When condensation is carried out on the preheated base, equilibrium is established then, but at the expence of the surface diffusion, which progresses considerably faster than volume diffusion at the lower temperatures.

CONCLUSIONS

1. A method has been developed for the preparation of "massive" (about 0.15 mm thickness) samples varying in composition in the Al-Cu-Mg system, giving alloys within a wide range of conditions, varying from very unstable to very near equilibrium.

2. The equilibrium state in the above alloys is reached either by annealing (about 250°C) by volume diffusion, or in the process of preparation – condensation on a hot base (about 200°C) by surface diffusion. The agreement of results obtained on these samples of variable composition with results on phase equilibrium and hardness for massive, samples of constant composition the literature has been established for several points and sections through the diagram.

3. The microhardness diagrams for a section $C_{Zl} = 0.025$; 0.035 have been constructed for the aluminium corner of the three component system Sl-Cu-Mg after condensation and natural ageing and also after annealing at 150-200°C; after annealing at 250°C they were constructed for sections $C_{Zl} = 0.015$; 0.025; 0.035; 0.050.

4. Metastable compounds of type $Al_x CuMg_2$ and $Al_x CuMg$, have been found by the microhardness methods, and these cause the high hardness of condensed alloys.

Translated by N.Peters

REFERENCES

1. V.G. Kuznetsov and L.N. Guseva, *Izv. Akad. Nauk SSSR*, OkhN, 6, 905 (1940).

2. G.G. Urazov and M.S. Mirgalovskaya, *Izv. CFKhA*, 19, 514 (1949).
3. M.S. Mirgalovskaya and E.S. Makarov, *Izv. CKhFA*, 18, 117 (1949).
4. G.G. Urazov and D.A. Petrov, *Zh. fiz. khim.* 20, 387 (1946).
5. D.A. Petrov and G.S. Berg, *Zh. fiz. khim.* 20, 1475 (1949).
6. H.H. Hardy, *J. Inst. Metals*, 83, 17 (1954).
7. S.M. Voronov and M.Kh. Rabinovich, *Trud. Mosk. Aviats. Tekhnol. Inst.* 30, 10 (1956).
8. S.A. Vekshinskii, *Novyi metod metallograf. issled. splavov*, Gostekhizdat, (1944).
9. L.S. Palatnik and G.V. Federov, *Dokl. Akad. Nauk SSSR*, 120 1, 79 (1958).
10. Iu.F. Komnik, L.S. Palatnik and G.V. Fedorov, *Akad. Nauk SSSR*, 11, 193 (1957).
11. L.S. Palatnik, and G.V. Federov, *Dokl. Akad. Nauk SSSR*, 110, 100 (1957).
12. L.S. Palatnik and G.V. Federov, *Izv. Akad. Nauk SSSR, otd. tekh. nauk.* No.9, 119 (1957).
13. N.N. Posokhin, *Zav. Lab.* No.6, 733 (1957).
14. G. Knudsen, *Ann. Phys.*, 50, 472 (1916).

VOL.
8
1959

ELECTRON MICROSCOPIC INVESTIGATION OF ETCHING FIGURES IN AGED ALUMINIUM ALLOYS*

N.N. BUINOV, T.V. SHCHEGOLEVA, V.G. RAKIN,
M.F. KOMAROVA and R.R. ZAKHAROVA

(Received 12th August 1958)

The results of electron microscopic study of the dimensions, shape and structure of etching figures on ageing aluminium alloys are surveyed. The relationship between the dimensions and shape of etching figures and the thermal processing of alloys is shown. Reasons are given for assuming that etching figures are related to mosaic structure.

1. In papers [1-5] it is suggested that etching figures on alloys Al-Cu, Al-Zn-Cu, and Al-Ag correspond to mosaic blocks, in that the strengthening of alloys during ageing is accompanied by disintegration of blocks and increased disorientation between them. However, so far, no convincing evidence has been obtained to show that etching figures correspond to mosaic blocks, although it was possible to show that in ageing alloys disintegration took place predominantly along their boundaries.

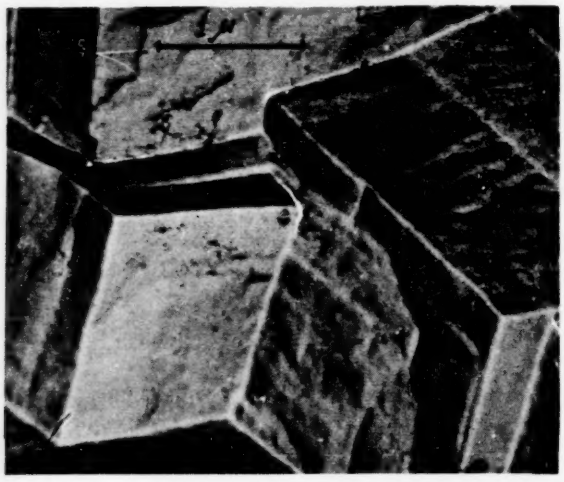

Fig. 1. Alloy Al-Si (1.2% Si); tempered at 530°C; x 15,750.

The purpose of the present investigation was a further study of the connexion between etching figures and mosaic blocks. The details of etching figures structure were examined in the light of the latest published data.

Data on the dimensions and shape of etching figures for various alloys are shown in the table. The figure-size varies from several microns to a fraction of a micron. It is characteristic of the majority of tempered and weakly aged samples, that etching figures have a rectilinear shape (Fig. 1), while those on strengthened samples are oval (Fig. 2), The dimensions of the above decrease (while the hardness of the alloys increases) depending on the artificial ageing time.

The etching figures of some alloys had spiral steps [4-5]. On this basis it was assumed that these are connected with the appearance of screw dislocations on the surface.

As the height of the steps in the spiral, etching figures of aluminium alloys reached several hundreds of angstroms and even as much as 0.1 μ, this led to the hypothesis [4-5] that the etching figures are connected, not with simple but with gigantic screw dislocations, which form groupings in the volumes corresponding to the above figures. Our observations and assumptions have contradicted the theory of dislocations [5] for the following reasons:

1. The spiral axes are parallel to type (001), while screw dislocations (or better their Biugers vectors) in cubic face-centred

* *Fiz. metal. metalloved.* 8, No.3, 387-399, 1959.

VOL. 8 1959

TABLE 1

The size and shape of etching figures

Alloy	Condition of alloy	Etching figures	
		Size (μ)	Shape
Al–Cu(4%Cu)	Tempered, naturally and artificially aged at temperatures below 150°C.	1-5	Octahedral and dodecahedral
	Ageing at 150-190°C (Max. hardness)	0.2-0.5	Irregular
	Ageing at 200-400°C	0.5-1.0	Octahedral
	Deformation and Ageing at 150°-210°C	0.5-1.0	Octahedral, dodecahedral and cubical
Al-Cu-Mg(3%Cu. 1.15%Mg)	Natural ageing	2-3	Octahedral
	Ageing at 218°C from 15 min to 2 hr	0.3-0.5	Irregular
Al-Si(1.2%Si)	Natural ageing	5	Cubical
	Ageing at 210-255°C (below Max. hardness)	2	Cubical and Oval
	Artificial Ageing at 210-255°C upto Max. hardness	0.5-1.0	Oval
	Deformation by 13.5% and ageing at 260°C from 5 min to 1 hr.	0.6	Oval
Al-Ag (10-20%Ag)	Natural ageing	1-5	Cubical
	Artificial ageing (175-220°C)	1-2	Oval
D1	Natural ageing	1-3	Octahedral
	Ageing at 180°C up to Max. hardness	0.3-0.5	Irregular
	Ageing at 225-275°C	0.2-0.3	Irregular
AK4	Ageing at 180°C 10 hr.	0.1-0.2	Irregular
	Ageing at 225-275°C	1-3	Irregular etching figures, occasionally with spiral steps
AK4-1	Stepped tempering at 200°, 275°, 350°C (exposure 1 min.) and ageing at 180°C 10 hr.	0.1-0.4	Irregular
	Tempered condition	1-5	Oval, occasionally with spiral steps
	Ageing at 180°C 10 hr.	0.2-0.4	Irregular
	Isothermal tempering at 225°C 1 hr.	0.2-0.3	Oval
Al-Zn-Cu(10%Zn,4%Cu)	Tempered and naturally aged	5-10	Octahedrons and dodecahedrons
	Ageing at 150°C (close to Max. hardness	0.2-1.0	Octahedrons and figures of irregular shape

lattices should be parallel to dodecahedral directions.

Fig. 2. Alloy Al-Si (1.2% Si); ageing at 255°C; x 15,750.

Fig. 3. Alloy Al-Zn-Cu (10% Zn and 0.5% Cu); deformed under pressure by 15% and aged at 180°C for 6 hr; x 21,000.

2. The dislocations theory does not recognise the possible existence of gigantic dislocations in the metals.

Spiral etching figures have already been observed by Ameliuckx and Votava [6] on NaCl after thermal etching. Spiral figures with steps of considerable height were obtained on germanium and silicon by Ellis [7], and on α-brass by Bassi and Fur'e [8]. Step-like etching figures were observed in many other investigations (See references in [6]).

As a result of recent work on spiral etching figures on germanium, silicon and α-Brass (7,8) and helical dislocations in NaCl and CaF_2 [9-12], new interpretations of these figures have been put forward. Let us examine some of them.

Lang [13] considers that spiral figures of growth and etching can be explained as evidence of foliated growth and dissociation, without reference to the dislocations theory. In his opinion, foliated structures are formed under conditions in which tightly-packed atomic layers form a small angle to the crystal surface, and that growth or dissociation takes place mainly by precipitation or removal of atoms from the side of the layers. Energy considerations suggest that single-atom steps would not continue to exist, but would unite and form microscopically observable steps. Lang explains the appearance of spiral figures with a single-atom step as a result of "errors" in growth or dissociation, while the appearance of spiral figures with microscopic steps is taken to be a result of the regular displacement of the centres of concentric single-atom layers. In the latter case a microscopic step consists of a number of single-atom steps.

We disagree with Lang's explanation because of the rigid conditions he attaches to the formation of spiral figures, conditions which might well be only rarely fulfilled and result in the formation of only a small number of etching figures. Lang's supposition makes it impossible to explain the existence of spiral steps on three different sides of cubic etching figures (Fig.3).

An explanation of the dislocation of spiral etching figures in Ge, Si and CaF_2, which is based on the observations of Boutinck, Ameliuckx and others [9-11] is given in papers [7-12]. The above authors noticed that some decorated dislocations in synthetic Fluorite crystals and NaCl have a helical shape. They are formed at high temperatures, when dislocations are capable of creeping as soon as a vacancy occurs. Ameliuckx and others [12] consider that if such dislocations exist in Ge and Si and if the axis of the spiral forms only a small angle with normal to the etching surface, then in the process of etching the step of the figure will spread out in a circular fashion from the origin of the etching. In the cases where anisotropy in the etching rate is strongly expressed, multi-angular spiral etching figures are formed as a result of multi-angular helical dislocations (10). During study [9-11] of CaF_2 and NaCl crystals it was found that helical dislocations, as a rule, have an axis

parallel to their Biurgers vector; the screw radius is approximately constant, while screw spacing can considerably exceed the Biurgers vector value. Boutinck was able, using decoration as well as the etching method, to observe helical dislocations which develop in pairs out of one point and form angles close to 60 and 120° between one another. On the basis of the above observations it was established that the dislocation axes are parallel to type (110) directions, which is in agreement with the dislocations theory [14].

Weertman [15], has shown by theoretical calculations that the equilibrial form of a dislocation line should be helical. If the helical dislocation contains many coils, then its axis should be practically parallel to the Biurgers vector. In addition to this, pure screw dislocations can spontaneously take helical shape from many coils at great stresses. Prismatic and helical dislocations, caused by stresses, were observed by Johnson and Mitchell in the crystals of silver chloride [16] by introducing into them spherical glass impurities. On cooling to to room temperature from 370°C, the stresses created near the spherical particles due to the different expansion coefficients of glass and silver chloride, caused the formation of helical and prismatic dislocations.

2. Spiral etching figures on our alloys, i.e. Al-Zn.Cu, were observed both in the cast state (after cooling in air), and also after homogenization and slow cooling in an oven, followed by prolonged ageing at 150°C to 200°C. If these figures actually correspond to helical dislocations, the latter could have developed at high temperature, when dislocation creep and the condensation of vacancies on them is possible. Cottrell atmospheres and G.P. zones strengthen these dislocations and in doing so create favourable conditions for their development.

The helical dislocations in the alloys could have formed on account of the stresses that always exist in ageing alloys which are in the saturated non-equilibral solid solution state. Therefore, conditions for the development of helical dislocations are present in the alloys studied.

The spiral character of the etching figures is better detected when one of the alloy components is present in small quantity, i.e. in the alloy Al-Zn when 0.5% Cu is present, in the non-ageing aluminium alloys with 0.25% and 0.50% Cu, and in some industrial aluminium alloys when small additions of alloy components are made (see Table). Under these circumstances there is a great probability of the formation of helical dislocations at high temperature.

Fig. 4. Alloy Al-Cu4%Cu); Ageing at 220°C 5 min; x 21,000.

Helical dislocations can explain the existence of a large step in spiral etching figures (it's height is determined by the spiral spacing) and make it easier to understand the formation of a G.P. zone or phase separation nucleus on steps which correspond to individual dislocation sections. However, there are factors which either contradict the supposition of a connexion between etching figures and helical dislocations, or support the existence of a link between etching figures and large screw dislocations. Direct observations have shown that the helical dislocations in NaCl and CaF_2 have an approximately constant coil radius. No conical helical dislocations with a sharply varying coil radius (as in the case of the spirals in the aluminium alloys) were observed. Moreover, it has not yet been proved that spiral etching figures with large steps on NaCl and CaF_2 correspond to helical dislocations. The radius of the helical dislocations in these crystals is constant, while the spiral radius in the figures varies sharply. Tentative attempts only have been made to explain spiral etching figures in various materials by the existence of helical dislocations.

No interrupted or dotted spirals were found

VOL. 8 1959

on the alloys, as one might expect if they are in fact related to helical dislocations, because the coils of the latter are formed of alternate screw and edge parts, and should have been differently etched. The presence of craters at the apexes of the octahedra in Al-Cu type (Fig. 4) alloys tends to confirm the existence of large screw dislocations, and not helical ones. The stability of spiral etching figures in relation to deformation and thermal treatment also indicates their connexion with large screw dislocations. The above material does not give sufficient grounds for a definitive answer to the question: are etching figures connected with helical or with large screw dislocations?

3. The formation of spiral etching figures, the axes of which are parallel to the cube directions and which have large steps, can be explained on the basis of a special feature of the octahedral etching figures on Al-Cu alloys, which is that the ribs of the octahedral etching figures as a rule are poor in G.P. zones (See Fig. 4). These ribs are parallel to (011) type directions and the cube planes pass through tem. From this one can conclude that the planes, or rather the regions that are parallel to them, 0.1-0.2 in width, in which for some reason G.P. zone formation is impeded, are characteristic. In view of the fact that in the etching of aluminium and aluminium alloys with small copper addition (0,25% and 0.50%) cupe-shaped etching figures are formed, one might take the impoverished regions which are parallel to the (001) planes as a boundary of the initial mosaic blocks formed by the hardening of the alloys. The appearance on cooling of great distortions in atom positions at the boundaries of the blocks and at points of contact in particular, is possibly similar to that which should be observed near screw dislocations. These points can serve as centres of formation of new recrystallized blocks at high temperature. The arrangement of the initial blocks is shown in Fig. 5 (the possible axis of formation of new blocks shown by arrows). An analogous diagram in which not blocks but individual atoms are cubically shown is ordinarily used to demonstrate the development of screw dislocations (14).

Cubic spiral etching figures in such alloys as Al-Zn-Cu and Al-Cu (with small copper additions) are apparently formed according to the above scheme. Yet, even here it is not clear whether these figures are related to large screw dislocations or helical dislocations developing from single screw dislocations by vacancy condensation on them, since according to the diagram mentioned above the appearance of single screw dislocations which are parallel to the cube axes, is possible. Similar difficulty is experienced regarding octahedral etching figures. The presence of craters on them might indicate a possible connexion with large screw dislocations.

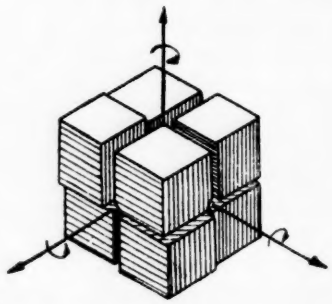

Fig. 5. Diagram of arrangement of initial mosaic blocks in a crystalizing alloy. The possible axes of newly formed blocks are indicated by arrows.

It is still not clear why old boundaries are poor in G.P. zones, while on the octahedral boundaries of etching figures they are present in great numbers. It is possible that displacements along plane (111) lead to a considerable reduction of elasticity stresses along the octahedral borders. Displacements along old boundaries which are parallel to (001) are impeded and serve as points of local elastic deformation. According to Koval'skii and Umanskii [17], elastic strains can inhibit dissociation in solid solutions.

Irrespective of whether the etching figures are connected with large screw or with helical dislocations, the figures correspond to mosaic blocks for following reasons,

If the initial premise is right, then the dislocation theory [14] gives a stress value (in the case of an elastic isotropic medium) in the direction of the displacement for helical dislocations as

VOL 8 195

$$\sigma_{\theta z} = \frac{Gb}{2\pi r},$$

where G = displacement modulus, b = Biurgers vector, r = the distance from the dislocation axis.

For ageing alloys on an aluminium base $G \simeq 2700$ kg/mm^2. For Al-Zn-Cu alloy $b = 2 \times 10^{-5}$mm (200Å) and $r \simeq 10^{-3}$mm. For $\sigma_{\theta z} \simeq 9$ kg/mm^2, a value which is close to the elastic limit of duraluminium. If we consider that each etching figure is connected with several dislocations, then the volume corresponding to it could be easily disorientated in relation to the matrix by such stresses, and therefore it can be regarded as a mosaic block. In the case of etching figures having a connexion with helical dislocations, they also correspond to mosaic blocks, because on the boundaries of the etching figures in alloys such as Al-Zn-Cu there are sufficiently closely disposed steps, which correspond to the separate links of the helical and prismatic dislocations. The combinations of such dislocation links form the boundaries of the mosaic blocks.

Both the gigantic screw and the helical dislocations have very little mobility. The former due to the great value of the Biurgers vector, the latter due to the formation around them of Cottrell atmospheres, G.P. zones and the nucleus of the separation phase. The greatly reduced mobility of the dislocations is also due to the fact that their axes are parallel to type (001) directions. Compactness of these dislocations should give alloys great strength. The strength and heat-resisting properties of Al-Cu could probably be explained by the great compactness of one of these types of dislocation. The study of the above of this type of mosaic in the strengthening of alloys confirms the dependence of hardness on the dimensions and shape of the etching figures.

CONCLUSIONS

1. The shape and dimensions of the etching figures on aluminium alloys vary according to the duration and temperature of ageing.
2. The connexion of etching figures with large screw or helical dislocations makes possible the suggestion that they correspond to mosaic blocks.

Translated by Peters

REFERENCES

1. N.N. Buinov and R.M. Lerinman, *Dokl. Akad. Nauk SSSR*, 74, No.4, 707 (1950).
2. N.N. Buinov and R.R. Zakharova, *Fiz. metal. metalloved.*, 6, 289 (1958).
3. N.N. Buinov, *Fiz. metal. metalloved.* 1, 339 (1955).
4. V.G. Rakin and N.N. Buinov, *Fiz. metal. metalloved.* 6, 686 (1958).
5. N.N. Buinov and T.V. Shchegoleva, *Fiz. metal. metalloved.* 5, 566 (1957).
6. S. Amelinckx and E. Votava, *Naturwissenschaften* 41, 422 (1954).
7. S.G. Ellis, *Phil. Mag.* 2, 1285 (1957).
8. G. Bassi and I.T. Fourie, *Acta Met.* 5, 678 (1957).
9. W. Bontinck and S. Amelinckx, *Phil. Mag.* 2, 94 (1957).
10. S. Amelinckx, W. Bontinck and W. Maenhout-van der Vorst, *Phis.* 23, 270 (1957).
11. W. Bontinck, *Phil. Mag.*, 2, 561 (1957).
12. S. Amelinckx, W. Bontinck and W. Dekseyser, *Phil. Mag.* 2, 1264 (1957).
13. A.R. Lang, *J. Appl. Phys.* 28, 497 (1957).
14. V.T. Rid, *Dislokatsii v Kristallakh, Metallurgizdat*, (1957).
15. J. Weertman, *Phys. rev.*, 107, 1259 (1957).
16. D.A. Jones and I.W. Mitchell, *Phil. Mag.*, 3, 1 (1958).
17. A.E. Koval'skii and Ya.S. Umanskii, *Zh. fiz. khim*, 20, 769; 773 and 929 (1946).

HOMOGENEOUS AGEING OF UNSATURATED SOLID SOLUTIONS*

A. A. PRESNIAKOV, L. I. DUATOVA and Iu. F. KLIUCHNIKOV

Nuclear Physics Institute of the Academy of Sciences of the Kazakhstan S. S. R.

(Received 27 November 1958)

MATERIAL AND METHOD OF INVESTIGATION

Specimens were examined of the following simple brasses corresponding in composition to the brands L95, L90, L85, L80, L75, L70, L65, L60 and of aluminium bronzes of brands Br. A1, A2, A3, A4, A5, A6, A7, A8, A9, A10. All these alloys were prepared from brand MO copper, A00 aluminium and brand TsV zinc.

The alloys were prepared for X-ray analysis as follows: Cast billets of 18 mm diameter and 120 mm length were forged (beginning the forging at about 800°) to a degree of deformation of the order of 30 per cent. Cylindrical "vessels" were out from the forged billets with a thickness at the bottom of 1.5-2 mm, their end surface (to be used for X-ray photographing) was ground and polished; then the specimens were annealed for six hr in air at 800°. After annealing the working surface was again ground, polished and etched in nitric acid to remove the deformed layer.

X-ray photographs were made with copper K_α radiation. The diffraction spots from the planes (420) and (331) were obtained after an exposure of 45 min. The specimens remained in the electric furnace during the exposure. The temperatures of the specimens were 20, 100, 200, 250, 300, 350, 400, 450 and 500° and were controlled with an accuracy of ± 10-20°.

EXPERIMENTAL DATA

Leaving aside the quantitative differences caused by the change in the composition of the alloys and the temperature of the investigation, the majority of the X-ray photographs reveal qualitatively the same picture characterized by the presence of a limited number of more or less large, well defined diffraction spots (Fig. 1a-c). This diffraction picture fully corresponds to the preparation of the specimens for X-ray photography which imparted to them a very large grained structure; in certain cases a single crystal structure was obtained at the working surface.

In the X-ray photographs of L90 brass and A2 bronze, however, as a result of strong azimuthal washing, certain spots formed almost continuous rings. Their X-ray photographs somewhat recall the picture of incomplete recrystallization, with the difference, however, that the individual spots are very ill defined against the background of the rings.

A second X-ray photographing of all the brass series after about four months showed that in all the alloys without exception and also in copper a certain process had occurred as a result of which almost continuous rings like those in the X-ray photographs of L90 and Br A2 drscribed above appeared (Fig. 2a-b). A similar phenomenon was observed in the second X-ray photographing of the alloys Cu-Al after 3-4 weeks (Fig. 1d). The conditions for the recovery of the alloys between the X-ray photographing was the following: During the first cycle of X-ray photographs all specimens were heated to 500° in stages, holding for about one hr at each temperature. Then they were cooled and held at room temperature for 4 months until photographed again.

The washing of the spots in the azimuthal direction may be a sign of a considerable breaking up of the mosaic blocks and their misorientation to each other [3, 9].

* *Fiz. metal. metalloved.* 8, No. 3, 394-399, 1959.

The rate of the breaking up process of the blocks proved to different for alloys of different composition. In the alloys L90 and Br A2 this process manages to take place during annealing and is revealed in the first X-ray photographs; in the alloys L85 and Br A3, where the beginning of washing of the spots is seen in the first X-ray photographs, the structure changes at a somewhat lesser rate. Hence, solid solutions with a relative composition of 20-30 per cent are most subject to change.

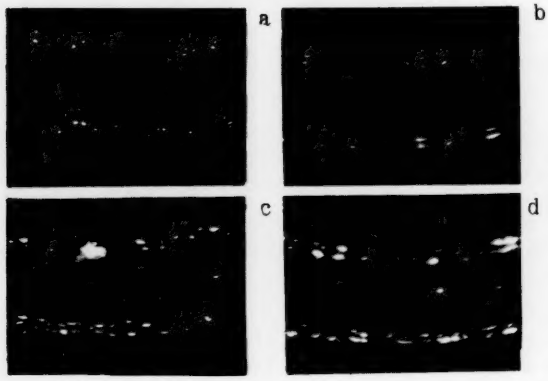

Fig. 1. X-ray photograph of the solid solutions
(a) L80, first X-ray photograph after annealing;
(b) L80, second X-ray photograph after recovery;
(c) Br. A5, first X-ray photograph after annealing;
(d) Br. A5, second X-ray photograph after recovery.

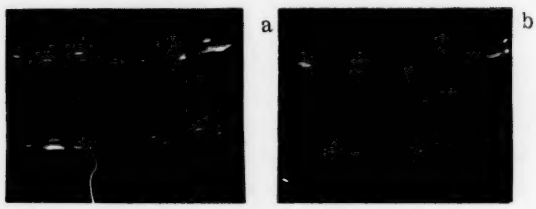

Fig. 2. X-ray photographs of alloys with "incomplete recrystallization": (a) L90; (b) Br. A2.

Both in the system Cu-Zn and in the system Cu-Al there is also another range of compositions where this process occurs with some speed. These are the solid solutions with relative composition of about 70-80 per cent, such as L70 and L65 and the bronzes A6 and A7. In alloys of intermediate composition the rate of the transformation is at a minimum.

L90 brass was X-rayed after quenching from 800°. In this case Laue spots appeared in the X-ray photograph and the number of spots of the Debye type was very small. A second investigation a week after the first cycle of photographs at different temperatures revealed a considerable increase in the intensity of the Debye spots and in their size (Fig. 3b). With the further recovery of the specimen the intense spots begin to become smaller and washed.

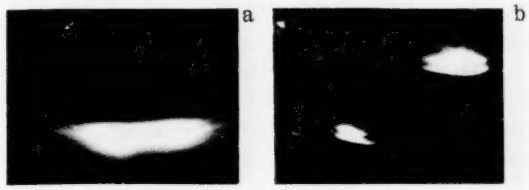

Fig. 3. X-ray photographs of specimens of brass quenched from 800° in water after annealing for 6 hr Temperature 20°:
(a) Brass L70 immediately after quenching;
(b) Brass L90 after quenching and ageing.

Special experiments in which all the specimens were annealed a second time indicate the reversibility of the process of the breaking up of the mosaic blocks. The rate of the reverse process depends on the composition and varies like the direct process. The more rapid the diminution of the blocks, the less time is needed for the second annealing to eliminate this effect. Thus, in L90 brass quenched after the second annealing at 800° the breaking up of the blocks is almost completely eliminated. In alloys of intermediate composition very long annealing is required to obtain the initial structure after recovery, as annealing for 6 hr only reduces the washing of the spots but does not eliminate it completely.

DISCUSSION OF THE RESULTS

During prolonged annealing after plastic deformation fairly large blocks of the mosaic

structure similar to those which occur in the recrystallization of steel [1, 2] develop in alloys which we investigated. The presence of well defined, not washed spots in the X-ray photographs shows that the blocks are of a size not smaller than 10^{-3} cm [3].

The observed change in the interference picture of solid solutions shows firstly that the equilibrium reached as the result of hot plastic deformation and high temperature annealing is metastable. On the other hand, slow cooling at a rate of 2°/min does not bring the alloy into the state of equilibrium at room temperature but, on the contrary, causes a kind of "quenching" of the high temperature state of the alloy.

The possibility of quenching solid solutions which do not suffer a phase transformation must now be considered as proved [1, 5-8]. In all previously mentioned cases, however, quenching was studied with rapid cooling. Our data shows that the processes of restructuring of the crystal lattice of solid solutions is fairly slow and does not always manage to take place when the specimen is furnace cooled.

If a metastable high temperature state is fixed during annealing it is quite natural to suppose that the alloy will in this case tend to pass into a state which is stable under the given structural conditions. Another consequence of this transition is apparently the considerable reduction in the size of the mosaic blocks and their misorientation to each other which causes the azimuthal washing of the spots in the X-ray photographs of papers [3, 9].

This process in the solid solutions is skin in nature to the ageing of supersaturated solid solutions (which, by the way, also shows itself in the washing of the spots [4]), since in both cases an approximation of the metastable alloy to the equilibrium for the given temperature conditions takes place; it is, however, not connected with a change in the phase composition of the alloy and not accompanied by the precipitation from the supersaturated solid solution. Taking both the similarity and the difference into account, the effect we have observed has been called by us homogeneous ageing of non-saturated solid solutions.

The diminution of the blocks as the result of homogeneous ageing shows that for room temperatures a very small mosaic structure is typical, close to the state which is obtained after plastic deformation. This state is preserved down to temperatures of 350-400° above which the blocks become larger by "recrystallization" (Fig. 4).

Fig. 4. "Recrystallization" after ageing in the alloy Br. A2 (400°).

The homogenization process is evidently preceded by short range ordering which is shown by the unusually sharp increase in the intensity of the spots in the X-ray photograph of L90 (see Fig. 3b). A similar growth in intensity also occurs in annealing brass L70 (see Fig. 3a).

Many authors have pointed out that it is possible for chemical affinity to show itself in the solid solutions of metals of the transition group [5-8, 10-15]. For us, the paper by Grigor'yev, Sokolovskaia and Piatnickii is of particular interest, which indicates an ordering of the solid solutions of copper with zinc [16], i.e. in alloys which do not contain metals of the transition group.

The fact that we obtained spots incomparably stronger than under ordinary conditions provides a basis for suggesting that the creation of short range order goes fairly far, i.e. that "long range ordering of a short range ordered solid solution" occurs "as a consequence of which a compound of variable composition may be formed at not very high temperatures" [15]. This kind of ordering together with the formation of a compound close to Cu_3Zn has been observed in brasses with a content of about 25% Zn [16]. Our data on the quenching of brand L70 brass confirms the possibility of the existence of such a compound. Besides, if one accepts Lesnik's point of view [15], the results of the quenching of L90 speak for the possibility of the existence of another compound in brasses,

which is close to the stoichiometric formula Cu_9Zn.

The rate of homogeneous ageing depends on the composition and is a maximum in solid solutions where the increase in the strength of the bond is most apparent.

We have not made experiments in quenching aluminium bronzes. But, taking into account the connexion between ageing and the short range ordering of solid solutions, one may suggest that in these systems, too, one should expect manifestations of chemical affinities in alloys with relative composition of 20-30 per cent and 70-80 per cent.

Summarizing what has been said one can give the following explanation for the effect of homogeneous ageing. In quenching solid solutions their high temperature state becomes fixed in which the atoms of the components are statistically distributed. The transition of the metastable state to one closer to the low temperature equilibrium is preceded by the development of short range order and an increase in the strength of the bonds between the atoms as a consequence of the appearance of chemical affinity. This in turn causes the compression of individual lattice volumes 6 which should evidently be the greater, the further the ordering process has gone. In the temperature investigations of the lattices of the above mentioned alloys we observed a reduction of the lattice parameter in the region of 100-200° which was greatest for relative compositions of 20-30 per cent and 70-80 per cent. This compression causes a distortion of the lattice of the block as a whole and is probably the cause of the breaking up of the mosaic blocks and their misorientation to each other, i. e. the cause of the homogeneous ageing of non-saturated solid solutions.

A parallel investigation of the microhardness of the experimental alloys showed that homogeneous ageing is accompanied by a change in this property (see Table 1).

Clearly to connect these two phenomena is, however, difficult for the time being because of the insufficiency of experimental material.

Homogeneous ageing of non-saturated solid solutions compels one to approach the study of the structure and properties of alloys at high temperatures and in quenching with great caution. In order to judge the properties and structure of alloys it is in this case necessary to make temperature investigations and not to confine oneself to the measurement of these properties in the state of quenching from the temperature to which they are referred.

VOL. 8 1959

CONCLUSIONS

1. The phenomenon of homogeneous ageing in non-saturated solid solutions, unaccompanied by a change in the phase composition of the alloy or the precipitation of an excess phase is observed, which consists in the very marked diminution of the size of the mosaic blocks and their misorientation to each other.

2. The presence of an ageing process in solid solutions which have undergone hot deformation and subsequent annealing shows that the high temperature state of the crystal structure of the alloy is "quenched" during slow cooling.

3. The diminution of the block size in the ageing process and their "recrystallization"

TABLE 1

Alloy	Value of microhardness, kg/mm² (from 100-120 measurements)					
	Immediately after annealing			After ageing for two months		
	Minimum	Most often repeated	Maximum	Minimum	Most often repeated	Maximum
L90	43.7	60.2	78.4	38.6	47.6	63.5
L70	40.5	54.9	67.6	47.6	63.5	90.8
L60	63.5	80.9	107.0	54.9	70.6	107.0

at higher temperatures shows that for various temperature conditions there exist corresponding equilibrium mosaic structures to which the alloy tends under all conditions, including room temperature.

4. The "ageing" process of solid solutions is reversible. The rate of the reverse process is the greater, the greater the rate of the direct process.

5. The process of homogeneous ageing is preceded by the short range ordering of the solid solutions; this, apparently, explains its slowness.

Translated by B. Ruhemann

REFERENCES

1. L.I. Lysak; *Voprosy metallovedeniia i fiziki metallov (Questions of metallography and the physics of metals)* sb. No.7 (1956).
2. L.S. Moroz, *Tonkaaia struktura i prochnost' stali (The fine structure and hardness of metals)* Metallurgizdat, p.60 (1957).
3. B.M. Rovinskii, *Zh. tekh. fiz.* 12, No.11-12 (1942).
4. A.M. Yelistratov, S.D. Finkel'shtein and T.Iu. Gol'dshtein, *Dokl. Akad. Nauk SSSR*, 88, No.4 (1953).
5. V.K. Kritskaia, G.V. Kurdiumov and L.V. Tikhonov, *Dokl. Akad. Nauk SSSR*, 102, No.2 (1955).
6. Sh.Sh. Ibragimov and B.G. Lifshits, *Fiz. metal. metalloved*, 4, No.2, (1957).
7. V.A. Il'ina, V.K. Ktitskaia, G.V. Kurdiumov, Iu.A. Osip'ian and T.I. Stelletskaia, *Fiz. metal. metalloved* 4, No.3 (1957).
8. H. Thomas, *Z. Phys.* 129, 219 (1951).
9. B.M. Rovinskii, *Zh. tekh. fiz.* 18, No.10 (1948).
10. N.V. Grum-Grzhimailo, *Izv. S.F.Kh.A.* 19, p.531 (1949).
11. N.V. Grum-Grzhimailo, *Izv. S.F.Kh.A.* 23, p.101 (1952).
12. N.V. Grum-Grzhimailo, *Dokl. Akad. Nauk SSSR*, 87, No.1 (1952).
13. G.A. Badayeva, *Izv. S.F.Ka.A.* 19 (1949).
14. A.G. Lesnik, *Vopr. fiz. metal. i metalloved. (Questions of metal physics and metallography)* sb. No.5, Kiev (1954).
15. A.G. Lesnik, *Vopr. fiz. metal. i metalloved. (Questions of metal physics and metallography)*, sb. No.5, Kiev (1954).
16. A.G. Grigor'yev, Ye.M. Sokolovskaia and V.N. Piatnitskii, *Zh. neorgan. khim.* 2, No.7 (1956).

INVESTIGATION OF THE TEMPERING OF COLD DEFORMED K40NKhM ALLOY*

B. G. LIFSHITS and N. G. MAKHUKOV

(Received 12 August 1958)

Investigation of spring alloys of the K40NKhM type with the methods of measuring their hardness, electrical resistance, thermal expansion, elastic constants and internal friction showed that the ageing process of these alloys (after cold hardening) consists of two independent stages. One of these, which occurs principally at 300-550°, consists apparently in the formation of a *K* state; the other, mainly at temperatures of 550-700°, in the precipitation of a second phase.

VOL. 8 1959

The K40NKhM alloy, developed by the precision alloy institute of the Central Scientific Research Non-Ferrous Metals Institute, is used as spring material for spiral cylindrical springs working in corrosive media, for spiral cylindrical heat resistant springs working at temperatures of up to 300-400°, for non-magnetic corrosion resistant winding springs with heightened durability, for the expansion members of instruments and for certain other parts.

The alloy has a complex chemical composition. Its basis is the Co-Cr-Ni-Fe system. Borodkina, Makhukov and Sol' ts have shown [1, 2] that if quenched from a temperature of 1100-1150° the alloy has a single phase structure with a face centred cubic lattice.

The high elastic properties, the strength and hardness of the alloy are imparted to it by cold plastic deformation, rolling or drawing, and subsequent tempering at temperatures of 400-500°. As Fig. 1 shows a maximum is observed at 500-550° in the curves for the dependence of the hardness, the elastic limit and the electric resistance of the alloy on the temperature of tempering (for 2-4 hr). Investigation of the microstructure of the cold deformed alloy has shown [2, 3] that at tempering temperatures of up to 600° no precipitation of any excess phase from the solid solution is observed. The hardening of the alloy in tempering is caused [3] by great microstrain of the crystal lattice (up to 4 x x 10^{-3} cm) and the breaking down of the mosaic blocks (to 2 x 10^{-6} cm).

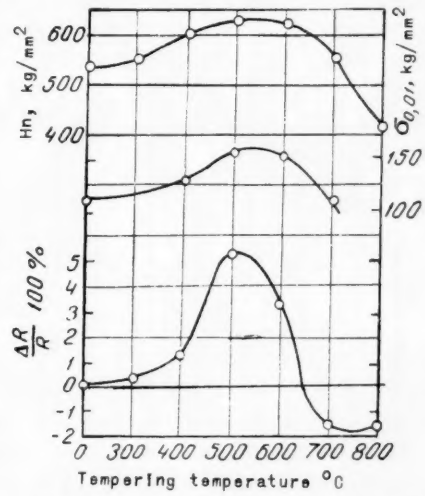

Fig. 1. Change in the hardness, elastic limit and electric resistance of a K40NKhM alloy with 0.05 per cent carbon on tempering (holding for 2-4 hr) after 70 per cent cold deformation.

We made a study of the alloy in order to establish the mechanism of the hardening process during tempering. The chemical composition of the alloys investigated is given in Table 1.

The following methods of investigation were employed: measurement of the hardness, the electrical resistance, the dilatometric method, the measurement of the elastic

* *Fiz. metal. metalloved.* 8, No. 3, 400-405, 1959.

TABLE 1

Chemical composition of the alloys

No. of alloy	% content of elements									
	C	Co	Cr	Ni	Mo	W	Nb	Mn	Si	Fe (difference)
1	0.120	40.75	20.31	15.58	2.51	3.95	0.61	2.20	0.29	13.68
2	0.050	41.00	20.26	15.60	2.47	4.00	0.60	2.20	0.31	13.51
3	0.015	42.10	20.65	15.00	6.25	–	–	0.39	0.30	14.70
4	0.015	43.85	22.30	17.15	–	–	–	0.39	0.39	15.90

properties, the measurement of internal friction.

The electric resistance was measured on a double bridge (with a UTV-2 type arrangement). The dilatometric investigation was carried out in a Chevenard differential optical dilatometer. Young's modulus was determined by the dynamic method from the measurement of the resonance frequency of the transverse oscillations of a specimen of round cross-section (diameter 0.7 mm, length 170-180 mm), the internal friction from the damping of the free torsional oscillations of wire specimens (diameter 0.7 mm, length 310 mm) in the temperature interval from 20 to 600° (the Kê method). The rate of heating was about 4°/min. The frequency of the oscillations was 0.7-0.8 c/s the quantity

$$Q^{-1} = \frac{1}{\pi \times n} \ln \frac{A_1}{A_n},$$

was taken for the measure of the internal friction, where A_1 is the initial amplitude of the torsional oscillations of the specimen; A_n the final amplitude of the torsional oscillations of the specimen; n the number of oscillations when measuring the amplitudes from A_1 to A_n.

The investigation should that in quenched and cold deformed alloys of K40NKhM type at temperatures of 400-500° a state is stable (tests took up to 100 hr) which can apparently be described as a concentration inhomogeneity of the solid solution. Such a phenomenon has earlier been established for a number of single phase alloys containing transition metals and has been given the name of *K* state [4]. It has been shown [5-7] that the same state of the solid solution is also observed in certain ageing alloys. In such a case, as also in oversaturated aluminium alloys [12], the occurrence of two independent processes is observed. At low temperatures of ageing zones of segregation of atoms of the same kind are formed which at higher temperatures are resorbed into the matrix, while the nuclei of the second phase develop and grow, which is an independent process.

The results of the dilatometric investigation show that in alloys of K40NKhM type there also occur two independent processes. Fig. 2 shows clearly the separation of these processes with temperature. Both processes cause a reduction of the volume of the alloy. The first process occurs at temperatures in the interval 300-550°, the second in the interval 550-700° and amounts to the separation from the solid solution of a second phase and the acceleration of the processes of relaxation and recrystallization. The first process of volume reduction occurs at the same temperatures at which an increase in the electric resistance, the hardness and the elastic properties is observed (see Fig. 1). The nature of these processes is apparently the formation of zones of atom segregation (*K* state).

We suggest that the segregations of atoms of the same kind are points of additional scattering of conduction electrons and reduce their mobility, as a result of which the electrical resistance increases. The alloy hardens because the zones of segregation are formed at temperatures below the temperature of recrystallization, strong internal stresses arise at the boundaries of the accumulations and the alloy is in an inhomogeneously strained state. The formation of the *K* state

VOL 8 195

in the alloy causes an increase in the strength of the bonds which shows itself in an increase in the modulus of elasticity. As the investigations showed, the atoms of molybdenum and tungsten play the main part in the formation of zones of segregation in the alloys of K40NKhM type.

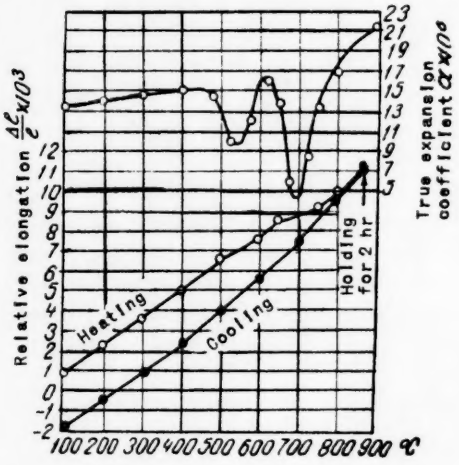
Relative elongation $\frac{\Delta l}{l} \times 10^3$
True expansion coefficient $\alpha \times 10^6$
Heating
Cooling
Holding for 2 hr
100 200 300 400 500 600 700 800 900 °C

Fig. 2. Relative elongation and true expansion coefficient of cold deformed (40 per cent compression) K40NKhM alloy with 0.12 per cent carbon.

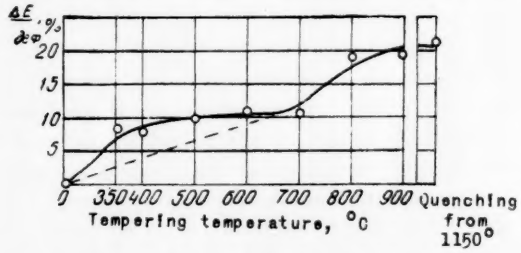

Fig. 3. Change in the modulus of the normal elasticity of a cold deformed specimens (40 per cent compression) of a K40KhM alloy with 0.12 per cent carbon depending on the tempering temperature.

In the curves for the dependence of Q^{-1} on the temperature in the testing of the alloy in the region of 300-350° a peak of the internal friction is observed. Fig. 4 shows one of these curves for the alloy with 0,12 per cent carbon content, on which the peak can very clearly be seen. A possible mechanism for the appearance of a peak of the internal friction in alloys with face centred cubic lattice containing carbon has been described in paper [8]. The occurrence of the peak is explained by the suggestion that a foreign atom which finds itself in a substitional solution forms an atomic pair with the carbon atom which creates distortions in the lattice different for the three crystallographic directions.

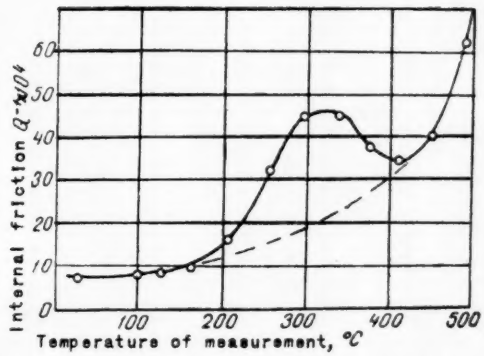

Fig. 4. Temperature dependence of the internal friction of a cold deformed (70 per cent compression) specimen of a K40NKhM alloy with 0.12 per cent carbon after tempering at 200° for two hr.

The relative displacement of these atoms under the influence of the stresses during the testing of the specimen generates internal friction. Apparently, the peak in the internal friction of the K40NKhM alloy is produced by the same cause. The elementary act of the process is the displacement of the carbon atom from one octahedral intermodular position to the other. The role of the foreign atom in the alloy of K40NKhM type is played by Mo and W (their atomic diameters are 2.80 and 2.82 kX respectively).

The atomic diameters of Co, Cr, Ni and Fe are within the limits of 2.49-2.57 kX. As has been observed, in alloy No. 4 (without Mo and W) no peak of internal friction appears at 300-350°, irrespective of the type of treatment, whether quenching or tempering. In alloy No. 3, which has the same amount of carbon but contains 6.85 per cent molybdenum, the peak of internal friction is observed (see Fig. 5).

A peak of internal friction is observed in the testing of specimens quenched from 1100° and cold deformed (Fig. 6). The height of the peak increases with increasing degree of cold plastic deformation of the specimens. This is apparently so because after deformation the solid solution becomes more homogeneous

VOL. 8 1959

due to the destruction of the zones of atom segregation which are formed in the process of quenching. Here the number of carbon-foreign atom pairs increases and their movement in the alternating field of tension during the testing process causes energy losses and the peak in the internal friction.

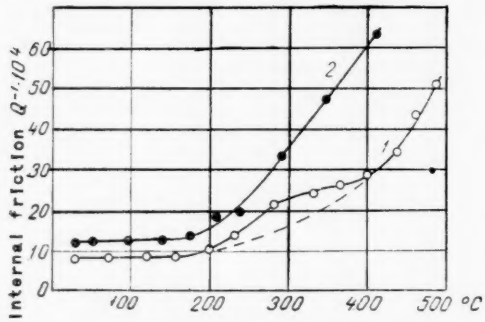

Fig. 5. Temperature dependence of the internal friction of cold deformed 70 per cent deformation) specimens of K40NKhM alloys with 0.015 per cent carbon after tempering at 200° for 2 hr: (1) with 6.85 per cent molybdenum; (2) without molybdenum.

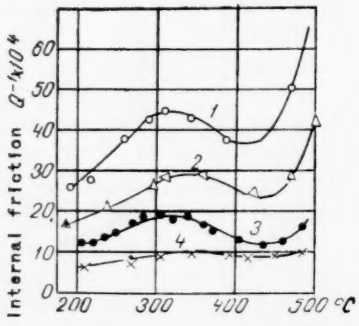

Fig. 6. Temperature dependence of the internal friction of quenched and cold deformed specimens of a K40NKhM alloy with 0.12 per cent carbon.

As Fig.7 shows, tempering at temperatures above 200° reduces the peak, since with such treatment segregation zones of molybdenum and tungsten atoms are formed as a result of which the number of carbon-foreign atom pairs capable of displacement in the field of tension is reduced.

Curves of internal friction similar to those shown in Figs. 6 and 7 for the alloy with 0.12 per cent carbon content are also obtained for alloys with smaller carbon content (alloys No.2 and 3), Fig.8a-c shows data for the height of the peak of internal friction (taking account of the background) of the alloys investigated.

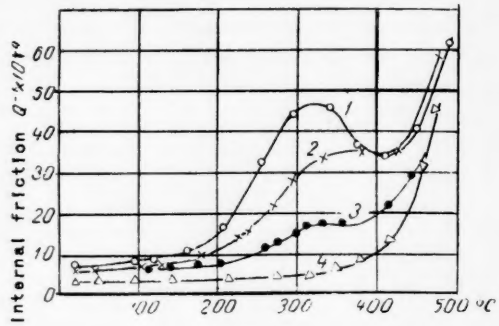

Fig. 7. Temperature dependence of the internal friction of cold deformed (70 per cent compression) specimens of a K40NKhM alloy with 0.12 per cent carbon after tempering at various temperatures for 2 hr.

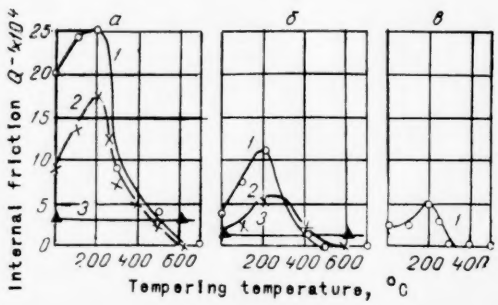

Fig. 8. Effect of the tempering temperature (holding for 2 hr) on the height of the peak of the peak of the internal friction of K40NKhM alloys with carbon contents:
(a) 0.12%; (b) 0.05%; (c) 0.015%.
State of the alloys before tempering:
(1) deformation 70%; (2) deformation 30%;
(3) quenching from 1100° in water.

For the same degree of compression and tempering temperature the alloy with 0.12 per cent carbon content shows a greater height of the peak of internal friction than the alloy containing 0.05 per cent carbon. For instance, the maximum height of the peak in curves 1 (70 per cent compression) for the alloy with 0.12 per cent carbon is 25 x 10^{-4}, but for the alloy with 0.05 per cent carbon only 11 x x 10^{-4}. The height of the peak for the alloy with 0.015 per cent carbon (Fig.8c) is still less. It follows that the height of the peak

depends on the carbon content of the alloy. The greater the carbon content, the higher the peak of internal friction, all other conditions being equal.

The increase in the peak of internal friction of deformed alloys after tempering to 200° can be explained by the recovery of internal friction [9]. It has been shown that cold hardening not only increases the background of internal friction because slip planes develop and spread [10], but also tends to lower the height of the peak on the curve of the temperature dependence of the internal friction caused by intrusion atoms [11]. Low temperature tempering, which does not substantially lower the other properties, can restore to the internal friction caused by cold hardening the value it had before cold hardening. This explanation for the effect of low tempering (up to 200°) on the cold deformed K40KhNM alloy appears to be correct, since at 300-350° the peak is caused by the presence of carbon together with Mo and W in the solution.

VOL. 8 1959

CONCLUSIONS

1. In investigations of the tempering of cold deformed alloys of type K40NKhM it is shown that in these alloys two independent processes take place. One of them occurs mainly in the temperature interval 300-550° and probably amounts to the formation of atom segregations of the type of Guinier Preston zones (*K* state). The second process occurs mainly in the temperature interval 550-700° and consists of the precipitation from the solid solution of a second phase and also in the acceleration of the relaxation and recrystallization processes.

2. The low temperature process is accompanied by an increase in the hardness, the elastic limit, the modulus of elasticity, the electrical resistance and by a reduction of the volume and the true expansion coefficient of the alloy.

3. In the homogeneous solid solution of the alloys of type K40HKhM (after deformation), which contain atoms of metallic components of different diameters and carbon atoms a peak of internal friction appears on the curve Q^{-1} *(T)* at 300-350°. This peak is caused by the relative displacement of the carbon atoms and the atoms with large atomic diameter (Mo, W).

4. The height of the peak of internal friction increases with the carbon concentration and the degree of deformation (with the homogeneity of the solid solution).

5. The formation of segregations of Mo and W atoms is regarded as the cause of the reduction of the peak of internal friction during tempering after cold hardening. This makes it possible to study the process of the formation of the *K* state by the method of internal friction. In such an investigation the carbon atom is an indicator for the formation of segregations of the atoms of the metallic components.

Translated by B. Ruhemann

REFERENCES

1. A.S. Boleukh, E.Po Belova and V.A. Sol'ts, *Sbornik Trudov TsNII-chermet, Pretsizionnyye splavy (Precision alloys)* No.22, p.41, Metallurgizdat (1959).
2. M.M. Borodkina, N.G. Makhukov and V.A. Sol'ts, *Sbornik trudov TsNII-chermet, Pretsizionnyye splavy (Precision alloys)* No.22, p.136, Metallurgizdat (1959).
3. Iu.A. Skakov and Ia.S. Umanskii, *Shestoye nauchno-tekhnickeskoye soveshchaniye po primeneniiu rentgenovskikh luchei k issledovaniiu metallov, Tezisy dokladov sektsii "Rentgenografiia splavov" (Sixth scientific-technical conference on the application of X-rays to the study of metals, theses of the lectures in the section "X-ray study of alloys")* p.25, Leningrad (1958).
4. H. Thomas, *Z. Phys.*, 129, 219 (1951).
5. B.G. Lifshits, Sh.Sh. Ibragimov, Iu.S. Avraamov and Iu.K. Konov, *Issledovaniia po zharoprochnym splavam (Studies of refractory alloys)* Izd. Akad. Nauk SSSR, 2, p.471 (1957).
6. Iu.S. Avraamov and B.G. Lifshits, *Issledovaniia po zharoprochnym splavam (Studies of refractory alloys)*, Izd. Akad. Nauk. SSSR, 2, p.198 (1957).
7. Van-Zhun' and B.G. Lifshits, *Nauchnyye doklady vysshey shkoly (Scientific lectures at higher schools)* No.1, 163, Metallurgizdat (1958).
8. Ke Tin-sui and Tazen Chi-Tszian, *Fiz. metal.*

metalloved. 4, 291 (1957).

9. A.S. Novik, *Uspekhi fiziki metallov, 1 sb. statei (Achievements of metal physics, first collection of articles)* Metallurgizdat (1956).
10. *Uprugost' i neuprugost' metallov, sbornik pod redaktsiyei S.V. Vonsovskogo (Elasticity and Inelasticity of metals, a collection of articles edited by V.S. Vonsovskii)* I.I. Leningrad (1954).
11. W. Koster and H. Stolte, *Z. Metallk.* 45, 6 (1954).
12. A. Guinier, *J. Metals*, p.673 (1956).

VOI
8
19

TRANSFORMATION OF AUSTENITE INTO MARTENSITE UNDER HIGH PRESSURE*

A.I. STREGULIN and L.A. MEL'NIKOV
Physics of Metals Institute of the
Academy of Sciences of the U.S.S.R.

(Received 16 October 1958)

VOL. 8 1959

The study of the effect of pressure on the phase transformations in steel has long interested metallographers, since pressure is one of the parameters which determine the phase composition of alloys.

According to the Le Chatelier rule pressure should arrest the $\gamma \rightarrow \alpha$ transition since this process takes place with an increase in volume. The theoretical calculations of Tamman [1], Bigeyev [2], Cohen [3], Crussard [4] and others confirm this. The experimental data of Bratskii [5], Yefremov, Selisskii and Georegievskii [6] and also of Prosvirin [7] have shown that pressure increases the temperability of steel, increases the amount of residual austenite and slows down its decomposition on tempering.

In these papers compression from one end of the specimen was employed, accompanied by plastic deformation. The latter complicates the process of the $\gamma \rightarrow \alpha$ transformation and the analysis of the results of the investigation.

Stregulin and Chuprakova [8] have studied the effect of hydraulic pressure on the transformation of austenite into martensite. This study also suffered, however, from a number of defects of method. The amount of martensite, for example, which is formed in the specimen under pressure, was determined after the pressure had been removed and the specimen had assumed room temperature. An improved method was necessary.

We succeeded in designing and producing a magnetometric device for the study of the austenite-martensite transformation under a pressure of 30,000 kg/cm^2. It consists of a hydraulic press, a magnetometer and a high-pressure chamber.

The hydraulic press was made from high grade austenite steel so that its mass should not affect the magnetic measurements.

The magnetometer was built after the well known Shteinberg and Ziuzin type of magnetometer. The amount of a magnetic phase is determined by it with the aid of a ballistic mirror galvanometer connected to a measuring coil placed between the poles of a strong electromagnet.

The high-pressure chamber is a cylinder with a bore of 7-8 mm diameter. It was also made from stable austenite steel of great strength and is placed between the free ends of the core of the electromagnet. From the ends the poles of the electromagnet were screwed into the high pressure chamber. The measuring coil is between the poles of the electromagnet and is part of the high pressure chamber.

In the centre of the poles and the measuring coil there is a through channel in which a lead or paraffin wax ampulla with the specimen is placed. The pressure on the ampulla is transmitted from the hydraulic press from the ends with the aid of punches. Lead, paraffin wax or some other plastic substance serves as the medium transmitting the hydraulic pressure to the specimen. No noticeable plastic deformation of the specimen was observed.

The investigation of the transformation of the austenite into martensite under pressure was made on two austenite steels of the following composition (see Table 1).

The specimens made from these steels had a diameter of 4 mm and a length of 25 mm.

* *Fiz. metal. metalloved.* 8, No.3, 406-411, 1959.

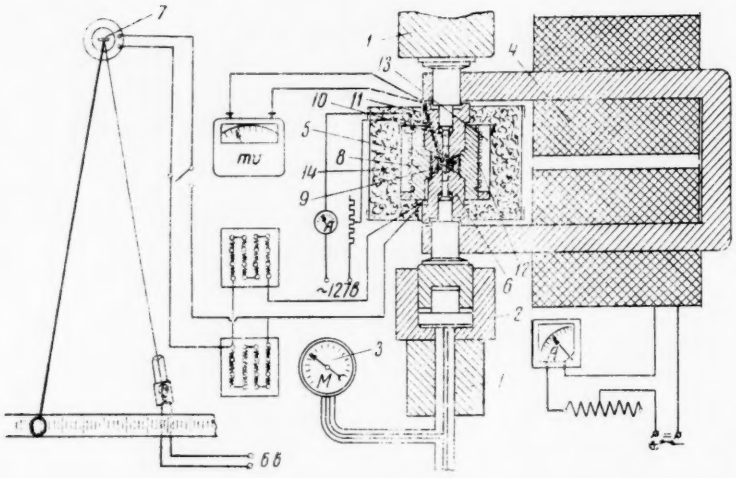

Fig. 1. Schematic drawing of magnetometric arrangement for the study of the transformation of austenite into martensite at high pressure: (1) Upper and lower gravers of the hydraulic press; (2) cylinder of the hydraulic press; (3) manometer; (4) electromagnet; (5) measuring coil; (6) pole of the electromagnet; (7) ballistic galvanometer; (8) high-pressure chamber; (9) specimen of the steel to be investigated; (10) punch; (11) thermocouple; (12) chrome-nickel heater; (13) liquid nitrogen reservoir; (14) heat insulation.

Before the investigation the specimens were homogenized at 1150° for several hr and then stabilized at 100°.

To measure the curve of the austenite-martensite transformation during cooling the specimen was room temperature enclosed in a paraffin wax ampulla. The ampulla with the specimen fitted closely into the bore of the high-pressure chamber. The chamber with the specimen and the poles was placed in the hydraulic press. After that the compression of the ampulla with the specimen was effected in the chamber.

The pressure on the specimen was determined by means of multiplying the pressure measured in the cylinder of the hydraulic press by the ratio of the area of the piston to the area of the cross-section of the ampulla. The temperature was determined with a chromel-copel thermocouple inserted in a special opening in the upper pole.

After the specimen had been compressed the high-pressure chamber together with the specimen was gradually cooled with liquid nitrogen. Simultaneously the temperatures and the deflexions of galvanometer mirror were measured. The rate of cooling while the curve of the austenite-martensite transformation was measured was 2-3°/min.

The investigation was made on the two above

TABLE 1

Steel	% content of elements						Point T_m
	C	Ni	Mn	Si	P	S	
7N4G4	0.66	4.20	3.74	0.22	0.05	0.03	5° C
4N19G	0.39	19.30	1.00	0.15	–	–	0° C

mentioned steels. The same results were obtained for both. Here the austenite-martensite transformation of 7N4G4 steel is described.

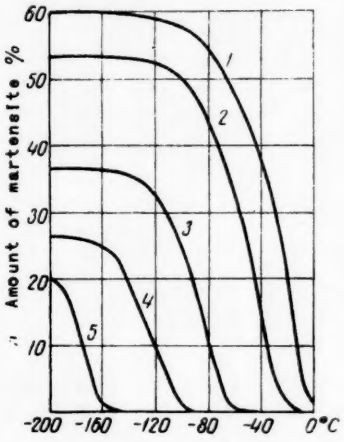

Fig. 2. Effect of pressure on the transformation from austenite into martensite in 7N4G4 steel: (1) 1 kg/cm^2; (2) 5000 kg/cm^2; (3) 10,000 kg/cm^2; (4) 15,000 kg/cm^2; (5) 20,000 kg/cm^2.

Fig. 2 shows the curves for the austenite-martensite transformation on cooling and for various pressures. As the diagram shows, the higher the pressure, the lower the temperature of the beginning of the martensite transformation (point T_M). At atmospheric pressure the point T_M is at about 5°. At a pressure of 10,000 kg/cm^2 it is at -60°, and at 20,000 kg/cm^2 at about -160°. At a pressure of 25,000 kg/cm^2 no austenite-martensite transformation is observed in either steel, even if the temperature is lowered to that of boiling liquid nitrogen (-196°).

Fig. 3 shows the curve of the change in the position of the martensite point as a function of the pressure.

The amount of martensite (the effect of the transformation) which is formed on cooling to -196° decreases with increasing pressure. If at atmospheric pressure it forms about 65 per cent, at a pressure of 10,000 kg/cm^2 it forms about 37 per cent and at a pressure of 20,000 kg/cm^2 about 20 per cent.

It was interesting to find out how the pressure affects the isothermal transformation of austenite into martensite.

The investigation of the isothermal austenite-martensite transformation was done by the following method. The specimen of the steel to be investigated, as usual in an ampulla, was placed in the high pressure chamber. After that it was subjected to a pressure of 25,000 kg/cm^2 and cooled to the given temperature of isothermal holding. At such a pressure the specimen remained austenite to a temperature of -196°.

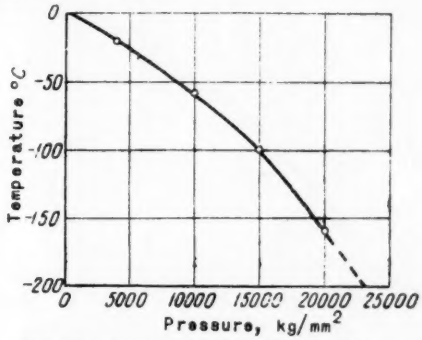

Fig. 3. Effect of pressure on the position of the martensite point in 7N4G4 steel.

After reaching the given temperature of isothermal holding the pressure was reduced to atmospheric, if the transformation was to studied at atmospheric pressure. If the isothermal transformation was effected at a higher pressure (in our case at 10,000 kg/cm^2), then after cooling to the given temperature the pressure was reduced to 10,000 kg/cm^2 at which the isothermal transformation took place.

In the first two or three seconds after the lowering of the pressure the transformation proceeded very rapidly, since the pressure which had prevented the transformation had been taken off. The amount of martensite was in this case the greater the lower the temperature and pressure. Fig. 4 shows that the curves for the austenite-martensite transformation lie the higher, the lower the temperature of the transformation. It is known that the greater the degree of cooling, the more martensite is formed.

Half a minute after the pressure had been lowered the rapid transformation came to an end. After that the magnetometric measurement of the amount of martensite formed during prolonged isothermal holding was begun. Fig. 4 shows the curves of the isothermal transformation at atmospheric pressure by continuous lines, the transformations at a pressure of 10,000 kg/cm^2 by dotted lines.

VOL. 8 1959

The latter lie lower, since the pressure reduces the amount of martensite formed.

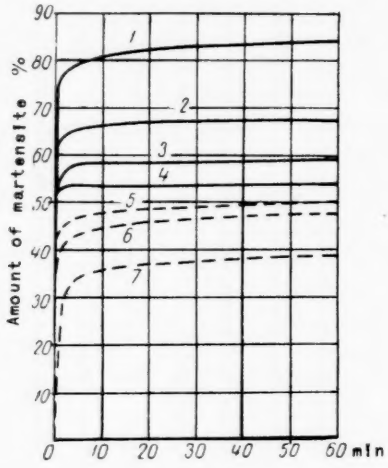

Fig. 4. Isothermal austenite-martensite transformation in 7N4G4 steel: (1) at -160°; (2) at -120°; (3) at -93°; (4) at -65° and atmospheric pressure; (5) at -150°; (6) at -120°; (7) at -85° at a pressure of 10,000 kg/cm^2.

If on the curves of Fig. 4 we take away the initial part which is obtained as a result of taking the pressure off, we obtain the curves for the isothermal transformation of austenite into martensite at the given pressure. Figs. 5 and 6 show such curves at atmospheric pressure and at a pressure of 10,000 kg/cm^2. But these curves reflect the kinetics of the isothermal austenite-martensite transformation transformation incorrectly. Kurdiumov and

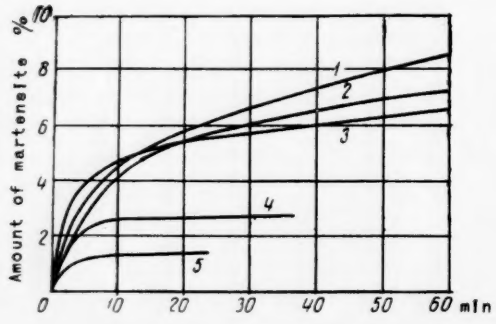

Fig. 5. Curves for the isothermal austenite-martensite transformation in 7N4G4 steel at atmospheric pressure:
(1) at -180 ; (2) at -160 ; (3) at -120 ; (4) at -93°; (5) at -65°.

Maximova [9] have suggested that the amount of martensite formed in isothermal holding should refer not to the whole amount of martensite in the specimen but only to the maximum amount of martensite formed only during the isothermal holding.

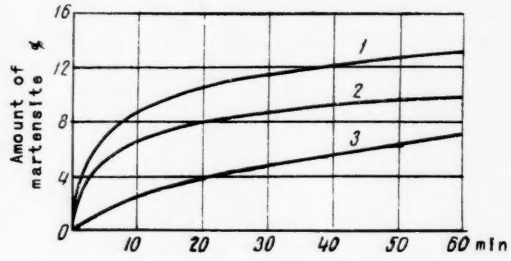

Fig. 6. Curves for the isothermal austenite-martensite transformation in 7N4G4 steel at a pressure of 10,000 kg/cm^2:
(1) at -85°; (2) at -120°; (3) at -150°.

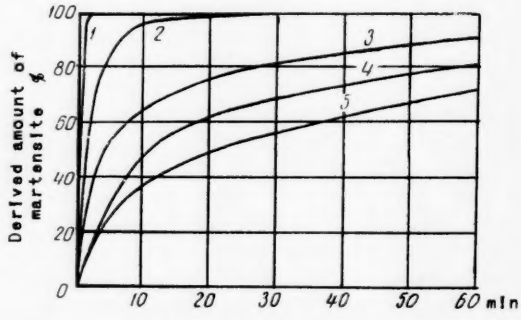

Fig. 7. Derived amount of martensite formed at constant temperature and atmospheric pressure in 7N4G4 steel:
(1) at -65°; (2) at -93°; (3) at -120°; (4) at -150°; (5) at -180°.

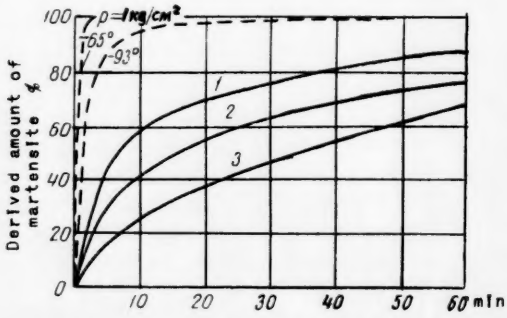

Fig. 8. Derived amount of martensite formed at constant temperature and a pressure of 10,000 kg/cm^2 in 7N4G4 steel:
(1) at -85°; (2) at -120°; (3) at -150°.

Treating the curves of Figs. 5 and 6 in this way we obtain curves for the derived amount of martensite formed in isothermal holding (see Fig. 7-8). They show that the lower the temperature, the less the rate at which the isothermal austenite-martensite transformation proceeds. The dotted curve in Fig. 8 which refers to the transformation at atmospheric pressure rises higher than the continuous curve for a pressure of 10,000 kg/cm^2. At one and the same temperature the isothermal transformation at atmospheric pressure ends earlier than at a pressure of 10,000 kg/cm^2.

Similar results were obtained for 4N19G steel the isothermal transformation for which was studied at a pressure of 5000 kg/cm^2.

CONCLUSIONS

1. A magnetometric arrangement for the study of the austenite-martensite transformation under a hydraulic pressure of up to 30,000 kg/cm^2 was designed and tested.

2. It was found that pressure considerably reduces the temperature of the beginning of the martensite transformation (the point T_m) and reduces the effect of the transformation.

3. The isothermal austenite-martensite transformation proceeds more slowly at high pressures than at atmospheric pressure.

Translated by B. Ruhemann

REFERENCES

1. G. Tamman, *Metallovedeniye (Metallography)*, p. 317 (1935).
2. M.M. Bigeyev, *Trud. Urals Fil. Akad. Nauk. SSSR*, No. 9, p. 13 (1937).
3. M. Cohen, *Acta Met.* 1, (1953).
4. C. Crussard, *C. R.* No. 25, 237 (1953).
5. M.V. Bratskii, *Zh. tekh. fiz.* 5, No. 7, 1178 (1935).
6. Ia.I. Selisakii, N.I. Yefremov and P.I. Georiyevskii, *Metallurg*, No. 1, 20 (1938).
7. V.I. Prosvirin, *Vliianiye vneshnego davleniia na fazovyye prevrashcheniia v stali i chugune (The effect of external pressure on the phase transformations of steel and cast iron)*, Mashgiz (1948).
8. A.I. Stregulin and N.P. Chuprakova, *Fiz. metal. metalloved.* 1, 368 (1955).
9. G.V. Kurdiumov and O.P. Maximova, *Probl. metalloved. i fiz. metal. (Problems of metallography and the physics of metals)* No. 2, p. 64 (1951).

VOL. 8 1959

STRUCTURE CHANGES AND ANOMALOUS TEMPERATURE DEPENDENCE OF THE MAGNETIC PROPERTIES OF Ni-Fe ALLOYS (50% Ni)*

M.V. DEKHTYAR and N.M. KAZANTSEVA

Moscow State University, M.V. Lomonosov College

(Received 8 August 1958)

The temperature relationship of magnetic properties of nickel-iron alloys (50% Ni) has been studied. It is shown that it has a different form depending upon the structure of the alloy after heat treatment.

On quenching the alloy from 1200° an anomalous temperature relationship of magnetic saturation, maximum susceptibility and coervice force is discovered when the alloy is heated in the 300-360° range. This is due to the formation of short range order which occurs on heating the disordered, rapidly-quenched alloy. Hence the anomalous properties which the alloy receives on heating to 300-360° are retained after cooling and at room temperature.

The anomalous temperature – magnetic properties relationship is not observed in the temperature range mentioned, in samples which have undergone an ordering quench.

The magnetic properties of rapidly-quenched alloys of Ni_3Fe and Permalloy have an anomalous temperature relationship [1-4]. The anomalous temperature – magnetic properties behaviour of these alloys below the critical temperature for the formation of long range in Ni_3Fe is subject to structural changes which are produced on heating the rapidly-quenched alloy [3]. These changes are caused by the formation of short range order in the disordered alloy and aid in producing a heterogeneous structure. The results of other methods of testing also indicate the existence of such a structure [5-7]. Heidenreich and Nesbitt [7] have reported that the heterogeneous structure in Permalloy and in Ni-Co alloy (50% Co) can be revealed by electron diffraction. The authors connect the latter with distortions of the crystal lattice** in regions where the face-centred cubic lattice changes into the hexagonal.

It is very probable that these distortions in the lattice of the alloy arise from the initial coherent stage of formation of short range order regions inside the disordered solution. These considerations are prompted by the results of the work of Wakelin and Yates [8] who showed that the parameter of the lattice of the ordered structure of Ni_3Fe is 0.002 Å less than that of the disordered.

In the present work the temperature relationship of the magnetic properties of the Ni-Fe alloy with a large nickel content (50%) has been studied.

We have studied the temperature relationship of the magnetic properties of samples quenched from 1200° and after an ordering anneal. Measurements were taken on samples, 200 mm in length and 0.3 mm in diameter. The samples were placed in thin silica tubes which were evacuated down to a pressure of 10^{-4} mm Hg and then sealed. After maintaining a temperature of 1200° for 48 hr the silica tube and sample were removed for quenching in water.

* *Fiz. metal. metalloved.* 8, No. 3, 412-416, 1959.

** Stacking faults.

Magnetic measurements were carried out by means of an astatic magnetometer. For high temperature measurements a furnace with non-magnetic bifilar winding of Pt wire, was inserted into one of the coils of the astatic magnetometer. To even up the temperature along the sample in the furnace a non-magnetic metal tube was installed, inside which was placed the silica tube and the sample under test was surrounded directly by the metal tube.

In Fig. 1 curve *a* the temperatures magnetic saturation curve is given for a sample quenched from 1200° and in Fig. 1 curve *b* for a sample which after quenching had been soaked at 480° for 100 hr. In curve *a* Fig. 1 a break can be seen which indicates increased magnetization in the region 300-360° caused by formation of short range order. The lower portion of this curve is displaced towards the right which shows that the Curie temperature of the newly-arising short range order structure is higher than the Curie temperature of the disordered alloy.*

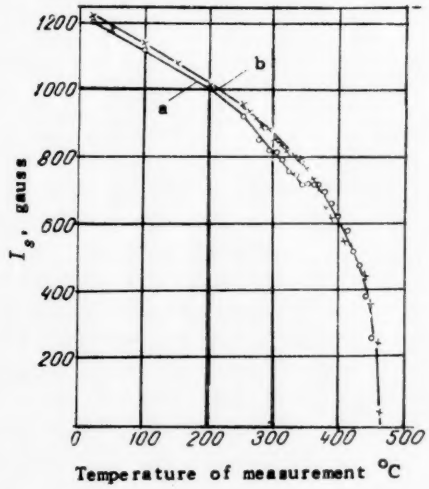

Fig. 1. Curve *a* temperature relationship of magnetic saturation of the Ni-Fe alloy (50% Ni) quenched from 1200°. Curve *b* temperature relationship of the magnetic saturation of the Ni-Fe alloy (50% Ni) which has been given a 100 hr ageing at 480° after quenching from 1200° in water.

* The dependence of I_s and the Curie point on the degree of short range order has been indicated by Vonsovskii [9, 10].

For the sample whose structure had been ordered by prolonged soaking there is no break in the curve $I_s(t)$ and the magnetization decreases regularly with rising temperature (Fig. 1. curve *b*). Formation of short range order is more clearly shown on the curves giving the temperature relationship of coercive force and maximum permeability of samples quenched from 1200° (Fig. 2).

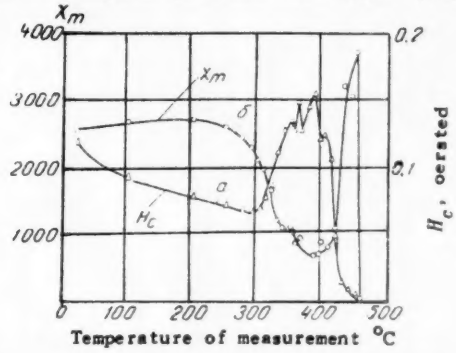

Fig. 2. Curve temperature relationship of the coercive force of the Ni-Fe alloy (50% Ni) quenched from 1200°. Curve *b* temperature relationship of the maximum susceptibility of the alloy quenched from 1200°.

The coercive force of the quenched sample falls albeit insignificantly, on heating from room temperature to 300°. This reflects the stage of coherent formation of regions with short range order in the disordered Ni-Fe solution and may be the consequence of coherent stresses which arise.

A similar conclusion may be drawn from the temperature relationship curve of maximum permeability of the quenched alloy (Fig. 2 curve *b*). χ_{max} decreases on heating in the 280-360° range by four times. Fluctuation of the value of H_c within certain limits in the 350-390° range is probably caused by the break in coherency of the freshly formed ordered regions.

The sharp increase of χ_{max} and decrease of H_c at about 400° in this case indicates the stage in the breakdown of coherency in the newly formed regions of short range order and disordered solution.

The short range order structure arising from heating the quenched sample is stable at room temperature. From this it is evident that the observed anomalous changes in the magnetic properties are not reversible. The

alloy under study, being held in the stated temperature range also has anomalous properties after cooling to room temperature. This is illustrated in the temperature vs. maximum susceptibility curve (Fig. 3 curve *a*) and the temperature vs. coercive force curve (Fig. 3 curve *b*), (the temperature in this case being the ageing temperature of the quenched specimen). According to the curves shown in these figures it seems that the structure which is produced by ageing the quenched sample in the 300-400° range has double the coercive force at room temperature and less than half the χ_{max} compared with the sample quenched from 1200°.

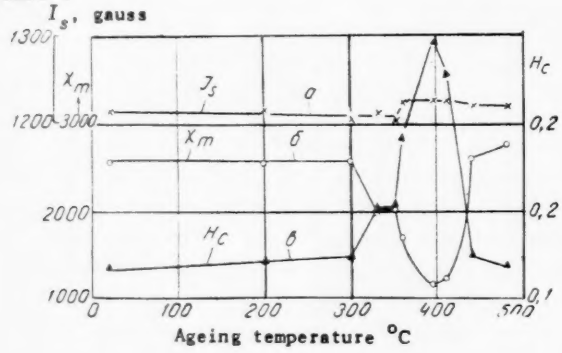

Fig. 3. Curve *a*. Relationship of maximum susceptibility of the quenched sample to the ageing temperature. Curve *b*. The relationship of H_c of the alloy quenched from 1200° to ageing temperature.

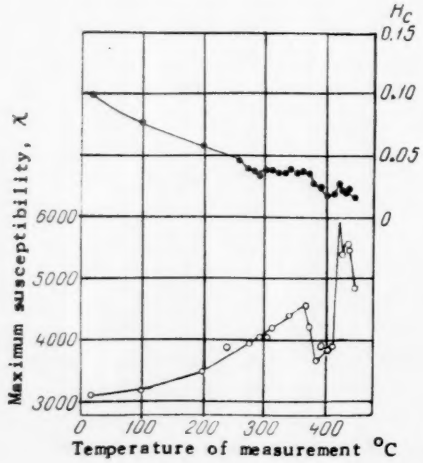

Fig. 4. The temperature relationship of the coercive force and the maximum susceptibility of the alloy quenched from 1200° to 600° with a rate of 5°/min, and then quenched in water.

The growth of I_s in particular indicates the part played by ordering when the sample is aged in the 300-400° range (Fig. 3 curve *a*). If the sample which has been held at 1200° is slowly cooled to 600° (at the rate of 5°/min) and then quenched in water, the anomalous effects on the temperature relationship curves, although they are still appreciable, are considerably less. As can be seen in Fig. 4 the maximum susceptibility at about 360° is 20 per cent lower* (from 4500 to 3700 units) and at the same time for the quenched sample it is four times less at this temperature, (from 2800 to 700 units). On the $H_c(t)$ curve the fall of H_c with temperature in the 300-400° range is delayed (Fig. 4) and in this region the increase of H_c is not as sharp as when the sample quenched from 1200° is heated (Fig. 2 curve *a*). Thus, the heat treatment indicated helps to produce regions of short range order in that stage when coherency of these regions and of the disordered solution is already disrupted.

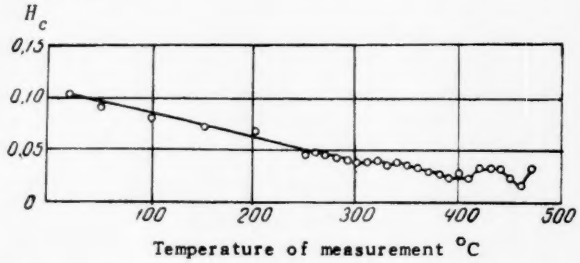

Fig. 5. The temperature relationship of the coercive force of the alloy quenched from 1200° and then held for 100 hr at 480°.

Anomalous temperature behaviour of the magnetic properties in the 300-400° range are not observed in samples which have been given a 100 hr ageing at 480° after quenching from 1200° (Fig. 1 curve *b* and Fig. 5).

---

* This behaviour of the curve $\mu_{max}(t)$ for the alloy with 50% Ni is shown in the article of Zaimovskii (see Fig. 21 in Ref. [11]). The effect of heat treatment of the alloy (with the original structure) on the temperature vs. magnetic properties curve has not been studied in ref. (11).

CONCLUSIONS

The temperature effect on the magnetic properties of the Ni-Fe alloy (50% Ni) quenched from 1200° has an anomalous character – on heating this alloy the magnetic properties change sharply in comparitively narrow temperature range (300-360°). The coercive force increases and the maximum susceptibility decreases by several times. The magnetic saturation is also increased. This anomaly is not observed in samples which have been given a 100 hr ageing at about 480°.

Comparing these results with those obtained earlier on the Ni_3-Fe [2,3] we may make the following conclusions: On heating the rapidly quenched Ni-Fe alloy (50% Ni) to about 300°, formation of short range order commences in the disordered alloy. This is indicated by the increase in magnetic saturation and rise in the Curie temperature. In the initial coherent stage of the formation of regions with short range order in the disordered solution, distortions occur in the crystal lattice which cause increased coercive force and sharp lowering of the maximum susceptibility.

Holding the quenched alloy in the 300-400° range leads to a structural condition with less free energy than that of the disordered (quenched) solid solution. This state is is preserved during cooling to room temperature. So the anomalous changes in magnetic properties acquired by the quenched alloy by ageing in the temperature range indicated are irreversible and are maintained after cooling the alloy to room temperature.

Translated by W.J. King

REFERENCES

1. M.V. Dekhtyar, *Fiz. metal. metalloved.* 3, 55, (1956).
2. M.V. Dekhtyar, *Zh. eksp. teor. fiz.* 34, 772 (1958).
3. M.V. Dekhtyar, *Izv. Akad. Nauk SSSR*, series physics 23, 271 (1959).
4. M.V. Dekhtyar, and N.M. Kazantseva, *Fiz. metal. metalloved.* 7, 453 (1959).
5. B.G. Livshits, Izv. Akad. Nauk SSSR Series physics, 21, 1225 (1957).
6. B.G. Livshits and M.P. Ravdel', *Dokl. Akad. Nauk*, SSSR 93, 1033 (1953).
7. R.D. Heidenreich and E.A. Nesbitt, Phys. Rev. 1957, 105, 1678.
8. R. Wakelin and E. Yates, *Proc. Phys. Soc.*, 66, 221 (1953).
9. S.V. Vonsovskii, *Dokl. Akad. Nauk*, SSSR 26, 564 (1940), *Zh. teor. fiz.* 18, 131 (1948).
10. S.V. Vonsovskii and Ya.S. Shur, *Ferromagnetism*, State United Publishing Houses (1948).
11. A.S. Zaimovskii, Izv. *Sek. fiz.-khim. anal.* 16, 126 (1941).

VOL. 8 1959

MECHANICAL PROPERTIES OF NICKEL-ALUMINIUM ALLOYS*

V.A. PAVLOV and I.A. PERETURINA

Institute of Physics of Metals

(Received 21 August 1958)

A study is made of the dependence of the yield point of Ni-Al alloys on concentration of the solid solution (from 0.025 to 2.93% Al), as well as on the temperature and rate of deformation. When Ni is alloyed with Al consolidation of the solid solution takes place, excluding the region of low Al content (from 0.025 to 0.05% Al), where yield point initially decreases with increase of alloying metal. As the content of Al is raised, there is a stronger dependence of yield point on temperature and rate of deformation. For alloys with 1.5 and 2.93% Al, an irregular change of yield strength with temperature is observed.

In a previous work, Al-Mg and Ni-Cu alloys have been studied with the object of discovering the effect on mechanical properties of inter-atomic cohesion forces and of the static distortion of the crystal lattice which arise in solid solutions from the effect of atoms of the alloying element [1,2].

These alloys were very suitable for making the intended studies since they differ amongst themselves as regards the nature of the variation of modulus of elasticity, characteristic temperature and static distortions with concentration of the solid solution.

In Al-Mg alloys in the range of concentrations studied, the modulus of elasticity and characteristic temperature are not dependent on the composition of the alloy; static distortion increases with increasing Mg content.

In Ni-Cu alloys the modulus of elasticity and characteristic temperature decrease with increasing Cu content, but the static distortion increases up to 40% Cu and then falls.

From these studies certain general principles have been established for both alloys with regard to change of yield point with solid solution content and deformation conditions.

1. It is not possible to explain the strengthening of the alloys by change in the interatomic forces. The relationship of yield point to solid solution content is correlated to the change of static distortion of the crystal lattice. On this basis, it is suggested that strengthening of alloys is mainly connected with change in the macrostructure (with the appearance of static distortion of the crystal lattice with the formation of non-uniform distribution of impurities throughout the solid solution, with change of block structure and so on) which increases the coefficient of performance of interatomic cohesion forces.

2. For pure metals change of the yield point with temperature when dynamically deformed is mainly determined by the temperature relationship of the modulus of elasticity. For alloys the yield point depends considerably more on temperature; moreover, irregular change of the yield point with temperature and deformation rate is observed. All these laws of change of yield point with temperature and deformation rate show that in the solid solutions studied, as the shearing plastic deformation develops certain thermally activated processes are brought about when deformation takes place.

In the present work, data will be quoted from the study of the relationship of yield point to alloy composition and deformation conditions of solid solutions of Ni and Al.

These alloys are characterized by the fact that the modulus of elasticity, characteristic temperature and static distortion of the crystal lattice increase with increased alloy

* *Fiz. metal. metalloved.* 8, No.3, 417-425, 1959.

content. An appreciable part of the increase of inter-atomic cohesion forces, it seems, is connected with close-packing since in plastic deformation at room temperature, the characteristic temperature falls, approaching the value for pure Ni. [3].

PREPARATION OF THE ALLOYS AND METHOD OF TESTING

The alloys were melted in a vacuum of 10^{-5}mm Hg, from electrolytic Ni mark H0000 of high purity, and aluminium mark AB000. The castings after homogenization were forged into small bars 10 x 10 mm. These bars were planed to a thickness of 0.5-1.0 mm to remove the surface layer and then rolled and drawn into wires of about 1 mm diameter. The drawing was carried out at room temperature annealing in a vacuum at 800° at certain intervals.

After the last intermediate anneal the wires received a deformation of about 80 per cent less than the square of the cross-section and in that condition were crystallized in the temperature range 850-1000°C in a vacuum. The temperature of recrystallization for each alloy was chosen so as to obtain identical grain size in all the alloys. The linear measurement of the grain in all alloys was about 1 mm.

Elongation of the samples was carried out on a special machine while the temperature was varied from 77 to 973°K. The rate of deformation was changed 300 times.

RESULTS OF THE EXPERIMENTS

In Fig. 1 are curves showing the temperature relationships of yield point of pure Ni and Ni-Al alloys with 0.025, 0.05, 0.5, 1.5 and 2.93% Al.

The yield point of pure Ni, as follows from previous studies, depends relatively slightly on temperature in the range 200 to 500-550°K. Change of the creep limit of Ni at these temperatures is determined mainly by the modulus of elasticity with temperature. In the high temperature range it changes more strongly. Microscopic studies of the plastic deformation and measurement of internal friction serve to explain the reinforcement of the temperature relationship of the creep limit by deformation along the grain boundaries. An explanation of the rise in yield point at low temperatures has been given in ref. [5,6].

With low concentrations of solid solutions

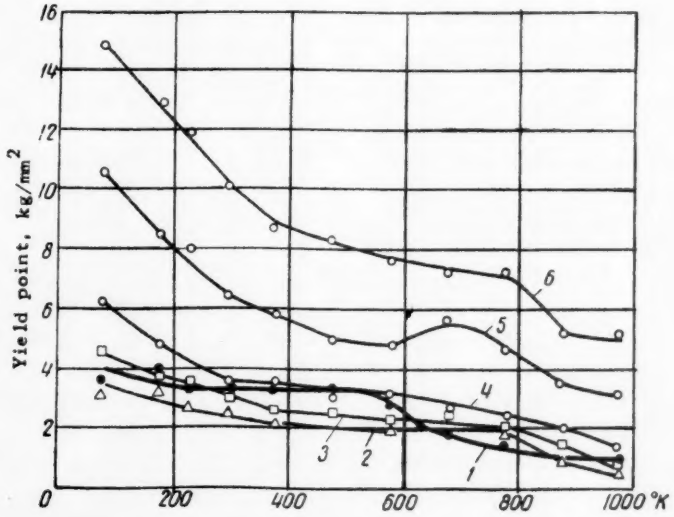

Fig. 1. Temperature vs. yield point of pure Ni and Ni-Al alloys at a deformation rate of 6.4 x 10^{-3} cm/sec:
1. Pure Ni; 2. Ni - 0.025% Al; 3. Ni - 0.05% Al;
4. Ni - 0.50% Al; 5. Ni - 1.5% Al; 6. Ni - 2.93% Al.

VOL. 8 1959

a lower yield point is observed compared with pure Ni. The temperature-yield point curves for alloys with 0.025 and 0.05% Al are found in a fairly wide range of temperatures perceptibly lower than the curve for pure Ni. Further increase of solid solution concentration is accompanied by increase in the yield point. For alloys with 1.5 and 2.93% Al the yield point is appreciably higher than for pure Ni in the whole temperature range studied. Particularly strong strengthening of the alloys is observed at the lower temperatures. Thus, at 77°K the magnitude of yield point for the alloy with 2.93% Al is almost four times that of pure Al.

In Fig. 2 yield point vs solid solution concentration curves are shown for two rates of deformation differing from each other by 300 times. From the figure the nature of the relationship of yield point to solid solution concentration and the softening action of small quantities of Al alloy are plainly seen; yield point concentration curves for two deformation rates do not run parallel with one another but diverge with increasing Al content. This denotes that with increased solid solution concentration the yield point deformation relationship is strengthened.

A stronger relationship of yield point to deformation temperature is observed particularly at low temperatures. In the low temperature range already for solid solutions with small amounts of Al there is a notably greater increase in the yield point at lower temperatures than for pure Ni. Because of this the softening effect at low temperatures is only feebly expressed. As the solid solution concentration is increased the dependence of the yield point on temperature is continuously strengthened.

As to the change of temperature relationship of yield point to solid solution concentration the conclusions can be made from the curve in Fig. 3. In this drawing the change of difference of yield point between −196 and 100°C ($\sigma_{-196} - \sigma_{100}$) in relation to the Al content is shown. The temperature relationship of the yield point rapidly rises with low Al content and more slowly with higher Al content.

Change of yield point with reciprocal of temperature curve for low temperatures of deformation (from 77 to 600°K) is shown in Fig. 4. Two peculiarities of the temperature relationship of the yield point are plainly evident from these curves. Firstly, in the 600 to 200°K range (approximately) there exists a fairly strong linear relation of yield point to reciprocal of temperature; secondly, at temperatures below 200°K the yield point is only slightly dependent on temperature. A similar character of change of the yield point is observed for iron with additions of carbon [20].

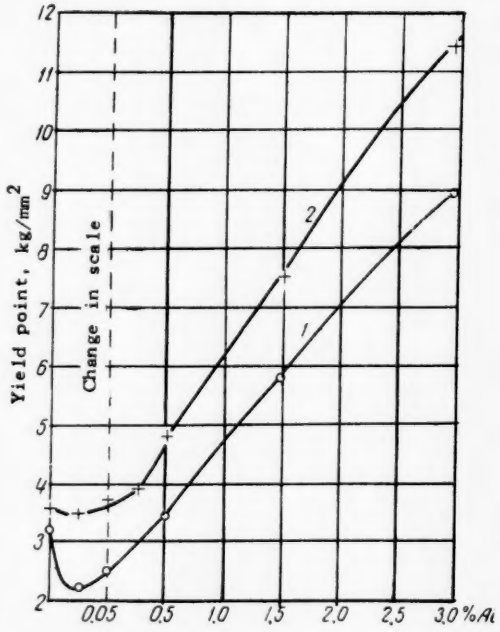

Fig. 2. Yield point of Ni-Al solid solution vs. Al content curves.
1. Deformation rate 6.4×10^{-3} cm/sec.
2. Deformation rate 2×10^{-1} cm/sec.

For alloys with 1.5 and 2.93% Al a maximum yield point is observed in the temperature range 700-800°K. For alloys with 2.93% Al the maximum is less marked because it is masked by increase of yield point at low temperatures.

DISCUSSION OF RESULTS

In the alloys studied, the following basic principles of yield point in relation to solid solution concentration and deformation

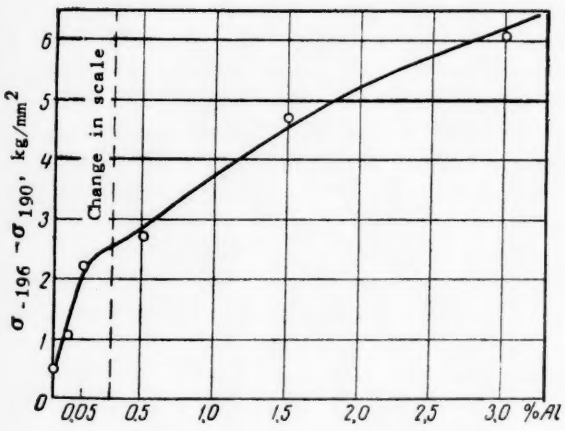

Fig. 3. Change of difference in yield point between -196 and 100°C vs. Al content

conditions were established:

1. There is a strengthening of the solid solution when Ni is alloyed with Al. But in the low alloy range an initial lowering of yield point is observed.
2. As the Al content is increased the relation of yield point to temperature and deformation rate is strengthened. The change of yield point with temperature is particularly marked in the low temperature range.
3. Alloys with 1.5 and 2.93% Al show an irregular relation of yield point to temperature.

Laws of changes of yield point to alloy composition, temperature and deformation rate were observed also for the earlier studies of Al and Mg alloys and Ni-Cu alloys. Strengthening of Ni-Al alloys may be connected, generally speaking, with increase of interatomic forces of cohesion, and variation of their macro-structure. But change of stability of alloys has been observed already in very low Al contents when still, as the tests show, [4] change in value of the dynamic distortions is practically non-existent. Moreover, the yield point depends to a large extent on concentration (decreased at low concentrations and increased at higher) which cannot be explained by variation in the interatomic cohesion forces. All this leads to the assumption that the peculiarities of relationship of yield point to Al content in Ni and the observed strengthening to a marked extent are conditioned by the variation of their macro-structure which increases the extent of the use of the interatomic cohesion forces.

The observed stronger relationship of yield point of the alloys to temperature, which

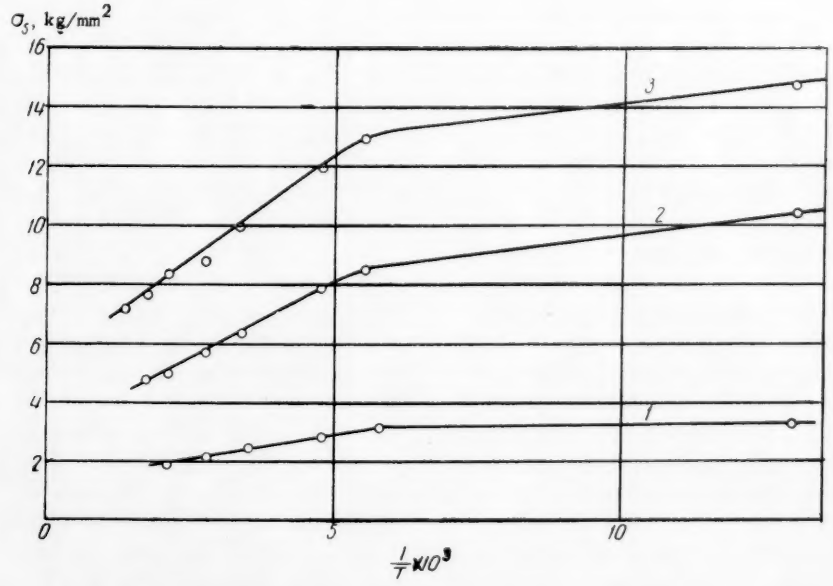

Fig. 4. Relationship of yield point to reciprocal of temperature. 1. NI - 0.025% Al. 2. Ni - 1.5% Al; 3. Ni - 2.93% Al.

VOL. 8 1959

does not succeed in explaining the temperature relationship of the modulus of elasticity, and in a similar manner the appearance of an irregular relationship of yield strength to temperature indicate that with increased alloy content the effect of the thermally activated processes on the progress of the plastic deformation is increased.

On the basis of theoretical and experimental studies in the literature the following fundamental principles can be stated, which to a smaller or larger extent may lead to strengthening and improving the relationship of yield point to temperature and deformation rate.

1. Analysis of temperature relationship in alloys of substitution with a face-centred cubic lattice has been carried out by Suzuki [18]. Basing his considerations on theory he came to the conclusion that in these alloys two types of clouds of impurity atoms can arise around the dislocations: Cottrell clouds, associated with elastic interactions of the dislocations with impurity atoms and clouds of impurity atoms in a defect of packing between two extended dislocations. In Suzuki's opinion strengthening of solid solution of the substitution of type with grain-centred cubic lattice is determined by three types of non-uniform distribution of impurity atoms: by forming two kinds of clouds of impurity atoms around dislocations and by the appearance of short range order. Variation of the temperature relationship in the low temperature range of deformation is connected chiefly with the effect of the Cottrell atmospheres and at high temperatures with the effect of the clouds in the defects of the packing. Short range order in Suzuki's opinion does not have an effect on the temperature relationship of the yield point if the degree of short range order is not changed thereby with temperature.

Suzuki compared theoretical considerations with experimental data for the alloys Ni-Cu, Ag-Au and Cu-Zn in wide limits of variation of solid solution concentration. Qualitative agreement has been established in all these alloys between theoretical and experimental significance of the yield point but quantitative agreement has only been seen two or three times. These agreements should be considered close enough, since variation of yield point in these alloys under the influence of impurity has much the same order of magnitude.

In substitutional alloys with face-centred cubic lattice, the effect of clouds of impurity atoms on resistance to deformation depends strongly on the average concentration of the impurity in the solid solution; therefore the effect of the clouds on the yield point in small concentrations of impurity will be insignificant, particularly when the distortions caused by the impurity atoms are not large. On this basis Seeger 19 considers that low concentrations of impurity in these alloys causes only an indirect effect on resistance to deformation, through increased density of dislocation. Hence the temperature relationship of the yield point will be identical for the pure and the impure metals. But in many cases a variation in the temperature relationship of the yield point is observed already at fairly low impurity concentrations. On this basis, it can be thought that there are certain other principles which affect the temperature relationship of the yield points.

2. Other reasons may exist for the strong temperature relationship of yield point in alloys. Studies [7] of Al-Cu alloys showed that for age-hardened single crystals with Guinier-Preston zones a more marked strengthening and a stronger yield point relationship in the low temperature range are observed than for annealed single crystals. The effect of inhomogoneous concentrations on the yield point is generally explained by the fact that a moving dislocation has to by-pass or even disrupt regions with higher impurity content [8-10].

It is possible that in favourable conditions of deformation both these processes will take place by means of the thermo-dynamic energy of the atoms. In this case a strong relationship of yield point to temperature is observed.

As far as the alloys investigated by us are concerned, there may exist some deviation from the static distribution of atoms in the solid solution, which does not exclude the possibility of the reasons mentioned above playing a definite role in strengthening the alloys and intensifying the yield point relationship.

VOL 8 195

3. When observing the yield point of the alloys being studied one ought to take into account the anomalous dependence of yield point on temperature and the rate of deformation.

Similar laws were observed first during the deformation of metastable solid solutions and were usually explained by the decomposition of the solid solution at the time of the deformation. But to an irregular dependence of deforming stresses on temperature and deformation rate one can probably assign other diffusion processes which occur in alloys during deformation under the influence of stresses, e.g. variation in the extent of short range order, transorientation of pairs of atoms or vacancies, uphill diffusion and so on. A similar redistribution of atoms can occur in small volumes, where dislocations are created or even in the stress fields of moving dislocations. They will be accompanied by relaxation of the stresses, decrease in the energy of dislocations and at the same time an arresting of their movement or creation [11,12].

Recently, Shoek [13] has examined one of the possibilities of local redistribution of atoms of dissolved elements in the stress. fields of moving dislocations, when these atoms cause a disturbance of the symmetry of the lattice or when the parameter of the lattice depends on the degree of short range order. In this case, in the field of the moving dislocation there arises a short range order which is broken down on account of thermal movement on removing the dislocation movement. Because of this reconstruction a frictional force arises which depends on the rate of dislocation movement. With infinitely small and infinitely rapid dislocation movement, the arresting force stays equal to zero. At a certain critical rate of dislocation movement which depends on the radius of the ordered zone and vibrating frequency of the atoms, the dislocation will experience a very great resistance from the side of the ordered zone.

From this point of view, one can probably explain the irregular relationship of deforming stresses to temperature and deformation rate.

It should be noted, however, that experimental data existing at the present time does not allow definite conclusions to be drawn about the nature of the processes which accompany shearing plastic deformation in alloys under these or other deformation conditions, the processes which change the temperature relationship of the deforming stresses and the processes which also affect the whole behaviour of alloys under load.

Further investigations, obviously, must be directed towards study of those processes which occur in alloys during shearing plastic deformation.

Disordering of the alloys under the influence of small quantities of impurities is difficult to understand from the point of view of the more widely distributed dislocation hypotheses. According to these theories, plastic deformation is then only the movement of dislocations since the creation of new dislocations occurs during the motion of the old ones. The appearance of foreign atoms or other distortions of the crystal lattice will always only check the movement of the dislocations. However the hypothesis existing formerly allowed the possibility of generating dislocations on distortions of the crystal lattice [14-16]. These presentations have gained greater foundation at the present time, because in Gilman's experiments [17] the possibility was actually shown of forming dislocations during plastic deformation, on certain defects of the crystal lattice. From this point of view disorder of alloys can be explained at low concentrations of impurities by facilitating the generation of dislocations by static distortions of the crystal lattice which occur under the influence of atoms or groups of atoms of the impurity. This does not exclude the possibility of other reasons existing, for instance, interaction of the impurity.

CONCLUSIONS

1. The dependence of the yield point on the solid solution concentration temperature and deformation rate, for Ni-Al alloys has been studied.
2. Strengthening of the solid solutions takes place on alloying Ni with Al, excluding the low concentration region where a decrease of the yield point is initially observed.

VOL. 8 1959

3. As solid solution concentration rises the dependence of the yield point on temperature and deformation rate is strengthened. An irregular relationship of yield point to temperature exists in alloys with 1.5 and 2.93% Al.

4. Experimental data obtained in the present work and also in the study of other alloys in previous works, show that the main reason for strengthening of alloys in shearing plastic deformation is the change in the nature of the fine structure of the solid solution which leads to a fuller use of the interatomic forces of cohesion.

5. More marked in alloys than in pure metals, the change of yield point with temperature and with deformation rates and also the phenomenon of irregular dependence on the temperature show that in the solid solutions studied, the thermally activated processes, which occur at the time of the deformation, affect the growth of shearing plastic deformation.

Translated by W.J. King

REFERENCES

1. A.V. Grin', V.A. Pavlov and I.A. Pereturina, *Fiz. metal. metalloved.* 5, 493 (1957).
2. V.A. Pavlov and I.A. Pereturina, *Fiz. metal. metalloved.* 6, No.4 (1958).
3. N.I. Noskova and V.A. Pavlov, *Fiz. metal. metalloved.* 7, No.3, 400 (1959).
4. M.A. Adams and A.N. Cottrell, *Phil. Mag.* 46, 1187 (1955).
5. M.I. Makin, *Phil. Mag.* 3, 27, 309 (1958).
6. A. Seeger, *Phil. Mag.* 46, 1194 (1955).
7. A. Kelly and O. Chion, *Acta Met.*, 6, No.9, 565 (1958).
8. J.C. Fisher, *Acta Met.*, 2, 9 (1954).
9. Thomas Gurdica and J. Nutting, *J. Inst. Metals*, 58, 86, 7 (1957).
10. P.B. Hirsch, *J. Inst. Metals.*, 86, 13 (1957-58).
11. V.A. Pavlov, *Dokl. Akad. Nauk*, SSSR, 95, 1201 (1954).
12. V.A. Pavlov, M.G. Gaidukov, A.V. Grin' and I.A. Pereturina, *Studies on heat-resisting alloys.* 2, p.257 (1957). Izv. Akad. Nauk. SSSR.
13. G. Shoek, *Phys. Rev* , 102, No.6, 1458 (1956).
14. E. Orowan, *Z. Phys.* 89, 605 (1934), 98, 382 (1936).
15. W. Burgers and G. Burgers. First report on Viscosity and plasticity. Amsterdam (1935).
16. M.V. Yakutovich. Trud. Inst. fiz. metal. Trans. Unit of Physics of Metals. *Urals. fil. Akad. Nauk*, No.12 (1947).
17. J.J. Gilman and W.F. Johnston, G.E.C. Research Lab. Report No.57, RL-1662.
18. H. Suzuki, *Dislocations and Mechanical properties of Crystals.* New York, p.361 (1956).
19. A. Seeger, *Dislocations and Mechanical Properties of Crystals.* New York, p.243 (1956).
20. N. Loudt, *Proc. Phys. Soc.* 1369, 495 (1956).
21. J.S. Erickson and J.R. Low, *Acta Met.* 5, 405 (1957).

VOL 8 195

RELATIONSHIP OF CREEP OF NICKEL-COPPER ALLOYS TO SOLID SOLUTION CONCENTRATION AND DEFORMATION CONDITIONS*

M.G. GAIDUKOV and V.A. PAVLOV

(Institute of Physics of Metals, Academy of Sciences of the U.S.S.R.)

(Received 2 August 1958)

The creep of nickel-copper alloys with 10, 20, 40 and 60% Cu in the temperature range 500-700° is studied. At high deforming stresses, comparable to the yield point and at relatively low temperatures, alloys with high yield point have the smallest creep rate. Under small deforming stresses, appreciably lower than the yield point, and at high temperatures the creep rate increases with higher alloy content. The difference in behaviour of the alloys with variation of deformation conditions is explained by the varying degree of participation of shearing and diffusion plastic deformation in the general process.

VOL. 8 1959

The heat resistance of single-phase solid solutions depends not only on the concentration of alloying elements but also on the test temperature and on the rate of deformation. Thus, for example Kornilov and Pryakhina [1], working with solid solutions of Al-Mg, have shown that at low temperatures of deformation alloys are more resistant with high Mg content but as the temperature is raised, alloys with less Mg become more resistant.

Properties of Al-Mg alloys also depend on the deformation rate. Alloys rich in magnesium, at high creep rates have a high resistance, but at lower rates, the resistance approaches that of pure aluminium [2].

In this way, it can be seen from the example of study of the heat resistance of Al-Mg alloys relative to deformation conditions, that at low temperatures and high creep rates, alloys with high concentration of impurity have the greatest resistance whereas at high temperatures and low creep rates, alloys with a low impurity concentration are more resistant.

This characteristic variance of the heat resistance of alloys with deformation conditions, can be explained, it seems, by a change in the part played by shearing and diffusion deformation [2].

In the present work the creep of nickel-copper alloys of various compositions is studied.

This alloy system is characterized by the fact that with rise of solid solution content the amount of static distortion increases as the copper is increased to 40 per cent and then decreases; the critical temperature and modulus of elasticity fall in the whole range of concentrations [3,4]. The critical temperature depends on the thermal and mechanical treatment [3]. This, apparently, is connected with variation in the degree of short range order (the *K*-state) which may arise in nickel-copper alloys [5,6].

The yield point and temporary resistance increase as the copper content is increased up to 40 per cent and then they decrease. Simultaneously with an increase in the resistance of the alloys, the relationship of yield point to deformation temperature is strengthened [7-9]. The observed principles of change of the mechanical properties with solid solution concentration and deformation temperature in the alloys studied cannot be explained merely by changes in the interatomic cohesion forces.

Strengthening of the alloys, as the tests

* *Fiz. metal. metalloved.* 8, No.3, 426-433, 1959.

show is connected with peculiarities in their fine structure. Change of the yield point with solid solution concentration coincides with the change in the static distortions of the crystal lattice, caused by impurity atoms. This shows that in the case stated static distortion is one of the reasons for strengthening of the alloys. Also it is probable that the unsymmetrical distribution of atoms through the volume of the solid solution plays a not unimportant rôle in increasing the yield point: the formation of atmospheres of impurity atoms around the dislocation and the appearance of short range order. All these factors increase the coefficient of utilization of the interatomic cohesions forces.

Strengthening of the temperature relationship of the yield point in alloys compared with pure nickel shows that in nickel-copper solid solutions to a large extent the effect is that of thermally activated processes of the interaction of the moving dislocation, e.g. with atoms or groups of impurity atoms [9, 10].

The aim of the present studies was to find out the effect of change of composition in the alloys of the Ni-Cu system on their behaviour under creep conditions, when plastic deformation is brought about chiefly by shearing or diffusion mechanism.

MATERIALS AND INVESTIGATION METHODS

The nickel-copper alloys were melted in the precision alloy laboratory of the Institute of the Physics of Metals in a h.f. furnace under a vacuum of 10^{-5} mm Hg. The starting materials were electrolytic nickel mark N0000 (99.99% Ni) and electrolytic copper with overall impurity content of not greater than 0.05 per cent (of which 0.02 per cent was oxygen).

The nickel and copper were melted beforehand in a vacuum to expel any gases present. The ingots were forged into rods of diameter 18 mm from which samples were turned with the headers cut off. The diameter of the working section of the sample was 6 mm, the length of the test section was 50 mm. The samples were annealed at specially selected temperatures in the range 800-900° so as to obtain approximately identical grain size in all the alloys. The experiments were carried out on the TsKTI-2 machine. The temperature during the experiments was maintained constant within the limits $\pm$ 2° and was measured with 2 thermo-couples attached to the samples. The time for testing the samples was as much as 500 hr in some cases.

RESULTS OF THE TESTS

In order to study the behaviour of alloys under load in conditions of shearing or diffusion plastic deformation, the temperature and magnitude of the deforming stresses were selected accordingly.

In order to obtain predominantly shear plastic deformation during the period of creep, the experiments were conducted at relatively low temperatures and high deforming stresses commensurable with the yield point. Diffusion plastic deformation could predominate at high temperatures and low stresses.

Yield point of pure nickel and Ni-Cu alloys is shown in the table [9].

In Figs. 1-3 curves are shown of deformation changes obtained at the moment of loading and for a specified period of creep against alloy contents at a temperature of 500° and effec-

TABLE 1

Temp. °C	Yield point (kg/mm²) for Ni-Cu alloys (Copper content, %)				
	0	10	20	40	60
500	1.5	4.5	6.3	7.5	5.3
600	1.3	4.2	5.6	6.8	5.0
700	1.0	4.0	4.9	6.0	4.7

tive loads corresponding to 9, 2 and 5 kg/mm^2.

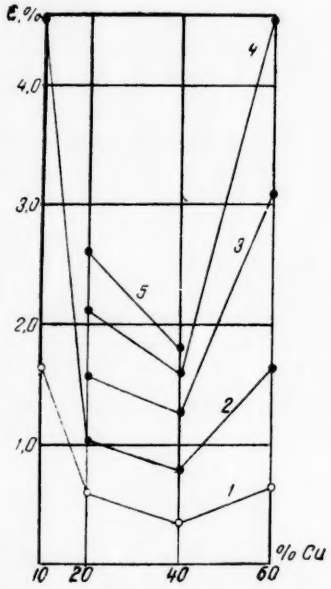

Fig. 1. Relationship of creep elongation at a temperature of 500° and stress of 9 kg/mm^2 to alloy concentration for various testing times:
1. deformation at the moment of loading; 2. 10 hr; *3.* 50 hr; 4. 100 hr; 5. 150 hr.

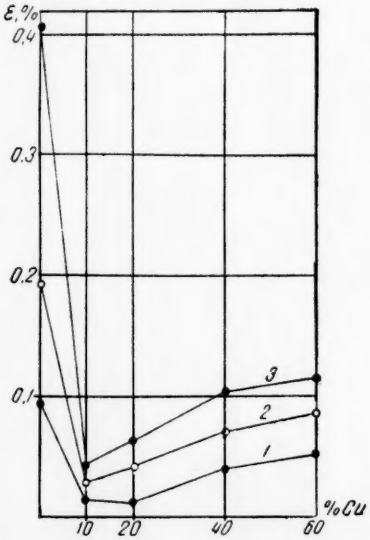

Fig. 2. Relationship of creep elongation at a temperature of 500° and stress of 2 kg/mm^2 to alloy concentration for various testing times.
1. 50 hr; 2. 200 hr; *3.* 500 hr.

Under a load of 9 kg/mm^2 which exceeded the value of the yield point for all the alloys, an appreciable amount of plastic deformation occurs already at the moment the load is applied. As the duration of the experiment is extended, so the deformation gradually increases but the character of the solid solution content plastic deformation curve does not change. For all ranges of creep, the extension at first decreases with increased copper content, reaches a minimum in the 40% Cu alloy, and then starts to increase. Hence the 40% Cu alloy has the lowest creep rate. (See Fig. 1). In this case the creep of pure nickel could not be studied since its yield point was too small.

It is interesting to compare the change of deformation of the creep and yield point in relation to the alloy content. It seems that in a given case, the elongation obtained for a given period of time, or, in other words, the creep rate, bears an inverse relationship to the yield point. At first the yield point rises with increased solid solution content and the creep elongation falls. In 40% Cu alloys the yield point reaches a maximum value and the elongation a minimum. As the added metal concentration is further increased, the yield point falls and the elongation increases.

Consequently, in these deformation conditions, the heat resistance of alloys of different concentration is determined by the level of the yield point. The higher the yield point, the greater the heat resistance of the alloys.

This relationship between yield point and creep rate is explained by the fact that with large deforming loads and therefore, appreciable deformation rates, plastic deformation at low temperatures is brought about by a predominantly shearing mechanism. Because of that, the yield point as a characteristic of the resistance to the plastic shearing deformation for normal elongation maintains a significance also for creep.

Another picture is observed for creep under a load of 2 kg/mm^2 (Fig. 2). In this case the smallest elongation and thus the lowest creep rate is observed for the 10% Cu alloy. This load is considerably lower than the yield strength of all the alloys, so the plastic deformation probably proceeds as a predominantly diffusion mechanism, through diffusion of copper atoms under the influence of thermal movement and the application of external

VOL. 8 1959

loads. Consequently the higher value of the elongation in alloys with a greater copper content in comparison with 10% Cu alloys is apparently connected with higher intensity of the diffusion processes within the volume of the grains. As the solid solution content rises so the number of copper atoms taking part in the diffusion rises besides which the diffusion and auto-diffusion rate rise because the inter-atomic cohesion forces decrease with increased copper content.

The resistance of pure nickel is lower than that of the 10% Cu alloy. In pure nickel plastic deformation may proceed both by a shearing mechanism (so long as the deforming loads are close to the yield point), and also probably to an appreciable degree along the grain boundaries.

The grain boundaries in alloys of all concentrations are strengthened as the tests show. [11]. Hence the higher resistance of the 10% Cu alloy compared with nickel can presumably be explained by the grain boundary strengthening and the higher resistance of the deformation shear. The intermediate case of the relationship of creep to concentration of alloys is observed when the deforming loads equal 5 kg/mm^2. Here plastic deformation proceeds apparently by both the shearing and the diffusion mechanism (Fig.3). A fairly large plastic deformation at the moment when the load is applied is obtained only with the 10% Cu alloy, where as it is appreciably less in alloys of higher copper content. The dependence of the magnitude in alloys of higher copper content. The dependence of the magnitude of deformation on the alloy content corresponds to the development of plastic shear deformation. But the difference in properties among alloys from 20 and 40% Cu was noticeably lowered, which fact evidently is connected with stronger occurrence of diffusion plastic deformation in the 40% copper alloys.

Similar principles are observed in the 600° temperature range at deforming stresses of 5 kg/mm^2. (Fig.4).

The 20-40% copper alloys have the smallest elongations. But because of the great intensity of the diffusion plastic deformation the creep rate of the 60 per cent copper alloy approximates that of the 10 per cent copper alloy.

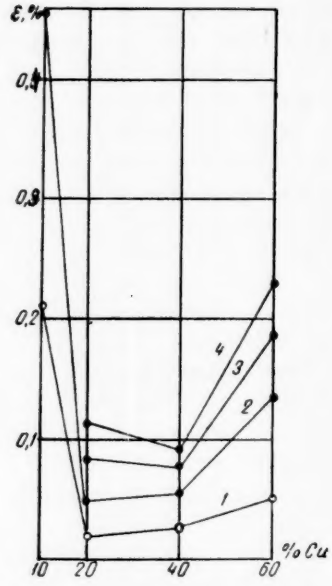

Fig. 3. Relationship of creep elongation at 500° and 5 kg/mm^2 load to alloy concentration for various testing times:
1. deformation on loading; *2.* 50 hr; *3.* 100 hr; *4.* 150 hr.

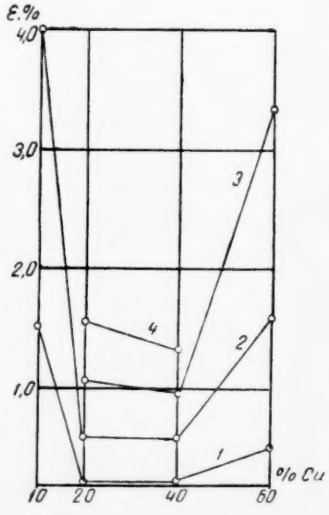

Fig. 4. Relationship of creep elongation at 600° and 5 kg/mm^2 load to alloy concentration for various testing times:
1. 10 hr; *2.* 50 hr; *3.* 100 hr; *4.* 150 hr.

alloy.

Lowering the stress to 2 kg/mm^2 (Fig.5) is accompanied by change in the relationship of elongation to concentration corresponding to

the picture of the development of diffusion plastic deformation. The 10 per cent copper alloy has the greatest resistance. Raising the temperature of deformation from 500 to 600° intensifies the occurrence of the diffusion processes, hence the deformation increases appreciably approaching the time when creep begins; the difference in the deformation, between the 10 per cent copper alloy and alloys of higher copper content is increased because of a softening of the alloys rich in copper (compare Fig. 2).

Similar results however, from a qualitative angle were obtained at a temperature of 700°.

According to test results of several samples of each alloy in similar conditions (test temperature and stress) mean deformation rates on a fixed section of the creep curve were calculated.

Figs. 6 and 7 show these data in logarithmic co-ordinates of deformation vs. alloy composition at temperatures of 500, 600 and 700° and two deforming stresses. It can be seen from Fig. 6 that with a stress of 5 kg/mm^2 and temperature 500° the 20-40% copper alloys have the lowest deformation rate, i.e. alloys with the highest yield point.

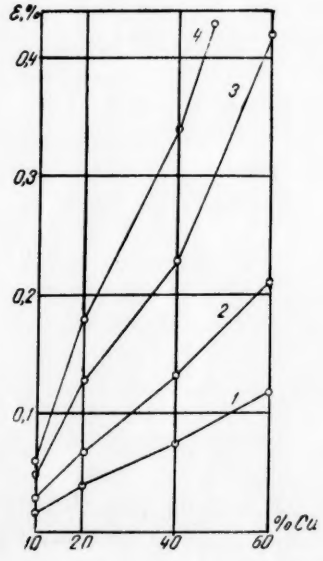

Fig. 5. Relationship of creep elongation at 600° and 2 kg/mm^2 load for various loading times: *1*. 50 hr; *2*. 100 hr; *3*. 200 hr; *4*. 300 hr.

Raising the testing temperature from 600 to 700° still does not change the character of this relationship, but in the 700° temperature range the deformation rate of the 20-40 per cent copper alloys remains equivalent to that of 10 per cent copper. These changes, it seems, are connected with the increased part played by diffusion plastic deformation in the high temperature range in copper-rich alloys.

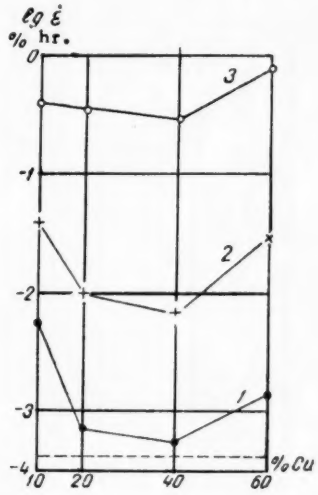

Fig. 6. Relationship of the logarithm of the creep rate to concentration of Ni-Cu alloys with load of 5 kg/mm^2 and temperatures: *1*-500°; *2*-600°; *3*-700°.

Under the influence of a stress of 2 kg/mm^2 (Fig. 7) in all temperature ranges studied the above-mentioned principle is observed for small stresses. The deformation rate of 10 per cent copper alloys appears to be the smallest compared with that of alloys of higher copper content.

It is necessary to note also that at 500° experimental data on creep tests agree with results of experiments on relaxation of stresses carried out earlier on these same alloys. [12].

In Fig. 8. for comparison, values of external stresses are shown as those remaining after relaxation of 84 hr for two initial stresses σ_0, 2 and 4 kg/mm^2. With the higher initial stress (4 kg/mm^2) the residual stress in the 10 per cent copper alloy was less, hence the rate of relaxation of this alloy was greater compared with that of the 20-40 per cent copper alloys. With initial stresses of 2 kg/mm^2 conversely, the 10 per cent copper

VOL. 8 1959

alloy had a lower rate of relaxation. Thus, despite the difference in methods of testing for creep and for relaxation of stresses the relationship of resistance to composition of an alloy and to deformation conditions appears to be qualitatively identical.

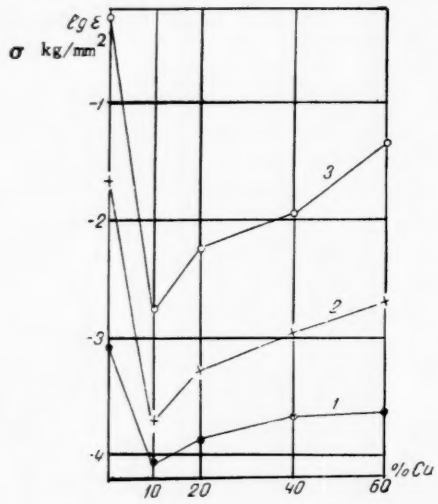

Fig. 7. Relationship of the logarithm of creep rate to concentration of Ni-Cu alloys with load of 2 kg/mm^2 and temperatures:
1. 500°; *2.* 600°; *3.* 700°.

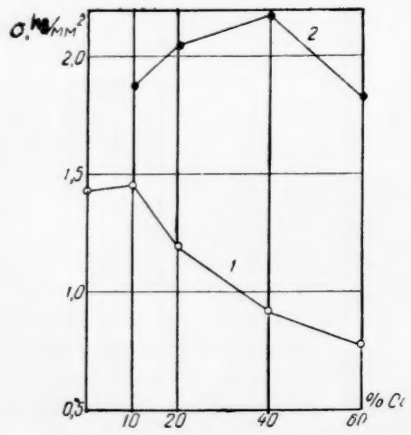

Fig. 8. Relationship of the residual external stresses in the alloys after tests on relaxation of stresses for 84 hr at 500°:
1. σ_0 = 2 kg/mm^2; *2.* σ_0 = 4 kg/mm^2.

CONCLUSIONS

1. The creep rate of nickel copper alloys in the temperature range 500-700° depends on the composition of the alloy and on deformation conditions.
2. At relatively low temperatures and high deformation stresses commensurate with the yield point at which the deformation in all probability proceeds primarily by a mechanism the creep rate is inversely dependent on the yield point. The higher the yield point the lower the creep rate. Under these deformation conditions the 40 per cent copper alloys have the highest resistance.
3. In the high temperature range and at fairly low deforming stresses, appreciably less than the yield point the deciding factors are the diffusion processes which occur under loading. In this case creep rate increases with increasing solid solution content.
4. In the general case the behaviour of alloys under loading is determined by the part played by shearing and diffusion plastic deformation.

Translated by W.J. King

REFERENCES

1. L.I. Kornilov and LII. Pryakhima, *Dokl. Akad. Nauk. SSSR.*, 87, No.6, 971 (1952).
2. M.G. Gaidukov and V.A. Pavlov, *Fiz. metal. metalloved.* 7, No.2, 254 (1959).
3. N.I. Noskova and V.A. Pavlov, *Fiz. metal. metalloved.* 6, No.2, 334 (1958).
4. V.A. Pavlov, N.F. Kryuchkov and I.D. Fedotov, *Fiz. metal. metalloved.* 5, No.2, 374 (1957).
5. H. Thomas, *Z. Phys.*, 129, 219 (1951).
6. W. Koster and W. Schule, *Z. Metall.*, 48, 592 (1957).
7. E. Osswald, *Z. Phys.*, 83, No. 1-2, 55 (1933).
8. W. Broniewski, S. Kulesza, *Metaux a. Corrosion*, 12, No.140, 67 (1957).
9. V.A. and Pavlov and I.AO Pereturina, *Fiz. metal. metalloved.* 6, No.4, 717 (1958).
10. A.V. Grin', V.A. Pavlov and I.A. Pereturina *Fiz. metal. metalloved.* 5, No.3, 493 (1957).
11. V.I. Syutkina and E.S. Yakovleva, *Fiz. metal. metalloved.*, 7, No.5 (1959).
12. M.G. Gaidukov and V.A. Pavlov, *Fiz. metal. metalloved.* 6, No.3, 517 (1958).

SOME PECULIARITIES OF TRANSFORMER STEEL ON RAPID HEATING. II. KINETICS OF TEXTURE FORMATION*

P.D. IZBRANOV, V.A. PAVLOV and H.M. RODIZIN

Institute of the Physics of Metals Academy of Sciences of the U.S.S.R.

Sverdlovskii Pedagogic Institute

(Received 13 August 1958)

The formation of a recrystallization texture in transformer steel was studied in relation to the rate of heating of samples by an electric current or in a salt bath. The highest heating rate was 1000-1100°/sec. It was shown that the first stage of recrystallization has a texture similar to the deformation texture. During the subsequent development of recrystallization this texture is gradually replaced by another generally observed in transformer steel when it is isothermally annealed.

VOL. 8 1959

During a study of the mechanism of the nucleation of recrystallization, the question which arises above all others, is that concerning the structure of those regions of the deformed crystal in which the nucleation rate of new grains is a maximum. Investigators usually strive to obtain these data by comparing orientation distribution of new grains with the orientation distribution of particles of the deformed crystal [1].

However, investigations which have been carried out up to the present time, as a rule, were done at small rates of heating and for rather long holding times. Moreover, collective recrystallization may have occurred in the material in the process of which an essential change in the character of the orientation distribution of the grains is possible. This may lead, in particular, to an incorrect conclusion about the relative orientation relationship of recrystallization nuclei with the deformed crystal portions.

To obtain more reliable data it is expedient to conduct studies on the orientation of recrystallization nuclei obtained by high heating rates such as can be obtained either by passing an electric current through samples or by heating thin samples in a salt bath.

Similar studies are also interesting from the point of view of studying the peculiarities of recrystallization at high heating rates by the electric current. To explain high recrystallization rates which are observed in this case an assumption is made concerning the non-uniform heating of microparticles which have different specific electrical resistance [2, 3]. The influence of the electric current on the nucleation of recrystallization if in a given case it takes place, apparently, can be observed from the variation of the character of the orientation distribution of new grains.

It is expedient to use a high rate of heating also to study the process of the formation and development of the recrystallization texture particularly in transformer steel. In this case reliable information can be obtained about the texture arising in the first stage of recrystallization and the nature of its further development.

On the basis of much work devoted to the study of the recrystallization texture of transformer steel, it can be considered an established fact that this texture depends on previous deformation not only for sharpness

* *Fiz. metal. metalloved.* 8, No.3, 434-439, 1959.

but also for its type. For large deformations where the reduction is 90-95 per cent, Barret, Ansel and Mehl [4] have established by the X-ray diffraction method that the recrystallization texture is characterized basicly of two predominant orientations.

1. The plane of type $\{100\}$ parallel to the plane of rolling, direction of type $\langle 011 \rangle$ makes an angle of 17° with the direction of rolling.

2. The plane $\{112\}$ parallel with the plane of rolling and the direction $\langle 011 \rangle$ making an angle of 17° with the direction of rolling (RD).

These orientations can be expressed in the following manner:

1. $\{100\}$, $\langle 011 \rangle \sim 17°$ with RD
2. $\{112\}$, $\langle 011 \rangle \sim 17$ with RD

The said authors also note that there is a third predominant orientation, not so easily perceptible.

3. $\{111\}$, $\langle 112 \rangle$.

They came to the conclusion also that this type of recrystallization texture does not depend on the total reduction in the 60-95 per cent range.

But, Bozorth [5] and Burwell [6] also studying the recrystallization texture by X-ray diffraction methods of transformer steel prepared by Goss's method, came to the conclusion that it can be characterized on the basis of one principal orientation of type $\{110\}$, $\langle 011 \rangle$, i.e. the plane $\{110\}$ parallel to the plane of rolling and direction $\langle 001 \rangle$ parallel to the direction of rolling.

Yakovleva [7] studied the recrystallization texture by an optical method, for a 67 per cent reduction of transformer steel. Her results were in agreement with those of Bozorth.

Grigorov and Izbranov [8] also by an optical method determined the recrystallization texture in transformer steel, both for larger deformations – 95 per cent and for smaller – 75 per cent. According to their data for large deformations the first orientation indicated by Barret ($\{100\}$, $\langle 011 \rangle \sim 17°$) is expressed appreciably more strongly than the second ($\{112\}$, $\langle 011 \rangle \sim 17°$). With a deformation of 75 per cent their results coincided with those of Yakovleva.

It has also been found by a magnetometric method that the character of the magnetic anisotropy changes as the deformation increases on rolling prior to recrystallization.

All the above tests were carried out on transformer steel which had been given an isothermal recrystallization anneal. The annealing time was several hours in the various cases. The aim of the present work is to study the formation and development of the recrystallization texture of transformer steel at high heating rates.

MATERIALS AND MEASURING METHODS

Transformer steel with a silicon content of 3.54 per cent served as material for the tests. The reduction was 75 per cent in one case and 95 per cent in the other. Samples in the form of small bars 15 x 100 mm with a thickness of, 0.25 mm were heated without any holding time by an electric current. Other samples of thickness 0.11 mm were heated to the desired temperature. The samples were cooled in air.

The temperature of the samples during heating with the electric current was measured by means of a ballistic galvanometer connected to the metal of a thermocouple. All experiments on heating the samples by the electric current were conducted on the apparatus of Rodigin [10].

The microstructure in the recrystallized samples was studied and the texture was determined by X-ray diffraction. A special camera was prepared for radiography which permitted the sample to be displaced during exposure in two mutually perpendicular directions.

RESULTS OF THE TESTS

In Figs. 1, 2 and 3 X-ray diffraction patterns are shown corresponding respectively to a cold-deformed sample, one recrystallized by heating by the current to 770° at the rate of 1100°/sec. and one recrystallized in a salt bath by holding it at 770° for a period of about 2 sec.

VOL 8 195

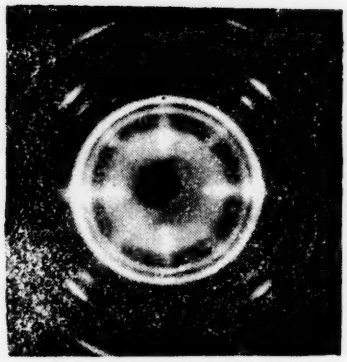

Fig. 1. X-ray diffraction pattern of cold-deformed sample.

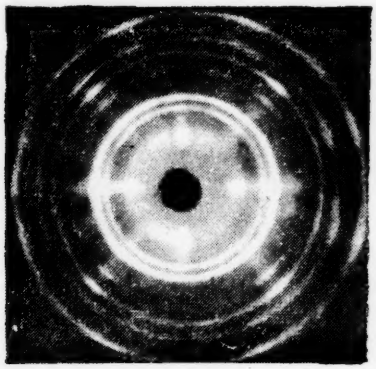

Fig. 2. X-ray diffraction pattern of sample recrystallized by heating with a current at a rate of 1100°/sec to a temperature of 770°.

The reduction of these samples was 75 per cent. In Fig.4 an X-ray diffraction pattern of a sample reduced 95 per cent and recrystallized in a salt bath at a temperature of 725° is shown. Time held at this temperature was about one second. In Fig.5 is shown the structure of a sample which is obtained by this method of recrystallization. From Fig.5 it can be seen that the first stage of recrystallization has already set in, and the whole volume of the sample is filled with new equiaxed grains.

Comparing Figs. 1, 2, 3 and 4 it is easy to note that in these conditions of experiment, independent of the method of heating, the orientation distribution of new grains in recrystallized samples corresponds to the orientation distribution of portions of the deformed material. In other words, the texture of the first stage of recrystallization corresponds to the deformation texture.

But it is known, that the deformation texture remains unchanged in the polygonization process [11] which is shown more precisely when course-grained samples are annealed predominantly those given only slight deformation. In poly-crystalline, heavily-deformed metals clearly defined polygonization before recrystallization is not usually observed [12].

In our experiments the material was heavily deformed, hence the structure shown in Fig.5 more likely exhibits not sub-grains or blocks (which are not equiaxed) but new equi-axed grains arising as a result of the first recrystallization stage.

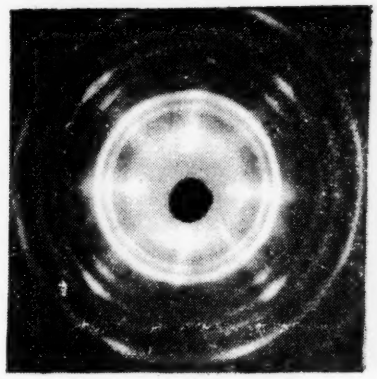

Fig. 3. X-ray diffraction pattern of sample recrystallized in the salt bath at a temperature of 770°; held for about 2 sec.

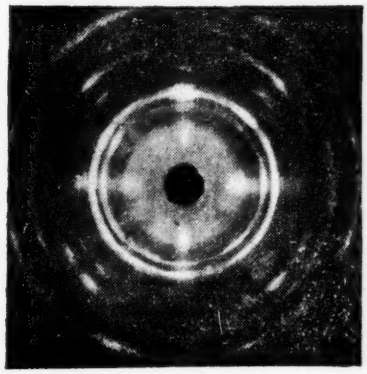

Fig. 4. X-ray diffraction pattern of sample recrystallized in the salt bath at a temperature of 725°; held for 1 sec.

VOL. 8 1959

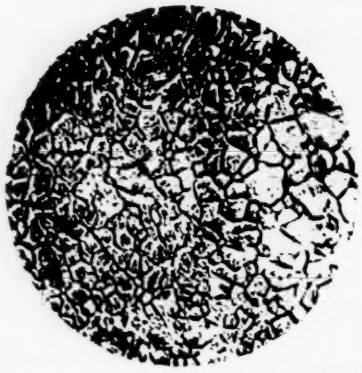

Fig. 5. Photo-micrograph of the structure of the recrystallized samples x 320.

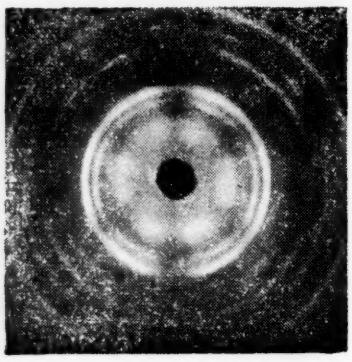

Fig. 6. X-ray diffraction pattern of sample recrystallized in the salt bath at a temperature of 725°; held for 1 min.

Comparing the diffraction patterns of Figs. 1 and 2, we may conclude that the recrystallization texture in the case (Fig. 2) is expressed even somewhat more strongly than the deformation texture (Fig. 1). This strengthening of the texture at the beginning of annealing of the deformed samples was observed by Grigorov [13] by means of the magnetometric method. But he explained this strengthening as a process of recovery and not as the first recrystallization stage.

On increasing the annealing time in the salt bath and as the recrystallization process progresses, a gradual break-up of the first texture takes place and it is replaced by a new texture, the one usually observed in transformer steel recrystallized by isothermal annealing for long periods.

At a certain period in the recrystallization process such a condition is reached that almost complete absence of a texture is revealed. In Figs. 6 and 7 X-ray diffraction patterns are given for samples, reduced 95 per cent and recrystallized in a bath at 725° with holds of 1 min and 5 hr. By holding for 1 min there is almost an recrystallization texture corresponding to the type of deformation condition but a new texture is not yet produced to any marked extent. After annealing for a period of 5 hr intensity maxima can be plainly seen on the X-ray diffraction pattern corresponding to a new texture.

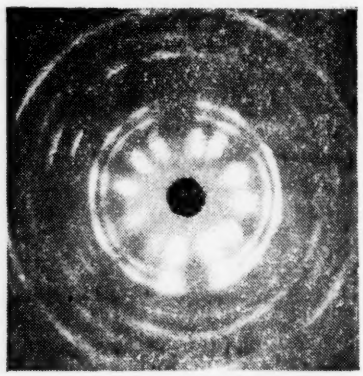

Fig. 7. X-ray diffraction pattern of a sample recrystallized in the salt bath at a temperature of 725°; held for 5 hr.

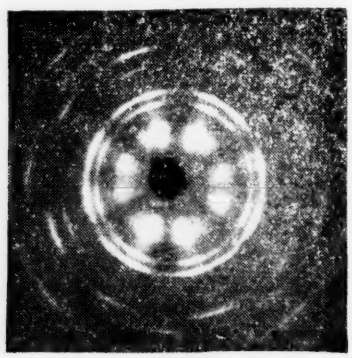

Fig. 8. X-ray diffraction pattern of a sample recrystallized by heating with electric current at the rate of 840°/sec to 1170°.

As the annealing temperature is raised when the samples are heated by the electric current the nature of the texture change is similar to that obtained with longer periods of annealing in the salt bath. In Fig. 8 an X-ray diffraction pattern is shown of a sample reduced also by 95 per cent and recrys-

tallized by heating with the current at a rate of 840° sec to 1170°. On the X-ray diffraction pattern it is clearly seen that the type of recrystallization texture is the same as that obtained by annealing in the salt bath for a period of 5 hr.

This is probably explained by the fact that despite the short interval of time to heat to high temperatures the recrystallization develops so rapidly that it is practically impossible to capture the first stage of formation of a texture.

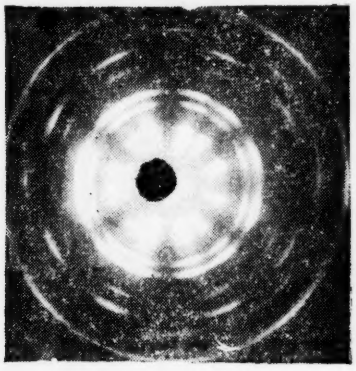

Fig. 9. X-ray diffraction pattern of sample recrystallized at a temperature 1000°: held for 1 hr.

In Fig. 9 an X-ray diffraction pattern is shown of a sample reduced 95 per cent and recrystallized by heating in the usual furnace (in a vacuum) at 1000° for a period of 1 hr. Comparing Fig. 9 with Figs. 7 and 8 one may conclude that the nature of the recrystallization texture in these samples is fundamentally the same.

In all the X-ray diffraction patterns the rolling direction is vertical.

CONCLUSIONS

From the results obtained, the following conclusions can be made:

1. Textures of two types are observed in the recrystallization of transformer steel.
2. When heavily deformed transformer steel is recrystallized (with a clearly defined deformation texture) those recrystallization nuclei whose orientation coincides with that of the particles of the deformed crystal are most likely to be produced. Hence the texture of the first stage of recrystallization is similar to that of deformation texture.
3. As the process of recrystallization progresses further, this pattern is replaced by another which is usually observed in transformer steel after isothermally annealing.
4. The indicated rates of electrical heating and density of current, do not show a marked effect on the mechanism of the formation of new grains from the point of view of orientation relations.
5. High rates of recrystallization which are observed for rapid heating by the electric current or by heating thin samples in a salt bath are connected it seems, with the fact that to a significant extent the interval of recovery before recrystallization is decreased; also, it is possible that there is less redistribution of impurities.
6. When transformer steel is heated rapidly to high temperatures by the electric current (above 1000°) a recrystallization texture arises substantially similar to that of recrystallization by isothermal annealing.

Translated by W.J. King

REFERENCES

1. M. Kornfel'd, *Zh. eksp. teor. fiz.* 7, 450 (1937).
2. N.V. Geveling, Superficial electro-tempering United Scientific and Technical Press, 1936.
3. A.I. Gardin, *Metallurg.* No.3 (1938).
4. Barret, Ansel and Mehl. *Trans. A.I.M.E.*, 125 (1937).
5. R.M. Bozorth, *Trans. Am. Soc. for Metals.* 33, 1107 (1935).
6. J.T. Burwell, *Metals Technology*, 7 (1940).
7. E.S. Yakovleva, *Zh. teor. fiz.* 9, No.14, 1280 (1939).
8. K.V. Grigorov, and P.D. Izbranov, *Fiz. metal. metalloved.* 7, No.2 (1959).
9. K.V. Grivorov, G.P. Blokhin, E.A. Korzun and M.Ya. Zakutner, *Fiz. metal. metalloved.* 1, No.1 (1955).
10. N.M. Rodigin, *Trud. Inst. fiz. metal. Urals fil. Akad. Nauk SSSR.* No.9 (1946), No.13 (1951).
11. S. Grussard, *Metaux Corrosion-Industries,*

VOL. 8 1959

No. 330, 47 (1953).

12. A. Guinier, *Metaux Corrosion-Industries*, No. 337, 339 (1953).

13. K.V. Grigorov, *Izv. Akad. nauk SSSR. ser. fiz.* 9, No. 6, 679 (1947).

INTERNAL FRICTION OF METASTABLE SOLID SOLUTIONS*

B.G. LIVSHITS, Iu.S. AVRAAMOV, V.B. OSVENSKII, S.O. MEBZENNAIA AND L.N. BELIAKOV

-Experimental results of work on the study of solid solutions of different composition are given. It is shown that phase transformations in alloys can be investigated by means of the method of internal friction even in cases in which the difference between the atomic diameters of the solvent and the dissolved element is small.

VOL. 8 1959

The feasibility of an effective use of the method of internal friction in investigating phase transformations of metals and alloys has been mentioned in a number of works [1, 2]. The majority of them are associated exclusively with the study of the processes of ageing of different alloys possessing a structure of interstitial solid solutions. In this case the method of internal friction is exceptionally sensitive structurally, and can be used for determining the change in the composition of solid solutions [3-5] in the course of their phase evolution.

Attempts have also been made to apply this method to investigations of phase transformations which take place during the heat treatment of alloys with the structure of a substitutional solid solution. In the course of his researches on brass (30% Zn), Ke Tin-sui [5] obtained a characteristic peak due to relaxation conditioned by the migration of zinc atoms in the field of elastic stresses. A similar effect was observed by Nowick [7] in connexion with a silver-zinc alloy. The difference in atomic diameters in the latter case is greater than in the case of a copper-zinc alloy, and the effect is correspondingly greater. It is shown by the authors of this work that the extent of the effect depends on the difference between the atomic diameters of the dissolved component and the solvent: the greater the difference, the greater the effect. A likely mechanism of relaxation in substitutional solid solutions has been suggested by Zener [6] and Nowik [7] The method of internal friction was also used in investigating the process of the formation of an ordered arrangement of β-brass [9], and iron with 16% aluminium [8]. The authors showed that the behaviour of a solid solution in a perfectly ordered state is the same as that of pure metal, its internal friction being a gradually increasing function of the temperature. When measuring the internal friction of alloys in a disordered condition, the effects resulting from relaxation conditioned by the migration of the dissolved atoms in the field of elastic stresses are observed in the temperature relation of internal friction. In each case the difference between the atomic diameters of the solvent and the dissolved component (structural factors) was found to be considerable.

It was, therefore, assumed that the method of internal friction could also be applied to investigations of substitutional solid solutions, provided their structural factor was high enough. Obviously, this concept requires elucidation. Even in cases in which the difference between the atomic diameters is small and the content of the alloying element low, a relaxation peak connected with the presence of that element in a solid solution, can appear on the temperature relation, provided there is a tendency in the system towards a change in the structural condition, i.e. when that system is in a state of metastability (for example, a tendency towards orderliness, or phase separation, or formation of K-state).

* *Fiz. metal. metalloved.* 8, No.3, 440-448 1959.

Fig. 1

Alloy No.	Element content in %						
	Fe	Ni	Cr	Mo	Mn	C	S
1	0.36	75.1	–	Traces	22.8	0.037	0.15
2	0.16	74.5	–	1.34	23.2	0.037	0.08
3	0.24	75.3	–	2.77	21.8	0.040	0.17
4	24.15	75.0	–	–	–	0.0094	–
5	22.50	76.8	–	1.04	–	0.0094	–
6	20.95	74.5	–	3.08	–	0.0093	–
7	18.80	76.0	–	5.15	–	0.0092	–

The assumption is borne out by the results of the experiments given below.

The method of measuring the temperature relation of internal friction was used in investigating Ni_3Mn alloy of a stoichiometric composition and the alloys of a similar composition with molybdenum, with the content of the latter amounting to 1.34 and 2.77 per cent. The same method was also used when investigating the Ni_3Fe type of alloys, with and without molybdenum, as well as an alloy of the EI437A type (nimonic).

The chemical composition of the alloys examined is recorded in the table above.

The measurement of internal friction was carried out on a wire specimen 300 mm long and 0.7 mm in diameter by means of a vacuum relaxator.

Ni_3Mn is an alloy assuming an ordered arrangement, its Kurnakov point being in the neighbourhood of 350° [10, 11]. Two peaks *A* and *B* with their maxima at 120° and 290° (fig. 1) were revealed on the temperature relation of internal friction of Ni_3Mn quenched from a temperature above that of the formation of an ordered arrangement.

The maximum height of the peaks above the base was 21 per cent. In form, they were washed out maxima.

In its quenched condition, Ni_3Mn is a solid solution assuming an ordered arrangement. The atoms of nickel and manganese are statistically distributed over the crystal lattice points, the solid solution being in a state of metastability resulting from the high level of free energy of the system. An increase in the degree of orderliness should result in a lowering of the level of free energy. During the determination of internal friction a quenched alloy does its best to lower the level of free energy by forming an ordered arrangement in the stress field. This process has its fixed times of relaxation for each atom taking part in the formation of an ordered arrangement, and results in the appearance on the curves of the temperature relation of internal friction of two peaks which can be suitably termed "the peaks of metastability during the period of formation of an ordered arrangement."

The emergence of the effects in the case of a comparatively small structural factor – (the difference in atomic diameters of nickel and manganese is small) – is evidently connected with the relaxation which is taking place in torsional vibrations, this relaxation being due to the movement of nickel and manganese atoms as they strive to depress the common level of free energy. In such a case an increase in the degree of adjustment in the course of tempering should lead to a decrease in the size of peaks of metastability, whilst on attaining a complete order there should take place uniform fading away of internal friction with the temperature.

Such a result, experimentally obtained, is illustrated in fig. 1. After a temper at 320° lasting fifteen min, the size of the peaks *A* and *B* decreased from 21 to 14 per cent. On raising the period of tempering to twenty min, their size was reduced to 9.5 per cent, and after a half hour temper, the peaks

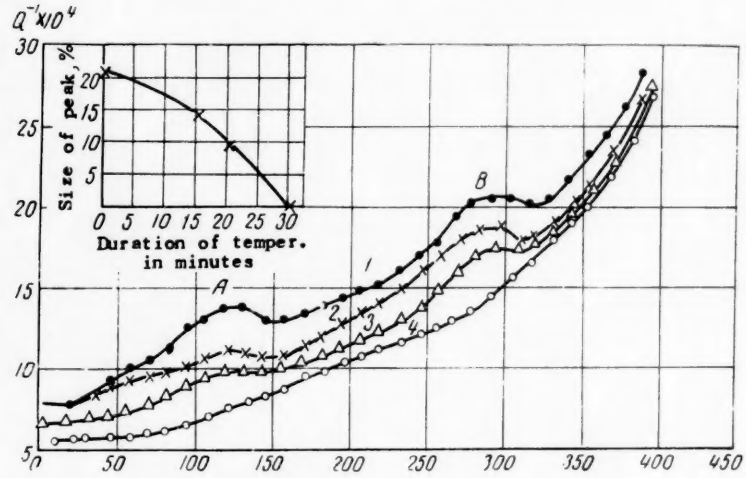

Fig. 1. Effect of heat treatment on temperature relation of internal friction of Ni_3Mn alloy:
1. Quenching; 2. Quenching – temper. for 15 min; 3. Quenching – temper. for 20 min; 4. Quenching – temper. for 30 min. Frequency 0.5 c/s.

VOL. 8 1959

disappeared. Furthermore, on increasing the period of tempering the level of internal friction fell. These facts confirm our assumption that *A* and *B* have a connexion with the orderly disposition of the atoms and represent peaks of metastability during the process of the formation of an ordered arrangement. The absence of any connexion of the peaks with the presence of carbon in the alloy, as well as their non-deformational origin, are verified by the following experiment.

The peaks *A* and *B* are preserved in the temperature relation of internal friction in the case of the deformed (to the extent of 75 per cent) Ni_3Mn alloy, the common level of internal friction at the same time rising considerably (fig. 2). The presence of the deformation peak *D* can similarly be attributed to the state of metastability. The system of a deformed metal posses a higher level of free energy in comparison with the state of recrystallization. For this reason the field of elastic stresses causes additional relaxation – (with its collection of relaxation periods) – due to the change of position of the atoms striving to depress the level of free energy.

There is an additional peak *C* with its maximum at 316° in the carburized Ni_3Mn alloy (containing 0.35% C). The emergence of this peak is explained by the diffusion of carbon atoms into the field of elastic stresses. In this instance peak *A* retains its shape and value and peak *B* does not appear at all, apparently owing to the rapid rise of the curve of internal friction due to the diffusion of carbon atoms under stress.

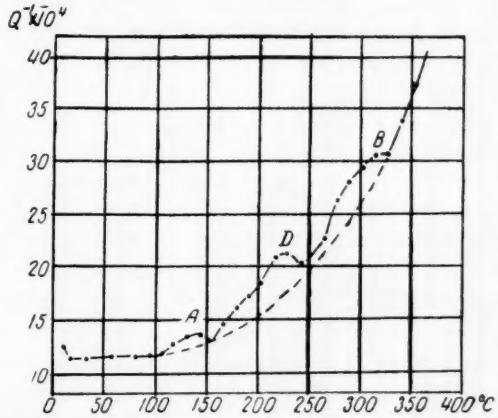

Fig. 2. Effect of deformation on internal friction of Ni_3Mn alloy. Frequency 0.5 c/s.

The same diagram illustrates the influence of heat treatment on the temperature variation of internal friction. These results bear out the results earlier arrived at.

The study of the effect of the alloying of Ni_3Mn solid solution with molybdenum has

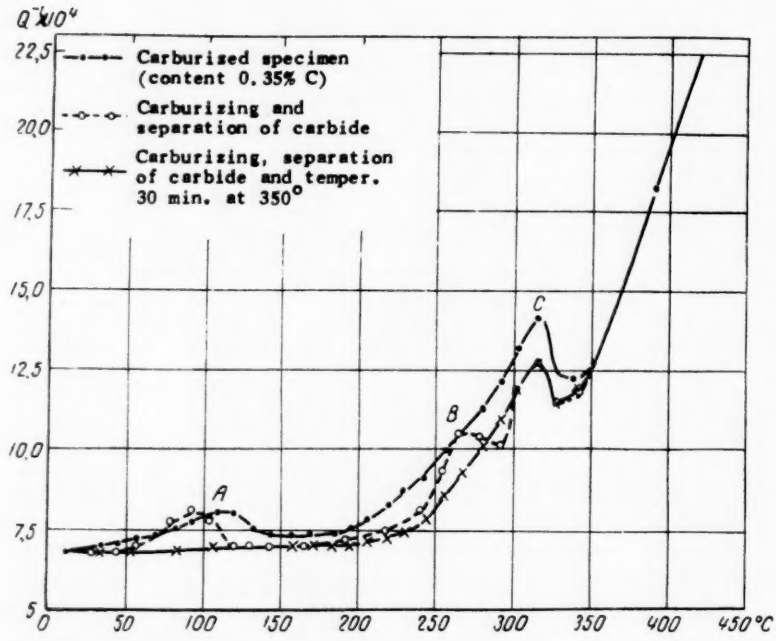

Fig. 3. Effect of carbon content on temperature relation of internal friction of Ni_3Mn alloy. Frequency 0.56 c/s.

shown that two other maxima, *M* and *C*, appear on the temperature relation of internal friction at the temperatures of 52° and 316° (see fig. 4). The maxima at 120° and 290° are slightly displaced in temperature and decrease in size. In our study of the temperature relation of internal friction of Ni_3Mn without molybdenum, the peak at 316° was found to be due to the diffusion of carbon atoms into the field of stresses, but it only appeared when the carbon content of the alloy was sufficiently high (tenths per cent). In the case of Ni_3Mn alloyed with molybdenum, the peak at 316° emerges when the entire content of carbon is only 0.037%. This carbon origin of the peak is confirmed by the fact that the height of the peak at 316° rises simultaneously with the raising of the carbon content to 0.23%.

The appearance of a maximum at 316° in Ni_3Mn alloyed with molybdenum when the content of carbon is low can be explained according to the pattern suggested by Ke Tin-sui [12, 13]. Upon the introduction of molybdenum into the solid solution of Ni_3Mn – (it is hypothetically assumed that the peak at 52° is due to the diffusion of the atoms of molybdenum in the field of elastic stresses) – a carbon peak of relaxation is formed at 316° even when the amount of carbon in the solid solution is low, which fact is due to the spinning of a molybdenum-carbon couple in the field of elastic stresses (carbon-molybdenum exchange).

An experimental verification of the possibility of the appearance of relaxation peaks even in the case of a low content of dissolved atoms, at the expense of the emergence of similar exchange couples, is set forth in Makhukov and Livshits' work [14].

It has been shown by experiment that the addition of molybdenum to Ni_3Mn results in a decrease of the degree of development of an ordered arrangement, i.e. molybdenum has the effect of concentrational derangement. This explains the decrease in size of peaks *A* and *B* upon the introduction of molybdenum into the solid solution.

During the process of the formation of an ordered arrangement the height of the peaks of metastability is the greater the bigger the difference of free energies of an alloy in that condition, and in the ordered state. Upon the introduction of molybdenum into Ni_3Mn a deterioration in the degree of order

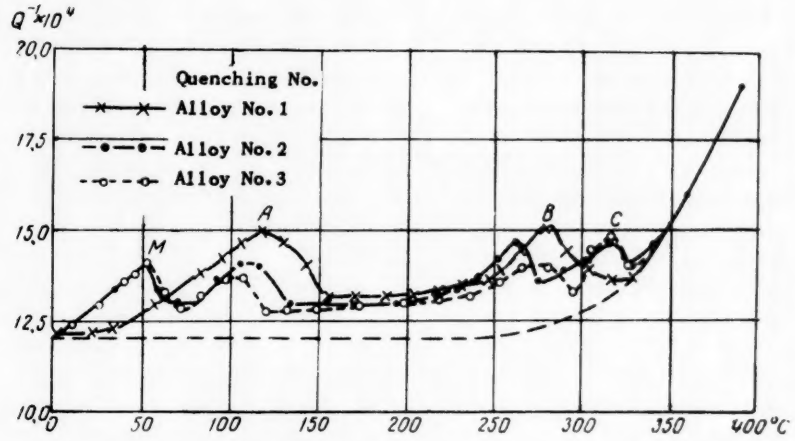

Fig. 4. Temperature relation of internal friction of alloys of Ni_3Mn type differently alloyed with molybdenum. Frequency 0.59 c/s.

takes place and with it also a decrease of free energy in its quenched and tempered states, and, therefore, the size of the peaks of metastability should likewise decrease in the course of the formation of an ordered arrangement.

This can be seen when comparing the temperature relation of internal friction of Ni_3Mn containing molybdenum with the alloys with 1.34-2.77 per cent of the latter element.

Fig. 5 shows the effect of heat treatment on the temperature relation of Ni_3Mn with 1.34% molybdenum. A similar result is also obtained when the content of molybdenum amounts to 2.77 per cent.

Peaks *M*, *A* and *B* gradually decrease in size with the increase of the periods of tempering, and after one hour's tempering these peaks completely disappear. At the same time the temperature dependence of internal friction of Ni_3Mn alloyed with molybdenum becomes a gradually increasing function of the temperature. There is only one maximum on the curve at 316° due to carbon diffusion. The reduction of peak *M* in size in the case of short periods of tempering and its subsequent complete disappearance, indicates that the atoms of molybdenum do not just cause a concentrational derangement in the solid solution but in some way they react chemically with the atoms of nickel and manganese. It is probable that during the process of tempering the atoms

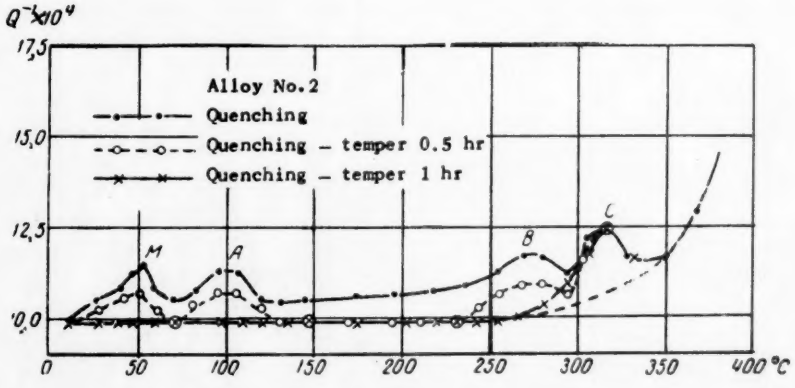

Fig. 5. Effect of heat treatment on temperature relation of Ni_3Mn alloy containing 2.77% molybdenum. Frequency 0.59 c/s.

of molybdenum form stable zones with nickel and manganese (of the Guinier-Preston type), as a result of which they are rendered incapable of exchanging freely their position in the field of elastic stresses, with the result that the characteristic peak at 52° is absent from the temperature relation of internal friction.

No peaks of metastability can be observed in Ni_3Fe during the formation of an ordered arrangement in spite of the fact that it is an alloy which assumes such an arrangement. This is possibly due to a small difference in free energies of the adjusted and unadjusted states, i.e. difference of the bonding energies of these two states is small. This is also borne out by the fact that the addition of molybdenum to Ni_3Fe results in the elimination of the process of formation of an ordered arrangement [16, 17], and the alloy becomes inert towards any change in electric resistance during the heat treatment. However, the introduction even of 4% molybdenum into the solid solution of Ni_3Mn reduces the relative degree of adjustment only by 50 per cent.

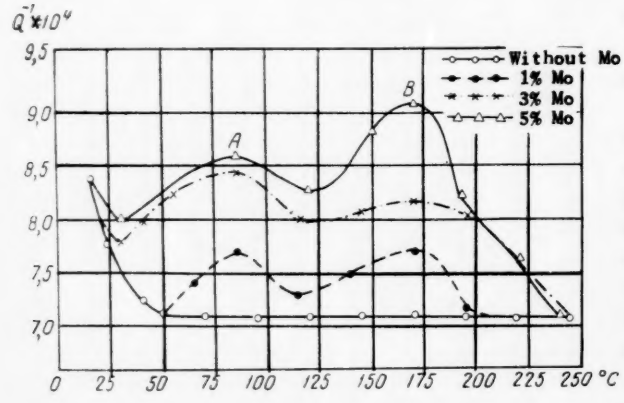

Fig. 6. Variation of internal friction in relation to molybdenum content in Ni_3Fe alloy. Frequency 0.8 c/s.

Livshits and Ravdel' [16] established the fact that in Fe-Ni-Mo alloys containing more than 1% molybdenum the *K*-state, characterized by an abnormal rise in electric resistance and volumetric effect, develops within the temperature range of 350-450°. This state apparantly has a connexion with the formation in the solid solution of zones of the Guinier-Preston type. In measuring the internal friction of Ni_3Fe alloyed with molybdenum (fig. 6), two peaks were observed in the range of low temperatures, one around 85° (peak *A*), the other at 170° (peak *B*). Apparently in the interval between 100 and 150° there takes place a superimposition of the two peaks, and, therefore, the internal friction does not come down to the level of an alloy containing no molybdenum. When the molybdenum content amounts to 1%, the size these peaks is 8 per cent, which figure is above that of the error of observation. On increasing the molybdenum content to 3% the size of peaks of *A* and *B* rises to 19 per cent, and when the content of molybdenum is raised to 5%, it rises to 27%. Here it should be noted that not in all cases of different specimens containing 5% of molybdenum, there was obtained an independent peak *A* at 85°, as it sometimes degenerated into an inflexion and appeared as though it were part of peak *B*. This was probably due to the fact that peak *A* had been superimposed by the greater in size peak *B*.

We failed in our endeavours to determine the configuration of small peaks. However, in all cases the maximum of internal friction was observed at 170° (peak *B*), and it was also found that nearly every specimen had a second maximum at 85° (peak *A*).

It is clear from the above results that the size of peaks increases with the rise in the content of molybdenum. The absence of such peaks in the case of Ni_3Fe alloy confirms our assumption that peaks *A* and *B* have some connexion with the presence of molybdenum atoms in the solid solution. Moreover, in these alloys a carbon peak appears at 260° when the content of carbon in them is high, and in the case of deformed specimens, a peak is obtained at 220°. The above mentioned peaks *A* and *B* can be observed when measuring internal friction of the specimens quenched in water from high temperatures (of the order of 900°). In this case there is no formation of *K*-state in the solid solution, and molybdenum yields its characteristic peaks (*A* and *B*). If a quenched specimen has been previously tempered to the temperature of the formation of *K*-state, the height of peaks *A* and *B* on the graph of the temperature relation of internal friction gradually decreases with the increase of the duration of the preliminary temper. After a

period of twelve hour tempering at 400° the peaks *A* and *B* disappear. The graph in fig. 7 of this article relates to an alloy containing 3% molybdenum. A similar variation of internal friction in thermal treatment was observed during the testing of all Ni_3Fe alloys containing molybdenum.

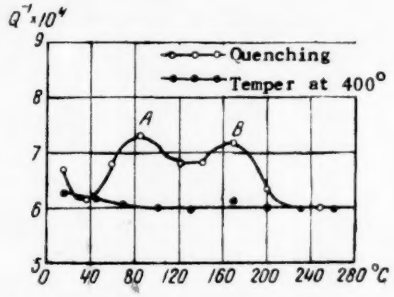

Fig. 7. Effect of heat treatment on temperature relation of internal friction of Ni_3Fe alloy. Frequency 0.8 c/s.

The results obtained can be explained as follows. In quenched solid solution Ni_3Fe alloyed with molybdenum the atoms of the latter element are statistically distributed over the crystal lattice points. A state is considered to be stable when molybdenum atoms are surrounded in a certain way by the nickel and iron atoms, i.e. when the *K*-state has been reached. But at low temperatures the process of the formation of *K*-state is hampered by the low speeds of diffusion. Therefore, the atoms of molybdenum are in an unstable condition (energetically), and at the time of the measurement of internal friction a relaxation takes place due to the movement of molybdenum atoms in the field of elastic stresses, having a fixed number of relaxation times, which causes the emergence of peaks *A* and *B*. This large collection of relaxation times is apparently due to the state of unequal energy of different atoms of molybdenum. In tempering with the object of obtaining the formation of *K*-state as a result of diffusion processes, the atoms of molybdenum, possibly, form zones and the alloy goes over to a stable state. At the same time the alloy behaves as though there had taken place within it an "interphase segregation". For this reason the atoms of molybdenum are not any longer taking part in relaxation processes, and consequently the peaks of internal friction are at first reduced in size, and after a protracted tempering disappear altogether.

Similar results were obtained when investigating the nichrome and nimonic (EI437A) alloys.

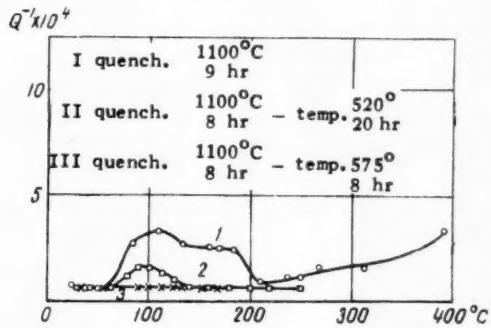

Fig. 8. Effect of heat treatment on internal friction of nimonic alloy.

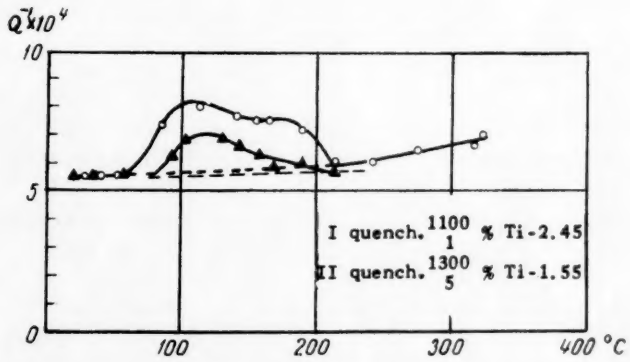

Fig. 9. Variation of internal friction in relation to titanium content in the nimonic alloy.

It is known that *K*-state is also formed in these alloys when they are tempered at 400-500° [18,19]. In the case of quenched nichrome there was regularly observed a maximum at 100-200° conditioned by the respective migration of nickel and chrome atoms. Since the atomic diameters of these two elements differ extremely little, the size of the peak was likewise very small. The size of the peaks was found to be within the limits of experimental error. On the addition of 2.5% titanium (nimonic) to the solid solution, the peak of internal friction increased considerably at 100-200° and exceeded the error of measurement; and in tempering for the formation of *K*-state (575° – 8 hr) this peak disappeared (fig.8). A relationship of this maximum with the presence of titanium in the solid solution has been proved by the results of our investigations (see fig.9). The maximum at 100°-200° due to relaxation in the field of stresses of titanium atoms is found in the case of the measurement of internal friction of quenched specimens only. If the *K*-state is brought about by tempering, the value of the maximum at 100°-200° gradually diminishes, and after tempering for 10 hr, completely disappears. This is similarly explained by the transition of titanium into a state of stability (*K*-state). In addition to that a carbon peak was obtained in the alloy nimonic at 240°.

Therefore, the results of the foregoing experiments make it possible to assume that when measuring the temperature relation of internal friction of metastable solid solutions, characteristic effects can be expected even when the structural factor is very small. In such a case the intensity of the effects should be greater, the greater the difference of free energies of a quenched and tempered alloy.

A comparison of internal friction of the alloys assuming an ordered arrangement with the same characteristic of the alloys which form *K*-state at low temperatures, is of extremely great interest (see fig.4 and 6).

Upon introduction of molybdenum into ordering alloys (Ni_3Mn), the peak of metastability decreases in proportion to the decrease of the extent of the possible order in molybdenum. On the other hand, the introduction of this element into alloys with a *K*-state (Ni_3Fe–Mo), increases the peak of metastability since the increase of the concentration of molybdenum seemingly increases the extent of atomic segregation (*K*-state) in a solution. The same holds good in the case of titanium in the EI437 alloy (fig.9).

Therefore, it is possible to differentiate between the formation of an ordered arrangement and the *K*-state by measuring internal friction (peaks of metastability).

Translated by H.G. Condover

REFERENCES

1. Symposium. *Elasticity and rigidity of metals, Foreign Literature Publishing House,* (1954).
2. A.S. Nowick, *Progress of Physical Sciences,* I (1956).
3. J.T. Stanley and C.A. Wert, *Acta Metallurgica,* 3, No.1 (1955).
4. W. Kostev and H. Bangert, *Archiv fid. Eisenhuttenn.* 25, No.11-12 (1954).
5. Ke, Tin-sui. *Symposium Elasticity and rigidity of metals. Foreign Literature Publishing House,* (1954).
6. C. Zenner, *Phys. rev.,* 71, 34 (1947).
7. A.S. Nowick, *Progress of physics of metals. Metallurgizdat,* I (1956).
8. C. Wort, *j. Appl. Phys.* 26, No.5 (1955).
9. A. Artman, *Symposium Elasticity and rigidity of metals. Foreign Literature Publishing House* (1954).
10. S. Kaya and A. Kussmann, *Zs. f. Physik,* 72, 6 (1931).
11. N. Vol'kenshtein and A. Komar, *Zh. teor. exp. fiz.* 11, No.6 (1941).
12. Ke, Tin-sui and L. Mag, *Acta Physica Sinica,* 13, No.1 (1957).
13. Ke, Tin-sui and Ch.T. Tsien, *Acta Physica Sinica,* 12, No.6 (1956).
14. N.G. Makhukov and B.G. Livshits, *Scientific papers of the Universities, Metallurgiia,* 3-4 (1958).
15. B.G. Livshits, B.V. Molotilov, N.N. Miuller and N.A. Savostianova, *Fiz. metal. metalloved.* 3, 3 (1956).
16. B.G. Livshits and M.P. Ravdel, *Dokl. Akad. Nauk. SSSR,* 93, 1033 (1953).
17. Iu.S. Avraamov and V.B. Osvenskii, *Scientific reports of Universities.* Metallurgiis, I, No.2 (1958).

18. B.G. Livshits, Sh.Sh. Ibragimov, Iu.S. Avraamov and Iu.Ko Konov, *Researches on fire-resistant alloys, Akad. Nauk SSSR,* 2 (1957).

19. Iu.S. Avraamov and B.G. Livshits, *Researches on fire-resistant alloys. Akad.Nauk.SSSR,* 2 (1957).

VOL.
8
1959

DETERMINATION OF THE NUMBER OF ARBITRARY PARAMETERS OF THE SHORT RANGE ORDER FOR MULTICOMPONENT ALLOYS*

A.N. MEN'

Consider a n-component alloy containing λ sublattices. Let us denote with M_ν the number of nodes in sublattice ν ($\nu = 1,2....\lambda$); N_i the number of atoms of the i ($i=1,2...n$) kind with N_i; the number of atoms of the i kind in the nodes of the ν type with $a_{i\nu}$; and the number of nodes in sublattice ν the closest to a given node in sublattice μ with $Z_{\mu\nu}$. Then let us build up matrix Z

$$Z = \{Z_{\mu\nu}\}. \tag{1}$$

Let us further denote the number of elements in this matrix Z with m_z, and the number of elements $Z_{\mu\nu}$ in matrix Z, for which $\nu > \mu$ with m_1.

The distribution of the atoms over the nodes is determined by matrix A

$$A = \{a_{i\nu}\}, \tag{2}$$

where

$$\sum_{i=1}^{n} a_{i\mu} = M_\mu, \quad \sum_{\mu=1}^{\lambda} a_{i\mu} = N_i \quad \begin{pmatrix} \mu = 1,2...\lambda \\ i = 1,2...n \end{pmatrix}. \tag{3}$$

Again, let us denote the number of the nearest neighbours made up of atoms of the i kind of a sublattice of the μ type, and of atoms of the j kind in a sublattice of the ν type with $Q^{ij}_{\mu\nu}$. Then according to matrix Z build up matrix Q which determines all the possible pairs

$$Q = \{Q_{\mu\nu}\}, \tag{4}$$

where

$$Q_{\mu\nu} = \begin{pmatrix} Q^{11}_{\mu\nu} \dots Q^{1n}_{\mu\nu} \\ Q^{n1}_{\mu\nu} \dots Q^{nn}_{\mu\nu} \end{pmatrix}. \tag{5}$$

and then determine the number of independent parameters of $Q^{ij}_{\mu\nu}$.

Since $Q^{ij}_{\mu\nu} = Q^{ij}_{\nu\mu}$, the total number of the unknown $Q^{ij}_{\mu\nu}$ will be

$$T = \frac{n\,[m_z(n+1) - 2m_1]}{2}. \tag{6}$$

The T unknown $Q^{ij}_{\mu\nu}$ are connected by $m_z n$ equations

$$\sum_{j=1}^{n} \gamma^{ij}_{\mu\nu} Q^{ij}_{\mu\nu} = Z_{\mu\nu} a_{i\mu} \quad \begin{pmatrix} i = 1,2...n \\ \mu,\nu = 1,2...\lambda \end{pmatrix}, \qquad \gamma^{ij}_{\mu\nu} = 1 + \delta_{\mu\nu}\delta_{ij}. \tag{7}$$

Of these equations only the linearly independent ones must be left, for which purpose we build up matrix X consisting of the coefficients of the unknown equations (7).

We shall now proceed to examine the rank of matrix X. In order to simplify the calculation of the rank of matrix X, let us arrange the elements in a definite manner (see figures).

Matrices B, D and C satisfy the following relationships

$$B^{(i)}_r = B^{(i)}_1, \quad C^{(i)}_{21} = C^{(i)}_{r,r-1},$$
$$D^{(i)}_{12} = D^{(i)}_{r-1,r}, \quad D^{(i)}_{21} = D^{(i)}_{r,r-1} \quad \begin{pmatrix} i = 1,2 \\ r = 2,3...\lambda \end{pmatrix} \tag{8}$$

and can be expressed in the form

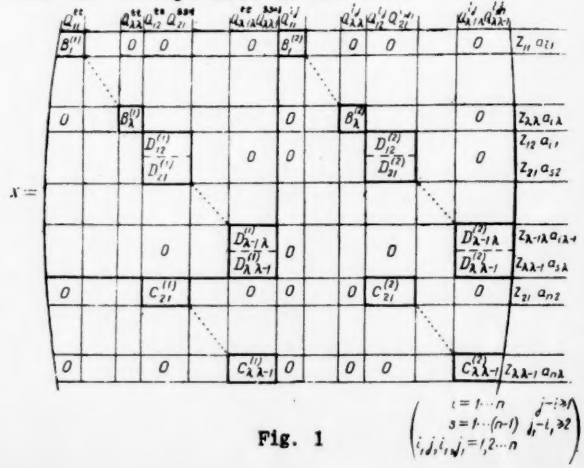

Fig. 1

* *Fiz. metal. metalloved.* 8, No.3, 449, 1959.

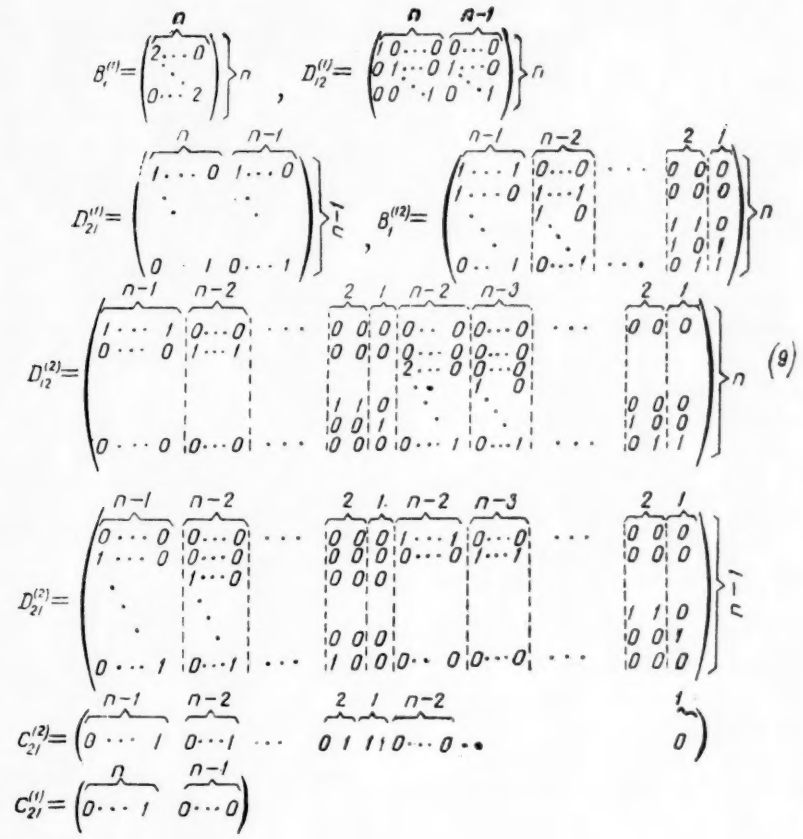

Fig. 2

It can be shown that the determinant of the order $m_z n - m_1$ at the top left hand corner of matrix χ differs from zero, but all the determinants of a higher order are equal to zero, i.e. the rank of matrix χ is equal to $m_z n - m_1$. The rank of the expanded matrix is similarly equal to $m_z n - m_1$, since the determinant of the expanded matrix resolved conforming to the last column produces $z_{\mu\nu} M_\mu - z_{\nu\mu} M_\nu$, after taking into account (3), – but this expression is equal to zero (it expresses the fact that the number of the nearest bonds $\mu\nu$ is equal to the number of $\nu\mu$ bonds). Consequently the rank of matrix χ is equal to

$$r = m_z n - m_1. \qquad (10)$$

It is now easy to find the number of independent parameters of the short range order

$$N_s = T - r = \frac{(n-1)(m_z n - 2m_1)}{2}. \qquad (11)$$

It can be clearly seen from the form of matrix χ which of the $Q^{ij}_{\mu\nu}$ parameters should be taken for independent ones. It must be pointed out that $Q^{ij}_{\mu\nu}$ determine the number of pairs of the nearest neighbors, so that the independent parameters of the short range order relate to the first co-ordination sphere*.

Let us consider a few examples.

I. An unordered n-component alloy:

a) a simple, body-centred and face-centred lattice (l=1)

$$Z = Z_{11},\ m_z = 1,\ m_1 = 0,\ N_s = \frac{n(n-1)}{2}; \qquad (12)$$

b) a lattice of the spinel type (one sub-

* The proposed method of calculating the number of independent parameters of the short range order cannot be applied directly in the case of other co-ordination spheres, since the parameters $Q^{ij}_{\mu\nu}$ for other spheres are not independent.

lattice-tetrahedral nodes, the other – octohedral) (l=2)

$$Z=\begin{pmatrix} Z_{11}Z_{12} \\ Z_{21}Z_{22} \end{pmatrix},\ m_z=4,\ m_1=1,\ N_z=(n-1)(2n-1), \tag{13}$$

we have three parameters of the short range order for a bi-component alloy (n=2)

II. An ordered n-component alloy below the temperature:

a) a body-centred lattice (one sublattice-cube centres, the other – top of cubes) (l=2)

$$Z=\begin{pmatrix} 0Z_{12} \\ Z_{21}0 \end{pmatrix},\ m_z=2,\ m_1=1,\ N_z=(n-1)^2, \tag{14}$$

for a bi-component alloy of the CuZn type (n=2) we have one parameter of the short range order

b) Face-centred lattice (one sublattice – top of cubes, the other – centre of faces) (l=2)

$$Z=\begin{pmatrix} 0 & Z_{12} \\ Z_{21} & Z_{22} \end{pmatrix},\ m_z=3,\ m_1=1_1,\ N_z=\frac{(n-1)(3n-2)}{2}, \tag{15}$$

for a bi-component alloy of the Cu_3Au type (n=2) we have two parameters of the short range order

c) A Heusler type of alloy (l=3)

$$Z=\begin{pmatrix} 0 & Z_{12}Z_{13} \\ Z_{21} & 0\ 0 \\ Z_{31} & 0\ 0 \end{pmatrix},\ m_z=4,\ m_1=2,\ N_z=2(n-1)^2, \tag{16}$$

for a tri-component alloy of Cu_2MnAl type (n=3) we have eight parameters of the short range order.

If the fact be taken into consideration that $a_i\mu$ are connected with the parameters of the long range order [1] in the case of an ordered, alloy, the formula (7) gives the connexion of the parameters of long and short range orders.

Having a clear form of expression for free energy $F(Q^{ij}_{\mu\nu})$ and introducing the parameters of the short range σ_k and the long range s_m 3 orders, it is possible to find from the system

$$\frac{\partial F}{\partial \sigma_k}=0,\ \frac{\partial F}{\partial S_m}=0,\ \begin{pmatrix} k=1,2\ldots N_z \\ m=1,2\ldots p \end{pmatrix}$$

a connexion among equilibrium σ_k, s_m and the temperature.

In conclusion I express my gratitude to A.N. Orlov for his valuable remarks in the course of our discussion in this paper.

Translated by H.G. Condover

REFERENCES

1. A.N. Men', *Fiz. metal. metalloved.* 7, 633 (1959).
2. L. Guttman, Solid State Phys. 3, 145 (1956).
3. K.K. Voitsekhovskii, *Acta Phys. Polonica* (in press).

VOL 8 195

STUDIES OF REACTION DIFFUSION IN BINARY SYSTEMS OF THE "METAL - GAS" TYPE*

V.I. ARKHAROV and E.B. BLANKOVA

A.M. Gor'kii State University of Ural'sk

(Received 31 March 1959)

VOL. 8 1959

In studying reaction diffusion, which is of such an immense importance to the chemico-thermal treatment of metals and the prevention of gas corrosion, one meets with great difficulties. These difficulties are due to the complexity of the mechanism of this phenomenon and the diversity of the nature of the developing phases.

In order to find a means of controlling these phenomena, it is necessary to work out a systematism of the reaction diffusion.

The mechanism of reaction diffusion is primarily determined by the type of chemical bond between the reacting elements, the structural characteristics of the phases developing in the course of the process of diffusion, and the relationship between the the dimensions of the diffusing particles.

In order to be in a position to demonstrate the regularity of the variation of the mechanism of diffusion in binary systems, it is found expedient to examine the reaction of the elements placed in the periodic system within one period, with the same second component, using different elements in succession the selection of which is based on their position in the periodic table.

In this work the principal results of research on the mechanism of reaction diffusion with sulphur in binary systems formed by transition elements of period IV (from Ti to Ni) are set forth.

Diffusional annealing was carried out in pyrex or quartz ampoules evacuated to a pressure of the order of 10^{-3} to 10^{-4} mm Hg, so designed that the specimen should be in an atmosphere of sulphur vapours in one part of the ampoule and sulphur in the other. In every case the sulphur vapour pressure was approximately 1 atm. The investigation of diffusion was conducted within the range of temperatures from the beginning of the observable formation of the skin (400-500°) to 1000°. For the purpose of analysis of the mechanism of diffusion, the phase composition (by the Debye method) and the presence or absence of texture in the scale, were, as usual, [1] investigated after annealing and determined by means of X-ray photographs. In addition to this, experiments were carried out using workers of an inert substance such as platinum wire.

The results of the investigation are recorded in Table I. From these results a conclusion can be drawn to the effect that in all the systems investigated the transition metal-sulphur mechanism of diffusion is the same in its main features. In effect, in every case the scale consisted of a more or less close outer crust and a friable layer continguous to the metal. An X-ray phase analysis showed that the outer crust consisted of one or two closely joined phase layers.

It was established by means of metallographic research that the inert marker was located between the outer crust and the layer contiguous to the metal. The thickness of the scale layer, forming by diffusion of metal towards the outer surface as well by diffusion of metalloid towards the scale-metal interface, was found to be of the same order of magnitude in all cases.

The texture in the outer crust of the scale and its absence in the inner layer was determined by means of a texture analysis.

* *Fiz. metal. metalloved.* 8, No.3, 452-454, 1959.

TABLE 1

Investigating results of the systems transition metal-sulphur

System	T°range °C	Number of layers revealed metallographically	Skin phase composition	Position of inert marker	Presence of texture in skin layers
Ti-S	600-1000	2	TiS_x in outer and inner skin layers (phase acc. ord. to Debye line location, intermediate between TiS and TiS_2 (2-5))	Between 2 layers of phase TiS_x	Texture in outer layer of skin
V-S	400-1000	2	VS_x (by X-ray photo VS_x is close to VS, but differs from it by the presence of extra lines and variations relating to intensiveness (2,3,6,7)	-	Ditto
Cr-S	400-1000	2	CrS (monoclinic) in outer and inner layers. CrS (superstructure) in a very thin layer adjacent to metal (2,3,8,9)	Between two layers of phase CrS (monoclinic)	Ditto
Mn-S	500-1000	2	MnS (structural type NaCl) in outer and inner layers (2,3)	Between two layers of MnS phase	Ditto
Fe-S	400-600	3	FeS_2 (pyrites) very thin outer layer. FeS (struct. type NiAs) constit. main layer of outer crust and inner layer	Between two layers of FeS phase	Texture in layer FeS cons. tit. main thickn. of outer crust
	600-980	2	FeS in outer and inner layers (2,3,10,11) at 980°	Between two layers	Texture in outer layer
Co-S	600-800	2	CoS_x in outer layer Co_9S_8 in inner	Between two layers	Texture in outer layer
	800-960	2	Co_9S_8 in outer and inner layers. Melts at 950° (2,3,12-14)	Ditto	Ditto
Ni-S	400-650	3	NiS_2 in v. thin outer layer (on Debyegram a row of extra lines not fitting NiS picture) constit. main thickn. of outer crust and inner layer. Melts at 650° (2,3,15,16).	Between two layers of NiS	Texture in outer layer NiS is main thickn. of outer crust.

All this makes it possible to assume that in all the systems investigated a bilateral diffusion of the metal and sulphur takes place.

The rate of diffusion of both components grows with the rise of temperature, and increases in a more or less equal proportion. In the case of a successive passage from one set of systems to another in the direction of Ti-S → Ni-S under identical conditions (temperature and duration of annealing, pressure of sulphur vapours) the rate of the growth of the scale increases.

The system Co-S, in which the rate of scale formation is somewhat lower than in the systems adjacent to it, constitutes an exception.

Translated by H.G. Condover

REFERENCES

1. V.I. Arkharov, *Proceedings of the All-Union Conference on the use of X-rays in researches on materials* (1949).
2. G.B. Bokii, *Introduction to crystallochemistry. Izd. MGU* (1954).
3. Landolt-Bornstein, *Atom und Molekularphysik*, part 4, Springer-Verlag, Berlin (1955).
4. P. Ehrlich, Zs. anorg. allg. Chem., 260, 1-3, 19 (1949).
5. P. Ehrlich, Angew. Chem., 60A, 68 (1949).
6. W. Blitz and A. Kocher, Zs. anorg. allg. Cehm., 241, 324 (1939).
7. E. Hoschek and W. Klemm, Zs. anorg. allg. Chem., 242, 49 (1939).
8. H. Haraldsen, Zs. anorg. allg. Chem., 234, 372 (1937).
9. F. Jellinek, Acta Cristall., 10, 10, 620 (1957).
10. G. Hagg and J. Sucksdorf, Zs. Phys. Chem., B22, 444 (1933).
11. H. Haraldsen, *Zs. anorg. allg. Chem.*, 246, 195 (1941).
12. W. Jong and H.W.V. Willems, *Zs. anorg. allg. Chem.*, 161, 311 (1927).
13. O. Hulsmann and F. Weibke, *Zs. anorg. allg. Chem.*, 227, 113 (1936).
14. D. Lundqvist and A. Westgren, *Zs. anorg. allg. Chem.*, 239, 85 (1938).
15. A. Westgren, *Zs. anorg. allg. Chem.*, 239, 82 (1938).
16. D. Lundqvist, *Arkiv. Kemi. Mineral. Geol.*, 24A, 21, 12 (1947).

VOL. 8 1959

SOME PECULIARITIES IN THE DISPOSITION OF CORROSION FIGURES IN THE ALLOY Al-Zn-Cu*

N.N. BUINOV and T.V. SHCHEGOLEVA

Institute of Physics of Metals Akad. Nauk SSSR

(Received 12 August 1958)

One of the basic questions of the theory of dislocations is the origination and multiplication of dislocations. However, experimental data on this question are insignificant, particularly for metals and metallic alloys. In the current report, some observations are brought forward concerning the disposition of corrosion figures on the ageing alloy Al-Zn-Cu, which probably give a representation of the sources of dislocation. Upon investigation of the electro-polished and corroded (by aqua regia) surface of the alloy Al-Zn-Cu (10% Zn, 0.5% Cu) which had first been deformed by compression of less than 1%, spirals were discovered which possibly illustrate either the action of the mechanism of Frank and Read [1], or the existence of spiral or helical dislocations. Together with them, loops were observed, similar in form to the dislocation loops emitted by the sources of Frank and Read.** They were observed not only inside the granules (Fig. 1, 2), but also on the intergranular boundaries (Fig. 3). In the first instance, they are found more often in groups, into each of which enter from two to seven loops. In those instances when the loops are not closed, they have the form of small brackets with ends folded inwards (Fig. 1-6), indicating their non-accidental origination. Light photographs on a dark field (Fig. 3) show that the loops consist of corrosion figures.

However, in the disposition of the loops there is one peculiarity which gives doubt as to whether they arise from Frank-Read sources. In the central section of certain groups of loops a small "claw" is observed at times, with a different orientation (shown by an arrow on Fig. 1).

Fig. 1. The alloy Al-Zn-Cu; deformation by compression of less than 1%; ageing at 150° for 96 hr; corrosion by aqua regia; X 140.

Fig. 2. As Fig. 1; X 140.

It is difficult to understand this peculiarity arising from the mechanism of multiplication of dislocations by Frank and Read.

** It must be noted that on undeformed specimens of the alloy, loops and spirals were very rarely observed. On severely deformed specimens, they were not observed at all.

* *Fiz. metal. metalloved.* 8, No.3, 455-457, 1959.

Jones and Mitchell [2] observed the formation of helical and prismatic dislocations in silver chloride after the addition of glass globules and after rapid cooling from a temperature of 370°. The authors concluded that the dislocations arose from the effect of pressures which appeared around the glass particles due to variations in the expansion coefficients of glass and silver chloride.

Fig. 3. The alloy Al-Zn-Cu; deformation by compression of less than 1%; ageing at 150° for 96 hr; corrosion by aqua regia; X 140.

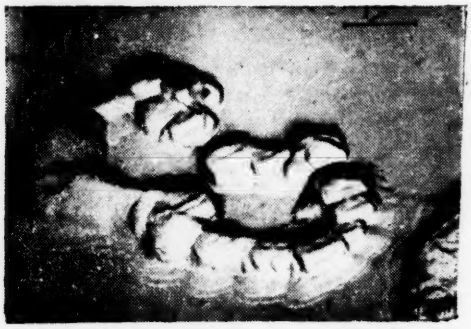

Fig. 4. The alloy Al-Zn-Cu; ageing at 150° for 5 hr; corrosion by aqua regia; X 10,500.

Sources of this type may probably emit dislocations not singly but in a whole batch or even in several batches of differently orientated slip planes. The formation of dislocations without the action of Frank-Read sources was observed by Gilman and Johnston [3] in crystals LiF under the action of pressures.

If it is granted that we are dealing not with the sources of multiplication (which demand the existence of a dislocation network in the alloy) but with sources of the origin of dislocations arising around impurities or places of localization of pressures, then the observed loops and their peculiarity are easily explicable. This conception is found to be in accord with the fact that sources are observed in all crystals of the specimen, which were randomly orientated. The latter is possible only when the source works in comparatively thick batches of planes. If it is assumed that each group of loops is connected with one source then the density of such sources inside the crystal can be estimated as approximately equal to $10^4/cm^2$. Along the boundaries of the crystals the loops are displaced with a larger density than inside and interweave among themselves; because of this it is difficult to calculate the density of the sources.

Fig. 5. The alloy Al-Zn-Cu; ageing at 150° for 5 hr; corrosion by aqua regia; X 10,500.

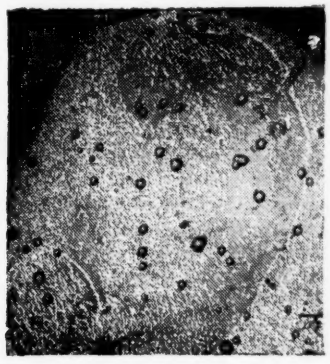

Fig. 6. The alloy Al-Zn-Cu; deformation by compression of less than 1%; ageing at 150° for 96 hr; corrosion by aqua regia; X 3480.

It must be noted that in our laboratory, groups of loops in the alloy Al-Cu were observed by decoration. From this it was concluded [4] that these groups correspond to

VOL. 8 1959

Frank-Read sources. It is probable that in this instance, too, we are also dealing with the sources of dislocations around the impurities and places of localization of deformation.

CONCLUSION

1. In the alloy Al-Zn-Cu small chains of corrosion figures are discovered which apparently have a dislocation origination.
2. The assumption is expressed that the observed loops arose not from Frank-Read sources but by the effect of pressures localized in separate regions of the alloy. We

express gratitude to A.N. Orlov for discussing the results of the work.

Translated by J. Harvey

REFERENCES

1. V.T. Read, *Dislokatsiya v kristallakh, (Dislocations in crystals), Metallurg.*, (1957).
2. D.A. Jones, and I.W. Mitchell, *Phil. Mag.* 3, 1 (1958).
3. J.J. Gilman and W.G. Johnston, *Dislocations and Mechanical Properties of Crystals.* John Wiley and Sons, Inc., New York, 116 (1957).
4. V.G. Rakin and N.N. Buinov, *Dokl. Akad. Nauk SSSR*, 121, 271 (1958).

SOME REGULARITIES OF THE CHANGE OF FORCES OF THE INTER-ATOMIC BOND IN THE ALPHA-SOLID SOLUTIONS OF SYSTEMS WITH ELECTRON COMPOUNDS*†

G.P. KUSHTA and O.I. RYBAILO

Chernovitskii State University

(Received 31 March 1959)

VOL. 8 1959

Changes of forces in the inter-atomic link in alpha-hard solutions of the systems Cu-Zn and Cu-Sn are investigated in the current work. An estimate of changes of forces of the inter-atomic bond in the alloys was carried out by means of X-ray determination of the characteristic temperature of the alloy, according to the method developed by G.V. Kurdiumov [1] of exposure at two temperatures: room temperature and the temperature of liquid air.

To obtain the alloys Cu-Zn, first an alloy was prepared, containing about 30% Cu and 70% Zn. Electrolytic copper and granulated zinc free from arsenic were used.

By fusion of the alloy with the appropriate quantity of copper in sealed graphite crucibles, alloys were obtained with a zinc content: 4.33; 8.74; 19.78; 29.24 and 38.62 at. %.

An alloy to produce the alloys Cu-Sn contained about 60% Sn. Tin of mark ChDA was used. The content of tin in the obtained alloys Cu-Sn was: 1.09; 2.19; 4.46; 6.95 and 9.31 at. %.

The composition of the alloys was carefully controlled by chemical and spectral analyses and also by X-ray determination of the lattice parameter of the solid solution.

From the alloys, powders were produced by filing and a fraction was withdrawn giving continuous lines on the X-ray photograph. To relieve the strain arising with filing, the powders were annealed in evacuated glass ampoules at a temperature of 360° for 4 hr. X-ray photographs were obtained from cylindrical specimens with a diameter of 0.6 mm, prepared by the application of annealed powder on a fine glass filament moistened with cellulose nitrate varnish. Iron K-emission was used. Extinction in the specimens was absent.

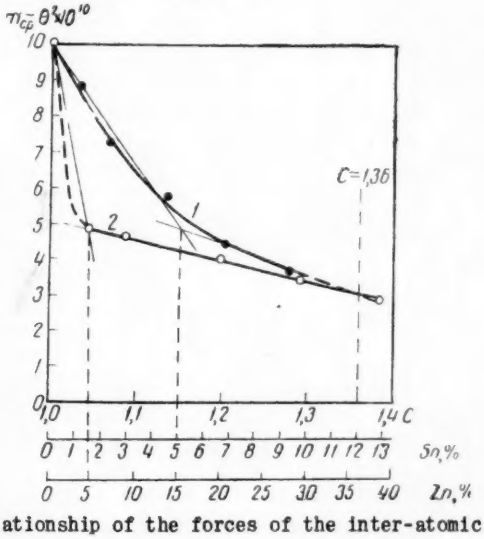

Relationship of the forces of the inter-atomic link in the alpha-solid solutions of the systems Cu-Zn and Cu-Sn from the electron concentration: (1) for Sn; (2) for Zn.

Cooling of the specimen to the temperature of liquid air was accomplished by means of the continuous spraying of it by a jet of liquid air in an open chamber, in accordance with the method described in [2].

X-ray photographs taken from the same specimen at varying temperatures were developed simultaneously. The photographs were

---

* *Fiz. metal. metalloved.* 8, No.3, 457-459, 1959.

† N.P. Skochelyas and I.V. Ugorchuk participated in the experimental work.

measured on the micro-photometer, MF-2, and the ratio of intensity I_{111}/I_{222} was defined. The value of the amounts of I_{111}/I_{222} for each of the samples at two temperatures, from which the characteristic temperature of the alloy was determined, represent the average result of several measurements from two to three X-ray photographs.

These normalized data were used for calculating the amount $m_{ep}\theta^2$ being the measure of the inter-atomic bond in the network of the alloy.

On the figure these values are depicted in relation to the calculated value of the electron concentration for the alloys under investigation. As is evident from the figure, the (decrease) of the force of the inter-atomic bond as a function of the electron concentration for solid solutions in the systems Cu-Zn and Cu-Sn is characterized by complex curves converging to a point which corresponds to the maximum electron concentration of alpha-phase. Each of these curves may be approximated, however, by two straight lines intersecting at points which in practice correspond to the same value of the force of inter-atomic bond for both systems and to the same content of added atoms ($\sim$5 at. %.) The observed decrease of forces of the inter-atomic bond only qualitatively corresponds to the increase of forces of repulsion in the lattice but is not determined uniquely by these forces.

From the actual course of curves for the alloys Cu-Zn and Cu-Sn, it may be concluded that the influence of local disturbances of the potential of the lattice, induced by the presence of ions of another valence, which distort the electron energy band of the alloy, prevail over the influence of the electron concentration. The indicated influence is limited by the action of the well known Hume-Rothery law.

Translated by J. Harvey

REFERENCES

1. V.A. Il'ina, V.K. Kritskaya and G.V. Kurdiumov, *Problemi metallovedeniya i fiziki metallov, (Problems of metal behaviour and physics of metals)*, edition 2, metallurgizdat, page 222 (1956).
2. V.I. Iveronova, *Izv. Akad. Nauk SSSR, physics series* 75 No.1 (1951).

VOL 8 195

TEMPERATURE DEPENDENCE OF MAGNETIC PROPERTIES OF THE ALLOY IU 16 (ALFENOL)*

O.N. ALTGAUZEN and I.K. KUPALOVA

Central Scientific Research Institute of Ferrous Metallurgy

(Received 13 September 1958)

In the current work, results are given of an investigation of magnetization curves of the alloy IU16 at temperatures from -78° to 300°. The iron-aluminum alloy IU 16 with an aluminum content of 16 wt. %, being a soft magnetic material, finds an application with the preparation of small heads for sound-recording apparatus and cores of communication equipment [1,2]. An investigation of magnetic properties of this alloy at varying temperatures presents interest in connexion with the expansion of the interval of temperatures in which this apparatus finds an application.

The alloy was melted in a high frequency furnace, subjected to hot rolling and later to warm rolling to a thickness of 0.35 mm. From the ribbon so obtained, rings were were stamped and afterwards assembled in piles for subjecting to heat treatment.**

Magnetic measurements were carried out by a ballistic method. On Fig. 1-3 and in the table, magnetic properties of this alloy at

TABLE 1

Magnetic properties of the alloy IV 16 at varying temperatures

	Heat treatment number	Initial state at 21-24°	Concerning the initial state (%) at temperatures, °C									
			-78	22-23	100	23	200	23	255	26	300	21-26
Maximum penetrability gc/e	1	52,000-60,000	60	–	70-75	99	55-60	99	17	65	35	48-53
	2	38,000	60	99	94	–	71	–	–	–	47	33
Coercive force e	1	0,028-0,029	102	107	102-110	102	115-120	104	124	166	124	218
	2	0.33	98	98	91	–	102	–	–	–	102	272
Induction in field 8 e, gc	1	6200-6600	102	97	92	99	80	100	75	102	65	100
	2	7300	103	100	93	–	84	–	–	–	66	97

Heat in treatment. 1. Heating to 900°, Ageing 30 min. Cooling with furnace to 600°, ageing 10 min, hardening water. 2. Heating to 1000°, ageing and cooling as indicated above, hardening in oil.

* *Fiz. metal. metalloved.* 8, No.3, 459-461, 1959.

** The material for the investigation was submitted by C.A. Golovanenko.

VOL. 8 1959

varying temperatures are indicated. Magnetic properties of the alloy depend essentially on the temperature. Upon cooling to -78° and heating to 200°, maximum permeability in both instances decreases practically reversibly, whilst upon heating to 255°-300° and subsequent cooling, the change is irreversible – maximum permeability does not attain the initial value.

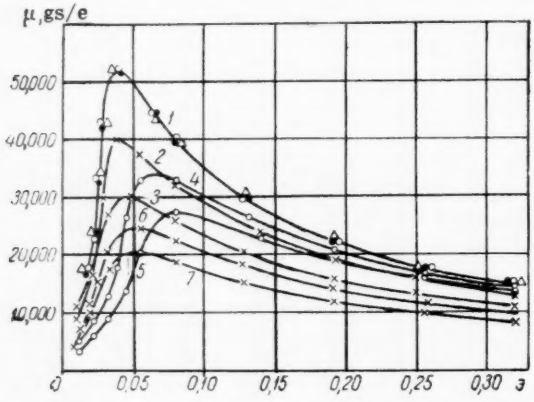

Fig. 1. Temperature relationship of magnetic penetrability of the alloy IU 16. Specimen No. 1: *1* – initial, 22° (0); 23° after 100° (•); 23° after 200° (△); *2* – at 100°; *3* – at 200°; *4* – 26° after 255°; *5* – 26° after 300°; *6* – at 255°; *7* – at 300°.

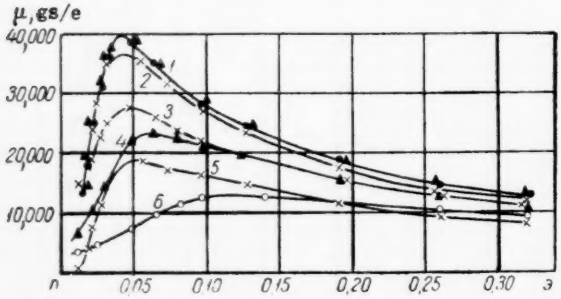

Fig. 2. Temperature relationship of magnetic penetrability of the alloy IU 16. Specimen No. 2: *1* – initial, 22° (△); 22° after – 78.5° (•); *2* – at 100°; *3* – at 200°; *4* – at 78.5°; *5* – at 300°; *6* – 21,5° after 300°.

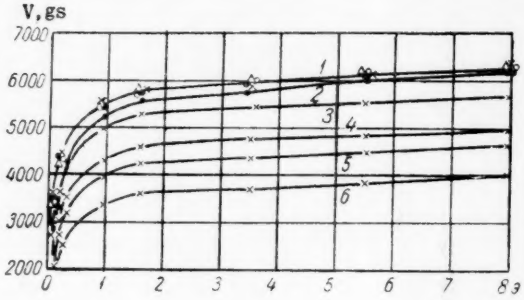

Fig. 3. Magnetization curves of the alloy IU 16 at a varying temperature. Specimen No. 1: *1* – initial 22° (0); 23° after 100° (×); 23.5° after 200° (△); 25° after 255° (0); 2– 26° after 300°; *3* – at 100° *4* – at 200°; *5* – at 255°; *6* – at 300°.

In practice, the coercive force remains unchanged with the change of temperature from -78° to 200° but with higher temperatures increases irreversibly.

The irreversible change of magnetic properties is apparently connected with the beginning of the process of ordering in the alloy [3] and imposes a substantial limitation on the possibility of applying it in apparatus working at temperatures higher than 200°.

Some stabilization of properties may be obtained by changing the heat treatment (specimen No. 2) in such a way that partial ordering may already have taken place during the process, lowering the level of properties of the alloy to some extent, but raising its temperature stability upon heating to 100°-200°.

Translated by J. Harvey

REFERENCES

1. C. A. Golovanenko, *Metallovedeniya i obrabotka metallov (Metal behaviour and working of metals)*, No. 2 50 (1958).
2. W. I. Shotnikow, Hutnik, 24, No. 7-8, 282 (1957).
3. Y.P. Selisskii, *Fiz. metal. metalloved.*, 4, 191 (1957).

VOL 8 195

THE INCREASE IN THE COERCIVE FORCE OF MIXED FERRITES-CHROMITES OF LITHIUM IN THE REGION OF THE COMPENSATION TEMPERATURE*

K. M. BOL'SHOVA and T. A. YELKINA

Moscow State University named after M. V. Lomonosov

(Received 10 October 1958)

Ferri-magnetic spinels, the composition of which is described by the formula $Li_2O \cdot (5-2a)\,Fe_2O_3 \cdot 2a\,Cr_2O_3$, possess in the region from $a = 1$ to $a = 2$ the distinctive peculiarity that their spontaneous magnetization returns to nil not only at the Curie temperature but also at a lower temperature – the so-called compensation point [1, 2].

A detailed experimental investigation was carried out by us of the temperature course of spontaneous magnetization of the indicated materials in the region of the compensation temperature and Curie temperature.

An anlysis of these results led to the conclusion that in ferrites of the type indicated, the increase of H_c must be observed in the region of the compensation temperature T_k, connected with a sharp decrease of magnetization with the approach of the measurement temperature to T_k.

The measurements carried out of H_c of specimens of the system LiFeCr in annealed and hardened states confirmed this assumption (cf. Fig. 1 on which are given data for a specimen of the composition $Li_2O \cdot 2{,}5\,Fe_2O_3 \cdot 2{,}5\,Cr_2O_3$ in an annealed state). As is evident from the figure, the increase of H_c takes place not exactly at T_k but in a significant interval of temperatures adjoining T_k on both sides.

Two possible causes of this effect may be pointed out. Evidently the main reason for the growth of H_c in the area of the compensation temperature is connected with some heterogeneity of the chemical composition according to the volume of material (which may take place even with the most careful technology in the preparation of ferrites).

The fact that minor heterogeneity by composition takes place, results from the existence of "incomplete compensation", i.e., of small spontaneous magnetization at the compensation temperature. The existence of of such chemical heterogeneity of material and the relationship of T_k to the composition must lead to sharply expressed magnetic heterogeneity in the region of T_k with an increasing degree of dispersion of ferrimagnetic impurities with the approach of the measurement temperature to T_k. With sufficiently low dimensions of such impurities (approaching the dimensions of separate domains) the process of magnetization in them may originate only by means of the rotation of the vector of magnetization and the coercive force will be defined by the formula:

$$H_c \approx \frac{K}{I_s},$$

where K – constant of anisotropy; I_s – magnetization saturation.

The second possible reason for the increase H_c is connected with the powdered character of the ferrite materials. Whilst any ferrite is a pressed and baked powder, the separate particles of this powder will be uncoupled to some measure in magnetic relationship. With sufficiently small dimensions of the "powder grains", they may appear as single domain particles. The single domain criterion is connected with the constant of anisotropy and with the spontaneous magnetization of the

* *Fiz. metal. metalloved.* 8, No. 3, 461-463, 1959.

VOL. 8 1959

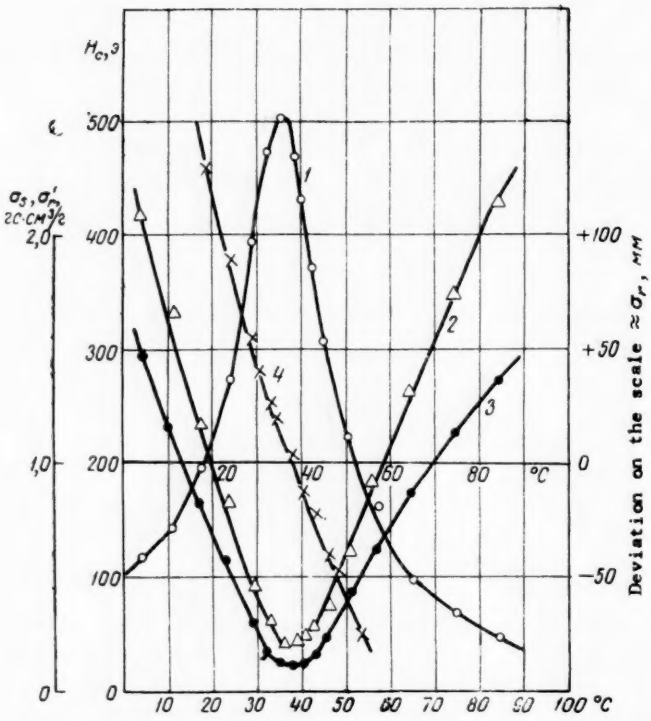

Fig. 1. Temperature relationship of magnetic properties of the ferrite $Li_2O \cdot 2{,}5\,Fe_2O_3 \cdot 2{,}5\,Cr_2O_3$ in the region of the compensation temperature:
1 – Temperature relationship of the coercive force; *2* – Temperature relationship of spontaneous magnetization $\sigma_s(t)$; *3* – Temperature relationship of residual magnetization created with each given temperature $\sigma_r(t)$; *4* – Temperature relationship of residual magnetization created at room temperature $\sigma_r(t)$.

material: the greater K is and the smaller I_s is, then the particle becomes single domained with large dimensions. Consequently, with $T \to T_k$, when I_s decreases strongly, a better approach to a single domain structure may be expected than when the temperatures are far from T_k. In such an instance the coercive force of the material in the region of temperatures adjoining T_k may also be expressed by the formula

$$H_c \approx \frac{K}{I_s},$$

In view of the fact that we are dealing with a pressed and baked powder and not with single domain particles in a pure state, the indicated formula may not be applied for the calculation of H_c in the region of T_k but it may be used for qualitative assessment of the temperature course of H_c in the area of the compensation temperature.

The curves of magnetization obtained earlier for ferrites of the system LiFeCr, according to the measure of the approach to the compensation temperature, become still more sloping, testifying the increasing role of the mechanism of rotation in the processes of magnetization of the ferrite, i.e., in the use of the possibility of applying formula (1) for assessing the temperature course of H_c in the region of T_k.

Translated by J. Harvey

REFERENCES

1. E.W. Gorter, *Phil. Res. Rep.*, 9, 295 *(Russian translation in Progress of Physical Sciences* 10-11 (1955).
2. L. Neel, *Ann. de Phys.*, 3, 137 (1948).
3. K.P. Ryelov, K.M. Bol'shova and T.A. Yelkina, *Zaitseva M.A. Izv. Akad. Nauk SSSR, physics series*, 10, 1282 (1958).
4. E.I. Kondorckii, *Dokl. Akad. Nauk SSSR*, 82, 365 (1952).

VOL.
8
1959

ON THE POLYGONAL STRUCTURE OF IRON-ALUMINIUM ALLOYS*

B. V. MOLOTILOV

(Received 16 March 1959)

We studied the structure of a high permeability alloy of iron and 16% aluminium. After slow cooling in the interval 980-590° and abrupt quenching from 590° the alloy had the maximum magnetic permeability of 71,000 G/Oe.

A typical grain microstructure in a plane near (111) is shown in Fig. 1. A fragment of the same structure near the grain boundary with large magnification is shown in Fig. 2. It will be seen from Figs. 1 and 2 that the grain of the alloy is divided into blocks of 0.01-0.05 mm in size, whose boundaries form proper lines of etching pits placed at regular intervals. Structures, similar to those described, were observed by Lacombe and Cahn [1] in aluminium, by Dunn, Daniels and Hibbard [2] in ferro-silicon alloys and by a number of other authors in non-metallic crystals. The origination of such structures during annealing after deformation may be connected with polygonization, consisting of a formation of regulated dislocation systems as a result of their displacement in the crystal lattice at the annealing temperature [3]. Heat treatment of the studied alloy was carried out after warm rolling, i.e. the original condition was that of partial recrystallization. Etching did not disclose grain boundaries in the original condition.

The presence of more than one slip system during deformation, as well as different grain orientations resulted in a complex deformation of each grain and consequently in a complex orientation of grain boundaries of the blocks formed during the polygonization anneal. The order of the angle of the bend of the blocks which have a common boundary may be determined by the known formula for a small angle boundary [3]: $\theta \approx \frac{b}{D}$ ($\vec{b}$ – Burger's vector, D – distance between the etching pits of the dislocation). The appraisal gives a θ value of about one minute.

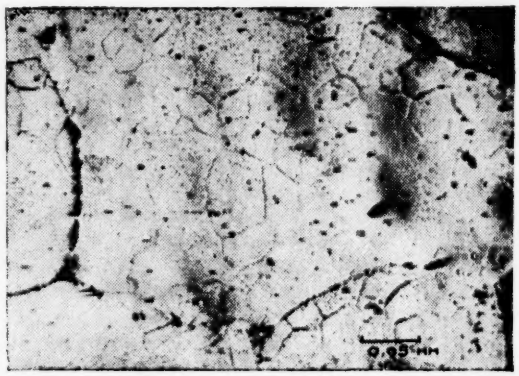

Fig. 1. Grain structure of iron and 16% aluminium alloy in a polygonized condition.

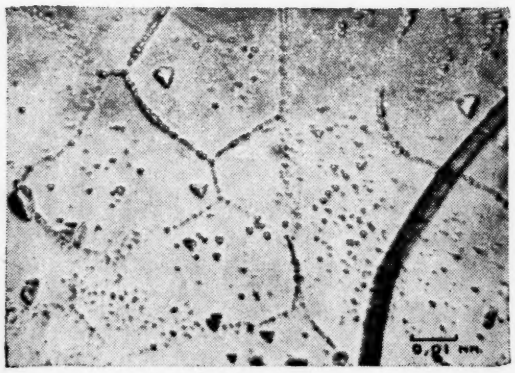

Fig. 2. Structure of polygonized alloy near the grain boundary.

The polygonized alloy was slightly deformed plastically by tension. It will be seen in Fig. 3 that the slip line spread freely across the block boundaries without suffering any noticeable breaks. This is possible only in a case of very close orientation of the

* *Fiz. metal. metalloved.* 8, No. 3, 463-465.

blocks. At the same time the block boundaries do not alter the directions of the walls of the ferro-magnetic domains, whose position was ascertained by the magnetic colloid method [4]. This circumstance, apparently, facilitates the movement of the domain wall during magnetization in a polygonized structure compared with its movement in a field of chaotically distributed defects.

An analogous structure was also observed in other specimens of high permeability alloys of iron and 16% aluminium.

Translated by A. Allan

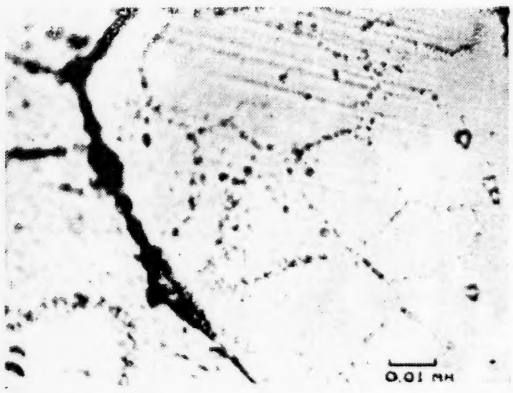

Fig. 3. Process of plastic deformation flow in a grain split up into blocks.

REFERENCES

1. P. Lacombe and L. Beaujard, *Journ. Inst. Metals.* 74 (1948); R.W. Cahn, *Journ. Inst. Metals.* 76, 121 (1949).
2. C. Dunn and W. Hibbard, *Acta Metallurgica,* 3, 409 (1955).
3. A. Cottrell, *Dislokatsiya i plasticheskoye techeniye v kristallakh (Dislocation and plastic flow in crystals), State United Scientific and Technical Publishing House,* (1958). *Forti A.Dzh. Neposredstvennoye nabliudeniye dislokatsii v kristallakh (Direct observation of dislocation in crystals), Metallurgizdat,* (1956).
4. B.V. Molotilov, *O. magnitnoi strukture splava zheleza s 16% alluminia (On the magnetic structure of an iron and 16% aluminium alloy), Bulletin TsNIIChM* (in print).

VOL. 8 1959

ON THE TYPE OF DEFECTS IN AN ALPHA-LEBOITE*

F. A. Sidorenko, P. V. Gel'd and L. B. Dubrovskaya

(Received 2 June 1959)

Based on the fact of a reduction of lattice parameters with an increasing silicon content in ζ_α-phase (α-leboite) in the system Fe-Si, the assumption was made [1] about the formation of solid substitutional solutions on a base of disilicide of iron. A precision determination of the density of leboite alloys and of the lattice parameters produce results which contradict such an assumption.

The investigation was carried out on alloys prepared in a tungsten vacuum furnace from chemically pure silicon (99.95% Si) and iron carbonyl P-4. The alloys were homogenized in vacuo at 1080° for 100 hr. Densities of the powders, ground in an agate mortar, were measured by the pycnometric method with the loading of the pycnometers in vacuo. A VRS-3 camera was used for determining the lattice parameters. Their values for alloys of different composition show (Table 1) that the phase under consideration is stable in a region of concentrations of 53.5 to 56.5% Si, which conforms with Haughton's and Becker's data.

The number of iron and silicon atoms per elementary cell were computed on the basis of the values of density and lattice parameters (Table 1). It was found that in the whole region of α-leboite existence, each cell contained almost exactly two atoms of silicon (1.99) and that the number of iron atoms is reduced regularly from 0.87 (53.5%Si) to 0.77 (56.5% Si) which points to the appearance of vacancies in the iron sub-lattice. A comparison of the X-ray and experimental densities confirms these conclusions.

An X-ray determination of thermal expansion coefficients along α-leboite lattice axes has shown that the expansion coefficient grows particularly in plane (001) along the iron atoms, which conforms with the vacancy type of structure of the ξ_α-phase.

Translated by A. Allan

TABLE 1

Weight, % Si	Lattice parameters		Density g/cm³	Number of atoms	
	a, Å	c, Å		n_{Si}	n_{Fe}
50.0	2.6937	5.139	4.68	–	–
52.5	2.6937	5.139	4.71	–	–
53.0	2.6937	5.139	4.69	–	–
53.2	2.6937	5.139	4.68	–	–
53.5	2.6937	5.139	4.65	1.99	0.87
54.0	2.6932	5.136	4.64	2.00	0.86
54.5	2.6923	5.135	4.57	1.99	0.83
55.0	2.6901	5.134	4.54	1.99	0.82
56.5	2.6872	5.128	4.44	1.99	0.77
57.0	2.6869	5.128	4.41	–	–
58.0	2.6870	5.128	4.30	–	–

* *Fiz. metal. metalloved.* 8, No. 3, 465-466.

REFERENCES

1. G.J. Phragmen, *Iron and Steel Inst.* 114, 397 (1926).

2. J.L. Haughton and M.L. Becker, *J. Iron and Steel*, 121, 315 (1930).

VOL.
8
1959

A FINE STRUCTURE IN BRITTLE AND DUCTILE FRACTURE OF EI531 STEEL TUBES IN TESTS OF EXPANSION BY A CONE*

E. Iu. Chemadurova

(Received 13 October 1958)

The breakdown of tubes during their production in a cold condition as well as in tests of expansion by a cone and with the same external stresses is apparently connected not only with differences in the microstructure but also the character of the fine structure.

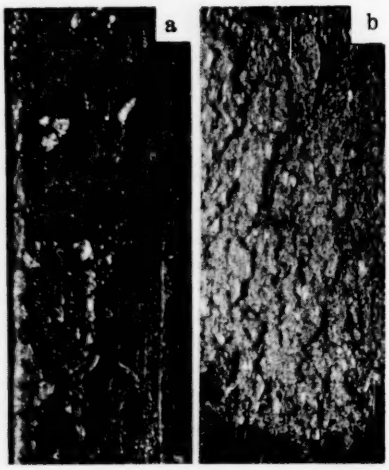

Fig. 1. Appearance of fractures of EI531 steel: *a* – steel which passed technological test; *b* – steel which failed to pass this test.

To establish a difference in the fine structure of tube specimens of heat-resisting EI531 steel, passing or failing to pass technological tests of expansion by a cone, distortions of the secondary lattice and the size of blocks were determined by the widening of the interference lines. Tube specimens were selected which were tested in expansion by a cone and which displayed fractures of a different character.

Cone expansion tests are carried out after heat treatment in a cold condition by a mandrel with 1/10 taper up to a 6% expansion of the outside diameter. Another kind of the same test is to expand the tube until it breaks. This happens at varying increases of the outside diameter (the break may occur in a section which is not being deformed). The type of the fracture depends on the plastic properties of the steel.

In the illustration are shown photographs of the fractures of specimens which passed and which failed to pass this test. In the first case (Fig. 1, *a*) the fracture is dull-grey, fibrous, denoting the high plastic properties of the metal. In the second case (Fig. 1, *b*) the break is crystalline, lustrous, bright with small tears, brittle. The microstructure of these specimens was practically identical – fine grained, consisting of equiaxial polyhedra and globular carbides.

For the investigation, specimens were cut from undeformed parts of tubes of the following composition:

TABLE 1

Composition of the examined steel, %

C	0.08-0.12	Nb	0.5-0.8
Mn	0.4 –0.7	Ti	0.1
Si	0.4 –0.7		
Cr	2.1 –2.6	Cu	0.25
V	0.2 –0.35	Ni	0.3
Mo	0.5 –0.7	S	0.03
		P	0.03

The deformed layer, produced by mechanical working, was removed by anodic dissolving to a depth of 0.15 mm.

For the separation of the widening of the interference line on account of secondary

* *Fiz. metal. metalloved.* 8, No.3, 466-468.

TABLE 2

Values of secondary distortions, size of blocks and of hardness

Specimen No.	Breakdown characteristics	$\frac{\delta a}{a} \cdot 10^{-3}$	$D \cdot 10^{-5}$ cm	Hardness
31	Passed cone expansion test ..	0.13	4.3	80
30	Passed cone expansion test ..	0.17	5.3	80
29	Failed to pass cone expansion test	0.1	7.2	82
28	Failed to pass cone expansion test	0.1	8.3	82

distortions and because of the small size of the blocks, a method was utilized, proposed by Lysak [1], of taking X-ray photograms in two radiations (inasmuch as EI531 is a low carbon steel).

The X-ray photograms were taken by the reflex method in a chrome radiation from face (211) and in a molybdenum one from face (651), which have the same reflection angles $\sim 78^{\circ}$.

The widening of the interference lines due to the exposure geometry was excluded from the total by deducting the width produced by a standard specimen. A specimen of EI531 steel, annealed for 6 hr at 700°, served as the standard. The X-ray photograms were photometrically evaluated by a MF-2 photometer. The width of the lines was determined as the ratio of integral intensity to the height of the maximum.

Experimental and computed values of secondary distortions $\frac{\delta a}{a}$, a size of blocks D (regions, coherently diffusing X-rays) and of hardness (Rockwell scale B) are given in table 2.

As it will be seen from Table 2, the hardness is low in both cases.

The measurements show that there are no substantial differences in the values of secondary distortions of the crystal lattice of the specimens cut from the tubes which passed and those, which failed to pass the cone expansion tests. A measurement of the blocks of these specimens has shown that they are not of the same size. The specimens which did not pass the test, i.e. the size of blocks of the more plastic specimens (specimens Nos. 30 and 31) is 1.5 times smaller than the size of the blocks in the second case.

A comparison of the data of microstructure, hardness, secondary distortions and of the blocks, allows one to draw the conclusion that the difference in the character of the fractures in technological tests of cone expansion is linked up with the size of the regions coherently diffracting X-rays (of the blocks).

Translated by A. Allan

REFERENCES

1. L.I. Lysak, *Voprosy fiziki metallov i metallovedeniye (Problems of the physics of metals and metallurgy), Izd. Akad nauk U.S.S.R.* p.45 (1954); p.40 (1955).

VOL. 8 1959

ON THE PROBLEM OF INTERMEDIATE CARBIDE PHASES IN CARBON STEELS*

N.V. GUDKOVA and V.P. KUZNETSOVA

(Received 18 September 1959)

Based on the data of a magnetic phase analysis, Apayev [1] expressed the opinion about a difference in the phase composition of annealed carbon steel depending on the carbon content. The difference is introduced by the intermediate carbide phase $\chi - Fe_xC$, which is not detected by the magnetic method in steel containing less than 0.4% carbon.

However, electron diffraction analysis of carbide precipitates of annealed carbon steel reveals the same intermediate carbide phases independently of the carbon content.

Two intermediate phases were found during a previous investigation of U12 steel [2]: hexagonal in a specimen annealed at 150°, and a rhombic in a specimen annealed at 200°. The same phases were found during examinations of steel 30. Carbide precipitates for the analysis were obtained by electrolytic solution of the specimens by Popova's method [3].

Specimens of steel 50 mm long and 13 mm in diameter were first quenched in alkali from a temperature of 880° and then annealed for 1 hr at 150, 200, 250, 300 and 350°.

The best diffraction pictures of intermediate carbide phases were obtained in carbon steel 30: hexagonal (Fig. 1) from a specimen annealed at 250° after it was dissolved for 6 hr, and a rhombic (Fig. 2) from a specimen annealed at 300° after dissolving for 6 hr.

In Tables 1 and 2 are given the values of interplane distances and line intensities of the hexagonal phase (Table 1) and of the rhombic (Table 2) for steels 30 and U12 [2].

Fig. 1. Electron difraction patterns of a hexagonal carbide phase.

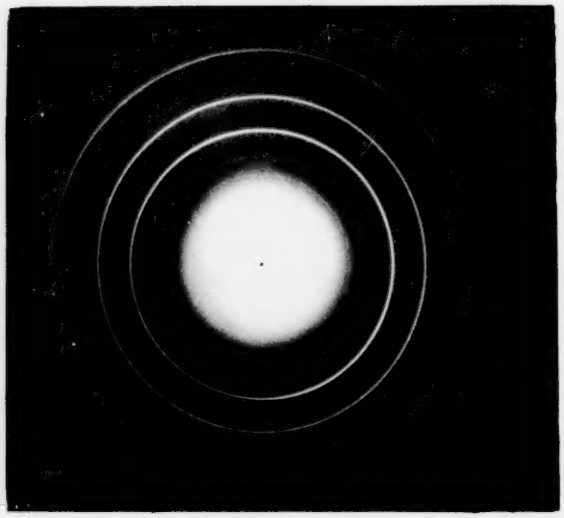

Fig. 2. Electron diffraction patterns of a rhombic carbide phase.

* *Fiz. metal. metalloved.* 8, No.3, 468-470.

TABLE 1

d, Å		I		hkl
Steel 30	U12	Steel 30	U12	
2.730	2.730	Strong	Average	200
2.060	2.060	Weak	Weak	210
1.815	1.820	Average weak	Average strong	300
1.570	1.575	Average strong	Very very strong	220
1.532	1.540	Average strong	Average strong	223
1.360	1.360	Weak	Average strong	400
0.910	0.907	Average weak	Weak	600

TABLE 2

d, Å		I		hkl
Steel 30	U12	Steel 30	U12	
2.815	2.815	Strong	–	103
2.500	2.500	Weak	–	005
2.360	2.362	Strong	Very weak	020
2.055	2.050	Very weak	Very weak	023
1.910	1.912	Very very strong	Very very strong	122
1.775	1.770	Average	–	210
1.705	1.703	Very weak	Average	212
1.540	1.550	Very very strong	Very very strong	030
1.425	1.430	Average	Average weak	027
1.324	1.335	Very weak	Average strong	035
1.200	1.200	Very very strong	Very very strong	230
0.960	0.982	Strong	Very weak	330
0.815	0.821	Strong	Average strong	250
0.767	0.770	Average	Average strong	060
0.714	0.726	Average	Average	260

Comparison shows a satisfactory coincidence of the values of interplane distances and consequently of the periods of the elementary nuclei (hexagonal – $a = 6.27$ Å, $c = 21.40$ Å and rhombic – $a = 3.82$ Å, $b = 4.72$ Å, $c = 12.50$ Å) and intensities of the produced lines.

It should be mentioned, firstly, that intermediate carbide phases were detected in steel U12 and, secondly, that it was not possible to obtain sharp diffraction pictures from steel 30 with a large number of reflections, such as those previously obtained for steel U12 [2].

Both facts, it seems, may be explained by the small number of intermediate carbide phases in carbon steel 30.

Apparently for the same reason intermediate phase χ was not detected by the magnetic method. It is possible that its quantity lies in annealed steel 30 outside the sensitivity limits of the magnetic method used in work [1].

Translated by A. Allan

REFERENCES

1. B.A. Apayev, *Metallovediniye i obrabotka*

VOL. 8 1959

metallov (Metallurgy and the working of metals), 1 (1957).
2. N.V., E.I. Levina and V.A. Tolomosov, *Fiz. metal. metalloved.* 4, vyp.3 (1957); 5, vyp.1 (1957).
3. N.M. Popova, *Karbidnyi analiz stali (Carbide analysis of steel)* Monograph M., Oborongiz (1957).

INFLUENCE OF THE DURATION OF TREATMENT ON THE PHASE COMPOSITION OF IRON WHICH HAS BEEN ELECTRICALLY HARDENED WITH GRAPHITE*

B.P. KOLESNIK

Institute of ferrous metallurgy Ac.Sc. U.S.S.R.

(Received 15 November 1958)

VOL. 8 1959

The hardening of machine and instrument components by means of electrically applied graphite is extensively used in industry [1]. The micro-hardness and resistance to wear of the hardened layer of a steel toughened with hard alloys depends on the specific duration of the treatment [2], [3]. However in the papers cited no investigation was carried out on the influence of the duration of the hardening process on the phase composition of the surface layer of the iron. Meanwhile, a study of this question appears to be of great practical interest.

We have made examinations, employing specimens of Armco iron which were prepared in the shape of thin sections as used for X-ray analysis. A low ash-content electro-technical quality graphite was used for the hardening. The electric arc hardening of the specimens was carried out in the following conditions: voltage 80V, capacitive load 28 microfarads, short circuit current 1.4A. The apparatus was equipped with a power regulator which was adjusted in such a way that the rate of charging of the condensers remained constant. The adjustment of the regulator and the control of the constancy of the charging was accomplished with the aid of an oscillograph of type EO-5, connected up with the circuit in a specially devised plan [4]. The X-ray photographs were taken with chrome irradiation in a camera with a drum radius of 114.6 mm. Microphotometry was carried out by means of a microphotometer of type MF-2.

As will be seen from the figure a *gamma*-phase appears in the first minute of treatment and appreciable distortions occur in the *alpha*-phase lattice, facts supported by the increase in the width of the interference line (110) $_{\alpha}$ from 0.4 to 0.73 mm. Relation of the phase composition of the iron's surface to the duration of the electric hardening of the graphite.

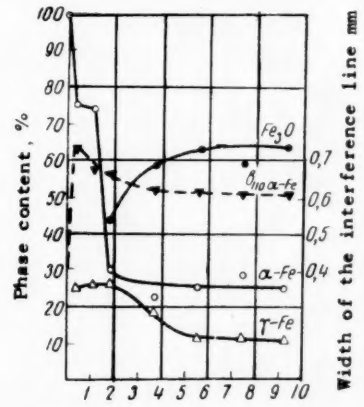

Fig. 1. Specific duration of treatment, min/cm^2.

Increase of the duration of the process up to 2 min/cm^2 results in a very slight rise in the amount of the *gamma*-phase and in the appearance of cementite. The distortions of the *alpha*-phase lattice decrease slightly; the width of the interference line (119) decreases from 0.73 to 0.66 mm. Thus, in the first 1-2 min of electric hardening in the basic process there is an occurrence of spot tempering of small regions of the specimen, with the formation of austenite and martensite. The quantity of carbon in the surface layer of the specimens is small.

A further increase in the duration of treatment up to 6 min/cm^2 results in some

* *Fiz. metal. metalloved.* 8, No.3, 470-472, 1959.

decrease in the distortion of the *alpha*-phase lattice, the amount of which in the surface layer hardly varies, and to a decrease in the quantity of the *gamma*-phase from 26 to 11 per cent. The amount of cementite increases from 44 to 63 per cent. The possibility of the formation of such large amounts of cementite in the surface layer of the specimen is foreshadowed in the metallographic investigations made by Mogilevskii and Chepovaya [5]. They showed that the surface layer of iron electrically hardened by graphite consists of ledeburite and needles of primary cementite. Here, it frequently happens that the formation of large crystals of cementite is made possible and even cases where the surface layer consists wholly of primary cementite. It follows that an increase of the duration of the treatment to 6 min/cm^2 results in an intensive saturation of the surface layer of the specimen with carbon, which gives rise to the appearance of cementite and increases in its quantity. The disintegration of the austenite and the decrease in the distortion of the *alpha*-phase grid, obviously takes place because of the heating of the specimen's surface by the subsequent discharges. Here, the disintegration of the austenite is followed by an increase in the amount of cementite.

An increase of the duration of treatment from 6 to 9 min/cm^2 results in practically no change in the phase composition of the surface layer or in the distortion of *alpha*-phase.

As can be seen from the data obtained the duration of treatment exercises its maximum influence on the phase composition of the surface layer at 6 min/cm^2 in the conditions stated. But the phase composition and, consequently, also the properties of the surface layer change over a very wide range. The hardening of instruments and components is generally carried out for a duration of 0.5-2.5 min/cm^2, that is to say, in the region of maximum influence of the duration of treatment on the phase composition, as can be seen from the graphs. Therefore if the time for the treatment is not strictly determined different effects for the hardening may be obtained notwithstanding the maintenance of a constant electric treatment.

Translated by A.J. Gibson

REFERENCES

1. B.R. Lazarenko and N.I. Lazarenko, *Elektroiskrovaya obrabotka metallov (Electric spark treatment of metals) Gosenergoizdat*, 1950; *Elektroiskrovaya obrabotka tokoprovadyashchikh materialov (Electric spark treatment of electric current conducting materials) Izd. Akad. Nauk SSSR*, (1958).
2. A.V. Polyanichenko, *Vestnik mashinostroeniya*, No.7 (1954); Trud. LONITO-Mash, Kn. 36, Mashgiz; (1955).
3. G.P; Ivanov, *Tekhnologiya elektroiskrovogo uprochneniya instrumentov i letalei mashin (Technology of electric spark hardening of instruments and machine components)* Mashgiz, (1957).
4. B.P. Kolesnik, *Vestnik machinostreoniya*, No.4 (1957).
5. I.Z. Mogilevskii and S.A. Chepovaya, *Elektroizkrovaya obrabotka metallov (Symposium: Electri spark treatment of metals), Izd. Akad. Nauk SSSR*, issue No.1 (1957).

ELECTRICALCONDUCTIVITY AND THE HALL EFFECT IN IRON-SILICON ALLOYS CONTAINING LEBOITE WHEN SUBJECTED TO HIGH TEMPERATURES*

A.I. GOL'DBERG, V.A. LIPATOV and P.V. GEL'D

S.M. Kirov Ural polytechnic Institute

(Received 14 July 1958)

VOL. 8 1959

Results were given in a previous publication 1 of an investigation dealing with the electrical properties of β-leboite at room temperature, which constituted the basis of an assumption regarding the semiconductor nature of the $\zeta\beta$-phase (in distinction to the $\zeta\alpha$-phase). In order to confirm this conclusion investigations were undertaken to establish the dependence of the temperature of the electroconductivity and of the constancy of the Hall effect for iron-silicon alloys which contained from 40 to 80 per cent by weight of Si, the temperature range used being 20 to 350°

The alloys were smelted in an induction furnace, using a silicon of brand Kr. 0 and Armco-iron. The specimens were prepared by drawing the molten alloy by suction into quartzite capillaries with a diameter of 2.5 to 4.0 mm.

A low temperature modification of leboite was stabilized by annealing at 800° [2, 3].

All measurements were made with the aid of an ordinarily used compensating device. Contacts with the specimen were of the rubbing type.

Results of the resistance measurements showed that for alloys containing more than 47% of Si a typical semiconductor character was observable in the variation of resistance with temperature. The exponential relation of resistance to temperature was especially clear in specimens containing 49-51% of Si. These specimens were most closely allied by composition to the $\zeta\beta$-phase and the maximum specific resistance, the Hall coefficient and the differential thermo-electromotive forces (not only at room but at higher temperatures) correspond to them, in the investigated region of temperatures, on the curve "composition-properties".

In the region beyond leboite all the speci-

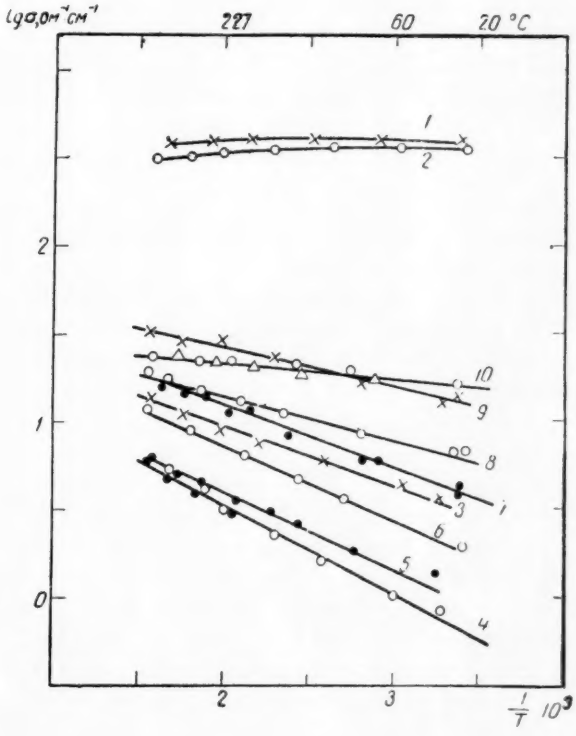

Fig. 1. Polytherms for the electroconductivity of alloys of iron and silicon:
1 - 40; 2 - 45; 3 - 47; 4 - 49; 5 - 53; 6 - 55; 7 - 57; 8 - 59; 9 - 65; 10 - 80; 85 wt. % Si.

* *Fiz. metal. metalloved.* 8, No.3, 472-475, 1959.

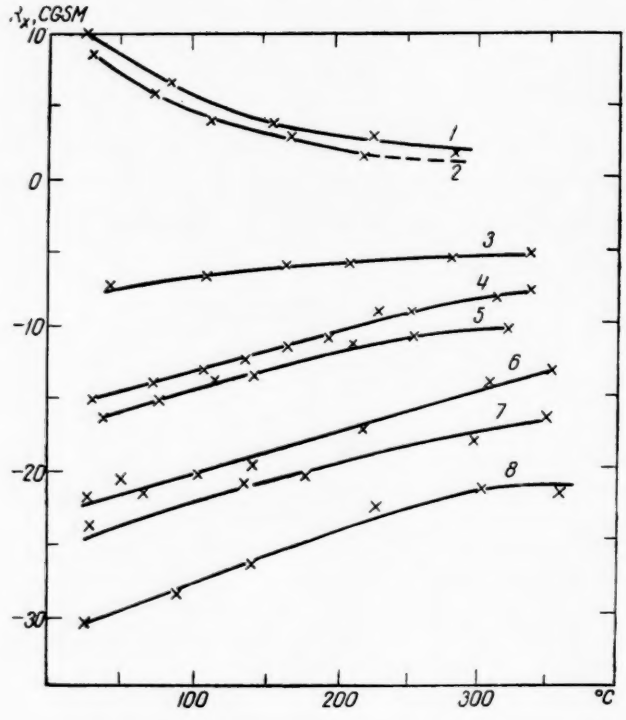

Fig. 2. Influence of the temperature on Hall's constant: 1 – 49; 2 – 51; 3 – 57; 4 – 59; 5 – 65; 6 – 70; 7 – 75; 8 – 80 wt.% Si.

mens gave evidence of possessing semiconductor properties but more weakly.

In alloys containing 40-45% of Si metallic conductivity is, apparently, in the ascendant.

Experimental data for some specimens are given in Figure 1 in a system of co-ordinates $\log \sigma - \frac{1}{T}$.

As can be seen from the graphs, the conductivity of the specimens containing 40-45% of Si is considerably larger than in the others. The smallest value of conductivity is possessed by specimens containing 49-51% of Si. The data recorded in Figure 1 opens up the possibility of evaluating the energy of activation of the alloys for which the following values were found.

Therefore, here also the dependence of E_{act} on the Si percentage is of an experimental character, attaining its maximum in alloys which by their composition coincide with leboite.

The temperature relationship of the Hall coefficient was measured on the same specimens as were employed in the conductivity investigation. It is to be regretted that failure has to be recorded where measurements of some of the alloys were concerned because of the small values and large fluctuations in the Hall electromotive force. The investigations were carried out in fields of 10,000 e by means of the usual method with two directions for the field and the current. The results obtained are given in Figure 2.

TABLE 1

Weight per cent Si:	48	49.51	53	55	57	59	65	75.80
E_{act} eV	0.13	0.20	0.18	0.17	0.13	0.12	0.08	0.04

As can be seen from the graphs, the Hall coefficient decreases (in absolute magnitude) in the case of all the specimens with increase in temperature. This circumstance indicates apparently that the concentration carriers in the alloy increases with the rise in temperature. Specimens containing 49 and 51% of Si are characterized by a positive Hall coefficient, which is evidence of their hole conduction. This point agrees with the results of the previous measurements of the thermoelectromotive force [1].

In alloys in the range beyond leboite the Hall coefficient is negative and in the range of 53-54% of Si changes sign. It is worthy of note that a change of sign is observed in the very same region of compounds, and with a differential thermoelectromotive force. It is conditioned by an accumulation of silicon crystals in the system.

The measurements made open up the possibility of computing the values of the concentration and mobility of the carriers. For instance, with readings at room temperature, using alloys of leboite composition, their concentration is approximately equal to 7×10^{18} $1/cm^3$ if in the expression $Rx = A\ 1/ne$ the multiple A is taken to have value unity.

The mobility of the current carriers for the same set of specimens was 0.7 cm^2/e sec.

The data obtained, in this way, confirm and add detail to the conclusion arrived at previously [1]on the semiconductor properties of the low temperature modifications of leboite.

Translated by A.J. Gibson

REFERENCES

1. A.I. Gol'berg, V.A. Lipatova and P.V. Gel'd, *Zh. tekh. fiz.* (in the press).
2. P.V. Gel'd, N.N. Serebrennikov and P.M. Sokharev, *Fiz. metal. metalloved.* 2, 244 (1956).
3. I.N. Strukov and P.V. Gel'd. *Symposium: trud - Ural'skogo politekh inst,,* No.72, 149 (1957).

VOL. 8 1959

AN INVESTIGATION OF PEARLITE TRANSFORMATION IN SEGREGATED AUSTENITE POWDER*

A.P. GULYAEV and V.DO ZELENOVA

The Central Scientific-Research Institute for motor cars and automobile motors

(Received 10 February 1959)

The procedure for obtaining the powder of segregated austenite from hardened steel by the method of anodic solution was described in paper [1] cited in the references. The separation by the method mentioned of segregated austenite made it possible to study the features of the transformation of this austenite in different temperature zones in comparison with conversions in massive specimens.

The investigation of the martensite transformation in powder form, obtained by electrolytic separation from hardened steel showed that martensite transformation does not take place in segregated austenite, though in the case of uniform specimens the reaction proceeds in normal fashion [2].

Results are given in the present paper of the investigation of the pearlite transformation of segregated austenite. The pearlite transformation of segregated austenite was investigated with a powder, separated by the method of electrolytic solution from a hardened steel type X 12F1 (1.49%C; 12%Cr; 0.28%V). A comparison was made of the graphs of the isothermal transformation of the austenite of the hardened steel type X12F1 and of the segregated austenite separated out from this steel.

The curves for the isothermal transformation of the powder and for the uniform specimens were based on the N.S. Akulov system of anisometry for which purpose the austenite powder and the uniform specimens were heated and soaked in a temperature range of 300-700°. The powder, obtained by electrolytic solution of the steel, was packed into a quartz tube fitted with a ground quartz stopper. After taking the curve for the isothermal decomposition of the austenite of the uniform specimen, the latter was put into a quartz tube, as done in the case of the powder, in order to secure as far as possible identical conditions for heating to constant temperature. The samples and powders after soaking in an isothermal bath were examined, as a supplementary measure, by means of X-rays.

In the steel type X12F1 being investigated observations were made, in the pearlite region of transformation, of the isothermal transformation both of the austenite of the uniform specimen and of the austenite in powder form. Graphs of the isothermal decomposition of the austenite of the uniform specimen and of the powder are given in Fig. 1.

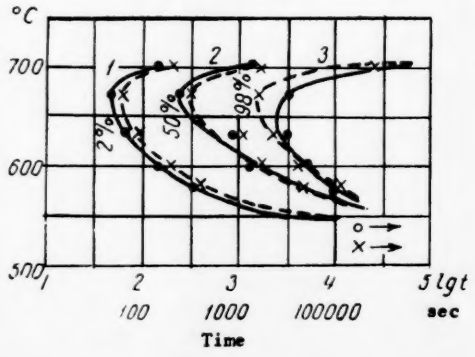

Fig. 1. Diagram showing the isothermal transformation of austenitic steel type X12F1 (hardening temperature for the samples 1150°) 1 — 2%; 2 - 50%; 3 - 98%. Continuous line curves refer to the uniform specimens, the broken line curves to the powders.

* *Fiz. metal. metalloved.* 8, No.3, 475-476, 1959.

As will be seen from Fig. 1 the curves for the isothermal decomposition of the austenite in the region of pearlite transformation coincide for the segregated and unsegregated austenite. The beginning of the austenite decomposition (the incubation period) for the cases of both the powder and the specimen are the same over the whole range of temperatures in the pearlite transformation. There were some divergencies in the time of the decomposition end-point of the austenite of the uniform specimen and of the powder which can be attributed to error in measurement (it was difficult to determine the change of position the light spot on the anisometer at the end of the transformation).

The X-ray photographs of the powder taken up to the isothermal soaking only showed the austenite lines, consisting of separate spots. The X-ray photographs of the powder taken after the isothermal treatment showed the presence of unbroken diffraction lines of the alpha-lattice, the X-ray photographs being absolutely identical for both the powder and the uniform specimen. Thus, it is seen that the pearlite transformation of the segregated austenite proceeds analogously to the pearlite transformation of the austenite of the uniform specimen of the steel. The incubation period of time and also the velocity of transformation are identical for the segregated crystals of austenite and for the austenite of the pearlite transformation.

The fundamental difference in the original condition of the segregated austenite and the austenite of the uniform specimen lies in the fact that in the powder obtained by the method of electrolytic solution from the hardened steel there is no sign of stresses of the second order.

The complete coincidence of the curves for the isothermal decomposition of the segregated austenite and the austenite of the uniform sample in the region of the pearlite transformation can be explained by the fact that the stresses of the second order exercise no appreciable influence on the diffusional transformation process, which takes place at high temperatures or, because there are no stresses of the second order in this range of temperatures, neither in the uniform specimen, nor in the segregated crystals of austenite.

Translated by A.J. Gibson

REFERENCES

1. V.D. Zelenova, *Zavodskaya laboratoriya*, No.1, 60 (1958).
2. A.P. Gulyaev and V.D. Zelenova, *Fiz. metal. metalloved.* 6, No.5, 945 (1958).

VOL. 8 1959

AN INVESTIGATION OF INTERMEDIATE TRANSFORMATION IN SEGREGATED AUSTENITE POWDER*

A.P. GULYAEV and V.D. ZELENOVA

The Central Scientific-Research Institute for Motor Cars and Automobile Motors

(Received 10 February 1958)

In the paper [1], it is shown that there is no martensite transformation observable in the monocrystalline austenite powder produced by the method of electrolytic solution of hardened steel.

The object of the present study was to ascertain the nature of the transformation of the segregated austenite in the intermediate region of temperatures in comparison with the transformation of the austenite of the uniform specimen. Intermediate transformation of segregated austenite was investigated with a powder separated by the method of electrolytic solution from hardened steel of type 144X3 (1.44%C; 3.45Cr; 0.21%Si; 0.36%Mn). The procedure adopted for producing austenite powder from steel of type 144X3 was analogous to that used for the separation of segregated austenite from steels marks X12M and X12 Fl, [2].

The investigation of the isothermal conversion of austenite from hardened steel of type 144X3 and of the separated electrolytic deposit was carried out with the aid of N. S. Akulov's system of anisometry. The curves from the isothermal decomposition were recorded for temperatures of 300 and 400°. The specimens of hardened steel and of the electrolytic deposit were heated in the anisometer bath and soaked for varying periods of time (from 8 to 20 hr) and then quenched in water.

For the uniform specimens of steel type 144X3 the transformation was observed in the temperature range of 300 to 400°.

Fig. 1 shows the curve for the isothermal decomposition of austenite at a temperature of 400° (a 100% decomposition of austenite was taken to be the declination of the light spot indicator of the anisometer corresponding to a temperature of 400° for the tempered specimen). As can be seen from the figure the magnetic induction of the electrolytic deposit separated out from the hardened steel type 144X3 as the result of soaking at a constant temperature in the mean temperature range hardly increases, which points to the absence of transformation.

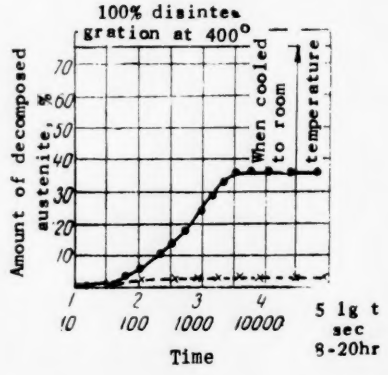

Fig. 1. Curve showing the isothermal transformation of austenite from steel type 144X3 at 400°. 1 – uniform specimen: 2 – powder.

An X-ray investigation of the electrolytic deposit showed that the small increase in the magnetic induction of the powder as the result of soaking at the temperature of intermediate transformation is linked up with the formation of oxides Fe_3O_4, that is the oxidation of the powder at the temperature of

* *Fiz. metal. metalloved.* 8, No.3, 476-478, 1959.

the experiment. X-ray photographs of the powder after isothermal soaking are analogous to X-ray photographs taken of the original powder, with the exception of the oxide lines. Attempts to avoid the formation of oxides by first putting the powder into ampoules from which the air had been exhausted did not lead to positive results. After soaking at temperatures of 300-400° the oxide lines are visible on the X-ray photographs of the annealed powder; however, no lines of the alpha-lattice were disclosed.

It follows that, as in the case of the martensite transformation, the intermediate stage in segregated austenite obtained by the method of electrolytic solution does not occur, while with the uniform specimen this process proceeds normally.

The transformation of austenite in the intermediate range of temperatures has features in common with the martensite transformation. This led to the concept that transformation in the intermediate range of temperatures proceeds via martensite formation. This point of view, supporting the existence of an intermediate conversion is expressed in the works of Shteinberg [3], Minkevich [4] and Kurdyumov [5].

Absence of evidence of transformation of segregated austenite in the range of temperatures where intermediate transformation takes place strengthens the hypothesis of the martensite character of the gamma-alpha transition in the bainite transformation.

Translated by A.J. Gibson

VOL. 8 1959

REFERENCES

1. A.P. Gulyaev and V.D. Zelenova, *Fiz. metal. metalloved.* 6, No.5, 945 (1958).
2. V.D. Zelenova, *Zavodskaya laboratoriya*, 24, No.1, 60 (1958).
3. S.S. Shteinberg, *Metallurg.* Nos.9-10, 58 (1937).
4. N.A. Minkevich, *Kachestvennaya stal'*, No.5, 25 (1935).
5. G.V. Kurdyumov, *Izv. Akad. Nauk SSSR, ser. Khimich.*, No.2, 271 (1963).

THE X-RAY K-ABSORPTION AT THE TEMPERATURE OF LIQUID NITROGEN*

S.A. NEMNONOV and K.M. KOLOBOVA

The Institute of Physics of Metals
Academy of Science U.S.S.R.

(Received 1 April 1959)

The experimental material available today on investigations regarding the K-absorption in the low temperature range is insignificant in quantity and contradictory in content. In the paper [1], (the dispersion was 20.75 XE/mm) it was shown that the fine structure of the K-absorption edge of copper at the temperature of liquid air shows up in greater contrast, supplementary extremes make their appearance, fluctuations of the absorption coefficient are expressed more strongly and spread to a greater distance from the principal edge than that obtained at room temperature. However for chromium [2] the transition from room temperature to the temperature of liquid nitrogen produces no change of any sort in the structure of the basic K-edge. Kurelenko investigated the fine structure of the K-absorption edges of iron and copper at + 20 and - 180° [3]. From the tabular data published in his study it can be seen that some extremes of the K-absorption spectrum of iron shift to the short-wave side while others travel in the opposite direction; the principal edge moves to the long-wave side at 1.4 eV. However, because of the poor quality of the spectrograms (for instance, the fine structure of the principal absorption edge of iron did not show up at all) the results of his investigations [3] appear to be somewhat unconvincing.

We carried out an investigation of the K-absorption spectrum of pure iron at two temperatures: + 20 and -180°. The specially constructed vessel to contain the liquid nitrogen was held in a vacuum together with the spectrograph. The temperature of the absorbing material was determined by means of a copper-constantan thermo-couple welded to the absorption apparatus and corresponded to - 180°. The spectra were photographed in the first order of reflexion from the crystallographic plane of the quartz ($13\bar{4}0$). The dispersion in the region being investigated was 2.5 XE/mm. Fig. 1 shows the curves of the K-absorption edges of iron, obtained at temperatures of + 20 and - 180°. The microphotograms of these edges recorded on MF - 4 are reproduced in Fig. 2. All the spectra were obtained from one and the same absorbent.

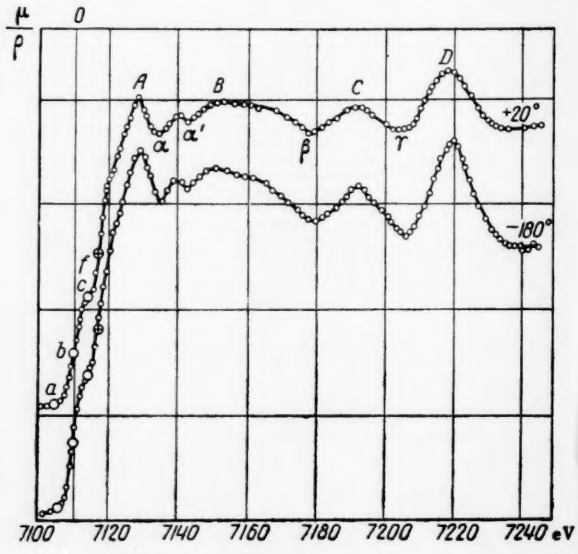

Fig. 1. K-absorption spectra of iron at + 20 and - 180°.

An examination of Fig. 1 and 2 showed that the contrast in the fine structure of the K-absorption of iron at a low temperature

* *Fiz. metal. metalloved.* 8, No.3, 478-480, 1959.

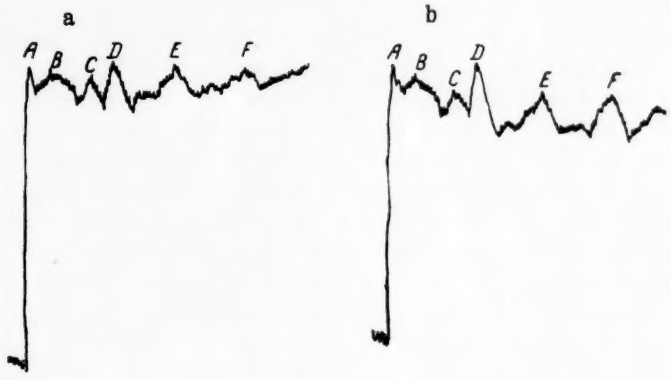

Fig. 2. Microphotograms of K-absorption edges of iron at + 20 (a) and -180° (b).

had improved appreciably, that is to say the relative sizes of the fluctuations of the absorption coefficient had grown larger. During this examination it was noticed further that the relative sizes of the different fluctuations in absorption did not change to an identical degree: for extremes situated at greater distances from the principal edge the difference in size of the corresponding amplitudinal fluctuations in the temperature change from + 20 to - 180° is more marked than when these distances are smaller, the result being an increase in the energetic spacing, the extension of which has a direct bearing on the emergence of the fine structure. Because of the limited nature of the length of film investigated by us and of the presence of identifiable K_{α_1} lines for nickel we were unable to trace the appearance of new fluctuations extending further from maximum F towards the short-wave side (Fig. 2).

Table 1 shows the relation of the fluctuations amplitudes (from the fourth to the first) which definitely indicate the increase in contrast of the fine structure of the K-absorption edge of iron at a temperature of -180° as compared with room temperature, which apparently is due to the decrease in the amplitude of the thermal vibrations of the atoms in the lattice.

As the temperature is lowered from + 20 to -180° the lattice parameter of metallic iron decreases correspondingly from 2860 to 2857 Å. In consequence, and in agreement with Kronig's [4] theory the extremes disposed at 50-70 eV from the principal edge should travel towards the short wave side. Such migration, to judge from our own data is actually observable. For instance the maximum D moves to 1.6 eV (Table 1). Travel towards the side of large energy is also observable for either extremes (γ, C, β), when the fact emerges that the nearer they (the extremes) are placed to the principal edge the smaller is their displacement. The change of position of the maximum A already no longer exceeds the experimental error (Fig. 1 and Table 1).

TABLE 1

Characteristics of the K-absorption edge in iron	Temperature, °C	
	+ 20°	- 180°
b, eV	7110,0±0,2	7109,6±0,2
$(^3/_4-^1/_4)_{abc}$, eV	2,2±0,2	1,8±0,2
$\frac{(\mu/\rho)_r}{(\mu/\rho)_A}$	0,35	0,38
f, eV	7117,1±0,2	7116,6±0,2
A, eV	7129,3±0,2	7129,5±0,2
C, eV	7187,0±0,2	7187,6±0,2
γ, eV	7205,0±0,2	7206,0±0,2
D, eV	7218,6±0.2	7220,2±0,2
$\frac{\Phi_\partial}{\Phi_A}$	1,78±0,06	1,95±0,06

Data regarding changes in the fine structure of the basic K-absorption edge of iron at the temperatures investigated are also

included in the table. From the table it is evident that both the central portion of the curve of the basic edge (point *f*) and the central portion of the curve of the initial absorption (point *b*) migrate to the long-wave side (in contrast with the change of position of the extremes). We suppose that, as the result of the decrease of the lattice parameter the extent of the coverage of the $3d$ – $4s$ – and $4p$ – bands of the metallic iron increases, the result of which might be an alteration in the distribution of the energy density of states and in the probability of the corresponding transitions. One cannot exclude the possibility, that as the result of such re-distribution of electrons by state, due to the fall in temperature, the energy of the Fermi surface (in the case of reversible metals) can decrease and that this decrease can become one of the factors resulting in the travel of the central portion of the curve of the initial absorption towards the side of the smaller energy. This assumption does not contradict either the tendency for the energetic width of the portion of the initial absorption (measured in the range of 3/4 to 1/4 of the maximum height of the curve *abc*) to undergo constriction, or the increase of the relation of the size of the initial absorption to the whole change in the coefficient of absorption $(\mu/\rho)_c/(\mu/\rho)_A$. Actually, because of the large coverage of the external energy bands in the general band of conductivity an increase is to be expected in the alloy of the *p*-states, and that means an increase in the magnitude of the initial change of absorption. A more pronounced increase in the initial absorption must result in a contraction of the width of this region and, consequently in a reduction of the difference existing in the range 3/4 – 1/4. The reduction in diffusion of the Fermi boundary at -180°, in comparison with room temperature, may also influence the contraction of the energetic width of a portion of the initial absorption.

Translated by A.J. Gibson

REFERENCES

1. N. Sedenborg and M. Claesson, *Ann. d. Physik*, 28, No.2 (1937).
2. Boke Klaus, *Zs.f. Phys. Chem.*, 10, H 1/8 (1957).
3. C.J. Kyrilenko, *J. de Physique Rad.*, 1, 139 (1940).
4. M.A. Blokhin, *Fizika rentgenovskikh luchei, (X-ray physics)*, (1953).

VOL.
8
1959

No. 4

		PAGE
Investigation of the stability of cracks in a microscopic model of a crystal	A. N. Orlov	1
The dispersion of current carriers in compounds of the PbS group	I. M. Tsidil'kovskii	16
Superconductivity of metals taking into account overlapping of the energy bands	V. A. Moskalenko	25
The effect of geometrical distortions on the distribution of the background intensity of X-ray and neutron diffraction photographs	M. A. Krivoglaz	37
The influence of thermomechanical treatment in which the stresses are created by twisting the sample, on the magnetic properties of the alloy vicalloy	M. G. Iuzhinskaia, Ia. S. Shur and N. N. Iagovkina	52
A magnetic method for the quantitative carbide analysis of carbon steels	Ia. I. Kagan and S. V. Bronin	56
Magnetic properties, electrical characteristics and hardness of high-carbon alloy steels in hardened state	M. N. Mikheev and G. .S Tomilov	63
Nickel-cadmium ferrites	N. A. Smolkov and S. A. Guschina	76
Generator of ultra-high magnetic fields	I. G. Fakudov and E. A. Zavadskii	81
An investigation of reaction diffusion in binary systems of the " metal-gas " type 2	V. I. Arkharov and E. S. Blankova	87
The problem of the state of carbon and iron in steel	I. N. Frantevich, D. F. Kalinovich and I. Io. Kovenskii	93
Treatise on recrystallization of the matrix in the process of decomposition of supersaturated solid solution aluminium-silver	R. M. Leriman and M. I. Turchinskaia	98
Electron microscope investigation of the distortion of Guinier-Preston zones in ageing alloys	N. N. Buinov	103
Plasticity of transformer steel after heat treatment at temperatures of 300-900°	S. I. Doroshek	109
Carbide eutectic in nickel carbon alloys	R. A. Sidorensko	114
An investigation of internal friction in powder products	B. Ia. Pines and Den Ge Sen	117
Some features of the recrystallization of transformer steel during rapid heating. 3. The dependence of grain growth rate and activation energy on heating rate	P. D. Izbranov, V. A. Pavlov and N. M. Rodigin	124
Small flow and after-effect deformations of spring phosphor bronze Br OF 6.5-0.15	S. O. Tsobkallo	129
Hardness and brittleness of metal-like compounds	G. V. Samsonov, V. S. Neshpor and L. M. Khrenova	137
On the question of the mechanism of the initial stage of deformation of polycrystalline metals	Y. R. Rausin	145

Letters to the Editor

A study of the reactional diffusion in binary systems of the type "metal-gas". 3	V. I. Arkharov, E. B. Blankova, N. A. Sukhova and R. A. Entelis	150
The change in the electrical resistance of a monocrystal of magnetite in a magnetic field in the region of its low-temperature transformation	T. D. Zotov	154

VOL
8
195

INVESTIGATION OF THE STABILITY OF CRACKS IN A MICROSCOPIC MODEL OF A CRYSTAL*

A.N. ORLOV

The Institute of the Physics of Metals Akad. Nauk. S.S.S.R.

(Received 14 February 1959)

The conditions are determined for the existence of a minimum in the potential energy for a simple microscopic model of an elastically extended crystal of finite dimensions which contains a crack. The form and dimensions of the crack are described by three variable parameters.

VOL. 8 1959

1. INTRODUCTION

According to the modern presentation, the process of brittle fracture in a crystal under tensile stresses can be divided into three stages: 1) The formation of a crack nucleus on account of local stresses arising close to dislocation concentrations [1], as a result of a concentration of vacant sites [2] or a combination of both these effects or as the results of the transfer of atoms in phase changes; 2) the growth of the nucleus accompanied by relief of the stresses caused by the external load; this stage ends when the dimensions of the crack are so large that its further growth continues without further increase of the external load; 3) the crack spreading over the whole cross section of the crystal.

In this article the conditions of equilibrium for the cracks in the second stage are reviewed. Although microscopic distortions of the lattice (dimensions of the order of an interatomic distance) play, apparently, a decisive role in the mechanism of the nucleation of the cracks, in the second stage of the crack growth its stability in the actual lattice is determined by nearly the same conditions as in the ideal one. Therefore, it is sufficient to consider the ideal lattice with a crack.**

Griffith [5] first of all studied the problem of a crack from this viewpoint (conforming to an amorphous medium) within the framework of elasticity theory. He determined the reduction in the elastic energy of a sample upon the opening of a crack, using the stress distribution in the vicinity of the crack which had been calçulated according to elasticity theory. In this straightforward problem the equilibrium form of the cross section of the crack is an ellipse, the length of the major semi-axis being $2c$. The difference in energy U between the elastically strained crystal without a crack, and the crystal with a crack so that the elastic stresses have been partially relieved is illustrated as a function of the dimension c by a curve with a maximum at

$$c = c^* = 2\gamma E/\pi\sigma^2, \tag{1}$$

where γ - the surface energy; E - Young's modulus; σ - the stress at large distances from

---

* *Fiz. metal. metalloved.* 8, No.4, 481-493, 1959.

** As experimental [3] and theoretical [4] studies show, microscopic defects at the edge of the cracks may substantially effect the mechanism by which it spreads and the second stage.

the crack. The study of the three dimensional problem leads to an analogous results [6, 7].

Griffith's theory possesses a number of faults: 1) The large distortions of the lattice close to the edge of the crack are described using the linear theory of elasticity. 2) It does not take into account the interaction of the opposite walls of the crack (q.v. however, [6]). 3) For a finite crystal the problem is solved only in a general way and the dependence of the critical dimensions of the crack on the parameters of the problem cannot be studied on account of the cumbersome nature of the solutions. 4) As Elliott [6] remarked and Frenkel [8] emphasised (q.v. also [9]) according to Griffith's theory a crack which has not achieved the critical dimension c^* will heal up again of its own accord. Stable nucleating cracks of dimensions $c < c^*$ are impossible. In order for such cracks to exist the graph $U(c)$ should have a minimum at $c < c^*$[1]

In the works mentioned the stability of cracks under tensile stresses was considered. It can be shown (q.v. e.g. the review [11]) that in the presence of distortions which impede the process of shear deformation (the movement of dislocations) and lead to the formation of incompleted shears, it is possible for cracks to be formed where the energy of the crystal, as a function of the dimension of the crack c, has a minimum. In other words in a lattice with distortions of a definite type stable cracks are possible in the presence of stress concentrations.

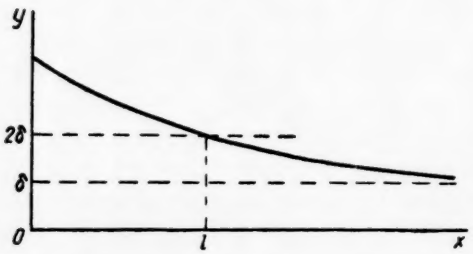

Fig. 1. The transition from the wide to the crevice like part of the crack in Frenkel's model

Under tensile stresses the possibility of the existence of stable cracks even in the ideal lattice is not excluded *a priori* because the energy of the elastically extended crystal with a crack of some optimum dimension $c = c_0$ may be smaller then the energy of a crystal with a smaller or larger crack. For this it is necessary that, with the growth of $c > c_0$, the energy of the elastically distorted region G_1 (Fig. 2) at the edge of the crack should grow faster than the elastic energy due to the relief of stresses in the region G_0 under the central part of the crack decreases, and that with the decrease of $c < c_0$ the energy of the region G_0 should grow faster than the energy in the region G_1 diminishes.

Frenkel [8] studied a model of an elastic body with a crack, actually – a plate with a longitudinal crack spreading under the action of the force F which was directed along the normal to the surface of the plate. The "chipped off" layer of the plate may be considered as a separate cantilever [12]. In such a model equilibrium is possible when the elastic energy of the bent "cantilevers" and the energy coupling it to the remaining part of the plate is compensated by the work of the force F. However, on enlarging the crack, both the

[1] The expression for the energy accepted in Shil'krut's paper also does not give a minimum U but has a maximum at the critical value for the dimension of the crack which was mentioned by the author. Besides we notice that the elliptical form of the crack is not "chosen" by Griffith, as is confirmed in [10] but it is obtained as a result of solving equations of the theory of elasticity. On doing this the edge of the crack may appear to be extremely "sharp"; [8].

energy U_1 of the free surfaces (the walls of the crack) and also the elastic energy U_2 of the bent "cantilevers" grow so that this model poorly reflects the state of things when cracks appear inside an elastically extended body when the elastic energy is increased and decreased only by the energy of the free surfaces.

Apart from this, in Frenkel's calculation [8] (which was published after his death) there are mistakes. As Rzhanitsyn [13] noticed formula (8a) is not true. Further, as has just been pointed out, in the expression for the energy (formula 13 in [8]) all the items should be positive and in the formula mentioned the energy $U_2 < 0$. Finally, the formula (12) for the energy U_3 of the "crevice like" part of the crack (q.v. our Fig. 1), where according to the definition of the length of the crack l (on page 1861) the distance between the planes $y + \delta$ varies from the normal δ to 2δ, is also not true. In fact by considering that in this region the force of the interaction of the walls of the crack is equal to (p. 1863) $f = 2Ey/\delta$, we obtain Ey^2/δ for the energy of interaction on unit surface. This quantity must be integrated with respect to x, from l to infinity when the co-ordinate of the edge of the crack l is not an arbitrary point but, by definition, is found from the condition

$$y(l) = \delta. \tag{2}$$

If we accept according to Frenkel (formula (10)), that in the region considered

$$y = F\delta/Ex, \tag{3}$$

then we obtain

$$U_3 = \frac{\delta F^2}{E}\int_l^\infty \frac{dx}{x^2} = \frac{\delta F^2}{El},$$

where in agreement with (2) and (3) $l = F/E$. Thus $U_3 = \delta F$ and distinct from the formula (12) U_3 does not depend on the size of the crack l but only on the slope of the graph (3) determined by the force F.

Hence it follows that in Frenkel's work the question concerning the existence of stable cracks with dimensions less than critical ones are not decided; although, as we shall show further on, the fundamental idea of Frenkel, that such cracks are possible, is true.

Frenkel considered a body of finite dimensions (plate in the direction along the normal to the plane of the crack while calculations according to the theory of elasticity for Griffith's cracks were carried out for an infinite body. A body of finite dimensions differs from an infinite one in that in it, upon forming a crack and completely relieving the stresses, a finite elastic energy is released $U_v = L\epsilon^2 E$ per unit area of the crack. This is determined by the dimension of the body L and the size of the relative extension ϵ. If L and ϵ are small then the elastic energy is insufficient to compensate for the free surface energy and the formation of cracks is disadvantageous. And in the infinite crystal ($L \to \infty$ at as small a finite ϵ as you like) the energy $U_v \to \infty$ and the formation of cracks is always advantageous. Therefore the conditions for the stability of the cracks in a finite and an infinite body should not be the same. However since a strict calculation within the framework of the elasticity theory gives, for a finite body, a solution that is being criticized, we shall consider a simple microscopic model that enables the qualitative aspects of the problem to be clarified.

2. THE MODEL

We shall consider the model of a crystal composed of point atoms which interact according to the law

VOL. 8 1959

$$v(l) = -a_1 l^{-\mu} + a_2 l^{-\nu},$$

where v is the potential energy of the interaction of two atoms situated at a distance l; a_1 $a_2, \mu < \nu$ are constants. We shall denote

$$l/l_0 = x, \; v l_0^{\mu}/\mu a_1 = u, \; l_0 = (\nu a_2/\mu a_1)^{\frac{1}{\nu-\mu}}. \tag{4}$$

l_0 is the equilibrium distance between two free atoms. The instead of $v(l)$ can be written:

$$u(x) = -\mu^{-1} x^{-\mu} + \nu^{-1} x^{-\nu}. \tag{5}$$

We assume that the energy $u(x)$ does not depend on the distribution of the other atoms surrounding a given pair. By this we are taking only the central forces into account and we are not considering the changes in the energy of the lattice due to changes in the valence angles. We further assume that it suffices to be limited to the calculation of the interaction of only the nearest neighbour atoms.

The model described reflects the non-linear character of the inter-atomic forces at large distances, in particular in the "fissure like" part of the crack. In addition to this it is based on essential simplifying assumptions. Therefore in studying the model one cannot expect to obtain quantitative results. Hence in the calculations there is no sense in considering the actual symmetry of the lattice and it is sufficient to consider a simple cubic lattice*.

In the accepted approximation the total energy of the crystal at absolute zero is equal to

$$U = \sum_i u_i(x). \tag{6}$$

The summation is carried out over all the interatomic bonds. In order to find the values $x_i = x_{io}$, corresponding to the minimum U, the set of equations for $\partial U/\partial x = 0$, must be solved and the derivatives $\partial^2 U/\partial x_i \partial x_j$ should satisfy the conditions for a minimum and the variable x_i – the boundary conditions for a given form of the external surface of the crystal.

During the development of the ideas of Born [16] and Frenkel [17] in references [14, 15] this problem was solved for the one dimensional case (a chain of given length L, the atoms of which interact according to the law (5), or a pile of hard parallel planes, interacting according to the same law). If the number of atoms $N+1$ in the chain (or the planes in the pile) is sufficiently large ($N \lesssim 10^3$), then even for an insignificant relative extension of it ($(L - L_0)/L_0 = \epsilon \approx 10^{-2}$, L_0 is the length of a chain with free ends) assymetrical configurations of the atoms are possible. In these configurations one interatomic distance $x_{N_0} = \eta$ is considerably larger than the rest $x_{10} = x_{20} = \ldots = x_{N-1.0} = \xi$ and fulfills the minimum potentail energy conditions which have the appearance of

$$\varphi(\xi) = \varphi(\eta), \; (N-1)\frac{\partial \varphi(\xi)}{\partial \xi} + \frac{\partial \varphi(\eta)}{\partial \eta} > 0,$$

where $\phi(x) = du/dx$. Since the average interatomic distance is L/N is given so ξ and η are

* It is known that in the presence of central forces only the lattice with the most densely packed atoms is stable and the stability of crystals with any other symmetry cannot be explained. Thus it was necessary to carry out the calculation for a densely packed lattice. Although we shall apply the method of calculation given below to such a lattice, the working is greatly simplified in the case of a simple cubic lattice which has been considered below. It can be assumed that its stability is provided by certain additional forces depending, for example, on the valency angles which obstruct only a large shear deformation and secure a minimum for the energy of the simple cubic structure.

connected by the condition

$$(N-1)\xi+\eta=L. \tag{7}$$

In the case of a "pile" of planes such a configuration corresponds to a crack going right through.

Here we shall show that in the three dimensional model for an inconsiderable uniaxial tension a configuration with large interatomic distances is also possible in a limited region in the crystal, that is limited cracks which correspond to a potential energy minimum.*

In order to do this we shall assume that in a lattice with central symmetry all the lines joining the nearest neighbour atoms are parts of straight lines which form $z/2$ families (z is the co-ordination number), all the straight lines of one family are parallel to each other and through each atom one line of each of the families passes. Each straight line may be regarded as a chain of atoms to which all the results of [14, 15] apply. On deforming the lattice these chains stretch and in the general case they bend. However, since we are not considering the dependence of the energy on the valence angles the energy is determined only by the size of the interatomic distances and not by the form of the chains.

VOL. 8 1959

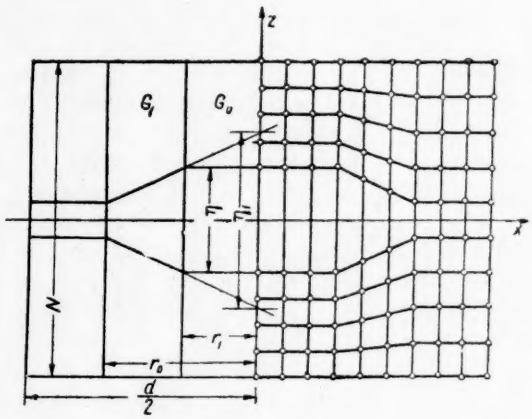

Fig. 2. The distribution of the atomic planes in a crystal with a crack

We shall consider a crystal that is infinite in the x and y directions and has a thickness of $N-1$ atomic layers along the z axis; the direction in which the stress** is applied. We shall divide the crystal into prisms with axes in the oz direction and with a basal area of

* This does not mean that for a given deformation of the outer surface of the crystal other atomic configurations are not possible, in particular those with a different lattice symmetry whose energy is lower than the ones studied below. The ascertainment of a configuration corresponding to the absolute energy minimum is not included in the present work in which is considered only a narrow group of configurations + cracks with a definite form.

** In future the linear dimensions will be expressed in units which are equal to the equilibrial interatomic distance in the unstressed crystal. According to (4) it is equal to $x = a = 1$. Therefore the length L of the unstressed crystal is numerically equal to the number of atomic layers.

such a size d^2 that on average one crack* is projected onto this area. Due to their small number the average distance d between the points of their projection is so large that the interaction of the cracks' elastic fields may be neglected.

We shall call the interatomic bonds along the x, y and z axes x-, y- and z- bonds respectively and the energy of interaction of the atoms joined by them – the energies of the bonds corresponding to the x- and y- bonds together will be called r-bonds and those composed from the z- and r-bonds of the chain – z- and r-chains. Let the lattice be subjected to a relative extension ϵ in the Oz direction and in it let it have, at a height $z = 0$ between the $N/2$ and the $N/2 + 1$ layers, a crack in the form of a disk, radius r_0 with sharp edges (Fig. 2). The radius of the plane part of the disk is r_1, the thickness of this part is η. The apices of the cones which form the truncated part of the disk lie above the centre of the disk at a height of $\pm\eta/2$. From the theory of elasticity [18] it is known that the linear dimensions of the region in which, near to the crack, the stresses are relieved are of the order of the radius of the crack r_0. Therefore at a distance of the order of $N/2 \approx r_0/2$ atomic layers on both sides of the crack, the z-chains should be found not in the equilibrially extended state but in a configuration containing one large interatomic space. On the other hand from the point of view of the model [14] the z-chains in the G_0 region (Fig. 2) can be considered as being isolated since in this region all the z-chains are similar and the resultant force with which the neighbouring chains act on the given one is equal to zero. But according to [14] in the isolated chain all the small spaces are equal to each other. In accordance with this we suggest that the stresses are relieved in all the G_0 region and the shear deformation is distributed uniformly over the whole of the G_1 region which is projected onto the ring of width $r_0 - r_1$. If it turns out that the dimension of the stable crack $r_0 \geqslant N$ then our assumption concerning the stresses being relieved over the wole thickness of the crystal (as takes place in Frenkel's thin plate) will be justified and the result will not contradict the theory of elasticity. If $r_0 < N$, then strictly speaking, we shall apply the result only to an hypothetical crystal with a Poisson coefficient equal to zero for which the configuration given in Fig. 2 corresponds to a minimum of the elastic energy for any thickness of N.

The length of the largest interatomic space in the plane part of the crack is equal to η and in the conical part is

$$\eta' = \eta_1 - (\eta_0 - 1)\, r/r_0. \tag{8}$$

The length ξ of the short spaces in the G_0 region where $\eta' = \eta$ is equal to ξ_0 and ξ_0 is connected to η by equation (7). In the G_1 region

$$\xi - 1 = \delta = \delta_0 + (\varepsilon - \delta_0)\,(r - r_1)/(r_0 - r_1),\ \ \delta_0 = \xi_0 - 1. \tag{9}$$

In order to simplify the calculation we suggest further that the angle at the edge of the crack should be so sharp that $\alpha \equiv (\eta_1/2r_0)^2 \ll 1$ and in the calculations it is sufficient to limit oneself to the first degree of α.

3. THE CALCULATION OF THE ENERGY OF A CRYSTAL CONTAINING A CRACK

We shall calculate the energy of the model described for the part of a crystal containing a

* As is mentioned above we are not reviewing the growth mechanism of the cracks. However it must be assumed that the number of cracks which form for a definite extension of the crystal is predetermined by the number of weak places in the lattice (the assumulations of dislocations and also the accumulations of vacant sites) where the growth of cracks is facilitated. For a small extension only the largest distortions, which are few, are effective.

crack and having the form of a prism height $N-1$ and a basal area of d^2. We shall denote

$$u(1) = u_1, \left(\frac{\partial^2 u}{\partial x^2}\right)_{x=1} = u_1''.$$

Then the energy of one bond extended to a size ϵ is equal to

$$u = u_1 + u_1'' \varepsilon^2 a^2/2, \tag{10}$$

the energy of all the Nd^2 z- bonds in the equilibrially extended lattice is obtained by multiplying (10) by Nd^2, but the energy of the same volume with a crack considering the x- and y-bonds is equal to

$$3Nd^2u_1 + Nd^2u_1''\varepsilon^2a^2/2 + U, \tag{11}$$

where U is the enery change on forming the crack at a fixed ϵ.* U is a function of the parameters r_0, $\beta = r_1/r_0 > 1$ and η which should be determined from the conditions for minimum U (if it exists) at given ϵ, N and β, ν. We shall present U as the sum of the items which are related to the r- and z-bonds

$$U = U_r + U_z. \tag{12}$$

The energy of the short bonds is calculated according to formula (10), the energy of the long bonds, intersecting the crack we are writing down in the form of (5)**

The energy of these bonds in the G_1 region, which are projected onto a ring width $r_0 - r_1$ and length $2\pi r_0$ (since the largest portion of the energy is donated to the short bonds near $r = r_0$, $2\pi r_0$ and not $(r_0 + r_1)$ must be taken as the length of the parameter of the ring), is equal to

$$U_{G_1} = 2\pi r_0 \int_{r_0}^{r_1} u(x)\,dr = -\pi r_0^2 \frac{4}{\eta}\left(1 - \frac{1}{\beta}\right)\bar{u}_1, \tag{13}$$

where

$$\bar{u}_1 = [\mu(\mu - 1)]^{-1} - [\nu(\nu - 1)]^{-1} \tag{14}$$

and the value of the integral at the upper limit is omitted since at $\eta > 1$ it is considerably smaller than u_1 and, as the calculation shows, also does not affect the values of the derivatives of U.

Also omitting the imaginary items in the sum (12) which represent the elastic energy of the practically unextended z-bonds in the G_0 region, i.e. considering $\xi_0 = 1$, it is possible

---

* For a fixed load on the sample the change in energy will be different since on the formation of a crack the stress over the continuous section of the sample is increased. For a large enough d this condition may be neglected. Then the conclusions are applicable to a crystal under a load proportional to ϵ.

** When the width of the crack is $\eta \gg 1$ there are no grounds for considering that the last atom in the z-chain belonging to the plane $z = \eta/2$ interacts only with that atom in the plane $z = -\eta/2$ which comes into the same z-chain. One must consider its interaction with all the atoms in the opposite wall of the crack. It is possible however to arrange to calculate that this case is discounted in choosing the constants μ and ν in (5) so that $u(x)$ for large x is the energy of interaction of all the atoms of one plane with all the atoms of a neighbouring plane which apertains to one z-chain. We shall assume that μ and ν are chosen in this way.

VOL. 8 1959

to write (12) in the form

$$U = A_T \pi r_0^2 + \frac{N u_1'' a^2}{96} \frac{\gamma_1^4}{r_0^2} \left(\frac{\beta}{\beta-1}\right)^2 \left[\left(\frac{\beta}{\beta-1}\right)^2 I_1 - \frac{1}{(\beta-1)^2} I_1'\right] = \tag{15}$$

$$= A_T \pi r_0^2 + D/r_0^2,$$

where

$$I_1' = I(r_1), \quad I_1 = I(r_0) = 0{,}219026,$$

$$I(r) = \frac{1}{r^2} \int_0^r \sqrt{r^2 - y^2} \left(\frac{r_0 - y}{r_0 + y}\right)^2 dy, \quad r_1 = \frac{r_0}{\beta}. \tag{16}$$

$$A_T = A + A_{G_1} \tag{17}$$

$$A_{G_1} = -\frac{4}{\gamma_1}\left(1 - \frac{1}{\beta}\right)\bar{u}_1,$$

$$A = A_0 + A_1\gamma_1 + A_2\gamma_1^2, \quad A_0 = -u_1 - u_1''\varepsilon^2 a^2/2, \tag{18}$$

$$A_1 = -2\varepsilon A_1' u_1'' a_1^2, \quad A_1' = \frac{1}{6}\left(1 + \frac{1}{\beta} + \frac{1}{\beta^2}\right),$$

$$A_2 = u_1'' a^2 A_2'/N, \quad A_2' = \frac{1}{12}\left(5\,\frac{\beta+1}{\beta-1} + \frac{\beta-3}{\beta^2(\beta-1)}\right),$$

$$D = \frac{N}{96} u_1'' a^2 \left(\frac{\beta}{\beta-1}\right)^4 \Phi_0(\beta)\,\gamma_1^4, \tag{19}$$

$$\Phi_0(\beta) = 0{,}0547566 - \frac{1}{\beta^2}\left(2 - \pi\beta + \frac{\pi}{16\beta} + \frac{2\beta^2 - 1}{\sqrt{\beta^2 - 1}} \cos^{-1}\frac{1}{\beta}\right). \tag{20}$$

The term $r_0^2 A_T$ in (15) represents the energy of the z-bonds and D/r_0^2 the energy of the extended r-bonds in the G_1 region.

In future it will be more suitable to give the value of A in the form

$$A = A_0\,[1 - (2A_1' - A_2'\gamma_{10})\,\gamma_{10} q], \tag{21}$$

$$\gamma_{10} = \gamma_1/N\varepsilon, \tag{22}$$

$$q = N\varepsilon^2 u_1'' a^2/A_0 \approx N\varepsilon^2 u_1'' a^2/|u_1|. \tag{23}$$

We note that A_0, and u''_1 are of the order of the unit $a = 1$.

4. AN EXAMINATION OF THE DEPENDENCE OF THE ENERGY ON THE PROBLEM'S PARAMETERS

The co-ordinates r_0, β, η of the points Q_i at which the energy U is a minimum should satisfy the conditions

$$\partial U/\partial r = 0, \quad \partial U/\partial\eta = 0, \quad \partial U/\partial\beta = 0 \tag{24}$$

and furthermore at these points the following determinant should be positive;

$$D = \begin{vmatrix} U''_{rr} & U''_{r\eta_1} & U''_{r\beta} \\ U''_{r\eta_1} & U''_{\eta_1\eta_1} & U''_{\beta\eta_1} \\ U''_{r\beta} & U''_{\eta_1\beta} & U''_{\beta\beta} \end{vmatrix}, \tag{25}$$

it is composed of the second derivatives of U and all its chief minors, e. g.

$$U''_{rr},\ U''_{\eta_1\eta_1},\ U''_{\beta\beta} \text{ и } D^{(2)} = \begin{vmatrix} U''_{rr} & U''_{r\eta_1} \\ U''_{r\eta_1} & U''_{\eta_1\eta_1} \end{vmatrix}. \tag{26}$$

At first we shall find the points at which the necessary conditions of (24) are fulfilled.

From the conditions

$$U'_r = \partial U/\partial r_0 = 2\pi A_1 r_0 - 2D/r_0^3 = 0 .$$

it follows that

$$r_{0\,min} = (D/\pi A_1)^{\frac{1}{4}} = M\left(\frac{\Phi_0}{A_1}\right)^{\frac{1}{4}} \frac{\beta}{\beta - 1}\,\eta_1, \tag{27}$$

where

$$M = (Nu''_1 a^2/96\pi)^{\frac{1}{4}}.$$

Consequently the necessary condition for the existence of a minimum is $A_1 > 0$. In accordance with (16), (17) and (21) the condition for $A_1 = 0$ has the form

$$A_0[1 - (2A'_1 - A'_2\eta_0)\,\eta_0 q] - \frac{4a}{\sqrt{N}q\eta_0}\sqrt{\frac{u''_1}{A_0}}\,\bar{u}_1\,\frac{\beta - 1}{\beta} = 0. \tag{28}$$

We shall limit the investigation of the case to quite large N and not very small deformations ϵ, when the second term in (28) is considerably smaller than the first and can be omitted (the conditions for a minimum obtained below $N \sim 10^4$, $g > 10$, $\eta_0 \approx 0.3$, $\beta \approx 3$ do not contradict this assumption).

The second condition (24) is written in the form

$$U'_{\eta_1} = \partial U/\partial\eta_1 = 4A_0 + 5A_1\eta_1 + 6A_2\eta_1^2 = B(\eta_1) = 0, \tag{29}$$

if after differentiating r_0 is substituted in accordance with (27) in

The last condition in (24) comes to

$$U'_\beta = \partial U/\partial\beta = 2\pi r_0^2 u''_1 a^2(\varepsilon B_1\eta - B_2\eta_1^2/N) + \pi N^4\eta_1^4\Phi_1(\beta)/r_0^2, \tag{30}$$

where

$$B_1 = u''_1 a^2(\beta + 2)/6\beta^3,\ B_2 = \frac{u''_1}{12(\beta - 1)^2}\,[5 + \beta^{-1} - 5\beta^{-2} + 3\beta^{-3}], \tag{31}$$

$$\Phi_1(\beta) = \frac{\beta^2}{(\beta - 1)^5}\left[2 - 0{,}2190263 + \frac{6\beta + 5}{\beta(\beta + 1)} - \pi\left(3 + \beta - \frac{3\beta + 1}{16\beta^2}\right) + \right.$$

$$\left. + (2\beta^2 + 6\beta - 1) - \frac{3\beta + 2}{\beta(\beta + 1)}(\beta^2 - 1)^{-\frac{1}{2}}\ \cos^{-1}\frac{1}{\beta}\right]. \tag{32}$$

VOL. 8 1959

It can be transformed into the form

$$\frac{Ar_0^2}{\Phi_1 M^4 \pi \gamma_1^4} \frac{\partial U}{\partial \beta} = A_0 - 2\varepsilon C_1 \eta_1 + \frac{C_2}{N} \eta_1^2 \equiv C(\eta_1) = 0, \tag{33}$$

where

$$C_1 = A_1' + B_1 \Psi_1, \quad C_2 = A_2 + 2B_2 \Psi_1, \quad \Psi_1 = -\frac{\Phi_0}{\Phi_1} \left(\frac{\beta}{\beta - 1}\right)^4. \tag{34}$$

In solving (29) and (30) the terms containing A_{G_1} are omitted on the same grounds as in (27).

Equation (27) determines a certain surface $r_0 = r_0(\beta, \eta_1)$. The conditions $U_{\eta'} = 0$ and $U_{\beta'} = 0$ determine two other surfaces $r_{0\eta}$ and $r_{0\beta}$. They intersect the surface r_0 along curves whose projections on the plane of $r_0 = 0$ are determined by the equations (27) and (31). The points of intersection $Q_i(\beta_M, \eta_{1M})$ of these curves are the projections on the plane $r_0 = 0$ of the unknown points Q_i of the intersection of the three surfaces r_0, $r_{0\eta}$, and $r_{0\beta}$; r_0 – we find the co-ordinates of the points Q_i by substituting β and η in (27).

We shall find the co-ordinates of the points Q_i. We shall write the equation of the curves $B = 0$ and $C = 0$ in the form.

$$\eta_1^B = \frac{5}{6} N\varepsilon \frac{A_1'}{A_2'} \left(1 \pm \sqrt{1 - f_B/q}\right), \tag{35}$$

$$\eta_1^C = N\varepsilon \frac{C_1}{C_2} \left(1 \pm \sqrt{1 - f_C/q}\right), \tag{36}$$

where

$$f_B = 24A_2'/25A_1'^2, \quad f_C = C_2/C_1^2. \tag{37}$$

By equating the expression (35) and (36) and giving the parameter q a different value we shall find the abscissa β_M of the points of intersection Q_i. It is easier to express q through β_M*

$$q^* = q(\beta_M) = \frac{2g - f_B - f_C}{g^2 - f_B f_C},$$

$$g = \frac{2}{5}\left(\frac{25}{24} f_B \frac{A_1'}{A_2} \frac{C_2}{C_1} + \frac{3}{2} \frac{A_2'}{A_1'} \frac{C_1}{C_2} f_C\right). \tag{38}$$

The graph of $q^*(\beta)$ is shown in Figure 3. It is seen that the intersection of the curves $B = 0$ and $C = 0$ is possible only at $q > 13.75 = q_{min}$ and $\beta > \beta_M$. Substituting q in (35) and (36) we obtain the equation of the geometrical position of the points of intersection of the curves $B = 0$ and $C = 0$. The curve of $\eta_M = \eta_1(\beta_M)$ is given in Figure 4. It is cut short at $\beta = 1.55$ where $q = \infty$.

Now we shall establish under what conditions the curve η_A lies in the region where $A > 0$. The boundary of the region $A = 0$ for a given q is described by the equation

---

* The equation $\eta^B = \eta^C$ is also satisfied at $q^{-1} = 0$. However this solution is not of interest since for this $\eta = 0$ and there are no cracks.

$$\eta_i^A = N\varepsilon \frac{A_1'}{A_2'}\left(1 \pm \sqrt{1 - A_2'/A_1'^2 q}\right). \tag{39}$$

The point of intersection of the curves η^A and $\eta(\beta_M)$ can be found most simply of all graphically. If, for a given q and values of β_M, corresponding to it, according to equation (38) equation (39), has real values for η_1^A and η_2^A such that $\eta_1^A < \eta_i(\beta_M) < \eta_2^A$, then at the point $\eta_i(\beta_M)$ it will be true that $A < 0$. If (39) does not have real values or $\eta_i(\beta_M)$ lies outside the interval (η_1^A, η_2^A), then at the point $\eta_i(\beta_M)$ $A > 0$. Therefore one must find the points of intersection of the graph $\eta_i(\beta_M)$ and the two branches of the graph $\eta^A(\beta, q^*(\beta))$, which correspond to the two values β_M for a given q and shown in Figure 4. The area $A > 0$ is shaded.

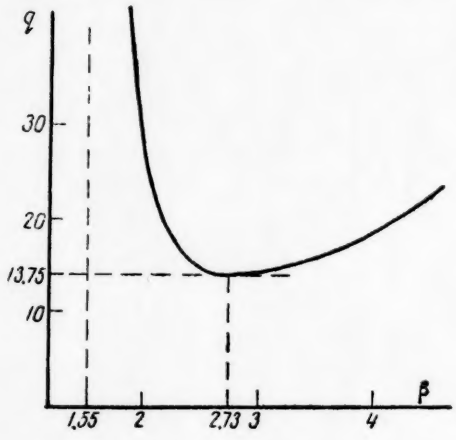

Fig. 3. A graph of the function $q^*(\beta)$

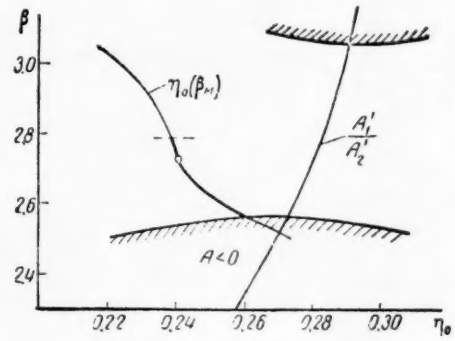

Fig. 4. A graph of the function $\beta_M(\eta)$

We move on to the determination of the sign of the determinant D and its minors. Differentiating U and using (27) we obtain:

$$\begin{aligned}
U_{rr}'' &= 8\pi A = 2\pi A_0 \{4[1 - (2A_1' + A_2'\eta_0)\eta_0 q] - \lambda(\beta - 1)/\beta\},\\
U_{r\eta}'' &= 2\pi r_0 A_0 \eta^{-1}\{-4 + (6A_1' - 2A_2'\eta_0)\eta_0 q + \lambda(\beta - 1)/\beta\},\\
U_{r\beta}'' &= 2\pi r_0 A_0\{[1 + (2B_1\Psi_1 - 2A_1 + (A_2' - 2B_2\Psi_1)\eta_0)\eta_0 q]\Psi_1^{-1} - \lambda/\beta^2\},\\
U_{\eta\eta}'' &= 2\pi r_0^2 A_0 \eta^{-2}\{6 + (-12A_1' + 7A_2'\eta_0)\eta_0 q - \lambda(\beta - 1)/\beta\},\\
U_{\eta\beta}'' &= 2\pi r_0^2 A_0 \eta^{-1}\{[-2 + (4A_1' + B_1\Psi_1 - (2A_2' + 2B_2\Psi_1)\eta_0)\eta_0 q]\Psi_1^{-1}\} + \lambda/2\beta^2,\\
U_{\beta\beta}'' &= 2\pi r_0^2 A_0\{[1 + (-2A_1' - E_1\Psi_2 + (2A_2' + E_2\Psi_2)\eta_0)\eta_0 q](2\Psi_2)^{-1} + \lambda/\beta^2\},
\end{aligned} \tag{40}$$

$$E_1 = 2(\beta + 3)/3\beta^4,\ E_2 = (10\beta^4 + 3\beta^3 - 21\beta^2 + 25\beta - 9/6\beta^4(\beta - 1)^3, \tag{41}$$

$$\Psi_2 = \Phi_0\left(\frac{\beta}{\beta - 1}\right)^4 \Big/ \frac{\partial\Phi_1}{\partial\beta},\quad \lambda = \frac{4\bar{u}_1}{\eta A_0}. \tag{42}$$

The second terms in the curly brackets in (40) are obtained by differentiating U_{G_1}. We shall denote the limited U_{G_1} fraction of the derivatives of U and also the determinant D and its chief minors by the index 1 and the remaining terms of U, D and $D^{(2)}$ by the index 0. The investigation shows that in the region where $A > 0$ the terms U_0'' in the curly brackets are

normally of the order 0.1-1 while the terms U_1'' contain the additional factor $\eta^{-1} \sim 10^{-2}-10^{-1}$. Therefore at first we shall find points at which D_0 and its chief minors revert to zero. The substitution of $\eta_i = \eta_i(\beta_M)$ in (40) shows that U''_{0rr}, $U''_{0\eta_i\eta}$ and $U''_{0\beta\beta}$ are positive for all $\beta > 1$, and D_0 and $D_0^{(2)}$ change sign close to $\beta = 3$. We shall denote the general factors in D and $D^{(2)}$ by

$$H = (2\pi r_0 A)^3/\eta_i^2, \quad H^{(2)} = (2\pi r_0 A_0/\eta_i)^2.$$

The dependence of D_0/H and $D_0^{(2)}/H^{(2)}$ on β is shown in the table. From it and Fig. 4 it is seen that only in the narrow interval of β varying from ~ 2.56 to ~ 2.79 are the conditions for minimum U satisfied. Now we shall check whether these conditions are broken if the terms U_{G_1}

TABLE 1

Parameters	N	The values of β.			
		2,60	2.75	2.80	3.00
η_{i0}	–	0.254	0.239	0.238	0.223
q	–	13.93	13.78	13.78	13.87
D_0/H	–	0.00036	0.00015	-0.00003	-0.00052
$D_0^{(2)}/H^{(2)}$	–	0.031	0.022	0.007	-0.098
D/H	10^3	-0.00007	-0.00010	–	–
$D^{(2)}/H^{(2)}$		-0.003	-0.005		
D/H	10^4	0.00032	0.00013	–	–
$D^{(2)}/H^{(2)}$		0.020	0.014		
D/H	10^5	0.00037	0.00014	–	–
$D^{(2)}/H^{(2)}$		0.027	0.020		

are considered. We shall calculate D and its chief minors at $\beta = 2.60$ and $\beta = 2.75$. Taking for estimation $q = 14$, $\eta_0 = 0.24$ and $\frac{u_1''}{A_0} = 1$, we find that $N\varepsilon^2 = 14$, $N\varepsilon = 3{,}7\sqrt{N}$ and $\eta_i = N\varepsilon\,\eta_0 \approx 0{,}9\sqrt{N} \approx \sqrt{N}$. If further it is assumed that $\bar{n}_1/A_0 = 1$ then the factor $\bar{n}_1/A_0 = 1$, $4\,\bar{u}_1/\eta A_0 = 4N - \frac{1}{2}$ for $N = 10^3$; 10^4; 10^5 is equal to 0.13; 0.04; 0.013 respectively and

$$\varepsilon = \varepsilon_{kp} = \sqrt{14N} \tag{43}$$

is equal to 0.13; 0.04; 0.013. The values of D/H and $D^{(2)}/H^{(2)}$ considering these additions are shown in the following lines of table 1. As is seen for $N \geqslant 10^4$ the conditions for minimum U are fulfilled in the narrow interval close to $\beta = 2.7$ and at $N = 10^3$ in general are not fulfilled.

In accordance with (27) the size of a stable crack at $\beta = 2.7$ is

$$r_0 = \frac{1}{2}\left(\frac{u_1'' a^2 \Phi_0}{6\pi A_0}\right)^{1/4} \frac{\beta}{\beta - 1}\eta_i N^{\frac{1}{4}} = \frac{1}{2}\left(\frac{0{,}049}{6\pi\, 0{,}050}\right)^{1/4} 1{,}6N^{3/4} \approx 0{,}4N^{3/4}. \tag{44}$$

At $N = 10^4$; 10^5; 10^6 the ratio $100r_0/N$ is equal to 4; 2.2; 1.3 respectively.

Consequently the mode we have considered of an elastically extended crystal without defects shown in Fig. 2 permits the existence of stable cracks and the conditions for stability are fulfilled only within the narrow interval of the values of the problem's parameters. However, since, in accordance with (44) the size of the stable crack is considerably smaller than the dimensions of the crystal and, in accordance with the theory of elasticity, the model of Fig. 2 is correct only when the size of the crack is of the order of the thickness of the crystal or larger then the configuration of a crystal with a stable crack is normally unrealized* and the fundamental result of our calculation must be to consider that in a crystal without defects stable cracks which do not extend to the surface of the crystal are impossible.

5. A COMPARISON WITH THE RESULTS OF GRIFFITHS AND RZHANITSYN

We shall now consider what relation the conclusion we have obtained bears to Griffith's theory and Rzhanitsyn s result [13] according to which stable cracks are impossible. Griffith's formula (1) is obtained for an infinite crystal or one so large that the region G_0, in which the stresses are relieved on the formation of a crack, does not reach the surface of the crystal. We have considered the opposite case when the G_0 region extends to the surface. Therefore our results complete Griffith's theory in the case of a limited crystal**

VOL. 8 1959

Rzhanitsyn [13] considered a rod of finite cross section with a crack, the plane of which was perpendicular to the axis of the rod. The length of the rod can be finite. On comparing the results of [13] with ours it must be mentioned that in our formula (15) the term D/r_0^2 which leads to the existence of a minimum of $U(r)_0$ depends essentially on the form of the crack. Its dependence on ϵ, through the values of β and η minimizing the energy, outlines the redistribution of the elastic energy between the G_0 and G_1 regions on varying ϵ. Also if the value of the elastic energy in the region G_1 is considered to be independent of ϵ and proportional to the perimeter of the crack $2\pi r_0$ as assumed in [13], when the size of the diagram area of the additional stresses R in the region G_1 is considered constant, then the function $U(r_0)$ will have a maximum.

In fact we shall consider a crack with a narrow G_1 region, i.e. the case of $\beta \approx 1$. We shall denote $r_0 - r_1 = \rho \ll r_0$ ***. Since for $\rho \to 0$ $I_i \to I_1$, then (15) can be presented in the form

$$U = A(\beta) r_0^2 + \frac{N u_1'' a^2 \eta^4}{96 r_0^2} \frac{r_0^2}{\rho^2} I_1 \left(\frac{r_0^2}{\rho^2} - \frac{(r_0 - \rho)^2}{\rho^2} \right) = \tag{45}$$
$$= A(\beta) r_0^2 + \text{const} \cdot r_0 + O(\rho^2).$$

For small ε $A > 0$ and the function $U(r_0)$ does not have an extreme value, remaining positive.

---

* In the model in Fig. 2 the proposed relief of the stresses along the whole length of the z-chains in the case of $r \ll_0 N$ can take place only in a strongly anisotropic crystal in which the z-bonds are considerably stronger than the r-bonds.

** The formal expression of (27) does not contradict Griffith's theory because at $N \to \infty$ and finite ε $q \to \infty$ and in agreement with (28) $A < 0$, that is in an infinite crystal, according to the model described in Fig. 2, stable cracks of finite dimensions are impossible.

*** In (13) the difference $r_0 - r_1$ is denoted by a, which is considered "sufficiently small" so that the tensile force acting in the G_1 region may be written in the form $2\pi r_0 R$.

For a sufficiently large ε $A<0$, and from the condition $\partial U/\partial r_0 = 0$ we find r_0 corresponding to maximum U.

$$r_0 = -\frac{Nu_1'' a^2}{96}\frac{I_1}{\rho^3}\frac{1}{A}. \tag{46}$$

It is easy to see that the function $U(r_0, \rho)$ has a minimum with respect to ρ at $\rho = 3r_0$ and at $\rho \ll r_0$ it varies monotonically with ρ. Therefore in our model the energy U as a function of r_0 and ρ at the point where $\rho \ll r_0$ and r_0 satisfied (46) has neither a maximum nor a minimum. Our calculation shows that if a crystal with a crack is described by several parameters (r_0, ρ, R in the case of (13)) it is necessary to study the energy as a function of all these parameters at its extreme values.

6. CONCLUSIONS

1. The energy of an elastically extended crystal N atomic layers thick with a crack of radius r_0 and of the form shown in Fig. 2 is expressed by formula (15) and has a minimum at known values of problem's parameters N, ε, μ, ν, actually $N \geqslant 10^4$, $N\varepsilon^2\beta\nu \approx 14$. Also the parameters r_0, η, β, describing the form of the stable crack have the following values: $\beta \approx 2{,}75$; $\eta = 0{,}24N\varepsilon$; r_0 is determined by formula (44).

2. Since in accordance with the theory of elasticity the model examined must be considered to be applicable to r_0 N and the conditions found for the stability of the crack are realized only at $r_0 \approx 0{,}4N^{3/4} < N$, stable cracks inside an elastically extended ideal crystal are not possible.

Translated by: J.H. Dempster

REFERENCES

1. N.F. Mott, *Proc. Roy. Soc.* 220, 1. (q.v. review 11) (1953).
2. J.C. Fisher, *Acta Met.* 3, 109, 1955; R. Green, *Phys. Rev.* 102, 376, (1956).
3. J.J. Gilmah, C. Knudsen and W.P. Walsh; *J. Appl. Phys.*, 29, 601, (1958).
4. G.M. Bartenev, *Izv. Akad. Nauk. S.S.S.R., Department of Technical Sciences*, No.9, 53, (1955).
5. A.A. Griffith, *Phil. Trans. Roy. Soc.*, A, 221, 180, (1921).
6. H.A. Elliott, *Proc. Phys. Soc.*, 59, 208, (1947).
7. Sneddon. *Fourier transformations* (Preobrazovaniia Fur'ye) *Foreign Literature Publishing House*, para. 54, (1955); R.A. Sack, *Proc. Phys. Soc.*, 58, 729, (1946).
8. Ia.I. Frenkel', *Zh. Tekh. Fiz.*, 22, 1857, (1952).
9. P.A. Rebinder, *A jubilee symposium dedicated to the thirtieth anniversary of the Great October Socialist Revolution*, (Iubil) einyi sbornik, posviashch. 30-letiiu Velikoi Oktiabr'skoi sotsialisticheskoi revoliutsii), chap. 1, 533, (1947).
10. D.I. Shil'krut, *Dokl. Akad. Nauk. SSSR*, 122, 69, (1958).
11. V.I. Likhtman and Ye.D. Shchukin, *Progress of Physical Sciences*, 66, 213, (1958).
12. I.V. Obreimov, *Proc. Roy. Soc.*, A, 127, 290, (1930).
13. A.R. Rzhanitsyn, *A study of the problems of structural mechanics and the theory of plasticity*, (Issledovaniia po Voprosam

stroitel'noi mekhaniki i teorii plastichnosti) Moscow, p. 66, (1956).

14. A.N. Orlov, Iu.M. Plishkin and I.M. Shepeleva, *Fiz. metal. metalloved*, 4, 540, (1957).
15. Iu.M. Plishkin, *Works from the Physics of Metals Institute Akad. Nauk. SSSR*, No.22, (1958).
16. M. Born and M. Goppert-Mayer, *The theory of the solid body*, (Teoriia tverdovo tela), *United Scientific and Technical Press*, (1938).
17. Ia. I Frenkel', *Acta Physicoch. U.S.S.R.*, 3, 633, 915, (1935).
18. K. Ziner, *The elasticity and inelasticity of metals*, (Uprugost' i neuprugost' metallov), *Foreign Literature Publishing House*, p. 137, (1954).

VOL.
8
1959

THE DISPERSION OF CURRENT CARRIERS IN COMPOUNDS OF THE PbS GROUP*

I.M. TSIDIL'KOVSKII

The institute of the Physics of Metals Akad. Nauk. SSSR.

(Received 9 July 1959)

Much research has been devoted to the study of the physical properties of semiconductors of the PbS type. This group of crystals attracted attention, on one hand because lead sulphide and its analogues, thanks to their sensitivity to infra-red radiation and their transistor properties, can be used as infra-red receivers and crystal amplifiers and detectors; on the other hand the physical properties of the compounds of the lead sulphide group are distinguished by a number of properties which are of great theoretical interest [4].

Thus for example normally in the homologous series for semi-conductors the width of the forbidden band decreases as the atomic number of the constituent elements increases, in accordance with the fact that the binding energy of the valency electrons decreases with the growth of the atomic number. In the PbS group an anomaly is observed: the width of the forbidden band $\triangle \epsilon$ of lead selenide is smaller than that of lead telluride. As distinct from the majority of semiconductors from compounds of the PbS group a positive temperature dependence is observed for the width of the forbidden band with a coefficient of $\approx +4\times10^{-4}$ eV/degree. As is shown in the account of [1], a change in the permanent lattice should be considered the fundamental case of the anomalous temperature dependence $\triangle \epsilon$. The thermal vibrations of the lattice should take the negative sign for the temperature coefficient.

Usually semiconductors of the $A^{IVB}{}_{B}{}^{VIB}$ group, in the first place lead sulphide, are related to ionic crystals [2-5]. We think that there are insufficient grounds for this in particular with respect to lead telluride and selenide. We shall dwell briefly on the problem of determining the type of chemical bond.

In spite of the large amount of attention which has been and is being devoted to the problem of the chemical bond, so far there are not sufficiently simple or reliable methods for determining the type of bond. In crystal chemistry in order to determine the type of bond they use such characteristics as the lattice energy, the dimensions and polarizability of the ions, the difference of the electronegativities of the compound's components. If for example the difference of the electronegativities is large they consider that the crystal possesses an ionic bond, if this difference is small – it possesses a covalent bond. However all these methods are extremely inaccurate and do not give a simple solution to the problem. Besides this, on account of the experimental difficulties information about a number of the properties of crystals is missing, the knowledge of which is essential to ascertaining the type of bond. This concerns first of all the majority of the semiconducting compounds..

Ascertaining the character of the chemical bond is undoubtedly one of the most important tasks of both crystal chemistry and also solid state physics. Moreover it must be remembered that for the majority of real crystals there exists an intermediate type of bond and the bond approaches some sort of "pure" type for only a few substances. Besides this, for the most part, crystals possess an heterodesmic structure, i.e. a

* *Fiz. metal. metalloved.* 8, No.4, 494-502, 1959.

VOL
8
195

structure in which bonds of different types may act between the atoms. Therefore usually it is apparently possible to speak only about a lesser or greater degree of predominance of one or other type of bond in a given crystal and not about a "pure" type of bond.

An analysis of the data from other works concerning the physical properties of the crystals of the lead sulphide group supports our view that, in them, the covalent bond predominates over the ionic bond. We shall give a few examples.

1. The formation of one type of bond* or another is determined chiefly by the ability of the ions of the compound to polarize themselves or to polarize the neighbouring ions. The larger is this ability then the more strongly is the covalent bond expressed and more weakly the ionic. The electric moment of unit volume, which characterizes the degree of polarization, depends both on the induced moment of each ion and also on their concentration. Consequently one may judge the degree of polarization from the value of α_e/R^3, where α_e - is the electronic polarizability, R is the radius of the ion. Comparing the values for the polarizibility and the radii of different ions** [6] it can be seen that for Pb^{++}, Cu^{+}, Ag^{+}, Hg^{++} α_e/R^3 is much greater than for ions of the alkali and alkaline earth metals*** but for O^{--}, S^{--}, Se^{--}, Te^{--} α_e/R^3, is greater than for the ions of the haloids. Consequently in compounds containing Pb^{++} and other cations and S^{--} and other anions the covalent bonds should be more strongly expressed than for compounds containing the cations Na^{+} and others and the anions Cl^{-} and others.

2. The lattice energies of lead sulphide and lead selenide found experimentally by the circular Born-Haber process (731 and 735 kcals/mol) differ significantly from the values for the energies calculated according to the Born theory for ionic crystals (705 684 kcals/mol), while for the alkali haloid crystals or such oxides as Li_2O, NiO and ZnO the theory agrees well with experiment: for KCl, for example, theory and experiment give one and the same value, for NiO the disagreement is all of 2kcal/mol.

3. An important criterion which permits one to distinguish the ionic crystal from the covalent one is the ratio of the values of the electronic and ionic polarizabilities which is found from the ratio of the static (χ) and optical ($\varkappa_0 = n^2$) dielectric constants. We shall compare the values of and χ for lead sulphide - for other compounds of this group the value of χ is unfortunately unmeasured. According to Landolt's tables [7] for PbS χ = 17.9, and χ_0 17.5 (for $\lambda = 6\mu$) according to the results of [8] and in the reference [9] the value χ_0 = 15.3 is given for the D-lines of sodium. The difference between the values of χ and χ_0 is small and consequently for lead sulphide the electronic polarization should predominate over the polarization produced by the displacement of the ions. The authors [4] give a value of the order of 70 for χ estimated from the compressibility and the frequency of the residual rays, however the truth of these results is not clear.

In S.I. Pekar's monograph [2] where lead sulphide is regarded as an ionic crystal a value of 2.81 is taken for χ_0 which differs sharply from the experimental data given above. If it is accepted that χ_0 = 17.5 then the criterion of the existence of F'-centres, the presence of which is used essentially in [2] to explain a number of the properties of PbS, in particular the metallic character of the electrical conductivity, is fulfilled much more poorly than when χ_0 = 2.81.

4. In order to explain the problem of which type of bond is predominant in a given

---

* The discussion concerns the covalent and ionic types of bond.

** It should be noted that the value of the polarizibility of an ion depends on the compound which the ion has entered and it may only approximately be considered that the α_e of a given ion is the same for different compounds.

*** There is a general rule in accordance with which cations with an 18-electron outer shell polarize neighbouring ions and are polarized themselves more strongly than cations with an 8-electron shell corresponding to an inert gas.

VOL. 8 1959

compound the study of the kinetic effects affords definite interest. In accordance with the theory of ionic crystals the mobility of the current carriers u at temperatures lower than the characteristic (θ) should decrease exponentially with the temperature rise: $u = u_0(e^{\theta/T} - 1)$ and for $T > \theta$ the theory predicts a power law for the decrease: $u = u_0 T^{-\frac{1}{2}}$.

In the assumption that lead sulphide is an ionic crystal S.I. Pekar [2] approximates to the graph for the temperature dependence of the mobility of the electrons obtained experimentally by Iu.A. Dunayev and Iu.P. Maslakovets [10] by an exponential. Thus in the low temperature region a discrepancy between the experimental and theoretical graphs is noticed. On comparing these curves for $u(T)$ the value of the characteristic temperature was found to be equal to 865°K in [2] while in [9] for lead sulphide a value of $\theta \simeq 223°$ K is given and the authors of [11], measuring the specific heat, established that θ lay within the limits 150-230°K. But in this case the measurements carried out by Iu.A. Dunayev and Iu.P. Maslakovets refer to temperatures above the characteristic for which the ionic crystal theory is demanded for $u \sim T^{-\frac{1}{2}}$, while in the work [10] the function $u \sim T^{-2.3}$ approximates well to the experimental curve over the whole temperature interval.

Thus for lead sulphide the temperature dependence of the mobility of the electrons does not correspond to the ionic crystal theory. Also with reference to lead selenide and telluride $u \sim T^{-5/2}$ above ~100°K as for PbS. (q.v. for example [12]). In connexion with this, one must point out the error in Chazmar and Putli's [13] interpretation of the temperature dependence of the mobility of the electrons for lead telluride which assumed that PbTe was an ionic crystal with a high Debye temperature. From the temperature dependence of the electron mobility above ~450°K they determined θ = 1300°K which sharply contradicts the experimental results of [11] according to which $\theta \approx$ 120-130°K. Petritz and Scanion [14] attempted to explain the temperature dependence of the mobility of the current carriers in lead sulphide as arising from the presence of a simultaneous dispersion by the acoustic and optical vibrations of the lattice. However they did not succeed in obtaining the $u \sim T^{-5/2}$ law. L.S. Stil'bans and others [15, 16] suggested that the dependence of the type $T^{-5/2}$ observed for lead telluride by these authors is caused by a multiphonic mechanism for dispersing the current carriers the probability of which grows with the rise in temperature. The suggestion concerning the multiphonic dispersion mechanism not only allows the relation $u \sim T^{-5/2}$ to be explained but also shows that it can take place in crystals in which the covalent bond is predominant.

Of great interest is the study of the thermomagnetic effects which are very sensitive to the form of the interaction of the current carriers with the crystal lattice. For different types of chemical bond the solid state theory predicts different mechanisms for the dispersion of the current carriers [17]. In crystals with an atomic lattice the current carriers are dispersed by acoustic oscillations, in ionic crystals chiefly by optical oscillations which are accompanied by the polarization of the substance.

Each form of dispersion corresponds to a definite relation between the relaxation time of the current carriers (naturally in those cases when it can be introduced) and the energy and temperature [17]. It is usually difficult and sometimes quite impossible to establish definitely a law for the temperature variation of the relaxation time using the temperature dependence of the galvanic and thermomagnetic effects. This can be illustrated from the example of semiconductors for which the mobility of the current carriers varies proportionally to $T^{-5/2}$, or those like copper oxide for which, in different temperature intervals, the mobility of the holes varies according to different power laws which are in complete disagreement with the theory. The dependence of the relaxation time τ on the energy ϵ effects the galvanomagnetic phenomena slightly (with the exception of the Ettingshausen effect [18]) but decisively influences the thermomagnetic phenomena, chiefly, the Nernst-Ettingshausen effect.

In the case of weak magnetic fields, iso-

VOL 8 195

thermal conditions $\left(\frac{\partial T}{\partial y} = \frac{\partial T}{\partial z} = 0\right)$ and impurity conduction, the dimensionless fields of the Nernst-Ettingshausen effects are expressed by the formulae [19, 20]:

$$F_y = \frac{E_y}{\frac{k}{e}\frac{\partial T}{\partial x}} = \left(\frac{1}{2} - r\right) a_r \frac{uH}{c}, \qquad (1)$$

$$F_x = \frac{E_x}{\frac{k}{e}\frac{\partial T}{\partial x}} = (1-2r)\left(b_r - \frac{a_r^2}{2}\right)\left(\frac{uH}{c}\right)^2, \qquad (2)$$

where E_y and E_x are the electric fields formed in the directions of the x and y axes, and the temperature gradient is directed along the x axis and the magnetic field along the z axis; the value of r is determined by the dependence of the relaxation time of the current carriers on the energy: $\tau = \tau_0(T)\,\varepsilon^{r-1/2}$; a_r and b_r are some constants depending only on r and are of the order of unity.

From formulae (1) and (2) it is seen that only one sign of the transverse or longitudinal Nernst-Ettingshausen effect in the case of impurity conduction permits the value of the index of r to be estimated which is characteristic of the type of dispersion: it is larger or smaller than a half. A joint study of both effects in the region of weak magnetic fields permits the value of r to be determined and in the regicn of high fields r can be found immediately from the longitudinal effect alone ($F_x = \frac{1}{2} - r$). As is known [17] different mechanisms for the dispersion of the current carriers correspond to different values of r: for dispersion by acoustic oscillations $r = 0$, for dispersion by optical oscillations in a polar crystal at temperatures below the Debye temperature $r = \frac{1}{2}$, above the Debye temperature $r = 1$, for dispersion on the ions of the impurity $r = 2$.

We shall analyse the results of the research we carried out (they were published in part earlier [21]) on the transverse and longitudinal Nernst-Ettinshausen effects for a number of samples of PbS, PbSe and PbTe. For comparison we shall give the results of Putli's [22] measurements of the transverse effect for lead selenide (In [22] there is also given a graph of the temperature dependence of the transverse effect for a sample of lead telluride which is analogous to the corresponding graph for our third sample).

In Table 1 are given the basic electrical properties of all our samples for $T = 300°K$. For the sample of PbTe-3 the data are given also at $T = 125°K$ since at 300°K the conductions for it is composite.

The samples PbS, PbSe-1, PbSe-2, PbTe-1 and PbTe-3 are polycrystals, PbSe-3 and PbTe-2 are monocrystals. The samples of PbSe-1 and PbTe-3 are obtained by slow cooling of the synthesized substance, and PbS, PbSe-2 and PbTe-1 by hot pressing.

In all the samples the temperature coefficient of the electrical conductivity in the region of impurity conductivity is negative. The region of intrinsic conductivity depending on the impurity content begins at different temperatures for different samples: for PbSe-1 – at $\approx 500°K$, for PbSe-3 – at 700°K, forPbTe-3 – at $\approx 380°K$, for the remaining samples impurity conductivity exists up to $\approx 750°K$.

In Figs. 1-5 graphs of the temperature dependence of the transverse Nernst-Ettingshausen effect are shown. At low temperatures, for all samples with the exception of PbTe-3, the effect is positive. In the region of composite conductivity the effect becomes negative in complete agreement with the theory [23].

The positive sign of F (or the coefficient $Q^{\perp} = \frac{E_y}{H\frac{\partial T}{\partial x}}$) denotes, in agreement with (1) that the index of $r < \frac{1}{2}$. In order to calculate the value of r we shall use the results of the measurements of the longitudinal Nernst-Ettingshausen effect. Since the thermal conductivity governed by the current carriers, is significantly smaller than the lattice thermal conductivity for compounds of the lead sulphide group (only if the electron gas is not strongly degenerate)*, it is possible to use formulae for the isothermal

* Thus for example for a sample of lead sulphide [10] with a high concentration of electrons (8×10^{18} cm^{-3} at $\approx 300°K$) $\frac{\lambda_e}{\lambda_\varphi + \lambda_e} \simeq 0.07$, λ_e and λ_φ are the electronic and phonic components of the thermal conductivity.

TABLE 1

Electrical characteristics	PbS	PbSe-1	PbSe-2	PbSe-3 [22]	PbTe-1	PbTe-2	PbTe-3	
							125°K	300°K
σ (Ω^{-1}. cm^{-1})	450	165	126	359	240	1600	1100	100
R (cm^3/C)	-1.15	+3.8	-0.92	+2.9	-2.0	-1.45	-14.9	-0.9
N. 10^{-18} (cm^{-3})	6.5	1.95	8.0	2.55	3.7	5.1	0.42*	–
u (cm^2/V. sec).	430	530	98	880	400	1950	16,400*	–

* The mobility and the concentration of the electrons in PbTe-3 are calculated from the equations for strong magnetic fields since the measurements were carried out in conditions where $\frac{u_- H}{c} > 1$.

case in interpreting the experimental results.

From equations (1) and (2) we have

$$\frac{F_y^2}{F_x} = \frac{(1/2 - r)\, a_r^2}{2b_r - a_r}. \qquad (3)$$

In table 2 the values of F_y^2/F_x are given which have been calculated with the aid of (3) for different r.

The experimental values of F_y^2/F_x are the following: for PbS 0.1-0.25 in the interval 130-330°K; for PbSe-1 0.15-0.3 in the interval 130-300°K and 0.32-0.34 in the interval 300-350°K; for PbSe-2 0.1-0.22 in the interval 135-330°K; for PbTe-1 0.2-0.31 in the interval 200-320°K; for PbTe-2 0.15-0.25 in the interval 200-300°K; for PbTe-3 0.01-0.03 in the interval 125-220°K (in the temperature region where holes still do not influence the Nernst-Ettingshausen effect for PbTe-3). At high temperatures the longitudinal effect which decreases with the rise in temperature in proportion to the square of the carrier mobility, becomes so small that it cannot be measured with a sufficient degree of accuracy and consequently the relation F_y^2/F_x cannot be determined

A comparison of the experimental results with the theoretical ones shown that for all samples with the exception of PbTe-3 the value of F_y^2/F_x corresponds best of all to $r = 0$. For PbSe-1 and in a somewhat smaller temperature interval for PbTe-1 the experimental value of F_y^2/F_x agrees well with the theoretical ones for $r = 0$. For the other samples the disagreement between the experimental and theoretical results is larger. On reducing the temperature the agreement becomes worse for all samples including PbSe-1. The deviation of the experimental results from those calculated according to equation (3) is governed by the partial degeneration of the electron gas which increases on reducing the temperature. Judging by the thermoelectromotive force it may be concluded that for PbTe-3 the gas of the current carriers is not degenerate in the whole of the temperature interval studied, for PbSe-1 and PbSe-3 weak degeneracy should occur at very low temperatures, for PbTe-1 partial degeneracy occurs at temperatures lower than $\approx$250°K, for PbTe-2 degeneracy is widespread up to $\approx$300°K, for PbS – up to

TABLE 2

r	0	1/2	1	2
F_y^2/F_x	+0,323	0	–0,426	–0,702

≈350°K, for PbSe-2 – up to ≈400°K.

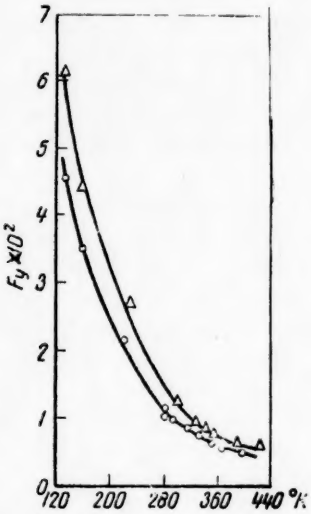

Fig. 1. The dependence of the dimensionless field of the transverse Nernst-Ettingshausen effect on the temperature for samples of lead sulphide (△) and for the first sample of lead telluride (○). H = 9200 oersted.

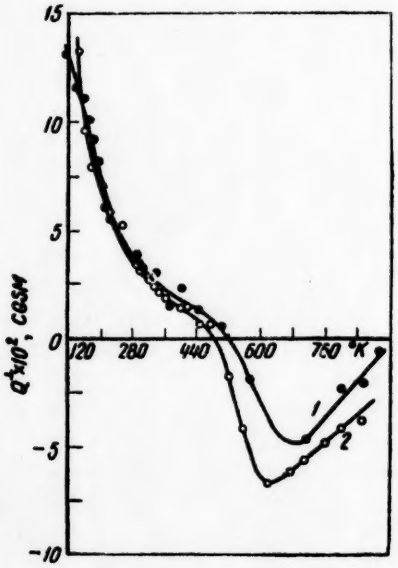

Fig. 2. The dependence of the coefficient of the transverse Nernst-Ettingshausen effect on the temperature for the first (2) and the third (I) [22] of the samples of lead selenide.

The negative sign for E_y and the small values of F_y^2/F_x at low temperatures can be explained for PbTe-3 by the influence of excitation effects on the thermomagnetic phenomena. This is also confirmed by the temperature variation of the coefficient of

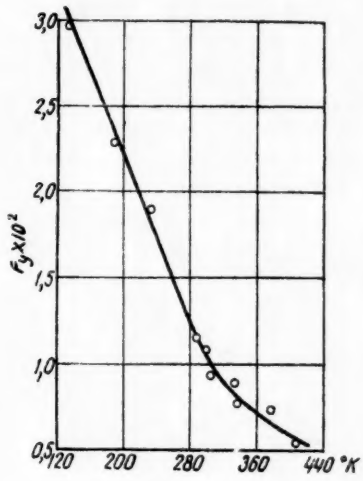

Fig. 3. The dependence of the dimensionless field of the transverse Nernst-Ettingshausen effect on the temperature for the second sample of lead selenide. H = 9100 oersted.

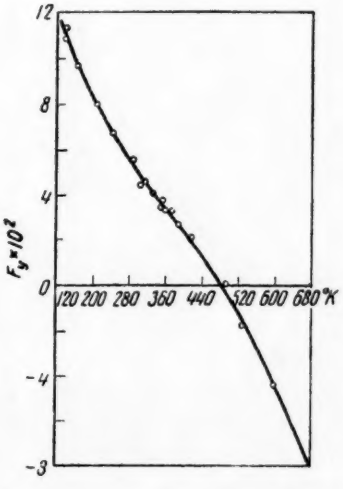

Fig. 4. The dependence of the dimensionless field of the transverse Nernst-Ettingshausen effect on the temperature for the second sample of lead telluride. H = 9950 oersted.

the thermoelectromotive force α: below 180°K $|\alpha|$ noticeably begins to increase on reducing the temperature.

Thus the combined measurements of the longitudinal and transverse Nernst-Ettingshausen effects for compounds of the PbS group showed that for a region of temperature where the current carriers interacted with the lattice vibrations $r = 0$, i.e. the acoustic oscillations are predominant in the dispersion. And this signifies that the dominant type of bond is the covalent bond.

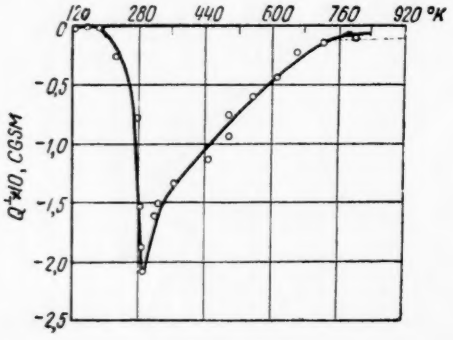

Fig. 5. The dependence of the coefficient of the transverse Nernst-Ettingshausen effect on the temperature for the third sample of lead telluride.

A.V. Ioffe and A.F. Ioffe, studying the connexion between the electronic thermal conductivity and the electrical conductivity of lead telluride [24], also came to the conclusion that $r = 0$. The value $r = 0$ was obtained by L.S. Stil'bans and others [15, 16] in analysing the measurements of the thermoelectromotive force and the mobility for a number of samples of lead telluride with different impurity contents.

Knowing that $r = 0$ it is possible to calculate with the aid of equation (1) the mobility of the current carriers in the temperature region where $F_\nu > 0$. Such calculations showed that above 200-250°K for all samples the mobility of the holes and electrons vary proportionally to $T^{5/2}$, at lower temperatures $u_{\frac{1}{2}} \sim T^{-1} - T^{-1.8}$, and for PbTe-3 $u \sim T^{-5/2}$ up to 120°K. The temperature dependence of the mobilities found from the transverse Nernst-Ettingshausen effect for all samples coincide exactly with the corresponding graphs of the mobilities determined from the electrical conductivity and the Hall effect. However the quantitative agreement is not equally good in all cases. The values of the Hall and Nernst mobilities agree in the temperature interval where $F_\nu > 0$ (within the limits of experimental error) for PbSe-1 and PbSe-3. For the remaining samples apart from PbSe-2 the Hall mobility is 1.5-2.0 times larger than the Nernst and the discrepancy is increased on reducing the temperature. The disagreement between the results of the Hall and Nernst-Ettingshausen effects can be explained by the stronger influence of the degeneracy of the gas of current carriers on the latter effect. The degeneracy leads to a considerable reduction in the coefficient of $Q^\perp$ [25] and changes Hall's constant comparatively little. On increasing the temperature, that is on approaching the region of composite conductivity, where the field F_ν becomes negative the Nernst mobilities calculated from (1) should also be smaller than the Hall ones due to the substantial influence on the value of F_ν of carriers possessing the other sign.

For PbSe-2 the opposite phenomenon is observed: the Nernst mobilities of the electrons are approximately 2-2.5 times larger than the Hall mobilities. It may be thought that this difference is connected with the loose packing of the sample's grain structure which brings distortions into the value of the electrical conductivity and moreover immaterially effects the thermomagnetic phenomena.

It should be mentioned that the research carried out on samples of lead selenide containing holes and electrons confirmed that the sign of the transverse Nernst-Ettingshausen effect was independent of the sign of the current carriers. Besides this an interesting fact is established: on decreasing the temperature the fields F_y and F_x increase without any tendency being found towards either a change in sign or even saturation. This should testify to the extremely small role of the impurity ions in the dispersion of the current carriers and

consequently also in the temperature dependence of the mobilities and the kinetic effects. So far the reason is not clear why such a large concentration of impurity ions (10^{18} -10^{19} cm^{-3}) hardly effects the dispersion of the current carriers while for germanium, silicon, indium arsenite and other semiconductors at an impurity ion concentration of $\sim 10^{16}$ cm^{-3} dispersion by them predominated up to room temperatures.
Stil'bans and others [16] suggested that the causes of the weak interaction of the current carriers with the impurity ions at large concentrations of the latter could be: 1) the formation of impurity zones, 2) the formation by donors and acceptors of neutral complexes (dipoles), 3) the interaction of the current carriers with the impurity lattice and not with individual impurity ions (if the distance between them is smaller than the wavelength of the electron).

In conclusion one's attention must be turned to an interesting peculiarity of the transverse Nernst-Ettingshausen effect which was noticed for lead selenide. It appears that the constant $Q^{\perp}$ has almost the same value for polycrystalline and monocrystalline samples of PbSe with close values for the mobilities and the concentrations of the current carriers (qv. the graphs of $Q^{\perp}(T)$ for the samples PbSe-1 and PbSe-3). This lets one consider that the variation of the energy surfaces of the holes and electrons from the spherical which, according to measurements of the resistance in a magnetic field [26], looks as though it should take place for lead selenide, does not lead to any noticeable changes of the numerical coefficient in the constant $Q^{\perp}$. The question concerning the structure of the energy surfaces for compounds of the lead selenide group still remains open and requires further research.

Translated by J.H. Dempster

REFERENCES

1. D.G. Bell, D.M. Hum, L. Pincherle, D.W. Sciama and P.M. Woodward, *Proc. Roy. Soc.*, 217A, 71, (1953).
2. S.I. Pekar, *Research on the electronic theory of crystals, (Issledovaniia po elektronnoi teorii kristallov) Gostekhteoretizdat* (1951).
3. F. Zeitts, *A modern theory of the solid state, (Sovremennaia teoriia tverdogo tela) Gostekhteovetizdat,* (1949).
4. E. Burstein and P. Eglix, *Problems of modern physics (Problemy sovremennoi fiziki) vyp.* 8, 5 (1957).
5. G. Bush, *Progress of Physical Sciences,* 47, 258, (1952).
6. G.I. Skanavi, *The physics of dielectrics (Fizika dielektrikov), Gostokhteoretizdat,* (1949).
7. Landolt, *Phys. Chem. Tabellen.*
8. D. Avery, *Proc. Phys. Soc.,* B67, 2, (1954).
9. *Intern. Crit. Tabl.* 5, 90, (1929).
10. Iu. A. Dunayev and Iu.P. Maslokovets, *Zh. Eksp. Teor. Fiz.* 17, 902 (1947).
11. D. Parkinson and J. Guarrington, *Proc. Phys. Soc.,* A67, 569, (1954).
12. R.S. Allgaier and W.W. Scanlon, *Phys. Rev.,* 111, 1029 (1958).
13. R. Chazmar and E. Putli, *Semiconducting materials, (Poluprovodnikovyye materialy) Foreign literautre publishing house,* p.275 (1954).
14. R. Petritz and W.W. Scanlon, *Phys. Rev.* 97, 1620 (1955).
15. L.S. Stil'bans, B.I. Bok and E.L. Lifshitts, *Dokl. Akad. Nauk. SSSR,* 111, 1011 (1956).
16. E.Z. Gershtein, T.S. Stavitskaia and L.S. Stil'bans, *Zh. tekh. fiz.* 27, 2742 (1957).
17. A.H. Wilson, *Theory of Metals, University Press, Cambridge,* (1954).
18. I.M. Tsidil'kovaskii, *Zh. Tekh. Fiz.* 28, 1171 (1958).
19. K.B. Tolpygo, *Works of the Institute of Physics (Trudy Inst fiziki) Akad. Nauk. Ukr. S.S.R., vyp.* 3, 52 (1952).
20. F.G. Bass and I.M. Tsidil'kovskii, *Zh. Tekh. Fiz.* 24, 1834 (1954).
21. I.M. Tsidil'kovskii, *Dokl. Akad. Nauk SSSR,* 102, 737 (1955).
22. E. Putley, *Proc. Phys. Soc.* B68, 22, 35 (1955).
23. F.G. Bass and I.M. Tsidil'kovskii, *Zh. Eksp. teor. fiz.* 31, 671 (1956).
24. A.V. Ioffe and A.F. Ioffe, *Izv. Akad. Nauk*

VOL. 8 1959

SSSR ser. fiz. 29, No.1 (1956).
25. V.Ye. Vzdornov and I.M. Tsidil'kovskii, *Fiz. metal metalloved.* 7, 801, (1959).
26. R.S. Allgaier, *Phys. Rev.*, 112, 828, (1958).

VOL
8
195

SUPERCONDUCTIVITY OF METALS TAKING INTO ACCOUNT OVERLAPPING OF THE ENERGY BANDS*

V.A. MOSKALENKO

The Moscow State University – M.V. Lomonosov

(Received 31 October 1958)

Using Bogoliubov's method [1] the effect of the overlapping of energy bands of metals on their properties of superconduction was studied. The possibility of the transfer of a pair of electrons with opposite momenta and spin from one energy band to another due to the action of the lattice vibrations is considered.

Under certain conditions the energy band with the higher density of electrons close to the Fermi surface plays the more important role in superconductivity.

VOL. 8 1959

1. INTRODUCTION

Considerable success has been achieved recently in the theory of superconductivity. A new method has been developed by N.N. Bogoliubov [1] for the theoretical study of this problem; this method depends on the close analogy which exists between the superfluidity of an imperfect Bose-gas and the superconductivity of electrons in a metal. An important role in the new theory is played by pairs of electrons with opposite momentum and spin which belong in the vicinity of the Fermi surface.

The conception of the above mentioned pairs was put forward by Cooper [2] and is based on Bardeen, Cooper and Shrieffer's [3] approximate variation method. It should be mentioned that the actual role of the pair of electrons, according to [1], is somewhat different from the initial proposals of Cooper.

However up to the present day a quantitative study of the role of the periodic field of the lattice in the properties of superconductivity has been absent, since in the works devoted to this problem in recent years the lattice was in fact replaced by an oscillating continuum.

Due to the periodic structure of the lattice the energy of the electron may take values belonging to the allowed bands.

Thus it is possible to have the energy zones overlapping so that the boundary Fermi energy may, in general, appertain to several zones; therefore the role of the different zones must be clarified and the probability of transfers between them estimated. Furthermore a study of the role of the Peierls transfer processes (umklapprozess) in the theory of superconductivity is of interest (Pines [4] pointed out the necessity of considering them).

In this article our main attention is devoted to the first question and for simplicity the second is neglected.

A study of the role of overlapping zones is necessary in view of the existence, apparently, of similar overlapping in all known superconducting metals. Thus, for example, for super-

*Fiz. metal. metalloved. 8, No.4, 503-513, 1959.

conductors belonging to the main groups of the periodic table of elements, the s- and p-bands overlap. For metals of the transition groups the d- and s-bands overlap.

d-electrons as well as s- and p-electrons will be described by the band system alhtough, as is known, the single electron approximation in the first instance has an extremely limited sphere of application.

For simplicity we shall neglect the magnetic degeneracy of the p- and d-bands, taking into consideration several effective densities of the electronic states close to the Fermi surface and the average matrix elements for transition caused by the thermal vibrations of the lattice.

The Hamiltonian of the electron-phonon system being considered may be obtained in our case of overlapping energy bands as a direct generalization of Bardeen's [3] model Hamiltonian. We shall denote the energy of the electron in the first energy band by $E_1(\vec{k})$, the chemical potential of this band, corrected for the interaction, by λ_1 and the annihilation and creation operators for electrons in the first band by a_{ks}, a^+_{ks}. The intensity of the electron-phonon interaction within the limits of the first band is denoted by I_1.

The corresponding quantities for the second band are denoted by $E_2(\vec{k})$, λ_2, b_{ks}, b^+_{ks}, I_2.

The intensity of the electron-phonon interaction corresponding to transitions between the energy bands is denoted by I_{12}. Using this notation we have:

$$\begin{aligned} \mathbf{H} = &\sum_{\vec{k},\, s} \left[(E_1(\vec{k}) - \lambda_1)\, a^+_{\vec{k}s} a_{ks} + (E_2(\vec{k}) - \lambda_2)\, b^+_{\vec{k}s} b_{\vec{k}s}\right] - \\ &- \frac{1}{V} \sum_{\vec{k} \neq \vec{g}} \left[I_1^2 a^+_{\vec{k}\uparrow}\, a^+_{-\vec{k}\downarrow}\, a_{-\vec{g}\downarrow}\, a_{\vec{g}\uparrow} + I_2^2 b^+_{\vec{k}\uparrow}\, b^+_{-\vec{k}\downarrow}\, b_{-\vec{g}\downarrow}\, b_{\vec{g}\uparrow}\right] - \\ &- \frac{I_{12}^2}{V} \sum_{\vec{k} \neq \vec{g}} \left[a^+_{\vec{k}\uparrow}\, a^+_{-\vec{k}\downarrow}\, b_{-\vec{g}\downarrow}\, b_{\vec{g}\uparrow} + b^+_{\vec{k}\uparrow}\, b^+_{-\vec{k}\downarrow}\, a_{-\vec{g}\downarrow}\, a_{\vec{g}\downarrow}\right], \end{aligned} \tag{1}$$

where V is the volume of the system; s denotes the spin index. The summation in (1) over momentum space is limited by the proximity of the Fermi surface $2h\omega$* wide (ω is some average acoustic frequency).

The model Hamiltonian (1) can be proved if one uses a method analogous to Tolmachev and Tiablikov's method [6] for proving the usual Bardeen model from Frӧhlich's accurate Hamiltonian.

Without resting in detail on this aspect of the problem we shall just note that the model Hamiltonian (1) takes into account the most important, for the superconducting state, coupled correlations of electrons with opposite moment and spins. On the grounds of [1, 8, 9] it is possible to affirm that, contained in (1), are the important mathematical characteristics of Frӧhlich, initial Hamiltonian (completed by the consideration of overlapping bands) which are essential for the correct description of superconductivity.

2. THE CALCULATION OF THE THERMODYNAMIC POTENTIAL

For the study of the superconducting state of a metal, in the Hamiltonian (1), we shall complete the transition to the new Fermi-amplitudes according to N.N. Bogoliubov's equations:

$$\begin{aligned} a_{\vec{k}\uparrow} &= u_{\vec{k}}\, \alpha_{\vec{k}1} + v_{\vec{k}}\, \alpha^+_{-\vec{k}0}; \quad b_{\vec{k}\uparrow} = x_{\vec{k}}\, \beta_{\vec{k}1} + y_{\vec{k}}\, \beta^+_{-\vec{k}0}; \\ a_{\vec{k}\downarrow} &= u_{\vec{k}}\, \alpha_{\vec{k}0} - v_{\vec{k}}\, \alpha^+_{-\vec{k}1}; \quad b_{\vec{k}\downarrow} = x_{\vec{k}}\, \beta_{\vec{k}0} - y_{\vec{k}}\, \beta^+_{-\vec{k}1}. \end{aligned} \tag{2}$$

* Both here and later h will denote Planck's constant divided by 2π.

then H takes the form:

$$\mathbf{H} = \mathrm{U} + \sum_{i=0}^{5} \mathbf{H}_i, \tag{3}$$

where

$$\mathbf{H}_i = \mathbf{H}_{i\alpha} + \mathbf{H}_{i\beta},$$

$$\mathrm{U} = 2 \sum_{\vec{k}} (\varepsilon_1(\vec{k})\, v_{\vec{k}}^2 + \varepsilon_2(\vec{k})\, y_{\vec{k}}^2),$$

$$\mathbf{H}_{0\alpha} = \sum_{\vec{k}} \Omega_1(\vec{k})\, (\alpha_{\vec{k}1}^{+}\, \alpha_{\vec{k}1} + \alpha_{\vec{k}0}^{+}\, \alpha_{\vec{k}0}),$$

$$\mathbf{H}_{1\alpha} = \sum_{\vec{k}} [\varepsilon_1(\vec{k})\, (u_{\vec{k}}^2 - v_{\vec{k}}^2) - \Omega_1(k)]\, (\alpha_{\vec{k}1}^{+}\, \alpha_{\vec{k}1} + \alpha_{\vec{k}0}^{+}\, \alpha_{\vec{k}0}),$$

$$\mathbf{H}_{2\alpha} = \sum_{\vec{k}} 2\varepsilon_1(\vec{k})\, u_{\vec{k}}\, v_{\vec{k}}\, (\alpha_{\vec{k}1}^{+}\, \alpha_{-\vec{k}0}^{+} + \alpha_{-\vec{k}0}\, \alpha_{\vec{k}1}),$$

$$\mathbf{H}_{3\alpha} = -\frac{1}{V} \sum_{\vec{k}\,\vec{g}} u_{\vec{k}}\, v_{\vec{k}}\, (\alpha_{-\vec{k}0}\, \alpha_{-\vec{k}0}^{+} - \alpha_{\vec{k}1}^{+}\, \alpha_{\vec{k}1})\, [I_1^2 u_{\vec{g}}\, v_{\vec{g}}\, (\alpha_{-\vec{g}0}\, \alpha_{-\vec{g}0}^{+} - \alpha_{\vec{g}1}^{+}\, \alpha_{\vec{g}1}) + \tag{4}$$

$$+ I_{12}^2\, x_{\vec{g}}\, y_{\vec{g}}\, (\beta_{-\vec{g}0}\, \beta_{-\vec{g}0}^{+} - \beta_{\vec{g}1}^{+}\, \beta_{\vec{g}1})],$$

$$\mathbf{H}_{4\alpha} = -\frac{1}{V} \sum_{\vec{k}\neq} u_{\vec{k}}\, v_{\vec{k}}\, (\alpha_{-\vec{k}0}\, \alpha_{-\vec{k}0}^{+} - \alpha_{\vec{k}1}^{+}\, \alpha_{\vec{k}1})\, [I_1^2\, (u_{\vec{g}}^2 - v_{\vec{g}}^2)\, (\alpha_{\vec{g}1}^{+}\, \alpha_{-\vec{g}0}^{+} + \alpha_{-\vec{g}0}\, \alpha_{\vec{g}1}) +$$

$$+ I_{12}^2\, (x_{\vec{g}}^2 - y_{\vec{g}}^2)\, (\beta_{\vec{g}1}^{+}\, \beta_{-\vec{g}0}^{+} + \beta_{-\vec{g}0}\, \beta_{\vec{g}1})],$$

$$\mathbf{H}_{5\alpha} = -\frac{1}{V} \sum_{\vec{k}\neq\vec{g}} (u_{\vec{k}}^2\, \alpha_{\vec{k}1}^{+}\, \alpha_{-\vec{k}0}^{+} - v_{\vec{k}}^2\, \alpha_{-\vec{k}0}\, \alpha_{\vec{k}1})\, [I_1^2\, (u_{\vec{g}}^2\, \alpha_{-\vec{g}0}\, \alpha_{\vec{g}1} - v_{\vec{g}}^2\, \alpha_{\vec{g}1}^{+}\, \alpha_{-\vec{g}0}^{+}) +$$

$$+ I_{12}^2\, (x_{\vec{g}}^2\, \beta_{-\vec{g}0}\, \beta_{\vec{g}1} - y_{\vec{g}}^2\, \beta_{\vec{g}1}^{+}\, \beta_{-\vec{g}0}^{+})].$$

$H_{i\beta}$ is obtained from $H_{i\alpha}$ by exchanging all the terms referring to the first band by all the terms of the second band and vice verse.

In (4) the renormalized energies of the elementary excitations $\Omega_1(\vec{k})$ and $\Omega_2(\vec{k})$ are introduced which together with u, v, x, and y are due to be determined further on.

By $\varepsilon_l(\vec{k})$ we have in mind $E_l(\vec{k}) - \lambda_i$.

To calculate the thermodynamic potential of the system we shall use Bloch and Dominisis's statistical theory for disturbances. [7]

$$\Psi = \Psi_0 - \frac{1}{\beta} \sum_{p\geq 1} (-1)^p \int_0^{\beta} dt_1 \ldots dt_n \langle V'(t_1) \ldots \tag{5}$$

$$\ldots V'(t_p) \rangle_c \beta > t_1 > t_2 > \ldots t_n > 0.$$

$\langle\ \rangle$ denotes the statistical average over a large Gibb's ensemble with the Hamiltonian H_0 while the index c shows that only the connected diagrams must be considered $\left(\beta = \frac{1}{\theta}\right)$.

By V' is understood the last five terms of (3), and

$$V'(t) = e^{H_0 t} V' e^{-H_0 t}.$$

The thermodynamic potential of the zero approximation is equal to

$$\Psi_0 = U - \frac{2}{\beta} \sum_{\vec{k}} \sum_{i=1}^{2} \ln (1 + e^{-\beta \Omega_i (\vec{k})}). \tag{6}$$

We move on to the calculation of a first order correction of V' for the thermodynamic potential.

In addition to Bloch and Diminisis's rules [7] for calculating a group of diagrams we shall show that the self formed Fermi loop is compared with $N_i^-(k)$, if its direction is clockwise and $N_i^+(\vec{k})$ in the opposite case.

Also

$$N_i^- (\vec{k}) = \frac{1}{1 + e^{\beta \Omega_i (\vec{k})}}, \quad N_i^+ (\vec{k}) = 1 - N_i^- (\vec{k}).$$

The dotted line between the nearest points of the diagrams correspond to the potential of the quadruple interaction of the quasiparticles.

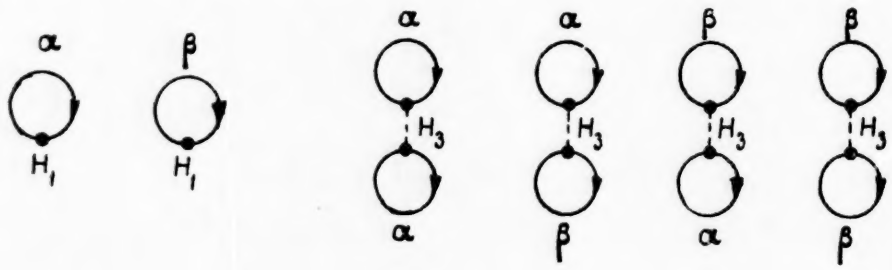

The parts of the diagrams which refer to particles of the first band are denoted by the index α, and to the second by β.

For the first order in V' the group of diagrams of Fig. 1 must be considered. Then we shall obtain:

$$\begin{aligned}
\Psi = \Psi_0 &+ 2 \sum_{\vec{k}} [\varepsilon_1 (\vec{k}) (u_{\vec{k}}^2 - v_{\vec{k}}^2) - \Omega_1 (\vec{k})] N_1^- (\vec{k}) + \\
&+ 2 \sum_{k} [\varepsilon_2 (\vec{k}) (x_{\vec{k}}^2 - y_{\vec{k}}^2) - \Omega_2 (\vec{k})] N_2^- - \\
&- \frac{I_1^2}{V} \left(\sum_{\vec{k}} u_{\vec{k}} v_{\vec{k}} (1 - 2N_1^- (\vec{k})) \right)^2 - \frac{I_2^2}{V} \sum_{\vec{k}} x_{\vec{k}} y_{\vec{k}} (1 - 2N_2^- (\vec{k}))^2 - \\
&- 2 \frac{I_{12}^2}{V} \sum_{\vec{k}} u_{\vec{k}} v_{\vec{k}} (1 - 2N_1^- (\vec{k})) \sum_{g} x_{\vec{g}} y_{\vec{g}} (1 - 2N_2^- (\vec{g})).
\end{aligned} \tag{7}$$

We shall determine the parameters u, v; x, y; Ω_1, Ω_2 from the following conditions. We

shall require that the diagrams which already appear in the second order (Fig. 2) are fully compensated for, and secondly, we shall compensate for the remaining diagrams of the second order, the number included of which is proportional to the volume of the system.

All the same the asymptotic higher approximations at $V \to \infty$ will not add further to the thermodynamic potential of the system (Fig. 3). Both the conditions are equivalent to the procedure of compensating the diagrams given earlier by Zubarev and Tserkovnikov [8].

It must also be mentioned that the conditions formulated are equivalent to the minimum condition of equation (7).

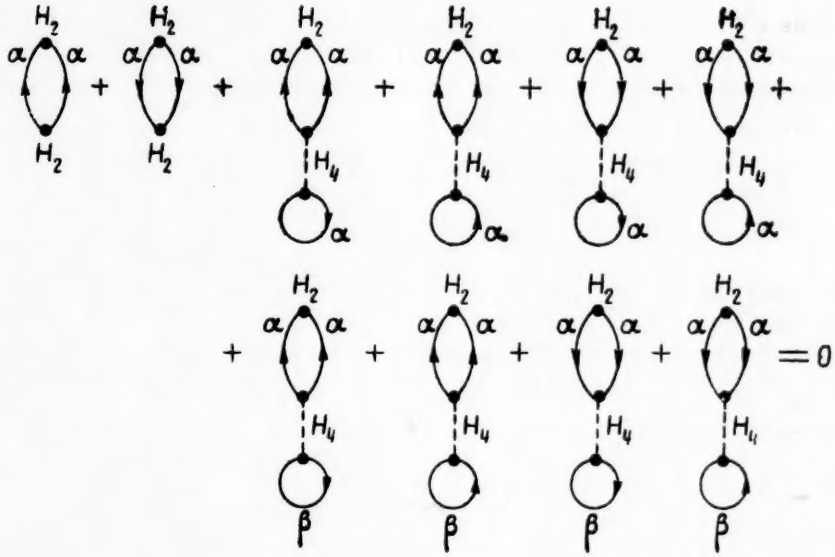

Fig. 1. Compensation diagram (Analogue equation of site for quasi-particles of the second order)

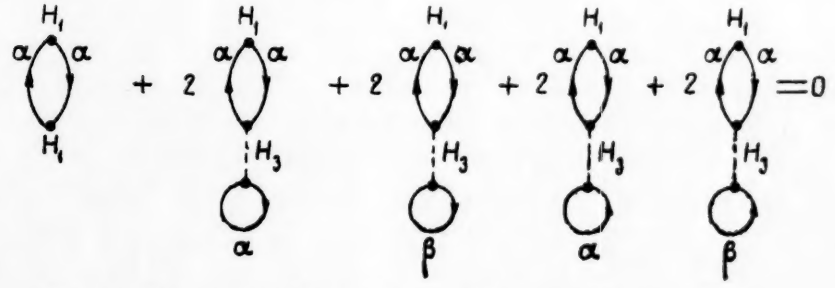

Fig. 2. Compensation diagram "correct energy consumption" (Analogue figure for quasi-particles β)

As a result of the calculations we obtain:

$$u_{\vec{k}}^2 = \frac{1}{2}\left(1 + \frac{\varepsilon_1(\vec{k})}{\Omega_1(\vec{k})}\right), \quad v_{\vec{k}}^2 = \frac{1}{2}\left(1 - \frac{\varepsilon_1(\vec{k})}{\Omega_1(\vec{k})}\right); \tag{8}$$

$$x_{\vec{k}}^2 = \frac{1}{2}\left(1 + \frac{\varepsilon_2(\vec{k})}{\Omega_2(\vec{k})}\right), \quad y_{\vec{k}}^2 = \frac{1}{2}\left(1 - \frac{\varepsilon_2(\vec{k})}{\Omega_2(\vec{k})}\right);$$

VOL. 8 1959

where

$$\Omega_i(\vec{k}) = \sqrt{\varepsilon_i^2(\vec{k}) + C_i^2},$$

$$C_1 = \frac{I_1^2}{V}\sum_{\vec{k}} u_{\vec{k}} v_{\vec{k}} (1 - 2N_1^-(\vec{k})) + \frac{I_{12}^2}{V}\tau_2 \sum_k x_k y_k (1 - 2N_2^-(\vec{k})),$$

$$C_2 = \frac{I_2^2}{V}\sum_k x_{\vec{k}} y_{\vec{k}} (1 - 2N_2^-(\vec{k}) + \frac{I_1^2}{V}\tau_1 \sum_{\vec{\kappa}} u_{\vec{k}} v_{\vec{k}} (1 - 2N_1^-(\vec{k})), \tag{9}$$

$$\tau_1 = \frac{I_{12}^2}{I_1^2}, \quad \tau_2 = \frac{I_{12}^2}{I_2^2}, \quad \tau = \tau_1\tau_2.$$

Taking (6), (8) and (9) into account equation (7) takes the form

$$\Psi = \sum_{\vec{k}}\sum_{i=1}^{2}(\varepsilon_i(\vec{k}) - \Omega_i(\vec{k})) - \frac{2}{\beta}\sum_{\vec{k}}\sum_{i=1}^{2}\ln(1 + e^{-\beta\Omega_i(\vec{k})}) + \tag{10}$$
$$+ \frac{V}{I_1^2} C_1 \frac{C_1 - \tau_2 C_2}{1 - \tau} + \frac{V}{I_2^2} C_2 \frac{C_2 - \tau_1 C_1}{1 - \tau}.$$

The terms C_1 and C_2 play the role of gaps in the spectrum of the elementary disturbances. On the basis of (9) and (8) we obtain the following equations for their determination:

$$C_1 = \frac{I_1^2}{2V} C_1 \sum_k \frac{1}{\Omega_1(k)} \tanh\frac{\beta\Omega_1(\vec{k})}{2} + \frac{\tau_2 I_2^2}{2V} C_2 \sum_{\vec{k}} \frac{1}{\Omega_2(\vec{k})} \tanh\frac{\beta\Omega_2(\vec{k})}{2},$$
$$C_2 = \frac{I_2^2}{2V} C_2 \sum_{\vec{k}} \frac{1}{\Omega_2(\vec{k})} \tanh\frac{\beta\Omega_2(\vec{k})}{2} + \frac{\tau_1 I_1^2}{2V} C_1 \sum_{\vec{k}} \frac{!}{\Omega_1(k)} \tanh\frac{\beta\Omega_1(\vec{k})}{2}. \tag{11}$$

3. THE DETERMINATION OF THE CRITICAL TEMPERATURE AND OF THE PARAMETERS C_1 AND C_2 IN ITS VICINITY

A non-trivial solution only exists below a certain critical temperature $T = T_c$. On approaching this point the parameters C_1 and C_2 tend to zero according to the law $C_1 = \delta\gamma_1$, $C_2 = \delta\gamma_2$, where $\delta(T = T_c) = 0$.

The constants γ_1, γ_2 satisfy the linear equations (11):

$$\gamma_1 = \frac{I_1^2}{2V}\gamma_1 \sum_{\vec{k}} \frac{1}{\varepsilon_1} \tanh\frac{\beta_c\varepsilon_1}{2} + \tau_2 \frac{I_2^2}{2V}\gamma_2 \sum_{\vec{k}} \frac{1}{\varepsilon_2} \tanh\frac{\beta_c\varepsilon_2}{2};$$
$$\gamma_2 = \frac{I_2^2}{2V}\gamma_2 \sum_{\vec{k}} \frac{1}{\varepsilon_2} \tanh\frac{\beta_c\varepsilon_2}{2} + \tau_1 \frac{I_1^2}{2V}\gamma_1 \sum_{\vec{k}} \frac{1}{\varepsilon_1} \tanh\frac{\beta_c\varepsilon_1}{2}. \tag{12}$$

Equating the determinant of this system to zero we obtain an equation for determining T_c

$$1 - (\rho_1 + \rho_2)\xi + (1 - \tau)\rho_1\rho_2\xi^2 = 0, \tag{13}$$

where

$$\xi = \int_0^{\hbar\omega} \frac{1}{\varepsilon} \tanh \frac{\beta_c \varepsilon}{2}\, d\varepsilon$$

$$N_1(0) = \frac{1}{8\pi^3} \iint_{E_F} \frac{dS_1}{|\mathrm{grad}_k E_1(k)|}; \quad N_2(0) = \frac{1}{8\pi^3} \iint_{E_F} \frac{dS_2}{|\mathrm{grad}\, E_2(k)|}; \tag{14}$$

$$\rho_1 = I_1^2 N_1(0); \quad \rho_2 = I_2^2 N_2(0).$$

$N_1(0)$ and $N_2(0)$ are the densities of the electronic states close to the Fermi surface for the first and second energy bands respectively.

On the grounds of (13) and (14) we obtain the following expression for the critical temperature:

$$\Theta_c = 1{,}14\hbar\omega\, e^{-\xi}, \tag{15}$$

where

$$\xi_{\pm} = \frac{\rho_1 + \rho_2 \pm \sqrt{(\rho_1 + \rho_2)^2 - 4\rho_1\rho_2(1-\tau)}}{2\rho_1\rho_2(1-\tau)}. \tag{16}$$

The sign before the root in equation (16) for should be chosen so that is positive. In those cases when this condition is not sufficient for the determination of the sign, the condition for the minimum thermodynamic potential of the superconductor is decisive.

We shall also quote the ratio of the terms γ_1 and γ_2 at the critical point

$$\frac{\gamma_1}{\gamma_2} = \frac{1 - \rho_2\xi}{\tau_1\rho_1\xi}. \tag{17}$$

We shall proceed to find out the expression for C_1 and C_2 close to the critical temperature.

With this aim we shall analyse the functions $\frac{1}{\Omega_i(k)} \tanh \frac{\beta\Omega_i(k)}{2}$, which come into (11), in steps $(\beta - \beta_c)$ and we shall limit ourselves to the first term of this analysis.

Equations (11) simplified in this way give

$$\frac{\beta_c^3}{F}\left(\frac{dC_1^2}{d\beta}\right)_c = 1 + \frac{\rho_2}{\rho_1}\,\frac{1-(1-\tau)\rho_1\xi}{1-(1-\tau)\rho_2\xi}\left(1 - \frac{\beta_c^3}{F}\left(\frac{dC_2^2}{d\beta}\right)_c\right), \tag{18}$$

where

$$F = 2\int_0^{\infty} f(x)\,dx \simeq 9{,}39; \quad f(x) = \frac{\sinh x - x}{2x^3 \cosh^2 x/2}$$

The second relation between the derivatives we obtain from (17)

$$\left(\frac{dC_1^2}{d\beta}\right)_c = \left(\frac{1-\rho_2\xi}{\tau_1\rho_1\xi}\right)^2 \left(\frac{dC_2^2}{d\beta}\right)_c. \tag{19}$$

On the grounds of (18) and (19) we obtain the following expressions for the derivatives:

$$\left(\frac{dC_1^2}{d\beta}\right)_c = \frac{F}{\beta_c^3}\,\tau_2(1-(1-\tau)\rho_1\xi)\,\frac{\rho_1+\rho_2-2(1-\tau)\rho_1\rho_2\xi}{\rho_1\tau_2(1-(1-\tau)\rho_2\xi)^2 + \tau_1\rho_2(1-(1-\tau)\rho_1\xi)^2}, \tag{20}$$

VOL. 8 1959

$$\left(\frac{dC_2^2}{d\beta}\right)_c = \frac{F}{\beta_c^3}\tau_1(1-(1-\tau)\rho_1\xi)\frac{\rho_1+\rho_2-2(1-\tau)\rho_1\rho_2\xi}{\rho_1\tau_2(1-(1-\tau)\rho_2\xi)^2+(1-(1-\tau)\rho_1\xi)^2\tau_1\rho_2} \quad (20)\ \textit{contd.}$$

Thus it is obvious that the parameters C_1 and C_2 themselves have the form

$$C_1^2 = \left(\frac{dC_1^2}{d\beta}\right)_c(\beta-\beta_c)+\ldots, \quad C_2^2 = \left(\frac{dC_2^2}{d\beta}\right)_c(\beta-\beta_c)+\ldots \quad (21)$$

4. THE DETERMINATION OF THE JUMPS IN THE THERMODYNAMIC QUANTITIES

It is not difficult to check that a phase transition of the first order is absent at the critical point.

Actually in accordance with (10) we have

$$\frac{\partial\Psi}{\partial C_1} = \frac{\partial\Psi}{\partial C_2} = 0.$$

Therefore

$$\frac{d\Psi}{d\theta} = \frac{\partial\Psi}{\partial\theta} = -2\sum_{\vec{k}}\sum_{i=1}^{2}\ln(1+e^{-\beta\Omega_i(\vec{k})}) - 2\beta\sum_{\vec{k}}\sum_{i=1}^{2}\Omega_i(\vec{k})N_i^-(\vec{k}). \quad (22)$$

The entropy S of the system

$$S = -\frac{d\Psi}{d\theta}$$

thus has the form of the entropy of a free Fermi gas with energies $\Omega_1(k)$, $\Omega_2(k)$. It is obvious that $(S-S_n)_{T_c} = 0$ where the index n refers to the normal state. However a phase transition of the second order exists at the critical point. The sp. ht. of the system in the superconducting state has the form

$$\sigma = 2\beta^2\sum_{\vec{k}}\sum_{i=1}^{2}\Omega_i^2(k)e^{\beta\Omega_i(\vec{k})}(1+e^{\beta\Omega_i(\vec{k})})^{-2} + \beta^3\sum_{i=1}^{2}\frac{dC_i^2}{d\beta}\sum_{\vec{k}}e^{\beta\Omega_i(k)}(1+e^{\beta\Omega_i(k)})^{-2}, \quad (23)$$

then as in the normal state we have

$$\sigma_n = 2\beta^2\sum_{i}\sum_{\vec{k}}\varepsilon_i^2(\vec{k})e^{\beta|\varepsilon_i(\vec{k})|}(1+e^{\beta|\varepsilon_i(\vec{k})|})^{-2} = \frac{2\pi^2}{3\beta_c}V(N_1(0)+N_2(0)). \quad (24)$$

Thus at the critical point there is a jump in the sp. ht.

$$(\Delta\sigma)_c = V\beta_c^2\sum_{i=1}^{2}N_i(0)\left(\frac{dC_i^2}{d\beta}\right)_c. \quad (25)$$

Using (20), (25) can be rewritten in the form

$$(\Delta\sigma)_c = \frac{V}{\beta_c} F \frac{\tau}{I_{12}^2} \frac{[\rho_1 + \rho_2 - 2(1-\tau)\rho_1\rho_2\xi]^2}{\tau_2\rho_1(1-(1-\tau)\rho_2\xi)^2 + \tau_1\rho_2(1-(1-\tau)\rho_1\xi)^2}. \tag{26}$$

We shall also quote the expression for the critical magnetic field which is necessary to destroy the superconducting state in the vicinity of the critical temperature:

$$\frac{H_c^2}{8\pi} = \Psi_n - \Psi = \frac{(\Delta\sigma)_c}{2\theta_c}(\theta - \theta_c). \tag{27}$$

The larger the jump in the sp. ht. ($\Delta\sigma > 0$) the more stable will the superconducting state be. This condition together with the condition $\xi > 0$ fully determines the value of ξ.

5. THE ENERGY OF THE GROUND STATE

When the temperature tends to zero the thermodynamic potential goes into the energy of the ground state

$$E_0 = \sum_{i=1}^{2}\sum_{\vec{k}}(\varepsilon_i(\vec{k}) - \Omega_i(\vec{k})) + \frac{V}{I_1^2} C_1 \frac{C_1 - \tau_2 C_2}{1-\tau} + \frac{V}{I_2^2} C_2 \frac{C_2 - \tau_1 C_1}{1-\tau}. \tag{28}$$

Thus the parameters C_1 and C_2 are determined from the equations:

$$\begin{aligned} C_1 &= \frac{I_1^2}{2V} C_1 \sum_{\vec{k}} \frac{1}{\sqrt{\varepsilon_1^2(k) + C_1^2}} + \frac{\tau_2 I_2^2}{2V} C_2 \sum_{\vec{k}} \frac{1}{\sqrt{\varepsilon_2^2(k) + C_2^2}} \\ C_2 &= \frac{I_2^2}{2V} C_2 \sum_{\vec{k}} \frac{1}{\sqrt{\varepsilon_2^2(k) + C_2^2}} + \frac{\tau_1 I_1^2 C_1}{2V} \sum_{\vec{k}} \frac{1}{\sqrt{\varepsilon_1^2(k) + C_1^2}}. \end{aligned} \tag{29}$$

Completing the summation over the k-space, instead of (29) the following equations can be obtained:

$$\begin{aligned} C_1 &= C_1\rho_1 \ln \frac{\hbar\omega + \sqrt{(\hbar\omega)^2 + C_1^2}}{C_1} + C_2\rho_2\tau_2 \ln \frac{\hbar\omega + \sqrt{(\hbar\omega)^2 + C_2^2}}{C_2}; \\ C_2 &= C_1\rho_1\tau_1 \ln \frac{\hbar\omega + \sqrt{(\hbar\omega)^2 + C_1^2}}{C_1} + C_2\rho_2 \ln \frac{\hbar\omega + \sqrt{(\hbar\omega)^2 + C_2^2}}{C_2}. \end{aligned} \tag{30}$$

Equations (30) have the solution $C_1,\ C_2 \ll \hbar\omega$, therefore we can proceed to the simplified equations:

$$C_1 = C_1\rho_1 \ln \frac{2\hbar\omega}{C_1} + C_2\rho_2\tau_2 \ln \frac{2\hbar\omega}{C_2};\ C_2 = C_1\rho_1\tau_1 \ln \frac{2\hbar\omega}{C_1} + C_2\rho_2 \ln \frac{2\hbar\omega}{C_2}. \tag{31}$$

Further we shall denote the ratio of $C_1C_2^-$ by z, then

$$C_1 = 2\hbar\omega z \exp\left[-\frac{\tau_1 z - 1}{\rho_2(\tau - 1)}\right],\ C_2 = C_1/z. \tag{32}$$

where z is determined from the following equation:

$$\frac{1}{\rho_1} - \frac{1}{\rho_2} + \frac{\tau_1}{\rho_2} z - \frac{\tau_2}{\rho_1} \frac{1}{z} = (\tau - 1) \ln z \tag{33}$$

If it is possible to neglect the transitions of pairs between the zones, i.e. if it is assumed that $\tau_1 = \tau_2 = \tau = 0$, then

$$z = exp\left(\frac{1}{\rho_2} - \frac{1}{\rho_1}\right),$$
$$C_2 = 2\hbar\omega\, exp\left(-\frac{1}{\rho_2}\right), \quad C_1 = 2\hbar\omega\, exp\left(-\frac{1}{\rho_1}\right). \tag{34}$$

If τ_1, $\tau_2 \neq 0$, then the solution of (33) can be obtained in the form $z = z_0 + z_1 + \ldots$ where

$$z_0 = \frac{1}{2\tau_1}\left[1 - \frac{\rho_2}{\rho_1} + \sqrt{\left(1 - \frac{\rho_2}{\rho_1}\right)^2 + 4\tau \frac{\rho_2}{\rho_1}}\right],$$
$$z_1 = \frac{\rho_2 (\tau - 1) \ln z_0}{\tau_1 + \tau_2 \rho_2 / \rho_1 z_0^2}. \tag{35}$$

For the reasons mentioned above one sign is chosen in these formulae. Finally we obtain:

$$C_2 = 2\hbar\omega\, e^{-\xi} exp\left[-\frac{z_0 \tau_1 \ln z_0}{\sqrt{\left(1 - \frac{\rho_2}{\rho_1}\right)^2 + 4\tau \frac{\rho_2}{\rho_1}}}\right], \quad C_1 = z_0 C_2, \tag{36}$$

where ξ is determined by equation (16).

The transition to the superconducting state is accompanied by a loss of energy

$$W = E_0 - E_N = -\frac{1}{2} V (N_1(0) C_1^2 + N_2(0) C_2^2). \tag{37}$$

6. DISCUSSION OF THE RESULTS

If the matrix element I_{12} is equal to zero ($\tau_1 = \tau_2 = 0$), then the electrons of the two bands form two independent sub-systems with different critical transition temperatures in the superconducting state (T_{1c}, T_{2c}).

At temperatures above the highest critical temperature both systems are found in the normal state. On lowering the temperature at first one system of electrons moves into the superconducting state while the second remains in the normal state. And only on further cooling does the second system of electrons move into the superconducting state.

However if the matrix element I_{12} for a transition between the bands is other than zero then the transition to the superconducting state comes simultaneously for both the sub-systems.

Actually, as is seen from equation (11), the parameter C_1 reverting to zero leads to C_2 also being equal to zero and vice verse.

The expressions given in the earlier paragraphs can be simplified for several particular values of the parameters in the theory.

We shall consider the particular case $\tau = 1$.

Then

$$\xi = (\rho_1 + \rho_2)^{-1} \tag{38}$$

and consequently,

$$\Theta_c = 1{,}14\hbar\omega \exp\left(-\frac{1}{\rho_1+\rho_2}\right),$$
$$\frac{(\Delta\sigma)_c}{\sigma_N} = \frac{3}{2\pi^2} F \frac{(\rho_1+\rho_2)^2}{\tau_1\rho_2+\tau_2\rho_1}. \tag{39}$$

It is also possible to quote expressions for the parameters C_1 and C_2 at zero temperature:

$$C_1(0) = 2\hbar\omega(\tau_2)^{\frac{\rho_2}{\rho_1+\rho_2}} \exp\left(-\frac{1}{\rho_1+\rho_2}\right),$$
$$C_2(0) = 2\hbar\omega(\tau_1)^{\frac{\rho_1}{\rho_1+\rho_2}} \exp\left(-\frac{1}{\rho_1+\rho_2}\right). \tag{40}$$

If the parameter τ is not equal to unity a certain simplification of the formulae can nevertheless be obtained if one takes into account the fact that the densities of the electronic states are different in the different energy bands.

Before carrying out the simplification one must choose the sign for ξ. For the conditions where $\rho_2 - \rho_1$ and $N(0) - N_1(0)$ have the same sign for ξ, ξ_- can be chosen (16).

As is known the density of the states in the d-band is considerably larger than in the s-band ($N_1(0) \gg N_2(0)$), then, if τ is not much bigger than unity, for ξ may be written

$$\xi \simeq (\rho_1 + \tau\rho_2)^{-1},$$

and

$$\Theta_c \simeq 1{,}14\hbar\omega \exp\left(-\frac{1}{\rho_1+\tau\rho_2}\right),$$
$$(\Delta\sigma)_c/\sigma_N \simeq \frac{3F}{2\pi^2}\left(1+\frac{\rho_2\tau}{\rho_1}(2-\tau^{-2}-\tau_1^2)\right),$$
$$C_2(0) \simeq 2\hbar\omega\left(1-\frac{\rho_2}{\rho_1}(\tau-1+\tau\ln\tau_1)\right)\exp\left(-\frac{1}{\rho_1+\tau\rho_2}\right). \tag{41}$$

Thus the energy band with a high density of electronic states close to the Fermi surface (the d-band) plays the chief part in the determination of the parameters of the superconducting state.

The second band with the lower density alters the value of the physical quantities by the order of $\tau\rho_2/\rho_1$.

The earlier discussions of this paragraph were based on the assumption that I_1^2, I_2^2, I_{12}^2 are positive.

However a calculation of the coulomb interaction leads to a number of the quantities enumerated being reduced and in particular a number of them can become negative in accordance with the repulsive nature of the coulomb interaction.

Since the existence of a superconducting state in the present model is linked with such quantities as ξ and $\Delta\sigma$ being positive we see that in the model considered the criterion of superconductivity is less rigid than in Bardeen's usual model ($\rho > 0$).

The present work was undertaken at the suggestion of S.V. Tiablikov to whome the author expresses deep gratitude for the help given in its completion.

I take this opportunity of expressing the warmest thanks to D.N. Zubarev for his discussion

VOL. 8 1959

of this work and critical comments.

Translated by J.H. Dempster

REFERENCES

1. N.N. Bogoliubov, *Zh. eksp. teor. fiz.*, 34, 58, (1958). N.N. Bogoliubov, V.V. Tolmachev and D.V. Shirkov, *A new method in the theory of superconductivity (Novyi metod v teorii sverkhprovodimostri), Izv. Akad. Nauk. SSSR*, Moscow, (1958)
2. L.N. Cooper, *Phys. rev.* 104, 1189, (1956).
3. J. Bardeen, L. Cooper and J. Schrieffer, *Phys. rev.* 108, 1175, (1957).
4. D. Pines, *Phys. rev.*, 109, 280, (1958).
5. R. Peierls, *The quantum theory of the solid state (Kvantovaia teoriia tverdykh tel)* Foreign Literature Publishing House, Moscow, p.153, (1956).
6. V.V. Tolmachev and S.V. Tiablikov, *Zh. eksp. teor. fiz.*, 34, 66, (1958).
7. C. Bloch and C. Dominisis, *Nuclear Phys.* 7, 459, (1958). *Russian translation "Problems of modern physics"* No.6, (1958).
8. D.N. Zubarev and Iu.A. Tserkovnikov, *Dokl. Akad. Nauk. SSSR.*, 122, 999, (1958).
9. V.A. Moskalenko, *Dokl. Akad. Nauk. SSSR.*, 123, 434, (1958).

VOL 8 195

THE EFFECT OF GEOMETRICAL DISTORTIONS ON THE DISTRIBUTION OF THE BACKGROUND INTENSITY IN X-RAY AND NEUTRON DIFFRACTION PHOTOGRAPHS*

M.A. KRIVOGLAZ

Institute of Metal Physics Akad. Nauk Ukr.S.S.R.

(Received 7 January 1959)

A study has been made of the characteristics of the background distribution close to the lines or spots of Debye, Laue X-ray photographs which were obtained by scattering monochromatic radiation with a single crystal. The scattering is controlled by the difference between the atomic scattering factors and the atomic radii of the components of the solution. An abnormally large scattering is observed close to the critical point. Equations are given which enable the correlation parameters to be determined (taking into account the geometrical distortions) for the distribution of the background intensity found experimentally for a Debye photograph.

VOL. 8 1959

1. INTRODUCTION

A study of the diffuse scattering of x-rays and thermal neutrons enables a whole series of results to be obtained concerning the order in the distribution of the atoms in the solid solution, the lattice vibrations, the constants for interatomic interaction etc. Apparently the best method in principle which enables the largest number of such results to be found with sufficient accuracy, is the ionization method for studying the scattering of monochromatic radiation by a single crystal, which enables one to find the distribution of the intensity at all points of a cell in the reciprocal lattice. However in the experimental study of diffuse scattering less clumsy methods are often used, in which, somehow, there is determined the average distribution of the intensity (Debye or Laue photograph) or the distribution of the intensity at some surface in the space of the reciprocal lattice (in the photographic study of the scattering of monochromatic radiation by a single crystal).

In connexion with this it is interesting to find theoretically the distribution of the background intensity in an x-ray photograph using the research methods already mentioned. Moreover the effect of the geometrical distortions on the distribution of the intensity of the diffuse scattering in the space of the reciprocal lattice* is mainly studied in the theoretical works. In the present work will be studied the distribution of the background intensity in a Debye, Laue, and x-ray photograph obtained using scattered monochromatic radiation with a single crystal.

* *Fiz. metal. metalloved.* 8, No. 4, 514-530, 1959.

* In [1] the background in a Debye photograph is reviewed. However in this work an assumption, which does not correspond to reality, is accepted in which the distance between two atoms in the solid solution depends only on the kind of atoms they are (and does not depend on the kind of atoms neighbouring those considered). Besides this, in [1], only that part of the scattering was considered which corresponded to the "interference" between the scattering connected with the geometrical distortions and the scattering linked with the difference between the atomic scattering factors. The scattering which is governed only by the geometrical distortions (which is obtained in

The main attention will be devoted to the study of the background characteristics which are connected with the presence, in the expression for the intensity of a term which tends to infinity in the neighbourhood of the reciprocal lattice points. Thus we shall proceed from expressions for the intensity of the diffuse scattering of monochromatic radiation by a single crystal $I\phi$ which were obtained in [3]. Also as in [3] we shall calculate only the scattering at non-uniformities which are created by the variation in the factors for scattering and the atomic radii.

In the case of binary disordered solutions for the substitution A–B in the vicinity of reciprocal lattice points the expression for $I\phi$, according to [3] has the form**

$$I_\phi = \frac{N}{\Delta}\frac{kT}{\varphi_{cc}+\beta q^2}\left(a_q \bar{f}\frac{q_1 e_q}{|q|} - f_A + f_B\right)^2. \quad (1)$$

Here $I\phi$ is expressed in electronic units; N is the number of atoms in the crystal; k is Boltzmann's constant; T is the absolute temperature; Δ is the volume of an elementary cell; $\varphi_{cc} = \frac{\partial^2 \varphi}{\partial c^2}$ is the second derivative of the thermodynamic potential of a unit of volume for a concentration c; q_1 is the difference between the wave vectors for the scattered and the incident waves; $q = q_1 - 2\pi K_n$, where K_n is a vector of the reciprocal lattice which is drawn to the centre of the cell into which drops the end of the vector $q_1/2\pi$; β is a quantity of the order $kT\Delta^{-1/3}$; f_A and f_B are the atomic scattering factors for the atoms A and B;

$$\bar{f} = f_A \exp\left(-\frac{L_A}{2}\right) + f_B \exp\left(-\frac{L_B}{2}\right),$$

where $\exp(-L_A/2)$ and $\exp(-L_B/2)$ are the factors determining the reduction in the amplitude of the scattering for the atoms A and B on account of the distortions; e_q is a unit vector lying in the direction parallel to the displacements of the atoms in the q wave of the fluctuations of the components; a_q represents the amplitude of these displacements. In the case of cubic crystals a_q and e_q are equal:

$$a_q e_{qx} = \frac{1}{3}\frac{c_{11}+2c_{12}}{D}(1+\varepsilon n_y^2)(1+\varepsilon n_z^2)\frac{1}{\Delta}\frac{\partial \Delta}{\partial c} n_x,$$

$$D = c_{11} + \varepsilon(c_{11}+c_{12})(n_x^2 n_y^2 + n_x^2 n_z^2 + n_y^2 n_z^2) + \varepsilon^2(c_{11}+2c_{12}+c_{44}) n_x^2 n_y^2 n_z^2, \quad (2)$$

where the axis of the co-ordinates are taken along the cubic axes; $n = q/|q|$, c_{ij} is the modulus of elasticity; $\epsilon = (c_{11} - c_{12} - 2c_{44})/c_{44}$. The expressions for $a_q e_{qy}$ and $a_q e_{qz}$ are obtained from equations (2) by a cyclic permutation. For other structures the equations for $a_q e_q$ are given in [4]. In the isotropic continuum approximation ($\epsilon = 0$) $e_q \| q$, a_q does not depend on q and is equal to (σ is Poisson's coefficient)

$$a_q = a = \frac{1+\sigma}{3(1-\sigma)}\frac{1}{\Delta}\frac{\partial \Delta}{\partial c}; \quad e_q = \frac{q}{|q|} = \vec{n}. \quad (3)$$

For large $|q|$ equation (1) ceases to be applicable. In this case it is possible for example to express $I\phi$ by the correlation parameters $\varepsilon(\rho)$

$$I_\phi = N\left[c(1-c) - \sum_{\rho \neq 0}\varepsilon(\rho)\cos q\rho\right]\left(a_q \bar{f}\frac{q_1 e_q}{|q|} - f_A + f_B\right)^2. \quad (4)$$

Here ρ is a lattice vector and $\varepsilon(\rho) = c^2 - p^\rho_{AA}$, where p^ρ_{AA} is the probability of the occupation of a pair of points, separated by the vector ρ, by A atoms. For larger q equation (2) also ceases to be applicable. The corresponding equations for the calculation of $a_q e_q$ are given in [3, 4]. For example,

---

continuation

the second term, which is not accounted for in [1] of the analysis of the expression for the intensity according to the powers of the difference of the atomic radii of the components) is not considered in [1] although in certain cases, for example, in the neighbourhood of reciprocal lattice points (2), it can give a more intense background (especially when the components have close atomic scattering factors). Therefore the background distribution for a Debye photograph obtained in [1] may differ substantially from the actual distribution.

**Here and below q_1, q, K_1, R, ρ, e denotes vectors

for solutions with a face centred cubic lattice $a_q e_q$ are determined by equations (28) (29) of 4.

2. THE DISTRIBUTION OF THE BACKGROUND INTENSITY IN A DEBYE PHOTOGRAPH

It is easy to see that the intensity of the diffuse scattering by a polycrystal I_D is connected to the intensity of the scattering by a single crystal $I\phi$ by the relation

$$I_D = \frac{1}{4\pi q_1^2} \int_S I_\phi(q)\, dS, \tag{5}$$

where integration is carried out over the surface of a sphere of radius $|q_1|$ in the space of the reciprocal lattice.

First of all we shall consider scattering by an ideal solution. We shall proceed from equation (4) in which we shall assume that $\varepsilon(\rho) = 0$. First of all it is interesting to study which characteristics in the background distribution of a Debye photograph are brought forward by the term, proportional to q^{-2}, which tends to inifinity at several points of the reciprocal lattice. It is obvious that these characteristics will be displayed close to the lines on the Debye photograph. For the lines $|q_1| = q_0 = 2\pi K_n$, themselves and for points lying close to the lines, on integrating in (5) over sectors of the sphere which are situated near the ends of the vectors $2\pi K_n$, the term in the expression under the integral, proportional to $q^{-2} = |q_1 - 2\pi K_n|^{-2}$ becomes very large. In order to ascertain whether I_D has a peculiarity close to the lines we shall integrate the square of the first term in the bracket of equation (1) over the sectors of the sphere S_1 mentioned above which with sufficient accuracy may be replaced by flat disks perpendicular to the vectors $2\pi K_n$, the radius of which r_m is considerably larger than the shortest distance Q from the end of the vector $2\pi K_n$ to the sphere, but considerably less than the dimensions of a cell of the reciprocal lattice

$$I'_D = \frac{pNc(1-c)\bar{f}^2}{4\pi q_1^2} \int_0^m \int_0^{2\pi} a_q^2 \frac{(q_1 e_q)^2}{r^2 + Q^2}\, r\, dr\, d\varphi, \tag{6}$$

where p is the number of lattice points for which the vectors $2\pi K_n$ lie at the surface of the sphere (the recurrence factor); r and ϕ are the co-ordinates of the points on the flat part. In the isotropic continuum approximation, considering that, in accordance with (3) $e_q q_1 = Q/\sqrt{Q^2 + r^2}$, and carrying out the integration in (6), we obtain

$$I'_D = \frac{1}{4} Npc(1-c)\bar{f}^2\bar{a}^2. \tag{7}$$

In this approximation I_D has no peculiarities close to the lines.

In calculating the elastic anisotropy qualitatively different results are obtained depending on whether the given vector $2\pi K_n$ is perpendicular to the isodiffuse surface $I\phi = 0$ which crosses the end of this vector. In the first case on account of the symmetry of the crystal in the plane for which $q \perp q_1$, e_q is also perpendicular to q_1 and the isodiffuse surface is parallel to the sector S_1. Such a case exists, for example, for the scattering points *(hOO)* and *(hhO)* in cubic crystals. In this case as in the isotropic continuum approximation the expression in the integral in (6) differs significantly from zero only in the sector of the circle with radius $\sim Q$, and I'_D is determined from an equation like (7) in which a^2 must be written as

$$\bar{a}^2 = \int_0^\infty \frac{a^2(x)}{(1+x)^2}\, dx;$$

$$a^2\left(\frac{r^2}{Q^2}\right) = \frac{r^2 + Q^2}{2\pi Q^2 q_1^2} \int_0^{2\pi} a_q^2 (q_1 e_q)^2\, d\varphi \tag{8}$$

The values of $\bar{a}^2$ for different crystals can be determined by means of numerical integration or with the help of approximate equations. For example, in the case of ϵ weakly anisotropic cubic crystals analysing (2) according to the powers of and considering only the linear terms we obtain for *(hOO)* points

$$\bar{a}^2 = \frac{1}{9}\left(1 + \frac{7}{12}\varepsilon - \frac{5}{12}s\varepsilon\right)(1+2s)^2\left(\frac{\tau}{\Delta}\frac{1}{\partial c}\frac{\partial \Delta}{\partial c}\right)^2,$$

where $S = C_{12}/C_{11}$.

Qualitatively another result is obtained in the second case when the observed point in the reciprocal lattice does not correspond to a particular symmetry and as a result of the anisotropy of the crystal in the plane $q \perp q_1$, the vector e_q is not perpendicular to q_1 and the surface $I\phi = 0$ lies at an angle to the sector S_1 in this case in the immediate vicinity of the line on the Debye photograph I_D', in agreement with (6) takes the assymptotic value:

$$I_D' = \frac{1}{2} pNc(1-c)\bar{f}^2 a_0^2 \ln \frac{r_m}{|Q|}\ ;\ a_0^2 = \overline{a_q^2 \frac{(e_q q_1)^2}{q_1^2}}\ ;$$
$$Q = |q_1| - 2\pi |K_n| \cong |q_1| \cot\theta \cdot \Delta\theta = \frac{4\pi}{\lambda} \cos\theta \Delta\theta, \quad (9)$$

where λ is the wave length, 2θ is the angle of scatter $\Delta\theta = \theta - \theta_0$ (θ^0 corresponds to a line on the Debye photograph) and in calculating a_0^2 the mean is taken over all the directions of the vector a in the plane $q \perp q_1$. In the particular case of cubic crystals with an accuracy to the square of terms in

$$a_0^2 = \frac{5}{144}(1+2s)^2 \varepsilon^2 \left(\frac{1}{\Delta}\frac{\partial \Delta}{\partial c}\right)^2 \cdot$$
$$\frac{h^2(k^2+l^2)^3 + k^2(h^2+l^2)^3 + l^2(h^2+k^2)^3 - 2(h^4k^4 + h^4l^4 + k^4l^4)}{(h^2+k^2+l^2)^4}.$$

As it follows from (9)*, in calculating the elastic anisotropy close to the line corresponding to junctions in the reciprocal lattice of the type being considered, I_D has a particular value and for $\Delta\theta \to 0$ it tends logarithmically to infinity.* (Equally as in (9), I_D' also contains a term similar to that in (7)). However the line always has a finite value and in studying the background $\Delta\theta$ cannot be made as small as one likes. Therefore, considering how weak the characteristic is, it is not easy to find it experimentally. Thus if $r_m \sim 10^{-1}|q_1|$ then for $\theta \sim 45^0$ on altering $\Delta\theta$ from the order of 10^{-3} to 10^{-2} I_D' is doubled.

In contrast to the square of the first term in the last factor of equation (1) the square of the second term and the doubled product on integration over the allotted sectors in the vicinity of the reciprocal lattice points give an expression which tends to zero if $r_m \to 0$, $Q \to 0$. In order to determine I_D it is necessary to add to the expression for I_D' the mean value of the expression for $I\phi$ over the remaining part of the surface of integration. The corresponding integration for actual crystals can be carried out numerically. The result obtained will give a term in I_D which increases as $|q_1|$ increases (although generally speaking not monotonically).

We shall now consider the non-ideal solutions in which $\varepsilon(\rho)$ are other than zero. As follows from (4), (5) in this case I_D has the following form:

$$I_D = N\left[c(1-c)\varphi_0(|q_1|) - \sum_{l=1}^{\infty} z_l \varepsilon_l \varphi_l(|q_1|)\right]. \quad (10)$$

* In equation (9) in included a somewhat indetermined quantity – the radius of the area of integration r_m (r_m, of course, arises from the expression for the sum I_D' and the integral over the remaining part of the sphere). For very small Q ($Q \ll r_m$), i.e. close to a line on the Debye photograph, the value of I_D' is not very sensitive to the value of r_m and even increasing or decreasing it a few times leads to a relatively small change in I_D.

* Thus as in the calculation of the anisotropy considering the reciprocal lattice points of the second type, the distribution of the intensity, close to the lines corresponding to points of the first type, alters (mainly quantitatively) if the isodiffuse curves have a non-lemniscular form which is determined by the equations (1), (4), and an oval form. Such a form should occur close to certain points of the reciprocal lattice in nucleated solutions in which the atoms introduced occupy assymtrical positions of several kinds, and also in substituted solutions in which the fluctuations of the correlation parameters play the essential role. An analogous kind of logarithmic characteristics close to the lines in the Debye photograph should occur for the distribution of the intensity of diffuse scattering by the thermal vibrations of the lattice.

Here l is the number of the co-ordination sphere, z_1 is the co-ordination number, $|q_1| = \frac{4\pi}{\lambda}\sin\theta$ and

$$\varphi_0(|q_1|) = \frac{1}{4\pi q_1^2}\int_S dS\left(a_q \bar{f}\frac{q_1 l_q}{|q|} - f_A + f_B\right)^2$$

$$\varphi_l(|q_1|) = \frac{1}{4\pi q_1^2}\int_S dS\left(a_q \bar{f}\frac{q_1 e_q}{|q|} - f_A + f_B\right)\cos\vec{a}_{xl}\,q_1, \qquad (11)$$

where $\vec{a}_{xl}$ is the vector of one of the points of the l th co-ordination sphere*. If geometrical distortions are absent then, obviously

$$\varphi_0(|q_1|) = (f_A - f_B)^2;\ \varphi_l(|q_1|) = (f_A - f_B)^2\frac{\sin|q_1|\,|\rho_l|}{|q_1|\,|\rho_l|}$$

and (10) are converted into the usual expression for the background intensity on a Debye photograph of a non-ideal solution. If the distortions are present then $\varphi_0(|q_1|)$, and $\varphi_e(|q_1|)$ apparently cannot be calculated analytically and must be determined for actual crystals by numerical integration over the surface of the sphere. For example, for solutions with a face centred cubic lattice such a calculation can be carried out by determining $a_q e_q$ for each cell of the reciprocal lattice into which falls the end of a vector $q_1/2\pi$ on integrating over the surface of the sphere, according to the equations (28), (29) of [4] (we consider the centres of the cells to be positioned at the scattering points of the reciprocal lattice). While the numerical integration is carried out and the values of the functions $\varphi_0(|q_1|)$, $\varphi_l(|q_1|)$ are found for all q_1, equation (10) permits (if $\varepsilon(\rho)$ are known) one to determine I_D including the calculation of the distortions. In addition this equation enables one to determine, (e.g. by the methods of least squares) according to the values of I_D found experimentally, the correlation parameters for several of the first co-ordination spheres with a correction for the geometrical distortions of the lattice.

In order to examine the characteristics of the background distribution in the neighbourhood of lines on the Debye photograph of a non-ideal solution which correspond to the term in $I\phi$ proportional to q^{-2} we shall use equation (1) for $I\phi$. In the isotropic continuum approximation the integration of the square of the first term in (1) over the sectors of the surface mentioned above which lie close to the ends of the vectors $2\pi K_n$ $(2\pi K_n \gg r_m \gg Q)$, in agreement with (1), (3), and (5), leads to the following expression for I_D':

$$I_D' = \frac{pNkT\bar{f}^2a^2}{4\varphi_{cc}\Delta}\left[1 + \frac{\beta Q^2}{\varphi_{cc}}\ln\frac{(\varphi_{cc}+\beta r_m^2)\,Q^2}{(\varphi_{cc}+\beta Q^2)\,r_m^2}\right] \qquad (12)$$

Enormous interest is presented by the case of solutions the composition and temperature of which are close to the composition $c = c_k$ and the temperature $T = T_k$ corresponding to the critical point on the graph of the solubility. At the most critical point $\phi_{cc} = 0$. Close to it it is possible to assume that $\varphi_{cc} \ll \beta r_m^2$. In this case

$$I_D' = \frac{pNkT\bar{f}^2a^2}{4\varphi_{cc}\Delta}f\left(\sqrt{\frac{\beta}{\varphi_{cc}}}\,Q\right);$$
$$f(x) = 1 + x^2\ln\frac{x^2}{1+x^2} \qquad (13)$$

For very small deviations from the line in the Debye photograph $\beta Q^2 \ll \varphi_{cc}$, $I_D' = pNkT\bar{f}^2a^2/4\varphi_{cc}\Delta$. This equation is correct also if ϕ_{cc} is large and the condition accepted in deducing equation (13) is not fulfilled. In so far as $\varphi_{cc} \ll \beta r_m^2$ $\varphi_{cc} = \frac{kT}{(1-c)\Delta}\frac{1}{a_A}\frac{\partial a_A}{\partial c}$, where a_A is the

---

* For the values of q_1 corresponding to the neighbourhood of a line in the Debye photograph on numerical integration over sectors of the surface of the sphere which lie close to the ends of the vectors $2\pi K_n$, one must take a considerbly smaller step in the integration or employ analytical expressions of the type (7)-(9) (for these sectors $\cos\vec{a}_{xl}\,q_1 \approx 1$).

We notice that the equations (10), (11) are correct only in the case of lattices which are not very strongly distorted when $L \ll 1$ and a_q is not very large, i.e. as follows from the criterion (9) of [3] all the terms thrown out in the conclusion of equation (4) are considerably smaller than the terms retained. In doing this however the first term in brackets in equation (11), generally speaking, is not smaller in comparison with the second particularly if $|f_A - f_B| \ll \bar{f}$.

VOL. 8 1959

activity of the A atoms, the given equation permits I_D' to be calculated according to thermodynamic data. As is seen from this equation on approaching the critical point when $\varphi_{cc} \to 0$, the background intensity close to the lines becomes extremely large. We notice that in this case the integral over the remaining part of the surface of the sphere has a value of the same order as it is far from the critical point and I_D determines the main part of the background intensity connected with the distortions.

For larger angular deviations from the line when $\beta Q^2 \gg \varphi_{cc}$, I_D' is equal to $I_D' = pNkTf^2a^2/8\Delta\beta Q^2$. In so far as according to (9) $Q\,\Delta\theta$, I_D' for this are inversely proportional to the square of the angular deviation from the line. The graph of the function $f(x)$ is drawn in Fig. 1. For comparison a graph of the function $(1 + 2x^2)^{-1}$ is drawn in the same figure; this function coincides with $f(x)$ at $x \gg 1$ and $x = 0$. The difference between the graphs is not great. Thus close to the critical point in the vicinity of each line on the Debye photograph the distribution of the background intensity has the form of a bell shaped curve the position of the maximum of which coincides with the position of the line*. Half the width of the curve (the distance between the points at which the intensity is half that at the maximum) is equal to

$$\delta\theta = \frac{\delta Q}{|q_1|\cot\theta} = 1{,}262\sqrt{\frac{\varphi_{cc}}{\beta}}\,\frac{1}{|q_1|\cot\theta} = \tag{14}$$

$$1{,}262\sqrt{\frac{\varphi_{cc}}{\beta}}\,\frac{\lambda}{4\pi\cos\theta}.$$

and decreases proportionally to $\sqrt{\varphi_{cc}}$ on approaching the critical point. Thus the maximum of the curve rises in proportion to $1/\phi_{cc}$. On increasing the angle of scatter 2θ the half width increases in proportion to $1/\cos\theta$. For the width of the curve which is defined as the ratio of its area to its maximum height we obtain the same equation as (14) in which the numerical coefficient of 1.262 is replaced by 1.047. For a rough estimate of the width of the curve and the maximum value of I_D' we assume, in the case of, $c = c_\kappa$ $\varphi_{cc} \sim \frac{kT_k}{\Delta}\frac{T-T_k}{T_k}$; $\beta \sim \frac{kT_k}{\Delta^{1/3}}$; $q_1 \sim \Delta^{-1/3}$; $\cot\theta \sim 1$. Then $\delta\theta \sim \sqrt{\frac{T-T_k}{T_k}}$, and the value of I_D' at the maximum point of the graph is $\sim \frac{T_k}{|T-T_k|}$ times larger than for ideal solutions. If for example $T_k \sim 1000°K$, $T - T_k \sim 3°K$ then $\delta\theta$ is equal to several degrees and I_D' at the maximum is increased several hundred times.**

In the case of the reflections of the first type reviewed above for which the surface $I\phi = 0$ which passes through a junction in the reciprocal lattice is perpendicular to the vector q_1, including the anisotropy in the calculation does not alter the distribution I_D in the neighbourhood of the line. As before close to the critical point this distribution is described by a bell shaped curve. At $\beta Q^2 \ll \varphi_{cc}$ for the determination of I_D' it is possible to use the equation given earlier if a^{-2}, determined by equation (8), is substituted for a^2 in it. For $\beta Q^2 \gg \varphi_{cc}$ it is necessary to replace a^2 by the quantity $a_1^2 = \int_0^\infty \frac{a^2(x)}{(1+x)^3}\,dx$, where $a^2(x)$ is determined by equation (8). In the particular case of reflections of the type $(h00)$ for cubic crystals to an accuracy up to and including the linear terms with respect to ϵ, this quantity is equal to

* Far from the critical point the oscillations of the background on the Debye photograph are governed chiefly by the correlation parameters in several of the first co-ordination spheres and the maxima of these oscillations do not coincide with the lines. On the contrary the narrow curves for the background distribution close to the critical points, which are observed here, whose maxima coincide with the lines, are governed by the correlations at large distances.

** In order to separate the intensity distribution corresponding to diffuse scattering and lines in the Debye photograph (the maxima of these distributions coincide) it is essential that the width of the lines is small.

VOL 8 195

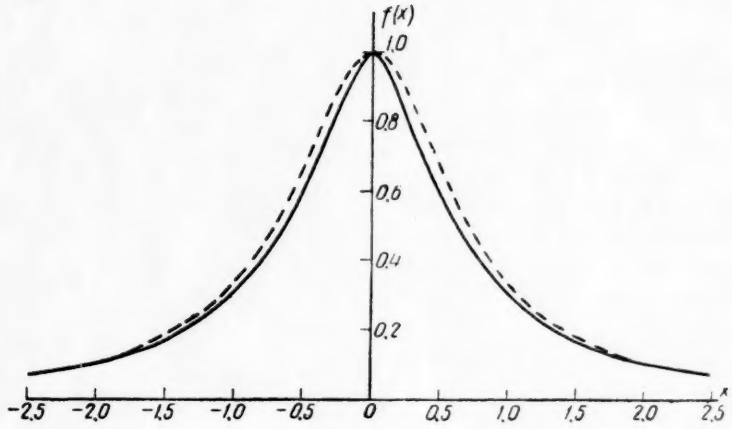

Fig. 1

$$\frac{1}{18}(1+2s)^2\left(1+\frac{7}{24}\varepsilon-\frac{3}{8}s\varepsilon\right)\left(\frac{1}{\Delta}\frac{\partial\Delta}{\partial c}\right)^2.$$

In the case of second order reflections when the surface $I\phi = 0$ passes through a junction and is not perpendicular to the vector $q_1/2\pi$ another picture is obtained for the background distribution. At $\beta Q^2 \ll \varphi_{cc}$ the graph of I_D' against Q does not achieve its maximum value and tends to infinity according to a logarithmic law. Close to the critical point at $\beta r_m^2 \gg \varphi_{cc}$ I_D' is equal to

$$I_D' = \frac{pNkT\bar{f}^2a_0^2}{4\varphi_{cc}\Delta}\ln\frac{\varphi_{cc}}{\beta Q^2}, \qquad (15)$$

where a_0^2 is determined from equation (9). For $\varphi_{cc} \to 0$ I_D' increases even more quickly than for first order reflection (or than in the isotropic continuum approximation). Far from the critical point when $\beta r_m^2 \ll \varphi_{cc}$, I_D' is equal to

$$I_D = \frac{pNkT\bar{f}^2a_0^2}{2\varphi_{cc}\Delta}\ln\frac{r_m}{|Q|}. \qquad (16)$$

This expression differs from (9) only in the substitution of the factor $c(1-c)$ by $kT/\varphi_{cc}\Delta$. At $\beta Q^2 \gg \varphi_{cc}$ it is defined by the same equation as in the case of first reflextions in which it is necessary however to replace a^2 by a_1^2.

Earlier an addition to the expression for I_D was considered which corresponded to the square of the first term in the brackets of equation (1). If the distortions are small then it can be expected that close to the critical point a noticeable addition to the expression for I_D near the line gives an integral from the doubled product of the terms lying within the brackets of equation (1). In the isotropic continuum approximation integrating over those parts of the sphere's surface lying close to the ends of the vectors $2\pi K_n$ ($Q \ll r_m$), we find that the corresponding term I_D' in the vicinity of the critical point ($\varphi_{cc} \ll \beta r_m^2$) is equal to

$$I_D'' = -\frac{pNkT\bar{f}(f_A - f_B)aQ}{4|q_1|\varphi_{cc}\Delta}\ln\frac{\varphi_{cc}+\beta Q^2}{\beta Q^2}. \qquad (17)$$

Comparing (17) with (12) it is not difficult to convince oneself that $|I_D''|$ is $\frac{\bar{f}|q_1|a}{|f_A - f_B|Q}$ times smaller than I_D' and in so far as $|Q|/|q_1| \ll 1$, these quantities can be compared only for small a (almost the same atomic radii). Depending on the signs of $f_A - f_B$, a and Q, I_D'' can be both positive and negative. Along both sides of the line the sign of I_D'' is different.

A similar quantity of the same order is obtained for I_D'' when anisotropy is taken into account in the case of first order reflections. For second order reflections at $\beta Q^2 \gg \varphi_{cc}$

$$I_D'' = -\frac{\pi p N k T \bar{f} (f_A - f_B)\, a'(\infty)}{4 |q_1| \sqrt{\beta \varphi_{cc}}\, \Delta}, \qquad (18)$$

where

$$a'\left(\frac{r^2}{Q^2}\right) = \frac{1}{2\pi |q_1|} \int_0^{2\pi} a_q (q_1 e_q)\, d\varphi.$$

Thus I_D'' has a value of the same order as in the isotropic continuum approximation. For $\beta Q^2 \ll \varphi_{cc} \ll \beta r_m^2$

$$I_D'' = -\frac{\pi p N k T \bar{f} (f_A - f_B)\, a'(\infty)}{4 |q_1| \sqrt{\beta \varphi_{cc}}\, \Delta}. \qquad (19)$$

The ratio of the expression (19) for I_D'' and (15) for I_D' is of the order

$$\frac{f_A - f_B}{af} \sqrt{\frac{\varphi_{cc}}{\beta q_1^2}} \Big/ \ln \frac{\varphi_{cc}}{\beta Q^2}$$ and for example for $af \sim \frac{1}{10}(f_A - f_B)$ can be equal to unity.

In an analogous way it is possible to carry out a study of the characteristics of the background distribution on a Debye photograph close to the point of a second order phase transition.*

3. THE DISTRIBUTION OF THE BACKGROUND INTENSITY IN A LAUE PHOTOGRAPH

In research on the scattering of x-rays by the Laue method they use a non-monochromatic ("white") parallel beam incident on a stationary crystal. By $I_0(|k|)$ we shall denote the density of the intensity distribution of the incident radiation according to the value of the wave vector. Then the intensity of the scattered radiation in the Laue photograph is determined by the equation $I_s = A \int I_0(|k|)\, I_{\phi}\, d|k|$, where the constant A determines the intensity of the radiation scattered by one electron (under the same conditions) for unit integral intensity of the incident radiation.

A spot on the Laue photograph corresponds to values k_{20} and k_{10} of the wave vectors of the scattered and incident waves. We shall consider the wave vectors k_2 and k_1 of the scattered and incident waves corresponding to some neighbour of the marked spot ($k_1 \| k_{10}$ but k_2 is not parallel to k_{20} and $|k_2| = |k_1| \neq |k_{20}| = |k_{10}|$). By $\vec{m}$ we shall denote the difference between the unit vectors parallel to k_2 and k_{20}. It is obvious that in the second approximation $\vec{m} \perp \vec{k}_{20}$. The vector $\vec{m}$ indicates the direction of the emission of the observed scattered ray. Further by k_0 we shall denote the modulus of the wave vectors which correspond to a spot and by $\Delta k = |k| - k_0$ the difference between the modulus of the wave vector k of the scattered wave and k_0. Since to an accuracy including terms of second order smallness

---

* If the geometrical distortions are neglected then, in this case, in the neighbourhood of the lines on the Debye photograph I_D has a particular logarithmic value [6] which is difficult to find experimentally. Taking the distortions into account leads to the appearance of an additional term, proportional to q^{-2}, in the expression for $I\phi$.

In a number of cases, for example, in the control of the substitution alloys, the coefficient for this term is small and taking the distortions into account hardly alters the intensity distribution. However in crystals which do not possess central symmetry in which both below and above the transition point, a wave of the fluctuations of the remote order parameters cause a wave of displacements proportional to it (e.g. in the case of seignette's salt or KH2PO4) and also in crystals in a less symmetric phase close to the critical point in which a graph of the second order phase changes, is transformed into a graph of first order phase changes (e.g. in crystals of the

contd.

type BaTiO3), as is shown in [7] the coefficient at q^{-2} on approaching the transition point tends to infinity.

This coefficient also tends to infinity in ordered substitution alloys which are close to the critical point, in which the graph of the second order phase changes, is transformed into the solubility curve [3]. In these cases an anomalously large diffusion scatter should be observed close to the lines on the Debye photograph, and the qualitative distribution of the background intensity should be the same as in the case of the solutions considered earlier close to the critical point on the solubility curve.

VOL 8 195

$k_2 = k_{20} + k_0 \vec{m} + \Delta k \frac{k_{20}}{k_0}$, $k_1 = k_{10} + \Delta k \frac{k_{10}}{k_0}$ and $k_{20} - k_{10} = 2\pi K_n \approx q_1$, the vector $q = k_2 - k_1 - 2\pi K_n$ is approximately equal to

$$q = k_0 \vec{m} + \frac{\Delta k}{k_0} q_1. \qquad (20)$$

The fundamental part of I_1 close to the spot gives the square of the first term in the brackets of equation (1). Firstly we shall consider this part of the background

$$I_1' = A \frac{NkTf^2}{\Delta} \int I_0(|k|) \frac{a_q^2 (q_1 e_q)^2}{q^2 (\varphi_{cc} + \beta q)^2} d|k| \qquad (21)$$

far from the critical point when it is possible to neglect βq^2 side by side with φ_{cc}. In the isotropic continuum approximation substituting (3) and (20) in (21) and carrying out the integration we obtain:

$$I_1' = \frac{B}{\varphi_{cc}} \frac{q_1^2}{\sqrt{q_1^2 m^2 - (q_1 m)^2}} = \frac{B}{\varphi_{cc}} \frac{|q_1|}{m \sin\psi} =$$

$$= \frac{B}{\varphi_{cc}} \frac{|q_1|}{m'} = \frac{B}{\varphi_{cc}} \frac{|q_1|}{\sqrt{m_\perp^2 + \left(\frac{q_1}{|q_1|} \frac{k_{20}}{k_0}\right)^2 m^2}},$$

$$B = A I_0(k_0) \frac{\vec{\pi} NkTf^2 a^2}{2\Delta}. \qquad (22)$$

Here γ is the angle between $\vec{m}$ and q_1; $m' = m \sin\psi$ is the projection of the vector $\vec{m}$ on the plane perpendicular to the vector q_1; $m_\perp$ is the projection of $\vec{m}$ on the plane going along the vectors k_1, k_2 and q_1, $m_\perp$ is the component of $\vec{m}$ in the direction perpendicular to this plane (obviously $m_\parallel$ and $m_\perp$ are the angular deviations of the scattered ray from the direction corresponding to the spot in the plane k_1, k_2 and perpendicular to this plane respectively).

From (22) it is seen that on approaching a spot on a Laue photograph the background intensity tends to infinity as $1/m$ and the value of m is proportional to the distance from the spot. For a given m $I' \sim |q_1| = \frac{4\pi}{\lambda} \sin\theta$, i.e. I_1' grows on increasing the angle of scatter and reducing the wavelength. The intensity distribution I_1' in the plane perpendicular to the direction of the scattered beam k_2 is characteristic of isodiffuse curves which in agreement with the last equation (22) have the form of an ellipse for I_1'. One of the main axes of the ellipse (the longer axis) lies perpendicular to the plane crossing the vectors k_1 and k_2 and the other axis lies in this plane. The eccentricity of the ellipse is equal to $\cos\theta$, i.e. the isodiffuse curves are close to a circle for scattering angles close to 180° and for small θ these curves are strongly elongated ellipses.

The double product of the terms in the brackets of equation (1) after integration give a term in I_1' of the order

$$\frac{f_A - f_B}{af} \frac{k_0^2}{q_1^2} \frac{\delta k}{k_0} m^2 I_1',$$

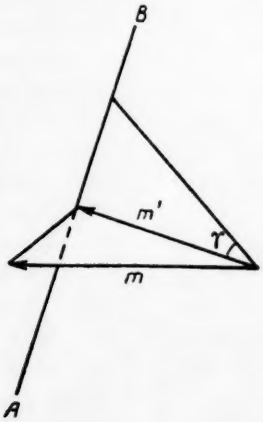

where δk is the region of the values of the wave vector moduli for which $I(k)$ is large. As the scattering of "white" radiation is being considered $\delta k \sim k_0 \sim |q_1|$ and since $m \ll 1$ the term considered is much smaller than I_1'. It is obvious that the square of the second term in the brackets of equation (1) also gives a uniform background without any peculiarities close to the spots. Therefore close to the spots the main part of the background intensity is made up from I_1.

Taking the anisotropy into account little alters the qualitative picture of the distribution of the background intensity close to the spot. As it is easy to see from the equations (20), (21) that taking the anisotropy into account leads to the replacement in (22) of a^2 by a_1^2, where

$$\overline{a_1^2} = \frac{2}{\pi} \int_{-\pi/2}^{\pi/2} \overline{a_q^2} \left(e_q \frac{q_1}{|q_1|} \right) d\gamma. \qquad (23)$$

Here γ is the angle between the vector $\vec{m}$ which is a projection of the vector $\vec{m}$ on the plane perpendicular to the vector q_1 and a line dropped from the beginning of the vector $\vec{m}$ to some point on the straight line AB parallel to q_1 and passing through the end of this vector (Fig. 2). The values of a_q and e_q included in equation (23) correspond to the vector

$$\vec{n} = q/|q| = \frac{\vec{m'}}{m} \cos\theta + \frac{q_1}{|q_1|} \sin\theta.$$

In the case of ideal solutions (high temperatures) $\phi_{cc'}$ which, in agreement with (22) determines the temperature dependence of I_1' is equal to $\frac{kT}{c(1-c)\Delta}$. On reducing the temperature in the case of self ordered alloys ϕ_{cc} increases and I_1' decreases. In the case of soluble alloys ϕ_{cc} decreases on reducing the temperature and I_1' increases. An especially large increase in I_1' should be observed about the critical point on approaching which $\varphi_{cc} \to 0$. In this case in (21) it is not possible to neglect $\beta q^2 a$ side by side with ϕ_{cc}. Proceeding with the calculation of I_1' according to the equations (21), (3) taking into account the term in the isotropic continuum approximation, we obtain

$$I_1' = B \frac{|q_1|}{m'} \frac{1}{\left(\sqrt{\varphi_{cc} + \beta k_0^2 m'^2} + \sqrt{\beta} k_0 m' \right)^2} \qquad (24)$$

(the value of m' in agreement with (22) can be replaced by

$$\sqrt{m_\perp^2 = m_1^2 \left(\frac{q_1}{|q_1|} \frac{k_{20}}{k_0} \right)^2}$$

For very small m' when $\beta k_0^2 m'^2 \ll \varphi_{cc}$, equation (24) is tranformed into (22). In this region of the values of m', I_1' as before is inversely proportional to m' but the coefficient of proportionality close to the critical point is very large and I_1' on approaching this point increases sharply. Close to the critical point for comparatively small m' the opposite inequality $\beta k_0^2 m'^2 \gg \varphi_{cc}$ starts to be fulfilled. In this region $I_1^1 \cong B|q_1|/\beta k_0^2 m'^3$ i.e. I_1' is inversely proportional to the cube of m'. The value of $m' = m_0'$ at which $\beta k_0^2 m'^2 \sim \varphi_{cc}$ and the transition from the law $I_1' \sim m'^{-2}$ to the law $I_1' \sim m'^{-3}$, is proportional to $\sqrt{\varphi_{cc}}$, inversely proportional to k_0 and decreases on approaching the critical point and on reducing the wavelength. The form of the isodiffuse curves close to the critical point is the same as far away from it.

Analogous effects to the radpid growth of I_1 should also be observed close to points of the second order phase change in the above mentioned cases when the lattice distortions are substantial (when they increase anomalously on approaching the transition point). If the distortions can be neglected then the characteristics of I_1 are shown more weakly so that at the transition point itself I_1' is proportional to $1/m'$ [6] and not to $1/m'^3$ as at the critical point in the solubility curve (equation (24)) or at the point of the second order phase transition in the above mentioned cases when the distortions were substantial.

The equations obtained determine the intensity distribution depending on the direction of the scattered ray and enable us with the aid of purely geometrical constructions to determine the intensity distribution in a Laue photograph taken under different possible conditions.

VOL. 8 1959

4. THE DETERMINATION OF THE BACKGROUND INTENSITY IN AN X-RAY PHOTOGRAPH WHEN MONOCHROMATIC RADIATION IS SCATTERED BY A SINGLE CRYSTAL

Now we shall consider the scattering of monochromatic radiation by a single crystal the position of which is slightly displaced in relation to the position which gives correct Bragg reflection. Since scatter by a stationary crystal is being considered in this case correct reflection is absent. However as it is easy to see applying Ewald's construction to the intensity distribution determined by equation (1) (c.f. [8], chap.5) close to a point on the x-ray photograph corresponding to Bragg reflection (which would be obtained if the photograph was taken with a rotating crystal) intense maxima of the diffuse scattering should be observed. In this paragraph the intensity distribution close to these maxima will be studied.

By K_{no} we shall denote the vector being examined in the reciprocal lattice at a position in the single crystal which corresponds to Bragg reflection. By K_n we shall denote the vector at the displaced position in the crystal. Then $K_n - K_{no} = |K_n|\vec{\psi}$, where $\vec{\psi}$, which represents the angular inclination of the crystal, is equal to the difference between the unit vectors parallel to K_n and K_{no} and to a first approximation is perpendicular to K_{no}. If the axis of rotation is perpendicular to K_{no} then the modulus of the vector $\vec{\psi}$ is equal to the angle of rotation ϕ. If also the axis of rotation makes an angle with K_{no} then obviously $\psi = \phi \sin\beta$. Further we shall denote by k_{20} the wave vector of the scattered wave which corresponds to Bragg reflection (in an undistorted crystal) and by k_2 – the wave vector of the diffusely scattered wave being considered ($|k_{20}| = |k_2| = k_0$). We shall represent the angular inclination of the scattered beam to the direction of k_{20} by the vector $\vec{m}$ which is equal to the difference between the unit k_2/k_0 and k_{20}/k_0. Then $k_2 = k_{20} + k_0\vec{m}$. Noticing that $k_{20} - k_1 - 2\pi K_{no} = 0$, we find that the vector $q = k_2 - k_1 - 2\pi K_n$ is equal to

$$q = k_0\vec{m} - 2\pi|K_n|\vec{\psi}. \qquad (25)$$

First of all we shall consider the case of small ψ when the region of the maximum intensity the chief role is played by the square of the first term in the brackets of equation (1). In the isotropic continuum approximation, substituting in (1) the expression (25) for q (in doing this $2\pi K_n$ can be replaced approximately by q_1) and expression (3) for a_q and e_q, we obtain

$$I' = \frac{N}{\Delta}\frac{kTa^2\bar{f}^2}{\varphi_{cc} + \beta\left(k_0^2m^2 + q_1^2\psi^2 - 2k_0|q_1|\vec{m}\vec{\psi}\right)}, \qquad (26)$$

$$\frac{k_0^2(\vec{m}q_1)^2}{\left(k_0^2m^2 + q_1^2\psi^2 - 2k_0|q_1|\vec{m}\vec{\psi}\right)^2}.$$

We shall resolve $\vec{m}$ into the component $\vec{m}_1$ lying in the plane passing through q_1 and $\vec{\psi}$, and the component $\vec{m}_2$ normal to this plane. We shall denote the angle between $\vec{m}_1$ and q_1 by α. In the case of reflections for which the vectors k_1, k_{20}, q_1 and $\vec{\psi}$ lie in one plane the angle α is equal to $\bar{\bar{\theta}}$ (Fig.3). In the general case as is seen from Fig.3, α and $\bar{\bar{\theta}}$ are connected by the relation $\tan\alpha = \frac{\tan\theta}{\cos\Gamma}$, where Γ is the angle between the planes passing along the vectors q_1, $\vec{\psi}$ and the vectors k_1, k_{20}.

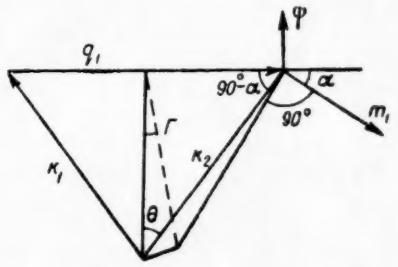

Fig.3

If one excludes the region near the critical point then for small rotations of the crystal in the region of the maximum intensity it is possible to neglect the term standing together with ϕ_{cc} in the denominator of equation (26). Paying attention to the fact that

$$\vec{m}q_1 = m_1|q_1|\cos\alpha; \quad \vec{m}\vec{\psi} = m_1\psi\sin\alpha;$$

$$|q_1| = 2k_0 \sin\theta \text{ и } m^2 = m_1^2 + m_2^2,$$

we shall rewrite equation (26) in the form:

$$I = \frac{C}{\varphi_{cc}} f(m_1, m_2); \quad C = \frac{NkTa^2\bar{f}^2}{\Delta};$$

$$f(m_1, m_2) = \frac{4m_1^2 \sin^2\theta \cos^2\alpha}{\left(m_1^2 + m_2^2 - 4m_1\psi \sin\theta \sin\alpha + 4\psi^2 \sin^2\theta\right)^2}.$$

The dependence of the diffuse scattering in the x-ray photograph on the angular inclinations of m_1 and m_2 for the angle of rotation of the crystal α and the reflection which are being considered (giving the values of θ and ϕ) is determined by the function $f(m_1, m_2)$. For a given m_2 this function takes maximum values at the points $m_1 = \pm\sqrt{m_2^2 + 4\psi^2 \sin^2\theta}$, which are symmetrically placed with respect to the axis m_2. These quantities are euqal to

$$f_{max}(m_2) = \frac{\sin^2\theta \cos^2\alpha}{\left(\sqrt{m_2^2 + 4\psi^2 \sin^2\theta} \mp 2\psi \sin\theta \sin\alpha\right)^2}.$$

Between the maximum values the function $f(m_1, m_2)$ at $m_1 = 0$ takes a minimum value equal to zero*. If $f(m_1, m_2)$ is considered as a function of both variables m_1 and m_2 then it has its maximum values

$$f_{max} = \frac{\cos^2\alpha}{4\psi^2 (1 \mp \sin\alpha)^2}$$ at the points

$m_1 = \pm 2\psi \sin\theta$. Thus the maximum value of the background intensity is inversely proportional to the square of the angular inclination of the crystal to the position giving Bragg reflection. The widths of the spots which form a double spot corresponding to diffuse scattering, as well as the distance between their maxima, are proportional to the angular inclination. The most intense background should be observed with the crystal in the position which gives Bragg reflection ($\psi = 0$), when $f(m_1, m_2) = 4\frac{m_1^2}{m^4}\sin^2\theta\cos^2\alpha$ and the intensity tends to infinity on approaching the point on the x-ray photograph at which a spot which corresponds to Bragg reflection is observed.

Considering the second derivative of $f(m_1, m_2)$ with respect to m_1 it is easily seen the graph of I' against m_1 has a very sharp peak close to the maximum where f_{max} is larger. The larger value of the maximum corresponds to the angular inclinations of m_1 pointing in the same way as the vector $\vec{\psi}$, which determines the direction of rotation of the crystal. The maximum value of the intensity is particularly large if the angle of scatter is close to 180° and the angles θ and α close to 90°. For small α the assymetry of the curves $f(m_1, m_2)$ for given m_2 is expressed more weakly and the distance between the maxima decreases. For illustration in Fig. 4 are drawn graphs of functions $f(m_1, m_2)$ at $m_2 = 0$, $m_2 = \frac{\sqrt{2}}{2}\psi$ and $m_2 = \psi$ for $\alpha = \theta = 45°.°$. (27)

We notice that the picture obtained on the intensity distribution in the "extra-spot" differs from the intensity distribution in the "extra-spot" created by the thermal vibrations of the lattice.

Taking into account the double product of the terms standing in the brackets and the square of the second term in (1) leads to the replacement of expression (27) in the isotropic continuum approximation by the expression

$$I = \frac{C}{\varphi_{cc}}\left(\sqrt{f(m_1 m_2)}\frac{\cos\alpha}{|\cos\alpha|} - \frac{f_A - f_B}{af}\right)^2. \quad (28)$$

The second term in the brackets of this equation is significant only at large ψ (or at large $\frac{f_A - f_B}{a\bar{f}}$). In so far as $\cos\alpha$ changes sign on changing the direction of m_1 this term increases one of the maxima of the intensity and decreases the other (exactly which maximum is increased depends on the signs of $f_A - f_B$ and α). The position of

* On account of the small terms, thrown out of the numerator of equation (26), which are proportional to $m\psi^2$ and ψ^4, at $m_1 = 0$ $f(m_1, m_2)$ takes a value other than zero, but a small (of the same order as far from the spot) one.

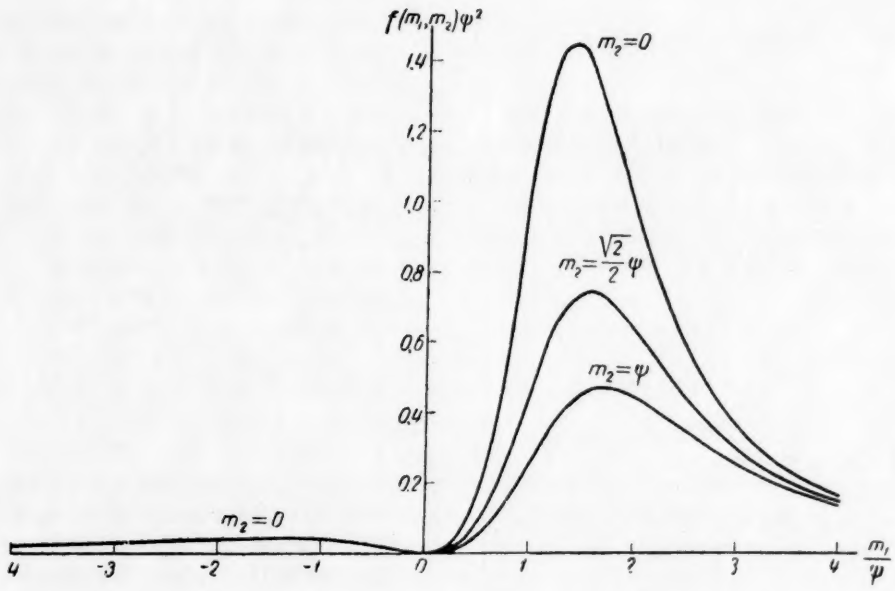

Fig. 4

the maximum and the general view of the function $I(m_1, m_2)$ which is determined by equation (28) are the same as for the function $f(m_1, m_2)$.

If the anisotropy of the crystal is substantial and the isotropic continuum approximation is not applicable then a general study of the intensity distribution in the "extra-spots" cannot be carried out. For actual crystals this distribution is not difficult to find by substituting in (1) the expression (25) for q and determining a_q and e_q corresponding to these values of q by equation (2) or by analogous equations from [3,4] for cubic crystals. Also taking the anisotropy into account can noticeably change the character of the intensity distribution. A particularly obvious difference from (28) should occur in the cases (not considered here of nucleation alloys in which the foreign atoms occupy nonsymmetrical positions between lattice points of various types, if the fluctuations of the correlation parameters play a substantial role in the alloys and in the case of strongly distorted lattices (e.g. ageing alloys in the first stages of ageing). In these cases the isodiffuse surfaces in the space of the reciprocal lattice have a non-lemniscate and oval form and the qualitative intensity distribution connected with vibrations than to the picture considered above.

As in the cases considered in the previous sections on approaching the critical point $\varphi_{cc} \to 0$, the intensity of the spot, with respect to the diffuse scattering, increases rapidly. Thus for small angular deviations of the crystal from the position giving Bragg reflection and small deflections m of the scattered beam from the direction corresponding to Bragg reflection, when the conditions $\beta q_1^2 \psi^2 \ll \varphi_{cc}$, $\beta k_0^2 m^2 \ll \varphi_{cc}$, it is possible as before to use equation (27) for I' (but in this equation close to the critical point ϕ_{cc} is very small and at $f(m_1, m_2)$ the coefficient is very large). If these angular deviations are not small and the opposite $\beta q_1^2 \psi^2 \gg \varphi_{cc}$ or $\beta k_0^2 m^2 \gg \varphi_{cc}$), then in the denominator of equation (26) ϕ_{cc} can be neglected. In this case

$$I'(m_1, m_2) = \frac{C}{\beta k_0^2} \frac{4m_1^2 \sin^2\theta \cos^2\alpha}{\left(m_1^2 + m_2^2 - 4m_1\psi \sin\theta \sin\alpha + 4\psi^2 \sin^2\theta\right)^3}. \quad (29)$$

For a given m_2 this function takes maximum values at the points

$$m_1 = \frac{1}{2}\psi \sin\theta \sin\alpha + \quad (30)$$

$$\frac{1}{2}\sqrt{2m_2^2+8\psi^2\sin^2\theta+\psi^2\sin^2\theta\sin^2\alpha}. \quad (30)$$ *contd.*

As is seen from (30) both maxima are displaced in proportion to ψ and the distance between the maxima is almost $\sqrt{2}$ times smaller than at a distance from the critical point. The values of the function I' at the maximum points is equal to

$$I'_{max}(m_2)=\frac{64C}{27\beta k_0^2}\frac{\left(\psi\sin\theta\sin\alpha\pm\right.}{\left(-3\psi\sin 0\sin\alpha\pm\right.}\cdots\rightarrow$$

$$\rightarrow\cdots\frac{\left.\pm\sqrt{2m_2^2+8\psi^2\sin^2\theta+\psi^2\sin^2\theta\sin^2\alpha}\right)^{-1}\sin^2 0\cos^2\alpha}{\left.\pm\sqrt{2m_2^2+8\psi^2\sin^2\theta+\psi^2\sin^2\theta\sin^2\alpha}\right)^3} \quad (31)$$

$I'(m_1, m_2)$ takes the maximum values

$$I'_{max}=\frac{64C}{27\beta k_0^2}$$

$$\frac{\cos^2\alpha}{\left(-3\sin\alpha\pm\sqrt{8+\sin^2\alpha}\right)^3\left(\sin\alpha\pm\sqrt{8+\sin^2\alpha}\right)\sin^2\theta}\frac{1}{\psi^4} \quad (32)$$

at the points

$$m_1=\frac{1}{2}\psi\sin\theta\left(\sin\alpha\pm\sqrt{8+\sin^2\alpha}\right);\ m_2=0.$$

As is seen from (32) these values are inversely proportional not to ψ^2, as they are at a distance from the critical point, but to ψ^4, I'_{max} for a given ψ increases abruptly as $\theta\to 0$ and particularly as $0\alpha\to\frac{\pi}{2}$.

The equations obtained determine the intensity of scattered radiation depending on the angular deviations of the scattered beam and the crystal from the directions corresponding to Bragg reflection. With the aid of geometrical constructions it is simple to proceed from these equations to the determination of the intensity distribution in an x-ray photograph taken under various conditions. It is particularly simple to carry out the construction for the case when the rotation of the crystal is carried out around the axis perpendicular to the plane passing along the vectors k_1, k_{20} and k_n (the spot on the equatorial plane of the film). In this case the vector $\vec{\psi}$ lies in the plane mentioned, ψ is equal to the angle of rotation, m_1 also lies in this plane, m_2 is normal to it and the angle α is equal to half the scattering angle θ.

In experimental research both characteristics and "white" radiation are frequently used. In this case when taking the photograph from a single crystal one should observe the correct Bragg Laue reflections, the "extra-spots" which correspond to the diffuse scattering of the characteristic radiation, and (usually more weakly) the background maxima corresponding to the diffuse scatter of "white" radiation.

In conclusion as an illustration of the effect of anisotropy on the form of the isodiffuse scattering surfaces in the space of the reciprocal lattice we have drawn (for the case when $f_A - f_B$) the isodiffuse curves in the plane (001) close to the

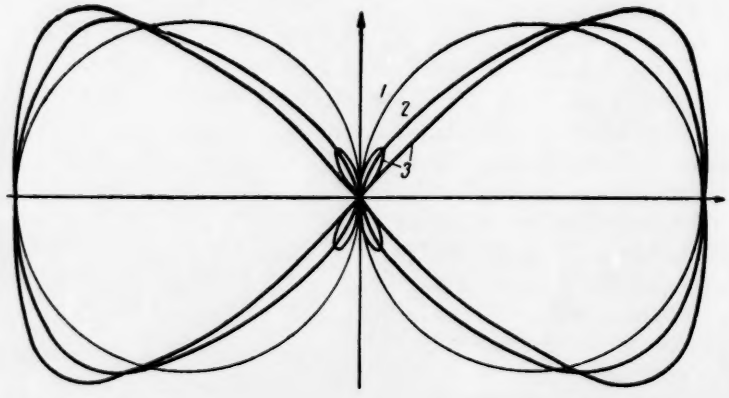

Fig. 5

VOL 8 195

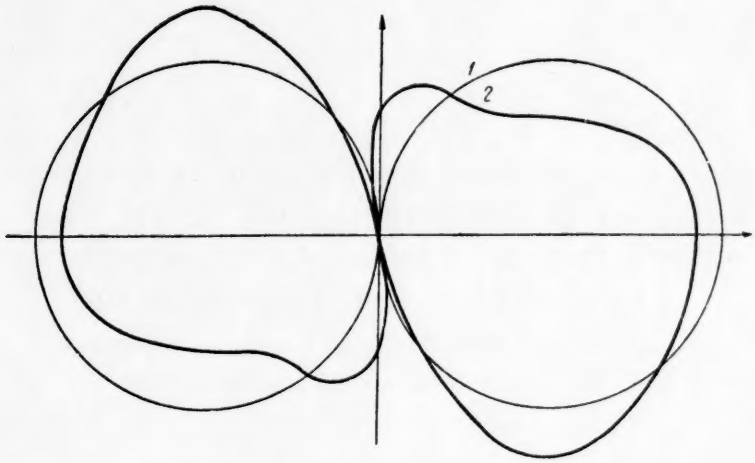

Fig. 6

scatter point ($h00$) (Fig. 5) and the point ($2h,h,0$) (Fig. 6) for a cubic crystal where the values of the constant are $\epsilon = 0$ (graph 1), $\epsilon = -1$ (graph 2) and $\epsilon = -1.5$ (graph 3 in Fig. 5). The graphs are drawn in arbitrary units.

We note also that it would be interesting to carry out a detailed experimental study of the characteristics of the background distribution, which have been considered, in particular, close to the critical point and the points of the second order phase transition both with the help of photographic and, especially, with the help of ionization methods.

Translated by J.H. Dempster

REFERENCES

1. B.E. Warren, B.L. Averbach and B.W. Roberts, *J. Appl. Phys.* 22, 1493, (1954).
2. K. Huang, *Proc. Roy. Soc.*, 190, 102, (1947).
3. M.A. Krivoglaz, *Zh. eksp. teor. fiz.*, 34, 204, (1958).
4. M.A. Krivoglaz and Ye.A. Tikhonova, Ukr. Fizichn. zhurn., 3, 297, (1958).
5. M.A. Krivoglaz, *Problems of the Physics of metals and metallurgy (Problemy fiziki metallov i metallovedniia), Akad. Nauk. Ukr. S.S.R.*, No.8, p. 199, (1957).
6. L.D. Landau, *Zh. eksp. teor. fiz.*, 7, 1232, (1937).
7. M.A. Krivoglaz, *Zh. eksp. teor. fiz.*, 34, 405, (1958).
8. R.W. James,, *The optical principles of x-ray diffraction, (Opticheskiie printsipy difraktsii rentgenovykh luchei)* 1950.
9. M. Born, *Rep. Ptog. Phys.*, 9, 294, (1942-1943).

VOL. 8 1959

THE INFLUENCE OF THERMOMECHANICAL TREATMENT, IN WHICH THE STRESSES ARE CREATED BY TWISTING THE SAMPLE, ON THE MAGNETIC PROPERTIES OF THE ALLOY VICALLOY*

M.G. IUZHINSKAIA, Ia.S. SHUR and N.N. IAGOVKINA

Institute of metal physics Akad. Nauk. SSSR

(Received 23 March 1959)

The elastic stresses which are created by twisting are applied to a sample of the alloy vicalloy during heat treatment as a result of which this alloy acquires a high coercive force. Such thermomechanical treatment at definite torsional angles leads to the growth of the coercive force linked with a rise in the total magnetic anisotropy and also to a decrease in the residual induction caused by a reduction in the degree of perfection of the longitudinal magnetic texture.

VOL
8
195

1. Earlier we showed [1, 2] that thermomechanical treatment has a substantial effect on the magnetic properties of certain highly coercive alloys: alloys of the Fe-Co-V system (the vicalloy type) and an alloy of Fe with 15% Mn. The high coercive force in these alloys is obtained after normalizing at temperatures of about 500-600°. The thermomechanical treatment consists of applying a tensile stress to samples in the form of wires during the normalizing period mentioned. Such treatment under certain conditions leads to an increase, in the direction of the extension, of the coercive force H_c, the residual induction B_r and the maximum magnetic energy $(BH)_{max}$.

On the grounds of a study of the effect of the different types of thermomechanical treatment on the magnetic and several other characteristics of the alloys a conclusion was drawn that the increase of B_r which can be obtained as a result of thermomechanical treatment is governed by the increase in the order of the magnetic texture along the sample's axis. An increase in H_c is connected chiefly with a growth in the total magnetic anisotropy of the structural formations, which are isolated magnetic domains, however it is suggested that the increase in the order of the longitudinal texture also leads to a certain increase in H_c.

In the experiments carried out earlier on thermomechanical treatment, it was not possible to estimate immediately which role each of the factors mentioned played in the increase of H_c. One of the methods of separating the effects of the changes in the texture and the increase in the anisotropy of the single domain formations is to study the influence of thermomechanical treatment, by which stresses of another type are created, other than those which arise with the stresses used before. With this aim we have studied the effect of twisting the samples, during heat treatment, on their magnetic properties.

On twisting a wire, stresses are produced in it which tend to turn the vector of self magnetization to an angle of 45° to the axis of the sample. Such stresses as those which arise on extension will increase the anisotropy of the single domain formations. However on twisting as distinct from extension, the direction of the additional anisotropy will not coincide with the axis of the sample.

*Fiz. metal. metalloved. 8, No. 4, 531-534, 1959.

Therefore in the case when the sample after the usual treatment has a clearly expressed longitudinal texture (as happens for samples of the observed alloys in the form of wires), twisting should cause the destruction of this structure.

A comparison of the effects of extending and twisting we carried out in a paper on the study of the effects of elastic extensions at room temperature on the magnetic properties of the alloy, vicalloy, which enabled the mechanism of this effect to be explained [3].

2. In the present paper the results are given of research on the influence of thermomechanical treatment, in which the stresses are created by twisting, on the magnetic properties of the alloy, vicalloy, containing 12% V, 52% Co, and the rest Fe.

As is known the high coercive state of this alloy is achieved as a result of normalizing previously deformed samples at a temperature of about 600 . During this normalizing process the precipitation of a finely dispersed non-ferromagnetic γ-phase in the ferromagnetic α-phase occurs.

The samples are wires 0.6 mm in diameter extended with a relative extension of 89%. The length of the samples is about 100 mm. In the heat treatment one of the ends of the sample which is being twisted, is held still, the other end is attached firmly to the axis of the block on which is wound a thread from which hangs a weight. The size of the weight is chosen to be such that it keeps the sample twisted at the given angle. Thus the twisted sample is normalized at a constant torsional moment. Close to the twisted sample is fastened a control sample which is not subjected to the stresses. Over the samples is moved an oven heated to the required temperature. The magnetic properties of the samples (the graphs of the magnetization and the hysteresis loops) are measured by a ballistic method.

3. In Fig. 1 the quantities H_c, $4\pi I_r(B_r)$ and $4\pi I_s'$ (where I_s' is the magnetization in a field of 2000 oersteds, close to the value of the saturation magnetization I_s) are given for samples with a diameter of 0.6 mm normalized at one and the same temperature 600° for 30 minutes but with different angles of twist α from 0 to 1.5 degrees per millimetre length of sample.

From Fig. 1 it is seen that on increasing the angle of twist, H_c of the samples at first increases, reaches a maximum, and then becomes smaller than for the sample which was not twisted. The value of B_r on increasing α only decreases. The value of $4\pi I_s'$ at small angles α remains the same as for the untwisted sample, at large angles $4\pi I_s'$ decreases.

Analogous results were obtained at normalizing temperatures of 500, 550 and 620°. In doing this it was established that on increasing the normalizing temperature the maximum H_c and the beginning of the rapid drop of $4\pi I_s'$ started at smaller α than it did for lower normalizing temperatures. At lower temperatures it is possible to obtain a relatively larger increase in H_c than at high ones. For all normalizing temperatures the value of B_r only decreases on increasing α. As a result of the reduction in B_r on twisting samples during heat treatment it is not possible to obtain an increase in $(BH)_{max}$ in comparison with the $(BH)_{max}$ for samples normalized in the optimum regime without the application of stresses.

In Fig. 2, for comparison, have been shown the extension σ during the heat treatment of samples of vicalloy of the same composition with a diameter of 1 mm, normalized at 575° for 20 minutes.* As is seen from Fig. 2 for small σ the quantity $4\pi I_s'$ remains unchanged, on increasing σ further the quantity $4\pi I_s'$ decreases. The value of H_c on increasing σ at first rises and then falls. $4\pi I_r$ on increasing σ at first rises somewhat and then, for all σ which cause a reduction in I_s', falls.

From a comparison of the laws obtained concerning the effect of twisting and extension in the heat treatment of the alloy vicalloy it follows that both types of stresses with heat treatment have a qualitatively analogous effect on such magnetic characteristics as H_c and I_s. The effect of extension and twisting on B_r is different. As a result of the extension an increase in B_r can be obtained; only under the influence of very large extending loads, as the result of a sharp reduction in I_s is a reduction in B_r observed. Under the influence of twisting B_r only decreases. This reduction is observed even for those at which I_s remains unchanged.

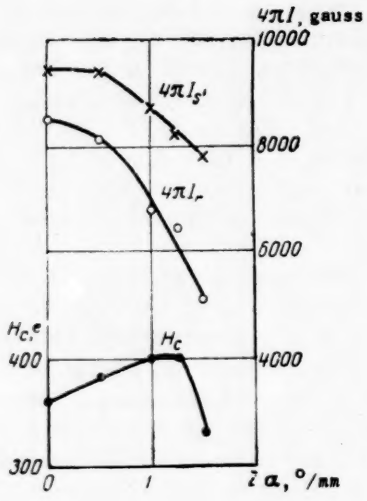

Fig. 1. The dependence of the magnetic properties on the size of the angle to which the samples were twisted during their heat treatment.

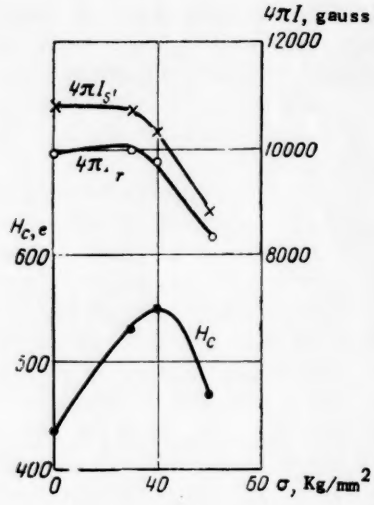

Fig. 2. The dependence of the magnetic properties on the size of the load extending the samples during the heat treatment.

4. One explanation can be given for the laws obtained concerning the effect of the stresses in the heat treatment (both the extension and the twisting). It is that the application of elastic stresses effects the course of the structural changes during the normalizing process. Small stresses (in Fig. 2 $\sigma <$ 30 kg/mm^2; in Fig. 1 $\alpha < 0.5$ o/mm) do not effect the relation of the phases (the constancy of I_s) leading apparently only to a growth in the anisotropy of the single domain formations and also to a change in the magnetic texture. The growth of the anisotropy leads to an increase in H_c both on extension and on twisting. The texture on extension remains more completely along the axis of the sample therefore B_r increases. On twisting the longitudinal texture is destroyed as a result of which B_r increases.

Consequently the growth of H_c on thermomechanical treatment is not determined fundamentally by the change in the magnetic texture since it can occur also on increasing the strength of the longitudinal magnetic texture (extension) and on its destruction (twisting). Large stresses which are created both by extension and by twisting lead to the additional decomposition of the γ-phase which is accompanied by a decrease in I_s, B_r and H_c.

5. In the present work it has been established that thermomechanical treatment for which stresses are created by twisting the sample, have a substantial influence on the magnetic properties of the alloy, vicalloy. For thermomechanical treatment with relatively small angles of twist it is possible to obtain an increase in H_c in comparison with the H_c of the untwisted sample normalized at the same temperature. The value of I_s for this does not alter, however B_r becomes smaller. Thermomechanical treatment at large angles of twist leads to a reduction in I_s, H_c and B_r.

The physical processes which lead to a change in the magnetic properties on twisting during heat treatment obviously are analogous to the processes which occur on extension during heat treatment.

The results obtained are explained on the basis of hypotheses concerning the thermomechanical treatment of highly coercive alloys which were suggested earlier [1].

Translated by J.H. Dempster

REFERENCES

1. Ia.S. Shur, M.G. Luzhinskaia and L.A. Shubina,

VOL 8 195

Fiz. Metal Metalloved 4, 60, (1957).
2. M.G. Luzhinskaia and Ia.S. Shur, *Fiz. Metal Metalloved* 4, 239, (1957)
3. Ia.S. Shur, M.G. Luzhinskaia and L.A. Shubina, *Fiz. Metal Metalloved* 4, 54, (1957).

VOL.
8
1959

A MAGNETIC METHOD FOR THE QUANTITATIVE CARBIDE ANALYSIS OF CARBON STEELS*

IA. I. KAGAN and S. V. BRONIN

Khar'kov electromechanical works,
The Khar'kov polytechnic Institute

(Received 10 October 1958)

The carbide composition of the carbon steels U8 and U12 are studied by the magnetic method. The presence of three carbide phases is confirmed: Fe_3C, χ Fe_xC and ϵ Fe_xC. The quanitiative relation between the carbide phases at different tempering temperatures was also studied and their stable zones more precisely determined.

1. INTRODUCTION

A great number of works have been devoted to the experimental study of the process of carbide formation on tempering a quenched carbon steel. Concrete evidence concerning the intermediate carbide phase were communicated by Arbuzov and Kurdiumov [1]. In a number of the succeeding papers the intermediate phase secured a position in metallurgical terminology and processes arising from the "third transition" are linked with transitions in just this phase.

Papers [2,3] recently published show that on tempering quenched carbon steels three carbide phases are formed: Fe_3C, χ Fe_xC and ϵ Fe_xC. However up to the present time there is no single point of view with regard to the number and nature of the carbide phases observed on tempering. None of the research workers has given a well defined relation between the quantity of carbide phases formed and the tempering temperature and time. A quantitative determination of the χ- and ϵ-carbides generally speaking has thus far not been carried out by anyone. In connexion with this we have attempted to develop a method for the quantitative analysis of the carbide phases of carbon steels.

2. THE BASIS OF THE METHOD OF ANALYSIS

The physical basis of the proposed method is the simple connexion of the magnetic saturation with the phase composition of the heterogeneous system. Analytically the connexion of the magnetization with the phase composition when the heterogeneous system is saturated is expressed by the equation.

$$I_s = \frac{1}{100}\sum_{i=1}^{n'} I_{si} P_i, \qquad (1)$$

and

$$\sum_{i=1}^{n'} P_i + P_0 = 100, \qquad (2)$$

where I_s and I_{si} are the magnetization at saturation for the system studied and its i-phase; P_i is the volume percentage content of the i-phase; P_0 is the percentage content by volume of the non-ferromagnetic phases.

Usually the magnetization of the non-ferromagnetic phases can be neglected, therefore the sum in equation (1) is taken over only n ferromagnetic phases. The given relations (1) and (2) can be used for calculating the quantity of the phase which interests us.

By quenching the samples being studied to

* *Fiz. metal. metalloved.* 8, No. 4, 535-542, 1959.

martensite and cold working them it is possible later to exclude the retained austenite from the observations and to consider that in the tempering process only the transformation of martensite with the separation of the carbide phases occurs.

Firstly we shall consider a normalized sample. The structure of such a sample has two phases; ferrite + cementite. On the grounds of equations (1) and (2) we can write in the given case

$$I_0 = \frac{1}{100}(I_\phi P_\phi + I_c P_c), \qquad (3)$$

and

$$P_\phi + P_c = 100, \qquad (4)$$

where I_0, I_ϕ and I_c are the magnetization at saturation of the sample, ferrite and cementite; P_ϕ and P_c are the percentage contents by volume of the ferrite and the cementite. Finding P_ϕ in terms of P_c in (4) and substituting it in equation (3) we obtain

$$I_0 = \frac{1}{100}[I_\phi(100 - P_c) + I_c P_c]. \qquad (3')$$

Transforming equation (3) we obtain an equation for calculating the percentage content by volume of the cementite

$$P_c = \frac{I_\phi - I_0}{I_\phi - I_c} 100. \qquad (5)$$

For calculations with equation (5) it is necessary to know the magnetization at saturation of the ferrite and cementite and to measure the magnetization at saturation of the samples each time The accuracy of the results obtained will be determined by the accuracy with which the numerator in equation (5) is calculated. From this point of view one must carry out the measurements by the differential method, i.e. measuring directly the difference between the magnetization at saturation of the ferrite and that of the sample.

However even with the differential method the measurements will contain quite significant errors if the quantity of the cementite in the sample is small since in this case the magnetization at saturation of the ferrite and the sample differ little from one another. Therefore it is sensible to increase this difference for a given cementite content, which can be done by carrying out the measurement at a temperature exceeding the Curie point for cementite (210°) for example at 250°.

In such a case equation (5) changes into the following equation:

$$P_c = \frac{I_\phi^{250} - I_0^{250}}{I_\phi^{250}} 100. \qquad (6)$$

If the sample contains all three carbides (Fe3C, χ Fe_xC, and ϵ Fe_xC) it is necessary to translate them consecutively into the paramagnetic state and carry out the measurements. This is quite possible due to the difference between the Curie points of these phases. Thus heating to 300° causes not only the cementite but also the χ-carbide, whose Curie point is 260-270°, to transform into the paramagnetic state. In the same way as for equation (6) we obtain in this case an equation for calculating the sum of the percentage contents by volume of cementite and the χ-carbide

$$P_c + P_\chi = \frac{I_\phi^{300} - I_0^{300}}{I_\phi^{300}} 100, \qquad (7)$$

where I_ϕ^{300} is the magnetization at saturation at 300° of the remaining ferromagnetic phases of the sample.

On heating to 425° all three carbides go into the paramagnetic state (the Curie point of the ϵ-carbide is 380-400°), we obtain in this case an equation for calculating the total percentage content by volume of all three carbides similar to equation (6)

$$P_c + P_\chi + P_\epsilon = \frac{I_\phi^{425} - I_0^{425}}{I_\phi^{425}} 100, \qquad (8)$$

where I_ϕ^{425} is the magnetization at saturation at 425° of the remaining ferromagnetic phases of the sample.

Successive calculation according to the equations (6), (7) and (8) permit the percentage content by volume of each carbide to be determined individually. But in order to carry out the calculation according to these formulae it is necessary to have standards

VOL. 8 1959

which would be identical to the phase of the sample which remains ferromagnetic at the temperatures 250, 300 and 425°. The character of this phase and its magnetic properties depend on the thermal history of the sample being tested. Armco iron can be considered with a sufficient degree of accuracy, as the standard for the normalized state. For the annealed states it is not possible to choose standards immediately. However there is another way of calculating the quantity of carbides in a sample which does not require the presence of such a standard. Actually in connexion with the equalities (1) and (2) it is possible to write down a number of other relations

$$I_0^{20} = \frac{1}{100}\{I_\phi^{20}(100 - P_c) + I_c^{20} P_c\}, \quad (9)$$

$$I_0^{250} = \frac{1}{100} I_\phi^{250}(100 - P_c), \quad (10)$$

$$I_0^{20} = \frac{1}{100}\{I_\phi^{20}[100 - (P_c + P_\chi)] + I_c^{20} P_c + I_\chi^{20} P_\chi\}, \quad (11)$$

$$I_0^{300} = \frac{1}{100} I_\phi^{300}[100 - (P_c + P_\chi)], \quad (12)$$

$$I_0^{20} = \frac{1}{100}\{I_\phi^{20}[100 - (P_c + P_\chi + P_\varepsilon)] + I_c^{20} P_c + I_\chi^{20} P_\chi + I_\varepsilon^{20} P_\varepsilon, \quad (13)$$

$$I_0^{425} = \frac{1}{100} I_\phi^{425}[100 - (P_c + P_\chi + P_\varepsilon)], \quad (14)$$

where I_ϕ^{250}, I_ϕ^{300} and I_ϕ^{425} is the saturation magnetization at the respective temperatures of the remaining ferromagnetic phases in the sample.

Subtracting equation (10) from equation (9) and rearrangement of the results yields an equation for calculating the percentage content by volume of cementite in the sample

$$P_c = \frac{(I_0^{20} - I_0^{250}) - (I_\phi^{20} - I_\phi^{250})}{I_c^{20} - (I_\phi^{20} - I_\phi^{250})} 100. \quad (15)$$

The subtraction of equation (12) from equation (11) and rearrangement gives an equation for calculating the percentage content by volume of the χ-carbide in the sample

$$P_\chi = \frac{(I_0^{20} - I_0^{300}) - (I_\phi^{20} - I_\phi^{300}) - [I_c^{20} - (I_\phi^{20} - I_\phi^{300})]\frac{P_c}{100}}{I_\chi^{20} - (I_\phi^{20} - I_\phi^{300})} 100. \quad (16)$$

Subtracting from equation (13) equation (14) and carrying out the suitable rearrangement we obtain an equation for calculating the percentage content by volume of the ϵ-carbide in the sample

$$P_\varepsilon = \frac{(I_0^{20} - I_0^{425}) - (I_\phi^{20} - I_\phi^{425}) - [I_c^{20} - (I_\phi^{20} - I_\phi^{425})]\frac{P_c}{100} - [I_\chi^{20} - (I_\phi^{20} - I_\phi^{425})]\frac{P_\chi}{100}}{I_\varepsilon^{20} - (I_\phi^{20} - I_\phi^{425})} 100. \quad (17)$$

In order to calculate the quantity of the carbide phases from the equations (15), (16), (17) one must measure the saturation magnetization of the samples being tested at room temperature and at a temperature somewhat above the Curie point of the corresponding carbide and, besides this, one must know the temperature dependence of the saturation magnetization of the ferromagnetic base of the sample and the saturation magnetization of the carbides at room temperature.

The relative change in the saturation magnetization of the ferromagnetic base of the samples of carbon steel ($K(t)$) with the change in temperature is practically independent of the carbon content in the steel and of its structural state:

$$\frac{I_\phi^{20} - I_\phi^{250}}{I_\phi^{20}} 100 = 4\%, \quad \frac{I_\phi^{20} - I_\phi^{300}}{I_\phi^{20}} 100 = 4{,}9\%, \quad \frac{I_\phi^{20} - I_\phi^{425}}{I_\phi^{20}} 100 = 9{,}4\%.$$

In order to calculate the absolute values ($I_f^{20} - I_f^t$) for samples which are in different structural states it is possible to proceed from the following considerations.

At tempering temperatures above 300° the ferromagnetic base of the sample differs little in its magnetic properties from ferrite [4]; the transition of tetragonal martensite into cubic which proceeds in tempering at low temperatures, is not very evident in the value of the saturation magnetization of martensite [5]. Therefore for tempering at low temperatures (up to 200°)

one may with a sufficient degree of accuracy write

$$I_{\phi}^{20} - I_{\phi}^{t} = k(t)\, I_{\alpha}^{20},$$

where I_{α}^{20} is the saturation magnetization of the martensite of the steel being studied: for tempering at high temperatures (above 300°)

$$I_{\phi}^{20} - I_{\phi}^{t} = k(t)\, I_{a}^{20},$$

where I_{a}^{20} is the saturation magnetization of Armco iron; for intermediate tempering (from 200 to 300°) one may take a temperature dependence half way between those mentioned above. There is extremely poor and insufficiently well grounded evidence in other works concerning the saturation magnetization of the carbides of carbon steel. Therefore these quantities were determined by us experimentally in the following way.

For the normalized state calculations by the first method give reliable results. Therefore the quantity of cementite in the normalized form was calculated from equation (6) (the normalized samples will not contain the other carbides) and then the saturation magnetization of cementite was calculated from equation (15). The method of determining the saturation magnetization of the α and ϵ-carbides is somewhat more complicated. Samples were taken which contained all three types of carbide tempered in the temperature interval 150-200 and 300-400°). The quantity of cementite in these samples was calculated according to equation (15). These calculations were carried out by taking martensite (for samples tempered at 150-200°) and armco iron (for samples tempered at 300-400°) respectively as standards. Equation (6) was used to calculate the difference between the saturation magnetization of the standard and that of the sample at a temperature of 250° for a given cementite content in the sample

$$(I_{e}^{250} - I_{0}^{250})_{true} = I_{e}^{250}\,\frac{P_c}{100}\,. \qquad (18)$$

The actual value of this difference was measured. It was shown that it differed from that calculated according to equation (18) by the quantity Δ since the ferromagnetic base of the sample was somewhat different from the standard in its magnetic properties. Taking this different to the actual saturation magnetization of the sample at a temperature of 250° they obtained the relative difference between the magnetization of the ferromagnetic base of the sample and the magnetization of the standard at the given temperature

$$\delta = \frac{(I_{s}^{250} - I_{0}^{250})_{act} - (I_{s}^{250} - I_{0}^{250})_{true}}{I_{0}^{250}} = \frac{\Delta}{I_{0}^{250}}\,. \qquad (19)$$

This quantity will have practically the same value on heating to a temperature of 300 and 425° since the temperature dependence of the saturation magnetization of the ferromagnetic base of the sample and the standard may be considered the same. By calculating the value δ from equation (19) it was possible to decide what the difference between the saturation magnetization of the standard and the sample at temperatures of 300 and 425° should be in order to obtain the correct values for the quantities of the χ and ϵ-carbides in the sample:

$$(I_{s}^{300} - I_{0}^{300})_{true} = (I_{s}^{300} - I_{0}^{300})_{act} \pm \delta I_{0}^{300}, \qquad (20)$$

$$(I_{s}^{425} - I_{0}^{425})_{true} = (I_{s}^{425} - I_{0}^{425})_{act} \pm \delta I_{0}^{425}. \qquad (21)$$

Substituting the corrected values in equation (7) and (8) for the difference in the saturation magnetizations of the standard and the sample obtained from equations (20) and (21) we obtain the true quantities of the χ and ϵ-carbides in the sample. Knowing these quantities, we calculated the saturation magnetization of these carbides from equation (16) and (17). Thus having determined the temperature dependence of the saturation magnetization of the ferromagnetic base of the samples and the values of the saturation magnetization of the carbides we can use equations (15), (16), (17) to calculate the quantity of each carbide phase in the carbon steels on tempering them in any temperature interval.

3. THE EXPERIMENTAL METHOD AND MATERIALS

For the research the carbon tool steels U8

VOL. 8 1959

TABLE 1

Phase	$4\pi I_{\phi}^{20} - 4\pi I_{\phi}^{250}$, gauss	$4\pi I_{\phi}^{20} - 4\pi I_{\phi}^{300}$, gauss	$4\pi I_{\phi}^{20} - 4\pi I_{\phi}^{425}$, gauss
Armco-iron	835	1030	1980
Martensite U8	770	950	1820
Martensite U12	725	885	1700

and U12 were taken which have a carbon content of 0.78 and 1.20% respectively.

The samples were prepared in the form of cylinders with a diameter of 8 mm. and length 20 mm.

The quenching of the samples to martensite was carried out in water from a temperature of 880°. Cold working followed immediately after quenching and was concluded by cooling the quenched samples to a temperature of -120°, holding them at this temperature for one hour and heating them in air. This led to the additional transformation of the remaining austenite into martensite and permitted the remaining austenite to be excluded from further observations.

Tempering of the samples was carried out for 5 hr. in an oil bath at temperatures: 120; 160; 180; 190; 200; 210 and 240° and in a salt bath at the temperatures: 260; 280; 320; 370; 400; 450; 500 and 600°. The quantity of carbide phases in these samples was calculated from the formulae (15), (16) and (17). The measurement of the values $(4\pi I_0^{20} - 4\pi I_n^t)$ was carried out by the method of pressing. This method of determining the quantity of carbides requires measurements to be carried out, heating the samples sometimes to a temperature above that at which they are tempered, which can lead to a certain additional transformation of the martensite and separation of the carbides. In connexion with this the heating period up to each temperature was chosen to be as small as possible and was of the order of 3 min.

The preliminary data, essential for the calculations, of the temperature dependence of the saturation magnetization of the ferromagnetic base of the samples are given in Table 1.

The values of the saturation magnetizations determined by us for the carbide phases are equal to: $4\pi I_u^{20} = 10\,020$ G, $4\pi I_\chi^{20} = 19\,890$ G, $4\pi I_\varepsilon^{20} = 19\,470$ G.

4. A DISCUSSION OF THE RESULTS OF THE RESEARCH

The nature of the dependence of the amount of the carbide phases on the tempering temperature for the steels U8 and U12 (Fig. 1) obtained as a result of the experiments are completely identical, therefore we shall limit the description of the graph of the dependence to only one steel, U8 (Fig. 1*a*). The graph of the dependence for the steel U12 (Fig. 1*b*) differs from the graph for the desteel U12 (Fig. 1*b*) differs from the graph for the steel U8 only in that at corresponding tempering temperatures the quantity of carbides is approximately 1.5 times larger than for the steel U8*.

An examination of the graph given shows that on increasing the tempering temperature the rate of formation of all the carbides noticeably increases. The rate of formation of the lowest temperature ϵ-carbide, which achieves a maximum in quantity at a tempering temperature of 200°, increases particularly rapidly. Further increase of the tempering temperature leads to a rapid decrease in the quantity of the ϵ-carbide which testifies to the instability of this carbide above 200°.

The quantity of the intermediate χ-carbide increases on increasing the tempering temperature and reaches a maximum at 400°. At a tempering temperature of the order of 250° some increase in the rate of formation of the

* The somewhat elevated course for the graph of cementite in the steel U12 is explained by the fact that on quenching, part of the cementite was not transformed into a solid solution.

VOL 8 195

χ-carbide is observed. Above 400° this carbide is unstable and decomposes.

The quantity of cementite increases continually on raising the tempering temperature. The decomposition of the δ-carbide above 200° leads to a noticeable increase in the rate of formation of the cementite from which it follows that the decomposing ϵ-carbide is transformed partially into cementite.

It is probable that part of the ϵ-carbide is transformed into the χ-carbide which is confirmed by the increase in the quantity of the χ-carbide in the temperature interval 200-250° where the rate of decomposition of the ϵ-carbide is the largest.

In the temperature interval 300-400° the chief product of the decomposition of the ϵ-carbide is, in all probability, the χ-carbide since in this interval considerable increases in the quantity of χ-carbide are observed and the growth of the quantity of cementite is retarded. At much higher temperatures (above 400°) the formation of cementite is intensified on account of the decomposition of both carbides.

In the graph of the dependence of the total quantity of the carbides on the tempering temperature there is a clearly expressed fall in the region 210-250°. In this region intense decomposition of the ϵ-carbide occurs. A reduction in the total quantity of the carbides can be explained only by the intense reaction, in this temperature region, of the decomposition of the carbide which is low in carbon with respect to the cementite, i.e. considering the index x in the formula Fe_xC is greater than 3. This conclusion that the index is greater than 3 is also obtained from the higher ferromagnetic properties of of χ- and ϵ-carbides, which we found, and also from the increased rate of separation of the ϵ-carbide at tempering temperatures up to 200° when the rate of diffusion of the carbon is small.

It is possible to carry out a purely qualitative calculation of the values of x, assuming that the ϵ-carbide is completely transformed into cementite and that the cementite forms only on account of the decomposition of the ϵ-carbide. In this case, in the temperature interval 200-250°, the intense reaction below occurs

$$\varepsilon\ Fe_xC \rightarrow Fe_3C + (x-3)\,Fe.$$

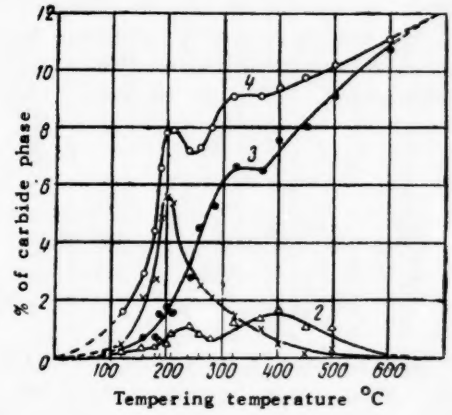

Fig. 1a. The dependence of the quantity of the carbide phases, which are formed on tempering, on the tempering temperature. The steel U8: 1—$\varepsilon\ Fe_xC$; 2—$\chi\ Fe_xC$; 3—Fe_3C; 4— the total quantity of the carbides.

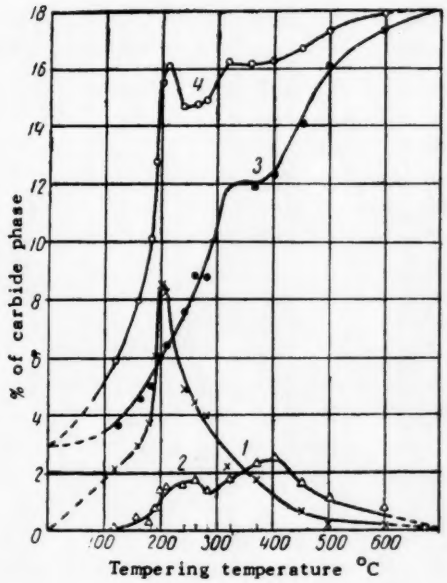

Fig. 1b. The same as for Fig. 1a for the steel U12: 1—$\varepsilon\ Fe_xC$; 2—$\chi\ Fe_xC$; 3—Fe_3C; 4— the total quantity of the carbides.

In this the quantity of the ϵ-carbide is reduced by 2.7% and the quantity of the cementite increases by 2%. On the grounds of the reaction given above, having assumed that

the volume percentage differs little from that by weight, we compose a ratio, taking into consideration the molecular weight of the cementite, equal to 180, and the ϵ-carbide (56 $\pm$ 12). Whence we find a value 4.1 for x. A value of the same order was found in an analogous calculation for the steel U12.

CONCLUSIONS

1. A method has been developed for the determination of the content of the carbides in carbon steels using a magnetic method without separating them.
2. The saturation magnetizations of cementite, χ and ϵ-carbides have been determined.
3. The quantitative ratio of cementite, χ and ϵ-carbides in U8 and U12 steels at various temperatures in the interval 120-600° have been studied.
4. The stable zones of ϵ-carbide, χ carbide and cementite have been made more precise: ϵ-carbide is formed chiefly at low temperatures and is stable up to 200°: at higher temperatures it decomposes vigorously changing into cementite and χ-carbide: χ-carbide is stable up to 400° changing at higher temperatures into cementite; χ and ϵ-carbides practically completely disappear only at 600°.
5. The results obtained allow it to be assumed that the χ-and ϵ-carbides contain little carbon ($x > 3$); a qualitative calculation shows that for the ϵ-phase $x > 4$.

Translated by J.H. Dempster

REFERENCES

1. M.P. Arbuzov and G.V. Kudriumov, *Zh. teor. fiz.* 10, vyp. 13 (1940).
2. N.V. Gudkova, E.Io Levina and V.A. Tolomasov. *Fiz. Metal Metallov*, 4, vyp. 3 (1957).
3. VoG. Permiakov and M.V. Belous, *Fiz. Metal. Metallov*, 4, vyp. 3 (1957).
4. B.A. Apayev. *Hot working of metals, (Termicheskaia obrabotka metallov) Symposium materialov konferentsii. State United Scientific and Technical Publishing House*, Moscow (1950).
5. R.I. Ianus, *A magnetic defect detection (Magnitnaia defektoskopiia) Gostekhizdat* (1946).

VOL 8 195

MAGNETIC PROPERTIES, ELECTRICAL CHARACTERISTICS AND HARDNESS OF HIGH-CARBON ALLOY STEELS IN HARDENED STATE*

M.N. MIKHEEV and G.S. TOMILOV

Metal Physics Institute of the Academy of Sciences of U.S.S.R.

(Received 3 February 1959)

An investigation was made of coercive force and magnetic saturation in comparison with the hardness and microstructure of a number of high-carbon steels alloyed with tungsten, chromium and manganese, after hardening treatment from a wide range of temperatures (780-1250°C). A study was made of the dependence of the magnetic properties after hardening on the starting structure of steel ShKH15SG and, on the basis of such results, a method is put forward for the control of the quality of hardening processes for steel parts [22].

VOL. 8 1959

It is a well known fact that the magnetic properties of steel are extremely sensitive to variations in the chemical composition and microstructure and thereby also to the mechanical properties of steel [1]. It is exactly because of this sensitivity that the magnetic methods of investigation and control found a wide field of practical applications.

Earlier investigations of the magnetic properties of straight carbon and alloy steels in quenched condition were undertaken in connexion with the search for a most effective and economic alloy for permanent magnets [2]. Subsequently, studies were made mainly for the purpose of developing magnetic methods suitable for the control of quality of the thermal treatment of steel products and for elucidating the nature of the coercive force of hardened steel [3-7].

In the present series of investigations, a study was made of the magnetic properties after quenching of a number of instrument steels for industrial applications, the chemical composition and the magnetic proper-

TABLE 1

Chemical composition and properties of test steels in their initial state

Steel	Chemical composition, by weight %									H_c, ergs	H_B (Brinnel)
	C	Cr	Mn	Si	W	Ni	V	S	P		
KhV-5	1.42	0.51	0.23	0.25	5.2	0.25	–	–	–	11.6±0.2	270
KhG3**	0.90	1.35	2.43	0.50	–	–	–	< 0.02	< 0.03	12.8±0.6	217
ShKh15	1.00	1.50	0.30	0.30	–	–	–	< 0.02	< 0.03	12.0±0.5	215
ShKh15SG	1.06	1.45	1.07	0.50	–	–	–	< 0.02	< 0.03	12.0±0.5	230
Kh12F1	1.44	11.60	0.28	0.34	–	0.23	> 0.86	0.022	0.018	14.9±0.2	223

**Steel KhG3 was made by re-melting of steel ShKh15SG with an addition of 1.5 % Mn. This opportunity is taken for expressing our thanks to L.V. Smirnov for his supervision of this operation.

*Fiz. metal. metalloved., 7, No.4, 543-556, 1959.

of which (H_c, H_{RC}) in the initial state after annealing are tabulated in table 1.

1. TEST MATERIALS AND PROCEDURES

The steels to be investigated were in annealed state and had the structure of grained pearlite. Steel KhG3 was also annealed, after forging to rods 15 x 15 mm, in order to ensure that it had the structure of grained pearlite. The tests were carried out on testpieces, as used for impact tests, whose dimensions were 10 x 10 x 68 mm. The heating prior to quenching from the temperature of 780-950°C was by means of a laboratory muffle furnace. The quenching from the temperatures of 1000-1250°C was carried out after the testpieces were heated in a salt bath consisting of $BaCl_2$ deoxidized with borax. The period of testpiece holding at a given temperature was 15 min, after which the testpiece was oil-quenched at room temperature. At least four testpieces were quenched from each temperature; two of them were either heated in air (in the case of quenching from the temperature of the order of 780-980°C) or in $BaCl_2$ salt (for quenching temperatures of 1000-1250°C), whereas the other two testpieces were heated to the quenching temperature in a protective atmosphere†. In order to follow the degree of decarburization and degradation, the testpiece was weighed, with an accuracy of ± 0.01g, before and after quenching.

The variation in volume of the testpieces during the process of treatment with cold, was followed by means of measurement of the length l of the testpieces using a micrometer giving an accuracy of the order of ± 0.02 mm. For steel Kh12F1, an additional determination was also made of the length L before and after testpiece quenching; testpieces of this steel were heated to the quenching temperature in a protective atmosphere. The results of changes in the weight and dimensions of the testpieces (Δp, Δl and ΔL) are given in Table 2.

Coercive force measurements were repeated thrice: 1) 1-2 hr after quenching; 2) after truing of the testpiece surface (removal of surface layer with a thickness of 0.2-0.3 mm); and 3) after final polishing to the dimensions of 8 x 8 x 65 mm. After the second and third

TABLE 2

Variation in weight (Δp) of testpieces of various steels in the process prior to quenching and their length changes (ΔL) during annealing and subsequent quenching (Δl).

Quenching temperature, °C	KhV-5		KhG 3		ShKh-15		ShKh15SG		Kh12F1		
	Δp, г	Δl, мм	Δp, г	Δl, мм	Δp, г	Δl, мм	Δp, г	Δl, мм	Δp, г	Δl, мм	ΔL, мм
780*	—0.22	0.00	—0.12	+0.02	—0.37	0.00	—0.41	+0.03	—0.03	0.00	—
780**	—0.05	—	0.00	—	0.00	—	+0.05	—	+0.02	—	0.00
850*	—0.25	+0.04	—0.35	+0.08	—0.37	+0.04	—0.37	+0.06	—0.07	0.00	—
850**	—0.05	—	—0.03	—	0.00	—	0.00	—	0.00	—	0.00
900*	—0.31	+0.09	—0.63	+0.24	—0.57	+0.08	—0.55	+0.12	—0.14	+0.01	—
900**	—0.02	—	0.00	—	—0.05	—	0.00	—	0.00	—	0.00
950*	—0.32	+0.17	—0.64	+0.30	—0.77	+0.17	—0.65	+0.21	—0.13	0.00	—
950**	—0.03	—	0.00	—	0.00	—	0.00	—	0.00	—	0.00
1000***	—0.30	+0.30	—0.30	+0.30	—0.37	+0.18	—0.40	+0.35	—0.04	+0.01	—
1000**	0.00	—	0.00	—	—0.08	—	—0.10	—	0.00	—	0.00
1100***	—0.25	+0.30	—0.30	+0.32	—0.25	+0.18	—	+0.34	—0.09	+0.08	—
1100**	—0.05	—	0.00	—	—0.03	—	—0.10	—	—0.05	—	—0.10
1200***	—0.80	+0.30	—	—	—	—	—1.40	+0.35	—0.46	+0.24	—
1200**	—0.03	—	—	—	—	—	—0.17	—	—0.06	—	—0.35

* Heating in air ** Heating in a container *** Heating in a salt bath

† The testpiece was placed inside a special cylindrical vessel made in ShKh15SG steel (ext. dia. d = 27 mm, height ~ 120 mm).

of the above operations, the measurement was also made of other properties (I_s, H_{RC}, ρ). It was noted that in the test specimens quenched from $T > 950^{\circ}C$, there is a significant drop in the coercive force values already after surface polishing (3-5%). The measurement of coercive force was made by means of the ballistic and magnetometric methods with an accuracy of $\pm$ 1.0%. Measurement of saturation magnetisability was by means of a differential method which involves placing the test specimen between two electromagnets in the field of 1000, 2000 and 3000 ergs. The difference in the specimen magnetisation and that of the standard was calculated from the expression:

$$\Delta I = I_{stand} - I_{spec} = \frac{C_B}{8\pi N S_{stand}} \alpha - \left(I_{spec} \frac{S_{stand} - S_{spec}}{S_{stand}}\right)_A - \left(\frac{H_{stand} - H_{spec}}{4\pi}\right)_B \quad (1)$$

The correction terms A and B can be ignored in most cases, because $S_{stand} = S_{spec}$ (this was ensured in the specimen preparation). The difference in fields $H_{stand} - H_{spec}$ did not exceed 50 ergs, as it was proved by special tests, provided that the proportion of austenite in the specimen did not exceed 50% The error in the relative magnetizability values of the specimens did not exceed $\pm$ 6 gaus, or $\pm$ 0.5%. During tests on specimens in which the proportion of austenite was higher than 50%, the standard was trimmed. This enabled a reduction to be achieved in the type B error, which is conditioned by the field difference $H_{stand} - H_{spec}$. By extrapolating to zero $H \to \infty$ the values were found of saturation magnetisation I_s, for which purpose the magnetisation curve was traced for the pearlitic standard specimen, on the basis of carefully carried out preliminary measurements.

2. EVALUATION OF EXPERIMENTAL RESULTS

1. It is clear from the curves given in Fig. 1-4, that the coercive force maximum corresponds to quenching for the maximum hardness of $H_{RC} = 65$. This is the structure of "gardenite" or pseudo-crystalline martensite. Depending on the carbon concentration and that of the alloying elements, there is a change in the form and position of the H_c maximum on the scale of quenching temperatures, which is associated with different solubilities in austenite of the various carbide phases. Thus, at comparatively low concentrations of chromium and manganese in the KhG3, ShKh15 and ShKh15SG steels, only the cementite type carbides are present in the initial structure $(Fe,Me)_3C$ [8]. In accordance with a higher solubility of the manganese-type cementite, the position of the maximum H_c in Fig. 2 corresponds to $\sim 810^{\circ}C$. Tungsten is only little soluble in cementite and it is present in annealed steel either in the composition of binary carbides Fe_2W_2C, or as a constituent of special carbides of tungsten: W_2C and WC [9, 10]. All these carbides are practically non-ferromagnetic and have a low solubility in austenite during the heating to the quenching temperature.

The maximum in the H_c curve for steel KhV-5 (Fig. 1) has a very diffuse appearance (810-950°C). This fact is explained by the presence in the initial structure of steel KhV-5 of a whole series of carbide phases with various stability degrees during heating. If judged in terms of variation in the saturation magnetisability, coercive force and the specific resistance as functions of increasing quenching temperatures, it can be assumed that, during the heating to 1000°C and specimen holding at this temperature for 15 min., all the carbides which are at all soluble, pass fully into the γ-solid solution.

Depending on the carbon and alloying elements contents in steel, which fix the position of the martensite point, the maximum amount of the residual austenite in steels KhV-5 and KhG3 is of the order of 70%, while in steels ShKh15SG and ShKh15 it reaches the values of 40 and 30%, respectively.

In Kh12F1 steel (Fig. 5), the martensite point is lowered within a wide range (400-0°C) as the quenching temperatures are increased. The final point of the martensitic transformation is reduced from +300°C (for quenching from the temperature of 900°C) to -180°C (for quenching from 1200°C) [11]. This makes it possible to modify the phase composition of steel after its quenching over almost the whole of its composition range (from 0 to 98%), i.e. it is possible to obtain residual

VOL. 8 1959

austenite concentrations up to 98%.

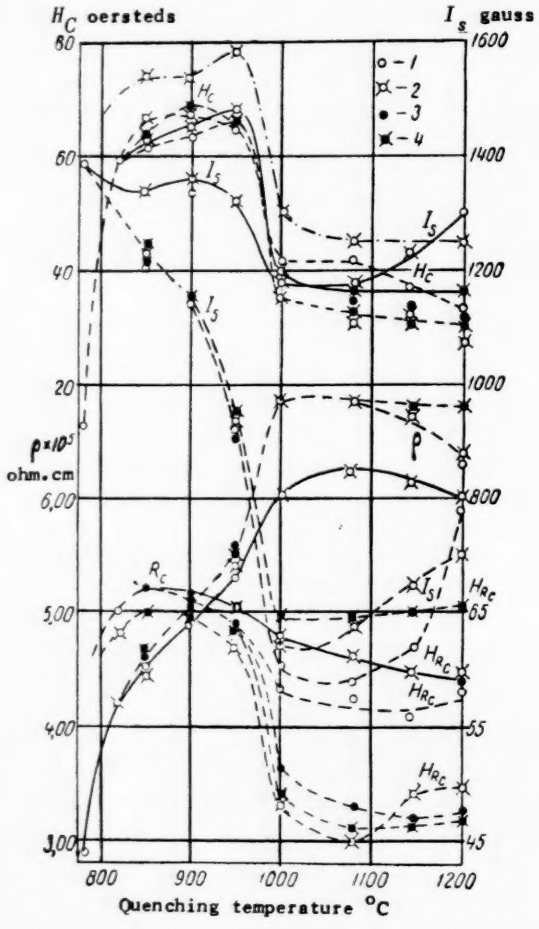

Fig. 1. Magnetic (H_c, I_s) electrical (ρ) and mechanical (HR_C) properties of KhV-5 steel after its quenching from various temperatures into oil at room temperature. The holding period at the quenching temperature was 15 min
– – – – after quenching; ——— after treatment with cold (-196°C); –.–.–.–. at the liquid nitrogen temperature (-196°C); 1 – specimen heating without any special protective measures. The specimen dimensions were checked after polishing to see that there has been no change; 2 – the specimen dimensions after grinding were corrected exactly to 8 x 8 x 65.5 mm; 3 – specimen heated inside a vessel; its dimensions were checked for accuracy after grinding; 4 – specimen heating inside a vessel; its dimensions were corrected after grinding to be exactly 8 x 8 x 65.5 mm.

During the homogenization and annealing treatments of this steel, there are formed, apart from the cementite-type carbide $(Fe,Cr)_3C$, also special chromium carbides: $(Cr,Fe)_7C_3$ and $Cr_{23}C_6$ [8, 12].

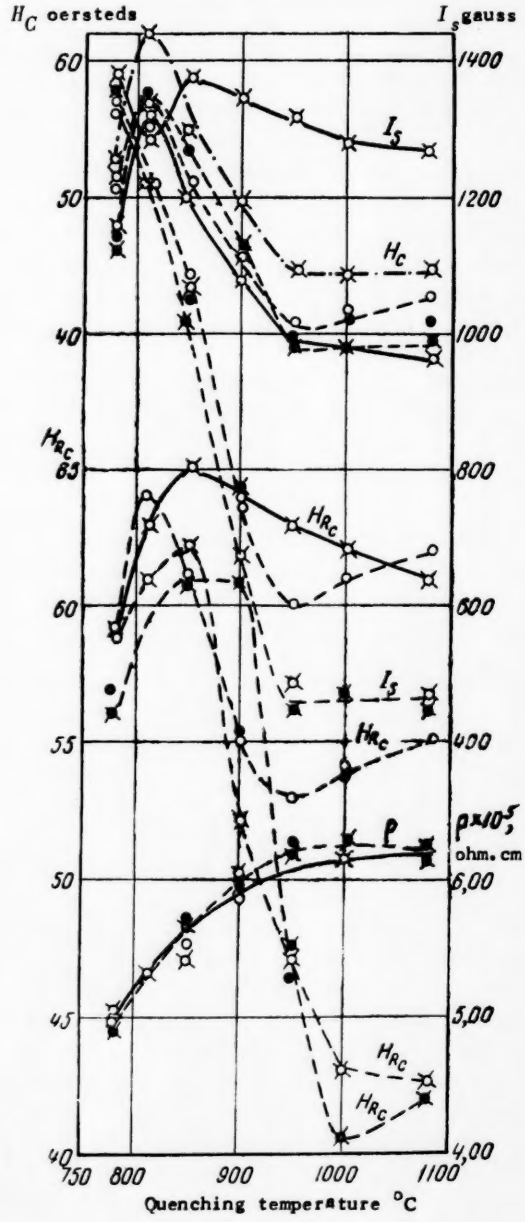

Fig. 2. Magnetic (H_c, I_s), electrical (ρ) and mechanical (HR_C) properties of steel KhG3 after its quenching from various temperatures in oil at room temperature. The duration of holding at the quenching temperature was 15 min.

Consequently, in the quenching temperatures

interval from 800-950°C (Fig. 5), there sets in a transition of the $(Fe,Cr)_3C$ carbide, of the cementite type, into the γ-solid solution. The rate of increase in the coercive force, hardness and resistivity values drops progressively as all carbides of the $(Fe,Cr)_3C$ type pass in the γ-solid solution.

A certain increase in the saturation magnetisability, because of an increase in the residual austenite content in this interval, is compensated by a rise of magnetisability on account of the transition of weakly-magnetic carbides into the γ-solid solution. The net result is that the saturation magnetisability remains constant right up to the quenching temperature of 950°C.

Starting with the temperature of 950° and up to 1080°C, it is mainly the trigonal chromium carbide $(Cr,Fe)_7C_3$ [12] which passes into γ-solid solution. Because of this, there is found a new rise in the coercive force, hardness and resistivity values and a rapid drop in the saturation magnetisability, which is associated with overcoming of the effect of the rising content of the residual austenite, in comparison with the influence of the reducing concentration of the weakly, magnetic carbides.

During a further increase in the quenching temperature, the effect of the specimen surface layer depletion begins to manifest itself both in the value of the surface hardness and in the values of the saturation magnetisability and coercive force. However, it is clear from the properties shown by specimens, which were heated to the quenching temperature in a protective atmosphere, that, parallel with a rapid drop in the residual austenite contents, there is also a rapid increase in the coercive force values. Such a rapid variation in the phase composition and properties within the quenching temperature interval from 1080-1250°C, is associated with a rapid increase in the austenite grain size after the cubic chromium carbide, and perhaps also the special vanadium carbide VC, have passed into the γ-solid solution. It is extremely likely, that a full dissolution of the above two carbides (and especially of VC) is not achieved even at the temperature of 1250°C. Furthermore, according to the phase composition diagram of the Fe-C-Cr system, steel melting along the grain boundaries sets in after heating to the temperature of 1250°C, this fact being shown in microscopic thin sections in the form of an eutectic (ledeburite).

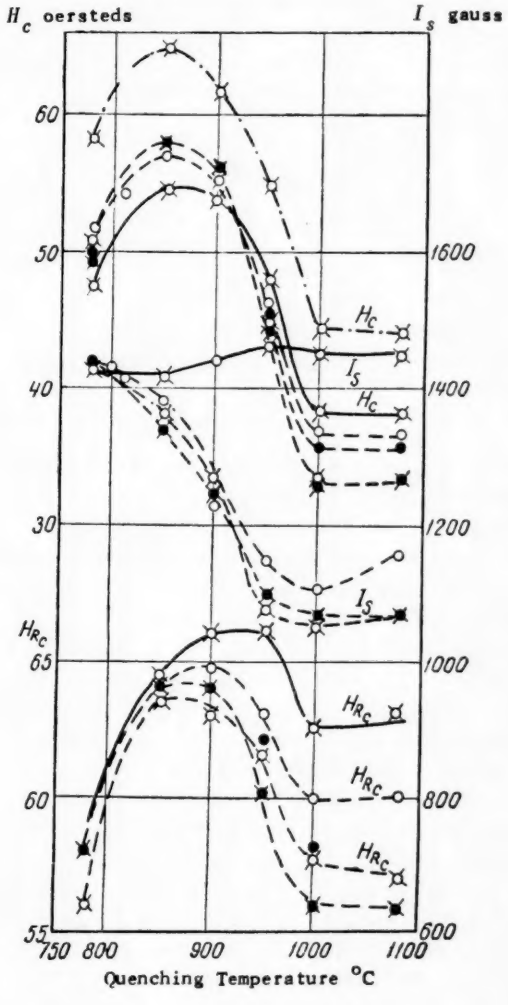

Fig. 3. Magnetic (H_c, I_s) properties and hardness (H_{RC}) of steel ShKh15 after its quenching from various temperatures into oil at room temperature. The duration of specimen holding at the quenching temperature was 15 min.

2. The modern theory of technical magnetisation and re-magnetisation, i.e. the theory of critical field $H_0 \sim H_c$, the value of which,

in the first approximation, also determines the coercive force H_c, provides a fully satisfactory explanation of the behaviour of the magnetic properties of steel as a function of changes in the steel structure and stresses [13-17]. According to the stress theory [13], and bearing in mind the high level of the second order stresses present in steel quenched for martensite [18], as well as the high dispersion of these stresses [19], we can expect that:

$$H_c \sim H_0 =$$

$$= p\frac{\lambda_s \cdot \Delta\sigma_i}{I_s} \simeq 1\,\frac{5 \times 10^{-6} \cdot 2 \times 10^{10}}{1{,}5 \times 10^{3}} = 70\ \text{ergs} \qquad (2)$$

But, a high degree of stress dispersion $\left(p \sim \frac{\delta}{l} \sim 1\right)$ is, obviously, reached in the structure of what is known as gardenite or pseudo-crystalline martensite. In this stage, the solid solution concentration has not, as yet, reached its limiting value and, consequently, the value of stresses $\Delta\sigma_i$ is slightly below its maximum one.

High values of H_c could also be expected according to the theory of inclusions [14-16], but no inclusions are present in non-annealed martensite and therefore the stress theory mechanism is operative inside the needle-shaped particles [13]. In this case, as inclusions can be regarded the excess carbides and residual austenite.

A drop in the coercive force in the region of a high overheating of steel (coarse, acicular structure with a high concentration of residual austenite) should be considered as being associated with the effect of "inclusions" of the residual austenite according to the inclusions theory, as well as with the influence of these "inclusions" on the re-magnetisation mechanism inside the needle-shaped martensite particles (stress mechanism).

With the rising coarseness of the acicular particles of martensite and with increasing concentration of the residual austenite, there is a decrease in the 2nd order stresses in the martensite particles and, consequently, the values of coercive force drop according to equation (2). If a testpiece, quenched for the maximum concentration of the residual austenite, is cooled, then depending on the rise in the dispersion p and on the level of the $\Delta\delta_i$ values of the second order stresses in the newly formed and old martensite needles, there will again be a rise of the coercive force, the maximum of which, as it is shown by experiments [5] corresponds to about 12% of the residual austenite.

In the case of non-annealed martensite in the presence of slightly higher concentrations of the residual austenite, we can assume that, as put forward in work [15], the following relationship holds:

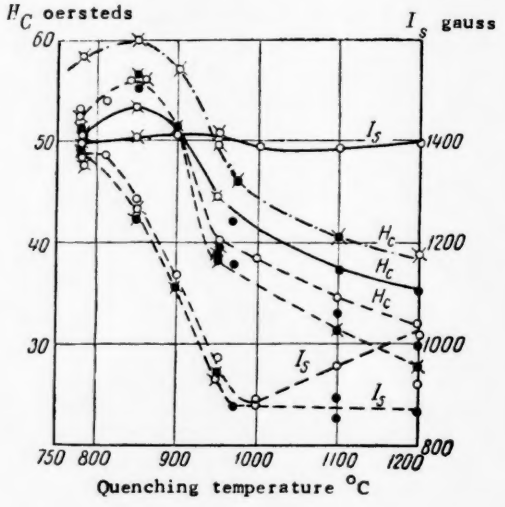

Fig. 4. Coercive force and saturation magnetisability of steel ShKh15SG after quenching from various temperatures into oil maintained at room temperature. The duration of specimen holding at the quenching temperature was 15 min.

$$H_c \simeq p_1\frac{\lambda_s \Delta\sigma_i}{I_s} + p_2\frac{k}{I_s}\beta^{\frac{2}{3}};\ p_2 \sim \frac{\delta}{d}, \qquad (3)$$

where, k – magnetic anisotropy constant ($k \simeq 4 \times 10^5$ ergs/cm^3); $\delta = 10^{-5}$ – width of the domain wall; d – diameter of inclusion; β – relative bulk concentration of inclusions.

As the temperature is increased during the specimen heating prior to quenching, there is a rise in the grain size, coarseness of the martensite needles and in the mean diameter

of the residual austenite inclusions. At the same time, the value of $p_2\beta^{3/4}$ drops, in spite of the fact that there is an increase in the values of β. Simultaneously, there is also a reduction in the dispersion $p_1 \sim \frac{\delta}{l}$ of the internal stresses in martensite needles.

A particularly extensive reduction in the coercive force during the overheating of the specimens (to temperatures greater than 950°C) is observed in the case of steels KhV-5, ShKh15SG and ShKh15 (Fig. 1, 3 and 4). The extent of this reduction is of the order of 25-35 erg, whereas in the case of straight carbon steel, in which the concentration of the residual austenite is small, the reduction in the coercive force arising in consequence of overheating does not exceed 10-15 ergs [2]. In the underheating region of the high-carbon steels, i.e. during quenching so as to produce a troostosorbite structure, the coercive force rises rapidly with rising quenching temperature. Such a rapid increase of coercive force in the narrow interval of quenching temperatures (750-820°C) affects strongly the specific electrical resistance ρ and hardness values. As it is known, this is associated with increasing concentration of the solid solution, and a rising level of internal stresses $\Delta\delta_i$, at the maximum value of their dispersion $p_1 \sim 1$. Therefore, in the pseudo-crystalline state of martensite, when maximum values are reached of the dispersion factors p_1 and p_2, the coercive force achieves also its maximum.

During overheating, according to the theory of inclusions, a rise in the coercive force should be produced by an increase in the quantity of the residual austenite β only. However, a reduction in the dispersion factors p_1 and p_2, strengthened by some reduction in the level of stresses $\Delta\delta_i$ in martensite, overcomes the effect of β and leads to a reduction in the coercive force.

The treatment with cold (-196°C) leads to a reduction in the contents of "inclusions" of the residual austenite β and to an increase in the degree of dispersion of the stresses in martensite.

In the region of strong overheating (900-1000°C), this leads to an increase in the coercive force, whereas in the interval of normal quenching temperatures necessary for obtaining pseudo-crystalline martensite, the coercive force drops. Depending on the residual austenite concentration and on the degree of dispersion of the "inclusions" and stresses before and after the treatment with cold, it is reasonable to expect that different steels should show different changes in the coercive force values. However, the qualitative picture of the changes remains the same (see Fig. 1-4). In steel KhG3, there is practically no change in the coercive force before and after the treatment with cold, which is clearly due to the special nature of its grain structure. Consequently, the effect of changes in the austenite β content was compensated by the influence of the dispersion factors p_1 and p_2.

In the case of steel ShKh15SG, values of the coercive force drop off gradually right up to the highest quenching temperature used (1200°C). This can be regarded as indicating that the grain growth in this steel ceases as a result of its alloying with a small amount of manganese.

3. More complex changes are observed in the properties of steel Kh12F1 in consequence of raising it quenching temperature. As already mentioned above, the break in the coercive force growth in the quenching temperature intervals from 850-960 and 1000-1080°C is associated with an inhibition in the rise of the solid solution concentration if the carbide of one type has already dissolved fully in austenite, while the more stable carbide did not, as yet, start to dissolve. This indicates that the coercive force, after specimen quenching so as to produce the structure of pseudo-crystalline martensite, is proportional to the concentration of the solid solution. The same direct proportionality relationship is shown also by variations of the specific electrical resistance and hardness (see Fig. 5). If it is assumed that the 2nd order stress (deformation) p_1 in pseudo-crystalline martensite is approximately constant over the whole temperature interval of 800-1080°C, one must conclude that, according to equation (1), the level of $\Delta\sigma_i$ stress values rises continuously with rising solid solution concentration.

VOL. 8 1959

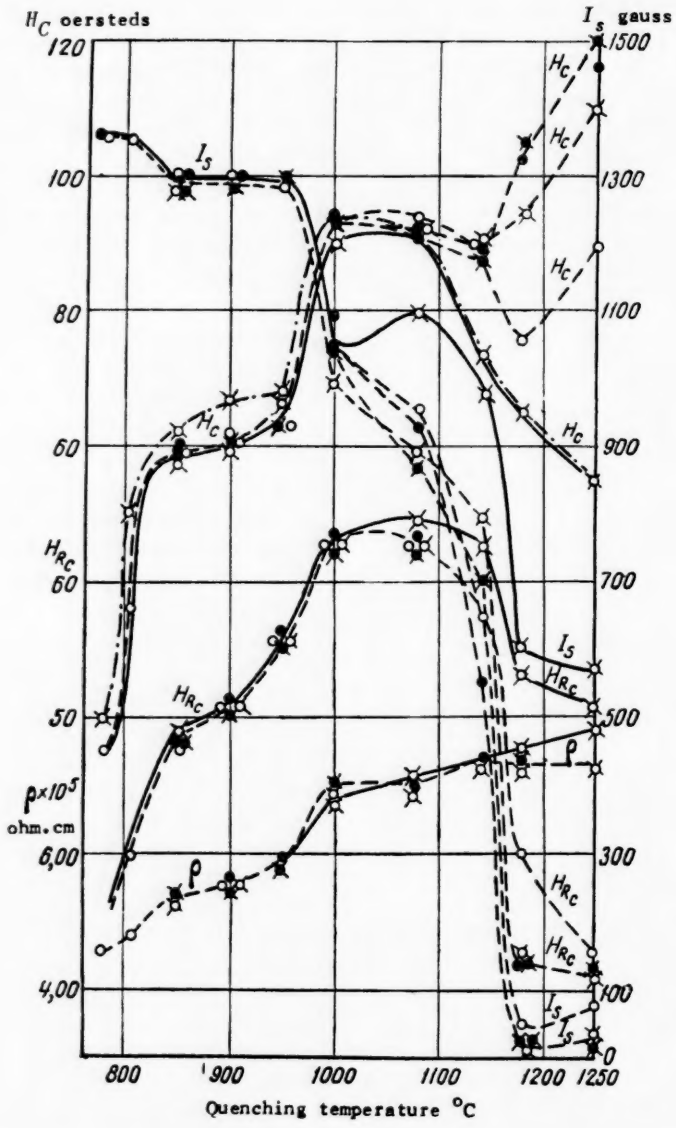

Fig. 5. Magnetic (H_c, I_s), electrical (ρ) and mechanical (H_{R_C}) properties of steel Kh12F1 after quenching from various temperatures into oil maintained at room temperature. The duration of specimen holding at the quenching temperature was 15 min.

However, the rapid rise in the coercive force values as observed after quenching from temperatures of $T > 1140^{\circ}C$ no longer corresponds to a small increase in the concentration of the solid solution because of the dissolution of a small amount of the cubic carbide of chromium $Cr_{23}C_6$ and of the vanadium carbide VC.

The specimen with depleted surface layer, in which the martensite transformation has penetrated deeper, shows that its coercive force value is much lower, while after treatment with cold, the value of coercive force drops instead of rising. Finally, the coercive force value, was measured at the liquid nitrogen temperatures, was found to be

practically identical with that determined at room temperatures. All such considerations, point to the fact that the nature of the coercive force is, in this case, quite different from the typical "martensitic" coercive force as determined according to equation (3).

It can be assumed that the martensite needles have a two-dimensional magnetic anisotropy of form and stresses in the needle plane, owing to the action of compressive, homogeneous stresses acting from the direction of the surrounding austenite. Thus, additional limitations are thereby imposed on the displacement processes and a basically different mechanism of remagnetisation is postulated, i.e. the rotation mechanism [15,17].

3. EFFECT OF INITIAL MICROSTRUCTURE ON THE MAGNETIC PROPERTIES AFTER QUENCHING

The above subject was partly dealt with in work [3] and all of the work [6] was devoted to it. It is known [20,21] that the coarse globular pearlite passes into solid solution on heating at a much slower rate than the fine-grained one. The plastic and especially fine, lamellar carbides dissolves in austenite much faster than the grained ones. Under all conditions, the rate of dissolution is affected also by the grain size of ferrite [21].

The present investigation was carried out on two steel ShKh15SG specimens with completely different initial structures, the specimens being in the form of cylinders with the height of h = 23 mm and 25 mm in diameter (D = 25).

The first group of test specimens (II) had in its initial state the structure of regular grained pearlite with coercive force of 9-11 ergs and a hardness of the order of 190-230 H_B.

The second group of test specimens (IV) had the structure of lamellar pearlite with coercive force of 21-28 ergs and a Brinell hardness of 293-326.

The coercive force before and after quenching was determined at the maximum magnetizing field of 7000 ϵ, while the saturation magnetisability was determined by the differential method in fields of 3000-7000 ϵ.

The testpieces were quenched under the same conditions as used for impact strength testing, with the only difference in that the holding period during heating was increased to 60 min.

The curves given in Fig. 6 show that the lamellar pearlite (IV) has, after quenching from the temperatures of 780-900°C, a higher coercive force than that of grained pearlite (II). After quenching from temperatures exceeding 900°C, on the other hand, the position is reversed: the lamellar pearlite (IV) gives a lower coercive force than the grained one (II).

During quenching from 780-900°C, this is, obviously, connected with the fact that, in the case of a more highly dispersed initial structure, the highest concentration of the solid solution is reached earlier than in the case of the grained pearlite.

During quenching from temperatures exceeding 900°C, the influence of different grain growth rates begins to make its contribution as the quenching temperature is increased. Of course, retarded grain growth is to be expected in the case of grained pearlite. In a close relation with this fact is also the difference in the saturation magnetisability values (different contents of residual austenite) after quenching of the group (II) initial structures. In fact, specimens of groups (II) have a higher saturation magnetisability (less austenite) than those of group (IV), in spite of the use of identical quenching temperature and other conditions.

In Fig. 7 is shown the relationship between coercive force and the residual austenite concentration, % $A = \frac{\alpha_g}{11,5}$ for the two groups of test specimens: (II) and (IV).

It could be expected that, irrespectively of the initial micro structure, the presence of acicular martensite (overheating) will be detected in the quenched steel at approximately the same value of the residual austenite content ($\sim$20%). A detection of overheating e.g. during the quenching of ball bearings, represents an important problem.

In Fig. 7, the structure-less pseudo-crystalline martensite has corresponding to it a band limited by a semi-open rectangle

ab. Line *a* divides troostite on the left, arising from underheating, while line *b* separates the acicular martensite on the right.

Line *a-b* separates from below the material rejected because of underheating, the initial structure of which is in the form of coarse-grained, (globular) pearlite possessing a characteristic and very irregular carbides content.

Numerous comparisons of microstructure and hardness with coercive force values and magnetisability as determined on specimens of roller bearing shafts (steel ShKh15 and ShKh15SG) after their quenching, show that the concepts put forward above are correct. The same ideas served as a basis of methods developed for the control of quenching quality in terms of variations in the coercive force and saturation magnetisability of steel [22].

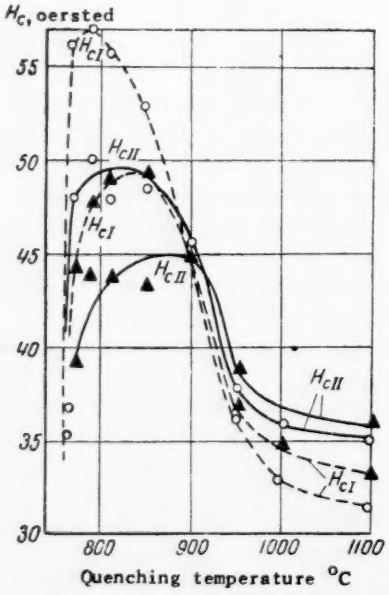

Fig. 6. Coercive force of steel ShKh15SG after quenching from various temperatures into oil at room temperature and subsequent treatment with cold (-196°C): H_{cI} - after quenching; H_{cII} - after cold treatment; ▲ initial structure of grained pearlite; o initial structure of lamellar pearlite.

Overheating of steel Kh12F1 to temperatures higher than 1100°C leads to an intensive grain growth and to a concentration of the remaining insoluble carbides in the vicinity of grain boundaries. This results in a rapid lowering of the mechanical strength properties (hardness, strength, etc.). An underheating (<1000°C) leads usually to a lowering in hardness.

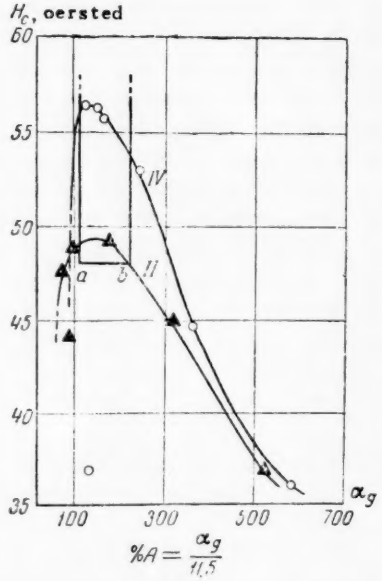

Fig. 7. Coercive force and the residual austenite content (%A) after quenching of grained (II) and lamellar (IV) pearlites in steel ShKh15SG from various temperatures in oil maintained at room temperature.

According to Fig. 5, both types of failure can be detected quite clearly from magnetisability measurement data at a sufficiently high magnetic field.

4. ON THE MAGNETIC PROPERTIES AND HARDNESS OF SPECIMENS WITH SURFACE LAYER DEPLETION DURING THE PROCESS OF HEATING PRIOR TO QUENCHING

As it is clear from Table 2, the specimens heated prior to quenching without the provision of any means of protecting them against chemical interaction with the surrounding medium, have shown a considerable loss in weight Δp. This loss in weight was accompanied by an extensive depletion of their chemical composition, as it can be seen by examining the chemical analysis data. In Table 3, are given the results of chemical analyses carried out on shavings taken from

TABLE 3

Chemical analysis data on shavings removed from ring-shaped specimens at various depths below the surface

Depth below surface, in mm	KhV-5			ShKh15SG		Kh12F1	
	%C	%Cr	%W	%C	%Cr	%C	%Cr
0-0.40	0.47	0.05	–	0.60	1.30	1.30	11.2
0.40-0.60	0.72	trace	–	0.60	1.30	1.25	12.3
0.60-1.00	0.91	as above	–	0.75	1.40	1.20	12.5
1.00-1.40	1.38	0.33	5.2	–	–	–	–

various depths of ring-shaped specimens heated to 1200°C for 15 min in a slat bath consisting of $BaCl_2$.

The thickness of the ring-shaped specimen was 5 mm, i.e. it was only half of the thickness of impact strength testpieces.

The presence of an extensive depletion in test specimens heated prior to their quenching to a temperature $T > 1000°C$ (in $BaCl_2$ salt bath) is shown also by H_{R_C} hardness test data, which are given in Fig. 1-3 and in Fig.5, as well as by the magnetic properties data shown in Fig. 1-5.

The hardness of specimens with a depleted layer is higher by more than ten Rockwell hardness units than that of the same specimens whose surface layer has been ground away to a depth of 1 mm. On the other hand, the hardness of specimens heated to the same high temperatures but in a protective atmosphere, remains at the same value before and after the removal of a surface layer with a thickness of 1 mm and it is equal to the hardness value of the depleted specimens after this depleted surface layer has been removed by grinding.

The saturation magnetisability of the depleted specimens, as well as their coercive force, have a clearly shown tendency to higher values and this is the higher the higher the temperature to which the specimen is heated prior to its quenching (see Fig. 1-4).

The changes in the magnetic properties and hardness as observed in the case of depleted test specimens is associated with the simple fact that there is a deeper penetration of the martensitic transformation in their surface layers (up to 1-1.5 mm), which is brought about by an *increase of the martensite point in the surface layer**.

The difference in the structure of the surface layer and that of the body of the specimens, as indicated above, was detected microscopically.

CONCLUSIONS

1. The course of coercive force variation after quenching for the pseudo-crystalline martensitic structure of high-carbon chromium, manganese and tungsten steels, reflects the degree of saturation of the solid solution with carbon and the alloying elements present and, therefore, it is parallel to the variations in the hardness and specific resistance values. Owing to this fact, the measurement of coercive force can serve as in indication of the solubility of the various carbide phases during the process of steel heating.

A regular pattern of coercive force variation has been detected with increasing quenching temperature, this being true provided that the structure of steel after quenching remains pseudo-crystalline.

After the dissolution of all carbides, the

* In a series of investigations [7], use was made of specimen heating in atmospheric air right up to very high temperatures (1000-1100°C) and of prolonged holding periods (up to 30 min.). Additional tests showed that an extensive depletion affects in this case the whole of the specimen volume and the hardness value of H_{R_C} = = 58 ~ 60 at the depth of 2-3 mm below the surface, points exactly to the presence and not to the absence of depletion.

steel becomes overheated and this fact is manifested by an intensive grain growth, an acicular nature of martensite particles, a drop in the mechanical strength properties, a rapid rise in the residual austenite concentration and by a drop in the hardness value.

Once the overheating has set in, there occurs a drop in the coercive force of the martensitic class steels, while austenitic steels, containing only small proportions of martensite after quenching, show a rapid increase in their coercive force values.

The pattern of coercive force variation after quenching, as described above, is explained satisfactorily by the stress and inclusion theories [13-16]. On the other hand, a rapid rise in coercive force in steels, which are almost austenitic (of the Kh12F1 class) and which are subjected to a high degree of overheating is, clearly, connected with the anisotropy of the form and stresses of martensite lamellae (needles) [15, 17].

2. An investigation of the behaviour pattern of coercive force and magnetisability during the quenching of specimens with clear differences in their initial structure (grained pearlite, lamellar pearlite) points to a relationship between the magnetic characteristics and the grain size of steel. Numerous comparisons of the microstructure and hardness values with the coercive force and magnetisability after quenching, give results which lend support to the method of controlling the quality of quenching by the data obtained from the measurement of the coercive force and magnetisability. This method, the use of which was put forward by the present authors some time ago, is capable of detecting unequivocally both of the two types of defective quenching treatments: underheating and overheating [22].

3. In the region of high quenching temperatures, $T > 950°C$, even during heating in a bath of molten $BaCl_2$ and its periodic deoxidation, there sets in a certain surface depletion in the chemical composition of the specimens (to a depth of the order of several mm, depending on the period of its holding at the quenching temperature) and, as a result, there is a considerable increase in the hardness value at the specimen surface in comparison with that in the body of the specimen, while the saturation magnetisability and coercive force values rise, the rate of this increase being the higher is the quenching temperature employed. By removing the depleted surface layer by means of grinding, or by taking precautions in order to prevent the chemical interaction of the specimen with the surrounding medium, it is possible to prevent the depletion of the surface layers and thereby to guard against the setting in of highly anomalous variations in the magnetic properties of steel.

Translated by H. Cygielski

REFERENCES

1. S.V. Vonsovskii and M.N. Mikheev, *Zavodsk. laboratoriia*, No.10, 1221 (1957).
2. V.S. Mes'kin, Ferromagnitnye splavy (Ferromagnetic alloys), State United Scientific and Technical Publishing House, 1937.
3. R.S. Deah and C.Y. Clayton, *Trans. Amer. Soc. for Metals*, 26, 237 (1938).
4. M.V. Dekhtiar, V.I. Malovitskaia and V.I. Shur, *Zavodsk. laboratoriia*, No.1, 70 (1946).
5. V.K. Vainshtein and B.G. Livshits, *Zh. tekh. fiz.*, 19, 871 (1949).
6. Ia.R. Rauzin and V.I. Malovitskaia, *Zh. tekh. fiz.*, 21, 1504 (1951).
7. M.N. Mikheev, I.A. Kuznetsov, V.A. Kruikova and B.M. Neizvestnov, *Fiz. met. metalloved.* 3, 229 (1956).
8. I. Mirkin and M.E. Blanter, *Metallurg*, No.8 (1940).
9. Ia.S. Umanskii and N.T. Chebotarev, *Izv. Akad. Nauk SSSR*, 15, No.1 (1951).
10. A.P. Guliaev *Novoe v metallovedenii (News in metal working)*, Mashgiz, (1948).
11. A.P. Guliaev and E.A. Lebedeva. *Issledovanie stali marki Kh12F1 (Investigation steel Kh12F1)*, All-Union Instrument Scientific Research Institute, Mashgiz, (1952).
12. M.E. Blanter, *Zh. tekh. fiz.*, 17, No.5 (1947).
13. E.I. Kondorskii, *Zh. exp. tekh. fiz.*, 7, 1117 (1937).
14. M. Kersten, *Phys. Zh.*, 44, 63 (1943).
15. S.V. Vonsovskii and Ia.S. Shur, *Ferromagnetism (Ferromagnetism)*, State United Publishing Houses, Moscow, (1948).
16. E.I. Kondorskii, *Dokl. Akad. Nauk SSSR*, 63, 5 (1948); 68, 1 (1949).

17. E.I. Kondorskii, *Izv. Akad. Nauk SSSR*, No.4, 398 (1952).
18. G.V. Kurdiumov, *Problemy metallovedenia i fizyki metallov (Problems in metal working and metal physics)*, Symposium No.4, 321 (1955).
19. B.Ia. Pines, *Dokl. Akad. Nauk SSSR.*, 103, No.4, 601 (1955).
20. Goran Molinder, *Acta Metallurg.*, 4, No. 6, 565 (1956).
21. M.I. Maslennikova and Ia.R. Rauzin, *Zh. tekh. fiz.*, 20, 694 (1950).
22. M.N. Mikheev, G.S. Tomilov, M.F. Pomukhin, K.G. Riaznikin and V.A. Utkina, *Zavodsk. laboratoriia*, No.5 (1956).

VOL.
8
1959

NICKEL-CADMIUM FERRITES*

N.A. SMOLKOV and S.A. GUSHCHINA

M.V. Lomonosov Moscow State University

(Received 12 February 1959)

The results are reported of an investigation of the Curie point and static magnetic characteristics of the solid solution of nickel and cadmium ferrites. A determination was made of compositions having good characteristics at ultra-high frequencies.

Nickel-zinc ferrites have found wide applications in the field of telecommunications [1-3] and their solid solutions with lithium ferrite as shown by Weicz [4] give magnetic materials with a small tangent to the angle of loss at radio frequencies of tens of megacycles.

According to Weicz's data, the zinc ferrite can be replaced fully in the above solutions with cadmium ferrite, which, at identical molar ratios as in the case of zinc ferrite, lowers considerably the Curie point. Lithium-cadmium ferrites were studied previously [5] whereas, to our knowledge, no data have been reported as yet with regard to the properties of the solid solutions of nickel-cadmium ferrites.

For the purpose of our investigations, we have prepared by the ceramic technology techniques, eleven compositions with the general formula of $Ni_{1-x}Cd_xFe_2O_4$, in which the value of x varied from 0 to 1, through the steps of 0.10. Fe_2O_3 and CdO of the "ChDA" class and NiO of "Ch" class were used as starting materials. The test specimens were pressed under a pressure of 3 tons/cm^2. In order to obtain material with high magnetic properties, the batch was dried after its grinding and sieving and it was then subjected to a preliminary firing for 3 hr at 950°C, which was followed by regrinding and mixing with a plasticizer (polyvinyl alcohol). From the compressed-powder material thus obtained, the specimens were now prepared by firing at the temperature of 1245°C for 3 hr. Test specimens prepared without a preliminary firing stage were found to have low magnetic characteristics.

CURIE POINT AND STATIC MAGNETIC CHARACTERISTICS OF FERRITES

The Curie point Θ_k of ferrites was determined from the drop in the values of induction of a coil with ferrite core during heating, while the static characteristics: initial and maximum magnetic permeabilities, μ_0 and μ_{max}, the coercive force H_c and the residual and maximum magnetic inductions, B_r and B_m were determined on torroidal specimens using a ballistic apparatus. The results obtained in measurements of Θ_k, μ_0, μ_{max}, H_c, B_r and B_m as a function of the chemical composition are given in Fig. 1-4.

The nature of these results can be explained as follows. Nickel ferrite has the structure of inverse spinel, i.e. in the $NiFe_2O_4$ molecule, one Fe^{3+} atom is situated in the tetrahedral centre, or at the point *A*, whereas a second Fe^{3+} atom and the Ni^{2+} ion occupy the octahedral centres or points *B*. Cadmium ferrite has the structure of the normal spinel, i.e. in the molecule of $CdFe_2O_4$, position *A* is occupied by the Cd^{2+} ion while both of the Fe^{3+} ions are at point *B*. Inasfar as in ferrites, there exists, according to Neel's theory [6], a strong negative interaction between the ions situated at *A* and those situated at *B*, or, in other words, there

*Fiz. metal. metalloved., 7, No. 5, 557-561, 1959.

exists a strong negative interaction *AB* and a less strong negative interaction *AA* and *BB* and, since the magnetic moments $2S$ of the ions are equal to $2S_{Fe^{3+}}=5\mu_5$, $2S_{Ni^{2+}}=2\mu_5$ and $2S_{Cd^{2+}}=0$ (where μ_5 is the Bohr magneton), then the theoretical molecular magnetic moments of ferrites are: of the nickel ferrite: $n=2S_{Fe^{3+}}+2S_{Ni^{2+}})-2S_{Fe^{3+}}=2\mu_5$ and of the cadmium ferrite $n=(2S_{Fe^{3+}}-2S_{Fe^{3+}})-2S_{Cd^{2+}}=0$.

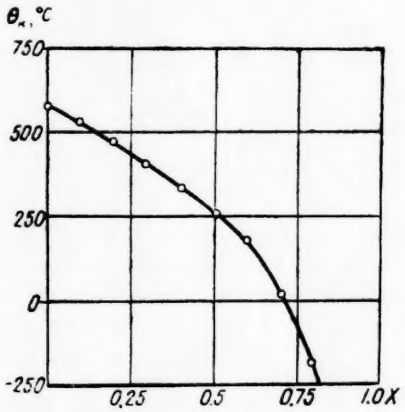

Fig. 1. Variation of the Curie point with the composition of the $Ni_{1-x}Cd_xFe_2O_4$ ferrites.

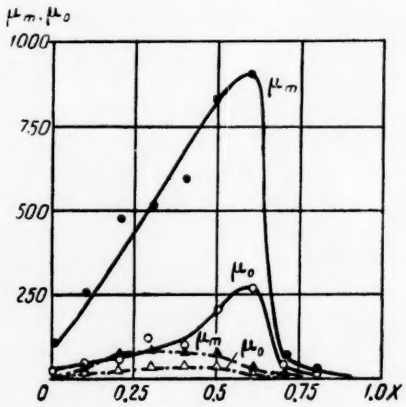

Fig. 2. Dependence of the initial and maximum magnetic permeabilities of the $Ni_{1-x}Cd_xFe_2O_4$ ferrites on their composition.

It is known from Gorter's experiments [7], that the molecular magnetic moment n of $NiFe_2O_4$ is equal to 2.3 μ_5 and that for $CdFe_2O_4$ it is zero. The deviation of the experimental n from the theoretical value of 2 μ_5 for $NiFe_2O_4$ is explained as being due to addition of the orbital moment to the spin moment, which is also confirmed by the cleavage factor of the nickel ferrite, whose value is higher than 2 ($q>2$).

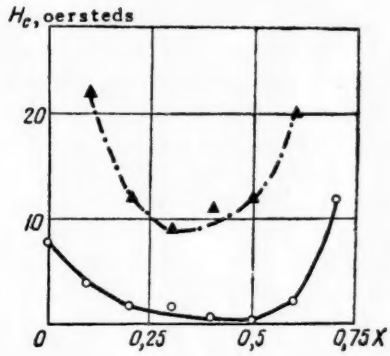

Fig. 3. Dependence of coercive force H_c of the $Ni_{1-x}Cd_xFe_2O_4$ ferrites on their composition. Continuous line curve refers to ferrites with preliminary firing and the discontinuous one to those prepared without it.

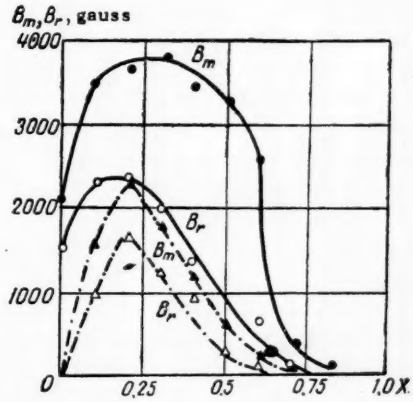

Fig. 4. Dependence of the residual and maximum magnetic inductions (B_r and B_m) on the ferrites composition. Continuous line curves refer to ferrites with preliminary firing and the discontinuous ones to those prepared without it.

On substituting Ni^{2+} ions in the nickel ferrite with Cd^{2+} ions, the *AB* interaction diminishes, i.e. there is a reduction in the exchange interaction and, consequently, the Curie point Θ_k is lowered. But, as long as the interaction *AB* will, irrespective of its reduction, continue to overcome the weaker interactions *AA* and *BB*, there will occur a

drop in the partial magnetization at A and a rise at B, in consequence of which the molecular magnetic moment n will diminish and this will manifest itself in the increased induction B_m of the material, as it is shown in Fig. 4. But, when the interaction AB weakens to such an extent that the weak interaction BB begins to play a significant role, the partial magnetization will diminish not only at A but also at B and then n, and consequently also B_m (Fig. 4) will begin to diminish and the lowering of the Curie point will be much sharper as it is shown in Fig. 1.

A reduction in Θ_k in a mixed ferrite with increasing extent of nickel ions replacement by the cadmium ions, leads, in fact, to a drop in H_c and to a rise in μ_o and μ_{max}. But, since the data given in Fig. 2 and 3 refer to room temperature, T_{room}, then the drop in H_c and the rise of μ_o and μ_{max} will continue until the Curie point of the solid solution becomes $\Theta_k \leqslant T_{room}$, after which H_c will rise again and μ_o and μ_{max} will drop sharply.

HIGH FREQUENCY PROPERTIES OF FERRITES

With the help of a previously developed test procedure [8], a study was made of Faraday's effect on ferrite test specimens, which were cylindrical in shape and had the length of 55 mm and diameter of 5 mm, at room temperatures and a frequency of 9370 kc/s. In Fig. 5 is shown a curve of the relationship between the polarization plane angle of rotation ϕ in $Ni_{1-x}Cd_xFe_2O_4$ ferrites, at a fixed value of the magnetizing field of H = 460 oersted, and the ferrite chemical composition. An examination of the curve shows that the highest value of angle ϕ is given by the following compositions: $Ni_{0.9}Cd_{0.1}Fe_2O_4$ and $Ni_{0.8}Cd_{0.2}Fe_2O_4$.

Using also the above frequency, a determination was made of the high-frequency efficiency Q of ferrites at a constant magnetizing field H = 600 oersted. The measurements were made on ferrite, flat needle-shaped specimens, 3 x 7.5 x 95 mm in dimensions, using an apparatus whose diagram is shown in Fig. 6. This apparatus served for determination of the phase shift $\Delta\phi$ and of the damping δ in decibels. The data thus obtained were used for claculation of the high-frequency performance index Q, i.e. $Q = \frac{\Delta\varphi}{\delta}$.

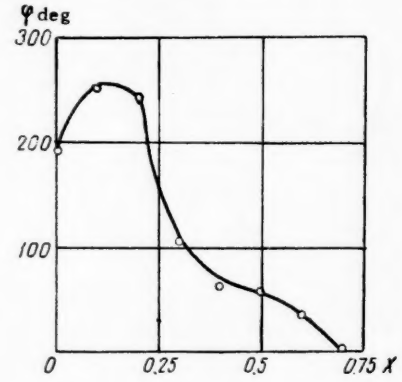

Fig. 5. Dependence of the polarization plane rotation angle ϕ on the composition of $Ni_{1-x}Cd\ Fe_2O_4$ ferrites at a constant magnetizing field equal to H = 460 oersted and for a frequency of 9370 kc/s.

The following method was used for the measurement of phase shift $\Delta\phi$. As it is clear from Fig. 6, the signal produced by the generator 51-I is passed into the resonator of the measurement line by two paths. The phase of the signal, passing through a directional coupler and a waveguide-coaxial transition, is constant with respect to the phase of the generator signal. The wave, however, passing through the ferrite, suffers a phase shift with respect to the generator signal phase and, consequently, also with respect to the phase of the signal fed into the resonator through the coupler and the coaxial transition. By displacing the probe and the resonator of the measurement line along the waveguide, it is possible to make the phases of the two signals which have passed through the measurement line coincide. The coincidence of the phases is detected from the maximum reading of the amplifier No. 1.

The distance Δl, by which the probe of the measurement line is displaced, enables a calculation to be made of the phase displacement $\Delta\varphi = \frac{360°\Delta l}{\lambda}$, where λ is the wavelength in the waveguide. The experimental accuracy in phase displacement measurements is $\pm 2^o$.

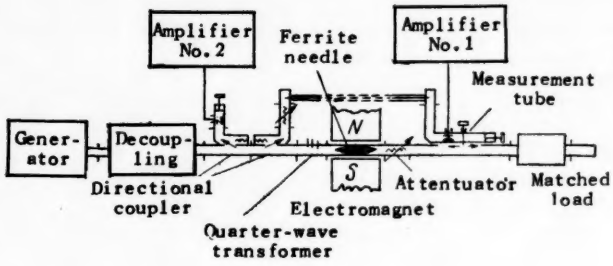

Fig. 6.

In order to determine the loss δ, simultaneously with the measurement of $\Delta\phi$ a determination was also made of the maximum of the signal being transmitted using for this purpose amplifier No. 1, while the maximum of the reflected signal is determined by means of amplifier No. 2. After the above measurements have been carried out, the ferrite needle is removed from the waveguide and, with the help of a quarter-wave transformer, a reflected wave is now created artificially in such a way that its intensity is exactly the same as that obtained during reflection by the magnetized ferrite.

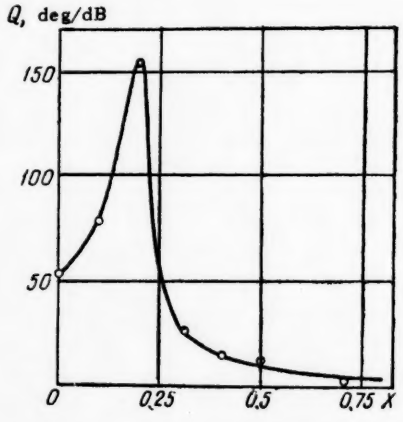

Fig. 7. Dependence of high-frequency performance Q of $Ni_{1-x}Cd_xFe_2O_4$ ferrites on their composition, at the frequency of 9370 kc/s and under a field of H = 600 oersted.

Using a precision attenuator 67-I, the intensity of the signal passing through is reduced to the value corresponding to the ferrite transmission. The readings of the attenuator 67-I give the damping δ produced in the waveguide by the ferrite. As it is clear from Fig. 7, the highest high-frequency performance in the ferrites system here studied was given by the following compositions: $Ni_{0.9}Cd_{0.1}Fe_2O_4$ and $Ni_{0.8}Cd_{0.2}Fe_2O_4$.

CONCLUSIONS

In solid solutions of the nickel and cadmium ferrites, an increase in the cadmium ferrite concentration produces a lowering of the Curie point, an increase in the initial and maximum values of the magnetic permeability, whose maximum is reached in the region of 60% of the cadmium ferrite content and is then followed by a rapid drop, the coercive force reaches its minimum when the cadmium ferrite content is 50%, the residual and maximum values of the magnetic induction (B_r and B_m) reach their maxima in the region corresponding to 20% cadmium ferrite content and the highest value of the polarization plane angle of rotation ϕ and the best high-frequency performance are given by the following chemical compositions: $Ni_{0.9}Cd_{0.1}Fe_2O_4$ and $Ni_{0.8}Cd_{0.2}Fe_2O_4$.

Translated by H. Cygielski

REFERENCES

1. G.A. Smolenskii, *Izv. Akad. Nauk SSSR*, 16, No. 6, 728 (1952).
2. L.I. Rabkin and B.Sh. Epshtein, *Nematel-*

licheskie ferromagnetiki (ferrity) v apparature sviazi (Non-metallic ferromagnetic materials (ferrites) and their applications in telecommunication instruments), Sviazizdat, Moscow, 1955.

3. V.I. Evseev, *Elektrichestvo*, No.9, 23 (1956).
4. R.S. Weicz, *Ceram. Ind.*, 58, No.4, 130 (1952); No.5, 76 (1952).
5. N.A. Smolkov and S.A. Dovba, *Vestnik Moscow State University*, No.4, 155 (1958).
6. L. Neel, *Ann. de Phys.*, 3, 137 (1948).
7. E.V. Gorter, *Progress of Physical Sciences*, 57, No.2, 279 (1955).
8. N.A. Smolkov, *Izv. Akad. Nauk SSSR*, 18, No.3, 378 (1954).

VOL
8
195

GENERATOR OF ULTRA-HIGH PULSE MAGNETIC FIELDS*

I.G. FAKUDOV and E.A. ZAVADSKII

Metal Physics Institute of the Academy of Sciences of USSR

(Received 28 February 1959)

A description is given of a generator of ultra-high pulse magnetic fields (GSMP) capable of producing magnetic field intensities of up to 700,000 oersted by discharge of a battery of condensers. Details are given of the power characteristics of the generator, together with a discription of the electrical circuitry and construction of the coil producing the magnetic field and an account of the magnetic field measurement procedure.

VOL. 8 1959

I. INTRODUCTION

The application of ultra-high magnetic fields widens essentially the range of experimental investigations in the field of solid state physics and enables a complete study to be made of the properties of metals and semiconductors. High-pulse magnetic fields can, obviously, be used also in the investigation of the electro-magnetic properties of liquid metals. Valuable data can also be obtained in this wwy with regard to the mechanism of magnetic phenomena in antiferromagnetic and ferromagnetic materials, by studying their behaviour in ultra-high magnetic fields. The progress made in theoretical physics in the last few years, demonstrates that studies of the magnetic and electro-magnetic properties of solids in the region of high and ultra-high magnetic and electro-magnetic fields and low temperatures, enables important deductions to be made with regard to the character and form of the limiting energy surface of the conductivity electrons.

Ultra-high magnetic fields were first produced by Academician P.L. Kapitsa more than 30 years ago. As a source of energy, Kapitsa employed a special battery of accumulators [1] and, in later work, he used a special generator capable of producing magnetic fields up to 360,000 gauss in a volume of 2 cm^3 [2].

Rault [3] was the first to use a charged condenser as a source of energy for producing magnetic fields up to 50,000 gauss.

In the years that followed, Myers [4] used this latter method and, by employing several coils of his design, he produced fields up to 250,000 gauss.

Subsequent developments in the methods of producing strong magnetic fields went along the line of constructing special coils capable of withstanding mechanically the colossal strains produced during the discharge [5, 6].

In a brief note published by the present authors [7], it was reported that a generator was designed for the production of ultra-high pulse magnetic fields, which were created by discharge of a battery of condensers through a specially constructed coil.

In the present report, a detailed description is given of one of the existing variants of GCMP and a determination is made of the optimum parameters of the apparatus so that magnetic fields up to 700,000 oersted can be achieved.

In the course of our investigations, we have designed, constructed and experimented with numerous types of single-layer and polylayer coils. In the present article, a detailed description is also given of the construction of coils at present in use.

*Fiz.metal. metalloved., 8, No.4, 562-568, 1959.

2. DESCRIPTION OF THE GENERATOR

The design and dimensions of a generator to be used in the production of ultra-high magnetic fields depend to a great extent on the number of condensers and their working potential. Among the serial production condensers at present manufactured in the U.S.S.R., the most effective were found to be the pulse condensers of the IM-3/100 type. In the equipment here described we have used 16 such condensers, which ensures an accumulation of 7200 joules of energy at the nominal potential 3 kV.

By reducing the resistance and inductance of the discharge circuit, it is possible to increase in the coil the portion of energy which is used up directly for the creation of magnetic field. We have succeeded by such means in raising the coil energy utilization coefficient to 17%. To achieve this purpose, we had to use copper busbars with cross-section of 250 mm^2, which were arranged parallel and were separated with textolitic sheets 2.5 mm in thickness.

The discharge of condensers through the coil has an oscillatory character. The damping decrement of the oscillatory discharge, as expressed by the formula: $\Delta = \frac{I_t}{I_{t+T_0}}$, varies in its value from 4 to 6 V depending on the coil dimensions. The oscillation frequency also depends on the coil dimensions and varies in the interval of 3000 to 3500 c/s.

Owing to the comparatively small dimensions of the condensers, the whole apparatus is compact in size and has a form making it ideal for the use in research investigations. The general view of the equipment, as shown in Fig. 1, shows that the magnetic coil is positioned below the busbar plane, which enables the immersion of the whole of the coil, together with the specimen being investigated, into a Dewar flask. In the case of coils of greater diameter, a Dewar flask can be inserted directly inside the coil. The coils can be positioned with their axes both vertically and horizontally.

As a result of prolonged experiments, we have succeeded in constructing a coil with such a strength that it could be used almost indefinitely. The coils used in our present investigations have produced already more than a hundred discharges, during which the current passing through the coil reached values up to 60,000 amps.

3. ELECTRICAL CIRCUITRY OF THE GENERATOR

A battery of condensers is charged through a high-voltage rectifier fed through a

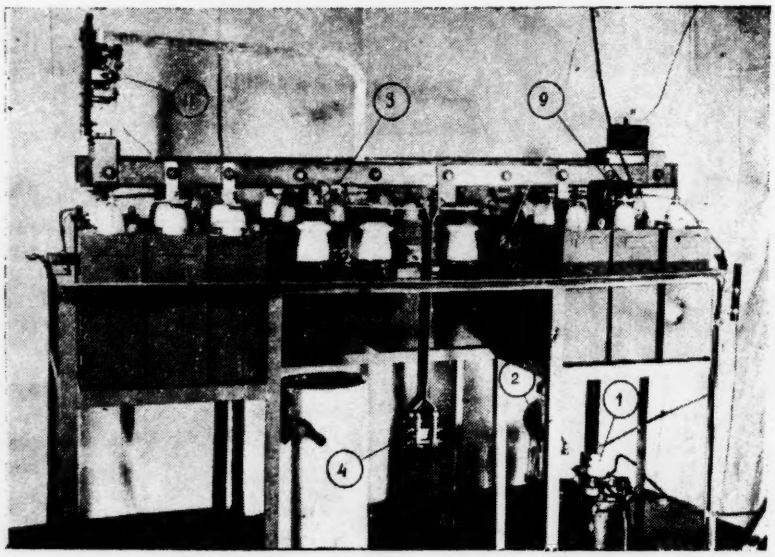

Fig. 1. General view of the apparatus

current-limiting resistor R (Fig. 2). The presence of this resistor limits not only the charge, but it also slows down the rate of discharge, which enables a more accurate control of the potential value at the condensers.

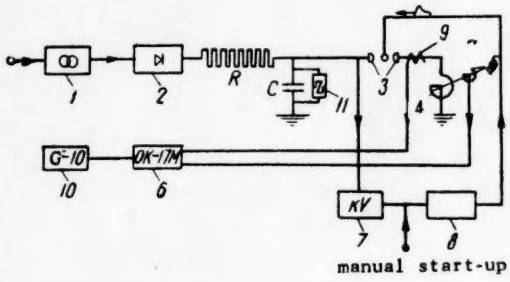

Fig. 2. Block-diagram of the equipment.
1 – step-up transformer; 2 – gas-filled rectifier; 3 – step-by-step discharger with control electrode; 4 – working coil of the generator; 5 – measurement coil; •6 – pulse oscillograph; 7 – contact voltmeter; 8 – control block; 9 – coil of the external switch of the oscillograph scan; 10 – sound generator; 11 – shunting contactor.

The discharge of condenser batteries is carried out through a step-by-step discharger by means of a control electrode *3*. The igniter pulse on the control electrode is fed from a coil either by hand operation, by compressing the hand discharge knob, or automatically, when the required potential is reached on the condensers. The value of this potential is pre-set on a contact kilovoltmeter.

The diagram shown in Fig. 3 enables the discharge process to be carried out automatically, as well as to achieve an optical and sound warning signalling.

The set-up is controlled by means of a control key (*KCh*). The shifting of the key into "in" position closes the contactor K_1 circuit and switches in the control autotransformer connected with the step-up transformer of the charging circuit of the apparatus. On reaching a voltage approaching in value the pre-set discharge voltage, the contact 7-8 KV is closed and the contactor K_2 is switched in, which, in its turn, switches in the coil and RV_1 timer circuit. After the elapse of a short time (during

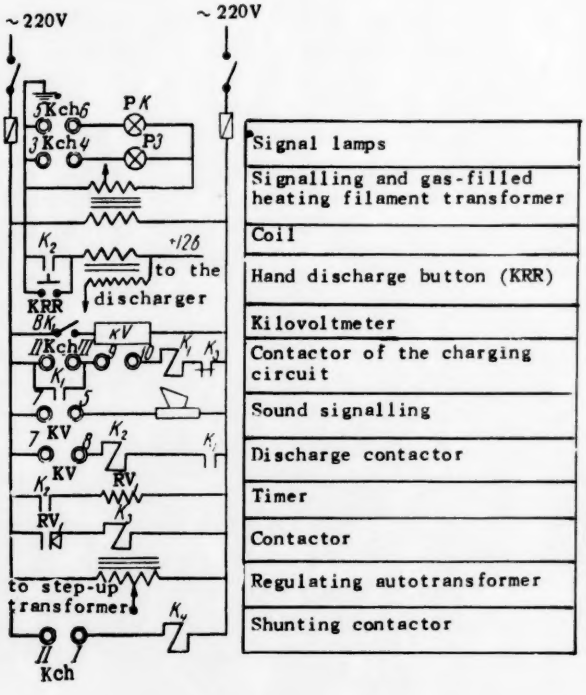

Control key contacts closing programme (KCh)

Key position \ No. of contactors	I–II	II–III	1–2	3–4	5–6	7–8	9–10
Open	–	–	×	×	–	–	–
Pre-closure	–	×	–	–	×	×	×
Closed	–	–	–	–	×	×	×
Pre-opening	×	–	×	×	–	–	–

Program of kilovoltmeter contacts closure (KV)

Position of pointer on the scale \ No. of contactors	7–6	7–5	7–8
Not enough	×	–	–
Too high	–	×	–
Normal	–	–	×

× – contact closed
– – contact open
* – heating filament

Fig. 3. Diagram of control and signalling equipment

TABLE 1

Symbol	Description	Type
KCh	Control key	KUV-1
K_1, K_2, K_3	A.C. Contactors	EP-41/21-B
RV_1	Timer..	EV-214
K_4	Shunting contactor	P-311
	Gas-filled rectifier	VG-236
	Control autotransformer	Lstr-1
	Filament-supply and signalling transformer	OSO-0.25 220/12
KV	Kilovoltmeter	MRShPr-54 with external scale.

which the coil current is established), the timer RV_1 closes the contact RV_1 in the K_2 contactor circuit. Then, contact K_1 opens contactor K_1 thereby shutting off the current in the step-up transformer and passing it to contactor K_2. On opening contactor K_2, an igniter pulse is created in the coil circuit and this produces a discharge of the condenser battery through the coil.

After discharge, the control key should be put in the open position. Shortly after that, the shunting contactor K_4 short-circuits the condenser battery. Simultaneously, a green lamp lights up, which indicates that the apparatus can be safely examined.

An explanation of the symbols used in the description of the apparatus is given in Table 1.

4. DESCRIPTION OF COIL CONSTRUCTION

The essential part of the coil, i.e. its winding, is in the form of a precision-machined spiral (1, Fig. 4). In between the spiral turns textolite collars were inserted 2, 0.4 mm in thickness. The external diameter of the spiral was 30 mm. The internal diameter of the coils, intended for the creation of magnetic fields, was from 4.5 to 16 mm. The total number of windings in the various coils was varied from 12-20, and correspondingly, the coil constant also varied from 7-11 $\frac{\text{erg}}{\text{A}}$. The thickness of each winding was from 1-1.5 mm. The spiral was made in beryllium bronze BRB-2, which was annealed and aged in order to impart to it a high mechanical strength.

In the first variants of the coil, the spiral was in a direct contact with current-carrying face plates 5, but this had to be modified because of spiral burning. A prolonged search for a solution, led to the development of a spiral with massive end-faces, which were in direct contact with the face-plates.

For protecting the spiral against radial expansion, use was made of a steel ring 3 with a textolite bushing 4. In the axial direction, the coil is held together by means of brass rods 6, which are insulated from the face-plates by means of textolite sleeves 7. Although the construction of the coil might appear to be weak, it was good enough to ensure that it had sufficient strength for resisting considerable mechanical stresses, acting in the coil in radial directions, during the passage through it of the discharge current.

The current distribution in the spiral is not uniform. The highest current density, and therefore the maximum mechanical stresses act at the internal surface of the spiral.

Approximate calculations, the results of which were confirmed by test results, showed that a magnetic field of 700,000 oersted is the maximum permissible for a heat-treated beryllium bronze alloy BRB-2 inasfar as its capacity to resist mechanical stresses is concerned.

An extremely important aspect of the work to be carried out concerns the region of the

TABLE 2

Internal diameter in mm	External diameter, in mm	Spiral height, in mm	3% region of field uniformity, in mm
4.5	30	30	9.0
5.5	30	30	8.0
7.5	30	30	7.5
9.0	30	30	7.0
16.0	30	30	5.0

homogeneous magnetic field in the coil. In coils with internal diameters of up to 9 mm, the field along the coil radii can be considered as uniform. In the case of a coil 16 mm in dia., the distribution of the magnetic field is shown in Fig. 5.

VOL. 8 1959

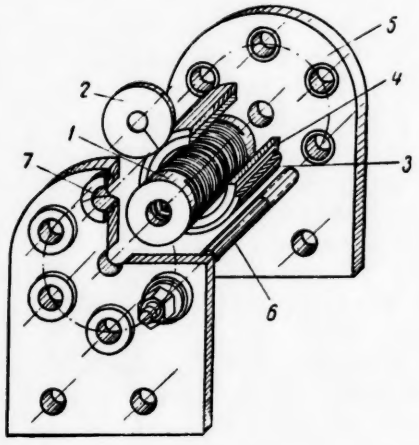

Fig. 4. Coil construction

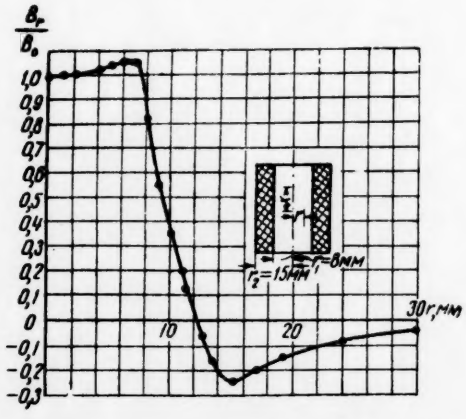

Fig. 5. Radial topography of magnetic field in a coil with 16 mm external diameter.

In Table 2 are given the regions of magnetic field homogeneity, within which the constancy of the field intensity is maintained with an accuracy up to ± 3%.

5. MEASUREMENT OF MAGNETIC FIELD

The induction method is the most suitable for the determination of pulse magnetic field intensity. For this purpose use is made of a measuring coil 5 (Fig. 2), which is placed in the field to be measured and connected through an integrator with a pulse oscillograph. For the synchronization of the scanning, use is made of the pulses from an external coil 9 (Fig. 2).

When the usual R-C integrator is used, the oscillograph output voltage at $\mu = 1$ is:

$$u = \frac{k}{RC}\int u_{vkh}\,dt = \frac{kws}{RC}H, \qquad (1)$$

where, R, C – resistance and capacity of integrator;

k – amplification coefficient of amplifier;

w, s – number of turns and cross-section of the measurement coil;

$u_{vkh} = w\frac{d\Phi}{dt}$ – integrator input voltage.

The factor $\frac{k}{RC}$ can be easily found by feeding a known standard voltage in the integrator input.

It is known from the theory of the R-C integrator operation that the voltage u_1 at the integrator input and u_2, at its output stage, are connected by the following relationship:

$$u_2 = \frac{ku_1}{R\omega C}. \qquad (2)$$

By making use of the expressions (1) and (2), we find quite easily an expression for calculating the magnetic field intensity:

$$H = u_{1k} \frac{1}{\omega_k w s} \frac{u}{u_{2k}} . \qquad (3)$$

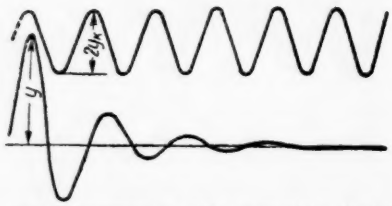

Fig. 6. Oscillograms of the magnetic field intensity and of calibrated voltage, 3 kc/s, 10 V.

In Fig. 6 is shown an oscillogram of a magnetic field and another one of the calibrated voltage. Using the actual value of the calibrated input voltage and expressing the cross-section of the measurement coil in cm^2 and the frequency in c/s, we arrive at an expression for the field intensity:

$$H = u_k \frac{10^8}{\sqrt{2} \pi f_k w s} \frac{y}{y_k} . \qquad (4)$$

Ultra-high pulse magnetic fields were employed by us for studies of electromagnetic phenomena and in investigation of the Kikoin-Noskov effect (photoelectro-magnetic effect) in various semiconductors. Furthermore, we are at present investigating by means of strong magnetic fields the magnetization curves of ferrites.

The experimental techniques employed and the results obtained so far will be reported in other articles.

At the time when the ultra-high magnetic pulse equipment was being developed, an identical apparatus was constructed at the Low Temperature Physics Department of the State Moscow University. For the opportunity of inspecting this apparatus, we wish to express our thanks to Prof. A. I. Shalnikov, Corresponding Member of the Academy of Sciences of the U. S. S. R.

Grateful acknowledgement is also made of the help given in the construction of the equipment here described by I. I. Kuntsevich and A. A. Teterina.

Translated by H. Cygielski

VOL 8 195

REFERENCES

1. K.R. Kapitsa, *Proc. Roy. Soc.* A 105, 691 (1924).
2. P. Kapitsa, *Proc. Roy. Soc.*, A 115, 658 (1927).
3. G. Rault, *Ann. Phy. (Paris)*, 4, 369 (1949).
4. W.R. Myers, *J. Sci. Instr.*, 30, 237 (1953).
5. H.P. Furth and R W. Waniek, *Rev. Sci. Instr.*, 27, 195 (1956).
6. S. Foner and R. Kolm, *Rev. Sci. Instr.*, 27, 547 (1956).
7. I.G. Fakidov and E.A. Zavadskii, *Fiz. met. metalloved.*, 6, 569 (1958).

AN INVESTIGATION OF REACTION DIFFUSION IN BINARY SYSTEMS OF THE "METAL-GAS" TYPE. II*

V.I. ARKHAROV and E.B. BLANKOVA

A.M. Gorkii Ural State University

(Received 20 May 1959)

VOL. 8 1959

In work [1], the principal facts were outlined in connexion with the peculiarities of the diffusion mechanism in systems formed by the transition metals of group IV of the periodic table of elements with sulphur.

Our investigations concerned the behaviour of systems based on the same group of metals, but, as the second component of the system, we used selenium or tellurium instead of sulphur.

Sulphur, selenium and tellurium belong to to the same group VI of the Periodic Table and they are close in their chemical properties. However, on passing from S to Se and Te, the polarizability of atoms increases with rising number of the peripheral electrons around the nucleus. This rise of polarizability, should, in its turn, affect the nature of the bond forces in analogous compounds of sulphur, selenium and tellurium with the same metals.

Chalcogenides of the transition group metals are characterized by the simultaneous presence of various types of bond forces. Thus, in monochalcogenides with the structure of NiAs, ionic bond forces are present side by side with the homopolar and metallic bonds, while in dichalcogenides of the CdI_2, the ionic, homopolar and residual Van der Vaal forces (between the layers) are present simultaneously [2-5]. On passing from sulphur to the more easily polarizable selenium and tellurium, there should be a gradual increase in the relative importance of the homopolar and metallic bond forces. It should be noted that according to Ehrlich's data [6], in a number of transition metals from Ti to Ni, the influence can be observed also of the elements that are the most inclined to the formation of homopolar bonds. To this type belong V and Co; Ti resembles them closely in this respect. On the other hand, the ionic bond forces are shown more in manganese compounds than in similar compounds but of different metals.

In Table 1 are given the results of our investigation of the reaction diffusion mechanism in the Ti-Se, V-Se, Cr-Se, Mn-Se, Fe-Se, Co-Se and Ni-Se systems. The mechanism of diffusion is the same in most of the selenium systems as it is in the sulphur systems. Namely, in the Cr-Se, Mn-Se, Fe-Se and Ni-Se systems there is, in the whole interval of the temperatures investigated (up to 1000°C), a two-directional diffusion of the metal and selenium, which is analogous to the corresponding sulphur systems. In the Ti-Se, V-Se and Co-Se systems, on the other hand, no metal diffusion was detected in the temperature range from the moment of a noticeable scaling to the temperatures of 850, 800 and 700°C, respectively, and practically all the scale formation was as a result of a one-sided diffusion of the metalloid toward the metal-scale internal surface.

It is only at temperatures above the temperature range mentioned that diffusion of Ti, V and Co could be detected. It should be emphasized that a change in the diffusion mechanism occurs exactly in such systems [6] in which homopolar bonds manifest themselves the strongest.

As it was already pointed out previously, the transition from Se to Te as the second component should be accompanied by a *still higher intensification* of the role played by

*Fiz.metal. metalloved., 8, No.4, 569-573, 1959.

TABLE 1

System	Temperature interval, °C	Number of macroscopic layers	Phase composition of scale	Macroscopic characteristics of the diffusion mechanism	Presence of grain in scale layers
Ti-Se	500-850	1	Phase resembling TiSe inasfar as the X-ray analytical data are concerned, but differing from the above compound with regard to the relative line intensity and the presence of additional lines	F*	No
	850-1000	2	In the outermost and innermost layers the presence was found of the same phase that was present at lower temperatures [7,8,10,11]	No change in the specimen shape after annealing	Signs of graininess in the external scale layer
V-Se	450-800	1** –	Phase resembling VSe (of the CdI_2 type) but differing in that it produces additional lines and that its relative line intensity is deformed.	F	No
	800-1000	2 –	Identical phase in the external and internal layers [6-8,11].	F less sharply shown	Grains in the thin external layer
Cr-Se	450-700	1*** –	Phase close to that of β-CrSe (monoclinic structure) but distinguished the presence of additional lines on Debye radiographs	–	Grains indications
	700-1000	2 –	The phase present in the external and internal layers is closely allied to β-CrSe (NiAs type) [7,8,12,13].	–	Graininess of the external scale layer
Mn-Se	600-1000	2	MnSe (Type NaCl) in the external layer of scale; $MnSe_x$ in the internal layer (no identification was possible with phases reported in technical literature [7,8,14].	The specimen has the appearance of a predominant metal diffusion	Graininess in external layer.
Fe-Se	400-940	3	All the three scale layers consist of phases similar to each other roentegonographically. The position of the basic lines resembles that of β-CrSe (phase close to NiAs, but showing an extensive monoclinic deformation, [13,15, 17,20]. Melting point of 950°C	No change in the specimen appearance after diffusional annealing	Graininess in external layer

Table 1 *(continued)*

System	Temperature interval, °C	Number of macroscopic layers	Phase composition of scale	Macroscopic characteristics of the diffusion mechanism	Presence of grain in scale layers
Co-Se	450-700	2	$CoSe_2$ in the external layer (T_h^6), but CoSe in the internal one (structural type of NiAs)	An inert mark is left on the external scale surface.	No
Co-Se	700-950	2	CoSe phase in both the external and internal layers, [7,8,16,19]. The scale melts at 950°C.	An inert mark between the external and internal layers.	Graininess in external layer
Ni-Se	400-700	3 -	$NiSe_2$ in a very thin external layer; NiSe (of the NiAs type) forms the basic thickness of the external skin; Ni_3Se_2 in internal layer. The scale melts at 670°C.	The specimen appearance is characteristic of a predominantly metallic diffusion.	Graininess in the external scale surface.

* F = specimen appearance characteristic of one-sided diffusion of the metalloid.

** *1* or *2* (subscript to figures) means that the number of layers was confirmed by metallographic examination.

***In the interval of the phase layer, the presence was detected of micro-layers.

the homopolar bond forces in the corresponding compounds of the transition metals. According to our postulation, this should be associated with an increase in the significance of the role of tellurium and in a reduction of the role played by metals in the diffusion process (a detailed analysis of the experimental results will be made on another occasion).

In fact, it is clear from Table 2, that in all the metal-tellurium systems, the influence of the metalloid diffusion has a predominant character. For all of the systems investigated, a temperature interval was established in which practically all the scale formation is caused by the diffusion of tellurium, whereas the metal diffusion was detected only at very much higher temperatures.

In the Cr-Te system, no diffusion of Cr was found to occur right up to the temperature at which the scale melts (750°C). But, even at high temperatures, a predominant role in all the systems investigated is played by Te. A somewhat special case is shown by the Mn-Te system in which the diffusion of Mn is detectable already at the temperature of 600°C.*

Thus, a comparison of the experimental data, obtained by us with regard to the diffusion mechanism with the data for the changes in the character of the bond forces in chalcogenides of the transition group metals, enabled us to derive a correlation between the intensification of the relative role of the atomic bonds in the compounds and an increase in the relative role of

* In spite of the fact that MnTe has a higher melting point (1000°C) than CrTe, FeTe, CoTe and NiTe.

TABLE 2

System	Temperature interval, °C	Number of macroscopic layers	Phase composition of scale	Macroscopic characteristics of the diffusion mechanism	Presence of grain in scale layers
Ti-Te	500-600	1	$TiTe_2$ (structural type of CdI_2)	F*	No
	600-850	2	$TiTe_2$ in the external layer; $TiTe_x$-phase intermediate between TiTe and $TiTe_2$.	F	No grains in external layer but signs of graininess in the internal one
	850-1000	2	Both the external and internal layers consist of the $TiTe_y$ phase ($\leqslant y \leqslant 2$) with a very weak diffraction picture, [7-10].	Diffusional annealing has no effect on the specimen appearance	Graininess in external layer
V-Te	500-850	2	VTe_x in the external layer and VTe_y in the external one resemble closely each other on radiograms.	F	No
	850-1000	2	VT_y in the external and internal layers [6-8, 13].	F shown less clearly	Grain in a thin external scale layer.
Cr-Te	500-600	1 (?)	A very thin scale layer consisting, clearly, of the CrTe phase (monoclinic) [7,8,12].	-	No
	650-700	3	$CrTe_x$ (monoclinic). $CrTe_y$ (monoclinic) differs slightly from $CrTe_x$. CrTe has a structure close to that of NiAs. Melting point of 750°C.	An inert mark remains on the external scale surface	No
Mn-Te	500-1000	2	A phase resembling MnTe (structural type of NiAs) present in both the external and internal layers, but it differs by the presence of some additional weak lines in radiograms. Melting point of 1000°C [7,8,14].	No change in the specimen appearance after annealing	In the temperature interval of 600-700°C there are signs of grains in the thin external layer. Between 700-1000°C grain are present in the external scale layer.
Fe-Te	500-700	2	$FeTe_x$ phase with a low symmetry structure, which in line distribution, resembles closely $FeTe_2$ but differs from it in the relative line intensity.	An inert mark is left on the external surface	No

Table 2 *(continued)*

System	Temperature interval, °C	Number of macroscopic layers	Phase composition of scale	Macroscopic characteristics of the diffusion mechanism	Presence of grain in scale layers
Fe-Te	700-1000	2	$FeTe_x$ in the external and internal layers; Melting point of 950°C. [16-19].	–	Signs of graininess in external layer.
Co-Te	500-600	2	The phase present in the external layer resembles $CoTe_2$ (D^3_{3d}) and that of the internal layer is similar to CoTe (structural type of NiAs).	An inert mark left on the external surface	No
	600-750	2	In the external layer the structure of $CoTe_x$, which resembles $CoTe_2$ (rhombohedral) and in the internal layer the structure is similar to CoTe.	An above	No
	850-950	2	$CoTe_x$ in the external and internal layers. Melting point of 950°C. [16, 20].	Masked inert mark	Signs of grains in the external layer.
	400-800	2	$NiTe_x$ in the external layer and $NiTe_y$ in the external one; phases with structure of low symmetry and could not be identified as resembling any known compound phase.	–	No
	800-950	2	Phases forming the external and internal layers resemble closely $NiTe_y$. Melting point of 950°C. [21, 22].	–	No

* For meaning of symbols see footnote to Table 1.

metalloids during diffusion.

Translated by H. Cygielski

REFERENCES

1. V.I. Arkharov and E.B. Blankova, *Fiz. met. metalloved.*, In print.
2. N.V. Ageev, *Prirodw khimicheskoi sviazi (The nature of chemical bond)*, *Acad. of Sci. of the USSR*, Moscow-Leningrad, 1947.
3. E.S. Makarov, *Izv. Akad. Nauk SSSR*, 4, 201 (1944).
4. A.J. Cornish, *Acta Metallurgica*, 6, 5, 371 (1958).
5. E. Mooser and W. Pearson, *Phys. rev.*, 101, 5, 1608 (1956).
6. P. Erlich, *Zs. anorg. allg. Chem.* 260, 1-6, 19 (1949).
7. G.B. Bokii, *Vvedenie v kristallochimiu (Introduction to crystal chemistry)*, *Moscow State University*, 1954.
8. Landlot-Bornstein, *Atom und Molekularphysik*, 4, Berlin, Springer-Verlag, 1955.
9. P. Erlich, *Zh. angewand. Chem.*, 60A, 68 (1948).
10. P. Erlich, *Zs. anorg. allg. Chem.*, 260, 1-6, 1 (1949).

VOL. 8 1959

11. E. Hoschek and W. Klemm, *Zs. anorg. allg. Chem.*, 242, 49 (1939).
12. H. Haraldsen, *Zs. anorg. allg. Chem.*, 239, 1-4, 369 (1938).
13. H. Haraldsen, *Zs. anorg. allg. Chem.*, 234, 372 (1937).
14. N. Elliot, *J. Amer. Chem. Soc.*, 59, 1958 (1937).
15. G. Hagg and A.L. Kindstrom, *Zs. Phys. Chem.*, 22, 453 (1933).
16. S. Tengner, *Zs. anorg. allg. Chem.*, 239, 126 (1938).
17. F. Gronvold and H. Haraldsen, *Acta Chem. Scand.*, 8, 1927 (1954).
18. Sh. Chiba, *J. Phys. soc. Japan*, 10, 837 (1955).
19. R.H. Tompson, *The Amer. Mineralogist*, 32, 3-4, 210 (1947).
20. H. Haraldsen and F. Gronvold, *Zs. anorg. allg. Chem.*, 283, 143 (1956).
21. G.R. Levi and A. Baroni, *Zs. Kristallogr.*, 92, 211 (1935).
22. R.P. Agarvala and A.P. Sinha, *Zs. anorg. allg. Chem.*, 289, 203 (1957).

THE PROBLEM OF THE STATE OF CARBON AND IRON IN STEEL*

I.N. FRANTEVICH, D.F. KALINOVICH and I.IO KOVENSKII

Institute of Metalloceramics and Special Alloys,
Academy of Sciences of USSR

(Received 25 August 1958)

It has been demonstrated that all carbon atoms in austenite are in the form of positive ions. It has been concluded from the literature that there exists an analogous state of carbon in ferrite. It has been demonstrated that part of the iron atoms in austenite are negatively ionized, at which the extent of ionization drops in the same proportion as the temperature increases from 900°. The mean value of ionic charges of carbon and iron has been computed.

It has been proved that the conceptions of Hume-Rothery concerning the presence of a covalent combination of carbon atoms in austenite and the formation of positive and negative carbon ions compensating each other during the decomposition of these combinations under high temperatures, appear to be incorrect.

VOL.
8
1959

The clarification of the problem of interrelations between the iron and carbon atoms in ferrite and austenite appears to be extremely important for the development of the theory of iron-carbon alloys. It is known that these interrelations have been studied over a long period of time by a number of authors from the point of view of neutral atoms existing in the mentioned solid solutions. However, even in 1934 Lebedev came to the conclusion that the existence of atomic species in the ionic state [1] must be assumed in the solid solution of carbon in iron, whereby carbon must exist in this solution in the form of ions C^{4+}.

The ionic state of carbon in α and γ iron was experimentally demonstrated by other authors. In these experiments, a migration of carbon atoms in the solid solution in the direction of the cathode was observed under the influence of a constant electrical field. We shall call this phenomenom electro-migration. The papers of Seith, Kubaschewski [2], Prosvirin [3], Lebedev [4], Pomadin [5], Guterman and Lebedev [6,7], Dayal and Darken [8], were devoted to the study of electro-migration in austenite.

The applied metallographic or chemoanalytical methods of recording the effect of electro-migration severely limited the possibilities of research in these operations with regard to the quantitative definition of the obtained results. It should be borne in mind that the visible effects of migration can take place under considerable densities of current passing through the specimens during the experiments to create an electric field as well as to heat the test-pieces, and that in order to ensure the high current density, light-gauge specimens have to be used, which are inadequate for usual chemo-analytical determinations. A methodical inadequacy of a greater number of investigations was, that the electro-migration has been observed indirectly, through the resultant gradient of concentration along the specimen, which had a uniform composition in its initial state. No correction for the usual diffusion developing in the process of electro-migration was made at the expense of the appearing gradient of concentration.

Some investigators made attempts to deter-

* *Fiz. metal. metalloved.* 8, No.4, 574-578, 1959.

mine the value of the charge of carbon ions in austenite on basis of self-consistent experimental data. As Lebedev and Guterman [9] report, the most likely value of the charge approximates apparently 3 or 4 units. Dayal and Darken [8], having made a number of assumptions, find the value of the charge roughly equal to 4. It must be stressed however, that they obtained this approximate result by discarding the data of one of the experiments, on account of which the value of the charge would be brought down.

Thus, the papers [1-9] have shown that there are positive carbon ions in austenite possessing, in the opinion of the authors [8-9], a charge from 3 to 4 units. However, for some time past, Hume-Rothery questions the presence of permanently existing ions C^{4+} in austenite, considering as unlikely the departure of 4 electrons from each carbon atom in the lattice of austenite under an insufficiently high acceptor-capability of iron atoms. To explain the perceptible effect of electro-migration of carbon to the cathode in austenite, Hume-Rothery submits the following hypothetical description of the mechanism of this phenomenon. In his opinion, the carbon atoms in austenite are found in a co-valent bond with iron atoms. The thermal motions of atoms under high temperatures tend to destroy the bonds and bring about a partial disintegration of these bonds. At the same time, a certain number of carbon ions are formed with an excessive positive charge and an equivalent number of carbon atoms with an excessive negative charge, the latter having been produced at the expense of the migration of electrons to the atoms released by the positive carbon ions. Due to their small size, the positive carbon ions migrate in the lattice of austenite in the process of "electrolysis" and serve, at the same time, as carriers of electricity. The motion of the negative carbon ions is obstructed by their considerable dimensions and their bond with surrounding electro-positive shells of iron atoms.

Investigations carried out by us into the electro-migration of carbon and iron in austenite show conclusively that the explanation of electro-migration of carbon in austenite suggested by Hume-Rothery is erroneous.

In contrast to investigations having been carried out previously, we used in our experiments radioactive isotopes ^{14}C and ^{59}Fe for the indication of atoms participating in the electro-migration.

A radioactive isotope of the element, the electro-migration of which was investigated, was introduced into the central part of the wire specimen made of pure iron. The position of the radioactive zone on the specimen was fixed. A new position of the zone was determined through measuring the distribution of the activity of radiation along the test-piece, after a prolonged high-temperature heating of the specimens with direct current. This measurement was carried out by means of computing the activity of consecutive small parts of the specimens. The results were plotted in co-ordinates on diagrams: the distance of the centre of the part from the end of the specimen indicates the position of this part.

One of the diagrams illustrating the migration of carbon under the action of a permanent electric field is shown in Fig. 1. The experiments were carried out at temperatures of 950, 1000, 1050, 1100, 1150°. The effect of usual diffusion was taken into account by means of carrying out parallel tests on alternating current.

The experiments have shown that all carbon occurring in austenite participates in the process of electro-migration. It can be seen in Fig. 1 that the carburized zone shifted entirely toward the cathode. An analogous picture is observed in all tests.

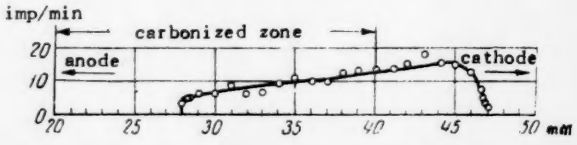

Fig. 1. Shifting of carburized zone as a result of heating the test-piece by direct current at 1100° during 8 hours.

The cited data demonstrate clearly that there are no un-ionized carbon atoms in austenite. All the carbon ions possess a positive charge, which is proved by the complete disappearance of radioactivity at the anode part of the initial carburized

zone. (Fig.1). If negative carbon ions had formed in austenite as well as Hume-Rothery presumes, then the retention of some activity would have been observed at that part. These findings are corroborated also by microstructural analysis of the specimens. Microstructures of a cross-section of the test-piece at the anode part of the initial carburized zone before (Fig. 2,a) and after (Fig. 2,b) the transmission of the direct current through the specimen, are given in Fig. 2. As it is obvious from these figures, the anode part of the specimen freed itself completely of carbon in the process of electro-migration.

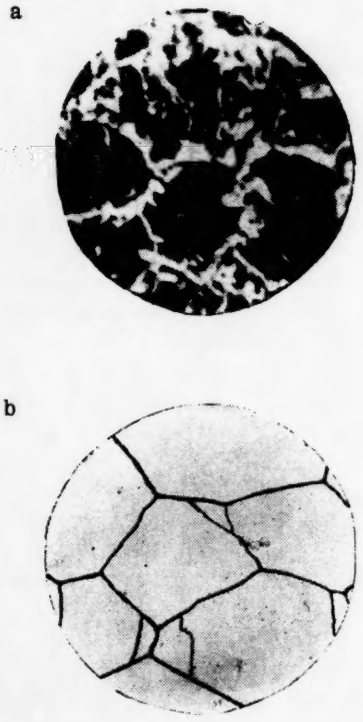

Fig. 2. Microstructure of cross-section of test-piece on anode part of initial carburized zone before (a) and after (b) transmission of direct current through test-piece; 266x.

It was shown in the papers [6,7] that the presence of negative carbon ions is observed in ferrite as well. The authors of treatise [11] demonstrated that all the carbon atoms in ferrite are in the form of positive ions (experiments, beginning at 530° and higher, were carried out). Thus, the description by Hume-Rothery of the formation of ionized carbon as a result of the disintegration of bonds in consequence of thermal motion of the atoms at high temperatures, also turns out to be incorrect.

If, in the absence of carbon, iron atoms behave neutrally during the transmission of direct current [12], then, in the presence of carbon, as was demonstrated by our investigations, the electro-migration of iron atoms to the anode is quite clearly established. Experiments were conducted at temperatures of 900, 950, 1000, 1050, 1100° on iron specimens carburized along their whole length with constant carbon and having in the centre a clearly confined zone of the radioactive isotope ^{59}Fe. One of our diagrams, illustrating the results of our tests, is shown in Fig. 3.

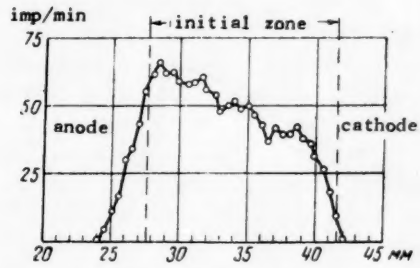

Fig. 3. Shifting of iron zone as a result of heating the testpiece by direct current at 950° during 30 hours.

As it is evident from the figure, a considerable shifting of the anode boundary of the radioactive zone toward the anode takes place. A small shifting of the cathode boundary is brought about by usual diffusion, which is corroborated by the coincidence of the size of the mentioned shifting and the shifting produced in the tests on alternate current. This gives proof of the fact that in the process of electro-migration to the anode not all iron atoms participate, but only some of them, apparently those from the number nearest to the carbon atoms, with which they are in a reciprocal donor-acceptor relationship.

In the paper [13] a formula was deduced permitting the computation of the charges of ions of elements participating in the electro-

migration. The computations have shown that carbon atoms in the lattice of austenite do not lose actually 3-4 electrons but only 1.4 electrons per atom in the whole range of tested temperatures. Iron atoms taking part in the electro-migration accept 4 electrons each at a temperature of 900°, that is a number equivalent to the defect in the 3*d* layer. Their acceptor capacity drops at higher temperatures (at 950°-1100°), the assumption of Hume-Rothery regarding the insufficient acceptor capacity of iron atoms, is not confirmed.

The donor or acceptor role of atoms of the impurity element in the solid metallic solution is determined by the reciprocal distribution of the energy levels of electrons of incomplete shells of the impurity atom and of the Fermi level of the electronic spectrum of the base. The appearance in the lattice of a solution of impure atoms with an excess charge, if these atoms possess a donor capacity, is connected with the development of a nearby deformation of the conduction band and with the appearance of a charge of the opposite sign screening the excess charge of the impurity. This screening charge is distributed partly in the conduction band, and partly in the inner incomplete *d*-shell of the base atoms. The thermal motion of the ions of the lattice of the solution shows a diffusing action on electrons of the conduction zone. It is easy to demonstrate [14] that in all probability the diffusion of electrons will be accomplished not in connexion with $s \rightarrow s$ migrations, but in connexion with $s \rightarrow d$ migrations of electrons, that is, by migrations of electrons from the conduction band to the incomplete *d*-layer of the base atoms. The probability of these migrations will be particularly great in the vicinity of impurity atoms, increasing the share of the potential of perturbation, entering into the value of the square of the matrix term of the form

$$\int \psi_2^* \Delta v \psi_1 d\tau, \text{ where } \Delta v = \xi \frac{\partial v}{\partial x}$$

is the potential of perturbation, appearing in connexion with the migration of the ion accomplishing a thermal fluctuation in an interval ξ in the direction x ψ_1 and ψ_2 are the wave functions, determining the state of the electron in the initial and final state; τ – time of relaxation being determined by the conditions of thermal motion of normal base atoms and impurity atoms with excessive charge. These descriptions comply with the contemporary conceptions regarding the electronic structure of solid metallic solutions [15].

Translated by W.A. Curtis

REFERENCES

1. T.A. Lebedev, *Metallurg (Metallurgist)*, No.5 (1934).
2. M. Seith and O.Z. Kubashewski, *Electrochemie*, 41, no.7, B, 551 (1935),
3. V.I. Prosvirin, *Vestnik metallopromyshlennosti (Bulletin of the Metal Industry)*, No.12, 102 (1937).
4. T.A. Lebedev, *Metallurg (Metallurgist)*, No.11-12, 61 (1940).
5. K.P. Romadin, *Elektroliticheskii perenos v metallicheskikh zhidkikh i tberdykh rastvorakh, Trudy Voyennovozdushnoi inzhenernoi akademii (Electrolitic migration in metallic liquid and solid solutions, Works of the Air-Force Engineers Academy)*, No.167 (1947).
6. T.A. Lebedev and V.M. Guterman, *Koroziya, zashchita ot korrozii i elektroliz, Trudy TSNIITMash, (Corrosion, protection from corrosion and electrolysis, Works of Central scientific Research Institute)* No.11, 156 (1948).
7. V.M. Guterman, *Izv. sektora fiz.-khim. analiza Akad Nauk SSSR, (Bulletin of physico-chemical analysis Academy of Sciences USSR)* 19, No.4, 452 (1949).
8. P. Dayal and L.S. Darken, *Trans. Indian Inst. Metals*, 7, No.3, 241 (1953).
9. T.A. Lebedev and V.M. Guterman, *Dan SSSR (Reports of Academy of Sciences USSR)*, 60, No.7, 1201 (1948).
10. Hume and W. Rothery, *Journ. Iron and Steel Inst.*, 188, 2, 113 (1958).
11. Iu.F. Babikova and P.L. Iruzin, *Fiz. Metal Metalloved*, 5, 255 (1957).
12. I.N. Frantsevich, D.F. Kalinovich, I.I. Koveniskii and V.V. Pen'kovskii, *Ukrain'skii fizichnii zhurnal (Ukrainian Journal of Physics)*, 3, No.1, 155 (1958).
13. I.N. Frantsevich and D.F. Kalinovich, *Voprocy*

VOL 8 195

poroshkovoi metallurgii i prochnosti materialov (Problems of Powder Metallurgy and Strength of Materials), No.3, 45 (1956).

14. W.F. Mott and H.H. Wils, *Proc. Roy. soc.*, 153 No.880, 699 (1936).
15. J. Fridel, *Advan. Phys.*, 3, No.12, 446 (1954).

VOL.
8
1959

TREATISE ON RECRYSTALLIZATION OF THE MATRIX IN THE PROCESS OF DECOMPOSITION OF SUPERSATURATED SOLID SOLUTION ALUMINUM-SILVER*

R.M. LERIMAN and M.I. TURCHINSKAIA

Institute of Metal Physics, Academy of Sciences, U.S.S.R.

(Received 16 December 1958)

During the decomposition of a supersaturated solid solution the formation of laminated areas of a two-phase composition: an equilibrium solid solution and a stable phase of segregation (two-phase decomposition) is observed in many alloys under certain conditions. These areas of a pearlitic type grow from the grain boundaries.

In Geisler's review on ageing of alloys (1951), the transformation starting from the grain boundaries is fully described. Observing many experimental data, the author came to the conclusion that transformation always follows the general single-phase decomposition of the alloy, since the stresses accompanying the single-phase decomposition are the cause of the reaction starting from the boundaries (the two-phase decomposition).

Geisler considers this reaction as one of recrystallization, since it is accompanied by the reorientation of the matrix. Moreover, the transformation of the meta-stable phase of precipitation to a stable one occurs through diffusion of the first and formation of the second one. However, Elistratov [2] and some other investigators assume that during the two-phase precipitation no recrystallization of the matrix, but only the formation of thoroughly contracted and expanded small blocks, with a high degree of separation, takes place. With a view to obtaining additional material for the solution of the problem of recrystallization of the matrix in the process of decomposition of the supersaturated solid solution, a comparative electron-microscopic study of the processes of the change starting from the grain boundaries in the non-deformed alloy with the process of recrystallization of the matrix after the deformation, was undertaken.

In 1943, Geisler, Barrett and Mehl [3] observed the reaction beginning from the grain boundaries in the alloy aluminum-silver, with 10, 20 and 30% of silver. In the present investigation, the decomposition of the supersaturated solid solution aluminum-silver with 38% Ag was investigated. The specimens were quenched from 535° in water and were tempered at 300° during 5, 20, 30 min and 1 hr with subsequent cooling in water. The change from a γ'-into a γ-phase through formation of two-phase laminated areas of a pearlitic type at the grain boundaries, (Fig.1), was also observed here. These "pearlitic" areas start only from the grain boundaries, and only on one side from the boundaries. Inside the grains, the Widmanstatten pattern of laminae of the γ'-phase remains. The area, where the change γ'-phase + matrix $\rightarrow \gamma$-phase + matrix originated, is split into segregated areas – colonies, where all laminae of the γ-phase have only one direction, (Fig.2). As in the paper [3], it was observed that the direction of the laminae of the γ-phase in the colony does not coincide with anyone of the directions of γ'-laminae in that grain into which this colony grows, (Fig.1). Besides, we note that the direction of laminae of the γ-phase in the colony coincides with one of the directions of γ'-laminae in the grain adjacent to that into which the colony grows, (Fig. 1, see directions of arrows).

* *Fiz. metal. metalloved.*, 8, No.4, 579-583 (1959).

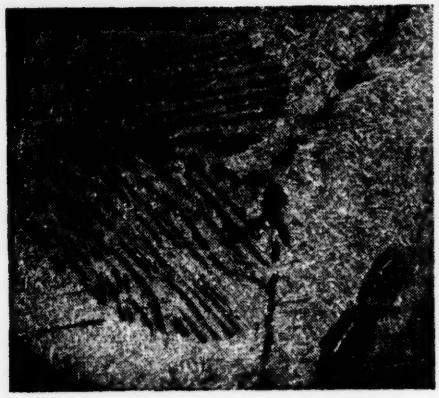

Fig. 1. Quench from 535° in water. Temper at 300°-20 min. X8500. Oxide replica.

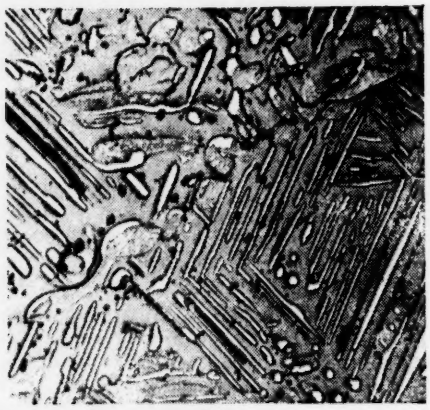

Fig. 2. Quench from 535° in water. Temper at 300°-30 min. X20,000. Oxide replica

VOL. 8 1959

Smith [4] also demonstrated by X-ray and inspection of the polished section in polarized light, on the alloy Zn with 2% Cu, tempered at 200° to obtain a two-phase decomposition, that the matrix in the laminated colony has an orientation coinciding with the orientation of the grain adjacent to that into which it grows. Smith thinks that this adjacent grain serves as a nucleus for the new unstressed area. The process of growth of areas of the pearlitic type, both in the alloy investigated and in the alloy Zn-Cu, resembles the process of recrystallization of the slightly deformed aluminum of high purity taking place through the movement of boundaries without formation of new nuclei [5]. It is known that a greater free energy is necessary for the formation of a new nucleus than for the advance of an already existing grain boundary. The measurements of the micro-hardness have demonstrated that the hardness inside the grain with γ'-precipitates, (in the first case, the hardness was 104 kg/mm^2, but in the second - 156 kg/mm^2). When the tempering period is extended to 30 min and longer, the "pearlitic" colonies occupy almost the whole area, (Fig. 2).

A parallel investigation of the decomposition of a supersaturated solid solution of the same alloy after a cold deformation of 51%, after quenching from 535° and a recrystallizing anneal for 25, 40 min and 1 hr at 165°; 25 min at 215°, and 25 min at 315°, followed by water cooling, was carried out. After a 25 min anneal at 165°, zones in form of bright specks enriched with silver, are visible on the whole area of the polished section. At this tempering temperature, new recrystallized grains appear in isolated grains, both at their boundaries and inside them, (Fig. 3).

Precipitation in these new grains is a much later stage not zones, but laminae of the γ'-phase. Consequently, the process of recrystallization "releases" the decomposition - the process of precipitation in recrystallized grains precedes that in unrecrystallized ones. This, apparently, can be explained thus; that the process of reorganization of the lattice occurs at the moment of recrystallization. It is known from the literature, that it is not the degree of preliminary deformation, but recrystallization which affects the rate of formation of the σ-phase in stainless steels [6]. In contrast to γ'- precipitates in the undeformed alloy, (Fig. 1), where laminae of the γ'-phase can in any region have directions parallel to the surface (III), in recrystallized grains the γ'-phase precipitates in form of colonies that are parallel only to one direction. One or several such colonies are in each recrystallized grain, (Fig. 3, 4). The hardness of recrystallized grains is considerably lower than the hardness of unrecrystallized parts: 110.4 kg/mm^2 for the first, and 210 kg/mm^2 for the second ones.

In the first colonies the laminae of the γ'-phase are distorted, (Fig. 3). The number of zones with distorted γ'-laminae decreases with the increase of temperature and time of tempering, (Fig. 4). The laminae of the

γ-phase have a fine structure. In colonies not combined with each other but distributed in one old grain, precipitating γ-laminae have often the same direction, (Fig. 3).

Fig. 3. Quench from 535° in water. Deformation 51%. Temper at 165°-25 min. X20,000. Oxide replica,

Fig. 4. Quench from 535° in water. Deformation 51°. Temper at 165°-1 hr. X20,000. Oxide replica.

Recrystallized regions after tempering at 165° for 25 min occupy approximately 1/6 of the size of the specimen, after 40 min – 2/5, after 1 hr tempering few unrecrystallized parts remain, (Fig. 4). After a 1 hr temper at 165°, very fine, distorted, densely distributed laminae of the γ-phase appear in the remaining unrecrystallized parts, (Fig.4); after tempering at 215° for 25 min the laminae are less distorted and form the Widmanstatten pattern, (Fig.7, see part A). It should be noted that in specimens not subjected to deformation, no formation of a γ-phase is observed after the above mentioned tempering. The deformation contributes to the decomposition of the solid solution, accelerating the formation and increasing the number of nuclei of the new phase [7-8]. After a 25 min tempering at 215° the unrecrystallized region are found very sparsely. The whole remaining field consists of colonies of very fine and straight laminae of a γ'-phase distributed along one direction in each colony, (Fig. 5).

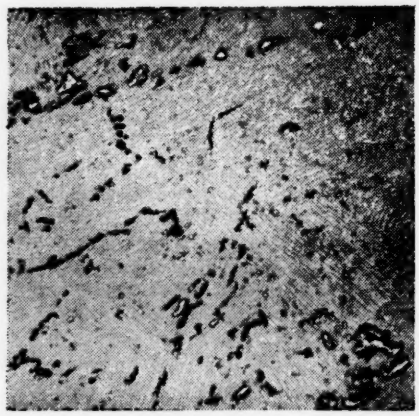

Fig. 5. Quench from 535° in water. Deformation 51%. Temper at 215°-25 min. X21,000. Oxide replica.

Fig. 6. Quench from 535° in water. Deformation 51°. Temper at 215°-25 min. X21,000. Oxide replica.

At 165°, after a 40 min soak, the beginning of the transition of the meta-stable γ'-phase

to the stable γ-phase is observed, with further increase of the temperature and annealing time, a further transition of $\gamma' \rightarrow \gamma$ and an enlargement of the latter, takes place, (Fig. 6,7). After a 25 min anneal, only colonies of precipitates of the γ-phase are visible, (Fig.8). Geisler, Barrett and Mohl [3] concluded from the results of X-ray investigations that the cold-deformed matrix in the alloy Al-Ag is recrystallized during the formation of the γ-phase.

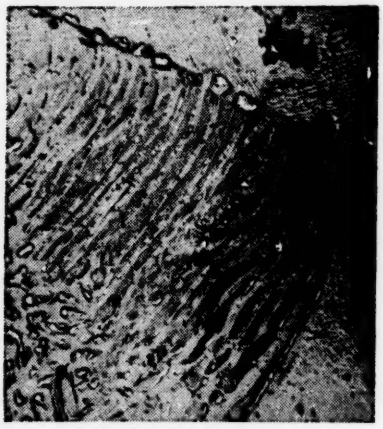

Fig. 7. Quench from 535° in water. Deformation 51%. Temper at 215°-25 min. X21,000. Oxide replica.

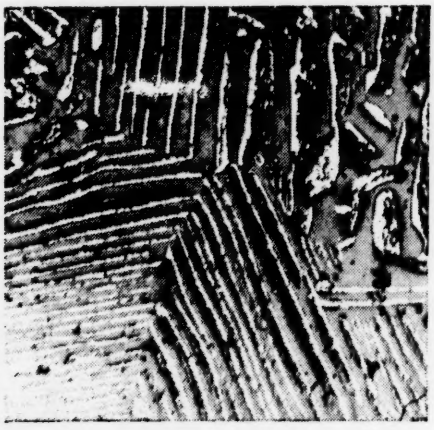

Fig. 8. Quench from 535° in water. Deformation 51%. Temper at 315°-25 min. X20,000. Oxide replica.

The electron-microscopic observations of the operation in question lead to the conclusion that the cold-deformed matrix in the alloy Al-Ag is recrystallized simultaneously with the formation of the γ'-phase, which changes into a γ-phase only when increasing further the temperature and time of tempering.

A corroboration of the conception that the growth of laminated areas from grain boundaries in an undeformed alloy during the transition of $\gamma' \rightarrow \gamma$ is accompanied by the recrystallization of the matrix, are the following observations:

1. During the growth of two-phase laminated areas in an undeformed alloy, just as during the growth of recrystallized grains after their deformation, the separating phase grows as colonies of parallel laminae;
2. In both cases, a phase develops that conforms to a much later stage of decomposition than that in the remaining grain;
3. The orientation of the laminated area does not coincide with the orientation of the grain into which it grows.

CONCLUSION

The comparison of the structural picture of the formation at the grain boundaries of laminated areas of the equilibrium phases of precipitation and matrix in the alloy Al-Ag with the picture of recrystallization after the cold deformation of the same alloy and also with the picture of recrystallization of lightly deformed aluminum of high purity, leads to the conclusion that the first process is accompanied by the recrystallization of the matrix.

Translated by W.A. Curtis

REFERENCES

1. A.H. Geisler, *Phase Transformations in Solids*, (1951).
2. A.M. Elistratov, *Dokl. Akad. Nauk SSSR*, 101, 69, 473 (1955).
3. A.H. Geisler, C.S. Barrett and R.F. Mohl, *Trans. AIMME*, 152, 182 (1943).
4. C.S. Smith, *Trans. Amer. Soc. Metals* 45, 56, 2-573 (1953).
5. P.A. Beck and P.R. Sperry, *Trans. Amer. Soc.*

VOL. 8 1959

Metals, 21, 150 (1950).
6. A.I. Lena and W.F. Curry, *Appl. Phys.*, 47, 193 (1955).
7. S.T. Konobeyevskii, *Zh. eksp. teor. fiz.*, 13, 200 (1943).
8. N.N. Buinov and V.P. Savinykh, *Dokl. Akad. Nauk SSSR*, 88, No.2, 257 (1953).

VOL
8
195

ELECTRON-MICROSCOPE INVESTIGATION OF THE DISTRIBUTION OF GUINIER-PRESTON ZONES IN AGEING ALLOYS*

N.N. BUINOV

Institute of the Physics of Metals, U.S.S.R. Academy of Sciences**

(Received 16 January 1959)

1. Much valuable information on the structure and structural changes of the matrix of supersaturated solid solutions may be obtained by the electron-microscope investigation of the distribution of Guinier-Preston zones (G.P.) and their precipitation through the volume of the alloys. The references include only the series of reports [1-7, 18] devoted to the study of the distribution of precipitates. The present article gives only the results of the study of the G.P. zone distribution in ageing alloys.

VOL. 8 1959

TABLE 1

Name of alloys	Network formed by G.P. zones			Network formed by diffused "veins" and relief	
	Limits of network dimensions (μ)	Average dimensions of network (μ)	Distance between G.P. zones in the dimensions (μ)	Limits of network dimensions (μ)	Average dimensions of network (μ)
1. Al-Cu (4% Cu), with quenching and low-temperature ageing to 150°	0.07-0.2	0.15	0.01-0.02	0.05-0.2	0.15
Ageing at 150-190°	0.05-0.2	0.10		0.07-0.2	0.10
Strain and ageing at 150-210°	0.1 -0.2	0.15		–	–
Ageing at 340° (1 hr.) and straining to 90%..	0.1 -0.2	0.15		–	–
Ageing at 350° (2 hr.) and rapid anneal at 500°	–	0.10		–	–
2. Al-Cu (1% Cu). Low-temperature ageing	0.1 -0.2	0.15		–	0.1
3. Al-Cu (2% Cu). Natural ageing	–	0.10		–	0.15
4. Al-Cu (5.7% Cu). Natural ageing	–	0.2		–	–
5. Al-Cu (4% Cu – 1% Fe). Low-temperature ageing	–	0.2		–	–
6. Al-Cu-Mg (3% Cu and 1.15% Mg). Natural Ageing	0.01-0.2	0.15		–	0.10

* *Fiz. metal. metalloved.*, 8, No.4, 584-589, 1959.

** Use has been made of electron photographs taken at the phase transformations laboratory of the Institute of the Physics of Metals of the Academy of Sciences of the U.S.S.R.

Table 1 *(continued)*

Name of alloys	Network formed by G.P. zones			Network formed by diffused "veins" and relief	
	Limits of network dimensions (μ)	Average dimensions of network (μ)	Distance between G.P. zones in the dimensions (μ)	Limits of network dimensions (μ)	Average dimensions of network (μ)
7. Al-Si (1.2% Si). Quenched	–	–	–	0.2-0.3	0.25
Ageing at 210-255° (to maximum hardness)	–	–	–	0.1-0.2	0.15
Straining to 13.5% and ageing at 260° from 5 min to 1 hr	–	–	–	0.1-0.2	0.15
8. Al-Ag (10-20% Ag) Natural ageing	0.04-0.07	0.05	0.015	–	–
Artificial ageing (175-220°)	0.03-0.05	0.04	0.02	–	–
9. Aluminium (99.95%) strained	–	–	–	0.1-0.2	0.15
	–	–	–	–	0.05
10. Dl. Natural ageing	0.01-0.15	0.10	0.01-0.02	–	–
Ageing at 180°	0.1-0.2	0.15		–	–
Ageing at 300° 1 hr	0.1-0.2	0.15		–	–
11. AK4. Quenching and annealing at 180°	0.1-0.2	0.15		0.1-0.2	0.15
Idem. at 225-275°	0.1-0.2	0.15	–	–	–
Idem. at 325-425°	0.1-0.2	0.15	–	0.1-0.2	0.15
Isothermal hardening at 225-250° for 1 hr.	0.1-0.2	0.10	–	–	–
12. AK4-1. Quenched	0.1-0.2	0.15	0.01-0.02	–	–
Ageing at 180° 10 hrs	0.1-0.15	0.10	0.01-0.02	–	–
Gradual quenching 275° 1 min, quenching and annealing at 250° 1 min	–	0.1	0.01-0.02	–	–
13. Ni-Be (1.9% Be). Ageing at 425-500°	–	–	–	0.03-0.2	0.07
14. Magniko. Quenched ($H_c = I_e$)	0.15-0.5	0.3	0.02	0.2 -0.3	0.25
Treated to a highly coercive state ($H_c = 470_e$)	0.2-0.3	0.2	0.02	–	–
Furnace cooled from 1280°	–	–	–	0.2 -0.3	0.25
15. Cunife. Thermo-mechanically treated to a highly coercive state ($H_c = 305\ I_e$).	0.07-0.3	0.15	–	–	–
16. Permalloy (66; 78.5 and with Mo). Quenched and partially regulated	0.02-0.3	0.1	–	–	–
17. Transformer steel	0.05-0.07	0.06	–	–	–
18. Al-Zn (10%)-Cu (0.5%). Ageing at 180° 12 hr.	0.1 -0.2	0.1	–	–	–

2. In the second column of the table are given the dimensions of the "network" formed by G.P. zones* in various alloys. The network consists of equiaxial, and sometimes also of oblong cells (Figs. 1a-c). For almost all alloys the dimensions of the cells of this network are the same in diameter, 0.01-0.2μ**: The average measurement, however, is nearer

* On the electron photographs the light equiaxial-shaped specks correspond to the G.P. zones. This correspondence follows from a comparison of the electron-microscope and X-ray data which has been partially published [19-21].

** Information on the existence of networks of this scale, formed by G.P. zones in the alloys Al-Ag and Al-Cu, is given in [8].

VOL 8 195

0.1μ. Variations on these values are slight and are observed mostly in the Al-Ag alloy (0.03-0.07μ).. The shape of the cells at times approaches that of a hexagon. In some cases the alignment of the links almost coincides with the alignments of type [100] and [110], but this is usually arbitrary. The networks can be seen in alloys subjected to widely differing heat treatments, as for instance in the alloy Al-Cu (4% Cu), as can be seen from the table, after quenching, natural ageing, artificial ageing (Fig. 1c), ageing under high temperatures (Fig. 2), ageing and straining etc. The development of such a network was particularly successful in this alloy after quenching from 530°, polishing electrolytically, subjecting it to a strain (1-9% in tension), and annealing for one hour at 150°C (Fig.3).

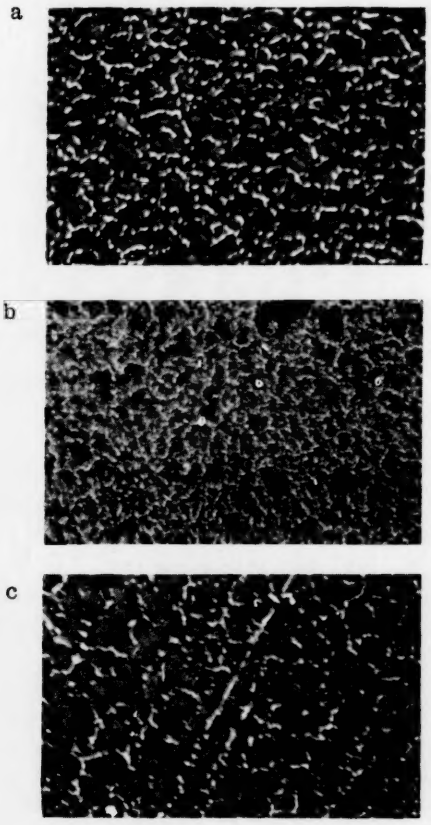

Fig. 1. a – alloy Al-Cu (4% Cu); after natural ageing; b – alloy Al-Ag (10% Ag); after natural ageing; c – alloy Al-Cu (4% Cu); ageing at 180° for 30 min.; X 50,000.

A regular distribution of cells in a network relative to each other is often observed. In Fig. 3, for example, cells of approximately similar dimensions and shape are arranged in rows and form an almost rectangular network. The regular distribution of cells is seen also in Fig. 1a and 1c.

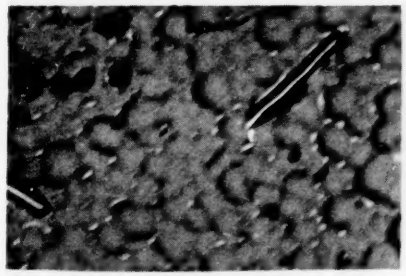

Fig. 2. Alloy Al-Cu (6.3%) – Mn (0.7%) – Ti (0.14%); Annealing 250° – 10 hr and testing for prolonged stability at 350° during 100 hr. with stress of 3 kg/mm^2; X 50,000.

In some crystalline alloys Al-Cu, Al-Zn-Cu, and Al-Cu-Mg the G.P. zones form straight or almost straight traces several microns long and at a distance of 0.05-0.2μ from each other (Fig.4). Here the zone distribution recalls the distribution of etch pits in the polygonized alloy Fe-Se studied by Dunn and Hibbard [9]. The distance, however, between the traces of the zones is considerably less than between the traces of the etched pits.

Together with the submicroscopic network formed by the G.P. zones the electron photographs show a network formed by dark diffused "veins" (Fig. 5) and a contour. The second network is probably developed at the expense of the uneven distribution of the atoms of the metal alloy components. The shape and dimensions of the cells of this network (cf. column three of the table) are approximately the same as those of a network formed by G.P. zones.

3. As has already been observed, the dimensions of both types of submicroscopic networks coincide. Moreover, both types of network are stable for the various heat treatments and strains. They are, it seems, of identical origin. This is confirmed by the electron photographs in which the network is formed simultaneously with the G.P.

zones and the diffused "veins" (Fig. 6).

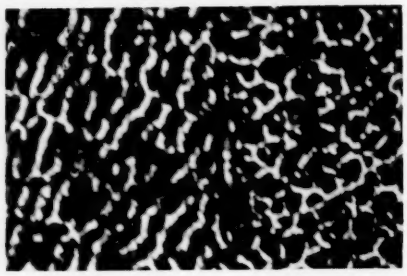

Fig. 3. Alloy Al-Cu (4% Cu) polishing electropolytically, strain to a certain degree (1-9% with tension) and ageing at 150° for 1 hr; X 50,000.

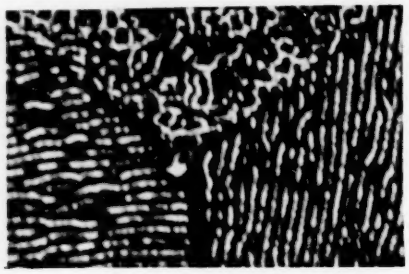

Fig. 4. Alloy Al-Zn-Cu (10% Zn and 4% Cu); ageing at 150° for 1 hr; X 50,000.

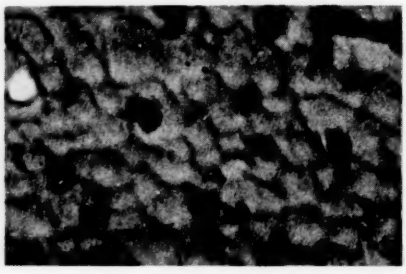

Fig. 5. Alloy Al-Si (1.2% Si); etching, quenching from 525° and ageing at 255° for 8 min; X 50,000.

A detalied study of tne distribution of G.P. zones leads one tc conclude that the networks very often occur in adjacent grains also, and almost always in deformed alloys. If the networks were plane or 2-dimensional they could be observed only under the particularly favourable conditions when the plane of the networks coincided with the polished sample surface. In the as-quenched state and in the initial stages of decomposition, 3-dimensional networks may not yet have spread through the entire volume of the alloy. The networks have both equiaxial and elongated cells. After deforming the alloys, cells of equiaxial from only were seen in the electron photographs (Fig. 7). These networks should correspond to the submicromosaic structure of the alloys, which will agree with the results of X-ray investigations [10]. Inasmuch as the dimensions of the cells depend but little on the nature of the metal of the alloy component, on deformation and on heat treatment, a submicromosaic structure of a scale of 0.1-0.2 μ may be considered as characteristic for both metals and alloys. This is confirmed also by data given in the references. It follows from the electron-microscope research cited in Hirsch's survey [10] that a submicromosaic structure of 0.1μ is to be found in strained copper, of 0.15μ in beaten gold foil, of 0.1μ in steel (3% Cr and 1% Mo).

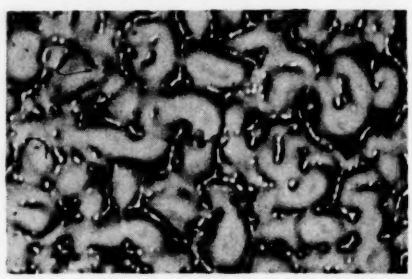

Fig. 6. Alloy Al-Cu (1% Cu); natural ageing; X 50,000.

In the last case the submicro-mosaic structure is shown by precipitates, their distance being equal to 300 Å. According to data given by Masin [11], in martensite (steel with 1% C) annealed at 550-700°C the size of the mosaic blocks is 0.2μ . Moreover, this depends neither on the temperature nor on the time of annealing. Finally Biussi's data [12] on the substructural dimensions for aluminium and aluminium alloys with copper coincides with that given in our table.

It must be noted that in the electron photographs in which the network is formed both by G.P. zones and dark "veins" (Fig. 6), double boundaries of the cell are to be seen. Some of the boundaries are marked by the G.P. zones and others by accumulations of the

alloy components. Sub-boundaries in the form of dark "veins" are more frequently observed in strained alloys and also in dilute alloys (for instance, in aluminium alloys with 1-2% copper). A small degree of supersaturation and, consequently, a slight tendency to age, probably leads more often not to the formation of G.P. zones on the boundaries of the cells of the submicro-mosaic structure, but to the formation of elongated zones of a comparatively weak concentration of the alloy component.

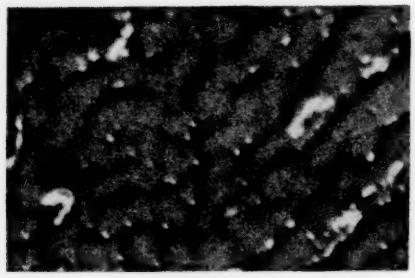

Fig. 7. Alloy Al-Cu (4% Cu); ageing at 340°, 1 hr; straining by compression to 90%; X 50,000.

4. As has already been shown, it has not been possible to observe any substantial change in the dimensions of the submicro-mosaic structure of the type described (or in the dimensions of the cells) in relation to heat treatment and strain. On this basis we formerly made the mistaken preliminary assumption that the submicro-mosaic structure of the type we have considered, plays no part in the strengthening of alloys produced by ageing. But in actual fact the submicro-mosaic structure seems to play a significant role in the increase of alloy strength. In support of this assumption is the fact that the etch patterns, corresponding to mosaic blocks of a larger scale, decrease with the period of ageing and the increase in strength of the aluminium alloys to dimensions of the order of several tenths of microns [14-15], i.e. to dimensions approaching the size of the blocks of the submicro-mosaic structure described.

The strengthening of metals by alloying, ageing and plastic deformation at the expense of the submicro-mosaic structure may be described as follows. If the submicro-mosaic structure is not fully developed in the whole volume of the metal then the alloying, ageing and plastic deformation lead to the extension of this mosaic throughout the entire volume of the alloy and to an increase in disorientation between sub-grains. But if submicro-mosaic structure of the scale observed is always found in metals and alloys then the strengthening must be connected with the increase in the disorientation.

The formation of zones of straight line traces may be considered as the result of the regular rotation of the blocks of the submicro-mosaic structure about some axis or alignment. That this rotation may occur in separate grains of the alloy is shown by X-ray investigations [16-17]. In the Ni-Be alloy [17], judged by the different degree of diffuseness of the anomalous two-dimensional effects, the rotation of the blocks during ageing takes place chiefly about one of the [110] directions. The boundaries of mosaic blocks parallel to the axes of the rotation will have larger angles of disorientation. Because of this, it is in them that the process of the principal accumulation of the formation of the G.P. zones will occur.

SUMMARY

1. 3-Dimensional networks with cell dimensions of the order of 0.1 μ are found along the distribution of G.P. zones and the alloying component in alloys.
2. We have established that the dimensions of the cells do not change with heat treatment and strain.
3. The data obtained experimentally and given in the references allows us to conclude that the networks observed correspond to the blocks of a submicro-mosaic structure.
4. We have stated a theory on the role of the submicro-structure in the strengthening of alloys.

Transalted by J.H. Gwynn

REFERENCES

1. P. Lacombe, and A. Berghezan, *Compt. Rend.*, 226, 2152 (1948).

2. P. Lacombe, *Physics.*, 15, 161 (1949).
3. R. Castaing, *C.R.*, 228, 1341 (1949).
4. J. Nutting, and J. Thomas, *International Conference on Electron Microscopy*, London, (1954).
5. H. Wilsdorf and D. Kuhlmann-Wilsdorf, *Phil. Mag.*, 45, 1096 (1954).
6. H. Wilsdorf and D. Kuhlmann-Wilsdorf, *Report of Conference on Defects in Crystalline Solids, Bristol, 1954.* (Phys. Soc., London, 175 1953).
7. J.M. Hedges and J.W. Mitchell, *Phil. Mag.*, 44, 223 (1953). 44, 357 (1954).
8. N.N. Buinov and R.M. Lerinman, *Dokl. Akad. Nauk. SSSR.* 74, 707 (1950).
9. C. Dunn and W. Hibbard, *Acta Metallurgica*, 3, 409, (1955).
10. P.B. Hirsch, *Progress in Metal Physics*, 6, 236 (1956).
11. A. Masin, *Ann. d. Physik*, 19, 257 (1957).
12. P. Biussi, *Primeneniye elektronnoi mikroskopii* (Use of the Electron Microscope), Metallurgizdat, 149 (1957).
13. N.N. Buinov, *Trud. Inst. Fiz. Metallov. Ural. Filial. Akad. Nauk.*, Vol. 20, 283 (1958).
14. N.N. Buinov and R.R. Zakharova, *Fiz. Metal. Metalloved.*, 6, 289 (1958).
15. V.G. Rakin and N.N. Buinov, *Fiz. Metal. Metalloved.*, 6, 686 (1958).
16. A.M. Yelistratov, *Dokl. Akad. Nauk. SSSR.*, 101, 69 (1955).
17. N.N. Buinov, *Izv. Akad. Nauk. SSSR* , ser. fiz., 5, 648 (1959).
18. V.G. Rakin wnd N.N. Buinov, *Dokl. Akad. Nauk. SSSR.* 121, 271 (1958).
19. N.N. Buinov, *Fiz. Metal. Metalloved.*, 1, 339 (1955).
20. R.M. Lerinman and N.N. Buinov, *Fiz. Metal. Metalloved.*, 5, 279 (1957).
21. N.N. Buinov, and L.I. Podrezov, *Fiz. Metal. Metalloved.*, 1, 349 (1955).

PLASTICITY OF TRANSFORMER STEEL AFTER HEAT TREATMENT AT TEMPERATURES OF 300-900°*

S.I. DOROSHEK

Urals Scientific Research Institute of Ferrous Metals

(Received 17 July, 1958)

A general picture is given of the change in the plasticity of transformer steel within the temperature range of 300-900° both in the cooling process after annealing and in the annealing process after quenching. In this range the plasticity of transformer steel has three minimum and two maximum values of ductility.

Some of the kinetic rules for the change in plasticity in the low-temperature maximum and medium-temperature minimum range of ductility are studied. By gradual cooling or quenching with annealing the plasticity of transformer steel may change in any direction.

VOL. 8 1959

Contemporary technology of the annealing of transformer steel only takes into account recrystallization and low-temperature changes according to a stable and metastable variant. Meanwhile a number of works [1, 2] point to the possible occurrence of different phase transitions in microvolumes of transformer steel with commercial proportions of carbon and silicon, which cannot be reflect on the mechanical and magnetic properties. Actually, as has been shown in articles [3,4], the change in steel ductility in the cooling process after annealing is of a complex character which cannot be explained merely by the diffusion and precipitation of cementite [5, 6]. There is as yet no data in the reference on which to base a general picture of the change in ductility of transformer steel after heat treatment at temperatures of 300-900°. The present work gives some of the experimental data relating to this problem.

Research was undertaken on four commercial medium-alloyed melts of transformer steel, the chemical composition of which is given in the table.

Samples in the form of strips measuring 0.5 x 30 x 250 mm were subjected to heat treatment: a) annealing at a temperature of 900°, soaking for two hours, furnace cooling at a rate of 50° per hour with oil fixation

TABLE 1

Melts	Content of the elements, %								
	Si	C	Mn	P	S	Cr	Ti	Al	Cu
A	3.60	0.047	0.17	0.022	0.020	0.12	0.009	0.036	0.16
B	3.74	0.036	0.23	0.033	0.017	0.12	0.009	0.065	0.15
C	3.58	0.050	0.14	0.020	0.011	0.10	0.010	0.055	0.12
D	3.56	0.070	0.18	0.020	0.015	0.10	–	0.050	0.16

* *Fiz. Metal Metalloved.*, 8, No.4, 590-594, 1959.

every 25-30°; b) quenching from 900° after a two-hour soaking in oil with subsequent anneal over two hours in the 350-875° range; c) quenching from 900° after a two-hour soaking in oil with subsequent anneal at 475-675° over 2-8 hours; d) samples fixed at temperatures of 875, 775, 725, 675, 550 and 425°, after treatment according to variant *a*, were annealed at 580° for 1-8 hr and at 400° for 1-12 hr.

The samples treated were tested at room temperature on a special bending device, the radius of the bit being 5 mm. Each point on the graphs represents the mean value, 10-20, of the tests. The dispersion of the readings is shown on some of the graphs.

Part of the experiments were undertaken on Menage samples subjected to hardening from 950° after a 2 hr soaking in oil with subsequent annealing in the 300-900° range every 25° for 2 hr. In each case the cooling after the anneal was effected in oil. The Menage samples were tested on a ram impact machine at a power of 30 kgm at 130°. Each point corresponds to 3-5 samples.

In individual cases a chemical analysis of the carbon was undertaken, and also a microstructural analysis with a magnification of X 600.

In Fig. 1 are shown the results of tests for melt brittleness in relation to the temperature for quick cooling. With a fixation temperature of 875° the number of bends for this melt levels to an average of 12. With a lowering of the fixation temperature to 725° a sharp decline in plasticity was most clearly observed, with a maximum plasticity at 675° and also an analogical minimum and maximum at 550 and 425°.

Analogical tests were made in other melts to check the rules obtained. In Figs. 2a-b are shown the graphs of change in the number of bends in relation to the fixation temperature for melts *C*, *D*. It will be seen from the graphs shown that the general rules for the change in plasticity in the cooling process after annealing remain the same as for melt *A*; but the character of the increase and decrease in plasticity and also the distribution of the extreme points differ somewhat as a result of the individual peculiarities of each melt.

The carbon content of the strips tested was 0.004-0.008 per cent. The grain seemed pure in all melts and no structural changes at the boundaries (X 600) were detected. Stringers of a thin cementite network were very rarely encountered, but their connexion with brittleness was not clearly observed.

It was expedient to study the plasticity of transformer steel with annealing in the 300-900° range after high-temperature quenching at 900-950°. For this, samples of melts *B* and *D* were treated according to variant *b*.

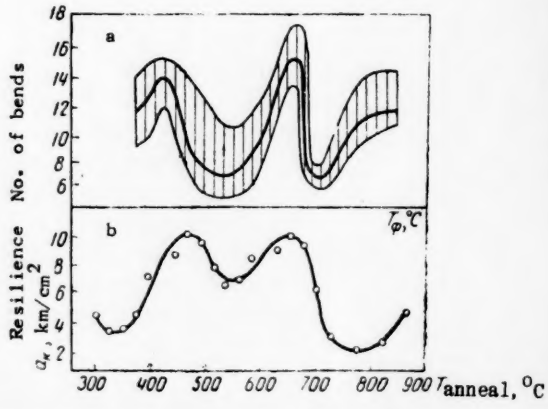

Fig. 1. Change in plasticity of transformer steel of smelting *A* with heat treatment in the temperature range 300-900°:
a – relation of the number of bends at room temperature in the cooling process after annealing (T_{anneal} = 900°; τ_{anneal} = 2 hr., speed of cooling after anneal 50° per hr);
b – relation of resilience to annealing temperature. ($T_{quenching}$ = 950°; τ_{anneal} = 2 hr; $t_{testing}$ = 130°).

After testing the relation between the number of bends and the temperature of annealing became apparent and the curve is shown in Fig. 2 (graphs 3, 4). At a temperature of 350° both melts had 13 bends. With an increase in temperature to 450° the number of bends increased somewhat, and at 550° noticeably decreased. Thus, as a result of the anneal, maximum plasticity was also observed at 450°. The increase in the temperature of annealing from 550 to 690-700° is accompanied by a decrease in brittleness, and with annealing at 775-800° a decrease in ductility is again observed.

As in the case of cooling after annealing, two maximum values of plasticity are observed

upon the hardening of transformer steel (at temperatures of 450 and 690-700°) and three minimum values (350, 550, 775-800°).

The extreme points of change in brittleness after annealing were clearly detected while testing the Menage samples for resilience (Fig. 1b). In this case three minimum readings for brittleness were clearly visible at 350, 550, 800°, and maximum readings at 470 and 670°.

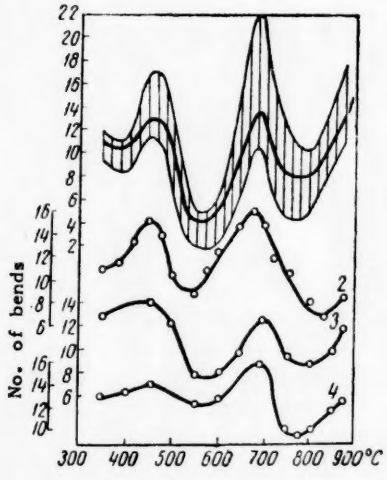

Fig. 2. Influence of treatment-temperature of the samples on the number of bends: 1 – smelting *D*, T_{anneal} = 900°, time of anneal 2 hr., $v_{cooling}$ = 50° per hr. 2 – smelting *C*, T_{anneal} = 900°, time of anneal 2 hr, $v_{cooling}$ = = 50° per hr. 3 – smelting *B*, $T_{quenching}$ = 900°, time of quenching 2 hr., time of anneal 2 hr. 4 – smelting *D*, $T_{quenching}$ = 900°, time of quenching 2 hr., time of anneal 2 hr.

Existing technology of the finishing heat treatment of transformer steel in Soviet factories envisages slow cooling (5-10° per hr) to a temperature of 550-600°, with a subsequent fast cooling of 40-60° per hr. Thus of greatest interest from the point of view of practical heat treatment are the medium-temperature minimum (525-575°) and the low-temperature maximum (425-450°) plasticity observed above.

Kinetic graphs for the isothermic treatment of transformer steel within the range of the low-temperature maximum and the medium-temperature minimum brittleness are shown in Figs. 3, 4.

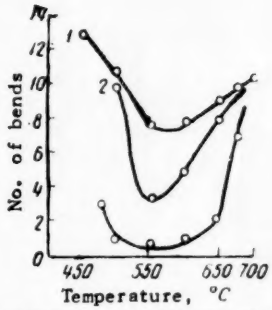

Fig. 3. Kinetic drop in brittleness of transformer steel at medium-temperature minimum of ductility (smelting *D*, $T_{quenching}$ = 900°, oil cooling): 1 – τ_{anneal} = 2 hr. 2 – τ_{anneal} = 4 hr. 3 – τ_{anneal} = 8 hr.

After tests for bends, samples of melt *D*, treated according to variant *c*, gave the following picture of the development of brittleness at the medium-temperature minimum plasticity (Fig. 3).* With a 2 hr soaking in the 450-700° temperature range the drop in plasticity at temperatures of 550-600° is clearly defined, characterized by 7.5 bends. Increasing the soaking to 8 hr led to an even greater development of brittleness (0-0.5 bends). It should also be noted that an 8 hr soaking is fully sufficient to induce a sharp drop in plasticity not only at 550° but also at 475-650°, i.e. the longer the soaking the greater the drop in plasticity.

Samples fixed at different temperatures in the cooling process after annealing noticeably lowered the plasticity on annealing in the range of the medium-temperature drop. Strips of melt *A*, treated according to variant *d*, were annealed at 580°. Moreover, samples rapidly cooled from a temperature of 875° after a 9 hr soaking at this temperature lowered the plasticity on an average from 12 to 4 bends (Fig. 4c, graph 2). Samples rapidly cooled from a temperature corresponding to maximum plasticity (675°) lowered the plasticity from 16 to 11 bends with a soaking lasting 1 hr, and to 6.5 bends with a 9 hr soaking (Fig. 4a, graph 1). But after rapid

* In the case under consideration the "cork" sheets taken of this melt were of a rather smaller absolute plasticity than sheets of the same melt observed earlier.

VOL. 8 1959

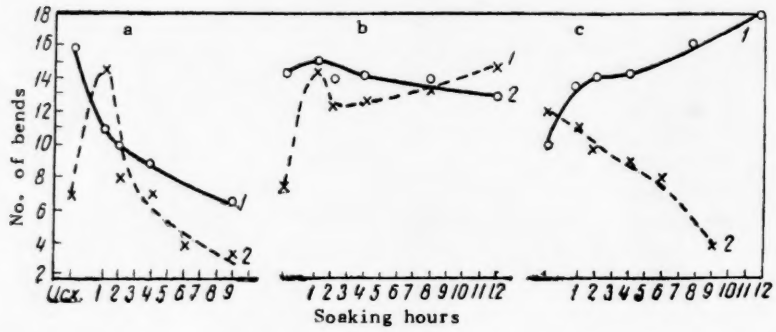

Fig. 4. Relation of plastic rapid cooling of transformer steel to time of soaking with anneal at 400 and 500°.
a – T_{anneal} = 580°, oil cooling; 1 – $T_{fix.}$ = 675°, 2 – $T_{fix.}$ = 725°.
b – T_{anneal} = 400°, oil cooling; 1 – $T_{fix.}$ = 550°, 2 – $T_{fix.}$ = 425°.
c – 1 : $T_{fix.}$ = 775°, T_{anneal} = 400°; 2 – $T_{fix.}$ = 875°, T_{anneal} = 580°.

cooling from the temperature of the high-temperature minimum brittleness (725°) the sample's plasticity after annealing for 1 hr suddenly increases (from 7 to 14.5 bends), and with further soaking invariably drops (down to 3-4 bends after 6-9 hr) to a value lower than the corresponding value after fixation at 675° (Fig. 4a, graph 2).

Imported (French) steel known for its high plasticity is also impaired by annealing at about 550°. Sheets with 4.3% Si, 0,5 mm thick in their initial state, similarly sustained 4-6 bends; but after a 3 hr anneal at 550° not one of them sustained even 0.5 bends, although with a magnification X 600 no changes were discerned in the structure, which contained a large number of titanium and graphite carbonites.

Thus the plasticity of transformer steel, both with a small carbon content (0.004-0.008%), close to the solubility limit, and with combined carbon (in the form of graphite or titanium carbonites precipitating at high temperatures), invariably deteriorates after annealing at the temperatures for the medium-temperature minimum (525-575°).

The results of the survey of plasticity obtained by annealing samples of melt *A* at 400°, after being treated according to variant *d*, are given in Figs. 4 b/c. After a 12 hr anneal at 400° the number of bends in samples rapidly cooled from the low-temperature maximum (425°) was reduced from 14.5 to 13.0. But the brittle sheets obtained as a result of the rapid cooling from 550°, characterized by 7.0-7.5 bends, noticeably increased in plasticity of samples fixed at the high-temperature minimum (Fig. 4c, graph 1) changes analogically. With an increase in the soaking time to 12 hr during anneal the number of bends is almost doubled. Thus the brittleness of transformer steel can be rectified after appropriate treatment by annealing in the range of the low-temperature maximum ductility (400-450°).

The complex character of the change in plasticity after heat treatment within the range of the temperatures investigated, and without noticeable structural changes after the usual magnification (x 600), is characterized by the general kinetic rules for diffusion processes and indicates the occurrence of transitions in volumes of a microscopic and submicroscopic order. Similar transitions may, evidently, occur in the boundary regions of grains (blocks where the increased reserve of free energy favours a considerable variation in the chemical composition of intercrystalline zones from the average composition of steel [7].

CONCLUSIONS

1. In the process of cooling transformer steel after annealing in the temperature

range of 300-900° three minimum and two maximum values of ductility are observed. The high-temperature minimum is located in the 725-825° range, the medium-temperature at 525-575°, the low-temperature at 350-400°. Correspondingly, the maximum readings are at 650-700° and 425-450°.

2. The plasticity of transformer steel may deteriorate by annealing at minimum temperatures but improve, on the other hand, by annealing at temperatures of maximum ductility. The longer the metal stays at temperatures characterizing the extreme values of ductility the greater the extent of the occurrence of decrease or increase in the brittleness of transformer steel.

3. Extreme change in the plasticity of transformer steel treated in the temperature range of 300-900° indicates the occurrence within that range of complex diffusion processes in volumes of a microscopic and submicroscopic order.

Translated by J.M. Gwynn

VOL. 8 1959

REFERENCES

1. R.L. Ricket and N.C. Fick, *Metals Technology*, Fabr., (1946).

2. E.D. Harry, *Journ. of the Iron and Steel Inst.*, 167, 3 (1951).

3. S.I. Doroshek and N.I. Lapkin and G.N. Shybin, *Fiz. Metal. Metalloved.*, 4, Vol.1, 171 (1957).

4. S.I. Doroshek and G.N. Shybin, *Ural. Nauch-Issled. Inst. Chernyx Metallov. Bulletin of scientific-technical information, No.4, Metallurgizdat.* (1958).

5. M.M. Steinberg, I.N. Bogachev, G.A. Zykov and R.Sh. Shkliar, *Fiz. Metal. Metalloved.*, 1, Vol. 1, (1955).

6. V.A. Koroleva and M.I. Sherstiuk, *Stal* , No. 545 (1956).

7. V.I. Arkharov, *Trud. Inst. Fiz. Metallov. Ural. Filial. Akad. Nauk. SSSR.* Vol. 8, 54 (1946).

CARBIDE EUTECTIC IN NICKEL-CARBON ALLOYS*

R. A. SIDORENKO

S.M. Kirov Urals Polytechnic Institute

(Received 27 December 1958)

Alloys of iron, cobalt and nickel with carbon have much in common. In these systems a graphite eutectic is formed, in connexion with which cobalt-carbon and nickel-carbon alloys are repeatedly used as models of graphite-forming processes in cast iron. In iron-carbon and cobalt-carbon alloys the formation of a metastable carbide eutectic as well as a graphite eutectic is possible. However, if this structure is well-known and is easily formed in iron-carbon alloys, it has been obtained in cobalt-carbon alloys only by sudden quenching from a liquid state [1, 2]. As regards the carbide eutectic in nickel-carbon alloys, judging from reference data this structure has not yet been observed.

According to the abstract of Khansen's data [3], in the structure of nickel-carbon alloys only graphite and a solid solution of carbon are observed in the nickel. The presence at 2100° of a bending point on the carbon solubility curve in liquid nickel and an exact correspondence of the carbon content at this temperature to the composition of Ni_3C allowed Ruff and Martin [4] to deduce the existence of this carbide. They saw in the structure of certain alloys, together with nickel and graphite, a structural element, brown in colour, inside the eutectic and this, in their opinion, could only be nickel carbide. Morrogh and Williams [1] maintain that Ruff and Martin's microphotographs do not confirm the presence of carbide in the structure of their alloys. Ruff and Martin had been the first to observe disintegrated carbides whose carbon was unable to spread to the graphite impurities. These disintegrating carbides have been observed by the author in cobalt-carbon alloys in a joint study with A. Goroshkov [2], and these also were brown in colour. Khansen's general conclusion is such that although the existence of nickel carbide cannot be doubted nevertheless it cannot be present as a structural component in alloys obtained by a diffusion of carbon in liquid nickel.

Morrogh and Williams [1] melted 6 g of nickel into a graphite crucible, soaked the alloy for a long period at a temperature of 1500°, slowly cooled it over half an hour to 1450° and then rapidly quenched it in water. Together with the graphite they observed in the structure of this alloy a Widmanstatten pattern (Fig. 1) which they believe to be nickel carbide. The absence of this pattern near graphite impurities and its disappearance with annealing proved, in the author's opinion, that this was nickel carbide, although Scheil [5] justly observes that this pattern does not resemble that of a eutectic and was probably already formed in a solid state with the disintegration of the supersaturated solid solution of carbon in the nickel.

From the above summary we are forced to conclude that inasmuch as nickel carbide exists it is probably possible to obtain a carbide eutectic in nickel-carbon alloys also preventing its decomposition by a very rapid cooling of the alloy from a liquid state to room temperatures. In connexion with this the present study was also undertaken.

Electrolytic nickel, type H000 of 99.9% purity, was used for this work. For the preparation of the crucibles pure graphite with 0.1% ash content was used. The crucibles had an inside diameter of 10 mm, the thickness of the sides being 2 mm and the height 30 mm. To increase the rate of cooling after quenching the lower half of the crucibles was ground off with an abrasive till the thickness of the side was about 1 mm, so that the

* *Fiz. Metal. Metalloved.* 8, No.4, 595-598, 1959.

VOL 8 195

weight of the melting process was 3 g.

Fig. 1. Nickel carbides according to Morrogh and Williams; X 1200.

Fig. 2. Carbide eutectic and acicular Widmanstatten component in nickel-carbon alloys; Etched; X 666.

The meltings were undertaken in a carbon resistance furnace, the combustion space of which was insulated from the oxidization products of the heater by a porcelain shaft. The temperature was measured by an optical pyrometer with a disappearing thread, adjusted by a platinum thermocouple. The crucible with a hanging of pure nickel was placed in the furnace at a temperature of 1400° and after the melting of the metal was kept at that temperature for 3-4 min when it was taken by pincers, removed from the furnace as quickly as possible and immediately quenched in a 5% aqueous solution of caustic soda, vigorously revolving the crucible in the cooling medium.

A low superheat temperature (the hardening of graphite eutectic in a nickel-carbon system occurs at 1318°) and a short exposure to it proved essential inasmuch as previous tests showed that a heavy carbon saturation increases the tendency of liquid alloys to harden with graphite eutectic formation.

A study of the microstructure of the alloys obtained has shown that they can provide a metastable eutectic of nickel carbide and nickel (a solid solution of carbon in nickel). The alloys were of a hypoeutectoid structure. The eutectic was found in the interdendritic spaces and occupied about 5-10 per cent of the microsectional area. Besides the eutectic and the primary solid solution a small number of fairly large graphite impurities, mostly globular, was observed in the structure. In unetched microsections the carbide eutectic stood out faintly against the background of the matrix and had a bluish tint. After etching with a solution of bromine in alcohol the eutectic component stood out celarly and was of a blue colour, the intensity of which depended on the degree of etching. In Fig. 2 is shown a microphotograph of the structure of the alloys obtained. In it, apart from impurities of the carbide eutectic, is seen an acicular Widmanstatten component very similar to the pattern obtained by Morrogh and Williams (Fig. 1). That there was less of this component in our alloys is evidently connected with the lower temperature and the shorter time of superheating and, consequently, with the smaller concentration of carbon in the solid solution compared with the alloys of the authors quoted.

The eutectic component was extremely finely dispersed and despite the use of maximum-capacity immersion objectives it was possible to observe their complex structure only in a few large impurities (Fig. 3). It will be seen from a study of Fig. 3 that the shape and structure of the impurities of the carbide eutectic obtained are similar to the cementite eutectic in white hypoeutectoid iron.

Measurement of the micro-hardness of the structural component showed that it averages 518 kg/mm^2 for the carbide eutectic and 303 kg/mm^2 for the matrix. The matrix was probably heavily supersaturated with carbon. Sections near the graphite, and from which carbon may partially precipitate, have a smaller micro-hardness, equal to 175 kg/mm^2.

An alloy with a carbide eutectic structure was subjected to annealing at a temperature of 1000° for 1.5 hr, with subsequent quenching. The carbide eutectic in this alloy completely disintegrated and a fine compact graphite

formed in it (Fig. 4). In certain sections of the microsection graphite was observed whose precipitation repeated the pattern of the impurities of carbide eutectic, and graphite precipitated at the grain boundary of the alloy. All these graphite precipitations are visible in Fig. 4.

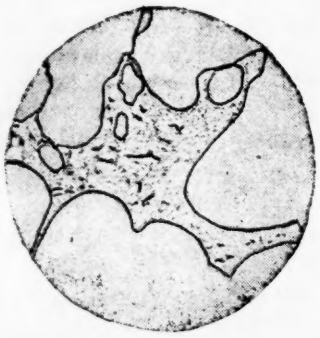

Fig. 3. Structure of carbide eutectic in nickel-carbon alloys; Etched; X 666.

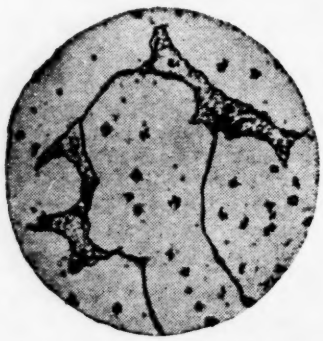

Fig. 4. Graphite formed after annealing an alloy with carbide eutectic in the structure; Etched; X 666.

The similarity of the structural components, obtained by the extremely rapid cooling of liquid nickel-carbon alloys, with the cementite eutectic in hypoeutectoid iron, its high micro-hardness in comparison with the matrix, the disintegration of this component with graphite formation upon annealing, and also the absence in the alloys of any significant number of constituents of other elements besides nickel and carbon, leave no room for doubt that the structure obtained is in fact a metastable eutectic of nickel carbide – a solid solution of carbon in nickel.

The acicular Widmanstatten pattern (Fig. 1) obtained by Morrogh and Williams [1], and also in our present investigation, is also observed in cobalt-carbon alloys [1, 2]. This structure is probably formed by the disintegration of the supersaturated solid solution of carbon in the nickel or the cobalt. It is difficult to say whether the acicular precipitates forming at the same time are carbides. They are possible similar to the acicular precipitates formed by the disintegration of supercooled austenite at the second or third degree.

Thus we have been able to show in the present investigation that a metastable carbide eutectic may also be obtained in nickel-carbon alloys. This fact graphically proves the close relationship of the properties of nickel-carbon alloys to iron and serves as an additional argument to justify the use of these alloys as models for iron. It is evident that the study of "white" nickel-carbon and cobalt-carbon alloys will help to widen our knowledge of the graphitization of cementite in iron carbide alloys, and of the properties of carbides in general.

Translated by J.M. Gwynn

REFERENCES

1. H. Morrogh and W.J. Williams, *Journ. of the Iron and Steel Inst.* 155, No.3, 321 (1947).
2. A.A. Gorshkov and R.A. Sidorenko, *Isv. Vysshix Ucheb Zavedenii Chern. Metallurg.* No.8, 39 (1958).
3. M. Khansen, *Struktury binarnyx splavov (Structures of binomial alloys), Metallurgizdat,* 1, p.367 (1941).
4. O. Ruff and M. Martin, *Metallurgie,* 9, 143 (1912).
5. E. Scheil, *Archiv. f. d. Eisenhuttenwesen,* 25, No. 1/2, 71 (1954).

AN INVESTIGATION OF INTERNAL FRICTION IN POWDER PRODUCTS*

B.Ia. PINES and DEN GE SEN

Khar'kov State University

(Received 12 May 1958)

An investigation was made of the relationship between temperature and the logarithmic decrement of torsional oscillations Q^{-1} in sintered specimens of Cu, Ni and Fe powders and Cu-Ni and Cu-Fe powder mixtures. The activation energy E' was determined from the frequency shift of the internal friction peaks and E'' from the "background" of the curve $Q^{-1} = Q^{-1}(T)$. The relationship between E' and E'' and concentration was found for specimens of the Cu-Ni and Cu-Fe systems. For specimens made from powder mixtures of different metals, three peaks are obtained on the $Q^{-1} = Q^{-1}(T)$ curves, two of which relate the processes at similar grain contacts and one to processes at dissimilar grain contacts.

VOL. 8 1959

1. The study of internal friction in solids, which has led to many fruitful results in the work of Ke T'ing-sui [16], A.S. Nowich [2], L. Rotherham and S. Pearson [3, 4], W. Köster [5], B.N. Finkel'shteyn [6], V.S. Postnikov [7] and others has, in general, not yet been sufficiently widely applied, especially in regard to alloys. At the same time, the results of an internal friction investigation cannot always be interpreted simply and uniquely.

The investigation of internal friction in metallic bodies compacted from powders of different metals is of great interest inasmuch as in such bodies it is possible to create a given non-homogeneity in composition and structure and trace the relation between this non-homogeneity and the internal friction effects.

Internal friction in sintered specimens of Cu, Ni and Fe powders is investigated experimentally in the present paper, as also is internal friction in specimens made from powder mixtures of the above metals.

2. The investigation was carried out in a vacuum "relaxator" for torsional oscillations of the usual type [8], using specimens 70 mm long and 3 x 3 mm in cross-section, with heads of larger cross-section (6 x 3 mm) 10 mm long. The specimens were produced by compacting the powders in a special die. The heads of the specimens were secured rigidly in stainless steel clamps and the frequency of the free oscillations controlled by the magnitude of the loads put on the horizontal rod suspended from the lower specimen clamp. The oscillation frequency was ordinarily 1.0-2.7 c/s. The oscillations were excited by solenoids attracting iron armatures.

Typical curves of the logarithmic decrement of vibration damping Q^{-1} against temperature are shown in Fig. 1. This gives two curves for a specimen prepared from pure copper (compacted from electrolytic powder with a linear particle size of under 50 and porosity of approximately 26%). Curve 1 was obtained with loads which gave an oscillation frequency $f_1 = 0.86$ c/s; curve 2, for an oscillation frequency $f_2 = 1.94$ c/s.

Fig. 2 shows similar curves for specimens made from a Cu and Ni powder mixture (75% Ni). Here the corresponding frequencies were $f_1 = 0.85$ c/s, $f_2 = 2.01$ c/s. As can be seen, in all cases there are internal friction "peaks" on the curves at some temperature and, moreover, a rapid monotonic growth of Q^{-1} is observed with increase of temperature.

* *Fiz. metal. metalloved.* 8, No.4, 599-606, 1959.

According to the literature [3], internal friction curves of a similar type have been observed for cast copper specimens.

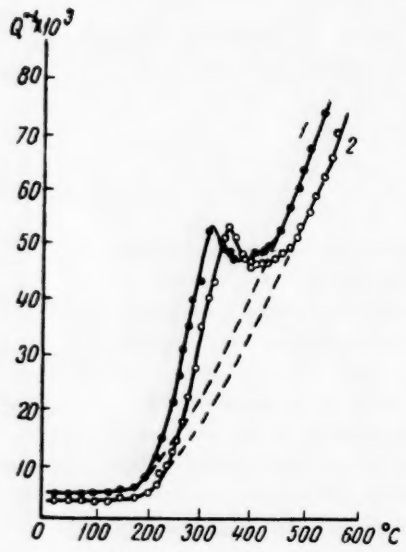

Fig. 1. Variation with temperature of internal friction of pure copper sintered specimens. Q^{-1} is the logarithmic decrement of torsional oscillation damping. Specimens instered at 1000° for 30 min. 1 – Oscillation frequency f_1 = 0.86 c/s (for 20°); 2 – oscillation frequency f_2 = 1.94 c/s (for 20°).

3. The activation energies of the processes determining the internal friction were obtained from measurements of the temperature dependence of the logarithmic decrement. They were obtained by two distinct methods:-

a) from the shift of the observed internal friction peak in relation to the oscillation frequency. In this method the activation energies E were calculated from the formula

$$E = R\,\frac{\ln f_1/f_2}{\frac{1}{T_1}-\frac{1}{T_2}}, \qquad (1)$$

where T_1 and T_2 are the temperatures of the maximum of the peaks at oscillation frequencies f_1 and f_2 and R is the gas constant;

b) from the temperature trend of the smooth part of the curve $Q^{-1} = Q^{-1}(T)$ i.e. from the so-called "background" curve. Here it was assumed that the smooth part of the curve Q^{-1} or "background" varies with temperature according to the law $Q_1^{-1} = \frac{A}{T}\exp\left(-\frac{E}{RT}\right)$ (where A is a constant).*

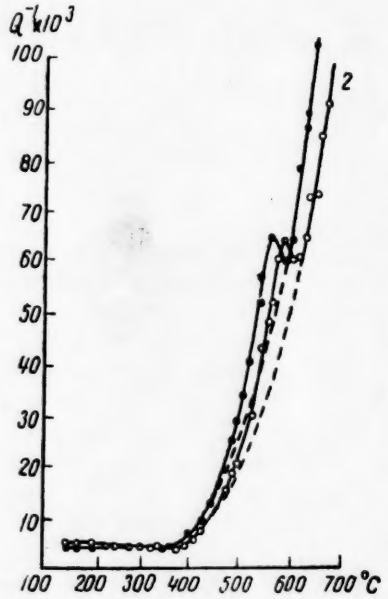

Fig. 2. Variation with temperature of internal friction of specimens sintered from Cu and Ni (75% Ni) powder mixtures. Specimens sintered for 2.5 hr at 1000°. 1 – Oscillation frequency f_1 = = 0.85 c/s; (for 20°); 2 – oscillation frequency f_2 = 2.01 c/s (for 20°).

For pure Cu and Ni the values of E determined from the internal friction peak shift and from the "background" trend were identical, viz. E_{Cu} = 34 cal/mole; E_{Ni} = 43 cal/mole.

The figures quoted relate to specimens sintered at 1000° for 5 hr. In general, the values of activation energy obtained depend on the temperature and duration of sintering as is shown by the data given in Fig. 3. For pure copper, for example, the activation energy (from the "background" and from the frequency shift of the maximum) for specimens sintered for 30 min at 1000° is only 27 kcal/mole. The activation energy rises when the sintering time is increased. The same applies to specimens compacted from nickel

* This relationship between background and temperature was also used when isolating the peak and constructing the background curve.

powder. It should be noted that although the magnitude of the activation energy is not very accurately determined in an internal friction investigation (the calculated error is 7%) the changes in activation energy with increased sintering time are fixed sufficiently reliably as they exceed 20%.

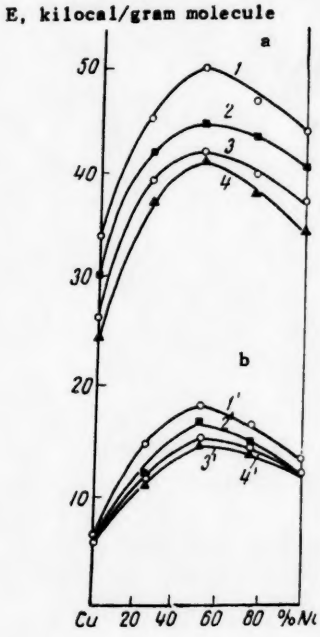

Fig. 3. Relationship between activation energy and volumetric concentration of components for specimens sintered from Cu-Ni powder mixtures. The specimens were sintered at 1000° for: 1 – 300; 2 – 150; 3 – 60 and 4 – 27 min. The values of E were determined by the frequency dependence of the peak temperature. Sintering time of specimens (at 1000°): 1′ – 300, 2′ – 150, 3′ – 60 and 4′ – 25 min; E found from the "background" curve.

4. Figs. 4a and 4b show the internal friction curves for sintered specimens made from mixed Cu-Ni powders. The general trend of the curves is the same as for the pure metals but the number of maxima on the curves is increased. In addition to the maximum corresponding to the pure copper and the maximum corresponding to the pure nickel, additional, third maxima are observed which in our opinion should be attributed to internal friction effects (diffusion effects) at the grain boundaries, primarily appertaining to the *dissimilar* metals Cu and Ni. The maxima corresponding to the pure metals are shifted to different temperatures in the specimens prepared from powder mixtures, which was to be expected as there are no pure component grains in these specimens, which were sintered at 1000°, but only solid solution grains.

Assuming that the maxima observed on the internal friction curve correspond to grain boundary effects, it must be concluded that the three maxima on the $Q^{-1} = Q^{-1}(T)$ curves are due to processes primarily corresponding to Cu-Cu, Ni-Ni and Cu-Ni grain junctions.

From the data given in the curves of Figs. 4a and 4b, the activation energy was also determined by the two methods – from the "background" and from the frequency shift of the additional internal friction peak corresponding to the boundary of the fundamentally dissimilar grains of the Cu-Ni system. In order that the error in determining the magnitude of E should not here exceed ~10%, the peak shift was measured only on specimens with a high Ni content (25, 50 and 75%).

Fig. 3 shows the results of the determination of E. It appears that the activation energy determined from the "background" of the Q^{-1} curve depends linearly on the concentration of the powder mixtures. On the other hand, the magnitude of the activation energy found by the frequency shift of the maximum displays a concentration dependence in the shape of a convex curve. In plotting this curve, it is assumed that as a result of the sintering, the concentrations of solution directly on the boundary of dissimilar grains have been able to equalize themselves (i.e. have become the same in both grains). This justified drawing a curve through points corresponding to pure components.

The data given show that the "background" effects and the appearances of the maxima observed during the internal friction investigation are essentially different although in the case of pure metals the activation energy values coincide for the two effects.

During an investigation of the diffusion creep of specimens made from Cu-Ni powder mixtures [9] it was found that the relationship between concentration and activation energy of constant creep is also linear, and

VOL. 8 1959

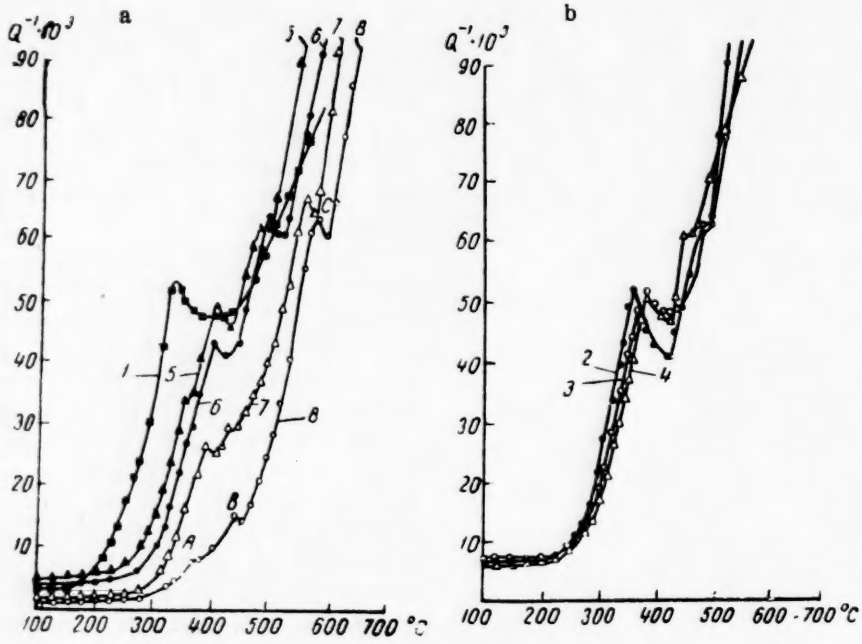

Fig. 4 a-b. Internal friction plotted against measurement temperature for specimens sintered from Cu-Ni powder mixtures. Specimens sintered at 1000° for 30 min. Oscillation frequency f = 1.5 c/s (for 20°):
1 – pure copper; 2 – Cu-Ni (Ni ~ 0.5%); 3 – Cu-Ni (Ni ~ 1%); 4 – Cu-Ni (Ni ~ 3%); 5 – Cu-Ni (Ni ~ 5%); 6 – Cu-Ni (Ni ~ 10%); 7 – Cu-Ni (Ni ~ 25%); 8 – Cu-Ni (Ni ~ 50%); A – peak for Cu-Cu; B – peak for Cu-Ni; C – peak for Ni-Ni.

that the magnitude of the activation energy has approximately the same values as those obtained from the internal friction experiments. This gives grounds for suggesting that the background on the $Q^{-1}(T)$ curve is determined by creep effects in the neighbourhood of the grain boundaries. On the other hand, the peaks, which also represent a surface effect, are associated with some diffusion process. Possibly they are associated with passages of atoms across the grain boundaries.

Fig. 5 gives some data on the maximum temperatures of "similar" and "dissimilar" peaks (corresponding to the contact of dissimilar and similar grains) in relation to concentration. The data relate to specimens sintered at 1000° for 30 min. The maximum corresponding to the dissimilar grain contacts is obtained at the highest temperature for a 50% mixture. The maximum for "similar" contacts (which in the initial state corresponded to Cu-Cu and Ni-Ni grain boundaries) is displaced towards the high temperature side in the case of the powder mixture specimens, in comparison with the position for the pure component specimens.

In order to test the suggestion concerning the link between the maximum on the $Q^{-1}(T)$ curve and the processes at the grain boundaries, a comparison was undertaken between the height of the maximum corresponding to the contact of the "similar" Cu-Cu grains and the height expected for mixtures of various concentrations according to the above suggestion. For specimens made from powder mixtures, the height of this maximum must decrease in proportion to the decrease in the area of contact of similar grains. In the case of isomeric Cu and Ni powders, the contact area S of the Cu-Cu grains must alter with concentration according to the law $S = S_0 (1 - x^2)$ (where x is the concentration of Ni by volume). Fig. 6 shows the calculated

and experimental relationships of the height of the maximum. Within the limits of unavoidable error, due to the scatter in the grain sizes of the specimen, both curves coincide.

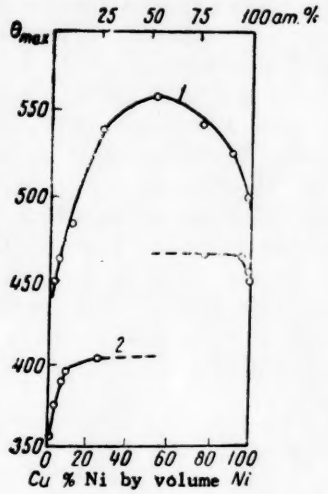

Fig. 5. Peak temperature plotted against component concentration: 1 – peak obtained only in specimens made from Cu-Ni powder mixture; 2 – peak observed also in specimens of pure copper; 3 – peak occurring in specimens of pure nickel.

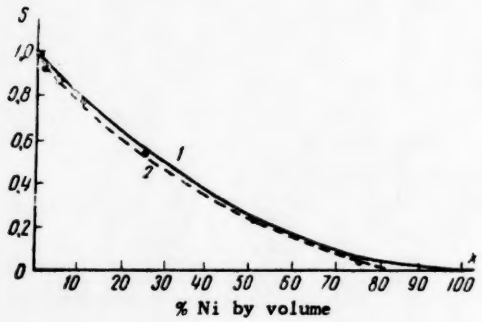

Fig. 6. Variation of the height of the maximum with concentration of the second component (Cu+Ni system):
1 – calculated curve $S/S_0 = (1 - x^2)$; 2 – experimental curve.

5. In powder products which are in a state of disequilibrium, the values of activation energy obtained depend on the duration of the high temperature soak. Fig. 7 shows more detailed data for specimens subjected to sintering of various durations at 1000°. The values of activation energy shown here were found from the frequency shift of the internal friction peak. For specimens made from pure Cu and Ni powders the values of E correspond to the peaks on the "similar" contacts. For specimens made from powder mixtures of various compositions the activation energies were determined from the frequency shift of the peak corresponding to "dissimilar" contacts. In spite of a prolonged soak, the growth of the values of E with increased sintering duration is not slowed down much. Hence it can be expected that a considerable increase in the soak period up to tens of hours may noticeably increase the values obtained for E.

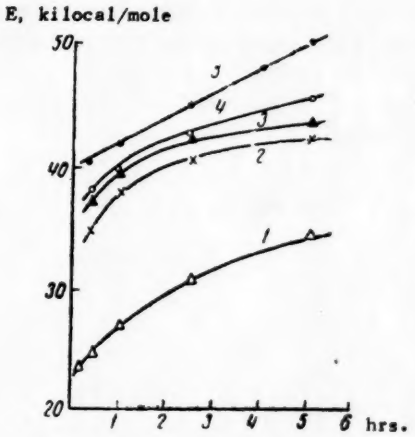

Fig. 7. Activation energy plotted against duration of sintering at 1000°: 1 – pure copper; 2 – pure nickel; 3 – Cu-Ni(25%Ni); 4 – Cu-NI (75%Ni); 5 – Cu-Ni(50%Ni).

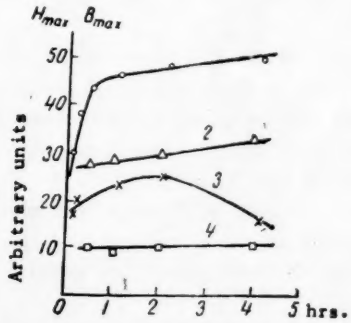

Fig. 8. Height H_{max} and breadth B_{max} of internal friction peak plotted against duration of sintering at 1000°:
1 – height of peak for pure copper; 2 – height of peak for solid solutions (Cu-Ni, 50%); 3 – breadth of peak for pure copper; 4 – breadth of peak for solid solutions (Cu-Ni, 50%).

VOL. 8 1959

Fig. 8 shows the alteration in the height H_{max} and breadth B_{max} of the internal friction peaks in specimens made from Cu powder and from a mixture of Cu and Ni powders (50%) subjected to sintering of various durations at 1000°. The height and breadth of the peaks also change to a notable extent, depending on the change of state in the specimen as a result of sintering.

Fig. 9 also gives data on the dependence of the magnitude of the activation energy of internal friction processes on the volumetric concentration of the components for specimens made from Cu-Fe powder mixtures. Here also the magnitude of E was determined in two ways:

a) from the frequency shift of the internal friction peak (curve 1, fig. 9) and

b) from the "background" of the $Q^{-1}(T)$ curve (curve 2, fig. 9).

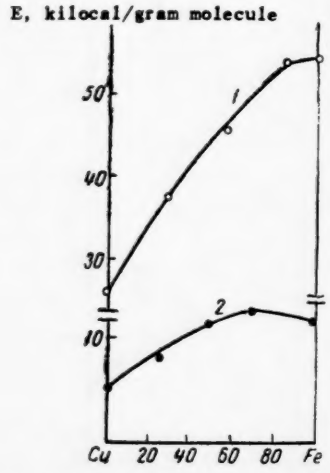

Fig. 9. Activation energy plotted against component concentration for specimens made from Cu-Fe powder mixtures. Specimens sintered at 1000° for 30 min.
1 – values of E found from the frequency shift of the internal friction peak; 2 – values of E calculated from the background curve.

In this case also the values of E determined from the trend of the "background" depend linearly on the concentration. Curve 2 on fig. 9 is almost indistinguishable from a straight line. The values of E found from the frequency shift of the peak in this system also form a convex curve. It should be noted that in specimens made of Cu and Fe powder mixtures three peaks were observed on each $Q^{-1} = Q^{-1}(T)$ curve (fig. 10). As before, it was possible to consider that two peaks (A and C) correspond to processes on the Cu-Cu and Fe-Fe grain boundaries and the third peak (B) to processes on the boundaries of dissimilar grains.

The points on curve 1 Fig. 9 correspond to the frequency dependence of the dissimilar grain peak. We shall note that in this case this peak may correspond to heterodiffusion phenomena, although mutual solubility in the Cu-Fe system is not very great [10] (about 5% Cu in Fe and 3% Fe in Cu at 1000°). The specimens made from Cu-Fe powder mixtures which were investigated in the "relaxer" were sintered at 1000° for 30 min.

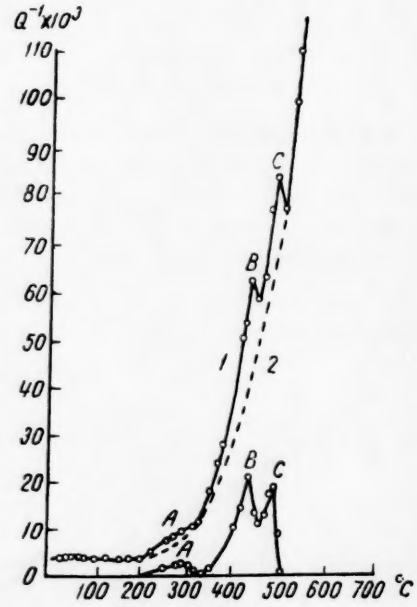

Fig. 10. Internal friction plotted against temperature for a specimen made from a Cu-Fe (50%) powder mixture. The specimen was sintered at 1000° for 30 min: A – peak for Cu-Cu; B peak for Cu-Fe; C – peak for Fe-Fe: 1 – experimental curve of internal friction $Q^{-1}(T)$; 2 – calculated "background" curve, plotted in accordance with the formula:

$$Q_1^{-1} = \frac{A}{T} \exp\left(-\frac{E}{RT}\right).$$

CONCLUSIONS

1. The activation energy, and the height and

breadth of the internal friction peaks for specimens made from pure metals and Cu-Ni powder mixtures depend on the duration of sintering of the specimens; the activation energy rises with increased duration of soak, as does the height of the peaks.

2. In specimens made from Cu-Ni and Cu-Fe powder mixtures, the activation energy determined from the "background" depends linearly on the volumetric concentration of the mixtures.

3. The activation energy found from the frequency shift of the peak, which corresponds to the contact of dissimilar grains, depends on the concentration in a non-linear manner, forming a convex curve.

4. Three peaks are observed on each curve showing the relationship between temperature and logarithmic decrement for specimens made from Cu-Ni and Cu-Fe powder mixtures. Two of these correspond to the contact of similar grains and one to the contact of dissimilar grains.

5. In powder mixtures where the component grain sizes are approximately the same, the height of the peak which corresponds to the contact of similar grains varies approximately as the area of grain contact, i.e. according to the law $(1 - x^2)$, where x is the volumetric concentration.

VOL. 8 1959

REFERENCES

1. Ke T' ing-sui. *Phys. rev.*, 71, 533 (1947); 72, 41 (1947); 73, 268 (1948); 74, 914 (1948). *Journ. Appl. Phys.*, 19, 285 (1948); 20, 274 (1948); 21, 414 (1950).
2. A.S. Nowick. *Phys. rev.*, 88, 925 (1952); symposium *"Uspekhi fiziki metallov"*, *Metwllurgizdat*, Moscow, 1, p.7 (1956).
3. L. Roterham and S. Pearson. *Journ. Metals.*, No.8, 881 (1956).
4. S. Pearson and L. Rotherham. *Journ. Metals.*, No.8, 898 (1956).
5. W. Koster. *Zs. Metallkunde*, 47, 228 (1956); 46, 34 (1955).
6. B.N. Finkel'shteyn and K.M. Rozin. *Dokl. Akad. Nauk SSSR*, 91, 811 (1953).
7. V.S. Postnikov. *Dokl. Akad. Nauk SSSR*, 91, 79 (1953); *Zh. Teor. fiz.* 24, 9 (1954); *Fiz. Metal. Metalloved.* 4, issue 2 (1957).
8. V.S. Postnikov. *Tr. Kemerovskogo gornogo in-ta*, issue 1 (1954).
9. B.Ya. Pines and A.F. Sirenko. In symposium *"Issledovaniya po zharoprochnym splavam"*, 4, published by U.S.S.R. Academy of Sciences, Moscow (1958).
10. M. Khansen. *Struktura binarnykh splavov, (The Structure of Binary Alloys)*, Metallurgizdat, Moscow, 1 p. 533 (1941).

Translated by R. Hegarty

SOME FEATURES OF THE RECRYSTALLIZATION OF TRANSFORMER STEEL DURING RAPID HEATING

III. THE DEPENDENCE OF GRAIN GROWTH RATE AND ACTIVATION ENERGY ON HEATING RATE*

P.D. IZBRANOV, V.A. PAVLOV and N.M. RODIGIN

Institute of the Physics of Metals USSR Academy of Sciences
Sverdlovsk State Educational Institute

(Received 25 January, 1959)

In previous papers [1, 2] it was suggested that the high recrystallization rates occurring during rapid heating of cold deformed metals, in particular transformer steel, could be explained by a considerable reduction in recovery immediately before recrystallization.

Such a change in the state of the metal before recrystallization must affect the grain growth rate and the activation energy of grain growth. Rafalovich [3] has done some work in this direction, determining the activation energy of grain growth during rapid induction heating of low-carbon steel. According to his data, it was about a third of the activation energy of grain growth during slow heating. He determined the grain growth rate and also the nucleation rate by the technique devised by I.L. Mirkin [4]. He did not measure the grain growth rate directly as was done, for example, in references [5, 6].

It is of interest to determine the grain growth rate and activation energy for transformer steel during both rapid and slow heating and to compare the data obtained with the results mentioned above, and this is the object of the present paper.

The material used for the investigation was transformer steel with the following composition: carbon – 0.08%, silicon – 3.54%, manganese – 0.15%, sulphur – 0.018% and chromium – 0.10%.

1. *Rapid Electric Heating.* In order to distinguish the new grains which appeared in the recrystallization process from the old grains of the deformed matrix, a large-grained material was selected for the preparation of the specimens. The material was subjected to the following treatment with the object of obtaining large grains. Strips of raw material 0.5 mm thick were cold rolled to 40% shrinkage, after which they were ann annealed at a temperature of 1000° for 40 min. They were then given a small deformation by cold rolling (2-3%) after which they were re-annealed at 1000° for 6 hr. As a result of this treatment, the mean grain size in the specimens was of the order of 2-3 mm. To reduce the number of recrystallization centres during the subsequent rapid annealing, the material was lightly cold rolled after re-annealing, to 10% elongation.

The specimens prepared in this manner were subjected to rapid electric heating without soaking to various temperatures (from 1000° to 1360°). Cooling took place in air. In each annealed specimen, the size of the 10 largest isolated grains formed in the recrystallization process was measured and their mean value calculated (the area of the prepared sections was approximately the same). In this connexion, the mean deviation of the grain size from the mean value in individual specimens did not exceed ± 10%.

* *Fiz. metal. metalloved.* 8, No.4, 607-612, 1959.

VOL 8 195

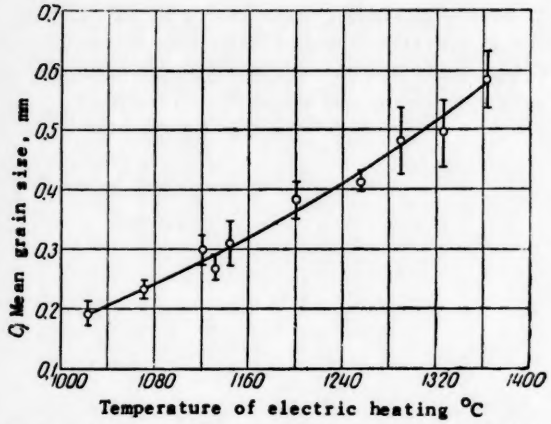

Fig. 1. Mean grain size plotted against electric heating temperature.

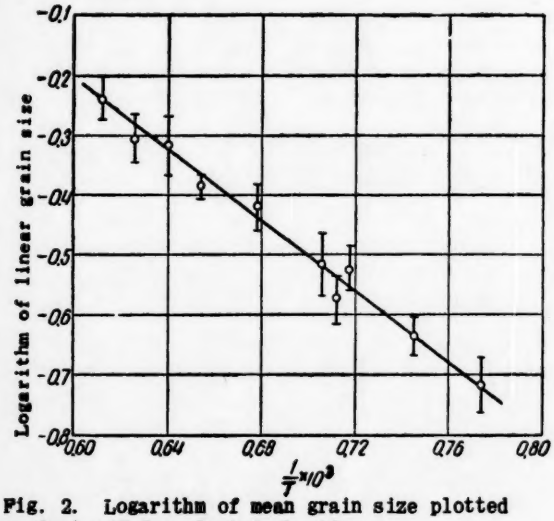

Fig. 2. Logarithm of mean grain size plotted against $1/T$ for electric heating.

The results of the experiment are presented in Fig. 1, which shows the relationship between grain size and electric heating temperature. As can be seen from the diagram, the grain growth rate increases with temperature; with a final temperature of 1020° the mean size of the largest isolated grains in the specimen is of the order of 0.2 mm, and with a temperature of 1360° approximately 0.6 mm. The magnitude of the deviation of grain size from the mean value is indicated on the diagram by means of the vertical intercepts.

The results of the above experiment enable the activation energy of the grain growth during rapid electric heating to be determined. In fact, if a graph is plotted showing the logarithm of mean size against $1/T$ (where T is the absolute temperature), the experimental points should lie on a straight line, the tangent of whose angle of slope is a measure of the activation energy of grain growth. From the data in Fig. 2, which was constructed by the method indicated above, the activation energy of grain growth is found to be equal to 13,500 ± 2,500 cal/mole.

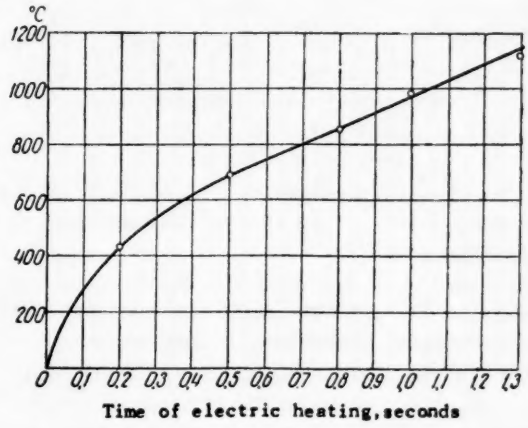

Fig. 3. Annealing temperature plotted against electric heating time.

To determine the grain growth rate it is necessary to know, in addition to the data in fig. 1, the time in which this growth took place. The relationship between temperature and heating time was determined experimentally for one particular specimen. This relationship is shown in fig. 3, from which it can be seen that from 700° onwards the rate of temperature rise becomes practically constant and (for this specimen) equal to about 500°/sec. With some approximation it may be considered that all the specimens of the above experiment were heated from 1000° to higher temperatures at this rate.

Knowing the heating rate and the temperature difference over a particular section of the curve in fig. 1, the duration of the temperature rise over this portion can readily be determined. On the assumption that the incubation period of the measured grains is the same in all specimens and the increase in mean grain size over a particular section of the curve in fig. 1 occurred during the time determined by the method indicated above, it is possible to determine the grain growth rate in this temperature range. The grain growth rate calculated by this method varies

VOL. 8 1959

from 0.2 mm/sec to 0.4 mm/sec in the temperature range 1000-1360°.

The activation energy determined from the relationship between the logarithm of grain growth rate and $1/T$ was approximately the same as that obtained from the data in fig. 2.

2. *Slow Heating.* In isothermal annealing the grain growth rate is often determined from the results of observing the growth of individual grains [5]. Anderson and Mehl [6] used a statistical method to determine the grain growth rate, which involves determining the grain growth rate, which involves determining the sizes of the largest isolated grains in each specimen and thence determining the mean value. This method was used by us in this experiment.

The specimens prepared for this experiment underwent the same treatment as before. After 10% deformation they were heated in an ordinary resistance furnace to a temperature of 870° at a mean rate of 0.2°/sec and then annealed in a salt bath at the same temperature for 45 min. After this the sizes of the 20 largest isolated grains were measured and the mean value found. Then they were again annealed at 870° for 15 min. The sizes of the 20 largest isolated grains were again measured and the mean value calculated. In both cases, the only grains considered were those whose mean deviation from their mean value did not exceed ± 10%. From the values found for mean grain size before and after the repeat annealing, the grain growth rate was determined for the given temperature. In the present experiment, a mean grain growth rate equal to 6.0×10^{-5} mm/sec was obtained.

Other batches of specimens were annealed in a salt bath at temperatures of 900, 942 and 975°. The mean grain growth rates at those temperatures were, respectively, 10×10^{-5}; 19×10^{-5} and 31×10^{-5} mm/sec.

Fig. 4, plotted from these data, expresses the relationship between the logarithm of the grain growth rate and $1/T$. The activation energy, calculated from the tangent of the angle of slope of the straight line of the diagram, is approximately equal to 44,000 cal/mole. Allowing for the maximum error, which in this case is ± 25%, the minimum value of the activation energy of grain growth during slow heating is 33,000 cal/mole. This is over twice the maximum value of the activation energy of grain growth during rapid heating.

The grain growth rates were determined in the temperature ranges 1020-1360° for rapid electric heating and 870-975° for slow heating.

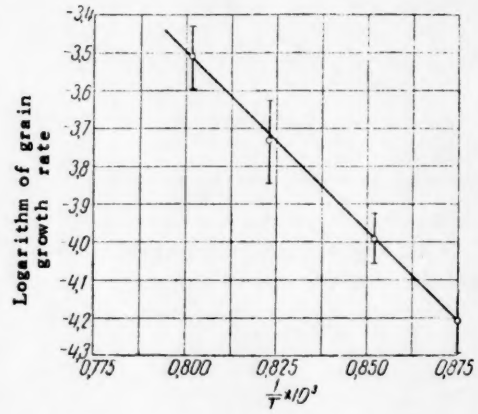

Fig. 4. Relationship between the logarithm of grain growth rate and $1/T$ during slow heating.

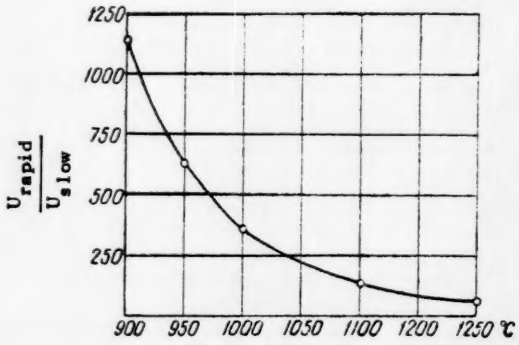

Fig. 5. Variation with temperature of ratio of grain growth rates during rapid electric heating and slow heating.

TABLE 1

T °C	Grain growth rate, mm/sec.	
	during rapid heating U_{rapid}	during slow heating U_{slow}
900	0.11	10×10^{-5}
1000	0.16	44×10^{-5}
1100	0.21	155×10^{-5}
1200	0.27	474×10^{-5}

On the assumption that the activation energies of grain growth during rapid and slow heating do not alter in the 900-1200° temperature range, it is possible to determine the grain growth rates in this range by extrapolating the straight lines which represent the logarithm of the grain growth rate plotted against $1/T$. The results of these calculations are given in the table.

The ratio of the grain growth rates decreases with increase of temperature, as is shown in Fig. 5.

DISCUSSION OF THE RESULTS OBTAINED

In the 900-1200° temperature range, the grain growth rate during rapid electric heating is 100-1000 times greater than the grain growth rate during slow heating. The ratio of these rates diminishes with increase of temperature.

The activation energy of the grain growth process during rapid heating is approximately one-third of the corresponding value slow heating. This result, obtained for transformer steel, is of the same magnitude as the results of reference [3] for low-carbon steel. It should be noted that the technique used by us to determine the grain growth rate was different from that used in reference [3].

The following considerations may be used to explain the results obtained.

1) During rapid heating, material with increased free energy will be passing into the high temperature zone; consequently a reduction in the activation energy of the recrystallization process is possible. During slow heating, on the other hand, recovery processes are occurring during the period between the commencement of heating and the attainment of the recrystallization temperature of the material and as a result of these processes a proportion of the most unstable distortions of the crystalline lattice is removed.

3) As has been previously pointed out [1], redistribution of the alloying elements can affect the grain growth rate. In fact, during slow heating the alloying elements may accumulate on the boundaries of the nuclei and hinder their growth. During rapid heating, on the other hand, it is possible that the alloying elements do not have time to diffuse to the boundaries of the nuclei, which would favour their growth.

3) On a "micro" scale, transformer steel, like all steels, is a heterogeneous substance not only in composition and crystal lattice structure but also in thermal and electrical conductivity. Due to this heterogeneousness, heating of the various microsections by an electric current may be non-uniform. During slow heating there is time for temperature equalization to occur, while during rapid heating various temperature gradients may arise, depending on the heating rate. The greater the heating rate, naturally, the greater will be the non-uniformity of the heating, and this can play a part in the nucleation and growth of the grains.

Of the above three considerations, the third is the least likely and for the following reason. At the heating rates used in this paper, an increased recrystallization rate was observed not only with rapid electric heating but also when thin specimens of cold-deformed metals were heated in a salt bath, when the soak time is a fraction of a second. Thus, for example, in reference [2] it was established that specimens of cold-deformed transformer steel 0.11 mm thick (95% shrinkage) recrystallize completely at a temperature of 725° in less than one second. In the same paper it was shown that the rate of electric heating was of the order of 1000°/sec and the corresponding current densities had no noticeable effect on the mechanism of new grain formation from the point of view of orientation relationships. Regardless of the method of heating (electric current or salt bath), the recrystallization centres with the greatest probabilities of forming nuclei are those whose orientation coincides with that of the portions of the deformed crystal.

A more probable governing factor affecting the recrystallization rate is the condition of the metal at high temperatures.

From this point of view the work of Masing and his co-workers [7] is of interest. In this the relationship between recovery activation energy and toughening has been established experimentally. According to their results, when the toughness is approximately tripled, the activation energy of recovery

VOL. 8 1959

is almost halved.

In view of the above, it appears desirable to investigate in subsequent work the effect of preliminary recovery before recrystallization on the magnitude of the grain growth activation energy during rapid electric heating.

CONCLUSIONS

1. An investigation was made of the relationship between temperature and grain growth rate in the process of the first stage of recrystallization of cold-deformed transformer steel using both rapid and slow heating.

In the 900-1200° temperature range the grain growth rate with rapid heating was 100-1000 times greater than with slow heating. The ratio of these rates decreases with increased temperature.

2. The activation energy of grain growth with rapid electric heating is approximately one-third of that with slow heating.

Translated by R. Hegarty

REFERENCES

1. P.D. Izbranov, V.A. Pavlov and N.M. Rodigin. *Fiz. Metal. Metalloved.* 7, 915 (1959).
2. P.D. Izbranov, V.A. Pavlov and N.M. Rodigin. *Fiz. Metal. Metalloved.* 8, 434 (1959).
3. Ts.N. Rafalovich. *Fiz. Metal. Metalloved.* 2, 259 (1956).
4. I.L. Mirkin. *Sb. Moskovskogo in-ta stali (Symposium of the Moscow Steel Institute)*, 18 (1941).
5. M. Kornfel'd and V. Pavlov. *Zh. Eksp. teor. fiz.* 4, 982 (1934).
6. W.A. Anderson and R.F. Mehl. *Trans. AIME*, 161, 140 (1945).
7. D. Kuhlmann, G. Masing and I. Raffelsiper. *Zs. Metallkunde*, 40, 241 (1949).

SMALL FLOW AND AFTER-EFFECT DEFORMATIONS OF SPRING PHOSPHOR BRONZE Br. OF6.5-0.15*

S.O. Tsobkallo

Leningrad Polytechnic Institute named after M.I. Kalinin

(Received 6 August 1958)

Using new and accurate methods, a study was made of the direct and reverse elastic after-effect in bending, and also of the elastic limit of Br. OF6.5-0.15 at normal temperature. The elastic limit was determined allowing for the time of action of the stress from curves which it is proposed to term elastic limit curves. An analysis of these curves in the paper leads to the establishment of a phenomenon termed proportional flow. In comparison with an annealed specimen, an increase in elastic limit and a decrease in the direct elastic after-effect accompanied by increased reversibility were established for a cold-worked alloy with over 32% deformation. The paper gives an analysis of the physical nature of the phenomena established in connexion with structural changes in the alloy during cold-working.

VOL. 8 1959

1. STATEMENT OF THE PROBLEM

The physical property of the elasticity of metals, which is the basic one for spring materials, is defined by two mechanical characteristics: the modulus and the elastic limit. The latter, as has been shown in previous papers by the writer [1, 2] depends on the time of action of the force and is determined by the phenomenon of after-effect elasticity. This phenomenon is also very important for the evaluation of the mechanical properties of spring materials used for the manufacture of spring elements in instrument construction [20]. It is important to study the elastic after-effect [4-6, 21] in materials at the large stresses used in practice (of the order of tens of kg/mm^2). A new and effective method recently devised [1, 11] has made it possible to state the problem [2] of a broad, systematic comparative study of the effect of various physical and technological factors on the imperfect elasticity. In this plan, the present paper is a link in a cycle of investigations devoted to materials [2, 3, 15-18] in a cold-worked state.

* *Fiz. metal. metalloved.* 8, No.4, 613-621, 1959.

2. MATERIAL AND TECHNIQUE OF THE INVESTIGATION

The work was carried out using spring phosphor bronze of the Sn 6.5 P0.15 type with the following composition: Sn 6.52% P 0.18% Cu 93.22%. The material was used in the form of a flexible ribbon 0.2 mm thick rolled with three different degrees of deformation ϵ_s 32-35; 49 and 60%. The time between cold-working and the investigation was about one month.

Study of the elastic after-effect and elastic limit was done in bending [1, 2, 11] which gives the best correspondence with the conditions of work of sheet spring material. The specimens were of an extremely simple shape, being rectangular strips 20 x 110 mm in size. The quantity $E/1 - \mu^2$ (where E is the modulus and μ Poisson's ratio) which is needed for the calculation of the stresses in the specimen was computed on the basis of measurements of E by a new infrasonic method [7-9]. E was found to be equal to 1.13×10^4 kg/mm^2 and remains practically the same for all the cold-workings shown with an accuracy of up to 1%. μ was taken as 0.36.

In this manner, the required value of $E/1 - \mu^2 = 1.30 \cdot 10^4$ kg/mm^2

3. THE RELATIONSHIP BETWEEN THE ELASTIC LIMIT AND COLD-WORKING

A new treatment of the elastic limit as a relaxation characteristic depending on the time of action of the force on the substance leads [1] to the necessity of testing a series of identical specimens which are given different stresses for a predetermined time (10 min). The values of residual deformation during this time $\Delta\epsilon_{10}$ are plotted as a function of the stresses σ acting on the specimen. As a result, a curve is obtained which in what follows will be termed the elastic limit curve (Fig. 1). By setting off along the ordinate the required allowance for residual deformation (for example, 0.001; 0.003; 0.005% etc.) it is possible to read off on the abscissa the corresponding values of the elastic limits.

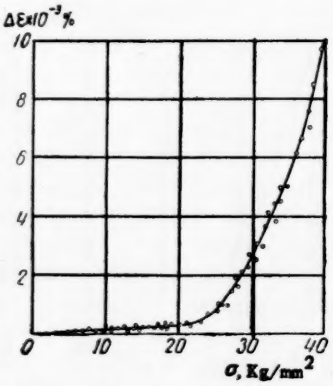

Fig. 1. Curve of elastic limits of bronze Sn 6.5 P0.15 cold-worked with 49% deformation.

In order to study the effects of cold-working on the elastic limits, curves were plotted for three degrees of plastic deformation and for completely annealed material (Fig. 2). On the basis of these data, values were obtained for the conventional (according to the universally accepted assumptions) elastic limits (Table 1) and their change in relation to cold-working was shown (Fig. 3).

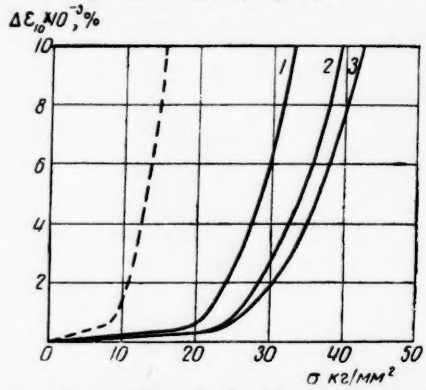

Fig. 2. Alternation of elastic limit curves of Sn 6.5 P0.15 bronze with cold-working. Degree of deformation: 1 – 32-35%; 2 – 49%; 3 – 60%. The dotted curve corresponds to fully annealed material.

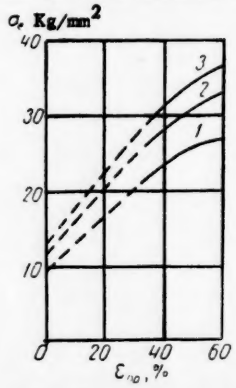

Fig. 3. Increase in conventional elastic limits of Sn 6.5 P0.15 bronze (in accordance with three tolerances for residual deformation) during cold-working:
1 – $\sigma_{0.001}$; 2 – $\sigma_{0.003}$; 3 – $\sigma_{0.005}$.

TABLE 1

State of material	Elastic limits kg/mm²				
	σ_{Pb}	$\sigma_{0.001}$	$\sigma_{0.003}$	$\sigma_{0.005}$	$\sigma_{0.01}$
Annealed at 650°	8	9.5	11.5	13.0	15.0
Deformation 32-35%	17	21.5	26.0	28.5	33.0
Deformation 49%	20	25.5	30.5	34.0	39.5
Deformation 60%	21	27.0	33.0	36.5	42.5

4. DEPENDENCE OF THE ELASTIC AFTER-EFFECT ON COLD-WORKING

The process of direct and reverse elastic after-effect is represented in the form of a family of curves of after-effect deformation $\Delta\epsilon$ against time (Figs. 4 and 5); the parameter of these curves is stress. These stresses were selected so that they were close to the corresponding values of the elastic limits. In this way a fuller characteristic of the imperfect elasticity properties is obtained for the material. Obviously, the better the material, the higher its elastic limit and the lower its elastic after-effect.

For the best quantitative description of the after-effect process it is appropriate to introduce the following numerical characteristics: 1) the magnitude of the deformation of the direct elastic after-effect during 10 min $\Delta\Sigma_{10}(\%)$; 2) the difference between the magnitudes of the direct elastic after-effect for 2 hr and for 10 min $m = \Delta\Sigma_{120} - \Delta\Sigma_{10}(\%)$ 3) the ratio of the deformation of the direct after-effect during 2 hours to the deformation during 10 minutes $k = \Delta\Sigma_{120}/\Delta\Sigma_{10}$; 4) the reverse after-

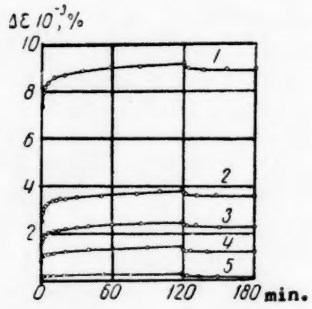

Fig. 4. Curves of direct and reverse elastic after-effect of Sn 6.5 P 0.15 bronze cold-worked to a 32-35% degree of deformation at the stresses: 1 – 32 kg/mm^2; 2 – 26.3 kg/mm^2; 3 – 24.3 kg/mm^2; 4 – 21.7 kg/mm^2; 5 – 11.5 kg/mm^2.

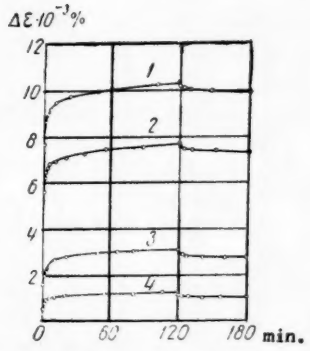

Fig. 5. Curves of direct and reverse elastic after-effect of Sn 6.5 P 0.15 bronze cold-worked to a 60% degree of deformation at the stresses: 1 – 41.8 kg/mm^2; 2 – 39 kg/mm^2; 3 – 32 kg/mm^2; 4 – 27 kg/mm^2.

TABLE 2

Deformation during cold-working, %	σ, kg/mm^2	$\Delta\varepsilon_{10}\,10,^{-3}\%$	$m \times 10,^{-3}\%$	k	$\Delta\varepsilon_{rev60}\,10,^{-3}\%$	α, %
32—35	11.5	0.20	0.05	1.25	0.12	50.0
32—35	21.7	1.10	0.30	1.27	0.20	14.0
32—35	24.3	2.05	0.40	1.20	0.21	8.5
32—35	26.3	3.35	0.45	1.13	0.22	6.0
32—35	32.0	8.55	0.60	1.07	0.30	3.5
49	21.6	0.40	0.17	1.44	0.15	22.0
49	26.6	1.45	0.35	1.24	0.22	12.0
49	32.0	3.70	0.50	1.14	0.27	6.5
49	37.6	7.60	0.70	1.09	0.30	3.5
49	39.5	10.33	0.80	1.08	0.32	3.0
60	27.0	1.02	0.20	1.20	0.20	16.0
60	32.0	2.65	0.60	1.16	0.28	9.0
60	39.0	6.95	0.72	1.10	0.35	4.5
60	41.8	9.42	0.85	1.09	0.37	3.5

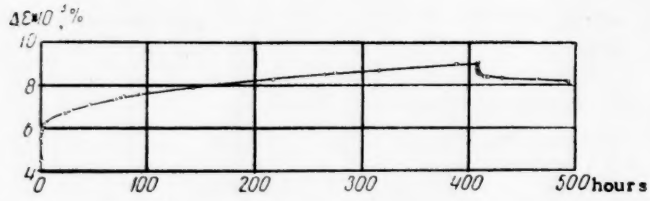

Fig. 6. Process of direct and reverse elastic after-effect over a prolonged period in Sn 6.5 P 0.15 bronze cold-worked to a 60% degree of deformation. Stress 37.2 kg/mm^2.

effect during 1 hr $\Delta\Sigma_{rev\ 60}$ (%); 5) the reversibility of the after-effect process $\alpha = \Delta\Sigma_{rev\,60}/\Delta\Sigma_{dir\,120}$. The values of these quantities, which in what follows will be termed the criteria of the elastic after-effect, are given in Table 2.

In addition to the main experiments, in which the direct after-effect was studied for 2 hr and the reverse after-effect for 1 hr, experiments of greater duration were carried out for several hundred hr (Fig. 6). From these data it was seen that the flow process under normal temperature conditions at a stress near the elastic limit $\sigma_{0.005}$ does not cease even after this prolonged time, continuing to the end of the experiment at the low rate of 4 x 10^{-6}%/hr.

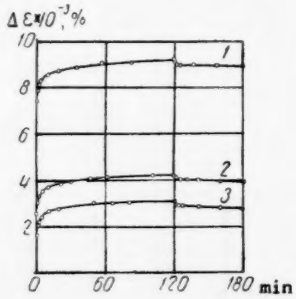

Fig. 7. Effect of cold-working on the process of direct and reverse elastic after-effect. Stress 32 kg/mm^2 for all curves. Degree of deformation: 1 – 32-35%; 2 – 49%; 3 – 60%.

The effect of cold-working on the process of direct and reverse elastic after-effect is shown best of all in the experiments using the same stress (Fig. 7).

5. DISCUSSION OF RESULTS

All the processes examined in the present paper are governed by flow of the polycrystal at normal temperature and small stresses. Analysis of this phenomenon is possible with the help of the elastic limit curves (see Figs. 1 and 2). In effect there are two portions on these curves: the initial, linear, and the steeper, curvilinear. The existence of the linear portion is confirmed by calculating the linear correlation coefficient, which has a value not less than 0.8. This value can be considered sufficiently large, in view of the considerable scatter of the numerical characteristics which is inherent in the elastic after-effect.

The presence of a linear portion on the elastic limit curve gives grounds for suggesting the existence of a special mechanism for the onset of small deformations of the polycrystal. The peculiarities of this mechanism are that the flow deformation in unit time (or, which amounts to the same thing, the flow rate) is proportional to the stress. The length and slope of the linear portion varies depending on the state (cold-working) of the material. In what follows this phenomenon will be termed proportional flow.

The writer also observed proportional flow when investigating a large number of materials – aluminium bronze [15], brass [18], dispersion hardening alloys [19] (beryllium bronze and others), steels of various types in the hardened and tempered conditions, and also in technically pure metals. It is appropriate to remark that the presence of proportional flow causes a linear distribution of stresses along the height of the bent

VOL 8 195

specimen, in spite of the fact that plastic deformation is taking place.

2. The appearance of a linear portion on the elastic limit curves makes it possible to introduce a new material characteristic defining the boundary of the linear portion with respect to stress. This quantity is a unique elastic limit, fixed, not by an arbitrary deformation tolerance, but on the basis of the physical characteristic of the flow process.

We shall agree to call this quantity the *proportional limit of elasticity* and denote it by σ_{pb} (proportional boundary). In order to exclude arbitrariness in finding the boundary of the transition of the linear portion into the curvilinear, we shall agree to regard this boundary as the point where the tangent of the angle of slope of the tangent is 25% larger than for the angle of slope of the linear portion. The values of σ_{pb} determined in this manner are shown in Table 1.

The existence of the linear portion of the elastic limit curve down to extremely low stresses (see Fig. 1) and the passage of the end of this portion through the origin gives grounds for considering the absolute elastic limit as being equal to zero. However, strict experimental proof of this conclusion is limited by the inaccuracy of measurement of the residual deformations and is obviously impossible. Moreover, modern ideas concerning the great mobility of atoms in the neighbourhood of defects in real crystals and possible energy fluctuations in different parts of the lattice give grounds for considering that a temperature other than absolute zero a theoretical elastic limit does not exist.

In the present paper, the employment of merely arbitrary elastic limits is based on a tolerance for the residual deformations caused by a force acting during a definite time. From this point of view, difficulties arise when using elastic limits given [36] without particulars of the deformation tolerance applied when they were determined.

3. A characteristic feature of proportional flow is its comparatively rapid attenuation (Fig. 4 curve 5). However, when the stress is increased above σ_{pb}, a significant momentary deformation appears on the flow curves, and this later changes into a slow flow (see Fig. 6). Hence σ_{pb} is the stress at which there is a "disruption" of proportional flow.

The proportional flow process is governed by elementary slips occurring in individual, highly stressed places in the polycrystal. A measurable quantity of deformation is composed of these slips, and is fixed by their number and the width of their propagation path. From this point of view it becomes possible to explain the decrease in the gradient of the linear portion with cold-working, which increases the number of slip locations. Therefore the tension decreases and there is a corresponding decrease in slip mobility. The decrease in the gradient is also facilitated by possible decrease in the propagation path with increased cold-working.

To explain the physical nature of proportional flow it is appropriate to introduce the ideas developed by Cottrell [25] concerning the segregation of solute atoms by distorted parts of the lattice, which had been stated as early as 1933 by Konobeyevskiy and Selisskiy [24]. The formation of such an "atmosphere" of atoms around the dislocation hinders its movement. As was shown [26], the speed of movement of this complex dislocation is small and proportional to the applied stress. Cottrell explained by this mechanism the phenomenon of microcreep observed by Chalmers [27] in monocrystals of tin at small stresses of the order of 0.1 kg/mm^2.

In spite of the external similarity of the phenomena of proportional flow and microcreep, the following principal differences between them should be pointed out:
1) proportional flow is observed on a polycrystal and microcreep on a monocrystal;
2) proportional flow occurs at stresses approximately 100 times greater than microcreep; 3) as a result of proportional flow, residual stresses arise which cause reverse elastic after-effect, whereas there is none with microcreep; 4) proportional flow is more clearly defined on severely cold-worked materials, but microcreep was observed only on annealed materials.

4. Proportional flow with its disruption at σ_{pb} is essentially the transition mechanism of the material to greater plastic deformations. In this connexion the quantity σ_{pb} acquires the meaning of the physical yield point. However, the area of yield in many

cases cannot be clearly observed during ordinary tensile tests. It will be apparent only during an especially sharp breakdown of the proportional flow process. Support is lent to this view by the manifestation of a greater area of yield [34] in phosphor bronze when the material is heated to 100° after cold-working. Furthermore it has been shown [15-19] in a number of alloys (including phosphor bronze [16]) that low temperature annealing after cold-working leads to an increase in σ_{pb}. Hence the presence of a visible area of yield indicates that the difference in materials is quantitative rather than fundamental [23].

5. Considering the universality of the proportional flow phenomenon and also its existence up to comparatively high stresses, of the order of tens of kg/mm^2 (see Fig. 2), this phenomenon must be regarded as of direct practical interest. The linear portion on the elastic limit curve gives a fundamental limitation of the relative minimum error caused by imperfect elasticity of the material. Therefore the specification of stresses below σ_{pb} in the operation of spring elements is meaningless.

The concepts of the segregation of solute atoms around dislocations are very promising for the creation of a new kind of heat treatment – the annealing of alloys after cold-working with the object of improving the imperfect elasticity characteristics. It is important to note that an improving annealing of this kind, formally compatible with the structure, can be carried out even on single-phase alloys and need not necessarily be accompanied by the segregation of new phases. In a heat treatment of this type there may be little or no change in the mechanical characteristics usually defined in industry (breaking point, elongation, hardness), as has been shown by Sachs [29] and later by Rovenskiy [35] and the writer [10, 12]. However, due to the atom localization of the process, as has been shown [2, 3, 16], the practically important characteristics of resistance to small plastic deformations (elastic limit and σ_{pb}) and imperfect elasticity (elastic after-effect and also vibration damping) may change many times.

The mechanism of proportional flow will appear in the majority of cases when the plastic deformations are commensurate with the elastic deformations possible in the given solid. For this reason the mechanism must occur during stress relaxation, during recovery, and also when residual stresses of the first order are removed.

6. An examination of the after-effect process (see Table 2, Figs. 4-7) shows that this phenomenon is more sensitive to cold-working than is the elastic limit. In fact, while the elastic limit rose by 25% when the deformation was altered from 32-35% to 60%, the elastic after-effect, according to the criterion $\Delta\Sigma_{10}$ (for various values of σ) decreased over 300%. At the same time the reversibility of the process α increased considerably. However, the absolute magnitude of the reverse elastic after-effect (criterion $\Delta\Sigma_{\text{rev }60}$ for various values of σ) was practically unaltered. These data indicate that with such severe cold-working there is little alteration in the magnitude of the slip accompanying residual stress relaxation in individual places during the reverse after-effect. This agrees [14] with the observation of the "saturation" of the process of crushing crystallites into blocks during plastic deformation. However, with increase of stress the absolute value of the reverse elastic after-effect rises continuously.

The reduction in direct elastic after-effect with increased cold-working mentioned above conflicts with the results of Davidenkov [21], Belyaev [30], Rovenskiy and Lyuttsau [31] where the opposite effect was observed – increased elastic after-effect and reduced relaxation stability with increased cold-working. This discrepancy is explained by the fact that these writers were dealing with cold-working. This discrepancy is explained by the fact that these writers were dealing with cold-working deformations smaller than those in the present paper; moreover in Davidenkov's work [21] the experiments were carried out at high temperatures and the method used did not take account of the deformations due to the after-effect in the first 5 min after the load was applied In this connexion it was shown in a paper by the present writer that the elastic after-effect and the elastic limit do not increase monotonically with cold-working.

7. The direct elastic after-effect (the flow rises with increased stress (see Figs. 4 and 5).

There is also a continuous rise in both the deformation rate (criterion n) and the deformation occurring shortly after the load application ($\Delta\Sigma_{10}$). However its rise predominates over a further increase in deformation in the flow process. For this reason the criterion k falls continuously. Its values show that most of the deformation occurs in the first 10 min after loading. This circumstance is an argument in favour of selecting a 10 min soak when taking the elastic limit curve (see Figs. 1 and 2).

Prolonged experiments (see Fig. 6) have shown the duration of the flow process; however, even in this case the direct after-effect deformation during the first 2 hr is over 2/3 of the deformation during 17 days and the reverse after-effect reaches in 1 hr half the amount observed in 3.5 days. Thus the comparatively short 3 hr experiments described above constitute a basis for a description of the after-effect processes. However, this circumstance does not diminish the importance of further study of the flow phenomenon for a prolonged period at normal temperature of a number of high-melting metals and their alloys.

8. The flow phenomenon investigated in this paper should be compared with the phenomenon studied by Zhurkov [32,33] and his co-workers concerning the relation between the strength of solids and the time of action of the load. It is natural to suppose that the flow of the material governs the process of its gradual destruction. From this point of view, all the factors (plastic and heat treatment) which decrease flow and increase the proportional flow region must increase the strength of materials against long term attack and make the strength less sensitive to the time of action of the force. There is a need to devise experiments to check this hypothesis.

9. It should be pointed out that it became possible to obtain the new results of the present paper thanks to the high accuracy with which the residual deformations were measured. Flow deformation was measured with an absolute error $\Delta\Sigma = 5 \times 10^{-6}\%$ which is 100 times more accurate than measurements on Martens' apparatus in tension testing and twice as accurate as the deformation measurements in Chalmers' well-known paper [27] in which an interferometer was used as a tensometer.

6. CONCLUSIONS

1. In Sn 6.5 P 0.15 phosphor bronze at normal temperature, flow (direct elastic after-effect) was established at stresses at an order below the minimum conventional elastic limit.
2. To determine conventional elastic limits it is necessary to plot special curves termed elastic limit curves, obtained in a series of experiments in which various stresses are applied for equal periods.
3. It is advisable to select a loading time not greater than 10 min when taking the elastic limit curves, as most of the flow deformation occurs during this period.
4. It was established that the flow rate is proportional to the stress when the stresses are not too large. This phenomenon is termed proportional flow.
5. The boundary of the proportional flow stress range, termed the proportional elastic limit σ_{pb}, is a characteristic whose deformation tolerance is not expressed as an arbitrary value, but has a physical basis. The value σ_{pb} should be regarded as the physical yield point, even in a case where the yield area is not observed on the stress diagram.
6. The proportional elastic limit is of practical significance when selecting the maximum permissible stress below which the amount of the relative elastic after-effect (the relative error caused by the after-effect) does not diminish during the operation of the elastic element.
7. After a considerable degree of cold-working the elastic limit of the material increases, but the direct elastic after-effect decreases while its reversibility rises. The elastic after-effect is extremely sensitive to the structure of a material and can alter many times within the confines of a single material.
8. It is feasible to use the proposed quantitative criteria of the process to describe the elastic after-effect.
9. The high accuracy of the fixed deformation method used to measure the elastic limit and elastic after-effect of sheet spring materials is associated with the possibility of obtaining data of direct practical interest.

Translated by R. Hegarty

VOL. 8 1959

REFERENCES

1. S.O. Tsobkallo, *Fiz. metal. metalloved.* 2, 149 (1956).
2. S.O. Tsobkallo. In symposium: *Voprosy proyektirovaniya, izgotovleniya i sluzhby pruzhin (Problems of the design, manufacture and service of springs)*, Mashgiz (1956).
3. S.O. Tsobkallo. *Nauchnyye doklady vysshey shkolv, Metallurgiya*, 3 (1959).
4. S.O. Tsobkallo and N.A. Golubev. *Trud. Leningr. politekh. inst.* No.197 (1959).
5. S.O. Tsobkallo and Yu.F. Balandin, *Tsvetnyye metally*, No.2, 26 (1956).
6. S.O. Tsobkallo and Yu.F. Balandin, *Trud. Leningr. politekh. inst.* No.202, 68 (1959).
7. S.O. Tsobkallo, G.N. Slavskiy and N.A. Chetyrkina. *Izmeriltel'naya tekhnika*, No.1, 24 (1958).
8. S.O. Tsobkallo and Z.A. Vashchenko. *Trud. Leningr. politekh. inst.* No.208 (1959).
9. S.O. Tsobkallo and Z.A. Vashchenko. *Zavodskaya laboratoriya*, 24, 68 (1958).
10. S.O. Tsobkallo and V.V. Latsh. *Trud. Leningr. politekh. inst.* No.180, 87 (1955).
11. S.O. Tsobkallo and Yu.F. Balandin. *Izmerit. tekhnika*, No.9, 74 (1956).
12. S.O. Tsobkallo and V.V. Latsh. *Izv. Akad. Nauk SSSR, ser. fiz.*, 17, 373 (1953).
13. S.O. Tsobkallo and B.I. Smirnov. *Zh. teor. fiz.*, 27, 1912 (1957).
14. S.O. Tsobkallo and Yu.F. Balandin. *Trud. Leningr. politekh.* No.202, 79 (1959).
15. S.O. Tsobkallo and Z.A. Vashchenko. *Nekotoryye problemy prochnosti tverdogo tela, posvyashchennyy 80-letiyu N.N. Davidenkova (Some Problems of the Strength of Solids, Dedicated to the 80th Anniversary of N.N. Davidenkov)*, published by U.S.S.R. Academy of Sciences (1959).
16. S.O. Tsobkallo and N.A. Likhacheva. *Izv. vysshikh uchebnykh zavedeniy, Seriya fiziki*, No.1 (1959).
17. S.O. Tsobkallo and Z.A. Vaschenko. *Izv. vysshikh uchebnykh zavedeniy, Seriya tsvetnoy metallurgii*, No.2 (1959).
18. S.O. Tsobkallo and Z.A. Vashchenko. *Metallovedeniye i obrabotka metallov*, No.8 (1959).
19. S.O. Tsobkallo and Z.A. Vashchenko. *Tsvetnyye metally*, No.9 (1959).
20. D.A. Braslavskiy, S.S. Logunov and D.S. Pel'por. *Raschet i konstruktsiya aviatsionnykh priborov. (Design and Construction of Aviation Instruments)*. Oborongiz (1954).
21. N.N. Davidenkov and G.A. Kusmirskaya. *Zh. teor fiz*, 16, 1261 (1946).
22. N.A. Shaposhnikov. *Mekhanicheskiye ispytaniya metallov (The Mechanical Testing of Metals)*, Mashgiz, (1954).
23. Ya.B. Fridman. *Mekhanicheskiye svoystva metallov (The Mechanical Properties of Metals)* Oborongiz. (1952).
24. S.T. Konobeyevskiy and I. Selisskiy. *Phys. Zn. d. Sow.*, 4, 455 (1933).
25. A.H. Cottrell, *Rep. Conf. on Strength of Solids*, London, 30 (1948).
26. A.H. Cottrell a. M.A. Jaswon. *Proc. Roy. soc;*, A199, 104 (1949).
27. B. Chalmers, *Proc. Roy. soc.*, A156, 427 (1936).
28. A. Cottrell. *Uspekhi fiziki metallov (Progress in the Physics of Metals)*, 1, Metallurgizdat, (1956).
29. G. Sachs, *Mechanische Technologie der Metalle*, Leipzig, 166 (1925).
30. A.N. Belyayev, *Dissertation. Inst. of Mechanics, USSR Academy of Sciences*, Moscow (1954).
31. B.M. Rovinskiy and B.G. Lyuttsau. *Izv. Akad. nauk SSSR, Department of Technical Sciences* No.6, 54 (1954).
32. S.N. Zhurkov and B.I. Narzulayev, *Zh. teor. fiz.* 23, 1677 (1953).
33. S.N. Zhurkov and T.P. Sanfirova. *Dokl. akad. nauk SSSR*, 101, 237 (1955).
34. N.H. Polakowski. *Journ. Inst. Met.*, 81, 617 (1953).
35. B.M. Rovenskiy. Quoted in book by Ya.S. Umanskiy et al. *"Fizicheskiye osnovy metallovedeniya" "The Physical Principles of Metallography,"* Metallurgizdat, p.400 (1955).
36. A.P. Smiryagin. *Promyshlennyye tsvetnyye metally i splavy (Industrial Non-Ferrous Metals and Alloys)*, Metallurgizdat, (1956).

HARDNESS AND BRITTLENESS OF METAL-LIKE COMPOUNDS*

G.V. SAMSONOV, V.S. NESHPOR AND L.M. KHRENOVA

Institute of Powder Metallurgy and Special Alloys USSR Academy of Sciences

(Received 1 November 1958)

The high hardness of metal-like compounds – carbides, nitrides, borides and silicides of the transition metals of groups IV-VIII of the periodic system – is one of the most characteristic properties of these substances. In view of the brittleness of the compounds in question, the only feasible method of investigating their hardness is the microhardness method. Values previously obtained for the microhardness of metal-like compounds were given in references [1, 2].

The present paper describes an investigation of the effect of the load on the diamond pyramid, on the value of the microhardness numbers of the above compounds as measured with the PMT-3 instrument [3]. The brittleness of the specimens was also estimated from the nature of the surface impression left by the pyramid.

VOL. 8 1959

1. MEASUREMENT OF MICROHARDNESS

Specimens of the carbides of titanium, zirconium, vanadium, tantulum, chromium, molybdenum and tungsten, the nitrides of titanium and zirconium, the borides of titanium, zirconium, niobium, tantalum, chromium, molybdenum, tungsten, calcium, barium, lanthanum and cerium and the silicides of titanium, zirconium, niobium, tantalum, chromium, molybdenum, tungsten, iron, cobalt and nickel, consisting of a single phase, were prepared by sintering hot compressed powders of these compounds followed by prolonged high temperature annealing to remove internal stresses. The polished sections prepared from these specimens were etched to reveal the grain boundaries and to remove the surface layer which was cold worked during polishing. Microhardness was investigated on a PMT-3 instrument adjusted as recommended by Khrushchev and Berkovich [3]. Loads from 20 to 200g were used when obtaining the impressions and 10 indentations were made at each load. The experiments showed that the microhardness number depends on the load used and that this dependence is found to exist above the limits of accuracy of the measurements.

The dependence of the microhardness number on the load was first established with certainty by Bochvar and Zhadayeva [4] for comparatively soft materials – copper, zinc and Armco iron. The relationship between microhardness and load was established for other metallic and non-metallic materials quoted in references [5-7]. Gogoberidze and Kopatskiy [8] point out that the relationship between the microhardness number and the load must evidently be of a universal kind, as the instrument for measuring microhardness, even after being specially adjusted so as to indicate microhardness numbers for a given material independent of the load, still indicates this dependence when harder materials are investigated. On the other hand, the independence of microhardness number of the load applied is asserted in references [9-10].

The microhardness investigations described in the present paper, carried out on very hard materials, in all cases confirm the existence of a fully defined relationship between the microhardness numbers and the

* *Fiz. metal. metalloved.* 8, No.4, 622-630, 1959.

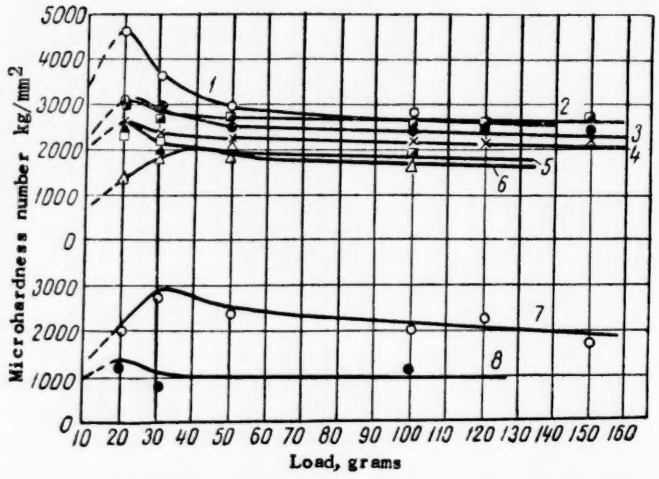

Fig. 1. Variation with load of microhardness numbers of carbides and nitrides of transition metals.
1 – VC 2 – TiC 3 – Zrc 4 – Cr_3C_2 5 – WC, Mo_2C 6 – TaC 7 – TiN 8 – ZrN

load applied. See Figs. 1-4). In the general case, when the load on the diamond pyramid of the instrument is increased, the microhardness number increases at first and then decreases, reaching a practically constant value at loads of 60-200 g. A similar relationship was established by Bochvar and Zhadayeva [4] for copper, zinc and aluminium. Thus this relationship is of the same kind for both comparatively soft and very hard substances.

The existence of such a relationship can evidently be explained by the following considerations. The size of the impression measured after the load has been removed is determined both by the magnitude of the plastic deformation under the action of the load applied through the diamond pyramid of the instrument and by the elastic after-effect

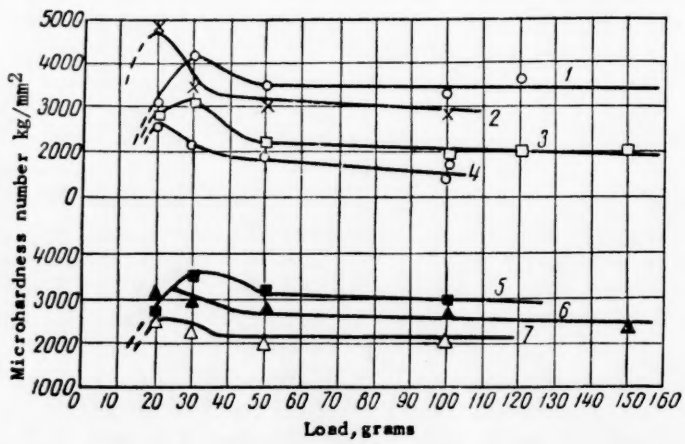

Fig. 2. Variation with load of microhardness numbers of borides of transition metals.
1 – TiB_2; 2 – NbB_2; 3 – TaB_2; 4 – ZrB_2; 5 – Mo_2B_5; 6 – W_2B_5; 7 – CrB_2.

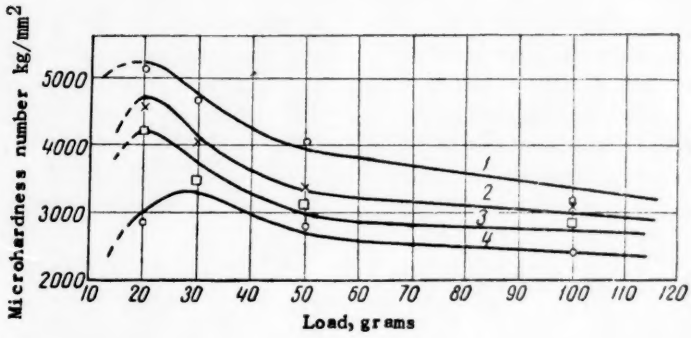

Fig. 3. Variation with load of microhardness numbers of hexaborides of alkali and rare earth metals.
1 – CaB_6; 2 – BaB_6; 3 – LaB_6; 4 – CeB_6.

of the material after load removal. The latter is proportional to the elastic part of the surface deformation. Taking the elastic deformation, as usual, as directly proportional to the stress and, consequently, to the applied load, and the plastic deformation as proportional to the square of the stress (see, for example, [11]), and, consequently, to the square of the load, we obtain that the size of the impression

$$s \cong AP^2 - BP + C, \qquad (1)$$

where P is the load; and A, B and C are constants depending on the physical characteristics of the material. Then we obtain the following expression for the microhardness number

$$H_\mu \sim \frac{P}{s} \sim \frac{P}{AP^2 - BP + C}. \qquad (2)$$

The graph of function (2) 12 corresponds fairly well with the experimental graphs in Figs. 1-4. It should be noted that in many cases in Fig. 1-4 the rising part of the graph for the function $H_\mu = f(P)$ is not realised. Smaller loads are required to reveal it, and these are difficult to arrange in view of the high hardness of the materials investigated and the practical impossibility of measuring impressions obtained at loads less than 20 g.

It follows from the above that when making comparative measurements of the microhardness

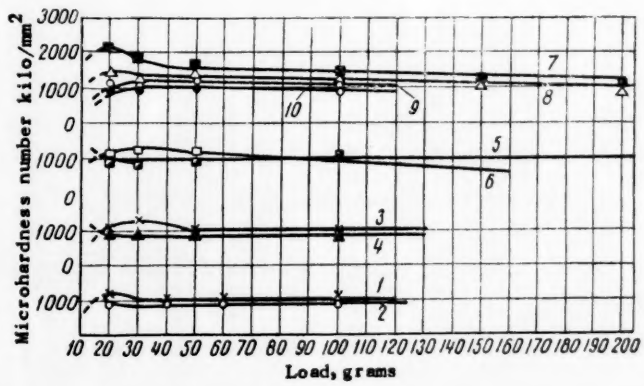

Fig. 4. Variation with load of microhardness numbers of silicides of transition metals.
1 – $MoSi_2$; 2 – $NbSi_2$; 3 – $FeSi_2$; 4 – $NiSi_2$; 5 – $CoSi_2$; 6 – $CrSi_2$; 7 – WSi_2; 8 – $TaSi_2$; 9 – $TiSi_2$; 10 – $ZrSi_2$.

of various materials the microhardness numbers should be determined at various loads and compared in the region where the variation of H_m with load is of no practical importance.

In this connexion the following sets of microhardness numbers may be quoted for the compounds investigated (for a load of 120 g).

1. Carbides:

Phase	TiC, VC	ZrC	Cr_3C_2	Wc, Mo_2C	TaC
H_m	2600	2400	2160	1800	1630

2. Nitrides:

Phase	TiN	ZrN
H_m	2100	930

3. Borides MeB_2 (Me_2B_5):

Phase	TiB_2	Mo_2B_5	NbB_2	W_2B_5	CrB_2
H_m	3400	2950	2900	2500	2150

Phase	TaB_2	ZrB_2
H_m	2000	1500

4. Borides MeB_6:

Phase	CaB_6	BaB_6	LaB_6	CeB_6
H_m	3150	2900	2500	2350

5. Silicides:

Phase	WSi_2	$TaSi_2$	$TiSi_2$	$CoSi_2$	$MoSi_2$
H_m kg/mm^2	1430	1200	1100	1030	950

Phase	$ZrSi_2$ $NbSi_2$	$CrSi_2$ $NiSi_2$
H_m kg/mm^2	900	800

Thus the hardness of metalline compounds in general increases in the order; silicide, nitride, carbide, boride. This is in agreement with the crystalline structure and strength of the interatomic bond in these compounds [2].

2. BRITTLENESS OF METAL-LIKE COMPOUNDS

At an earlier date we made an attempt at estimating the brittleness of some metal-like compounds from the packing rate of powders of these compounds during compacting [13], inasmuch as the main type of deformation of the powder particles during packing is brittle disintegration of irregularities on the surface of the particles and also of the partic-

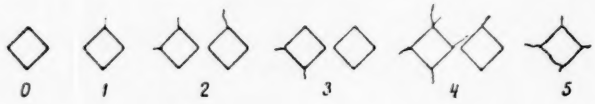

Fig. 5. Nature of impressions for estimating destruction mark.

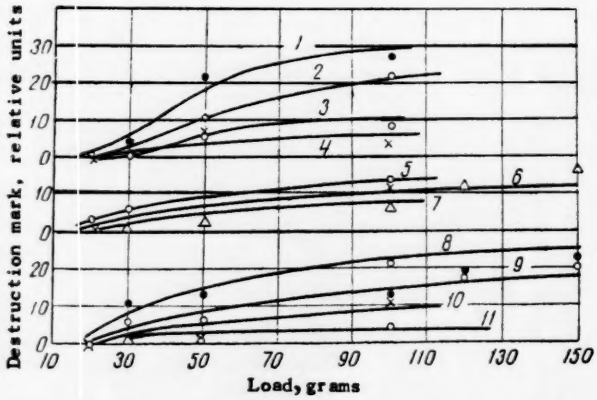

Fig. 6. Variation with load of the total destruction mark of borides.

1 – CeB_6; 2 – BaB_6; 3 – LaB_6; 4 – CaB_6; 5 – Mo_2B_5; 6 – TaB_2; 7 – CrB_2; 8 – W_2B_5; 9 – TiB_2; 10 – NbB_2; 11 – ZrB_2.

les themselves. It was shown [14] that the degree of brittleness of metal-like compounds established in reference [13] decreases in proportion to the increase of the root-mean-square displacement of the centres of molecular complexes in the crystal lattices of the compounds during thermal oscillations, to which corresponds a decrease in the rigidity of the interatomic bonds and, consequently, an increase in the possibility of stress relaxation.

In the present work the microbrittleness method was used to estimate the brittleness of the metal-like compounds. This was first suggested by Ikornikova [15] for estimating the brittleness of carborundum, in conjunction with the determination of a mean brittleness mark, as was done in a paper by Kotelnikov [16].

The essence of this procedure is the obtaining impressions with the diamond pyramid of the PMT-3 instrument at various loads and estimating the quantity and nature of the cracks and other defects produced. To reduce the subjectivity of this estimate, the so-called mean brittleness mark is introduced. This is computed from the degree of destruction manifested by the nature of the impression. The degree of destruction is estimated according to a five-mark scale (see Fig.5 and Table 1).

The total destruction mark is determined from this according to the formula

$$Z = 0n_0 + 1n_1 + 2n_2 + 3n_3 + 4n_4 + 5n_5, \quad (3)$$

where n_0, n_1, n_2 ... are the relative quantities of impressions with the given mark or character of destruction.

Naturally, the greater the number of appraisable marks, the less subjective the results given by the sum $Z = \sum_{i=0}^{i=k} a_i \cdot n_i$ However, even with the five-mark system results are obtained which permit a fairly objective comparison of the brittleness of the investigated materials to be made.

Values of the total destruction mark calculated in accordance with formula (3) are presented in relation to load on Fig. 6-7 for borides and silicides. Allowing for the scatter of the experimental results, the nature of the variation of Z with respect to load is the same for all the materials investigated. It is conspicuous that no traces of destruction at any load are observed on the impressions of the carbides of tantalum and wolfram (W_2C) and niobium silicide. This is practically true for Mo_2C also. At the same time these compounds, like the other metal-line phases, have considerable brittleness.

Thus, it was remarked that specimens of niobium and tantalum silicides prepared by hot pressing powders of these compounds are very subject to spontaneous cracking in the unannealed state under the action of internal stresses. Evidently, the absence of visible defects in the impressions on the slides of these compounds merely indicates that the shear stresses set up in the surface layer of the slide by the diamond pyramid indentation is for these materials less than their yield strength. For the silicides of tantalum for example, the destruction of the impressions is observed only at loads exceeding 50 g. From this it follows that a single total destruction mark must not be taken as a characteristic of the brittleness of the material. Such a characteristic should reflect the rate factor of growth of the destruction of the material with increased load (that is, the stresses in the material). This factor may be characterized by the value of the derivative of the total destruction mark with respect to the applied load. Table

TABLE 1

Destruction mark	Nature of the impression
0	Impression without visible cracks or chips
1	One small vertical or horizontal crack
2	1-2 cracks
3	2-3 cracks, chip from one side of the impression
4	More than 3 vertical cracks
5	Complete destruction of form of the impression

TABLE 2

Brittleness Indices of Metal-like Compounds

Phase	Crystalline structure	$\sqrt{\overline{u_{291}^2}}$	Brittleness factor (Z_{90})	$\left(\frac{\partial Z}{\partial p}\right)_{90}$	Brittleness index γ X 10	Brittleness index A from data of refs [13-14]
WC	Hexagonal	0.058 [14] 0.055 [17]	20.5	0.200	40.9	18
TiC	Cubic	0.067 [14] 0.085 [17]	20.0	0.175	35.0	9
ZrC	Cubic	0.074 [14]	32.5	0.100	32.5	2.67
VC	Cubic	0.088 [14]	18.5	0.175	32.3	–
Cr_3C_2	Rhombohedral	0.091 [17]	16.0	0.150	24.0	–
Mo_2C	Hexagonal	0.055 [14] 0.090 [17]	3.0	0.025	7.5	–
W_2C	Hexagonal	0.062 [14] 0.070 [17]	0	–	–	–
TaC	Cubic	0.082 [14, 17]	0	–	–	–
TiN	Cubic	0.091 [14] 0.160 [14]	29.0	0.085	24.7	1.11
ZrN	Cubic	–	–	–	Less brittle than TiN	–
W_2B_5	Hexagonal	–	21.0	0.125	26.2	–
TiB_2	Hexagonal	0.073 [14]	13.5	0.100	13.5	2.66
Mo_2B_5	Rhombohedral	–	13.0	0.075	9.7	–
TaB_2	Hexagonal	–	9.5	0.06	5.7	–
NbB_2	Hexagonal	–	8.0	0.065	5.2	–
CrB_2	Hexagonal	0.121 [14]	2.0	0.05	1.0	–
ZrB_2	Hexagonal	0.072 [14]	3.0	0.025(?)	0.75	3,27
CeB_6	Cubic	–	28.5	0.15	41.0	–
BaB_6	Cubic	–	19.0	0.175	33.3	–
LaB_6	Cubic	–	9.5	0.05	4.75	–
CaB_6	Cubic	–	5.5	0.045	2.48	–
$FeSi_2$	Tetrahedral	–	37,0	0.10	37.0	–
$TaSi_2$	Hexagonal	0.073*	10.0	0.25	25.0	–
$CrSi_2$	Hexagonal	0.082*	26.5	0.075	19.9	–
$TiSi_2$	Rhombohedral	0.087*	41.0	0.045	18.5	–
$ZrSi_2$	Rhombohedral	0.087*	42.5	0.04	18.0	–
WSi_2	Tetrahedral	0.073*	12.0	0.06	7.2	–
$CoSi_2$	Cubic	–	15.0	0.045	6.8	–
$NiSi_2$	Cubic	–	10.0	0.045	4.5	–
$MoSi_2$	Tetrahedral	0.076	8.0	0.05	4.0	–

* Calculated from the melting point and the molecular volume by the method of reference [18] without taking account of the anisotropy of the thermal oscillations of the atoms in crystals of non-cubic symmetry.

VOL 8 195

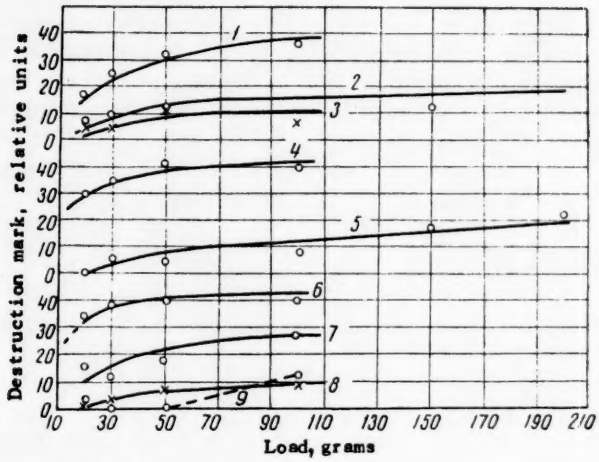

Fig. 7. Variation with load of the total destruction mark of silicides.
1 – $FeSi_2$; 2 – $CoSi_2$; 3 – $NiSi_2$; 4 – $TiSi_2$; 5 – WSi_2; 6 – $ZrSi_2$; 7 – $CrSi_2$; 8 – $MoSi_2$; 9 – $TaSi_2$.

VOL. 8 1959

2 gives values of the total destruction mark Z_{90} for a load of 90 g and the value of $\left(\frac{\partial Z}{\partial P}\right)_{p=90}$ The product of the total destruction mark and the value of its derivative with respect to load, that is, the quantity

$$\gamma = Z_{P_i}\left(\frac{\partial Z}{\partial P}\right)_{P_i} \qquad (4)$$

may be regarded as an index of the brittleness of the material which reflects both the nature of the destruction and the rate of growth of the destruction with increased load.

The brittleness indices calculated in this way (column 6 table 2) are in satisfactory agreement with the hardness indices found for certain compounds in reference [13], and also with the cohesion characteristics of the atoms in the lattices of the compounds, decreasing with increase of the root-mean-square displacements of the centres of the molecular complexes (column 3 Table 2) in accordance with the relationship established established in reference [14].

The values of the root-mean-square displacements $\sqrt{\overline{u^2_{291}}}$ given in column 3 of table 2 for silicides were calculated by the method proposed by one of the authors [18] which is applicable with adequate reliability only to substances with cubic symmetry of the crystal lattice. However, for substances with the same lattice and close values of the lattice constants, the values of $\sqrt{\overline{u^2_{291}}}$, calculated in this way are obviously a fairly good indication of the rigidity of the bond. Comparison of these values with the brittleness indices for isostructural silicides shows that for these compounds also the brittleness increases as $\sqrt{\overline{u^2_{291}}}$, decreases, that is, as the rigidity of the interatomic bonds increases.

By comparing the values of the total destruction mark of the impressions and the brittleness indices for the various compounds it can be seen that brittleness in general increases in the order: silicide, boride, nitride, carbide.

3. CONCLUSIONS

1. The microhardness of a number of metal-like compounds of the transition metals was investigated at various loads. It was established that the microhardness numbers depend on the load at which the investigation is

made. The nature of the relationship between microhardness numbers and load is the same for materials with very high and comparatively low hardness and is determined, apparently, by the nature of the plastic deformation of the surface of solids when their microhardness is tested.

2. The brittleness of metal-like compounds was investigated by a microbrittleness method. The brittleness indices obtained in the present paper are in satisfactory agreement with the brittleness indices which we previously established for some compounds.

3. The brittleness of the compounds increases as the root-mean-square displacements of the centres of the molecular complexes in the crystal lattices of the compounds increase, that is, as the rigidity of the interatomic bond increases and as the possibility of stress relaxation in the material decreases.

4. The hardness of metal-like compounds increases in the order: silicide, nitride, carbide, boride; and the brittleness in the order: silicide, boride, nitride, carbide.

Translated by R. Hegarty

REFERENCES

1. G.V. Samsonov, *Dokl. akad. nauk SSSR*, 86, 329 (1952).
2. G.V. Samsonov and V.S. Neshpor, *Voprosy poroshkovoy metallurgii i prochnosti materialov*, No.5 p.3 (1958) published by the Uk.S.S.R. Academy of Sciences.
3. M.M. Khrushchev and Ye.S. Berkovich, *Pribory PMT-2 i PMT-3 dlya ispytaniya na mikrotverdost' (The PMT-2 and PMT-3 Instruments for Microhardness Testing)*, published by the USSR Academy of Sciences, Moscow (1950).
4. A.A. Bochvar and O.S. Zhadayeva, *Izv. Akad nauk SSSR, Department of Technical Sciences*, No.10-11, 108 (1945); No.3, 341 (1947); No.4, 419 (1947).
5. R. Campbell, K. Gonderson and M. Donlevy *Trans. Amer. soc. Metals*, 40, 954 (1948).
6. D.B. Gogoberidze and N.A. Kopatskiy, *Zh. teor. fiz.*, No.8, 910 (1950).
7. W. Rostoker, *Journ. Inst. Metals*, No.77, 175 (1950).
8. D.B. Gogoberidze and N.A. Kopatskiy, *Trudy Vsesoyuzn. nauchnogo inzhenerno-tekhn. ob-va metallurgov*, Metallurgizdat, Moscow, 2, p.156 (1954).
9. B.I. Kostetskiy, *Iznosostoykost detaley mashin (The Durability of Machine Parts)*, Mashgiz, Moscow, (1950).
10. B.I. Kostetskiy and P.K. Topekha, *Zavodskaya laboratoriya*, No.8, 972 (1948).
11. Ya.S. Umanskiy, B.N. Finkel'shteyn, M.Ye. Blanter, S.T. Kishkin, N.S. Fastov and S.S. Gorelik, *Fizicheskiye osnovy metallovedeniya, (The Physical Principles of Metallography)*, Metallurgizdat, Moscow, p.417 (1955).
12. M.Ye. Blanter, *Matodika issledovaniya metallov i obrabotki opytnykh dannykh (Procedure for Investigating Metals and Processing Experimental Data)*, Metallurgizdat, Moscow (1952).
13. G.V. Samsonov, V.S. Neshpor, *Dokl. akad. nauk. SSSR*, 104, 405, (1955).
14. V.S. Neshpor and G.V. Samsonov, *Fiz. metal. metallov*, 4, 182 (1957).
15. N.Yu. Ikornikova, *Mikrotverdost' (Microhardness)*, published by U.S.S.R. Academy of Sciences, Moscow, p.211 (1951).
16. P.B. Kotel'nikov, *Avtoreferat dissertatsii* (Thesis Review), Mintsvetmetzoloto, (Moscow Institute of Gold and Non-Ferrous Metals), Moscow (1956).
17. I.N. Frantsevich, *Voprosy poroshkovoy metallurgii i prochnosti materialov*, published by the Uk.S.S.R. Academy of Sciences, Kiev, No.3, p.14 (1956).
18. V.S. Neshpor, *S svyazi mezhdu nekotorymi termicheskimi kharakteristikami tverdykh tel, (On the Relationship between Certain Thermal Characteristics of Solids)*, *Fiz. metal. metallov*, (in the press).

ON THE QUESTION OF THE MECHANISM OF THE INITIAL STAGE OF DEFORMATION OF POLYCRYSTALLINE METALS*

By Y.R. RAUSIN

(Received 25 September 1958)

VOL. 8 1959

B.A. Sidorov [1] has expressed doubt in the correctness of a series of conclusions made by us on the basis of experimental observations of the initial stage of plastic deformation [2,3]. Comments on the method, which were the consequence of an insufficiently exact description of the methods used by us, could probably be excluded from the differences of opinion noted. In particular, the method of observation used by us from the beginning of the appearance of slip lines could possibly have been incorrect if we had used it as B.A. Sidorov supposes. We not only observed under the microscope the beginning of the appearance of slip lines in a polycrystal with different grain sizes, but also compared it with the appearance of slip lines in a monocrystal of the same metal. If, at one and the same stage of deformation (under identical conditions of observation), the slip lines had appeared in the monocrystal, but not in the polycrystal, that is, if slip had appeared in the grains of the polycrystal at a greater degree of general deformation than in the monocrystal, then we were correct to suppose that the beginning of the appearance of slip lines in the polycrystal is preceded by some other, pre-slip deformation. Also, by deformation by slip, we presuppose deformation characterized by the formation of localized planes of slip.

Besides this, the inspection under the microscope was carried out at various magnifications (100-600) with control checks on an electron microscope (x 8000). No change was observed in the degree of deformation at which the first slip appeared.

It is also impossible to accept the supposition expressed by Sidorov, that the slip lines "taper" with a decrease in grain size. In detailed surveys, Kuhlman [5] and Brown [4] have examined about two hundred papers devoted to slip lines. From these papers it follows that the number of elementary slip planes included in a slip band, or, in other words, the width of the slip band visible to us under a microscope in the form of slip lines, depends on the physical nature of the metal and on the conditions of deformation, but not on the size of the crystal.

However, not only the absence of slip lines in the deformation of polycrystals forces us to suppose that slip takes place later in them than in the monocrystal, that is, that the appearance of slip in the grains of the polycrystal is preceded some other form of deformation. The reason for this is a whole series of direct and indirect observations described in the references and partly carried out by us. They also allow us to maintain that at this stage of deformation intergranular processes take place. Are they peculiar to this stage or not? It is most probable that the intergranular deformation is accompanied by processes corresponding to those which take place in the monocrystal before the beginning of the appearance of slip. Such an idea was expressed as early as in 1931 by Shchapov, who was the first to establish the absence of slip lines in fine-grained iron [6]. Bochvar [7] and a series of other authors [8,9] consider that the initial deformation of monocrystals consists of the uniform displacement of atomic planes which do not leave visible traces on coming to the surface. Yet another idea exists, according to which pre-slip deformation leads to fragmentation of the grain with the formation of nuclei of substructure [10], among them also the usual low-temperature deforma-

* *Fiz. metal. metalloved.* 8, No.4, 631-635, 1959.

tion [11, 12]. Unfortunately, even X-ray observations do not give a single answer to this question. At the same time a series of experimental observations allows us to consider that at this stage of the deformation of polycrystals intergranular processes are prevalent.

The possibility of the relative displacement of grains because of the flow at the boundaries is acknowledged also by Sidorov. However, he doubts whether this flow can prevail over the intragranular processes before some stage of deformation. He considers that the prevalent role of inter-granular processes at the beginning of the deformation is unproved, mainly because no direct measurements of the displacement of grains have been made. As a matter of fact it is necessary to solve the question in another way.

The localization of deformation on the boundaries of the grains was observed experimentally in a series of metals: zinc [8], magnesium [26] and low-carbon steel [27, 28]. As the amount of displacement is very small, an authentic quantitative comparison of the micro- and macroscopic deformation is made difficult and is not a reliable criterion for well-founded conclusions. Mass statistical observations of the change in the diameter of grains of steel in the direction of expansion and across it (which, by the way, did not show any change in these two dimensions within the limits of 5-6% deformation), cannot be quoted by us because of insufficient accuracy. Rachinger, [13], who is referred to by Sidorov, carried out such observations with deformation of 50%. But this has nothing in common with those small deformations which were examined in our articles. Therefore we consider it more reliable to support our propositions with indirect observations of the initial stage of plastic deformation. The results of such observations give us sufficient grounds to confirm that deformation, called "critical" by Ivanova, does exist, with which one mechanism of deformation alternates with another. The amount of "critical" deformation is not constant. It changes depending on a series of factors, and mainly on those which determine the state and extent of the boundaries, that is, the degree of purity of the metal and the grain size. Therefore the supposition of Sidorov is quite correct, that the difference in the degree of intergranular displacement that we and Rachinger had, apart from the above-mentioned reason, is explained by the content of various impurities in aluminium.

At the present time there is a great deal of experimental material which confirms the position expressed earlier, that a change from one mechanism of deformation to another exists. We will limit ourselves to a brief enumeration of some of them.

1. In proportion to the decrease in the quantity of impurities in the metal and the increase in the grain size, the following decrease:

a) the degree of deformation at which the slip lines appear [2, 3, 5, 6];

b) the degree of deformation* at which collective recrystallization on annealing is replaced with recrystallization of the worked material (see work [23]);

c) the size of the yield point [3, 24, 25];

d) the degree of deformation before which the Bauschinger effect is observed [16].

It is characteristic that the parameters enumerated, progressively decreasing in proportion to the freedom of the metal from impurities and the increase in the grain, in several cases reach zero value. In this case there is an absence of the inter-granular displacement as well as the yield point and the Bauschinger effect and others; there is seen, as in the monocrysta, only deformation by slip.

2. The presence of "critical" deformation was established by Crussard, who analysed the course of load-extension curves of a large number of metals which do not show a yield point. The author established that within the limits of 6-7% of deformation there is an inflexion in the load-extension curve, which bears witness to the change in the deformation mechanism [17]. Crussard does not give an answer to the question of the form of the mechanism of deformation up to the point of inflexion, but the substantial role of intergranular processes does not, in the opinion of the author, give rise to any doubt. Consequently one may consider that "critical" deformation is a property of all metals, with

* Critical degree of deformation before recrystallization.

the exception of very pure and coarse-grained, metals in which there occurs inter-granular displacement, and the "critical" deformation becomes equal to zero.

3. The increase in the hardness at the boundaries of the grains, especially after ageing, and the absence of such inside the grain is a very important confirmation of the inter-granular character of the initial stage of deformation. (see work [14]).

4. Continuing the exposition of the facts which confirm the special mechanism of the initial stage of deformation, one must point out the unusual change here of a series of physical properties [18] and, in particular, the decrease in electrical resistance in the zone of critical deformation [19-21]. This decrease is greater, the smaller the grain [21]. An increase was also noted in the density of iron at a deformation within the limits of the yield point; this increase appears when there is a lesser degree of penetration of hydrogen as a result of cathodic charging [22].

We do not identify the existence of inter-granular displacement and "critical" deformation with the definite presence of a yield point. Like Crussard [17], we consider the presence of a yield point a particular case of a change in the deformation mechanism. In the explanation which appears below we attempt to answer very briefly the puzzling question which Sidorov poses: why is the yield point absent in the metals in which, as we maintain, inter-granular displacement exists?

First of all one must note that the existing ideas about the mechanism of the formation of a yield point (the hypotheses of the "brittle skeleton") proved not to be in the position to explain the series of experimental observations. The failure of these hypotheses is explained, from our point of view, by the fact that in them, the boundaries of the grains were considered as the zones of greatest strength. On the basis of the hypothesis about the nature of the yield point modern ideas about the grain boundaries must be proposed, in accordance with which they are an intermediate layer between grains of different orientation, with disturbed atomic packing, with a large quantity of dislocated atoms and the accumulation of vacancies. Deformation at the grain boundaries approaches, in its character, viscous flow. In connexion with this, the boundaries of the grains are often weaker than the body of the grains, especially in technical metals and alloys.

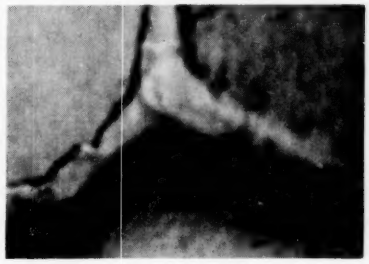

Fig. 1. The boundaries of the grains of annealed technically pure iron; X7500.

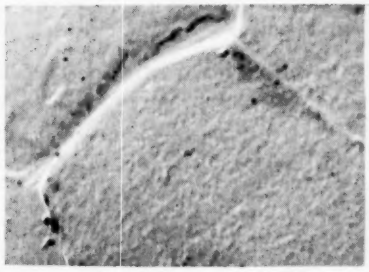

Fig. 2. The boundaries of the grains of the same iron after quenching from 900° in water; X7500.

The undissolved impurities and the impurities which enter the solid solution are concentrated, to a large extent, in these boundary layers [15], which intensifies the defects of the atomic packing and broadens the disintegrated intermediate zone. The electron-microscope photographs reproduced in Figures 1 and 2 in particlar bear witness to this. In connexion with this, the difference in the strength in the boundaries and the grains themselves aggravates the relative weakness of the boundaries. Therefore, the quantity of impurities at the boundaries of the grains is one of the important reasons for the larger or smaller inter-granular displacement in the initial stage of deformation. As Rachinger showed visually [13] on models made of bubbles, the movement of whole grains is greater, the broader the boundaries are between them. With a narrow boundary grain boundary slip quickly changes to intragranular deformation with elongation of the grains;

VOL. 8 1959

with a broad boundary the grains (bubbles) slide over one another for a long time without changing their internal form.

The inter-granular displacement is one of the reasons for the formation of the yield point. However, this condition is necessary but insufficient. The second necessary condition for the formation of the yield point is the sensitivity of the metals to stress concentration. In fact, the yield point in the load extension curve is accompanied by localization of deformation. Both these phenomena are inseparable and caused by the same reasons. What does the existence of such a sharply defined localization of deformation mean? It bears witness to the large concentration of stresses in the zone of the origin of the deformation. It is known that local deformation originates as a rule, at the ends of the specimens. If the transition from the shank to the ends of the specimens is made more smoothly, then the formation of the local deformation is preceded by a large "peak" of an upper yield point. In this case also a large local overstress precedes the beginning of yielding.

With the effect of the local increased stress there takes place the first group displacement of grains* in the direction of the maximum tangential stresses and the first Chernov-Luders line is formed.

Not all metals are sensitive to the concentration of stresses and capable of supporting local overstresses. In soft non-ferrous metals it is impossible to create high local stresses in the zone of the concentrator, because consequence of the low value of the yield stress, the effect of the concentration quickly weakens. Such metals do not have a yield point on the load-extension curve in spite of the presence of inter-granular movement. However, even aluminium, if it is strengthened by a very fine grain size (0.002-0.005 mm) which simultaneously raises the sensitivity to a concentration of stresses, and tendency to inter-granular movement elongates with the formation of a yield point.

The sharp rise in the yield stress and the increase in the sensitivity to a concentration of stresses, but not an increase in inter-granular movement, is explained by the increase in the yield point at low temperatures. Conversely, the decrease in the yield stress and sensitivity to a concentration of stresses explains its disappearance on heating.

Sidorov correctly considers that it is impossible to consider the present opinion expressed about the mechanism of the initial stage of deformation as sufficiently well-founded. It is clear that the considerations stated here are far from an exhaustive treatment of necessary basis of the hypothesis discussed. With the present article the author wants to bring attention to numerous experimental observations which could be simply explained from the point of view of the suggested mechanism of deformation. The broadening of the circle of these observations may lead, in time, to making more precise the theory of the plastic deformation of polycrystals.

Translated by R. J. Coleman

* In a series of cases the formation of slip lines is observed simultaneously in separate, as a rule, coarse and non-equiaxed grains. This does not exclude the prevalent inter-granular character of deformation, spreading over the greater part of the grain of the metal.

REFERENCES

1. B.A. Sidorov, *Fiz. metal. metallov*, 6, 191 (1958).
2. Y.R. Rausin and A.R. Zheleznyskova, *Fiz. metal. metallov*, 3, edition 1, 146 (1956).
3. Y.R. Rausin and A.R. Zheleznyakova, *Fiz. metal. metallov*, 3, edition 1, 154 (1956).
4. A. Brown, *Phil. Mag.* (1952).
5. D. Kuhlman, *Zs. f. Metallk.*, 41, H.5 (1950).
6. N.P. Shchapov, *Zh. tekh. fiz.*, 1, edition 1 (1931).
7. A.A. Bochvar, Y.A. Preobrazhenskaya, *Dokl. Akad. Nauk SSSR*, 113, No.3 (1957).
8. D.G. Kurnosov, N.M. Tronina and M.V. Yakutovich, *Zh. tekh fiz.* 18, No.2, 197 (1948).
9. G.N. Kolesnikov, *Dissertation*, Sverdlovsk. (1945).
10. W. Wood and R. Scrutton, *J. Inst. Metals*, 77, 423 (1950).
11. B.M. Rovinskii and L.M. Rybakova, *Izv. Akad. Nauk SSSR, physica series*, 20, No.6, YRU.647 (1956).

VOL 8 195

12. A. Gunier, *Proc. Phys. soc.*, 57, 4 (1945).
13. M. Rachinger, *J. Inst. Metals*, 81, 33 (1952).
14. V.S. Ivanova, *Dokl. Akad. Nauk SSSR*, 44, No.2 (1954).
15. V.I. Arkharov, *Institute of Applied Mathematics SSSR*, edition 8, page 54 (1946).
16. S.I. Ratner and Y.S. Danilov, *Factory Laboratory*, No.4, 468 (1950).
17. Ch. Crussard and B. Jaoul, *Rev. d. Metallurgie*, 47, No.8, 589 (1950).
18. J. Fast, *Philips techn. Rundschau*, 14, 27 (1952).
19. R. Bardenheuer and H. Schmidt, *Miteilungen Inst. f. Eisenforschung*, 10, No.10 (1928).
20. B.G. Livshits, *Vestnik metallopromyshlennosti (Metal-industry news)*, No.10, 53 (1932).
21. Y.R. Rauzin and A.R. Zheleznyakova, *Metalloved i obrab metallov (Metallography and working of metals)*, No.12 (1957).
22. J. Duflot, *Rev.de metallurgie*, No.1, 35 (1952).
23. Y.R. Rausin and A.K. Zhekznyakova, *Metallovedenie i obrabotka metallov, (Metallography and metal working)* No.12 (1957).
24. N.N. Davidenkov, *Mechanischeskie svoistva i ispytwnie metallov (The mechanical properties and test of metals)*, page 128 Leningrad (1933).
25. J. Low and M. Gensammer, *Metals Technology*, 10, 207 (1943).
26. F. Hauser, C. Starr, L. Tietz and I. Dorn, *Trans. Amer. soc Met.*, 47, 102 (1955).
27. P.O. Pashkov and V.A. Bratukhina, *Symposium: Metallovedenie, Subpromgiz*, page 165 (1958).
28. I.V. Navrotskii, Y.S. Kurmanov, Y.S. Gomenko and Z.F. Yanushevskaya, *Biulleten' Ukrainskogo instituta metallov (Bulletin of the Ukrainian institute of metals)*, No.7 (1958).

VOL.
8
1959

LETTERS TO THE EDITOR

A STUDY OF THE REACTIONAL DIFFUSION IN BINARY SYSTEMS OF THE TYPE "METAL-GAS" III*

By V.I. ARKHAROV, E.B. BLANKOVA, N.A. SUKHOVA and R.A. ENTELIS

(Received 19 June 1959)

For checking the supposition [1] about the correlation between the strengthening of tne relative role of the homopolar bonds in the products of reactional diffusion and the increase in the relative role of the metalloid in the process of diffusion we carried out a supplementary study of the mechanism of diffusion in the systems Fe-P, Co-P, Zr-S, Zr-Se, Zr-Te and Nb-Z, Nb-Se, Nb-Te.

The coice of systems was determined by the following considerations. It is known [3,4] that homopolar bonds in combinations of transitional metals with metalloids are stronger, the greater the polarizability of the metalloid and the stronger the polarizing effect the metal has on the metalloid. For instance phosphorous, placed in the periodic table next to sulphur, but to the left of it, is polarized more strongly than sulphur, consequently, in combinations of phosphorous the homopolar bonds will be expressed more strongly than in combinations of sulphur with the same metals.

In the article [2] it was stated that in the system Fe-S and Co-S in the whole of the temperature interval studied, (from the beginning of the dross formation, revealed by X-rays, to the temperature of melting of the dross) there takes place a bilateral diffusion of the metal and the sulphur and also the thickness of the layers of dross, formed because of the diffusion of the metal and the sulphur and also the thickness of the layers of dross, formed because of the diffusion of the metal and the diffusion of the metalloid, are approximately the same. If the supposition expressed by us is correct, then in the systems Fe-P and Co-P the relative role of phosphorous in the diffusion must be greater than the role of the sulphur in the diffusion in the systems Fe-S and Co-S.

On the other hand, our supposition may be checked if, instead of the transitional metals of the IV period, for example Ti and V, transitional metals of the V period – Zr and Nb are taken, placed respectively in the same groups of the periodic system, but having a greater polarizing effect on the metalloid (which once again leads to the strengthening of the relative role of the homopolar bonds in the sulphides, selenides and tellurides of these metals in comparison with the analogical combinations on the basis of titanium and vanadium.

The results of the study of the reactional diffusions in the systems Fe-P, Co-P, Zr-S, Zr-Se, Zr-Te, Nb-S, Nb-Se and Nb Te are shown in the table.

A comparison of the data obtained by different methods of study allows us to deduce that in the systems Fe-P and Co-P, in the temperature interval 400-600°, there takes place a unilateral diffusion of phosphorous; in all the systems on the basis Zr and Nb the unilateral diffusion of the metalloids (S, Se and Te) is observed in the interval of 400-1,000°. We recall that in the systems Ti-S and V-S in the same temperature interval was observed bilateral diffusion of the metals and sulphur, but in the systems Ti-Te, V-Se and V-Te the bilateral diffusion of the metals and metalloids was observed in the

* *Fiz. metal. metallov.* 8, No.4, 636-638, 1959.

TABLE 1

System	Temperature interval °C	No. of macroscopic layers	No. of metallographically exposed layers	Phase compound of dross	Presence of texture in the layers of dross	Macroscopic characteristics of the type of reaction diffusion
Fe-P	400-600	1	–	FeP_x (unable to identify it with the phases described in the references) [5, 6]	None	–
Co-P	400-600	1	–	X-ray picture of the phase close to the picture of CoP [7]	None	–
Zr-S	600	1	1	ZrS_3 [8]	None	Neutral on outside layers of dross
	700	1	2	In outer layer – ZrS_3 [8], in inner layer – ZrS_2 [8].	None	Neutral on outside layers of dross
	800-1000	1	1	X-ray picture of the phase close to that calculated theoretically for ZrS_2 [8]	None	Neutral on outside layers of dross, *F**
Zr-Se	400-600	1	1	X-ray picture of phase close to that calculated theoretically for $ZrSe_2$ [9]	None	*F** (at 600°)
Zr-Te	400-1000	1	1	$ZrTe_x$ (unable to identify with phases known in references [9])	None	*F**
Nb-Se	640	3	–	In outer layer–NbS_{z2}** in middle and inner layers – phases close according to X-ray picture to NbS_2 [10]	None	Patches of dross along the edges of the specimen
	820	1	–	A phase close, according to X-ray picture, to that calculated theoretically for NbS_2 [10]	Texture with a low degree of perfection.	Patches of dross along the edges of the specimen
	1000	1	1	Low-symmetrical phase NbS_x (unable to identify it with the phases known in the references [10])	Texture with a low degree of perfection.	The same on the outer surface of dross.

Table 1 *continued*

System	Temperature interval °C	No. of macroscopic layers	No. of metallographically exposed layers	Phase compound of dross	Presence of texture in the layers of dross	Macroscopic characteristics of the type of reaction diffusion
Nb-Se	650-800	1	–	In outer layer – NbSe**, in inner layer – $NbSe_y$**	Texture with low degree of perfection.	Patches of dross along edges of specimen
	820	2	–	In outer layer – low symmetrical phase $NbSe_z$**, in inner layer – $NbSe_x$**	Texture with low degree of perfection	Patches of dross along edges of specimen
	1000	1	2	In outer layer – phase $NbSe_x$**, the inner, very fine layer was not exposed by X-rays	Texture with low degree of perfection	The same on the out surface of dross
	640	1	–	A phase close, by the position of the lines, to phwses with structural type NiAs	None	Patches of dross along edges of specimen
Nb-Te	820	2	–	In the outer and inner layers – phases close by X-ray picture to phases from structural type CdI_2	None	Patches of dross along edges of specimen
	930	2	2	In outer layer – $NbTe_x$**, in inner layer – $NbTe_x$	None	*F** of outer surface of dross

* Form of specimen after diffusional annealing characteristic for a case of unilateral diffusion of the metalloid.

**Impossible to identify with the phases described in the references.

temperature region starting from 700-800° and higher.

Thus, the selection of binary systems on the principle of the gradual strengthening of the relative role of the homopolar bonds in the chalcogenides of the transitional elements leads to the expected conclusion – an increase in the relative role of the metalloid in the process of reactional diffusion.

Translated by R.J. Coleman

REFERENCES

1. V.I. Arkharov and E.B. Blankova, *Fiz. metal. metallov*, 8, 569 (1959).
2. V.I. Arkharov and E.B. Blankova, *Fiz. metal. metallov*, 8, 452 (1959).
3. N.V. Ageyev, *Priroda khimicheskoi svyazi v metallicheskikh splavakh. (The nature of the chemical bond in metallic alloys) edition Akad Nauk SSSR*, (1947).
4. P. Ehrlic, *Zs. phys. Chem.*, 260, 1-6, 19 (1949).

5. K. Meisel, *Zs. phys. Chem.*, 218, 360 (1934).
6. O. Oerstad and H. Novotny, *Zs. phys. Chem.*, 38, 356 (1937).
7. G.B. Bokii, *Vvedenie v kristallokhimiyu (Introduction to crystallo-chemistry) Pub. Moscow State University* (1954).
8. E.F. strotzer, W. Biltz and K. Meisel, *Zs. phys. Chem.*, 242, 249 (1939).
9. H. Hahn and P. Ness, *Naturwisenschaften*, 44, 20, 534 (1957).
10. G. Hagg and N. Schonberg, *Arkiv. Kemi.*, 7, 371 (1954).

VOL.
8
1959

THE CHANGE IN THE ELECTRICAL RESISTANCE OF A MONOCRYSTAL OF MAGNETITE IN A MAGNETIC FIELD IN THE REGION OF ITS LOW-TEMPERATURE TRANSFORMATION*

By T.D. ZOTOV

(Received 13 April 1959)

It is known that magnetite (Fe_3O_4) cooled below 111°K sharply changes its physical properties [1-5]. The change in the physical properties is usually connected with the low-temperature transformation in magnetite. Vervey supposed [6] that this transformation is explained by the ordering of the divalent and trivalent ions of iron in the octahedral conditions of the magnetite lattice.

In the present work the temperature dependence of the change in electrical resistance in a longitudinal magnetic field is studied at a temperature of from 78 to 213°K on a natural magnetite monocrystal. The specimen was in the form of a small rod of diameter 1.33 mm and length 7 mm. The shaft of the rod was set along a crystallographic axis [100]. Electrical measurements and chemical analysis showed that the magnetite monocrystal studied was close to the stoichiometric composition. According to the spectrum analysis, titanium formed the basic additive within the limits 0.01 to 0.3%. Besides this, traces of Al, Cu, Cr, Mg and several other elements were observed. The statistical alteration of the crystal lattice of the magnetite

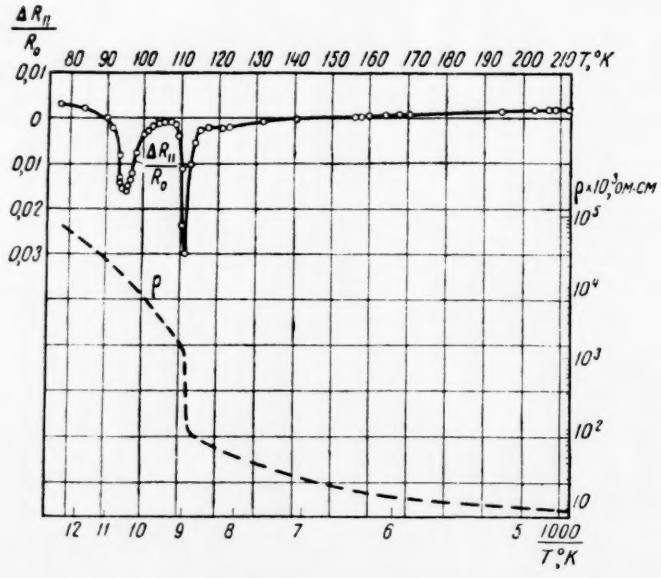

Fig. 1. Dependence of relative electrical resistance in a longitudinal magnetic field on temperature.

* *Fiz. metal. metallov*, 8, No.4, 639-640, 1959.

monocrystal was not observed by X-ray examinations. The determination of the amount of the change in electrical resistance was carried out by slowly heating the specimen from the temperature of liquid nitrogen in a longtitudinal magnetic field of 20,000 oersteds, which is significantly stronger than the field which is necessary for the saturation of the specimen. The specimen was cooled to the temperature of liquid nitrogen in the absence of the magnetic field.

On the drawing the dependence of the relative change in electrical resistance in a longitudinal magnetic field on the temperature is represented by the continuous curve. The dotted curve represents the temperature dependence of the specific electrical resistance. Both curves were obtained on one and the same specimen. As is seen from the drawing, on the curve $\frac{\Delta R_{\parallel}}{R}(T)$ two minimums are observed. Besides this, the curve $\frac{\Delta R}{R}(T)$ has yet another peculiarity: it crosses zero twice, in the regions 88 and 140°K.

The first minimum is explained by the transition of the magnetite, on heating, from an ordered to a disordered state. With regard to the second minimum, it is apparently connected with the scattering of the conduction electrons in the fluctuations of electronic density, the magnetizability and density of the substance, analogous to the process of the scattering of the conduction electrons in the fluctuations of magnetizability, which should take place slightly lower than the Curie temperature, in accordance with the work of Krivoglaz and Ribak [7]. On switching on the magnetic field the fluctuations decrease and, because of this, the movement of the electrons increases. This leads to a decrease in electrical resistance.

In conclusion, I express thanks to N.V. Volkenstein for continuous attention and interest in the work, and to B.S. Borisov for the X-ray study of the specimen.

Translated by R.J. Coleman

VOL. 8 1959

REFERENCES

1. E.J.W. Verwey, *Nature*, 144, 327 (1939).
2. Ching Hsin Li, *Phys. rev.*, 40, 1002 (1932).
3. R.M. Millar, *J. Amer. Chem. soc.*, 51, 215 (1929).
4. P.A. Khalileyev, *Sow. Phys.*, 7, 108 (1935).
5. C.A. Domenicali, *Phys. rev.*, 78, 458 (1950).
6. E.J. Verwey, P.W. Haayman and F.C.J. Romeijn, *Chem. Phys.* 15, 181 (1947)
7. M.A. Krivoglaz and S.A. Ribak, *Zh. tekh. fiz.* 28, 940 (1958).

No. 5

	PAGE
On the determination of conditions for the autoradiographic exposure of inhomogeneities in adsorptive concentration — V. S. Galishev, A. N. Orlov and I. A. Shvarte	1
On the effect of fluctuations in the parameters of correlation upon scattering of X-rays and thermal neutrons by solid solutions — M. A. Krivoglaz	8
Relaxation absorption of ultrasound in ferromagnetics — V. T. Shmatov	27
A diabetic galvanomagnetic and thermomagnetic phenomena in semiconductors. 2. Mixed conductivity — V. Ye. Vzdornov and I. M. Tsidil'kovskii	31
On the temperature dependence of the magnetic properties of magnetically textured specimens of MnBi alloy powders — Ia. S. Shur, Ye. V. Shtolts, G. S. Kandaurova and L. V. Rebneva	38
On the reforming of the domain structure of magnetically uni-axial ferromagnetics in a magnetic field — Ia. S. Shur, Ye. V. Shtolts and A. A. Glazer	44
On the dependence of the field of a defect of the crack type on the thickness of the covering metal layer — V. V. Vlasov and R. Ye. Yeršhov	47
The thermoelectric properties of magnetite in the temperature region of 80-400°K — A. A. Samoklvalov and I. G. Fakidov	52
X-ray study of the temperature dependence of defects in the crystal lattice of metals — G. A. Sirenko and V. I. Khotkevich	57
Some peculiarities in the structure of anomalous effects in powder diffraction patterns of ageing Al-Ag and Al-Ag-Cn alloys — R. R. Zakharova and N. N. Buinov	62
Effect of small amounts of admixtures on the diffusion coefficients of polycrystalline materials. 3. Effect of thallium on auto-diffusion of silver — V. I. Arklarov, S. M. Kliutsman and A. N. Timofeev	66
Investigation of the causes of diffusional "activity" of deformed crystalline bodies. 2. On the sintering of electrolytic metals in the light of model tests data — Ia. E. Geguzin and N. N. Ovcharenko	70
To the determination of surface tension on the boundaries of phases — I. V. Salli	76
The effect of additions of vanadium on the self-diffusion of iron — M. S. Zelinskii, B. M. Noskov, P. V. Pavlov and E. V. Shitov	79
High temperature study of alloys, the phases of which have identical lattices with nearly the same parameters — I. I. Titarenko and B. M. Rovinskii	84
The nature of ζ-phase of the system Fe-Si — F. A. Sidorenko, P. V. Gel'd and L. B. Dubrovskaya	88
On the reduction of copper ferrite with graphite — N. M. Stafeeva, V. N. Bogoslovskii, G. I. Chufarov and V. A. Subbotina	93
The effect of vacuum on variation of critical temperatures structure and chemical composition of cast iron — V. P. Chernobrovkin, V. S. Belyaev and A. A. Dobryden'	98
Hot-rolled transformer steel with low specific losses — N. F. Dubrov	103
Analysis of the kinetics of two-phase precipitation of Cu-Be alloy by an electrical resistance method — A. S. Kagan and Ya. S. Umanskii	108
Study of the patterns of deformation and recrystallization of iron-nickel alloy (48% Ni) in relation to the degree of deformation on cold rolling — M. M. Borodkina and N. P. Gromov	111
The influence of phosphorous on structural transformations and properties of low-alloy electro-technical steel — S. I. Doroshek	118
The influence of cold plastic deformation on the modulus of elasticity in carbon steels — A. V. Gur'yev	123
Determination of the period of relaxation at the polymorphic transformation of iron — R. I. Garbyer and A. I. Kovalev	129
The influence of the temperature of the experiment on the fatigue strength of specimens of carbon steel with stress concentrators under the action of a molten environment of the eutectic Pb-Sw — M. I. Chayevskii	132

VOL. 8 195

Letters to the Editor

The problem of the mechanism of intercrystalline internal adsorption in dilute solid solutions
V. I. ARKHAROV, B. S. BORISOV, S. D. VANGENGEIM and G. G. TALUTS 135

On additional weakening of X-ray diffraction lines in powder specimens
A. YE. KOVAL'SKII and S. V. SEMENOVSKAIA 138

Dispersion equation for electron plasma in a magnetic field L. I. PODLUBNYI 140

Contribution to the treatment of anomalous effects on X-ray photographs of alloys in the process of ageing R. R. ZAKHAROVA and N. N. BUINOV 142

VOL.
8
1959

VOL
8
195

ON THE DETERMINATION OF CONDITIONS FOR THE AUTORADIOGRAPHIC EXPOSURE OF INHOMOGENEITIES IN ADSORPTIVE CONCENTRATION*

V.S. GALISHEV, A.N. ORLOV and I.A. SHVARTE
Institute of Physics of Metals, U.S.S.R. Academy of Sciences
(Received 28 July 1959)

The criterion suggested in paper [3] for autoradiographic exposure of intergranular boundaries enriched by a radioactive isotope is more accurately defined. The more accurate specification consists of taking into consideration the space distribution of electrons emitted by the boundary and the relationship between the sensitivity of photographic emulsions and the energy of the electrons.

VOL. 8 1959

1. In the work by Arkharov, Galishev et al [1] conditions were discussed for the exposure of inhomogeneity in adsorptive precipitation by the autoradiographic method using β-emitting isotopes. The calculation of electron density $F(r, \vec{r})$ of energy E, defined by symbolic growth τ (cm² in dimension) at point $\vec{r}$ inside or on the surface of a specimen, was carried out taking multiple scattering into consideration for the following model.

The specimen is a plane-parallel plate of thickness b along the y-axis and infinitely extended along the x and z axes. A portion of the plane $x = 0$, cut out by the $y = 0$ and $y = b$ planes, forms an infinitely thin intercrystalline zone on which β-emitting atoms are adsorbed. By the method in paper [2] the question of finding the function $F(r, \vec{r})$ is reduced to the diffusion problem, the solution of which has a simple form when the thickness of the specimen is

$$b \ll \lambda\pi^2/6, \tag{1}$$

where $\lambda(E)$ is the free path of the electron of energy E [3]. In this case the density of electrons of symbolic growth τ emitted by the intercrystalline zone near the specimen surface at a distance x from the zone is equal to

$$F(x, 0, \tau) = F(x, b, \tau) = \frac{s_0}{2\sqrt{\pi\tau}} exp\left(-\frac{x^2}{4\tau} - \frac{6\tau}{b\lambda}\right), \tag{2}$$

where s_0 is the number of electrons emitted from 1 cm² of the zone surface. The electron density emitted by sources evenly distributed in the grain space near the zone surface, is equal to

$$F'(0, \tau) = F'(b, \tau) = \frac{v_0}{\sqrt{2\pi}} exp\left(-\frac{6\tau}{b\lambda}\right), \tag{3}$$

where v_0 is the number of electrons emitted from unit volume of the grain. The spectral density of the electron beam through the planes $y = 0$ and $y = b$ is equal to

$$n(x, 0, \tau) \equiv \frac{dn}{d\tau} = \frac{\partial F}{\partial y}\Big|_{y=0} = \frac{3}{\lambda} F(x, 0, \tau). \tag{4}$$

Galishev and Shvarte [3] defined the results of [1] more accurately for application to Al + 0.1 per cent ^{110}Ag and Cu + 0.1 per cent ^{124}Sb systems by assuming that the concentration of the active

component in the intercrystalline zone is equal to 10 per cent and that the criterion for the exposure of the zone is the fulfilment of the inequality

$$s_{\text{zone}} - s_{\text{background}} > 0.1, \tag{5}$$

where

$$s = aD$$

denotes the intensity of blackening of the film; D is the radiation dose, a the coefficient of proportionality*. The quantity D is associated with the number of electrons n falling on the emulsion and the time of exposure t by the relationship

$$D = n\nu t c'(E) E, \tag{6}$$

where ν is the coefficient of absorption of the photographic emulsion and $c'(E)$ is the efficiency of the absorbed electron of energy E in producing the latent photographic image. In paper [3] it was, in fact, assumed that the product

$$c = c'\nu aE$$

is independent of energy so that the equation $\Delta = s_z/s_{bg} = n_z/n_{bg}$ (as follows from formula (31) of paper [3]) holds; Δ is the ratio of electrons beams and not of the intensities which are equal to

$$I = \int n'(E) E dE).$$

For evaluation of the difference (5), the value of $n(x, r)$ at the point $x = 0$ was taken as the n_{zone}, where, according to (2), $n(x)$ reaches peak value, and the rate of fall of function $n(x)$ with rise of x was disregarded. For these assumptions, expression (5) holds when

$$\Delta = s_z/s_{bg} > 1.1 - 1.5, \tag{7}$$

whereupon the lower limit corresponds to the intensity of blackening $s = 1$, and the upper to $s = 0.2$. For the enriched zone, 0.1 μ thick, condition (7) is fulfilled for ^{110}Ag – lines with a mean energy of 29 and 170 keV (1/3 of maximum energy).

The purpose of this report is to make the conditions (7) of exposure more accurate by taking into consideration the type of the function $n(x)$ and the dependence of coefficient c on energy.

2. It can be seen from (2) that for small r the integrand in the expression

$$n(x, \tau_0) = \int \frac{3}{\lambda} F(x, \tau) d\tau$$

falls sharply with rise of x, and for large r it falls slowly. If the fall is sharp and $n(x)$ is noticeably different from zero only in a region a few microns thick, the intercrystalline zone will occur as a thin strip of width of the order of emulsion grains. If, however, the fall of $n(x)$ is too slow (takes place at a distance of a crystal grain), the intercrystalline zone will then not appear even if Δ satisfies the inequality (7). Finally, if the spectrum of β-emitting atoms contains lines of various maximum energy, the fulfilment of conditions (7) for one or several lines of the spectrum is then not sufficient

* The function $s(D)$ is in fact more complicated (see e.g. [6]) but for a small section of variation of s it may be approximated to be linear.

for the exposure of the zone, because the electrons of high energy and free path L of the order of specimen grains, practically, will just intensify the background blackening.

It is known (see e.g. [4]) that in visual examination of a film the exposure of an image (as uneveness in blackening) is defined by the brightness element of the image i.e. by the value $\Delta_i = \log (B_1/B_2)$, where B_1 and B_2 are the brightness of the image and the brightness of the background respectively which can still be distinguished by the eye at a given illumination of the film. If the film is examined in a plane-parallel beam of in transmission light, the difference then, by the definition of the intensity of blackening s, is

$$\Delta s = \Delta_i$$

Δ_i depends on the background brightness, the size of image, its contrast range (the distance at which B changes from B_1 to B_2) and other factors. Precise forms of these relations are unknown. For a rough estimation of Δ, we take into consideration that in the γ-detection of defects a very small difference in blackening $\Delta s = 0.05$ [5] is sufficient for a clear detection of them. Since the autoradiographic images are usually examined under a microscope when they are less clear due to fluctuations in the background blackening (this also concerns the examination of microphotographs on which the fluctuations are reproduced), we shall assume, as in [3], that

$$\Delta s_{min} = 0.1 \tag{8}$$

and require that the change of

$$s \text{ from } s_{\text{background}} \text{ to } s_{\text{background}} + \Delta\, s_{\text{min}}$$

take place over a distance of the order of $0.1\, L$, where L is the grain size of the specimen.

We shall now define more accurately formula (6) which was assumed in [3]. The relation between the intensity of blackening s and the amount of energy absorbed by the emulsion, or more accurately the dose of incident radiation, is described by a curve known as the characteristic curve of emulsion which in general case is of a complex form [6]. Experiments show [7] that for electrons of energy up to 50 keV the relation between s and the number of electrons falling in 1 sec on 1 cm² is linear

$$s = c\,(E)\, nt. \tag{9}$$

The coefficient $c\,(E) = c'\nu\, aE$ increases with electron energy faster than required by linear law and the form of this relationship on the type of emulsion.

Expressing E in terms of the symbolic growth, we write $c = c\,(r)$. Let the intensity (a number of electrons per decay) of the ith line of β-ray spectrum be denoted, by a by n_{i_0} the electron-beam density of the ith line for $x = 0$, by n_{i_1} for $x = 0.1\, L$, and by n_{ibg} the density of the electron beam of the ith line from the bulk of the grain. By rewriting then equation (9) in the form of

$$s = \sum_i \alpha_i t \int_0^{\tau_{i0}} c\,(\tau)\, n_i'\,(\tau)\, d\tau, \tag{10}$$

where

$$n' = \frac{dn}{d\tau},$$

instead of (8) we obtain the exposure condition as

$$t \left[\sum_i \alpha_i \int c\,(\tau)\, n_{i0}'\,(\tau)\, d\tau - \sum_i \alpha_i \int c\,(\tau)\, n_{i1}'\,(\tau)\, d\tau \right] > 0{,}1. \tag{11}$$

VOL. 8 1959

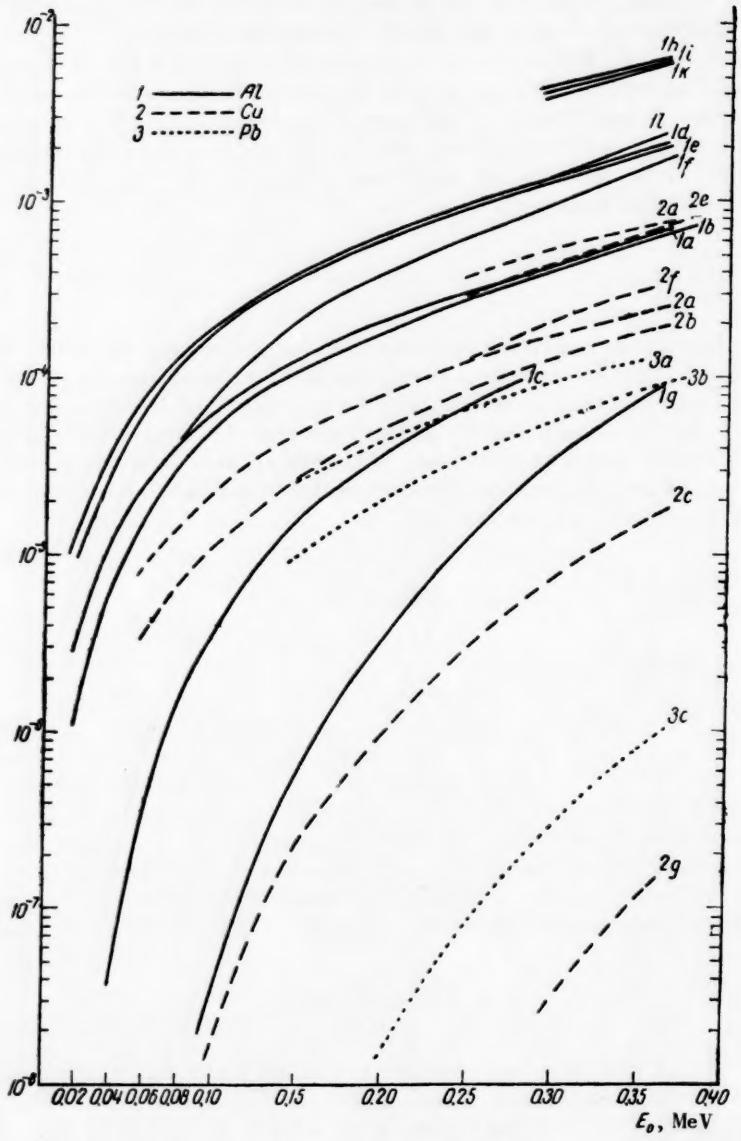

FIG. 1. Integral (15) as a function of mean electron energy E_0. Figures on the curves denote: 1 – Al; 2 – Cu; 3 – Pb. Values of b – the thickness of the specimen – and x – the distance of enriched zone from the centre – see in Table 2.

The time t is obtained from the condition that the intensity of background blackening

$$s_{bg} = \sum \alpha_i \int c(\tau)\, n'_{i\,bg}(r)\, d\tau\, t \tag{12}$$

is optimum for exposing the image, i.e. about 2 [5]. We obtain then

$$S_{opt}\ \frac{\sum \alpha_i \int c(\tau)\left(n'_0 - n'_1\right) d\tau}{\sum \alpha_i \int c(\tau)\, n'_{bg}\, d\tau} > 0.1. \tag{13}$$

In the particular case when (as assumed in [3]) c is independent of E (or the dependence is of such a form that in formula (13) for the spectrum of dispersed electrons discussed it practically vanishes) and in the spectrum of primary electrons there is only one line, we obtain

$$s_{opt} \int (n_0' - n_1')\, d\tau / \int n_{bg}'\, d\tau > 0.1. \tag{14}$$

Finally, if n' falls with x so sharply that practically $n' = 0$, the relation (7) is obtained.

3. It is shown in [3] that in certain conditions two lines of the ^{110}Ag β-spectrum satisfy the condition of exposure (7). Let us verify by using the more general condition (13) whether the intercrystalline zone appears if the assumptions assumed in [3] about c being independent of E and n falling rapidly with x are not fulfilled.

For this purpose it is necessary to know the function $c(E)$ for the film used in the experiments with the Al-Ag system mentioned in [1]. Unfortunately, no such data are available. We assume, therefore, that $c(E)$ is linear. This does not differ much from the data quoted in [7] and agrees with the results of the X-rays in [8]. Instead of (13) we then obtain:

$$s_{opt} \frac{\sum a_i \left[\int_0^{\tau_{0i}} n_{i0}'(\tau)\, E(\tau)\, d\tau - \int_0^{\tau_{0i}} n_{i1}'(\tau)\, E(\tau)\, d\tau \right]}{\sum a_i \int_0^{\tau_{0i}} n_{ibg}'(\tau)\, E(\tau)\, d\tau} > 0.1. \tag{14'}$$

VOL. 8 1959

The integral

$$I(x) = \frac{2\sqrt{\pi}}{s_0 h_0} \int_0^{\tau_0} n'(x, \tau)\, E(\tau)\, d\tau = \int_0^{\tau_0} e^{-\frac{2h_0\tau}{b} - \frac{x^2}{4\tau}} E(\tau)\, \tau^{-1/2}\, d\tau \tag{15}$$

was calculated graphically for the following values of the problem: β-electron energy from 0.02 to 0.35 MeV; absorbers of Al, Cu, Pb used; thickness of specimens $b = 10^{-4}$; 10^{-3}; 10^{-2} cm; distance of the points of observation from the centre of enriched zone $x = 0$; 10^{-4}; 10^{-3}; 10^{-2} cm. All the combinations of these values which do not satisfy the condition (1) were excluded. The integrals in the denominator of formula (14′), which define the blackening of background, were approximately calculated by means of the formula:

$$\frac{I_{bg}}{h_0} = \int_0^{\tau_0} e^{-\frac{2h_0\tau}{b}} E(\tau)\, d\tau \approx E_0 \frac{b}{2h_0} \left(1 - e^{-\frac{2h_0\tau_0}{b}}\right), \tag{16}$$

in which the electron energy function $E(r)$ is substituted by its maximum value E_0. The examination of the integrand in (16) for the values of the parameters of the problem indicates that its variation differs from an exponential function only in the vicinity of the point $r = r_0$ (and even here insignificantly).

The results of calculations are shown in the figure. By interpolation and using formulae (16) and (14′), the conditions for the autoradiographic exposure of irregularities in concentration discussed can be determined from these data for a wide group of systems. Let us examine two examples:

a. Al with admixture of ^{110}Ag for the values of parameters of the problem adopted in [3]: thickness of the specimen $b = 0.001$ cm; thickness of the intercrystalline zone $d = 10^{-5}$ cm; concentration of ^{110}Ag in the zone $c_2 = 10$ per cent; and in the bulk $c_1 = 0.1$ per cent so that, when $s_{opt} = 2$, $ds_{opt}c_2/c_1 = 2 \times 10^{-3}$ cm. The results of calculations are given in Table 1. It is evident that the blackening of the film by the line of 29 keV decreases quite sharply at a distance of $10^{-4} - 10^{-3}$ cm from the zone, and that by the line of 170 keV at this distance is nearly the same as for $x = 0$. By comparing the values from the last line of Table 1 with the inequality (14′) we come to the

TABLE 1

System	Mean energy E_i	Relative intensity a_i	$I(x)h_0$		
			$x=0$	$x=10^{-4}$ cm	$x=10^{-3}$ cm
Al—Ag	29 keV	0.65	0.061	0.051	0.006
	170 keV	0.33	0.080	0.073	0.045
	$\frac{a_1 h_{01} I_1 + a_2 h_{02} I_2}{I_{bg}}$		0.066	0.057	0.019
	Left-hand side of (14′) $\times \frac{c_1}{ds_{opt} c_2}$		3.7×10^{-5}	3.7×10^{-5}	3.7×10^{-5}
			0	1.7×10^{-2}	8.9×10^{-2}
Fe—C	55 keV left hand Side of (14′) $\times \frac{1}{I_{bg}} \frac{c_1}{ds_{opt} c_2}$		0.058	0.023	3.72×10^{-6}
			2.6×10^{-6}	$2,6\times10^{-6}$	2.6×10^{-6}
			0	0.95×10^{-4}	1.6×10^{-4}

TABLE 2

Values at b	Values of x			
	0	10^{-4}	10^{-3}	10^{-2}
10^{-4}	*a*	*b*	*c*	—
10^{-3}	*d*	*e*	*f*	*g*
10^{-2}	*h*	*i*	*k*	*l*

conclusion that at a distance of $x = 10^{-4}$ cm from the centre of the intercrystalline zone the intensity of blackening of the film is already appreciably lower than that over the zone so that for the size of grain $L > 10^{-3}$ cm – in agreement with the conclusions of [1, 3] – the intercrystalline zones in the specimen investigated appear when the emulsion is used in which the increase of $c(E)$ with E is linear or sharper. In the experiments described in paper [1] they did not appear evidently because the specimen used was very thick.

b. The Fe-C system investigated experimentally by Zav'yalov and Bruk [9] on massive specimens. Here C^{14} with one line of the β-spectrum is the radioactive isotope ($E_{max} = 0.155$ MeV, $E_0 = 1/3\ E_{max} = 0.05$ MeV). In this case expression (14′) is simplified because the sums contain but one item. Assuming an effective thickness of the layer from which electrons hit the film to be equal $b = 10^{-4}$ cm and using the curves of the figure (see Table 2), we shall obtain the figures given in Table 1. If – according to [9] – we put $d = 5 \times 10^{-6}$ cm; $c_1 = 0.23$ at.% and assume c_2 to be equal to the limiting solubility of carbon in γ-iron (about 7 at.%), then $ds_{opt}\, c_2/c_1 = 10^{-6} \times 7/0.23 \approx 3 \times 10^{-4}$ cm so that the blackening of the film at a distance of $x = 10^{-4}$ cm from the centre of the enriched zone should be appreciably less than over the zone. This conclusion holds even if the concentration of carbon in the enriched zone is a fraction of the above.

As the thickness of the layer emitting electrons to the surface is in fact greater than 10^{-4} cm (in [9] it is estimated to be 3×10^{-3} cm), the contrast range is decreasing and the blackening falls rise of x slower than the rate calculated in Table 1. Owing to the fact that in this case condition (1) is violated, it is impossible to estimate the dependence of film blackening on x more accurately by the approximate method used here. It is possible that the broad image of the intercrystalline zone (of the order of 10^{-3} cm) obtained in work [9] is caused by the fact that the width of the zone enriched

by carbon was appreciably greater than that assumed by the authors.

In order to estimate conditions of exposing the boundaries correctly it is important to have experimental data concerning the function $c(E)$ for various emulsions. Any reliable theoretical calculation of the coefficient $c'(E)$ is scarcely possible in the present state of knowledge on the mechanism of developing the latent photographic images produced by the action of β-particles.

In addition to the conclusions of paper [3], the emulsions should be recommended for use which are sensitive to the electrons of low energy and insensitive to the electrons of high energy, because the latter produce homogeneous blackening of the background due to their long free paths even when the β-emitting atoms are concentrated on the intercrystalline boundaries.

Translated by B. Cynk

REFERENCES

1. V.I. Arkharov, V.S. Galishev, C.M. Klotsman and A.N. Timofeyev, *Issledovaniya po zharoprochnym splavam* (Investigations on heat-resistant alloys), 3, p. 421, Izd. Akad. Nauk SSSR (1958).
2. H.A. Bethe, M.E. Rose and L.P. Smith, *Proc. Am. Phil. Soc.*, 78, 573 (1938).
3. V.S. Galishev and I.A. Shvarte, *Works of the Institute of Physics of Metals, U.S.S.R. Academy of Sciences*, No. 22, 0. 37* (1958).
4. G.S. Baranov, *Voprosy teorii fotograficheskogo vosproizvedeniya* (Questions of the theory of photographic reproduction), Goskinoizdat (1949).
5. N.P. Grazhdankina and I.G. Fakidov, *Sb. Gamma-defektoskopiya metallov* (Collection, Gamma-detection of defects), p. 54, Izd. Akad. Nauk SSSR (1955).
6. A.N. Orlov, *Sb. Gamma-defektoskopiya metallov* (Collection, *Gamma-detection of defects*), p. 5, Izd. Akad. Nauk SSSR (1955).
7. L. Granberg and J. Halpern, *Rev. Sci. Instr.*, 20, 641 (1949) (Translation in the symposium: Radiography, p. 292, Foreign Literature Publishing House, (1952).
8. G.J. Hine, *Nucleonics*, 7, No. 4, 18 (1950) (Translation in collection: Radiography, Foreign Literature Publishing House, p. 28, 1952).
9. A.S. Zav'yalov and B.I. Bruk, *Sb. Metallovedeniye* (Collection: *Metallography*), 1, p. 206 (1957).

* In work [3] the spectral density was denoted by n, in this articel by n'.

VOL. 8 1959

ON THE EFFECT OF FLUCTUATIONS IN THE PARAMETERS OF CORRELATION UPON SCATTERING OF X-RAYS AND THERMAL NEUTRONS BY SOLID SOLUTIONS*

M.A. KRIVOGLAZ

Institute of Physics of Metals, U.S.S.R. Academy of Sciences

(Received 8 January 1959)

Scattering of X-rays and thermal neutrons by substitutional solid solutions associated with a variety of atomic scattering factors and geometric distortions are discussed. Heterogeneity associated with fluctuating changes not only in the composition but also in the parameters of correlation is considered.

It is shown that accounting for fluctuations in the parameters of correlation order may lead to substantial changes in the shape of isodiffusion curves. Ideal solutions and solutions near the point of the phase transition of the second order are discussed in detail. Formulae are given for the quantities which determine the weakening due to static distortions in intensity of normal reflections.

1. INTRODUCTION

When scattering of various types of waves (X-rays, thermal neutrons, light) by solutions is analysed, only the scattering from fluctuating concentrations of components at various lattice points is usually taken into consideration (the fluctuations in composition and parameters of long-range order). Meanwhile, in addition to the composition fluctuations, fluctuations in the parameters of correlation (p.c.) usually occur measured by the number of pairs of similar atoms at a definite distance from one another in a given element of volume. In general, a degree of heterogeneity which causes scattering of a given type of waves (the extent of irregularities in refractive index in the case of light dispersion, or lattice distortions in the case of X-ray scattering) should depend not only on the fluctuations in composition but in the p.c.

Irregularities associated with fluctuations of p.c. should result in the occurrence of additional scattering.

Moreover, the value of the coefficient correlating the extent of irregularities with fluctuations in concentration c is usually assumed to be equal to the equilibrium (not fluctuating) change of c per unit change in composition of the whole specimen. However, in such an equilibrium change of c, the p.c. also change in a definite way, whereas in fluctuating changes of c the p.c. may remain constant (or vary by quantities having no relation to their equilibrium changes). For this reason the above mentioned coefficients to Δc in the degree of heterogeneity resolved into fluctuations in composition and in the p.c. should be determined for constant values of p.c; they may noticeably differ from the equilibrium coefficients.

Thus, the results obtained without accounting for fluctuations in the p.c. may undergo some changes.

In connexion with the above statement, it is of interest to find out the effect of p.c. fluctuations upon scattering. Evidently, the simplest way of studying this effect is to use the scattering of X-rays (or thermal neutrons†) by solid solutions, because in this case the relation can be established between the lattice distortions and the fluctuations in composition and p.c. by means of quite a simple model, which will also reveal all the properties of the effects. In paper [1] the theory of scattering from irregularities of solid solutions, associated with difference of atomic factors and atomic radii

---

* *Fiz. metal. metalloved.*, 8, No. 5, 648-666, 1959.

† The following account will be given in terms referring to the scattering of X-rays. For studying the thermal neutron scattering from irregularities of the type discussed here it is in fact sufficient to simply change the notations.

VOL
8
195

of components, was developed without accounting for the fluctuations in the p.c.. Such an approximation is evidently applicable in the cases when the proportionality factors between the lattice distortions and the fluctuating change of p.c. are sufficiently small.

As was noted in [1], the applicability criterion of this approximation is fulfilled in the solutions obeying the Vegard principle (of linear relation between lattice constant and composition) and in those with low concentration of one of their components. In our present report the effect of p.c. fluctuations upon scattering will be explicitly taken into consideration. Such an analysis will enable one to estimate corrections associated with these fluctuations, to formulate more accurately the criterion of insignificance of their influence and to investigate changes in the distribution of scattering intensities contributed by them. The calculations will be made for the same case as in [1], i.e. for the monochromatic scattered radiation from statical irregularities of a single crystal.

Within limitations of the kinematic theory of dispersion, the intensity of X-ray dispersion by a binary disordered substitutional solid solution A-B with the lattice containing one atom in its unit cell may be expressed in electron units in the known form:*

$$I = \overline{\left|\sum_s f_s \exp\left(iq_1,\ R_s + \delta R_s\right)\right|^2}. \tag{1}$$

Here f_s is the scattering factor of the atom in the sth lattice point; q the difference of wave vectors of scattered and incident waves; R_s the vector of sth point of the ideal "mean" lattice; δR_s the vector of displacement of the atom from this point. It is obvious that f_s may be represented in the form: $f_s = c_s f_A + (1 - c_s) f_B$, where f_A and f_B are the scattering cross-section of A and B atoms respectively, and $c_s = 1$ if atom A occupies the sth point, or $c_s = 0$ if atom B is at the point. Let us expand c_s and δR_s by Fourier's series:

$$c_s - c = \sum_k{}' \left(c_k e^{-ikR_s} + c_k^* e^{ikR_s}\right);$$

$$c_k = \frac{1}{N} \sum_s (c_s - c)\, e^{ikR_s}, \tag{2}$$

$$\delta R_s = i \sum_k{}' \left(R_k e^{-ikR_s} - R_k^* e^{ikR_s}\right);$$

$$R_k = -\frac{i}{N} \sum_s \delta R_s\, e^{ikR_s}. \tag{3}$$

Here c is the concentration of atoms A; N are the number of atoms in the crystal, the summation for k is performed over vectors $k/2\pi$ lying in the half-space of the first structure cell of the reciprocal lattice (we assume that the reciprocal lattice point is in the centre of the structure cell). The imaginary unit i is taken out in (3) for facility.

Substituting expansions (2) and (3) in (1), performing the same transformation as done in [1] and using, as in [1], only quadratic items referring to R_k and c_k (which is right for lattices not much distorted when the condition (9) of paper [1] is satisfied), we obtain

$$I = 8\pi^3 \frac{N}{\Delta} \bar{f}^2 \delta(q) + N^2 \overline{|f q_1 R_q - (f_A - f_B) c_q|^2}, \tag{4}$$

where Δ is the volume of the unit cell; $q = q_1 - 2\pi K_n$; K_n is the vector of reciprocal lattice lying in the same cell as vector $q_1/2\pi$; the first term, containing the δ-function, determines the intensity of regular reflections, and the second one determines the intensity of diffuse scattering. In contrast to [1], where $\bar{f}$ denoted the mean atomic scattering factor, in the present work $\bar{f}$ is given by

* Here and below q_1, q, k, K, R and ρ denote vectors

$$f = cf_A \exp\left(-\frac{L_A}{2}\right) + (1-c) f_B \exp\left(-\frac{L_B}{2}\right), \tag{5}$$

where

$$\exp\left(-\frac{L_A}{2}\right) = \overline{\exp(iq_1 \delta R_{sA})};\ \exp\left(-\frac{L_B}{2}\right) = \overline{\exp(iq_1 \delta R_{sB})};$$

$$L_A = \overline{(q_1 \delta R_{sA})^2};\ L_B = \overline{(q_1 \delta R_{sB})^2}. \tag{6}$$

Here

$$\exp\left(-\frac{L_A}{2}\right) \text{and} \exp\left(-\frac{L_B}{2}\right)$$

are the factors which account for reduction of scattering amplitudes of A and B atoms due to static distortions; averaging in (6) is performed along the lattice points occupied by atoms A and B respectively. In expressing L_A and L_B in formulae (6) in terms of mean squares of atom displacements the Gaussian distribution of displacement probability was used. Although, as shown in [2] the displacements do not in general obey this distribution, formulae (6), however, hold with sufficient accuracy because, in the case of substitutional homogenized solutions in question the deviations are small. As is evident from formula (4) it is necessary to know the Fourier transforms of lattice distortions in order to determine intensities of diffuse scattering. In chapter 2 these values will be expressed in terms of Fourier concentrations and p.c.

2. DETERMINATION OF FOURIER TRANSFORMS OF ATOM DISPLACEMENTS

Static displacements δR_s are determined as equilibrium positions for the thermal oscillations of atoms. These values can be found from the condition for minimum of free energy of the solution F. Let us assume a harmonic model according to which the expression for F may be written in the form:

$$F = F_0 - \sum_{s,\,s'} w^{\alpha\alpha'}_{ss'i}\, \delta R_{si} + \frac{1}{2} \sum_{ss'} V^{\alpha\alpha'}_{ss'ij}\, \delta R_{si}\, \delta R_{s'j}, \tag{7}$$

where the indices $\alpha, \alpha' =$ A, B denote the kind of atom occupying sth or s'th lattice points respectively; i,j. number Cartesian co-ordinates of vectors and the summation with respect to the twice repeated indices i and j is carried out here and below in the text from 1 to 3. The quantities

$$w^{\alpha\alpha'}_{ss'i} \text{ and } V^{\alpha\alpha'}_{ss'ij}$$

are not constant but depend on the composition of solution, the p.c. and temperature. In working out the expression (7) for F, it was taken into consideration that the force acting on sth atom from the s'th atom depends on the displacement of the latter and on the type of both atoms. In this case, however, it is not taken into account that this force may also depend on types and dislocations of all the remaining neighbouring atoms. As will be evident from the results obtained below, these effects (which can easily be calculated when data on interatomic interactions in solutions are more accurately defined) do not change the evidence obtained on the distribution of scattering intensity (and evidently lead to small quantitative changes). The model adopted is more accurate than the model corresponding to the case when Vegard's principle holds, used in [1] in which it was assumed that

$$V^{\alpha\alpha'}_{ss'ij}$$

are independent of α and α' and that $w^{\alpha'}_{ss'i}$ are independent of α.

The quantities $w_{ss'i}^{aa'}$, which take three values

$$w_{ss'i}^{AA}, \quad w_{ss'i}^{AB} \text{ and } w_{ss'i}^{BB},$$

may evidently be written in the form

$$w_{ss'i}^{aa'} = w_{ss'i} + w'_{ss'i}(c_s + c_{s'} - 2c) + w''_{ss'i}(c_s - c)(c_{s'} - c), \tag{8}$$

where

$$\begin{aligned} w''_{ss'i} &= w_{ss'i}^{AA} + w_{ss'i}^{BB} - 2w_{ss'i}^{AB}; \\ w'_{ss'i} &= w_{ss'i}^{AB} - w_{ss'i}^{BB} + cw''_{ss'i}; \\ w_{ss'i} &= w_{ss'i}^{BB} + 2cw'_{ss'i} - c^2 w''_{ss'i}. \end{aligned} \tag{9}$$

The quantities $V_{ss'ij}^{aa'}$ for $s \neq s'$ may be presented in a similar way as

$$\begin{aligned} V_{ss'ij}^{aa'} &= V_{ss'ij} + V'_{ss'ij}(c_s + c_{s'} - 2c) + V''_{ss'ij}(c_s - c)(c_{s'} - c); \\ V''_{ss'ij} &= V_{ss'ij}^{AA} + V_{ss'ij}^{BB} - 2V_{ss'ij}^{AB}; \\ V'_{ss'ij} &= V_{s'ij}^{AB} - V_{ss'ij}^{BB} + cV''_{ss'ij}; \\ V_{ss'ij} &= V_{ss'ij}^{BB} + 2cV'_{ss'ij} - c^2 V''_{ss'ij}. \end{aligned} \tag{8a}$$

By taking derivatives of expression (7) for free energy with respect to δR_{si} zero, we obtain a system of equations for the determination of displacements:

$$\begin{aligned} \sum_{s'} [V_{ss'ij} + V'_{ss'ij}(c_s + c_{s'} - 2c) + V''_{ss'ij}(c_s - c)(c_{s'} - c)](\delta R_{s''j} - \delta R_{sj}) = \\ = \sum_{s'} [w'_{ss'i}(c_s + c_{s'} - 2c) + w''_{ss'i}(c_s - c)(c_{s'} - c)]. \end{aligned} \tag{10}$$

In the right-hand side of equation (10) the sum $\sum_{s'} w_{ss'i}$, is omitted as zero, because by the Newton third law,

$$w_{ss'i}^{aa'} = -w_{s's i}^{a'a} = -w_{s'si}^{aa'} \quad (w_{ssi}^{aa'} = 0).$$

Below in the text we shall regard $V'_{ss'ij}$ and $V''_{ss'ij}$ as appreciably smaller than the corresponding values of $V_{ss'ij}$, and solve the system (10) by a method of consecutive approximations. This assumption is true if the differences of elasticity moduli of solutions of various compositions are smaller than the moduli themselves. In the zero approximation we assume that

$$V'_{ss'ij} = V''_{ss'ij} = 0.$$

Multiplying equation (10) by e^{ikR_s}, adding the results and considering (2) and (3), we obtain a system of three linear equations for determining three components of the vector R_k

$$V_{kij} R_{kj} = w'_{ki} c_k + \sum_{\rho \neq 0} w''_{ki}(\rho) c_k(\rho). \tag{11}$$

Here the following notations are introduced:

$$V_{kij} = \sum_s V_{ss'ij}\, e^{ik,\, R_s - R_{s'}};$$
$$w'_{kl} = -i \sum_s w'_{ss'i}\, e^{ik,\, R_s - R_{s'}};$$
$$w''_{ki}(\rho) = w''_i(\rho) = -i w''_{ss'i}; \tag{12}$$
$$c_k(\rho) = \frac{1}{N} \sum_s^{(\rho)} (c_s - c)(c_{s'} - c)\, e^{ikR_s},$$

where $\rho = R_s - R_{s'}$ is one of the lattice vectors ($V_{ss'}$ and $w_{ss'}$ evidently depend on the difference $R_s - R_{s'}$ alone) and in the summation for s, s' in the expression for $c_k(\rho)$ passes through the values identically related to s by the formula $R_s = R_s - \rho$.

As follows from (11), the Fourier transforms of atomic displacements, R_{kj}, are now linear functions not only of the Fourier transforms of concentration fluctuations, c_k, but also of the Fourier transforms of various p.c., $c_k(\rho)$. Here the p.c. between probabilities of substitution of sth and s'th lattice points by atoms A are found as average values $(c_s - c)(c_{s'} - c)$ (in [1] $\epsilon(\rho)$ designated the p.c. between the substitution of the pair of lattice points by atoms A and B and was equal to the value introduced here with the opposite sign). Obviously, $c_k(\rho)$ is the kth Fourier transform of the p.c., $\epsilon(\rho)$. The solution of equations (11) can evidently be represented in the following form:

$$R_{ki} = A_{ki}\, c_k + \sum_{\rho \neq 0} A_{ki}(\rho)\, c_k(\rho), \tag{13}$$

where A_{ki} and $A_{ki}(\rho)$ are the respective solutions of the systems of equations:

$$V_{kij} A_{kl} = w'_{ki};\quad V_{kij} A_{kl}(\rho) = w''_{ki}(\rho). \tag{11a}$$

On the other hand, by expressing $c_k(\rho)$ by means of formulae (12) and (2) in terms of combinations of c_k, we obtain:

$$R_{ki} = A_{ki}\, c_k + \sum_{k'}{}' \Big[c_{k'} (c_{k-k'} + c^*_{k'-k}) \sum_{\rho \neq 0} A_{ki}(\rho)\, e^{ik'\rho} +$$
$$+ c^*_{k'} (c_{k+k'} + c^*_{-k-k'}) \sum_{\rho \neq 0} A_{ki}(\rho)\, e^{-ik'\rho} \Big], \tag{14}$$

where, in the summation for k', the items to be considered are only those in which the indices in both factors $c_{k'}$ and $c_{k''}$ divided by 2π enter the chosen half of the reciprocal lattice cell. When written in this way, R_{ki} transforms appear to be expressed in the Fourier transforms of concentration fluctuations alone; in this case, however, R_{ki} is not a linear but a quadratic function of the fluctuations. Both forms of writting, (13) and (14), are evidently equivalent and may be conveniently used for different cases.

We shall now consider the first approximation in which $V'_{ss'ij}$ and $V''_{ss'ij}$ are different from zero but small. When determining R_{ki} by the method of consecutive approximations, $\delta R_{s'j}$, standing by V' and V'', may be substituted by the values of $\delta R^{(0)}_{sj}$, obtained by the zero approximation. According to (13) and (3) these values are equal to:

$$\delta R^{(0)}_{si} = \sum_{s'} A_{ss'i}(c_{s'} - c) + \sum_{\substack{s's'' \\ (s' \neq s'')}} A_{ss's''i}(c_{s'} - c)(c_{s''} - c), \tag{15}$$

where

$$A_{ss'i} = -\frac{2}{N} Im \sum_k{}' A_{ki} e^{ik,\, R_{s'} - R_s},$$

$$A_{ss's''i} = -\frac{1}{N} Im \sum_k{}' A_{ki} (R_{s'} - R_{s''}) (e^{ik\, R_{s'} - R_s} - e^{ik\, R_{s''} - R_s}). \tag{15a}$$

Substituting (15) in the terms of (10) containing V' and V'' we find that R_{kj}, as the first approximation of the perturbation theory, are determined by the following system of equations:

$$V_{kij} R_{kl} = W_{ki} c_k + \sum_{\rho \neq 0} W_{ki}(\rho)\, c_k(\rho) + \sum_{\rho_1 \neq \rho_2 \neq 0} W_{ki}(\rho_1\rho_2)\, c_k(\rho_1\rho_2) + \\ + \sum_{\rho_1 \neq \rho_2 \neq \rho_3 \neq 0} W_{ki}(\rho_1\rho_2\rho_3)\, c_k(\rho_1\rho_2\rho_3), \tag{16}$$

where

$$W_{ki} = -i \sum_s W'_{ss'i} e^{ik\, R_s - R_{s'}};$$

$$c_k(\rho_1\rho_2) = \frac{1}{N} \sum_s^{(\rho_1\rho_2)} (c_s - c)(c_{s'} - c)(c_{s''} - c)\, e^{ik\, R_s}, \tag{17}$$

$$c_k(\rho_1\rho_2\rho_3) = \frac{1}{N} \sum_s^{(\rho_1\rho_2\rho_3)} (c_s - c)(c_{s'} - c)(c_{s''} - c)(c_{s'''} - c)\, e^{ik\, R_s}.$$

VOL. 8 1959

In expressions for $c_k(\rho_1\rho_2)$ and $c_k(\rho_1\rho_2\rho_3)$, s', s'' and s''' in the summation for s are identically related to s by the formulae: $\rho_1 = R_s - R_{s'}$, $\rho_2 = R_s - R_{s''}$, $\rho_3 = R_s - R_{s'''}$. The differences $W'_{ss'i} - w'_{ss'i}$ and $W_{ki}(\rho) - w_{ki}(\rho)$, as well as the quantities $W_{ki}(\rho_1\rho_2)$ and $W_{ki}(\rho_1\rho_2\rho_3)$ are linear items in relation to V' and V''. Formulae which express these quantities in terms of V', V'' and A can easily be obtained from (10) and (15) but are omitted here for brevity. It can be seen from (16) that when various values of $V^{a\,a}_{ss'ij}$ are considered, R_{kj} in the first approximation are linear functions of the Fourier transforms of p.c. adequate not only to pairs but to three and four lattice points.

The same terms in R_k would appear if in the expression for F the items of the type

$$\sum_{ss's''} w'''_{ss's''l} (c_s - c)(c_{s'} - c)\, \delta R_{s''i}, \quad \sum_{ss's''s'''} w^{IV}_{ss's''s'''l} (c_s - c)(c_{s'} - c)(c_{s''} - c)\, \delta R_{s'''l}$$

were considered. These items may evidently be calculated from (16) by changing the physical meaning of coefficients W_{ki}. In the following discussions we shall regard that this change has been already made. In the subsequent approximations, as well as for calculating the items of the

$$\sum_{ss's''} V'''_{ss's''ij} (c_s - c)(c_{s'} - c)(c_{s''} - c)\, \delta R_{s'i}\, \delta R_{s''j}$$

type in the expression for F, terms will occur in the expression for R_k which are proportional to the Fourier transforms of p.c. between substitutions of a great number of lattice points. However, since no detailed evidence on the interatomic interactions are available, the calculation of these items (as well as the items proportional to $c_k(\rho_1\rho_2)$ and $c_k(\rho_1\rho_2\rho_3)$) is inexpedient because they evidently play an unimportant part and do not alter the qualitative aspect of the influence of the p.c. fluctuations upon the scattering; in the following discussions, therefore, they will be disregarded.

A certain relation can be established between the constants V and w on one side and on the other the elasticity moduli λ_{iljm} and the quantities which specify the size and form of the lattice cell as a function of composition and p.c. For this purpose we shall consider an ultimate case of long waves. It is easy to see that the expansion of V_{kij} by a k power series begins with quadratic terms, that of W_{ki} with terms of first power and the expansion of $W_{ki}(\rho)$, $W_{ki}(\rho_1\rho_2)$, $W_{ki}(\rho_1\rho_2\rho_3)$ with terms of zero power. Expanding by k and considering the relationship between $V_{ss'ij}$ and λ_{iljm} (compare the formula (27,12) in [3]), we shall find that in a range of long waves the equation (16)

acquires the following form:

$$\Delta\lambda_{ilmj}\, k_l k_m R_{kj} = \sum_s W'_{ss'i}(k,\ R_s - R_{s'j})\, c_k + \sum_{\rho\neq 0} W_{ki}(\rho)\, c_k(\rho) + \\ + \sum_{\rho_1\neq\rho_2\neq 0} W_{ki}(\rho_1\rho_2)\, c_k(\rho_1\rho_2) + \sum_{\rho_1\neq\rho_2\neq\rho_3\neq 0} W_{ki}(\rho_1\rho_2\rho_3)\, c_k(\rho_1\rho_2\rho_3). \tag{18}$$

In the ultimate case of long waves, macroscopic calculations of R_k may be conducted by considering the free energy as a function of components of the deformation tensor u_{mj} and continuous fluctuating variations of composition and p.c. Carrying out the same calculations as in deriving the formula (16) in [1], we obtain:

$$\lambda_{ilmj}\, k_l k_m R_{kj} = \lambda_{ilmj}\, k_l \left[\left(\frac{\partial u_{mj}}{\partial c}\right)_\varepsilon c_k + \sum_{(\rho_x>0)}^{\rho} \frac{\partial u_{mj}}{\partial \varepsilon(\rho)}\, c_k(\rho) + \right. \\ \left. + \sum_{(\rho_{1x}>0,\ \rho_{2x}>0)} \frac{\partial u_{mj}}{\partial \varepsilon(\rho_1\rho_2)}\, c_k(\rho_1\rho_2) + \sum_{\rho_1\rho_2\rho_3} \frac{\partial u_{mj}}{\partial \varepsilon(\rho_1\rho_2\rho_3)}\, c_k(\rho_1\rho_2\rho_3)\right], \tag{19}$$

$$(\rho_{1x}>0,\ \rho_{2x}>0,\ \rho_{3x}>0).$$

Here the following p.c. are introduced:

$$\varepsilon(\rho) = \overline{(c_s - c)(c_{s'} - c)};$$

$$\varepsilon(\rho_1\rho_2) = \overline{(c_s - c)(c_{s'} - c)(c_{s''} - c)};$$

$$\varepsilon(\rho_1\rho_2\rho_3) = \overline{(c_s - c)(c_{s'} - c)(c_{s''} - c)(c_{s'''} - c)},$$

where

$$\frac{\partial u_{mj}}{\partial \varepsilon}$$

is defined by the variation of u_{mj} with composition for p.c. constant. The formula (19) makes it possible to find A_{kj} and $A_{kj}(\rho)$ etc. from experimental data on the dependence of size and form of the lattice cell on the composition and the p.c. However, while

$$\left(\frac{\partial u_{mj}}{\partial c}\right)_\varepsilon$$

is easy to find experimentally, the experiments on the effect of annealing (which establishes the order) upon the lattice constant provide only the sum of quantities

$$\left(\frac{\partial u_{mj}}{\partial \varepsilon(\rho)}\right)_\varepsilon$$

over ρ and for obtaining these tensors for individual ρ, special complicated experiments are to be performed on the study of changes in the lattice constant with the order arrangement in the presence of elastic stresses or magnetic field (in a ferromagnetic substance).

By comparing coefficients to Fourier transforms of composition and p.c. in (18) and (19), we obtain the relations between $W'_{ss'i}$, $W''_{ss'i}$ and derivatives of u_{mj} with respect to c and $\epsilon(\rho)$:

VOL 8 195

$$\frac{1}{\Delta}\sum_{s} W'_{ss'i}(R_{sl}-R_{s'l}) = \lambda_{ilmj}\left(\frac{\partial u_{mj}}{\partial c}\right)_{\varepsilon};$$
$$\frac{1}{\Delta} W''_{ss'i}(R_{s'l}-R_{sl}) = \lambda_{ilmj}\frac{\partial u_{mj}}{\partial \varepsilon(\rho)}. \qquad (20)$$

In the case of cubic crystals, the formulae (20) establish one relation for $W'_{ss'i}$ and one for $W''_{ss'i}$, because, as already noted, only the sum of quantities

$$\frac{\partial u_{mj}}{\partial \varepsilon(\rho)},$$

can be found by usual experiments. When only one value of W' and one of W'' is different from zero in approximation to nearest neighbours, formulae (20) render it possible to determine these quantities from experiments. In a similar way, the relations between $V_{ss'ij}$ and λ_{ilmj} enable one to find from experiment three values of $V_{ss'ij}$ in the case of a cubic crystal.

3. DIFFUSE SCATTERING BY IDEAL SOLUTIONS

The simplest expressions for scattering intensities are obtained for ideal solutions in which the distribution of atoms amongst the lattice points is random and the mean of p.c. is zero (the fluctuation of the p.c. is of course different from zero). To simplify the problem, we confine ourselves to the case when in the expression for R_k only the items proportional to c_k and $c_k(\rho)$ can be calculated (i.e. the case of relatively small values of $W_{ki}(\rho_1\rho_2)$ and $W_{ki}(\rho_1\rho_2\rho_3)$ in (16), which usually occurs, when elastic moduli depend only slightly on concentration). The intensity of diffuse scattering I_ϕ is defined by the second item of formula (4). We substitute R_q in this formula by expression (13) (whereupon by A_{ki} and $A_{ki}(\rho)$ we shall subsequently understand the solutions of equations (11a) in which w_{ki} and $w_{ki}(\rho)$ are replaced by W_{ki} and $W_{ki}(\rho)$. By averaging the random distribution of atoms, we find:

$$I_\phi = I_\phi^{(1)} + I_\phi^{(2)} = Nc(1-c)|\bar{f}(q_1\vec{A}_q) - f_A + f_B|^2 + \\ + Nc^2(1-c)^2\sum_\rho |q_1\vec{A}_q(\rho)|^2(1-\cos q\rho), \qquad (21)$$

where the fact that $\vec{A}_q(\rho) = -\vec{A}_q(-\rho)$. is accounted for. The first item, $I_\phi^{(1)}$ in (21) determines the scattering associated with the concentration fluctuations while the second item, $I_\phi^{(2)}$ determines that associated with fluctuations of p.c.

Since, as already mentioned, for small $|k|$ $V_{ki'}$ is proportional to the second, W_{ki} to the first and $W_{ki}(\rho)$ to the zero power of $|k|$, A_q is proportional to $|q|^{-1}$, and $\vec{A}_q(\rho)$ proportional to $|q|^{-2}$ according to (11a). For this reason, as evident from (21), for $q \to 0$ near the reciprocal lattice points, the intensity of diffuse scattering from geometrical distortions of the lattice associated with both the fluctuations of composition and the fluctuations of p.c., tend to infinity proportionally to $|q|^{-2}$. However, the angular variations in the distribution of scattering intensities in the reciprocal lattice space are substantially different for these two items. While the isodiffusion curves of scattering proportional to $|q|^{-2}$, associated with composition fluctuations, have a lemniscate-like form as discussed in [1, 4] (in [1] the quantity $a_q\vec{q}'/|q|^2$), played part of $\vec{A}_q$), the isodoffusion curves of scattering associated with fluctuations of the p.c. are of more oval form, as will be shown. In order to investigate $I_\phi^{(2)}$ we consider crystals with body-centred and face-centred cubic lattices and use the approximation of nearest-neighbours i.e. we shall regard values of $W_{ss'i}$ as different from zero only for the nearest neighbouring atoms*. Then for small values of $|q|$, A_{qi} and $A_{qi}(\rho)$ are defined

* For every pair of lattice points in the face-centred cubic lattice, two components of $W_{ss'i}$ are different from

(continued to the next page)

by the following system of equations:

$$[c_{44} + (c_{11} - c_{44})\, n_x^2]\, A_{qx} + (c_{12} + c_{44})\, n_x\, (n_y\, A_{qy} + n_z\, A_{qz}) =$$
$$= \frac{1}{3\,|q|}\,(c_{11} + 2c_{12})\,\frac{1}{\Delta}\left(\frac{\partial \Delta}{\partial c}\right)_{\varepsilon} n_x \qquad (22)$$

. . . . . .

$$[c_{44} + (c_{11} - c_{44})\, n_x^2]\, A_{qx}(\rho) +$$
$$+ (c_{12} + c_{44})\, n_x\, [n_y\, A_{qy}(\rho) + n_z\, A_{qz}(\rho)] = -\frac{i}{q^2 \Delta}\, W''_{ss'x}, \qquad (23)$$

. . . . . .

where c_{ij} are the elastic moduli in Voigt's ($\vec{n} = q\ |g|$) and in every system of three equations, two can be obtained from the above written equations by cyclic change of x, y and z indices. The components $|W''_{ss'i}| = W$ different from zero for the structures discussed as follows from (20), are equal to

$$\frac{W a_0}{\Delta} = \frac{1}{6}\,(c_{11} + 2c_{12})\,\frac{1}{\Delta}\left|\frac{\partial \Delta}{\partial \varepsilon}\right|, \qquad (24)$$

where a_0 is in the length of the edge of cubic cell and $\partial\Delta/\partial\epsilon$ is determined by the variation of Δ with the change of p.c. for all the pairs of neighbouring atoms (and not for one pair as in the case of derivative

$$\frac{\partial \Delta}{\partial\, \varepsilon\,(\rho)}\Big).$$

Substituting the solutions of equations (22), (23) in (21) and considering (24), we find:

$$I_{\phi}^{(1)} = Nc\,(1-c)\left[\frac{\bar{f}}{|q|}\sum_{i=x,\,y,\,z} a_i(\vec{n})\, q_{1i} - f_A + f_B\right]^2, \qquad (25)$$

$$I_{\phi}^{(2)} = Nc^2\,(1-c)^2\,\frac{\bar{f}^2}{q^2}\left[\sum_{i=x,\,y,\,z} f_i(\vec{n})\, q_{1i}^2 + 2\sum_{\substack{i,\,j=x,\,y,\,z \\ (i<j)}} f_{ij}(\vec{n})\, q_{1i}\, q_{1j}\right]. \qquad (26)$$

Here

$$a_x(\vec{n}) = \frac{1}{3}\,\frac{c_{11} + 2c_{12}}{D}\,(1 + \xi n_y^2)\,(1 + \xi n_z^2)\,\frac{1}{\Delta}\left(\frac{\partial \Delta}{\partial c}\right)_{\varepsilon} n_x, \qquad (27)$$

(equation (27) continued on the next page)

(continued from previous page)
zero and of equal values. For example, for the lattice points (000) and (110), $W''_x = W''_y = W$, $W''_z = 0$; for the points (000) and (1-10), $W''_x = W''_y = W$, $W''_z = 0$. For the pair of lattice points in the body-centred cubic lattice these components take equal values

$$\pm W''_x = \pm W''_y = \pm W''_z = W,$$

where for each pair a corresponding sign + or − is assigned.

(equation (27) continued from previous page)

$$D = c_{11} + \xi (c_{11} + c_{12}) (n_x^2 n_y^2 + n_x^2 n_z^2 + n_y^2 n_z^2) + \\ + \xi^2 (c_{11} + 2c_{12} + c_{44}) n_x^2 n_y^2 n_z^2,$$

$$f_x(\vec{n}) = \frac{(c_{11} + 2c_{12})^2}{288 c_{44}^2 D^2} \left(\frac{1}{\Delta} \frac{\partial \Delta}{\partial \varepsilon}\right)^2 \sum_{b_1 b_2 b_3} \{b_1 [c_{44} + (c_{11} - c_{44}) (n_y^2 + n_z^2) + \\ + \xi (c_{11} + c_{12}) n_y^2 n_z^2] - b_2 (c_{12} + c_{44}) n_x n_y (1 + \xi n_z^2) - \\ - b_3 (c_{12} + c_{44}) n_x n_z (1 + \xi n_y^2)\}^2 (b_1 n_x + b_2 n_y + b_3 n_z)^2;$$

$$f_{xy}(\vec{n}) = \frac{(c_{11} + 2c_{12})}{288 c_{44}^2 D^2} \left(\frac{1}{\Delta} \frac{\partial \Delta}{\partial \varepsilon}\right)^2 \sum_{b_1 b_2 b_3} \{b_1 [c_{44} + (c_{11} - c_{44}) (n_y^2 + n_z^2) + \\ + \xi (c_{11} + c_{12}) n_y^2 n_z^2] - b_2 (c_{12} + c_{44}) n_x n_y (1 + \xi n_z^2) - \\ - b_3 (c_{12} + c_{44}) n_x n_z (1 + \xi n_y^2)\} \cdot \{- b_1 (c_{12} + c_{44}) n_x n_y (1 + \xi n_z^2) + \\ + b_2 [c_{44} + (c_{11} - c_{44}) (n_x^2 + n_z^2) + \xi (c_{11} + c_{12}) n_x^2 n_z^2] - \\ - b_3 (c_{12} + c_{44}) n_y n_z (1 + \xi n_x^2)\} (b_1 n_x + b_2 n_y + b_3 n_z)^2,$$

where $\xi = (c_{11} - c_{12} - 2c_{44}) c_{44}$ and variables b_1, b_2, b_3 take values of $+1$, and -1 in the case of crystals with body-centred cubic lattice, and values of $0, +1, -1$ (only one variable takes 0 in every item) in the case of the face-centred cubic lattice. The remaining functions $a_i(\vec{n})$, $f_i(\vec{n})$, $f_{ij}(\vec{n})$ are obtained from (26) by cyclic permutation of indices.

Expressions for

$$a_i(\vec{n}), \quad f_i(\vec{n}), \quad f_{ij}(\vec{n})$$

are simplified in the case of elastic-isotropic crystals, for which $\xi = 0$. In this case

$$a_i(\vec{n}) = a n_i = \frac{3p - 1}{3(1 + p)} \frac{1}{\Delta} \left(\frac{\partial \Delta}{\partial c}\right)_\xi n_i;$$
$$f(\vec{n}) = \frac{(3p - 1)^2}{72 (1 + p)^2} \left(\frac{1}{\Delta} \frac{\partial \Delta}{\partial \varepsilon}\right)^2 f'(\vec{n}), \tag{28}$$

where

$$p = \frac{c_{11} - c_{44}}{c_{44}} = \frac{c_{12} + c_{44}}{c_{44}} = \frac{1}{1 - 2\sigma} \quad (\sigma - \text{Poisson's ratio}),$$

$$f_x(\vec{n}) = 1 + n_x^2 + 2p (1 - n_x^2)^2 + p^2 [(1 - n_x^2)^3 + n_x^4 (1 - n_x^2) + 2 n_x^2 n_y^2 n_z^2] \\ f_{xy}(\vec{n}) = n_x n_y [2 - p (1 + n_z^2) - p^2 (1 - n_z^2 + 2n_z^4 - 2 n_x^2 n_y^2)] \tag{29}$$

for crystals with face-centred cubic lattice, and

$$f_x(\vec{n}) = 2 + 4p (1 - n_x^2) (1 - 2n_x^2) + 2p^2 [(1 - n_x^2) (1 - 2n_x^2) + 4 n_x^2 n_y^2 n_z^2] \\ f_{xy}(\vec{n}) = 2 n_x n_y [2 - 2p n_z^2 - p^2 (1 + 4n_z^2 - 4 n_x^2 n_y^2)] \tag{30}$$

VOL. 8 1959

for crystals with body-centred cubic lattice.

As can be seen from (25), (28), the coefficient to q^{-2} in $I_{\phi}^{(1)}$ is proportional to $(\vec{n}q_1)^2$ in the case of elastic isotropy and goes to zero for $\vec{n} \perp q_1$, in consequence, the isodiffusion curves corresponding to this item have the lemniscate-like forms. As follows from (26)-(30), the $I_{\phi}^{(2)}$ in this case does not go to zero and the isodiffusion curve for $I_{\phi}^{(2)}$ has an oval-like form. In the figure the isodiffusion curves are shown for illustration (in conventional units), $I_{\phi}^{(1)}$ (for $f_A = f_B$) and $I_{\phi}^{(2)}$ (the curves 1 and 2) in the plane (001) of the reciprocal lattice space near the point (h00), and also the isodiffusion curves of the function $I_{\phi} = I_{\phi}^{(1)} + I_{\phi}^{(2)}$ for

$$c(1-c)\left(\frac{\partial \Delta}{\partial \varepsilon}\right)^2 \Big/ \left(\frac{\partial \Delta}{\partial c}\right)^2 = 0.2$$

(curve 3) and for

$$c(1-c)\left(\frac{\partial \Delta}{\partial \varepsilon}\right)^2 \Big/ \left(\frac{\partial \Delta}{\partial c}\right)^2 = 0.08$$

(curve 4). The curves are constructed for the body-centred cubic lattice with $\xi = 0$, $p = 2.5$.

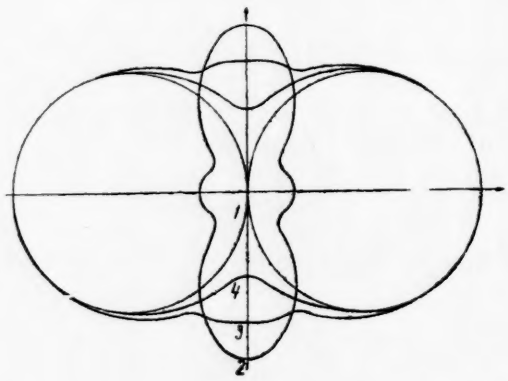

FIG. 1. Isodiffusion curves.

In order to make qualitative estimation of a relative part played by scattering from the fluctuations of the p.c. and the composition fluctuations, we compare for a given $|q|$ the maximum value of the item in $I_{\phi}^{(1)}$ proportional to q^{-2} and the maximum value of $I_{\phi}^{(2)}$ for the reflection of the (h00) type. According to (25)-(30) for the isotropic case, the second quantity is appreciably smaller than the first one, if

$$\left(\frac{\partial \Delta}{\partial c}\right)_{\varepsilon}^2 \gg \frac{1}{4} c(1-c)(1+p)^2 \left(\frac{\partial \Delta}{\partial \varepsilon}\right)^2. \tag{31}$$

For crystals with a face-centred lattice the right-hand side of the inequality is half of the left one. The derivative $\partial\Delta/\partial\epsilon$ can be found from the evidence concerning the change of crystal volume during annealing when the short-range order is established. Such data, however, are available only for a few solutions. For this reason, for evaluation of $\partial\Delta/\partial\epsilon$ it may be considered that, according to (20) and (9),

$$2\frac{\partial \Delta}{\partial \varepsilon} \sim \frac{\partial^2 \Delta}{\partial c^2} + \frac{2}{3\Delta}\left(\frac{\partial \Delta}{\partial c}\right)^2.$$

if the dependence of $W''_{ss'i}$ on composition is neglected. The other (evidently, more accurate) evaluation gives for $\partial\Delta/\partial\epsilon$ the values $\partial\Delta/\partial\epsilon \sim \delta\Delta/\delta\epsilon$, where $\delta\Delta$ is the change of the lattice cell volume in the transition from the fully-ordered to disordered alloy in which not only the long-range but also the short-range order does not exist, and $\delta\epsilon$ is equal to ¼ for alloys of the β-brass type, and 1/16 for alloys of the AuCu type. If these evaluations are accepted, the criterion (31) may be rewritten in the form:

$$\left(\frac{\partial\Delta}{\partial c}\right)^2 \gg c(1-c)\left(\frac{\partial^2\Delta}{\partial c^2}\right)^2 \quad \text{if} \quad \left(\frac{\partial\Delta}{\partial c}\right)^2 \gg 4c(1-c)\left(\frac{\delta\Delta}{\delta\varepsilon}\right)^2 \tag{32}$$

whereupon the fact that

$$\frac{(1+p)^2}{16} \sim 1.$$

is taken into consideration.

Thus, in accordance with the assumption made in [1], the scattering by fluctuations of p.c. may be neglected if the lattice constant only slightly depends on the p.c. or (less accurately) if the dependence of the lattice constant on concentration does not differ much from linear (deviations from the Vegard principle are small). In many cases inequalities (31) and (32) are satisfied with sufficient accuracy and in the expression for I_ϕ the item $I_\phi^{(1)}$ alone, discussed in detail in [1]*, may be considered. However, cases may occur when these inequalities are not satisfied and $I_\phi^{(1)}$, hence the character of angular distribution of scattering power in the reciprocal lattice space changes. It may be expected that $I_\phi^{(2)}$ plays an appreciable part in solutions with large deviations from Vegard's principle. In particular, at the points of maximum and minimum values of the concentration curve Δ, when $(\partial\Delta/\partial c)_\epsilon \approx 0$, the items in $I_\phi^{(1)}$ proportional to q^{-2} and $|q|^{-1}$ vanish (only the Laue background remains, having no relation to distortions) and $I_\phi^{(2)}$ plays a predominat part in the vicinity of the reciprocal lattice points†. The effects associated with fluctuations of the p.c. should evidently be appreciable for subtractional alloys (Gerzriken and Lesnik drew attention to the fact). As shown in [5], oval isodiffusion curves should also be found in the diffusion by vacancy pairs.

If V and W are known, formulae (21), (11a) and (17) evidently enable one to find the distribution of intensity I_ϕ not only in the vicinity of reciprocal lattice points but also for large $|q|$. In approximation to nearest neighbours for $V' = V'' = 0$, V and W may be expressed in terms of c_{ij} and derivatives

$$\left(\frac{\partial u_{mj}}{\partial c}\right)_\varepsilon \text{ and } \frac{\partial u_{mj}}{\partial \varepsilon},$$

which renders it possible to calculate $\vec{A}_k$ and $\vec{A}_k(\rho)$, hence also I_ϕ, for any k from independent experimental data. In particular, for crystals of face-centred lattices these quantities are determined by the equations:

---

* Calculation of the relation between the lattice constant and the p.c. for non-ideal solid solutions leads to substituting, in formulae for A_{qi}, the derivative $\partial u_{jm}/\partial c$ – in calculation of which the dependence of the p.c. on composition is accounted for – by the derivative $(\partial u_{jm}/\partial c)_\epsilon$. The latter is expressed in terms of $\partial u_{jm}/\partial c$ by means of the relation

$$\left(\frac{\partial u_{jm}}{\partial c}\right)_\varepsilon = \frac{\partial u_{jm}}{\partial c} - \frac{\partial u_{jm}}{\partial \epsilon}\frac{\partial \varepsilon}{\partial c},$$

whereas for the ideal solution both derivatives coincide. The difference between them is small when the lattice constant is only slightly dependent on the p.c.

† It is easy to prove that the pattern obtained for the distribution of scattering intensities and the estimation of orders of magnitude would not change if in calculatin I_ϕ the items in R_k proportional to $c_k(\rho_1\rho_2)$ and

(continued on the next page)

VOL. 8 1959

$$|k|\, Q_{ij} A_{kj} = \frac{1}{3} \frac{1}{\Delta} \left(\frac{\partial \Delta}{\partial c}\right)_{\varepsilon} P_i;$$
$$Q_{ij} A_{ki}(\rho) = -iN \frac{a_0^2}{24} (c_{11} + 2c_{12}) \frac{1}{\Delta} \frac{\partial \Delta}{\partial \varepsilon} b_i. \tag{33}$$

Here Q_{ij} and P_i are fractions of k and c_{ij} and are determined by the formulae (28) of paper [6], and b_i the components in expansion of ρ according to the crosscut d_i directed along cubic axes:

$$\rho = \frac{a_0}{2} \sum_{i=1}^{3} b_i \vec{d}_i.$$

The formulae (21) and (33) enable one to calculate $I_{\phi}^{(1)}$ and $I_{\phi}^{(2)}$ for any q.

It is also not difficult to obtain expressions for the scattering power of non-ideal solutions. In this case, however, the p.c. for three and four atom groups will also enter the formulae. Since these parameters are hitherto unknown, we shall not quote the quite cumbrous formulae obtained for this case. We shall only note that in individual cases the scattering from fluctuations of p.c. in non-ideal solutions may appreciably exceed that in ideal ones. If, e.g., admixed atoms in diluted solutions are located mainly in pairs (diatomic molecules) or groups containing several atoms, $I_{\phi}^{(2)}$ then is proportional to c and not to c^2 as in ideal solutions. The occurrence of oval isodiffuse scattering curves associated with fluctuations in the p.c. may be expected in the vicinity of some reciprocal lattice points close to a temperature of phase transition in crystals of the CuAu type and in other cases when regions with large values for parameters of short-range order are formed, corresponding to the laminated structure formation.

4. DIFFUSE SCATTERING FROM FLUCTUATIONS IN THE PARAMETERS OF CORRELATION IN VICINITY OF THE PHASE TRANSITION POINT OF THE SECOND ORDER

It is interest to investigate the scattering from fluctuations in the p.c. in the vicinity of the point of the phase transition of the second order. This effect was investigated in [7] for the case of dispersed light in which the influence of p.c. fluctuations was calculated by considering quadratic items in the expansion of dielectric constant by power series of fluctuations in the parameter of long-range order. We shall investigate X-ray scattering for the case of transition into ordered structure in which the structure cell contains one lattice point of the first and one of the second kind, while each is a centre of symmetry (e.g. crystals of the β-brass type). We shall analyse the scattering in the domain of structural reflections since, in the domain of superlattice reflections, distortions in these alloys have insignificant effect upon the scattering (see [1]) and abnormally large scattering takes place associated only with variety of atomic (see [8], [9]). For simplicity we confine to the case when $\vec{A}_k(\rho)$ corresponding to the nearest neighbours only are different from zero. As follows from (4) and (13) for finding I_{ϕ} it is necessary to calculate mean values of

$$\overline{|c_k|^2},\ \overline{c_k c_k^*(\rho)} \text{ and } \overline{c_k(\rho)\, c_k^*(\rho')}.$$

For small k, corresponding to the domain of structural reflections, these quantities may be expressed in terms of second derivatives of the thermodynamic potential per unit volume, ϕ, with respect to c and ϵ. In this case it should be considered that thermodynamically c and ϵ are not independent variables because, in general, $\partial^2\phi/\partial c\partial\epsilon$ is different from zero. However, $\partial^2\phi/\partial c\partial\epsilon = 0$ for the value of c for which $\partial\epsilon/\partial c = 0$. For simplicity we subsequently confine ourselves to the concentration for which c and ϵ are statistically independent. Such a concentration is usually close to that in which the phase transition temperature T_0 is maximum. In this case, the quantities $c_k\, c^*_k(\rho)$ proportional

---

(continued from previous page)
$c_k(\rho_1\rho_2\rho_3)$ are taken into consideration. The corrections obtained in the case of ideal solutions are proportional to $c^3(1-c)^3$ or $c^4(1-c)^4$ and are particularly small for small concentrations.

to $\partial^2\phi/\partial c\partial\epsilon$ turn to zero. $\overline{c_k(\rho)\,c_k^*(\rho')}$ could be expressed in term of $\partial^2\phi/\partial\epsilon^2$. Since, however, the behaviour of this function near T_0 is unknown, we shall represent $c_k(\rho)$ in the form of a quadratic function of c_k, i.e. we shall define R_{ki} by formula (14). Substituting (14) in (4) and considering that $\vec{A}_{ki}(\rho) = -\vec{A}_{kl}(-\rho)$, we then find that for small $|q|$

$$I_\phi = N^2\overline{|c_q|^2}\,|\overline{f}(q_1\bar{A}_q) - f_A + f_B|^2 +$$
$$+ N^2\overline{f}^2\sum_k{}'\,\overline{|c_{k+q/2}|^2}\,\overline{|c_{k-q/2}|^2}\,|\sum_\rho(q\rho)\,(q_1\vec{A}_q(\rho))e^{-ik\rho}|^2 +$$
$$+ \sum_{kk'}{}'\,c_{k+q/2}\,\dot{c}_{k-q/2}\,c_{k'+q/2}\,\dot{c}_{k'-q/2}\sum_\rho(q\rho)\,(q_1\vec{A}_q((\rho))\,e^{-ik\rho}\times \tag{34}$$
$$\times\sum_\rho(q\rho)\,(q_1\vec{A}_q(\rho))\,e^{ik'\rho}.$$

For small $|q|$,

$$\overline{|c_q|^2} = \frac{\varkappa T}{N\Delta}\,(\varphi_{cc} + \beta q^2)^{-1},$$

where $\varkappa$ is the Boltzmann constant and

$$\varphi_{cc} = \frac{\partial^2\varphi}{\partial c^2}.$$

For values of k near to $2\pi K_1$, where K_1 is the vector of reciprocal lattice corresponding to superlattice reflection, $|c_k|^2$ is equal to (compare with [1]):

$$\overline{|c_k|^2} = \frac{\varkappa T}{4N\Delta}\,\frac{1}{\varphi_{\eta\eta} + \alpha k'^2}, \tag{35}$$

where $k' = k - 2\pi K_1$ is a small vector; $\varphi_{\eta\eta} = \frac{\partial^2\varphi}{\partial\eta^2}$; η is the degree of long range order*. Since $\phi_{\eta\eta} = 0$ at the point of phase transition of the second order, the summed up expression in the last but one summation of formula (34) and the sum itself sharply increase near this point. The last summation of (34) is, in general, of the same order as the last but one. However as in [7], we shall not discuss the scattering associated with the last item of (34) in our investigation of characteristics of the transition point. A reason for either neglect or calculation of this item could only be provided if accurate characteristics of thermodynamic quantities at the transition point were known. As noted in [11] the neglect of the above item may result in appreciable error in the close vicinity of the transition point. From (35), considering only the main part of summation tending to infinity at the transition point, we find that

$$\sum_{\vec{k}}{}'\,\overline{|c_{\vec{k}+\vec{q}/2}|^2}\,\overline{|c_{\vec{k}-\vec{q}/2}|^2} = \frac{N\Delta}{16\pi^3}\int d\vec{k}\,\overline{|c_{k+q/2}|^2}\;\;\overline{|c_{\vec{k}-\vec{q}/2}|^2} =$$
$$= \frac{(\varkappa T)^2}{128\pi N\Delta\alpha^2 q}\,\tan^{-1}\sqrt{\frac{\alpha q^2}{4\varphi_{\eta\eta}}}. \tag{36}$$

---

* This formula is true only for disordered alloys at temperatures above the transition temperature T_0 and also for the composition for which T_0 has a maximum. For ordered alloys of other compositions, according to [9], $\partial^2\phi/\partial\eta^2$ must be substituted by the quantity

$$\frac{\partial^2\varphi}{\partial\eta^2} - \left(\frac{\partial^2\varphi}{\partial c\partial\eta}\right)^2\Big/\frac{\partial^2\varphi}{\partial c^2},$$

which usually is of the same order of magnitude. Below in the text $\phi_{\eta\eta}$ may mean this quantity.

VOL. 8 1959

Considering further that for $k \approx 2\pi K_1$ which mainly contribute in integral (36), $e^{ikp} - 1$, we find from (34), (36) and (22) that for crystals of the β-brass type, near temperature T_0:

$$I_\phi = \frac{N\varkappa T}{\Delta(\varphi_{cc} + \beta q^2)}\left(\frac{\overline{f}}{|q|}(q_1\vec{A}_q) - f_A + f_B\right)^2 + \\ + \frac{N\overline{f}^2(\varkappa T)^2}{128\pi\Delta\varkappa^2|q|^3}\tan^{-1}\sqrt{\frac{\alpha q^2}{4\varphi_{\eta\eta}}}(q_1\vec{B}_q)^2, \tag{37}$$

where

$$B_{qx} = \frac{2}{3}\frac{c_{11}+2c_{12}}{c_{44}D}\left[c_{44} + (c_{11}-c_{44})(n_y^2+n_z^2) + \xi(c_{11}+c_{12})n_y^2n_z^2\right]\frac{1}{\Delta}\frac{\partial\Delta}{\partial\varepsilon}n_x. \tag{38}$$

The second item $I_\phi^{(2)}$ in formula (37) describing diffuse scattering associated with fluctuations of p.c. is simplified if $\alpha q^2 \ll 4\phi_{\eta\eta}$

$$I_\phi^{(2)} = \frac{N\overline{f}^2(\varkappa T)^2(q_1\vec{B}_q)^2}{256\pi\Delta\varkappa^{3/2}\sqrt{\varphi_{\eta\eta}}\,q^2}. \tag{39}$$

For small $|q|$, $I_\phi^{(2)}$ as well as $I_\phi^{(1)}$ are proportional to q^{-2}. Since at the transition point $\phi_{\eta\eta} = 0$, the coefficient of proportionality to q^{-2} greatly increases with the approach to temperature T_0. In this case $\phi_{\eta\eta}$ tends to zero at a different rate above and below T_0 and $I_\phi^{(2)}$ increases more sharply below the transition point. Since no accurate characteristics of $\phi_{\eta\eta}$ and values of α at the transitions point are hitherto available, the principle of change of

$$\alpha^{3/2}\sqrt{\varphi_{\eta\eta}} \text{ and } I_\phi^{(2)}$$

in the vicinity of this point cannot be strictly determined. However, an order of magnitude of $I_\phi^{(2)}$ can be estimated by using the thermodynamic theory of phase transitions or statistical theory of solution ordering which qualitatively give the same results. The estimation by this theory [9] leads to

$$\varphi_{\eta\eta} \sim \frac{\varkappa T_0}{\Delta}\frac{|T-T_0|}{T_0}, \quad \alpha \sim \frac{1}{10}\frac{\varkappa T_0}{\Delta^{1/3}}.$$

In this case

$$I_\phi^{(2)} \sim 0{,}04N\overline{f}^2(q_1\vec{B}_q)^2\left(\frac{|T-T_0|}{T_0}\right)^{-\frac{1}{2}}.$$

According to this estimation, for $T \to T_0$, $I_\phi^{(2)}$ tends to zero as $|T - T_0|^{-1/2}$. By comparing the expression for $I_\phi^{(2)}$ obtained with formula (25) for ideal solutions (for $c = 1/2$), we find that near the transition point the peak value of $I_\phi^{(2)}$ for a given $|q|$ is about

$$\sqrt{\frac{T_0}{|T-T_0|}}$$

times greater than that for ideal solutions. Since $I_\phi^{(1)}$ near the transition point is of the same order as that for ideal solutions, i.e.

$$\frac{\varkappa T}{\Delta\varphi_{cc}} \gtrsim c(1-c) \sim \frac{1}{4},$$

for small $|q|$, $I_{\phi}^{(2)}$ becomes equal in order of magnitude to $I_{\phi}^{(1)}$ at the temperature T for which the condition

$$\left(\frac{\partial \Delta}{\partial c}\right)^2 \sim \left(\frac{\partial \Delta}{\partial \varepsilon}\right)^2 \sqrt{\frac{T_0}{|T-T_0|}}.$$

holds. Since B_{qi}, according to (38), contains factors n_i, it is easy to see that for any q_1 such a value of q can be found that the corresponding vector $\vec{B}_q$ is perpendicular to q_1 i.e. $I_{\phi}^{(2)} = 0$. For this reason the isodiffusion curves of $I_{\phi}^{(2)}$ and those of $I_{\phi}^{(1)}$ should have a lemniscate-like shape. Since $\vec{A}_q$ and $\vec{B}_q$ become perpendicular, generally speaking, for different q, the distribution of total intensity $I_{\phi}^{(1)} + I_{\phi}^{(2)}$ in the vicinity of reciprocal lattice points not lying on high-symmetry planes and which also pass through the (000) point of intersection, may not turn to zero for any q.

It should be noted that the calculation of the last item of (34) and accurate calculation of the last but one would provide the expression for $I_{\phi}^{(2)}$ with a term describable by isodiffusive curves of oval shape.

The expression for $I_{\phi}^{(2)}$ is also simplified if

$$\alpha q^2 \gg 4\varphi_{\eta\eta} \quad \text{or} \quad q \gg 3\Delta^{1/3}\left(\frac{|T-T_0|}{T_0}\right)^{1/2},$$

but $|q|$ being still sufficiently small ($|q| \ll \Delta^{1/3}$) for the use of macroscopic approximation to be allowed. In this case

$$I_{\phi}^{(2)} = \frac{N\overline{f^2}(\varkappa T)^2 (q_1 \vec{B}_q)^2}{256\Delta\alpha^2 |q|^3}. \tag{40}$$

In this case $I_{\phi}^{(2)}$ is inversely proportional to $|q|^3$ and not to q^2 as it is far away from the transition point. The quantity $|q|$ which separates the applicability regions of formulae (39) and (40) is proportional to

$$\sqrt{\varphi_{\eta\eta}/\alpha}$$

and tends to zero with approach to the transition point.

In a similar way the expression for $I_{\phi}^{(2)}$ can be obtained in the vicinity of the critical point on the decomposition curve in approach to which $\phi_{ce} \to 0$. Since for small $|q|$ in this case

$$I_{\phi}^{(1)} \sim \frac{1}{\varphi_{cc}}, \text{ and } I_{\phi}^{(2)} \sim \frac{1}{\sqrt{\varphi_{cc}}},$$

the latter scattering may usually be neglected. Scattering from fluctuations in the p.c. plays a relatively small part near the points of phase transition also in the cases when a geometric distortion near the transition becomes anomalously large (Seignette's salt, in which the piezoelectric effect is observed on both sides of the transition point, or crystals at a state near the critical point on the curves of the phase transition of the second order) [10, 9], because in these cases the principal part is played by the scattering associated with fluctuations in the parameters of long-range order.

5. DETERMINATION OF THE WEAKENING IN INTENSITY OF NORMAL REFLECTIONS

Quantities L_A and L_B which define the weakening of regular reflections can be expressed, according to (6), in terms of mean square values of displacements of atoms A and B. These quantities may also be written in the form:

$$L_A = \frac{1}{c}\overline{c_s (q_1 \delta R_s)^2}; \quad L_B = \frac{1}{1-c}\overline{(1-c_s)(q_1 \delta R_s)^2}; \tag{41}$$

VOL. 8 1959

where the averaging is now carried out over all the lattice points and not only over the atoms A and B as in (6). We shall initially assume that the lattice constant is independent of p.c. so that in determining the atom displacements only the first items in (15) and (13) may be used and that

$$\delta R_s = \sum_{s'} \vec{A}_{ss'} (c_{s'} - c).$$

Substituting this expression in (41) and considering (3), we obtain

$$L_A = L + \frac{1}{c} L'; \; L_B = L - \frac{1}{1-c} L', \tag{42}$$

where

$$\begin{aligned} L &= \overline{(q_1 \delta R_s)^2} = \sum_{s's''} (q_1 \vec{A}_{ss'}) (q_1 \vec{A}_{ss''}) \overline{(c_{s'} - c)(c_{s''} - c)} = \sum_k (q_1 \vec{A}_k)^2 |\overline{c_k}|^2, \\ L' &= \overline{(c_s - c)(q_1 \delta R_s)^2} = \frac{1}{N} \sum_{ss's''} (q_1 \vec{A}_{ss'}) (q_1 \vec{A}_{ss''}) \overline{(c_s - c)(c_{s'} - c)(c_{s''} - c)}, \end{aligned} \tag{43}$$

whereupon $\vec{A}_{s\,s''} = 0$. (In paper [1], where in principle the diffusive scattering was investigated and not the weakening of lines, no distinction was made between the mean square values of displacements of atoms A and B, i.e. the items in L_A and L_B containing L' were diseregarded and $L_A = L_B = L$ assumed). It can be seen from (43) that in the case of ideal solutions – when $\overline{(c_{s'} - c)(c_{s''} - c)} = 0$ for $s' \neq s''$ and $\overline{(c_{s'} - c)^2} = c(1-c)$, L' is zero and

$$L_A = L_B = L = c(1-c) \sum_{s'} (q_1 \vec{A}_{ss'})^2 = \frac{1}{N} c(1-c) \sum_k (q_1 \vec{A}_k)^2. \tag{44}$$

The value of L' is also small when $c \approx \frac{1}{2}$. Indeed, it is easy to see that for $c = \frac{1}{2}$ in a model of pair interaction the probability of substitution of any three lattice points by A atoms is equal to the probability of substitution by B atoms, i.e. $\overline{c_s c_{s'} c_{s''}} = \overline{(1-c_s)(1-c_{s'})(1-c_{s''})}$. Whence it follows that $(c_s - \frac{1}{2})(c_{s'} - \frac{1}{2})(c_{s''} - \frac{1}{2}) = 0$ and $L' = 0$ for $c = \frac{1}{2}$. L' is also small in the case of sufficiently small concentration of one of the components because in this case the p.c. are small.

For evaluating L' we shall consider slightly less than ideal solutions in which one may consider the correlation only between the nearest atoms only so that quadratic terms of ϵ may be neglected. In the sum (43) then the terms for L' with $s' = s''$ alone remain. In this case

$$L' = (1-2c)\, \varepsilon \sum_{s'}{}' (q_1 \vec{A}_{ss'})^2,$$

where the summation with respect to s' is performed over the atoms of the first co-ordinated domain. For the evaluation of ϵ, the formula can be used as obtained in the approximation of Kirkwood theory of ordering:

$$\varepsilon = -c^2 (1-c)^2 \frac{w}{\varkappa T},$$

where w is the energy of ordering. From this evaluation and from formulae for L and L' it follows that $|L'| \ll L$, if

$$c(1-c)\,|1-2c|\, \frac{|w|}{\varkappa T} \ll 1,$$

i.e. in the case of solutions of small concentration of close to $c = \frac{1}{2}$ also in the case of high temperatures. In general case of non-ideal solutions, L' may, however, be appreciable.

Even in the case of ideal solutions, L_A and L_B may differ if the lattice constant depends on the p.c. In order to determine R_s in this case it is necessary to calculate not only the first but also the second item in (15). Substituting (15) in (16) and performing the averaging we find that L_A and L_B may be represented in the form of (42), but now L_A and L' are defined by the formulae:

$$L = c(1-c)\sum_{s'}(q_1\vec{A}_{ss'})^2 + 2c^2(1-c)^2\sum_{s's''}(q_1\vec{A}_{ss's''})^2,$$
$$L' = 4c^2(1-c)^2\sum_{s'}(q_1\vec{A}_{ss'})(q_1\vec{A}_{sss'}) + 4c^2(1-c)^2(1-2c)\sum_{s'}(q_1\vec{A}_{sss'})^2. \tag{45}$$

If $\vec{A}_{sss'} = 0$, i.e. the displacement of a given atom is independent of the kind of the atom and the lattice constant independent of ϵ, then $L' = 0$, and the formula (45) for L turns to formula (44). One may think that the difference between L_A and L_B becomes relatively larger (as compared with L) in the region of concentrations lying near the extreme points on the concentration curve of the lattice constant (if these extreme points do not lie at $c \approx \frac{1}{2}$).

If L_A and L_B is appreciably less then one, then the quantity $\bar{f}$, which defines the intensity of regular reflections, is equal, by (5) and (41), to

$$\bar{f} \cong c_A f_A + c_B f_B - \frac{1}{2}(c_A f_A L_A + c_B f_B L_B) =$$
$$= (c_A f_A + c_B f_B)\left(1 - \frac{L}{2}\right) - \frac{1}{2}L'(f_A - f_B). \tag{46}$$

As was already noted [2], since $c_A f_A + c_B f_B$ and $f_A - f_B$ are dependent on $|q_1|$ in different ways the presence of the item containing L' in (46) may result in the variation of the logarithm of the ratio $\bar{f}/(c_A f_A + c_B f_B)$ (or the ratio of intensity of regular reflections to $(c_A f_A + c_B f_B)^2$) with q_1^2 not being linear but of a more complex form. Deviations from the linear variation is evidently small for small concentrations, the concentrations close to $c = \frac{1}{2}$, in case of nearly ideal solutions in which the lattice constant only slightly depends on the p.c. and also in the case of atomic scattering factors, f_A and f_B being close to one another. The greatest deviations from the linear functions may be expected for the scattering by solutions with very different atomic scattering factors in which values of the p.c. are great (or there are large deviations from Vegard's principle) and concentrations appreciably differ from $c = 0$, $c = 1$, $c = \frac{1}{2}$. One may suppose that also in these cases deviations from the above mentioned linear dependence, associated with the difference between L_A and L_B, will be smaller than the deviations associated with the difference between the distribution of probabilities of atom displacements and a Gaussian distribution, which were discussed in [2].

CONCLUSIONS

Simultaneous calculations of scattering from fluctuations in the composition and in the p.c. lead, firstly, to a certain change of the coefficient correlating the lattice distortions with the fluctuations in the composition and, secondly, to the occurrence of an additional scattering. Isodiffusive curves of scattering from fluctuations in the p.c. are not of a leminiscate but close to oval shape. The effects associated with fluctuations in the p.c. play a relatively important part when the lattice spacing greatly varies with the p.c. and deviations from Vegard's principle are large. In ideal solutions the scattering power of fluctuations in the p.c. is proportional to $c^2(1-c)^2$ and becomes insignificant for small concentrations. In non-ideal solutions the part played by these fluctuations may strengthen. Near the phase transition point, in particular, they may lead to the occurrence of strong diffusive scattering in the vicinity of structural reflections (in addition to the usual scattering in the vicinity of superlattice reflections) the intensity of which tends to infinity with $T \to T_0$.

Translated by B. Cynk

VOL. 8 1959

REFERENCES

1. M.A. Krivoglaz, *Zh. eksp. teor. fiz.*, 34, 204 (1958).
2. M.A. Krivoglaz, *Fiz. metal. metalloved.*, 7, 650 (1959).
3. M. Born and K. Huang, *Dinamicheskaya teoriya kristallicheskikh reshetok (Dynamic theory of crystal lattices)*, Foreign Literature Publishing House (1958).
4. K. Huang, *Proc. Roy. Soc.*, 190, 102 (1947).
5. H.J. Kanzaki, *Phys. Chem. Solids*, 2, 107 (1957).
6. M.A. Krivoglaz and Ye.A. Tikhonova, *Ukr. fiz. zh.*, 3, 297 (1958).
7. V.L. Ginsburg and A.P. Levanyuk, Sb. posvyashchennyi pamyati G.S. Landsberg (Collection devoted to the memory of G.S. Landsberg) (in print).
8. L.D. Landau, *Zh. eksp. teor. fiz.*, 7, 1234 (1937).
9. M.A. Krivoglaz, *Zh. eksp. teor. fiz.*, 31, 625 (1956); 32, 1368 (1957).
10. M.A. Krivoglaz, *Zh. eksp. teor. fiz.*, 34, 405 (1958).
11. A.P. Levanyuk, *Zh. eksp. teor. fiz.*, 36, 810 (1959).

VOL
8
195

RELAXATION ABSORPTION OF ULTRASOUND IN FERROMAGNETICS*

V.T. SHMATOV

Institute of Metal Physics U.S.S.R. Academy of Sciences

(Received 19 January 1959)

On the basis of the thermodynamic theory of relaxation phenomena [1, 2] equations have been obtained for the coefficient of absorption and dispersion of ultrasound in ferromagnetics.

VOL. 8 1959

When a sound wave is propagated in a ferromagnetic, the degree of the ferromagnetic order does not, generally speaking, coincide at every moment with the equilibrium magnetization, since the relaxation time of the degree of the ferromagnetic order is finite. Only at sonic frequencies which are much lower and much higher than the inverse magnitude of the relaxation time can the process of sound propagation in ferromagnetics be regarded as being in equilibrium. In the first case the degree of the ferromagnetic order permits one to follow the change of state of the ferromagnetic, and the velocity of the sound is determined by the full value of the modulus of elasticity. In the second case there is no variation whatever in the degree of the ferromagnetic order, and the velocity of the sound is determined by the value of the modulus of elasticity after subtracting the portion arising through the existence of the ferromagnetic order. In the intermediate frequency range there will be a phase lag between the variation in the degree of the ferromagnetic order and the variation in the elastic state of the ferromagnetic; this will bring about the dissipation of sonic energy. In order to calculate the coefficient of absorption and dispersion of ultrasound in ferromagnetics, we will employ the general thermodynamic concepts adduced in references [1, 2].

For linear vibrations, the square of the complex velocity of sound of frequency ω can be obtained by substituting in the well-known equation for the velocity of sound, instead of Young's static modulus, its dynamic value [2, 8].

$$C_\omega^2 = C_0^2 \frac{1 + i\omega\tau^{\sigma S}}{1 + i\omega\tau^{\varepsilon S}}, \tag{1}$$

where C_0 is the normal Laplace velocity of sound; $\tau^{\sigma S}$ and $\tau^{\epsilon S}$ are the relaxation times of the degree of the ferromagnetics order γ for constant values of the parameters represented by the upper indices (σ = stress, ϵ = deformation, S = entropy). From this we obtain by the usual method [1, 3] the expression for the velocity of the sound and the coefficient of absorption over the length of the wave:

$$C_\omega = C_0 \left[1 + \frac{(\omega\tau^{\varepsilon S})^2}{1 + (\omega\tau^{\varepsilon S})^2} \cdot \frac{\Delta}{2}\right], \tag{2}$$

$$\mu = \pi \frac{\omega\tau^{\varepsilon S}}{1 + (\omega\tau^{\varepsilon S})^2} \Delta. \tag{3}$$

The degree of relaxation of Young's adiabatic modulus may be represented as follows:

$$\Delta = \frac{E_T'}{E_T} \cdot \frac{c_\sigma' c_\varepsilon}{c_\varepsilon' c_\sigma} - 1, \tag{4}$$

---

* *Fiz. metal. metalloved.*, 8, No. 5, 667-670, 1959.

where E_T is Young's isothermal modulus; E'_T is the non-relaxing part of Young's modulus, i.e. that part of the modulus minus the portion arising through the ferromagnetic order; c_σ and c_ϵ are specific heats; c'_σ and c'_ϵ are specific heats with no account taken of the ferromagnetic order. Since the modulus and specific heat ratios are close to unity, we can write with a fair degree of accuracy

$$\Delta = E'_T\left(\frac{1}{E_T}\right)'' + \left(\frac{c'_\sigma c_\epsilon}{c'_\epsilon c_\sigma} - 1\right), \tag{5}$$

where $(1/E_T)''$ is the contribution of the ferromagnetic order to that value which is reciprocal to the isothermal modulus. The second component in equation (5) is equal to 10^{-4}, since the specific heat ratios deviate from unity in the second decimal place. The degree of relaxation will therefore be determined by the first component, which is the degree of relaxation of Young's isothermal modulus.

As will be seen from equation (3), sound absorption attains its maximum value at $\omega\tau^{\epsilon s} = 1$, and thus possesses a resonance character. The value of the degree of relaxation of Young's isothermal modulus can be expressed by the degree of the ferromagnetic order, employing the thermodynamic equation obtained in reference [10],

$$\Delta_T = E'_T \frac{\left(\frac{\partial y}{\partial \sigma}\right)^2_T}{T\left(\frac{\partial v}{\partial T}\right)^2_\sigma} c''_\sigma, \tag{6}$$

where c''_σ is the additional specific heat due to the existence of the ferromagnetic order.

Employing the results of Weiss's phenomenological theory of ferromagnetism [3], according to which

$$\ln\frac{1+y}{1-y} = \frac{2\Theta}{T}y;\quad c''_\sigma = -Nk\Theta y\left(\frac{\partial y}{\partial T}\right)_\sigma, \tag{7}$$

we obtain

$$\Delta_T = E'_T Nk\left(\frac{\partial\Theta}{\partial\sigma}\right)^2 \frac{y^2(1-y^2)}{T-\Theta(1-y^2)}, \tag{8}$$

where Θ is Curie temperature; k is Boltzmann's constant; and N is the number of non-compensated spin moments per unit volume. As equation (8) shows, the degree of relaxation, and hence also the absorption of sound at frequencies $\omega\tau^{\epsilon s} \simeq 1$, increase with rising temperature and attain a maximum at Curie point, where

$$\Delta_T = E'_T\frac{Nk}{\Theta}\left(\frac{\partial\Theta}{\partial\sigma}\right)^2. \tag{9}$$

If the ferromagnetic is located in an external magnetic field of intensity H, instead of equation (7) we will have [3]

$$\ln\frac{1+y}{1-y} = \frac{2\Theta}{T}y + \frac{2\mu_0}{kT}H;\quad C''_\sigma = -(Nk\Theta y + N\mu_0 H)\left(\frac{\partial y}{\partial T}\right)_\sigma, \tag{10}$$

where μ_0 is Bohr's magneton. On the basis of equation (6), we find from this that the degree of relaxation is here again determined as in equation (8), but in this case the degree of the ferromagnetic order is a function of the external field and thus the degree of relaxation is determined not by spontaneous,

but by true, magnetization. The increase in magnetization caused by the field is, however, so slight that it is of no practical significance for a wide range of field and temperature values. Only when the Curie temperature is approached does the influence of the external field increase and must for this reason be taken into account.

A disadvantage of Weiss's theory of ferromagnetism is the fact that it ignores ferromagnetic order at short range; it is essential that this factor be taken into account, since the exchange forces which determine ferromagnetism operate at short range. Taking account of short-range ferromagnetic order, we have [3, 4] instead of the first equation in (7)

$$\ln \frac{1+y}{1-y} = \frac{z}{z-2} \ln \frac{\alpha+y}{\alpha-y}; \quad \alpha^2 = 1 + (1-y^2)\left(e^{\frac{4A}{kT}} - 1\right) \tag{11}$$

and, according to equation (6), we obtain

$$\Delta_T = E'_T \frac{T}{\Theta^2} \left(\frac{\partial \Theta}{\partial \sigma}\right)^2 \cdot c''_\sigma, \tag{12}$$

where z is the co-ordination value and the exchange integral $A \sim k\ \Theta$.

Direct measurement of the displacement of Curie point in ferromagnetics under the influence of elastic stresses is difficult to achieve; only approximate evaluations of this displacement are known in a number of ferromagnetic materials [7], and these can at best be used only for determining the ferromagnetic order (12). In the case of nickel

$$\frac{\partial \Theta}{\partial \sigma} = 1{,}47 \times 10^{-4} \frac{\text{deg.cm}^2}{\text{kg}} \text{ [7]}; \quad E'_T = 2 \times 10^6 \frac{\text{kG}}{\text{cm}^2}; \quad \Theta = 631^\circ\text{K};$$

$$c''_\sigma = 0{,}037 \frac{\text{cal}}{\text{g.deg.}} \text{ [6]}$$

and in the region of Curie point we obtain $\Delta_T = 0.001$. In Invar steels the displacement of the Curie point is of the order of 10^{-3} and for this reason the degree of ultrasound absorption to be expected in these steels is presumably 100 times greater.

It follows from these examples that in ferromagnets near the Curie points at frequencies of $\omega\, \tau^{es} \simeq 1$ there should be observed an anomalously large absorbtion of ultrasound.

The derivative $\partial\Theta/\partial\sigma$, which enters into the equation for the degree of relaxation of Young's isothermal modulus (12), as does also E'_T, is an anisotropic value in ferromagnetic monocrystals*. Therefore the relaxation absorption of ultrasound in a ferromagnetic monocrystal has different values for the different directions in which the sound is propagated. In polycrystalline specimens the derivative $\partial\Theta/\partial\sigma$ represents a value, averaged in all directions, for the displacement of Curie point under the influence of elastic stresses (the same is true for E'_T) and, consequently, relaxation absorption of ultrasound in these specimens is not dependent on the direction of propagation.

The relaxation time of the degree of the ferromagnetic order τ^{es}, which enters into the equations derived here, is simultaneously the spin-lattice relaxation time, since it characterizes the establishment of equilibrium between the spins and the lattice. It follows from thermodynamic considerations that

---

* In Artmann's experiments [9] it was found that in β-brass $(1/E_T)''$ (part of the reciprocal value of Young's modulus, arising from long-range order) is different for the different crystallographic directions. Employing equation (6), it can be shown that in β-brass, as in ferromagnetics,

$$(1E_T)'' \sim (\partial\Theta/\partial\sigma)^2$$

Consequently, in alloys which are well ordered, the displacement of Curie point is an anisotropic value. Since ferromagnetics present an analogous case, this circumstance applies also to them.

VOL. 8 1959

$$\tau^{sS} = LF_{yy}^{-1}\left(1 - \frac{c_\sigma''}{c_\sigma}\right), \tag{13}$$

where L is the knimetic coefficient, which is a function of temperature and magnetization; F_{yy} is the seond derivative of the free energy of the ferromagnetic order, taken as being in a state of equilibrium. If Weiss's theory of ferromagnetism [3] is employed, we obtain

$$\tau^{sS} = \frac{L(1-y^2)}{NkT\left[1 - \frac{\theta}{T}(1-y^2)\right]}\left(1 - \frac{c_\sigma''}{c_\sigma}\right). \tag{14}$$

If L does not possess a characteristic property at Curie point, the relaxation time must increase strongly as Curie temperature is approached. An experimental evaluation of the spin-lattice relaxation time has been made in a paper by Bloembergen and Wang [5], who found, in the case of nickel at room temperature, that $\tau^{sS} \simeq 10^{-10}$ sec.

My thanks are due to S.V. Vonovskii for his help in this work.

Translated by C.M. Burnell

REFERENCES

1. L.M. Mandel'shtam and M.A. Leontovich, *Zh. eksp. teor. fiz.*, 7, 432 (1937).
2. V.T. Shmatov, *Zh. eksp. teor. fiz.*, 33, 1359 (1957).
3. S.V. Vonsovskii and Ia. S. Shur, *Ferromagnetism*, Gostekhteoretizdat (1958).
4. L.S. Stil'bans, *Zh. eksp. teor. fiz.*, 9, 432 (1937).
5. N. Bloembergen and S.Wang, *Phys. Rev.*, 93, 72 (1954).
6. G.I. Dorfman and P.I. Janus, Zeitschr. für Phys., 54, 277 (1929).
7. K.P. Belov, *Elastic and Other Phenomena in Ferromagnetic Materials*, Gostekhteoretizdat, (1951).
8. V.T. Shmatov, *Fiz. metal. metalloved.*, 6, No. 6 (1958).
9. R.Artman, *J. Appl. Phys.*, 23, 475 (1952).
10. V.T. Shmatov, *Fiz. metal. metalloved.*, 7, No. 3 (1959).

ADIABATIC GALVANOMAGNETIC AND THERMOMAGNETIC PHENOMENA IN SEMICONDUCTORS. II. MIXED CONDUCTIVITY*

V. Ye. VZDORNOV and I.M. TSIDIL'KOVSKII

Institute of Metal Physics, U.S.S.R. Academy of Sciences

(Received 21 July 1959)

A theoretical examination is made of adiabatic galvanomagnetic and thermomagnetic phenomena in semiconductors with mixed conductivity, based on the hypothesis of the isotropy of effective masses and the relaxation times of conductors.

VOL. 8 1959

The theory of adiabatic galvanomagnetic and thermomagnetic phenomena in impure semiconductors has been expounded by Tolpygo [1] and by one of the authors of the present paper [2]. An account is given below of the results of a calculation of adiabatic transfer phenomena for semiconductors with mixed conductivity. The calculation is carried out on the same plan, and is based on the same hypotheses, as in reference [2]†.

Moreover, it is assumed that the mechanisms by which electrons and holes are dispersed are identical, i.e. $n_+ = n_- = n$, where n is determined by the dependence of the relaxation time of the conductor on the quasi-impulse:

$$\tau = \Phi(T)\left(\frac{p}{m}\right)^{n-1}$$

the symbols (+) and (−) refer to holes and electrons respectively. We will select a conductor distribution function as follows:

$$f_0 = N(2\pi mkT)^{-3/2} exp\left\{-\frac{1}{2kT}\left(\Delta\varepsilon + \frac{p^2}{m}\right)\right\}.$$

The electric and thermal fluxes are determined as the sum of the electron and hole fluxes:

$$\vec{j} = \vec{j}_+ + \vec{j}_-,\ \vec{W}_e = \vec{W}_{e+} + \vec{W}_{e-}.$$

The expressions for the total electron and hole fluxes are the same as in the case of impurity conductivity (equations (1) and (2) in reference [2]), if the integrals I_{ij} are re-defined in the following manner:

$$I_{10} = I_{10}^+ + I_{10}^-;\ I_{20} = I_{20}^+ - I_{20}^-;\ I_{30} = I_{30}^+ + I_{30}^-;$$

$$I_{11} = (I_{10}^+ - I_{10}^-)\frac{\Delta\varepsilon}{2} + I_{11}^+ - I_{11}^-;$$

$$I_{21} = (I_{20}^+ + I_{20}^-)\frac{\Delta\varepsilon}{2} + I_{21}^+ + I_{21}^-;$$

$$I_{31} = (I_{30}^+ - I_{30}^-)\frac{\Delta\varepsilon}{2} + I_{31}^+ - I_{31}^-; \qquad (1)$$

---

* *Fiz. metal. metalloved.*, 8, No. 5, 671-677, 1959.

† All the nomenclature adopted in reference [2] has been preserved here.

$$I_{12} = (I_{10}^{+} + I_{10}^{-})\left(\frac{\Delta\varepsilon}{2}\right)^2 + (I_{11}^{+} + I_{11}^{-})\Delta\varepsilon + I_{12}^{+} + I_{12}^{-};$$

$$I_{22} = (I_{20}^{+} - I_{20}^{-})\left(\frac{\Delta\varepsilon}{2}\right)^2 + (I_{21}^{+} - I_{21}^{-})\Delta\varepsilon + I_{22}^{+} - I_{22}^{-};$$

$$I_{32} = (I_{30}^{+} + I_{30}^{-})\left(\frac{\Delta\varepsilon}{2}\right)^2 + (I_{31}^{+} + I_{31}^{-})\Delta\varepsilon + I_{32}^{+} + I_{32}^{-}.$$

The calculation has been carried out for weak and strong magnetic fields:

$$\left(\frac{u \pm H}{c}\right)^2 \ll 1 \text{ and } \left(\frac{u \pm H}{c}\right)^2 \gg 1.$$

1. GALVANOMAGNETIC PHENOMENA

Let us suppose that the primary current is an electric one and is directed along the axis x, while the magnetic field is located in a plane xz and at an angle of θ to it. The conditions

$$j_y = j_z = W_y = 0 \text{ and } \frac{\partial T}{\partial x} = \frac{\partial T}{\partial z} = 0$$

determine a system of equations for the fields E_y and E_z and the temperature gradient $\partial T/\partial y$.

Ettingshausen effect

Weak magnetic fields.

$$\frac{\partial T}{\partial y} = \frac{a_n}{2}\frac{kT}{e\lambda}\frac{1}{(N_+ u_+ + N_- u_-)^2}\{(1-n)(N_+^2 u_+^3 + N_-^2 u_-^3) - N_+ N_- u_+ u_- (7 + 3n + 2\varepsilon)\} j_x \frac{H}{c}\sin\theta, \tag{2}$$

where $\lambda = \lambda_f + \lambda_{en}$ is the overall thermal conductivity in the magnetic field; $\epsilon = \Delta\epsilon/kT$

Strong magnetic fields.

$N_+ \neq N_-$;

$$\frac{\partial T}{\partial y} = \frac{a_n'}{2}\frac{kT}{e\lambda_f}\frac{1}{(N_+ - N_-)^2}\left\{(1-n)\left(\frac{N_+^2}{u_+} + \frac{N_-^2}{u_-}\right) - \frac{N_+ N_-}{u_+ u_-}(u_+ + u_-)(11 - n + 2\varepsilon)\right\} j_x \frac{c}{H}\sin\theta. \tag{3}$$

The connexion between E_x and j_x is given in this case by the equation

$$E_x = \left\{\cos^2\theta + \frac{a_n' \sigma_0}{e(N_+ - N_-)^2}\left(\frac{N_+}{u_+} + \frac{N_-}{u_-}\right)\sin^2\theta\right\}\frac{j_x}{\sigma_0}, \tag{4}$$

where

$$\sigma_0 = e(u_+ N_+ + u_- N_-).$$

Since in the first approximation the integrals I_{20} and I_{22} when $N_+ = N_- = N$ revert to zero in the region of strong magnetic fields, expressions for effects containing I_{20} and I_{22} are obtained only in the second approximation and are naturally bound to differ from the corresponding equations for $N_+ \neq N_-$.

$$N_+ = N_- = N:$$

$$\frac{\partial T}{\partial y} = -\frac{kTN}{\lambda_f}(5+\varepsilon)\frac{E_x}{\sin\theta}\frac{c}{H}, \tag{5}$$

or

$$\frac{\partial T}{\partial y} = -\frac{kTN}{\lambda_f}(5+\varepsilon)\frac{j_x}{F\sin\theta}\frac{H}{c}, \tag{6}$$

where F is determined by the relationship between j_x and E_x when $N_+ = N_-$:

$$F = \frac{j_x}{E_x}\frac{H^2}{c^2} = \left\{a_n'\frac{u_+ + u_-}{u_+ u_-} + \frac{k^2T}{e\lambda_f}N(5+\varepsilon)^2\right\} eN(1+\cos^2\theta) +$$
$$+\left\{d_n\frac{u_+^3+u_-^3}{u_+u_-} - \frac{a_n'}{2}\frac{k^2T}{e\lambda_f}N\left[(6-n)(u_+^2+u_-^2) + \right.\right.$$
$$\left.\left. + 2u_+u_-(42-13n+n^2-2n\varepsilon+12\varepsilon+\varepsilon^2)\right]\right\}\frac{eN}{u_+u_-}\cos^2\theta, \tag{7}$$

$$d_n = a_n'\frac{\Gamma\left(4-\frac{3n}{2}\right)\Gamma\left(2+\frac{n}{2}\right)}{\Gamma^2\left(3-\frac{n}{2}\right)}.$$

Hall effect

Weak magnetic fields.

$$E_y = \frac{a_n}{4}\frac{k^2T}{e^2\lambda}\frac{1}{(N_+u_+ + N_-u_-)^2}\left\{A_1(N_+^2u_+^3 - N_-^2u_-^3) + \right.$$
$$+B_1N_+N_-u_+u_-(u_+-u_-) + \tag{8}$$
$$\left. + \frac{4e^2\lambda_f}{k^2T}(N_+^2u_+ - N_-^2u_-)\right\}\frac{j_xH}{c}\sin\theta + \alpha\frac{\partial T}{\partial y},$$

where

$$A_1 = 12 - n - n^2 + (1-n)\varepsilon,\quad B_1 = 36 + 21n + 3n^2 + 5(3+n)\varepsilon + 2\varepsilon^2;$$

thermoelectric force coefficient:

$$\alpha = \frac{k}{\sigma_0}\left\{u_+N_+\left(2+\frac{n}{2}-\mu_+^*\right) - u_-N_-\left(2+\frac{n}{2}-\mu_+^*\right)\right\};$$

$$\mu_-^* = \frac{\mu_-}{kT}$$

is the adduced chemical potential of the electrons; $\mu_+^* = -\epsilon - \mu_-^*$ is the adduced chemical potential

of the holes.

*Strong magnetic fields**.

$N_+ \neq N_-$:

$$E_y = \frac{j_x H}{e(N_+ - N_-)c} \sin\theta + \frac{k}{2e} \varepsilon \frac{\partial T}{\partial y} . \tag{9}$$

$N_+ = N_- = N$:

$$E_y = \frac{1}{F} \left\{ \frac{c_n}{a_n'} \frac{u_+ - u_-}{u_+ u_-} + \frac{k^2 T}{2e\lambda_f} N(5+\varepsilon) \frac{u_+(6-n+2\varepsilon) - u_-(6-n)}{u_+ + u_-} \right\} \cdot \frac{j_x}{\sin\theta} \frac{H}{c} . \tag{10}$$

Equations (6) and (10) for $\partial T/\partial y$ and E_y are true at fairly large angles of θ. If θ is small, the terms of the fourth order relative to $1/H$ must be taken into account in resolving the integrals I_{ij}. The nature of the dependence of $\partial T/\partial y$ and E_y on

$$\frac{u_\pm H}{c}$$

will in this case be the same as when $N_+ \neq N_-$.

Resistance variation in a magnetic field

Weak magnetic fields.

In view of the unwieldiness of the general equation for $\Delta\sigma/\sigma_0$, we will adduce only the expression for the case of high values of ϵ (we will ignore both those terms which do not contain ϵ, and those $\sim \epsilon$, leaving only the terms $\sim\epsilon^2$)

$$\frac{\sigma_0 - \sigma}{\sigma_0} = \left(b_n - \frac{a_n^2}{2} \right) \frac{k^2 T}{e\lambda} \frac{N_+ N_- u_+ u_-}{(N_+ u_+ + N_- u_-)^2} (N_+ u_+^3 + N_- u_-^3) \varepsilon^2 \frac{H^2}{c^2} \sin^2\theta. \tag{11}$$

In strong magnetic fields the adiabatic variation of resistance coincides with the corresponding isothermal value (equations (35) and (37) in reference [3]) correct to the terms $\sim H^{-2}$.

Nernst effect

The expressions for the Nernst effect are extremely cumbersome, and will not be adduced here.

It should be noted that equation (17) in reference [2] is erroneous. The expression for $\partial T/\partial x$ in the case of impurity conductivity and strong magnetic fields is as follows:

---

* In equations (8) and (8a) reference [2], the expression in parentheses

$$-T \frac{d\,lnN}{dT} + \frac{3}{2}$$

is erroneous; it should be replaced by the expression

$$T \frac{d\,lnN}{dT} + 1.$$

Then the correlation:

$$R_{ad} = R_{is} + \overline{PQ}_{is}^{||}$$

is obtained.

$$\frac{\partial T}{\partial x} = \frac{kT}{2e} J_x \frac{5 + (n-1)\cos^2\theta}{\lambda_f} . \tag{12}$$

2. THERMOMAGNETIC PHENOMENA

Let us suppose that the primary thermal flux is directed along the axis x, and the magnetic field along the axis z, i.e. $\theta = \pi/2$. The conditions $\vec{j} = 0$ and $W_y = 0$ determine the system of equations for the fields E_x and E_y and the temperature gradient $\partial T/\partial y$.

Righi - Leduc effect

Weak magnetic fields.

$$\frac{\partial T}{\partial y} = \frac{a_n}{4}\frac{k^2T}{e\lambda}\frac{1}{(N_+u_+ + N_-u_-)^2}\{(7+2n+n^2)(N_+^3u_+^4 - N_-^3u_-^4) - \\ - A_2N_+N_-u_+^2u_-^2(N_+ - N_-) - B_2N_+N_-u_+u_-(N_+u_+^2 - N_-u_-^2)\}\frac{H}{c}\frac{\partial T}{\partial x} , \tag{13}$$

where

$$A_2 = 55 + 46n + 9n^2 + 4(7+3n)\varepsilon + 4\varepsilon^2; \quad B_2 = 2[1 - 8n - 3n^2 + 2(1-n)\varepsilon].$$

Strong magnetic fields.

$$N_+ \neq N_-: \\ \frac{\partial T}{\partial y} = \frac{k^2T}{e\lambda_f}\frac{1}{N_+ - N_-}\left\{\frac{5}{2}(N_+^2 + N_-^2) - N_+N_-(30 + 10\varepsilon + \varepsilon^2)\right\}\frac{c}{H}\frac{\partial T}{\partial x} . \tag{14}$$

$$N_+ = N_- = N: \\ \frac{\partial T}{\partial y} = \frac{1}{a_n'}(u_+ - u_-)\frac{a_n'^2(6 - n + \varepsilon) - c_n(5+\varepsilon)}{u_+u_-(5+\varepsilon)^2 + \frac{a_n'}{N}\frac{e\lambda_f}{k^2T}(u_+ + u_-)}(5+\varepsilon)\frac{c}{H}\frac{\partial T}{\partial x} . \tag{15}$$

Nernst - Ettingshausen transverse effect

Weak magnetic fields.

In view of the unwieldiness of the general equation, we will adduce the expressions for E_y in the special case of high values of ϵ (we will retain those terms proportional to ϵ^3).

$$E_y \approx -\frac{a_n}{2}\frac{k}{e}\frac{k^2T}{e\lambda}\varepsilon^3 N_+N_-u_+u_- \cdot \\ \frac{N_+u_+(u_+ + u_-) + N_-u_-(u_+ - u_-)}{(N_+u_+ + N_-u_-)^2}\frac{H}{c}\frac{\partial T}{\partial x} . \tag{16}$$

Strong magnetic fields.

$$N_+ \neq N_-: \\ E_y = E_y^{us} + \frac{5}{2}\frac{k}{e}\frac{k^2T}{e\lambda_f}\frac{1}{(N_+ - N_-)^2}\left\{\frac{5}{2}(N_+^2 + N_-^2) - \right. \\ \left. - N_+N_-(30 + 10\varepsilon + \varepsilon^2)\right\}\left\{N_+ + \left(1 + \frac{2\varepsilon}{5}\right)N_-\right\}\frac{c}{H}\frac{\partial T}{\partial x} , \tag{17}$$

VOL. 8 1959

where the field of the isothermal effect E_y^{is} is determined by the equation

$$E_y^{is} = \frac{a_n'}{2}\frac{k}{e}\frac{1}{(N_+ - N_-)^2 u_+ u_-} \cdot \\ \cdot \{(1-n)(N_+^2 u_- + N_-^2 u_+) - N_+ N_- (u_+ + u_-)(11 - n + 2\varepsilon)\}\frac{c}{H}\frac{\partial T}{\partial x}. \tag{18}$$

In the case of equal concentrations of electrons and holes, the adiabatic field E_y coincides with the isothermal fields [3] correct to the terms proportional to H^1.

Nernst - Ettingshausen linear effect

The expression for E_x in the case of weak magnetic fields is extremely cumbersome and will not be adduced here.

In the case of strong magnetic fields and unequal concentrations, the adiabatic field E_x coincides with the isothermal field correct to the terms $\sim H^{-2}$. When $N_+ = N_- = N$:

$$E_x = E_x^{is} + \frac{1}{a_n'^2}\frac{k}{e}\frac{u_+ - u_-}{u_+ + u_-}(5+\varepsilon)^2 \\ \frac{a_n'^2(1-n)(5+\varepsilon) - c_n + a_n'^2}{(5+\varepsilon)^2 + a_n'\dfrac{u_+ + u_-}{u_+ u_-}\dfrac{e\lambda f}{k^2 TN}}\frac{\partial T}{\partial x}, \tag{19}$$

where

$$E_x^{is} = \frac{k}{e}\frac{c_n - a_n'^2}{a_n'^2}\frac{u_+ - u_-}{u_+ + u_-}(5+\varepsilon)\frac{\partial T}{\partial x}.$$

Maggi - Righi - Leduc effect

Owing to the extreme unwieldiness of the equation for weak magnetic fields, it will not be adduced here.

Strong magnetic fields.

$N_+ \neq N_-$:

$$\lambda_{en} = \frac{kT}{2}\left\{\frac{k}{2e}\left[a_n'\left(\frac{N_+}{u_+} + \frac{N_-}{u_-}\right)(48 - 14n + n^2 + 2(6-n)\varepsilon + \varepsilon^2)\frac{\partial T}{\partial x} + \right.\right. \\ + (N_+ - N_-)(35 + 10\varepsilon + \varepsilon^2)\frac{H}{c}\frac{\partial T}{\partial y}\Big] - a_n'\left(\frac{N_+}{u_+} - \frac{N_-}{u_-}\right)(6 - n + \varepsilon)E_x^* - \\ \left. - (N_+ + N_-)(5+\varepsilon)\frac{H}{c}E_y^*\right\}\frac{c^2}{H^2}\left(\frac{\partial T}{\partial x}\right)^{-1}, \tag{20}$$

where

$$E_y^* = E_y + \frac{k}{2e}\varepsilon\frac{\partial T}{\partial y}, \quad F_x^* = E_x - \frac{k}{2e}\frac{N_+ u_+ - N_- u_-}{N_+ u_+ + N_- u_-}(4 + n + \varepsilon)\frac{\partial T}{\partial x}.$$

When $N_+ = N_- = N$ λ_{en} equals:

$$\lambda_{en} = \frac{1}{a_n'} \frac{k^2 T}{e} N \frac{u_+ u_-}{u_+ + u_-} (5 + \varepsilon)^2. \tag{21}$$

3. CONCLUSIONS

1. The nature of the dependence of all transverse galvanomagnetic and thermomagnetic effects on the magnetic field for semiconductors with unequal concentrations of electrons and holes is the same as in the case of impurity conductivity: in the region of weak fields these effects are proportional to H, while in the region of strong fields they are inversely proportional to H (in the case of the Hall effect this is true not of the field E_y but of the current j_y.)

2. Where there are equal concentrations of conductors the transverse effects may be divided into two groups: (1) Hall and Righi-Leduc effects, for which the nature of the magnetic field dependence is the same as in the case of unequal concentrations, and (2) Ettingshausen and Nernst-Ettingshausen effects, which are directly proportional to H whatever the magnetic field.

3. The nature of the dependence of all linear effects on the magnetic field is the same as in the case of impurity conductivity. Characteristic properties of the Maggi-Righi-Leduc effect are to be observed in the presence of strong fields and equal concentrations of electrons and holes. While the dependence of electronic thermal conductivity on the magnetic fields, obtained when $E_y = 0$, is identical for different correlations of concentrations [3], when $j_y = 0$ and

$$N_+ = N_- = 0 \text{ and } \left(\frac{u_+ H}{c}\right)^2 \gg 1$$

the electronic thermal conductivity tends not towards zero, as in the case of $N_+ \neq N_-$, but towards some constant value. When the values of ϵ are sufficiently high (as for example in Ge and Si) the symbol for the Maggi-Leduc effect may even vary, i.e. there must be an increase in thermal conductivity when the transition from impurity to natural conductivity occurs.

4. Attention must be paid to the essential difference between adiabatic effects and corresponding isothermal effects, based on their relation to the width of the forbidden energy band. Thus, the Hall field and resistance variation in a magnetic field will contain terms proportional to ϵ^2, while in isothermal conditions they are not dependent on ϵ. The Nernst-Ettingshausen transverse effect in weak magnetic fields and in strong fields when $N_+ \neq N_-$ contains terms $\sim\epsilon^3$, but in isothermal conditions it contains terms $\sim \epsilon$. Electronic thermal conductivity in both weak and strong magnetic fields when $N_+ \neq N_-$ contains components $\sim \epsilon^4$, while in isothermal conditions $\lambda_{en} \sim \epsilon^2$.

Thus, in equations for adiabatic effects ϵ is at a power twice as high as in equations for corresponding isothermal effects.

Translated by C. M. Burnell

REFERENCES

1. K.B. Tolpygo, Proceedings of the Institute of Physics of the U.S.S.R. Academy of Sciences, No. 3, 52 (1952).
2. I.M. Tsidil'kovskii, *Zh. teor. fiz.*, 28, 1171 (1958).
3. F.G. Bass and I.M. Tsidil'kovskii, *Zh. eksp. teor. fiz.*, 31, 672 (1956).

VOL. 8 1959

ON THE TEMPERATURE DEPENDENCE OF THE MAGNETIC PROPERTIES OF MAGNETICALLY TEXTURED SPECIMENS OF MnBi ALLOY POWDERS

Ia.S. SHUR, Ye.V. SHTOL'TS, G.S. KANDAUROVA and L.V. REBNEVA

Institute of Physics of Metals of the Academy of Sciences of the U.S.S.R.

(Received 18 July 1959)

This paper gives the results of an investigation of the magnetic properties of magnetically textured specimens of fine powders of the MnBi alloy in the temperature interval from + 20 to − 150°. It was observed that with a lowering of the temperature the nature of the anisotropy of the coercive force, the magnetization curves and the residual magnetization in individual cycles as a function of the magnetizing field change. It is shown that from these features one can judge the magnetic structure of powders of magnetically uniaxial materials.

1. INTRODUCTION

The study of the magnetic properties of powders of various materials has shown that the magnetic characteristics of powders change in a regular manner with the grain size of the powder. This change in the magnetic properties of the powders is caused by the change in the magnetic structure of the ferromagnetic: with a reduction of the size of the ferromagnetic, the magnetic structure is transformed from a multi-domains into a transitional and then into a single domain structure. The cause of this reforming of the structure is that with decreasing size d of the particles the appearance of boundary layers between the regions and the development and growth of nuclei of remagnetization become energetically disadvantageous. This reforming of the magnetic structure should in different materials occur at different particle sizes. The critical size d_k of the particles below which a single domain state begins, depends on the first place on the anisotropy parameters K and the magnetic saturation I_s it increases with increasing K and decreases with increasing I_s [1]. Hence, one must expect that in small grained powders of certain ferromagnetics in which in a certain temperature interval a sharp temperature dependence of the anisotropy parameter is observed together with a slight change in the magnetic saturation it should be possible to cause a reforming of the magnetic structure by changing the temperature of the ferromagnetic without changing its particle size [2]. The latter process should in turn cause a regular change in the magnetic properties [3].

The purpose of the present paper was to study the temperature dependence of the magnetic properties of specimens of MnBi alloy powders which at room temperature have a record high value of the parameter of magnetic anisotropy [4], as a result of which this material has a high value of d_k. With decreasing temperature K decreases rapidly [4], which causes a reduction in the critical size. Hence, in MnBi alloy powders, as the temperature decreases, the form of the magnetic structure will change and certain magnetic characteristics will change in a certain way as a consequence. This in turn should make it possible to draw certain qualitative conclusions on the form of the magnetic structure of powders of magnetically uniaxial materials from the observed regularities of the magnetic properties.

2. SPECIMENS AND METHODS OF MEASUREMENT

The MnBi alloy which was investigated was obtained by means of sintering powders of magnesium and bismuth at a temperature of 300°; it had a coercive force of the order of 1000 oersted. By mechanical breaking up the alloy was turned into a powder which was then separated into fractions according to grain size by means of a special device. The average diameter of the particles of the various fractions varied from 20 to 2μ. The powders of the individual fractions were mixed with an adhesive and the mixture filled into disk-shaped moulds which were placed between the poles of an electromagnet, the particles of the powder were glued together in the presence of a magnetic field.

* *Fiz. metal. metalloved.*, 8, No. 5, 678-684, 1959.

As a result magnetically textured specimens were obtained and the axis of the texture proved to be that direction in the specimen along which the magnetic field was applied during the preparation of the specimen.

The measurement of the magnetic properties of the specimens was done with the ballistic method. A special device was used to cool the specimen to low temperatures; it made it possible to lower the temperature evenly down to −150°. The specimens were demagnetized at the temperature of measurement by selecting a reverse permanent magnetic field. The curves of the angular dependence of the coercive force and the residual magnetization were measured, as well as the curves of the magnetization and residual magnetization in individual cycles as a function of the maximum field originally used to magnetize the specimen.

3. RESULTS OF THE MEASUREMENTS

The main results of the measurements are given in Figs. 1-4. Fig. 1 shows the angular dependence of the coercive force of the specimen with 6μ particle size at various temperatures. The angle ϕ is plotted on the abscissae; it represents the angle between the angle of the direction of the magnetic field during the preparation of the specimen (the axis of the texture) and the direction of the magnetic field during the measurement of the magnetic properties. The ordinates represent the ratio of the coercive force under a certain angle ϕ to the coercive force along the axis of texture (ϕ = 0°). As can be seen from the figure, at temperatures of + 20 and − 40° the coercive force for an increase in the angle ϕ from 0 to 90° only decreases. At temperatures of − 65°, for values close to ϕ = 45° an increase in the coercive force is observed (for ϕ = 45°, H_c/H_c^0 = 1.02); when ϕ is further increased the coercive force diminishes and for ϕ = 90°, H_c/H_c^0 = 0.77. At a temperature of − 90° the coercive force increases with increasing angle ϕ right up to ϕ = 75°, and then decreases slightly, remaining, however, greater than the value of the coercive force at ϕ = 0°. At lower temperatures (−150°) H_c only increases when ϕ is increased from 0 to 90°.

Thus, in one and the same specimen three kinds of curve can be observed for the dependence of the coercive force on the angle ϕ during the measurement of the magnetic properties of that specimen, depending on the temperatures: (*a*) when the angle ϕ is increased from 0 to 90° the coercive force only diminishes; (*b*) when the angle ϕ is increased from 0 to 60-70° the coercive force increases, and then decreases; (*c*) when the angle ϕ is increased from 0 to 90° the coercive force only increases.

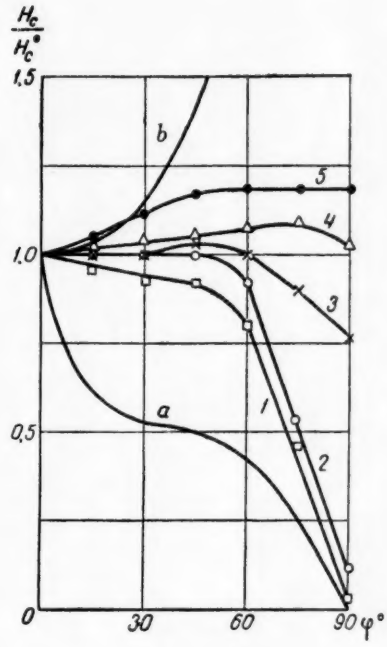

FIG. 1. Angular dependence of the coercive force of a specimen with a particle size of 6μ at the temperatures: 1 at + 20°; 2 at − 40°; 3 at − 65°; 4 at − 90°; 5 at − 150°.
Theoretically calculated curves for the angular dependence of the coercive force:
(*a*) for a single-domain structure;
(*b*) for a multi-domain structure.

Fig. 2 shows the dependence of the coercive force on the angle ϕ in specimens with different powder particle size at a temperature of − 65°. As the figure shows, specimens with 2 or 3 powder particle size the coercive force only diminishes with increasing angle ϕ. In specimens with 6 and 20μ particle size the anisotropy H_c was small and its nature changed as follows: with increasing angle ϕ the coercive force grows slightly up to ϕ = 45° and then decreases. Thus, a different nature of the angular dependence of the coercive force is observed in specimens of powders of different particle size.

From Fig. 3, which shows the temperature dependence of the relative residual magnetization along the axis of the texture of specimens with different particles sizes one can see that specimens with 20μ particle size the relative residual magnetization I_r/I_s decreases rapidly with decreasing temperature from + 20 to − 60°; in the temperature region of − 80 to − 130° the change in I_r/I_s is slight. The relative residual magnetization of a powder specimen with 3μ particle size remains virtually constant

VOL. 8 1959

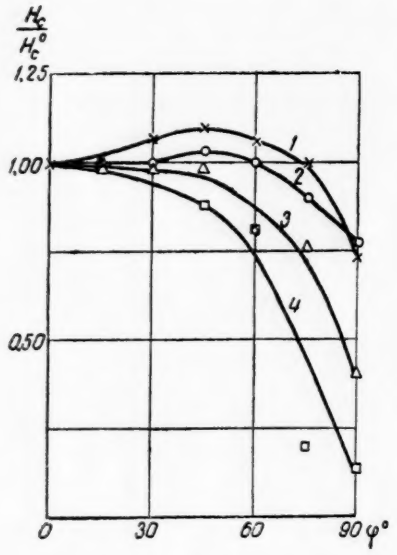

FIG. 2. Angular dependence of the coercive force at a temperature of − 65° for specimens of powders with particle sizes:
1.20μ; 2.6μ; 3.3μ; 4.2μ.

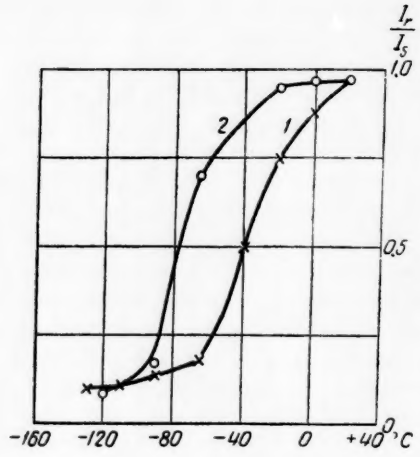

FIG. 3. Temperature dependence of the relative residual magnetization of powder specimens with particle sizes:
1.20μ; 2.3μ.

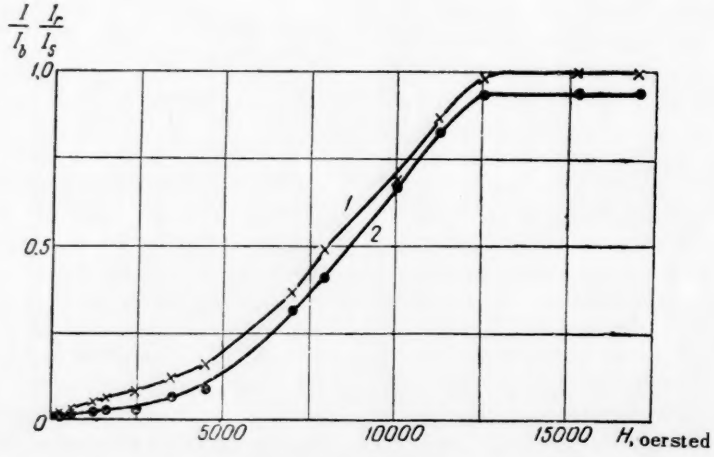

FIG. 4a. Dependence of the magnetization (curve 1) and the residual magnetization (curve 2) on the strength of the magnetic field. The curves are measured along the axis of the texture of the specimen made from powder with a particle size of 6μ at a temperature of + 20°.

when the temperature is lowered from + 20 to − 20°, but decreases rapidly in the temperature interval from − 40 to − 90° and then again hardly changes at all down to a temperature of − 130°. Hence, in specimens of comparatively large powder particle size a considerable decrease in the relative residual magnetization is observed when the temperature is lowered from + 20°. In specimens of finer powders a rapid decrease in the residual magnetization is observed at temperatures below − 20°.

Fig. 4a-b shows the dependence of the relative magnetization (curve 1) and the relative residual magnetization (curve 2) on the strength of the magnetic field oriented parallel to the axis of the texture of the specimen (the specimen is made of powder with 6μ particle size); the change of these curves with the change in temperature is shown. As can one see from the figure, at a temperature of + 20°

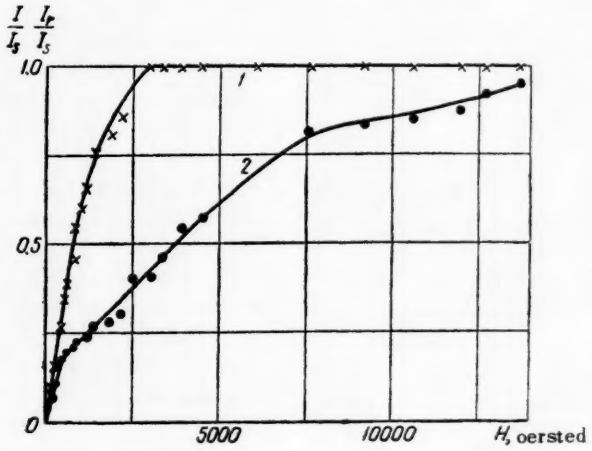

FIG. 4*b*. The same as Fig. 4*a*, for a temperature of – 37°.

VOL. 8 1959

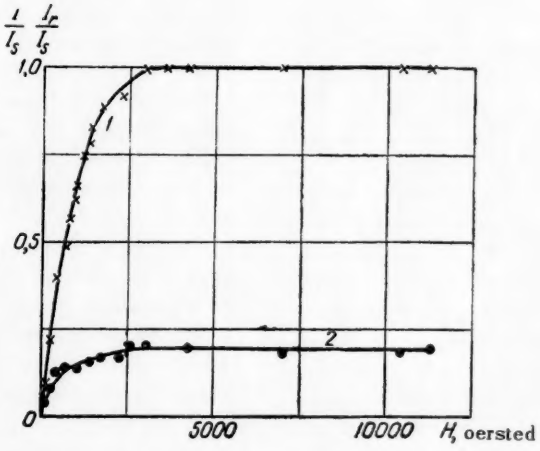

FIG. 4*c*. The same as Fig. 4*a*, for a temperature of – 60°.

(Fig. 4a), at all values of the maximum magnetizing field the value for the residual magnetization is close to the corresponding value for the magnetization in the same field. The maximum value of the relative residual magnetization is equal to 0.97 and is reached in a magnetic field which is close to the field of saturation H_c ($H_{max} \sim 13{,}000$ oersted).

At a temperature of – 37° (Fig. 4b) a great difference is observed between the values for the magnetization and the residual magnetization in "weak" fields. Thus, for example, in a field of 2000 oersted, $I/I_s = 0.88$, but $I_r/I_s = 0.32$. The magnetization reaches saturation in a field $H_s = 3000$ oersted, but to reach the maximum value of the residual magnetization even a field of 14,000 oersted is not sufficient. The maximum value of the residual magnetization is close to the saturation magnetization. At a temperature of – 60° (Fig. 4c) the maximum value of the residual magnetization is equal to $I_r/I_s = 0.19$. The field H_{max} is roughly equal to the field H_s and is about 4000 oersted.

Hence, along the axis of the texture of the specimens of fine powder of the alloy MnBi, when the temperature is lowered, (*a*) the process of magnetizing the specimen is made easier (H_s is reduced); (*b*) the value of the residual magnetization is reduced; (*c*) the ratio between the saturation field H_s and the field in which the maximum value for the the residual magnetization H_{max} is reached, changes. At certain temperatures H_s become less than H_{max}.

4. ANALYSIS OF THE RESULTS

As was shown above, in isotropically shaped ferromagnetic particles the critical size of single domain texture d_k is in the main determined by the quantities K and I_s. In the alloy MnBi in the temperature interval from + 20 to − 150° the value of K decreases rapidly (at 20° $K \sim 10^7$ erg/cm³, at − 150° $K \sim 10^5$ erg/cm³), while the quantity I_s changes only slightly. Hence, the quantity d_k also decreases rapidly in this temperature interval. From this it follows that if at 20° small particles of MnBi alloy have a single domain texture, it is possible by lowering the temperature to obtain a transitional or multi-domain texture in these particles, which will also be accompanied by the corresponding change in the magnetic properties which are determined by the processes of technical magnetization.

Starting from these concepts one can explain the change in the nature of the anisotropy curves H_c (ϕ) shown in Fig. 2. The point is that according to theoretical calculations the curve for magnetically uni-axial specimens should be of a different shape in the case of multi-domain (curve *b* in Fig. 1) and single-domain (curve *a* in Fig. 1) magnetic texture [5].

Comparison of the theoretically calculated with the experimental curves (Fig. 1) shows that at room temperature an angular dependence of the coercive force is observed which is characteristic for single-domain particles. For small values of the angle ϕ the relative change in the value of H_c in the experimental curves is less than in the theoretical curve. This indicates a certain difference in the magnetic structure of the particles from a single-domain structure. When the temperature is lowered the experimental curves differ more and more from curve *a*, although down to − 40° the basic regularity is preserved, namely the decrease in the coercive force with increasing angle ϕ. The curves for the dependence of H_c (ϕ) at low temperatures approaches the theoretical curve *b*, i.e. an angular dependence characteristic for particles with multi-domain structure. Hence, in the measure in which the critical particle size d_k decreases on account of the decrease in the quantity K, a reforming of the magnetic structure from a single − into a multi-domain structure is observed.

These concepts are also confirmed by investigations made on specimens with different powder particle sizes. Indeed, at one and the same temperature the curve H_c (ϕ) can have a different form depending on the size of the particles (Fig. 2). At a temperature of − 65° in specimens of fine powders the angular dependence of the coercive force corresponds to a magnetic structure which is close to the single-domain structure. At the same temperature in specimens of larger grained powders (6 and 20μ) the angular dependence of the coercive force is of a different nature and approaches H_c (ϕ) for uni-axial ferromagnetics with multi-domain structure. Hence, when the particle size decreases, a change in the nature of H_c (ϕ) is observed which corresponds to an approximation to a single-domain magnetic structure.

The transition from a single − to a multi-domain structure when the critical particle size decreases is also confirmed by the decrease in the residual magnetization along the axis of the texture with decreasing temperature (Fig. 3), which is evidently caused by the appearance of locking areas and areas with reverse magnetization.

In the case of a single-domain structure the residual magnetization along the axis of the texture should be equal, or in a real specimen close to the saturation magnetization. Besides, in a single-domain structure the saturation magnetization and the maximum residual magnetization should be reached in one and the same fields. As Fig. 4a shows, at room temperature I/I_s and I_r/I_s reach their maximum values in a field of 15,000 oersted, and $I_r/I_s = 0.96$. At a temperature of − 37°, however, the nature of these curves changes completely (Fig. 4b), namely, $H_{max} > H_s$. This regularity can be understood if it is assumed that at the given temperature the powder particles have a transitional structure. In the case of such a magnetic structure the process of magnetic reversal in individual hysteresis cycles occurs on account of the growth of the nuclei of reverse magnetism and the shift in the boundaries and at the maximum hysteresis loop, where all nuclei of magnetic reversal have already been destroyed by the field, on account of irreversible rotation. The proposal of a transitional structure of such a type is confirmed by visual observation of the domain structure with the aid of powder figures on small grains of the alloy MnBi [4]. At lower temperatures (below − 50°) only processes of growth of the nuclei of magnetic reversal occur evidently along the axis of texture together with shifts in the boundaries, hence $H_{max} > H_s$. This also explains the low value for the residual magnetization (Fig. 4b).

5. CONCLUSIONS

On the basis of a study of the temperature dependence of the magnetic properties of textured specimens of fine powders of MnBi alloy in the tempera-

ature interval from + 20 to − 150° it is found that when the temperature is lowered the following regularities are observed:

(1) A change in the nature of the angular dependence of the coercive force expressed in the fact that the lower the temperature of the specimen, the more the curves of the angular dependence of the coercive force differ from the theoretical curve H_c (ϕ) calculated for the case of a single-domain structure. This change in the angular dependence is caused by the decrease in the anisotropy parameter when the temperature is lowered, as a result of which the critical size of the particles decreases and the magnetic structure of the particles is transformed from a single-domain into a multi-domain structure.

(2) A change in the nature of the curves of the magnetization and the curves of the dependence of the residual magnetization in individual cycles on the strength of the maximum magnetic field along the axis of texture. For higher values of the anisotropy parameter (greater critical size) the value of the residual magnetization in individual cycles is close to the corresponding value of the maximum magnetization of the given cycle, and the maximum value of the residual magnetization is reached in the field of saturation (the magnetic structure comes closest to a single-domain structure). For smaller values of the anisotropy parameter, i.e. when the critical size is reduced, the maximum value of the residual magnetization which remains close to the saturation magnetization is reached in a field greater than the field of saturation (transitional structure). For small values of the anisotropy parameter, i.e. small values of the critical size, the value of the residual magnetization is small and reached in a field weaker than the field of saturation (multi-domain structure).

On the basis of the results obtained it is shown that it is possible to make a qualitative judgment on the magnetic structure in magnetically uni-axial ferromagnetics and on its change under the effect of various influences from certain magnetic characteristics.

Translated by B. Ruhemann

VOL.
8
1959

REFERENCES

1. Ch. Kittel, *Rev. Mod. Phys.* 21, 541 (1949).
2. Ia.S. Shur, Ye.V. Shtol'ts and V.I. Margolin, *Zh. eksp. teor. fiz.* (in the press).
3. Ye.V. Shtol'ts and Ia.S. Shur, *Dokl. Akad. Nauk SSSR* 95, 781 (1954).
   Ia.S. Shur, Ye.V. Shtol'ts and G.S. Kandaurova, *Fiz. metal. metalloved.* 6, 420 (1958).
4. C. Guillaud, *Cahiers des phys.* 15, (1943).
5. G.S. Kandaurova, Ia.S. Shur and Ye.V. Shtol'ts, *Fiz. metal. metalloved.*, 6, 229 (1958);
   Ye.V. Shtol'ts, Ia.S. Shur and G.S. Kandaurova, *Izv. Akad. Nauk SSSR, ser. fiz.*, 22, 1269 (1958).

ON THE REFORMING OF THE DOMAIN STRUCTURE OF MAGNETICALLY UNI-AXIAL FERROMAGNETICS IN A MAGNETIC FIELD*

Ia.S. SHUR, Ye.V. SHTOL'TS and A.A. GLAZER

Institute of Physics of Metals of the Academy of Sciences of the U.S.S.R.

(Received 21 August 1959)

The visual domain structure of ferromagnetics, including magnetically uniaxial ones, has been most fully studied with the method of powder figures. As we know, with this method it is assumed that the magnetic powder collects around the boundaries between the domains and thereby renders the domain structure on the surface of the ferromagnetic specimen visible. If by some external action the surface domain structure is altered the powder will shift to the new positions of the domain boundaries [1]. In the study of magnetically uni-axial single crystal of cobalt it was found, however, that the magnetic powder behaved in an unusual manner. If one regards the powder figures on that surface of the specimen which contains the hexagonal axis (the axis of easy magnetization), one sees the parallel lines of the boundaries between the domains with anti-parallel orientation of the vector of magnetic saturation $\vec{I}_s$. The boundary lines are parallel to the hexagonal axis. On switching on a field parallel to the easy direction one observes a change in the position of the boundaries caused by the shifting processes which follow from the well known concepts on the re-forming of the domain structure in a field. When a field is switched on which is perpendicular to the easy direction one set of lines (every other one) begins gradually to become weaker while the other set hardly changes or even becomes a little stronger; in strong fields the first set of lines disappears completely [2]. This behaviour of the powder figures is unusual and cannot be explained from the point of view of the present concepts on domain structure.

We have observed a similar effect on crystals of the magnetically uni-axial alloy MnBi. Fig. 1 shows photographs of powder deposits obtained on a crystal of MnBi alloy in which the hexagonal axis (the axis of easiest magnetization) almost coincides with the surface of the specimen.

As can be seen from Fig. 1a, in the absence of an external field the entire crystal is divided into domains the boundaries of which (made visible by the black lines formed by the powder deposit) separate the regions with anti-parallel orientation of the magnetization $\vec{I}_s$. When a field perpendicular to the orientation of $\vec{I}_s$ is switched on and gradually increased in strength (Fig. 1b) on some boundaries the area of the powder deposit becomes broader, on others it becomes narrower. On further increasing the field strength (Fig. 1c) the weakening set of lines disappears almost completely. Such a reforming of the domain structure contradicts the generally accepted concepts and therefore casts doubt on the correctness of the judgments on the domain structure of the surface of the crystal from the shape of the powder deposits. For this reason the study of the domain structure in the present paper was conducted not only with the method of powder figures but also with the help of the magneto-optic polarization of the Kerr effect [3]. With this method it is not the boundaries of the domains which are made visible (as is the case with the method of the powder figures) but the surface of the domains themselves.

The results we obtained with the help of the Kerr effect are shown in Fig. 2. Fig. 2a represents the photographs of the same domain structure as Fig. 1a. The dark and light bands correspond to the regions with anti-parallel orientation of $\vec{I}_s$. From a comparison of Fig. 1a and 2a by means of superimposing a tracing made from the second figure on the first it is apparent that the boundaries between the dark and light regions coincide accurately with the boundaries made visible by magnetic suspension. The application of a field perpendicular to the boundaries, under the influence of which the powder deposit on the boundaries becomes different in width (Fig. 1b) doest not cause a change in the domain structure shown in Fig. 2a. On further increasing the field strength until the powder deposits on one set of lines disappears

* *Fiz. metal. metalloved.*, 8, No. 5, 685-688, 1959.

VOL
8
195

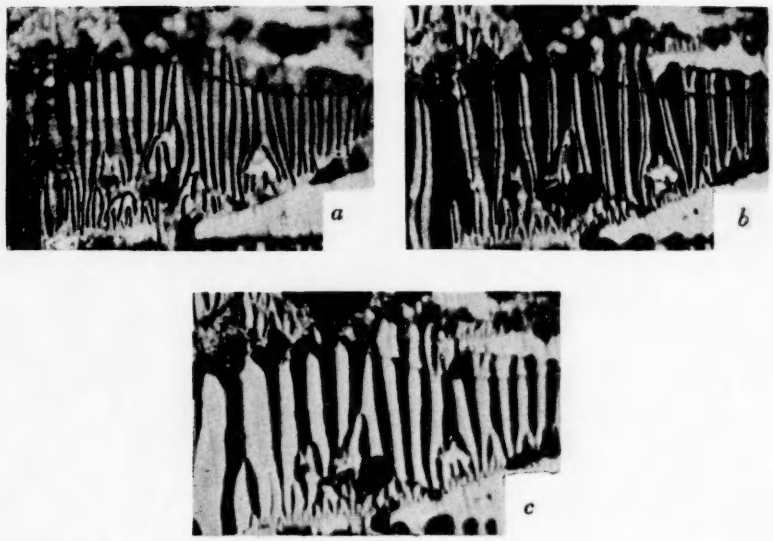

FIG. 1. Change in the powder figures on a MnBi crystal in a magnetic field applied perpendicularly to the easy direction (the direction of the field is horizontal); × 350:
a – demagnetized; *b* – H = 600 oersted; *c* – H = 3000 oersted.

VOL.
8
1959

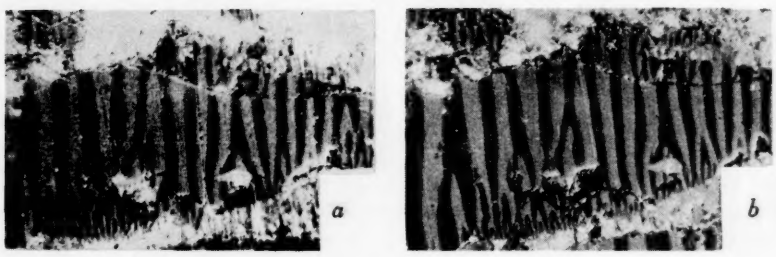

FIG. 2. Domain structure revealed with the help of the Kerr effect, for the same case as in Fig. 1; × 350:
a – demagnetized; *b* – H = 3000 oersted.

(Fig. 1c), the form of the domain structure obtained with the help of the Kerr effect hardly changes at all (Fig. 2b).

To compare the pictures obtained by the two methods it proved very convenient to make simultaneous observations of the domain structure with the aid of magnetic suspension and with the Kerr effect. If one observes the domain structure in a polarization microscope with the aid of the Kerr effect and at the same time covers the specimen with a magnetic suspension, then besides the dark and light domain surfaces made visible by the polarized light, the powder deposits on the boundaries between the domains will also become visible. The results of such a simultaneous observation of the domain structure by two independent methods on the surface of the earlier described MnBi crystal are shown in Fig. 3.

Fig. 3a shows the domain structure of a crystal in the demagnetized state. The dark and light bands correspond to the domains with anti-parallel orientation of the vector $\vec{I}_s$ shown up with the help of the Kerr effect; the black lines are the powder deposits along the boundaries between the domains. These powder boundaries coincide with the positions of the boundaries shown up with the aid of the Kerr effect. When a field perpendicular to $\vec{I}_s$ in the domains is switched on (Fig. 3b) it is seen that narrow and broad powder deposits appear on the boundaries between the domains which are shown up by the Kerr effect. In strong fields (Fig. 3c) the thin boundaries shown up by the powder disappear;

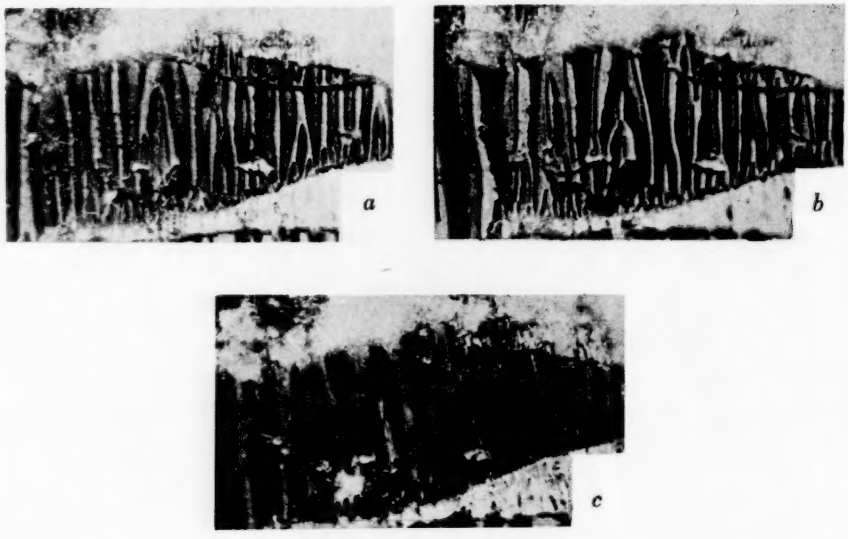

FIG. 3. Simultaneous showing up of the domain structure with powder figures and with the Kerr effect for the same case as in Fig. 1; × 350:
a – demagnetized; *b* – H = 600 oersted; *c* – H = 3000 oersted.

at the same time, to judge by the form of the domain structure revealed by the Kerr effect, the boundaries between the regions continue to exist. It follows from these experiments that in strong fields the method of the powder figures does not show up the domain structure in magnetically uniaxial crystals when they are magnetized in a direction perpendicular to that of light magnetization. One of the possible causes of this effect may be the interaction of the external magnetic field with the ferromagnetic particles of the suspension, as is pointed out in paper [2]. The possibility is not, however, excluded that we have here a case of more complex processes which occur on the boundary itself.

The observations of the change in the domain structure made by us with the help of the Kerr effect in fields perpendicular to the light direction showed that in weak fields the domain structure hardly changes at all. In the measure in which the field strength increases individual domains become contorted and split into parts, gradually disappearing in the measure in which saturation is approached. This enables us to suggest that the process of magnetization in a magnetically uniaxial ferromagnetic when the orientation of the external magnetic field is perpendicular to the light direction is not caused by the shifting of the boundaries but in all probability by a rotation of the magnetization vectors in each domain in the direction of the field.

Translated by B. Ruhemann

REFERENCES

1. H.J. Williams, R.M. Bozorth and W. Shockley, *Phys. Rev.* 75, 155 (1949); Ia. S. Shur and V.R. Abel's, *Fiz. metal. metalloved.*, 1, 5 (1955).
2. C.D. Mee, *Proc. Phys. Soc.* A63, 922 (1950).
3. B.W. Roberts and C.P. Bean, *Phys. Rev.* 96, 1494 (1954).

ON THE DEPENDENCE OF THE FIELD OF A DEFECT OF THE CRACK TYPE ON THE THICKNESS OF THE COVERING METAL LAYER*

V.V. VLASOV and R. Ye. YERSHOV

Physics of Metals Institute of the Academy of Sciences of the U.S.S.R.

(Received 31 March 1959)

VOL. 8 1959

The question of the dependence of the field of a defect on the thickness of the metal layer covering the defect is of considerable important for the detection of defects in various ferromagnetic products. The field of a defect as a function of the depth at which it lies has been studied in the case of an artificial defect in the shape of a cylinder [1-4] and for a natural fatigue crack unsymmetrically placed in the head of a rail [5]. The field of artificial defects of the crack type has been studied in one paper [6], but not as a function of the depth at which it lies but only of the degree of uncovering of the defect (the ratio of the dimensions of the defect in the direction of the field to its dimension transverse to the field).

At the same time there is a basis for expecting the field of the defect to decrease with decreasing thickness of the metal layer covering it. Thus, on the basis of experiments to study the dependence of a cylindrical defect on the depth at which it lies and taking certain theoretical considerations into account, Sapozhnikov [2] came to the conclusion that the field of scattering is affected not only by the walls of the defect, but also by the area of metal situated above the defect. With decreasing thickness of the covering the field of the defect should therefore increase, but only until this area of metal is touched. In the case of an open defect, however, this area does not exist at all, and the field of the defect should be still less.

To test these propositions work has been done [7, 8] with an artificial defect in the shape of a crack and with magnetically different covers [9]. It has been found that the field of a covered defect exceeds the field of an open defect if the covering is of a certain thickness (1.5 mm) [7] and that with increasing induction in the part, the former increases more rapidly than the latter [8].

It should be noted that the work described in papers [7, 8] was done on one and the same specimen. The defect in the shape of a transverse crack was imitated by the authors of these papers by a gap formed between the ends of two cylinders (of 25 mm diameter) between which a paper washer of 0.02 mm thickness was inserted. The covering of the defect was imitated by "sleeve" tubes of 1.5 mm thickness, tightly fitted both to each other and to the surface of the cylinders. The specimen with the defect, with or without the cover, was pressed between the poles of a magnet in such a manner that the field was directed along the axis of the specimen. In the experiments the tangential component of the field of the defect was measured by the ballistic method.

This method of investigation has, however, generally speaking, two shortcomings. In the first place, the covering of the defect is not a single whole with the material of the deficient part. Secondly, it is not possible to control the size of the defect in the direction of the external field in the presence of the covering. It was therefore of interest to study the field of the defect as a function of the thickness of the covering metal layer in more correct conditions than those in the papers mentioned above. The present paper describes investigations of the field of a defect which are free from these shortcomings.

SPECIMEN AND METHOD OF INVESTIGATION

A plate of strongly cold hardness ferrosilicon containing 1 per cent silicon was used as the object to be magnetized. The dimensions of the plate were as follows: length 120 mm, width 80 mm and thickness 9 mm.

The defect imitated a continuous transverse crack and was situated in the middle of the plate (Fig. 1); its length (across the plate was 25 mm, and the distance between the walls of the defect in the direction of the longitudinal axis of the plate was 1.3 mm.

* *Fiz. metal. metalloved.*, 8, No. 5, 689-693, 1959.

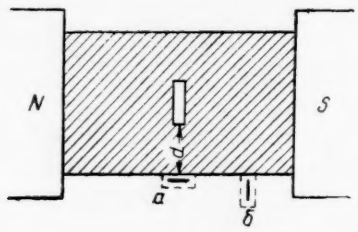

FIG. 1. Schematic drawing of the position of the defect in the plate, its position between the poles of the electromagnet and the orientation of the cores of the probe during the measurements of the tangential (a) and normal (b) components of the field of the defect.

An electromagnet with pole shoes of 150 × 48 mm size served to provide the field; the specimen was clamped between the poles of the magnet as shown in Fig. 1. It should be noted that the electromagnet in the absence of the defect in the plate created a homogeneous magnetization in the middle part of the plate to within 60 mm of its length.

The thickness of the covering layer was determined from the distance between the lateral edge of the plate and the edge of the gap which imitates the defect. It was changed by planing off the corresponding layers from the lateral surface of the plate.

The field of the defect is determined, as we know, by the relation

$$\vec{H}_d = \vec{H} - \vec{H}_0,$$

where $\vec{H}_d$ is the field of the defect; $\vec{H}_0$ the primary field and $\vec{H}$ the resulting field.

Iron probes were used to measure the fields $\vec{H}$ and $\vec{H}_0$. The cores of the probes were made from 4-79 permalloy subsequently annealed in a vacuum and had a length of 6 mm and a diameter of 0.3 mm. The primary winding of the probes consisted of 350 turns, the secondary winding of 360 turns. The probes operated at a frequency of 10 kc/s with an exciting current of 15 mA. The measurements were made both on the rising and the descending branch of the graduating curve and the moment of transition from the one to the other was easily fixed from the inertness of the electromagnet. The probes permitted measurements of magnetic fields within a range of from 2-3 to 300 oersted.

A schematic drawing of the circuit of the iron probes is given in Fig. 2. The exciting current was controlled with the aid of the voltmeter 5. The readings of voltmeter 6 enabled the field in which the probe finds itself to be determined with the aid of a correspondingly graduated curve. The following quantities were measured in the experiments:

1. The tangential component of the resultant field. For this purpose the probes were placed with their cores parallel to the lateral surface of the plate and moved along it until the maximum values were obtained.

2. The tangential component of the primary field. For its determination the place where the normal component of the resultant field becomes zero was first found. For this purpose the probe with its cores was placed perpendicularly to the lateral surface of the plate and moved along it until zero was indicated. After that the probe was rotated in that place for the measurement of the tangential component of the field.

3. The induction in the specimen. It was determined in the same section of the plate where the measurement of the tangential component of the primary field was made. The induction was measured with the ballistic method through the medium of one loop enveloping the plate, by means of reversing the current in the electromagnet.

RESULTS OF THE EXPERIMENT AND DISCUSSION

Fig. 4 shows the curve of the dependence of the field of the defect on the induction in the plate for various thicknesses of the cover over the defect. The curves given in this figure show that the field of the defect increases uniformly with decreasing thickness of the cover. This is in agreement with the data for the field of the cylindrical defect [1-4] but differs from that obtained in papers [7-8]. With the object of discovering the causes of this difference investigations were made to find out the degree of permanence of the width of the defect and the effect of any impermanence on the field of the defect. For this purpose we used the same cylindrical specimen which had been used for the study of the field of the defect in papers [7, 8] in the absence

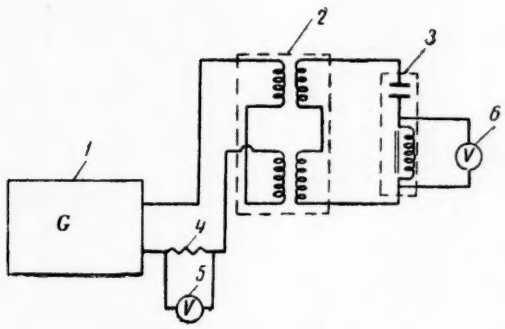

FIG. 2. Schematic drawing of the arrangement for measuring the fields:
1 – of the 3G-10 generator;
2 – of the iron probes;
3 – filter tuned to a frequency of 20 kc/s;
4 – resistance of 100 Ω;
5 – and 6 – electronvoltmeters.

VOL. 8 1959

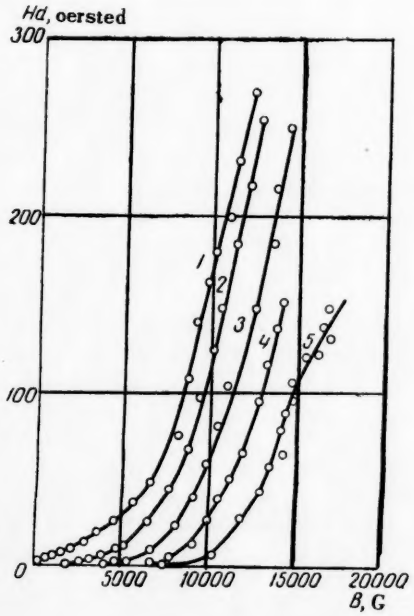

FIG. 3. Dependence of the tangential component of the field H of the defect on the induction B in the plate with a thickness of the cover of the defect of 1 – 0; 2 – 2.5 mm; 3 – 7.4 mm; 4 – 7.4 mm; 5 – 28.3 mm.

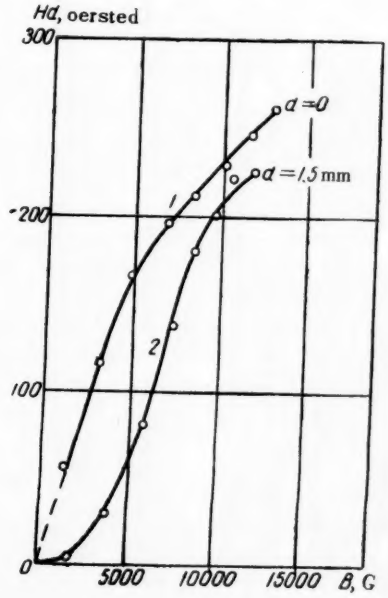

FIG. 4. Dependence of the tangential component of the field H of the defect on the induction B for specimens from paper [7] with a width of the defect of 0.24 mm:
1 – in the absence of a cover;
2 – in the presence of a cover of 1.5 mm thickness.

and in the presence of a cover.

1. The width of the defect in the direction of the primary field was made to be 0.24 mm by inserting three layers of graph paper. Then the tangential components of the resultant and the primary field were measured with the iron probes in the same order as in the case of the above described study of the field of the defect in the plate. The results of this investigation are given in Fig. 4. The figure shows that the field of an open defect is greater

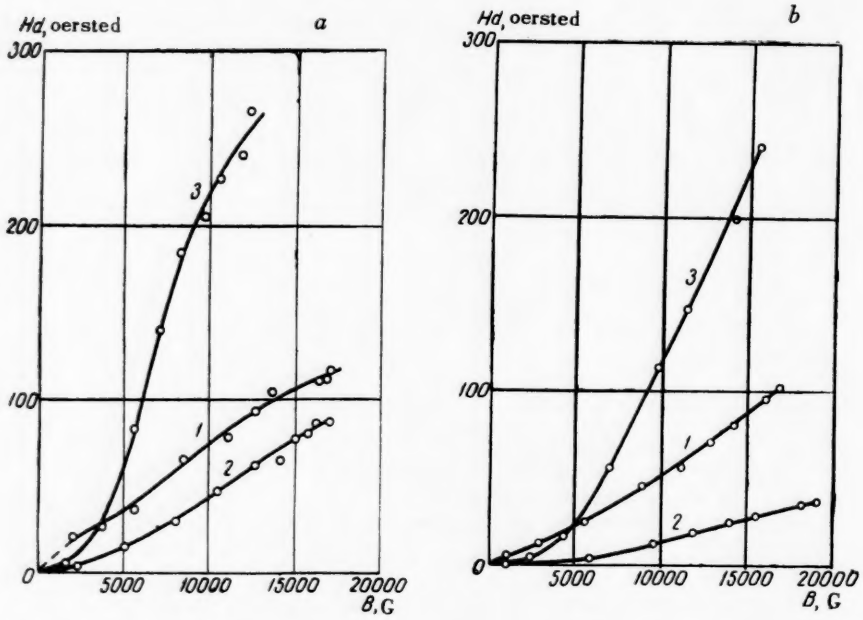

FIG. 5. Dependence of the tangential component of the field H of the defect on the induction B in the same specimen as in Fig. 4:
a — obtained with the method of the iron probes;
b — obtained with the ballistic method.
1 — in the absence of a cover;
2 — in the presence of a cover of 1.5 mm and an additional washer between one of the cylinders which from the defect and the pole shoes of the electromagnet;
3 — with the same cover, but in the absence of a washer between the cylinder and the pole of the electromagnet.

than that of a defect covered with a layer of metal.

2. The width of the defect in the direction of the primary field was 0.02 mm, but between the end of one of the cylinders which form the defect and the surface of the pole of the electromagnet a round disk of transformer iron of the same diameter as the cylinders and 0.35 mm thickness was placed. In this case the tube which covered the defect did not quite reach the surface of the pole of the electromagnet. The results of the investigation of the field of the covered defect in the presence and absence of the above mentioned washer are given in Fig. 5.

The figure shows that the field of the open defect in this case, too, is greater than the field of the covered defect. It should be noted that curve *3* of Fig. 5 agrees with curve *2* in Fig. 4. The first refers to a width of the defect of 0.24 mm, the second to the same defect but a width of 0.02 mm. It follows from this that in the absence of the 0.35 mm washer between the pole and the cylinder a movement of the cylinders away from other takes place underneath the tube which covers them when the field is switched on, causing an increase in the distance between them compared with the defect in the absence of the cover.

Thus, the increase in the field of the defect when the cover is put on it, which was observed in paper [7, 8], was the consequence of a change in the dimensions of the defect in the direction of the external field made possible because the sleeve was 0.24 mm longer than the length of the two cylinders.

3. The experiments made to obtain Fig. 5a were also repeated with the ballistic method. A flat measuring coil was used in this case, which had the following dimensions: 15.8 mm across the primary field and 5.2 mm in its direction. The centre of the coil was at a height of 4.3 mm above the surface of the specimen. The results obtained in this case are given in Fig. 5b.

As this figure shows, the order of the position of the curves remains the same as in Fig. 5a, but the curves themselves are situated a little lower. This is apparently a result of the greater neutralization of the field in the ballistic measurements compared

with the neutralization of the field in the measurements with the iron probes, and also of the inertness of the electromagnet which increases the ballistic error.

CONCLUSIONS

In this way it has been shown that the magnetostatic field of a crack defect increases with decreasing thickness of the cover, which is in agreement with data in the reference on the field of a cylindrical defect. The results which differed from this, which were obtained in paper [7, 8] are the consequence of an experimental error.

In conclusion we take the opportunity to express our gratitute to Professor R.I. Ianus for certain critical comments.

Translated by B. Ruhemann

REFERENCES

1. A.V. Talitskii and N.I. Pogozhev, *Vestnik metallopromyshlennosti* 2, 10 (1933).
2. A.B. Sapozhnikov and Ye.D. Malerevich, *Trud. Sib. fiz. tekh. inst.* No. 24, p. 240, Tomsk (1947).
3. N.V. Lambin, *Izv. Akad. Nauk BSSR* No. 4 (1952).
4. L.F. Il'iushenko, *Eksperimental'nyye metody magnitnoi defektoskopii (Experimental methods of the magnetic detection of defects), kandidatskaia dissertatsiia* (1953).
5. T.M. Sycheva and A.B. Sapozhnikov, *Trud. Sib. fiz. tekh. inst.* No. 28, p. 385, Tomsk (1949).
6. A.B. Sapozhnikov, *Trud. Sib. fiz. tekh. inst.* No. 26, Tomsk (1948).
7. V.V. Vlasov and E.E. Stoinskaia, *Fiz. metal. metalloved.* 4, 552 (1957).
8. V.V. Vlasov and L.Z. Piatigorskaia, *Fiz. metal. metalloved.* 5, 376 (1957).
9. V.V. Vlasov and L.Z. Piatigorskaia, *Fiz. metal metalloved.* 5, 377 (1957).

VOL. 8 1959

THE THERMOELECTRIC PROPERTIES OF MAGNETITE IN THE TEMPERATURE REGION OF 80-400°K *

A.A. SAMOKHVALOV and I.G. FAKIDOV

Physics of Metals Institute of the Academy of Sciences of the U.S.S.R.

(Received 15 May 1959)

With the object of obtaining new information on the energy spectrum of the conductivity electrons of the ferromagnetic semiconductor magnetite, its thermoelectric properties were studied in the temperature region which includes both the region of the ordinary ferromagnetic state of magnetite and the region of the low temperature transformation. Certain data on the chemical potential of the group of conduction electrons and on the low temperature transformation of magnetite has been obtained.

The question of the energetic spectrum and the nature of the interactions of the electrons of a ferromagnetic which are responsible for its magnetic and electric properties is very important for the physics of ferromagnetism. The theoretical and experimental clarification of this question will make it possible to solve a number of problems connected with the improvement of the properties of ferrites, in particular to explain the mechanism of their electric conductivity.

The present paper, which is part of a series of investigations of the electric properties of magnetite, gives the results of the study of its thermoelectric properties with the object of obtaining certain data on the energy spectrum of the conductivity electrons and the low temperature transformation in magnetite.

We know that magnetite is a semiconductor and an uncompensated ferromagnetic. In the temperature region of $\sim$ 118°K magnetite undergoes a transformation at which anomalies of the magnetic [3, 4], electric [4, 6], galvanomagnetic [4-6], thermal [2] and other physical properties are observed (see,e.g. [7, 9]). Thus, the investigation of magnetite in the temperature region of 80-400°K makes it possible to clarify the peculiarities of the energy spectrum of the conductivity electrons both in the region of the usual ferromagnetic state of magnetite and in the region of its low temperature transformation where the magnetic characteristics (for example the parameter of the magnetic anisotropy) change rapidly.

SPECIMENS AND METHOD OF MEASUREMENT

The thermo-e.m.f. was measured in six single crystal specimens of natural magnetite and one polycrystalline specimen. Specimens *1, 3, 4, 6* were cut from one large octahedral single crystal of magnetite, specimens *2* and *5* from two other single crystals of magnetite. Specimens *1-6* had the form of disks of the approximate dimensions 8.15 × 5.60 × 2.15 mm (specimen *4*) and 9.20 × 7.00 × 2.10 mm (specimen *6*). The other specimens were of similar dimensions. The polycrystalline specimen *7* was considerably larger: 50 × 12×6 mm.

During the measurements in the temperature region of 300-400°K the specimens were placed in a thermostat of the Gepler type. Beginning with the temperature of boiling nitrogen and above we used a cryostat similar to that described in [15]. This cryostat was altered a little so that measurements could be made in the gap between the poles of the electromagnet.

The design of the cyostat and its main dimensions are given in Fig. 1. The cryostat consists of two Dewar vessels: an outer one *1* and an inner one *2* placed bottom upwards in the outer vessel and projecting outwards into the space between the poles of the electromagnet. A copper tube or rod *3*, in the upper part of which the specimen *4* to be studied is mounted in section A, was placed inside the Dewar vessel *2*. The furnace *5* of 10-20 W capacity was wound on the tube. When the outer vessel is filled with liquid nitrogen a gas bubble forms in the inner vessel which prevents liquid nitrogen from entering vessel *2*. Some time after the vessel has been filled with liquid nitrogen

* *Fiz. metal. metalloved.*, 8, No. 5, 694-699, 1959.

VOL
8
195

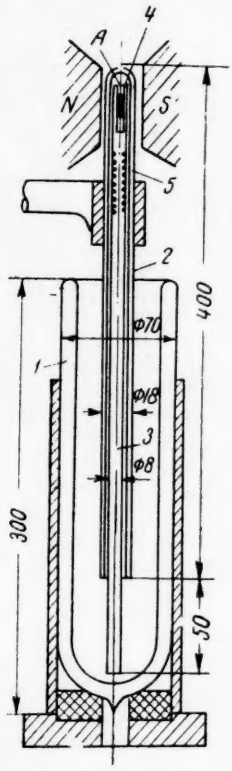

FIG. 1. Schematic drawing of cryostat.

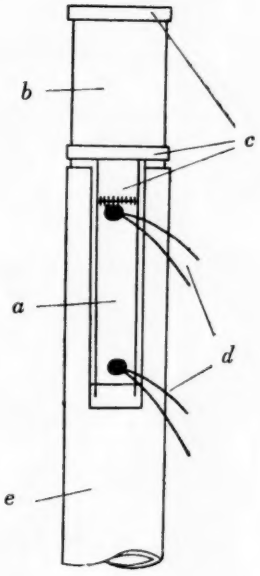

FIG. 2. Schematic drawing of arrangement for measuring the coefficient of the thermo-e.m.f.

the specimen *4* has cooled down to a temperature close to that of boiling nitrogen.

By changing the strength of the current in the furnace *5* (fed from a ferroresonance stabilizer) one can evenly change the temperature of the specimen to 300-400°K.

Fig. 2 shows the details of the arrangement for measuring the thermo-e.m.f. force. The difference in the temperatures on the specimen was created by the furnace *b* wound on the copper block *c*. The magnetite specimen *a* was soldered to the copper block and together with it was then placed in the gap of the upper part of the tube of the cryostat. The temperatures of the joints were measured by two copper-constantan thermocouples *d* soldered to the lateral edges of the specimen away from the main heat flow.

For the measurement of the thermo-e.m.f. force on specimen 7 (which was 50 mm long) the furnace creating the temperature difference ΔT was wound directly on the specimen. The thermocouples were also soldered to the lateral edges of the specimen. The specimen with the furnace and the thermocouples, surrounded by a second furnace for the changing of the temperature of the specimen as a whole, was placed in a test tube which in turn was placed in the Dewar vessel with liquid nitrogen.

The thermo-e.m.f. and the temperature of the joints of the specimens were measured by the compensation method with the aid of a low resistance potentiometer. By preliminary experiments the absence of a dependence of the coefficient of the thermo-e.m.f. α on the difference in the temperatures ΔT of the joints was established (see Fig. 3). The figure shows that for $\Delta T \geqslant 1°$ the coefficient of the thermo-e.m.f. does not depend on the difference in the temperatures of the joints. During the measurements in the temperature region of liquid nitrogen the temperature difference was usually 3-5°, and at higher temperatures 8-10°. The error of measurement of α at liquid nitrogen temperature was roughly 15 per cent and at higher temperatures 5-8 per cent

The electric resistance of the specimens was measured simultaneously with the measurement of the thermo-e.m.f. in order to establish the correlation between these characteristics. The temperature

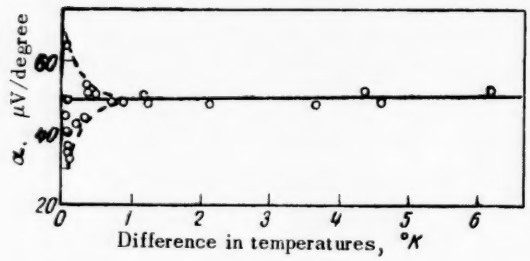

FIG. 3. Dependence of the coefficient of the thermo-e.m.f. on the difference in the temperatures of the joints.

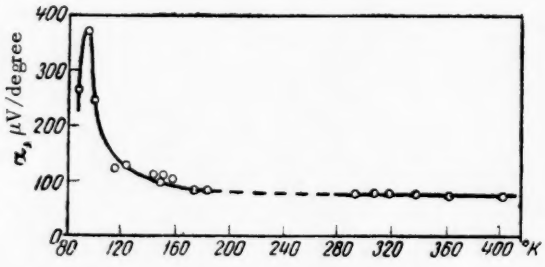

FIG. 4. Temperature dependence of the coefficient of the thermo-e.m.f. of a single crystal of magnetite (specimen *1*).

dependence of the initial magnetic permeability was also measured on certain specimens in order to determine the temperature of the transition from the jump in the magnetic permeability.

RESULTS OF THE MEASUREMENTS

All magnetite specimens had a negative sign of the thermo-e.m.f. corresponding to electron conductivity.

The results of the measurement of the thermo-e.m.f. in a single crystal of magnetite (specimen*1*) in the temperature region of 90-400°K are given in Fig. 4. In the region of room temperatures α changes slightly, then on lowering the temperature reaches a maximum and again decreases. The measurements of the thermo-e.m.f. in the other single crystal specimens gave a similar result. The maximum mentioned above occurs at a temperature of 95 ± 2°K.

Fig. 5 shows the results of the measurement of the temperature dependence of the thermoelectromotive force and the electric resistance of magnetite (specimen *6*) in the region of the low temperature transformation. The figure shows ln r and α as functions of the reciprocal temperature ($10^3/T$). The position of the maximum of α coincides with the break B in the curve ln r ($10^3/T$) at the transition into the temperature region lying below the region of the low temperature transformation. The other limit of the region of the transformation, as can be seen from the break A in the curve ln r ($10^3/T$), occurs at the temperature of 114 ± 2°K. A similar correlation was also observed for the other magnetite specimens. The magnetic permeability of these specimens changes at a temperature of 109 ± 2°K.

The results of the measurements of the electric resistance and for specimen *7* are given in Fig. 6.

The absence of a jump in the resistance (there is only a break) at the transition temperature, equal here to 109 ± 1°K correlates with the absence of a sharp increase in α when the specimen is cooled in the region of the low temperature transformation. On cooling below the temperature of the transformation the quantity α for specimen *7* decreases sharply. The absence of a noticeable jump from the curve ln r ($10^3/T$) for specimen *7* is apparently due to the fact that its chemical composition differs noticeably from the stoichiometric. Bearing in mind the results of papers [8, 10] on the connexion of the size of the jump and the temperature of the transition with the deviation of the chemical composition of the specimen from the stoichiometric, one can approximately estimate that for specimen *7* $Fe_2O_3/FeO = 1.05$,

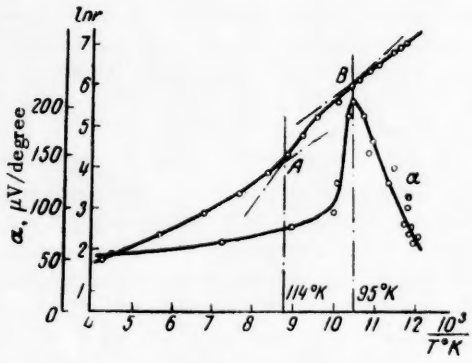

FIG. 5. Coefficient of the thermo-e.m.f. and the electric resistance of magnetite in the region of the low temperature transformation (specimen 6).

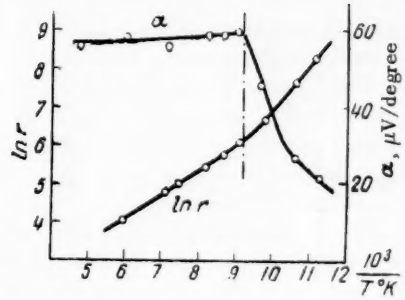

FIG. 6. Coefficient of the thermo-e.m.f. and the electric resistance of magnetite (specimen 7).

while for the composition of specimen *1* this ratio is considerably closer to one.

Hence, we find:

1. In a wide temperature region of the usual ferromagnetic state of magnetite the coefficient of the thermo-e.m.f. α is constant (with an accuracy of up to 5-8 per cent) and compared with other semiconductors small: 50-80 μV/degree.

2. In the region of the low temperature transformation the quantity α increases (which correlates with the jump in the curve for the electric resistance). The size of this effect is apparently linked with the deviation of the chemical composition of the magnetite specimen from the stoichiometric.

3. On cooling below the temperature region of the transformation the quantity α drops sharply for all specimens.

DISCUSSION OF THE RESULTS

At the present time the absence of a consistent multi-electron theory of electric (in particular thermoelectric) phenomena in ferromagnetics makes it very difficult to interpret our results. The application of the kinetic theory of semiconductors can in this case evidently not be regarded as valid, for a number of reasons. In paper [16] it was, e.g. shown that the conductivity electrons in magnetite have low mobility (several cm²/sec) at room temperature). But for substances with such low mobility the conclusions of the kinetic theory [1] lose their meaning. Another reason is the presence of antiferromagnetic bonds in magnetite which cannot be consistently accounted for with the single electron theory, but which can materially affect the energy spectrum of the conductivity electrons. Finally, Verwey's hypothesis suggests a mechanism for the electric conductivity in magnetite which differs essentially from the usual semiconductor mechanism of the electric conductivity with great length of the free path which lies at the basis of the kinetic theory.

One can, however, attempt to obtain data on the chemical potential of a group of conduction electrons by using the thermodynamic relations between the coefficient of the thermo-e.m.f. α and the flux of electrons S [1, 14]

$$\alpha = \frac{S}{e} = -\frac{k}{e}(\varepsilon^* - \mu^*), \qquad (1)$$

where $\overline{\epsilon}^*$ is the average reduced energy of the electrons which take part in carrying the current (in kT units) [11];

μ^* is the reduced chemical potential (in kT units);

k is the Boltzmann constant;

e is the electronic charge.

In estimating the size and temperature dependence of the chemical potential from formula (1) it is necessary to bear in mind the possibility of a strong degeneration of the electron gas in magnetite, which is indicated by the low value of α and its constancy in a temperature region and also by the predominantly ion nature of the chemical bonds in magnetite and the fact that the temperature region investigated is a region lying below the Debye temperature of magnetite. (Using the data of the paper on the technology of magnetite [2] one can estimate the Debye temperature as 540°K. The estimate of the Debye temperature from the elastic properties of magnetite gave 500°K).

VOL. 8 1959

Using the graphic solution of equation (1) given in [13] the following result was obtained. In the temperature region above 200°K the chemical potential has a positive value independent of the temperature, corresponding to a strong degeneration of the conductivity electrons in magnetite. When the temperature is lowered to below 200°K the chemical potential is reduced and in the region of the low temperature transformation goes over into the region of negative values which indicates a reduction in the degeneration. The result obtained for the strong degeneration of the conductivity electron collective is in agreement with the high concentration of the conductivity electrons of 10^{20} cm^{-3} obtained from the measurement of the Hall effect in magnetite [12, 16]. Thus, the measurement of the thermo-e.m.f. also confirm the result concerning the low mobility of the conductivity electrons (a few cm^2/sec) and its sharp drop when the temperature is raised, which was obtained from the Hall effect and the electric conductivity [16].

In the region of the low temperature transformation the coefficient α has a sharp anomaly. In attempting to interpret this anomaly one must bear in mind the parallel measurements of the electric resistance of magnetite. The comparatively sharp increase in the coefficient in the region of the transformation is apparently determined by the rapid decrease in the concentration of the conductivity electrons with electron ordering, which, according to Verwey's hypothesis, occurs in the low temperature transformation. The change in the temperature curve of the coefficient α below $\sim$ 95°K indicates a considerable change in the energy spectrum of the conductivity electrons in the low temperature transformation.

Comparison of the data of the parallel measurements of the thermo-e.m.f. and the electric resistance indicates that the anomaly connected with the low temperature transformation occurs 14-15° lower than the temperature of the transformation in magnetite. This is confirmed by the measurements of the Nernst-Ettinghausen thermomagnetic effects in magnetite [17].

Translated by B. Ruhemann

REFERENCES

1. A.F. Ioffe, *Fizika polyprovodnikov (Physics of semiconductors)*, Izd. Akad. Nauk SSSR (1957).
2. R.W. Millar, *J. Amer. Chem. Soc.* 51, 215 (1929).
3. P. Weiss and R. Forrer, *Ann. d. Phys.* 12, 279 (1929).
4. C.A. Domenicali, *Phys. Rev.* 78, 458 (1950).
5. P.A. Khalileyev, *Sow. Phys.* 7, 2, 108 (1935).
6. T. Okamura and Y. Torizuca, *Sci. Rep. Inst. Tohoku Univ. A*, 2, 3, 352 (1950).
7. M.E. Fine and N.T. Kenney, *Phys. Rev.* 94 (6), 1577 (1954).
8. E.I.W. Verwey, P.W. Haayman and F.C. Romeijn, *J. Chem. Phys.* 15, 181 (1947).
9. S.C. Abrahams and B.A. Calhoun, *Acta cryst.* 8, 257 (1955).
10. E.I.W. Verwey, *Phys.* 8, 979 (1941).
11. R. Wright, *Proc. Phys. Soc. A*, 64, 11 (1954).
12. A.A. Samokhvalov and I.G. Fakidov, *Fiz. metal. metalloved.*, 4, 2, 249 (1957).
13. A.G. Samoilovich and L.L. Korenblit, *Urals, fil. nauk.* 57, 4, 577 (1955).
14. F.I. Morin, *Phys. Rev.* 98, 6, 1194 (1954).
15. N.V. Zavaritskii, *Pribory i tekhnika eksperimenta* 2, 140 (1956).
16. A.A. Samokhvalov and I.G. Fakidov, *Fizika tverdogo tela (Physics of solids)* (in the press).
17. A. A. Samokhvalov and I.G. Fakidov, *Fiz. metal. metalloved.*, (in the press).

X-RAY STUDY OF THE TEMPERATURE DEPENDENCE OF DEFECTS IN THE CRYSTAL LATTICE OF METALS*

G.A. SIRENKO and V.I. KHOTKEVICH

Kharkov State University

(Received 4 June 1959)

The mean linear size of the areas of coherent scattering and the microstrains in Al and Pb plastically deformed in the temperature interval of from 90-293°K was studied with the method of harmonic analysis.

It is shown that when the temperature of the deformation is changed, the size of the areas of coherent scattering changes in such a way that (*a*) for every degree of deformation there exists a certain temperature limit above which deformation does not produce an observable decrease in the area of coherent scattering; (*b*) this temperature is the higher, the lower the degree of deformation and vice versa.

The residual microstrains in the lattice which emerge are linked with the temperature of the deformation in a similar manner. A certain limiting deformation corresponds to each deformation temperatures; for greater deformations no residual microstrains develop.

VOL. 8 1959

1. In previous papers [1, 2] it has been shown that a reduction in the temperature of the deformation causes a marked reduction in the size of the areas of coherent scattering (a.c.s.) and a growth in the microstrains.

It was of interest to make detailed study of the nature of the dependence of these properties of the temperature of the deformation in a large temperature interval, particularly for small deformations.

2. Large specimens of technically pure aluminium and spectrally pure lead were plastically deformed by uniaxial compression at 90, 195, 255 and 293°K.

Immediately after deformation, without heating in between, the specimen was placed in a low temperature camera [1] and during the X-ray photograph was kept at the temperature of liquid oxygen to prevent relaxation.

The X-ray photographs were taken with copper radiation by the back reflection method, using a sharp focus X-ray tube in which the size of the focal spot could be adjusted. The aluminium line (511) and the lead line (620) were studied.

The mean linear size of the areas of coherent scattering and the microstrains were determined with the method of harmonic analysis of the form of the interference line.

The method of X-ray photography and the treatment of the results have been described in greater detail earlier [2].

3. Figs. 1a and 2a show the curves of the mean linear size of the a.c.s. as a function of the amount of deformation for the metals studied at the above mentioned temperatures. As can be seen from the figures (and was noted earlier [2]), the lowering of the temperature of deformation reduces the linear size of the areas of coherent scattering.

A certain difference in the numerical data compared with those published earlier [2] must evidently be ascribed to the fact that in this work a different crystallographic direction was studied (the photographs were taken with a different radiation). The existence of an anisotropy in the distribution of the sizes of the areas of coherent scattering over different crystallographic directions has not been reported, but is quite probable. This suggestion is confirmed by the data of paper [3] in which the presence of a marked anisotropy of the microdeformations for different crystallographic directions was observed. An important role is probably also played by differences in the purity of the original specimens and by the considerable margin of error of the method of calculation itself.

Figs. 1b and 2b show the dependence of the mean linear size of the areas of coherent scattering $\bar{D}$ on the temperature of deformation. As can be seen from the figures, the size of the areas of coherent scattering decreases continuously with decreasing temperature of deformation. When this dependence is plotted in semi-logarithmic

* *Fiz. metal. metalloved.*, 8, No. 5, 700-704, 1959.

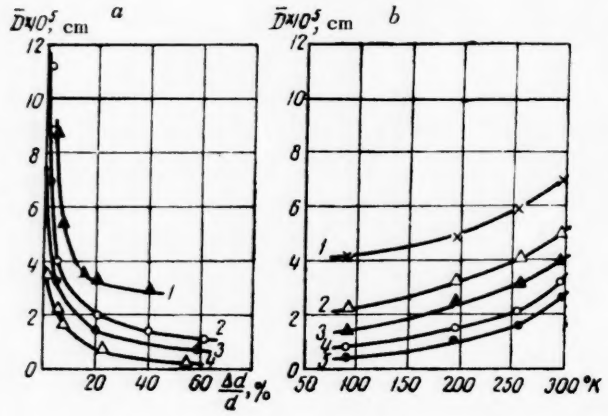

FIG. 1. *a* – Mean linear size of the areas of coherent scattering of aluminium as a function of the degree of deformation $\Delta d/d$ for various temperatures of deformation;
1 – 293°, 2 – 255°, 3 – 195°, 4 – 90°K.
b – Mean linear size of the areas of coherent scattering $\bar{D}$ as a function of the temperature of deformation for varying degrees of deformation;
1 – $\Delta d/d$ = 2%; 2 – $\Delta d/d$ = 5%; 3 – $\Delta d/d$ = 10%; 4 – $\Delta d/d$ = 20%; 5 – $\Delta d/d$ = 40%.

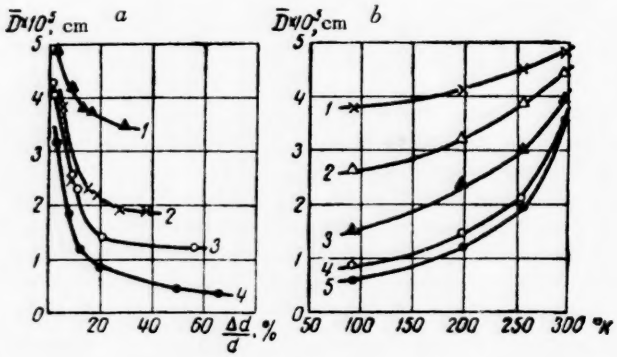

FIG. 2. *a* – Mean linear size of the areas of coherent scattering of lead as a function of the degree of deformation $\Delta d/d$ at various temperatures of deformation;
1 – 293°, 2 – 255°, 3 – 195°, 4 – 90°K.
b – Mean linear size of the areas of coherent scattering of lead *D* as a function of the temperature of deformation at varying degrees of deformation;
1 – $\Delta d/d$ = 2%; 2 – $\Delta d/d$ = 5%; 3 – $\Delta d/d$ = 10%; 4 – $\Delta d/d$ = 20%; 5 – $\Delta d/d$ = 40%.

co-ordinates it is seen that the points of each curve lie fairly well on a straight line which can be extrapolated to its intersection with a line, parallel to the axis of the abscissae, which corresponds to the equilibrium size of the areas of coherent scattering in the original material. Since there are no data on this size, we adopted conventionally the greatest size of the areas of coherent scattering observed in experiments for the equilibrium size.

Fig. 3 shows this dependence for aluminium. The lower limit for the equilibrium size of the areas of coherent scattering in the figure corresponds to the greatest size $\bar{D}$ observed in experiments (for specimens deformed at 500°K). The figure shows that the

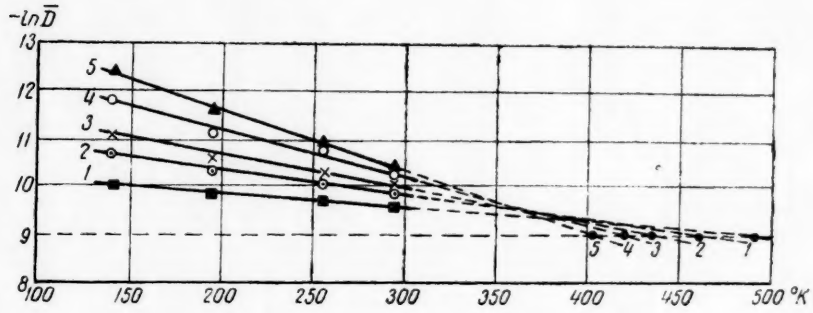

FIG. 3. Ln $\bar{D}$ ($\bar{D}$ being the mean linear size of the areas of coherent scattering) as a function of the temperature of deformation for varying degrees of deformation;
1 – $\Delta d/d$ = 2%; 2 – $\Delta d/d$ = 5%; 3 – $\Delta d/d$ = 10%; 4 – $\Delta d/d$ = 20%; 5 – $\Delta d/d$ = 40%.

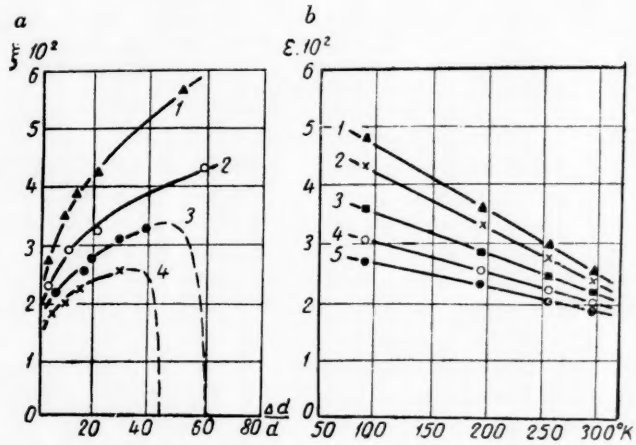

FIG. 4. *a* – Mean relative defo. mation

$$\bar{\varepsilon} = \frac{\sqrt{\Delta L^2}}{L}$$

of lead as a function of the degree of deformation at various temperature of deformation;

1 – 90°, 2 – 195°, 3 – 255°, 4 – 295°K.

b – Mean relative of deformation for varying degrees of deformation;
ation for varying degrees of deformation;

1 – 30%; 2 – 20%; 3 – 10%; 4 – 5%; 5 – 3%.

straight lines which correspond to various deformations intersect the line of the equilibrium size of the areas of coherent scattering at different temperatures, which are the lower, the greater the degree of deformation*.

The point of intersection evidently determines the temperature of deformation above which deformation to the given or a greater degree does not cause any reduction in the areas of coherent scattering. In other words, an increase in the degree of deformation causes a lowering of the temperature of deformation at which a reduction in the areas of coherent scattering ceases to be observed.

A low degree of deformation causes a reduction in the areas of coherent scattering at higher temperatures of deformation and vice versa, a greater

* The fact that we do not know the true equilibrium size of the areas of coherent scattering in the original material is irrelevant, for one can easily see that this will only slightly shift the point of intersection without changing the nature of the regularity itself.

VOL. 8 1959

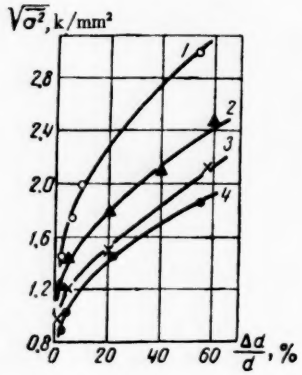

FIG. 5. Dependence of the microstrains

$$\sqrt{\overline{\sigma^2}}$$

on the degree of deformation $\Delta d/d$ in aluminium specimens deformed at various temperatures;
1 – 90°, 2 – 195°, 3 – 255°, 4 – 293°K.

deformation has no effect on the sizes $\bar{D}$ at lower temperatures. Data given in the literature on the dependence of the recrystallization temperature on the degree of deformation [4] in essence confirm the conclusion drawn here which is easy to understand if one bears in mind that at greater degrees of deformation the overwhelming part of the work of deformation is transformed into heat so that the relaxation processes occur to a considerable extent in the course of the deformation itself. This viewpoint is in agreement with the data of paper [5] where it is shown that for small degrees of deformation virtually all the work spent on deformation is transformed into the energy of the defects of the crystal lattice. With increasing degree of deformation the relative absorption of energy is sharply reduced. This is clearly confirmed by the observations on lead. The deformation of lead to 40-60 per cent at room temperature (photograph at 90°K), as was to be expected, yields sharp lines in the X-ray photograph which do not differ from the lines of the standard. Deformation to 2-3 per cent however, causes a marked washing of the reflections.

4. Besides the size $\bar{D}$ the values of the absolute

$$\sqrt{\overline{\Delta L^2}}$$

and relative deformation

$$\frac{\sqrt{\overline{\Delta L^2}}}{L} = \varepsilon$$

were also calculated. The nature of the changes in these quantities when the temperature of deformation is reduced agrees with the data of paper [2]: the lowering of the temperature of deformation continually increases

$$\sqrt{\overline{\Delta L^2}} \text{ and } \varepsilon.$$

By means graphic integration and averaging over the depth of the column (600 and 800 Å for lead and aluminium respectively) the value of the mean relative deformation $\bar{\epsilon}$ was calculated. The curves for the dependence of this quantity on the degree of deformation for specimens of lead deformed at various temperatures are given in Fig. 4. As the figure shows, for each temperature of deformation there exists a clearly marked region of deformations for which residual microstrains still exist. The lowering of the temperature of deformation widens this region so that at a temperature of deformation of 90°K it becomes impossible to stipulate a deformation at which there are no strains at all. This conclusion is in complete agreement with the conclusion drawn regarding the connexion of the sizes of the areas of coherent scattering with the degree of deformation and the temperature of deformation.

Using the value for ϵ it is easy to calculate the average size of the microstrains. For the correct calculation it is evidently necessary to use the value of the elasticity module which corresponds to the given crystallographic direction and temperature. This is proved possible to do for aluminium [6-8]; the results of this calculation are given in

Fig. 5 where $\sqrt{\overline{\sigma^2}}$ for various temperatures of deformation.

is plotted as a function of the degree of deformation

Translated by B. Ruhemann

REFERENCES

1. Iu.S. Terminasov and V.F. Mindukshev, *Kristallographiia* 2, 4, 514 (1957).
2. V.P. Golik, G.A. Sirenko and V.I. Khotkevich, *Fiz. metal. metalloved.*, (in the press).
3. O.N. Shivrin and B.M. Mimukhin, *Izv. vysshykh uchebnykh zavedenii razdel fizika* No. 3, 135 (1958).
4. M.P. Slavinskii, *Fiziko-khimicheskiye svoistva elementov (The physico-chemical properties of the elements)* Metallurgizdat (1952).
5. V.I. Khotkevich, E.F. Chaikovskii and V.V. Zashkvara, *Fiz. metal. metalloved.* 1, 2, 206 (1955).
6. *Spravochnik po rentgenovstrukturnomu analizu, (Handbook on X-ray structure analysis)* ed. A.I. Kitaigorodskii, Gostekhizdat (1940).
7. B. Shmidt and V. Boas, *Plastichnost' kristallov v osobennosti metalicheskikh (The plasticity of crystals, in particular metal crystals)* CONTI NKTP SSSR (1938).
8. P. Sutton, *Phys. Rev.* 91, 4, 816 (1953).

VOL.
8
1959

SOME PECULIARITIES IN THE STRUCTURE OF ANOMALOUS EFFECTS IN POWDER DIFFRACTION PATTERNS OF AGEING Al-Ag and Al-Ag-Cu ALLOYS*

R.R. ZAKHAROVA and N.N. BUINOV

Institute of Physics of Metals of the Academy of Sciences of the U.S.S.R.

(Received 7 February 1959)

The technique of anomalous scattering of X-rays serves as one of the effective methods of investigating structural changes associated with the process of supersaturated solid solutions breakdown. The method enables a correct interpretation to be made of the anomalous effects in the region of anomalous scatter (R.A.S.). In order to obtain additional information about the structure of the anomalous scatter region in a crystal undergoing the process of ageing, an analysis was made of the effects of anomalous scatter on the radiograms of the Al-Ag and Al-Ag-Cu alloys.

Powder diffraction patterns of coarsely-quenched specimens of the Al-Ag (20 % Ag) and Al-Ag (20%)-Cu (0.1, 1.0 and 5 % Cu contents)† show anomalous effects in the form of diffused spots and halos. After a short preliminary ageing, their intensity increases and the extent of them decreases. It was established in investigations [1] that, in the reciprocal space, there correspond to these effects certain regions of anomalous scatter in the shape of full spheres with the intensity maximum in the centre. On the basis of work [2], each of the spheres is regarded as being formed in consequence of a superimposition of two anomalous scatter regions on each other, the regions being spherical in shape but having different dimensions. One of them is conditioned by equi-axial Guinier-Preston zones, enriched with silver atoms, and the other depends on the dimensions and form of the matrix distortion regions in which the zones are situated ("hole" effect). In consequence of a small difference in crystalline lattice constants of the crystals in the matrix and in the zones, the anomalous scatter regions overlap one another. Hole and the Guinier-Preston zones produce an anti-phase type of X-ray scatter and therefore the overall intensity value is determined by the difference of the mean scatter capacity of zone atoms and that of the basic crystal lattice. Owing to different extents of the anomalous scatter regions of the zones and holes, the resultant distribution of the intensity around the centres of the reciprocal lattice assumes the form of a full sphere with intensity maximum corresponding to the sphere centre. The size of holes is greater than that of zones, because of a transitional layer, which exists between zones and the matrix.

The anomalous scatter regions which correspond to holes and are associated with crystal centres of the solid solution reciprocal lattice, were referred to by Elistratov as "type 1 regions", while the anomalous scatter regions corresponding to the Guinier-Preston zones, were termed "type 2 regions". (In radiograms, the effects of type 1 and 2 regions are separated by zero intensity regions, i.e. background intensity regions).

As a result of the investigations carried out, it was possible to establish the following characteristic features in the structure of the anomalous effects:

1. The intensity of that part of the halo, which is directed toward the centre of the radiogram (i.e. toward the trace of the primary X-ray beam) is higher than that of its reverse part (Fig. 1 a).

2. In the vicinity of Laue spots which overlap with the halo, there is found a rapid attenuation of the halo intensity, which diminishes right down to that of the background of the diffraction pattern. There appear "additional" regions of zero intensity* (in Fig. 1 b and c, this is shown by arrows).

The mechanism of formation of anomalous effects in X-ray diffraction patterns of Al-Ag alloys is shown in Fig. 2. According to the above mechanism, the higher intensity of a part of the halo directed toward the centre of the radiogram, is associated with the fact that the type 2 anomalous scatter

* *Fiz. metal. metalloved.*, 8, No. 5, 705-708, 1959.

† In all cases, the percentage content is expressed by weight.

* Further zero intensity regions can be seen more easily on the actual diffraction patterns.

VOL
8
195

FIG. 1. Form of anomalous effects in radiograms of the alloys:
a – Al-Ag (20% Ag content), quenched at 530°C;
b – Al-Ag (20% Ag) with 5% Cu; quenching temperature of 530°C;
c – Al-Ag (20% Ag content) with 0.1% Cu, quenched from 530°C.
Single arrow shows the direction of the primary X-ray beam spot; double arrow shows the position of the additional region of zero intensity.

region is displaced with respect to type 1 anomalous scatter region in the direction of co-ordinates origin of the reciprocal lattice. This fact indicates that the Guinier-Preston zone lattice constant is somewhat higher than that of the solid solution. If in the Al-Ag alloy, the Guinier-Preston zones are perfect, i.e. if the crystals in these zone have a non-deformed face-centred cubic lattice structure, then they should have a higher value of the lattice constant because the radius of the silver atom is higher than that of aluminium.

On the basis of radiograms and from the construction of the anomalous scatter regions, a diagram is shown in Fig. 3a,b,s of the intensity distribution near the reciprocal lattice centre, for the case when the lattice constants are identical in zone and matrix crystals, whereas in Fig. 3d,e,f, is shown the same intensity distribution but for the case when the lattice constants are slightly different (at the same time, Fig. 3b and 3f give a schematic representation of a halo during the passage of the reflection sphere through a crystal lattice in the reverse lattice matrix). According to the diagram (Fig. 3) the size of the type 2 anomalous scatter region is determined by the factor 0_2, this is by the external halo circumference, while the size of type 1 anomalous scatter region is determined by the distance between the halo blackening maxima, i.e. 0_1. The size of the zones and holes is found from the dimensions of the anomalous scatter regions. The difference in radii of zones and holes gives the width of the transition layer between the matrix and zones. It was found to be equal to 2-4 atomic layers (4-8 Å).

From the shift of one anomalous scatter region with respect to the other it is possible to determine the Guinier-Preston zone constant, provided that the crystal lattice constant of the solid solution is known. This shift does not exceed

$$\frac{x_1 - x_2}{2} = 0.2 \text{ mm}$$

(in Fig. 3f, x_1 and x_2 correspond to the halo width values in the direction radial with respect to the primary X-ray spot on the radiograph). It can be easily shown by calculation that the Guinier-Preston zone lattice constant should, in this case, not exceed 4.0463 ± 0.004 Å, while the crystal lattice constant of the solid solution matrix as determined by the Zaks's method is 4.0437 ± 0.0004 Å.

If it is assumed that, for the Al-Ag alloys system, Vegard's rule is true, then starting with the lattice constants for the aluminium and silver crystals, the Guinier-Preston zones should, according to the parameter determined above, consist of 14 at.% Ag (47 % by weight) and 86 % Al. A calculation of deviation from Vegard's rule was shown by Pines's investigations to be insignificant. If, on the other hand, in calculating this deviation, instead of the silver lattice constant use is made of that of the silver alloys with 19 at. % of Al (the crystal lattice constant of this alloy was determined by Westgren and Bradley [4] and its value was found to be 4.056 ± 0.002 Å) then the zones should consist of 24 at % of Ag and 76 % Al.

This rather low silver concentration value, as obtained by calculation for the above zones, should not be interpreted as being due to a lack of correlation between the Guinier-Preston zones constants and their composition in consequence of compression of their crystal lattice matrix. The occurrence of this phenomenon is possible owing to coherence of the zones and matrix and because of the fact that the matrix constant is lower than that of the zones. It is precisely on such grounds that the

VOL. 8 1959

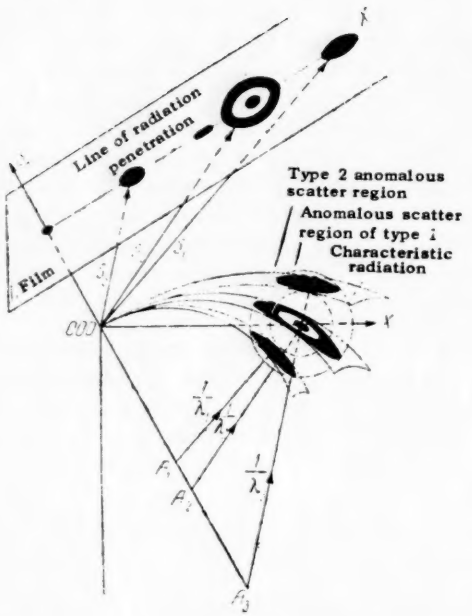

FIG. 2. Diagram of the anomalous effects formation in radiograms of the Al-Ag and Al-Ag-Cu alloys.

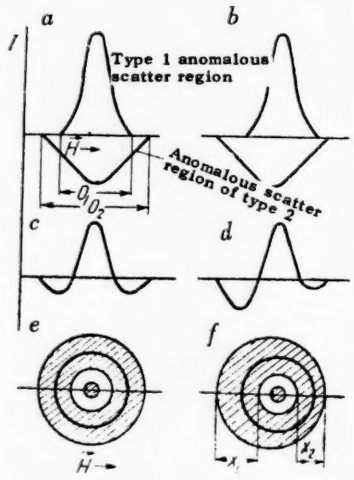

FIG. 3. Distribution of diffusional scattering in the vicinity of reverse crystal lattice centres.

anomalous behaviour of the crystal lattice constant during low-temperature ageing is often explained. In studying the effect of the additions of Mg, Zn and Si on the form of anomalous effects in the Al-Ag alloy, we have found that the first two of the above metals enter in the Guinier-Preston zones, while the last one enters into the composition of the solid solution only. The transformation of the anomalous effects observed at the same time in the radiographs, agrees well with the experimentally determined changes in the crystal lattice constant of the matrix. It is thus clear that, even if there is some effect of compression, its value in this alloy is quite insignificant.

The results obtained in the present investigation agree well with the previously reported [5-8] conclusions that the Guinier-Preston zones are relatively more depleted with regard to the alloying components concentration than the particles of the final segregation phase ($\gamma - AlAg_2$).

In the case of Al-Ag-Cu alloys, the same peculiarities were observed as for the Al-Ag alloy. Additions of copper (0.1, 1.0 and 5 %) have no effect on the dimensions and form of the anomalous scatter region and the intensity distribution in the halo is not affected, either. A thermal treatment producing a noticeable growth of the Guinier-Preston zones and a contraction of the anomalous scatter regions has also no effect on the halo intensity distribution.

These results show that the added copper is distributed uniformly throughout the whole alloy, i.e. there is no preferential concentration of copper either in the zones or in the matrix. It is possible that this phenomenon is associated with the fact that the solubility of copper at the temperature, at which the alloy is usually quenched (530°C), is approximately the same in both aluminium and silver.

An interpretation of the additional zero intensity regions in the radiograms of Al-Ag alloys will be given in a subsequent report.

Thus, a more detailed analysis of our concepts of the structure of the anomalous scatter regions and of the anomalous effects enables us to:

1. Determine the structure of the Guinier-Preston zones (in the sense, as to whether it resembles more closely that of the matrix or of the segregation phase);

2. Determine the width of the transition layer, and

3. Evaluate the composition of the Guinier-Preston zones and the distribution of copper in the alloy between the zones and the matrix.

Translated by H. Cygielski

REFERENCES

1. R.M. Lerinman and N.N. Buinov, *Fiz. metal. metalloved.*, 5, 279 (1957).
2. A.M. Elistratov, *Dokl. Akad. Nauk SSSR*, 87, 581 (1952).
3. B.Ia. Pines, *Zh. eksp. tekh. fiz.*, 11, 147 (1941).
4. A.F. Westgren and A.I. Bradley, *Phil. Mag.* 6, 280 (1928).
5. N.N. Buinov and R.M. Lerinman, *Dokl. Akad. Nauk SSSR*, 79, 69 (1951).
6. N.N. Buinov, *Fiz. metal. metalloved.*, 1, 339 (1955).
7. N.N. Buinov and L.I. Podrezov, *Fiz. metal metalloved.*, 1, 349 (1955).
8. N.N. Buinov, *Rost kristallov (Sbornik dokladov pervogo coveshchaniia po rostu kristallov). (Crystal growth). (Proceedings of the 1-st Crystal Growth Symposium).* Academy of Sciences of the U.S.S.R. p. 119 (1957).

VOL.
8
1959

EFFECT OF SMALL AMOUNTS OF ADMIXTURES ON THE DIFFUSION COEFFICIENTS OF POLYCRYSTALLINE MATERIALS
III. EFFECT OF THALLIUM ON AUTO-DIFFUSION OF SILVER*

V.I. ARKHAROV, S.M. KLIUTSMAN and A.N. TIMOFEEV
Institute of Physics of Metals of the Academy of Sciences of the U.S.S.R.

(Received 20 May 1959)

It was established in investigations [1, 2] that small amounts of antimony and beryllium alter significantly the coefficients of intercrystalline diffusion of silver. It was found that the extent of this change, in the case of beryllium addition to copper, depends on the method of thermal treatment preceeding the diffusional annealing. The interpretation of experimental data as given in the above reports, is based on the assumption that the diffusion of silver present in trace amounts produces no qualitative changes in the distribution of small amounts of impurities and in the structure of the intercrystalline elements of the alloy.

An investigation of the effect of small amounts of admixtures on the self-diffusion in polycrystalline materials enables a less unequivocal assessment of the experimental data.

In the present work, a study was made of the influence of small amounts of thallium on the self diffusion of silver. In investigations [3,4] it was established for the case of a silver alloy with 1 % thallium concentration, that thallium shows a positive adsorptive activity ("horophilia") in silver. In view of the fact that at high concentration the possibility is not excluded of the occurrence of certain effects which might alter the distribution of the dissolved element but which is conditioned not only by its adsorptive capacity [5], it is better to use in such investigations alloys with a smallest possible impurity concentration; in our case, we have chosen an alloy of silver with 0.1 % thallium.

MATERIALS AND EXPERIMENTAL PROCEDURE

As starting materials use was made of: silver of 99.99 % purity (re-melted in vacuum) and chemically pure thallium. The silver-thallium alloys were prepared in the atmosphere of argon. Slabs of pure silver and of the test alloy were cold-forged to rods with a cross-section of 12×12 mm. All the heat treatment operations and the diffusional annealing were carried out under vacuum of 10^{-1} to 10^{-2} mm Hg. The temperature during these operations was maintained constant with an accuracy of ± 1°C. After forging, all the specimens were recrystallized for 6 hr at the temperature of 900°C. The grain size was practically identical in all test specimens and equal to about 1 mm.

After recrystallization, the specimens of the pure silver and of the test alloy were subjected to one of the following heat treatments:

1. annealing at 350°C for 200 hr;
2. annealing at 285°C fro 200 hr;
3. annealing at 170°C for 200 hr, and
4. annealing at 170°C for 200 hr, followed by annealing at 350°C for a period of 100 hr.

Radioactive silver was deposited on the test specimens surface by vaporization in vacuum. All the specimens subjected to the various of the heat treatments as specified above, were subjected a simultaneous diffusional annealing, which was carried out at the temperature of 285°C for 200 hr.

The distribution of silver in the diffusion zone was determined layer-wise according to the integral residue method. The activity measurements were carried out according to a method described previously [1, 2], as was also the measurement of the thickness of the layers investigated.

EXPERIMENTAL RESULTS AND THEIR EVALUATION

In Fig. 1 and 2, the typical curves are given of the variation of the logarithm of relative residual activity with the diffusion depth in pure silver and the test alloy. Each of the cuves was constructed with the help of experimental points obtained for 5-6 test specimens tested independently in individual tests. Consequently, the scatter observed in

* *Fiz. metal. metalloved.*, 8, No. 5, 709-713, 1959.

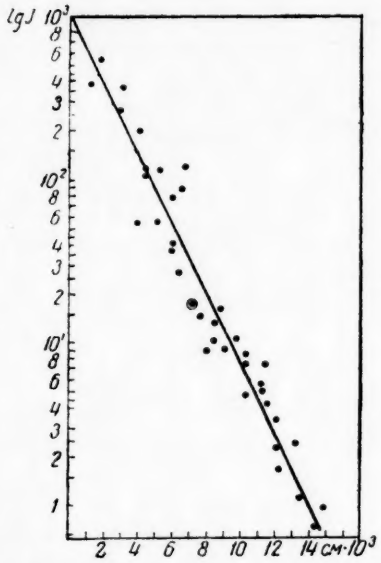

FIG. 1. Dependence of logarithm of the relative integral activity I on depth for the case of silver auto-diffusion at $T = 285°C$ and $t = 7.2 \times 10^5$ sec.

VOL. 8 1959

the test points is due not only to errors involved in the activity measurements and in the determinations of the layer thickness but also, perhaps, due to variations in the individual test conditions.

In Table 1 below, the values are tabulated of the intercrystalline diffusional permeability of silver in polycrystals of silver and of the silver alloy containing 0.1 % thallium. In order to calculate such data, we have assumed the value of the silver auto-diffusion coefficient at the temperature of 285°C as being: $D_{vol} = 2.4 \times 10^{-18}$ cm²/sec [6], whereas the volume diffusion coefficient of silver in the test alloy was taken as equal to the volume auto-diffusion coefficient, as proposed in accordance with the experimental data obtained in work [7]. It was also assumed [1, 2] that the value of the auto-diffusion coefficient D_{vol} in pure silver and in the silver alloy containing 0.1 % Th is independent of the previous heat treatments.

As it is clear from the above data, the rate of intercrystalline diffusion in the test alloy is much higher than that in pure silver. Thus, the effect of thallium on the auto-diffusion of silver is analogous to that exerted by it with respect to volume auto-diffusion [7].

In the case of pure silver specimens, there was found no relationship between the diffusional permeability of the intercrystalline mass and the type of heat treatment to which the test specimens have been previously subjected. In alloy test specimens, on the other hand, the diffusional permeability of the intercrystalline mass varies significantly with such prior heat treatments. Thus, a preliminary annealing at 170°C brings about a 2.6–fold reduction in the value of $\delta D_{boundary}$ in comparison with

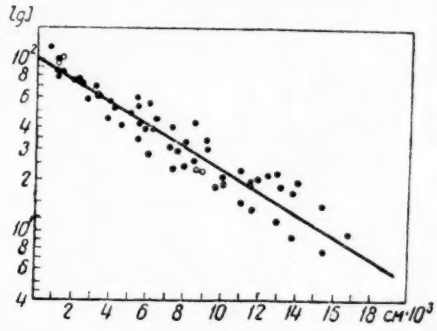

FIG. 2. Dependence of logarithm of the relative integral activity I on depth for silver diffusion in the alloy of silver with 0.1 % thallium, at $T = 285°C$ and $t = 7.2 \times 10^5$ sec. Preliminary heat treatment of the alloy: $T = 350°C$ and $t = 200$ hr.

the corresponding value of diffusional permeability of the intercrystalline mass in specimens previously annealed at the temperature of 350°C. As it follows from the data given in Table 1, these changes in the values of $\delta D_{boundary}$ are reversible, because in the tests with consecutive annealing first at 170°C for 200 hr and then at 350°C for 100 hr, the values obtained for $\delta D_{boundary}$ approach very closely those obtained after annealing at 350°C for a period of 200 hr.

Since the diffusional permeability ($\delta D_{boundary}$) in the intercrystalline boundaries in pure silver was found to be independent of the heat treatments to which the specimen was previously subjected, it can be expected that the variations in the values of $\delta D_{boundary}$, as observed experimentally in the alloy are conditioned by the composition of the intercrystalline mass. Such variations can occur, generally speaking, for two reasons. Firstly, it can be assumed that in the body of the grains there occur processes leading to changes in the admixture concentration throughout the *volume*. As a result, there occurs also a variation in the admixture concentration in the *intercrystalline mass* [5]. However, because the test alloy represents a *dilute* solid solution (its mean concentration at all temperatures is lower by one order than the limiting solubility), variations of such an order are improbable.

Secondly, if the admixture behaves as an adsorptively active material, then we should expect [8]

TABLE 1. Intercrystalline diffusional permeability in specimens subjected to preliminary thermal treatments. $D_{volume} = 2.4 \times 10^{-18}$ cm²/sec; $T = 285°C$ and $t = 7.2 \times 10^5$ secs.

Specimen composition	Heat treatment prior to diffusional annealing	$\delta D_{boundary}$ cm³/sec
Silver alloy with 0.1 % Th	900° 6 hours	$(7.48 \pm 0.3) \times 10^{-17}$
	900° 6 hours and 350° 200 hours	$(7.56 \pm 0.2) \times 10^{-17}$
	900° 6 hours and 285° 200 hours	$(3.65 \pm 0.15) \times 10^{-17}$
	900° 6 hours and 170° 200 hours	$(2.87 \pm 0.2) \times 10^{-17}$
	900° 6 hours and 170° 200 hours and 350° 100 hours	$(6.37 \pm 0.3) \times 10^{-17}$
Silver	900° 6 hours	$(7.44 \pm 0.4) \times 10^{-18}$
	900° 6 hours and 350° 200 hours	$(7.40 \pm 0.4) \times 10^{-18}$
	900° 6 hours and 285° 200 hours	$(7.49 \pm 0.4) \times 10^{-18}$

that at each temperature there exists a definite degree of adsorptive enrichement and a change in the annealing temperature should be accompanied by a redistribution of the admixture atoms between the volume and boundaries of the grains, whereby the concentration of the admixture would tend toward a range of values corresponding to the equilibrium concentration at a given temperature. In our opinion, it is this type of variation which occurs in the test specimens here investigated.

Thus, the results obtained so far enable us to conclude that thallium is adsorptively active in silver.

Since it was found that the value of $\delta D_{boundary}$ is higher in the alloy than in pure silver, it can be assumed that its increase in consequence of a suitable heat treatment is connected with an increase in the concentration of thallium in the intercrystalline mass, and vice versa. Starting with this assumption, we can now suggest that the data given in Table 1 above represent a qualitative variation of the degree of adsorptive enrichment with temperature. This dependence has a qualitative character not only because we do not know as yet the nature of the accurate dependence of the diffusional permeability as a function of adsorptive enrichment, but also because the values of the diffusional permeability of the intercrystalline mass as determined by us, are, in fact characteristic of the admixture distribution which is intermediate between that created by the *preliminary* heat treatment and the redistribution of the admixture atoms corresponding to the equilibrium position at the diffusional annealing temperature.

In fact, if the temperature of the preliminary heat treatment does not coincide with that of the diffusional annealing, then there will be a variation in the initial admixture redistribution during the process of the diffusional annealing and the concentration of the diffusing element will determine some value of an effective degree of the adsorptional enrichment of the boundaries. It is clear that the adoption of such an experimental procedure will diminish the values of the variations here investigated and that the degree of such stabilization will depend on the ratio between the diffusion velocities of the admixture atoms at the temperature of the preliminary heat treatment and that of the diffusional annealing. The starting distribution of the admixture atoms will remain constant for annealing at the temperature of 285°C, it remains practically constant for the annealing at 900°C and shows the highest variation in the case of annealing at the temperature of 170°C. Although the present series of investigations was designed to produce only qualitative data with respect to the temperature dependence of the degree of adsorptive enrichment, it can be assumed that the hypothesis put forward in work [8] has been thereby given experimental confirmation.

The sign of the temperature dependence of the adsorptive enrichment in the temperature interval investigated in the present work, coincides with that of the temperature dependence of the volume solubility of thallium in silver. On the basis of this observation, we can assume that [8] the interatomic interactions in the zone of adsorptive enrichment are qualitatively analogous to the interactions in the crystalline lattice of the alloy. This conclusion is confirmed by equal (in sign) effect of thallium on the diffusional permeability of the volume and the intercrystalline mass. Consequently, it appears reasonable that the lowering in the free energy of the intercrystalline transition zones is brought

VOL 8 195

about, principally, not because of a quantitative change in the nature of the interatomic interaction in the adsorption zone, as it obviously is the case in the copper alloy with 0.1 % Be [2], but because of a change in the geometric structure of the intercrystalline mass.

It follows from the above experimental data that the temperatures of the maximum degree of adsorptive enrichment of the intercrystalline mass and the maximum of the volume solubility do not coincide with one another. In a general case, when the adsorption of the admixture atoms leads to a change in the interatomic interaction in the intercrystalline mass, there is a chance that such a coincidence does occur.

CONCLUSIONS

1. On the basis of data concerning the independence of the diffusional permeability of intercrystalline transition zones in pure silver of the preliminary heat treatments, it is postulated that there is no change in the structure of these zones within the interval of the investigated temperatures.

2. It is postulated that thallium is adsorptively active in silver, this conclusion being based on the fact that the diffusional permeability of the intercrystalline mass in the alloy of silver with 0.1 % of thallium varies depending on the preliminary thermal treatment to which the alloy specimens were subjected.

3. Experimental verification was obtained for the hypothesis [8] concerning the temperature variation of the degree of adsorptive enrichment.

4. On the basis of an assumption to the effect that an increase in the degree of thallium adsorption leads to an increase in the diffusional permeability of the intercrystalline mass, a conclusion is drawn as to the sign of the temperature dependence of the intercrystalline internal adsorption of thallium in silver.

5. The postulate is made that during thallium adsorption, the free energy of the intercrystalline transition zones is reduced mainly because of a change in their geometric structure and not because of an interatomic interaction.

Translated by H. Cygielski

REFERENCES

1. V.I. Arkharov, S.M. Klotsman, I.I. Rusakova and A.N. Timofeev, *Issledovaniia po zharoprochnym splavam (Investigation of heat-resistant alloys)*, 3-rd edit., Akad. Nauk SSSR, (1958).
2. V.I. Arkharov, S.M. Klotsman and A.N. Timofeev, *Fiz. metal. metalloved.*, 6, 255 (1958).
3. V.I. Arkharov and S.D. Vangengeim, *Fiz. metal. metalloved.*, 4, 439 (1957).
4. S.D. Vangengeim, *Fiz. metal. metalloved.*, 5, 174 (1957).
5. V.I. Arkharov and S.D. Vangengeim, *Fiz. metal. metalloved.*, 4, 447 (1957).
6. C.T. Tomizuka and E. Sonder , *Phys. Rev.*, 103, No. 5, 1182 (1956).
7. R.E. Hoffman, *Acta metallurg.* 6, No. 2, 95 (1958).
8. V.I. Arkharov, *Tr.INF UFAN*, No. 8, 54 (1946).

VOL.
8
1959

INVESTIGATION OF THE CAUSES OF DIFFUSIONAL "ACTIVITY" OF DEFORMED CRYSTALLINE BODIES
II. ON THE SINTERING OF ELECTROLYTIC METALS IN THE LIGHT OF MODEL TESTS DATA*, †

Ia.E. GEGUZIN and N.N. OVCHARENKO

Gorki's Kharkov State University, Chemical Institute of Scientific Research

(Received 16 February 1959)

With the help of models consisting of copper wires of electrolytic copper, a study was made of the sintering kinetics of simple materials with a deformed crystal lattice. It is shown that the characteristics of the process, as observed in the investigations, agree with the concept of diffusional mechanism of high-temperature sintering.

VOL
8
195

I. INTRODUCTION

The phenomenon of sintering has been dealt with in a large number of experimental investigations both on powdered materials and on models, which serve for imitating powder compacts.

The results obtained in model investigations (sintering of wires and spheres to flat surfaces [1, 2].wire gaskets [3] etc), point to the fact that the basic concepts of the diffusional sintering theory [4, 6] can be used in arriving at a correct description of the sintering processes of products with a practically distortion-free crystalline lattice. Such concepts are further supported by coincidence of the values of the self-diffusion coefficient and the self-diffusion activation energy, as determined in sintering tests and in tests based on the use of radioactive isotopes.

Tests carried out on powdered metal compacts produced from "active" powders led to the conclusion that the experimentally observed kinetics of the compaction process differ from those anticipated on the basis of the diffusion theory. From the assumptions of the diffusion theory, it follows that the shrinkage of a powder compact should vary linearly as a function of time, while numerous dilatometric test data point to the fact that the speed of powder sintering diminishes with the sintering time. In the light of the concepts at present accepted [6], such a behaviour is explained as being due to a high structural sensitivity of the diffusion coefficient, the value of which diminishes under isothermal sintering conditions because of the spontaneous disappearance of distortions. This type of behaviour is therefore responsible for the experimentally observed reduction in the degree of shrinkage with time, i.e. the diffusional "activity" diminishes as a function of the duration of isothermal sintering. When referring to an increased diffusional "activity", especially of metals of the electrolytic origin, we mean that, all other conditions being equal, the diffusional processes proceeding in powder compacts with an increased diffusional "activity" occur at a speed higher than in "equilibrium" compacts.

Dilatometric tests data represent a source of valuable information as to the possibility of interaction between the state of the crystal lattice and its "activity" but they do not show up the conclusions with sufficient clarity. Among the drawbacks of powdered metal compacts as the specimens on which to study the relationships of interest to the present series of investigations we can mention the irregular shape of the powdered metal particles and pores, as well as the considerable scatter of the numerical distribution of particles within the range of particle dimensions.

In view of the above considerations, it appears advisable to investigate the sintering process with the help of models, which, while retaining the clarity characteristics of the models employed previously [1-3], will differ from them by a non-equilibrium condition of the crystal lattice.

In the present article, the results are reported of investigations in which the porous body was imitated with an assembly of metallic wires of electrolytic origin, i.e. of wires obtained in the same product-

---

* *Fiz. metal. metalloved.*, 8, No. 5, 714-720, 1959.

† The first article in the present series is that by Ia. Geguzin: "On excess vacancies in electrolytic metals", *Fiz. metal. metalloved.*, 5, No. 3, 1957.

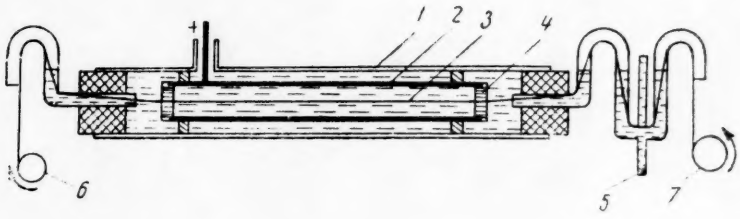

FIG. 1. Diagram of electrolytic bath:
1 – glass vessel;
2 – copper tube;
3 – copper wire serving as cathode;
4 – guide for the moving wire;
5 – U-shaped tube with wash water for the wire;
6,7 – driving and driven coils with wire.

ion process as employed for the preparation of "active" powders. Tests with such models can be regarded as a step following a previous one in which use was made of non-deformed lattices, the next step being a study of real powdered compacts. It can be assumed that tests with such models will provide additional data which might be capable of producing some new explanation of the reason for the increased activity and peculiar kinetics of volume shrinkage in powder sintering processes.

2. EXPERIMENTAL PROCEDURE *

Electrolytic copper wires were produced in a continuous electrolytic bath, the diagram of which is shown in Fig. 1. A previously annealed wire with a diameter of 50-70 μ was arranged coaxially with a cylindrical copper electrode, along the axis of which the wire could travel at a given speed. A layer of copper was deposited on the wire, the thickness of the deposit being controlled by varying the current density or the rate of travel of the copper thread. A U-shaped tube was arranged at the electrolytic bath outlet; it was filled with water for washing of the thread. A uniformly thick wire could be produced only by electrolytic deposition of copper on a slowly travelling thread. Attempts at producing such a wire under stationary conditions showed that the thread was conical in shape, as a result of a potential drop along its length. In our tests, the thread was produced in an acid bath under the following conditions: $I = 5$ A/dm^2, thread travel speed = 3×10^{-2} cm/sec. The thread obtained under such conditions was calibrated by drawing it through a diamond die the diameter of which was by about 5μ less than that of the thread. Using this procedure, it was possible to level off even the slightest uneveness in the wire surface.

The test specimens were prepared using the method employed in previous investigations [7,8]. The thread was wound in several layers onto a copper spool with a diameter of 8 mm. The winding operation was carried out with the help of special winder, in which the contact between the thread windings could be controlled under a microscope. During winding, one end of the thread was tensioned uniformly by suspending from it a weight of about 100 g, so that good contact could be ensured between the single coil turns. Thus the specimens were made of "electrolytic" and ordinary copper wires. The principal series of tests was carried out on wires 120 μ in diamter. The diffusional sintering of the wires was carried out in a vacuum furnace at the temperatures of 750, 870 and 1020°C. The sintered spools were mounted in AST-1 resin, which was then polished at the temperature of 30°C. Metallographic polished sections were prepared in the transverse spool cross-section. The structure was examined only after many repeat polishing operations and subsequent etching with ammoniacal solution of ammonium persulphate.

3. EXPERIMENTAL RESULTS AND THEIR EVALUATION

The results obtained in three series of isothermal sintering are shown in Fig. 2, a-c and in Fig. 3, a-d. An examination of the micrographs shows that:

1). Under conditions of isothermal sintering and as the time of sintering is extended, there occurs a burning on of the individual threads to their neighbours; this can be seen from the increasing thread

* A.A. Chernyshev participated in this part of the tests.

VOL. 8 1959

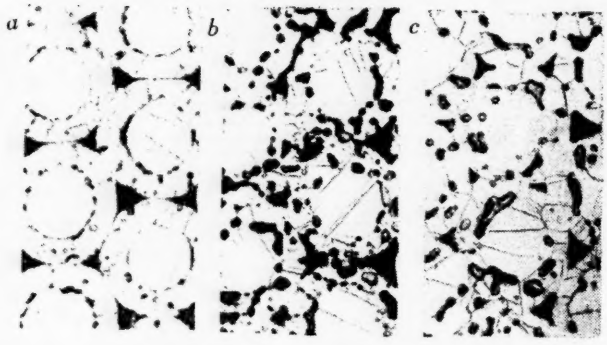

FIG. 2. Transverse section of wire coils with 120 μ wire diameter after burning for 20 hr:
$a - T = 750^{\circ}C$; $b - T = 870^{\circ}C$; $c - T = 1020^{\circ}C$.
Magnification × 200.

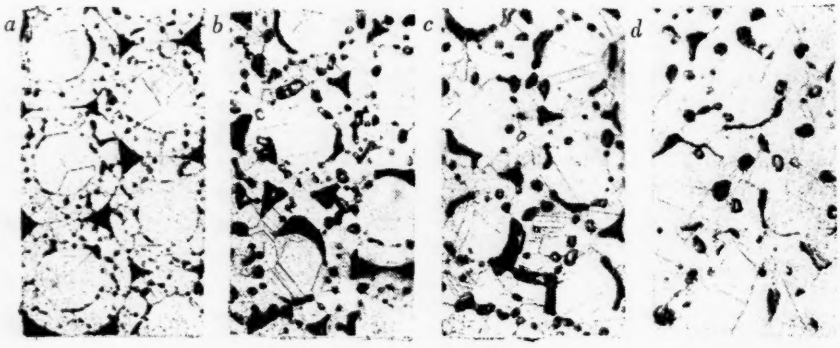

FIG. 3. Transverse sections of wire coils with 120 μ wire diameter after burning at $T = 1020^{\circ}C$.
$a - t = 3$ hr; $b - t = 10$ hr; $c - t = 20$ hr; $d - t = 58$ hr.
Magnification × 200.

thickness in the regions of contact with the adjacent threads (Fig. 3).

2). The sintering process is accompanied by the development of porosity. The mean linear diameter of pores increases with increasing sintering time. The pores appear in grain boundaries between the macrostructure elements and in boundaries between the central wire core and the electrolytically deposited metal (Fig. 2 and 3).

3). Recrystallization of the electrolytically deposited metal film proceeds at a slower rate than that of the wire core metal, with the result that the individual natures of the deposited metal film and of the ordinary metal core are retained up to latest stages of the sintering process. For instance, at the temperature of 750° and after a sintering period of 20 hr (Fig. 4), the mean linear size of the metallographically detectable grain is found to be by 1.0-1.5 orders smaller than that of the wire core metal.

4). At high temperatures and in the final stages of the process (Fig. 2,c) there sets in an intergrowth of the grains of the core and electrolytic metals. This grain growth occurs intensively when the coalescence of the individual pores leads to the formation of a smaller number of larger pores.

Some of the observations reported above were made in previous investigations of the sintering process of electrolytically produced metals [9]. It should therefore be of interest to compare qualitatively the characteristics of sintering, similarly as it was done in conjunction with the model tests [1, 2, 8]. Unfortunately, a subsequent quantitative treatment of the results obtained in our investigations, in which use is made of the known expressions for the establishment of a relationship between the self-diffusion coefficient and the size of the chord, cannot be carried out reliably because of the presence of a well developed network of diffusional porosity. However, certain qualitative and semi-qualitative data can be obtained, which are

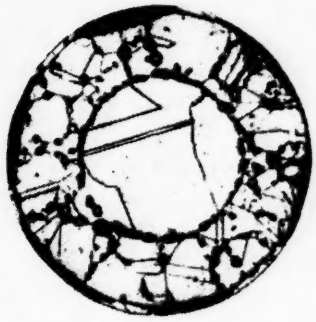

FIG. 4. Transverse section of wire after its burning at the temperature $T = 750^{\circ}C$ for $t = 20$ hr. Magnification × 500.

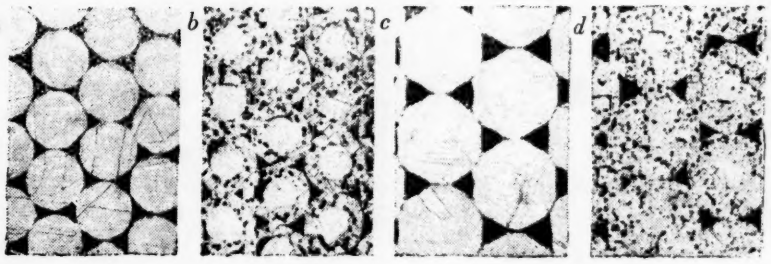

FIG. 5. Transverse sections of wire coils after sintering at the temperature $T = 1020^{\circ}C$, for 10 hr.
a – ordinary wires, 120 μ in diameter;
b – wire of electrolytic metal, 120 μ in diameter;
c – ordinary metal wires 200 μ in diameter;
d – electrolytic metal wire 200 μ in diameter.
Magnification × 100.

characteristic of the special sintering kinetics of wires drawn from an electrolytically produced metal.

The microstructure of the specimens made in ordinary wire and of those of the electrolytic origin, both of the specimens having been sintered under identical conditions (Fig. 5), points to the fact that the speed of sintering of wires produced from the electrolytic metal is much higher than that in the case of ordinary wires. This phenomenon is shown particularly clearly in the micrographs obtained with "combined specimens" in which the layers of ordinary wire and of the electrolytic one were alternated (Fig. 6 and 7).

By comparing the data obtained for wires of electrolytic origin with those of the ordinary ones (the sintering on the latter wires was investigated both by us and in work [8]) some information can be derived with respect to the temperature dependence of the ratio of the effective self-diffusion coefficients D_0 for the ordinary copper and that of the electrolytic copper D_i ($X = D_i/D_0$). In deriving such information, it was assumed that between the chord along which the sintering of two individual wires takes place (Y), the self-diffusion coefficient and the time of sintering a relationship of the following type holds true: $D \sim Y^4/t$ [6] (see Table 1).

The self-diffusion coefficient in the electrolytic metal at a given temperature can depend on the sintering period because it is conditioned by the coalescence of the pores [6, 10]. However, to the layer stages of isothermal sintering corresponds a quasi-stationary self-diffusion coefficient. The data as reported by us for the value of X refer to this quasi-stationary self-diffusion coefficient. That this is so, was confirmed by determining the values of X in the various sintering stages. At the temperature $T = 1020^{\circ}C$ we obtained the following values of X: $X_{t=}$ 10 hr = 4; X_t = 20 hr = 4. A determination of X was also made on the basis of experimental data obtained with wire 200 μ in diameter, (instead of wire with a diameter of 120 μ) and it was found that λ_t = 10 hr = 4.2.

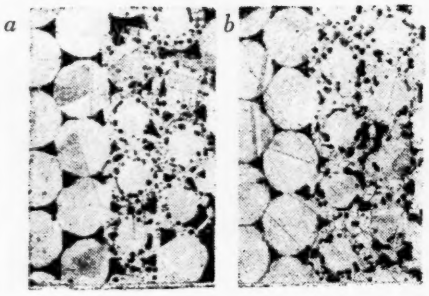

FIG. 6. Transverse cross-section of wire coils of the "combined" specimens after burning at $T = 1020^{\circ}C$:
a – burning time $t = 6$ hr;
b – $t = 15$ hr;
Magnification × 100.

T, °C	$\chi = \frac{D_i}{D_0}$	$\lambda = \frac{Q_0}{Q_i}$
750	~100	~1.30
870	~15	~1.14
1020	~4	~1.07

By making use of the experimental values of χ at three different temperatures and knowing the activation energy of the copper self-diffusion process in a crystal lattice at equilibrium (Q_0) [8], it is possible to determine the factor $\lambda = Q_0/Q_i$, in which: Q_i – activation energy of the process of sintering of wires of electrolytic metal.

It follows from the table given above that, as the melting point temperature is gradually approached, the values of both the diffusion coefficient and the activation energy tend to those corresponding to the equilibrium state, i.e. it can be assumed (without prejudicing the actual causes of such non-equilibrium values) that the lack of equilibrium present in the metal of electrolytic origin, which is responsible for an increase in the value of the diffusion coefficient, is retained right up to the pre-melting temperatures. The above conclusion agrees with the results obtained previously in dilatometric investigations of copper compacts [10].

Let us now consider again the problem of the burning-on of wires with different diffusional "activity". We are interest in the relations between the chords formed in the boundaries between two wires of electrolytic metal Y_{ii}, the wire of electrolytic metal and the ordinary wire chord Y_{i0} and that formed between two ordinary wires Y_{00}. The above relationships can be easily deduced if the following conditions are specified:

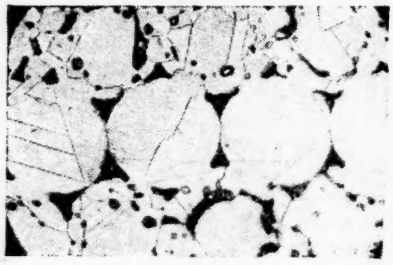

FIG. 7. Transverse section of wire coils of the "combined" specimens after its burning at $T = 1020^{\circ}C$ for a period $t = 10$ hr.
Magnification × 200.

1) The volume of the material V, which passed into the contact region by diffusional mechanism, is proportional to the current and, as it follows from geometric concepts (see [1], [6]) it is related with the chord value by the following expression:

$$V \sim \frac{Y^3 L}{a} \sim Y^3 \qquad (1)$$

(a – radius of the wire and L is its length).

2) The current of the material from each of the wires in contact is proportional to the self-diffusion coefficient in the wire crystal lattice

$$\vec{j} \sim V \sim D. \qquad (2)$$

After taking into consideration equation (1) and (2), we arrive at the following expression

$$Y_{ii} : Y_{i0} : Y_{00} = (2D_i)^{1/3} : (D_i + D_0)^{1/3} (2D_0)^{1/3}, \qquad (3)$$

where, D_i and D_0 are the autodiffusion coefficients in the wire metals of the electrolytic and ordinary origins, respectively.

By making use of a factor

$$\chi = \frac{D_i}{D_0}$$

which was defined previously, the equation (3) can be put in the following form:

$$Y_{ii} : Y_{i0} : Y_{00} = 1 : \left(\frac{1}{2} + \frac{1}{2\chi}\right)^{1/3} : \left(\frac{1}{\chi}\right)^{1/3}. \qquad (4)$$

It is of interest to check experimentally the correctness of equation (4), which was derived on the basis of the principal concepts involved in the diffusional mechanism of the sintering process.

In order to do so, we carried out tests at the temperature $T = 1020°C$ on combined specimens, the results of which are shown in Fig. 6 and 5. The choice of this particular temperature was made because, firstly, at lower temperatures the chords are small and it is difficult to measure them accurately and, secondly, the factor χ at this temperature was determined by us with the greatest accuracy ($\chi = 4$.)

Mean results of numerous measurements of the factors Y_{ii}, Y_{i0} and Y_{00} led to the following relation:

$$Y_{ii} : Y_{i0} : Y_{00} = 1 : 0.75\,(\pm 0.05) : 0.45(\pm 0.03).$$

A calculation of this expression according to equation (4) at $\chi = 4$, enabled us to derive the following relationship:

$$Y_{ii} : Y_{i0} : Y_{00} = 1 : 0.85 : 0.50,$$

which is in satisfactory agreement with the experimental behaviour.

CONCLUSIONS

1. A technique is formulated and used experimentally for the modelling of powdered compacts with deformed crystalline lattice.

2. Relationships are obtained, as functions of time and temperature, for variation in the sintering speed of wires drawn in metal of electrolytic origin (with deformed crystal lattice) and of ordinary metal wire (with crystalline lattice free of deformation).

3. Attention is drawn to the following characteristics of the phenomena investigated: the speed with which the electrolytic metal wires become joined to one another during sintering is considerably higher than that found with ordinary wires. Phenomenologically, this fact can be ascribed to an increase in the self-diffusion coefficient and a lowering of the activation energy of the sintering process of electrolytic metal wires.

4. Attention is drawn to the fact that the approach to equilibrium conditions in the electrolytic metal wires is accompanied by an increase in the size of the diffusion pores, which are distributed principally in the grain boundaries.

5. An examination is made of the problem concerning the burning-on of wires of the same metal, which show "different" degrees of diffusional activity. In special tests based on the use of combined specimens, which consisted of wires of the electrolytic and ordinary metals, it was shown that the experimentally determined chord values agree with those anticipated on the basis of the diffusion mechanism concept of high-temperature sintering.

Translated by H. Cygielski

REFERENCES

1. G. Kuczynsky, *J. Appl. Phys.*, 21, No. 7 (1950).
2. G. Kuczynsky, *Trans. AIME*, 185, 969 (1949).
3. Ia. E. Geguzin, *Zh. Tekh. Fiz.*, 24, No. 9 (1954).
4. Ia.I. Frenkel, *Zh. Exp. Teor. Fiz.*, 16, No. 29 (1946).
5. B.Ia. Pines, *Zh. Tekh. Fiz.*, 16, 737 (1946).
6. B.Ia. Pines, *Progress of Physical Sciences*, 52, No.4 (1954).
7. G. Geach and F. Jones, *Research*, 2, 493 (1949).
8. B. Alexander and R. Balluffi, *Acta metallurgica*, 5, No. 11 (1957).
9. Ia.E. Geguzin, *Fiz. metal. metalloved.*, 5, No. 3 (1957).
10. Ia.E. Geguzin, V.V. Makhonin, B.Ia Pines and *Uchenye zapiski KhGU, Trudy fiz. otd.*, 4, (1953).

VOL. 8 1959

TO THE DETERMINATION OF SURFACE TENSION ON THE BOUNDARIES OF PHASES †

I.V. SALLI
Dnepropetrovskii State University

(Received 11 November 1958)

The specific free energy of the interfaces between phases, or the so-called surface tension of interphase interfaces, represents a thermodynamic quantity which determines to a significan degree the conduct of systems in the process of crystallization and recrystallization. It is sufficient to say that this quantity comes into all the basic relationships of the thermodynamic and molecular-kinetic theory of crystallization and consequently, without knowledge of this quantity, any accurate quantitative calculations are impossible.

As is known, up to the present time reliable values of this quantity have been obtained only for the boundaries between the nuclei and the liquid during the solidification of certain metals and organic substances [1-7].

Besides this, the order of magnitude of the surface tension on the boundaries cementite, austenite, cementite ferrite and graphite austenite is determined in the work [8].

In the present information are introduced data obtained by the calculation of surface tension on the boundary of phases with the aid of known formulae used for the determination of the size of crystalline nucleus in the case of the crystallization of single-component systems, or in the separation of supersaturated solutions

$$r^* = \frac{2\sigma T_s}{L(T_s - T)\rho}, \qquad (1)$$

where σ – the surface tension on the interphase boundary;
ρ – the density;
T_s – the melting point;
$T_s - T$ – the supercooling;
L – the heat of transformation.

If r^* is expressed as $r^* = nr_0$, where r_0 is the minimum radius of the nucleus of the dividing substance (half the period of the lattice $a/2$) then the relation (1) may be rewritten in the following form:

$$n\frac{T_s - T}{T_s} = \frac{2\sigma M}{Lr_0}.$$

The right hand side of this equation is the size of the constant and consequently the product

$$n\ \frac{T_s - T}{T_s}$$

remains constant for any T. The maximum value of the quantity

$$\frac{T_s - T}{T_s} \to 1 \quad \text{for} \quad T \to 0,$$

however, the minimum value of the quantity n, which also cannot be less than one, should correspond to the maximum value of the relative supercooling. Therefore, for all values of T

$$\frac{2\sigma M v}{Lr_0} = 1$$

and consequently

$$\sigma = \frac{1}{2} L\rho r_0. \qquad (2)$$

In Table 1 are shown experimental values of the surface tension on the nucleus-liquid interface obtained in the work [2-7], in comparison with the amount of surface tension calculated by the formula (4). In the same table are shown all the other values which come into formula (4).

The coincidence of the experimental and calculated data is quite satisfactory.

Analogical reasonings can be introduced for the determination of the surface tension of the interphase boundary on the separation of a substance from supersaturated solutions.

In fact the radius of the critical nucleus of the isolating is

† *Fiz. metal. metalloved.*, 8, No. 5, 721-724, 1959.

VOL
8
195

TABLE 1.

Substance	L, $\frac{erg}{r}$	ρ, $\frac{g}{cm^3}$	$\frac{a}{2} \times 10^8$ cm	σ_{exp}, $\frac{Din}{cm}$	σ_{cal}, $\frac{Din}{cm}$	Reference sources
Al	$3,7\times10^9$	2.70	2.02	93.0	98.90	[4]
Sn	$5,6\times10^8$	7.30	2.90	59.0	61.60	[3]
Fe	$2,6\times10^9$	7.86	1.43	204.0	146.0	[4]
Ni	$2,9\times10^9$	8.90	1.70	255.0	232.0	[4]
Bi	$5,6\times10^8$	9.80	2.30	54.0	56.0	[2]
Co	$2,5\times10^9$	8.90	1.80	284.0	200.0	[4]
Pb	$2,2\times10^8$	11.30	2.56	33.0	32.30	[2]
Sb	$1,6\times10^9$	6.69	2.20	101.0	116.80	[4]
Ge	$4,0\times10^9$	5.36	2.80	181.0	240.0	[4]
Ag	1×10^9	10.50	2.00	126.0	105.0	[4]
Au	6×10^8	19.30	2.00	139.0	115.80	[4]
Pt	$9,4\times10^8$	21.40	2.00	240.0	200.0	[5]
Ga	$7,68\times10^8$	5.90	2.30	56.0	53.13	[6]
Pd	$1,52\times10^9$	11.50	1.90	209.0	174.0	[4]
Water	$3,2\times10^9$	1.00	2.20	32.1	35.20	[7]
Hg	$1,2\times10^8$	14.20	2.30	28.1	20.40	[2]
Na	$9,3\times10^8$	0.97	2.15	20.0	19.40	[4]

TABLE 2.

Boundary	T°K	ρ, $\frac{g}{cm^3}$	$a\times10^8$, cm	$r_0\times10^8$, cm	c_∞, %	σ_{exp}, $\frac{Din}{cm}$	σ_{cal}, $\frac{Din}{cm}$	Remarks
Cementite-ferrite	993 903 823	7.6	4.5	2.3	0.029 0.021 0.012	8.0 13.0 29.0	11.5 12.0 16.8	c_{max}=0,03%
Cementite-austenite	1023 1073 1123 1173	7.6	4.5	2.3	0.85 1.05 1.15 1.30	28,0 25.3 19(21)* 15.0	32.1 28.3 23.4 20.1	c_{max}=2%
Graphite-austenite	1123 1173 1273 1323	2.23	2.4	1.2	1.0 1.20 1.50 1.70	73.0 71(90)* 54(70)* 45(50)*	70.8 58.0 39.4 30.2	c_{max}=2%

* These values of the surface tension are derived as a result of a verification of the theoretical calculation of the coalescence carried out in [9]. In doing so the experimental data of [8] are employed.

$$\bar{r^*} = \frac{2\sigma_{12} Mv}{RT \ln \frac{c}{c_\infty}}. \qquad (3)$$

Here σ_{12} is the surface tension on the boundary of the precipitating phase and the parent solution; M is the molecular weight of this phase; v is its specific volume; R is the gas constant; T is the temperature at which transformations take place; c is the concentration of the mother phase and c_∞ is the equiponderant concentration.

If we once again substitute $r^* = nr_0$, then equation (5) can be rewritten in the following form:

$$n \ln \frac{c}{c_\infty} = \frac{2\sigma_{12} Mv}{RTr_0}. \qquad (4)$$

The right hand side of this equation is constant for the given temperature T. The minimum value $n = 1$ should once again correspond to the maximum value $\ln c/c_\infty$. The value $\ln c/c_\infty$ will be maximum in the case where c, the concentration of the mother phase is naximum. For cigar-shaped diagrams this will be 100 % concentration.

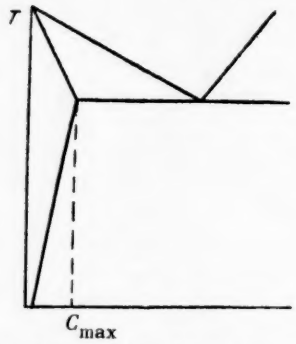

FIG. 1. Part of diagram of a binary system with limited solubility in the solid state. C is the limiting solubility of primary solid solution.

For diagrams with limited solubility this concentration corresponds to the point c, shown on the diagram.

Then the equation for determining the surface tension takes the form

$$\sigma_{12} = \frac{RT\rho r_0}{2M} \ln \frac{c_{max}}{c_\infty}. \qquad (5)$$

In Table 2 the experimental data introduced in [8] are compared with the calculated data obtained with the aid of formula (7).

The semi-empiric equations shown naturally need a further check, but the experimental data which exist at the present time compare quite satisfactorily with formulae (4) and (7). Apparently, an even better coincidence with the experimental data can be obtained with the aid of a coefficient, taking into account the difference of the structure of the mother phase and the substances crystallizing from it.

Translated by R.J. Coleman

VOL
8
195

REFERENCES

1. V.I. Danilov, *Problemi metallovedenie i fiziki metallov (Problems of metallography and physics of metals) Metallurgizdat* (1949).
2. D.J. Turnbull, *Chem. Phys.* 20, 411 (1952).
3. G.M. Pound and V.R.J. La Mer, *Amer. Chem. Soc.*, 74, 2323 (1952).
4. D. Turnbull and R.E.J. Cech, *J. Appl. Phys.*, 21, 840 (1950).
5. C.E. Mandenhall and L.R. Ingersoll, *Phil. Mag.* 15, 205 (1908).
6. D. Turnbull, *Trans. Amer. Inst. Min. Met.Eng.*, 188, 1144 (1950).
7. V.J. Schaefer, *Ind. Eng. Chem.*, 44, 1300 (1952).
8. I.V. Salli and V.I. Psarev, *Physics of metals*, 5, 268 (1957).
9. I.M. Livshits and V.V. Sledov, *Zh. eksp. teor. fiz.*, 35, 474 (1958).

THE EFFECT OF ADDITIONS OF VANADIUM ON THE SELF-DIFFUSION OF IRON*

M.S. ZELINSKII, B.M. NOSKOV, P.V. PAVLOV and E.V. SHITOV

The Research Physicial-Technical Institute of Gor'kii

(Received 29 May 1959)

With the aid of radioactive iron the self-diffusion of iron in iron-vanadium alloys with various vanadium and carbon contents is studied. The parameters are found for volume and grain boundary diffusion and their change with the concentration of the alloy. It is shown that the activation energy of self-diffusion of iron decreases linearly with increase in the vanadium concentration. The effect of additions of vanadium to the iron differs from the effect of additions of other transition metals (chromium, manganese, nickel), increasing the activation energy of self-diffusion. These peculiarities of vanadium are compared with other peculiarities in the behaviour of vanadium in its alloys with iron.

The activation energy for diffusion depends functionally on the bond energy, which is equal to the energy of sublimation. For the diffusion of foreign atoms this functional connexion has not yet been established exactly. For self-diffusion, that is the diffusion of atoms in the crystal lattice of the same metal, this connexion between the activation energy of self-diffusion Q and the bond energy E_{bond} has the form Q/E_{bond} = const, also the value of the constant equals 0.67 for a face-centred cubic lattice and 0.85 for a body-centred cubic lattice [1]. It is very important that this relationship between Q and E_{bond} is maintained also for dilute solid solutions. The latter is confirmed by the direct changes of Q and E_{bond} for iron-carbon alloys [2]. In this way, having determined experimentally the activation energy of self-diffusion in relation to the content of the additive, we can estimate the bond energy and the properties of the metal which depend on the stability of interatomic bonds.

There is still little systematic data on the effect of additions on the stability of interatomic bonds. For especially important, in a practical respect, alloys of iron with other metals, the existing data bear witness to the fact that within the defined limits of concentration the addition of chromium [3], manganese [4] and nickel [5] increases the activation energy of the self-diffusion of iron, that is raises the stability of the interatomic bonds in the crystal lattice of iron.

The results of the work on the determination of the strength of the inter-atomic bond, carried out in the laboratory of academician Kurdyumov by the X-ray study of dynamic distortions of the crustal lattice [6, 7], lead to this same conclusion. Accroding to this work chromium manganese, cobalt, molybdenum and niobium increase the strength of the bond in the crystals of iron, but vanadium weakens the inter-atomic bond strength in comparison with the same in pure iron.

The strengthening of the inter-atomic bonds on melting of transiton metals may be explained by the formation of additional bonds because of the interaction of 3*d*- and 4*s*-electrons. From this point of view, the difference in the behaviour of vanadium, which is also a transition metal, is extremely interesting. Inasmuch as other metals have a correspondence between the results of diffusional and X-ray examinations, some interest was presented by the study of the self-diffusion of iron in relation to the addition of vanadium

Zelinskii and Noskov undertook the study of the effect of vanadium on the self-diffusion of iron in three iron-vanadium alloys with vanadium concentrations of 0.48, 1.01 and 2.04 wt.% and in the temperature range of 1100-1340°. The results obtained confirmed the data of the X-ray investigations [7] in that vanadium weakens the inter-atomic bond strength in comparison with the same in pure iron.

The activation energy of the self-diffusion of iron decreased with the increase in the vanadium concentration.

Now the work Sanadze and Tsivisivadze [8], devoted to this same question has been published in the press. They studied alloys in the range of concentrations of 0.1-0.5 at.% in the temperature range 1050-1150°. The data of this work also confirmed the weakening effect of vanadium on the bond strength of the lattice of iron, but the decline in the activation energy of self-diffusion with the increase

* *Fiz. metal. metalloved.*, 8, No. 5, 725-730, 1959.

TABLE 1. The composition of iron-vanadium alloys

No of alloy	Mark of alloy	Content of elements wt %							
		Fe	V	C	Si	Mn	Ni	S	P
1	V—5	Осн.	0.48	0.025	0.09	0.083	0.092	0.021	0.004
2	V—10	Осн.	1.01	0.03	0.06	0.091	0.09	0.020	0.005
3	V—20	Осн.	2.04	0.045	0.05	0.121	0.123	0.020	0.004
4	10V—1	Осн.	0.096	0.820	0.12	0.688	0.106	0.013	0.004
5	2V—200	Осн.	2.46	0.25	0.07	0.140	0.140	0.021	0.06

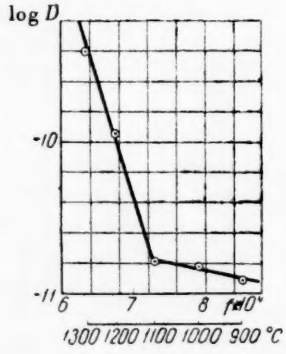

FIG. 1. The dependence of ln D on $1/T$ for alloy No. 1.

in the vanadium concentration was sharper than that obtained by Zelinskii and Noskov. Besides this, the authors of the work [8] pointed out that, in the temperature range studied by them, the process of bulk diffusion is prevalent. The latter raised doubt, inasmuch as that for all the previously studied alloys of iron in this temperature range two diffusional streams of different speeds were usually observed, which is expressed by a break in the direct temperature relation of the coefficient of self-diffusion [4, 5, 9]. Therefore we undertook a further study of the effect of vanadium on the self-diffusion of iron in a wider range of concentrations and temperatures.

For the study three alloys of Fe–V and two alloys of Fe–V–C were taken. The composition of the alloys is shown in Table 1.

Plane-parallel specimens of dimensions 5 × 8 × 25 mm were prepared from the alloys. First the specimens were subjected to homogenizing anneals at a temperature of 1100° for 20 hr. The radioactive isotope of iron ^{59}Fe was electrolytically deposited on one of the flat faces of the specimens. The thickness of the covering was about 0.005 mm. The specimens, laid in pairs with the active sides towards one another, were placed in a quartz tube evacuated to a residual pressure of 10^{-3} mm.hg, and were subjected to diffusional annealing. The time of isothermal annealing was varied, depending on the temperature, from 4 to 200 hr. The regulation of the temperature of the furnace was carried out automatically by a potentiometer with an accuracy of ± 5°. A check by a control thermocouple was made every 5 – 10 hr.

After the annealing the specimens were quickly cooled in a stream of water. During the time of annealing the depth of diffusional penetration of the radioactive isotope exceeded the thickness of the initial layer by 20 - 30 times. This ensured a sufficiently accurate determination of the coefficient of self-diffusion with the use of the solution of the equation of diffusion for the infinitesimally thin initial layer. In order to avoid the influence of boundary effects and accidental soiling from of the side faces of the specimen, a layer of thickness 0.5 - 0.7 mm was taken from all five unactivated faces.

For the determination of the coefficients of self-diffusion, the method of the removal of layers with the measurement of the integral γ-activity of the remaining part of the specimen [10] was chosen. The advantage of the method of the removal of layers lies in the possibility of excluding the effect of

diffusion on the boundaries of the grains. As the speed of volume diffusion is less than the speed of diffusion on the boundaries of the grains, during the time of the diffusional annealing, volume diffusion passes only to the depth of a few first layers, but the spreading of the diffusing substance in the last layers is explained mainly by diffusion on the boundaries of the grains. Thus, on the calculation of the coefficients of volume diffusion only the first points of the graph, corresponding to the first layers, were taken into consideration. A correction for absorption was not introduced, as the gamma-radiation of ^{59}Fe is only weakly absorbed by the diffused layer. By a graphical differentiation of the integral curve of activity the dispersion of the diffusing isotope on the layers was found.

The investigation was carried out for alloys 1-3 (see Table 1.) in the temperature range 900-1,300°, and for alloys 4-5 in the range 1,100-1,340°.

At every temperature the coefficient of self-diffusion was determined as an average of 2-4 independent measurements.

An analysis of the temperature dependence of the coefficients of self-diffusion showed that on the graphs $\log D = f(1/T)$ breaks are obtained in the straight lines at the points corresponding approximately to 1100° (Fig. 1). Thus, at temperatures lower than 1100° a strong influence of intercrystalline diffusion is present. Consequently, the assertion of the authors of the work [8], that in the temperature range studied by them volume diffusion is prevalent, is not confirmed. The effect of intercrystalline diffusion explains, apparently, the rather low values of the activation energy Q obtained in the work [8].

For determining the coefficients of volume diffusion and on the boundaries of the grains, independent determination is necessary of either volume or intercrystalline diffusion. Thus, on further examination of the results of the measurements for all the alloys, only the coefficients at temperatures of 1100° and higher, at which diffusion can be considered uniform, were taken into consideration. From these coefficients were determined, by the method of least squares, the parameters of volume diffusion for all the alloys studied. The values of the coefficients and the parameters of diffusion are shown in Table 2.

In Table 3 are shown the coefficients and parameters of intercrystalline diffusion for alloys 1-3, calculated by Fisher's formula [11].

$$D_{gr} = \frac{\sqrt{D_{o\delta}}\, 2\,(\lg e)^2}{\operatorname{tg}^2\beta \sqrt{\pi \times t \times \delta}}.$$

D_{vol} for the given temperature was obtained by the means of extrapolation of the straight line $\log D_{vol} = f(1/T)$, obtained for temperatures above 1100°. The thickness of the transitional layer on the boundary of the grains δ was taken as equal to the parameter of the lattice. Because of the arbitrarily taken value δ, the values of the coefficients of intercrystalline diffusion D_{gr} and D'^{P}_{o} also contain the arbitrary factor, but inasmuch as it is approximately equal for all the specimens, it does not have an effect on the value Q_{gr}, determined only by the slope of the straight line $\log D_{gr} = f(1/T)$.

The results obtained by us showed that for the iron-vanadium alloys studied, between the values D_0 and Q is the following relationship

$$\ln D_0 = A + B \times Q,$$

where A and B are constants. Such a connexion is explained by the fact that not only the activation energy Q, but also the pre-exponential factor D_0 are determined, in the first place, by the character and size of the inter-atomic bonds. Dekhtyar showed [12] that for pure volume diffusion, not distorted by diffusion on the boundaries of the grains, the connexion between D_0 and Q has the form

$$\ln D_0 = A + B \times Q/RT_{met},$$

where A and B are constants; R is the gas constant and T_{met} is the melting point of the alloy. Taking into account the fact that for the alloys studied by us the change in the melting point is less than 10 per cent, the formula shown above changes to $\ln D_0 = A + B'Q$, which coincides with the empirical regularity found by us

$$\ln D_0 = -24.5 + 3.61 \times 10^{-24} \times Q. \qquad (1)$$

This confirms that the values of the coefficients of self-diffusion obtained by us correspond sufficiently accurately to the volume diffusion. The dependence of $\ln D_0$ on Q for alloys 1-3 is shown in Fig. 2.

For all the alloys studied by us the activation energy of self-diffusion decreases with the increase in the concentration of vanadium. A quantitative survey can be carried out sufficiently strictly only for alloys 1-3, in which the carbon content is approximately equal and sufficiently small. For these alloys a linear dependence is obtained (Fig. 3)

VOL. 8 1959

TABLE 2. The parameters of volume diffusion in iron-vanadium alloys

Content of V, at. %	Temperature °C							D_0, cm²/sec	Q, cal/mol
	1100	1160	1200	1220	1280	1300	1340		
	Coefficients of self-diffusion $D \times 10^{11}$, cm²/sec								
0.53	1.62	—	11.3	—	—	39.0	—	1.46	68 900
1.09	1.78	—	10.1	—	—	26.9	—	$5.3 \cdot 10^{-1}$	66 200
2.11	1.94	—	8.73	—	—	33.6	—	$1.0 \cdot 10^{-1}$	61 500
0.102	0.718	1.91	—	5.9	12.9	—	32.1	$8.6 \cdot 10^{-1}$	70 200
2.67	1.72	2.73	—	6.43	16.1	—	36.3	$3.6 \cdot 10^{-1}$	66 900

TABLE 3. The parameters of intercrystalline diffusion in iron-vanadium alloys

Content of V, at. %	Temperature °C			D_0^{gr}, cm²/sec	Q_{gr}, cal/mol
	900	1000	1100		
	Coefficient of intercrystalline diffusion $D \times 10^6$, cm/sec				
0.53	0.378	2.09	5.74	1.59	43 000
1.09	0.605	2.55	7.59	1.06	40 900
2.11	0.278	1.11	3.21	0.34	38 700

$$Q = 71275 - 4617 \times C_V \text{ cal/mol}, \quad (2)$$

where C_V is the concentration of vanadium (at. %).

A similar relationship is obtained for the pre-exponential factor

$$\ln D_0 = 1.22 - 1{,}67 C_V. \quad (3)$$

Formulae 5 and 6 are obtained by the method of least squares. Formula 6 can also be obtained by the indirect substitution of the value Q according to formula 5 in formula 4.

The values of the activation energy of self-diffusion of iron in iron-vanadium alloys obtained in the work show that the introduction of atoms of vanadium, even in small quantities, into the crystal lattice of iron leads to a considerable weakening of the strength of the bond in the lattice. This agrees well with the X-ray work [7]. In this connexion it is interesting to compare the following data: in the work [7] the vanadium content was 2.3 at. %, for this alloy the value $m\theta^2$, characterizing the size of the strength of the bond, equals 1.48×10^{-17}, but for pure iron (Fe-armco) it equals 1.14×10^{-17}. It is obvious that the relationship of these two values will characterize the weakening of the strength of the bond. In the given case this relationship

$$\frac{m\theta^2_{\text{iron}}}{m\theta^2_{\text{alloy}}} = 1.15.$$

If we now take the activation energy of iron Q for the alloy with a vanadium content of 2.11 % as equal to $Q_{\text{alloy}} = 61{,}500$ cal/mol, and for pure iron we take $Q_{\text{iron}} = 71{,}100$ cal/mol (extrapolated from a series of investigations), then the relationship

$$\frac{m\theta^2_{\text{iron}}}{m\theta^2_{\text{alloy}}}$$

will be equal to ~ 1.16.

Transition metals of the fourth period of the Mendeleev system, such as chromium, manganese, cobalt and nickel, when introduced into the lattice of iron increase the strength of the bond and hamper self-diffusion. The data available at present are insufficient for a full explanation of this behaviour of vanadium. It is expedient, however, to compare with this certain other qualitative differences of the behaviour of vanadium in alloys.

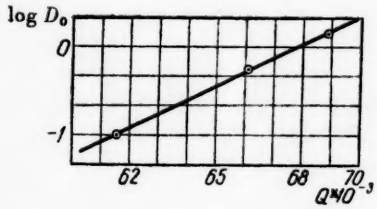

FIG. 2. The dependence of $\log D_0$ on the activation energy Q for alloys No. 1-3.

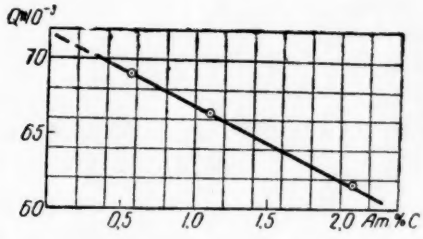

FIG. 3. The dependence of the activation energy Q on the concentration of vanadium in alloys No. 1-3.

According to the work of Owe Berg [13], systems formed by iron with elements which have a high ordinal number contain two phases: a complete solid solution α, characterized by "equal" electronic density, and phase α', having "unequal" electronic density, in which the s-electrons of the added element react chiefly with the s-electrons of the iron atom and do not react with its $3d$-electrons. With cobalt and nickel, iron forms α-alloys and, with sufficiently high concentrations of the added metal, α' alloys. With vanadium iron does not form α-phase and the region of α'-phase extends from 0 to 6.7 at.%.

One may suppose that the increase in the activation energy of self-diffusion (and consequently in the bond energy) is connected with the formation of α-phase, but in the α'-phase a decrease in the activation energy of self-diffusion occurs. Not only the decrease in the activation energy of self-diffusion in an iron-vanadium alloy consisting of α-phase, serves as a basis to this supposition. According to [13], in the system iron-nickel the α-phase extends from 0 to 12 at. % Ni, and subsequently α'-phase is formed. From the data of the work [14] an increase in the concentration of nickel in an iron-nickel alloy from 11.8 to 25 per cent leads to a decrease in the activation energy of self-diffusion of iron from 66,000 to 62,000 cal/mol. Considering the great similarity of atoms of Fe, Co and Ni, it is possible to examine from the same point of view the self-diffusion of cobalt in a cobalt-nickel alloy. From the data of Gruzin and Noskov [15], the activation energy of self-diffusion of cobalt at first rises (up to 8 % Ni) after which there is a fall in the activation energy, which at 30 % Ni becomes even less than the activation energy in pure cobalt.

The absence of interaction of s- and d-electrons in alloys of iron with vanadium does not give the formation of the additional strengthening bonds which arise in alloys of iron with other transition metals of the fourth period. Which physical factors lead to the decrease in the bond strength in comparison with pure iron still remains unexplained.

Translated by R.J. Coleman

REFERENCES

1. I.Y. Dekhtyar, *Zh. tekh. fiz.*, 20, 1015 (1950).
2. Y.V. Kornev, *Dokl. Akad. Nauk SSSR*, 93, 467 (1953).
3. P.L. Gruzin, *Dokl. Akad. Nauk SSSR*, 100, 65 (1955).
4. P.L. Gruzin, B.M. Noskov and V.I. Shirokov, *Dokl. Akad. Nauk SSSR*, 99, 247 (1954).
5. P.L. Gruzin and E.V. Kuznetsov, *Dokl. Akad. Nauk SSSR*, 93, 80, 9 (1953).
6. V.K. Kritskaya, G.V. Kurdyumov and G.I. Stelletskaya, *Dokl. Akad. Nauk SSSR*, 98, 63 (1954).
7. V.A. Il'ina and V.K. Kritskaya, *Dokl. Akad. Nauk SSSR*, 100, 69 (1955).
8. V.V. Sanadze and G.A. Tsivtsivadse, *Georgian politechnical institute*, No. 1, p. 141 (1956).
9. P.L. Gruzin, *Problemi metallovedeniya i fiziki metallov (Problems of metallography and physics of metals)* ed. 4, p. 475 (1955).
10. P.L. Gruzin, *Dokl, Akad. Nauk SSSR*, 86, 289 (1952).
11. J.C. Fisher, *J. Appl. Phys.*, 22, 74, (1951).
12. I.Y. Dekhtyar, *Dokl. Akad. Nauk SSSR*, 89, 49 (1953).
13. T.G. Owe Berg, *Journ. phys. et radium*, 15, 90 (1954).
14. S.T. Kishkin, S.Z. Bokstein, I.I. Mirskii and A.V. Kazakova, *Izv. Akad. Nauk SSSR, Department of Technical Sciences* No. 12, 18 (1955).
15. P.L. Gruzin and B.M. Noskov, *Problemi metallovedenie i fiziki metallov (Problems of metallography and physics of metals)* ed. 4. p. 524 (1955).

VOL. 8 1959

HIGH TEMPERATURE STUDY OF ALLOYS THE PHASES OF WHICH HAVE IDENTICAL LATTICES WITH NEARLY THE SAME PARAMETERS*

I.I. TITARENKO and B.M. ROVINSKII

All-Union Aviation Materials Scientific Research Institute

(Received 21 February 1959)

The results of a study of refractory nickel alloys at temperatures of up to 1250° are given.

Investigation at room temperature of complex refractory alloys on a nickel base [1], X-ray structure analysis of the Ni-Al system [2] and other studies of similar systems have shown that when these alloys are cooled from high temperatures, phases are precipitated which have the same lattice as the solid solution and differ from it only in the concentrations of Al, Ti and other elements. The lattices of the precipitated phase (γ' phase) and the impoverished solid solution (γ phase) are "interlinked" and differ little in their parameters.

The present paper is a study of complex alloys on a nickel base, ZhS6 and ZhS6K alloys and partly EI437. The alloy ZhS6K has the same composition as the alloy ZhS6, but is additionally alloyed with cobalt.

The chief task of the work was the study of the process of the solution of the γ' phase during annealing and the process of segregation of the solid solution into the γ and γ' phases on cooling the alloy from 1250°.

It was assumed that under certain conditions, when the previously cooled alloy is heated the lattices of the γ and γ' phases become segregated, which would make it possible to trace the process of the solution of the γ' phase. On the other hand, it should be possible to trace the process of the segregation of the solid solution into the γ and γ' phases by bringing the alloy into the state of the homogeneous solid solution and then reducing its temperature.

The X-ray photographs were taken in a special high temperature camera with a powerful sharp focus tube with rotating copper anode of Sergeyev's [3] design with a voltage of 30 kV and a current of 180 mA. Static single crystal specimens of the alloy were photographed at temperatures of from 900-1250°.

For a provisional estimate of the difference in the parameters of the lattices of the γ and γ' phases a series of X-ray photographs was taken at room temperature. By various methods and under various conditions we photographed specimens from a single crystal, from sediments of the γ' phase obtained electrochemically, shavings of the alloys, shavings mixed with 30 per cent of γ' phase sediment and others.

As a result of these photographs and of subsequent photographs taken at various temperatures with the specimens rotating back and forth through angles of from 3 to 9° and of photographs taken with monochromatic chromium K_β radiation it was established that the difference in the periods of the lattices of the γ and γ' phases is considerably less than 0.01 kX and probably of the order of 0.001 kX.

Fig. 1 shows in six-fold magnification photographs of the alloy ZhS6 obtained with the method of back reflection at a specimen temperature of 1125°. The photographs were taken after every 30 min of holding.

At room temperature and after 6 min holding at 1125° the spots were washed. After 30 min holding the splitting up of the spots into two reflections became noticeable; the sharpness of the reflections increased when the time of holding was prolongued to 5 hr. The distance between them changed little.

It is probable that when the time of holding at 1125° is prolongued, the segregation of the lattices of the γ and γ' phases occurs and possibly also an exchange of components between the phases by slow diffusion.

Fig. 2 shows photographs of the same specimen at a temperature of 1200°. The position of the specimen was not changed and the conditions of the photograph remained the same as at 1125°.

The spots split up into two reflections already after 30 min holding. As the time of holding was

* *Fiz. metal. metalloved.*, 8, No. 5, 731-734, 1959.

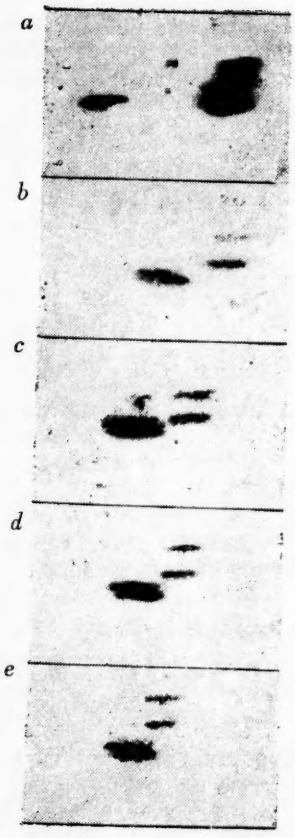

FIG. 1. X-ray photograph of the alloy ZhS6, taken at 1125° and holding
a – at room temperature;
b – for 6 min;
c – for 30 min;
d – for 3 hr;
e – for 5 hr; × 6.

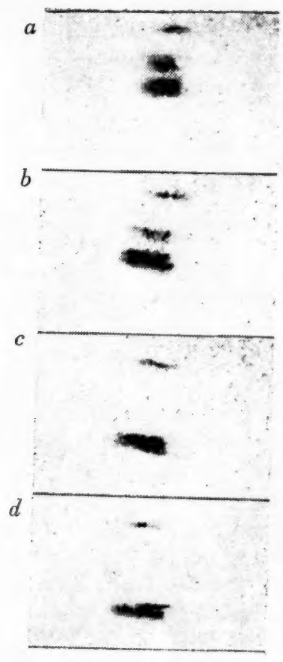

FIG. 2. X-ray photograph of alloy ZhS6 taken at 1200° and holding
a – for 30 min;
b – for 1 hr;
c – for 2 hr;
d – for 3 hr.

prolonged to two hr the distance between the reflections decreased in proportion. After two hr and on further holding to three hr the distance did not change. Moreover, in the course of holding both reflections shifted to smaller angles. The final shift corresponded to an increase in the lattice parameter of 0.005 kX for reflections with a large Bragg angle and of 0.004 kX for relfections with smaller Bragg angles. The maximum distance between the reflections in the spots at 1125 and 1200° corresponded to a difference in the lattice parameters of $\Delta a \simeq 0.0025$ kX with an accuracy of measurement of ± 0.0003 kX.

A difference in the lattice parameters of about 0.002 kX was also obtained in the measurement of the lattice periods of a single crystal of the alloy ZhS6 and a sediment of the γ' phase precipitated from it.

Evidently, diffusion displacement of the components from the γ' into the γ phase occurs during the holding at 1200° and leads to the evening out of the concentration in the alloy. Probably, alloy elements with smaller atomic radius leave the γ' phase first.

If one lowers the temperature of the alloy after previously holding it for 3-4 hr at a temperature of 1250 or 1200°, then at a temperature of about 1180° the spots split up again into two sharp reflections and then at a still lower temperature specific for each alloy the spots become completely washed. The degree of washing increases with further reduction of the temperature to room temperature. This washing of the spots occurs at 1100° for the alloy ZhS6K, at 1000° for the alloy ZhS6 and below 800° for the alloy EI437. Fig. 3 shows photographs of the alloy ZhS6K taken when the temperature was reduced to 1150 and 1100°.

The segregation of the homogeneous solid solution probably occurs in such a manner that first the γ' phase is precipitated and the "interlinking" of

VOL. 8 1959

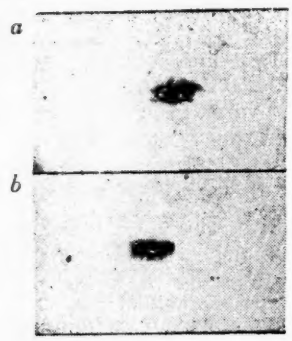

FIG. 3. X-ray photograph of the alloy ZhS6K taken at 1150° (*a*) and 1100° (*b*) in the process of cooling a specimen previously heated to 1250° and held at that temperature for 3 hr; × 6.

the lattices of the γ and γ' phases occurs at a lower temperature.

Increasing the complexity of the alloy leads to a slowing down of the diffusion processes and raises the temperature at which the "interlinking" of the lattices occurs.

We have not yet fully explored the mechanism of the segregation of the homogeneous solid solution into the γ and γ' phases and work with this end in view still continues.

One could have attempted to explain the effects shown in Figs. 1, 2 and 3 by the mosaic structure of the blocks, that is to say by the degree of disorientation. In papers [4, 5] an increase in the perfection and re-orientation of the elements of the substructure of the crystallites was observed in aluminium on plastic deformation and creep. The analysis of the effects obtained by us shows, however, that they are of a different nature and are not reflections from blocks of a single phase.

If the spots in Figs. 1 and 2 are examined under slight optical magnification, fine, more intense dashes are visible on the background of the reflections extended in the direction of the reflection. Fig. 4 shows them schematically in magnification. Such effects are sometimes called second order mosaics [6].

From the width of these dashes we have attempted to estimate the size of the reflecting particles and to compare them with the data of electron microscope observations.

As an example, Fig. 5 shows an electronmicrophotograph of the alloy ZhS6 obtained by Grekova, in which the details of the forms and distribution of the γ' phase formations can be clearly seen.

Measurements of the size of the γ' phase formations in electronmicrophotographs of the alloy ZhS6 showed that depending on the conditions of heating, holding and cooling the alloy, the size of the γ' phase formations changes within limits of from 5×10^{-4} to 3×10^{-3} mm.

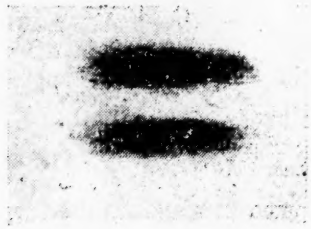

FIG. 4. Schematic position of dashes on the reflections of the X-ray photograph of Figs. 1 and 2.

Measurements made from the X-ray photographs obtained by us showed that the size of the reflecting particles is roughly 5×10^{-3} mm. Good agreement with the electronmicroscopic data is thus obtained. This gives grounds for suggesting that the dash-like reflections are really reflections from the elements of the substructure of the γ and γ' phases.

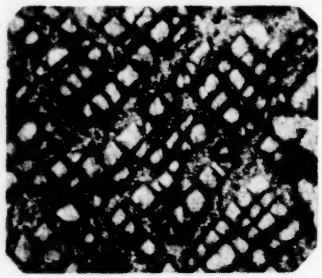

FIG. 5. Electronmicrophotograph of the alloy ZhS6; × 10,000.

CONCLUSIONS

1. The maximum difference in the parameters of the lattices of the γ and γ' phases in the alloy ZhS6 are about 0.002 kX both at high temperatures (1125° and after one hr holding at 1200°) and in their electrolytic separation.

2. Diffusion processes which occur in the alloy ZhS6 at a temperature of 1125° lead to the segregation of the lattices of the γ and γ' phases.

3. In the process of holding the alloy at a temperature of 1200° diffusion displacement of the components from the γ' phase into the solid solution occurs.

4. On cooling the solid solution from a temperature of 1250° the segregated γ' phase is first precipitated, but at a lower temperature the "interlinking"

VOL 8 195

of the lattices of the γ and γ' phases occurs.

In the carrying out of certain stages of this work the authors had advice and valuable advice from S.T. Kishkin and N.F. Lasnko, which they note with gratitude.

Translated by B. Ruhemann

REFERENCES

1. N.I. Blok, A.I. Glazove, O.A. Dubovnikova, S.T. Kishkin and N.F. Lashko, *Zavodsk. Lab.* No. 8 (1954).
2. Iu.A. Bagariatskii and Iu.D. Tiapkin, *Dokl. Akad. Nauk SSSR* 108, No. 3, 451 (1956).
3. I.I. Titarenko, *Zh. Inst. tekh. ekon. inform.* 3, No. 11-56.451 (1956).
4. B.M. Rovinskii and V.G. Liuttsau, *Izv. Akad. Nauk SSSR, ser. fiz.* 20, No. 6, 638 (1956).
5. B.M. Rovinskii and L.M. Rybakova, *Izv. Akad. Nauk SSSR* 20, No. 6, 646 (1956).
6. S.J. Weismann, *J. Appl. Phys.* 27, No. 11 (1956).

VOL.
8
1959

ON THE NATURE OF ζ_a-PHASE OF THE SYSTEM Fe–Si *

F.A. SIDORENKO, P.V. GEL'D and L.B. DUBROVSKAYA
Urals Polytechnic Institute named after C.M. Kirov

(Received 6 June 1959)

As is well known [1, 2] the physical properties of alloys of iron with silicon containing more than 50 % Si are very sensitive to the phase condition of the leboite. In connexion with this, numerous investigations of structural peculiarities and of conditions of stability [3, 7] of ζ_a-phase were carried out. By this it was proved [6, 8-11], that the high-temperature a-variety of leboite, inclined towards supercooling, it broken eutectically at 915-920° with the formation of the low-temperature ζ_β-phase and of silicon (Fig. 1). It was further shown [1,2] that a-leboite is characterized by metallic properties and β-leboite by semi-conductor properties. Finally, it was discovered [2, 13] that in technical varieties of ferrosilicon the presence of ζ_a-phase makes them predisposed towards dispersal.

Information on the structural properties of the high-temperature phase is insufficiently precise. In particular, rather large differences of opinion exist in the appraisal of the concentration boundaries of its stability [3-7]. This also follows with regard to the temperature of the eutectic and peritectic conversions [6, 8-11].

Appraisals of the construction of ζ_a-phase are more uniform. According to data by Phragmen [4], leboite possesses a tetragonal nucleus characterized by the spatial group D_{4h}^1 with the following position

$$\text{Fe} - [[000]]; \quad \text{Si} - [[\tfrac{1}{2}, \tfrac{1}{2}, z]]; \quad \left[\left[\tfrac{1}{2}, \tfrac{1}{2}, \bar{z}\right]\right],$$

where $z = 0.25$. The parameter of the networks diminish somewhat with the growth in the content of silicon in the leboite (from 53.0 to 55.0 weight % Si). This circumstance and also the fact that within the limits of the area of homogeneity of ζ_a-phase the content of silicon exceeds the appropriate stoichiometric compond $FeSi_2$ (50.1 weight % Si)

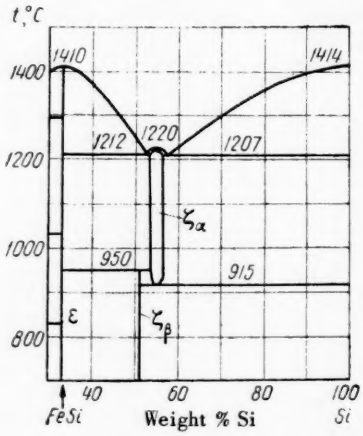

FIG. 1. The system FeSi–Si.

Phragmen explained by the substitution of a section of iron atoms with atoms of silicon.

Other investigators [5,7] do not object to this pattern of construction of the leboite although in the work [2] some doubts have been expressed in this connexion.

As far as the structural parameter of z ζ_a-phase is concerned, it was shown [12] that in the frame work of Phragmen's suppositions, the calculated and observed intensities agree better with each other if z is assumed equal to 0.28, not 0.25.

It must be noted that the considerations by Phragmen of the structure of a-leboite cannot be acknowledged as sufficiently convincing inasmuch as they bear an *a priori* character and do not permit an identical choice to be made between patterns of substitution and substration. In connexion with this an interesting aspect of investigation was presented not only of the boundaries of homogeneity of ζ_a-phase but also of the connexion of their parameters with densities of the alloy.

1. Specimens. Alloys of iron with silicon, containing 50.0 to 58.0 Si were prepared for investigation. Crystalline silicon (containing about 0.02 weight %

* *Fiz. metal. metalloved.*, 8, No. 5, 735-739, 1959.

TABLE 1. Comparison of measured and calculated densities of some silicides

Substance	Density, g/cm³	
	Calculated	Observed
Si	2.33	2.32
CrSi	5.20	5.18
$CrSi_2$	4.85	4.81
FeSi	6.16	6.14

TABLE 2. Influence of the content of silicon in alloys with iron on parameters of the network, density and number of atoms in the elementary nucleus of α-leboite

Weight % Si	Parameters of the network		Density, g/cm³			Number of atoms in the nucleus					
				Calculated		n_{Si}			n_{Fe}		
	a, Å	c, Å	Measured	Substitution	Subtraction	Experimental	Substitution	Subtraction	Experimental	Substitution	Subtraction
50.0	2.6937	5.139	4.86	—	—	—	—	—	—	—	—
52.5	2.6937	5.139	4.71	4.93	4.73	—	—	—	—	—	—
53.0	2.6937	5.139	4.69	4.90	4.70	—	—	—	—	—	—
53.2	2.6937	5.139	4.68	4.89	4.59	—	—	—	—	—	—
53.5	2.6937	5.139	4.65	4.88	4.67	1.99	2.00	2.09	0.87	0.91	0.87
54.0	2.6932	5.136	4.64	4.87	4.65	2.00	2.10	2.00	0.86	0.90	0.86
54.5	2.6923	5.135	4.57	4.86	4.59	1.99	2.12	2.00	0.85	0.88	0.84
55.0	2.6901	5.134	4.54	4.85	4.56	1.99	2.13	2.00	0.82	0.87	0.82
56.5	2.6872	5.128	4.44	4.82	4.45	1.99	2.16	2.00	0.77	0.84	0.77
57.0	2.6869	5.128	4.41	4.76	4.41	—	—	—	—	—	—
58.0	2.6870	5.128	4.30	—	—	—	—	—	—	—	—

of admixtures) and also carbonyl iron of mark R4 previously degasified served as initial materials. Batches of thinly ground reagents were carefully intermixed, pressed into tablets and fused (in quartz crucibles) in the tungsten furnace TVV-1 with a pressure of about 10^{-3} mm hg. The samples obtained were homogenized (in a vacuum) at 1080° for 100 hr and were then hardened in air to stabilize ζ_α-phase. Control experiments confirmed the conclusion reached earlier [13] that in these conditions the breaking up of α-leboite is slowed down completely.

Specimens prepared in this way were subjected to metallographic investigation and were then ground in an agate beater. For X-ray analyses the powder was again fired for an hour at 1080° (for relief of pressures) and was then cooled quickly in air.

2. Method of Investigation. X-ray analyses were carried out in the chambers VRC-3. Exposures were taken in cobalt emission (12 mA 32 kV) with asymmetrical insertion of the film. Measurements of the X-ray photographs were produced with the help of the comparator IZA-2. Parameters of the network of the leboite were determined according to the lines (220) and (204) with an accuracy to ± 0.0001 Å (for a) and ± 0.002 Å (for c).

Measurements of the densities were carried out pycnometrically in thermostatically-regulated conditions with the use of a middle fraction of refined kerosene. The charging of the pycnometer with a weighted portion of the preparation was carried out with kerosene in a vacuum. Verification of the accepted method of measurement of densities was carried out on the preparations of silicon and also of monosilicide of iron and silicides of chromium prepared in the Institute of metal-ceramics and special alloys Akad. Nauk Ukr. S.S.R. A comparison of the results obtained with densities calculated by structural characteristics is given in Table 1. It confirms the sufficient accuracy and reliability of the accepted scheme of measurements.

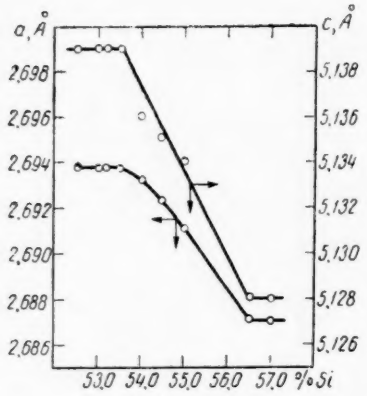

FIG. 2. Relationship of parameters of α-leboite with the content of silicon.

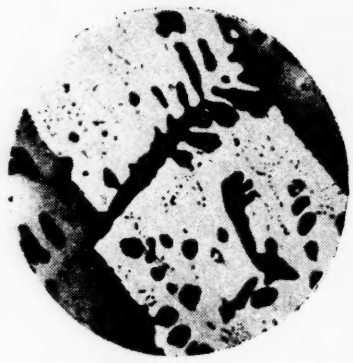

FIG. 3. Excessive monosilicide and eutectic ($\epsilon + \zeta_\alpha$) in an alloy with 50% Si; crossed nicols, × 60.

RESULTS OF MEASUREMENTS

A. Borders of homogeneity of α-leboite. Results investigations of parameters of the network of α-leboite of a varying composition are given on Fig. 2 and in Table 2. As is evident from these data, with a content in the alloys of less than 53.5 and more than 56.5 weight % Si the parameters of the network of ζ_α-phase prove not to be related to the composition. In those specimens in which the concentration of silicon was increased from 53.5 to 56.5 weight %, a regular decrease of the parameters of a and c was observed. Arising from this, the conclusion may be reached that α-leboite at 1080° is characterized by the area of homogenity from 53.5 to 56.5 weight % Si, the extent of which largely agrees with that established earlier by Haugton and Becker [7].

This conclusion is confirmed by results of metallographic investigations. In particular they disclosed a very considerable quantity (around 3%) of eutectic colonies ($\epsilon + \zeta_\alpha$) in the section of the alloy containing 53.5 weight % Si. With lesser contents of silicon the quantity of ϵ-phase increased quickly (Figs. 3, 4) – with 53.2% Si – 18%, with 52.5 Si – 60% eutectic ($\epsilon + \zeta_\alpha$). With larger contents of Si the alloy was single-phase and contained only ζ_α-phase. By a similar method the upper border of stability of the single-phase α-leboite was confirmed (Fig. 5). Microphotographs were produced in polarized light with a crossed polarizer and analyzer. In these conditions α-leboite is dark and light in relation to the orientation of the granule but the monosilicide is always dark.

B. Nature of the ζ_α-solid solution. The structural peculiarities of the α-leboite may be explained by the formation of solid solutions of either substitution or subtraction. Both this and other patterns agree qualitatively with observations over the decrease of parameters of the network of ζ_α-phase with the growth of the silicon content in it. It was decided to use the well-known procedure based on a comparison of experimental and calculated densities of the alloy and also an analysis of intensities of the reflexes for a well-defined establishment of the nature of the ζ_α-solid solution.

A claculation of the density was carried out by the formula

$$\rho = \frac{n}{a^2 c N_0}(A_{Fe} N_{Fe} + A_{Si} N_{Si}), \qquad (1)$$

where n – general number of atoms in the nucleus with parameters a and c;

N_0 – Avogadro number;

A_{Fe}, N_{Fe}, A_{Si}, N_{Si} – atomic weights and atomic parts of iron and silicon.

Apparently, for the pattern of substitution $n = 3$, but with the formation of perforated structures

$$n = \frac{2}{N_{Si}}, \quad (n_{Si} = 2).$$

By setting out data on the density of the leboite, it is not difficult to calculate the number of atoms of iron and silicon arriving at one nucleus:

$$n_{Si} = \frac{N_0 a^2 c \rho N_{Si}}{A_{Fe} N_{Fe} + A_{Si} N_{Si}}; \qquad (2)$$

$$n_{Fe} = \frac{N_0 a^2 c \rho N_{Fe}}{A_{Fe} N_{Fe} + A_{Si} N_{Si}}.$$

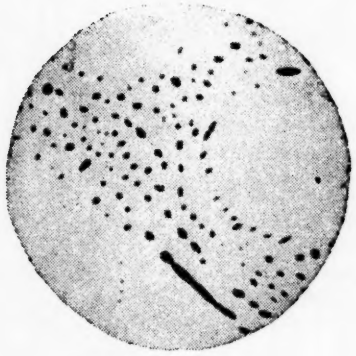

FIG. 4. Eutectic monosilicide in an alloy with 53.2% Si; crossed nicols, × 240.

FIG. 5. Eutectic silicon in an alloy with 57% Si; crossed nicols, × 240.

In Table 2 and on Fig. 6 a comparison is made of experimental and calculated densities (for patterns of substitution and subtraction) and also of the number of atoms in the elementary nucleus. As is evident from the data given in Table 2, within the limits of the area of homogeneity $n_{Si} \cong 2$ at the time when the number of iron atoms in the elementary nucleus diminishes with the growth of N_{Si} from 0.87 to 0.77. This cicumstance serves as a reliable indicator that α-leboite is not a solid solution of substitution (for which $n_{Si} > 2$ and must grow with the increase of N_{Si}) and is characterized by perforation in the sub-network of iron.

A comparison of experimentally measured and calculated densities of alloys of a varying composition supplies information on this point. In fact (see Table 2 and Fig. 6) densities of leboite calculated by Phragmen's patterns (solution of substitution) not only according to the absolute value bu' also according to the concentration course differ essentially from experimental data. On the contrary, the assumption concerning the formation of a solid solution of subtraction leads to results which in practice coincide with experimental results.

Evidently, the increase of perforation of the sub-network of iron with the growth in the concentration of silicon in α-leboite must be expressed on the relative intensities of the Debye lines. In particular, the intensity of the weak reflections (100) and (120), the structural amplitude of which is defined by the variation of the dispersal capacities of atoms located in positions [[000]] and

$$\left[\left[\frac{1}{2}, \frac{1}{2}, z\right]\right], \left[\left[\frac{1}{2}, \frac{1}{2}, \bar{z}\right]\right]$$

and do not depend on the parameter z, must increase

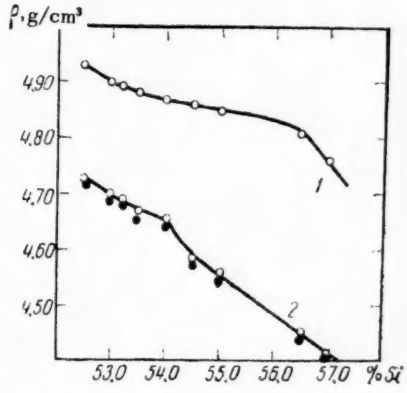

FIG. 6. Calculated and experimental densities of α-leboite.
1 — solution of substitution;
2 — solution of subtraction;
• — experimental results.

with the growth of N_{Si}. This is also observed in reality. It is hardly possible to explain the indicated regularity by substitution of iron atoms with silicon which can bring forth an effect considerably less than that observed. On the contrary, the intensities of lines (100) and (120 calculated on the assumption of perforation of the sub-network of iron agree satisfactorily with intensities of other weak lines observed.

Thus, experimental data on the concentration relationship of parameters of the network and density of the leboite and also on the intensities of reflexes of weak lines assert that the high-temperature ζ_α-phase, despite the foregoing statements, is a solid solution of subtraction of which the concentration of holes in the sub-network of iron changes from 13 to 23% within the limits of the

VOL. 8 1959

area of homogeneity.

Translated by J. Harvey

REFERENCES

1. P.V. Gel'd, *Zh. tekh. fiz.*, 27, 113 (1957).
2. P.V. Gel'd and O.A. Yesin, *Protsessy vysokotemperaturnovo vosstanovleniya (Processes of high-temperature restoration)*, *Metallurgizdat* (1957).
3. N.S. Kurnakov and G.G. Urazov, *Zhurnal russkovo fiziko-khimicheskovo obshchestva (Journal of Russian physical-chemical society)*, 45, 676 (1913).
4. G.J. Phragmen , *Iron and Steel Inst.*, 114, 397 (1926).
5. N.V. Ageev, N.S. Kurnakov, L.N. Guseva and O.K. Kononenko-Gracheva, *Metallurg.* No. 1, 5 (1940).
6. N.Kh. Abrikosov, *Izv. sektor fiziko-khimicheskovo analiza IONKh Akad. Nauk SSSR (News of the sector of physical-chemical analysis IONKh Akad. Nauk SSSR)*, 27, 157 (1956).
7. J.L. Haugton and M.L.J. Becker, *Iron and Steel Inst.*, 121, 315 (1930).
8. N.N. Serebrennikov and P.V. Gel'd, *Dokl. Akad. Nauk SSSR*, 97, 695 (1954).
9. P.V. Gel'd and N.N. Serebrennikov, *Dokl. Akad. Nauk SSSR*, 97, 827 (1954).
10. P.V. Gel'd and N.N. Serebrennikov, *Fiz. metal. metalloved.*, 2, 244 (1956).
11. I.N. Strukov and P.V. Gel'd, *Fiz. metal. metalloved.*, 4, 190; (1957); *Trud. Ural'skovo politekh. inst. Urals polytechnical institute)*, Symposium No. 72, page 149. (1957).
12. F.A. Sidorenko and P.V. Gel'd, *Nauchnye doklady vysshei shkoly Metallurgiya (Scientific reports of the higher school of metallurgy)*, No. 3 (1959).
13. I.N. Strukov and P.V. Gel'd, *Fiz. metal. metalloved.*, 3, 564 (1956); *(Trud. Ural'skovo polytech. inst.) Urals polytechnical institute*, Symposium No. 72, page 134 (1957).

ON THE REDUCTION OF COPPER FERRITE WITH GRAPHITE*

N.M. STAFEEVA, V.N. BOGOSLOVSKII, G.I. CHUFAROV and V.A. SUBBOTINA
Institute of Metallurgy Ural Branch, Academy of Sciences SSSR

(Received 19 March 1959)

Copper ferrite $CuFe_2O_4$ has a tetragonal structure at room temperature [1, 2]. At high temperatures it possesses a cubic structure which may be come metastable by quick cooling [3]. These structures may be represented in the form of a close-packed cubic array of oxygen ions in the intersticies of which are located cations. The disposition of ions in the unit cell of the tetragonal form of the ferrite approaches the distinctive distribution of the reverse spinel.

The cubic form represents an intermediate spinel in which there are both Fe^{3+} and Cu^{2+} ions in the tetrahedral and octahedral units.

Conversion of tetragonal into cubic ferrite takes place at 760° [1]. With this the character of the forces of the link between the ions is changed [4, 5]. The covalent reaction which plays a signification role in the network of tetragonal ferrite develops more weakly in cubic ferrite in which the interaction is basically ionic. Such a change in the character of the interatomic forces may exert influence on the kinetics of restoration.

In the current work the kinetics and the mechanism of reduction of tetragonal and cubic ferrites with graphite in a vacuum are investigated.

INITIAL MATERIALS

Graphite, being used in the nature of a reducer, was prepared by grinding Acheson electrodes and by annealing, first at a temperature of 1200° in a graphite crucible without an air inlet and later in a vacuum at a temperature of 1000°.

The ferrite was obtained by annealing a mixture of the composition $CuO.Fe_2O_3$ in air at a temperature of 1000° for 30 hr. With slow furnace cooling of the specimens a mixture of the cubic and the tetragonal forms was obtained, as shown by X-ray investigations. Such a mixture was also obtained by furnace cooling of the ferrite to 530° and subsequent quenching in water, although only the cubic form is to be expected in this case, according to [3].

A ferrite with a cubic lattice was obtained by quenching specimens in water immediately after the end of the annealing, i.e. those heated to 1000°. The data of X-ray analysis of such a specimen coincides with those given in the literature [5].

A ferrite with a tetragonal lattice is obtained by annealing at 1000° with subsequent exposure for three hr at 700° and slow furnace cooling.

METHOD OF CARRYING OUT EXPERIMENTS

Experiments on the reduction of copper ferrite were carried out in a vacuum apparatus [6] with spring quartz weights.

In all cases the weighed portion of the reduced specimen amounted to 0.5 g. 0.15 g of graphite was added i.e. almost triple the quantity necessary for full reduction.

The ferrite was elaborately intermixed and ground with graphite in an agate beater. The ground mixture was placed in a quartz crucible and suspended to a quartz sping, the tension of which was fixed by a micro-cathetometer.

The weighed portion was first degasified at 300° and with a pressure of 10^{-5} mm Hg. Later the furnace, heated to the given temperature, was moved near to it. The gases obtained as a result of the reaction were evacuated through a trap immersed in nitrogen. In the trap was frozen carbon dioxide the quantity of which was determined according to the pressure after evaporation in a known space. In the apparatus three such traps were sealed in parallel and were switched to the reactive space in sequence after a certain interval of time. Thus the quantity of carbon dioxide obtained as a result of the reaction after a defined interval of time was determined. According to the difference between the loss in weight determined by the shortening of the spring and the quantity of CO_2 frozen in the trap, the quantity of carbon dioxide obtained for the same interval of time was determined.

* *Fiz. metal. metalloved.*, 8, No. 5, 740-746, 1959.

VOL. 8 1959

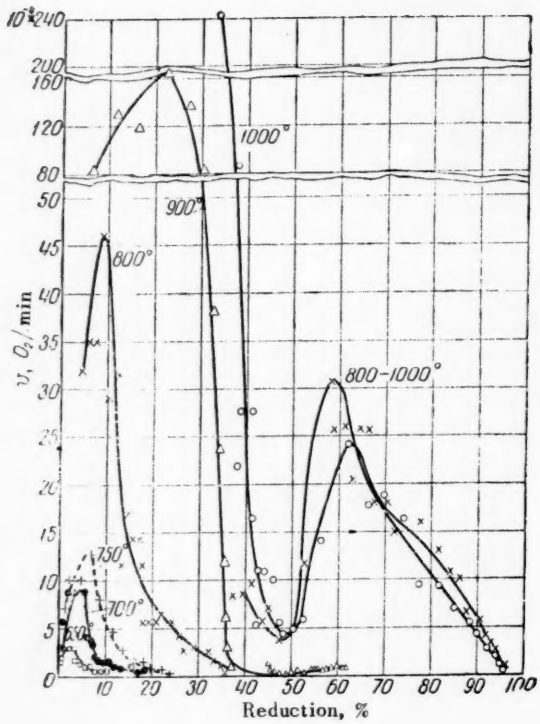

FIG. 1. Relationship of the reduction speed of tetragonal copper ferrite with graphite to the percentage of reduction at various temperatures.

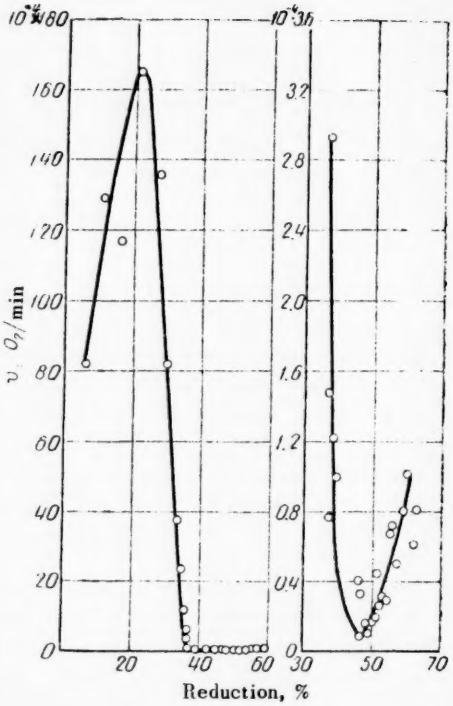

FIG. 2. Relationship of the reduction speed of tetragonal copper ferrite with graphite to the percentage of reduction at 900°.

The percentage of reduction was calculated from the quantity of oxygen removed from the weighed portion.

The solid products of reduction were investigated by X-rays. The lattice parameters of each phase were determined by a method of extrapolation from the graphite parameters.

RESULTS OF EXPERIMENTS AND THEIR DISCUSSION

Reduction of tetragonal ferrite was carried out at temperatures both lower than the transformation point (650, 700, 750°) and higher (800, 900, 1000°). Results of the experiments are given on Figs. 1 and 2.

At temperatures of 650, 700 and 750° a considerable percentage of reduction was attained (respectively 11; 18 and 24%). At 800° reduction proceeded somewhat more extensively but the process practically ceased toward 33-35%. At this stage, the reaction rate of the reduction has a clearly defined maximum. With a rise in temperature, the rate increases, and the transformations related to the lattice change from tetragonal to cubic, have an effect to some degree on the rate of the process, since the temperature coefficient of rate in the range 750-800° is considerably more than in the range 650-750°.

With a temperature of 800° the sample was reduced until such a time as it was practically possible to measure the speed of the process and the temperature was then raised to 1000° and reduction carried through to the end (see Fig. 1, curve for 800-1000°). From the diagram it is seen that up to 50 per cent, the speed of reduction continues to fall and afterwards begins to increase. At 900 and 1000° the speed is high at the beginning of the process.

All the peculiarities of the reduction of copper ferrite with graphite may be seen from the kinetic curve obtained at 900° (Fig. 2.). The initial stage, as is seen from Fig. 2, passes through a maximum reaction rate which afterwards falls sharply, and at 40-50% reduction the rate becomes very small. However, after 50 per cent the growth of the reaction rate may be observed and is clearly seen on section of the kinetic curve between 30 and 70 per cent of

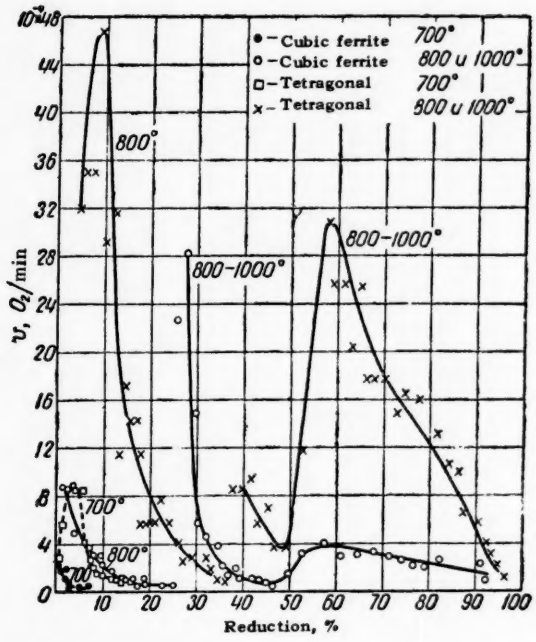

FIG. 3. Comparison of kinetic curves of reduction of tetragonal and cubic copper ferrites with graphite at 700° and 800-1000°.

reduction. This is portrayed on an enlarged scale on the right hand section of Fig. 2.

On Fig. 3 are compared kinetic curves expressing the relationship of reduction rate of tetragonal and cubic forms of copper ferrite from the degree of reduction at temperatures of 700, 800 and 1000°. From the diagram, it is seen that at the same temperatures the reduction speed of the cubic ferrite is less than the tetragonal. In addition, for the cubic form the maximum process speed does not develop at the first stage. Subsequent stages are similar in character for both forms.

Gaseous products of the reaction consist of a mixture of CO and CO_2. In the first stage of the process the content of CO_2 reaches 60-65 per cent. Between 33 and 50 per cent of reduction the gas phase contains 40-25 per cent of carbon dioxide, in the interval of 50-60 per cent reduction the content of CO_2 falls to 12 per cent, towards 70 per cent reduction down to 3 to 4 per cent; after 70 per cent to the end of reduction the gas phase consists practically of pure carbon oxide.

The results of X-ray investigations of the solid reduction products are given in Table 1.

At temperatures of 650, and 750°, the products of incomplete reduction consist of copper, the spinel phase and remains of the initial tetragonal ferrite.

The spinel phase in this case may correspond to either magnetite or cubic ferrite, the lattice parameters of which are so close to each other that it is impossible to differentiate between them by the usual methods of phase analysis.

X-rays taken of the specimens show, however, that a considerable quantity of copper is present in the reduction products as an independent phase and consequently cannot enter into the composition of the spinel. This permits consideration as to whether the spinel phase in these specimens is magnetite, containing, possibly, some quantity of dissolved copper which agrees with the instability of cubic ferrite at temperatures below 760°.

On X-ray photographs of the specimens reduced at 900° to 13-30 per cent, lines are also present which are peculiar to diffractional pictures of copper, spinel and tetragonal ferrite.

The spinel constituent of the specimen in these cases evidently represents a mixture of magnetite and cubic ferrite, the lattices of which, as noted above, are closely related. The latter is formed at the indicated temperature from tetragonal ferrite as a result of phase transformation. At 800° and 24 per cent reduction tetragonal ferrite is not found in the specimens, since under these conditions the reduction process proceeds comparatively slowly (Fig. 4),

VOL. 8 1959

TABLE 1. Results of X-ray investigation of solid products of reduction

Temperature °C	Reduction %	a_{Cu}, Å	$a_{Fe_3O_4}$, Å	a_{Fe}, Å	a_{FeO}, Å	Other phases
			Initial ferrite – tetragonal			
650	10	3.608	8.374	—	—	$CuFe_2O_4$ Tetragonal
700	18	3.608	8.372	—	—	Tetragonal
750	24	3.608	8.374	—	—	Tetragonal
800	24	3.600	8.375	—	—	Tetragonal
900	13	3.599	8.375	—	—	
900	30	3.599	8.375	—	—	—
900	40	3.600	8.374	—	4.280	—
900	63	3.599	—	2.861	4.292	—
1000	96	3.599	—	2.859	—	—
			Initial ferrite – cubic			
800	21	3.608	8.374	—	—	—
1000 After 800	74	3.608	—	2.862	4.280	—

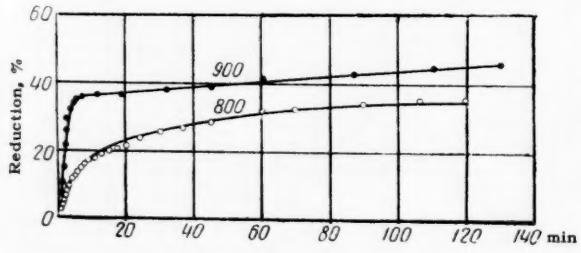

FIG. 4. Change of the percentage of reduction of tetragonal copper ferrite for a given time at 800 and 900°.

and the phase transformation of tetragonal ferrite to cubic goes to completion.

In specimens reduced at 900° to 40 per cent, in the solid phase, in addition to copper, wüstite is observed; with 63 per cent reduction, iron is also present. At 1000° the final products are copper and iron.

Upon reduction of cubic ferrite the following solid reduction products are obtained: in the first stage copper and the spinel phase, but after 50 per cent – copper, wüstite and iron.

It must be noted that copper obtained with the reduction of tetragonal ferrite above the transformation point has a lattice parameter somewhat lower (3.599 Å) in comparison with the tabulated data (3.6080 Å). In the case of the reduction of tetragonal ferrite below the transformation point and with the reduction of cubic ferrite, copper is obtained with a lattice parameter corresponding to pure metallic copper. The lowered lattice parameter of copper indicates that with reduction of tetragonal ferrite at temperatures above 760° some quantity of iron is dissolved in the copper. With the transformation of one modification into another a change of interatomic forces in the lattice takes place, apparently contributing to the solution of iron in copper. Proof of this is also served by the cicrumstance that the lattice parameter of copper does not change monotonically, as would be expected if the appearance of a solid solution was independent on the change of solubility with temperature, but with a rapid drop corresponding to the transition point (Fig. 5).

On the basis of the given experimental material the first stage of the process may be schematically recorded thus:

$$9CuFe_2O_4 + 7C \rightarrow 9Cu + 6Fe_3O_4 + 2CO + 5CO_2.$$

Calculated from this scheme, the degree of reduction is equal to 33.3 per cent. After this magnetite begins to be reduced to wüstite and after 50 per cent wustite to iron. At the second and third stage the process continues as with the reduction of

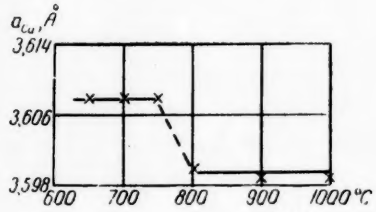

FIG. 5. Relationship of the parameter network of copper to the temperature of reduction of tetragonal ferrite.

simple iron oxides.

The probable mechanism of crystal-chemical transformations during the reduction of copper ferrite may be represented in this way: according to the removal rate of oxygen on the surface of the ferrite a surplus amount of iron and copper ions is formed. Copper, as the least firmly linked with oxygen, forms a metallic phase, but iron diffuses deeply into particles of the ferrite, displacing the copper. Part of the trivalent ions of iron are converted into the bivalent, due to the process of reduction. The ferrite structure approaches the structure of magnetite. After all the ferrite is converted into magnetite, reduction of the latter begins according to the scheme laid out in the work of Arkharov, Bogoslovskii, Zhuravleva and Chufarov [7].

Thus, metallic copper is obtained in the first stages of reduction and iron at the end as a result of the following transformations: copper ferrite → magnetite → wüstite → iron.

CONCLUSIONS

The reduction of tetragonal and cubic copper ferrites with graphite proceeds gradually

$$CuFe_2O_4 \rightarrow Cu + Fe_3O_4;$$

$$Fe_3O_4 \rightarrow FeO;\ FeO \rightarrow Fe.$$

At temperatures of 650, 700, 750 and 800° only the first stage of reduction is observed but at 900° and higher temperature – all three stages. The rates of reduction of the first and third stage are characterized by the presence of a maximum.

Upon the reduction of tetragonal copper ferrite at temperatures above the transformation points a solid solution of iron in copper is obtained. This is related to the simultaneously proceeding process of transformation of the tetragonal lattice of copper ferrite into the cubic.

The probable mechanism of crystal-chemical transformations during the reduction of copper ferrite with graphite is given.

Translated by J. Harvey

REFERENCES

1. L. Well, F. Bertaut, and L.J. Bochirol, *Phys. rad.*, 11, 208 (1950).
2. E.F. Bertaut, *J. phys. rad.*, 12, 252 (1951).
3. N.A. Toropov and A.I. Borisenko, *Zhurnal prikladnoi khimii (Journal of applied chemistry)*, 23, 11, 1163 (1950).
4. J.B. Goodenough and A.L. Loeb, *Phys. rev.*, 98, 391 (1955).
5. E. Prince and R.G. Treuting, *Acta cryst.*, 9, 12, 1025 (1956).
6. E.P. Tatiyevskaya and G.I. Chufarov, *Metallurg*, No. 7, 3 (1940).
7. V.I. Arkharov, V.N. Bogoslovskii, M.G. Zhuravleva and G.I. Chufarov, *Dokl. Akad. Nauk SSSR*, 98, 5, 803 (1954); *Zhurnal fizicheskoi khimii (Journal of physical chemistry)*, 29, 2, 272 (1955).

VOL. 8 1959

THE EFFECT OF VACUUM ON VARIATION OF CRITICAL TEMPERATURES STRUCTURE AND CHEMICAL COMPOSITION OF CAST IRON*

V.P. CHERNOBROVKIN, V.S. BELYAEV and A.A. DOBRYDEN'

Institute of metallurgy, Ural Branch, Academy of Sciences USSR

(Received 21 November 1958)

Vacuum finds many applications in metallurgy [1-3]. In particular, it is used for degasifying when transformer steel is smelted. It gives a significant increase to its plastic and transformer properties by removing the gases O_2, H_2, N_2, sulphur and similar types of impurity [4, 5].

The influence of vacuum on the properties of steel has not been completely studied especially from the metallographic point of view. Very little work has been done on the "vacuumization" of cast iron. This is explained by the fact that less stringent demands are made on cast iron than on steel, hence the expensive process of vacuumization for treating cast iron has not been applied as yet. Meanwhile, the study of the effect of vacuum on the properties of cast iron shows considerable interest.

Tavadze and Bairamashvilli [6] have described the structure of cast iron, obtained in a vacuum. The melts were made in a TGV-1 furnace in magnesite tubes at a residual pressure of 10^{-3} mm Hg. The cast iron was reheated to 1320° and held at that temperature for 20 min. The authors have noted the considerable variation in chemical composition of cast irons melted under a vacuum compared with ordinary cast irons. For example, a lower combined carbon content and appreciably smaller quantities of phosphorus and sulphur are observed. Vacuum also has a effect on the structure of cast iron; graphite accretions have a fine, scaly eutectoid character. Among the aggregates of fine graphite coarser, plate-like graphite is dispersed.

In another work of these same authors [7], the metallic basis of the vacuumization of cast iron is described. It shows isolated pearlite particles within the ferrite deposits.

Bunin and Salli [8] noticed an interesting phenomenon when annealing white cast iron in a vacuum. After holding at 950° and cooling, graphite separated out on the polished surface of the sample. The structure of the sample remained characteristic of white cast iron. As the annealing time was increased so the quantity of graphite on the surface increased and the superficial layer of austenite increased. Graifer and Salli [9] noticed the separation of carbon on the surface of steel graphitized in a vacuum.

In the last article some facts are given about the influence of low residual pressure on the situation of the critical points, the structure and the chemical properties of cast iron.

EXPERIMENTAL METHOD

The experiments were conducted in a vacuum furnace type TGV-1 with molybdenum heating elements (Fig. 1). A vacuum and a diffusion pump maintained a residual pressure of 1×10^{-4} mm Hg in the system. The molybdenum heating elements made it possible to melt the cast iron and re-heat it to a temperature of the order of 1250°.

Measurements of the residual pressure were made with a thermocouple monometric lamp LT-2 and a vacuum meter. Temperature was measured by means of a chromel-alumel thermocouple, the cold junction of which was at the temperature of melting ice; and also a compensating potentiometer. Time was reckoned with a seconds clock.

The cast iron was melted in a Tamman furnace. It was cast in a sand mould gear as applied for determining the properties of metals [10]. The critical temperatures of the cast iron were determined as it cooled in the mould.

A stock length of 35-36 mm was cut off the cooled sample. A sample for vacuum melting was prepared according to pattern by turning in a lathe. A porcelain crucible served as a pattern. Through the centre of the sample a hole 3.5 to 4 mm diameter was bored to admit the hot junction of the thermocouple, which was protected with a silica sheath. The sample and crucible were inserted in a large crucible which was placed on the fire brick support in the working region of the furnace.

* *Fiz. metal. metalloved.*, 8, No. 5, 747-751, 1959.

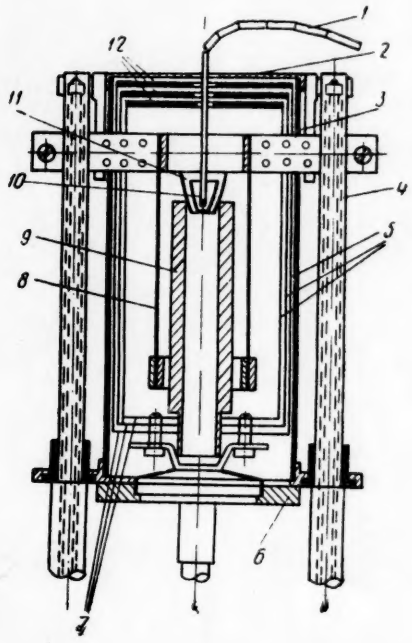

FIG. 1. Diagram of the arrangement of the sample and thermocouple in a vacuum furnace:
1 – thermocouple; 2 – furnace cover;
3 – furnace lining; 4 – conductors;
5 – side-screens; 6 – moveable platform;
7 – bottom screens; 8 – heaters;
9 – fireclay support; 10 – crucible for melting;
11 – protective crucible; 12 – top screens.

TABLE 1. Variation of critical points and composition of cast iron when melted in a vacuum

Melt No.	Melting conditions	Content of elements %				Temperature of eutectic arrest °C	Temperature of eutectoid arrest °C	Period of eutectic arrest, minutes	Period of eutectoid arrest, minutes
		Order C	Graph. C	Mn	S				
1	Normal	3.75	2.73	0.64	0.069	1139	726	1.0	2.0
	vacuum	3.87	3.56	0.14	0.008	1134	730	1.5	1.5
2	Normal	3.75	2.73	0.64	0.069	1139	726	1.0	2.0
	vacuum	3.80	3.52	0.11	0.008	1136	730	2.25	1.5
3	Normal	3.70	2.77	0.64	0.048	1147	—	1.25	2.5
	vacuum	3.80	3.50	0.04	0.008	—	—	1.75	1.25
4	Normal	3.90	3.04	0.54	0.042	1147	729	0.75	2.75
	vacuum	3.80	3.67	0.08	0.007	1129	731	1.75	1.0

Note: The contents of silicon (1.7%) and phosphorus (0.14%) in the cast iron remained the same.

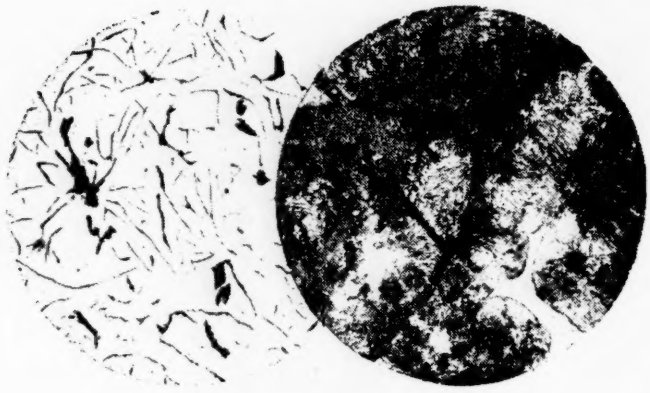

FIG. 2. Structure of ordinary grey cast iron.

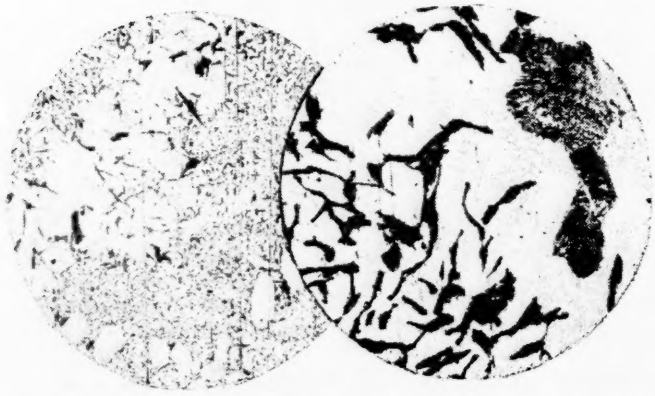

FIG. 3. Structure of grey cast iron, re-melted in the vacuum furnace.

The furnace was covered with three detachable screens and a lid, which had apertures for thermocouples.

A glass cover was placed on the furnace, under which a residual pressure of 1×10^{-4} mm Hg was created. The glass covered was protected by metal gauze which helped to carry away the heat and prevented it from being mechanically damaged. The furnace and the sample were heated up slowly so that the gases evolved could be removed uniformly and the vacuum not be destroyed.

The melted cast-iron was held for 30 min under a vacuum at the re-melting temperature. Later, cooling commenced, in which time, the critical points of the cast iron were determined. After the eutectic transformation has been passed the second heat was carried out, holding for 20 min and finally cooling. Then the vacuum was removed and the sample taken from the furnace.

The sample was now broken to determine the type of fracture. Part of it went to make a polished specimen. Turnings were taken from the other part for a sample for chemical analysis.

The results of the experiments are shown in Table 1.

CONSIDERATION OF RESULTS

To work out an experimental method, some preliminary melts were carried out. Subsequently four experimental melts were made. The chemical composition of the original cast iron is shown in the table.

The surface of the sample not adjacent to the walls of the porcelain crucible shown a smooth prominent plane after vacuumization, on which projections taking the form of grain boundaries are observed. On that surface the graphite is often seen in the form of fine particles.

The surface of the sample adjoining the walls of

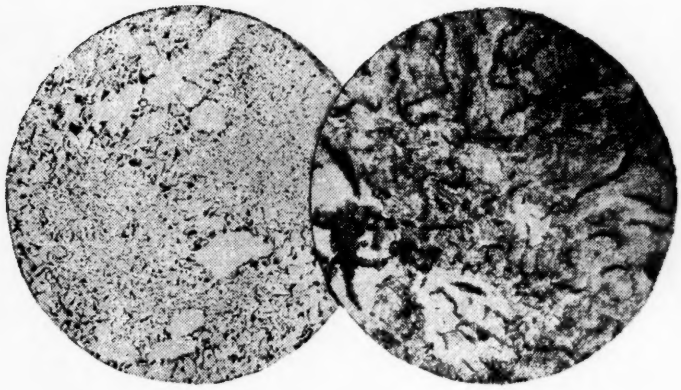

FIG. 4. Structure of white cast iron, re-melted in the vacuum furnace.

the crucible, on the other hand, is uneven with a great number of channels very like the channels from gas bubbles. The same is also observed in the region of the thermocouple.

The samples are very tough, quite flexible and do not fracture for a long time without previous defacing with a chisel.

The fracture of the samples is fine grained at the surface and shows a black periphery. In the centre of the bar the fracture is more coarse-grained and on the whole field white projections are seen which indicate that there is a prevalence of ferrite in the structure.

The chemical composition of the cast iron changes considerably. In all the melts the quantity of graphite increased, the manganese content was very much lower (from 0.64 to 0.14 and even down to 0.04%. Melt 3.), and the sulphur content was reduced by 6 to 8 times.

During the experiment the temperature of the sample was taken every 15 sec. The eutectic temperature of the vacuumized samples could be compared with the same temperatures in corresponding cast irons melted in the Tamman furnace. The general rule seems to be the lowering of the critical point on melting in a vacuum. For instance the eutectic arrest in ordinary cast iron, melt 1, was observed to be 1139°. That same cast iron re-melted in a vacuum had the arrest at 1134°. After repeated heating and finally cooling the eutectic temperature is still lower. For the melt given above it is 1132°.

The eutectoid temperature on cooling a vacuumized cast iron is almost identical for all melts and at 730° it is higher than for ordinary cast iron.

The period of the eutectic and the eutectoid arrest for the vacuum and ordinary cast iron is also shown in the table. The eutectic period of cast iron cooled in a vacuum is longer than that of ordinary cast iron.

It is possible that this is connected with the somewhat more rapid cooling of the latter. The period of eutectoid arrest, on the other hand, is longer for ordinary cast iron than for vacuumized cast iron.

As the microstructure analysis shows (Figs 2 and 3) the flaky form of graphite is maintained in vacuum treated cast iron, the basic mass of the pearlitic is transformed into the ferritic, coupled with which a large quantity 12 to 15%) of graphite inclusions are found amongst the grains of the specimen. The graphite is masked by colonies of medium degree of dispersion, the average length of the flakes being 13 microns. The graphite has a dendritic character in its distribution.

Vacuum treatment was also given to a cast iron of composition 4.1% C; 0.18% Si; 0.2% Mn; 0.3% P. This cast iron on cooling in a sand mould, diameter of the sample 30 mm had a white fracture. After remelting in a vacuum it became grey with a pearlito-ferritic basic mass (Fig. 4).

CONCLUSIONS

1. When cast iron is melted in a vacuum, its chemical composition is greatly changed, the Mn and S contents go down and the content of graphite rises.

2. Eutectic transformations on cooling cast iron in a vacuum occur at lower temperatures and eutectoid at higher temperatures.

3. Pearlitic grey cast iron after re-melting in a vacuum becomes ferritic and white cast iron pearlito-ferritic.

Translated by W.J. King

REFERENCES

1. E. Kalinnikov, *Stal'* No. 5, 608 (1957).
2. D.S. Kametskaya and I.B. Piletskaya, *Stal'* No. 1, 72 (1956).
3. O. Winkler, *Stahl and Eisen*, No. 20, 1261 (1953).
4. G.A. Chernykh and A.M. Samarin, *Stal'* No. 6, 514 (1956).
5. B.M. Borodulina, *Metallurgy*, No. 5, 16 (1957).
6. F.N. Tavadze and I.L. Bairamashvilli, *Foundry Industry*, No. 12, 23 (1956).
7. F.N. Tavadze and I.L. Bairamashvilli, *Foundry Industry*, No. 5, 15 (1956).
8. K.P. Bunin and I.V. Salli, *Dokl. Akad. Nauk SSSR* 83, No. 6, 841 (1952).
9. E.Z. Gaifer and I.V. Salli, *Dokl. Akad. Nauk SSSR* 97, No. 4, 663 (1954).
10. V.P. Chernobrovkin, *Trud. inst. metallurgii Ural Branch Academy of Sciences SSSR*, No. 2, p. 81 (1958).

VOL 8 195

HOT-ROLLED TRANSFORMER STEEL WITH LOW SPECIFIC LOSSES*

N.F. DUBROV

(Received 14 March 1959)

Industrial batches of hot-rolled transformer steel of sheet thickness 0.35 mm and with specific losses $P_{10/50}$ within the limits 0.75 - 0.85 v/Kg, $P_{15/50}$ within the limits 1.72 - 1.96 v/Kg (using sheets of experimental design) were first obtained at the Verkh-Isetsk metallurgical works. Interest was shown in determining the characteristics of chemical and structural composition of the steel with these low specific losses. As a basis of a method for determining these characteristics a comparison was made of the results of chemical, metallographic and electron microscope tests† on steel samples selected from batches of sheets with $P_{10/50}$ 0.75 - 0.85 v/Kg (best indices); $P_{10/50}$ 0.86 - 0.95 v/Kg) mean indices) and $P_{10/50}$ 0.96 - 1.25 v/Kg (worst indices).

A. CHEMICAL INVESTIGATION

For the chemical investigation samples were selected from 90 batches of steel, which had been annealed in vacuum furnaces at 1090° the overall weight being more than 700 tons. The contents of Si, C, Mn, S, P, Cr, Al, Cu, Ti, Ni, N_2, Al_2O_3 were determined in the samples.

In Table 1 the average content of the above-mentioned elements is given for the best, medium and worst indices.

In this table two groups of metal are shown: the first group-metal melted in electric furnaces, and the second-metal melted in Martens furnaces.

Comparing the figures of Table 1. there is hardly a noticeable difference in the contents of the various elements in the best and worst steel. This refers chiefly to impurities like N_2, S, Al, Al_2O_3. In the best steel they are less and in the worst, more. In Martens steel the sulphur content is notably higher than in electro steel, but the content of Al and Al_2O_3 in the first is lower particularly when compared with bad electro steel. The suggestion that there was a lower content of nitrogen in sheets rolled from Martens steel was not confirmed. From the figures of Table 1 it is seen that the higher Nitrogen content goes with the higher aluminium content, – this is particularly well observed in bad electrosteel.

B. METALLOGRAPHIC INVESTIGATION

Samples were taken in the form of small strips from the sheets with specific losses $P_{10/50}$ from 0.75 to 0.85, from 0.95 to 0.99 and from 1.22 to 1.27 v/Kg., for the metallographic tests.

Chemical analysis of the strips taken from the sheets for metallographic testing and data on specific losses of the sheets are given in Table 2.

The amount of non-metallic inclusions in the sheets, their nature and dimensions were determined by a metallographic method; the dimensions of the ferrite grains (by counting the number of grains to the square mm of surface) and micro-structural constants were also determined.

Non metallic inclusions. The number of non metallic inclusions in the unetched strips was found by a calculation method. The criterion for estimation was the average number of non-metallic inclusions in 1 mm² of surface, determined for 60 grain regions with a magnification of 600. The non-metallic inclusions observed in the various strips could be sorted out into 4 types, differing one from the other.

Type 1. – Globular silicate inclusions – simple and complex silicates; – SiO_2, $2FeOSiO_2$, $MnOSiO_2$, nFeO. mMnO. $pSiO_2$;

Type 2. – Finely dispersed acute angled (acicular) or rectangular inclusions of titanium carbo-nitride, Ti (CN);

Type 3. – Sulphide inclusions, FeS, MnS;

Type 4. – Acicular inclusions rich in alumina, Al_2O_3, $Al_2O_3.SiO_2$, Al_2O_3. FeO.

In Table 3 results are shown of the determination of the overall amount of non-metallic inclusions, their types and dimensions in the strips. From the figures given in this table, it is seen that there are less non-metallic inclusions in low-loss steels,

---

* *Fiz. metal. metalloved.*, 8, No. 5, 752-757, 1959.

† I.E. Volotov, A.A. Kozhurov, M.V. Lyasko, G.D. Susloparov and N.I. Shishkina, took part in the test.

VOL. 8 1959

TABLE 1. Average values of the chemical composition of transformer steel samples with different specific losses

No. of samples tested	Specific losses v/kg		Magnetic induction B_{25} gauss	Contents %					
	$P_{10/50}$	$P_{15/50}$		Si	C	Mn	S	P	Cr
I. Electro-furnace metal									
11	0.75—0.85	1.72—1.96	14800	4.25	0.022	0.08	0.005	0.015	0.05
10	0.86—0.95	2.00—2.06	14500	4.22	0.022	0.12	0.007	0.015	0.08
14	0.96—1.25	2.40—2.60	14700	4.20	0.018	0.09	0.006	0.018	0.08
II. Martens metal									
9	0.75—0.85	1.80—2.00	14700	4.25	0.022	0.14	0,014	0.015	0.08
36	0.86—0.95	2.10—2.15	14700	4.18	0.020	0.16	0,016	0.020	0.09
10	0.96—1.25	2.20—2.30	14700	4.20	0.018	0.14	0,018	0.018	0.09

No. of samples tested	Specific losses v/kg		Magnetic induction B_{25} gauss	Contents %					
	$P_{10/50}$	$P_{15/50}$		Al	N_2	Ti	Ni	Cu	Al_2O_3
I. Electro-furnace metal									
11	0.75—0.85	1.72—1.96	14800	0.010	0.004	0.008	0.10	0.17	0.018
10	0.86—0.95	2.00—2.06	14500	0.012	0.004	0.010	0.10	0.17	0.020
14	0.96—1.25	2.40—2.60	14700	0.050	0.007	0.010	0.12	0.19	0.026
II. Martens metal									
9	0.75—0.35	1.80—2.00	14700	0.010	0.005	0.008	0.10	0.22	0.014
36	0.86—0.95	2.10—2.15	14700	0.012	0.005	0.010	0.12	0.22	0.015
15	0.96—1.25	2.20—2.30	14700	0.012	0.006	0.009	0.10	0.20	0.020

inclusions of the first and second types predominate, however. The number of non-metallic inclusions in samples of steel with medium and bad specific losses is practically the same, in steel with bad specific losses inclusions of the fourth type predominate. The relationship of the number of non-metallic inclusions with different dimensions is almost the same in all the strips tested. The majority of the inclusions are those with dimensions up to 1.5 microns and then up to 2.5 microns.

Dimension of the grains and their boundaries. The samples were etched in a 4 per cent solution of nitric acid in alcohol to show the grains. The dimensions of the grains were determined at a magnification of 100 by the calculation method, the criterion being the average number of grains to 1 mm² of the samples of sheet calculated for 60 grain regions. Data about the number of grains to 1 mm² of the samples tested is shown in Table 3.

From these figures, it is seen that specific losses and grain dimensions have a fairly close connexion. As the specific losses increase the dimensions of the grains decrease.

Grain boundaries in steel with specific losses of 0.75 v/Kg are sharply outlined and have a straight line form. (Fig. 1).

Isolated grains with curvilinear boundaries (Fig. 2, lower photograph) are already observed in steel with specific losses $P_{10/50}$ 0.83 v/Kg along with a considerable number of grains with straight line boundaries (Fig. 2). As the specific losses increase so the curvilinear grain boundaries increase. In Fig. 3 grain of steel are shown with specific losses $P_{10/50}$ = 0.95 (*a*) and 1.26 v/Kg (*b*).

Structural components. The basic structural component in all the strips examined under the microscope at magnification 600 was ferrite.

In samples with the best specific losses graphite

TABLE 2. Chemical composition of steel samples, submitted to metallographic testing, %

No. of samples tested	$P_{10/50}$ v/kg	Contents %										
		Si	C	Mn	S	P	Cr	Al	Cu	Ti	N_2	Al_2O_3
1*	0.75	4.43	0.025	0.09	0.004	0.016	0.060	0.009	0.16	0.007	0.004	0.014
2	0.81	4.22	0.028	0.08	0.005	0.009	0.049	0.011	0.20	0.009	0.003	0.009
3*	0.81	4.21	0.026	0.13	0.011*	0.018	0.033	0.011	0.17	0.010	0.004	0.011
4	0.82	4.04	0.026	0.08	0.004	0.016	0.041	0.015	0.16	0.010	0.006	0.021
5	0.82	4.22	0.026	0.06	0.004	0.014	0.082	0.008	0.22	0.008	0.005	0.021
6**	0.82	4.14	0.020	0.13	0.015	0.021	0.15	0.010	0.18	0.012	0.004	0.013
7	0.84	4.18	0.019	0.09	0.005	0.014	0.037	0.008	0.18	0.010	0.003	0.032
8	0.84	4.07	0.014	0.07	0.005	0.009	0.058	0.018	0.16	0.010	0.006	0.017
9**	0.85	4.15	0.017	0.12	0.012	0.017	0.082	0.011	0.26	0.008	0.006	0.011
10**	0.95	4.06	0.017	0.13	0.011	0.015	0.066	0.013	0.18	0.010	0.006	0.015
11	0.95	4.19	0.039	0.06	0.005	0.017	0.009	0.035	0.16	0.012	0.010	0.030
12**	0.96	4.38	0.022	0.13	0.013	0.020	0.074	0.020	0.24	0.010	0.006	0.012
13	0.99	4.30	0.028	0.14	0.004	0.014	0.058	0.010	Not determined	0.008	0.004	0.031
14	1.22	4.17	0.006	0.11	0.006	0.013	0.140	0.037	»	0.008	0.008	0.032
15	1.22	4.25	0.026	0.11	0.003	0.013	0.054	0.060	»	0.011	0.010	0.084
16	1.26	4.01	0.017	0.10	0.004	0.012	0.076	0.048	0.17	0.008	0.005	0.028
17	1.27	4.08	0.017	0.07	0.006	0.013	0.074	0.048	0.18	0.010	0.006	0.028

* Metal vacuumized in the ladle before pouring;
** Metal melted in Martens furnaces.

dispersions are observed here and there in the mass of the grains, the grain boundaries being clear-cut as a rule.

In samples of steel with bad specific losses dispersions of structurally free cementite can usually be seen on the grain boundaries of the ferrite.

B. ELECTRON-MICROSCOPE TESTING

In addition to metallographic testing, three samples of steel having good (No. 1), medium (No. 10) and bad (No. 16) specific losses were submitted to electron microscope testing*.

After the samples had been polished, their surface was etched with a 4 per cent nitric acid solution in alcohol for 30 seconds, then silica replicas were prepared by depositing quartz in a vacuum. The replicas were separated by means of gelatine. The replicas were examined in the electron microscope EM-3 at a magnification of 20,000.

Characteristic electron microphotographs are shown in Figs. 4a-b. In the steel sample with good specific losses ($P_{10/50}$ 0.75 v/Kg) the grain boundaries in the majority of cases are shown as narrow lines only, now and then they are met by inclusions of the second phase of comparatively small dimensions. (Fig. 4a).

For steel samples with medium specific losses the characteristic sign is the considerable number of dispersions of the second phase on the grain boundaries, albeit these dispersions are more coarse. (Fig. 4b).

In steel with bad specific losses the greatest number of dispersions is observed on the grain boundaries and are of still coarser size compared with the steel with medium specific losses.

D. DISCUSSION OF RESULTS

The following have been defined as the most characteristic structural signs of transformer steel having optimum specific losses; fairly coarser ferrite grains, on average 6-10 grains per mm² of sheet; the grain boundaries are straight-lined and to the least extent adulterated by masses of dispersions of the second phase; one would suppose that formation of this structure is promoted in steel with optimum specific losses by comparatively small amounts of impurities which act as barriers, impeding the normal growth of ferrite grains during annealing, and particularly the various compounds of aluminium, amongst them nitrides, sulphur, carbon as structurally free cementite and others.

We should pay attention to the fact that Martens transformer steel (sample No. 5) with sulphur content 0.012 per cent has fairly low specific losses, $P_{10/50}$ = 0.81 v/Kg. Evidently in this case the

* Chemical and metallographic data of these samples are given in Tables 1 and 2.

VOL. 8 1959

TABLE 3. Metallographic data of transformer steel samples with different specific losses

No. of samples	$P_{10/50}$, v/kg	No. of non-metallic inclusions per mm² of strip							Basic type of inclusion	No. of grains per mm²	Form of the dispersed carbon
		Total No.	Dimensions of the non-metallic inclusions, mic.								
			0.9—1.5	1.6—2.4	2.5—4.2	4.3—5.4	5.5—7.5	7.5			
1	0.75	25	4	3	11	1	4	2		6	Graphite
2	0.81	49	25	6	8	3	3	4		7	Graphite
3	0.81	30	19	5	4	1	1	—		10	None
4	0.82	50	22	8	11	4	3	2		12	None
5	0.82	49	11	11	13	4	7	3	1+2	4.5	Graphite
6	0.82	95	23	34	25	7	5	1		16	None
7	0.84	105	49	16	16	9	10	4		8	None
8	0.84	74	53	5	9	2	4	1		9	Graphite
9	0.85	59	34	8	11	3	2	1		16	None
Mean value.	0.83	64	30	12	12	4	4	2		10	
10	0.95	68	40	8	10	4	5	1		25	Graphite
11	0.95	93	37	23	22	5	4	2	3+4	10	Graphite
12	0.96	164	110	25	16	7	4	2		25	Graphite
13	0.99	253	121	59	47	16	7	3		14.5	Coarse Cementite Graphite
Mean value.	0.96	144	77	29	24	8	5	2		19	
14	1.22	132	60	28	27	9	6	2		30	Cementite
15	1.22	199	83	51	27	16	18	4		33	Cementite
16	1.26	129	63	30	18	4	5	5	4+2	94	Cementite Graphite
17	1.27	109	48	30	24	3	2	2		100	Cementite Graphite
Mean value.	1.24	141	63	35	24	8	8	3		64	

FIG. 1. Grain boundaries of the ferrite in transformer steel with specific losses $P_{10/50}$ = 0.75 v/kg. × 66.

FIG. 2. Grain boundaries of the ferrite in transformer steel with specific losses $P_{10/50}$ = 0.83 v/kg. × 66.

unfavourable effect of the sulphur is compensated by the fairly small number of non-metallic inclusions, – in all only 30 inclusions, with an average content for a group of samples with optimum specific losses of 64 inclusions.

CONCLUSIONS

Hot-rolled transformer steel with specific losses $P_{10/50}$ = 0.75 - 0.85 v/kg compared with steel having higher losses is characterized by the following:-

1. Coarse grains of ferrite (6-10 grains per mm) based on straight-lines boundaries;

2. Grain boundaries, in the majority of cases, do not have dispersions of the second phase.

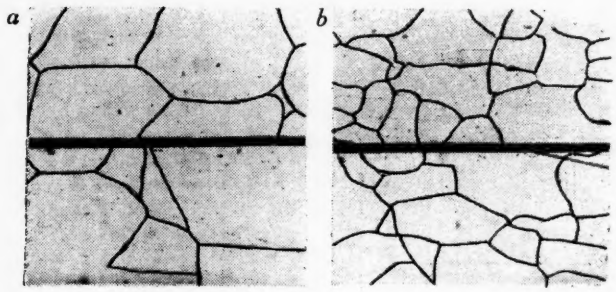

FIG. 3. Grain boundaries of the ferrite (× 66) in transformer steel with specific losses $P_{10/50}$ = *a*, 0.95 v/kg: *b* – 1.26 v/kg.

FIG. 4. Grain boundaries by electron microscope research $P_{10/50}$ = *a*, 0.75 v/kg: *b* – 0.96 v/kg.

3. A small number of non-metallic inclusions.
4. Basically low content of inclusions of Al_2O_3 and the chemical impurities, sulphur nitrogen, aluminium.

Translated by W.J. King

VOL. 8 1959

ANALYSIS OF THE KINETICS OF TWO-PHASE PRECIPITATION OF Cu-Be ALLOY BY AN ELECTRICAL RESISTANCE METHOD*

A.S. KAGAN and Ya.S. UMANSKII

(Received 14 March 1959)

By X-ray diffraction patterns it has been shown that there is a two-phase precipitation in Cu-Be Alloy with 1.9 % Be at temperatures up to 400°. A method of analysing the kinetics of the two-phased precipitation by using electrical resistance is suggested. The heat of activation of the precipitation is calculated.

The precipitation of the super-saturated solution of beryllium in copper with 1.9% Be at temperatures up to 400° bears a two-phase character. The position and intensity of the lines on the diffraction patterns show that on ageing, particles with a Be content of about 0.4% appear along with particles of solid solution containing 1.9% Be; hence the longer the time of holding at the stated temperature the less the amount of unprecipitated solid solution and the greater the amount of the precipitated (solid solution). By holding for a further period the pattern of the lattice of the impoverished solid solution is slowly enlarged, indicating that there is further precipitation due to breakdown of the colloidal equilibrium.

If should be noticed that the two-phased precipitation at 1.9% Be content at temperatures up to 400° contradicts the data given in work [1], where it is shown that the maximum temperature at which two-phase precipitation can still be observed is 350° for a Be content of 1.6%, and it is lower for higher Be contents. It can be suggested that this lack of agreement is due to varying amounts of other impurities in the alloys examined, and especially Ni, of which our alloy contained approximately 0.1%, and in alloys used in the work [1] nickel was absent. The rule about the two-phased precipitation in the alloy which we tested is borne out by the fact that the rates of precipitation in our case are appreciably lower in the solid solution precipitated after 10 min at 350° than in the 1.8% Be alloy used in work [1] – 40% under the same conditions. Hence it can be concluded that the two-phased ageing occurs in those circumstances where precipitation of the solid solution is difficult (either low temperature ageing, or, as in our case, the presence of Ni which delays ageing of beryllium bronze).

The kinetics of the two-phase precipitation were investigated by X-ray diffraction patterns when the martensite had been released, and investigated by Kurdyumov and Lycak [2] who showed that the quantity of solid solutions precipitated depends on the time according to the equation:-

$$V = V_0(1 - e^{-kt}). \qquad (1)$$

We undertook an attempt at analysing the kinetics of the two-phased precipitation of the super saturated solid solution of Be in Cu by an electrical resistance method.

If we accept the rule of precipitation according to Kurdyumov, then with certain stipulation it is easy to show that

$$x = Ae^{-kt} + B, \qquad (2)$$

Where X is the electrical resistance of the aged sample.

The stipulations which have to be fairly exactly fulfilled are the following:

(1) The electrical resistance is subject to the law of discharge, i.e.

$$x = x_1V_1 + x_2V_2 + x_3V_3,$$

where

$$x_1;\ x_2;\ x_3$$

and

$$V_1;\ V_2;\ V_3$$

are the electrical resistances of unit volume and volumes of unimpoverished solid solution, impoverished solid solution and the second phase;

(2) The overall volume of the sample is unchanged,

* *Fiz. metal. metalloved.*, 8, No. 5, 758-760, 1959.

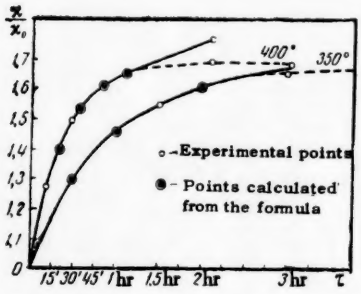

FIG. 1. Relationship of electrical resistance to ageing time.

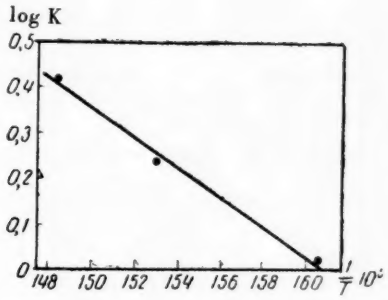

FIG. 2. Relationship of the logarithm of the precipitation rate to reciprocal of temperature.

i.e.

$$V_0 = V_1 + V_2 + V_3;$$

(3) Volumes of impoverished solid solutions and the second phase are in definite relationship to one another, i.e.

$$V_2 = CV_3.$$

The truth of equation (2) was verified with Cu-Be alloy samples as wire of diameter 0.75 mm and length 40 mm, heated to 850°, and aged in a salt bath at temperatures of 350°, 380° and 400°. The temperature was held constant within the limits ± 1°. The electrical resistance was measured on a double bridge with an accuracy of 0.0002 Ohm/Ohm.

In Fig. 1 the relationship is shown of the electrical resistance of the heated sample to ageing time at 350 and 400°. The electrical resistance curves up to a certain ageing time are well expressed by the equation (2), with values of A, B and K – 0.66; 1.69; 1.09 and – 0.69 ; 1.69 and 2.61 respectively. The dotted lines show curves drawn for these values of the constants in formula 2. It is seen that after definite ageing time these curves begin to deviate from the experimental and this may be connected with breakdown of the colloidal equilibrium. It is necessary to note that the time of break down of colloidal equilibrium, as revealed by electrical resistance (2.5 hr at 350°) is less than the time for maintaining equilibrium estimated by X-ray defraction method (3.5 hr under the same conditions), which leads us to add that the resistance method is very sensitive in connexion with the considerable changes of resistance on ageing Cu-Be alloys. From Fig. 1 it is seen that as the temperature is increased so the period of colloidal equilibrium is decreased.

From equation (1) it follows that the constant K is the rate of precipitation

$$K = -\frac{dV}{d\tau}\frac{1}{V}.$$

Assuming that on recrystallization in the solid state,

$$K = K_1 e^{-\frac{Q}{kT}},$$

the heat of the activation process, Q can be calculated from the relationship of precipitation rate to ageing temperature. From Fig. 2 it is seen that the value of log K is directly related to the inverse value of the absolute temperature. From the straight line rule the energy of activation can be calculated and appears to be in the region of 15,300 ± 600 cal/mol. This same factor determined by the internal friction method by Postinkov [3] was found to be 16000 cal/mol. Up till now the heat of activation of the precipitation of beryllium bronze with 1.9% Be (Ni absent) at temperatures from 200 to 500°, was determined in the work [4] by change in the electrical resistance (with different methods of calculation from the present work), of hardness and of area of precipitated grains. Values obtained were from 21,000 to 29,000 cal/mol. However, in the same authors' opinion, in view of the complexity of their precipitation curves, the values obtained correspond with the energy of activation not of a single process but of several super-imposed one on another.

Translated by W.J. King

VOL. 8 1959

REFERENCES

1. V.I. Elyutina and Ya.S. Umanskii, *Technological processes of treating steel and alloys. Symposium* No. 33 (1955).
2. G.V. Kurdyumov and L.I. Lysak, *Zh. teor. fiz.*, 16, 1307 (1946).
3. V.S. Postinkov, *Dokl. Akad. Nauk SSSR* 91, No. 1 (1953).
4. A.C. Guy, C.S. Barrett and R.F. Mehl, *Metals technology*, 15, No. 2 (1948).

STUDY OF THE PATTERNS OF DEFORMATION AND RECRYSTALLIZATION OF IRON-NICKEL ALLOY (48%Ni) IN RELATION TO THE DEGREE OF DEFORMATION ON COLD ROLLING*

M.M. BORODKINA and N.P. GROMOV

Central Scientific Research Institute of Ferrous Metallurgy

(Received 10 January 1959)

The pattern of deformation and recrystallization of thin ribbons (50 and 5 microns) of iron-nickel alloy (48% Ni) in relation to the degree of deformation on cold rolling were studied by an X-ray method by constructing quantitative polar figures. It is shown that only with definite deformations ($\sim$ 99%) the orientations (110) $[1\bar{1}2]$ + (110) $[3\bar{3}5]$ have maximum intensity. In this case, after tempering, a clearer cubic pattern of recrystallization is recorded (100) [001]. Increasing the deformation leads to transformation of orientations (110) $[1\bar{1}2]$ + (110) $[3\bar{3}5]$ into [112] $[11\bar{1}]$ and to weakening of the cubic recrystallization pattern to its complete destruction.

VOL. 8 1959

It is known that by patterning, the magnetic properties (right-angled hysteresis loops and magnetic permeability) of ribbons of the alloy 50 NP (50% Ni) can be increased. But for ribbon thicknesses of less than 50 microns these characteristics deteriorate. It has been shown that as ribbon thickness is decreased from 100 to 5 microns, a change occurs in the relationship of the deformation orientations, and the cubic recrystallization pattern gradually disappears. It is suggested that weakening of the cubic pattern as the ribbon thickness decreases can be explained by the greater part played by the surface layers which have a different deformation pattern and weakened cubic recrystallization pattern. As the deformation is increased from 96.8 to 99.8% while the ribbon thickness is reduced from 100 to 5 microns, it is still not clear what role the factor of increasing the deformation plays. The effect of the two factors – ribbon thickness and deformation must be studied in detail.

The present work is devoted to the study of the deformation and recrystallization patterns of ribbons of Fe-Ni alloy (48% Ni) of thickness 50 and 5 microns in relation to deformation on cold rolling.

SAMPLES AND INVESTIGATION METHOD

The alloy was melted in an induction furnace according to the usual technology and had the following composition, (wt.%): 47.75 Ni; 0.03 C; 0.55 Mn; 0.22 Si; 0.007 S, balance Fe.

A bar 6 mm thick was obtained by forging and hot rolling. By cold rolling the tempered isotropic under-roll ribbons of the alloy of thickness $\sim$ 50 microns were obtained with a reduction from 11 to 99.4% (the thickness of the under-roll varied from 54 microns to 6 mm) and a thickness of 5 microns with a reduction from 73.7 to 99.92% (the thickness of the under-roll from 19 microns to 6 mm), Table 1). The under-roll of a different thickness having no predominant orientations was obtained by cold rolling with a reduction of not more than 60%, followed by annealing at 950°. The hot-rolled annealed bar 6 mm thick was also homogenized. The homogeneity of the under-roll was confirmed by X-ray, photographic and ionization methods. The samples were annealed in a vacuum container (10^{-2} mm Hg) and held for 1 hr at a temperature of 1100°; cooling took place at the rate of 100°/hr down to 600°; then the container was cooled in the air. The magnetic properties were measured by the ballistic method.

The patterns were studied not only by X-ray photography, but the X-ray ionization method was also used to build up the quantitative polar figures. The intensity was registered by photographing the reflected beam through the slit and the complete polar figure was built up by means of a pattern attachment to the standard URS-50I equipment [2]. The intensity of a standard patternless sample, prepared by powder metallurgy was taken as unity; this also had an absorption factor μt (μ = coefficient of linear absorption; t = thickness of the sample). Standard samples were also used for calculating the corrections connected with the fall of intensity, when the sample was turned through a greater angle.

* *Fiz. metal. metalloved.*, 8, No. 5, 761-769, 1959.

TABLE 1.

Initial thickness	Final thickness	Deformation %	True deformation, ln d_0/d_1	Initial thickness	Final thickness	Deformation %	True deformation, ln d_0/d_1
54 μ	48	11.0	0.12	19 μ	5	73.7	1.33
63	48	24.0	0.27	28	5	82.2	1.72
66	48	27.3	0.32	49	5	90.0	2.28
70	47	32.9	0.40	125	5	96.0	3.22
82	48	41.5	0.53	200	5	97.4	3.69
125	49	60.8	0.94	300	5	98.3	4.09
200	49	75.5	1.41	500	5	99.0	4.60
300	48	84.0	1.84	600	5	99.2	4.80
500	49	90.3	2.32	1 mm	5	99.5	5.29
1 mm	49	95.1	3.00	2	5	99.7	6.00
2	49	97.8	3.70	3	5	99.8	6.40
3	48	98.4	4.15	5	5	99.9	6.90
5	49	99.0	4.63	6	5	99.92	7.10
6	49	99.4	4.82				

RESULTS OF THE EXPERIMENTS

The most characteristic X-ray diffraction patterns of the deformed, and tempered, samples of thickness 50 microns are shown in Fig. 1. As the deformation increases, so the deformation pattern becomes more clearly defined. A clearly defined cubic recrystallization pattern is observed in samples which have been deformed with a reduction of 98% and over. For ribbons of 5 microns thickness (Fig. 2) with a deformation of more than 99%, a split (bifurcation) is seen in the maximum ring {*111*}, perpendicular to the roll direction (azimuthal angle $\beta = 90°$). After tempering the cubic recrystallization pattern is only found in samples deformed with a reduction of 99.0 and 99.2%, that is, with those deformations where the pattern of deformation is clearly defined and yet not a significant split of the maximum.

The predominant orientations were studied by means of polar figures. In Fig. 3 the polar figures of some of the deformed, tempered samples are shown, which were obtained by the X-ray ionization method. Orientations observed for deformed samples correspond with ideal orientations set up in certain cold rolled cubic grain-centred metals and alloys. Besides the orientations (110) [$1\bar{1}2$] and (112) [$11\bar{1}$], [3-8], known as fundamentals, there should be noted the orientations (123) [$31\bar{2}$], [see 9], (236) [$53\bar{3}$], [see 10], (123) [$\bar{1}21$], [see 11], (479) [$94\bar{7}$], [see 12], (135) [533], [see 5] (Fig. 4a). However, the orientation (110) [$3\bar{3}5$], which, apparently, is also fundamental in the present instance, coincides most exactly with the intensity maximum, which is situated on the external ring of the polar figure of cold-rolled ribbons with deformation 84-99.4% (Fig. 3).

On deforming with reduction from 11 to 75%, the most intense orientation is (112) [$11\bar{1}$]. A recrystallization pattern is present in these samples after tempering at 1100°. Increasing the deformation to 99.0% leads to reinforcement of the orientations (110) [$\bar{1}12$] and (110) [$3\bar{3}5$]. At the same time, the cubic pattern is reinforced in the tempered samples. Besides the cubic orientation (100) [001], after tempering as a rule, weak orientations (123) [312]; (123) [$1\bar{2}1$] and (479) [$94\bar{7}$] (Fig. 4b) are present which are characteristic of the deformed condition. We did not discover orientations of the spinel type (122) [$21\bar{2}$], usually observed in the 30% Ni/Fe alloy tempered at 900° in ribbons of the 48% Ni alloy. Further increase of the deformation to 99.4% leads to weakening of the deformation pattern. After tempering, this sample, a weaker cubic recrystallization pattern is observed which accompanies orientations characteristic of deformation.

Results of measuring the magnetic properties of the tempered samples of 50 microns thickness correspond well with the pattern differences described above (Table 2). The maximum magnetic permeability μ_{max} and the rectangle of the hysteresis loop B_r/B_s are considerably increased with deformation greater than 95%. Maxima of the properties occur with a reduction of 99.0%, when the orientation of the cube is developed most strongly; further increase of deformation leads to a fall in the properties *.

* The general low level of the properties is explained the poor quality of the insulation of the ribbons

(continued on the next page)

VOL 8 195

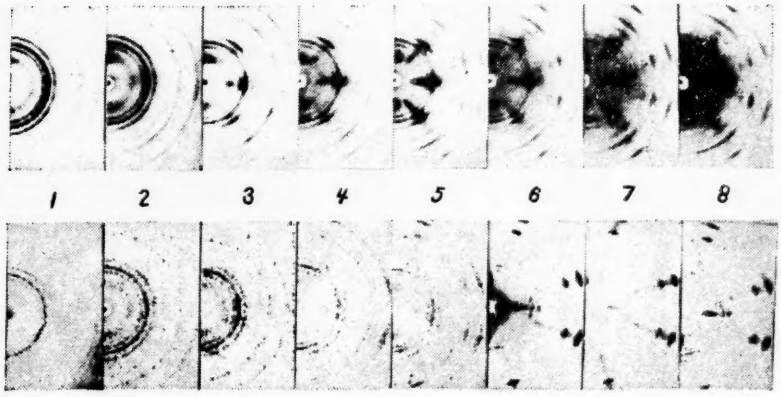

FIG. 1. X-ray diffraction patterns of samples 50 microns thick for various reductions, and the same samples after tempering at 1100° for 1 hr (the true deformation $\ln d_0/d_1$ where d_0 and d_1 are the initial and final thickness, is indicated in the brackets).

1—11.0% (0.12); *2*—41.5% (0.53); *3*—84.0% (1.84); *4*—90.3% (2.32); *5*—95.1% (3.00); *6*—98.4% (4.15); *7*—99.0% (4.63); *8*—99.4% (4.82).

VOL. 8 1959

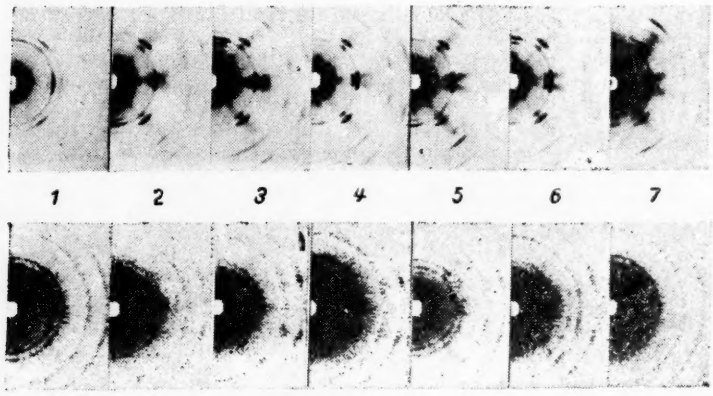

FIG. 2. The same as Fig. 1 for samples 5 microns thick, and for reductions.

1—73.7% (1.33); *2*—97.4% (3.69); *3*—99.0% (4.60); *4*—99.2% (4.80); *5*—99.7% (6.00); *6*—99.8% (6.40); 7—99.9% (6.90).

Polar figures of samples 5 microns thick are shown in Fig. 5. Increasing the deformation up to 99.0% causes the deformation pattern and the cubic recrystallization pattern to be reinforced. Further increasing the deformation produces a gradual transformation of the orientations (110) [$1\bar{1}2$] + (110) [335] into the orientation (112) [$11\bar{1}$], which is strongly reinforced, and leads to weakening of the recrystallization pattern and finally to its complete destruction.

DISCUSSION OF RESULTS

The results obtained give evidence of the fact that an orientation relationship exists between the cubic recrystallization pattern and the pattern from specific orientations. Only in the case of the strongly developed deformation orientations (110) [112] and (110) [335] is the cubic recrystallization pattern

(continued from previous page)
(insulated by talc). When they are insulated by cataphoresis (deposition of magnesium oxide filma by electrolysis) there is a considerable increase in the properties.

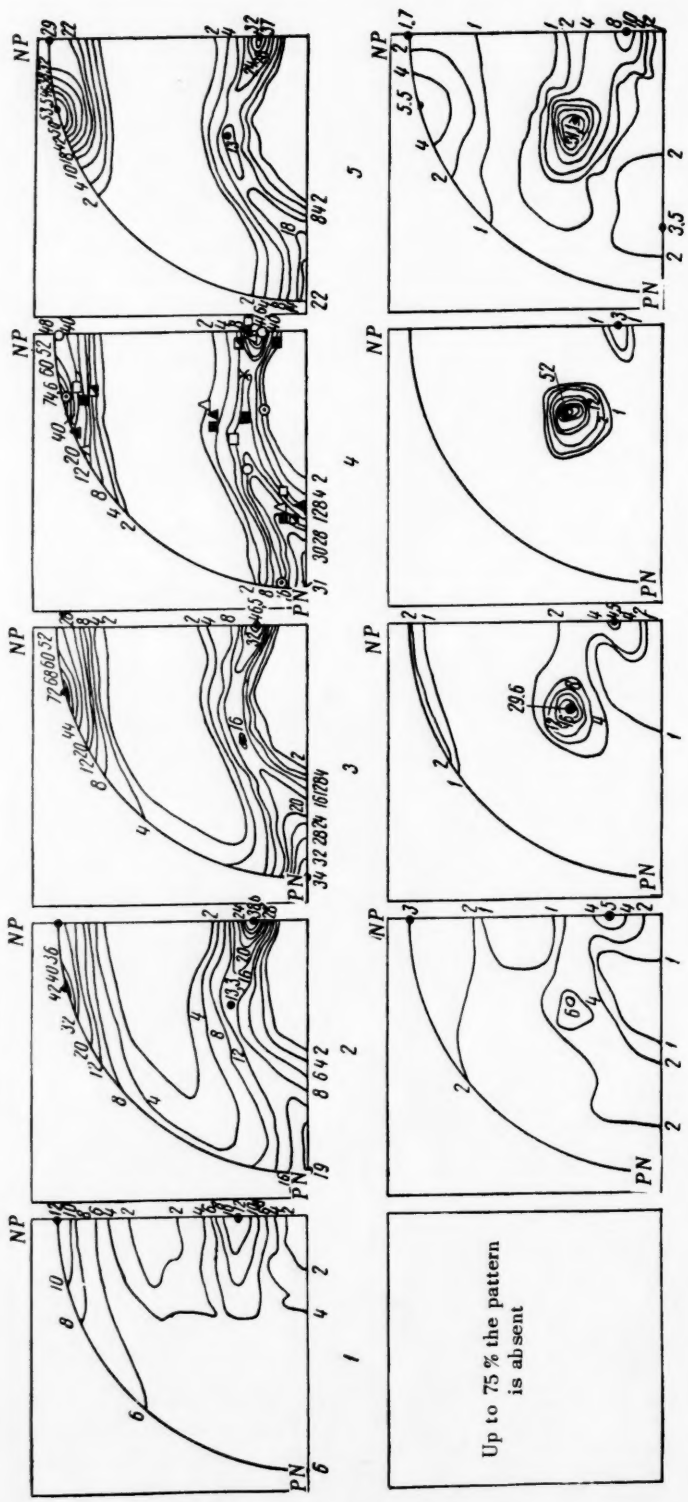

FIG. 3. Polar figures of deformed (upper series) and tempered (lower series) ribbons 5 microns thick:

1 — 11%; *2* — 84%; *3* — 95.1%; *4* — 99.0%; *5* — 99.4%.

TABLE 2.

Reduction, %	μ_0, gs/e	μ_{max}, gs/e	H_c, e	B_r, gs	B_s, gs	B_r/B_s, %
			Insulated with talc			
11.0	2800	22900	0.32	10600	13500	79
24.0	2800	25900	0.29	10700	13500	79
27.3	2800	23300	0.31	10350	13050	80
32.9	3000	26800	0.22	10700	13600	79
41.5	3100	25400	0.28	10500	13550	78
60.8	2900	26500	0.29	10700	13500	79
75.5	2800	27200	0.28	10750	13550	79
84.0	3100	29900	0.26	11050	13950	79
90.3	3000	31400	0.28	11000	13700	80
95.1	3100	32200	0.27	11500	14000	82
97.8	2500	41000	0.26	12400	14200	87
98.4	1400	41800	0.25	13250	14400	92
99.0	1100	44500	0.35	13600	14400	94
99.4	1800	35300	0.31	11600	13500	86
			Insulated by cataphoresis			
95.1	3100	37500	0.20	13500	14300	94
99.0	1300	60000	0.20	14100	14950	94

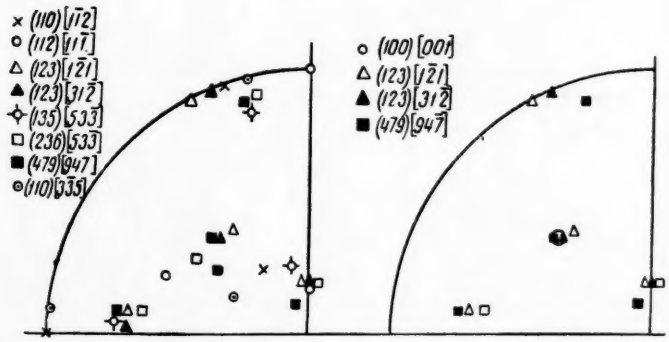

FIG. 4. Orientation pattern of Fe-Ni alloy (48% Ni) of the pole {111}:
a – deformation pattern;
b – recrystallization pattern.

formed.

With regard to the mechanism of the formation of the recrystallization pattern, several theories exist which can be brought together into two opposite points of view: 1) the hypothesis of Burgers [13] – Dunn [14], according to which an oriented formation of recrystallization nuclei occurs already in the deformed metal, thereupon the number of the nuclei should not exceed 5% of the sum of all the orientations; 2) the hypothesis put forward by Beck [15], who suggests that the recrystallization nuclei formed in the tempering process have a disordered orientation, but are distinguished by an orientation relationship of the rate of growth, that is, there is a predominant growth of nuclei with a favourable orientation.

In our investigation we did not discover any maxima corresponding to cubic orientation in the polar figures {111} and {200} of the deformed samples. Maybe the method is not sufficiently sensitive to be able to record the component of the pattern which makes up the whole 5%. The disappearance of the cubic recrystallization pattern when the deformation is appreciably increased, from the point of view of Dunn's theory, could be explained by the higher

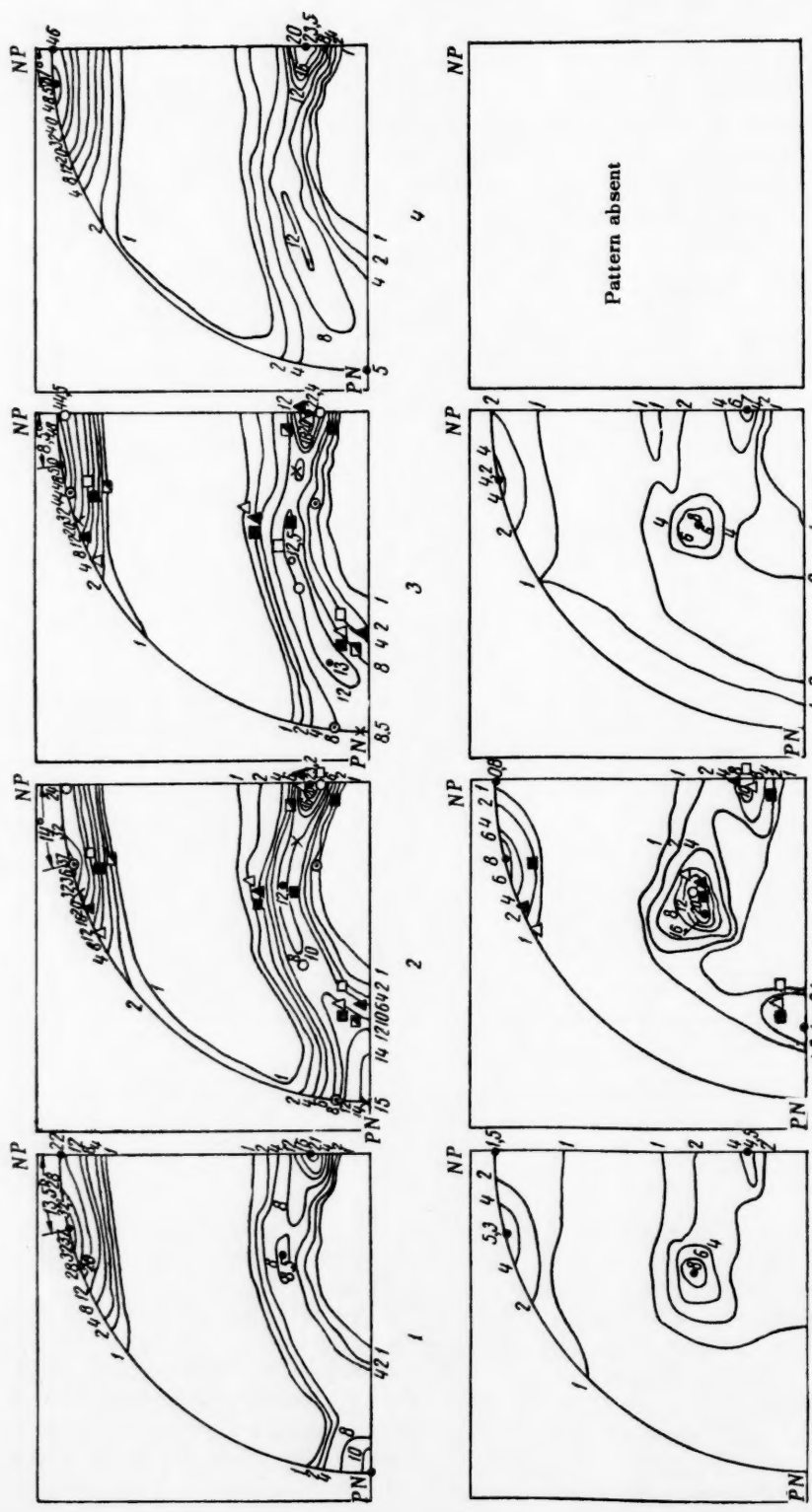

FIG. 5. Polar figures of deformed (upper series) and tempered (lower series) of samples 5 microns thick:

1 — 97,4%; 2 — 99,0%; 3 — 99,8%; 4 — 99,9%.

content (more than 5%) of the cubic orientation component. Yet, in the case where the same high deformation has been imposed (rolling from 6 mm to 5 microns without intermediate temper) the component (100) [001] is not observed in the deformation pattern. The view that the nuclei with cubic orientation appear at definite degrees of deformation and then disappear again is rather improbable.

Apparently, nuclei of cubic orientation are formed on tempering only in crystals having the orientations (110) [1$\bar{1}$2] and (110) [3$\bar{3}$5] which are adjacent to one another. It is possible also that nuclei of cubic orientation have the greatest rate of growth, so that in the case of the strongly developed deformation orientations (110) [1$\bar{1}$2] and (110) [3$\bar{3}$5] preferential growth of nuclei having cubic orientation occurs, which suppresses the development of almost all the remaining orientations.

As far as the patterns of ribbons 5 microns thick are concerned, from the results obtained, a deformation of 99.0% is recommended as the best for producing the most intense recrystallization pattern (100) [001]. However, in ribbons 5 microns thick it seems practically impossible to obtain such a clear-cut recrystallization pattern as in thicker ribbons. The bifurcation of the ring maximum {111} observeable in X-ray diffraction patterns of deformed ribbons of 5 microns thickness is connected with the transformation of the orientations (110) [1$\bar{1}$2] + (110) [3$\bar{3}$5] into (112) [1$\bar{1}$1]. From this it is evident that as the intense maximum of the onter ring of the polar figure approaches the direction of the roll, so there is a fall in the intensity in the direction transverse to the roll. As has been indicated earlier [1], this bifurcation of the maximum can be observed when passing from the centre of the surface of ribbons 50 microns thick. It seems that differing the deformation conditions of the outer and inner strata of the ribbon conditions (vb.) the variation in its pettern; as the total deformation increases so the depth of superficial layers increases. When the ribbon thickness is reduced, the deformation being unchanged, and conversely, when the deformation is increased, the thickness remaining unchanged, the superficial layers take a larger share, relative to the ribbon cross-section, in the effect on the pattern.

CONCLUSIONS

1). As the deformation increases, a change in the relative intensity of the orientations takes place.

2). After tempering the cubic recrystallization pattern is only observed in the case where the pattern with the intense components (110) [1$\bar{1}$2] and (110) [3$\bar{3}$5] is produced, which corresponds to a deformation of 99.0%. Further increasing the deformation leads to weakening of the orientations (110) [1$\bar{1}$2] and (110) [3$\bar{3}$5] and after tempering, to weakening of the cubic recrystallization pattern (100) [001] and to lowering of the magnetic properties.

3). Not only does the pattern of the superficial layers affect the cubic pattern of ribbons 5 microns thick, but also an excessively high deformation has a marked influence.

4). The nature of the variation of pattern of ribbons of Fe-Ni alloy (48% Ni) with increasing deformation confirms the fact that in the tempering process the formation and growth of recrystallization nuclei proceed in an oriented manner.

Translated by W.J. King

REFERENCES

1. M.M. Borodkina and N.P. Gromov, *Fiz. metal. metalloved.*, 6, No. 5, 812 (1958).
2. M.M. Borodkina, "*The Works Laboratory*", No. 5, 638 (1958).
3. S.T. Konobeyevski, *Zs.f. Phys.* 39, 415 (1926).
4. V.I. Iveronova and G.S. Zhdanov, *Zh. teor. fiz.*, 1, 64 (1934).
5. W.G. Burgers and J.L. Snoek, *Zs. Metall.* 27, 158 (1935).
6. G. Sachs and J. Spretnak, *Trans. Amer. Inst. Min. Met. Eng., Iron and Steel div.*, 140, 359 (1940).
7. E.Schmid and H. Thomas, *Zs. Metall.* 41, 45 (1950).
8. J. Grewen, A. Segmuller and G. Wassermann, *Arch. Eisenhuetten*, 29, No. 2 119 (1958).
9. W. Seymor and D. Harker, *J. Metals Trans.* AIME, 188, 1001 (1950)
10. Ch.S. Barret, *The structure of metals*, Metallurgizdat, p. 497 (1958).
11. R.E. Smallmann, *J. Metals*, 84, 10 (1955).
12. J.F. Custers, *J. Physics*, 8, 771 (1941).
13. W.G. Burgers, "*The Solid State*", Brussels, 431 (1951).
14. C.G. Dunn, *Acta metallurgica*, 2, No. 2, 173 (1954).
15. P.A. Beck, *Acta metallurgica*, 1, 230 (1953).

VOL. 8 1959

THE INFLUENCE OF PHOSPHORUS ON STRUCTURAL TRANSFORMATIONS AND PROPERTIES OF LOW-ALLOY ELECTRO-TECHNICAL STEEL *

S.I. DOROSHEK

Urals Scientific Research Institute of the Heavy Metals

(Received 21 April 1959)

Some of the results of the general research on the effect of phosphorus on the structure and properties of low-alloy silicon steel is presented.

Various questions are examined – recrystallization, critical grain growth, phase transformations and change of fundamental magnetic characteristics, as well as plasticity of the steel under the action of small additions of phosphorus.

It is shown that under certain conditions, magnetic properties can be obtained in low-alloy silicon steel, which correspond to a higher grade of high-alloy hot-rolled electro-technical steel.

The deciding factors in securing the highest magnetic properties in electro-technical steel are possibly coarser grain, the absence of phase recrystallization and high specific resistance. In connexion with these, the production of all grades of steel used in the electro-technical. Industry is based on alloying iron with silicon. It is an accepted fact that all other additions, with the exception of aluminium in some cases [1,2] are undesirable.

Meanwhile it is known that phosphorus sharply narrows the γ-region [3] in carbon steels and promotes considerable grain growth in pure iron [4]. The favourable action of the phosphorus should promote better magnetic characteristics. But information in the literature on this subject is very contradictory [5, 6].

The aim of this work is to determine the influence of phosphorus on the structure and properties of electro-technical steel.

The low alloy silicon steel (1.8% Si) chosen for the examination was melted in a 300-Kg induction furnace. All ingots of the steel under test had much the same composition, the other elements present (excluding phosphorus) being 0.24-0.30 % Mn; 0.21-0.30 % Cr; 0.08 % Ni; 0.04 % S; 0.15 % Cu; Al trace.

The phosphorus content of the ingots was 0.03; 0.06; 0.12; 0.21; 0.36; 0.56; 0.70 %. The ingots, rolled into sheets 0.50 mm thick in the Verkh-Isetsk metallurgical works in conditions favourable to this technology, were divided into two parts, one destined for laboratory reserach and the other for industrial experiments.

The carbon content after tempering is usually between 0.008 and 0.018 %, for the investigation of structural transformations, decarburized sheets containing 0.008 % C and raw sheets containing 0.03 % C were used.

The magnetic tests were made on individual bars in the same way as with one-kilogram Epstein trials. The specific resistance for each point was taken as the mean result of the tests on 10-15 bars. The plasticity was estimated in compliance with the requirements of GOST 802-58, from the least number of flexions at a temperature of 15-20°.

STRUCTURAL TRANSFORMATIONS IN SILICON FERRITE ALLOYED WITH PHOSPHORUS

At room temperature phosphorus is soluble in iron up to 1.2 %, forming a substitution of solid solution without any precipitation. Moreover it changes the inter-atomic cohesion forces and the activation energy of the system, and consequently, it must have a noticeable effect on the recrystallization process and grain growth.

With a carbon content of 0.008 % in the steel, no transformations connected with phase recrystallization are observed. Hence only recrystallization processes and grain growth have been studied.

After annealing at 950° for two hr, the samples with various phosphorus contents had differing types of grain. At the same time, increasing the phosphorus content from 0.03 to 0.70 % decreases the number of grains per square mm (× 100) by ten times (Fig. 1 curve *N*), which is about 4 or 5 times more than

* *Fiz. metal. metalloved.*, 8, No. 5, 770-776, 1959.

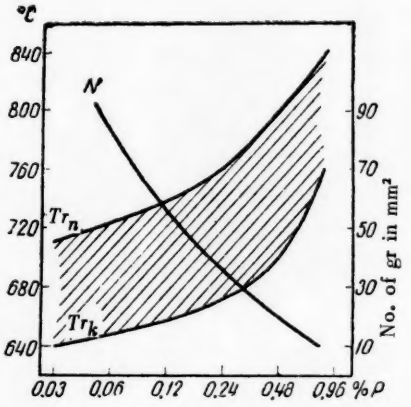

FIG. 1. The effect of phosphorus on the temperature interval of recrystallization and grain size of silicon ferrite ($T_{r.k}$ = temp. at commencement of recrystallization; treatment; $T_{r.n}$ = temp. at the end of recrystallization; N = no. of grains per mm² on annealing at 950° for 2 hr).

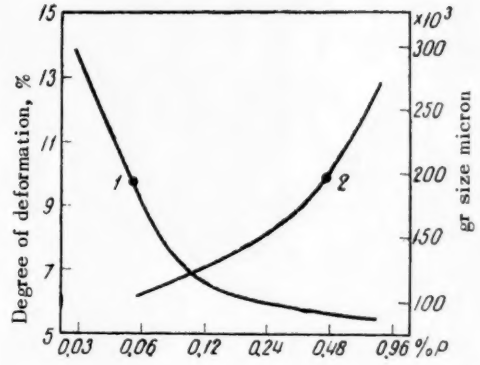

FIG. 2. The effect of phosphorus on the degree of critical cold work and grain size for critical growth:
1 – change of the critical degree of deformation;
2 – change of grain size resulting from critical growth the sample being held at 950° for 2 hr.

the analogous effect with the same amounts of silicon.

Thus phosphorus in silicon ferrite affects the tendency to grain growth very much more intensely than silicon.

In order to clear up this question of the influence of phosphorus on recrystallization processes of silicon ferrite, the samples, given a preliminary cold reduction of 50 per cent, were heated in a lead bath at temperatures 620-840° (every 20° interval) and held for 1 min.

Analysis of the microstructure of samples treated in this way showed that true recrystallization in samples with high phosphorus content takes place at higher temperatures than in samples containing small quantities of phosphorus.

The change of temperature of the beginning and end of the recrystallization treatment under the action of phosphorus is shown in Fig. 1 from which it is seen that increasing the phosphorus in the steel from 0.03 to 0.70% raises the recrystallization temperature by 100-120°. This is equivalent to the action of 3.5-4.5 % Si.

Thus, in regard to the effect on the temperature of recrystallization, phosphorus shows a more energetic action than silicon.

When hot-rolled electro-technical steel is produced by foreign works a critical cold working naklep is often used before the final annealing to improve the magnetic properties [7]. It seemed a useful exercise in the present work to study the effect of phosphorus on the change of critical cold working and the grain size of low-alloy silicon steel. For this, bars of the steel with varying phosphorus contents were given a reduction in the cold condition from 2ce to 18 % (by 1.0-1.5 % at each stage) and annealed in a laboratory furnace at 950° for 2 hr.

Analysis of the microstructure of samples so treated showed very fully the decided effect of phosphorus on the critical grain growth and the degree of cold working of dynamo steel. It indicates that increasing the phosphorus content from 0.03 to 0.7 % tends to lower the critical cold working by 8 % (Fig. 2, curve *1*). The relatively large grain size after annealing increases by more than 2.5 times compared with the effect of critical cold working in steel with a normal phosphorus content of 0.43 % (Fig. 2, curve *2*).

Thus, hindering recrystallization under heavy reduction, phosphorus promotes critical grain growth.

If we examine the secondary recrystallization which is connected with pattern formation as the particular case or the uniformity of grain growth then the phenomenon referred to has the greatest significance in the production and treatment of low-alloy cold-rolled patterned electro-technical steel.

PHASE TRANSFORMATIONS IN LOW-ALLOY SILICON STEEL WITH PHOSPHORUS

Increasing the carbon content in low-alloy silicon steel to values corresponding to the normal original carbon content in the sheets before the final

VOL. 8 1959

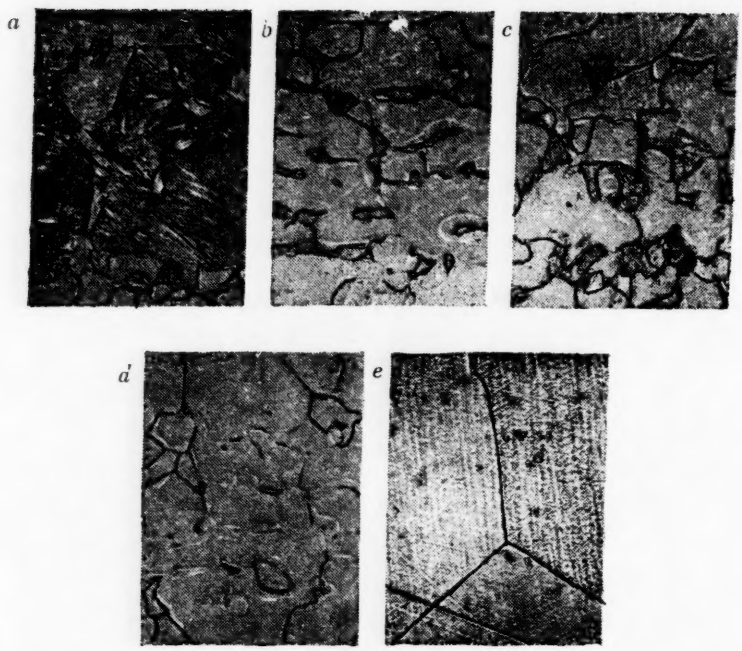

FIG. 3. The microstructure of samples with various phosphorus contents after holding at 1150° for 1 min.
a – *P* = 0.03 %;
b – *P* = 0.06 %;
c – *P* = 0.12 %;
d – *P* = 0.21 %;
e – *P* = 0.36 %. × 330.

tempering (0.03-0.05 %) leads to phase transformation coupled with formation decomposition of austenite [5, 8].

Since phase recrystallization refines the grain, it is undesirable for obtaining high magnetic properties. Phase transformations in dynamo steel containing up to 2.5% Si, are the main obstacle when high temperature tempering is applied [9].

When samples containing 0.03 %C and varying percentages of P were tested it was established that pearlite particles in the steel sharply lowered the favourable effect of phosphorus on the grain size even when critically tempered. Hence it seems a useful excercise to determine the effect of phosphorus on the amount of austenite to be decomposed on cooling.

The quantity of precipitated austenite was determined by heating previously copperised samples to the following temperatures 850; 950; 1050; 1100; 1150; 1200; 1300°.

To decrease the possibility of decarburizing samples by heating to high temperatures, they were held for not longer than 1 min in all cases*.

On soaking the samples containing 0.03 %P at various temperatures a gradual increase in the quantity of transformed austenite was observed with increase of temperature up to 1150°; further increase of temperature led to a smaller amount of martensite.

It is interesting to note that even by quenching from 1150° the whole volume is not transformed. It seems that even 0.03 % C with 1.8 % Si is not sufficient to give an homogeneous γ-region.

Fig. 3 a-e shows the effect of phosphorus on the amount of transformed austenite on quenching from 1150°. From the figure it is seen that even with an insignificant increase of the phosphorus content (from 0.03 to 0.06 %) the amount of transformed austenite diminishes sharply and with P content of 0.21 % phase recrystallization can only be stated to be present because of the fine grain, since the particles known as martensite do not exceed 3-5 %. The presence of 0.36 % phosphorus in steel eliminates the region $\gamma + \alpha$ completely; the very much

* Special experiments were carried out which established this time to be sufficient for the samples to attain the required temperature.

TABLE 1. The relation of the amount of converted austenite for different soaking temperatures to the phosphorus content in steel

Phosphorus content, %	Temperature of heating, °C						
	850	950	1050	1100	1150	1200	1300
	Ammount of converted austenite %						
0.03	10	30	50	80	90	60	25
0.06	10	30	40	50	40	30	15
0.12	15	25	30	25	20	15	5
0.21	15	25	25	20	5	0	0
0.36	15	15	5	0	0	0	0

TABLE 2. The influence of phosphorus on the properties of low-alloy silicon steel

Phosphorus content, %	Annealed in lab vacuum furnace (850° 4 hr)					Annealed in industrial vacuum furnace (1090° 24 hr)			Annealed in industrial vacuum furnace (1090° 24 hr) with preliminary critical cold work	
	H_c, oe	ρ, ohm/mm²/m	$B_{0,008}$, gs	B_1, gs	B_{100}, gs	B_{25}, gs	$P_{10/50}$, v/kg	Min. No. of bends	$P_{10/50}$, v/kg	Min. No of bends
0.03	0.87	0.375	2.53	5400	17550	15000	2.48	43.0	1.63	33.0
0.06	0.83	0.380	2.78	5500	17500	14850	1.83	32.0	1.54	26.0
0.12	0.74	0.385	3.05	7300	17400	14800	1.80	23.0	1.46	19.0
0.21	0.62	0.420	3.10	8200	17300	14950	1.71	11.0	1.34	9.5
0.36	0.56	0.460	3.25	9100	17200	14900	1.58	4.5	1.29	1.0

coarser grains of ferrite gives evidence of this. Repeated analysis of the samples after quenching show that by heating to 1150° the carbon content remain the same (0.028 - 0.031 %).

Thus, increasing the content of phosphorus in low alloy silicon steel with a carbon content of 0.03 % eliminates the γ-region promoting grain growth.

In Table 1 the amount of converted austenite (%) in relation to the quenching temperature and the phosphorus content is indicated. The results show that with increase in phosphorus content not only is the overall amount of decomposed austenite less, but also maximum decomposition is clearly noted in the lower temperature regions. With a phosphorus content of 0.36 % it is sufficient to heat to 1050 - 1100° in order to create normal conditions for intense growth of ferrite grains.

The latter must have great practical significance, since under industrial conditions where decarburization takes place on annealing the presence of increasing amounts of phosphorus permits effective use of high temperature treatment (annealing) in order to obtain maximum coarse grain. In this sense, increased phosphorus content in low-alloy silicon steel is still more useful for the reason that it promotes decarburization in a vacuum which acts on the tendency of carbon atoms to diffuse (relative to the surface of the sheet) similar to silicon [10].

Thus, even with a comparatively high carbon content (of the order of 0.03 %) phosphorus improves the structure making it possible to obtain high magnetic properties.

THE INFLUENCE OF PHOSPHORUS ON THE ELECTROMAGNETIC PROPERTIES AND PLASTICITY OF SILICON STEEL

Heat treatment of sheets with various phosphorus contents was carried out both under laboratory conditions and in the industrial furnaces of the Verkh-Isetsk metallurgical works.

In Table 2 results are shown of electromagnetic

experiments and the plasticity of steel with various phosphorus contents after low temperature annealing under laboratory conditions (850° 4 hr) and high temperature industrial annealing (1090° 24 hr). The figures obtained show that the magnetic induction in weak and medium fields increases with increased phosphorus content, and in strong fields it decreases somewhat. (B_{100}). This is in full agreement with the effect of phosphorus on the structure which was examined earlier. One should only note that the observed decrease of B_{100} does not completely reflect the true influence of the phosphorus on magnetic induction in strong fields, since with low temperature annealing the effect of the phosphorus on the change of the grain size of silicon ferrite is large (the difference in grain size in the cases of 0.03 and 0.36 % phosphorus is almost 6 or 7 times after annealing). With high temperature annealing under laboratory conditions (1150° 4 hr) where there was an insignificant difference in the grain size the samples with high and low phosphorus content (10-20 grains/mm²), the nature of the change of B_{100} was approximately as follows;

P contents %	0.06	0.12	0.36
B_{100} gauss	16,450	16,750	17,150

Thus, it can be stated that magnetic induction in general is increased under the effect of phosphorus. The same idea is confirmed by the small change of B_{25} after high temperature industrial annealing in a vacuum in sheets with varying phosphorus contents.

The specific resistance of steel with increased phosphorus content also increases, which should cut the loss in eddy currents and thereby lower the coercive force due to the growth of grain size which naturally reduces the hysteresis losses. Hence the overall specific losses must be reduced and this is clearly confirmed by $P_{10/50}$ data after industrial annealing in a vacuum.

It is interesting to note that increasing the phosphorus content up to 0.21 % does not reduce the plasticity below the limited value for dynamo steel complying with GOST 802-58. At the same time the magnitude of the specific losses ($P_{10/50}$) for the given phosphorus content greatly exceeds the limit fixed by GOST 802-58 for the best marks of dynamo steel.

Previous cold rolling of sheets of low alloy silicon steel for reductions equal to the critical for various phosphorus contents, improves the specific losses still more, their values approaching those obtained for high alloy transformer steel (E42, E43). In addition the plasticity is no worse than in high alloy silicon steel.

In this way increasing the content of phosphorus in low alloy silicon steel considerably improves its magnetic properties.

CONCLUSIONS

1. Increasing the phosphorus content in low alloy silicon steel promoted grain growth, raises the temperature of recrystallization, reduces the degree of critical cold working and relative volume occupied by the phase transformations.

2. The favourable effect of phosphorus on the structure promotes considerable improvement in the magnetic characteristics of electro-technical steel.

3. The addition of specified amounts of phosphorus to low alloy silicon steel and the use of critical cold working before the final anneal makes it possible to design new grades of electro-technical steel with high magnetic properties.

Translated by W.J. King

REFERENCES

1. F.U. Wefer and G. Hindrichs, *Mitteil aus dem Kais. Wiln. Inst. f. Eisenforschung*, 13, 23, 273 (1931).
2. N.F. Dubrov, G.A. Zykov and B.F. Trakhtenberg, *Bulletin TsNII Ch M*, No. 17, p. 10 (1956).
3. E. Gudremon, *A study of special steels*, United Scientific and Technical Press (1937).
4. B. Hopkins and H. Tipler, *Journ. Iron a Steel Inst.* 31, No. 6, 263 (1958).
5. T.D. Lensen, *Trans. Am. Inst. El. Eng.*, 43, 145 (1924).
6. E. Gumlick, *Zs.f. tech. Phys.* 670 (1925).
7. G. Rassman, *Neue Hutte*, H.4. 193 (1958).
8. R. Rickett and N. Fick, *Trans. of the Amer. Inst. of Mining and Metallurgical Eng.*, 167, 346 (1946).
9. A. Pomp and H. Wiibenhorst, *Stahl u Eisen.*, No. 23, 482 (1942).
10. E.D. Harry, *Journ. Iron and Steel Inst.*, 167, 3 (1951).

VOL 8 195

THE INFLUENCE OF COLD PLASTIC DEFORMATION ON THE MODULI OF ELASTICITY IN CARBON STEELS*

A.V. GUR'YEV
Stalingrad Engineering Institute

(Received 16 December 1958)

Results are set forth in the article of an investigation into the influence of cold plastic deformation on the change in the moduli of normal and tangential elasticity in carbon steels. Firm laws are established of the change in the true values of the moduli after prior plastic deformation. The conclusions are made on an accepted assumption that deformations in different microvolumes of the alloy are inhomogeneous, both in the plastic and elastic fields.

VOL.
8
1959

It was shown in study [1] that the true value of the modulus of normal elasticity determined as a derivative $E = \delta\sigma/\delta\epsilon$, changes after plastic extension of the specimen according to the linear dependence:

$$E = E_0 - \frac{E_0^2}{2P}\,\varepsilon. \qquad (1)$$

Here E_0 – the initial value of the modulus of elasticity (Young's modulus) which corresponds to zero stresses; ϵ – elastic deformation per unit length; P – the new constant of the material called the modulus of microplasticity [2].

It was established [1] that after a small amount of plastic extension (immediately after yielding) the initial modulus E_0 undergoes an insignificant decrease in comparison with Young's modulus determined for an undeformed material. The fact that Young's modulus decreases after cold plastic deformation is known in technical literature. In the majority of cases Young's modulus was determined by dynamic methods [3, 4] which have definite advantages over the static method. But the dynamic methods do not permit the establishement of a law for the change in the true values of the modulus with increased stresses, they merely determine a modulus more or less near in value to the initial modulus E_0. The establishment of laws for the change in the moduli of normal elasticity E and tangential elasticity G in the course of loading a material is very important from the point of view of explaining the influence of stresses on the change in the forces of interatomic bonds. We therefore selected the static method of determining moduli.

STUDY OF THE MODULUS OF NORMAL ELASTICITY

Experimental setup . Normal round specimens 10 mm in diameter were used in the experiments. Wherefore, prior to plastic extension by a given value, their diameter was taken such that after extension it proved to be equal to 10 mm. In those cases when, with plastic extension, the deformation in different directions of the cross-section went unevenly [5], the diameter was determined as the average of several measurements in different cross-sections and directions (perpendicular to the axis of the specimen).

The deformations were measured with high accuracy, using a tensometer of our design [6]. Four types of carbon steel were tested: St. 10, St. 15, St. 30, and St. 45 in conditions of annealing and normalization. The greatest plastic extension was limited by the commencement of necking, which was established on check specimens. The technique on the experiments has been described before in [1].

1. The region of low stresses. It can be seen from graphs given in Fig. 1 and 2 that in the region of very low stresses (region I) the function $E = f(\epsilon)$ differs substantially from the linear one. Also, the intensity of the decrease in E in this region is found to be the more marked, the greater the amount of prior plastic extension. This is why in study [1], where the minimum plastic deformation taken was that corresponding to passing the yield point, this

* *Fiz. metal. metalloved.*, 8, No. 5, 777-784, 1959.

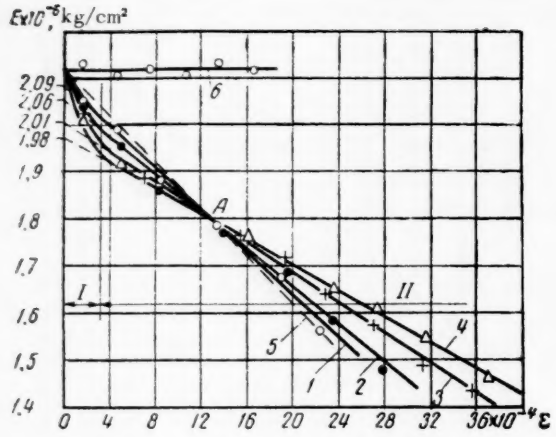

FIG. 1. Change in the true value of the modulus of normal elasticity. St. 30:
$1 - \epsilon_{pl} = 1.2\ \%$; $2 - \epsilon_{pl} = 2.6\ \%$;
$3 - \epsilon_{pl} = 6.9\ \%$; $4 - \epsilon_{pl} = 10.3\ \%$;
$5 - \epsilon_{pl} = 0\ \%$; 6 – the values of the modulus for a plastically undeformed specimen.

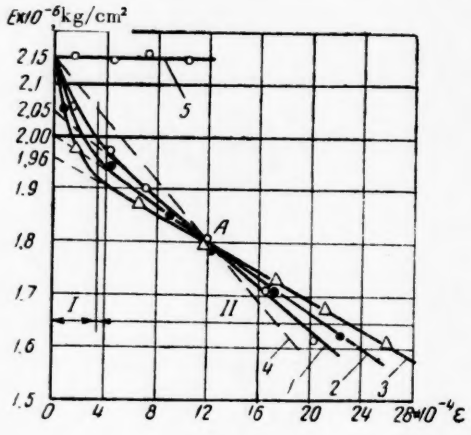

FIG. 2. Change in the true value of the modulus of normal elasticity. S. 15:
$1 - \epsilon_{pl} = 5.3\ \%$; $2 - \epsilon_{pl} = 10.2\ \%$;
$3 - \epsilon_{pl} = 17.6\ \%$; $4 - \epsilon_{pl} = 0\ \%$;
5 – the values of the modulus for a plastically undeformed specimen.

region of the change in E did not appear graphically.

The graphs given, force one to believe that no noticeable decrease in the initial value of the modulus of normal elasticity E_0 takes place as a result of plastic deformation, as was considered to be the case upt to the present, since continuing the curves $E = f(\epsilon)$ until they intersect with the ordinate axis gives, in all cases (and with sufficient accuracy), a constant value of E_0 which corresponds to Young's modulus for an undeformed material.

Conducting tests with small stresses involves as is known very great difficulties, which explains why researchers usually omit the initial steps of loading and do not take them into account. Then in fact, omitting the first region of loading, it would have been necessary to conclude that the modulus decreased steadily with increasing degree of prior plastic extension. On the ordinate axis of Fig. 1 and 2 these values of modulus E_0 are set forth, obtained by means of extrapolating the linear function $E = f(\epsilon)$ of the second region up to the values $\epsilon = 0$.

2. The region of medium and high stresses. In the region of medium and high stresses (region II in Figs. 1 and 2) the linear dependence of the change in modulus E for all the investigated steels is confirmed after any degree of plastic deformation. With increasing the prior plastic deformation, the straight lines $E = f(\epsilon)$ correctly change their slope, so that their angle of slope with the abscissa axes decreases. Therefore the modulus of microplasticity increases since [1]:

$$P = \frac{E_0^2}{2\operatorname{tg}\alpha}. \qquad (2)$$

The value of the modulus of microplasticity P shows the resistivity of the alloy to the development of elastic deformations into microplastic deformations along the weakest and most unfavourably orientated microvolumes [2]. Therefore the increase in the value of modulus P, points to the fact that plastic deformation increases the resistivity of the alloy to the subsequent onset and spreading of microplastic deformations, even with loads lower than the yield strength, that is, in that region which it is accepted to call the "elastic" region. Such a conclusion explains the effect of strengthening of steels due to plastic deformation (which has not yet been fully explained), indicating that this strengthening occurs as a result of increasing the resistivity of individual microregions of the alloy to the development of elastic deformations into microplastic ones, even with stresses lower than the yield strength. The question of the strengthening of steels by plastic deformation and the disclosure of the nature of this strengthening is outside the scope of the present investigation and will be dealt with in a separate report.

3. Concerning the surface-weakened layer. If plastic deformation leads to an increase in the restivity of microregions to the passing along themselves of plastic shears in a wide interval of stresses

TABLE 1.

Steel 15		Steel 30	
Plastic deformation ϵ_{pl} (%)	ΔR_{weak} (mm)	Plastic deformation ϵ_{pl} (%)	ΔR_{weak} (mm)
5.3	0.11	1.2	0.06
10.2	0.17	2.6	0.09
17.6	0.22	6.9	0.15
—	—	10.3	0.19

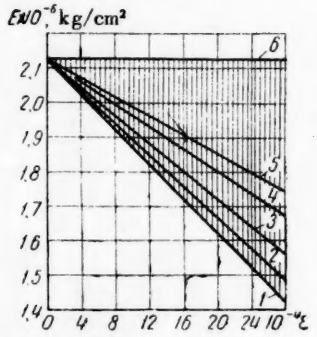

FIG. 3. Change in the true value of the modulus of normal elasticity after excluding the influence of the surface-weakened layer. St. 30:
1 – ϵ_{pl} = 0 %; 2 – ϵ_{pl} = 1.2 %;
3 – ϵ_{pl} = 2.6 %; 4 – ϵ_{pl} = 6.9 %;
5 – ϵ_{pl} = 10.3 %; 6 – plastically undeformed material.

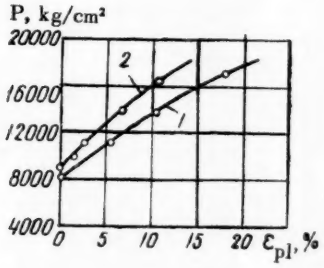

FIG. 4. Change in the modulus of microplasticity depending upon the degree of prior plastic deformation:

1 – St. 15

2 – St. 30

(region II in Figs. 1 and 2), then at first glance it appears incomprehensible why, in the region of low stresses (region I), on the contrary a sharp drop in this resistivity is noticed, which is noted on the graphs by a greater intensity in the decrease of modulus E. One of the explanations for this effect can be given by introducing the concept concerning the surface-weakened layer, taking into consideration that in the surface layer which is not reinforced from one side by the grains of the alloy, the onset of plastic shears and their development ought to be easier. Such an explanation does not contradict the dislocation theory either, according to which it is considered that grain boundaries and impurities form their own barriers to the path of displacements due to dislocations.

Several scientists [8, 9] confirm the existence of this layer on the basis of X-ray diffraction and mechanical studies, estimating their thickness to be in the limits of 0.06-0.2 mm. In one of the most recent studies Rovinskii and Mokeyeva [10], although they do not agree with the concepts of Davidenkov and Glikman about the surface-weakened layer, nevertheless indicate that a layer of metal adjoining the surface of steel specimens appears when loading, in a different way from the metal of the body as a whole, and introduce an idea of the elastic limit (the yield strength) of the specimen as a whole and of its surface layer.

At the moment it must not be considered that the question of the surface-weakened layer is completely solved. However the results of the investigation which has been conducted, permits one to estimate the approximate thickness of this layer and its change with an increase in cold hardening. The relative part of the area of the weakened layer [1] can

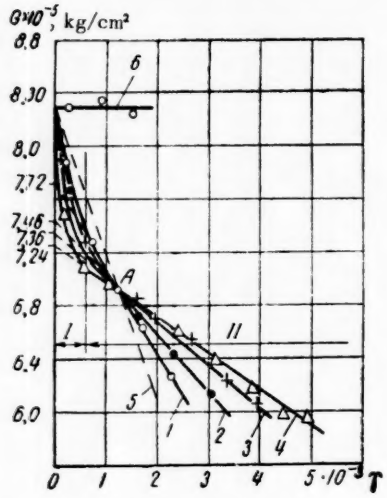

FIG. 5. Change in the true value of the modulus of tangential elasticity. St. 10:
1 – $\gamma_{pl} = 0.105$; 2 – $\gamma_{pl} = 0.227$;
3 – $\gamma_{pl} = 0.51$; 4 – $\gamma_{pl} = 1.25$;
5 – $\gamma_{pl} = 0$; 6 – plastically undeformed material.

be determined from:

$$f_{weak} = \frac{\Delta E_0}{E_0}. \qquad (3)$$

But

$$f_{oc} = \frac{\Delta F_{weak}}{F} = \frac{2\pi R \Delta R_{weak}}{\pi R^2} = \frac{2\Delta R_{weak}}{R}. \qquad (4)$$

Consequently

$$\Delta R_{weak} = \frac{\Delta E_0 R}{2E_0}. \qquad (5)$$

Table 1. sets forth value of ΔR_{weak} for two steels, calculated by formula (5). As can be seen from the table the thickness of this weakened layer, calculated by the analytical method, agrees well with the results of direct determination of its thickness carried out by other authors [8,9].

Since the thickness of the surface-weakened layer is insignificant, with increasing the stresses its influence ceases to be felt, and the change in modulus E at high stresses, determined experimentally, will reflect the properties of the basic mass of the metal.

INVESTIGATION OF THE MODULUS OF MICROPLASTICITY

Studying the graphs in Figs. 1 and 2 we note that all curves $E = f(\epsilon)$ intersect at one point A. This rule is probably not accidental, since it is repeated for all the investigated types of steel, and furthermore, as we shall see later, it is also confirmed by torsional tests. From this it may be concluded that, depending upon the selected step of loading when determining the modulus of normal elasticity, different and even contradictory results will be obtained.

Thus, if when testing one takes maximum stresses of the step of loading which are less than for point A, then one reaches the conclusion that Young's modulus decreases with increasing prior plastic extension. Increasing the step of loading (crossing point A) can give results with a constant value of Young's modulus, or even an increase with increasing the degree of prior plastic deformation. Since neither the initial not the final steps of loading are standardized, but are selected by each investigator independently, depending on the accuracy and reliability of the testing machine and the tensometers, it becomes understandable why there are still many results in this question which are inconsistent with one another. This is why, when conducting the present investigation, the change in the true value of the modulus ($E = \delta\sigma/\delta\epsilon$) was determined in the course of a smooth increase in stresses from zero to the yield strength, which allowed reliable laws to be established both in the qualitative and the quantitative respect.

Now it is possible to give a hypothetical law for

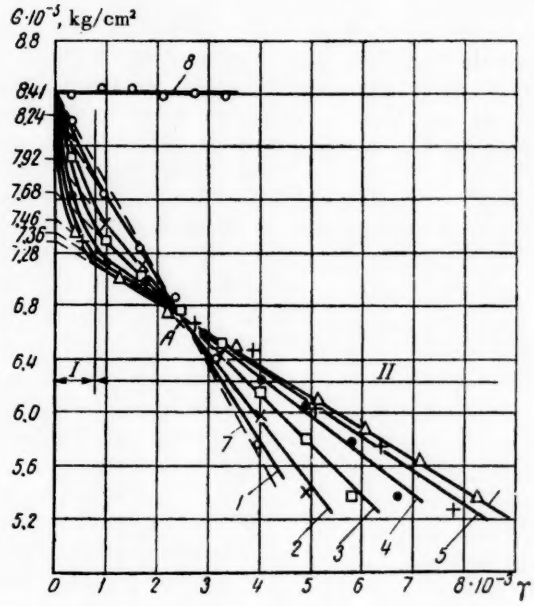

FIG. 6. Change in the true value of the modulus of tangential elasticity. St. 45:
1 – $\gamma_{pl} = 0.039$; 2 – $\gamma_{pl} = 0.079$;
3 – $\gamma_{pl} = 0.157$; 4 – $\gamma_{pl} = 0.314$;
5 – $\gamma_{pl} = 0.628$; 6 – $\gamma_{pl} = 0.942$;
7 – $\gamma_{pl} = 0$; 8 – plastically undeformed material.

the change in modulus E after very small plastic deformation within the limit equal to zero. With increasing degree of plastic deformation, curves ($E = f(\epsilon)$) in the first region of loading tend even more to develop into a straight line. Therefore when $\epsilon_{pl} = 0$ the change in modulus E will follow in accordance with a straight line passing through two points: point A and the point with co-ordinates $\epsilon = 0$, $E = E_0$. In Figs. 1 and 2 these straight lines are given by broken lines.

If the influence of the surface layer of the specimen is excluded, the graphs of the change in E in the whole region of loading appear as straight lines as indicated in Fig. 3. In this graph, the cross-hatching represents the region of possible change in modulus E for a given type of steel with any degree of plastic deformation.

The modulus of microplasticity P, upon whose value depends the intensity of the change in E with increasing stresses, can easily be calculated using formula (2). Modulus P, as can be seen from Fig. 4, increases steadily with the increase in the degree of plastic deformation.

STUDY OF THE MODULUS OF TANGENTIAL ELASTICITY

Torsion, as a more "gentle" way of loading [11], has certain advantages over tensile stressing, since with torsion considerably greater plastic deformations can be reached. This gives the opportunity of checking the laws established above in a considerably wider interval of plastic deformations. The maximum plastic tortional angle was chosen close to that torsional angle at which failure took place, which was established using the check specimens.

The true values of the modulus of tangential elasticity were determined as a derivative $G = \delta\tau/\delta\gamma$. The same types of steel were used as for the tensile tests.

Graphs are presented in Figs. 5 and 6 showing the change in the true value of the modulus of tangential elasticity $G = f(\gamma)$, and they repeat in all elements the laws for the change in the function $E = f(\epsilon)$. In this way the correctness of the basic assumptions in the first part of this article are confirmed. We shall not therefore repeat ourselves here by reviewing these graphs.

CONCLUSIONS

1. After plastic deformation (of any degree) the dependences of the change in the true values of the moduli of elasticity $E = f(\epsilon)$ and $G = f(\gamma)$ form two clearly distinct regions: the regions of low stresses with a sharp decrease in the moduli, and the

VOL. 8 1959

region of medium and high stresses with linear dependence of the decrease in the moduli. This indicates that in the second region the rate at which the microregion of the alloy enter into inelastic (plastic) deforming stabilizes itself and then remains constant.

2. The intense decrease in the moduli of elasticity in the first region can be explained by the action of the surface-weakened layer of the specimen, in which plastic shears can commence with smaller stresses.

3. An increase in the degree of prior plastic deformation leads to an increase in the modulus of microplasticity P, whose value indicates the rate of the development of elastic deformations into microplastic deformations along individual microregion of the alloy. Consequently, plastic deformation leads to the strengthening of individual weak microvolumes of the alloy, so that their entering into plastic deforming will take place with high stresses, which leads in the end to an increase in the overall yield strength of the metal, that is to say, to the well known effect of the strengthening of an alloy after plastic deformation.

4. The increase in the modulus of microplasticity P with increasing the degree of plastic deformation can be explained by the crushing of the units (which is made apparent by X-ray diffraction methods of research), as a result of which the number of obstructions in the path of displacement due to shearing (dislocations) is increased [12].

5. The results of the investigation show that plastic deformation gives rise to practically no decrease in the initial moduli of normal and tangential elasticity. The values of the moduli of elasticity E_0 and G_0 have a distinct connexion with the interatomic forces and the structure of the crystal [13], therefore plastic deformation which does not give rise to a change in the crystal structure should not lead to a noticeable change in the moduli of elasticity either. The opinion has already been expressed, that plastic deformation should not lead to a decrease in the moduli E_0 and G_0 [13], and in experiments at very low temperatures, when the passage of inelastic processes (relaxational) is made difficult, no decrease in the modulus should be observed. However such measurements were not carried out. The question of the constancy of the modulus of normal elasticity for steels which have not undergone deformation was studied in work [14].

Translated by J.J. Cornish

REFERENCES

1. A.V. Gur'ev, *Fiz. metal. metalloved.*, 7, No. 4, 586 (1959).
2. A.V. Gur'ev, *Zh. tekh. fiz.* 24, No. 9, 1644 (1954).
3. V.I. Korotkov, *Fiz. metal. metalloved.*, 2, No. 1, 160 (1956).
4. V.I. Korotkov, *Zavod. Lab.* 22, No. 1, 98 (1956).
5. A.V. Gur'ev, *Fiz. metal. metalloved.*, 2, No. 3, 457 (1956).
6. A.V. Gur'ev, *Pribory i tekhnika eksperimenta*, No. 4, p. 90 (1957).
7. N.F. Mott, *J. Iron and Steel Inst.* 183, 3, 233 (1956).
8. N.N. Davidenkov and Ye.L. Assur, *Primeneniye rentgenovskikh luchei k issledovaniiu materialov, (Application of X-rays to the study of materials)*, book 15, p. 61, Mashgiz, (1949).
9. L.A. Glikman and V.A. Stepanov, *Zh. tekh. fiz.* 16, No. 6, (1946).
10. B.M. Rovinskii and V.I. Mokeyeva, *Fiz. metal. metalloved.*, 5, No. 2, 331 (1957).
11. Ya.B. Fridman, *Mekhanicheskie svoistva metallov, (Mechanical properties of metals)*, Oborongiz (1952).
12. V.M. Golubkov, V.A. Il'ina, V.K. Kritskaia, G.V. Kurdiumov and M.D. Perkas, *Fiz. metal. metalloved.*, 5, No. 3, 465 (1957).
13. *Uprugost'i neuprugost' metallov, (Elasticity and inelasticity of metals)*, Edited by S.V. Vonsovskii, Foreign Literature Publishing House, (1954).
14. A.V. Gur'ev, *Nauchnye dokl. vysshei shkoly, Metallurgiia*, No. 4, 193 (1958).

DETERMINATION OF THE PERIOD OF RELAXATION AT THE POLYMORPHIC TRANSFORMATION OF IRON*

R.I. GARBYER and A.I. KOVALEV
Physico-Technical Institute, Academy of Sciences Ukrainian SSSR.

(Received 10 April 1959)

In the temperature range 20-1000° measurements have been made of the damping ratio of torsional vibrations in cylindrical specimens of technical iron with a carbon content of 0.04%. In the region of α-γ transformation, measurements were carried out at five different frequencies from 1.08 to 6.8 c/s. The frequency dependence of damping at transformation temperature has a maximum at 2.6 c/s, which corresponds to a relaxation period of 0.06 sec. Assuming that damping is connected with the activation process and that the natural frequency of the atomic vibrations amounts to 10^{13} sec^{-1}, a value for the activation energy can be obtained of 64 kcal/g-at.

VOL. 8 1959

In the region of the polymorphic transformation temperatures of cobalt [1] and zirconium [2] a considerable increase has been discovered in the damping ratio of elastic vibrations. This effect can be interpreted as a result of energy dissipation on the boundaries between grains of different phases. In actual fact, in each of the phases near to the transition temperature, internal friction is considerably lower than at a transition temperature when stable or unstable nuclei of a new phase arise. Unless one assumes special properties at the contact surfaces of crystals of different phases it is impossible to understand why such a sharp increase in internal friction is observed when approaching the transformation temperature. On the interphase boundaries transformation processes are localized. They take place due to heat energy necessary for maintaining constancy of temperature. Intensely progressing transformation processes can be the cause of additional dissipation of elastic energy of vibrations and can lead to a sharp increase in damping ratio. After the transformation process is completed, a sharp jump and a decrease in the damping ratio should be found, simultaneous with further temperature increase.

Since the position of the jump on the curve for temperature versus damping ratio can be displaced with change of frequency, serious difficulties arise when determining the relaxation characteristics of the phenomenon.

With a view to measuring the period of relaxation in similar cases one can, at a fixed temperature, determine the frequency dependence of the damping ratio of vibrations. Such a method is apparently, always applicable, and can be employed not only for studying polymorphic transformations. In particular, it is expedient to employ this method when studying the influence of cold working on internal friction, when there is a danger that heating can lead to uncontrolled annealing, when studying internal friction in the region of the melting point and the temperatures of recrystallization and phase transformations in alloys.

If the maximum of damping ratio is discovered at a definite frequency, one can consider that the period of relaxation of the process being studied τ satisfies the ratio

$$\omega\tau \approx 1, \qquad (1)$$

where ω – the cyclic frequency at which the damping value has its highest value. Results of such a method of investigating internal friction in iron at the temperature of α-γ transformation are set forth below.

SPECIMENS AND TECHNIQUE

A study was made of technical iron with a carbon content of 0.04%. The installation which was employed for the present study, and also the geometrical shape and dimensions of specimens are described in the previous article, which is devoted to the study of the temperature dependence of the moduli

* *Fi. metal. metalloved.*, 8, No. 5, 785-788, 1959.

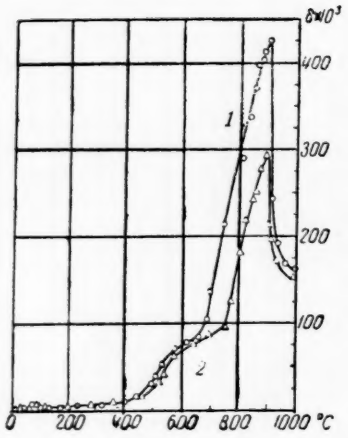

FIG. 1. Damping ratio of torsional vibrations of iron as a function of temperature:
1 – at a frequency of 2.6 c/s;
2 – at a frequency of 6.8 c/s.
Measurements were carried out at an increase of temperature. (The frequency is indicated for 900°).

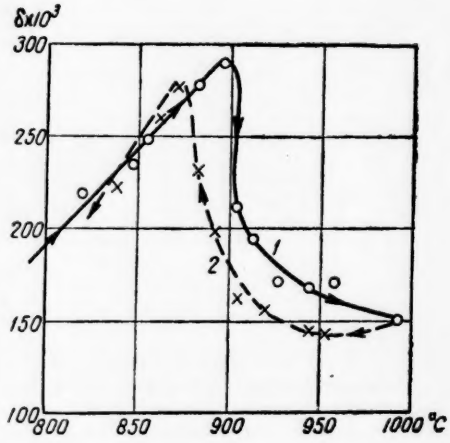

FIG. 2. Damping ratio of trosional vibrations of iron as a function of temperature:
1 – when heating;
2 – when decreasing the temperature.
In both cases the frequency at 900° was equal to 6.8 c/s.

of elasticity in iron [3].

After being machined the specimens were vacuum annealed at a temperature of 950° for 15 hr, and were then cooled to room temperature, after which the temperature was raised to the required value by a heating process at a rate of 1° per min. Prior to each oscillographic measurement the temperature was held constant for 15-20 min with a view to balancing the temperature along the whole specimen. Oscillographic measurements were carried out every 10-15°. In the most interesting region the temperature intervals were reduced to 8°. The damping ratio was determined on the results of measurements of photographically fixed oscillograms.

In all, five different series of measurements were made. In each series the moment of inertia of the pendulum gear was selected in such a way that at a temperature of about 900° the frequency of the torsional vibrations was approximately equal to the prescribed values. Measurement of the corresponding oscillograms showed that these frequencies amounted to 1.08, 1.80, 2.60, 5.00, 6.80 c/s. The greatest axial load of the specimen did not exceed 100 g/mm². The shear per unit length with torsional vibrations did not exceed 2×10^{-3}, which corresponds to a shearing stress of 45 g/,mm². An analysis of the possible mistakes showed that the error in determining the damping ratio does not exceed 5%.

DISCUSSION OF THE RESULTS OBTAINED

Fig. 1 shows the results of measuring the temperature dependence of the damping ratio of torsional vibrations obtained by conducting two series of measurements, corresponding to a frequency of 2.6 (curve 1) and 6.8 c/s (curve 2). Similar curves were obtained when carrying out the remaining three series of measurements. It is easy to see from the curves of Fig. 1, that up to 700° the temperature dependence of the damping ratio obtained from conducting the present work does not differ from well known literature data (cf [4]). When increasing the temperature further, a substantial increase in the damping ratio is observed and then a jump-like decrease, in the region of polymorphic α-γ transformation temperatures. Approaching a temperature of 1000° the decrease in the damping ratio ceases and apparently it can be expected that, with further temperature increase, an increase in the values of the damping ratio of vibrations will take place in the γ-phase.

Some measurements were carried out when cooling the specimens from 1000 to 800°. In this case, a displacement of 30-35° in the position of the jump on the curve towards the side of low temperatures was observed. Furthermore, when measuring in the reverse direction, the slope of the curve was substantially changed. Fig. 2 gives curves for temperature versus damping ratio when heating (the continuous curve) and when cooling (the broken curve). It is easy to see that when approaching the transformation temperature, the slope of the curves is somewhat flatter than when one is moving away from this temperature zone. However, in the γ-phase,

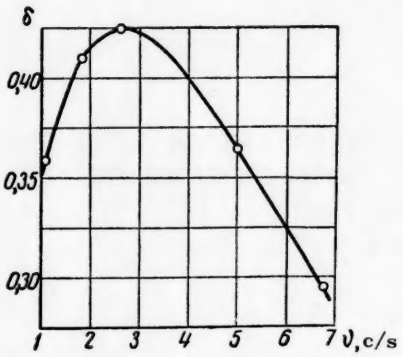

FIG. 3. Damping ratio as a function of the frequency of vibrations.
δ – the value of damping at transformation temperature;
ν – the value of the vibrational frequency (c/s).

both curves progress considerably more steeply than in the α-phase.

From a comparison of the curves in Fig. 1 for different vibrational frequencies, it follows that at one and the same temperature the damping ratio depends upon the frequency. The greatest difference is obtained for the temperature corresponding to the jump. Therefore in Fig. 3 the greatest values of the damping ratio, which are obtained at α-γ transformation, are placed along the ordinate axis, and along the abscissa axis are placed the corresponding values of the vibrational frequency of the specimen. The cuve in Fig. 3 has a clearly defined maximum at a frequency of about 2.6 c/s. This shows that at the temperature of the jump there is some kind of relaxation process, whose period, according to formula (1) amounts to 0.06 sec.

A value for the period of relaxation obtained in this way can be referred to the most diverse phenomena, for example, it could be suggested that relaxation occurs as a result of the relative displacement of adjacent grains of different phases. However, it is unlikely that simple friction between adjacent grains of different solid phases would greatly differ from the friction between grains of one and the same phase if the processes of phase transformation were not taken into account. Precisely the transformation processes which are localized on the interphase boundaries, can be the cause of relaxation of the type described. Therefore it is expedient to compare the value obtained for the relaxation period with processes of an activation character which are taking place at transformation temperature on the interface between the phases. For this purpose, the well known ratio can be used

$$\tau = \tau_0 e^{\frac{H}{RT}}, \qquad (2)$$

where $\tau_0 = 10^{-13}$ sec; H – activation energy; R – gas constant; T – temperature of transformation at which the value of the period of relaxation τ was determined. Substituting in expression (2) the corresponding values of the amounts indicated we obtain $H = 64$ kcal/g-at. It is expedient to compare the calculated value of H with the activation energy of self-diffusion, since polymorphic transformation can apparently be described as a process of detatchment of individual atoms from the lattice points of the old phase, and subsequent attachment to the lattice points of the new phase. Such a process must be localized on the interphase boundary, that is, in the very place where the energy of elastic vibrations is dissipated. Obviously H should not be greater than the activation energy of self-diffusion, which in the given case is so (according to the data of Golikov and Borisov [5] the activation energy of self-diffusion in the α-phase of iron amounts to 67 kcal/g-at). This circumstance, that the value of H was obtained close to the value of the activation energy of self-diffusion, can be interpreted as an argument in favour of the assumptions set forth above.

For the reverse transformation γ-α, τ and H can have somewhat different values, since the damping ratio in the jump zone when cooling can depend in a somewhat different way on the frequency, and the position of the maximum on the curve of the type in Fig. 3 can prove to be displaced. Unfortunately, at the present time, the authors do not have at their disposal enough data to explain this question.

Translated by J.J. Cornish

REFERENCES

1. W. Köster, *Zs.f. Metallk.* 39, 51 (1948).
2. W.J. Bratina and W.C. Winegard, *J. of Metals*, 8, No. 2, 186 (1950).
3. R.I. Garbyer and A.I. Kovalev, *Zav. Lab.* No. 4, 477 (1958).
4. Kê Ting-sui, *Metals Technology* 15, No. 4 (1948).
5. V.M. Golikov and V.T. Borisov, *Prob. metalloved. i fiz. metal* No. 4, M., 542.

THE INFLUENCE OF THE TEMPERATURE OF THE EXPERIMENT ON THE FATIGUE STRENGTH OF SPECIMENS OF CARBON STEEL WITH STRESS CONCENTRATORS UNDER THE ACTION OF A MOLTEN ENVIRONMENT OF THE EUTECTIC Pb-Sn *

M.I. CHAYEVSKII

Institute of Machinery and Automation, Academy of Sciences USSR

(Received 1 November 1958)

The article shows that under the action of a liquid metal molten environment the fatigue strength of steel can increase over a sufficiently wide temperature range.

One of the main factors impeding the development of high-temperature heat exchange systems in which liquid metal molten environments are used is the inability of the majority of materials to withstand the action of liquid metals at high temperatures. Therefore when investigating the fatigue strength of steels under the action of liquid metal molten environments, one must bear in mind that in the majority of cases only a limited ultimate fatigue strength can be determined, because under the action of the dissolution process the endurance of the steel being investigated will decrease with increasing the time scale.

The actions of liquid metal molten environments on steel which result in a change in the mechanical properties of the steel may be of several mutually interrelated types, for example: 1. Adsorption action; 2. Dissolution process of the basic part of the alloy or of the composite parts which bond the crystals together; 3. Chemical reaction between the steel and either the liquid metal or the inclusions contained in it (various types of oxide).

Diffusion processes proceed parallel with the types of action enumerated.

As the tests have shown (Fig. 1) one type of action or another can predominate; depending upon the testing temperature adsorption action may manifest itself the most strongly, whereas at higher temperatures the dissolution process may be of decisive significance. (Prior to conducting the tests, the same stress concentrators as in work [3] were applied to the specimens, only with a notch angle of 45°. Before testing in the molten environment of the eutectic Pb-Sn, the specimens were coated with a layer of the eutectic Pb-Sn by the hot-dipping method, (to ensure reliable wetting).

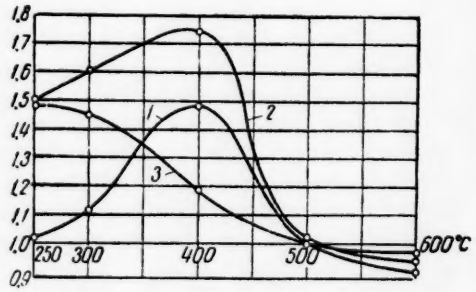

FIG. 1. Influence of temperature on the fatigue strength of specimens of carbon steel 35 with stress concentrators being tested in a molten environment of the eutectic Pb-Sn:

$1-\frac{\sigma_{-1\text{ action }t}}{\sigma_{-1\text{ action }20}}=f(t\,^{\circ}C)$; $2-\frac{\sigma_{-1\text{ environ}}}{\sigma_{-1\text{ action }20}}=f(t^{\circ}C)$;

$3-\frac{\sigma_{1\text{ environ}}}{\sigma_{-1\text{ action }t}}=f(t\,^{\circ}C)$.

$\sigma_{-1\text{ action}}$ – ultimate fatigue strength at a given temperature on the basis of 2×10^7 cycles;

$\sigma_{1\text{ action }20}$ – ultimate strength at room temperature;

$\sigma_{-1\text{ environ}}$ – ultimate fatigue strength in the molten environment of eutectic Pb-Sn at a given temperature on the base of 2×10^7 cycles.

The effect of adsorption action amounts first and foremost to facilitation of deformation in a steel placed under the action of a liquid metal molten environment which is a strong surface-active substance [1, 2]. As is shown in works [2, 3], the result of the effect of the facilitation of deformation of steel under the action of surface-active substances can be either an increase or a decrease in the fatigue strength of the steel.

* *Fiz. metal. metalloved.*, 8, No. 5, 789-791, 1959.

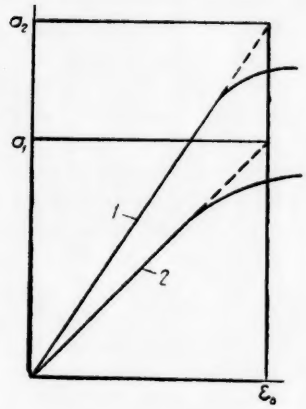

FIG. 2. Character of the change in the mechanical properties of metal with tensile stressing under the action of a surface-active substance:
1 – testing in air;
2 – testing in a surface-active medium.

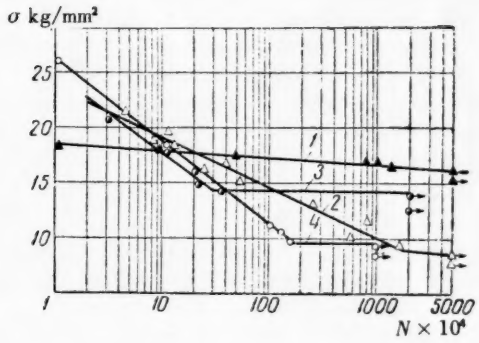

FIG. 3. Curves for fatigue strength of specimens of steel 35 with stress concentrators (H_{R_B} = 80 ± 1):
1 – tests of specimens precoated with a layer of eutectic Pb-Sn in a molten environment of eutectic Pb-Sn at 400° (n = 50 c/s);
2 – tests of specimens in a molten environment of eutectic Pb-Sn at 400°;
3 – test of specimens in air at 400°;
4 – tests of samples in air at 20°.

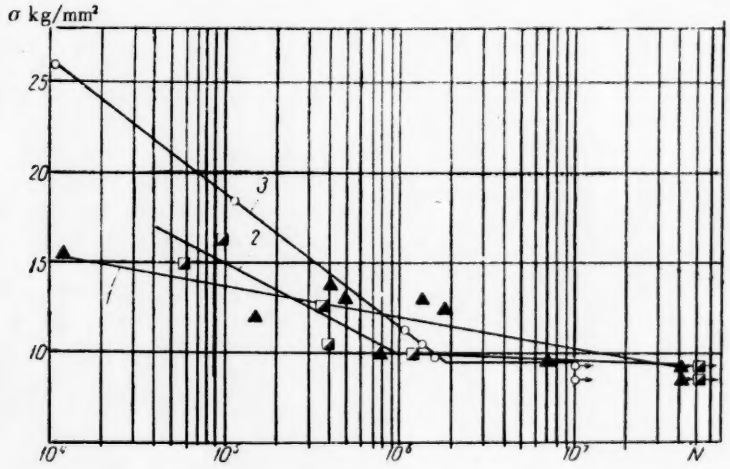

FIG. 4. Curves for fatigue strength of specimens of steel 35 with stress concentrators (H_{R_B} = 80 ± 1):
1 – test of samples precoated with a layer of eutectic Pb-Sn in a molten environment of eutectic Pb-Sn at 500°;
2 – test of samples in air at 500°;
3 – test of samples in air at 20°.

It is considered that facilitation of deformation and decrease in strength are explained by the fact that liquid metal molten environments diminish the surface energy of steel, promote the onset of plastic shear and the development of various defects [2]. There is little information in the literature [3-6] on the possibility of increasing the strength of steel under the action of surface-active media.

As can be seen from Fig. 1 in the temperature range 250-500°, the fatigue strength of steel specimens with stress concentrators, subjected to the action of a liquid metal molten environment of the

eutectic Pb-Sn, is higher than when testing in air. It must be assumed that the mechanism of such an increase in fatigue strength amounts to a decrease in stress concentration resulting from the softening of the surface layers of the metal under the action of a liquid metal molten environment. The latter leads not only to a decrease in the yield strength of the surface layers of the metal, but also to an alteration of the modulus of elasticity [2]. With cyclic straining of steel specimens at a given strain ϵ_0 (Fig. 2) the stress in the softened layer can only reach a magnitude of σ as a result of strengthening, whilst in steel specimens being tested in air the stress increases to a magnitude of σ_2 which can prove to be inadmissible [7, 8].

From the curves given in Fig. 1 one must not draw the conclusion that right up to 500° carbon steel specimens subjected to cyclic straining will work satisfactorily in a liquid metal molten environment. The fact is, that the points in Fig. 1 which correspond to the restricted endurance limit of steel specimens are determined on the basis of 2×10^7 cycles. In order to come to a conclusion about the possibility of employing steel which has undergone cyclic strain in structures with a liquid metal molten environment, it is necessary to determine the intensity of the drop in the limited endurance limit with increasing time scale of testing due to dissolution of the steel.

If, for example, during tests at $t = 400°$ (Fig. 3) the intensity of the drop in the limited ultimate fatigue strength is insignificant, then at a test temperature of 500° (Fig. 4) the limited ultimate fatigue strength drops considerably with increasing the basis of testing. Therefore, if at $t = 400°$ carbon steel, which is undergoing cyclic stressing, can still be employed for structures in which a molten environment of the eutectic Pb-Sn is used, then at a temperature of 500° it is inexpedient to employ carbon steel in the case of continuous operation.

Translated by J.J. Cornish

VOL 8 195

REFERENCES

1. P.A. Rebinder, *Iubileinyi sbornik Akad. Nauk USSR k XXX-letiiu Velikoi Oktiabr'skoi sotsialisticheskoi revoliutsii, (Jubilee symposium of articles of the Academy of Sciences USSR to celibrate the 30th anniversary of the great October socialist revolution), publ. Akad. Nauk USSR,* 1, 123 (1947).
2. V.N. Likhtman, P.A. Rebinder and G.V. Karpenko, *Vliianiye poverkhnostno-aktivnoi sredy na protsessy deformatsii metallov (The influence of a surface-active medium on the deformation processes of metals) Publ. Akad. Nauk USSR,* (1954).
3. M.I. Chayevskii, *Dokl. Akad. Nauk USSR,* 124, No. 4 (1959).
4. T.Iu. Liubimova and P.A. Rebinder, *Dokl. Akad. Nauk USSR* 63, No. 2 (1948).
5. T.Iu. Liubimova, *Zh. tekh. fiz.* 12, 331 (1950).
6. N.V. Pertsov and Iu.V. Goriunov, *Inzh-fiz.Zh.* No. 6 (1959).
7. E. Orowan, *The welding journal,* June (1952).
8. M.I. Chayevskii, *Dokl. Akad. Nauk USSR,* 125, No. 2 (1959).

VOL.
8
1959

LETTERS TO THE EDITOR

THE PROBLEM OF THE MECHANISM OF INTERCRYSTALLINE INTERNAL ADSORPTION IN DILUTE SOLID SOLUTIONS*

V.I. ARKHAROV, B.S. BORISOV, S.D. VANGENGEIM and G.G. TALUTS

Institute of the Physics of Metals Academy of Sciences U.S.S.R. Urals State University

(Received 19 June 1959)

The radiographic method of examining intercrystalline internal adsorption (measurement of the reversible chenges in the lattice parameter of a polycrystalline solid solution in relation to grain size of the alloy does afford much greater possibilities, in comparison with other methods, for a quantitive approach to the effect. Several binary and ternary systems [1, 2, 3] have been studied by this method, which has made possible various qualitative considerations concerning the factors which determine the nature of the intercrystalline internal adsorption in different alloys [4].

However, if the data obtained is to be used for a detailed analysis of the mechanism of the effect, it is necessary to define more accurately the ideas concerning the characteristics of the state of the atoms of the dissolved component in the lattice of the solvent.

On the basis of the models of Mott [5] and Friedel [6] it has been assumed that there are atomic nuclei of the solvent and the dissolved additions in the nodes of the lattice; electrons in the inner shells of these and other atoms form an electrical field which is the same for the whole lattice. It is exclusively the external valence electrons which are responsible for a change in potential. These may be observed as an electron gas. It is assumed that the impurity atoms are to be found at great distances from one another and their interaction may be ignored.

In this model only the differences are considered, between atoms which are bonded with their different valences. Here the valency of the solvent element must be less certain than that of the dissolved component.

In the case of solid solutions of elements in the II-V groups of the periodic system with copper, silver and gold, the model gives a picture of many different effects which corresponds very satisfactorily to experiments.

It has been shown that, as a result of the interaction of the electron shells of the atoms of the solvent and the atoms of the solute a local redistribution of electric charge "(screen redistribution") must arise close to the latter. This may be described as an increase in the effective atomic radius in the atoms of the solute. This change is much less in the atoms of the solvent and it may virtually be ignored.

This effect of "screen redistribition" has been observed, for example, in diffusions in weak solid solutions [7], in the changes in electric resistance [8] and paramagnetic susceptibility [9, 10] of solid solutions in relation to the concentration of the dissolved component, in more or less all effects and processes connected in any way with the further interaction in solid solutions.

The influence of impurities in similar phenomen opens up a way for the detemination of the significance of a "screened" atomic radius. In the work of Henry and Rogers [9] in particular, which is devoted to the study of the paramagnetic susceptibility of dilute alloys with a copper base, the ratio relating the value of paramagnetic susceptibility χ_A to the screen-redistributed atomic radius of impurity $\bar{r}$ is derived:

$$\chi_A = \frac{Ne^2}{6m}\bar{r}^2.$$

It follows from all that has been said that the interaction of the electron shells of the atoms included in the composition of the dilute solid solution may have a considerable effect on the behaviour of the atoms of the impurity in this solid solution. In particular this may have some bearing on the intercrystalline internal adsorption. In considering electron interaction it should be possible to describe the atomic mechanism of internal adsorption

* *Fiz. metal. metalloved.*, 8, No. 5, 792-794, 1959.

TABLE 1.

Composition %	Screen redistributed atomic radius $\bar{r}$, Å Calculated acc. [9]	Increased (+) or decreased (–) grain size	Change in grain size by how many times	$\Delta a_{teor} \times 10^4$, Å Calculated acc. [11]	$\Delta a_{exp} \times 10^4$, Å [2, 3]
Ag+1% Tl	2.68	–	15	–91	–71
		+	20	+98	+109
		–	30	–95	–71
		+	1,5	+32	+26
		–	1,2	–4	–4
		+	1,4	+29	+23
Ag+5% Zn	2.61	+	4	–21	–21
		–	4	+21	+32
		+	4	–21	–15
		–	4	+21	+18
		+	4	–21	–28
Ag+1% Pb	2.59	–	3,5	–56	–78
		+	3,5	+56	+47
		–	3,5	–56	–72
		+	3,5	+56	+63
		–	3,5	–56	–60
Cu+1% Mg	2.86	+	5	+15	+11
		–	6	–18	–7
		+	6	+18	+7
		–	12	+28	+22
Cu+1% Sn	4.21	+	3	+20	+27
		–	3	–20	–18
		+	3	+20	+17
		+	2	+12	+11

and to relate it to quantitative data available in this field.

If there are any defects or structural heterogeneities in the lattice, interaction will occur between them and the atoms of the impurity. This is an interaction of long range order and consequently one can here speak of "screen redistribution", that is to say, the atoms of the impurity should behave here as if they were subject to a "screen redistribution" atomic radius.

As any structural heterogeneity (including grain boundaries) may be regarded as a system of dislocations, for an approximate description of the interaction of the atoms of an impurity in a solid solution with the distortions of the lattice, Webb's [11] calculation may be used for a number N_0 of atoms diffused from the depth of the grain to the system of dislocations, which models the intercrystalline boundary, that is for the number of atoms subject to intercrystalline internal adsorption.

A similar calculation was carried out by us for the solid solutions Ag-Tl, Ag-Zn, Ag-Pb, Cu-Mg and Cu-Sn. The concentrations of surface active elements in these alloys were substantially lower than their volumetric solubility.

The results of the calculation are set out in Table 1.

As can be seen from Table 1, with calculations and experimental data corresponding quite well, divergencies are to be observed, which in certain cases exceed the absolute errors of measurement of the lattice parameter. The following may be put forward as possible causes for this divergence. First of all, the question of the use of Webb's formula, consisting as it does of macroscopic values, for the definition of an effect of atomic dimensions is justifiable only as an initial approximation. Secondly, the effect of the mutual orientation of neighbouring grains has not been clarified. This might lead to a change in the width of the intercrystalline zone and, connected with this, a change in the lattice parameter, which changes from one

group of grains to another. Thirdly, block formation which might be changed from experiment to experiment and, as a result of the internal adsorption on the boundaries of blocks might bring about some change in the lattice parameter; these factors are to be the subject of further investigation.

Translated by V. Alford

REFERENCES

1. V.I. Arkharov and N.N. Skornyakov, *Trud. IFM Ural Branch of the Academy of Sciences SSSR*, 16, (1955).
2. V.I. Arkharov and S.D. Vangengeim, *Fiz. metal. metalloved.* 4, No. 3 (1957).
3. V.I. Arkharov, S.D. Vangengeim and I.B. Klyueva, *Fiz. metal. metalloved.* 7, 3 (1959).
4. V.I. Arkharov and S.D. Vangengeim, *Fiz. metal. metalloved.* 4,3 (1957).
5. N.F. Mott, *Proc. Camb. Phil. Soc.* 32, 281 (1936).
6. J. Friedel, *Phil. Mag.* 43, 153 (1952).
7. D. Lazarus, *Phil. Rev.* 93, 654 (1954).
8. F. Blatt, *J. Phys. Rev.* 108, 285 (1957).
9. W.G. Henry and J.L. Rogers, *Phil. Mag.* 1, 237 (1956).
10. E. Vogt and H. Friedewohl, *Ann. d. Phys.* 17, 281 (1956).
11. W.W. Webb, *Acta met.* 5, 89 (1957).

VOL.
8
1959

ON ADDITIONAL WEAKENING OF X-RAY DIFFRACTION LINES IN POWDER SPECIMENS*

A.YE. KOVAL'SKII and S.V. SEMENOVSKAIA

All-Union Scientific Research Institute for Hard Alloys

(Received 5 April 1959)

It is well known that correct structural interpretation of diffraction is impossible without taking into account the influence of the factors of submicrostructure on intensity (primary and secondary extinction, third-order distortions, errors in the superposition of atomic layers). Furthermore, as was shown by Wilchinsky [1], additional weakening of intensity is observed in powder specimens which takes place as a result of "entanglement" of reflected rays in coarse-grained uncompact specimens. Such entanglement, according to the data in work [1] is constant for all angles of reflection.

If calculations are made, not by the absolute intensity of any one line, but by the ratio of the intensities of several lines, as is done in the most recent works [2, 3], then the constant factor is excluded and consequently the "powder" factor of intensity may, it would appear, be disregarded. However in actual fact this factor apparently changes with the angle of reflection. This was discovered by Mckeehan and Warren [4] for tungsten powder. We checked this circumstance further on three tungsten powders: *a*) coarse-grained; *b*) unground fine-grained; *c*) fine-grained, ground in spirit.

By means of compacting (by hand) under various pressures, specimens of different compactness were obtained from each powder. Measurement of the intensity of four lines for each specimen was carried out on installation URS-501 using Co$K\alpha$-radiation with an iron filter; the rotation rate of the specimen was 0.5°/min, the chart speed of the recorder was of 600 mm/hr, width of the slits was 2, 1, 0.5 mm. The intensity values obtained were referred to like values for the same lines of the most compact specimen of the given series. The results are set forth in Table 1.

The data from Table show:

In a fine-grained unground powder, the degree of compactness exerts a relatively small influence on the intensity.

In a coarse-grained powder, and also in a fine-grained powder ground in spirit, the influence exerted by the compactness on the intensity is substantial. The similar behaviour of what would appear to be such very different powder is possibly brought about by the formation in the latter powder of conglomerates, in which rays "get entangled" in the same way as in large grains.

The weakening of the intensity, in contrast to the data of Wilchinsky, depends on the angle of reflection, but this dependence is not regular in character, as was obtained in one specimen by Mckeehan and Warren, but random. We consider that this conclusion of ours is reliable, because the magnitudes of the fluctuations in intensity set forth in the table are, in the majority of the tests, outside the limits of error for the test (5%).

The presence of such random fluctuations in intensity depending upon the angle of reflection and the compactness make the interpretation of the intensity of powder specimens unreliable.

As can be seen from the data of the same table, the fluctuations in the values of the physical half-width of the lines depending upon compactness are not in practice outside the limits of measurement error, that is to say, the values of the half-width of the lines are not dependent upon the compactness of the specimen.

Translated by J.J. Cornish

REFERENCES

1. Z. Wilchinsky, *Acta cryst.* 4, 1 (1951).

2. A. Kochanovska, *Casopispro pestovani fysiky*, 7, 455 (1957).

* *Fiz. metal. metalloved.*, 8, No. 5, 794-796, 1959.

VOL. 8 195

TABLE 1.

Initial tungsten powders	No. of the sample	Degree of compactness (%)	Weakening of the intensity integral in comparison with the most compact specimen				Physical broadening by half the height, (degrees).			
			(110)	(200)	(211)	(220)	(110)	(200)	(211)	(220)
Series A ground for 2 days	1	22	0.62	0.53	0.85	0.85	0.358	0.475	0.771	0.780
	2	27	0.99	0.89	0.96	0.84	0.332	0.400	0.795	0.745
	3	32	1.00	1.00	1.00	1.00	0.368	0.442	0.772	0.815
Series B homogenous, fine	4	35	0.71	0.89	0.88	0.93	—	—	—	—
	5	40	0.95	0.95	0.90	1.01	—	—	—	—
	6	43	1.00	1.00	1.00	1.00	—	—	—	—
Series C inhomogeneous powder: 40% of series B + 60% of coarse homogeneous powder	7	43	0.61	0.57	0.81	0.58	—	—	—	—
	8	53	0.84	0.97	0.95	0.69	—	—	—	—
	9	65	1.00	1.00	1.00	1.00	—	—	—	—

VOL. 8 1959

3. V.I. Ivyeronova and A.A. Katsnel'son, *Zh. tekh. fiz.* 25, 696 (1955).

4. M. Mackeehan and B.E. Warren, *Journ. Appl. Phys.* 24, No. 1 (1953).

DISPERSION EQUATION FOR ELECTRON PLASMA IN A MAGNETIC FIELD*

L.I. PODLUBNYI

Odessa Pedagogic Institute

(Received 31 March 1959)

Recently a method has been developed in a number of works [1, 2] for calculating concrete characteristics (energy spectrum, distribution functions) of Bose-Fermi systems of quasi-particles by means of their Green's functions. In particular, having solved the corresponding Schwinger equation, one can track the change in the spectrum of the oscillations of an electron plasma placed in a constant uniform field.

The use of Green's function, for example, for an electron in the field

$$\varphi(r) = -(\vec{E}\,\vec{r}) \tag{1}$$

$$G(r, t) = \left(\frac{im}{2\pi t}\right)^{\frac{3}{2}} exp\left\{\frac{imr^2}{2t} + \frac{it}{2}(\vec{E}\vec{r}) - \frac{it^3E^2}{24m}\right\}$$

would allow one to explain the dependence of $\omega(E)$ (or $\chi(H)$) for the contribution of the "neutral" component to the specific inductive capacitance (or susceptibility). But in this case one would have to overcome considerable difficulties in calculation. In as much as in the pulse concept

$$\varphi(k) = -i\delta(k_0)(\vec{E}\vec{\nabla}_k)\delta(\vec{k}), \tag{2}$$

it is much simpler to confine oneself to expanding the first two terms of Green's electron-hole function so that

$$G(p) = G_0(p) - \tag{3}$$
$$- i(2\pi)^4 g G_0(p)(\vec{E}\vec{\nabla}_k) G_0(p_0, \vec{p}-\vec{k})|_{\vec{k}=0}$$

An analogous expansion can also be written in the case of the constant uniform magnetic field $\vec{H}$; by way of a vector potential it is convenient to select

$$\vec{A}(k) = \frac{i}{2}\delta(k_0)[\vec{H}\vec{\nabla}_k]\delta(\vec{k}). \tag{4}$$

Proceeding exactly as in work [2] (the legend is the same as in work [2]); the Lagrangian coincides with the Lagrangian in work [2] complemented by the term $(\vec{j}\vec{A})$ we shall obtain for Green's function of the plasma $D^F(k)$

$$[D^F(k)]^{-1} = [D_0^F(k)]^{-1} + \tag{5}$$
$$+ 2ig^2(2\pi)^8 P_1(k) - \frac{ig^4}{8}(2\pi)^{16} P_2(k, H),$$

where $P_1(k)$ corresponds to the self-energy of the plasmon (and coincides with the analogous expression in [2]), and the term $P_2(k, H)$ of the "light-field scattering" type containing the outer field has the form (if one confines oneself to isotropic approximation):

$$P_2(k, H) = \tag{6}$$
$$= \frac{(2\pi)^8}{m^2}\int d^4p G_0^3(p) G_0^3(p-k)[\vec{H}\vec{p}][\vec{H}(\vec{p}-\vec{k})].$$

Hence, having expanded the integrand into a $\vec{k}$ series, for the dispersion equation

$$[D^F(k)]^{-1} = 0$$

we shall find (with regard to the approximation and the system of units cf. [2]):

$$k_0^2 - \frac{2g^2}{3\pi^2}\left(1 + \frac{12}{5}\frac{\varkappa^2}{k_0^2} + \ldots\right) + \tag{7}$$
$$+ \frac{g^4H^2}{\pi^2 k_0^4}\sin^2\psi + \ldots = 0, \quad \varkappa = \sqrt{\vec{k}^2};$$

*Fiz. metal. metalloved., 8, No. 5, 796-798, 1959.

the terms which have not been copied out here contain k_0, χ, H and the angle ψ between vectors $\vec{H}$ and $\vec{k}$. We calculated term $P_2(k, H)$ accurately, but as a result we obtained a most massive expression.

From equations (5)-(7), as is usual, it ensues that the outer magnetic field changes the boundary of the spectrum and can destroy the plasma oscillations. It stands to reason that in the case of strong fields our method of investigation is unsuitable, but in this case one never has to talk about the separation of plasma oscillations on longitudinals and cross-sectionals.

The various generalizations of (6)-(7) (anisotropy, calculation of the following approximation of the perturbation theory and so on) can be obtained in the same way as in [2,3]. No special difficulties occur in the case of a variable field either, when it is only necessary to bring about the substitution

$$\delta(k_0) \to \delta(k_0 - \omega).$$

in equation (4). For the plasma in a constant uniform electric field results similar to (6)-(7) occur

$$-\frac{ig^4}{8}(2\pi)^{16} P_2(k, H) = \tag{8}$$

$$= 4\pi^3 g^4 E^2 \frac{\chi^2}{k_0^6} \cos^2\psi + \ldots,$$

but the corresponding expansion for Green's electron-hole function is more successive (besides, in the case of a weak magnetic field the Schrödinger equation can also be considered as linear for H; in this case the integration in (6) is considerably complicated).

In conclusion we shall note that the use of such a method is not exhausted by the evolution of "the polarization operator" which is carried out, but can be comparatively easily extended with a view to investigating self-energy induced by interaction between an electron and crystal lattice vibrations (cf [1]). This would enable one to conduct a mass renormalization in the presence of an outer field and to determine, for example, the correction for susceptibility (in work [4] which appeared recently, with this aim, a calculation is made, by means of solving the Heisenberg equations of motion, of an accurate transformation function for an electron in a constant uniform magnetic field, which also takes into account temperature effect.

Translated by J.J. Cornish

REFERENCES

1. V.L. Bonch-Bruyevich, *Zh. eksp. teor. fiz.* 30, 342 (1956). 32, 1092. (1957).
2. V.L. Bonch-Bruyevich, *Fiz. metal. metalloved.*, 4, 547 (1957) 6, 590 (1958).
3. A. Voloshinskii and L. Kobyelev, *Fiz. metal. metalloved.*, 6, 356 (1958).
4. A.V. Tulub, *Zh. eksp. teor. fiz.* 36, 565 (1959).

CONTRIBUTION TO THE TREATMENT OF ANOMALOUS EFFECTS ON X-RAY PHOTOGRAPHS OF ALLOYS IN THE PROCESS OF AGEING. * II

R.R. ZAKHAROVA and N.N. BUINOV

Institute of Metal Physics Academy of Sciences U.S.S.R.

(Received 7 February 1959)

In work [1] it is shown theoretically that when X-rays are scattered by a crystal in the process of ageing, the anomalous effects observed on the X-ray photographs can be regarded as effects of shape. Such treatment of the anomalous effects has been employed when analysing the results of an X-ray diffraction study of ageing in the alloy Al-Ag [2]. However for proving that the anomalous effects actually are effects of shape, it is desirable to have an experimental setup with which it would be possible to predict beforehand their shape and disposition. Therefore it was interesting to study alloys in the process of ageing with added agents which, depending upon whether they enter the Guignier-Preston zone or remain for the most part in the solid solution, will change in different ways the relative position of the regions of anomalous scattering corresponding to them. For the first attempt in this direction, a study was made of the alloy Al-Ag (20%) with 0.6% Mg.

The choice of the Al-Ag alloy was governed by the fact that after hardeing and low-temperature ageing the most simple anomalous effects, in the form of haloes and diffuse spots, are observed on Laue diffraction patterns from coarse-grained specimens of this alloy. In works [2, 3] it was considered that in the reciprocal space the regions of anomalous scattering of the first and second types superimposed upon one another correspond to these haloes and diffuse spots (these regions of anomalous scattering are connected with the points of the reciprocal lattice of the matrix and Guignier-Preston zone, respectively).

To explain the results of the present investigation diagrams are given (Fig. 1 (*a*), (*b*) and Fig. 2 of work [3]) of the formation of anomalous effects on X-ray photographs depending on the relative position of regions of anomalous scattering of the first and second types, graphed with the aid of concepts of the reciprocal lattice and on the basis of work [3].

When selecting Mg as the addition agent, it was assumed that, because of its greater atomic radius in comparison with the atomic radii of Al and Ag, the shape of the anomalous effects ought to change sharply, both in the case of the magnesium atoms gathering in the silver-rich zones and in the case of preferred distribution of magnesium in the solid solution. It was considered unlikely that zones based on magnesium would form because Al-Mg binary alloys age very little with hardening and low-temperature annealing. Moreover, in our tests the magnesium addition was very insignificant (lower than its solubility limit in aluminium at room temperature).

On the basis of what has been stated one might have expected the following.

1. If the magnesium enters the silver-rich Guignier-Preston zones in considerable quantity, then the lattice constant of these zones will increase in comparison with the matrix lattice constant. In accordance with this the regions of anomalous scattering of the second type will be "displaced" to the origin of the co-ordinates of the reciprocal lattice of the matrix. Diffuse spots in the form of "half-moons", with their convex side to the path of the primary beam (Fig. 1 (*a*)) ought to be obtained on the X-ray photographs.

2. If, in the main, Mg atoms enter the lattice of the solid solution, then the regions of anomalous scattering of the first type will be "displaced" to the point (000). In this case effects, also in the shape of "half-moons", will be obtained on the X-ray photographs, but placed the other way round, that is, with the concave part facing the path of the primary beam (Fig. 1 (*b*)).

3. When the magnesium additions are uniformly distributed in the Guignier-Preston zones and solid solution alike, no preferred displacement of one of the regions of anomalous scattering takes place,

---

* *Fiz. metal. metalloved.*, 8, No. 5, 798-800, 1959.

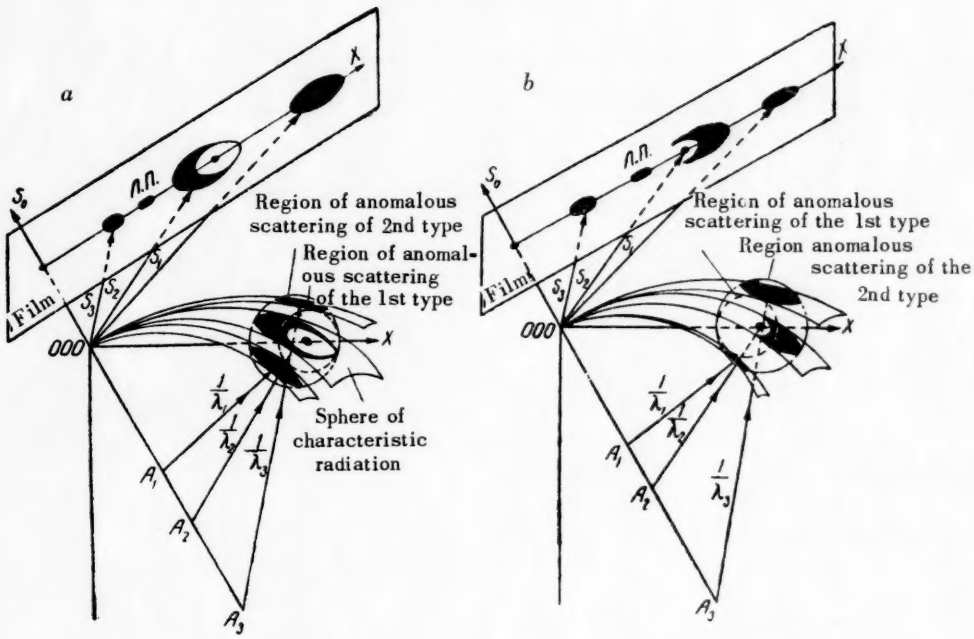
a
b
Region of anomalous scattering of 2nd type
Region of anomalous scattering of the 1st type
Sphere of characteristic radiation
Region of anomalous scattering of the 1st type
Region anomalous scattering of the 2nd type
Film
000

FIG. 1. (*a*), (*b*). Diagram of the formation of anomalous effects on X-ray photographs of alloys.

FIG. 2. The shape of anomalous effects on a Laue diffraction pattern of the alloy Al-Ag (20%) with 0.6% Mg after low-temperature ageing; the arrow indicates the position of the path of the primary beam of X-rays.

and diffuse spots in the form of rings should be obtained on the X-ray photographs (Fig. 2 of work [3]).

X-ray photographs of alloy Al-Ag with Mg addition showed the validity of the first assumption (Fig. 2).

Thus, the results obtained, confirm the correctness of the interpretation of diffuse anomalous effects from alloys in the process of ageing as effects of shape. In the future, tests will be continued using other additions.

In conclusion it must be noted that in the opinion of Ewald [4] only centrosymmetry of the region of anomalous scattering is proof that anomalous effects are effects of shape. A certain amount of centrosymmetry of the region of anomalous scattering is observed in the case of the Al-Ag alloy [3], it is strong in the case of Al-Ag-Mg and very strong in the alloy Al-Zn [5, 6]. However, this does not contradict Ewald's point of view because it is merely apparen t centrosymmetry (superposition and displacement of the centrosymmetrical regions of anomalous scattering take place relative to one another).

Translated by J.J. Cornish

VOL. 8 1959

REFERENCES

1. A.M. Yelistratov, *Dokl. Akad. Nauk SSSR*, 87, 581 (1952).
2. R.M. Lerinman and N.N. Buinov, *Fiz. metal. metalloved*, 5, 279 (1957).
3. R.R. Zakharova and N.N. Buinov, *Fiz. metal. metalloved*, 8 (1959).
4. P.P. Ewald, *Proc. Phys. Soc.*, 52, 67 (1940).
5. A.M. Yelistratov, *Dokl. Akad. Nauk SSSR*, 88, 803 (1953).
6. N.N. Buinov and L.I. Podrezov, *Fiz. metal. metalloved.* 1, 349 (1955).

VOL.
8
1959

No. 6

	PAGE
Electrical conductivity of ferromagnetic metals in a radio-frequency field — P. S. Zyrymanov, T. G. Izyumova and G. V. Skrotskii	1
The role of dipole-dipole interaction in ferromagnetic resonance — Iu. A. Izyumov	6
Development of metal physics and physics of metallurgy in the Chinese Peoples' Republic during ten years — Chou Chih-Hung, Ko Tsun and Tsin Lin-Chao	16
Mechanism of production of internal friction impurity peaks — V. T. Shmatov and A. V. Grin	24
The Hall effect in ferromagnetics — V. N. Novogrudskii, A. A. Samokhalov and I. G. Fakidov	28
A method for the direct measurement of magnetic anisotropy in thin films — W. Schuppel, O. Stemme, W. Andra and Z. Malek	30
Electric conductivity of iron at elevated temperatures — V. S. Gumenyuk and V. V. Lebedev	38
The temperature relation of the Nernst-Ettingshausen thermomagnetic effect in nickel and ferro-nickel alloys — R. P. Ivanova	42
The X-ray diffraction study of the reduction processes in some ferrites — V. N. Bogoslovskii	47
On the question of concentration inequalities experimentally detected in solid bodies — V. I. Arkharov	51
A study of the internal friction in powder metallurgical bodies. 4. Specimens from binary powders of noninteracting components Cu-Mo, Cu-W — B. Ia. Pines and Den Ge Sen	56
The wear resistance of case-hardened steel and its substructure — I. M. Lyubarskii, A. P. Lyubchenko and G. N. Bakakin	61
On the existance of the silicide W Si — N. N. Matiushenko, L. N. Yefimenko and D. P. Solopikhin	67
The fine structure of the intercrystalline transition zones of mild steel — B. S. Kasatkin and G. F. Darovskii	70
The formation of a cubic texture in ferro-silicon alloys — Chou P'en Hsin, Wang Wei Ming and Cheng Nen Huang	74
The components of specific loss and magnetic permeability of dynamo steels alloyed with phosphorous — S. I. Doroshek and V. V. Druzhinin	80
On the nature of the strain hardening which occurs when quench hardended high-speed steel is tempered — P. M. Yushkevich	84
The influence of cyclic heat treatment on uranium bicrystals — S. Ya. Zalivadnyi and V. M. Mikhailovskii	91
The failure of a martensite crystal under the simultaneous action of external tensile and compressive stresses — A. Mashin	95
The effect of the original structure and temperature of deformation on phase transformations during plastic formation — B. A. Apaev and Yu. A. Sysuev	101
Study of the mechanical properties of solids particularly metals, at and below temperatures of 4.2°K. 3. The mechanical properties of iron, titanium, tantalum and 2 steel at and below temperatures of 4.2°K. — O. V. Kliavin and A. V. Stepanova	107
The influence of the size effect on the deformability of metals — I. A. Razov, Ye. M. Shevandin and A. V. Yefimov	113
To the question of the dependence of the hardness on the composition of multi-phase alloys — V. P. Shishokin and A. E. Nikerov	119
Effect of the rate of heating and cooling on the irreversible deformation of iron — S. F. Kovtun	123

VOL 8 195

ELECTRICAL CONDUCTIVITY OF FERROMAGNETIC METALS IN A RADIO-FREQUENCY FIELD*

P.S. ZYRYANOV, T.G. IZYUMOVA and G.V. SKROTSKII

Ural Polytechnical Institute

(Received 13 April 1959)

VOL. 8 1959

1. INTRODUCTION

We know that ferromagnetic metals have additional specific resistance compared with non-ferromagnetic metals. This additional resistance is usually explained by dispersion of conductance electrons on thermal fluctuations in the degree of magnetization.

In metals which are in conditions of ferromagnetic resonance the character of the fluctuations in the degree of magnetization can be materially altered.

The specific resistance ρ of a metallic ferromagnetic can be considered to consist in the following parts

$$\rho = \rho_{\text{lattice}} + \rho_{fm} + \rho'_{fm}, \qquad (1)$$

where ρ_{lattice} and ρ_{fm} are respectively the resistances caused by dispersion of conductance electrons on lattice variations thermodynamically in equilibrium (phonons) and on variations in magnetization (ferromagnons) and ρ_{fm} is the additional resistance caused by a change in magnetization in a radio-frequency field. The temperature relation and order of magnitude of ρ_{lattice} are well known; ρ_{fm} was calculated by Turov [1] for low temperatures on a spin wave model. The temperature relation of ρ_{fm} agrees qualitatively with experience. Here an attempt is made to construct a qualitative theory for the increase in resistance of ferromagnetics in a radio-frequency field.

2. FORMULATION OF THE PROBLEM. THE ENERGETIC SPECTRUM OF A SYSTEM OF SPIN WAVES INTERACTING WITH EXTERNAL ELECTROMAGNETIC EMISSION

When far from ferromagnetic resonance a radio-frequency field does not in practice change the amplitude of the spin waves excited by thermal movement and ρ'_{fm} will be near zero.

When near ferromagnetic resonance the energy of a radio-frequency electromagnetic field is passed to spin waves with a wave number close to zero; this corresponds to the increase in the precession angle of the magnetization vector. Since in this instance the magnetization remains uniform no supplementary dispersion of conductance electrons will arise owing to the absence of non-uniformities in magnetization. However for a ferromagnetic metal in a radio-frequency field the magnetization in the skin layer will be non-uniform already and the radio-frequency field will increase this non-uniformity exciting a spin wave with the wave number $k \sim 1/\delta$ (δ the depth of the skin layer). A growth of non-uniformity in magnetization in a skin layer close to resonance will cause additional dispersion of conductance electrons and thus the resistance of the skin layer will have a resonance character. It should be noted that as the radio-frequency field interacts with the spin wave field the dispersion laws of these fields are altered.

We shall use the following form for Hamilton's function of spin waves interacting with a radio-frequency field:

$$\mathbf{H} = \int \left\{ \frac{A}{M_s^2} [(\nabla M_x)^2 + (\nabla M_y)^2] + \right.$$
$$\left. + \frac{H_0}{2M_s}(M_x^2 + M_y^2) \right\} + \frac{1}{8\pi}(\vec{e}^2 + \vec{h}^2) - (\vec{M}\vec{h}) d\tau. \qquad (2)$$

Here the first addend D is the energy of

---

* *Fiz. metal. metalloved.* 8, No.6, 801-806, 1959.

the free fluctuations of spin density in a constant magnetic field [2].

Developing the amplitudes of the free fields in series by Fourier-components and correspondingly standardizing them, the Hamiltonian (2) can be written;

$$H = 2\sum \omega_k^2 q_k^* q_k + 2\sum_{\alpha=1}^{2} \omega_0^2 p_{x\alpha}^* p_{x\alpha} + \\ + 2\sum_{\alpha=1}^{2} \omega_{12}^2 \{(e_{x\alpha}^x - ie_{x\alpha}^y) q_x p_{x\alpha}^* + (e_{x\alpha}^x + ie_{x\alpha}^y) q_x^* p_{x\alpha}\}. \quad (3)$$

Here

$$\omega_k = \frac{2g\gamma A}{M_s} k^2 + g\gamma H_0;\ \omega_{12}^2 = (4\pi c^2 x^2 \omega_x\ g\gamma M_s)^{1/2}, \quad (4)$$

where in the expression for the spin waves frequency - ω_k, the generally accepted symbols are used [2]; ω_0 is the frequency of the external electromagnetic field;

$$q_k \sim e^{i\omega_k t},\ q_k^* \sim e^{-i\omega_k t}$$

are the spin field amplitudes;

$$p_{x\alpha} \sim e^{i\omega_0 t},\ p_{x\alpha}^* \sim e^{-i\omega_0 t}$$

are the amplitudes of a radio-frequency field with polarization α; $\vec{e}_{x\alpha}$ is the unit vector of polarization. Spin waves with $\vec{k} \neq \varkappa$ are not changed by the radio-frequency field and consequently they can not be considered in the following calculations. In (3) we omit only one item with $\vec{k} = \vec{\varkappa}$ from the sum on k.

We shall consider the linear-polarization radio-frequency wave in the direction x. Then after diagonalization of (3) the energy can be represented as the sum of the energies of two non-interacting oscillators

$$H = \sum_{\mu=1}^{2} \Omega_\mu^2 \xi_{x\mu}^* \xi_{x\mu} \quad (5)$$

with frequencies

$$\Omega_{12}^2 = \frac{1}{2}(\omega_x^2 + \omega_0^2) + \sqrt{\frac{1}{4}(\omega_x^2 - \omega_0^2)^2 + 4\omega_{12}^4}. \quad (6)$$

The amplitudes ξ_{x_1} and ξ_{x_2} are linked with $p_{x\alpha}$ and q_x by the relations

$$\xi_{x1} = -\frac{p_x + \varepsilon_2 q_x}{\varepsilon_1 - \varepsilon_2}\sqrt{1+\varepsilon_1^2};\ \xi_{x2} = \\ = \frac{p_x + \varepsilon_1 q_x}{\varepsilon_1 - \varepsilon_2}\sqrt{1+\varepsilon_1^2}, \quad (7)$$

where

$$\varepsilon_1 = \frac{\omega_x^2 + 2\omega_{12}^2 - \Omega_1^2}{\omega_0^2 + 2\omega_{12}^2 - \Omega_1^2};\ \varepsilon_2 = \frac{\omega_x^2 + 2\omega_{12}^2 - \Omega_2^2}{\omega_0^2 + 2\omega_{12}^2 - \Omega_2^2}.$$

The interaction constant is $\omega_{12} \sim 5 \times 10^{10}$ sec.$^{-1}$ and therefore, in the conditions which interest us and are not too far from resonance ($\omega_x \sim \omega_0$), a true relation for ferromagnetics with a line width of $\gamma \Delta H < \omega_{12}$ will be

$$\frac{\omega_x^2 - \omega_0^2}{2\omega_{12}} \ll 1, \quad \text{then} \quad \xi_{x1} = \\ = \xi_{x2} = \frac{4\sqrt{2}\,\omega_{12}^2}{(\omega_x^2 - \omega_0^2)}(p_x + q_x). \quad (8)$$

Performing the quantization of the Hamiltonian (5) in the normal way in a system of spin waves interacting with radio-frequency emission we separate two types of quasi-particles not interacting with one another with energy

$$H = \hbar\Omega_1 \zeta_{x1}^+ \zeta_{x1} + \hbar\Omega_2 \zeta_{x2}^+ \zeta_{x2}. \quad (9)$$

The operators ζ_x and ζ_x^+ are subordinated to Bozev's inverse relations. When $\omega_{12} = 0$, $\Omega_1 = \omega_x$, $\Omega_2 = \omega_0$,

$$\zeta_{x1} = \sqrt{\frac{2\omega_x}{\hbar}}\xi_{x1};\ \zeta_{x2} = \sqrt{\frac{2\omega_0}{\hbar}}\xi_{x2},$$

then, as must be, the quasi-particles of the first type correspond to the spin field quanta or to ferromagnons and the electromagnetic field quanta, photons, are the quasi-particles of the second type.

When $\omega_{12} = 0$ the quasi-particles of both types can be interpreted as quanta of some electromagnetic fields (with the fluctuation frequencies Ω_1 and Ω_2 from (6)) which do not interact and can be described by the vector potentials

$$A_{q\mu}^x + iA_{q\mu}^y = A_{q\mu}^+ = 2i\sqrt{\frac{8\pi\hbar\Omega_\mu}{V}}\frac{[q\,e_q]_+}{q^2}\zeta_{q\mu}\,e^{iqr} \quad (10)$$

$$A_{q\mu}^x - iA_{q\mu}^y = A_{q\mu}^- = \\ = 2l\sqrt{\frac{8\pi\hbar\Omega_\mu}{V}}\frac{[\vec{q}\,\vec{e}_q]_-}{q^2}\zeta_{q\mu}^+ e^{-i\vec{q}\vec{r}}. \quad (11)$$

The vector $\vec{q}$ has the same sense as $\vec{x}$ and where $\omega_{12} = 0$ $\vec{q} \equiv \vec{\varkappa}$.

VOL. 8 1959

3. CALCULATION OF ELECTRICAL CONDUCTIVITY

We shall calculate the electrical conductivity for the common instance where a constant field $\vec{H}_0$ is sensed along the axis z and the vector of the electrical field E coincides with the radio-frequency field's direction of propoagation. The conductance electrons accelerated by the electrical field will be scattered on the quasi-particles with a spectrum as determined by (9).

In a representation of the secondary quantization the operator of electron interaction with both types of these quasi-particles has the form

$$H'_\mu = a_\mu \sum_k 1/q^2 \{[\vec{q}\vec{k}]_- a^+_{k+q} a_k \zeta_{q\mu} + [\vec{q}\vec{k}]_+ a^+_k a_{k+q} \zeta^+_{q\mu}, \quad (12)$$

$$a_\mu = -2\mu_0 \left(\frac{8\pi h}{V}\, \Omega_k e^2_{qx}\right)^{1/2}, \quad [\vec{q}\vec{k}]_\pm = [\vec{q}\vec{k}]_x \pm i\,[\vec{q}\vec{k}]_y. \quad (13)$$

We write the full Hamiltonian of the system in the form

$$H_\mu = \sum_k \varepsilon_k a^+_k a_k + h\Omega_\mu \zeta^+_{q\mu} \zeta_{q\mu} + H'_\mu. \quad (14)$$

The scattering of conductance electrons on both the spectrum's branches (9) is calculated using the statistical theory of disturbances worked out by Kubo and Tomita [3] and first used to calculate electrical conductivity in a work by Nakano [4]. This method is based on the linear theory of irreversible processes and via the relaxation function introduced by Kubo it gives an expression for electrical resistance.

We consider the movement of a system where there is a pulse in the electrical field and which can be described by the Hamiltonian

$$\mathrm{H} = H_\mu - 1/c\,(\vec{j}\vec{A}(t)), \quad (15)$$

where $\vec{A}(t)$ is the graduated function of time

$$\vec{A}(t) = \begin{cases} c\,\vec{E}(t_0)\,dt, & t \leqslant t_0 \\ 0, & t > t_0. \end{cases} \quad (16)$$

Taken conventionally at the moments $t > t_0$ the average current density is expressed via an equilibrium matrix of density $\rho(t_0) = \rho_c$ when there is an electric field at the moments $t \leqslant t_0$. In a linear approximation to the disturbance $\frac{1}{c}(jA)$ the current is

$$j_\nu(t) = \sum_\rho \int_0^\infty d\tau\, E_\rho(t-\tau)\, \varphi_{\rho\nu}(\tau), \quad (17)$$

where $\varphi_{\rho\nu}$ is the relaxation function equal to

$$\varphi_{\rho\nu}(t) = \int_0^\beta d\lambda\, \mathrm{spur}\left\{\varphi_c\, e^{\lambda H_\mu} j_\rho\, e^{-\lambda H_\mu} j_\nu\right\}, \quad \beta = 1/kT;\ \rho,\ \nu = x,\ y,\ z. \quad (18)$$

Taking into account that $H_\mu < kT$, $\vec{E}(t) = \vec{E}$ and the energy ϵ_k is the function of the square of the modulus of the electron $\vec{k}$ vector we shall obtain an expression for the specific resistance

$$\rho_{\nu\nu} = \frac{2\pi kT}{h^2 \langle j^2_\nu \rangle^2} \sum_\omega \langle [j_\nu,\ H^1_\omega]\,[H'_{-\omega},\ j_\nu] \rangle\, \delta(\omega). \quad (19)$$

Here

$$H'_\omega = a_\mu (a^+_{k+q} a_k \zeta_{q\mu} + a^+_k a_{k+q} \zeta^+_{q\mu}),$$

$$\pm h\omega = \varepsilon_{k+q} - \varepsilon_k - h\Omega_\mu,\ j_\nu = \sum_k \left(\frac{\partial \varepsilon_k}{\partial k}\right) \frac{k_\nu}{k} a^+_k a_k. \quad (20)$$

Using the Fermi inverse relations for a^+_k and a_k and the Bozev inverse relations for $\zeta^+_{k\mu}$ and $\zeta_{k\mu}$, we find the average value of the commutator entering into (19):

$$\sum_\omega \langle [j_\nu,\ H'_\omega]\,[H'_\omega,\ j_\nu] \rangle\, \delta(\omega) = \frac{e^2}{h^2} a^2_\mu \sum_k \frac{[\vec{q}\vec{k}]^2_x + [\vec{q}\vec{k}]^2_y}{q^4} \frac{q^2_\nu}{k^2} \left(\frac{\partial \varepsilon_k}{\partial k}\right)^2 \cdot \{f_{k+q}(1-f_k)(\langle \zeta^+_q \zeta_q \rangle + 1) + f_k(1-f_{k+q}) \langle \zeta^+_q \zeta_q \rangle\}\, \delta\left(\frac{\varepsilon_{k+q} - \varepsilon_k - h\Omega_\mu}{h}\right), \quad (21)$$

where $f_k = \dfrac{1}{e^{\frac{\varepsilon_k - \zeta}{kT}} + 1}$ is the Fermi dispersion function. Proceeding from summarization on the quasi-particles to integration we obtain

$$\sum_{\omega} \langle [j_\nu, H'_{\omega}][H'_{-\omega} j_\nu] \rangle \delta(\omega) =$$

$$= \frac{e^2}{\hbar} \alpha_\mu^2 \frac{V}{(2\pi)^2} \int_0^{\pi} (1 - \cos^2\theta)\, d(\cos\theta)\, d\theta \cdot$$

$$\cdot \int_0 k^2\, dk\, \frac{1}{q} \left(\frac{\partial \varepsilon}{\partial k}\right) \delta\left(\cos\theta - \frac{\hbar\Omega_\mu}{q} \frac{\partial k}{\partial \varepsilon_k} + \right.$$

$$\left. + \frac{q}{2k}\right) (f_k - f_{k+q}) \cdot$$

$$\{ \langle \zeta^+_{q\mu} \zeta_{q\mu} + 1 \rangle n_{q\mu} + \langle \zeta^+_{q\mu} \zeta_{q\mu} \rangle (n_{q\mu} + 1)\} = \frac{e^2 V \alpha_\mu^2}{\hbar (2\pi)^2} \cdot$$

$$\cdot k_0^2 \left[1 - \frac{q^2_{min}}{q^2}\right] \frac{\hbar\Omega_\mu}{q} \{ \langle \zeta^+_{q\mu} \zeta_{q\mu} + 1 \rangle \to n_{q\mu} + \quad (22)$$

$$+ \langle \zeta^+_{q\mu} \zeta_{q\mu} \rangle (n_{q\mu} + 1)\},$$

where

$$n_{q\mu} = \frac{1}{e^{\frac{\hbar\Omega_\mu}{kT}} - 1}, \quad q_{min} = \frac{2g\mu_0 H}{\left(\frac{\partial \varepsilon_k}{\partial k}\right)_0} \sim 10^{-1}.$$

The derivative $\left(\frac{\partial \varepsilon_k}{\partial k}\right)_0$ is taken on a Fermi surface. Disregarding q^2_{min}/q^2 compared with unity and considering that

$$\langle j_\nu^2 \rangle = \frac{e^2}{\pi^2 \hbar^2} kT \cdot k_0^2 \left(\frac{\partial \varepsilon_k}{\partial k}\right)_0,$$

we obtain for the specific resistance ρ_μ in the direction $\vec{q}$

$$\rho_\mu = \frac{\pi^3 \hbar V \alpha_\mu^2}{4kT} \frac{1}{e^2 k_0^2 \left(\frac{\partial \varepsilon}{\partial k}\right)_0^2} \frac{\hbar\Omega_\mu}{q} \{ \langle \zeta^+_{q\mu} \zeta_{q\mu} + 1 \rangle n_{q\mu} +$$

$$+ \langle \zeta^+_{q\mu} \zeta_{q\mu} \rangle (n_{q\mu} + 1)\}. \quad (23)$$

Here

$$\langle \zeta^+_{q\mu} \zeta_{q\mu} \rangle = \frac{32\omega_{12}^4}{(\omega_q^2 - \omega_0^2)^2} \cdot \frac{2\Omega_\mu}{h} (p_q^2 + q_q^2 + 2p_q q_q).$$

As

$$q_q^2 \simeq h/2\omega_q kT/h\omega_l, \quad \text{a} \quad p_q^2 = h_0^2/2\omega_0^2,$$

then the value q_q may be ignored in comparison with p_q

$$\langle \zeta^+_{q\mu} \zeta_{q\mu} \rangle \simeq \frac{2\Omega_\mu}{h} \cdot \frac{32\omega_{12}^4}{(\omega_q^2 - \omega_0^2)^2} \cdot \frac{h_0^2}{\omega_0^2}. \quad (24)$$

(24) shows that the number of quasi-particles of one or the other type is almost wholly determined by the radio-frequency field and does not depend on temperature. Substituting the values of α_μ in (23) we obtain

$$\rho_\mu = \frac{32\pi^4 c\mu_0^2 \hbar\Omega_\mu}{2e^2 k_0^2 \left(\frac{\partial \varepsilon}{\partial k}\right)_0^2} \cdot \frac{32\omega_{12}^4}{(\omega_q^2 - \omega_0^2)^2} \cdot \frac{h_0^2}{\omega_0^2} \quad (25)$$

(ρ'_{fm} is the sum of ρ_μ for $\mu = 1$ and $\mu = 2$).

The instance $\mu = 1$ corresponds to the dispersion of electrons on ferromagnons with a wave vector $\vec{q}$, being modulated by the radio-frequency field we summarize on all the quasi-impulses of the ferromagnons and express the operators ζ_{q1} and $\zeta^+_{q'}$ via the operators of the origin and destruction of the free ferromagnons b_q and b^+_{q1}, linked with the magnetization as follows:

$$M_q^+ = M_{qx} + iM_{qy} = \left(\frac{2q\mu_0 M_s}{V}\right)^{\frac{1}{2}} b_q \exp(i\vec{q}\vec{r}),$$

$$M_q^- = M_{qx} - iM_{qy} = \left(\frac{2q\mu_0 M_s}{V}\right)^{\frac{1}{2}} b_q^+ \exp(-i\vec{q}\vec{r}), \quad (26)$$

and we obtain a value for ρ_{fm} first calculated by Turov [1]

$$\rho_{\phi M} = \frac{4\pi^3 g\mu_0^3 \hbar M_s}{e^2 k_0^2 \left(\frac{\partial \varepsilon_k}{\partial k}\right)_0} \int_{q_{min}}^{\infty} \frac{(1 - q^2_{min}/q^2)}{(e^y - 1)(1 - e^{-y})} y dq^2,$$

где $y = \frac{\hbar\omega_q}{kT}$.

4. CONCLUSIONS

The calculated effect of an increase in the resistance of a ferromagnetic metal in conditions of resonance can be seen in thin films of the order of skin depth. In samples considerably thicker than skin depth this effect will be very inconsiderable and possibly unobservable as the alteration in resistance will only occur in the surface layer.

Since in (25) an approximation of the spin waves was used which is true only for deviations that are not excessively large from the equilibrium of magnetization, our results are true only for a range of temperatures below Curie's temperature. Since in our calculation we only retained terms linear according the amplitude of the radio-frequency field one must consider that this amplitude h_0 is considerably less than the width of the ferro-

magnetic resonance line.

Taking these limitations into account and substituting the values of the constants in (25) we obtain close to resonance ($\omega_q \sim \omega_0$)

$$\rho'_{fm} \sim 10^{18} \frac{h_0^2}{2\omega_q^2 (\Delta\omega_q)^2} \qquad (27)$$

As we have not taken attenuation of the spin waves into account the addend corresponding to the attenuation is missing from the denominator of (27); it is in order of value equal to the fourth power of the width of the resonance $\gamma \Delta H$.

Close to resonance $\rho'_{fm}/\rho_{\text{lattice}}$ can be approximately written in the form

$$\rho'_{fm}/\rho_{lattice} \sim 10^2 \frac{h_0^2}{(\Delta H)^2}$$

(the order of value for ρ_{lattice} is taken for iron at 100°K).

The relation $\rho'_{fm}/\rho_{\text{lattice}}$ is proportional to the value $(h_0/\Delta H)^2$ which was considered low in our calculations. Thus when far from saturation of ferromagnetic resonance and $h_0 < \Delta H$ the change in electrical resistance $\rho'_{fm}/\rho_{\text{lattice}}$ is small. This result can be obtained immediately by developing $\rho'_{fm}/\rho_{\text{lattice}}$ in series by powers of the relation $\frac{h_0}{\Delta H}$.

Apparently there must be a considerable change in the electro-resistance when there is saturation of ferromagnetic resonance. Unfortunately we do not know of any available methods of calculating the electromagnetic field of the fluctuations in spin density in this instance.

It would be interesting to study experimentally the relation $\rho'_{fm}/\rho_{\text{lattice}}$ as a function of $h_0/\Delta H$.

Translated by P.J.H. Saunders

REFERENCES

1. E.A. Turov, *Fiz. metal. metalloved.*, No.2, 6 (1958).
2. C.A. Kittel and E. Abraham, *Rev. of Mod. Phys.*, 25, 233 (1953).
3. R. Kubo, *Journ. of Phys. soc. of Japan*, No.6, 12, (1957), No.11, 12 (1957).
4. H. Nakano, *Prog. Theor. Phys.* 77, 15 (1956).

VOL. 8 1959

THE ROLE OF DIPOLE-DIPOLE INTERACTION IN FERROMAGNETIC RESONANCE*

Iu.A. IZYUMOV

Ural State University im. A.M. Gor'kii

(Received 15 April 1959)

The general theory of Kubo and Tomita [1] for magnetic resonance absorption is used to calculate the form of the line in ferromagnetic resonance including exchange and dipole-dipole interactions of electrons. It is shown that dipole-dipole interaction leads to Kittel's expression for the resonance frequency and causes the line to widen to a degree increasing with temperature. At absolute zero the width of the line appears, although finite, extraordinarily small in value.

1. INTRODUCTION

A characteristic feature of ferromagnetic resonance is the dependence of the resonance frequency on the form of the sample. Kittel [2] showed that if a constant magnetic field is applied along axis z and a variable field along axis x the resonance frequency is determined by the formula

$$\omega_0 = \frac{g\mu_0}{h}\sqrt{|H + (N_y - N_z)M|\,|H + (N_x - N_z)M|}, \tag{1.1}$$

where μ_0 is Borh's magneton; g is Lande's factor; M the magnetization along axis z and N_x, N_y, N_z, are the demagnetizing factors along the axes x, y, z, where $N_x N_y N_z = 4\pi$; h is everywhere Plank's constant divided by 2π.

On the basis of quantum theory Van-Vleck [3] has given a microscopical derivation of (1.1) considering the dipole-dipole interaction of the spins and linking in the same way the demagnetizing factors with the dipole-dipole sums along the lattice angles.

Using the method of moments [5] in an earlier work [4] Van-Vleck studied the combined role of dipole-dipole and exchange spin interaction in paramagnetic resonance establishing the effect of exchange reduction which consists in the line width, conditioned by dipole-dipole interaction, decreasing in the presence of exchange interaction by as many times as the exchange energy of the two neighbouring spins exceeds the dipole-dipole energy. Application of the moments method for ferromagnetics comes up against difficulties of principle but Van-Vleck showed qualitatively [3] that for ferromagnetic resonance the exchange reduction effect must be strongly dependent on the temperature and the line width, conditioned by dipole-dipole interaction, moves strongly towards nil at zero temperature. Here Van-Vleck does not work from the full operator of the dipole-dipole interaction but only from that part of it which is linked with the basic resonance line.

Keffer [6] calculated the second moment of the basic line by Van-Vleck's method using the dipole-dipole interaction terms omitted by Van-Vlecks and found that it does not disappear at zero temperature. From this Keffer [6] and Kittel and Abrahams [7] also, concluded that the line width at zero temperature is finite and its order of value is experimentally observable.

This result was criticized by Bloembergen and Wang and also in a recent work by Clogston and others [9]. They pointed out that the second moment found by Keffer which does not

* *Fiz. metal. metalloved.* 8, No.6, 807-819, 1959.

disappear at zero temperature is not linked to the width of the basic line but to the contribution made to it by satellite lines. However, there is still no convincing solution for this problem and to solve it the width of the absorption line must be calculated directly.

But in the application to ferromagnetics there is only difficulty; the dipole-dipole interaction in them can not be considered as a small disturbance, although it is already evident from (1.1). However, by applying the method of normalization to the energy of dipole-dipole interaction we shall avoid this difficulty and we use the formal method of the theory of disturbances which is developed in the following section.

2. THE THEORY OF DISTURBANCE FOR THE ANALYSIS OF MAGNETIC RESONANCE ABSORPTION

Let the system of magnetic moments be acted upon by a periodic magnetic field $h_\beta(t)$ ($\beta = x, y, z$) of radio-wave emission frequency ω. The absorption of emission energy is characterised in substance by the imaginary part of the tensor of complex susceptibility $\chi_{\alpha\beta}$, which is defined by the relation

$$M_\alpha(t) - M_\alpha^0 = \sum_\beta (\chi'_{\alpha\beta} - i\chi''_{\alpha\beta})\, h_\beta(t), \quad (2.1)$$

where $M_\alpha(t)$ is the projection of the sample's magnetic moment at an instant of time t and M_α^0 is the equilibrium magnetization of the sample. According to Kubo and Tomita's [1] general quantum-statistical theory $\chi_{\alpha\beta}$ is determined as a Fourier-component from the derived relaxation function $G_{\alpha\beta}$,

$$\chi'_{\alpha\beta}(\omega) - i\chi''_{\alpha\beta}(\omega) = \int_0 -\frac{dG_{\alpha\beta}}{dt}\, e^{-i\omega t}\, dt, \quad (2.2)$$

which can be expressed by the dynamic operators of the system

$$\frac{dG_{\alpha\beta}}{dt} = \frac{i}{h} \langle [\hat{M}_\alpha(t),\ \hat{M}_\beta] \rangle . \quad (2.3)$$

Here $\hat{M}_\alpha$ is the operator of the sample's magnetic moment, $\hat{M}_\alpha(t)$ is the same operator in a Heisenberg presentation

$$\hat{M}_\alpha(t) = e^{\frac{i}{h}\hat{H}t}\, \hat{M}_\alpha\, e^{-\frac{i}{h}\hat{H}t}, \quad (2.4)$$

$\hat{H}$ is the Hamiltonian of the system and $\langle \ldots \rangle$ from each operator $\hat{A}$ signifies

$$\langle \ldots \rangle = \mathrm{Sp}\,(e^{-\beta\hat{H}}\hat{A})/\mathrm{Sp}\,e^{-\beta\hat{H}};\ [\hat{A},\ \hat{B}] = \hat{A}\hat{B} - \hat{B}\hat{A}.$$

If the Hamiltonian $\hat{H}$ can be broken down into two parts $\hat{H} = H_0 + H'$ and H' can be considered as a disturbance, then it is easy to develop $M_\alpha(t)$ by the powers of this disturbance:

$$\hat{M}_\alpha(t) = \hat{M}_\alpha^0(t) + \sum_{n=1}^{\infty} \frac{1}{(ih)^n} \int_0^t dt_1 \int_0^{t_1} dt_2 \ldots \int_0^{t_{n-1}} dt_n \cdot [\ldots[\hat{M}_\alpha^0(t),\ H'(t_1)], \ldots,\ H'(t_n)], \quad (2.5)$$

where

$$H'(t) = e^{\frac{i}{h}H_0 t} H' e^{-\frac{i}{h}H_0 t}. \quad (2.6)$$

Substituting this in (2.3) the relaxation function can be developed by the powers of H'.

We shall use this scheme to calculate the susceptibility of a crystalline dielectric with spins of the value s in its nodes, if it is placed in a constant field H, sensed along the axis z. Ignoring other forms of spin interaction except exchange and dipole-dipole interaction we put the Hamiltonian of the spins' system in the form

$$\mathrm{H}_0 = \mathrm{H}_e + \mathrm{H}_z;\ \mathrm{H}_e = -\sum_{j \neq k} J_{jk} \vec{S}_j \vec{S}_k;\ \mathrm{H}_z = -g\mu_0 H \sum_j S_j^z. \quad (2.7)$$

$$H' = \frac{g^2\mu_0^2}{2} \sum_{j \neq k} r_{jk}^{-5} \{r_{jk}^2 \vec{S}_j \vec{S}_k - 3(\vec{S}_j \vec{r}_{jk})(\vec{S}_k \vec{r}_{jk})\}. \quad (2.8)$$

Formally we shall consider the dipole-dipole interaction H' as a disturbance. In future it will be convenient to write H' in the form:

$$H' = \sum_\alpha H'_\alpha = \sum_\alpha \sum_{j \neq k} \Phi_{jk}^{-\alpha} \{jk\}_\alpha;\ \alpha = 0, \pm 1, \pm 2. \quad (2.9)$$

VOL. 8 1959

$$\{jk\}_0 = S_j^z S_k^z - \frac{1}{4}(S_j^+ S_k^- + S_j^- S_k^+); \quad (2.9)$$

contd.

$$S_j^{\pm} = S_j^x \pm iS_j^y;$$

$$\{jk\}_{\pm 1} = S_j^{\pm} S_k^z + S_j^z S_k^{\pm}; \quad \{jk\}_{\pm 2} = S_j^{\pm} S_k^{\pm};$$

$$\Phi_{jk}^0 = -\frac{g^2\mu_0^2}{2} r_{jk}^{-5}(3z_{jk}^2 - r_{jk}^2); \quad \Phi_{jk}^{\pm 1} =$$

$$= -\frac{3g^2\mu_0^2}{4} r_{jk}^{-5}(x_{jk} \pm iy_{jk}) z_{jk};$$

$$\Phi_{jk}^{\pm 2} = -\frac{3g^2\mu_0^2}{8} r_{jk}^{-5}(x_{jk} \pm iy_{jk})^2.$$

Such a break-down of the disturbance is more natural as it amplifies the laws of selection for the matrix elements.

Let us consider further an emission polarized along an axis x so that it is sufficient to calculate one component only of the tensor χ''_{xx}.

The operator of the magnetic moment $\hat{M}_x$ is expressed through the operator of the sum spin of the crystal S_x in the form

$$M_x = g\mu_0 S_x = \frac{1}{2} g\mu_0 (S^+ + S^-). \quad (2.10)$$

In order to use (2.3) it is necessary to express the operators $\hat{M}_x$ and H' in a Heisenberg presentation (with the Hamiltonian H_0). This task is simply solved if the inverse relations for the spin operator are used and the two evident equalities noted;

$$[\mathbf{H}_e, \mathbf{H}_z] = 0; \quad [\mathbf{H}_e, S_x] = 0. \quad (2.11)$$

Thus we obtain:

$$\hat{M}_x^0(t) = \frac{1}{2} g\mu_0 (S^+ e^{-i\omega_z t} + S^- e^{i\omega_z t}); \quad \omega_z = \frac{g\mu_0 H}{h}. \quad (2.12)$$

$$H'_\alpha(t) = e^{-i\alpha\omega_z t} \mathbf{H}'_\alpha(t); \quad \mathbf{H}'_\alpha(t) = e^{\frac{i}{h}\mathbf{H}_e t} H'_\alpha e^{-\frac{i}{h}\mathbf{H}_e t} \quad (2.13)$$

Substituting (2.12) and (2.14) in (2.5) and (2.3) we find for the first of these approximations of the values $\frac{dG_{xx}}{dt} \equiv -\frac{dG}{dt}$ the expressions:

$$-\frac{dG^{(0)}}{dt} = \frac{2i}{h}\left(\frac{g\mu_0}{2}\right)^2 \langle S^2 \rangle e^{-i\omega_z t} + \text{к. с.} \quad (2.14)$$

$$-\frac{dG^{(1)}}{dt} = \frac{1}{h^2}\left(\frac{g\mu_0}{2}\right)^2 \left[\sum_{\alpha \neq 0} \frac{1}{i\alpha\omega_z}(1 - e^{-i\alpha\omega_z t})(L_\alpha^{+-} + L_\alpha^{+-}) + (L_0^{++} + L_0^{+-})t\right] e^{-i\omega_z t} + \text{к. с.} \quad (2.15)$$

$$-\frac{dG^{(2)}}{dt} = -\frac{1}{h^2}\left(\frac{g\mu_0}{2}\right)^2 \sum_{\alpha\beta} \int_0^t dt_1 \int_0^{t_1} dt_2 e^{-i\omega_z(\alpha t_1 + \beta t_2)} \cdot [Z_{\alpha\beta}^{++}(t_1 - t_2) + Z_{\alpha\beta}^{+-}(t_1 - t_2)] e^{-i\omega_z t} + \text{к. с.} \quad (2.16)$$

Here for the sake of brevity the symbols are introduced:

$$L_\alpha^{\sigma\sigma'} = \langle [[S^\sigma, H'_\alpha], S^{\sigma'}] \rangle; \quad \sigma, \sigma' \quad +, -. \quad (2.17)$$

$$Z_{\alpha\beta}^{\sigma\sigma'}(\tau) = \langle [e^{\frac{i}{h}\mathbf{H}_e \tau}[S^\sigma, H'_\alpha] e^{-\frac{i}{h}\mathbf{H}_e \tau}, [H'_\beta, S^{\sigma'}]] \rangle + \langle [e^{\frac{i}{h}\mathbf{H}_e \tau}[[S^\sigma, H'_\alpha], S^{\sigma'}] e^{-\frac{i}{h}\mathbf{H}_e \tau}, H'_\beta] \rangle. \quad (2.18)$$

Simplification in (2.16) is possible by integrating clearly on a single variable. If one proceeds from the variables t_1 and t_2 to to the new ones $\tau = t_1 - t_2$ and $y = t_1 + t_2$, then instead of the double integrals of the following form come in:

$$\left.\begin{aligned} F_{\alpha\beta}(t) &= \int_0^t (Z_{\alpha\beta}^{++}(\tau) + Z_{\alpha\beta}^{+-}(\tau)) e^{-i\alpha\omega_z \tau} d\tau \\ \Phi_{\alpha\beta}(t) &= \int_0^t (Z_{\alpha\beta}^{++}(\tau) + Z_{\alpha\beta}^{+-}(\tau)) e^{i\beta\omega_z \tau} d\tau \end{aligned}\right\} \alpha \neq \beta \quad (2.19)$$

$$F_{\alpha,-\alpha}(t) = \int_0^t (t - \tau)(Z_{\alpha,-\alpha}^{++}(\tau) + Z_{\alpha,-\alpha}^{+-}(\tau)) e^{-i\alpha\omega_z \tau} d\tau; \quad (2.20)$$

through them the expression (2.16) is defined as follows

$$-\frac{dG^{(2)}}{dt} = -\frac{1}{h^2}\left(\frac{g\mu_0}{2}\right)^2 \left[i\sum_\alpha F_{\alpha,-\alpha}(t) + \sum_{\alpha+\beta\neq 0} \frac{F_{\alpha\beta}(t)}{\omega_z(\alpha+\beta)} + \right. \quad (2.21)$$

VOL. 8 195

$$+\frac{1}{2\omega_z}\sum_{\alpha+\beta=-2}\Phi^{*}_{\alpha\beta}(t)\Big]e^{-i\omega_z t}+\frac{1}{\hbar^3}\left(\frac{g\mu_0}{2}\right)^2\sum_{\alpha\beta;\ \alpha+\beta\neq 0;\ \alpha+\beta\neq -2}\Phi_{\alpha\beta}(t)\cdot e^{-i(\alpha+\beta+1)\omega_z t}+\text{K. C.} \qquad (2.21)$$

contd.

The commutators entering into (2.17) and (2.18) can be calculated for all the values of α:

$$[S^-,\ H'_\alpha]=C_{-\alpha}\sum_{jk}\Phi^{-\alpha}_{jk}\{jk\}_{\alpha-1},$$
$$[S^+,\ H'_\alpha]=-C_\alpha\sum_{jk}\Phi^{-\alpha}_{jk}\{jk\}_{\alpha+1}, \qquad (2.22)$$
$$[[S^+,\ H'_\alpha],S^+]=-C_\alpha C_{\alpha+1}\sum_{jk}\Phi^{-\alpha}_{jk}\{jk\}_{\alpha+2},$$
$$[[S^+,\ H'_\alpha],\ S^-]=C_\alpha C_{-\alpha-1}\sum_{jk}\Phi^{-\alpha}_{jk}\{jk\}_{\alpha},$$

$C_{-2}=2;\ C_{-1}=-4;\ C_0=3/2;\ C_1=2;\ C_2=0.$

All the relations obtained at this point have a general character and are true for both ferromagnetic crystals and paramagnetic and anti-ferromagnetic crystals etc. as well. Further calculation requires concretization of the type of system under study. Before proceeding to a ferromagnetic we shall first consider some general properties of various approximations of the function $-\frac{dG}{dt}$.

It is easily seen from (2.2) that the zero approximation determines the spectrum of the resonance frequencies. For the system under study with exchange and dipole-dipole interaction it will contain one frequency ω_z. The zero approximation does not give a finite width of the absorption line (the line has a b-form character). Satellite lines appear in the second approximation with frequencies divisible by ω_z (the last term from (2.21)). However, their intensity is low compared with that of the basic frequency.

Collecting all the terms at the basic frequency in the first three approximations we obtain some function of time in the form of a polynome on t starting from unity. Without out calculating the higher terms of $-\frac{dG}{dt}$ we we can consider the polynome thus obtained as a development of some function $\psi(t)$ by powers of t. We shall now consider that the full function $-\frac{dG}{dt}$ equals

$$-\frac{dG}{dt}=\frac{2}{ih}\left(\frac{g\mu_0}{2}\right)^2\langle S^z\rangle e^{\psi(t)+i\omega_z t}+\text{K. C.} \qquad (2.23)$$

The expression $e^{\psi(t)}$ describes the process of the system's relaxation in time and it must move strongly towards nil when $t\to\infty$. It is clear that calculation of X'' by (2.2) must lead to an absorption line of finite width. Thus the task of the specific calculation comes down to finding the function $\psi(t)$ by the first few approximations of the value $-\frac{dG}{dt}$. The properties of the function $\psi(t)$ determine the form and width of the absorption line.

3. THE EFFECT OF A SECULAR DISTURBANCE

Now we shall examine a ferromagnetic with the indicated forms of spin interaction close to saturation. In this case one can proceed from the operators of the spin S_j to a new dynamic exchange – Bose-amplitudes 10 b_j:

$$S_j^+=\sqrt{2S}\,b_j;\ S_j=\sqrt{2S}\,b_j^+;\ S_j^z=S-b_j^+b_j. \qquad (3.1)$$

Introducing their Fourier forms we find that the exchange operator is represented diagonally

$$\mathrm{H}_e=\sum_{\vec{g}}\varepsilon_{\vec{g}}\,b^+_{\vec{g}}b_{\vec{g}};\ \varepsilon_{\vec{g}}=2SJ(ag)^2, \qquad (3.2)$$

where J is the exchange integral between immediate neighbours; a is the lattice constant, $\vec{g}$ the quasi-impulse.

The following approximation consists in our ignoring the influence of the dipole-dipole disturbance terms on the function of spin wave distribution i.e. we shall consider that

$$\langle b^+_{\vec{g}}b_{\vec{g}}\rangle\equiv\langle n_{\vec{g}}\rangle=\left\{\exp\frac{\varepsilon_{\vec{g}}+h\omega_z}{kT}-1\right\}^{-1}. \qquad (3.3)$$

This is possible if excessively low temperature cases are ignored and one starts from several degrees K and above. At lower temperatures one would have to consider Holstein's and Primakoff's [10] spin wave spectrum taking dipole-dipole disturbance into account.

Using (3.1) it can be determined that averaged as canonically accepted the terms of dipole-dipole interaction $\langle H'_\alpha \rangle$, equal zero when $\alpha = \pm 1, \pm 2$, but when

$$\alpha = 0 \quad \langle H'_0 \rangle \sim \frac{g^2 \mu_0^2}{a^3} N \sim N \mu_0 M_0,$$

where M_0 is saturation magnetization.

This shows that at low temperatures H'_0 in ferromagnetics is not at all small but fully comparable with the Zeeman energy of a system of moments in an external field $\sim N \mu_0 H$, and, therefore, the term can not be considered as a disturbance. In line with [1] we shall call the term H'_0 a secular disturbance and the terms H'_α with $\alpha \neq 0$ non-secular disturbances. The term H'_0 is connected with static demagnetizing fields and the non-secular terms cause in the system transitions with a change in the magnetic quantum number to a value of $\alpha = \pm 1, \pm 2$. In this section we shall only consider the secular term. Not being able to consider it as a small disturbance we shall modify the calculation plan developed in the preceeding section. First of all we note that in the spin waves approximation

$$[\mathbf{H}_e, H'_0] = 0. \tag{3.4}$$

Regarding this as approximated we shall calculate the value $-\frac{dG}{dt}$ for the secular term directly from (2.2) without developing it in series by the powers of H'_0. Using the inverse relations for the spin operator and keeping (2.11) and (3.4) in mind we find

$$-\frac{dG_s}{dt} \equiv \frac{i}{\hbar} \langle [e^{\frac{i}{\hbar}\left(\mathbf{H}_e + \mathbf{H}_z + H'_0\right) t} \hat{M}_x e^{-\frac{i}{\hbar}\left(\mathbf{H}_e + \mathbf{H}_z + H'_0\right) t}, \hat{M}_x] \rangle \approx$$

$$\approx \frac{i}{\hbar} \left(\frac{g\mu_0}{2}\right)^2 \langle [e^{\frac{i}{\hbar} 3 \sum_k \Phi^0_{ek} S^z_k t} S^+, S^-] \rangle e^{-i\omega_z t} + \text{к. с.}$$

We shall write the last expression in the form

$$-\frac{dG_s}{dt} = \frac{i}{\hbar} \left(\frac{g\mu_0}{2}\right)^2 e^{-it\left(\omega_z - \frac{3s}{\hbar} \sum_k \Phi^0_{ek}\right)} \langle [e^{\frac{i}{\hbar} 3 \sum_k \Phi^0_{ek} \left(S^z_k - S\right) t} S^+, S^-] \rangle + \text{к. с.}$$

The expression standing in the exponent under the spur sign is now really small at low temperatures because

$$\langle S^z_k - S \rangle \sim \frac{1}{N} \sum_g \langle n_g \rangle,$$

therefore, we can develop the exponent in series. Then

$$-\frac{dG_s}{dt} = \frac{i}{\hbar} \left(\frac{g\mu_0}{2}\right)^2 e^{-it\left(\omega_z - \frac{3s}{\hbar} \sum_k \Phi^0_{ek}\right)} \Big\{ \langle [S^+, S] \rangle + \frac{i}{\hbar} 3t \langle [\sum_k \Phi^0_{ek} (S^z_k - S) S^+, S^-] \rangle +$$

$$+ \left(\frac{i}{\hbar} 3t\right)^2 \frac{1}{2} \langle [(\sum_k \Phi^0_{ek} (S^z_k - S))^2 S^+, S^-] \rangle + \ldots \Big\} + \text{к. с.}$$

The separate terms in the braces can be calculated by development (3.1). Taking out the first term behind the bracket we obtain a square polynome on t starting from unity. We shall consider that it represents the first terms of the development of some function $e^{\psi(t)}$ in series on t. Dropping all the conversions the last expression can be expressed in the form

$$-\frac{dG_s}{dt} = \frac{2i}{\hbar} \left(\frac{g\mu_0}{2}\right)^2 \langle S^z \rangle e^{-i\omega_0 t - \frac{1}{2}\sigma_0^2 t^2} + \text{к. с.}, \tag{3.5}$$

where,

$$\sigma_0^2 = \frac{9}{\hbar^2 N^2} \sum_{\vec{g}_1 \vec{g}_2} \left| \sum_{\vec{p}} \Phi^0_{\vec{p}} e^{i\vec{p}(\vec{g}_2 - \vec{g}_1)} \right|^2 \langle n_{\vec{g}_1} \rangle (1 + \langle n_{\vec{g}_2} \rangle), \tag{3.6}$$

$$\omega_0 = \omega_z - \frac{3s}{\hbar} \sum_k \Phi^0_{ek} \left(1 - \frac{\sum_g \langle n_g \rangle}{Ns}\right) = \omega_z - \frac{3}{2} \frac{g\mu_0}{\hbar} Ma^3 \sum_p \frac{r_p^2 - 3z_p^2}{r_p^5}. \tag{3.7}$$

Here M is the magnetization at a given temperature.

The last sum can easily be calculated for a cubic crystal with a transition to integration [10].

$$a^3 \sum_{\vec{p}} \frac{r_p^2 - 3z_p^2}{r_{\vec{p}}^5} = -\frac{4\pi}{3} + \int_S \frac{z n_z}{r^3}\, dS, \tag{3.8}$$

where n_z is the projection of the normal to the outer surface of the samples. The first term D of (3.8) represents Lorenz' field and the second is the demagnetizing factor at the surface in the direction z-N_z. Therefore, (3.7) for resonance frequency can be written in the form

$$\omega_0 + \frac{g\mu_0}{\hbar}\left[H + \left(2\pi - \frac{3}{2}N_z\right)M\right]. \tag{3.9}$$

We shall always consider the samples in the form of a solid of revolution with the sense of the constant magnetic field along the axis of revolution (axis z). In the next section we shall show that for this case the non-secular terms do not lead to an actual shift in the resonance frequency and therefore, (3.9) is Kitel's formula for a body of revolution when

$$N_x = N_y = \frac{4\pi - N_z}{2}$$

Substituting (3.5) in (2.2) we shall define the contribution of the secular part of the disturbance to X''. Integrating we find that close to resonance frequency

$$\chi_s'' = \left(\frac{g\mu_0}{2}\right)^2 \frac{\langle S^z \rangle}{\hbar\sigma_0} \sqrt{\pi}\, e^{-\frac{(\omega-\omega_0)^2}{2\sigma_0^2}}, \tag{3.10}$$

i.e. the absorption line has a gauss form with width $\sim \sigma_0$

And so the secular part of dipole-dipole interaction plays an important role in ferromagnetic resonance. It leads to Kittel's shift in frequency, creating the demagnetizing field on the surface of the sample. In addition, thanks to the presence of thermal fluctuations, the secular interaction leads to non-uniform local demagnetizing fields, causing the line to widen. At 0°K i.e. complete ferromagnetic order, this widening is zero.

4. THE EFFECT OF NON-SECULAR TERMS

We have already pointed out that the non-secular terms can be examined by the theory of disturbances developed in section 2. The values of $Z_{\alpha\beta}^{\gamma\gamma'}$ must be calculated for this. In a spin wave approximation they will contain the operators:

$$b_{\vec{g}}(\tau) \equiv e^{\frac{i}{\hbar}H_e\tau} b_{\vec{g}} e^{-\frac{i}{\hbar}H_e\tau} = \tag{4.1}$$

$$= e^{-\frac{i}{\hbar}\varepsilon_{\vec{g}}\tau} b_{\vec{g}};\ b_{\vec{g}}^{+}(\tau) = e^{\frac{i}{\hbar}\varepsilon_{\vec{g}}\tau} b_{\vec{g}}^{+},$$

therefore, the time part in $Z_{\alpha\beta}^{\gamma\gamma'}$ is separated at once. The expressions independent of time are the commutators from various products of Bose operators and many of them disappear when the spur is taken.

It is easily seen from (2.18) and (2.22) that

$$Z_{\alpha\beta}^{+-}(\tau) = 0,\ \alpha+\beta \neq 0;\ Z_{\alpha\beta}^{++}(\tau) =$$
$$= 0,\ \alpha+\beta \neq -2.$$

Moreover, if the remaining terms of $Z_{\alpha\beta}^{++}$ are calculated it is not difficult to ascertain that they are all equal to zero because they contain the sums

$$\sum_p \frac{z_p(x_p+iy_p)}{r_p^5};\quad \sum_p \frac{(x_p+iy_p)^2}{r_p^5},$$

equalling zero for a body of revolution.

$$Z_{0,0}^{+-}(\tau) = 18\,S^3 N \sum_p \Phi_p^{0\,2}. \tag{4.2}$$

$$Z_{1,-1}^{+-}(\tau) = 32\,S^2 \sum_{\vec{g}} (1 + 2\langle n_{\vec{g}} \rangle)\, D_{\vec{g}}^{(1)\,2} e^{-i\frac{2\varepsilon_{\vec{g}}}{\hbar}\tau},$$

$$Z_{-2,2}^{+-}(\tau) = 32\,S^2 \sum_{\vec{g}} (1 + 2\langle n_{\vec{g}} \rangle)\, D_{\vec{g}}^{(2)\,2} e^{i\frac{2\varepsilon_{\vec{g}}}{\hbar}\tau} \tag{4.3}$$

where,

$$D_{\vec{g}}^{(1)} = \sum_{\vec{p}} \Phi_{\vec{p}}^{1} e^{i\vec{g}\vec{p}} = \frac{\pi}{2}\frac{g^2\mu_0^2}{a^3} \sin 2\theta_{\vec{g}}\, e^{i\varphi_{\vec{g}}}$$

$$D_{\vec{g}}^{(2)} = \sum_{\vec{p}} \Phi_{\vec{p}}^{2} e^{ig\,p} = \frac{\pi}{2}\frac{g^2\mu_0^2}{a^3} \sin^2\theta_{\vec{g}}\, e^{-i2\varphi_{\vec{g}}}. \tag{4.4}$$

$\theta_{\vec{g}}$ and $\phi_{\vec{g}}$ are the polar and azimuth angles

of the wave vector $\vec{g}$.

(2.21) is now extraordinarily simplified and if the secular term is rejected from it for the non-secular term we have

$$-\frac{dG_{n.s}}{dt} = -\frac{i}{h^3}\left(\frac{g\mu_0}{2}\right)^2 \sum_{\alpha\neq 0} F_{\alpha,\,-\alpha}(t)\, e^{-i\omega_z t} + \text{к. с.} \tag{4.5}$$

How can the secular term which can not be considered as a disturbance be included in this scheme? We note that in the second approximation the secular term is not confused with the non-secular (see (4.3)), therefore, formally calculating the whole series of the theory of disturbances for the secular term then summarizing it, we can account the secular term effect together with the non-secular.

For this we shall write the whole series of the theory of disturbances for secular interaction

$$-\frac{dG_s}{dt} = \frac{i}{h}\left\{ \langle\, [\hat{M}_x^0(t),\ \hat{M}_x] \,\rangle + \right.$$

$$+ \sum_{n=1}^{\infty} \frac{1}{(ih)^n} \int_0^t dt_1 \ldots \int_0^{t_{n-1}} dt_n \cdot \tag{4.6}$$

$$\left. \langle\, |\ldots[\hat{M}_x^0(t),\ H'(t_1)], \ldots,\ H'(t_n)],\ \hat{M}_x] \,\rangle \right\}.$$

In the spin wave approximation

$$\hat{M}_x^0(t) = \frac{g\mu_0}{2}(2SN)^{1/2}\left(b_0 e^{-i\omega_z t} + b_0^+ e^{i\omega_z t}\right) + \ldots \tag{4.7}$$

$$[b_0,\ H_0'(t)] = -3S\sum_p \Phi_p^0 b_0 + \ldots \tag{4.8}$$

Substituting (4.7) in (4.6) we obtain

$$-\frac{dG_s}{dt} = \frac{i}{h}\left(\frac{g\mu_0}{2}\right)^2 2SN\left\{1 + \right.$$

$$+ \sum_{n=1}^{\infty} \frac{1}{(ih)^n} \int_0^t dt_1 \ldots \int_0^{t_{n-1}} dt_n \cdot$$

$$\left. \langle\, [\ldots[b_0,\ H_0'(t_1)], \ldots,\ H_0'(t_n)],\ b_0^+] \,\rangle \right\} e^{-i\omega_z t} + \text{к. с.}$$

Calculating the n-fold commutator with (4.8) we find

$$-\frac{dG_s}{dt} = \frac{i}{h} 2SN\left(\frac{g\mu_0}{2}\right)^2 e^{-i\omega_z t}\left\{1 \right. \tag{4.9}$$

$$\left. + \sum_{n=1}^{\infty} \frac{1}{(ih)^n}\left(-3S\sum_p \Phi_p^0\right)^n \frac{t^n}{n!}\right\} + \text{к. с.} = \frac{i}{h} 2SN\left(\frac{g\mu_0}{2}\right)^2 e^{-i\omega_z t + i3S\sum_p \Phi_p^0 t} + \text{к. с.}$$

(4.9) contd.

The last expression coincides exactly with (3.5) for $T=0^\circ K$, when $\sigma_0 = 0$. If we calculate the higher terms of the development of (4.7) and (4.8) we should obtain in (4.9) terms dependent on temperature but it is not necessary to do this as it has already been done when (3.5) was obtained. Here we showed, summarizing the whole series of the theory of disturbances for a secular disturbance that the secular effect acts together with the non-secular described by (4.5).

Thus summarizing our results one can write

$$-\frac{dG}{dt} = 2\left(\frac{g\mu_0}{2}\right)^2 \frac{\langle S^z\rangle}{hi} e^{\psi(t)+i\omega_0 t} + \text{к. с.}, \tag{4.10}$$

where,

$$\psi(t) = -\frac{1}{2}\sigma_0^2 t^2 - \frac{1}{h^2\langle S^z\rangle}\sum_{\alpha\neq 0} F_{\alpha,\,-\alpha}^{\cdot}(t). \tag{4.11}$$

(4.11) can be calculated with (2.22), (4.3), (4.4) and (3.6). In the sums on the wave vectors of $\vec{g}$ it is necessary for this to proceed from summarization to integration. After substituting the variables in the integrals so obtained, which are typical for Bose statistics, the expression for $\psi(t)$ can be approximately presented in the form

$$\psi(t) = -\frac{1}{2}\sigma_0^2 t^2 - \frac{1}{2}\sigma_n^2 t^2 + \psi_0(t), \tag{4.12}$$

where,

$$\sigma_0^2 = C\,\frac{Sg^6\mu_0^4}{a^6h^2}\left(\frac{kT}{2SJ}\right)^3. \tag{4.13}$$

$$\sigma_n^2 = \frac{8}{15}\sqrt{\pi}\,\xi\left(\frac{3}{2}\right)\frac{Sg^6\mu_0^4}{a^6h^2}\left(\frac{kT}{2SJ}\right)^{3/2}. \tag{4.14}$$

Here C is some numerical constant of the tenth power, $\xi\left(\frac{3}{2}\right) = 2{,}61\ldots$ — ξ is Riman's function;

$$\psi_0(t) = \frac{8}{15}\frac{Sg^6\mu_0^4}{a^6h^2}\left(\frac{h}{2SJ}\right)^{3/2}\frac{1}{\sqrt{2}}\,[I(\omega_z,\ t) + \tag{4.15}$$

$$+ I^*(2\omega_z, t)], \qquad (4.15)$$

contd.

where,

$$I(\alpha, t) = \int_0^\infty \frac{x^2 e^{ix^2 t}}{(x^2+\alpha)^2}\, dx. \qquad (4.16)$$

This integral is calculated in the appendix.

For us its essentially asymptotic behaviour at low t

$$I(\alpha, t) = \frac{\pi}{4\sqrt{\alpha}} - \sqrt{-i\pi t} + \ldots \qquad (4.17)$$

Taking only the part of (4.17) dependent on time we obtain from (4.15)

$$\psi_0(t) = -b\sqrt{t};\ b = \frac{8}{15}\sqrt{\pi}\,\frac{Sg^4\mu_0^4}{a^6 h^2}\left(\frac{h}{2SJ}\right)^{3/2}. \qquad (4.18)$$

As can be seen from (2.12)-(2.14), $\psi_0(t)$ is the value of $\psi(t)$ at absolute zero.

On the basis of (2.2) and (4.10) we find that at zero temperature

$$\chi''_{T=0}(\omega) = \frac{2SN}{h}\left(\frac{g\mu_0}{2}\right)^2 \mathrm{Re}\int_0^\infty e^{-b\sqrt{t}+i(\omega_0-\omega)t}\, dt. \qquad (4.19)$$

An integral of such a type can be expressed through an integral of probabilities;

$$K(b, x) \equiv \int_0^\infty e^{-b\sqrt{t}+ixt}\, dt = - \qquad (4.20)$$

$$-\frac{\sqrt{\pi}\,b}{2(-ix)^{3/2}}\, e^{-\frac{b^2}{4xi}}\left[1 - \Phi\left(\frac{b}{2\sqrt{-ix}}\right)\right] - \frac{1}{ix}.$$

For it the following asymptotic estimations are obtained

$$K(b, x) = \frac{2}{b^2}\left\{1 + i\frac{x}{b^2}3! - \left(\frac{\lambda}{b^2}\right)^2 \frac{5!}{2} + \ldots\right\},\ x \ll b^2. \qquad (4.21)$$

$$K(b, x) = \frac{\sqrt{2\pi}}{4}\,\frac{b}{|x|^{3/2}} + \frac{i}{x} + \ldots,\ x \gg b^2. \qquad (4.22)$$

As $K(b, -x) = K^*(b, x)$, $\mathrm{Re}K(b, x)$ is an even function of x, therefore, (4.19) determines a line, symmetrical relative to the centre. Its form is determined by (4.20) for $x = \omega - \omega_0$. We have a complex non-analytic dependence from $\omega_0 - \omega$, but it determines a sharp resonance peak. On the wings the curve falls according to the law $\chi'' \sim |\omega_0 - \omega|^{-3/2}$ and near the centre $\chi'' \sim 1 - \frac{(\omega_0-\omega)^2}{b^2}\frac{5!}{2}$, that is near the centre it has a Lorenz character but on the wings falls more sharply than the Lorenz curve. It is useful to note that a gauss curve is obtained when $\psi(t)$ is proportional to $-t^2$, a Lorenz curve if $\psi(t) \sim -t$, our curve is obtained when $\psi(t) \sim -\sqrt{t}$.

It is easy to see that the width $(\Delta\omega)_{T=0}$ of the curve (4.20) is proportional to b^2, i.e.

$$(\Delta\omega)_{T=0} \sim \frac{D}{h}\left(\frac{D}{J}\right)^3, \qquad (4.23)$$

where, $D = g^2\mu_0^2/a^3$ the dipole-dipole energy of two neighbouring spins. As far as $D/J \sim 10^{-3}$ the width of the line at zero temperature on account of dipole-dipole interaction appears very small even if finite. This is the "zero oscillations" effect assessed by Keffer [6].

Ignoring this zero width we leave only the first two terms in (4.12). Then X'' is expressed by (3.10), only instead of σ_0^2 one must write

$$\sigma^2 = \sigma_0^2 + \sigma_n^2. \qquad (4.24)$$

The first term of this expression (4.13) is conditioned by secular interaction, the second (4.14) by non-secular interaction. We see that at low temperatures ($kT \ll J$) the term σ_n^2 is predominant. As far as the line form is gaussian the expression σ^2 is exactly the second moment of the absorption line. The lines width according to (4.14) is

$$\Delta\omega \sim \sigma \sim \frac{D}{h}\left(\frac{kT}{2SJ}\right)^{3/4} \qquad (4.25)$$

It is useful to compare this result with the cases of a paramagnetic in which the line width is inversely proportional to the exchange integral. (4.25) demonstrates the

exchange reduction effect for ferromagnetics.

For paramagnetics account of the non-secular terms increases the line width $^{10}/_{3}$ times (the so called $^{10}/_{3}$ effect). (4.13) and (4.14) show that in the case of a ferromagnetic the contribution from non-secular interaction is definitive. The line width can be assessed easily from (4.25). Thus, for example, at $10°\,\mathrm{K}\,\Delta\omega \sim \frac{1}{100}\cdot\frac{D}{h}$, which makes approximately 100 oersteds.

Therefore, dipole-dipole interaction plays an important role in ferromagnetic resonance, producing, at first a Kittel shift in frequency and widening the absorption line to hundreds of oersteds at low temperatures. However, other interaction mechanisms have to be considered to explain the line's great width at low temperatures.

As Clogston and others [9] showed, in ferrites distributions of spin waves on natural non-uniformities in the lattice's magnetic structure are such interactions. Apparently conductance electrons play an important role for metallic ferromagnetics.

I express my gratitude to E.A. Turov for having shown the necessity of discussing the problem and for his advice during the work and also to L.A. Kobelev, A.A. Kobin and G.V. Skrotskii for their discussion of the results.

APPENDIX

Let us calculate the integral

$$I(\alpha, t) = \int_0^\infty \frac{x^2 e^{ix^2 t}}{(x^2+\alpha)^2}\,dx = i\frac{\partial^2}{\partial t\,\partial\alpha}\int_0^\infty \frac{e^{ix^2 t}\,dx}{x^2+\alpha}. \tag{A.1}$$

For the subsidiary integral

$$J(t) = \int_0^\infty \frac{e^{ix^2 t}\,dx}{x^2+\alpha} \tag{A.2}$$

it is not difficult to compose the differential equation

$$\frac{dJ}{dt} + i\alpha J = i\sqrt{i}\,\frac{\sqrt{\pi}}{2}\,\frac{1}{\sqrt{t}}\,;\quad J(0) = \frac{\pi}{2\sqrt{\alpha}}, \tag{A.3}$$

the solution of which is

$$J(t) = \frac{\pi}{2\sqrt{\alpha}}\,e^{-i\alpha t}\{1 - \Phi(\sqrt{-i\alpha t})\};\quad \Phi(x) = \frac{2}{\sqrt{\pi}}\int_0^x e^{-\xi^2}\,d\xi. \tag{A.4}$$

Substituting this expression in (A.1) and differentiating on the parameters we find

$$I(\alpha, t) = \frac{\pi}{4\sqrt{\alpha}}\left\{e^{-i\alpha t}(1 - i2\alpha t)\left[1 - \Phi(\sqrt{-i\alpha t})\right] - \frac{2}{\sqrt{\pi}}\sqrt{-i\alpha t}\right\} \tag{A.5}$$

The integral of probability $\Phi(x)$ from a complex variable can be expressed if desired through Frenel's integrals from a material variable

$$\Phi(\sqrt{-i\alpha t}) = \sqrt{-2i}\,[C(\alpha t) + iS(\alpha t)]. \tag{A.6}$$

For $\alpha t \ll 1$ it is easy to obtain an asymptotic development of the integral

$$I(\alpha, t) = \frac{\pi}{4\sqrt{\alpha}}\left\{1 - \frac{4}{\sqrt{\pi}}\sqrt{-i\alpha t} - i3\alpha t + \ldots\right\} \tag{A.7}$$

Translated by P.J.H. Saunders

REFERENCES

1. R. Kubo and K. Tomita, *Journ. Phys. Soc. Japan*, 9, No.6 (1954).
2. C. Kittel, *Phys. Rev.*, 73, 155 (1948).
3. J.H. Van-Vleck, *Phys. Rev.*, 78, 266 (1950).
4. J.H. Van-Vleck, *Phys. Rev.* 74, 1168 (1948).

5. I. Waller, *Zs. f. Phys.*, 79, 380 (1932).

6. F. Keffer, *Phys. Rev.*, 88, 386 (1952).

7. C. Kittel and E. Abrahams, *Rev. Mod. Phys.*, 25, 233 (1953).

8. N. Bloembergen and S. Wang, *Phys. Rev.*, *93*, 72 (1953).

9. A.M. Clogston, H. Suhl, L.R. Walker and P.W. Anderson, *J. Phys. Chem. Solids*, 1, 129 (1956).

10. T. Holstein and H. Primakoff, *Phys. Rev.* 58, 1098 (1940).

VOL.
8
1959

DEVELOPMENT OF METAL PHYSICS AND PHYSICS OF METALLURGY IN THE CHINESE PEOPLES' REPUBLIC DURING TEN YEARS*

CHOU CHIH-HUNG, KO TSUN and TSIN LIN-CHAO

Chinese Peoples' Republic

(Received 8 October 1959)

There has been much development in physics of metals and physical metallurgy in China since the time of the formation of the Chinese Peoples' Republic in 1949.

Before the liberation there were in China only a few scientific workers, who were working on the electronic theory of metals and the statistical theory of ordering of solid solutions.

Now under the leadership of the Chinese Communist Party investigations have been started in different fields and much has been done, particularly after the great leap forward in 1958.

In the present article an attempt has been made to describe briefly the work done in China during the last ten years.

In the period of establishment of the national economy and in the initial period of the first five-year plan, the attention of Chinese workers in metal physics and metallurgy was directed largely to the creation of teams of scientific investigators and to the solution of the then current problems of industry.

Large-scale scientific investigations have begun only since 1954-55. This work may be conveniently grouped as follows:

1. Physics of strength and plastic deformation of metals
2. Internal friction and diffusion
3. Phase transitions
4. Theory of metals and alloys.

1. PHYSICS OF STRENGTH AND PLASTIC DEFORMATION OF METALS

The greater part of the work carried out in this field was concerned with the problems of fabrication of alloys for use at high temperatures. The efforts of the whole collective of the faculty of metal physics at Gilin University were directed towards the study of the various properties of a range of tungsten ferrite steels [1], including physical properties, resistance to oxidation, fatigue, wear, and erosion. These investigations showed that addition of 3-5% tungsten in steel increases its modulus of rigidity, particularly at high temperatures. Kou Chen-Chuan and his co-workers [2] found that the energy of activation for viscous flow at the grain boundaries in iron was increased on addition of tungsten as an alloying element. This series of studies was begun by M.G. Morozovyi, who was consultant to the University's faculty of metal physics in 1956-1958. Wider investigations in this direction were begun in other scientific research establishments to find the best compositions of ferrite heat-resisting steels for practical use.

Attempting to make new austenite heat-resisting steels, scientific workers of the department of metal physics at the Peking Institute of ferrous metallurgy, and other research institutes investigated the effect of addition of other alloying elements on the heat-resisting properties of austenite chrome-manganese steels.

The effect of the σ-phase in stainless steel of type 18-8 with 3% molybdenum and 1% titanium was studied by Li Yo-ko and Chuang

* *Fiz. metal. metalloved.*, 8, No.6, 820-828, 1959.

VOL 8 195

Yu-chi [3], who observed that the presence of the σ-phase lowered the creep resistance at 560-680°C.

By a torsional pendulum method, Ke Ting-sui and Kung Chin-pin [4] investigated the effect of carbon on creep at grain boundaries in iron, and observed that traces of carbon of the order of 0.00004% increased the creep resistance of iron, the effect becoming more pronounced with increase in carbon content. These results were interpreted on the basis of a theory of grain boundary structure proposed by Kê.

Tsien Lin-chao, Hou Shou-an and Yang Ta-yu [5-7] carried out electron microscope studies of the slip process in single crystals. It was noted that in a single crystal of technically pure aluminium the size of the deformation due to each slip line was comparatively great, and that the slip line consisted of layers with a relative deformation of the order of 200 and 2000 Å in the same specimen.

The same authors have also studied the effect of preliminary local deformation on the plastic flow of single crystals of aluminium. Tsien Lin-chao, Yang Ta-yu and L.I. Vasiliev [8] (who was consultant to the department of metal state physics at Peking University, and is now working in Tomsk State University), having determined the effect of deformation at one temperature on the development of slip lines at another temperature, showed that there does not exist a mechanical equation of state in metals.

They found that previous deformation at -180°C accompanied by deformation at a higher temperature generated wavy slip lines, made up of parallel sections of slip lines connected by transverse sections, which on close examination were found to consist of groups of fine parallel slip lines, bent slip lines, or transverse slips.

The authors have suggested that deformation in the transverse sections occurs as a result of stress concentrations when two series of parallel slip lines come together in the process of development.

The effect of impurities and ordering on plastic deformation has been studied. Workers at the Department of Metal Physics of Peking University [9] have investigated the effect of ordering on plastic deformation of polycrystalline Cu_3Au and have shown that for a deformation rate of 1mm/hr the disordered alloy has a jagged extension curve at room temperature, like the extension curve of mild steel in the blue brittle region. Tsien Lin-chao and Liu Min-chi [10] observed that impurities in tin markedly lower the amount of microcreep and cause strengthening connected with the microcreep process. Specimens are not able to attain their initial characteristics by relaxation for several hours after the microcreep experiments, as distinct from the case of tin purified by zone melting or high-purity zinc, which was studied earlier by Chalmers [11].

Ke Ting-sui and his co-workers [12] have observed that internal friction in deformed iron, copper, and aluminium sharply increases immediately before the elastic limit is reached; when there is a well expressed creep strength, as in low-carbon iron, internal friction remains constant during extension.

The effect of rate of deformation and annealing after deformation at room and elevated temperatures on internal friction in deformed copper and aluminium has also been studied [13].

Using the back reflection method and accurately focused X-rays, some investigators have studied the formation of sub-structure in aluminium during deformation at room temperature or during annealing after deformation [14-18]. It was concluded that the substructure is formed in the course of the plastic deformation, and not as a result of polygonization caused by creeping of dislocations. The presence of grain boundaries promotes fragmentation of the grains.

Texture in copper, aluminium, and in pure and siliceous iron with various silicon contents has been investigated [19-24]. Sheet siliceous iron with Goss texture was obtained by Chen Neng-Kuan, Tai Li-chi and their co-workers, and with a cubic texture by Chou Ban-sin, Wang Wei-ming and Chen Neng-kuan, who studied the mechanism of formation of cubic annealing texture and expressed the opinion that the theory of orientated growth of recrystallization nuclei is in best agreement with their experimental results. Yen Ming-kao and his co-workers [23-24] have studied the recrystallization texture of copper and aluminium. It was found that

sheet copper, with the ordinary well-known rolling texture after reduction by 90%, gave on low-temperature annealing the textures (100) [001], (358) [352], and (122) [212], grains with the orientation (100) [001] being formed in the first instance. Increasing the annealing temperature decreased the number of grains with the texture (358) [352] and increased the texture (100) [001]. The pure texture (100) [001] was obtained when the annealing temperature reached 900°C. The authors have suggested that cubic texture is obtained from recrystallization in situ and from selective growth of nuclei. Tai Lin-chi and co-workers [25,26] have investigated the formation conditions of cubic texture in 50% nickel Permalloy.

2. INTERNAL FRICTION AND DIFFUSION

Investigations of internal friction in metals and alloys have been carried out in connexion with many problems, including diffusion, plastic deformation, phase transitions and so on. Of special interest is the work on internal friction due to the diffusion of carbon in the face-centred cubic lattice of iron or nickel [28-34]. Finkelshtein and Rozin [27] observed an internal friction peak in austenite stainless steel with 25% Cr, 20% Ni and 0.3% C at 300°C and at a frequency of of 1 c/s. The phenomenon was systematically investigated by Kê and his colleagues in type 18-8 stainless steel containing 2.6% Mo and 0.80% Ti, in iron-manganese alloys containing 18.5 to 36% Mn, in an iron-manganese-nickel alloy with 12% Mn and 4% Ni, in an iron-manganese-nickel-chromium alloy with 9.5% Mn, 8% Ni and 3% Cr, in pure nickel (99.8%) and in a nickel alloy containing 2% Al, 2% Mn and 1% Si. They have shown convincingly that an internal friction peak can be observed in face-centred cubic austenite or nickel lattices when carbon is present and that the peak is caused by the micro-diffusion of carbon.

The energy of activation of carbon diffusion, calculated from the temperature dependance of the internal friction peak, turns out to be the same as the energy of activation determined by macroscopic methods; the diffusion constants at 230-250°C, determined macroscopically at 1000-1200°C. They found also also that the height of the internal friction peak is proportional to the carbon content, and very slightly decreases with increasing manganese content. It is well-known that the carbon atoms are disposed in the holes in the austenite or nickel lattice. Due to the symmetry of the holes in a face-created cubic lattice, internal friction is not observed if the carbon atoms are situated singly in the lattice. In calculation of the internal friction peak observed, Ke Ting-sui and Tsien Chi-chiang [30] assumed that in the alloyed steel the carbon atom forms a pair with an atom of the alloying element and that the internal friction peak appears as a consequence of the reorientation of such a pair under the action of an applied external stress. In nickel or low-alloyed steel the carbon atom forms a pair with a vacant lattice site, which gives the same effect as that if the vacant site was replaced by an atom of the alloying element.

Another mechanism was proposed by Chen and his co-workers [32,35,36]. Chen Kai-cha earlier proposed an internal friction theory based on general thermodynamic theory of irreversible processes and the Boltzmann superposition principle. Applying the theory to the diffusion of carbon in a face-centred cubic lattice, Chen found that the intensity of internal friction must be proportional to the concentration of intersticial carbon and must essentially depend on the concentration of the alloying element. The latter conclusion does not agree with Ke's observations.

Chen showed that here another mechanism must apply, namely, the following: the carbon atom is situated in a vacant site and forms a pair with another carbon atom situated in a vacant site and forms a pair with another carbon atom situated in a hole close to the occupied vacancy. The height of the internal friction peak created in this way must be proportional to $Nc^2/B + c$ where N is the vacancy concentration, c is the concentration of atoms in interstices and B is a constant. This second mechanism was applied by Wu Tsu-liang and Wang Chi-min to the interpretation of the results of their internal friction investigations in the series of iron-nickel alloys containing 19 to 75% nickel. These authors found that the height of the internal friction peak increases

VOL 8 195

with increase in carbon content and is proportional to it if it exceeds 0.2%. For a given carbon content the height of the internal friction peak increases with the nickel content. In an alloy with 50% nickel the height of the peak also increases with increase in quenching temperature (900-1200°C); this effect is explained as a result of increasing numbers of vacancies. In another paper Tsien Chi-chiang [34] suggested that the appearance of internal friction is a result of formation of pairs of carbon atoms in the interstices.

An internal friction peak due to the presence of carbon and an alloying element was also observed by Ke and his colleagues [37,38] in alloyed martensite.

The peak appears at 156°C and at a frequency of 2 c/s. The authors have deduced that the atom of carbon are situated at the (00½) position in the martensite lattice, but due to distortions caused by the atoms of the alloying element, the carbon atom, under the action of the external stresses, changes its position between two iron atoms to a position between an atom of iron and an atom of the alloying element, creating thereby an internal friction peak.

Ke and his colleagues also showed [39] that in the region of 0.001-0.017% carbon and 0.002-0.03% nitrogen their concentration does not affect the rate of their diffusion. Addition of manganese (0.23%) and silicon (0.13%) weakly affects the diffusion of nitrogen. Manganese hastens the separation of nitrides.

The internal friction method was applied by Wang Yeh-ning and Chu Chiang-chung [40,41] to the study of the martensite transformation in ferromanganese and copper – aluminium alloys. They noted that internal friction increases during the direct and reverse martensite transformations the internal friction peak disappears if the transformation stops (if the temperature remains constant). The authors conclude that internal friction is created by the interaction of an applied external stress with non-uniformities caused by the changes in relative quantities of the two phases, having different constants of elasticity.

3. THE KINETICS OF PHASE TRANSFORMATIONS

Studies in this field were concerned mainly with transformations in steel. Li Ling and his co-workers [42-45] investigated the effect of boron on the hardenability of steel, in relation to carbon content and austenitization temperature. The effect of boron was also investigated on the rate of generation and growth of pearlite. They found that in chromium-manganese-silicon steel with 0.27%C an increase in hardenability when boron was present was caused by an increase in the period of incubation of hypoeutectic ferrite and perlite. In hypoeutectic and eutectic steels boron affects slightly the rate of generation of perlite at 650-700°C; the rate increases with increasing time of standing, but in the period after the the beginning of the reaction there is a small difference in generation rates in steel with boron and without boron. The rate of growth of perlite in the temperature region given, almost doubles when boron is present, as a result of which, in spite of the more lengthy incubation period in steels containing boron, the completion time of the transformation in steels with boron and without is little different.

The authors also observed that in boron steel with a sufficiently high titanium content for the combining of nitrogen, an increase in size of austenite grains caused by an increase in austenitization temperature does not lead to an increase in hardenability, as is normally the case for steels without boron. In steels without titanium an increase in quenching temperature lowers the hardenability of boron steel right up to 1200°C, when the hardenability is the same for boron steel and steel without boron. This indicates that presence of boron lowers the action of the surface energy of grain boundaries in generation of perlite. The nature of carbides in alloyed steels and their transformation has been extensively studied by Ko Ke-hsin [46,47].

The distribution of the alloying elements in perlite in its formation in alloyed steel has been investigated by Chang Pei-lin and his co-workers [48] in chrome steels. They observed that the type and composition of carbides formed initially in the perlite transformation depend on the ratio of concentrations of chromium and carbon in the austenite and are not fixed by the equilibrium

diagram. If the atomic ratio Cr: C is equal to 2: 1, then initially cementite separates from the austenite; if this ratio changes from 2: 1 to 13: 1, then $(Cr,Fe)_7C_3$ separates; if this ratio exceeds 13: 1, $(Cr,Fe)_{23}C_6$ separates.

Ko Tsun, continuing his work on the mechanism of the bainite transformation, has shown together with his colleagues [49,50] that the well-known Widmanstatten structure of alpha-iron in coarse-grained hypoeutectic carbon steel arises by way of a bainite transformation; during the transformation carbon diffuses from the bainite into the austenite. The authors further show that the bainite transformation can take place between the points A_1 and A_3.

Tsi Tseng-fon has observed that in 55-S-2 steel the bainite transformation is accelerated by the presence of a small quantity of martensite, and slowed down if the amount of martensite becomes large [51].

The mechanism of the transformation of residual austenite in high-speed cutting steel into martensite, after tempering at 500-560°C, was studied by Ko Tsun, Hsu Tsu-yao, and their comrades in the Peking Institute of Ferrous Metallurgy. Ko considers that "conditioning", that is the transformation of residual austenite in high-speed cutting steel after tempering, is the reverse effect to the mechanical and thermal stabilization which goes on in the initial period of formation of martensite. Ko Tsun and Chen Mengtse [52] showed that the transformation in martensite after tempering may be obviated by stabilization treatment at a temperature a little higher than that at which austenite transforms into martensite in the absence of this treatment. But the effect of stabilization can be eliminated if the steel is reheated to the tempering temperature. Such a process can be repeated up to seven times.

Hsu and others [53-55] have recently shown that residual austenite in high-speed cutting steel has a critical temperature, above which "conditioning" or destabilization occurs, while below it stabilization takes place, each of these two processes being the reverse of the other.

Chang Pei-lin and Chu Sui-chang have studied residual austenite in hardened ball-bearing steel below the point M_s, and believe that isothermal transformation of the residual austenite into martensite takes place [56].

The amount of residual austenite in high-strength structural steels increases with the size of the article made from the steel, due to the stabilization effect, caused by decrease in rate of cooling. The austenite transforms into martensite during use, causing brittleness in the steel. Sze Chang-hsu [57] found that silicon (1.5%) appreciably lowered the rate of decay of austenite, on tempering between 100 and 400°C, in low-carbon high-strength steel.

Chou Chih-hung continued his investigation of the martensite structure of iron and carbon-iron alloys and linked up the nature and mechanism of formation of the Widmanstatten structure [58].

The decay of delta-ferrite in molybdenum and titanium stainless steel was studied by Chuang Yu-chi and his co-workers [59-61]. They systematically studied the mechanism and products of decay at various temperatures (500-950°C). The kinetics of the processes of ordering and disordering were studied by Sze Shih-yuan and his colleagues [62-64]. They came to the conclusion that the formation of anti-phase domains is a process of generation and growth brought about by the diffusion of vacant lattice sites.

The rate of regrouping of atoms from a disordered to an ordered state depends on two opposing factors; the rate of diffusion and the difference in free energy of the two phases, which is proportional to $\left(\frac{1}{T}-\frac{1}{T_0}\right)$, where T_0 is the Curie ordering temperature. They have shown experimentally that there is a temperature at which the transformation rate is a maximum, as follows from their theory.

4. THEORY OF METALS AND ALLOYS

In studying the formation conditions of phases in ternary systems, Lu Hsueh-shan and Chang Tsung [65] observed that in the Al-Cu-Ni system the τ-phase undergoes a systematic structural change in the single-phase region, contrary to the normal assumption in intermetallic phases, characterized by a definite type of crystalline structure. In the given case there were structures of the defect

lattice type, each of which could be built up from rhombohedral structural elements. From a Hume-Rothery valency estimation one may consider that the average number of valency electrons in a structural element remains constant over the single-phase region, while the electron concentration changes with composition. The authors consider that for alloys in which there is no change in the unit cell, the average number of electrons in the structure element is equivalent to the number of electrons in a unit cell, and for intermetallic phases without defects it is effectively equivalent to the electron concentration. In studies of alloys of the silver-gold-zinc system with 50% zinc, Liu Yi-huan [66] and his co-workers observed a $AgAuZn_2$ phase; they found that this phase had the same structure as Heusler alloys.

The formation of the intermediate phases in the region 0-50% gold of the above system followed the Hume-Rothery rule.

Chang Chung-sui, Wang Tei-mi and Hsu Hong-chang [67,68] carried out investigations on the statistical theory of solid solutions. They have proposed a new method of determination of the configurational free energy of solid solutions, which is simpler, more reliable, and at the same time is of wider application, than previous methods. The new method was applied to the case of formation of superstructure in a face-centred cubic lattice; the change in degree of ordering and the latent heat of solid solution were calculated.

In investigations of the theory of spectra of crystal lattices, Chen Kai-cha has obtained a general proof of the theorem of possible presentation of the upper Brillouin zone by transposition of fragments of the zone. They have shown that this theorem must be accurate in the following manner. All the upper Brillouin zones may be accurately represented in the first Brillouin zone by a definite section of the zone fragments with the transpositions belonging to them. The Thomas-Fermi and Slater methods were used by Chen Kai-cha [70] in calculation of the bond energies and interatomic distances in metals, and he concluded that an electron on the surface of a sphere in the Seitz cell method on the average has a potential energy equal to $-e^2/R$, and not equal to zero, as was suggested by Slater and Crutter [71]. With this boundary condition, the total energy, determined by numerical integration, as a function of interatomic distance has a minimum, a result which could not be obtained from Slater and Crutter's calculation. Calculated interatomic distances agree well with observations for multivalent heavy elements, but are not in agreement for light monovalent elements.

From the above short account one may see that in the short period since the time of formation there has taken place in the Chinese Peoples' Republic a rapid development of metal physics and physical metallurgy, the tempo of which increased even more after the Great Leap Forward in 1958. It must be pointed out that such rapid progress would not have been possible without help on the part of the Soviet people. A great number of workers in metal physics and metallurgy were trained in Soviet universities, colleges and scientific research institutes. Many scientific workers of the Soviet Union, such as Professor V.D. Sadovskii, B.G. Livshits, M.G. Morosov and L.I. Vasiliev visited China last year and read a great quantity of reports and lectures. All this had a strong influence on the course of the successful development of the science.

A new generation of workers in metal physics and metallurgy has appeared, and a basis created for further rapid development.

Translated by D.G. Noel

REFERENCES

1. *Acta Phys. Sinica*, 15, 89 (1959); *J. of Natural Science of Gilin University*, 2, 43, (1958).
2. Kou Chen-Chuan, Ko You-ian, Xy Zhem-sun, Koxai-gyn, Hu Pei-iao, and Cheng Peen-gyn. *J. of Natural Science, Gilin University*, 1, 47 (1959).
3. Li Yo-ko and Chuang Yu-chi. *J. of the Chinese Society of Mechanical Engineers*, 5, 159 (1957).
4. Ke Ting-sui and Kung Chin-pin. *Acta Phys. Sinica*, 10, 365 (1954); *Scientia Sinica*, 4, 55 (1955).
5. Tsien Lin-chao and Hou Shou-an. *Acta Phys. Sinica*, 11, 287 and 290 (1955).
6. Tsien Lin-chao, Hou Shou-an and Yang Ta-yu. *Acta Phys. Sinica*, 12, 643 (1956).

VOL. 8 1959

7. Tsien Lin-chao and Ho Shou-an. *Acta Phys. Sinica*, 12, 647 (1956).
8. L.I. Vasiliev, Tsien Lin-chao and Yang Ta-yu. *Acta Phys. Sinica*, 13, 443 (1957).
9. Chen Hung-yi and Yin Tao-lo. In the press.
10. Tsien Lin-chao and Liu Min-chi. *Acta Phys. Sinica*, 12, 275 (1956).
11. B. Chalmers. *Proc. Roy. Soc.*, A 156, 427 (1936).
12. Ke Tin-sui, Yung Pao-taui and Chang Chao-yuan. *Science Record, Academia Sinica*, 1, 231 (1957).
13. L.I. Vasiliev, Chen Hung-yi, Bao Shien-ke. In the press.
14. Liu Yi-huan and Tao Tsu-tsong, *Acta Phys. Sinica*, 11, 363 (1955).
15. Liu Yi-huan and Tao Tsu-tsong. *Acta Phys. Sinica*, 11, 507 (1955).
16. Liu Yi-huan and Tao Tsu-tsong. *Acta Phys. Sinica*, 11, 12, 174.
17. Liu Yi-huan and Tao Tsu-tsong. *Acta Phys. Sinica*, 12, 550 (1956).
18. Chang Pei-lin and Lin Shu-chi. *Acta Phys. Sinica*, 12, 170 (1956).
19. Tai-Li-chi. *Acta Metallurg. Sinica*, 3, 227 (1958).
20. Tai Li-chi and Chang Shing-yu. *Acta Phys. Sinica*, 14, 22 (1958).
21. Tai Li-chi and Wang Chien-kang. *Acta Metallurg. Sinica*, 3, 47 (1958).
22. Chen Heng-kuan and Lin Chang-lo. *Acta Metallurg. Sinica*, 3, 30 (1958).
23. Yen Ming-kao and Chou Pan-hsin. *Acta Phys. Sinica*, 14, 120 (1958).
24. Yen Ming-kao and Chen Ke-min. *Acta Metallurg. Sinica*. In the press.
25. Tai Li-chi, Chang Hsing-yu and Lin Jen-pao. *Acta Metallurg. Sinica*, 4, 52 (1959).
26. Tai Li-chi, Lin Jen-pao and Wang Li-ko. *Acta Metallurg. Sinica*, 4, 60 (1959).
27. K.M. Rozin, B.N. Finkelshtein. *Dokl. Akad. Nauk SSSR*, 91, 811 (1958).
28. Ke Ting-sui and Wang Chi-min. *Acta Phys. Sinica*, 11, 387 (1955).
29. Ke Ting-sui, Tsien Chih-tsiang and Misck K. *Acta Phys. Sinica*, 11, 403 (1955); *Scientia Sinica*, 4, 519 (1955).
30. Ke Ting-sui and Tsien Chi-chiang. *Acta Phys. Sinica*, 12, 607 (1956); *Scientia Sinica*, 5, 625 (1956).
31. Ke Ting-sui and Yang Pen-wei. *Acta Phys. Sinica*, 13, 410 (1957); *Scientia Sinica*, 6, 623 (1957).
32. Chen Kai-cha and Chang Shen-kwei. *Acta Phys. Sinica*, 14, 71 (1958).
33. Wu Tsu-liang and Wang Chi-min. *Acta Phys. Sinica*, 14, 354 (1958); *Scientia Sinica*, 7, 1027 (1958).
34. Tsien Chi-chiang. *Acta Metallurg. Sinica*, 4, 69 (1959).
35. Chen Kai-cha. *Acta Metallurg. Sinica*, 11, 163 (1955).
36. Chen Kai-cha and Li Cheng-Chung. *Acta Phys. Sinica*, 12, 281 (1956).
37. Ke Ting-sui and Ma Ying-liang. *Scientia Sinica*, 5, 29 (1956).
38. Ke Ting-sui and Ma Ying-liang. *Acta Phys. Sinica*, 13, 69 (1957); *Scientia Sinica*, 6, 81 (1957).
39. Ke Ting-sui, Yung Pao-tsui and Wang Yeh-ning. *Acta Phys. Sinica*, 11, 91,(1955); *Scientia Sinica*, 4, 263 (1955).
40. Wang Yeh-ning and Chu Chiang Chung. *Scientia, Academia Sinica*, 7, 580 (1957).
41. Wang Yeh-ning and Chu Chiang Chung. *Acta Phys. Sinica*, 15, 341 (1959).
42. Chi Ming-wei and Li Ling. *Acta Metallurg. Sinica*, 1, 265 (1956).
43. Kwan Chi-hiao and Li Ling. *Acta Metallurg. Sinica*, 1, 255 (1956).
44. Li Lin, Chi Ming-wei, Tseng Chin-ling and Miao Yung-kwang. *Acta Metallurg. Sincia*, 2, 59 (1957).
45. Li Lin et al. *Acta Metallurg. Sinica*, 2, 69 (1957).
46. Ko Ke-hsin. *J. Iron and Steel Inst.*, 173, 363 (1953); 174, 223 (1953); 78, 39 (1958); 184, 258 (1956); *Acta Metallurg. Sinica*, 2, 383 (1957).
47. Ko Ke-hsin, L.E. Pearson, *J. Iron and Steel Inst.*, 185, 277 (1957).
48. Chang Pei-lin and Liang Chih-te. *Acta Metallurg. Sinica*, 2, 367 (1957).
49. Ko Tsun and Zhao Gia-zheng. *Acta Metallurg. Sinica*, 1, 201 (1956).
50. Ko Tsun. *Trans. of the Conference of Metals Research (Academia Sinica)*, 5, (1954).
51. Tsi Tseng-fon. *Acta Metallurg. Sinica*, 3, 62 (1958).
52. Ko Tsun and Chen Meng-tse. *Report read at the second conference on metals (Chinese Society for Metals*, (1956).
53. Hsu Tsu-yao and Chang Wan-chen. *Science Record, Academia Sinica*, 1, 65 (1957); *J. of the Peking Inst. of Ferrous Metallurgy*, 6, 85 (1958).
54. Hsu Tsu-yao. *J. of Peking Inst. of Ferrous Metallurgy*, 5, 57 (1958).

VOL 8 195

55. Hsu Tsu-yao. *J. of the Chinese Society of Mechanical Engineers*, 6, 203 (1958).
56. Chang Pei-lin and Chu Sui-chang. *Acta Metallurg. Sinica*, 1, 347 (1956).
57. Sze Chang-hsu. *Acta Metallurg. Sinica*, 1, 383 (1956).
58. Chou Chih-hung. *J. of the Shanghai Chiao-Tung University*, 2, 1 (1958).
59. Chuang Yu-chi and Li Yo-ko. *Acta Phys. Sinica*, 10, 321 (1954).
60. Chuang Yu-chi et al. *Acta Metallurg. Sinica*, 1, 337 (1956); 2, 81 (1957); 2, 299 (1957); 2, 377 (1957).
61. Sze Shih-yuan. *Acta Metallurg. Sinica*, 1, 189 (1956).
62. Sze Shih-yuan. *Acta Phys. Sinica*, 12, 245 (1957).
63. Sze Shih-yuan. *Scientia, Academia Sinica*, 9, 274 (1958).
64. Sze Shih-yuan et al. *J. of the Nanking University*, 4, 63 (1956); *Acta Phys. Sinica*, 12, 80 and 559 (1956).
65. Lu Hsueh-shan and Chang Tsung. *Acta Phys. Sinica*, 13, 150 (1957); *Scientia Sinica*, 6, 431 (1957); *Science Record, Academia Sinica*, 1, 41 (1957).
66. Liu Yi-huan and Hsu Chen Chia. *Acta Phys. Sinica*, 13 (1957); *Scientia Sinica*, 6, 1013 (1957).
67. Chang Chung-sui. *Acta Physo Sinica*, 15, 42 (1959).
68. Chang Chung-sui et al. *Acta Phys. Sinica*, 13, 515 (1957).
69. Chen Kai-cha. *Science Record, Academia Sinica*, 4, 51 (1951).
70. Chen Kai-cha. *Acta Phys. Sinica*, 14, 106 (1958).

VOL.
8
1959

MECHANISM OF PRODUCTION OF INTERNAL FRICTION IMPURITY PEAKS*

V.T. SHMATOV and A.V. GRIN

Institute of Physics of Metals of the Academy of Sciences of the U.S.S.R.

(Received 15 April 1959)

A possible mechanism is proposed for the production of internal friction impurity peaks, by migration of impurity atoms to the grain boundaries and back. The variation of internal friction with concentration of impurity and other parameters, calculated according to this mechanism, is in qualitative agreement with experimental results.

We know that for pure metals in the polycrystalline state there exists in the high-temperature region one internal friction peak. Since a similar peak is absent for single crystals of the pure metal, this phenomenon is linked with relaxation processes at the grain boundaries.

On addition to the pure metal of an impurity, together with the internal friction peak from relaxation at the grain boundaries of the pure metal, there appears in a definite temperature region a second, supplementary internal friction peak, which we will in future call the impurity peak. Most systematic studies were carried out in this direction in the works [1-5]. The general rules which one can derive from analysis of the results of these works, in respect to the impurity peak, come down to the following:

1. Even a very insignificant addition of impurity (0.03 atomic % [3]) can lead to the appearance of an internal friction impurity peak.
2. On increasing the impurity content, at first the height of the impurity peak increases. However, as has been found for several alloys, beginning at definite, higher impurity concentrations, a decrease or even disappearance of the peak is observed [6]. Decrease in height of the impurity peak with further increase in impurity concentration has been found for alloys of copper with zinc, gallium, silicon [1,3] and also for alloys of silver with indium and tin [2]. At the same time, for alloys of copper with aluminium, nickel, silver, germanium and arsenic [1,3,4], and silver with cadmium [2], only the increase has been observed in the ranges of concentrations used.
3. These results indicate that the energy of activation of the relaxation processes which lead to the creation of internal friction impurity peaks is evidently for a relatively high impurity level close to the energy of activation for diffusion of impurity atoms in the alloy. Such a relationship was observed for alloys of copper with zinc and silicon [2,6], and in alloys of silver with cadmium, indium, and tin [2]. In the region of lower concentrations, where in some measure the first internal friction maximum is still noticeable, the value of the activation energy for an impurity peak is somewhat higher.
4. With increasing impurity level the first maximum, from relaxation at the grain boundaries, decreases, and as several experiments have shown, may completely disappear [1-3, 6]. It is evident that this feature can be definitely connected with the enrichment of the grain boundaries with impurity atoms.
5. The internal friction impurity peak is observed only in polycrystalline specimens, and consequently, just as in the first case of internal friction, is connected with the grain boundaries.
6. The height of the internal friction impurity peak changes comparatively little with

* *Fiz. metal. metalloved.*, 8, No.6, 829-833, 1959.

change in the average diameter of the grains, gradually decreasing with its increase [3,6]. On the other hand, the relaxation time is essentially dependant on the average grain size and appreciably increases with increasing grain size, or, which is the same thing, with decrease in their number in unit volume [3,6].

In the works examined no mechanism is proposed to explain the appearance of internal friction impurity peaks in polycrystalline specimens on alloying of a pure metal by an impurity. In the following pages a possible mechanism is examined for creation of these peaks, which, it appears to us, explains the characteristic features considered above*.

As we know, the large impurity concentration at the grain boundaries occurs because of the lower energy of deformation applicable to an impurity atom at the boundary of a grain compared to its energy of deformation in the body of the grain. For this reason it is energectically favourable for part of the impurity atoms to diffuse to the boundary of the grain. Elastic deformation of the specimen, changing the value of its energy of deformation, can, depending on its character, either help or hinder the concentrating of impurity atoms at the grain boundaries. Therefore for a periodic deformation the concentration of impurity atoms at the grain boundaries must change periodically. For a sufficiently rapid deformation of the specimen, the change in concentration of impurity at the boundaries will not be able to follow the change in deformation; the process of change of state of the specimen will be a non-equilibrium one, which will lead to the dissipation of elastic energy, that is the creation of internal friction at this frequency.

This type of internal friction is a special case of internal friction in systems with additional parameters [8]. The additional parameters are the concentration of impurity atoms at the grain boundaries, which is equal [7] to

$$c = \frac{c_0 \exp \frac{Q}{RT}}{1 - c_0 + c_0 \exp \frac{Q}{RT}}, \qquad (1)$$

where c_0 is the concentration of impurity atoms in the volume of the grain;

$$Q = N(E - e), \qquad (2)$$

where N is Avogadro's number; E is the energy of deformation per atom in the grain; e is the energy of deformation per atom on the boundary of the grain.

The value of internal friction in an isothermal process will be equal [8] to

$$Q_T^{-1} = \frac{\omega \tau^{\varepsilon T}}{1 + (\omega \tau^{\varepsilon T})^2} \Delta E_T, \qquad (3)$$

where $\tau^{\varepsilon T}$ is the relaxation time of concentrations of impurity atoms at the boundaries at constant deformation and temperature (or, which comes to the same thing, the relaxation time of the stress σ under these conditions). The degree of relaxation of the isothermal modulus of elasticity is given by the expression [9]

$$\Delta E_T = E_T' \frac{\left(\frac{\partial c}{\partial \sigma}\right)_T^2}{T\left(\frac{\partial c}{\partial T}\right)_\sigma^2} [C_\sigma], \qquad (4)$$

where E_T' is the value of the isothermal modulus of elasticity in the absence of a distribution of impurity atoms predominantly at the boundaries of the grains (the so-called non-relaxation modulus of elasticity for $\omega = \infty$), and $[C_\sigma]$ is the part of the total heat capacity for unit volume which is due to the distribution of impurity atoms predominantly at the grain boundaries.

Using expression (1), we find

$$\Delta E_T = E_T' \frac{T}{Q^2} \left(\frac{\partial Q}{\partial \sigma}\right)^2 [C_\sigma]. \qquad (5)$$

The energy of deformation of a unit volume with L grains is equal to

$$U = L(aE + be), \qquad (6)$$

* One of the authors formerly was inclined to consider that this peak of internal friction was produced by relaxation at the boundaries of blocks of the structural mosaic [6].

VOL. 8 1959

where a and b are the number of impurity atoms dissolved in the body of one grain and at its boundary, respectively. To fix the heat capacity, taking into account (2), we have

$$[C_\sigma] = \left(\frac{\partial U}{\partial T}\right)_\sigma = -\frac{nL}{N} Q \left(\frac{\partial c}{\partial T}\right)_\sigma, \qquad (7)$$

(since $a + b = \text{const}$), where $n = \frac{a}{c}$ is the number of atoms at the boundary of the grain, and consequently nL is the number of atoms at boundaries within the unit volume. Thus we have the final expression for degree of relaxation of isothermal modulus of elasticity:

$$\Delta E_T = E_T' \left(\frac{\partial Q}{\partial \sigma}\right)^2 \frac{nL}{NRT} c(1-c). \qquad (8)$$

Since according to the determination $\Delta E_T < 1$, an appreciable value of internal friction is to be expected for a not too small impurity atom concentration at the boundary. We know that even for an insignificant addition of impurity, the concentration of impurity atoms at the grain boundaries may turn out high. Thus in [7] it is shown that in iron with 0.09% phosphorus, the concentration of phosphorus in the grain-boundary region may be 50 times greater than the concentration within the grain. Just such a mechanism of production of internal friction impurity peaks as we have examined explains the possibility of appearance of this peak even for insignificant addition of impurity.

As is seen from formula (8), the height of the internal friction impurity peak increases with increasing level at the grain boundaries, at $c = 0.5$ reaches a maximum, then for further increase in concentration falls to zero. This feature explains the property of the peak noted in point 2, since according to formula (1), with increase in impurity content in the metal, the concentration of impurity atoms at the grain boundaries increases continuously.

Points 4 and 5 of the features of internal friction impurity peaks considered above also serve, it appears, as confirmation of the mechanism of production proposed here.

We will derive an expression for time of relaxation. The process of transition of an impurity atom from the body of the grain to its surface (or the reverse transition) is an activation process, that is bound up with the transition of an atom through a potential barrier. The thermodynamic activation potential is equal to

$$\Delta \Phi = \Delta H - T \Delta S, \qquad (9)$$

where ΔH is the heat of activation; ΔS is the entropy of activation. Carrying through reasoning similar to that used in [9] in deriving time of relaxation in interstitial solid solutions and in alloys with long-range order, we have

$$\tau^{-1} = \frac{h}{F_{cc}(\delta c)^2} \exp\left(\frac{\Delta \Phi}{RT}\right), \qquad (10)$$

where h is Planck's constant; F_{cc} is the second derivative of free energy with respect to c, taken at the equilibrium composition; δc is the change after one elementary act in concentration of impurity atoms at the grain boundaries.

From the definition of concentration we find

$$\delta c = \delta\left(\frac{b}{n}\right) = \pm \frac{1}{n}. \qquad (11)$$

As shown in [10] (equation (7)),

$$F_{cc} = \frac{[C_\varepsilon]}{T\left(\frac{\partial c}{\partial T}\right)_\varepsilon^2}, \qquad (12)$$

and consequently

$$F_{cc} = -\frac{\frac{nL}{N} Q\left(\frac{\partial c}{\partial T}\right)_\varepsilon}{T\left(\frac{\partial c}{\partial T}\right)_\varepsilon^2} = \frac{nLRT}{Nc(1-c)}. \qquad (13)$$

After substitution of (9), (11) and (13) in (10), for relaxation time we find the following expression

$$\tau^{-1} = \frac{nLh\nu}{L^2 RT} c(1-c) \exp\left(\frac{\Delta H - T\Delta S}{RT}\right). \qquad (14)$$

Or, if we use the temperature relation of impurity atom concentration at the grain boundaries, then we get

VOL 8 195

$$\tau^2 T = \frac{nLhN}{L^2RT} \frac{c_0(1-c_0)\exp\frac{Q}{RT}}{\left(1-c_0+c_0\exp\frac{Q}{RT}\right)^2} \exp\left(\frac{\Delta H - T\Delta S}{RT}\right). \quad (15)$$

For low impurity concentrations, when

$$c_0 \exp\frac{Q}{RT} \ll 1; \quad c_0 \ll 1,$$

we have approximately that

$$\tau^2 T = \frac{nLhN}{L^2RT} c_0 \exp\left(\frac{\Delta S}{R}\right) \exp\left(\frac{\Delta H + Q}{RT}\right). \quad (16)$$

Consequently, in this case the well-known measurement of heat of activation from displacement of the peak with frequency gives an exaggerated result, equal to $\Delta H + Q$. For an increase of impurity atom concentration at the grain boundaries this difference will be diminished. This conclusion from the theory agrees with point 4 of the experimental results in measurement of heat of activation of the processes leading to the production of internal friction impurity peaks.*

It is not difficult to show that

$$nL = \alpha^2 L^{1/3}, \quad (17)$$

where α is a quantity of the order of the lattice constant. Therefore the degree of relaxation of the modulus of elasticity (8), and also the height of the internal friction impurity peak, is proportional to $L^{1/3}$ and consequently with change of concentration c depends feebly on the average grain size. On the other hand, the relaxation time under the same conditions is strongly dependent on the average grain size, since according to expressions (14) and (17)

$$\tau^2 T \sim L^{-5/3}. \quad (18)$$

These conclusions are in qualitative agreement with the experimental results for internal friction impurity peaks set out in point 6.

For further comparison of the theory with experiment, more systematic investigations of impurity peaks are necessary, for example an explanation of the quantitative influence of grain size on the peak, the effect of quenching temperature and annealing temperature and so on. The qualitative comparison we have made between the theory and the available experimental data evidently supports the mechanism proposed here for the production of internal friction impurity peaks in metals.

Translated by D.G. Noel

REFERENCES

1. L. Rotherham and S. Pearson, *J. of Metals*, 8, 881 (1956).
2. S. Pearson and L. Rotherham, *J. of Metals*, 8, 894 (1956).
3. S. Weinig and E. Machlin, *J. of Metals*, 9, 32 (1957).
4. Ke T.S., *J. Appl. Phys.*, 20, 1226 (1949).
5. K. Marsh, *Acta Met.*, 2, 530 (1954).
6. A.V. Grin, *Fiz. metal. metalloved.*, 4, 561 (1957).
7. M. Jumen, H. Tipler, *Acta met.*, 6, 73 (1958).
8. V.T. Shmatov, *Fiz. metal. metalloved.*, 6, 984 (1958).
9. V.T. Shmatov, *Fiz. metal. metalloved.*, 7, 321 (1958).
10. V.T. Shmatov, *Zh. eksp. teor. fiz.*, 33, 1359 (1957).

* The heat of activation ΔH in formulae (14)-(16) corresponds in sense to the volume diffusion of impurity atoms.

THE HALL EFFECT IN FERROMAGNETICS*

V.N. NOVOGRUDSKII, A.A. SAMOKHALOV and I.G. FAKIDOV

Institute of Physics of Metals of the Academy of Sciences of the U.S.S.R.

(Received 17 May 1959)

In spite of the fact that at present there is a considerable amount of experimental material accumulated from the study of the Hall effect in ferromagnetics, there is as yet no complete theory of this phenomenon; also there is not at the moment a unique way of choosing the constants to characterize the Hall effect in ferromagnetics. The Hall effect in ferromagnetics is most frequently described [1,2] by the formula

$$E_x = R_0 H + R_1 M, \qquad (1)$$

where R_0 is the Hall constant for the "normal" part of the effect; R_1 is the Hall constant for the ferromagnetic part of the effect; H is the intensity of the magnetic field inside the specimen, that is $H = H_e - NM$, where H_e is the intensity of the external magnetic field, N is the demagnetization factor of the specimen, and M is the intensity of magnetization of the specimen.

Sometimes a somewhat different way of writing the formula is used

$$E_x = R_0 (H + \alpha M), \qquad (2)$$

where H and M have the same meanings as in formula (1), and α is the effective magnetic field factor; it is obvious that $\alpha = R_1/R_0$.

The normal subject for theoretical study is the temperature dependance of R_0 and R_1 (or α). With reference to R_1 see works [3-6], and for R_0 see work [7].

In the given way of writing the Hall effect it is assumed that the "normal" Hall constant, as in non-ferromagnetic substances also, is determined by the concentration of conduction electrons n.

In the presence of a current carrier of one sign, $R_0 = \frac{1}{cen}$. The small temperature variation of the "normal" Hall constant R_0 in several ferromagnetic metals and alloys has been explained in a series of theoretical works [7,8], from the interaction of the s- and d- electrons in ferromagnetics. There is, however, another point of view [9,10], according to which the Hall effect in ferromagnetics should be described by the formula

$$E = R_1 M + R_i M_i, \qquad (3)$$

where R_1 and M have the same meanings as in formulae (1) and (2), and R_i is the Hall constant to go with the true intensity of magnetization of the ferromagnetic at saturation (in the spin paramagnetism region). According to this view, the constant R_i is connected with the Hall e.m.f. produced by a change in spontaneous magnetization, whereupon R_i is not determined in the given case by the concentration of conduction electrons as simply as was the constant R_0 in the previous treatise.

Experimental results support both the first and the second point of view. We know that the concentration of current carrier for ferromagnetic metals, calculated from the formula $R_0 = \frac{1}{cen}$, gives a value of about $\sim 10^{22}$ см^3 [11].

Studies made by us of the Hall effect in a ferromagnetic semiconductor, magnetite [12], have shown that the concentration of conduction electrons, determined by the value of R_0, is strongly temperature-dependent, and its value is found to be in conformance with the semiconducting character of the magnetite. The value for the conduction electron concentration calculated from the value of R_0 is in agreement with values obtained from measurements of thermal e.m.f.s. in magnetite [13].

* *Fiz. metal. metalloved.*, 8, No.6, 834-836, 1959.

VOL. 8 195

On the other hand, in [10] there is experimental confirmation of the viewpoint expressed by formula (3). It was shown that in an alloy of the Invar group (Fe-Ni) in the Curie temperature region the Hall effect is effectively described by formula (3).

In our opinion, in the general case the Hall effect in ferromagnetic metals and semiconductors should be described by a three-term formula, taking into account the possible mechanisms noted above for the production of the Hall effect in ferromagnetics

$$E_x = R_0 H + R_1 M + R_i M_i, \qquad (4)$$

where all the Hall constants and the magnetic characteristics have the same meanings as in formulae (1) and (3). Formula (4) is corroborated by all the available data on the Hall effect in ferromagnetics for any temperature region. It is evident that in a number of particular cases (4) can pass either into (7) or (3). i.e. in a number of metal ferromagnets and in a ferromagnetic semiconductor magnetite in the region far from the Curie temperature, the last $R_i M_i$ term is considerably less than the first two and plays no part. It is evident that in this case the Hall constant R_0, determined from the slope of the $E\chi - H$ graph in the saturation region can be used to give the concentration of conduction electrons. On the other hand, for certain metallic ferromagnetics with large values of spin paramagnetic susceptibility, the second and third terms may predominate, as the first term may be small (due to the high concentration of the current carriers in the metal). For the high-temperature Curie region the second term disappears and

$$E_x = R_0 H + R_i M_i. \qquad (5)$$

Since $M_i = \chi H$ where χ is the spin paramagnetic susceptibility, formula (5) may be rewritten in the form

$$E_x = (R_0 + \chi R_i) H. \qquad (6)$$

In the work [14] it was actually shown that in a Cu-Ni alloy in the paramagnetic region, the term χR_i is subject to the Curie-Weiss law, and R_0 is independant of temperature. The maximum of the Hall constant observed in many works at the Curie temperature, calculated from the slope of the $E\chi - H$ graph in the region of saturation, is evidently fixed by the maximum of the paramagnetic susceptibility χ in the term $(R_0 + \chi R_i)$, so that the quantity R_i is evidently almost temperature-independent, since the term χR_i follows with great accuracy the Curie-Weiss law above the Curie-Weiss law above the Curie temperature.

We should also note that a determination of R_1 from the initial part of the $E\chi - H$ curve in the area close to the Curie temperature should be made with care, since in this case even in a weak field there may be an appreciable true intensity of magnetization and correspondingly the term $R_i M_i$ in formula (4).

The maximum of the R_1-T curve observed in a series of works somewhat lower than the Curie temperature is possibly also determined by the appearance of the true intensity of magnetization with a decreasing spontaneous magnetization.

To test the proposals given it is necessary to make a detailed study of the Hall effect and intensity of magnetization above and below the ferromagnetic transition temperature in substance where three terms are commensurable.

Translated by D.G. Noel

REFERENCES

1. E.M. Pugh, N. Rostoker and N. Schindler, *Phys. Rev.*, 80, 680 (1950).
2. K.P. Belov, Ye.P. Svirina and Iu.V. Belous, *Fiz. metal. metalloved.*, 6, 621 (1958).
3. R. Karplus and J.M. Lutinger, *Phys. Rev.*, 95, 1154 (1954).
5. J. Smit, *Physica*, 24, No.1, 39 (1958).
6. N.P. Patrakhin, *Izv. Akad. Nauk SSSR, ser. fiz.*, 16, 58 (1952).
7. K. Meyer, *Zs. f. Naturforsch.*, 10a, 8, 656 (1955).
8. E.M. Pugh, *Phys. Rev.*, 97, 647 (1955).
9. D.I. Volkov, *Moscow State University Messenger*, No.3, 65 (1954).
10. N.V. Bakhanova, *Zh. eksp. teor. fiz.*, 33, 3(9), 567 (1957).
11. S. Foner and E.M. Pugh, *Phys. Rev.*, 91, 20 (1953).
12. A.A. Samokhvalov and I.G. Fakidov, *Fizika tverdogo tela* (in the press).
13. A.A. Samokhalov and I.GO Fakidov, *Fiz. metal. metalloved*, 7, 465 (1959).
14. I.K. Kikoin, *Sow. Phys.*, 9, 1 (1936).

A METHOD FOR THE DIRECT MEASUREMENT OF MAGNETIC ANISOTROPY IN THIN FILMS*

W. SCHÜPPEL, O. STEMME, W. ANDRÄ and Z. MÁLEK

Institute of Magnetic Materials of the
German Academy of Sciences, Jena.

Physical Institute of the
Czechoslavakian Academy of Sciences, Prague.

(Received 10 September 1959)

1. Introduction
2. Description of the anisometer.
3. Causes of errors arising during the measurements.
4. 3.1. Inhomogeneity of the magnetic field.
   3.2. Asymmetry of the torsional system.
   3.3. Misalignment of the film.
   Evaluation of errors arising during measurement.
   4.1. Inhomogeneity of the magnetic field.
      4.11. at a point in the specimen,
      4.12. about the pole tips.
   4.2. Asymmetry of the torsional system.
      4.21. Paramagnetic and diamagnetic rotation.
      4.22. Ferromagnetic impurities.
   4.3. Misalignment of the film.
      4.31. Misalignment of the film in general
      4.32. Surface irregularity of the layer.
      4.33. Imperfections of the surface of the support.
      4.34. Pick-up of ferromagnetic material on the sides of the support.
5. Elimination and reduction of distortion effects.
6. Example of the measurement of anisotropy.
7. Summary.

1. INTRODUCTION

The constants of uniaxial magnetic anisotropy in thin ferromagnetic films have hitherto been determined only indirectly from measurements of the magnitude of the anisotropy field [1]. The measurement of these constants of anisotropy is also possible in principle by the torque method [2]. However, this method requires high sensitivity of the anisometer, since the volume of the specimens is very small and the magnitude of the constants of uniaxial magnetic anisotropy are close to those of the lowest constants of crystal anisotropy. It is the purpose of the present paper to describe a sufficiently sensitive instrument for this measurement and also to discuss the errors arising during measurement and the possibility of their elimination.

2. DESCRIPTION OF THE ANISOMETER

The principle of the operation of anisometer shown in Fig.1 is similar to that of the usual instruments for measuring the constants of crystal anisotropy by the torque method. However, as the constants of uniaxial magnetic anisotropy are of the order of 10^3 erg/cm^3 and, consequently, the maximum magnetic moment of a film 1000 Å thick and 2 cm^2 in surface area amounts to 2×10^{-2} dyne cm, the instrument should be able to measure a torque of the order of 10^{-3} dyne cm. The required sensitivity can be readily achieved by an instrument in which the uncompensated twisting of a thin phosphor-bronze wire 0.07 mm in diameter and 34 mm long gives the magnitude of the effective torque. The wire dimensions

* *Fiz. metal. metalloved.* 8, No.6, 837-846, 1959.

VOL
8
195

are adopted to ensure that the deformation of the wire during the twisting is kept below the elastic limit. By means of a simple optical device very low angles of twist can be read off (some minutes of arc at a twisting moment of 10^{-1} dyne cm).

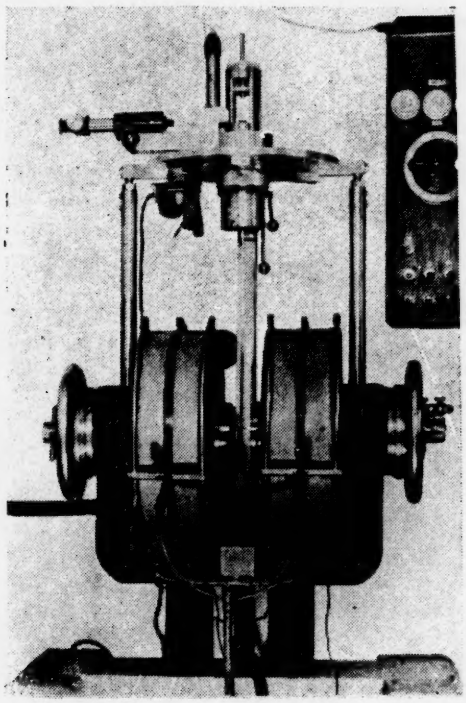

Fig. 1. Anisometer for thin ferromagnetic films (shown when not running). The glass cover has been removed to give a better view of specimen and holder.

The magnetic field necessary to saturate these specimens is obtained from a fixed Weiss-type magnet (diameter of the pole tips: 10 cm; distance between them: 3.7 cm). The specimen is attached to a machine component which revolves relative to the magneto at the near-homogeneous centre line of the magnetic field. To the upper end of this component a suspension thread is soldered; on this the specimen holder is fixed – a Vinidur adaptor tube into which a glass tube is pushed which has a tapered ground section on one end. The specimen is attached by means of paraffin to a copper stage which is placed into the ground section of the glass tube. By raising and compressing the Vinidur adaptor tube the whole torsion system can be arrested. To facilitate the positioning or removal of the specimen, the entire measuring unit is then tilted and the specimen is thus outside the magnetic field.

The high sensitivity of the apparatus can be exploited only when every influence which can introduce additional twisting moments is eliminated. Above all, it was necessary to avoid mechanical distortion of the torsion system. This purpose is served by the very sturdy construction of the whole machine which rests entirely on a stone bed; as a protection against air currents the torsion system is placed inside a glass cover; regularity of rotation for each torsion component is ensured (from $\phi = 0^{\circ}$ to $\phi = 360^{\circ}$) by a synchronous motor. In this way it has been possible to eliminate, nearly completely, non-periodic (with respect to ϕ) torques. It was still necessary to eliminate a number of distortion effects leading to a periodic torque curve which is superimposed on the periodic torque curve due to magnetic anisotropy.

3. CAUSES OF ERRORS ARISING DURING MEASUREMENTS

The distortion effects which give periodic torque curves are due partly to imperfections in the instrument itself and partly to the method of comparing specimens and the manner of fixing them in the anisometer. The errors arising in this way are considered more closely in the following sections.

3.1 Inhomogeneity of the magnetic field. Let dV be a body element at a distance r from the axis of rotation and $\vec{M}$ the magnetization of the element considered (for a ferromagnetic specimen $\vec{M}$ is equal to the saturation magnetization M_s; for paramagnetic and diamagnetic components with susceptibility χ, $\vec{M} = \chi \vec{H}$); then owing to inhomogeneity of the field there acts on the specimen when homogeneously magnetized the force

$$\vec{k} = \int (\vec{M} \operatorname{grad}) \vec{H} dV, \qquad (1)$$

that is, for a torque per unit volume we obtain

$$\frac{1}{V}\vec{D} = \frac{1}{V}\int \left[\vec{r}\left(\vec{M}\ \mathrm{grad}\right)\vec{H}\right] dV. \qquad (2)$$

Since in the middle of the field the component of the magnetizing force H_x (see Fig. 2) which is perpendicular to the pole tips is appreciably higher than the components H_y and H_z perpendicular to it, we have $|\vec{M}| \approx M_x$.

With this condition equation (1) is simplified

$$k_x = M_x \int \frac{\partial H_x}{\partial x} dV;\ k_y = M_x \int \frac{\partial H_x}{\partial y} dV;$$
$$k_z = M_x \int \frac{\partial H_x}{\partial z} dV. \qquad (3)$$

At $x = r\cos\phi$ and $y = r\sin\phi$ it follows from equation (2) (for the middle of the field) that

$$\frac{1}{V} D_z = \frac{1}{V} M_x \int \left[\frac{\partial H_x}{\partial y} r\cos\varphi - \frac{\partial H_x}{\partial x} r\sin\varphi\right] dV. \qquad (4)$$

In the upper part of the field near the centre line between the pole tips we always have $H_x > H_y, H_z$. Therefore

$$M_y,\ M_z < M_x \approx \mathrm{const}$$

and

$$\frac{\partial H_x}{\partial x} \geqslant \frac{\partial H_y}{\partial x},\ \frac{\partial H_z}{\partial x};\ \frac{\partial H_x}{\partial y} \geqslant \frac{\partial H_y}{\partial y},\ \frac{\partial H_z}{\partial y}.$$

Equations (3) and (4) are therefore approximately satisfied also at this point.

3.2. Asymmetry of the torsional system. Torques with periodic curves can also arise if paramagnetic or diamagnetic parts of the suspension system, or ferromagnetic contaminations of this system, are arranged asymmetrically with respect to the axis of rotation. Thus a shape anisotropy energy arises, which for an ellipsoid is equal to

$$E_N = \frac{1}{2}(N_2 - N_1) VM^2 \sin^2\varphi, \qquad (5)$$

where N_2 and N_1 are demagnetizing factors of the specimen in the direction of the secondary and principal magnetic axes, respectively, and ϕ is the angle between the magnetization vector and the principal axis. The angular dependence of this shape anisotropy energy produces the torque per unit volume

$$\frac{1}{V} D_N = \frac{1}{2}(N_2 - N_1) M^2 \sin 2\varphi \qquad (6)$$

3.3. Misalignment of the film. In the general case the magnetization vector of the film is parallel to its surface in the absence of external fields. However, when external fields are present components of the magnetization vector can be induced which are perpendicular to the surface of the film so that surface poles appear. The energy of the field of dispersion arising in this way is changed during the rotation of the film, if either the whole film or parts of it are not perpendicular to the axis of rotation. Thus torques arise which must also be attributed to the shape anisotropy.

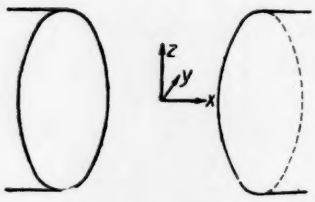

Fig. 2. For the calculation of the torque arising as a result of inhomogeneity of the field with eccentric positioning of the rotating parts. Orientation of the co-ordinate system in the magnetic field.

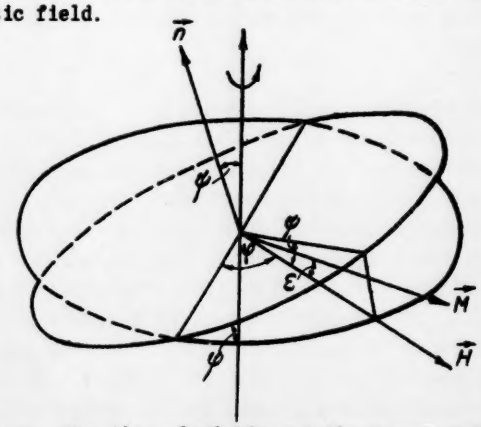

Fig. 3. For the calculation of the torque arising in the magnetic field $\vec{H}$ as a result of the deviation of the normal to the layer $\vec{n}$ from the axis of rotation.

Let ψ (Fig. 3) be the angle of inclination

of the normal to the film with respect to the axis of rotation. Then the magnetizing field $\vec{H}$ directed at an angle ψ^* to the surface of the film shifts the magnetization vector $\vec{M}$ by an angle $(\psi^* - \epsilon)$ away from the surface of the film so that it forms with the field an angle ϵ. This angle ϵ is determined from the condition of minimum total energy E of the specimen, which is composed of the magnetostatic energy

$$E_H = -VMH\cos\varepsilon \tag{7}$$

and the shape anisotropy energy

$$E_N = \frac{1}{2}\Delta NVM^2\sin^2(\psi^* - \varepsilon). \tag{8}$$

This condition, for small angles of ψ (i.e. $\psi \ll 1$ and

$$\psi^* \ll 1,\ \epsilon \ll 1)$$

is satisfied at

$$\varepsilon \approx \frac{4\pi M/H}{1+4\pi M/H}\psi^* \tag{9}$$

for the case when $N = 4\pi$.

At this value of ϵ the complete energy, considering that

$$\psi^* = \psi\sin\varphi \text{ (more precisely, } \sin\psi^* = \sin\psi\times\sin\varphi),$$

is equal to

$$E \approx -VMH\left[1 - \frac{1}{2}\left(\frac{4\pi M/H}{1+4\pi M/H}\right)^2\psi^2\sin^2\varphi\right] + 2\pi VM^2\psi^2\sin^2\varphi\left(\frac{1}{1+4\pi M/H}\right)^2, \tag{10}$$

where ϕ is the angle between $\vec{H}$ and the line at which the horizontal plane and the surface of the film intersect. The torque then acting on a unit volume of the specimen is

$$\frac{1}{V}D = \frac{1}{V}\frac{\partial E}{\partial\varphi} \approx 2\pi M^2\frac{1}{1+4\pi M/H}\psi^2\sin 2\varphi. \tag{11}$$

For $\psi = \frac{\pi}{2}$ (i.e., for the vertical position of the portion of the film being considered) an analytical expression for ϵ can be obtained only for the case $4\pi M/H = 2$. With this condition, the total energy has a minimum if

$$\varepsilon = \frac{2}{3}\varphi \quad \left(-\frac{\pi}{2} \leqslant \varphi \leqslant \frac{\pi}{2}\right) \tag{12a}$$

or

$$\varepsilon = \frac{2}{3}(\pi - \varphi) \quad \left(\frac{\pi}{2} \leqslant \varphi \leqslant \frac{3\pi}{2}\right). \tag{12b}$$

The magnitude of the total energy per unit volume is in this case equal to

$$\frac{1}{V}E = -MH\cos\frac{2}{3}\varphi + 2\pi M^2\sin^2\frac{\varphi}{3} \quad \left(-\frac{\pi}{2} \leqslant \varphi \leqslant \frac{\pi}{2}\right), \tag{13a}$$

or

$$\frac{1}{V}D = -2\pi M^2\sin^2\frac{(\pi-\varphi)}{3} \quad \left(\frac{\pi}{2} \leqslant \varphi \leqslant \frac{3\pi}{2}\right), \tag{13b}$$

Hence the torque acting on a unit volume of the film is equal to

$$\frac{1}{V}D = -2\pi M^2\sin\frac{2}{3}\varphi \quad \left(-\frac{\pi}{2} \leqslant \varphi \leqslant \frac{\pi}{2}\right), \tag{14a}$$

or

$$\frac{1}{V}D = -2\pi M^2\sin\frac{2}{3}(\pi-\varphi) \quad \left(\frac{\pi}{2} \leqslant \varphi \leqslant \frac{3\pi}{2}\right). \tag{14b}$$

The magnitude of the torque in the case $4\pi\frac{M}{H} \neq 2$ can be determined by either numerical or graphical solution; it increases as M/H increases. The expression following from equation (14) for maximum of minimum torque

$$\left(\text{for } \varphi = \frac{\pi}{2}, \quad \text{or} \quad \varphi = \frac{3\pi}{2}\right)$$

must in the case $4\pi M/H = 1$ be multiplied by ≈ 0.5; for $2 \leqslant 4\pi M/H \leqslant 5$ it does not differ greatly from the value obtained for $4\pi M/H = 2$.

4. EVALUATION OF ERRORS ARISING DURING MEASUREMENT

4.1. Inhomogeneity of the magnetic field. Appreciable torques due to eccentric position-

ing of the rotating parts can arise either if the magnetization or the volume of the specimen with a small field gradient have high magnitudes or if the field gradient or the specimen volume have high magnitudes with a small magnetization. The first case arises with eccentric positioning of a ferromagnetic specimen or holder component in the middle of the field, and the second case, if a paramagnetic or diamagnetic specimen holder is present in a field of very high gradient. We shall estimate the magnitude of these torques on the basis of the simplified equation (4).

4.11. Inhomogeneity of the field at a point of the specimen. The torque for a circular specimen (thickness d, radius R, with a displaced centre $r_0\,[x_0 = r_0 \cos\varphi_0,\ y_0 = r_0 \sin\varphi_0]$) is obtained from (4) under the condition that the field gradient is constant at the specimen surface

$$\frac{1}{V} D_z = \frac{1}{R^2 \pi d} M_x \left[\frac{\partial H_x}{\partial y} \int_0^d \int_0^{2\pi} \int_0^R (r \cos\varphi + x_0)\, r\, dr\, d\varphi\, dz - \right.$$

$$\left. - \frac{\partial H_x}{\partial x} \int_0^d \int_0^{2\pi} \int_0^R (r \sin\varphi + y_0)\, r\, dr\, d\varphi\, dz \right] =$$

$$= M_x r_0 \left(\frac{\partial H_x}{\partial y} \cos\varphi_0 - \frac{\partial H_x}{\partial x} \sin\varphi_0 \right); \qquad (15)$$

It is seen that the torque is equal to that of a film imagined to be centred at the centre of the specimen. To ensure that the total distorting torque does not influence significantly the magnitude of the anisotropy constant to be measured, it should be less than 5×10^{-3} dyne cm. Hence it follows that for

$$d = 1000\text{Å},\quad R = 0{,}8 \text{ cm},\quad \frac{\partial H_x}{\partial x} \approx \frac{\partial H_x}{\partial y} = 5 \text{ oe/cm},$$

the eccentricity r_0 should be not more than 0.7 mm in the case of Ni(M_s = 500 CGSM) and not more than 0.2 mm in the case of FE(M_s = = 1700 CGSM).

The torque described by equation (15) acts also on components of the specimen holder in the middle of the field if these components are positioned eccentrically with respect to the axis of rotation. To ensure that the torque does not exceed 5×10^{-3} dyne cm, for the value of the field gradient stated above, the distance between the axis of symmetry of the holder and the axis of rotation should be less than 1.8 mm if, as in the case of the described anisometer, the volume of the ground glass section ($\chi = -1.8 \times 10^{-6}$ is equal to 0.2 cm^3 and the volume of the copper stage ($\chi = -8.0 \times 10^{-7}$) is equal to 0.5 cm^3.

4.12. Inhomogeneity of the magnetic field at the edge of the pole tips. To ensure that the distorting torque does not exceed the indicated value, the eccentricity of the part of the holder located at the edge of the field must be very low; thus, for instance for glass ($\chi = -1.8 \times 10^{-6}$, $V = 0.3$ cm^3) at

$H_x = 5$ k oersted, $\frac{\partial H_x}{\partial x} \approx \frac{\partial H_x}{\partial y} = 100$ oersted/cm,

we obtain $D < 5 \times 10^{-3}$ dyne cm for $r_0 < 0.13$ mm.

4.2. Asymmetry of the suspension system.

4.21. Paramagnetic and diamagnetic parts of the suspension system. Numerical evaluation shows that the parasitic torque arising from the shape anisotropy in paramagnetic or diamagnetic parts of the nolder is very low.

4.22. Ferromagnetic inclusions. Ferromagnetic inclusions may produce quite considerable distortions. If such an inclusion is an iron cylinder, that is, a volume determined from (6) at $(N_2 - N_1) = 2\pi$, $M_s = 1700$ CGSM, it should not exceed the value indicated above.

4.3. Misalignment of the film. 4.31. Misalignment of the film as a whole. Positioning at an angle (misalignment) of the whole ferromagnetic film in the instrument for measuring anisotropy can be due either to an inaccurate plane parallel holder or to inaccurate fixing of the specimen to the suspension system. As the magnitude of the parasitic moment thus arising depends on the ratio $4\pi M/H$, and H in the set-up considered totals 6 k oersted, then M = 500 CGSM (Ni), i.e. $4\pi M/H \approx 1.0$, and M = 1700 CGSM (Fe), i.e. $4\pi M/H \approx 3.6$, should be considered the two limiting cases.

To keep the errors in the anisotropy constants small, i.e., the maximum parasitic moments not exceeding 5×10^{-3} dyne cm, for specimens 1000 Å thick and 2 cm^2 surface area,

VOL 8 195

the angle of misalignment ψ should not exceed 1° for nickel and $30'$ for iron.

4.32. Irregular surface of the film. If the support of the film is not flat but slightly corrugated, shape anisoptropy of the type considered will likewise arise. The torque due to this anisotropy is easily evaluated on the basis of calculations given in section 3.3 if the surface irregularity is sinusoidal in one direction with amplitude a and periodicity h, i.e. it is described by function $a \sin \frac{2\pi x}{h}$.

At point x of the surface the angle of inclination is equal to

$$\psi = \tan^{-1}\left(2\pi \frac{a}{h} \cos \frac{2\pi}{h} x\right)$$

or, for $a \ll h$, $\psi \approx 2\pi \frac{a}{h} \cos \frac{2\pi}{h} x$ and $\overline{\psi(x)^2} \approx 2\pi^2 \frac{a^2}{h^2}$. From (11) we obtain the torque acting on such an irregular film equalling

$$\frac{1}{V} D \approx 4\pi^3 M^2 \frac{a^2}{h^2} \frac{1}{1 + 4\pi M/H} \sin 2\varphi. \quad (16)$$

Hence it follows that, under the conditions described above, the value a/h should be less than 0.004 for nickel and less than 0.002 for iron. To indicate clearly how strictly this requirement must be met, we shall assume that the corrugation results from deflexion of the support (specimen radius 0.8 cm). Maximum deflexion should not exceed 0.13 mm in nickel specimens and 0.057 mm in iron specimens to ensure that the torque which thus arises does not exceed 5×10^{-3} dyne cm.

4.33. Distortions of the surface of the support. Exactly the same requirements should be made on the surface quality of the support. If this surface is marked with ridges, their sides will be covered with ferromagnetic material. These ridges are inclined to the surface of the film at varying angles and consequently produce shape anisotropy. To estimate the resulting torque, we shall assume that the ridges have side walls which are perpendicular to the specimen surface and are parallel to each other. Let l/h of such parallel ridges of depth a be present over a unit length of the support. Then, from equation (14), the torque acting (in the case $4\pi M/H = 2$) on the vertical walls of the ridges is

$$D = V_s \cdot 2\pi M^2 \sin \frac{2}{3}\varphi, \quad (17)$$

where V_s is the volume of these side walls. As the volume of the film $V = V_s \times \frac{h + 2a}{2a}$, the ratio of the moment (17) to the volume of the layer (at $a \ll h$) is equal to

$$\frac{1}{V} D \approx 4\pi \frac{a}{h} M^2 \sin \frac{2}{3}\varphi. \quad (18)$$

According to the conditions of section 3.3, this calculation is approximately correct for Fe.

To ensure that the torque due to the ridges does not greatly influence the measurement of anisotropy, $\frac{a}{h}$ should be less than 7.9×10^{-6} for Fe and $\frac{a}{h} < 1.8 \times 10^{-4}$ for Ni (with consideration of the factor ≈ 0.5). This means, for instance, that a single ridge over the whole support (diameter = 1.6 cm) can give a torque of 5×10^{-3} dyne cm, which cannot be neglected if its depth amounts to 1300 Å in the Fe layer or 29,000 Å in the Ni layer. It is understood that this case does not strictly occur in practice. The walls of the ridges produced when the support is machined are usually not perpendicular to the surface; but the important point is that the ridges are never parallel to each other. Consequently the torques due to the presence of the individual ridges are partially compensated. If the layers are produced on the support by an evaporation technique, then the covering of the ridge walls will vary in thickness only in the case of tilting of the walls or oblique evaporation.

4.34. Covering of ferromagnetic material on the sides of the support. On the basis of the preceding estimates it is seen immediately that covering (which is irregular with respect to the circumference of the specimen) of the sides of the support with ferromagnetic material may produce very great torques.

5. ELIMINATION OR REDUCTION OF DISTORTION EFFECTS

To eliminate the distortion effects of the

field gradient, best results would be achieved by homogenization of the magnetic field. For this end special devices can be employed, but while homogeneity improves in the middle of the field, inhomogeneity increases simultaneously near the edge of the pole faces where the influence is greatest. For this reason the specimen holder used in the described apparatus is a glass tube the curvature of which is corrected by extension at elevated temperature (500°C). A considerable reduction in the influence of the field gradient, which arises from the eccentric location of the glass tube, is obtained by filling the glass tube with an aqueous solution of $CuSO_4$ of suitable concentration (the susceptibility of $CuSO_4 \cdot 5H_2O = +1.3 \times 10^{-5}$); this compensates appreciably for the magnetization of the glass tube.

The relatively small influence of the field gradient on the specimen is further decreased by using a simple centering device for fixing the specimen on the copper stage.

Ferromagnetic inclusions can be eliminated by choosing appropriate materials for support (glass or very pure copper) and specimen holder (Vinidur for the coupling of the torsion system and the glass tube; glass; very pure copper; paraffin for bonding the specimen). Surface contamination of the high-purity copper stage is removed by periodic scouring. In the same way the supports for the specimens are cleaned prior to the application of the film.

Precise horizontal positioning of the ferromagnetic film is ensured by careful preparation of the specimen holder. Simple observation with the aid of a mirror will show that the angle of dip of the specimen relative to the horizontal plane does not exceed 0.3°.

Microscope cover glasses which are generally used as supports for the coating of the specimens are unsuitable in this case because of their surface corrugation. Optically polished glass plates (1 mm thick) are used instead. To eliminate the formation of directed corrugations and directed ridges during the preparation of the copper supports for electrolytic specimens, these copper disks are rotated during the polishing and perforated at the centre, to avoid indeterminate surface properties occurring at this point.

The side surfaces (and the rear end) are protected by a coat of lacquer from having ferromagnetic material settle on them; diaphragms suitably arranged during the coating serve the same purpose.

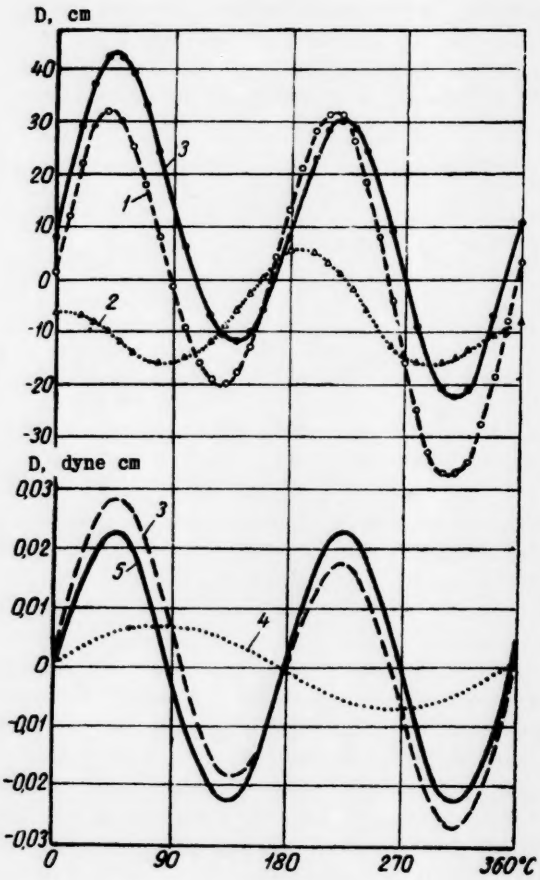

Fig. 4. Example of the measurement of anisotropy.
Top diagram:- correction to the curve of the torque, which is obtained when the specimen is absent.
1 – measured torque curve;
2 – curve when the specimen is absent;
3 – difference between curves 1 and 2.
Bottom diagram:- expansion of curve 3 in Fourier series.
4 – component of curve 3 with period 2π;
5 – component of curve 3 with period π (torque curve proper).

Parasitic moments arising in spite of all

VOL. 8 195

these precautionary measures can be partially eliminated from the measured curve. Thus, parasitic moments arising as a result of the field gradient, and also those due to ferromagnetic inclusions, can be determined by plotting – after the measurements are taken with the specimen in position – the curve of the torque without the specimen (but with the holder left in position). The curve thus obtained is subtracted from the previously measured curve. Errors due to eccentricity of the specimen can be eliminated by expansion in Fourier series if the conditions described in section 3.1 are satisfied.

6. EXAMPLE OF THE MEASUREMENT OF ANISOTROPY

A typical torque curve is shown in Fig. 4, curve 1. It is obtained on a permalloy (77 per cent Ni) film 1530 Å thick and 14 mm in diameter, produced in a magnetic field on a preheated support. It follows from the asymmetry of the curve that a number of parasitic moments still remain in spite of all the precautionary measures described above. The difference in the values measured at 0 and 360° is due mainly to starting the measurements too early when the deformation of the wire, which arises during the loading of the torsion system, is not completely recovered.

The curve measured subsequently, without the specimen, is represented by curve 2 in Fig. 4. The errors obtained on account of the specimen holder are eliminated by subtracting this curve from curve 1. The difference curve (curve 3) has the shape of superimposed plots of harmonic functions. It can be decomposed into components by the Fourier method. One component is curve 4 with period 2π due to the remaining eccentricity of the specimen; the other component is curve 5 with period π due to the presence of uniaxial anisotropy. From this curve the constant of uniaxial magnetic anisotropy is obtained at $k^* = 0.96 \times 10^3 \text{erg cm}^{-3}$.

7. SUMMARY

A description is given of a highly sensitive anisometer (10^{-3} dyne cm/mincron division) for the direct measurement of magnetic anisotropy in thin films. To obtain this high sensitivity, a number of parasitic effects must be eliminated. These effects are studied in detail, their influence on the measurement of anisotropy is estimated and methods of error elimination are proposed. An example illustrates how part of the remaining errors can be eliminated.

Translated by H. Nowottny

REFERENCES

1. D.O. Smith, *J.Appl.Phys.*, 29, 264 (1958); C.D. Olson and A.V. Pohm, *J.Appl.Phys.*, 29, 274 (1958); I.N. Mitchell, *J.Appl.Phys.*, 29, 286 (1958).
2. N.V. Kotel'nikov, *Dokl.Akad.Nauk SSSR*, 113, 97 (1957); *Fiz. metal. metalloved* 6, 222 (1958).
3. Z. Malék, W. Schüppel, O. Stemme and W. Ändra, *Ann. Physik*, 4, (7) (1959).

ELECTRIC CONDUCTIVITY OF IRON AT ELEVATED TEMPERATURES*

V.S. GUMENYUK and V.V. LEBEDEV

Physico-technical Institute of the Academy of Sciences, USSR

(Received 26 June 1959)

The paper gives data on the study of the temperature-dependence of the electric conductivity of high purity iron, which was obtained by vacuum distillation. The curve plotting the electric resistivity as a function of temperature shows clearly the points of magnetic and phase transition. Comparison is made with the measured values of the electric resistance for armco iron and with the results of other authors. A description is given of a high-temperature (up to 2500°C) furnace.

The study of the electric conductivity of iron at high temperatures presents a certain interest. Sal'dau [1] carried out measurements on chemically pure iron, but the author points out himself that the specimens studied may have become carburized to an appreciable degree while the test was being carried out. Ribbeck's investigations [2] were principally in the α-region, and measurements of the electric resistivity of iron in the γ-region were carried out only partially (up to 1000°C). Mokrovskii and Regel' [3] determined the temperature dependence of the electric resistance in the range between 900 and 1700°C for armco iron.

The object of the present work was to determine the electric resistivity of high purity iron in the range from 20 to 1450°C.

The measurements were carried out by the compensation method with the aid of a PPTV-1 potentiometer with a M-21 type galvanometer. The source of the current was a set of storage batteries which were charged continuously from a rectifier while the work was carried out. To ensure greater current stability, a barretter of type 1B5-9 which maintained current at 1 A was connected in series to the circuit. A standard resistance coil R-310 of 0.001 or 0.01 ohm of the class of accuracy 0.01 was connected in series to the specimen.

Specimens of the material studied were prepared in the form of cylinders 3-6 mm in diameter and 50-100 mm long, having recesses as shown in Fig. 1. The ends 1 and 2 served respectively for feeding the current and measuring the voltage drop in the portion l investigated (between the recesses). This specimen shape, which was suggested by Kan and Lazarev [4], eliminates the influence of the supply conductors since the points at which they are fixed do not enter into the effective portion of the specimen.

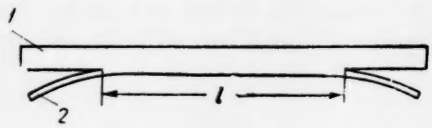

Fig. 1. Shape of specimen.

It was shown by precision measurements that the error introduced into the values of electric resistivity by the adopted form of specimens does not exceed the error of the potentiometric network.

The specimen was suspended vertically from one of the current-carrying conductors and extended into an electric resistance furnace which contained no ceramic material in the high-temperature zone [5].

An alundum support *11* ensuring thermal

* *Fiz. metal. metalloved.* 8, No.6, 847-850, 1959.

insulation was fixed on a metal base, and a screening case *8* which consists of a set of molybdenum sheets was placed on this support. An alundum ring - was fixed to the metal disc *4*, and with the aid of steel shells *6* there were introduced into this ring *5* the tungsten rods *9* which serve as supports for the heating coils *10*. The current source was connected to two of these rods across the terminals *3*. The "plug" which consists of an alundum ring *7* and a set of molybdenum screens is rigidly connected with plate *2*. On this plug the specimen is mounted. Bars *2* and *4* can be freely turned about guide stands *1*; this allows rapid mounting of the specimen in the furnace and replacement of defective heating coils.

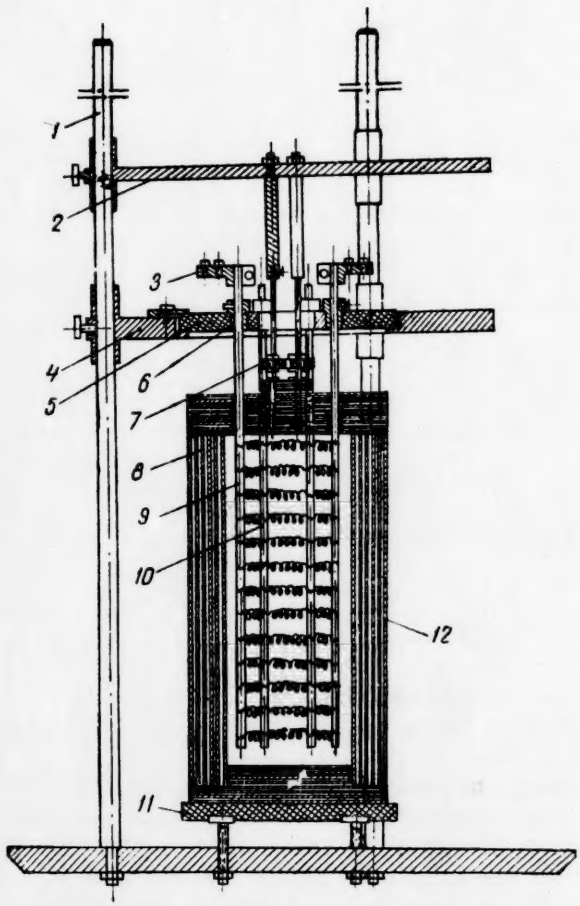

Fig. 2. Section through the high-temperature furnace.

The effective furnace space is 200 mm in height and 35 mm in diameter; temperatures up to 2500°C can be readily obtained at an input power of less than 6 kW.

The temperature can be measured either by thermocouples or by optical pyrometer across aperture *12*. During the work described here the temperature was measured by platinum, platinum-rhodium and chromel-alumel thermocouples and a PP type instrument.

The furnace together with the specimen was placed in a vacuum chamber which was evacuated by a steam-oil diffusion pump at the rate of 250 l./sec and a high-capacity pump. The vacuum maintained during the measurements was of the order of 10^{-5}-10^{-6} mm Hg.

The absolute error of the results in the work described concerning the determination of the electric resistivity does not exceed 1.5 per cent. The difference in the electric resistivity values for a given temperature between different specimens of the same batch did not exceed the error limits. The curves $\rho = f(T)$ are reversible.

On this apparatus we measured the electric resistivity of both armco iron and the iron produced by vacuum distillation [6]. Prior to the measurements the specimens were pre-annealed in a high vacuum at a temperature of 1100°C for 4 hr. The total impurity content of the distilled iron was approximately 0.02 per cent, which was estimated from the magnitude of the residual electric resistance* (see Table 1).

The results of the measurements are shown in Table 2 and graphically in Fig. 3.

TABLE 1

Temperature, °K	$R_{T°K}/R_{18°C}$
77	1×10^{-1}
20,4	$3,45 \times 10^{-2}$
4,2	$3,35 \times 10^{-2}$

For comparison the data of other authors are also plotted in Fig. 3. Curve 2 gives the

* The measurements of the residual electric resistance of the iron were carried out by B.N. Aleksandrov.

TABLE 2

Electric resistivity of distilled iron at various temperatures

Temperature (°C)	Electrical Resistance (Ω cm x 10^6)	Temperature (°C)	Electrical Resistance (Ω cm x 10^6)
20	9.89	800	100.0
100	14.0	900	107.8
200	20.2	1000	111.0
300	28.5	1100	114.2
400	38.5	1200	117.2
500	50.3	1300	119.7
600	63.7	1400	122.5
700	79.5	1450	125.0

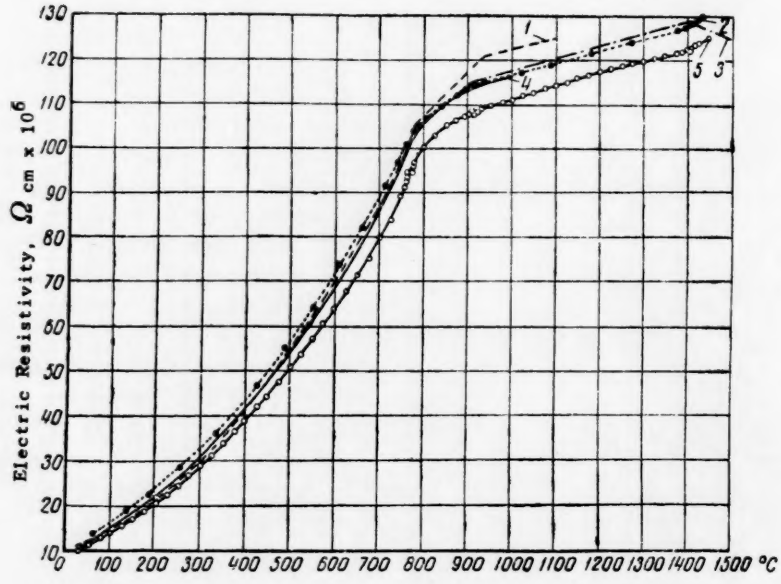

Fig. 3. Temperature dependence of the electric resistivity of iron from the data of various authors.
1. P.Ya. Saldau' [1]; 2. For armco iron; 3. N.P. Mokrovskii and A.R. Regel' [3]; 4. Ribbeck [2]; 5 Distilled iron.

results obtained by us for armco iron; they are in good agreement with the data obtained by Mokrovskii and Regel' up to a temperature of 1400°C (curve 3) for metal of the same degree of purity. Curve 5 constructed for distilled iron is lower than any curve known to us from the literature. According to the data of Sal'dau (curve 1) there is a marked change in slope at the points of magnetic and phase transformation; this was observed also by us for armco type iron. However, for pure iron the curve runs smoothly with a bend at 768°C (Curie point) and jumps at the points of allotropic transformations. A curve of a similar shape was obtained by Ribbeck (curve 4) for pure iron (0.00 per cent Ni, 0.00 per

cent C, 0.07 per cent Mn and traces of Si). The sharp bends in the curves for armco iron and for the iron studied by Sal'dau can probably be explained by the influence of carbon which is present to a considerable extent.

In contrast with the data of Mokrovskii and Regel', the electric resistivity of iron in the δ-region increased in our tests with the temperature, and this increase was more marked compared with γ-iron.

Translated by H. Nowottny

REFERENCES

1. P.Ya. Sal'dau, *Metod elektroprovodnosti pri vysokikh temperaturakh (The method of electric resistance at high temperatures)* Moscow-Leningrad (1952).
2. Ribbeck, *Zs. f. Phys.*, 39, 787 (1926).
3. N.P. Mokrovskii and A.R. Regel', *Zh. tekh. fiz.* 23, No.12, 2121 (1953).
4. L.S. Kan and B.G. Lazarev, *Dokl. Akad. Nauk. SSR*, 81, No.6, 1027 (1951).
5. A.G. Tyutyunik, *Zav. lab.* 9, 1126 (1957).
6. V.M. Amonenko, B.M. Vasyutinskii, V.V. Lebedev and B.I. Shapoval, *Fiz. metal. metalloved*, 7, 862 (1959).

VOL.
8
1959

THE TEMPERATURE RELATION OF THE NERNST-ETTINGSHAUSEN THERMOMAGNETIC EFFECT IN NICKEL AND FERRO-NICKEL ALLOYS*

R.P. IVANOVA

The "Lomonosov" State University, Moscow

(Received 8 May 1959)

The work studies the Nernst-Ettingshausen effect on nickel and ferro-nickel alloys in a wide temperature range. The relation between the effect and the magnetic field, the temperature relation of the effect and also the relation between the magnitude of the effect and the percentage composition of the alloy at different temperatures were found.

The present work is devoted to a study of the Nernst-Ettingshausen thermomagnetic effect in nickel and ferro-nickel alloys. As is known this effect consists in the formation of an electromotive force in metals and semiconductors placed in a magnetic field with a variation in the temperature in a direction perpendicular to the magnetic field. The electromotive force is produced in the direction perpendicular to the magnetic field and to the direction of the temperature gradient. The data available in the literature on the study of the Nernst-Ettingshausen effect is very disconnected [1-6]. The present work contains the results of a systematic study of this effect depending on a series of factors which influence its magnitude.

Ferro-nickel alloys with the following composition were studied:

1. 36% Ni – 64% Fe,
2. 45% Ni – 55% Fe,
3. 55% Ni – 45% Fe,
4. 65% Ni – 35% Fe,
5. 75% Ni – 25% Fe,
6. 85% Ni – 15% Fe,
7. Nickel.

Measurements of the Nernst-Ettingshausen electromotive force were taken for each of the specimens depending on the external magnetic field which varied to about 1600 oersted and the effect of the temperature on the magnitude of the effect was also studied.

METHOD OF MEASURING

Measurements were made on specimens which had a parallelepiped shape 5 x 15 x 150 mm in dimension. The temperature gradient was produced by using two furnaces consisting of nichrome spirals placed inside copper tubes and isolated from them by quartz. The copper tubes were inserted and tightly fixed into the slots cut along the narrow edges of the specimen. The temperature gradient obtained in this way was measured by two chromel-alumel thermocouples inserted in special holes drilled in the specimen. The distance between the thermocouples was about 1.4 cm (Fig. 1). The difference in temperature produced ΔT was about 5-10°.

Stability in the heat regime was achieved by using stabilized pressure for charging the furnaces. For this purpose the specimen under investigation was placed inside a tube of molybdenum glass evacuated to a pressure of 10^{-2} mm mercury column.

In addition before the measurements were begun the specimen was soaked for an hour with the furnaces switched on to set the heat regime at a given temperature. The temperature of the specimen was taken as the tem-

* *Fiz. metal. metalloved.* 8, No.6, 851-856, 1959.

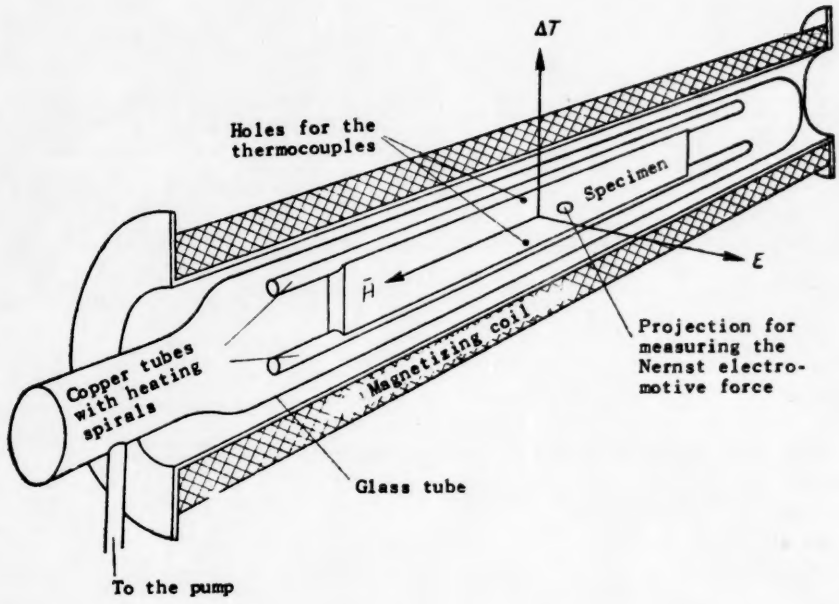

Fig. 1. A diagrammatic representation of the main part of the apparatus.

perature calculated as the average value from the readings of the upper and the lower thermocouples. The Nernst-Ettingshausen electromotive force was measured by the compensation method using a low-resistance direct current potentiometer and for small values of the electromotive force – a photcelectrooptical amplifier.

The contacts for recording the electromotive force were soldered in silver to special projections cut on the specimens and placed opposite each other at equal distances from the upper and lower edges. The electromotive force caused by the asymmetry of the contacts was compensated to the imposition of the outer magnetic field on the specimen.

It must be noted that as a result of the fine stability of the thermal regime the value of the temperature gradient during the test was kept constant with an accuracy of up to 0.05°. The temperatures were measured by a low-resistance type PPTN-1 potentiometer and a M-21/4 galvanometer.

The temperature measurements were taken before the beginning and after the end of the measurements at the given temperature.

THE RESULTS OF MEASURING

As a result of the measurements which were made the relation between the Nernst-Ettingshausen electromotive force magnitude and the external magnetic field was found for each of the seven specimens investigated at different temperatures. The curves for a specimen of pure nickel are shown in Fig. 2. The curves obtained for the alloys are of the same type and are not given. In Fig. 2 the relation $\frac{El}{\Delta Tb}$ $\frac{\text{volt}}{\text{degree}}$ was plotted along the Y-axis, where E is the Nernst-Ettingshausen electromotive force (in volts); l is the distance (cm) between the two thermocouples; b is the thickness of the specimen (cm); ΔT is the temperature difference (°C). Thus along the Y-axis are plotted the values of the Nernst-Ettingshausen electromotive force reduced to a temperature gradient of 1°C in 1 cm.

It is clear from the given diagram that there is a rapid increase in the electromotive force E in fields of the order of 75-100 oersted. For specimens with a small nickel content the relation between E and the field in these sections is linear. In more powerful fields the variation in E is small and the effect achieves saturation. There is an exception in certain curves measured at a temperature near to the Curie point for each

VOL. 8 1959

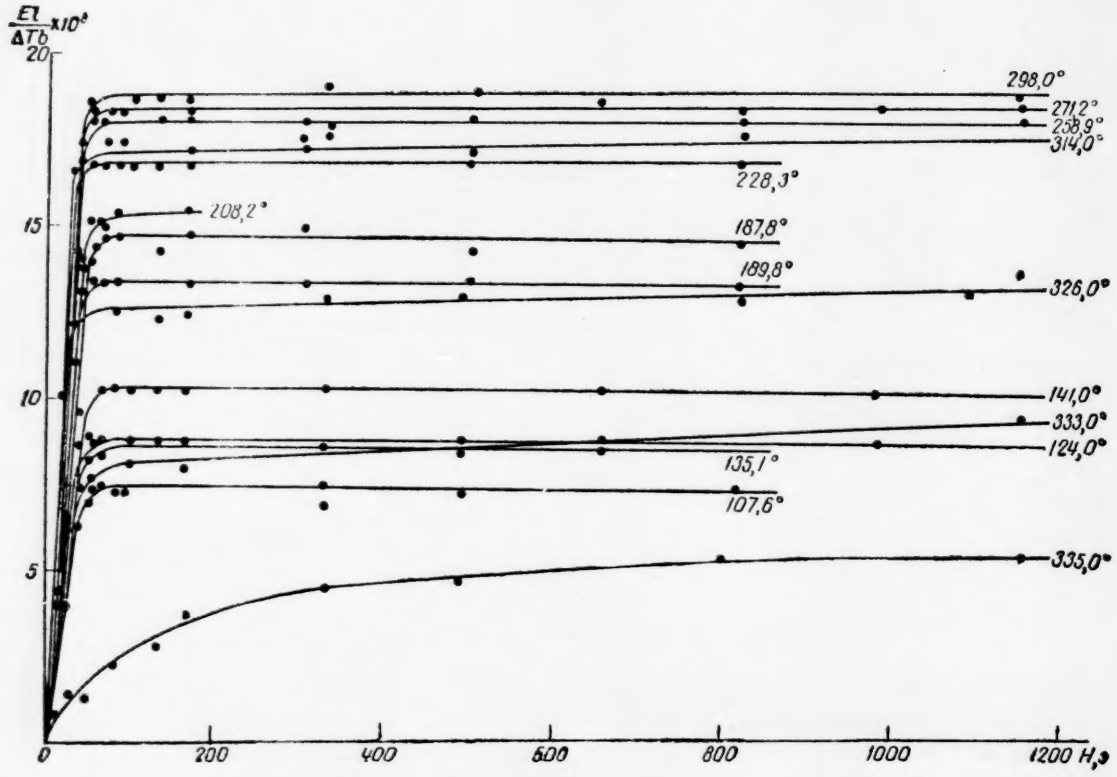

Fig. 2. The relation between the value $\frac{El}{\Delta Tb} \times 10^{-8}$ and the external magnetic field H for pure nickel.

composition which show a gradual increase in E with a growth in the H field.

The values obtained for the electromotive force in the saturation region are extrapolated till they intersect with the Y-axis ($H = 0$). Fig. 3 shows the relation between the values $\left(\frac{El}{\Delta Tb}\right)_{H=0} \times 10^{-8}$ and the temperature of all the compositions which were studied.

In the temperature range which was examined the curves corresponding to pure nickel and specimens containing 85; 75; 65 and 55% Ni have approximately the same shape. At the beginning with an increase in the temperature there is a linear growth in the value E and at a certain temperature (different for each of the compositions) the value E reaches a maximum. The maximum value of the effect for a composition of 55% Ni is reached at a temperature of the order of 260°, for 65% Ni the maximum is strongly blown up and is found in the temperature region from 300 to 400°, for 75% Ni the maximum is observed at about 460°, for 85% Ni – at 420° and for pure nickel – at 280°. A further increase in the temperature leads to a rapid reduction in the value of E as it approaches the Curie point for each composition. The figures showing the relation between the Nernst-Ettingshausen electromotive force and the temperature for specimens containing 45 and 36% Ni have the form of straight lines. The straight lines obtained are obviously the falling parts of the curves which are similar in shape to the curves examined above (for compositions of 85; 75; 65; 55% Ni and pure nickel), but lying in the lower temperature region not studied by us.

From the data shown in Fig. 3 it is easy to find the relation between the value of E and the composition at a given temperature. These curves are shown in Fig. 4. The dependence on

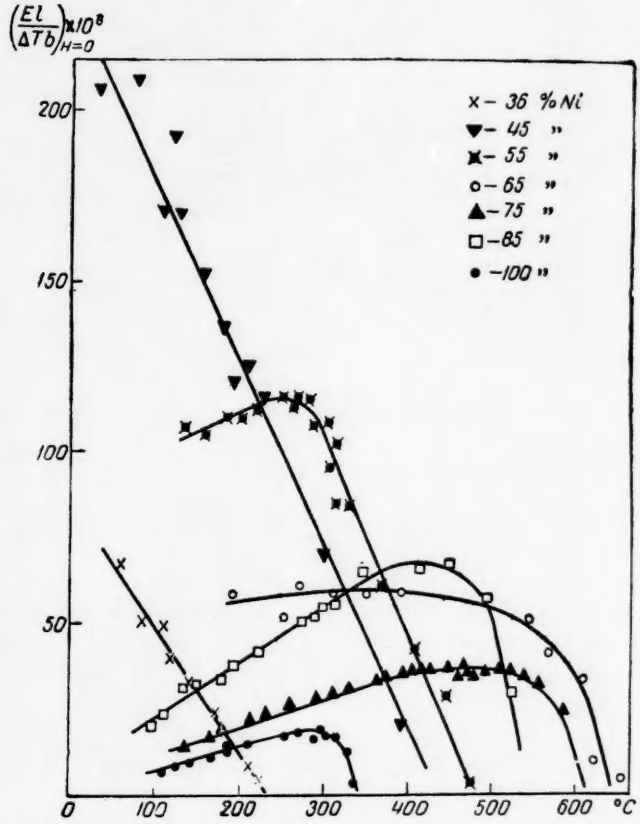

Fig. 3. The variation in the value $\frac{El}{\Delta Tb} \times 10^{-8}$ depending on the temperature for all the specimen alloys studied.

the composition is shown in this graph for the temperatures 100; 200; 300 and 400°.

It is seen from the figure that all the curves have two maxima. One of them for all temperatures corresponds to the composition with an 85% Ni content. The magnitude of the maximum value increases with a growth in the temperature. The position of the other maximum with an increase in the temperature is displaced to the side of the greater percentage nickel content. The value of this maximum decreases with an increase in the temperature.

The following maximum values of E were found from the tests carried out on each of the specimens (see Table 1).

The table does not include the data for compositions containing 36 and 45% Ni, because for these specimens no maximum was found on the curves, but the greatest values for E

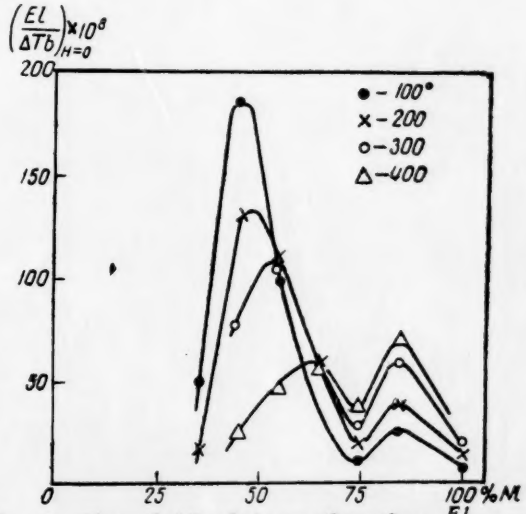

Fig. 4. The relation between the value $\frac{El}{\Delta Tb} \times 10^{-8}$ and the percentage composition of the alloys at different temperatures.

TABLE 1

Maximum values of E for each specimen

Ni content %	Temperature °C	$max\left(\frac{El}{\Delta Tb}\right)_{H=0} \times 10^{-8}$, $\frac{\text{volt}}{\text{degree}}$
55	260	117
65	300	60
75	460	36
85	420	68
nickel	280	18

$E\left(\frac{El}{\Delta Tb} \times 10^{-8} \sim 200\right)$ were observed just on the specimen with 45% Ni (for the lowest of the temperatures studied 40°).

Thus from the data obtained it is possible to obtain a fairly complete picture of the behaviour of E in ferro-nickel alloys with a change in the external field depending on the percentage composition of the alloys and with a variation in the temperature in the range from 40 to 200-600° (depending on the composition).

In conclusion I express my gratitude to Professor Ye.I. Kondorskii for his valuable advice and hints in carrying out the work.

Translated by J. Murray

REFERENCES

1. A. Smith, *Phys. Rev.*, 33, 295 (1911).
2. A. Smith, *Phys. Rev.*, 17, 23 (1921).
3. I.M. Nochan, *Zh. tekh. fiz.*, 25, 1003 (1955).
4. Holl, *Proc. Nat. Acad. Sci.*, 11, 416 (1925).
5. *Tekhnicheskaya entsiklopediya. Spravochnik, (Technical Encyclopaedia, Reference Book)*, Moscow., 4, 163 (1930).
6. I.K. Kikoin and I.G. Fakidov, *Zh. eksp. teor. fiz.*, 11, 113 (1941).

VOL. 8 1959

THE X-RAY DIFFRACTION STUDY OF THE REDUCTION PROCESSES IN SOME FERRITES*

V.N. BOGOSLOVSKII

The Metallurgical Institute of the Urals branch of the Academy of Sciences of the USSR

(Received 25 July 1959)

The study of the reduction process in complex metal oxides to which the ferrites belong is of great practical and theoretical importance. Oxides are the basic raw material for the production of many metals, and data on the mechanism of their reduction can assist the intensification of the existing processes and the development of new metallurgical processes.

The works of A. Le Chatelier, N.S. Kurnakov, A.A. Baikov, M.A. Pavlov, I.P. Bardin, I.A. Sokolov and many other scientists have studied in detail the thermodynamics and kinetics of the reduction processes of many oxides and natural compounds. However, despite the large amount of work devoted to the theory of metallurgical processes it needs further improvement. The important side of the reduction processes – the processes occuring in the solid phase – have not been sufficiently studied. In this connexion the reduction of metal oxides has had considerably less study than the reverse process – the oxidation of metals at high temperatures.

On the basis of data obtained from the X-ray diffraction study of solid products from the reduction of iron oxides carried out by the author under the direction of Arkharov [1,2], it was established that the diffusion of metal ions inside the crystal lattice of the oxide (volume diffusion) plays an important role in the reduction processes. In certain cases the migration of anions and cations through the free surface of the oxide and in the region of the coupling of the initial oxide with the the metallic phase – a product of its reduction (surface diffusion) also has considerable importance. The reduction of higher oxides to lower (Fe_2O_3 to Fe_3O_4 and Fe_3O_4 to FeO) takes place because of volume diffusion, but in the reduction of an oxide to a metal surface diffusion takes place.

The study of the reduction of ferrites is a further development of this work. The present report makes use of the results of investigating the solid products from the reduction of nickel ferrite by hydrogen at 400° and of nickel and copper ferrites by graphite. The reduction of the ferrites by graphite was carried out in a vacuum*. The phase composition and lattice parameters of the products of reduction were studied at various stages in the process.

THE PRODUCTS OF THE REDUCTION OF NICKEL FERRITE BY GRAPHITE

Ferrite obtained from the sintering of an equimolar mixture in air at 1200° for 30 hr served as the raw material for the reduction of nickel ferrite. The X-ray diffraction phase analysis showed that the sintering products are single-phase and have a spinel structure with crystal lattice parameters of $8,333 \pm 0.005$ Å, which agrees with the data on the nickel ferrite $NiFe_2O_4$ [3]. As the reduction takes place the parameter of the ferrite crystal lattice grows as shown in Fig. 1. Beginning with the 20% reduction the

* *Fiz. metal. metalloved.* 8, No.6, 857-860, 1959.

* Products from the reduction nickel ferrite were obtained by M.G. Zhuravleva and of copper ferrite – N.M. Stafeyeva. V.L. Subbotina took part in the investigation relating to the copper ferrite.

growth in the lattice parameter ceases and it remains practically constant until the spinel phase completely disappears in the specimens. A product of reduction at the beginning of the process is the phase with a face-centred crystal lattice, whose parameter agrees well with the parameter of the crystal lattice of pure nickel (3,517 Å). This indicates that in the reduction of nickel ferrite relatively pure nickel is a product of reduction. The growth of the lattice parameter of the spinel phase at this stage of the reduction means that the ferrite is transformed into magnetite.

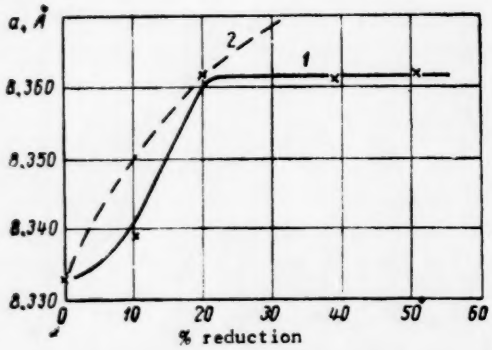

Fig. 1. The variation in the ferrite nickel lattice parameter in the graphite reduction process at 950°. 1 – experimental data; 2 – calculated data.

Since nickel ferrite and magnetite have an inverted spinel structure the change in the lattice parameter on the transition of ferrite to magnetite must agree with Vegard's law [4,5]. Stemming from this and taking into account that pure nickel is a product of the reduction, the dependence of the ferrite lattice parameter a on the degree of reduction X can be expressed in the form of the relation

$$a = 8{,}38 - 0{,}047\,\frac{1-3x}{1+3x}.$$

The comparison of this relation with test data shows as is seen from Fig. 1. that the variation in the ferrite lattice parameter with the reduction qualitatively agrees with Vegard's law at the beginning of the process. Some divergence at $X = 0.1$ is possibly connected with the fact that the degree of inversion at least for nickel ferrite is not known sufficiently accurately [6]. The comparison also shows that nickel ferrite obtained by the method described above obviously has a small amount of vacancies in the metallic part of the crystal lattice. If the amount of vacancies in the ferrite lattice were considerable a more rapid increase in the constant of its lattice at the beginning of the reduction would be expected.

It is also seen from Fig. 1 that the variation in the nickel ferrite lattice parameter in the reduction ceases before its value reaches the magnitude characteristic of pure magnetite (8.38 Å). The low value of the constant of the crystal lattice of the spinel phase indicates the presence in the latter of a certain amount of nickel ions which do not go over to the metallic phase in reduction.

The change in the nickel lattice parameter in the ferrite reduction process is shown in Fig. 2. The curve expressing this relation has two practically horizontal sections. The first from the beginning to 20% reduction corresponds to the growth in the parameter of the spinel phase. The transition of ferrite to magnetite takes place in this period. The second section – between 35 and 50% reduction – corresponds to the reduction of magnetite to wüstite. The latter agrees with the phase composition of products of reduction. Lines belonging to the wüstite phase are present in this section on the X-ray photographs of the specimens.

During the whole reduction process, apart from the two sections mentioned, the nickel lattice parameter increases which indicates the increase in the concentration of iron dissolved in it. This is understandable because at the beginning of the reduction the oxide phase becomes poor in nickel and later the metallurgical phase takes in mainly iron. The first signs of the phase with α-iron body-centered lattice appear only after 70% reduction. This phase can form either as a result of the iron concentration in the nickel reaching the limit of iron solubility in the γ-solution and the reducible iron forms an independent phase, or from the decomposition of the γ-solid solution when the specimens are cooled.

The data obtained enable the nature of the diffusion of metal ions in the reduction process to be judged. The variations in the crystal lattice parameter and in the structure

of the oxide phases with the constancy of the lattice parameter of the metal phase – a product of reduction indicates that volume diffusion is taking place in the oxide phases. On the other hand the changes in the lattice parameter of the metal phase while the lattice parameters of the oxides are unchanged indicates the pre-eminent role of surface diffusion and volume diffusion in the metal phase.

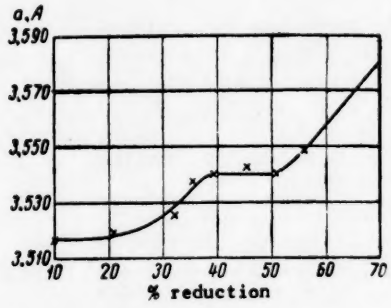

Fig. 2. The variation in the lattice parameter of the metal phase in the process of the graphite reduction of nickel ferrite at 950°.

From this point of view the beginning of the reduction process is marked by intense volume diffusion in the oxide phase. As a result of this process the ferrite becomes poor in nickel and turns into magnetite. Then for a time the volume diffusion slows down to a considerable extent and the reduction is accompanied by surface and volume diffusion in the metal phase. Later there is yet another period of intense diffusion in the oxide phase connected with the change-over of magnetite to wustite. Then the reduction of wustite to metal is again accompanied by surface diffusion. The existence of a period of intense surface diffusion after the transition of ferrite to magnetite is complete, before the formation of wustite, is obviously connected with the fact that wustite in contact with pure nickel is unstable. It does not form until the iron concentration in the metal phase increases to a value at which the chemical potential of the metallic solid solution is equal to the chemical potential of wustite containing a certain amount of dissolved nickel. Thus, the surface diffusion is the link connecting the separate stages of crystal chemical transformations in the reduction of complex oxides.

The phase composition of the products of reduction can also yield qualitative data on the relative magnitude of the binding forces between the metal ions and the oxygen in the complex oxide. The appearance at the beginning of the process in the metal phase – a product of reduction – of principally nickel ions indicates that the latter are less firmly bound with the oxygen in the ferrite lattice than the iron ions. This agrees with the data on the heats of dissociation of simple nickel and iron oxides [7], in which the metal ions have the same co-ordination as in the ferrite. Thus, the heat of dissociation of wüstite is equal to 129.0 kcal/mole, and of NiO 116.8 kcal/mole, i.e. somewhat lower for the second.

THE HYDROGEN REDUCTION OF NICKEL FERRITE

The composition of the solid products from the hydrogen reduction of nickel ferrite at 400° is substantially different from their composition after graphite reduction in the conditions described above. First of all the absence of noticeable variations in the ferrite crystal lattice parameter throughout the reduction attracts attention.

The composition of the metal phase also does not change and corresponds to the composition of the metal ions in the ferrite. Comparing this data with the ideas expressed above it is possible to assume that at a relatively low temperature the reduction is accompanied mainly by surface diffusion.

THE GRAPHITE REDUCTION OF THE COPPER FERRITE $CuFe_2O_4$

The reduction process of this copper ferrite has many features in common with the reduction of nickel ferrite in the same conditions. At the beginning of the process copper is the product of the reduction of copper ferrite at 700-900°. This indicates that the copper has a considerably looser bond with the oxygen in the ferrite lattice than the iron. In this case, however, it is not possible to use the values of the heats of dissocation of simple copper oxides for comparison because the copper ions have a different co-ordination in

VOL. 8 1959

them than in the ferrite. In addition the copper ferrite reduction process is considerably complicated by the existence of two modifications in the ferrite and by the limited reciprocal solubility of copper and iron.

CONCLUSIONS

1. The products of the graphite reduction of nickel and copper ferrites in a vacuum and of the hydrogen reduction of nickel ferrite were investigated by the X-ray diffraction method.

2. The data obtained enabled the role of volume and surface diffusion in the reduction process of complex oxides to be ascertained and also yielded qualitative information on the relative magnitude of the binding forces between the nickel and copper ions and the oxygen and iron ions in the ferrite.

Translated by J. Murray

REFERENCES

1. V.I. Arkharov, V.N. Bogoslovskii, M.G. Zhuravleva and G.I. Chufarov, *Dokl. Akad. Nauk SSSR*, 98, 803 (1954); *Zhurnal fizicheskoi khimii (Journal of Physical Chemistry)*, 29, 272 (1955).
2. *V.I. Arkharov and V.N. Bogoslovskii, Fiz. metal. metalloved.*, 3, 254 (1956).
3. E.J.W. Verwey and E.L. Heilman, *J. Chem. Phys.*, 15, 174 (1947).
4. A. Hoffman and W.A. Fischer, *Zs. Phys. Chem.*, 7, 80 (1956).
5. E.C. Romeijen, *Philips Res. Rep.*, 8, 304 (1953).
6. J.M. Hastings and L.M. Corliss, *Rev. Mod. Phys.*, 25, 114 (1953).
7. O. Kubashevskii and B. Gopkins, *Okisleniye metallov i splavov (Oxidation of metals and alloys)*, Foreign Literature Publishing House, Moscow., p. 28 (1957).

ON THE QUESTION OF CONCENTRATION INEQUALITIES EXPERIMENTALLY DETECTED IN SOLID BODIES*

(OBSERVATIONS ON THE WORK OF A.S. ZAV'IALOV and B.I. BRUK)

V.I. ARKHAROV

The Institute of the Physics of Metals of the
Academy of Sciences of the U.S.S.R.

(Received 20 July 1959)

VOL. 8 1959

1. One of the main directions in the development of modern physical metal studies consists of the study of inequalities in the concentration distribution in single-phase solid bodies.

Experimental data and certain general theoretical ideas developed in the last 10-15 years have resulted in the conception according to which definite concentration inequalities are to a greater extent inherent in solid bodies than the idealized uniformity in the distribution of atoms of different types throughout the points of the whole crystal lattice which until recently was considered the basis of the conception of a solid solution.

It is not a matter here of those macroscopic inequalities of concentration distribution which arise in the solidification of melts as a result of the finite cooling speed and which can be comparatively easily removed by subsequent homogenizing annealing which evens out the concentration in the macrospaces of the solid solution. Here it is a question of the quasi-stable inequalities of the concentration distribution influenced by deeper factors inherent in real solid bodies. These inequalities are not removed by homogenizing annealing but on the contrary they appear to a greater extent as a result of carrying it out.

The state of a real solid body in the presence of the inequalities of concentration examined here is nearer to the equilibrium state than with its uniform distribution throughout the volume of the solid solution.

Concentration inequalities of this kind arise from the internal adsorption of dissolved components in structural heterogeneities of solid bodies of a different kind [1].

The degree of stability of the concentration inequality from an adsorption origin is determined by the degree of stability of those structural heterogeneities which are influenced by internal adsorption. For example, intercrystalline internal adsorption creates a concentration of the intercrystalline transition zones by surface active components which is just as stable as the grain size of a given polycrystalline body.

Another kind of stable concentration nonuniformity in solid solutions is the so-called K-state characterized by the presence of volume microregions in them with a long lasting enrichment by atoms of certain dissolved components [2]. In the absence of rough structural heterogeneities the K-state microregions develop statically in a coherent crystal lattice.

When they form in the lattice of an unsaturated solid solution, concentration inequalities of the type K-state type regions reflect the action of chemical affinity forces. These forces (at a given temperature) are already capable of forming a structure corresponding to a much earlier stage of decomposition of the solid solution. These forces, however, are not sufficient to ensure the further growth of K-state regions which retain only a semimicroscopic size (in all three dimensions).

The sections of concentration inequality

* *Fiz. metal. metalloved.*, 8, No.6, 861-866, 1959.

influenced by internal adsorption have the scale of the structural heterogeneities by which they were influenced. In particular the zones of intercrystalline internal adsorption have the size of intercrystalline transition zones. The extension of these zones along the intercrystalline joints (in two dimensions) has a macroscopic size. In the third dimension (across the intercrystalline zones) their extension obviously has a semimicroscopic size. Estimates obtained even by indirect methods, but also from several experimental sources using different methods [1], give the order of magnitude of the average "thickness" of intercrystalline internal adsorption zones as several hundred angstrom units.

The very small thickness of these zones makes it extremely difficult to study them by direct experimental methods. In particular as it happens it is extremely difficult to use methods of contact autoradiography for this purpose which at first glance seem to be the most suitable.

II. The investigations published in a series of articles by Zav'ialov and Bruk [3-7] were carried out by these very methods. Phenomena of the appearance of concentration inequalities and then redistribution in solid solutions on an iron base containing carbon were found in these investigations. Using a radioactive carbon isotope these authors discovered non-uniformity in the distribution of the carbon itself in the alloyed iron and connected with it also the non-uniformity in the distribution of the other alloying elements.

The experimental results of Zav'ialov and Bruk are interesting and have great importance for physical metallography. The explanations of the observed phenomenon given by these authors which stem from the constitutional diagrams of alloys are also basically correct. The phenomena described and discussed by Zav'ialov and Bruk merit even more detailed discussion. We have limited ourselves here to formulating briefly a possible point of view on these phenomena: obviously we have here the particular preliminary (predecomposition) "stratifications" of the solid solution whose basic nature depends on the action of chemical forces. The presence of structural heterogeneities assists the development of these phenomena. The latter circumstance, however, is only concomitant and does not constitute the basic mechanism of these phenomena.

This constitutes the principal difference between the phenomena described Zav'ialov and Bruk on the one hand and the phenomena of internal adsorption described in a series of articles by Arkharov and his collaborators (see [1]) on the other hand.

In all the articles by Zav'ialov and Bruk [3-7] incidentally a point of view is directly expressed according to which both categories of phenomena are identified.

These authors mechanically transfer the conclusions from the examination of their experimental results to the phenomena of internal adsorption which leads them to conclusions which seem to us to be incorrect.

III. We notice first of all that the thickness of the zones of transcrystallite internal adsorption which as already stated can be considered as equal on the average to 10^2-10^3 Å, even from the calculation carried out by Zav'ialov and Bruk, lies in the limit of detectability by the autoradiographic method.

This calculation was carried out with such simplification that a difference in radiation was not determined between the intercrystalline zone enriched by the active component and the grain interior which contained a small but noticeable concentration of the component.

The calculation carried out by Galishev, Orlov and Shvarte [8], taking account of this circumstance shows that the autoradiographic method has even less sensitivity to the concentration inequalities of the fine layer type particularly if the effect of the thickness of the specimen is taken into account.

The zones of carbon concentration inequality which appear on the autoradiographs published in the articles by Zav'ialov and Bruk (taking into account the magnification indicated on them) exceed the upper limit of the thickness which could be allowed for the intercrystalline internal adsorption zones.

This confirms that the concentration inequalities studied by Zav'ialov and Bruk are not the result of internal adsorption and are an entirely different type.

IV. Practically speaking this is obvious from the fact that in examining the mechanism of the phenomena observed by them these authors never find it necessary to take into

VOL. 8 195

account the peculiarities of those sections of the solid medium which are enriched by one or other of the components; they only discuss the reasons which cause one or other of the components to be forced out from single sections of the crystallite thickness into other sections of it. In other words the reason for the redistribution of the concentration in the phenomena observed by Zav'ialov and Bruk is to be found in the characteristics of the state of the solid solution throughout the volume of the lattice.

In contrast to this, the phenomena of internal adsorption are influenced by the characteristics of the state of the solid solution in the structurally inhomogeneous portions into which is drawn one or other of the components with which the lattice volume is by no means supersaturated. When structural heterogeneities are absent in the solid solution of the given composition, adsorption does not take place.

The reason for the adsorption concentration redistribution is external with regard to the crystal lattice of the solid solution; the reason for the phenomena of concentration redistribution observed by Zav'ialov and Bruk is inherent in the lattice of the solid solution itself and it is found within it.

To establish finally the principal difference between the phenomena of "stratification" in solid solution observed by A. S. Zav'ialov and B. I. Bruk and the phenomena of internal adsorption we will record that the first is in principle only possible in ternary (or more complex) solid solutions and impossible in binary solutions, because the phenomena of internal adsorption can take place ir binary solid solutions on the same physical bases as in more complex solutions.

Since the phenomena of internal adsorption are in principle different from the phenomena observed by Zav'ialov and Bruk then all the bases are removed from the assertions expressed by these authors on the possibility of treating the phenomena of internal adsorption only on the basis of the constitutional diagrams of the alloys.

In fact the treatment of these phenomena is considerably more complicated. In their case, of greatest importance are, on the one hand, the variations in the forces of the interatomic bonds caused by the atoms of the dissolving substance in the lattice of the solvent, and, on the other hand, the local peculiarities of the structure and the excess energy of those structural heterogeneities through which internal adsorption takes place. In particular the nature and the degree of crystallographic disorientation of neighboring crystals is important for the intercrystalline internal adsorption.

V. Apart from this cardinal mistake in the method of treating the phenomena of internal adsorption in the quoted articles by Zav'ialov and Bruk they contain several other mistaken assumptions which must be corrected.

With regard to the relationship of the degree of enrichment of the intercrystalline transition zones ("boundary" or "surface" layers to use Zav'ialov and Bruk's expression) by impurities it is stated that "both the results of the tests and simple thermodynamic considerations lead to the conclusion that the action of factors which assist the enrichment decrease with a rise in the temperature".

In this connexion the following must be said. With regard to the "results of the tests" (by which Zav'ialov and Bruk obviously mean their own original tests described in the articles quoted by us) it has already been shown that they do not concern internal adsorption.

As far as "simple thermodynamic considerations" are concerned they were obviously too simple to be used in the problem under discussion. The fact is that Gibbs' equation derived for the concentration adsorption variation at the phase interface in connexion with the variation in the surface tension cannot be directly used for the phenomena of internal adsorption in a solid body in which first of all the absence of phase division must be noted (without mentioning the absence of an interface), and also instead of the surface tension the excess energy of the intercrystalline transition zone depending on the disorientation of neighboring crystallites must be examined.

If the similarity between the intercrystalline internal adsorption and the Gibbs' effect at the phase interface was not made in the first publications of Arkharov and his collaborators with sufficient explanation, then in later work (see in particular [1]) it was defined more precisely.

Also in the work published by Arkharov and his collaborators later it was pointed out that the temperature dependence of the adsorption enrichment of the zones of structural heterogeneities is not only determined by the volume solubility, the role of which was noted in the first articles, but also by certain other factors, and the combined action of all these factors can in certain cases give even a reverse relation of the adsorption enrichment and volume solubility with a variation in the temperature. The experimental data on this question have already been published; in some cases there is a direct connexion between the temperature dependence of the adsorption enrichment and the solubility and in other cases – a reverse relation [9-12]. It is scarcely necessary to comment that there is no need to discern the contradictions with the laws of thermodynamics in the case where the mechanism of the phenomenon is more complex than was supposed in the derivation of the thermodynamic equation.

Of course one and the same component of an alloy can with a different component ratio or even with the same ratio but at different temperatures be either "horophilic" or "horophobic" (or passive to adsorption). The whole series of fundamental ideas worked out for internal adsorption in solid bodies and the experimental data amassed illustrate this fact. The concentration relationship of the degree of horophilia of palladium relative to iron discovered in the work of Arkharov and Iunikov [13], and also the "competition" and "co-operation" of horophilic impurities when two (or more) of them are simultaneously present in a general solid solution with different concentration combinations [14-18] may be quoted as examples.

This, however, is the result of complex laws which are determined by the structure of the internal adsorption zones and by their energy, but by no means a result of those laws determined by the constitutional diagrams of alloys and not of those "simplest thermodynamic circumstances" by which Zav'ialov and Bruk correctly explain the phenomena of "stratification" of solid solutions observed by them in an incorrect, groundless and useless attempt to extend them to the phenomena of internal adsorption.

VI. In conclusion we must note two mistaken statements by Zav'ialov and Bruk which are closer to simple misunderstandings.

a) In trying to strengthen their argument in favour of an idea on the decrease in the enrichment of the intercrystalline boundaries with temperature during internal adsorption these authors write: "Finally if the process of the enrichment of the surface crystal layers by impurities is imagined as the result of a distortion of the crystal lattice in these layers, then in this case it must be admitted that an increase in the temperature must lead to a *reduction in the distortion of the lattice and to a relaxation of the stresses* existing in the boundary volumes examined". (our italics).

The lattice distortions inherent in intercrystalline zones are produced by the mutual action of differently oriented neighboring lattices and it is perfectly clear that until the nature of the disorientation changes, it is not possible to talk about either such a relaxation in "stresses" or about the reduction of the distortions in these zones with an increase in the temperature, because these distortions are just as stable as the existence of the intercrystalline boundary.

b) In trying to treat in their own way the results of the tests of Arkharov and Gol'dshtein [19] by analyzing the chemical composition of the surface layer of a stone-like fracture of over-heated steel 18KhNMA, Zav'ialov and Bruk taking the obviously overestimated numerical data obtain for the concentration of molybdenum in the surface layer the value of 160%, which as they reasonably remark "has no physical meaning". If, however, instead of the thousand-fold increase in the thickness of the etched layer over the assumed thickness of the adsorption layer taken by Zav'ialov and Bruk we take the five-hundred-fold increase (as indicated in the quoted article by Arkharov and Gol'dshtein), then the result is not 160 but 80% which has a physical meaning. If we also take into account that in the much later experimental work of Arkharov and his collaborators (quoted by Zav'ialov and Bruk, i.e. known to them) a much higher estimate of the thickness of the intercrystalline adsorption zones is given and, if according to this estimate we take this thickness as equal to 500 Å, then for the concentration in the adsorption enriched zone

VOL. 8 195

we obtain a much more accurate value of about 33% which not only has a physical meaning in general but also confirms the adsorption nature of enrichment.

VII. CONCLUSION

1. The phenomena of the appearance of concentration non-uniformity in alloys investigated by Zav'ialov and Bruk are different in their nature from the phenomena of internal adsorption.

2. The phenomena studied by Sav'ialov and Bruk can be explained on the basis of simple thermodynamic conditions influencing the form of the constitutional diagram of the alloy; however, these explanations are unsuitable for the phenomena of internal adsorption because of the completely different nature of the latter.

3. The thickness of the zones of intercrystalline internal adsorption estimated from the experimental data obtained by different methods has a value of 10^2-10^3 Å; direct autoradiographic detection of these zones is extremely difficult and possible only in particularly favourable conditions in exceptional cases. The zones detected in the work of Zav'ialov and Bruk have a thickness which exceeds the transverse size of the zones of intercrystalline internal adsorption.

4. The remarks of Zav'ialov and Bruk relating to some of the aspects of the phenomena of internal adsorption apart from the fact that they (the remarks) are made on the basis of incorrect identification of internal adsorption with the phenomena of stratification in solid solutions, contain also a series of misunderstandings caused by a much too simplified conception of the mechanism of internal adsorption.

5. Despite the short-comings noted in our article we consider that the work of Zavi'ialov and Bruk contains a description of phenomena which are important for metallography and a correct explanations of these phenomena on the basis of the laws represented by the constitutional diagrams of alloys.

Translated by J. Murray

REFERENCES

1. V.I. Arkharov, *Trud. Inst. Fiz. Met. Akad. Nauk SSSR*, No.20, p.201 (1958).
2. H. Thomas, *Zs. f. Physik*, 129, 219 (1951).
3. A.S. Zav'ialov and B.I. Bruk, *Dokl. Akad. Nauk SSSR*, 115, 94 (1957).
4. A.S. Zav'ialov and B.I. Bruk, *Metallovedeniy (Metallography)*, Sudpromgiz, p.206 (1957).
5. A.S. Zav'ialov and B.IO Bruk, *Fiz. metal. metalloved.*, 5, 127 (1958).
6. A.S. Zav'ialov and B.I. Bruk, *Metallovedeniye (Metallography)*, Sudpromgiz, p.35 (1958).
7. A.S. Zav'ialov and B.I. Bruk, *Fiz. metal. metalloved.*, 8, 349 (1959).
8. V.S. Galishev and A.N. Orlov and I.A. Shvarte, *Fiz. metal. metalloved.*, 8, (1958).
9. S.D. Vangengeim, *Fiz. metal. metalloved.*, 5, 174 (1957).
10. V.I. Arkharov, S.M. Klotsmwn, A.N. Timofeyev, *Fiz. metal. metalloved.*, 6, 255 (1958).
11. V.I. Arkharov, S.M. Klotsman, A.N. Timofeyev, *Fiz. metal. metalloved.*, 8 (1959).
12. V.I. Arkharov, B.S. Borisov, S.D. Vangengeim, G.K. Sokolova, *Fiz. metal. metalloved.*, (in print).
13. V.I. Arkharov and B.A. Iunikov, *Trud. Inst. Fiz. met. Urals branch of the Academy of Sciences of the U.S.S.R.*, No.16, p.62 (1955).
14. V.I. Arkharov and N.N. Skorniakov, *Trud. Inst. Fiz. Met. Urals branch of the Academy of Sciences of the U.S.S.R.*, No.16, p.75 (1955).
15. V.I. Arkharov and S.D. Vangengeim, *Fiz. metal. metalloved.*, 4, 439 (1957).
16. V.I. Arkharov, A.N. Moiseyev, I.P. Polikarpova, *Issledovaniya po zharoprochnym splavam (Studies on heat-resisting alloys)* 2, Izd. Akad. Nauk SSSR, p.92 (1956).
17. V.I. Arkharov, M.M. Belenkova, M.N. Mikheyev, A.I. Moiseyev, I.P. Polikarpova, *Fiz. metal. metalloved.*, 6, 633 (1958).
18. V.I. Arkharov and L.M. Magat, *Fiz. metal. metalloved.* 6,804; 809 (1958).
19. V.I. Arkharov and T.Iu. Gol'dshtein, *Trud. Inst. Met. Urals branch of the Academy of Sciences of the U.S.S.R.*, No.11, p.114 (1950).

A STUDY OF THE INTERNAL FRICTION IN POWDER METALLURGICAL BODIES. IV. SPECIMENS FROM BINARY POWDERS OF NONINTERACTING COMPONENTS Cu - Mo, Cu - W*

B. Ia. PINES and DEN GE SEN

The "A.M. Gorky" Khar'kov State University

(Received 4 May 1959)

The temperature relation of internal friction was determined by using a torsion pendulum for powder metallurgical specimens of binary mixtures of the powders Cu - Mo and Cu - W. On the curves of the temperature relation of internal friction $Q^{-1} = Q^{-1}(T)$ two maxima were obtained on each, one of which corresponds to the processes on the Cu grain contacts, and the other - on the contacts of grains of different kinds. The energies of activation were determined a) from the frequency shift of the maximum and b) from the background of the curve $Q^{-1} = Q^{-1}(T)$.

1. The present work is one of a series [1-3] devoted to the study of internal friction (i.f.) in powder metallurgical bodies. For a more detailed explanation of the laws of the development of i.f. maxima on similar and unlike grain contacts the investigation of powder metallurgical specimens from binary mixtures of the powders of noninteracting components of Cu - Mo, Cu - W was undertaken in this work.

The i.f. was measured on a vacuum torsion pendulum (relaxer) described previously [1]. The conditions and method of the measurements were the same as in the works [1-3]. The specimens were pressed from mixtures of differing composition of Cu (99.99% electrolytic) powders with a grain size of < 53 μ, Mo (99.98%) and W (99.98%) with a grain size of ~ 10 μ. Preliminary annealing of the specimens was carried out in the same relaxer at 1000° in a vacuum (at a pressure of 10^{-4} - -10^{-5} mm Hg) with different soaking.

2. The typical curves of the temperature relationship of i.f. in the studied specimens are shown in Fig. 1 (Cu - Mo) and Fig. 2 (Cu - W). The general shape of the curves is not different from that produced in the case of the specimens from pure metals and other binary powder mixtures. On all the curves there are two maxima (*A* and *B*) obtained at set temperatures and also a rapid growth in the internal friction is observed as the temperature increases.

The maximum A in the region of 300° corresponds to the similar grain contacts of pure copper and is influenced by the relaxation effect (diffusion slip) along the grain boundaries. It is also observed in single component specimens of Cu. The maximum *B* corresponds to the unlike contacts of Cu - Mo, Cu - W and is obtained at a temperature of 400-450°. Maxima corresponding to the grain contacts of the Mo-- Mo and W - W are not observed on the curves; these maxima must occur at considerably higher temperatures*.

Fig. 2 shows the i.f. curves obtained from Cu - W (10% W) specimens which have undergone

* *Fiz. metal. metalloved.*, 8, No.6, 867-871, 1959.

* According to the data of Shilling and Haspel [4] an internal friction peak appears on the $Q^{-1}(T)$ curve for pure W at a temperature of $\sim 1727°$.

VOL 8 195

preliminary annealing of various durations at 1000°. The curves correspond to an oscillation frequency of f = 0.9 c/s at room temperature (similar curves were obtained from specimens of the Cu-Mo system). It is clear that with an increase in the soaking time in preliminary annealing the level of internal friction drops at high temperatures. This can be explained by the "diffusion nature" of the processes influencing the "background" of internal friction because with an increase in the soaking time of the preliminary annealing the diffusion effects are slowed down.

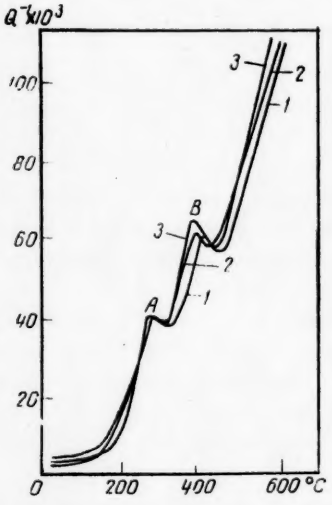

Fig. 1. Temperature relation of internal friction in powder metallurgical specimens from binary mixtures of Cu-Mo powders which have undergone preliminary annealing at 1000° for 30 min (oscillation frequency f ≅ 0.9 c/s). Curves 1, 2, 3 correspond to specimens with 5, 10 and 25% Mo. *A* – maximum of internal friction influenced by processes on the similar grain contacts (Cu-Cu); *B* – maximum of internal friction influenced by processes on the unlike Cu-Mo grain contacts.

3. The variation in the height of the i.f. maxima (*A* and *B*) corresponding to the similar and unlike grain contacts in metal ceramic specimens from mixtures of powders of Cu-Mo and Cu-W which have undergone preliminary annealing at 1000° with various soakings is shown in Figs. 3-6; curves 4, 5 in Fig. 3 and curves 3, 4 in Fig. 5 show that the height of the i.f. maximum *A* corresponding to the similar contacts (Cu-Cu) decreases with an increase in the addition of the second component. This is connected with a decrease in the contact area of the similar grains. With an increase in the soaking time of the preliminary annealing at 1000° the height of the maximum *A* also decreases (see curves 4-6 in Fig. 4 and curves 5, 6 in Fig. 6) which is caused by an enlargement of the Cu grains from the collective crystallization in the preliminary annealing process at 1000°.

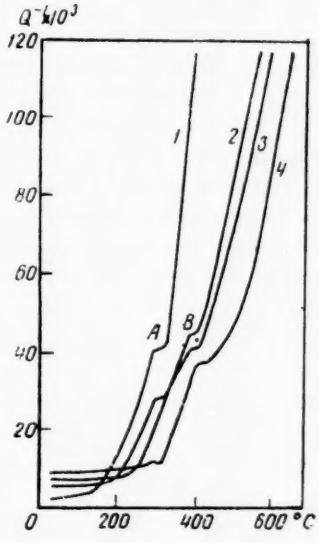

Fig. 2. Temperature relation of internal friction in a powder metallurgical specimen from a mixture of Cu-W powders (10% W) after preliminary annealing at 1000° with various soakings: 1 – heating and cooling; 2 – 30 min soaking; 3 – 2 hr soaking; 4 – 6 hr soaking. Oscillation frequency at room temperature f = 0.9 c/s.

The height of the i.f. maximum *B* influenced by the unlike grain contacts in the specimens of the Cu-Mo system increases with an increase in the Mo content (see curves 1, 2, 3 in Fig. 3) but it decreases with an extension of the preliminary annealing time at 1000° (curves 1, 2, 3 in Fig. 4). The height of the same maximum *B* in the Cu-W system on the other hand decreases with an increase in the W content (curves 1, 2 in Fig. 5) and increases with an increase in the duration of the preliminary annealing at 1000° (curves 1-4 in Fig. 6). The different effects are obviously connected with the different action of the preliminary annealing at 1000°. In mixtures of Cu-Mo powders at a temperature of 1000°

good contacts of the Cu grains with the Mo grains are obtained which influences the complete development of the possible height of the corresponding i.f. maximum. With an increase in the soaking time of the preliminary annealing at a given temperature the height of the maximum decreases probably in connexion with the decrease in the contact area (the growth of irregularities). In mixtures of Cu-W powders annealing at a temperature of 1000° still does not result in a sufficiently good contact of the Cu grains with the W grains and only with an increase in the soaking time at this temperature does the necessary contact which causes an increase in the height of the maximum gradually develop. The decrease in the height of the maximum *B* with an increase in the content of the second component W is obviously connected here with a deterioration in the contact influenced possibly by further difficulties in the pressing.

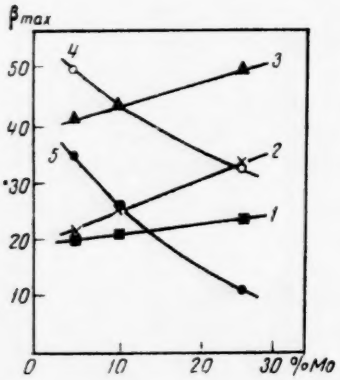

Fig. 3. Relation between the height of the maximum and the concentration in powder metallurgical specimens of Cu-Mo.
1-3 – correspond to the maximum *B* for specimens annealed at 1000° for a period of 6, 2 and 0.5 hr; 4-5 – correspond to the maximum *A* for specimens annealed at 1000° for a period of 0.5 and 2 hr.

In connexion with the assumptions quoted the rather greater "background" of the internal friction curve Q^{-1} *(T)* (see Fig. 2) in specimens of the Cu-W system deserves to be noted. With an increase in the duration of the preliminary annealing this background is removed. It must be noted that the porosity of the specimens from mixtures of Cu-W powders with the other conditions equal is higher than in specimens of the Cu-Mo system.

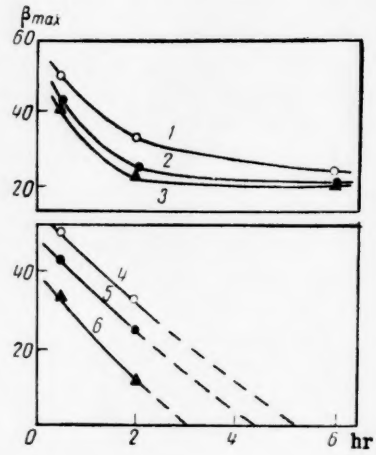

Fig. 4. Relation between the height of the maximum and the duration of the preliminary annealing at 1000° in powder metallurgical specimens of Cu-Mo.
1-3 – correspond to the maxima *B* for copper specimens with 5, 10 and 25% Mo; 4-6 – correspond to a maximum *A* for copper specimens with 5, 10 and 25% Mo.

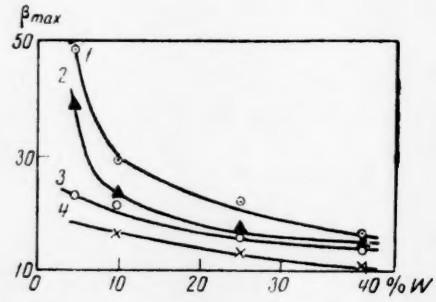

Fig. 5. Relation between the height of the maximum and the concentration in powder metallurgical Cu-W specimens:
1 and 2 – correspond to maxima *B* for specimens annealed at 1000° for a period of 6 and 2 hr; 3 and 4 – correspond to maxima *A* for specimens annealed at 1000° for a period of 0.5 and 2 hr.

To test the assumption which had been made on the connexion of the maximum on the internal friction curve with the processes on the

grain boundaries a comparison was made of the height of the maximum corresponding to the similar contacts of pure copper (i.e. to the contacts of the Cu-Cu grains) with what was expected from this assumption 1 . The height in the indicated maximum must decrease in proportion to the decrease in the contact area of the similar grains, i.e. in the case of binary mixtures of powders it must vary with the concentration according to the law $S = S_0 (1 - c)^2$ where c is the volume concentration of the second component. Fig. 7 shows the calculated and experimental relation

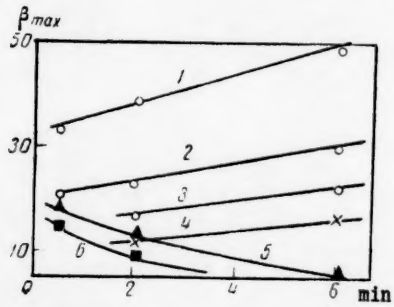

Fig. 6. Relation between the height of the maximum and the duration of the preliminary annealing at 1000° in powder metallurgical Cu-W specimens: 1-4 – correspond to maximum A for copper specimens with 25 and 40% W.

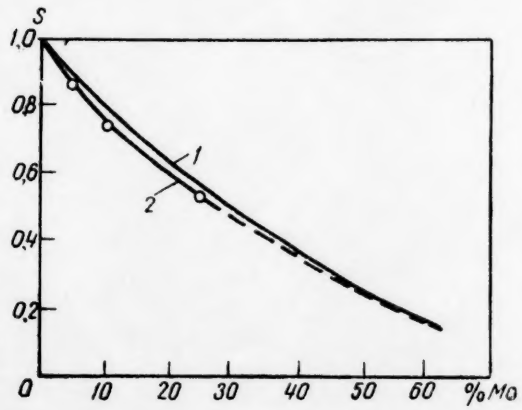

Fig. 7. Relation between the height of the maximum (contact area) and the concentration in powder metallurgical (contact area) and the concentration in powder metallurgical Cu-Mo specimens: 1 – calculated contact area; 2 – experimental curve of the height of the maximum.

between the height of the maximum A and the concentration in the specimens of the Cu-Mo system. Within the limits of error the measurements coincide well.

RESULTS

1. Using a torsion pendulum (relaxer) the internal friction in powder metallurgical specimens from binary mixtures of powders of the non-interacting components Cu-Mo and Cu-W was studied.

2. On the curves of the temperature relation of internal friction $Q^{-1}(T)$ two maxima (A and B) are observed, one of which (A) corresponds to the processes on the similar grain contacts (Cu-Cu) and the other (B) – to the unlike contacts (Cu-Mo, Cu-W).

3. For specimens of the Cu-Mo system the height of the maximum corresponding to the similar Cu grain contacts decreases changing with the concentration approximately as the the contact area of these grains i.e. according to the law $S = S_0 (1 - c)^2$, where c is the volume concentration of Mo.

4. The height of the maximum corresponding to the unlike grain contacts decreases in the Cu-Mo system and increases in the Cu-W system with a growth in the duration of the preliminary annealing at 1000°.

Translated by J. Murray

REFERENCES

1. B.Ia. Pines and Den Ge Sen, *Issledovaniye vnutrennego treniya u metallokeramicheskikh tel (Study of internal friction in powder metallurgical bodies) Fiz. metal. metalloved.*, (1959) (in print).
2. B.Ia. Pines and Den Ge Sen, *Issledovaniye vnutrennego treniya u metallokeramicheskikh tel. II. Troinaya sistema Cu-Fe-Ni (Study of the internal friction in powder metallurgical bodies. II. Ternary system Cu-Fe-Ni). Fiz. metal. metalloved.* (1959) (printing).
3. B.Ia. Pines and Den Ge Sen, *Issledovaniye vnutrennego treniya u metallokeramicheskikh tel III. Effekty, obuslovlennyye plasticheskoi deformatskiyei (Study of the internal friction in powder metallurgical bodies. III. Effects*

influenced by plastic deformation). Fiz. metal. metalloved., (1959) (in print).

4. W. Shilling and R. Haspel, *Zs. f. Metallk.* 48, 32 (1957).

VOL
8
195

THE WEAR-RESISTANCE OF CASE-HARDENED STEEL AND ITS SUBSTRUCTURE*

I.M. LYUBARSKII, A.P. LYUBCHENKO, G.N. BAKAKIN

Transport Machine Works, Khar'kov

(Received 9 March 1959)

VOL. 8 1959

1. In the reports [1, 2] it was suggested that the reason for the amibiguous effect of the gamma-phase (residual austenite) in the case-hardened steel layer on its wear-resistance (cf. with [3-5]) is dependent upon the different substructure of this phase, i.e. in the difference in the size and nature of the variations in the microdeformation of the crystal lattice and in the size and degree of disorientation of the subgrains. It was established that in the case when the microdeformation of the crystal lattice of the γ-phase is small ($\sim 2 \times 10^{-3}$) and homogeneous (homogeneous microdeformation regions ~ 150 Å) but the subgrain size is very great (< 1000 Å) then in certain friction conditions [1, 3] the case-hardened layer has good resistance to wear (even with a considerable amount of residual austenite (70-90%) . In this work, however, we only took into account the substructure of the γ-phase. Perhaps a correct conclusion about the influence of the substructure on the wear-resistance of steel can only be made on the basis of studying all the phases of the case-hardened layer.

The present report includes the results of the experimental study of the wear-resistance, substructure and alloying of the phases of the case-hardened steel layer containing different amounts of residual austenite.

2. A case-hardened layer of the steel 18KhNVA was used for the investigation and the variations in its thermal treatment are given in the table. The wear-resistance was determined by using radioactive isotopes ($^{59}_{26}$Fe and $^{60}_{27}$Co) to measure the radioactivity of the lubricant and by the autoradiography of the abrasion products brought to the conjugate friction surface. The specimens were worn in conditions of pure slip of the radioactive specimen on a standard disk and on a friction machine which simulated the work of transmission gear [6].

The substructure of the α- and γ-phases of the case-hardened layer (the size of the regions of coherent X-ray scattering δ, the magnitude of the sections of homogeneous microdeformation L_0, the saturation of the crystal lattice by inhomogeneous microdeformation L_i and the value of the relative microdeformation ϵ) was determined by the harmonic analysis of the "shape" of the diffraction line (311) (for the γ-phase) and (211) (for the α-phase) [7]. To take into account the possible variation in the substructure parameters within the depth of the case-hardened layer and the anisotropy of the microdeformation the X-ray photography was carried out at the same layer depth and the values of δ, L_0, L_i and ϵ_{max} are given in the table for the same crystallographic direction.

3. The results of the test are shown in the table and represented by Figs. 1 and 2 from which it follows that the nature of cooling the steel after case-hardening effectively influences its wear-resistance. In the case of slow cooling from the case-hardening temperature the wear-resistance of steel in conditions which reflect the real work parameters of a series of units and machines falls (No. 1-3 of the table) with an increase in the γ-phase content and with a practically unchanged submicrostructure of the α- and γ-phases. Rapid cooling speed after case-

* *Fiz. metal. metalloved.*, 8, No.6, 872-877, 1959.

Variations in the thermal treatment and results of studying steel 18KhNVA

	Nature of treatment	Content of γ-phase %	Hardness value from surface HR_C	Wear-resistance relative units	α-phase								γ-phase							
					before wear				after wear				before wear				after wear			
					ϑ, Å	L_0, Å	L_N, Å	$\epsilon_m \times 10^3$	ϑ, Å	L_0, Å	L_N, Å	$\epsilon_m \times 10^3$	ϑ, Å	L_0, Å	L_N, Å	$\epsilon_m \times 10^3$	ϑ, Å	L_0, Å	L_N, Å	
1	Case-hardening at 920° slow cooling tempering at 650° quenching from 810° in oil, tempering at 150° serial regime	⩾20	57-60	25	~400	Inhomogeneous microdeformation	~30	3.4	Monodispersed crystallite	15-20	~80	2.1	–	–	–	–	~200	~90	~70	~3
2	Case-hardening at 920° and cooling in air	40-50	~50	20	150	~70	~80	6.0	The same	30	70	2.3	~400	Inhomogeneous microdeformation	~50	4.5	~300	Inhomogeneous microdeformation	~50	4.5-4.0
3	Case-hardening at 920° and cooling with the furnace	60-70	~45	15	150	~70	~70	5.5	"	40	70	2.7	~400	The same	~50	7.0	~300	The same	~50	5.0 4.5
4	Case-hardening at 920° and quenching in oil	⩽90	50-60	100	~130	Inhomogeneous microdeformation	~30	5.0	"	~40	~60	2.5	monodispersed crystallite (>800)	150	Homogeneous microdeformation	1.9	~300	" "	~60	3.5
5	As in 4 and quenching from 810° in oil	~50	~60	60	300	20	80	5.0	"	20	190	3	~800	~80	120	2.2	~200	~30	60	3.3

VOL. 8 1959

hardening (see No. 4 and 5 of the table) results in high values for the wear-resistance of the case-hardened layer with practically the same concentrations of residual austenite (No. 2 and 5 of the table). In addition the substructure of the α- and γ-phases is considerably different from that which develops after slow cooling.

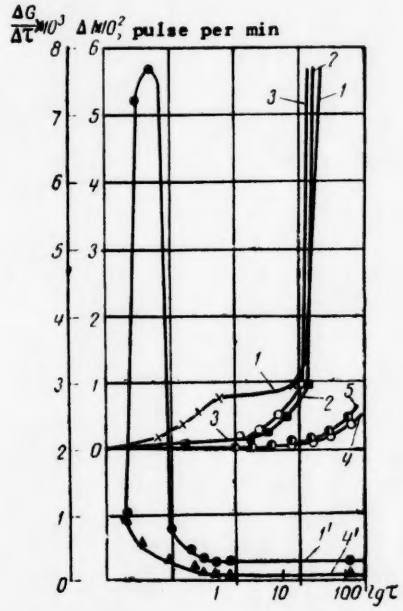

Fig. 1. The dependence of the magnitude of wear curves (1-4), rate of wear (1′-4′) of the case-hardened layer on the time of the test. The numbers of the curves correspond to the order of the thermal treatment regime according to the table.

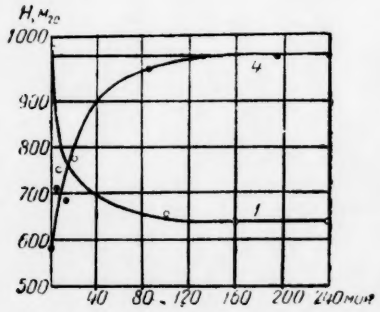

Fig. 2. The variation in the microhardness of the friction surface during the test: 1 – for the regime 1; 4 – for the regime 4.

What has been said on the question of wear-resistance can be illustrated by the curves of the dependence of the integral abrasion and the rate of abrasion on the time of the test (Fig. 1). The course of abrasion after rapid cooling (curve 4) is characterized by the very small separation of the abrasion products into the lubricant and by the migration to the conjugate surface [2] and the monotonous decrease in the rate of abrasion (curve [4]). At the same time after a series of industrial thermal treatment regimes the rate of abrasion rises sharply at the beginning of the test (curve [1]) and has very high values even after wearing in the conjugate friction surfaces.

It is also interesting to note the different variation in the value of the microhardness of the friction surfaces during the test. If the value of the microhardness after rapid cooling (Fig. 2, curve 4) increases continuously during the test, then for the friction surface treated by a serial regime it decreases with the passage of time (curve 1).

The substructure of the α- and γ-phases undergoes a regular variation which is the same for all the treatment regimes during the test (see table): hardening processes ("cold work") of the gamma-phase (δ small and ϵ_m large) and softening processes ("tempering") of the α-phase (δ large and ϵ_m small) take place under severe friction conditions.

It has been shown previously [2] that the magnitude of the cooling rate after case-hardening does not in practice change the nature of the carbide distribution throughout the depth of the case-hardened layer but affects the saturation of the carbide phase of the α- and γ-solid solution with alloying elements, in particular with chromium. Thus with a slow rate of cooling up to 40% of all the chromium in the steel goes from the solid solution into the carbides. With a high rate of cooling the chromium saturates the carbides and the solid solution in equal measure.

4. The experimental data stated above indicate that the phase composition unambiguously determines the capacity of the steel to resist wear. To evaluate correctly the effect of the γ-phase on the wear-resistance of steel not

only its content in the layer but also the substructure of the phases and the distribution of the alloying elements must be taken into account.

In fact, if the substructure and the alloyability of the phases does not change (see No. 1-3 of the table) then with an increase in the concentration of the residual austenite the resistance to wear decreases as it has been the custom to consider in practice. In the case of the variation in the alloyability of the phases and their substructure (see No. 4 and 5 of the table) with the same phase composition (cf. No. 2 of the table) the wear-resistance increases.

It is known that the solution of chromium in iron effectively influences the magnitude of the force of the interatomic bond in the crystals of the α- and γ-phases. Thus according to the data given in the works [8,9] the change in the concentration of the chromium from 0 to 1% results in an increase in the energy of activation of the self-diffusion of α- and γ-iron by $\sim 2\%$. Taking this into account with a variation in the cooling rate one must expect a variation in the magnitude of the energy of activation of the self-diffusion, for example, of γ-iron of 1000-1500 cal/g. atom^{-1}. Such a variation in the energy of activation will influence the size of the self-diffusion factor and the stability of crystals of α- and γ-iron.

However the magnitude of the self-diffusion factor D increases only 1.5-2 times [9], and the ultimate strength is not greater than by 5 kg x mm^{-2} [10]. Taking into account that the abrasion process does not take place at high temperatures (in any case lower than 700-800°) at which the self-diffusion processes can exert considerable influence on the stability of the material one must not relate the hardening of the steel by the variation in the cooling rate to the decisive effect of the alloyability of the phases.

Thus we come to the conclusion that in the case examined above the substructure of the α- and γ phases of the case-hardened layer determines its wear-resistance.

As is seen from the table the magnitude of the cooling rate after case-hardening does not exert substantial influence on the fine structure of the α-phase crystals. In the case of a small and a large cooling rate an intense breaking up of the crystallites takes place, a very inhomogeneous and high microdeformation of the crystal lattice of the α-phase. This is explained by the fact that irrespective of the magnitude of the cooling rate after case-hardening the nature of the α-phase crystallization does not change: in both cases it develops as a result of the martensitic γ-α transformation. With a high rate of cooling, however, purely diffusionless kinetics takes place and with a slow cooling rate – intermediate kinetics [1, 11].

The magnitude of the cooling rate after case-hardening influences the nature of the fine structure of the γ-crystallites. It follows from the data in the table that an increased cooling rate results in a small break up of the crystallites and in the small homogeneous microdeformation of the γ-phase crystal lattice.

The above-mentioned effect of slow cooling on the structure of the γ-phase can be connected with the peculiarities of the γ-α transformation in type KhNVA [1, 2, 11, 12]. Slow cooling results in the development of gradients of alloying elements and carbon in the microvolumes of the alloy, and also in an increase in the temperature of the γ-α transformation as a result of the redistribution of carbon in the intermediate transformation and as a result of this in a greater degree of deformation in the process of the $\gamma \rightarrow \alpha$ transformation [12] (on account of the greater plasticity of the γ-crystals).

The size of the microregion which has a carbon concentration gradient is obviously less or equal to the microvolume of the γ-crystal in which the process of carbon redistribution takes place (10^{-3} – 10^{-4} cm [2]). An evaluation of the size x of microregions which have concentration gradients of the alloying (Cr, W) can be made by using the relation $x^2 \sim D\tau$. where x corresponds to the way which the atom of the alloying element can take in the diffusion from the γ-crystal to the carbide phase in the time of slow cooling τ. Assuming that $\tau \leqslant 10^4$ sec and $D \leqslant 10^{-10}$ cm^2/sec, we get for the regions with chromium gradients $x_{chr} \leqslant 10^{-6}$ cm. Similarly for tungsten $x_t > 10^{-6}$.

Thus after slow cooling the crystal lattice of the γ-phase has gradients of carbon and

VOL 8 195

alloying elements in the microregions adjoining the carbide phase and undergoes intensive microdeformation which in turn lead to the above-mentioned diffraction picture of X-ray reflexion.

In the abrasion process the substructure of the α- and γ-phases undergoes, as has already been pointed out, a considerable variation. The different variation in the nature of the substructure of these phases in the abrasion process can be put down to the "cold-worked" α- and γ-crystals on account of the different effect of the heat of friction. In conditions of excessive lubrication the momentary initial heating of the "working" microvolumes of the alloy does not exceed 400-500° [13]. At these temperatures the coefficients of self-diffusion in the α-phase are 3-4 times higher than in the γ-phase [14]. For this reason with all the other conditions being equal the coherence recovery processes and the removal of the microstresses take place more intensely in the α-phase than in the γ-phase.

It is an established rule that the wear-resistance of a heterophase $\alpha + \gamma$ alloy is higher the greater the substructure of the γ-phase differs from that which characterizes the "cold worked" state of austenite. In the case when the γ-phase has already been intensely "cold worked" during the thermal treatment the wear-resistance is much lower (see Nos. 1-3 of the table). The optimum combination of "uncold-worked" γ-phase in an $\alpha + \gamma$ alloy ensures as is seen from the results of the present work high wear-resisting properties for an alloy.

The time of effective resistance to wear for a given alloy microvolume can obviously be connected with the time of the transition of the γ-phase to the "cold-worked" state. The rate of change in the mechanical properties of the alloy is clearly seen from the graphs in Fig. 2: the microhardness of the alloy sharply cooled after case-hardening increases monotonously during the test up to saturation, while the microhardness of the layer which had been already "cold-worked" during the thermal treatment constantly decreases.

It must also be noted that the alloy which has undergone sharp cooling after case-hardening has the further advantage in comparison with the case-hardened layer treated by a serial industrial regime that it contains a smaller amount of the α-phase which can be changed into the γ-phase in the friction process [15]. The $\alpha - \gamma$ transition and the appearance of the so-called "white zone" results in additional distortions of the crystal lattices on account of the difference in the parameter of the coupling cells of austenite and martensite [15].

The dynamics of the variation in the substructure was studied in the present work for definite parameters in the friction process. In other conditions the kinetics of the process can be different but the principal position put forward in the present work holds true in a very wide range of conditions which characterize the friction process.

CONCLUSIONS

1. From the point of view of wear-resistance the optimum steel structure can be produced from the correct evaluation of the processes which take place in the active layer and it is determined from the kinetics of hardening or softening different structural constituents in the friction process.

2. The wear-resistance of the case-hardened steel layer is determined not only by the phase composition but also by the structure of the phases. In accordance with this in the general case when the substructure and the phase composition vary the wear-resistance unambiguously depends on the austenite content.

The high resistance to wear in the friction conditions examined is attained with a considerable content of residual austenite in the case-hardened layer in which the crystals of the γ-phase are in an "un-cold-worked" and the crystals of the α-phase – in a "cold-worked" state.

The authors express their gratitude to Professor L.S. Palatkin for valuable advice in the execution of this work.

Translated by J. Murray

REFERENCES

1. L.S. Palatkin, I.M. Liubarskii, A.P. Liubchenko, I.A. Tananko, *Fiz. metal. metalloved.*, 1, 50 (1955).

VOL. 8 1959

2. L.S. Palatkin, I.M. Liubarskii, A.P. Liubchenko, *Tr. khimicheskogo fakul'teta i NII khimii Khar'kovsk. Gos. Univ. (Work of the Chemical Faculty and the scientific research Institute of Chemistry of the Kharkov State University)*, 18, p.75 (1958).
3. L.S. Moroz and S.S. Shurakov, *Problemy prochnosti tsementirovannoi stali (Problems of the stability of case-hardened steel)* Leningr., (1947).
4. A.I. Zhironkin, *Trud. Tsentr. Nauchno-Issled Inst. Narod. komitet tiazheloi prom-cti*, No.17 (1944).
5. Ia.I. Sagaradze, Dissertation, Lenin Library, Mosk.
6. I.M. Liubarskii, A.P. Liubchenko, V.G. Nesterenko, *Treniye i iznos v masinakh (Friction and wear in machines)*, No.12 (1958).
7. B.Ia. Pines, *Ostrofokusnyye trubki i prikladnoi rentgenostrukturnyi analiz (Sharp-focused tubes and applied X-ray structural analysis) Gostekhteoretizdat*, Moscow, (1955).
8. V.K. Kritskaia, G.V. Kurdiumov, T.I. Stelletskaia, *Problemy metallovedeniya i fiziki metallov, (Problems of metallography and the physics of metals) Metallurgizdat*, Moscow, p.408 (1955).
9. P.L. Gruzin, *Problemy metallovedeniya i fiziki metallov. (Problems of metallography and the physics of metals), Metallurgizdat*, Moscow, p.480 (1955).
10. S.Z. Bokshtein, *Struktura i mekhanicheskiye svoistva legirovannoi stali (Structure and mechanical properties of alloyed steel), Metallurgizdat*, Moscow, p.204 (1945).
11. L.I. Kogan and R.I. Entin, *Fiz. metal. metalloved.*, 6, No.1 (1957).
12. L.S. Palatkin and I.A. Tananko, *Doklad na VI Vsesoiuznoi rentgenokonferentsii (Report on the VIth All-Union X-ray conference)*, Leningrad (1958).
13. *Sb. Treniye i granichnaia smazka, (Collection. Friction and boundary lubrication)*, Foreign Literature Publishing House, Moscow (1955).
14. Ia.S. Umanskii and others, *Fizicheskiye osnovy metallovedeniya, (Physical basis of Metallography), Metallurgizdat*, (1956).
15. L.S. Palatkin, I.M. Liubarskii, B.T. Boiko, *Fiz. metal. metalloved.*, 1, 285 (1955).

VOL
8
195

ON THE EXISTENCE OF THE SILICIDE W_3Si*

N.N. MATIUSHENKO, L.N. YEFIMENKO, D.P. SOLOPIKHIN

Physical and Technical Institute of the Academy of Sciences of the Ukr.S.S.R.

(Received 26 June 1959)

VOL. 8 1959

At the present time the X-ray diffraction data on the silicides of the high-melting metals of VIth group of the periodic table have been sufficiently well elucidated in literature. In particular, the data on the silicides of molybdenum and tungsten are specially important: Mo_3Si, Mo_5Si_3, $MoSi_2$. There is a close analogy between the silicides of molybdenum and tungsten but up to the present the existence of silicide of the composition W_3Si [2, 3] has remained unestablished.

From the data of the X-ray diffraction study of the phases of the Mo-Si, W-Si systems it follows that the heating to high temperatures ($\sim 1700^0$) of specimens of Mo and W alloyed from the surface with silicon is accompanied by transitions of the higher silicides to the lower with the precipitation of silicon. In addition as in the thermal diffusion of silicon into molybdenum and tungsten a substantial role displayed by the peculiar chemical reaction which is influenced by the redistribution of the electrons in the *s*- and *d*-bands of the atoms of the metals which interact with the silicon. This reaction, taking into account the number of molecules in the volume of the elementary cell, is written in the following way:

$$30 \cdot 2MoSi_2 \rightleftarrows 3 \cdot 4Mo_5Si_3 \rightleftarrows 10 \cdot \underset{+84Si}{} \quad (1)$$

$$\underset{+100Si}{2Mo_3Si} \rightleftarrows 30 \cdot \underset{+120Si}{2Mo}.$$

The coefficients in front of the numbers of the molecules indicates the number of elementary cells. From this were found the volume percentages of the phases calculated on the basis of the literature data on the silicon compounds of molybdenum and tungsten [1]

TABLE 1

Phase	Atomic weight %	Syngony	Space group	z	Molybdenum			
					a, Å	c, Å	X-ray density (g/cm^3)	Volume percentage of phase
Mo	0	Cubic	O_h^9	2	3.14_7	–	10.2_2	$38._{5\pm2}$
Mo_3Si	25	cubic	O_h^3	2	4.89_0	–	8.9_7	$48._{1\pm2}$
Mo_5Si_3	37.5	tetragonal	D_{4h}^{18}	4	9.64_2	4.90_5	8.2_1	$56._{3\pm2}$
$Mo\ Si_2$	66.7	tetragonal	D_{4h}^{17}	2	3.20_6	7.87_7	6.2_4	$100._0$

* *Fiz. metal. metalloved.*, 8, No.6, 878-880, 1959.

Table 1 *(Cont.)*

Phase	Atomic weight %	System	Space group	z	Molybdenum			
					a, Å	c, Å	X-ray density (g/cm^3)	Volume percentage of phase
Mo	0	cubic	O_h^9	2	3.16_5	–	19.2_6	$38._{8\pm2}$
Mo_3Si	25	cubic	O_h^3	2	–	–	–	–
Mo_5Si_3	37.5	tetragonal	D_{4h}^{18}	4	9.60_5	4.96_4	14.5_6	$56._{0\pm2}$
$MoSi_2$	66.7	tetragonal	D_{4h}^{17}	2	3.21_8	7.89_6	9.7_5	$100._0$

(Table 1).

Taking into account this similarity it is natural to assume in accordance with the classical rule of isomorphism the existence of the silicide of the composition W_3Si belonging to the structural type β-W and to calculate its lattice parameter with accuracy influenced by the accuracy of the adduced parameters of all the other phases. It was found that the value of the W_3Si lattice parameter was equal to

$$a = 4{,}910 \pm 0{,}01\text{Å}.$$

With the object of confirming experimentally the fact of the existence of the silicide and to determine its lattice parameter more precisely we prepared specimens in which the W_3Si phase was observed metallographically and by X-ray diffraction.

Tungsten (99% W) cylindrical specimens 20 mm in diameter were saturated by the thermal-diffusion method in a neutral silicon medium (99% Si) to a depth of $\sim 100\mu$. As a result there formed layers of the phases: WSi_2 and W_5Si_3 (Fig. 1).

When these specimens are heated in air at $\sim 1700^\circ$ a decrease in the thickness of the disilicide layer and a growth of the W_5Si_3 layer on the boundary with the tungsten and under the oxide film is observed (Fig. 2) in the metallographic study. On the W-W_5Si_3

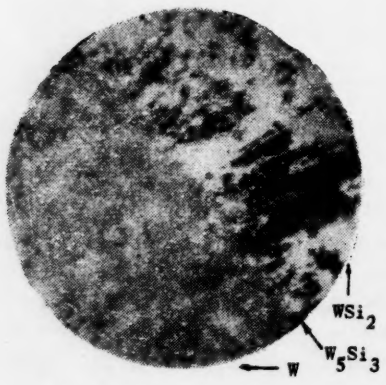

Fig. 1. Photograph of a section showing the formation of the silicides WSi_2 and W_5Si_3 in the silicidation of tungsten; X 186.

Fig. 2. Photograph of a section showing the formation of the silicide of the composition W_3Si as a result of prolonged heating of the specimen in air at ~ 1700; X 186.

TABLE 2

W_3Si: cubic system, structural type β-W, space group O_h^3, $z=2$, $a=4{,}91_{0\pm0{,}005}$ Å, density 16.2 g/cm^3.

hkl	d_{hkl}		hkl	d_{hkl}	
	calculated	experimental		calculated	experimental
110	3.47_2	–	332	1.04_7	–
200	2.45_5	2.46	422	1.00_2	1.00_1
210	2.23_6	2.24	510	0.962_9	–
211	2.00_5	1.99	520	0.911_8	0.913
220	1.73_6	1.72	521	0.896_5	–
310	1.55_3	1.54	440	0.868_0	–
222	1.41_7	1.40	530	0.842_1	–
320	1.36_2	1.35	531	0.829_9	0.828
321	1.31_2	–	600	0.818_3	0.816
400	1.22_8	1.23	610	0.807_2	0.804
411/330	1.15_7	1.15_8	611	0.796_6	0.795
420	1.09_8	1.09_3	620	0.776_3	–
421	1.07_1	1.07			

boundary is observed the formation of the new phase – W_3Si from which an X-ray photograph was made using copper radiation (Fig. 3) after removing the upper layers. As is seen from the diffraction lines (200), (400), the new phase has a texture which is influenced by the texture of the tungsten specimens. W_3Si and Mo_3Si – a silicide with a metal structure is formed as a result of the replacement of the tungsten atoms by silicon atoms without the radical reconstruction of the tungsten lattice.

The results obtained from interpreting the X-ray photograph are given in Table 2.

By the assymmetrical backing of the film and extrapolation to 90° values for the lattice parameter $a = 4.910 \pm 0.005$ Å and for the X-ray diffraction density of the new phase $d = 16.2$ g/cm^2 were obtained.

In this way the existence of the silicide with the composition of W_3Si was proved and its lattice parameter was determined.

Translated by J. Murray

Fig. 3. X-ray photograph obtained using copper radiation from a specimen after the removal of the upper layers. The lines of the W_3Si phase (200), (400) of the tungsten are visible.

REFERENCES

1. *J. of the Electrochemical Soc.* 104, 8, 521 (1957).
2. V.G. Samsonov and Ia.S. Umanskii *Tverdyye soyedineniya tugoplavkikh metallov, Metallurgizdat, (Solid compounds of high-melting metals)* (1957).
3. A.S. Berezhnoi, *Kremnii i ego binarnyye sistemy (Silicon and its binary systems)*, p.28, 172 (1958).

THE FINE STRUCTURE OF THE INTERCRYSTALLINE TRANSITION ZONES OF MILD STEEL*

B.S. KASATKIN and G.F. DAROVSKII

Inst. Electric Welding i/n Ye.O. Paton,
Academy of Sciences, Ukr.S.S.R.

(Received 31 March 1959)

In much earlier work a hypothesis was set forth concerning the amorphous nature of intercrystalline zones. The hypothesis however, met with great disapproval as it was not in agreement with many of the physical properties exhibited by polycrystalline metals. Later another hypothesis was put forth concerning the existence of a transition zone between neighbouring crystals of differing orientation; in this zone were atomic planes with a gradually increasing change from the orientation of the first crystal, to that of the neighbouring crystal [1].

In recent years a proposition was put forward and developed in a number of works abroad, concerning the dislocation structure of the intercrystalline zones [1, 2].

A dislocation model may be fairly easily constructed for low angle (less than 15°) boundaries. However, difficulties are encountered in the construction of a dislocation model for boundaries in which there are large misorientations between the crystals. For this type of boundary the "island" model has been suggested, which in schematic form is represented by alternating sectors of good and bad fit in the boundary zone between crystals [1].

A more universal model for intercrystalline boundaries been suggested by [3]. This model, based on the principle of a two-dimension vernier, may be used for all degrees of misorientation between crystals. In this model, intercrystalline linkage is characterized by the lack of a sharply defined surface separating the crystals, the multi-atom depth of the transition zone and the difference in the distribution of atoms in it compared to the correct crystal lattice. The linkage of lattices is based on the assumption of the existence of a skeleton consisting of coherent fields in the intervals between which there is a gradually increasing loss of cohesion. The greatest disregistry of the crystal order of distribution of the atoms occurs in regions of the transition zone halfway between neighbouring skeleton series.

From these islands of order there proceeds a gradually increasing irregularity in the arrangement of the atoms, both in the direction normal to the boundaries of each of the crystals, and along the boundaries of each of the neighbouring skeleton series.

The intercrystalline zone model proposed by Arkharov has, as the writer observes, been but poorly tested in experiments and remains to a large extent hypothetical. In the light of this, the experimental investigations of the fine structure of intercrystalline transition zones are of great interest.

This paper describes the attempt to carry out these investigations with the aid of an electron microscope. The tests were carried out on test pieces of hot rolled mild steel after hot forging and annealing (heating to 1100°, holding 3 hr followed by slow cooling in the furnace).

Microspecimens were prepared by electrolytic polishing and etching, as described in [4]. Electron microscope examination was carried out be means of collodion films shadowed with chromium, and carbon films. The advantage of the latter consists in the fact that a sufficiently contrasty representation of the fine

* *Fiz. metal. metalloved.*, 8, No.6, 881-884, 1959.

VOL
8
195

structure is possible without additional tinting. This is very important for studying the peculiarities of the fine crystalline structure at high magnifications.

1. Electron micrograph of the fine structure of twin-oriented ferrite grains, and the transition zone between them. Colloidal film, chrome shading; X 13,500.

Fig. 1 shows an electron micrograph of two adjacent grains and the transition zone between them. One deduces from the relative orientations of the blocks, that the grains are twins. Due to the very small misorientation of the grains, the transition zone between them is the minimum possible depth and very low in contrast. However, a close examination reveals that the blocks are slightly finer in the transition zones than in the linking grains.

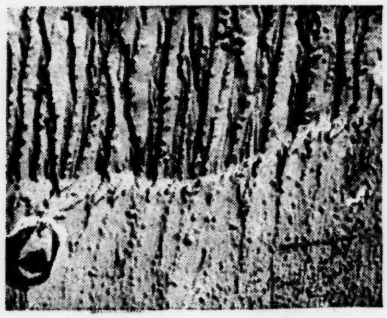

Fig. 2. Electron micrograph of the fine structure of ferrite grains having small relative misorientations, and the transition zone between them. Carbon film; x 18,000.

Fig. 2 shows the transition zone between grains with a fairly slight difference in orientation. The depth of the zone varies from 0.08 to 0.16 microns. The grains consist of laminar blocks whose boundaries are represented by chains of etch pits. These etch pits appear to correspond to the terminal points of dislocations [5]. The intergranular transition zone also has a block structure with boundaries consisting of a series of etch pits. However, the etching propensities of the transition zone are less, and the etch pits show less contrast; there is a somewhat greater regularity of the series of points than is the case in the grains. The boundary sections of the intergranular transition zone are eroded as a result of the "wedging" of grain blocks in the block structure of the zone. Fig. 3 shows a similar picture.

3. Electron micrograph of the fine structure of ferrite grains and the transition zone between them. Carbon film; X 7200.

Fig. 4 shows an electron micrograph of the fine crystalline structure of a fairly wide (about 0.8 microns) transition zone between two differently oriented grains. In one of the grains, there is, besides the blocks, a network of sub-grain boundaries [6]. The etching propensities of the zone are slightly different from the grains, but the peculiarities of its block structure are visible quite clearly. In the narrow etched out zone of transition from the grain to the inter-granular zone, the nature of the block structure becomes gradually the same as the block structure of the grain. It may be seen that the frequency of the nets of series of etch pits increases with distance from the grain

into the transition zone. The maximum density of distribution of the etch pits and the fine blocks is to be found halfway through the transition zone. Attention should now be turned to the "boundaries" of the sub-grains,

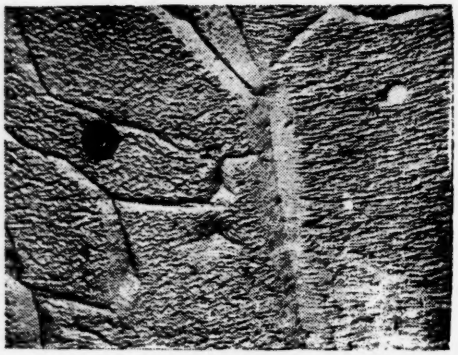

Fig. 4. Electron micrograph of the fine structure of ferrite grains of considerable misorientation, and the transition zone between them. In one of the grains there is a network of sub-boundaries. Carbon film X6750.

which are also transition zones, very similar in their fine structure to the intergranular transition zones.

Fig. 5. Electron micrograph of the fine structure of ferrite grains having different misorientations, and the transition zones between them. The arrows indicate the intergranular transition zones. Carbon film; X7200.

Fig. 5 shows the fine structure of sectors of some adjacent grains and the transition zones between them. The transition zone between the grains *1-2* is very narrow which fact evidently must be related to a twin orientation of the block structure of these grains.

The depth of the transition zone between grains *2-3* is about 0.5 microns. This zone has a fairly fine block structure with highly complex orientation.

The electron microscope examinations described are, in our opinion, to a very large extent in agreement with the model of a semi-regular intercrystalline transition zone proposed by Arkharov, and enable certain details of this model to be clarified.

The semi-regular fine structure of the intercrystalline transition zone in mild steel is formed of blocks. The existence of blocks within the grains themselves, and bounded by a series of dislocations, offers very favourable conditions for the formation of the block structure of the transition zone and the fused crystalline linkage of this zone with the grains.

As regards the model of the semi-regular intercrystalline transition zone itself, the blocks appear as an area of regular structure while the boundaries of the blocks are layers of deformed structure. The dislocation and the network density of dislocated series grow with the distance into the transition zone from the grain. As proposed by the model, the greatest disruption of the crystal order or atom arrangement is observed in sectors halfway through the transition zone. The depth of the transition zone and the increased density of the networks of dislocation series are determined by the relative orientations of the crystals. The greater the misorientation of linked grains, the wider will be the intergranular transition zone and the greater the difference in the size of the blocks and the density of dislocation between the periferal and central sectors of the zone.

As formation of intercrystalline transition zone occurs at high temperatures and is, apparently, accompanied by plastic deformation [5, 6], it may be suggested that the fine structure of this zone is further complicated (distorted) by the process of polygon formation which occurs fairly intensively at high temperatures.

Translated by V. Alford

REFERENCES

1. D. McLean, *Grain boundaries in metals*, London

(1957).

2. A.Kh. Kotrell, *Dislokatsiya i plasticheskoye techeniye v kristallakh (Dislocation and plastic flow in crystals)* Metallurgizdat (1958).
3. V.I. Arkharov, *Trud. instituta fizika metallov UFAN, SSSR, Izd. Akad. Nauk SSSR*, 16, 7 (1955).
4. B.S. Kasatkin, *Zav lab.*, No.7, 842 (1958).
5. N.P. Allen, *J. of the Iron & Steel Inst.*, 191, 1 (1959).
6. P. Samuel and A.G. Quarrell, *J. of the Iron Steel Inst.*, 182, 20 (1956).

VOL.
8
1959

THE FORMATION OF A CUBIC TEXTURE IN FERRO-SILICON ALLOYS*

CHOU P'EN HSIN, WANG WEI MING, CHENG NEN HUANG

Institute of Applied Physics, Chinese Academy of Sciences, Peking

(Received 15 August 1959)

Silicon sheet steel with oriented grains is widely used in the electrical industry; it has a texture of type (110) [001], that is, in most of the grains the planes (110) are parallel to the rolling plane and the directions [001] are parallel to the direction of rolling (Fig. 1, *a*). As [001] is the direction of easiest magnetization in the monocrystals of silicon iron magnetic permeability will increase as the texture increases in perfection, the loss in the core will be reduced.

In the last 25 years much research has been devoted to the question of the formation of this type of texture in silicon iron. At the same time there has been the hope of achieving a cubic texture of type (100)[00$\bar{1}$] in this kind of material Fig. 1, *b*). In material with this type of cubic texture it is the direction of rolling and the transverse direction which are those of easiest magnetization. The magnetic properties of this kind of cubic-textured transformer sheet steel are without doubt better in many respects than those of steel with a (110) [001] texture.

The formation of the kind of cubic texture described above is referred to in ferrosilicon alloys by, for instance, Sixtus [1] and Gol'dmann and Druzhinyi [2]. However, a highly perfect cubic texture, such as is found in most face-centred cubic metals, is but seldom achieved in silicon iron [3-5]. Experimental results show [4] that a transformer made out of sheets with a cubic texture, has a considerably lower energy of loss at all inductions, while at 17,000 c/s the losses are around 60% of those of a transformer made of steel with the usual

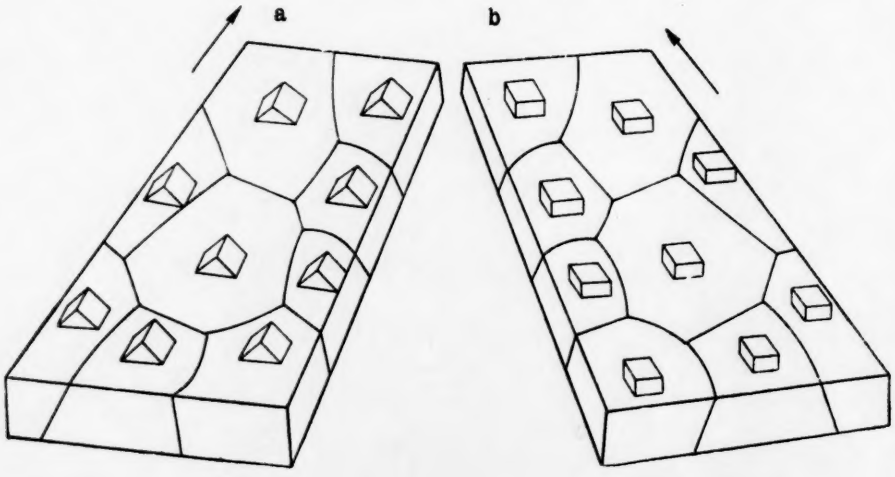

Fig. 1. *a* – diagram of texture (110) [001] in silicon iron;
b – diagram of texture (100) [001] in silicon iron.

* *Fiz. metal. metalloved*, 8, No. 6, 885-891, 1959.

texture (110)[00$\bar{1}$]. It is obvious from this that this new direction of development of magnetic materials will have considerable importance for the electrical industry.

In this report some of the results are described of our research into the formation of the cubic texture in ferrosilicon alloys containing 3.25% Si. It was found that in this alloy, it was possible to achieve a cubic texture either by a process of secondary recrystallization or simply by primary recrystallization. Furthermore, it was clear that there may, in silicon iron, be a partially cubic texture from cold rolling, if preliminary rolling has been in the direction [00$\bar{1}$] and the plane of rolling was not too different from plane (100). After annealing the recrystallization grains had for the most part the orientation (100) [00$\bar{1}$]. This observation is in agreement with published works of Chen and Maddin "The texture of cold rolling and annealing of molybdenum monocrystals" [6] and Walter and Hibbard "The Texture of Cold-Rolled and Recrystallized crystals of Silicon Iron" [7].

VOL. 8 1959

THE EXPERIMENTS AND THEIR RESULTS

The ferrosilicon alloy with 3.25% Si was produced in an electric arc furnace. It was oxidized and held in a vacuum during pouring. The ingots were rolled in the hot state to the required thickness and then annealed at a temperature of 850°. Different variations of cold rolling and intermediate annealing were tried out. Final annealing was carried out in an alundum tubular furnace under a vacuum of 10^{-4} mm, Hg col. The textures were analysed by X-ray diffraction, from the construction of the pole figures. For coarse-grained samples the Laue method of reverse reflexion was used for the determination of the orientation of individual grains.

Secondary Recrystallization. With one system of cold rolling and annealing (system *A*) secondary recrystallization in the test piece could be obtained on final high temperature annealing. Fig. 2*a* shows a photomicrograph which demonstrates the external form of the piece after the commencement of secondary recrystallization. In the photomicrograph the white sectors represent secondarily recrystal-

Fig. 2*a*. Diagram of sheet silicon iron on secondary recrystallization.

Fig. 2*b*. Etching figures of the cubic faces of silicon iron.

Fig. 3. Orientation of 32 secondary grains in silicon iron, pole figure (100).

lized grains which have cubic orientation, while the dark sectors represent primarily recrystallized grains. (Etching was carried out in a 25% solution of HNO_3). In Fig. 2b it can be seen that in the grains with cubic orientation, the etching figures are of a typically square shape which corresponds to the sides of a cube. (Etching agent: $FeSo_4$ – 100 gs., concentrated H_2SO_4 – 10 cc., dissolved in 1 l. H_2O). Using the Laue method, the orientation of thirty-two of the large grains was determined, after secondary recrystallization. These orientations are plotted in Fig. 3. The pole figure obtained in this way clearly shows a well-defined cubic texture in the test piece after secondary recrystallization. The dispersion in the orientation of planes (100) is approximately ± 5° while in direction [001] it is around ± 15° This result is similar to that

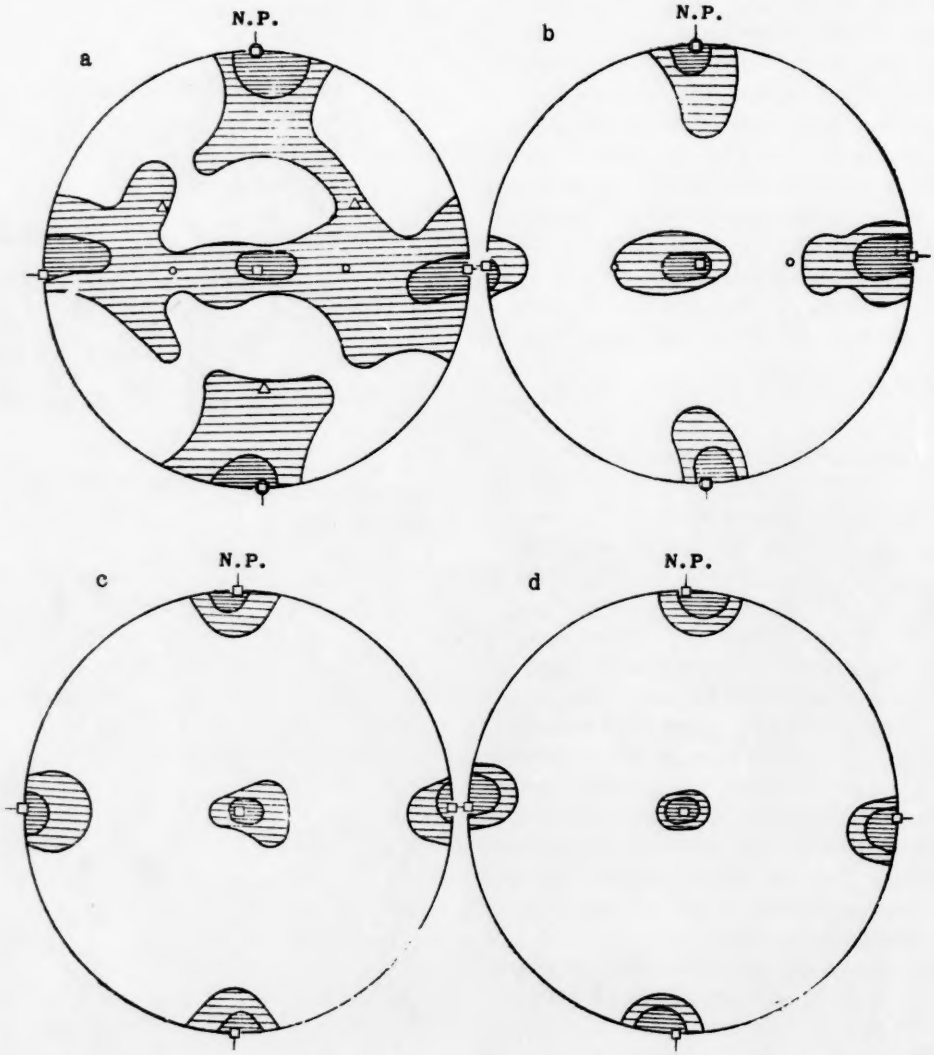

Fig. 4. Pole figures (100), showing the development of the cubic texture on primary recrystallization in silicon iron at increasing temperatures for the final annealing; *a* – immediately after complete recrystallization; *b-d* – increasing annealing temperatures
□ – (100) [001]; ○ – (110)[001]; △ – (111)[112].

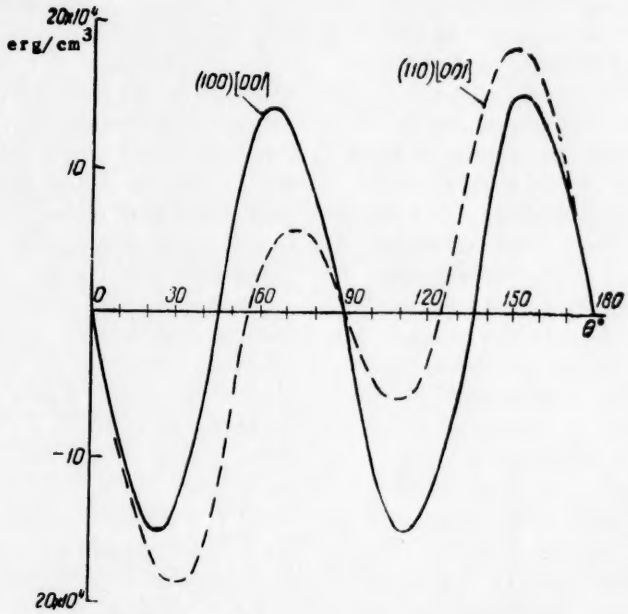

Fig. 5. Curve of magnetic torque of test piece with cubic texture (solid line) and with texture (110) [001] (dotted line).

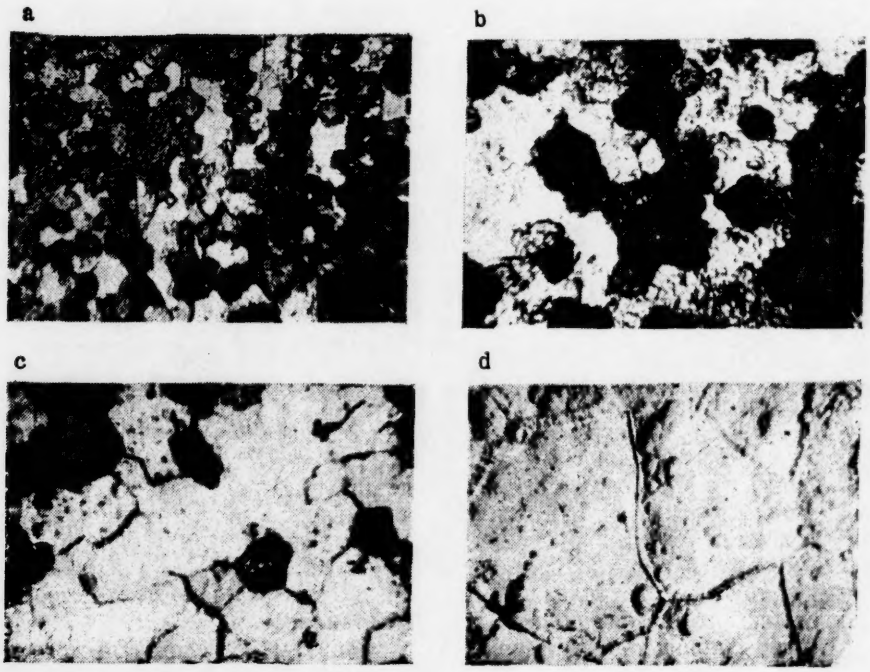

6*a-d*. Photomicrographs showing the development of the cubic texture in silicon iron in stages corresponding to those shown in Fig. 4*a-d*.

VOL.
8
1959

achieved by previous research workers [3-5].

Primary Recrystallization. It has already been noticed that it is possible to achieve a cubic texture in the monocrystals of molybdenum [6] and of silicon iron [7] after primary recrystallization. The same mechanism has been found to take place in the present research programme, where the starting material is a polycrystalline silicon iron. This is illustrated by Figs. 4*a-d*. First of all the prescribed test piece was rolled in the cold state and annealed according to the second system (system *B*). On completion of cold rolling the cubic texture of cold rolling was already observed on the pole figures. After final annealing at a low temperature a recrystallized cubic texture was obtained as the main component of the texture (Fig. 4*a*). Other weak components of the texture were (110)[001] and (111)[113], which were also recrystallization textures. When the temperature of the final annealing was increased (Fig. 4*b*), texture (111)[113] disappeared first, while texture (110)[001] still remained. With further increase of the final annealing temperature (Figs. 4*c* and *d*), texture (110) [001] became appreciably weaker and texture (100) [001] correspondingly stronger. The degree of preferred orientation of the grains was measured by the rotating magnetic pendulum. The number of (100) [001] orientations counted by this method was around 90% The experimental curve is shown in Fig. 5.

Deep etching is used for the metallographic detection of the various types of annealing texture in the process of the development of the cubic texture of the sample, in accordance with the conditions shown in Figs. 4*a-d*. Figs. 6*a-d* show a series of photomicrographs of these samples. Here again, the cubic orientations of the grain are clearly visible after etching, while the grains with orientation (110) [001] are quite dark. It may be seen from Fig. 6*a* that a fairly large number of cubically orientated grains have already formed at a low temperature of recrystallization. After this there is a growth of grains of all orientations, but that of the cubically orientated grains is greatest. The increased cubic texture at very high temperatures of annealing is, therefore, the result of ordinary grain growth. This distinguishes it from the secondary recrystallization described above.

CONCLUSIONS

1. The fact that a cubic texture may be obtained in silicon iron by either primary or secondary recrystallization is remarkable for two reasons. Firstly, it indicates that there is a broad and general basic principle behind the production of high grade transformer sheet steel with a cubic texture. Transverse rolling is not necessary for the production of this steel, nor is rolling with special compression or any other specific process. Secondly it indicates that the changeable "cubic texture" which is obtainable in many face-centred metals and alloys, is not a property existing only where there is a face-centred cubic lattice. A cubic texture in a body-centred lattice, besides being a practical possibility which would improve the magnetic properties, is a subject of great scientific interest.

2. It has been observed that the formation of a cubic texture by secondary recrystallization does not include the formation of nuclei. Nuclei with orientation (100) [001] already exist after primary recrystallization and are in most cases surrounded by grains with orientation (110)[001]. There is a pronounced and accelerated growth of the cubically oriented grains, while the normal growth of other primary grains is limited. The process, therefore, which is conventionally referred to as "secondary recrystallization" is not in fact a "recrystallization" process in its true meaning. In the case under review the secondary recrystallization may be regarded simply as a process of increased grain growth.

3. The conditions which determine the formation of a cubic texture on primary recrystallization with cold-rolling and annealing of polycrystalline silicon iron, are the same as those already described for monocrystals [6, 7]. A sharply defined cubic texture is already present under cold rolling conditions, then, with a low-temperature annealing, the cubic texture of annealing is obtained. This is the process of so-called "recrystallization in the moment of formation", which has been widely studied in aluminium and other metals.

The writers wish to extend their thanks to collaborators in the Iron and Steel Research Institute for providing the ferro-silicon

VOL 8 195

alloy used in these investigations.

Translated by V. Alford

REFERENCES

1. K. Sixtus, *Physics*, 6, 105 (1935).
2. A. A. Gol'dman and V. V. Druzhinin, *Sborn. posvyashch. akad. A.F. Ioffe (Symposium dedicated to the 70-year old Academician A.F. Ioffe*, 455 (1950).
3. F. Assmus, R. Boll, D. Ganz and F. Pfeifer, *Zs. Metallk.* 48, (6), 341 (1947).
4. J.L. Walter, W.R. Hibbard, H.C. Fiedler, H.E. Grenoble, R.H. Pry and P.G. Frischmann, *J. Appl. Phys.* 363 (1958).
5. G. Wiener, P.A. Albert, R.H. Trapp and M.F.J. Littmann, *J. Appl. Phys.*, 366 (1958).
6. N.K. Chen and R. Maddin, *J. of Metals*, 300 (1953).
7. J.L. Walter and W.R. Hibbard, *J. of Metals*, 1352; Fall Meeting Report, 44 (1957).

VOL.
8
1959

THE COMPONENTS OF SPECIFIC LOSS AND MAGNETIC PERMEABILITY OF DYNAMO STEELS ALLOYED WITH PHOSPHORUS*

S.I. DOROSHEK and V.V. DRUZHININ

Urals Ferrous Metals Research Institute/Verkh-Isetsk Metal Works

(Received 17 June 1959)

In the hot-rolled dynamo steels produced in this country according to GOST 802-58 (E11, E12, E13, E21 and E22), the main component of specific loss is hysteresis loss: at a point $P_{10/50}$ these losses amount to 1.6-2.2 w/kg at overall losses of 2.1-3.0 W/kg; loss from eddy currents is about 0.5-0.8 W/kg. Calculating the loss due to eddy currents by the formula known and used in paper [1], for a sheet thickness of 0.5 mm and specific electrical resistance of 0.35-0.24 ohms/mm^2/m, the resulting figure for $P_{e.o}$ is 0.4-0.5 W/kg. The difference between the actual P_e and the calculated $P_{e.o}$ losses on eddy currents, which is known as additional loss, is 5-10% for dynamo steel (it is about 50% for transformer steel E43). With coarser grain there is usually an increase in additional loss [2] but at the same time there is a sharp fall in hysteresis loss. As, therefore, when dynamo steels are heated to temperatures exceeding 950-1000°, grain refining occurs in some cases (as a result of phase recrystallization), while in others the grain becomes coarser (as a result of collective recrystallization), positive results are not always achieved by raising the temperature of annealing of dynamo steels for the purpose of improving their quality.

Meanwhile, it is well known that specific losses may be considerably reduced if dynamo steel is alloyed with phosphorus, which increases grain size and electrical resistance and thins out the gamma field, making possible the effective use of high-temperature treatment [3].

We have studied the components of loss of dynamo steel alloyed with up to 0.36% and having various grain sizes. The investigations were carried out on sheets 0.5 mm thick, produced by forging and hot rolling (according to the production process used in the Verkh-Isetsk Works) ingots weighing 35 kgs, which were produced from induction furnaces.

The Si content of the sheets was 1.8%, C was 0.03%. Other additions (Mn, Cr, S) did not exceed the limits accepted for industrial dynamo steels. The P content varied between 0.03 and 0.36%.

Strips of steel 250 x 30 x 0.5 mm., in packs, were annealed in a vacuum (residual pressure 10^{-1} mm Hg) at temperatures of 850, 950, 1050 and 1150° for 4 hr and then allowed to cool together with the furnace.

The following results were obtained from magnetic tests carried out on these samples.

In the steel which was not alloyed with phosphorus (P = 0.03%), there was coarsening of the grain at higher temperatures and a noticeable reduction in hysteresis loss (Table 1). Parallel with a certain reduction of specific electrical resistance, which appears to be caused by the partial removal from the solid solution of elements which possess electrical resistance (Si, C, Mn), there is an increase in calculated loss due to eddy currents (from 0.36 to 0.44 W/kg) and, because of the grain coarsening, there is a noticeable increase in additional losses (from 0.17-0.51 W/kgs).

When phosphorus is added to the steel a considerable coarsening of the grain is observed, which leads to reduction of the hysteresis loss. Table 2 gives figures for the components

* *Fiz. metal. metalloved.* 8, No.6, 892-895, 1959.

TABLE 1

Effect of annealing temperature on grain size, specific electric resistance and losses in dynamo steel without phosphorus

Annealing temperature °C	No. of grains per mm²	Specific resistance ohm. mm²/m	$P_{10/50}$ W/Kgs			
			P_{total}	P_h	P_e	P_a
850	200	0.38	2.20	1.67	0.36	0.17
950	150	0.38	2.03	1.55	0.36	0.12
1150	30	0.30	2.05	1.10	0.44	0.51

of loss, grain size and specific electrical resistance of dynamo steels with varying P contents, all annealed at 850°. It can be seen from the Table that, when the P content is increased to 0.36%, the grain size increases 6 times while hysteresis loss at point $P_{10/50}$ is reduced from 1.67 to 1.04 W/kg. This very considerable reduction in hysteresis loss is due to the reduction in coercive force (Fig. 1). The small reduction in losses due to eddy currents is brought about by a certain increase in the specific electrical resistance under the influence of the phosphorus.

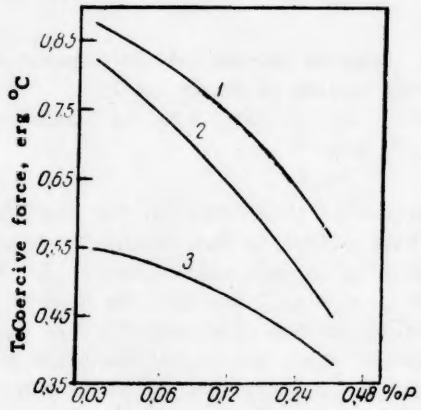

Fig. 1. Effect of phosphorus and annealing temperature on the coercitive force of dynamo steel: *1* - 850°; *2* - 950°; *3* - 1150°.

It is interesting to note that, despite the sharp increase in grain size (from 200 to 35 grains/mm²), the increase of additional losses is quite low (from 0.17 to 0.25 W/kgs). Such a phenomenon cannot be explained by increased resistance alone. It is also difficult to suggest that the phosphorus has a similar influence on additional losses, causing separation of the dispersoids, as that which has been observed from carbon [4] in steel (even at room temperature phosphorus dissolves, up to about 1.2%, in α iron) [5]. It appears that the phosphorus influences additional losses, not only via the grain, but also because of its immediate effect on the nature of the ferromagnetism and the structure.

The beneficial effect of the phosphorus on additional losses is particularly perceptible

TABLE 2

Effect of phosphorus on the components of specific loss and on specific electric resistance and grain size

P content	No. of grains per mm²	Specific resistance ohm. mm²/m	$P_{10/50}$, W/Kgs			
			P_{total}	P_h	P_e	P_a
0.03	200	0.380	2.20	1.67	0.36	0.17
0.06	160	0.375	2.07	1.52	0.36	0.19
0.12	120	0.385	1.91	1.37	0.34	0.20
0.36	35	0.420	1.61	1.04	0.32	0.25

if its influence on grain characteristics is excluded, that is, at constant grain size.

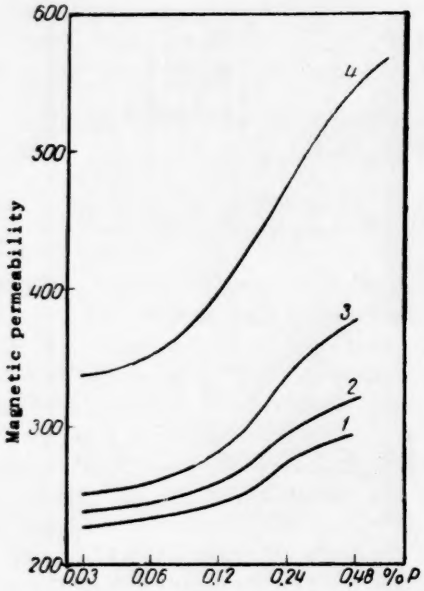

Fig. 2. Effect of phosphorus on the initial magnetic permeability at various annealing temperature *1* - 850°; *2* - 950°; 4 hr; *3* - 1050°, 4 hr; *4* - 1150°, 4 hr.

Table 3 gives the changes in the components of specific loss with various amounts of phosphorus and a practically constant grain size (10-15 grains/mm^2), with high temperature (1150°, 4 hr) annealing. It will be seen from the table that, with increasing P content and constant grain size, there is a reduction in additional losses.

A comparison of the figures in Tables 2 and 3 shows that phosphorus has in istelf a restraining influence on the change of additional losses due to grain size.

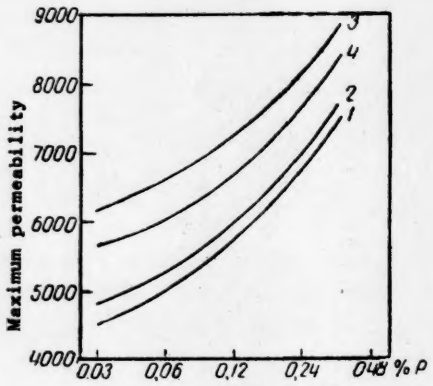

Fig. 3. Relation between maximum permeability and phosphorus content of dynamo steel; *1* - 850°, 4 hr, 2- 950°, 4 hr; *3* - 1050°, 4 hr; *4* - 1150°, 4 hr.

Additions of phosphorus to the steel have a beneficial effect in increasing the magnetic permeability in weak and medium fields, as may be seen from Figs. 2 and 3. The highest figures for maximum permeability are reached at a rather lower annealing temperature (1050°) than the highest figures for initial magnetic permeability (1150°).

A similar phenomenon is not infrequently observed in a 4% - Si steel [6-8] and is, apparently, due to the same causes as those which lead to reduction of permeability in the strong fields of coarse grained transformer steel [9].

TABLE 3

Effect of phosphorus on the components of specific loss, on specific electric resistance and grain size, with high temperature vacuum annealing

($T_{ann.}$ = 1150° 4 hrs.)

P content	No. of grains per mm^2	Specific resistance ohm. mm^2/m	$P_{10/50}$, W/Kgs			
			P_{total}	P_h	P_e	P_a
0.06	15	0.310	1.96	1.03	0.50	0.43
0.12	10	0.320	1.82	0.96	0.47	0.42
0.36	10	0.370	1.46	0.74	0.36	0.36

CONCLUSIONS

1. Small additions of phosphorus to dynamo steel lead to:

a) reduction in hysteresis loss due to grain growth;

b) reduction in loss from eddy currents due to increased specific resistance.

2. In coarse grained dynamo steel (10-20 grains/mm^2) increased phosphorus content leads to a marked reduction in additional losses.

3. Under the influence of phosphorus the levels of initial and maximum permeability are higher.

Translated by V. Alford

REFERENCES

1. K.A. Krug, *Osnovy elektrotekhniki (Principles of electrotechnics,* United Scientific and Technical Press, Peoples Commissariat of Heavy Industry, 2, 244 (1938).
2. V.V. Druzhinin and R.I. Yanus, *Zh. teor. fiz.* 6, 641 (1947).
3. S.I. Doroshek, *Tekh.-ekonom. byulleten' Sverdlovsk. sovnarkhoz,* No.4 (1959).
4. V.V. Druzhinin, Yu.P. Burdakova and V.A. Koroleva *Fiz. metal. metalloved.* 1, 75 (1955).
5. E. Gudremon, *Uchenie o spetsial' nykh stalyakh (Information on special steels)* United Scientific and Technical Press, Peoples Commissariat of Heavy Industry, pp.512 (1937).
6. A.S. Zaimovskiy, *Myakgie magnetnye materialy (Soft magnetic materials)* Moscow. Leningrad, Gosenergoizdat, p.38 (1941).
7. V.V. Druzhinin and V.A. Koroleva, *Trud. sektsii metalloved. i termich. obrabotka metallov (Proceedings of the Section of Metallography and Heat Treatment),* No.1, p.102 (1958).
8. N.I. Lapkin and G.A. Zykov, *Byulleten' UNIIChM,* No.3 (1957).
9. K.B. Vlasov, *Fiz. metal. metalloved.* 1, 70 (1955).

VOL. 8 1959

ON THE NATURE OF THE STRAIN HARDENING WHICH OCCURS WHEN QUENCH HARDENED HIGH-SPEED STEEL IS TEMPERED*

P.M. YUSHKEVICH

Ukrainian Pipe Research Institute

(Received 4 May 1959)

It has been shown in papers [1-4] that secondary hardness occurs as a result of secondary martensitic transformation. However, in paper [5] the opinion has been expressed that secondary hardness is not only the result of the transformation of residual austenite and martensite, but also of the dispersion hardening of the martensite and residual austenite. In paper [6] it has again been shown that secondary hardness is the result of the breakup of the martensite with the immediate formation of finely dispersed special carbides and the transformation of the cementite carbides into special carbides.

There are currently, therefore, two points of view on the nature of secondary hardness.

The work here presented was undertaken with a view to clearing up the nature of the secondary hardness and red hardness of high speed steel, and getting a more precise idea of the temperature ranges of carbide transformation, and of studying transformations in the fine crystalline structure of the α and γ-phases.

Three types of high speed steel were selected for these investigations: R18, 150R18 and EI184, the chemical compositions of which are set out in Table 1.

The test pieces were quenched in oil with transfer to iced water with austenitization temperatures of 190° for steel R18, 1200° for 150R18 and 1240° for EI184. Tempering was carried out in a vacuum furnace.

Measurement of the parameters of the crystal lattices, fields of coherent dispersion (blocks), distortion of the II and III type, was carried out on round test pieces 1 mm in diameter and flat pieces 4 x 8 x 20 mm in size respectively, in a powder chamber 149 mm across and on an ionization apparatus URS-501 in iron radiation.

Measurement of the size of the blocks and of distortion of the II type was made on the (110) and (211) reflections α phase, and (111) and (311) of the γ phase, in accordance with the method described in papers [10,11] in conditions in which the distribution of

TABLE 1

Mark of steel	Chemical composition, %							
	C	Cr	W	V	Mn	Si	S	P
P18	0.73	4.2	18.9	1.2	0.28	0.16	0.011	0.030
150P18+	1.50	4.3	18.0	1.6	0.26	0.15	0.010	0.027
184	0.87	7.5	4.9	1.2	0.32	0.17	0.016	0.025

+ Experimental

* *Fiz.metal.metalloved.* No.8, No.6, 896-903, 1959.

intensity was defined as a gaussien function.

The lattice parameters and the amount of residual austenite were checked both on the (110) and (111), (211) and (311) reflections.

THE RESULTS AND EVALUATION OF THE INVESTIGATIONS

Steel R18. In the annealed state the steel consists of 67% martensite, 18% austenite and 15% carbides. The extent of II type distortion and the size of the blocks were measured on the test pieces in the temperature range 300-760° at holding times of: 4 hr at temperatures above 540° and 8 hr in the range 300-540°, with the aim of approximating the α-hard solution to the metastable "rigid" state.

As can be seen from Fig. 1, in the range 640-760°, distortion of the II type changes parallel with hardness, which confirms the conclusions to papers [12-14]. Exceptions to this rule discovered between the two maxima (400-520° and 560-640°) may be explained by superimposing the effects of concentration heterogeneity and tetragonality, which are not allowed for in the method set out in papers [10, 11]. In this work an attempt has been made to make a qualitative evaluation of these effects.

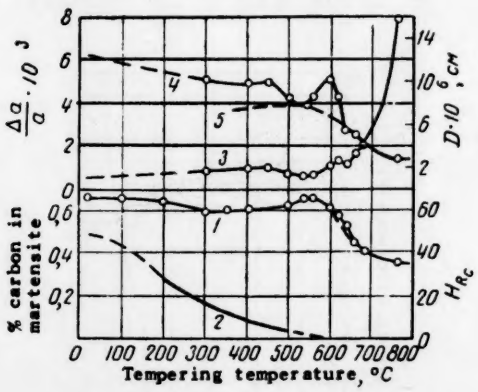

Fig. 1. Relation between hardness (curve 1), quantity of carbon (curve 2) in martensite [7], size of blocks (curve 3), summated distortions $\Delta a/a$ (curve 4) and type II distortions (curve 5), and temperature of tempering for steel R18.

From Fig. 1 it follows that the carbon content of the martensite [7] is steadily reduced as the tempering temperature increases, until about 540-560°, where it reaches the equilibrium state in the α phase. From this it may be anticipated that the expansion of the interference lines due to tetragonality, will also be steadily reduced until, in the range 520-560° it reaches an almost zero value. Furthermore it is well known that there is a steady reduction in II type distortion with increasing tempering temperatures for quench-hardened steels.

Proceeding from these figures it may be proposed that every deviation of curves $\Delta a/a$ from a steady course may be attributed to concentration heterogeneity of the α-hard solution.

In the 520-560° range, where $\Delta a/a$ has its minimum value, when the martensite breaks up into a ferritic-carbide mixture, $\Delta a/a$ is attributable, in the main, to distortion of the II type. This is confirmed by that distortion $\Delta a/a$ in the α phase and residual austenite, having passed through dispersion hardening on the steel reaching maximum hardness, now remain the same, $4.0\text{-}4.5 \times 10^3$ (See Fig. 4), which is only possible if no concentration heterogeneity is present in the α solution. A second confirmation of the accuracy of this view is given by the fact that, if the graph in Fig. 1 is reconstructed in the graph $\Delta a/a = (H_{R_C})$, the straight section corresponding to the temperature range 640-670° is extrapolated in the range 520-560°. From this, the emergence of maxima on the curve $\Delta a/a$ may be accounted for by the superimposing of distortions $\Delta a/a$, which are determined by the concentration heterogeneity (sectors between curves 4 and 5) on distortions of the II type (dotted curve 5).

When the tempering temperature is increased from 380 to 450°, with a slight increase in growth of the blocks of martensite, the concentration heterogeneity become noticeably greater. This is apparently due to the transfer of cementite type carbides, which are the poorest alloying elements and the greatest dispersing ones, to the chromium carbides. This bears out the findings in papers [8, 9] in which the possibility of the formation of cementite type carbides is pointed out, and their transformation, in the 400-450° range, into chromium carbides. The concentration

heterogeneity of tempered martensite, which increases with transfer of cementite carbides to chromium carbides, may be determined by irregular distribution of chromium and carbon in the martensite.

The reduction in $\Delta a/a$ which occurs above 450° is evidence of the levelling out of concentration heterogeneity in tempered martensite. The fact that this reduction is accompanied by an increase in hardness (Fig. 1) shows that concentration heterogeneity does not effect the strain hardening of the steel on dispersion hardening. This is particularly obvious in the 520-560° range, when concentration heterogeneity is practically non-existent, while the hardness of the steel reaches its maximum.

Concentration heterogeneity of the α solution in the 560-640° range is accompanied not only by a fall in hardness, but also by marked growth of the blocks and relaxation of II type distortion (dotted curve 4), and could be explained by the transformation in the 380--520° range, of the remaining undissolved cementite carbides, richer in alloying elements, into carbides of vanadium and tungsten with consequent coalescence. The reduction in concentration heterogeneity above 600° occurs, apparently, at the same time as the coalecence of the carbides of vanadium and tungsten. The growth of the α phase blocks and the reduction of type II distortion are determined by the coalescence of the carbides.

Between 620 and 650° there is a marked brake-up of the blocks, and a halt in the loss of hardness and type II distortion. According to the findings in paper [9], there is in this range an intensive enrichment of the carbides of vanadium and tungsten with vanadium and tungsten respectively, which may lead to a considerable change in their specific volume and, as a result, to break-up of the blocks and growth of II type distortion and hardness (See Fig. 1).

From a study of the kinetics of the softening of steel R18 the energy of activation has been calculated according to the rate of growth of the α phase blocks (Fig. 2). Up to 620° it comes to 60 kcal/mol, while above 650° it is 80 kcal/mol. This shows that, up to 620° it is the diffusion processes of the solution of cementite type carbides and the coalescence of chromium carbides, which act as checks in the growth of α phase blocks, while above 650° it is the coalescence of the vanadium and tungsten carbides. This is because the chemical affinity between the atoms of chromium and carbon is less than that between those of vanadium or tungsten and carbon, so that the coalescence of chromium carbides and the growth of α phase blocks will take place with greater intensity up to 620° than will the coalescence of vanadium and tungsten carbides and the growth of α phase blocks at 650°. This explanation fits in both with the figures obtained for the energy of activation, and with those for the rate of growth of the α phase blocks below 620° and over 650° (Fig. 2).

To make a more detailed analysis of the processes which occur on tempering, the system widely used in industry, of repeated tempering at 560° was also studied. It can be seen from Fig. 3 that at 560° there is in the course of ten seconds, a loss of hardness from 63 to 60 units, similar to that which occurs at 350° (see Fig. 1). At the same time there is a sharp diffusion-less increase in the lattice parameter of the residual austenite, from 3,608 to 3,635 Å, amalgamation of the martensite with carbon from 0.47 to 0.31% (this may be seen from the width of line (110), and relaxation of the II type distortion in the martensite. When the residual austenite is discharged in this way, plastic deformation occurs and is expressed by the brake-up of the

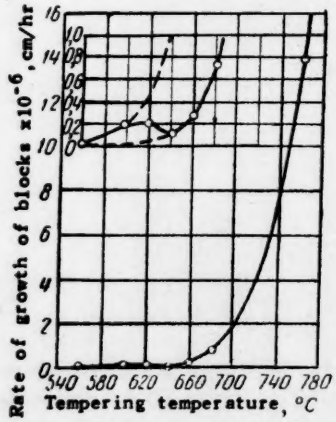

Fig. 2. Relation between the rate of growth of α phase blocks and tempering temperature (initial state of test pieces – thrice repeated tempering at 540°).

blocks. The impoverishment of the martensite for this short time suggests the formation of carbides of the cementite type.

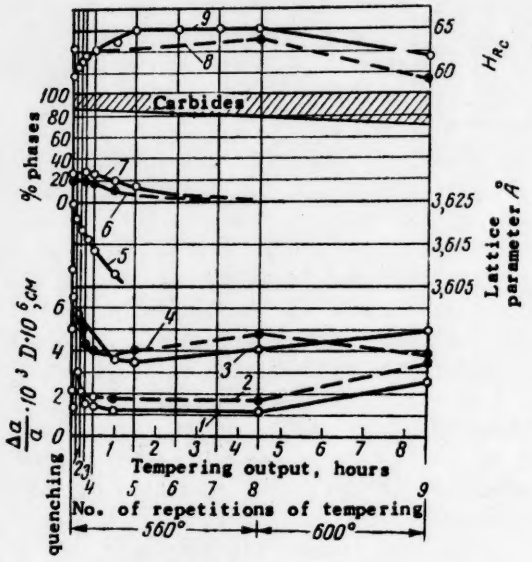

Fig. 3. The relation between the size of the blocks D (curves *1* and *2*) distortions $\Delta a/a$ (curves *3* & *4*) lattice parameters, residual austenite (curve *5*) amount of phases (curves *6* & *7*) and hardness in R_c units (curves *8* & *9*), and the number and duration of tempering treatments for steel R-18.
Solid lines – after quenching at 1290°;
dotted lines – after quenching at 1280°.

Subsequently, a 5 min thrice-repeated tempering leads to the rapid impoverishment of the residual austenite (the lattice parameter is reduced from 3.625 to 3.616 Å), breakdown of the α-phase blocks from 3 to 1.75 x 10^{-6} cm., further reduction of the summated $\Delta a/a$ and increased hardness of the steel; here radiography did not disclose secondary martensitic transformation. Increased hardness up to 65 units is accompanied by the further impoverishment of the residual austenite while the size of the blocks and the type II distortion of the α-phase remain constant until a fifth tempering. In this case secondary martensite transformation is observed (when the lattice parameter reaches 3.614 Å). Further increase in the number of temperings leaves the steel at the same hardness for quite a time, the size of the blocks becomes stable (1.25 x 10^{-6} cm after tempering quenched pieces from 1290°, and 1.75 x 10^{-6} cm for those quenched from 1280°), while the total distortions $\Delta a/a$ become greater with high quench-hardening temperatures, and then become stabilized. This second rise in $\Delta a/a$ corresponds to the concentration heterogeneity in the ferrite in exactly the opposite way to first tempering) in the tempered martensite (which may be seen from a comparison of curves *1* and *2* with curve *4* Fig. 1).

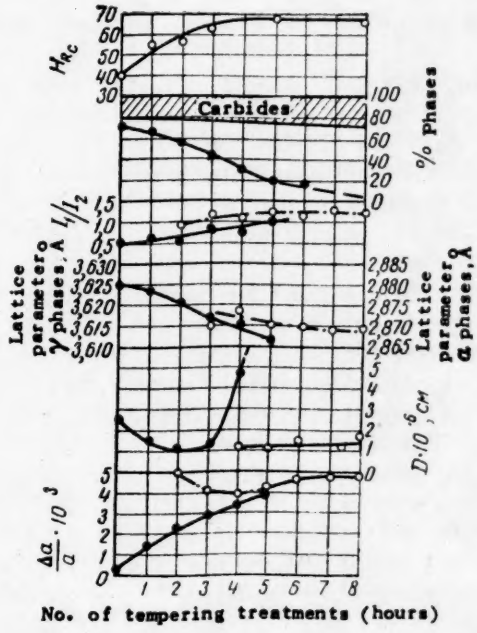

Fig. 4. The relation between hardness, amount of gamma phases, intensivity ratio I_1/I_2 of lines (111) and (311) of the γ phases and lines (110) and (211) of the α phase lattice parameters of α and γ phases, block size D, distortions $\Delta a/a$ of these phases, and the number of tempering treatments (in hours) at 560° for steel 150R18.
Solid lines – γ phase, dotted lines – α phase.

As the reduction in hardness on tempering at 560° in the course of the first 10 sec holding, is similar to that in the 300-400° range (See Fig. 1), it may be assumed that these reductions occur in the same manner. In both cases the martensite is deprived of carbon up to 0.31% (which causes its dispersion hardness) with simultaneously, the single diffusion-less increase in the lattice

VOL. 8 1959

parameter of the residual austenite of 0.016 Å (on account of the relaxation of type II distortion and reduction of volume). These facts show that the reduction in hardness is conditional upon a predetermined combination of quenching distortion of the II type and II type distortion arising as a result of the dispersion hardening of the martensite, and not on the recrystallization of the residual austenite, as no recrystallization of blocks of residual austenite has been discovered.

From the above it follows that the tempering of quenched high speed steel at 380° has much in common with the tempering of quenched carbon steel.

As to the higher temperatures, the tempering of high speed steel has many peculiarities among which are carbide transformations, two forms of concentration heterogeneity and changes in the fine crystal structure. The processes of dispersion hardening of martensite are common.

Steel 150P18. The large quantity of residual austenite in this steel (73%) make it possible to trace the influence of the phase hardening of the secondary martensite on the changes in the fine crystal lattice on tempering, both in the α- and in the γ-phases.

It can be seen from Fig. 4 that, according to the number of repeated temperings at 560° the reduction in the amount of residual austenite to 15-20% is accompanied by definite changes in its fine crystal structure: 1) reduction of the lattice parameter by 0.012 Å; 2) increase in II type distortion to 4×10^{-3} due to dispersion hardness and secondary martensite transformation: 3) increased distortion of type III; 4) grain refinement followed by growth of the blocks and 5) an increase in the hardness of the steel from 40 to 67 units.

Simultaneously with these changes in the fine structure of the residual austenite, definite changes take place in the tempered martensite (See Fig. 4): 1) the mean parameter of the martensite-ferrite is reduced from 2.877 to 2.869 Å after 7 hr) and, after a further 7 hr tempering at 600°, to 2.867 Å; 2) the blocks stabilise at 1.25×10^{-6} cm (their growth is observed only at higher temperatures); 3) the curve $\Delta a/a$ has two maxima of concentration heterogeneity, as in steel R18.

Investigation of the break-up of the martensite of steel EI 184 on tempering at 560° has shown that, as a result of the tempering, II-type distortions in the α-phase increase to 4×10^{-6} cm, and the size of the blocks to $1.5\text{-}2.0 \times 10^{-6}$ cm, i.e. the fine structure of this steel is hardly different from that of steel R18, with the exception of the somewhat greater size of the blocks. However, while in R18 the blocks grow to $2.8\text{-}3.0 \times 10^{-6}$ cm as the result of four temperings at 600°, in EI 184 they grow to $4.5\text{-}5.0 \times 10^{-6}$ cm, that is to say, the rate of growth of the blocks is one and a half times greater in EI 184. This shows that the tempering carbides of EI 184 are less stable than in R18 and the more easily coalesce; this, incidentally, might also explain the red hardness of EI 184.

In this work it has been established that red hardness increases according to the extent to which the martensite is alloyed, the α phase blocks are averse to growth and of the concentration heterogeneity in the 560-640° range is increased (in ferrite).

The nature of the red hardness of high speed steels may be explained by the great stability of the type II and III distortions and the fields of α phase blocks coherently diffused by the X-rays, as a result of the presence in the volume of the grains of a very large quantity of slowly coalescing high-dispersion carbides of vanadium and tungsten with strong interatomic bonds. But while in the high-speed steels there are carbides of chromium, which coalesce more easily than those of vanadium and tungsten, it is the coalescence of the chromium carbides which is one of the weakest links in the red hardness of steel. It is for this reason that the less chromium carbides there are in the steel, the greater will be its red shortness.

The great hardness of high speed steels with a martensitic structure, which undergo dispersion hardening, is due to the high dispersibility of the α-phase blocks (1.25×10^{-6} cm), the great distortions of the II (4×10^{-3}) and the III ($\sqrt{\overline{u^2}} = 0{,}3$ Å) types, the optimum dispersibility and extremely large amount, of vanadium tungsten and chromium carbides and to the presence of a large amount of ledeburitic carbides.

From measurements of the rate of separation of carbon from the residual austenite by

observation of the (110), reflection of the martensite in steel 150R18, and the rate of removal of carbon from the martensite (from the same lines) it has been found that the removal of carbon from the austenite at tempering temperatures of 540-580° takes place 260-300 times more slowly than does the impoverishment of the martensite. These figures. and also those on the fine crystal structure of these phases, show that the secondary hardness is not due to the transformation of residual austenite into martensite, as was indicated in paper [1-4], but to the dispersion hardening of the martensite. In the initial stages of ageing, the hardness of the martensite is reduced by 3-5 units, after which it grows again, due to dispersion hardening. This is explained by the fact that the martensite, which is very unstable on tempering, easily disintegrates, with the accompanying separation of carbides, as a result of which the reduction in hardness is rapidly changed into growth, which means that the nature of the hardening process is changed; the highly strain-hardened unstable martensitic state is followed by a highly hardened stable ferrito-carbide state. As the martensitic hardened state is unstable, then the secondary hardness also cannot be the result of secondary martensite transformation. It is, in fact, without accomanying phenomena.

The ageing of the austenite also is of secondary importance in the occurrence of secondary hardness; austenite has greater red hardness than martensite, so that with a long soaking at over 500° there is a considerable growth in the blocks in the residual austenite while the size remains the same in the ferrite.

Consequently, the strain hardened state of residual austenite is very unstable, and for this reason it plays only a negative role in secondary hardness. This latter factor would appear to explain also the considerably lower hot hardness of steel which after tempering contains residual austenite, as compared with that without residual austenite.

CONCLUSIONS

1. Secondary hardness is not the result of the transformation of residual austenite into secondary martensite, but the result of dispersion hardening of primary and secondary martensite. The dispersion hardness of residual austenite is of secondary importance.

2. The reduction in the hardness of the steel in the initial period of tempering is accompanied by the expansion without diffusion, of the lattice of the residual austenite, changing later into reduction of the lattice due to the residual austenite combining, mainly with carbon, but also to some extent with the alloying elements.

3. When the steel reaches maximum hardness on tempering, the distortions of the II type, in the α- and γ- phases, are the same, and equal to $4.0\text{-}4.5 \times 10^{-3}$.

4. The parameters established for the fine crystal structure are characteristic of the high hardness and red hardness of tempered high-speed steels.

5. The energy of activation, calculated according to the rate of growth of the blocks of α-phase in the 540-620° range, comes to 60 kcal/mol, while above 650 it is 80 kcal/mol.

6. Two types of concentration heterogeneity have been discovered: between 380 and 520° in the ferrite. With tempering at 560°, the concentration heterogeneity in ferrite is greater where the quench-hardening temperature was greater.

Translated by V. Alford

REFERENCES

1. A.P. Gulyaev, *Metallurg.* No.12 (1936).
2. I.Z. Yasnogorodskiy, *Kachestvennaya stal',* No.4 (1936).
3. A.P. Gulyaev, *Vestnik metallopromyshlennosti,* No.1 (1938).
4. V.Ya. Dubovoi, *Metallurg,* Nos.10-11 (1939).
5. S.S. Shteinberg, *Kachestvennaya stal',* No.3 (1937).
6. M.D. Perkas, *Problemy metalloved. i fiz. metallov. (Problems of metallography and the physics of metals),* 145 (1952).
7. G.V. Kudryumov and M.D. Perkas, *op cit.* p.161 (1951).
8. M.A. Nikanorov, *Metallovedenie i termich, obrabotka (Metallography and heat treatment),*

VOL. 8 1959

1st edit (1954).
9. Yu.A. Geller, *Izv. Akad. Nauk SSSR, Department of Technical Sciences*, No.5 (1954).
10. G.V. Kudryumov and L.I. Lysa, *Zh. teor. fiz.* 17, 9 (1947).
11. L.I. Lysak, *Voprosy fiz. metal. i metalloved.* No.3 (1952), No.6, Kiev (1955).
12. L.I. Lysak and L.G. Khandros, *Vopr. fiz. metal. i metalloved*, No.4, Kiev (1953).
13. L.I. Lysak and Ye.G. Nesterenko. *Vopr. fiz. metal. i metalloved.* No.4 Kiev (1948).
14. G.Ya. Kozyrskii, *Vopr. fiz. metal. i metalloved.* No.5, Kiev (1954).

VOL
8
195

THE INFLUENCE OF CYCLIC HEAT TREATMENT ON URANIUM BICRYSTALS*

S. Ya. ZALIVADNYI and V. M. MIKHAILOVSKII

Physico-Technical Institute, Academy of Sciences Ukr. S. S. R.

(Received 27 May 1959)

With cyclic heat treatment in the range 100-600° changes have been observed in bicrystals of uranium, inside the grain and along the adjoining boundaries, which are manifest in various forms including that of unilateral mutual slip of the crystallites. On one cycle the relative shift of the grains was in the region of 1×10^{-5}. The relative displacement of the grains coincides, according to the figures, with the displacements which occur in polycrystalline coarse-grained uranium in similar circumstances.

VOL. 8 1959

Much research has been devoted [1-3] to the investigation of the changes which occur in uranium on cyclic heat treatment. In our previous work [4] we studied the changes in the microstructure of uranium with coarse acicular grains. It was demonstrated how, on cyclic heat treatment, there occurred a reciprocal displacement of the grains due both to slip on the boundaries and to plastic deformation inside the grains.

The investigations here described were carried out on biocrystals of uranium for the purpose of finding out what effect the interaction of the grains has on the nature of the changes in the material on cyclic heat treatment, and of further clearing up the mechanism of this phenomenon under simplfiied conditions (without surrounding grains).

METHOD OF CONDUCTING THE EXPERIMENT

By the process already described [4] prismatic blanks with coarse acicular grains were prepared from technical uranium. From these blanks bicroystalline test pieces were out with a wire saw. Further preparation of the latter was done with abrasive paper and an electrolytic polisher. The finished test pieces were 3.2 x 1.3 x 0.7 mm. The bicrystals, electrolytically etched, could be seen in polarized light by means of a metallographic microscope. The orientation of the crystals in relation to one another was determined by the Laue method. In order to check the mutual displacement of the grains, lines perpendicular to the boundaries were traced across the testpieces. The lines were drawn with the diamond indenter of a micro-hardness tester.

For the cyclic heat treatment they were placed in an iron boat with a lid, which was lined with tantalum foil to prevent reaction between the uranium and the iron. They were heated by passing an electric current through the boat. Cooling was effected by heat transfer through large copper clamps round the boat, which were themselves cooled by water. Temperature measurement was by means of a platinum-platinorhodium thermocouple welded to the boat. The experiments were conducted in a vacuum with pressure not above 3×10^{-6} mm Hg. in the temperature range 100-600°. The procedure was the same as before, namely: heating to maximum temperature – 5 min, holding at 600° – 1 min, cooling to minimum temperature – 4 min. The investigation was carried to 1000 cycles with interruptions to examine the test pieces after 100, 200, 300,

* *Fiz. metal. metalloved.* 8, No.6, 904-907, 1959.

400, 500 and 750 cycles. After 1000 cycles the testpieces were given an electrolytic polishing and were etched, in order to disclose the changes of the microstructure.

RESULTS AND THEIR EVALUATION

The metallographic examination showed that, as a result of the cyclic heat treatment, there had been mutual displacement in all the bicrystals investigated. The displacement was judged by the difference in the length of the grain and, directly, from the nature of the distortion of the scratched lines. It would seem from this, therefore, that in uranium, the pair of grains is the elementary nucleus in which irreversible changes occur on cyclic heat treatment. Table 1 gives the results of the investigation of three pieces after 1000 cycles.

The value α_b was calculated from the data on mutual orientation of the grains by means of the tabulated data for α in the main direction. The negative values for α_b which appear in some cases, are due to the small angle between the axes of the testpieces and the direction [010], along which the coefficient of linear expansion for uranium is negative.

TABLE 1

Test piece No.	Grain No.	α_{zp} 10^6	$\Delta\alpha \times 10^6$	$\frac{\Delta l}{l} \times 10^6$
1	1	+6	14	+20
	2	−8		+ 6
2	3	−5	16	−10
	4	+11		+ 3
3	5	−8	14	0
	6	+6		+10

Note: α_b is the coefficient of linear expansion along the mutual boundary; $\Delta\alpha$ is the difference in the coefficients of linear expansion for the grains of bicrystals along their mutual boundaries; $\frac{\Delta l}{l}$ is the mean percentage change in the length of a grain after one cycle.

According to the data entered in Table 1, the value of $\Delta\alpha$ was more or less the same for all three pieces. It follows from this

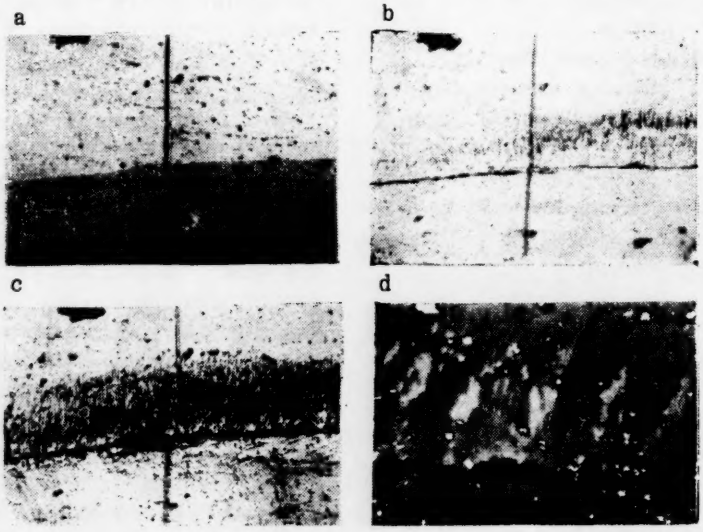

Fig. 1. Photomicrograph of a sector of a testpiece: *a* – initial state, polarized light, x40; *b* – the same after electrolytic polishing, x40; *c* – after 1000 cycles, x40; *d* – the same after electrolytic polishing etching, polarized light, x160.

that, in each pair of grains which together make one bi-crystal, the greater relative expansion is shown by the grain with the greater α_b, which is in agreement with the propositions developed by Burke and Turkalo [5].

If the relative figure for grain displacement in bicrystals is compared with the relative displacement of grains in polycrystalline test pieces, which have undergone cyclic heat treatment in similar circumstances [4], it will be seen that the figure is of the same order in both cases. The presence of surrounding grains, therefore, has little effect on the interaction of each pair of grains; at most, there might be a change of some percent in size due to irreversible changes.

As in the experiments with the polycrystalline pieces, mutual displacement of the grains occurred through slip along the boundaries and plastic deformation within the grains, mainly in the vicinity of the boundaries, which was detected from the rupture and distortion of the scratched lines. As in the previous tests, no migration of the boundaries was observed. Figs. 1*a-d* show photomicrographs of a testpiece after 1000 cycles of heat treatment. In the zone of greatest deformation at the boundary, new grains have arisen with close orientation. The phenomenon of the recrystallization of polycrystalline uranium on cyclic heat treatment has been described in the work of Bochvar and his collaborators [2].

In the bicrystals examined, in all cases where slip occurred along the boundaries, there was little change in the amount of mutual displacement of the grains per one cycle with an increasing number of cycles.

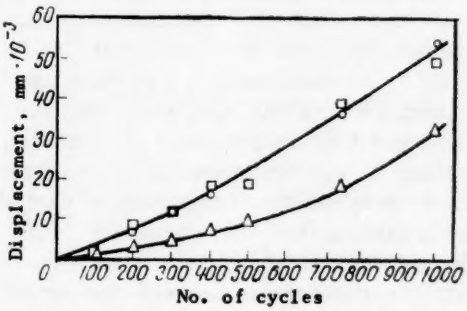

Fig. 2. Graph showing relation between extent of displacement along the boundaries and number of cycles, in bicrystalline uranium.
- displacement at the edges
- displacement in the middle.

Fig. 2 is a graph showing the relation between the extent of displacement and the number of heat treatment cycles, measured on three scratches which were made at the edges and in the middle of testpiece No. 3. With an increasing number of cycles the increase in the amount of mutual displacement per one cycle is insignificant. At one edge, and in the middle, the displacement was practically the same, for which reason there is a common line for these pieces in the graph.

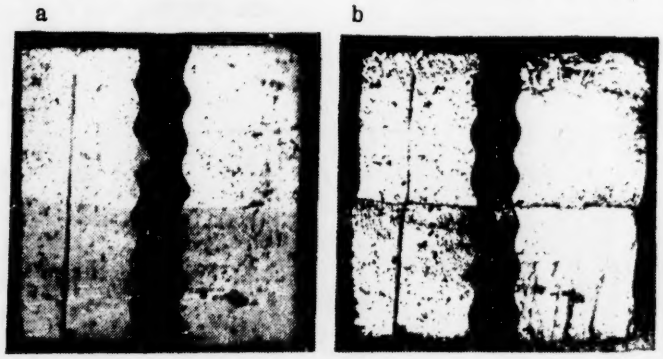

Fig. 3. Photomicrograph of a uranium testpiece with the centre removed; x40
a - prior to cyclic heat treatment, polarized light *b* - after 100 cycles

VOL. 8 1959

Metallographic examination disclosed in both crystals that additional displacement had occurred, of the whole grains in relation to one another, quite apart from the mutual displacement due to the difference in permanent extension of one of each grain pair. (Fig. 3). Although the reason for this has not been discovered, the fact that one grain, as a whole unit, is displaced in its relation to the other, may explain why, with the cyclic heat treatment of polycrystalline uranium, elongation in one direction does not occur mainly because of the corresponding elongation of the grains in the same direction. The sliding of the grain as a whole may also explain the discrepancy between the extent of slip on rupture of the scratched lines and the difference in the absolute elongation of the grains. In testpiece No. 3, for example, maximum displacement along the boundary after 1000 treatments comes to 0.06 mm, while the difference in the permanent elongation of the grains is 0.03 mm, i.e. half as much. It should be noted that curvature was observed in one of the bicrystals around the axis of the testpiece.

In conclusion we wish to express our thanks to Prof. R.I. Garber for checking our work and making valuable comments.

CONCLUSIONS

1. The relative displacement of grains of bicrystals after one cycle is of the same order as that which occurs in polycrystalline uranium testpieces in the same conditions of cyclic heat treatment.

2. Change in the disposition of the grains relative to one another may occur because of the difference in permanent elongation, or because of the displacement of one whole grain in relation to the other.

3. In general outline, these tests with bicrystalline uranium are in agreement with the propositions regarding the mechanism of irreversible changes in uranium on cyclic heat treatment, according to which these changes are brought about by a combination of slip along the boundaries, and plastic deformation inside the grains [3], which was established experimentally for polycrystalline uranium [4].

Translated by V. Alford

REFERENCES

1. A.A. Bochvar, S.T. Konobeevskii, A.S. Zaimovskii, G.Ya. Sergeev, V.I. Kutaitsev, N.F. Pravdyuk and B.M. Levitskii, *Atomnaya energiya*, No. 1, 5 (1958).
2. A.A. Bochvar, G.I. Tomson and N.T. Chebotareva. *Atomnaya energiya*, No. 6 555 (1958).
3. H.H. Chiswik and L. R. Kelman, *Metallurgiya yardernoi energetiki i deistvie obluchenia na materialy (the metallurgy of nuclear power and the action of radiation on material) (papers delivered by foreign scientists at the International Conference on Atomic Energy), Metallurgizdat*, (1956).
4. R.I. Garber, S.Ya. Zalivadnyi and V.M. Mikhailovskii, (received for publication in Zh. teor. fiz. 24 Feb (1958).
5. J.E. Burke and A.M. Turkalo, *J. of Metals*, 4, 651 (1952).

VOL 8 195

THE FAILURE OF A MARTENSITE CRYSTAL UNDER THE SIMULTANEOUS ACTION OF EXTERNAL TENSILE AND COMPRESSIVE STRESSES*

A. MASHIN

The Physics Laboratory of the Railway Research Institute,
Prague, Czechoslovakia

(Received 25 February 1959)

The present article deals with changes in a martensite crystal which is actually a martensite monocrystal, under the simultaneous action of external tensile and compressive stresses. It is found that the martensite crystals in failing, first form microcracks, break up, then fracture completely. The interpretation of these changes was based on an analysis of stresses acting on the martensite crystal during its loading. The crushing of the crystals is explained by the fact that the compressive stresses on one side of the crystal are not compensated in these cases. The problem considered here is solved in connexion with problems of propagation of elastic and plastic waves in an austenitic-martensitic medium.

VOL.
8
1959

INTRODUCTION

The aim of this work is to study changes in martensite crystals which are in an austenitic medium, in cases where the crystals are acted on simultaneously by external tensile and compressive stresses. This case can be encountered for example, during the propagation of elastic and plastic waves in a crystalline medium**(the propagation of plastic waves is also accompanied by plastic deformation of the medium).

The case mentioned was solved in connexion with this problem. The simultaneous action of stresses on the crystals was caused by simple extension of the specimen, containing a small amount of martensite crystals, in a perfectly pure austenitic medium. Thus, tensile stresses were applied to separate martensite crystals directly; The plastically deformed austenite in the neighbourhood of these crystals, due to the stress, simultaneously acts on them with compressive stress.

As far as we know, no work has been done on the study of changes in a martensite crystal during the action of external stresses.

EXPERIMENTAL METHOD

Some specimens with austenitic structure and singly included martensite crystals were obtained by quenching an iron alloy containing 5% manganese and 1.15% carbon from 1150°C (with 6 hr soaking in an electric vacuum furnace) with cooling in oil and subsequent supercooling to -55°C in a mixture of solid CO_2 and methyl alcohol. The high temperature and duration of the austenization process were selected in order to obtain coarse grains, which gave coarse martensite crystals on conversion. The specimens were in the shape of prisms measuring 70 x 15 x 5 mm. After quenching and supercooling, metallographic sections were prepared on a wider surface (70 x 15 mm) with subsequent electrolytic polishing. The composition of the electrolyte

* *Fiz. metal. metalloved.*, 8, No.6, 908-914, 1959.

** Corresponds to the structure during impact [1].

was: 133 ml glacial CH_3COOH, 25 gm CrO_3 and 7 ml H_2O. The thickness of the electrolytically polished layer was about 0.3-0.4 mm, which would make it reasonable to assume that the polishing had removed all of the surface layer which had been deformed during grinding. The specimens were rotated during the polishing.

The specimens were stretched statically on a hydraulic tensile machine at 18°C, they were clamped on their longer side in the direction of the axis of the machine, so that the direction of the tensile stress coincided with the longitudinal axis of the specimen. The state of the martensite crystals during the gradual increase in stresses was followed by the plastic relief which appeared on the polished but unetched surface. The observations were carried out with a vertical Vickers metallographic microscope.

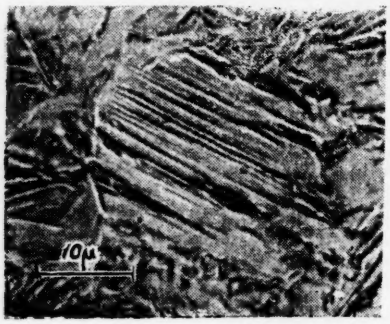

Fig. 1. Grain of austenite with martensite crystals in plastic relief.

To ensure that the observations were carried out on the same martensite crystals, the specimens were extended a little at first. This merely caused on the plastic relief the appearance of outlines of austenite grains and martensite crystals (Fig. 1). On this relief a place was selected and marked with the martensite crystals conveniently orientated with respect to the plane of the section (see below); the state of the crystals was then followed with further increase in stresses. There is very little risk that under stresses due to the plastic deformation that new martensite crystals might be formed due to the large difference in temperatures at the M_s point (the start of conversions to martensite) and the temperature of 18°C, at which the specimen was subjected to stresses. During the whole experiment, not one case showed the formation of new crystals.

VOL 8 195

RESULTS

Since the stress in the specimen was very small, only the austenite surrounding the martensite crystals was deformed, due to which the plastic relief acquired outlines only along its height. The martensite crystals did not fail. With increase in the stress, changes were also observed in some of the martensite crystals, an important role being played by their orientation with respect to the plane of the surface. The crystals with their wider surface in the direction of the plane of the

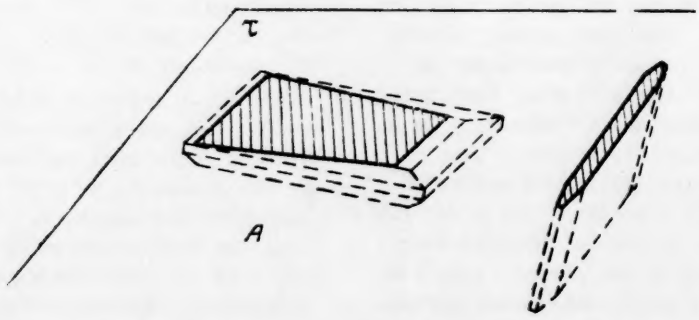

Fig. 2. Orientation of martensite crystals relative to the plane of the section. τ – plane of section.

section* (Fig. 2, case *A*), were broken up – showed microcracks measuring about 10^{-4} cm; with increased stress, the crystals fractured. On the other hand, in the case of crystals orientated with their wider surface approximately perpendicular to the plane of the section (Fig. 2, case *B*; in Figs. 3,4 they have the shape of fine needles), there were no micro-cracks or failure even when the specimen was loaded to the point of failure.

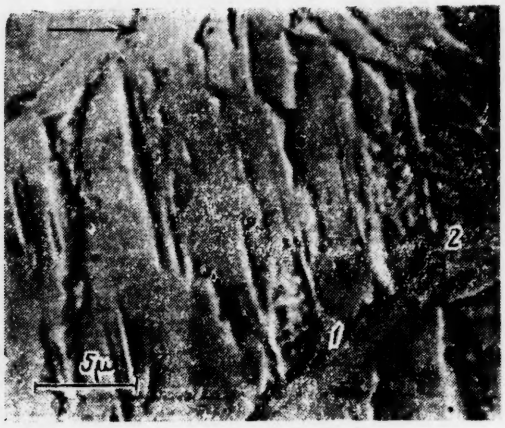

Fig. 3. Failure of the martensite crystals placed in the plane of the section (plastic relief). The arrow at the top left shows the direction of application of the tensile force.

The above described changes in the martensite crystals can be seen on the microphotographs of Figs3 and 4. In Fig. 3 a part of it (numbered 1) illustrates a cracked martensite crystal, and another part (numbered 2) shows the failure of this cracked crystal. On both diagrams, it is also possible to observe undestroyed narrow martensite needles (on Fig. 4 this needle is interesected by a line showing the magnification), corresponding to crystals orientated perpendicular to the plane of the section.

To decide whether failure of the martensite crystals takes place not only on the observed surface, but also inside the specimen, two heavily stressed samples, the section of which had failed martensite crystals, were cut down the middle along their longitudinal axis. A metallographic section wan then made on the two parts and subjected to electrolytic polishing. After etching it was found that here were martensite crystals which had failed, and that the failure coincided with the above type of failure. However, the number of failed crystals, determined by comparison, was less than on the surface of the specimen.

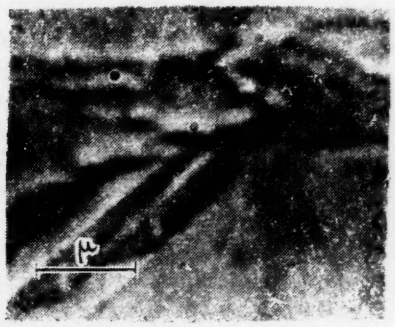

Fig. 4. Failed crystal of martensite (plastic relief).

It can therefore be concluded that stresses lead to the failure of martensite crystals inside the specimen also.

INTERPRETATION OF THE CHANGES

In the interpretation of the changes observed, it is possible to proceed from an analysis** of the individual stresses acting on martensite crystals when the specimen is in stress, and from the change in these stresses taking place for certain crystals.

As already mentioned, when the specimen is given tensile loading, the martensite crystal

* The dependence of the form of martensite crystals on their orientation (position) relative to the plane of the section. See [2].

** We decided against the mathematical treatment of the problem, since the experimental method used was unable to determine, except in a comparative fashion, either the value of the stress applied to the plastically deformed austenite crystals during the stress, or the degree of the plastic deformation of the austenite, which would means that the solution to the problem would be dependent on a number of assumptions.

is acted on not only by tensile stresses, but also compressive stresses caused by the plastically deformed austenite which is surrounding it. The value of these stresses will increase simultaneously with the increase in the stress of the specimens since the plastic deformation of the austenite also increases. In the case where the crystal is surrounded on all sides by austenite, and when the plastic deformation of the austenite is homogeneous throughout the whole medium, the compressive stresses acting on one side of the lamellar crystal will be opposed by stresses of the same magnitude on the opposite side. Consequently, for areas of the same value, given by the symmetry of the crystal, the resulting compressive forces, the value of which is equal to the product of these areas and the compressive stresses acting on them, are mutually compensated. An exact representation of this is given in Fig. 5.

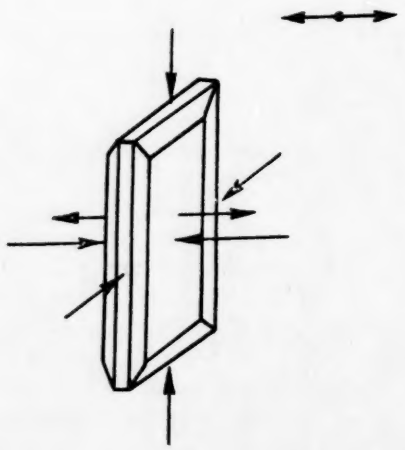

Fig. 5. Application of compressive and tensile forces to a martensite crystal in the case of homogeneous plastic deformation of the austenite in its neighbourhood.

However, on some sections of the loaded specimen, and also for some crystals, especially crystals in the plane of the section as will be shown later, the equilibrium of the compressive forces on one of the sides of the crystal can be destroyed. The reason for this phenomenon may be the different nature of the changes and the different degree of plastic deformation of the austenite (heterogeneous plastic deformation) or the absence of compressive stresses on one of the sides of the crystal. Heterogeneous plastic deformation arises for example, as a result of the presence in the immediate vicinity of the crystal of another martensite crystal, which alters the character of the changes in plastic deformation on this side; heterogeneous deformation also took place in martensite crystals lying at the boundaries of the austenite grains with a different crystallographic orientation due to the different character of the plastic deformation of the individual austenite grains, i. e. due to the heterogeneous plastic deformation of the austenite surrounding the martensite crystal (different compressive stresses act on different sides of the martensite crystal). In this way the equilibrium of the compressive forces is destroyed due to the asymmetrical shape of the martensite crystal itself. The case of complete absence of compressive forces on one of the sides of the crystal is encountered crystals lying close to the surface of the specimen (the metallographic section). In this case the compressive stresses applied by the plastically deformed austenite to the lower side of the crystal are not compensated by any stress from the opposite side (Fig. 6).

Thus, in all these cases concerning the martensite crystals, it is a case of partial or complete destruction of the equilibrium of the compressive forces: on reaching a certain value, the difference in these forces can cause destruction of the crystal. The value of this difference depends directly on the degree of plastic deformation of the austenite, and consequently on the value of the stress in the specimen.

The present work deals with martensite crystals at the surface of the sample – the metallographic section. Non-compensated compressive forces are applied towards the plane of the section (see Fig. 6), to all the martensite crystals without exception. However, under the influence of a different spacial orientation of the crystals relative to the plane of the section, the values of these forces and the reactions of the individual crystals to their action will be different. In the case of crystals disposed with their wider surface preferentially in the place of the section (case *A*, Fig. 2), the compressive

VOL. 8 195

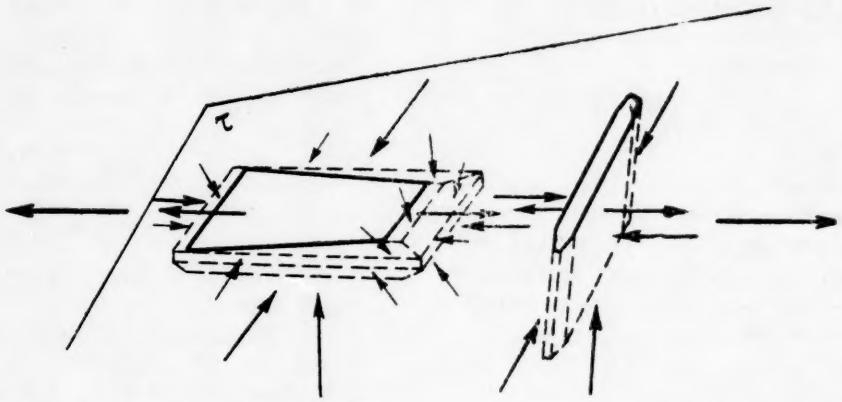

Fig. 6. Application of compressive and tensile forces to a martensite crystal at the surface of the specimen (section). τ - plane of the section.

forces reach a considerable value, since the size of the areas to which the stresses are applied, non-compensated on the side of the section, is also considerable. Due to the action of these forces deflexion (buckling) of the crystals takes place, which on reaching a fixed value, depending on a certain degree of stress in the specimen, leads to disturbance of the adherence of the crystals, which will result in the crystals being broken up into small particles. The simultaneously applied tensile forces (see Fig.6) readily cause fracture of these crystals in accordance with observed changes.

On the other hand, in the case of crystals which are orientated roughly perpendicularly to the plane of the section (case B, Fig.2), the areas on which the non-compensated compressive stresses act from the side of the section are small. The non-compensated compressive forces would therefore also be small. Furthermore, with the given geometrical arrangement (see Fig.6) the application of these forces cannot destroy the adherence of the crystals, as was the case previously. As a result, in the case of crystals orientated in this way, failure does not take place, which is borne out by the results obtained experimentally.

The above considerations would indicate that martensite crystals at the surface of the specimen (section) should break more often than inside the specimen because of the probability of non-compensated compressive forces on one side of the martensite crystal being greater than inside the specimen. This conclusion is in fact borne out by the above experiments in which the heavily stressed specimens were cut. It was found that the number of destructions of martensite crystals inside the specimen was less than at the surface.

DISCUSSION OF RESULTS

From the order of the succession of the changes during the failure of martensite crystals, microcracks fracture, and also from the interpretation of these changes, it follows that in the tests the compressive stresses predominated over the tensile stresses. However, the reverse is possible here, when the effect of the tensile stresses exceeds that of the compressive stresses. In this case also, it is probable that failure of the crystals occurs. However, if we suppose that the above conclusions are correct, then the reverse order of succession of the changes is nevertheless impossible, and the crystal simply fractures. The destruction of the adherence of the crystals and consequently their disintegration are excluded.

Proof of the fact that strong plastic deformation of the austenite can cause tearing of the martensite crystals can also be found in [3]. The authors, considering the plastic deformation of austenite in the neighbourhood of formation of the martensite crystals, found that there were broken martensite

crystals in regions of particularly strong plastic deformation of the austenite.

SUMMARY

The present work was carried out when the author was working in the Department of Mathematics and Descriptive Geometry of the Polytechnical Institute in Prague. It is his pleasant duty to pay tribute to the memory of the late Head of the Department, Professor F. Vyehikhla, Doctor of the Physical & Mathematical Sciences who was interested in the problems of which the present work forms a part.

The author also thanks Bakalikova from the IIVEP for certain comments on the work.

Translated by J. Thompson

REFERENCES

1. A. Masin and D. Tlusta, *Czechlosl. J. Phys.*, 7, 122 (1957).
2. A.P. Gulyaev and E.V. Petulina, *Zh. eksp. teor. fiz.*, 23, 502 (1953).
3. B. Edmondson and T. Ko, *Acta met.*, 2, 235 (1954).

VOL
8
195

THE EFFECT OF THE ORIGINAL STRUCTURE AND TEMPERATURE OF DEFORMATION ON PHASE TRANSFORMATIONS DURING PLASTIC FORMATION*

B. A. APAEV and Yu. A. SYSUEV

Gor'kov Physical and Technical Research Institute

(Received 1 January 1959)

VOL. 8 1959

Several papers express an opinion on the differences in processes caused by plastic deformation, when equilibrium and non-equilibrium alloys are subjected to plastic deformation. It is usual to consider that in the first case the deformation causes fragmentation of the phases, change in the block structure and stressed state of the alloy [1-4]. In the second case, as well as these processes, on reaching a certain degree of deformation more important changes can take place in the alloy, characterized by the formation of new phases, which can differ from the original phase both in their crystallographic structure and in the chemical composition [5-9].

In the light of a number of papers, this classification is more than arbitrary, since the results of these papers indicate the presence of phase transformations during deformation of the alloys in the equilibrium and states close to the equilibrium [10-14].

The opinion held by some authors that the deformation of equilibrium systems cannot cause the formation of new phases has led, in our opinion, to incorrect conclusions. Taking as a starting premise the fact that plastic deformation in equilibrium systems only causes those processes mentioned above, and observing the similar change of the physical properties during the heating of a plastically deformed alloy and also the alloy in the hardened state, these authors consider it sufficient proof that during tempering in the range of the "third transformation" processes occur which are caused only by the change in the block structure of the α phase, of its stressed state, by destruction of the coherent bonds and by the change in shape and dimension of the carbide particles [15-17].

If the equilibrium state of the alloy is characterized only by the ratio and chemical composition of the phases, then on the basis of the existing point of view the conclusion would be drawn that there should be no essential difference in the processes arising during the deformation of tempered steel, when the structure of the latter is characterized for example, by lamellar and granular cementite. In our opinion, this point of view should be made more specific, i.e. there should be a more complete determination of the equilibrium state of the system, taking into account the equilibrium of the form of the phases.

The present paper deals partly with problems similar to those already published [11, 12] and also studies the effect of the deformation temperature and the original structure on the character of phase transformations and the character of hardening during deformation.

MATERIAL AND METHOD OF INVESTIGATION

Industrial *U*12 and *U*10 steels were used in the investigation. Before deformation, the specimens of (4 x 40 mm cross-section) were subjected to heat treatment, as shown in Fig. 1 in order to obtain structures with a different form of cementite.

The deformation was accomplished by uneven compression on all sides in rings [18]. For the deformation in liquid nitrogen, the specimens held in the rings were given preliminary cooling in nitrogen in a Dewar flask; when

* *Fiz. metal. metalloved.*, 8, No.6, 915-921, 1959.

the nitrogen had finished boiling, the specimens were placed in a press-form, in a retort also filled with nitrogen. The volume of the retort was such that during the deformation, the specimen was constantly in a medium of liquid nitrogen. The compression was carried out on a 60-ton Gagarin press. The degree of deformation (ψ%) was determined from the change in height of the specimen and varied between 25 and 27%.

The main method used was the method of magnetic phase analysis. The phase composition was determined from magnetograms (curves $J_s(t)$), which were taken with a ballistic magnetometer in a 10,000 oersted field.

RESULTS OF INVESTIGATION

The phase composition of the specimens after the above-mentioned heat treatment is represented by the magnetograms of Fig. 1. It can be seen that steel U12 after normalization, tempering and isothermal quenching at 650°, and also annealing to granular pearlite (curves 1, 4, 5, 6), has an identical phase composition, characterized by the presence of two phases: cementite (Curie point 210°) and ferrite. The magnetograms taken with specimens after tempering and isothermal quenching at 450° (curves 2, 3), as well as the phases mentioned, exhibited the presence in the steel structure of a high-temperature intermediate carbide phase with a Curie point of 265°.

Fig. 2 gives the magnetograms obtained from these specimens after their deformation at room temperature. From a comparison of the magnetograms (Figs. 1, 2) it follows that in specimens having a 2-phase composition and structure of lamellar cementite the deformation leads to the formation of χ-carbide.

The deformation of the specimen having also 2-phase composition but the granular structure of the cementite, obtained by an oscillating anneal, does not cause phase changes (curves 6 on Figs. 1, 2). The deformation of steel after annealing, not leading to spheroidization of the cementite, as was indicated in papers [11, 12], leads to the transformation of the cementite phase with the formation of χ-carbide.

From an analysis of the magnetograms (Fig. 2), in accordance to the drop in the sections of the curves within the range 210-265° it can concluded qualitatively that the χ-phase is formed in the largest amount in the deformation of the normalized structure and in the smallest amount after tempering at 650°. After deformation of steel which had been given preliminary isothermal quenching at 450° and quenching plus tempering at this temperature, in which there was already the χ-phase, there is also an increase in the amount of the χ-carbide.

The opinion is stated in a number of papers that the plastic deformation causes strong heating of the metal [19], in local volumes. It can therefore be supposed that the χ-carbide, which is always observed in the structure of high-carbon tempered steel, is a product of the decomposition of the austenite which is formed.

To prevent heating of the specimens in the second series of experiments, the deformation was carried out in liquid nitrogen. Lowering the temperature of deformation at -196° shows that the action of plastic deformation remains the same (Fig. 3). In all cases where the structure of the specimen had the form of lamellar cementite, a high temperature carbide phase was formed. In the deformation of steel with the structure of granular cementite, no phase transformations were observed.

To find the degree of stability of the χ-carbide, the deformed specimens were tempered at 400, 500 and 600°. An analysis of the results shows that its stability depends on the original structure. In the steel after normalization the disappearance of the χ-carbide was observed after tempering at 600°. The least stability (disappearance at 400°) is observed in steel which was quenched and tempered at 650° before deformation. The results obtained therefore show that the character of the transformations caused by plastic deformation depend on the original structure of the steel. Reducing the temperature of deformation (from +20 to -196°) does not change this dependence.

Deformation by uneven compression on all sides leads to a sharp change in the shape of the specimen (uneven change in the diameter, bending, etc.) which complicates the quantitative comparison of the results obtained with different specimens. To overcome this problem, in the following series of experiments the samples were deformed by the method of cold

wire drawing. The original blank was *U*10 steel wire of 5.5 mm diameter. The blank was subjected to two types of heat treatment: normalization from 1000° and an oscillating anneal at 690-730° for 10 hr with subsequent slow cooling.

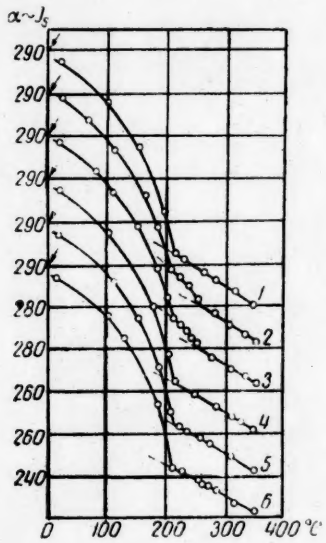

Fig. 1. Magnetograms of U12 steel after various heat treatment: 1 – normalization from 1000°; 2 – isothermal quenching from 1000° in tin at 450°, τ = 15 min; 3 – quenching from 1000° + tempering at 450°, τ = 60 min; 4 – isothermal quenching from 1000° in tin at 650°, τ = 25 min; 5 – quenching from 1000° + tempering at 650°, τ = 60 min; 6 – oscillating anneal at 690-730°, τ = 10 hrs., cooling with the furnace.

The degree of deformation was determined from the change in the cross-section and was 5, 16.6, 33.3, 46.6, 59.3, 70, 79.7, 86.85%. 50 mm samples were cut from the deformed wire.

The dependence of the change in magnetization on the specimen diameter is linear, therefore the results of the measurements obtained with specimens of different cross-section are easily comparable with one another. In these investigations all readings are related to a 4 mm diameter specimen.

It was found that altering the method of deformation did not change the dependence of the phase transformation on the original structure of the steel. Regardless of the degree of deformation in steel with a granular cementite structure, no phase transformations were observed. Fig. 4 shows magnetograms from an original specimen and specimens compressed at 46.6 and 86.85% (curves 2, 3, 4). The magnetogram is given here for the original normalized specimen (Curve 1). When these curves are drawn from one origin they all coincide (Curve 5), which points to the complete coincidence of the phase compositions of these specimens.

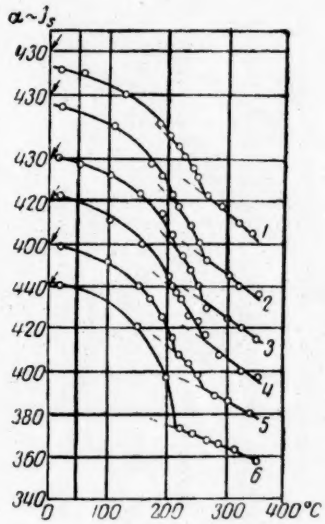

Fig. 2. Same as Fig. 1 after deformation at 20° (ψ = 25-27%).

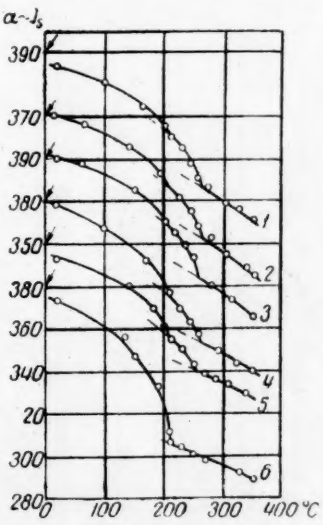

Fig. 3. Same as Fig. 1 after deformation at -196° (ψ = 25-27%).

The plastic deformation of steel with lamellar cementite structure leads to the formation of an intermediate carbide phase with a Curie point of 265°.

Increase in the total magnetization of the specimen and the magnetization at the ferrite section of the $J_s(t)$ curve (Fig. 5) with increase in the degree of deformation indicates that a larger amount of the cementite phase is converted and that this conversion leads to an increase in the amount of the α-phase. All curves in Fig. 5 were drawn from one origin.

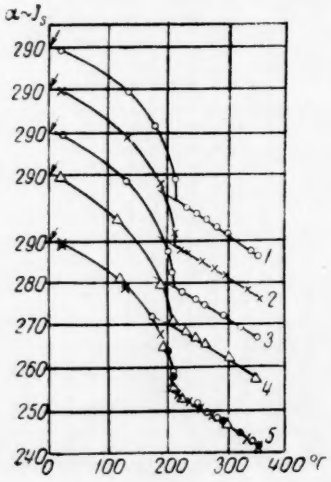

Fig. 4. Magnetograms of U10 steel: 1 – after normalization (lamellar cementite) $\psi = 0$; 2 – after oscillating anneal (granular cementite, $\psi = 0$; 3 – same – deformation, $\psi = 46.6\%$; 4 – the same – deformation, $\psi = 86.85\%$; 5 – magnetograms of all specimens drawn from the one origin.

Extrapolating the ferrite section of the $J_s(t)$ curve and the section of the χ-carbide curve (210-265°) to room temperature, we can determine the fractions of magnetization contributed by each of the phases to the total value J_s, and from them it is possible to determine the volume percentages of these phases. We used the Heisenberg approximation [20] in carrying out this extrapolation. The curves 1, 2, 3 of Fig. 6 characterize the change in the volume of the ferrite, cementite and χ-carbide respectively in dependence on the degree of deformation. The volume of the χ-carbide was determined from the formula

$$P_x = 100 - (P_{Fe_3C} + P_\alpha).$$

With degrees of deformation up to 60%, there is a reduction in the amount of cementite and an increase in the χ-carbide. The observed increase in volume of the α-phase indicates that the plastic deformation causes transformation of the cementite in accordance with the reaction: $Fe_3C \rightarrow \chi Fe_xC + m\,Fe$, which also points to the higher concentration of carbon in the χ-carbide in comparison with the cementite. For higher degrees of deformation ($\psi > 60\%$) there is a very small increase in the volume of the cementite phase and a sharp drop in the amount of the χ phase. The large increase in the amount of ferrite may

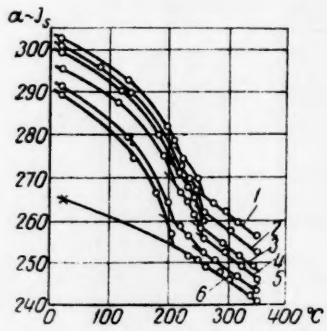

Fig. 5. Magnetograms of normalized U10 steel after various degrees of deformation: 1 – $\psi = 86.85\%$; 2 – $\psi = 79.7\%$; 3 – $\psi = 70\%$; 4 – $\psi = 33.3\%$; 5 – $\psi = 5\%$ 6 – $\psi = 0\%$.

be connected only with the transformation of the α-phase. It is still not known in what form the carbon exists which is separated during the decomposition of the intermediate carbide, whether it is in the form of graphite or dissolved in the α-phase.

The results indicate that the character of the phase transformations depends on the degree of deformation. In steels with granular cementite, no transformations are observed within the range of degrees of deformations investigated, whereas in steels with lamellar cementite, at first there is the formation of the χ-carbide, and with higher degrees of deformation this phase decomposes. In this connexion it was of interest to follow the development of the hardening process with the increase in the degree of deformation in steels with different original structure. Fig. 7 shows the change in hardness as a function of the degree of deformation for a steel

with granular and lamellar cementite. The hardness of steel with lamellar cementite changes very little with increase in the degree of deformation the hardening process develops more intensively.

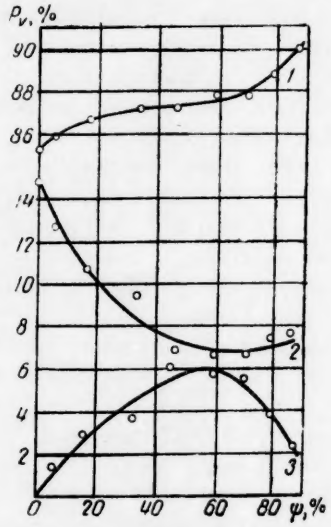

Fig. 6. Change in volume of the phase depending on the degree of deformation of the normalized U10 steel: 1 – change in the ferrite phase; 2 – change in the cementite phase; 3 – change in the high temperature carbide phase.

The change in the hardness during the deformation of steel with granular cementite has a different character: the main hardening of the steel is observed in the range of degrees of deformation up to 60%, whereas with higher degrees of deformation, the development of the hardening process is slowed down. Comparing the shape of the hardness curves with the change in the phase composition depending on the degree of deformation, it can be conluded that hardening during deformation of steel with granular cementite is caused by the change in the block structure and the stressed state of the ferrite. The maintenance of the phase composition during deformation of the granular structure should be connected with the fact that the cementite grains are in a state close to even compression on all sides, hindering their plastic deformation [21]. The different character of the change in hardness of the steel with lamellar structure of the cementite should be connected with the change in the phase composition caused by the plastic deformation. To reveal the nature of the processes leading to strengthening, it is desirable to obtain new experimental data establishing the inter-connexion between microhardness, structure and state of the α-phase during deformation from the original structure.

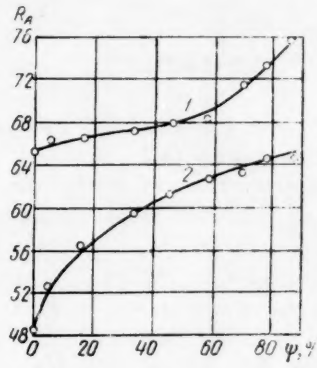

Fig. 7. Change in the hardness of U10 steel depending on the degree of deformation: 1 – normalized steel (lamellar cementite); 2 – steel with oscillating anneal (granular cementite).

The work shows that the more sharply the lamellar form of the cementite the more intense its decomposition with the formation of χ-carbide and α-iron. With reduction in the lamellar structure, this process weakens and when the cementite assumes a granular form, it disappears completely. In the light of these facts it is reasonable to assume that steel annealed to granular cementite is more stable than steel annealed to lamellar cementite.

Reducing the temperature of deformation does not change the general character of the conversion and its connexion with structure. Since the χ Fe_xC carbide phase is different in its carbon content from cementite, then that fact indicates the possibility of diffusion processes due to deformation at low temperatures. The mechanism of formation of this carbide remains uncertain: whether it is formed from austenite, obtained due to local heating, or due to crystallographic rearrangement of the cementite under the action of stresses.

We would like to express our gratitude to S. V. Vonsovskii, Corresponding Member of the

VOL. 8 1959

Academy of Sciences of the U.S.S.R. for his interest shown during the discussion of the preliminary experimental results and for suggesting the study of phase transformations during deformation in a liquid nitrogen medium.

Translated by J. Thompson

REFERENCES

1. V.I. Il'ina, E.Z. Kaminskii, V.K. Kritskaya and R.I. Entin, *Probemy metallovedeniya i fiziki metallov, N.3 (Problems of the Metallography and Physics of Metals)*, Metallurgizdat, p.178 (1952).
2. V.M. Golubov and V.K. Kritskaya, *(Problems of the Metallography and Physics of Metals)* Metallurgizdat, No.4, 461 (1955).
3. V.M. Golubov, V.I. Il'ina, V.K. Kritskaya, G.V. Kurdyumov and M.D. Perkas, *(Problems of the Metallography and Physics of Metals)*, No.5, Metallurgizdat, p.433 (1958).
4. D.M. Zlatoustovskii and Ya.S. Umanskii, *Nauchnye doklady vysshii shkoly (Scientific Reports of a College)* Metallurgiya, 1 (1958).
5. V.I. Prosvirin, *Vliyanie vneshnego davleniya na fazovye prevrashcheniya v stalyakh (The Effect of External Pressure on Phase Transformations in Steels)*, Mashgiz, (1948).
6. O.P. Maksimova, A.I. Nikanorova and R.I. Entin *(Problems of the Metallography and Physics of Metals)*, No.4, Metallurgizdat, (1955).
7. A.P. Gulynev and I.V. Chernenko, *Metalloved. i. obrab. met.* No.5 (1957).
8. S.T. Kishkin, *Izv. Akad. Nauk SSSR, Department of Technical Sciences*, No.12 (1946).
9. G.V. Kurdyumov and A.I. Lysak, *Zh. tekh. fiz.*, 16 (1946); 18 (1947).
10. S.V. Serensen, *Zav. lab.* No.4 (1958).
11. B.A. Apaev, *Fiz. metall. metalloved.* Vol.4, No.2 (1957).
12. B.A. Apaev and Yu.A. Sysuev, *Nauchnye doklady vysshii shkoly (Scientific Reports of a College)*, Metallurgiya, No.2 (1958).
13. T. Suzuki and T. Imura, *Rep.Conf. Defects in Cryst. Solids in Bristol*, London, 347 (1955).
14. P.W. Bridgman, *Recent Work in the Field of High Pressures*, (1948).
15. A.P. Gulyaev and N.I. Burova, *Metalloved. i. obrab. met.* No.1 (1955).
16. V.K. Babich and K.F. Starodubov, *Izv. vyssh. ucheb. zaved., Chernaya Metallurgiya*, No.2 (1958).
17. I.N. Bogoachev and Kh.D. Reshetnyak, *Izv. vyssh. ucheb. zaved., Chernaya Metallurgiya*, No.8 (1958).
18. B.D. Grozin, *Mekhanicheskie, svoistva zakalennoi stali (The Mechanical Properties of Hardened Steel)*, Mashgiz (1951).
19. K.A. Osipov, *Issledovaniya po zharoprochnym splavam (Studies of Heat-Resistant Alloys) Izd. Akad. Nauk. SSSR*, 3 (1958).
20. J. Grangle and W. Sucksmith, *J. Iron and steel Inst.* 168 (1951); 170 (1952).
21. Camo, Hucugzaba, *J. Japan Inst. Metals*, 20 (1956).

VOL. 8 195

STUDY OF THE MECHANICAL PROPERTIES OF SOLIDS, PARTICULARLY METALS, AT AND BELOW TEMPERATURES OF 4.2°K

III. THE MECHANICAL PROPERTIES OF IRON, TITANIUM, TANTULUM AND 2 STEEL AT AND BELOW TEMPERATURES OF 4.2°K*

O.V. KLIAVIN and A.V. STEPANOV

Physico-technical Institute of the Academy of Sciences of the USSR, Leningrad

(Received 29 September 1958)

The present paper is a continuation of the earlier published investigations [1, 2]. The data given below were obtained with the method and in the conditions described in [1]. The present paper gives the results of tests on polycrystalline specimens of armco iron, titanium, tantalum and 2 steel at temperatures of 300, 78, 4.2 and 1.6°K.

The accepted denotations and the dimensions of the specimens are the same as in [1, 2].

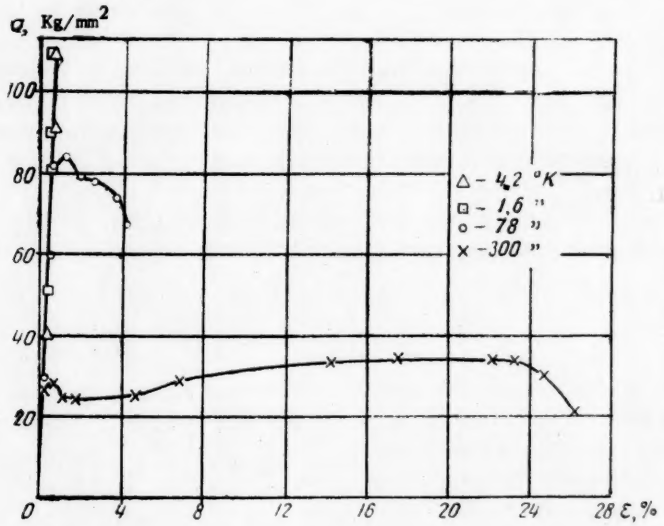

Fig. 1. Elongation diagrams at T = 300; 78; 4.2 and 1.6°K for specimens of armco iron.

* *Fiz. metal. metalloved.* 8, No.6, 922-927, 1959.
The work has been reported to the 11th scientific-technical conference on refractory, heat resistant alloys and cerametallic materials (Moscow, April 1957) and at the 4th All-Union conference on low temperature physics (Moscow, June 1957). The previous paper [2] was reported to the All-Union conference on low temperature physics (Leningrad, June 1956).

TABLE 1

Results of the testing of annealed armco iron

Number of experiments	T, °K	$\sigma_s\left(\frac{\text{upper}}{\text{lower}}\right)$, kg/mm^2	σ_B, kg/mm^2	σ_z, kg/mm^2	S_B, kg/mm^2	ψ_B, %	ψ_K, %	ε_K, %	S_K^*, kg/mm^2	S_K^{**}, kg/mm^2	S_K^{***}, kg/mm^2
3	300	$\frac{30}{26}$	36	22	42	16	88	27	$\frac{185}{172}$	$\frac{134}{115}$	92
5	78	$\frac{82}{78}$	83	68	83	0	54	4	$\frac{165}{137}$	$\frac{152}{133}$	143
7	4,2	106	106	106	106	0	73	0,6	$\frac{437}{325}$	$\frac{356}{278}$	210
2	1,6	112	112	112	112	0	74	0,5	$\frac{430}{429}$	$\frac{327}{300}$	226
*	300	22	34	—	—	—	73	—	74	—	—

* From data of paper [3].

Notes. Since the scattering of the values of S_k^* and S_k^{**} was considerable from the causes shown in paper [1], we give in all tables both the maximum and the minimum value of these quantities.

The values of S_k^* were obtained with the method and under the conditions described in [1], the values of S_k^{**} with the usual method of dividing the load at the moment of fracture by the area of the cross section which is determined after the fracture of the specimen from the average diameter in the neck at its narrowest point.

The values of S_k^{***} are calculated from the Markovets formulae [4] if the values of σ_B and ψ_k are known. These formulae have the following form:

$S_K = \sigma_B(0{,}8 \div 2{,}06\ \psi_K)$ for $\psi_B > 0{,}15$; $S_K = \sigma_B(1 \div 1{,}35 \cdot \psi_K)$ for $\psi_B < 0{,}15$.

1. Armco iron. The specimens for the tests of armco iron were drawn from rods of 12 mm diameter, their surface was treated with emery paper of 14 μ grain, they were annealed at 600°C for one hr in a vacuum of $\sim 10^{-4}$ mm.

The results of the tests are given in Table 1 and Fig. 1 which represents an elongation diagram.

At T = 4.2 and 1.6°K the specimen breaks with formation of a neck (ψ_k = 73-74%). Thus, the plasticity of the iron is preserved down to these temperatures.

Fig. 2 shows a photograph of the point of fracture of the armco iron specimen. The temperature of the test was 4.2°K (at 1.6°K a similar neck was observed). Neck formation is observed both in iron and in aluminium [1, 2]. With the lowering of the temperature, however,

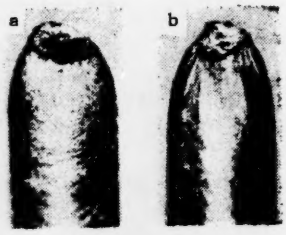

Fig. 2a and b. Photographs (x20) of the silhouettes of the points of fracture of specimens at a temperature of 4.2°K: a) annealed armco iron; b) annealed tantalum (99.74%).

the relative elongation of the iron drops, although the yield strength increases sharply. When the yield point is reached in the temperature region of 4.2-1.6°K the plastic deformation which sets in at once takes on a local character and a neck is formed, which causes fracture.

Thus, at low temperatures there is virtually no even plastic elongation of the specimen. Visual observation under a microscope of the behaviour of the specimen at the moment of fracture shows that neck formation takes place in a very brief time interval. The inertia of the device for measuring the force did not permit the drop in the load to be noted at the moment of fracture.*

It is interesting to note that, as can be seen from Table 1, the plasticity of iron is at a minimum at $T = 78°K$ (liquid nitrogen), if it is measured by the value of ψ_k.

After the present work on iron had been completed, Smith and Rutherford [5] and Basinski and Sleeswyk [6] in the United States obtained similar results independently of us; at $T = 4.2°K$ in superpure iron they also observed a residual elongation $\epsilon_k = 11\%$ and a jump in the elongation diagram which they explain by the appearance of twins.

2. *Titanium.* The titanium which was studied (99.6%) contained the following impurities (according to the certificate): 0.13% Fe, 0.14% Ni, 0.07% C, 0.072% N_2.

The specimens were turned in a lathe from rods of 10 mm diameter and polished with emergy paper of 14 μ grain. They were annealed at $T = 800°$ C for one hr in a vacuum of

TABLE 2

Results of the testing of annealed titanium

Number of experiments	T, °K	σ_s, kg/mm²	σ_B, kg/mm²	σ_z, kg/mm²	S_B, kg/mm²	ψ_B, %	ψ_K, %	ε_K, %	S_K^*, kg/mm²	S_K^{***}, kg/mm²
3	300	66	75	65	86	12	48	18	125/124	125
2	78	108	119	119	131	9	16	12	143/141	148
3	4,2	134	134	134	134	0	14	1	164/153	167
3	1,6	132	132	132	132	0	14	1	158/147	161
*	300	61—63	58—75	—	—	—	30—75	3—11	—	—

* From data of paper [7].

* For materials in which localized plastic deformation causing neck formation (without even elongation of the specimen) is observed at helium temperatures, the values of the quantities σ_s, σ_B, σ_z and S_k^* are given not in the usual meaning since the values of the stresses which correspond to these quantities are reached in a very brief interval of time and with our method [1] cannot be divided in time. It follows that the numerical values of the quantities σ_s, σ_B, σ_z, S_k^* for $T = 4.2$ and 1.6°K are exagerated and that $\sigma_s = \sigma_B = \sigma_z$.

The disagreement of S_k^* with the values in reference books [9] can be explained by the following causes: 1) the effect of the scale factor (which apparently depends on the temperature; 2) the more accurate method of determination of ψ_k [1, 2]; 3) by the error in the determination of the force at the moment of the fracture of the specimen.

$\sim 10^{-4}$ mm. The results of the tests are given in Fig. 3 and in Table 2.

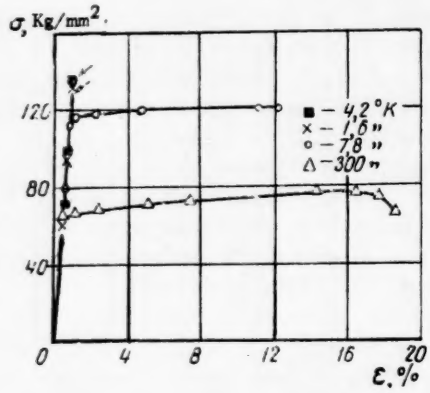

Fig. 3. Elongation diagrams at T = 300, 78, 4.2 and 1.6°K for specimens of annealed titanium (99.59%).

The changes in the mechanical properties of titanium when the temperature is lowered are similar to those observed in iron: the yield strength increases, the even elongation disappears at low temperatures. When plastic deformation begins it becomes at once localized and a neck is formed ($\psi_k \simeq 14\%$ at $T = 4.2^\circ$ and 1.6°K).

At $T = 4.2^\circ$K a jump was observed before fracture (stress $\simeq 130$ kg/mm^2) for each of three tested specimens.*

The temperature of 1.6°K is characterized by the fact that in two out of three tested specimens ($\sigma \simeq 126$ kg/mm^2) one or two jumps were observed before fracture, their amplitudes being:

$P = -0.5$ kg; $\Delta l = +0.005$ mm ($T = 4.2^\circ$K)

$P = -1$ kg; $\Delta l = +0.01$ mm (first jump)

$P = -2$ kg; $\Delta l = +0.01$ mm (second jump) } ($T = 1.6^\circ$K)

3. Tantalum. The tantalum specimens tested (Ta + Nb = 99.74%) contained the following impurities, according to the certificate: 0.63% Nb, 0.1% Ti, 0.004% Si, 0.025% Mo, 0.039% W. The study of tantalum was of special interest because it was possible to compare its properties in the ordinary and the superconducting state ($T_{cr} = 4.4^\circ$K). The specimens were turned in a lathe from rods of 8 mm diameter. The specimens were annealed at $T = 1100^\circ$C for 2 hr in a vacuum of $\sim 10^{-4}$ mm.

TABLE 3

Results of the testing of annealed tantalum

Number of experiments	T, °K	σ_s, kg/mm²	σ_B, kg/mm²	S_B, kg/mm²	σ_z, kg/mm²	ψ_B, %	ψ_k, %	ε_k, %	S_k^*, kg/mm²	S_k^{**}, kg/mm²	S_k^{***}, kg/mm²
4	300	56	62	67	43	7	79	13	236/181	152/125	130
4	78	103	103	103	88	0	69	6	328/268	248/205	200
3	4,2	115	115	115	115	0	74	0,6	474/381	362/275	230
2	1,6	120	120	120	120	0	77	0,5	530/530	413/350	245
*	300	—	35—52	—	—	—	—	25—40	—	—	—

* From data of paper [7].

* The beginning of the jump at low temperatures is indicated by arrows in all the elongation diagrams shown.

The results of the tests are given in Fig. 4 and in Table 3. The nature of the changes in the mechanical properties when the temperature is lowered is similar to that observed for iron. With decreasing temperature the yield strength increases, but the even elongation disappears. At low temperatures the plastic deformation which sets in is at once localized and a neck is formed ($\psi_k \sim 74\%$ at $T = 4.2^\circ K$), which causes the fracture of the specimen.

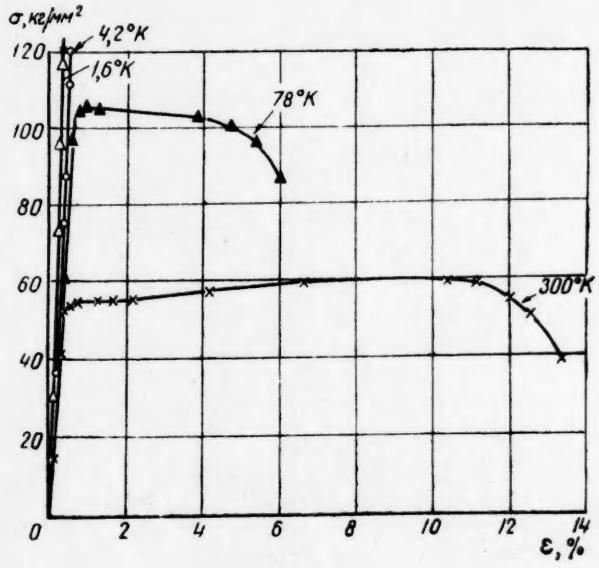

Fig. 4. Elongation diagrams at $T = 300$, 78, 4.2 and 1.6°K for specimens of annealed tantalum.

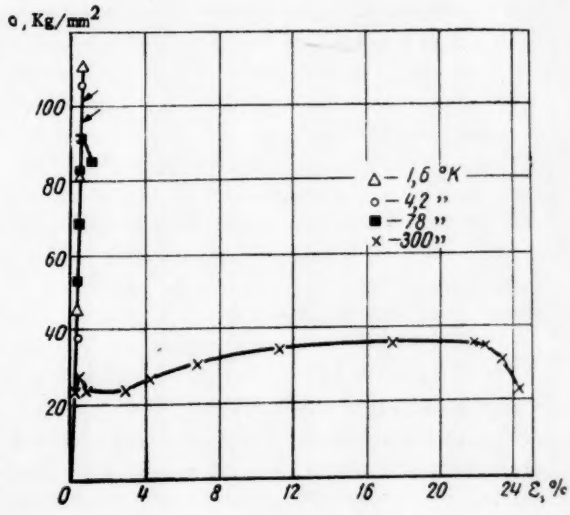

Fig. 5. Elongation diagrams at $T = 300$, 78, 4.2 and 1.6°K for specimens of annealed 2 steel.

TABLE 4

Results of the testing of annealed 2 steel

Number of experiments	T, °K	σ_s (upper / lower), kg/mm²	σ_B, kg/mm²	σ_z, kg/mm²	S_B, kg/mm²	ψ_B, %	ψ_K, %	ε_K, %	S_K^*, kg/mm²	S_K^{**}, kg/mm²	S_K^{***}, kg/mm²
3	300	27 / 23	33	21	41	14	74	25	94 / 83	90	71
5	78	86 / 81	91	88	91	0	12	1,2	99 / 88	99	106
3	4,2	—	106	106	106	0	0	0,4	107 / 105	107	106
6	1,6	—	110	110	110	0	0	0,5	121 / 103	121	110
*	300	29	43	—	—	—	76	30	—	—	—

* From data of paper [8].

Fig. 2b shows the photograph of the point of fracture of a tantalum specimen at $T = 4.2^{\circ}K$. Jumps were not observed in the elongation diagrams. The temperature of $1.6^{\circ}K$ is characterized by the fact that in both the specimens tested one jump was observed before fracture (stress $\simeq 118$ kg/mm^2) the amplitude of the jumps being $P = 0.5$ kg; $\Delta l = + 0.005$ mm.

No difference whatever was observed in the mechanical properties of the superconducting and non-superconducting state.

4. 2 *Steel.* The specimens of 2 steel (0.2% C) were turned from rods of 12 mm diameter and polished with emery paper of 14 μ grain size. The specimens were annealed at $T = 600^{\circ}C$ for one hr in a vacuum of $\sim 10^{-4}$ mm. The results of the tests are given in Fig. 5 and Table 4.

At $T = 4.2^{\circ}K$ three jumps were observed in the elongation diagram before fracture (stress $\simeq 101$ kg/mm^2) for one of the three specimens tested; the amplitude of the jumps was $P = -0.5$ kg; $\Delta l = + 0.02$ mm.

The temperature of $1.6^{\circ}K$ was characterized by the fact that in two out of six specimens tested (stress $\simeq 95$ kg/mm^2) 4-5 jumps were observed before fracture; the amplitude of the jumps was $P = -0.2$-0.4 kg; $\Delta l = -0.005$ mm. At 1.6° one of the specimens broke into three pieces. It is important that the fracture was virtually brittle beginning with temperatures of $78^{\circ}K$ and lower. As in the case described in [1] where the low temperature strength of aluminium was compared with that of its alloy B-95, the strength of iron is greater at low temperatures than that of 2 steel.

In conclusion we express our gratitude to our colleagues at the institute H.M. Reinov, N.G. Andreyev, G.A. Gukasov, Iu.M. Chernov, A.M. Poliakov, Iu.A. Burenkov, D.D. Baturin, who helped us in this work.

Translated by B. Ruhemann

REFERENCES

1. O.V. Kliavin and A.V. Stepanov, *Fizika tverdogo tela* 1, No.6 (1959).
2. O.V. Kliavin and A.V. Stepanov, *Fiz. metal. metalloved.* 8, 274 (1959).
3. P.M. Roitman and Ia.B. Fridman, *Mikromekhanicheskii metod ispytaniia materialov (The micromechanical method of testing materials)* Oborongiz (1950).
4. N.A. Shaposhnikov, *Mekhanicheskiye ispytaniia metallov (Mechanical metal tests)* Mashgiz, Moscow-Leningrad (1954).
5. I.K. Smith and R.T. Rutherford, *Journ. of Metals* 9, 857 (1957).
6. Z.S. Basinski and A. Sleeswyk, *Acta metallurgica*, 5, No.3, 176 (1957).
7. M.L. Filiand and Ye.I. Semenova, *Svoistva redkikh elementov (The properties of the rare elements)* Metallurgizdat (1953).
8. V.I. Kostenets, *Zh. tekh. fiz.* 16, 5 (1946).
9. *Entsiklopedicheskii spravochnik "Mashinostroyeniye" (Engineering Encyclopedic Handbook)* 3 (1947).

VOL 8 195

THE INFLUENCE OF THE SIZE EFFECT ON THE DEFORMABILITY OF METALS*

I.A. RAZOV, Ye.M. SHEVANDIN and A.V. YEFIMOV

Central *A.N. Krylov* Scientific Research Institute

(Received 24 Februsry 1959)

VOL. 8 1959

The size effect is now usually explained either from the standpoint of the statistical theory [1-7] or from that of the stored energy theory of strength [8-11]. The former regards the metal as a polycrystalline aggregate which includes a large number of defects; the distribution of the defects according to the degree of danger they represent is subject to a statistical Gauss law. Accordingly, the probability of being within the sphere of influence of the most dangerous defect increases with the sphere of influence. Therefore, the strength and plasticity of specimens of larger dimensions are always less than that of specimens of smaller size.

According to the second theory, which takes into account the kinetics of the fracture process, the onset of fracture does not depend on the size while the end of fracture is determined precisely by the size effect. This effect is linked with the stored elastic energy in a loaded system, which affects the rate of development of cracks and increases with increasing specimen size.

From the physical standpoint, the elastic energy takes effect by compensating the field of the excess stresses in the defect or crack the intensity of which decreases with the spreading of the crack.

From paper [12] it follows that for different materials of the same strength the size effect is determined not only by the external factor (the stored elastic energy), but also by an internal, structural factor (the physical properties of the material, i.e. in the final analysis by the atomic bonds).

There exists numerous considerations which speak in favour of both theories. In order to find out which of the two theories is valid it was necessary to make a special experiment. Such an experiment, at least for the region of viscous fracture, could be the determination of the plastic deformation which corresponds to the beginning and the end of fracture on two sets of specimens of different size and with different stored elastic energy, in both cases taking into account the statistical inhomogeneity of the metal as a polycrystalline aggregate.

The investigations were made on SKhL-4 steel* with large specimens of 20 x 20 x 110 mm size and a radius at the bottom of the incision of ρ = 6 mm and with small specimens of 5 x 5 x x 27.5 mm size and a radius at the bottom of the incision of ρ = 1.5 mm. The small specimens after the latter had been tested. The base of the incisions on both small and large specimens was always at the same level. In this way the maximum possible homogeneity of the material to be subjected to plastic deformation and fracture was ensured for specimens of both sizes. This made it possible to study the physical size effect almost completely excluding the effect of the technological factor. The specimens were tested for static bending under a concentrated force applied in the middle of the span; the relative deformation which corresponds to the beginning of the appearance of the first macro-cracks of a size of the order of 0.2-0.3 mm and the deformation at fracture which corresponds to the fracture crack going right through the entire length of

* *Fiz. metal. metalloved.* 8, No.6, 928-933 (1959).

* The mechanical properties are: σ_T = 42.1 kg/mm^2, σ_B = 61.0 kg/mm^2, δ_{10} = 29.5%, δ_p = 14.9%, ψ = 76.6%.

the bottom of the incision were determined for all specimens.

The method of determining the deformation during the testing of the large specimens was the same as the method described in paper [13]. For the testing of the small specimens a slightly different method was used. Several marks or "points" were made on the bottom of the incision instead of the usual dividing network. To distinguish this method from that of the dividing network it was accordingly called the "points" method.

Depending on the size of the radius of the bottom of the incision the size of the "points" was made equal to 0.3-0.5 mm. Before and during the testing process the size of the points was measured with an instrument microscope UIM-21 with an accuracy of 0.001 mm. Three to four "points" were made on each specimen in its centre third. The average of all measurements was taken as the final result.

The data obtained for all specimens is given in Table 1. From these results frequency curves of the deformation are plotted which correspond to the beginning of the appearance of the first cracks and to complete fracture (Fig. 1 and 2).

Fig. 1 shows that the distribution curves of the deformations which correspond to the appearance of the first cracks for large and small specimens are very close to each other and in form approximate a normal Gauss distribution curve. The maxima of the frequency curves the two cases coincide accurately.

Naturally, these results do not agree with

VOL. 8 195

TABLE 1

Values of the deformations for the beginning and end of the fracture of specimens of different sizes

Specimens of 20 x 20 x 110 mm size		Specimens of 5 x 5 x 27.5 mm size		Specimens of 20 x 20 x 110 mm size		Specimens of 5 x 5 x 27.5 mm size	
δ_{xb}, %	δ_{xe}, %	δ_{xb}, %	δ_{xe}, %	δ_{xb}, %	δ_{xe}, %	δ_{xb}, %	δ_{xe}, %
42.3	131	46.7	121	45.5	131	45.3	145
45.0	132	43.7	117	46.7	121	42.3	136
46.3	143	39.6	133	45.1	103	46.9	194
44.1	117	47.3	169	47.8	133	50.3	148
43.8	135	38.2	152	47.5	117	43.3	142
49.0	136	42.6	148	43.6	133	42.6	158
45.1	123	47.1	145	45.0	129	42.7	145
41.0	121	48.7	159	43.1	108	45.7	147
48.1	135	51.3	181	45.5	105	44.7	151
43.9	137	39.7	115	44.8	135	46.5	122
46.3	124	46.1	126	45.0	111	45.9	152
47.8	129	43.2	158	47.1	121	47.8	158
46.3	122	45.2	178	45.3	128	45.7	179
45.1	139	43.1	162	46.7	112	47.1	138
45.2	124	45.1	168	45.4	128	45.2	168
43.0	143	44.3	158	42.3	138	46.4	166
45.3	129	45.2	132	46.3	149	52.4	158
43.8	128	40.9	163	41.0	135	44.3	162
45.1	138	45.2	161	45.4	112	45.1	178
45.3	129	39.4	166	45.3	139	44.8	182

the statistical theory of strength, since according to that theory the maximum of the distribution curve (that is, the most probable value of the deformation which corresponds to the appearance of the first cracks) should for small specimens lie at relatively greater deformations than for large specimens. Besides, the scattering of the individual values of the deformations at the beginning of the appearance of cracks for small specimens compared with that for large specimens should have been much greater than was in fact observed. Hence, this result cannot be explained from the standpoint of the statistical theory of strength. Nevertheless, the very form of the curves reveals that a certain role is being played here by the statistical factor. This question will now be discussed in greater detail.

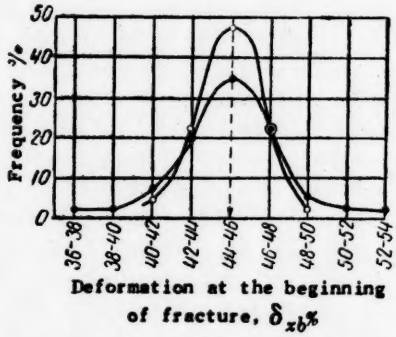

Fig. 1. Curves of the distribution of the deformations at the beginning of fracture for specimens of different sizes:
- o specimens of 20 x 20 x 110 mm size; ρ = 6 mm;
- • specimens of 5 x 5 x 27.5 mm size, ρ = 1.5 mm.

In the statistical theory of strength the nature and form of the "defects" are not established: therefore, dross or intermetallic inclusions, any defects in the structure of the crystal lattice itself such as dislocations or incipient microcracks (within the limits of the "holes" in the crystals) or any other kind of " defect" can be meant. Pashkov [14] gives a more precise definition of defect by assuming for it a certain region of given dimensions in which for some reason plastic deformation is made difficult and where as a result a volume stress arises.

Any interpretation of "defect" in the statistical theory leads, however, to a dependence of the deformation at the beginning of fracture on the scale, of a type shown in Fig. 3a, which contradicts the direct experimental data.

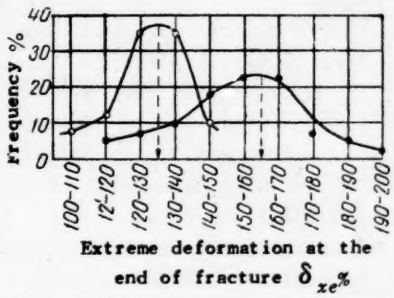

Fig. 2. Distribution curves of the extreme deformations at the end of fracture for specimens of different sizes:
- o specimens of 20 x 20 x 110 mm size, ρ = 6 mm;
- • specimens of 5 x 5 x 27.5 mm size, ρ = 1.5 mm.

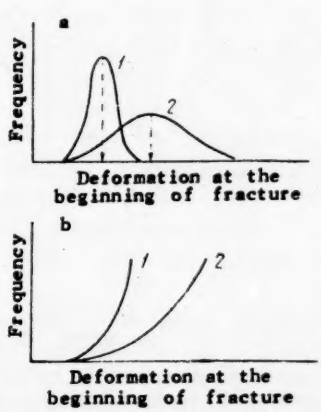

Fig. 3. Schematic position of distribution curves of the deformations at the beginning of fracture: a) with a Gauss, b) with a hyperbolic law for the distribution of the defects.
1) large specimens; 2) small specimens.

This difference between the theoretical and and experimental data becomes more understandable if one assumes that the main premise of the statistical theory concerning the Gauss distribution of the "defects" according to the degree of danger they represent is not valid. It is more natural to assume that in reality the " defects" are distributed according to a hyperbolic law, that is to say, the less dangerous the defect, the greater

the number of such defects in the material. This assertion is based firstly on the fact that there is not a single paper which experimentally confirms precisely the Gauss law of the distribution of the "defects". Secondly, the hyperbolic law of the distribution of the "defects" follows from the fact that the number of elementary defects such as dislocations, is of the order of 10^8 per cm^2, while the number of such defects as, for example, non-metallic inclusions (which are substantially larger in dimensions than dislocations) is many thousand times less.

From a hyperbolic law of the distribution of "defects" Gaussiun curves cannot be obtained at all for the distribution of the values of the initial deformations. Distribution curves constructed from the hyperbolic law have the form given in Fig. 3b.

Taking account of what has been said above, one must conclude that the appearance of the initial macrocracks cannot be connected with the " defects". The explanation of the results obtained must be based on different considerations.

In as much as the real metal represents a polycrystalline aggregate, the first macrocracks, according to paper [15] in particular, are inevitably linked with individual grains and depend on the orientations of the grains with respect to the direction of the acting force.

The first macrocracks which can be reliably determined in the incision while the investigation is being made with the instrument microscope are of the order of 0.2 mm. Hence, such an initial macrocrack covers a group of about 10 grains if the average grain size is 20μ. It is natural that the properties of this "group" may be very different depending on whether the grains included in it have different orientations and, hence, a different limit of plasticity. It is least likely that all the grains composing the "group" will have the same orientation and minimum or maximum limit of plasticity. It is most likely that all the grains of a given "group" will have different orientations, and, hence, some average limit of plasticity. It follows that the polycrystalline structure of the metal itself gives rise to a Gauss curve for the distribution of the values of the plasticity which correspond to the appearance of the first cracks.

Specimens of 20 x 20 x 110 mm size and ρ = 6 mm and specimens of 5 x 5 x 27.5 mm size and ρ = 1.5 mm have the same deformation as the first cracks appear because the working surface in the incision of even a small specimen, not to mention a large one, includes about 800 grains. With such a considerable number of grains the effect of the statistic factor connected with the orientation of the grains proves to be the same for specimens of different dimensions. From this standpoint the scattering of the values of the deformations which correspond to the beginning of fracture should differ little in large and small specimens, which is observed experimentally.

Thus, the statistic factor will have a certain influence on the beginning of fracture in very small specimens (of a size of the order of a few times ten millimetres), or in ordinary specimens (of a size of the order of 5 mm) when the grains are very large. In other words, the smaller the ratio d/M (where d is the grain size, and M a coefficient determining the size of the specimen), the less will be the effect of the statistic factor.

Fig. 2 shows that the curves of the distribution of the final deformations which correspond to fracture differ materially from each other. In the first place, the distribution curve for small specimens is displaced (at its maximum) by 30% compared with the distribution curve for large specimens. In the second place, the scattering of the values of the extreme final deformations for small specimens is substantially greater.

The shifting of the distribution curve is explained by the effect of the stored elastic energy in the specimen on the rate of development of the cracks [10]. With a large amount of stored elastic energy the cracks spread with great speed and this is not accompanied by any considerable plastic deformation. It is possible that this process is strongly localized and that plastic deformation develops only directly in the area of the fracture crack. In large specimens, therefore, the limit of plasticity which corresponds to fracture will always be less than in small specimens.

The form of the curves shown in Fig. 2 might seemingly be explained from the standpoint of

VOL. 8 195

the statistical theory of strength. In the first place, however, the extreme deformation which corresponds to the end of fracture is determined on the surface of the incision, while the process of fracture at that moment is penetrating to a considerable depth below the surface. Therefore one cannot speak here of the role of " defects" in the same sense as the statistical theory.

Secondly, one must take into account that the process of complete fracture does not represent a consistent development of one particular crack. At a certain stage individual small macrocracks begin to merge and in the final upshot form one main crack. Bearing this in mind one may suggest that the rate of merging of individual cracks and the formation of a main crack will be influenced both by the degree to which these cracks (by their length and the sharpness of the edge which determines the degree of localization of the process of fracture) represent a danger, and by the size of the specimen (by its elastic energy). In other words, the more dangerous the crack and the greater the dimensions of the specimen to be tested, the more rapidly and with less deformation will fracture occur in the end, and vice versa.

From the standpoint of the effect of the elastic energy it is possible to explain the form of the curves in Fig. 2 which correspond to complete fracture, that is to say, the greater scattering of the values of the extreme deformations for small specimens compared with that of the larger ones.

The latter becomes evident if one pays attention to the natural obstacles to the development of cracks in the form of differently orientated grains, their boundaries, various kinds of inclusions, small regions subject to uneven strengthening as a result of local plastic deformation, etc.

These obstacles have different effects on the rate of growth of the cracks depending on the size of the specimen.

In small specimens for which the amount of stored elastic energy is small the growth of the cracks may be held up to a different degree, since in different specimens of small size obstacles with different effects on the rate of spreading of the cracks may be encountered. This is the cause of the great scattering of the values of the extreme plastic deformation.

In large specimens for which the amount of stored elastic energy is great the cracks develop very rapidly in virtually all cases; they easily overcome the existing obstacles, and as a result the scattering of the values of the extreme plastic deformation is negligible.

Hence, the size effect as a whole represents a combination of energetic and statistical factors. The former plays the main, and the latter a subsidiary role, determining the position and form of the distribution curve respectively.

Nevertheless, it is necessary to take into account that under real conditions the so-called metallurgical factor acquires very considerable importance; it is dependent on the inhomogeneity of the metals, in particular steel, arising out of the technology of production, namely the circumstances of casting, rolling, etc. The role of the metallurgical factor may become so important that the distribution curve of the deformations for specimens of the same size may become substantially different both in position and in form, depending on the part of the examined sheet from which the specimens of the given series were cut, and also on the position of the examined material relative to the rolling axis and the edges of the sheet (bottom or head of the billet). As we know, the plasticity of the material of a given casting or sheet is worse in the axis of the billet and its ends, particularly in the head part. To obtain results which reliably characterize the dependence of the deformability of a sheet on size effect it is necessary to have test data on a large number of specimens of different sizes cut from different parts of the sheet.

Translated by B. Ruhemann

REFERENCES

1. W. Weibull, *Proc. Roy. Soc. Swed. Inst. Eng. Res.* Stockholm 151 and 153 (1939).
2. T.A. Kontorova and Ia.I. Frenkel', *Zh. tekh. fiz.* 11, 173 (1941).
3. Ye.M. Shevandin and Sh.S. Manevich, *Zh. tekh. fiz.* 16, 1223 (1946).
4. F.F. Vitman, *Zh. tekh. fiz.* 16, 961 (1946).

5. B.B. Chechulin, *Zh. tekh. fiz.* 24, 292 (1954).
6. I.M. Roitman and Ia.B. Fridman, *Mikromekhanicheskii metod ispytaniia metallov (The micromechanical method of metal testing)* (1950).
7. B.B. Chechulin, *Zh. tekh. fiz.* 24, 1101 (1954).
8. N.N. Davidenkov, *Predisloviye k knige L.S. Moroza i S.S. Shurakova "Problema prochnosti tsementovannoi stali" (Foreword to the book "The problem of the strength of case hardened steel" by L.S. Moroz and S.S. Shurakov)* (1947).
9. A.A. Wells, *Trans. N.E. Coast Inst. Eng. and Shipbuild.* 71, No.6, 277 (1955).
10. Ye.M. Shevandin, I.A. Razov, B.N. Serpeninov and R.Ye. Reshetnikova, *V sb., posviashchennom 80-letiiu N.N. Davidenkova (in the collection of papers commemorating the Eightieth anniversary of N.N. Davidenkov)* (1959).
11. I.L. Shemelevich, *v sb. Metallovedeniye (coll. Metallography)* p.70, (1957).
12. Ye.M. Shevandin, I.A. Razov and A.V. Yefimov, *v sb. posviashchennom 80-letiiu N.N. Davidenkova (in the collection of papers commemorating the eightieth anniversary of N.N. Davidenkov* (1959).
13. Ye.M. Shevandin, I.A. Razov and B.N. Serpeninov, *Zav. lab. toriia* 22, No.11, 1338 (1956).
14. P.O. Pashkov, *Plastichnost i razrysheniye metallov (The plasticity and fracture of metals)* Sudpromgiz (1950).
15. Ye.M. Shevandin, *Zh. tekh. fiz.* 8, 441 (1938).

VOL
8
195

TO THE QUESTION OF THE DEPENDENCE OF THE HARDNESS ON THE COMPOSITION OF MULTI-PHASE ALLOYS*

V.P. SHISHOKIN and A.E. NIKEROV

Leningrad M.I. Kalinin Polytechnical Institute

Leningrad A.I. Herzen Pedagogical Institute

(Received 17 February 1959)

It is shown that in the general case the dependence between the hardness and the composition of alloys which are mechanical mixtures will be non-linear. The form of the functional dependence is given which should govern any property so as to be a linear function of the composition in the general case.

VOL. 8 1959

For a long time it has been assumed that the hardness of alloys which form a mechanical mixture of the components should be a linear function of the composition. Already in 1907, however, A. Sapozhnikov and Ia Kanevskii [1, 2] observed that in the system lead-antimony the hardness changes along a curve with a maximum, while the eutectic composition has the most extreme hardness. Later [3-8] the number of similar examples increased.

The deviation of the functional dependence of the hardness of two-phase alloys from an additive straight line was at first explained by the alloys investigated not being of equilibrium composition [9, 10], but later, when this concept was rejected, by the presence of interactions between the phases [7, 11-14]. Although interaction between the phases plays an important role in the plastic deformation of alloys, such alloys cannot strictly speaking be called mechanical mixtures. Therefore, without denying the importance of taking account of such interaction, we shall attempt to explain the causes of the non-additive change in the hardness of two-phase alloys in the case of the absence of any kind of interaction between the phases.

According to one of the existing points of view [4, 9, 10, 15, 16], the absence of an additive dependence is explained by the faulty selection of units for the measurement of the concentration. We shall show that in the general case the hardness is a non-linear function of the composition in whatever units the latter may be measured. For this purpose we use the well known dependence of the hardness on the temperature

$$H = H_0 e^{\alpha\left(t^\circ - t_0^\circ\right)}, \tag{1}$$

where α depends on the composition and does not depend on the temperature.

Let the hardness at the temperature t_0° be a linear function of the composition

$$H_0 = ax + b; \tag{2}$$

then the dependence will be of a linear form at other temperatures only if

$$\alpha \neq f(x) \tag{3}$$

or if

$$\alpha = \text{const}. \tag{4}$$

Indeed, if condition (4) is fulfilled,

$$H = ae^{\text{const}\left(t^\circ - t_0^\circ\right)} x + be^{\text{const}\left(t^\circ - t_0^\circ\right)} = a_1 x + b_1;$$

but if the coefficient α is even a linear function of the concentration

$$\alpha = a_1 x + a_2,$$

then

* *Fiz. metal. metalloved.* 8, No.6, 934-938, 1959.

$$H = \left[ax\, e^{\alpha_1 x\left(t^\circ - t_0^\circ\right)} + be^{\alpha_1 x\left(t^\circ - t_0^\circ\right)}\right] e^{\alpha_2\left(t^\circ - t_0^\circ\right)},$$

that is, at

$$t^\circ \neq t_0^\circ$$

the hardness will depend on the concentration in a non-linear manner.

In the more general case, let

$$\alpha = f(x); \tag{5}$$

then

$$\ln H = \ln(ax + b) + (t^\circ - t_0^\circ) f(x). \tag{6}$$

Differentiating (6) with respect to t°, we get

$$\frac{H'_{t^\circ}}{H} = f(x)$$

or

$$\frac{\partial H}{\partial t^\circ} = Hf(x) = H\alpha. \tag{7}$$

If H is a linear function of the composition

$$\frac{\partial^2 H}{\partial x^2} = 0;$$

whence

$$\frac{\partial\left[\frac{\partial^2 H}{\partial x^2}\right]}{\partial t^\circ} = 0.$$

If (7) is twice differentiated with respect to x, one can obtain the following expression:

$$2\frac{\partial H}{\partial x}\cdot\frac{d\alpha}{dx} + H\frac{d^2\alpha}{dx^2} = 0 \tag{8}$$

or

$$\frac{d^2\alpha}{dx^2} + 2\frac{\partial \ln H}{\partial x}\cdot\frac{d\alpha}{dx} = 0;$$

whence

$$\alpha = c_2 - c_1\int H^2 dx. \tag{9}$$

Formula (9) contradicts the initial proposition that

$$\alpha \neq f(t^\circ);$$

hence, a linear dependence of the hardness on the composition can be observed at all temperatures only in the special case where

$$\alpha \neq f(x).$$

Incidentally, many investigations have shown that the composition has a very important effect on the heat coefficient of the plastic deformation (α). Hence, if the hardness is to be a linear function of the composition at some specific temperature (t_0°), then at any other temperature a linear dependence will not occur.

We can come to the same conclusion on the basis of the following graphic construction (Fig. 1).

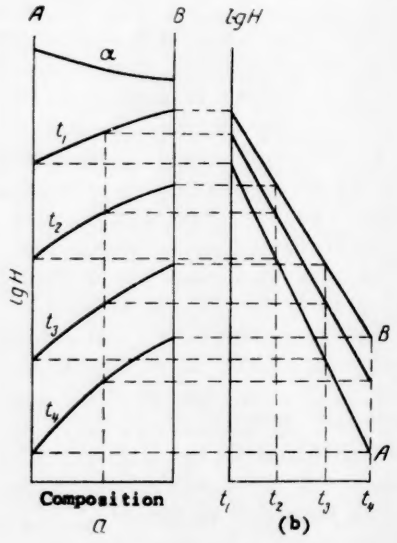

Fig. 1. Dependence between the logarithm of the hardness and the composition at different temperatures.

Let the dependence between the hardness H and the composition of systems which form mechanical mixtures of the components A and B at the temperatures t_0°-t_0° be a linear function. Then in Fig. 1a the dependence between lg H and the composition is expressed by curved lines (the curves t_1-t_4). Projecting these curves on Fig. 1b which shows the dependence between lg H and the temperature, we get three

straight lines with different angles of inclination, and for the average composition the straight line will lie closer to the straight line of component *B*. Accordingly, the curve for the change in the heat coefficient of the hardness as a function of the change in composition (Fig. 1a, curve α) will return to the axis of abscissae with a convexity. In reality, however, the curve of the heat coefficient of the hardness will in the case of alloys which are mechanical mixtures always return to the axis of abscissae with a convexity.

Similar results are obtained if instead of (1) another dependence is used, for example

$$H = a\tau^n,$$

where τ is the duration of the action of the load, etc.

Hence, for alloys which form mechanical mixtures of the components a linear dependence between the hardness and the composition can only occur for strictly defined values of the other factors which affect the hardness. In the overwhelming majority of cases the dependence will not be linear, however.

This is understandable: the hardness is a function not only of the composition of the alloy, but also of the temperature, the duration of the action of the load, the rate of deformation, etc., that is

$$H = H(\xi_1, \xi_2, \ldots, \xi_n, x), \qquad (10)$$

where x is the composition, and ξ_i the other variables. Incidentally, any property (A) which can be represented in the form (10) will be a linear function of the composition (in the general case) if it can be represented in the form

$$A = A(\xi_1, \xi_2, \ldots, \xi_n, x) =$$

$$= A_1(\xi_1, \xi_2, \ldots, \xi_n)\, x + A_2(\xi_1, \xi_2, \ldots, \xi_n). \qquad (11)$$

If, however, the property A cannot be represented in the form (11) (as, for example, the hardness), then a linear dependence of this property on the composition will be observed only in specific cases.

The concepts described above are close to the views expressed by A. A. Bochvar [17] who quite correctly has raised the question of the hardness not being a function of the composition alone. Further, the question was, however, reduced to a deviation from the rule of additivity caused by the change in the position of the structural components in the process of plastic deformation. Although the structure of the alloys undoubtedly has an effect also on their hardness, the general reason for the non-linear dependence of the hardness on the composition of alloys which form mechanical mixtures of the components is that the hardness is such a function of many variables as cannot be expressed by equation (11).

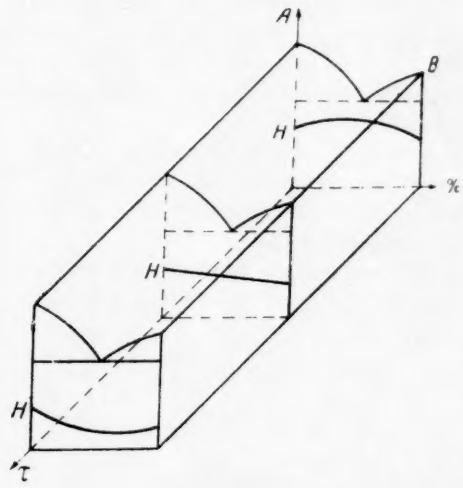

Fig. 2. Inversion of the isochrons and isotherms of the hardness with changing temperatures and rate of deformation.

Fig. 2 shows the inversion of the isotherms and isochrons of the hardness with the change in temperature and the rate of deformation in systems formed by a mixture of the components *A* and *B* (of the eutectic type). At a low temperature and a high rate of deformation (for example, in the case of the impact hardness or at short durations of the load τ) the isotherms and isochrons return to the axis of abscissae with a concaviety, but at high temperatures and low rates of deformation they return with a convexity to the axis of concentration; a linear form of the isotherms and isochrons is only possible as a special case at some average value of the temperature and the rate of deformation.

The concepts explained above can easily be put in a general form for the case of a mechanical mixture of more than two components.

VOL. 8 1959

If one demands a linear change of the property with changing composition in any section of a multi phase system equation (11) should have the form

$$A = A(\xi_1, \xi_2, \ldots, \xi_n, x_1, x_2, \ldots, x_m) = \sum_{i=1}^{m} A_i(\xi_1, \xi_2, \ldots, \xi_n)\, x_i + A_n(\xi_1, \xi_2, \ldots, \xi_n). \quad (12)$$

CONCLUSIONS

1. It is shown that a linear dependence of the hardness on the composition of alloys which form a mechanical mixture of the components can occur only in a special case. In the general case such a dependence will be non-linear.

2. The form of the functional dependence is given which should govern any property which is to be a linear function of the composition in the general case.

3. The concepts explained are given a general form for alloys containing any number of phases.

Translated by B. Ruhemann

REFERENCES

1. A. Sapozhnikov and Ia. Kanevskii, *Zh. rusek fiz.-khim. obshch.* 38, 246 (1906).
2. A. Sapozhnikov and Ia. Kanevskii, *Zh. russk. fiz.-khim. obshch.* 39, 901 (1907).
3. P.Ia. Sal'dau, *Zh. russk. fiz.-khim. obshch.* 61, 837 (1929).
4. V.P. Shishokin, *Izv. Akad. Nauk SSSR ser. khimich.* No.6, 1341 (1937).
5. V.P. Shishokin, *Zh. tekh. fiz.* 8, 1613 (1938).
6. A.A. Bochvar and Z.A. Sviderskaia, *Izv. Akad. Nauk SSSR OTN*, No.9, 821 (1945).
7. A.A. Bochvar, *Izv. Akad. Nauk SSSR, OTN*, No.9, 1463 (1948).
8. Ye.M. Savitskii and V.V. Baron, *Izv. sekt. fiz.-khim. analiza*, 27, 86 (1956).
9. N.S. Kurnakov and A.N. Akhnazarov, *Izv. SPb. politekh. inst.* 24, 1 (1915).
10. A.I. Glazunov and M.M. Matveyev, *Izv. SPb. politekh. inst.* No.9, 471 (1913).
11. V.P. Shishokin, V.A. Ageyeva and N.A. Vikhoreva, *Zh. tekh. fiz.* 10, 491 (1940).
12. A.A. Bochvar and O.S. Zhadayeva, *Izv. Akad. Nauk SSSR, OTN*, No.10-11, 1089 (1945).
13. A.A. Bochvar and Z.A. Sviderskaia, *Izv. Akad. Nauk SSSR, OTN*, No.7, 1001 (1946).
14. A.M. Korol'kov, *Izv. Akad. Nauk SSSR, OTN*, No.1, 114 (1949).
15. V.A. Nemilov, *Vestnik MGU*, No.9, 57 (1948).
16. V.P. Shishokin and A.A. Telitsyn, *Zh. tekh. fiz.* 22, 1572 (1952).
17. A.A. Bochvar, *Izv. Akad. Nauk SSSR, OTN*, No.5, 743 (1946).

VOL. 8 195

EFFECT OF THE RATE OF HEATING AND COOLING ON THE IRREVERSIBLE DEFORMATION OF IRON*

S.F. KOVTUN

Physico-technical Institute of the Academy of Sciences of the USSR

(Received 25 December 1958)

It has been shown in a number of papers [1-6] that metals with pronounced anisotropy of the physical and mechanical properties alter their dimensions as the result of repeated heating and cooling. The amount of the residual deformation depends on the number of heat changes.

It is to be expected that such irreversible thermal deformations will be particularly noticeable if the heat changes cover the region of polymorphous transitions; one may also suppose that the thermal deformations will strongly depend on the rate at which the boundary between the two phases is shifting. Preliminary experiments have shown that the results obtained may be seriously distorted by the oxide film which appears on the surface of the specimen; therefore, all our basic experiments were made in a good vacuum.

In the present paper we studied the effect of heat cycles and the rate of heating and cooling in the interval of the $\alpha \rightleftarrows \gamma$ transition on the dimensions and form of iron specimens.

APPARATUS

The experiments on heat changes were made in a vacuum apparatus (Fig. 1) which represents a cylindrical chamber of 80 in^3. On the lateral flanges of it were mounted a prechamber for admitting the specimens without destroying the vacuum, the leads for the electric current and inspection windows. The chamber was cooled with running water. The apparatus was evacuated with a diffusion pump with a pumping rate of 2000 l/sec and a prevacuum pump. A nitrogen trap mounted between the working chamber and the diffusion pump served as a protection against the penetration of oil vapours and as an additional evacuating pump for condensing gases.

A heater, representing a tube of 35 mm diameter and 500 mm length (*7*) with windings of molybdenum wire (*8*) was mounted in the chamber. To reduce heat losses through radiation and to create a uniform temperature in the furnace the tube was surrounded by

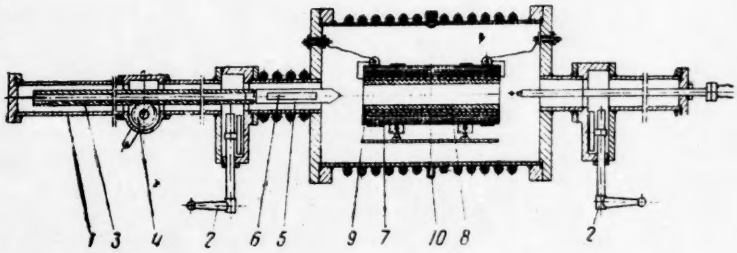

Fig. 1. Section of apparatus

* *Fiz. metal. metalloved.* 8, No.6, 939-945, 1959.

four screens, ceramic ones of Al_2O_3 (*9*) and an iron one. The vacuum lock consisted of tube *1*, divided by the excentric valve *2* in which was the rod *3* which moves along the tube *1* when the pinion *4* is turned. At the end of rod *3* the molybdenum carrier *5* for the specimens *6* was mounted. The specimens were loaded in the pre-chamber which was then evacuated to a pressure of 10^{-2} mm; after pumping the valve *2* was opened and the carrier with the specimen moved into the furnace.

A movable Pt-PtRh thermocouple was mounted on the other flange; it was enclosed in a double-channel tube which in turn was enclosed in a steel tube of 8 mm diameter. The tube with the thermocouple was introduced in the chamber through a greased packing which made it possible to measure the temperature of the specimens at any point of the working space of the furnace. To admit air into the chamber the needle valve *10* was used.

HEATING AND COOLING THE SPECIMENS *IN VACUO*

Cylindrical specimens of iron and carbon steel were subjected to repeated heating and cooling (heat changes) *in vacuo*. The chemical compositions and initial dimensions of the specimens are given in Table 1.

The first experiments with temperature cycles were made with the object of studying the effect of the phase transition on the irreversible deformation of the iron specimens. For this purpose the heating and cooling of the specimens was done with passing through the temperature of the $\alpha \rightleftarrows \gamma$ transition (910°C).

The experiments were conducted in the following manner: The specimens were placed in the molybdenum carrier and introduced into the vacuum furnace which had been heated to a temperature of $1000 \pm 20^{\circ}$. After thirty minutes holding they were taken out of the furnace and for 20 min cooled *in vacuo* to a temperature of 300°. Then the process was repeated. After every ten-twenty temperature cycles the specimens were cooled to room temperature, and taken out of the vacuum system for measurement and for the investigation of the surface. The specimens were laid horizontally so as to exclude the effect of the weight on the change in the length. The friction forces which occur between the specimen and the molybdenum carrier might somewhat weaken the effect of the change in length. To estimate this effect, the experiments were made on different carriers, made from molybdenum, tantalum, iron, etc., but since no noticeable effect of the carrier on the change in the length of the specimens was observed, this effect was subsequently neglected.

Preliminary experiments had shown that in a vacuum of the order of 10^{-2}-10^{-3} mm the specimens are covered with an oxide layer which affects the effect we wanted to study to a considerable extent. All experiments were therefore made at a pressure of 5×10^{-5} to 3×10^{-7} mm Hg. Cautionary measures were taken to prevent the formation of oxide films on the surface of the specimens. For this purpose the specimen was placed in an iron tube and before the beginning of the experiment was degassed for 30 to 40 min to a residual pressure of 4×10^{-7} mm. The rate of heating the specimen in the region of the $\alpha \rightleftarrows \gamma$ transition was 18°/min, the rate of cooling 45°/min. After several hundred heat changes the surface of the specimens which remained silvery-white became gradually

TABLE 1

Specimen	Impurities content in %							Length of specimen mm	Diameter of specimen mm
	C	Mn	Si	Cr	S	P	N		
Armco iron	0.04	0.14	0.20	–	0.02	0.010	0.026	100.00	8.05
3 steel	0.15	0.45	–	–	0.40	0.015	–	90.01	8.05
40 steel	0.40	0.55	0.25	0.1	0.20	0.020	0.030	96.11	8.00
UBA steel	0.80	0.30	0.30	0.2	0.20	0.030	–	84.86	6.55
Y12A steel	1.20	0.20	0.30	0.2	0.20	0.080	–	80.22	7.97

covered with creases.

Fig. 2 shows a section of the surface of the initial specimen and the same section after 300 heat changes. The length of the iron specimen as a function of the number of heat changes increases rapidly, and its diameter decreases correspondingly. With increasing number of heat changes the rate of increase of the length of the specimen increases.

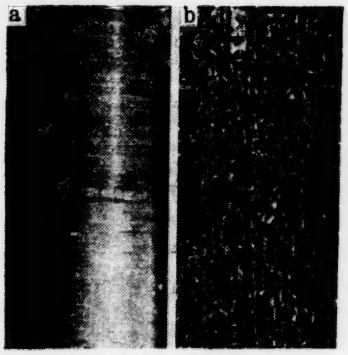

Fig. 2. Surface of the initial specimen (a) and the same section of the surface after 300 heat changes (b); x 6.

A set of specimens was subjected to heat changes in the temperature interval from 250 to 700°. The change in their length after 100 cycles did not exceed 0.2%. The form of the specimen did not change. With increasing number of heat changes a growth of the grains is observed in the specimens. Specimens consisting of large crystals change in length more markedly.

THERMAL CHANGES UNDER DIFFERENT HEAT TREATMENTS

To trace the effect of heating and cooling on the change in the length of the specimens, the experiments were in the main made under two heat treatments with the same specimen either 68 or 39 mm length and 8.0 mm diameter. In the beginning of the experiment and at the transition to a new heat treatment, the surface of the specimen was cleaned with fine emery paper. A thermocouple welded to the surface of the specimen made it possible to measure the rates of heating and cooling the specimen.

Under the first heat treatment a high rate of heating and low rate of cooling was achieved by heating the specimen to a temperature of 1000° by introducing it into the heated furnace, and by cooling it together with the switched off furnace.

Under the second heat treatment a low rate of heating and high rate of cooling was achieved by heating the specimen together with the furnace to a temperature of 1000° and by cooling outside the furnace to a temperature of 300°.

The measurements of the length of the specimen were made after every ten heat changes.

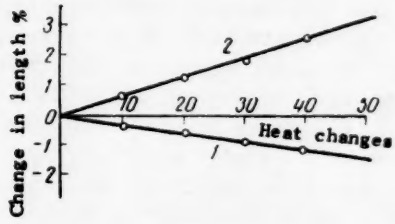

Fig. 3. Changes in the length of iron specimens as a function of the number of heat changes.

The results of the measurements of the length of the specimen are shown in Fig. 3. Here are presented two heat treatments under which the results of the change in the length of the specimen during the heat changes are diametrically opposite. Under the first heat treatment, where the rate of heating was 30°/min and the rate of cooling 6°/min, a rapid reduction in the length is observed (straight line 1, Fig. 3). At a rate of heating of 2°/min and of cooling of 80°/min a rapid increase in the length is observed (straight line 2).

As the experiments show, one can select such rates of heating and cooling that hardly any change in the length is to be observed. In our experiments this occurred at a rate of heating of 60°/min and a rate of cooling of 75°/min.

DISCUSSION OF THE RESULTS

The experiments show that when cylindrical

iron specimens are repeatedly heated and cooled in succession in the temperature interval which covers the $\alpha \rightleftarrows \gamma$ phase transition, irreversible changes in the length of the specimen occur. In the absence of an oxide film the changes in the length of a specimen of pure iron depend on the rates of heating and cooling.

It should be noted that the changes in the length of the specimens are recorded only for the transition through the point of the $\alpha \rightleftarrows \gamma$ phase transformation. For heat changes made *in vacuo* in the temperature interval below the $\alpha \rightleftarrows \gamma$ transition no noticeable change in length was observed.

The mechanism of the irreversible changes in iron specimens during the $\alpha \rightleftarrows \gamma$ transition is not yet sufficiently known; nevertheless, one may attempt to explain it in the following manner: We know that the $\alpha \rightarrow \gamma$ transition in iron occurs with a reduction in the atomic volume [7]. Hence, if one assumes that when the specimen is heated in the furnace the $\alpha \rightarrow \gamma$ transition begins at the surface and gradually spreads through the entire volume, one can reckon that the outer layers in the γ phase, which has a smaller volume, compress the inner parts of the specimen which are in the α phase. When the specimen is cooled, however, the outer layers which are in the α phase have a larger volume and exert stresses on that part of the specimen which is still in the γ phase.

Let us assume that the change in the linear dimensions of the iron specimen, when the phase transition occurs simultaneously throughout the entire volume, is ϵ % on account of the change in the atomic volumes. In the $\alpha \rightarrow \gamma$ transition the atomic volume of iron decreases from 12,1750 to 12.0512(kX)^3 [8]. If, however, the $\alpha \rightarrow \gamma$ transition is not completed simultaneously through the entire volume, but first in the upper layer of the cylindrical specimen and then in the following layers, the phase boundary will gradually spread inside the specimen. In our experiments the boundary between the α and γ phases moved from the outer surface into the specimen. If there were no link between the α and γ phase layers, or if the $\alpha \rightarrow \gamma$ transition were to proceed without the formation of a boundary between the α and γ phases, then, after the completion of the $\alpha \rightarrow \gamma$ transition the length of the specimen would be shortened by the quantity

$$\varepsilon = \frac{l_\alpha - l_\gamma}{l_\alpha} 100\%,$$

where l_α and l_γ are the lengths of the specimen in the α and γ phases during the $\alpha \rightarrow \gamma$ transition. Under real conditions the α and γ layers penetrate each other. Therefore, the inner layer of the α phase will on heating counteract the compressing forces of the γ phase layer. On cooling, however, the reverse process takes place: the inner layer of the γ phase will counteract the extending stresses of the γ phase layer. The resulting effect of compression or extension of the specimen will depend on the plastic properties of the one or the other phase.

In order not to complicate the question, we shall consider the irreversible change in the length of a cylindrical iron specimen as the result of the phase transition without taking into account its strength characteristics in the α and γ phases.

One can show that as a result of the gradual spread of the new phase inside the specimen an irreversible change in the length of the cylindrical specimen should occur if the rates of heating and cooling are different.

Let us examine two cases:

1) instantaneous heating and slow cooling of the specimen;

2) slow heating and instantaneous cooling.

By instantaneous heating or cooling we shall understand the simultaneous transition from the α to the γ phase throughout the entire volume without the formation of a shifting phase boundary.

With rapid heating throughout the entire volume, i.e. with instantaneous $\alpha \rightarrow \gamma$ transition the length of the specimen in the γ phase will be equal to $l_\gamma = l_{0\alpha}\ (1-\varepsilon)$, where l_γ and $l_{0\alpha}$ are the lengths of the specimen in the α and γ phases respectively, ϵ is the change in the length of the specimen without the formation of a phase boundary. If the specimen is now slowly cooled, the outer laye of α iron will extend the inner layer of γ iron and the length of the specimen after the transition to the α phase will be equal to

$$l_{1\alpha} = l_\gamma\ (1 + \varepsilon_1),$$

where ϵ_1 is the change in the length of the specimen for the $\gamma \rightarrow \alpha$ transition taking account of the interaction of the layers of the α and γ phases. Substituting the equation for l_γ we obtain

$$l_{1\alpha} = l_{0\alpha}(1-\varepsilon)(1+\varepsilon_1).$$

In this case $\varepsilon_1 < \varepsilon$, since the reverse transition $\gamma \rightarrow \alpha$ occurs gradually and the extending stresses of the α layer are partly compensated for by the counteraction of the γ layer. Therefore, the length $l_{1\alpha}$ is after one complete $\alpha \rightleftarrows \gamma$ transition irreversibly shortened by the amount Δl_1 (Fig. 4a)

$$\Delta l_1 = -l_{0\alpha}[(\varepsilon-\varepsilon_1)+\varepsilon\varepsilon_1] \cong -l_{0\alpha}(\varepsilon-\varepsilon_1).$$

In the second case, for slow heating, when the compressing forces of the γ layer which is being formed will be partly compensated for by the counteraction of the inner α layer, and the length of the specimen after a complete transition into the γ phase will be

$$l_\gamma = l_{0\alpha}(1-\varepsilon_2),$$

where l_γ is the length of the specimen in the γ phase after the $\alpha \rightarrow \gamma$ transition, $l_{0\alpha}$ the length of the specimen in the α phase up to the $\alpha \rightarrow \gamma$ transition; ϵ_2 is the change in the length of the specimen taking account of the interaction of the layers of the α and γ phases for slow heating. If this specimen is cooled instantaneously, its length in the α phase will be

$$l_{1\alpha} = l_\gamma(1+\varepsilon),$$

or, substituting the equation for l_γ, we obtain

$$l_{1\alpha} = l_{0\alpha}(1-\varepsilon_2)(1+\varepsilon).$$

Since $\varepsilon_2 < \varepsilon$ for the same reason stated above, after the complete $\alpha \rightleftarrows \gamma$ transition, if $\varepsilon_2 < \frac{\varepsilon}{\varepsilon+1} < \varepsilon$, the specimen will irreversibly increase in length by the amount l_2 (Fig. 4b)

$$\Delta l_2 = l_{0\alpha}(\varepsilon-\varepsilon_2-\varepsilon\varepsilon_2) \cong l_{0\alpha}(\varepsilon-\varepsilon_2).$$

Under real conditions the difference in the values of ϵ, ϵ_1 and ϵ_2 will be less, since interaction between the phase layers occurs both on heating and on cooling. By changing the relative rates of heating and cooling one can therefore change both the rate and even the sign of the deformation.

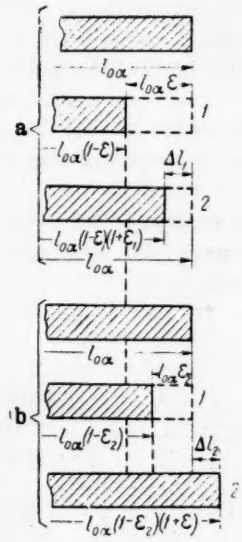

Fig. 4a. *1:* Shortening of the length by $l_{0\alpha}$ during heating without interaction; *2:* irreversible shortening after slow cooling with interaction of the phases α and γ,

$$\Delta l_1 = l_{0\alpha}[-(\varepsilon-\varepsilon_1)-\varepsilon\varepsilon_1].$$

Fig. 4b. *1:* Shortening by $l_{0\alpha}\epsilon_2$ for heating with taking the interaction of phases α and γ into account; *2:* irreversible lengthening on cooling without interaction between the phases α and γ,

$$\Delta l_2 = l_{0\alpha}(\varepsilon-\varepsilon_2-\varepsilon_1\varepsilon_2)$$

The explanation of the change in the length of iron specimens for heat changes in the temperature interval which covers the point of the $\alpha \rightleftarrows \gamma$ transition proposed by us is confirmed by the experimental data obtained by us and shown in Fig. 3.

With rapid (not instantaneous) cooling at a rate of 30°/min and slow cooling at a rate of 6°/min (Fig. 3, straight line *1*) a uniform shortening of the length of the specimen occurs. For every 10 heat changes the length of the specimen shortens by 0.28%.

VOL. 8 1959

With slow heating (2°/min) and rapid cooling (80°/min) a uniform increase in the length is observed (Fig.3, curve 2). For every 10 heat changes the specimen increases in length by 0.7%.

As the experiments have shown, one can change not only the amount of the residual deformation but also its sign by altering the rates of heating and cooling.

The grain growth observed during heat changes in the specimens affects the amount of the irreversible deformation, since in the process the plastic properties of the metal are altered. Therefore, one may suppose that adding impurities which change the mechanical properties of the metal one can also change the amount of irreversible deformation in phase transitions.

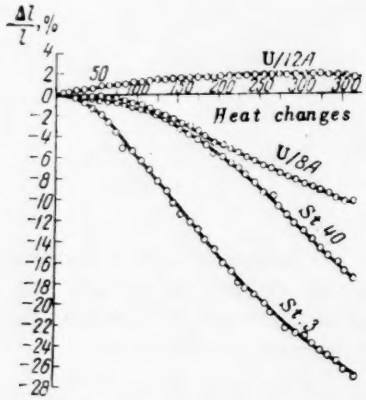

Fig. 5. Change in the length of specimens of steel of various brands as a function of the number of heat changes.

Fig.5 shows the results of the change in the length of steel specimens as a function of the number of heat changes. Since these experiments were made at a residual pressure of 10^{-3} mm, an oxide film was formed during the experiment.

With increasing number of heat changes longitudinal cracks appeared on the oxidized specimens, creases appeared on their ends, and the shape of the specimens became barrel-like. Specimens of 3 steel were shortened most in length, specimens of 40 steel a little less and specimens of U8A steel still less. A specimen of U12A steel increased in length.

CONCLUSIONS

1. Heat changes of cylindrical specimens of iron, 3 steel, 40 steel, U8A steel and U12A steel effected *in vacuo* by means of repeated heating and cooling in succession in the temperature interval which covers the point of the $\alpha \rightleftarrows \gamma$ transition cause considerable residual changes in the length of the specimens.

2. The amount of the irreversible change in the length of the specimens of iron during the phase transitions can be reduced by a corresponding selection of the per cent content of impurities, in particular carbon.

3. The rates of cooling and heating the specimens are the main factor which substantially affects the change in the length during repeated heat changes.

4. A possible mechanism is suggested for the change in the length of the metal specimens during repeated heating and cooling with passing through the point of the phase transformation.

I express my profound gratitude to Professor K.D. Sinel'nikov for guiding this work and to V.Ye. Ivanov for his help in carrying it out.

Translated by B. Ruhemann

REFERENCES

1. D.K. Chernov, *Zhurnal Russkogo metallurgicheskogo obshchestva*, No.5, part 1, p.706 (1912).
2. F. Berger, *Zs. Vereines Deutsch. Ingenieure*, 72, No.26 (1928).
3. L.A. Glikman, *Zh. tekh. fiz.* 7, 294 (1937).
4. W. Boas and K.W. Honeycombe, *Proc. Roy. Soc.* A188, No.1015, 427 (1947).
5. *Doklady Sovietskoi delegatsii na Mezhdunarodnoi konferentsii po mirnomu ispol'zovaniiu atomnoi energii "Issledovaniia v oblasti geologii, khimii i metallurgii" (Reports of the Soviet delegation to the International Conference on the Peaceful Utilization of Atomic Energy "Studies in geology, chemistry and metallurgy")* Akad. Nauk SSSR p.263, Moscow (1955).
6. F. Fut, *Fizicheskaia metallurgiia urana. Materialy Mezhdunarodnoi konferentsii po ispozovaniiu atomnoi energii v mirnykh tseliakh (The physical metallography of uranium. Materials of the International Conference for the*

utilization of atomic energy for peaceful purposes) M.M.K., Report 555 (1954).

7. V.D. Kuznetsov, *Kristally i kristallizatsiia (Crystals and crystallization)* p. 271, Moscow (1953).

8. Z.S. Basinski, W. Hume-Rothery and A.L. Sutton, *Proc. Roy. Soco* A229, 459 (1954).

VOL.
8
1959